Vidya Bharati Shaikshanik Mandal, Amravati's

VIDYA BHARATI MAHAVIDYALAYA, AMRAVATI

Affiliated to Sant Gadge Baba Amravati University, Amravati

Re-accredited 'A' Grade by NAAC (CGPA : 3.26 Second Cycle)

CPE Status by UGC-Thrice

Lead College identified by SGBAU, Amravati,

Mentor College under Paramarsha Scheme of UGC

C.K. Naidu Road, Camp, Amravati, Maharashtra State, India, PIN 444602

Phone: 0721-2662740, Fax 0721-2662740,

http://www.vbmv.org

Email: vm126@sgbau.ac.in, principal@vbmv.org

3.3.2 Number of research papers per teachers in the Journals notified on UGC website during the Academc Year 2014-15

SN	Title of paper	Name of the author/s	Department of the teacher	Name of journal	Year of publication	ISSN number	Link to the recognition in UGC enlistment of the Journal
1	Phytochemical screening and assessment of biomolecule compounds in Scilla hyacinthina Roth. Macbr. bulb	M.U.Ghurde & S.N.Malode	Botany	Journal of Global Biosciences	2014-15	23201355	Not listed in present UGC approved list as well as in deleted approved UGC List
2	Cytogenetic Effects of Tilt on Root Tip Meristem of onion Allium cepa L.	Pulate P.V. & Tarar J.L	Botany	International Journal of Plant and Environmental Science	2014-15	22314490	Not listed in present UGC approved list as well as in deleted approved UGC List
3	Liberalization of Indian Banking and Regulations, Page No.21-28	Dr. S. B. Kadu	Commerce	Journal of Research & Development, Vol.	2014-15	22309578	Not listed in present UGC approved list as well as in deleted approved UGC List
4	Priority Sector Lending for Agriculture in India	Dr. S. B. Kadu & Praneeta Deshmukh	Commerce	International Peer Reviewed Research Journal Special Issue	2014-15	22789308	Not listed in present UGC approved list as well as in deleted approved UGC List
5	Mahatma Gandhi National Rural Employment Guarantee Scheme: A Unique for Indian Rural Women, Page No.82-85	Dr. S. B. Kadu, Mr.S.K.Rodde	Commerce	"The Horizon" A Bi-annual Interdisciplinary Research Journal, Volume 5, No.2,	2014-15	22294554	Not listed in present UGC approved list as well as in deleted approved UGC List
6	Sensor Technoloies For Sensing The Heart beatSignal And Their Limitation	N.B.Raut	Electronics	Journal of the intrument society of india	2014-15		Not listed in present UGC approved list as well as in deleted approved UGC List
7	Total Quality Management in Dr. Panjabrao Deshmukh Agricultural University Library, Akola Maharashtra A Users' Study	Dr.Vishal R.Shekhawat	Library and Information Sciences	Indian Journal of Agriculture Library and Information Services	2014-15	9748776	Not listed in present UGC approved list as well as in deleted approved UGC List
8	Synthesis and characterization of photoconductive CdS thin Semiconductor Film by Sillar Method	S. K. Karande , Dr. F. C. Raghuwanshi	Physics	International Journal of Basic & Appl. Resech. Spe.	2014-15	22493352	https://www.ugc.ac.in/pdfnews/5283580_UGC-Cancelled-List.pdf
9	Synthesis and ammonia sensing properties of Bi_2O_3nanoparticles	S.D.Kapse, Raghuwanshi F.C., Kapase V.D	Physics	International Journal of Basic & Appl. Resech. Spe.	2014-15	22493352	https://www.ugc.ac.in/pdfnews/5283580_UGC-Cancelled-List.pdf
10	Preparation techniques and applications of spinel ferrite nanoparticle: An overview	Tatte T.R., Kapase V.D, Raghuwanshi F.C.	Physics	International Journal of Basic & Appl. Resech. Spe.	2014-15	22493352	https://www.ugc.ac.in/pdfnews/5283580_UGC-Cancelled-List.pdf
11	Miscibility studies of PVC/PMMA blends by FTIR analysis and measurements of AC Electrical conductivity of PVC/PMMA Blends.	Dakare,A.B., G.T.Lamdhade, F.C.Raghuwanshi	Physics	International Journal of Basic & Appl. Resech. Spe.	2014-15	22493352	https://www.ugc.ac.in/pdfnews/5283580_UGC-Cancelled-List.pdf

12	DC Conductivity of 2:1 (PVC:PMMA) polyblends: Temperature dependent	Dakare,A.B. ,G.T.Lamdhade,	Physics	International Journal of Basic & Appl. Resech. Spe.	2014-15	22493352	https://www.ugc.ac.in/pdfnews/5283580_UGC-Cancelled-List.pdf
13	Zn_2SnO_4modified ZnO thick film resistors as LPG sensor	V.S.Kalyamwar, N.S.Kadu, N.L.Jadhao, S.D.Charpe,	Physics	International Journal of Basic & Appl. Resech. Spe.	2014-15	22493352	https://www.ugc.ac.in/pdfnews/5283580_UGC-Cancelled-List.pdf
14	Electrical conductivity of surface activated Nanostructure ZnO thick films.	S.D.Charpe, F.C.Raghuwanshi, V.S.Kalyamwar	Physics	International Journal of Basic & Appl. Resech. Spe.	2014-15	22493352	https://www.ugc.ac.in/pdfnews/5283580_UGC-Cancelled-List.pdf
15	Study of variation dielectric constant of 4:1 PS PMMA polyblend thin films doped with Oxalic Acid in different weight proportions.	A. S.Wadatkar, T.S.Wasnik, S.G.Vidhale, N.G.Belsare	Physics	International Journal of Basic & Appl. Resech. Spe.	2014-15	22493352	https://www.ugc.ac.in/pdfnews/5283580_UGC-Cancelled-List.pdf
16	Effect of UV radiation exposure on the dielectric constant of salicylic acid doped polymer thin film of PMMA.	S.G.Vidhale, N.G.Belsare, A.S.Wadatkar	Physics	International Journal of Basic & Appl. Resech. Spe.	2014-15	22493352	https://www.ugc.ac.in/pdfnews/5283580_UGC-Cancelled-List.pdf
17	Temperature and Electric field dependence of DC electrical conductivity of 4:1 PVC-PMMA polyblend thin films doped with Cinnamic Acid	A.S.Wadatkar, S.G.Vidhale, N.G.Belsare, R.V.Waghmare, V.B.Gawali	Physics	International Journal of Basic & Appl. Resech. Spe.	2014-15	22493352	https://www.ugc.ac.in/pdfnews/5283580_UGC-Cancelled-List.pdf
18	Investigation of Temperature dependence of electrical conductivity of PVAC-PPy-$CrCl_3$ composite polymer film.	R. V. Joat, S.Bakade, S.Joshi, T.S.Wasnik, A.S.Wadatkar, P.Bodakhe	Physics	International Journal of Basic & Appl. Resech. Spe.	2014-15	22493352	https://www.ugc.ac.in/pdfnews/5283580_UGC-Cancelled-List.pdf
19	The Study of Molecular Interaction of Proton Polymer Electrolytes using Ultrasonic Technique	Joat,R.V, .,S.Bakade, S.Jadhao, P.Bodkhe, S.Binani	Physics	International Journal of Basic & Appl. Resech. Spe.	2014-15	22493352	https://www.ugc.ac.in/pdfnews/5283580_UGC-Cancelled-List.pdf
20	Stannic Oxide Doped with Zinc Oxide based for Co_2 gas Sensing	R. M. Agrawal, G. T. Lamdhade, K. B. Raulkar	Physics	International Journal of Basic & Appl. Resech. Spe	2014-15	22493352	https://www.ugc.ac.in/pdfnews/5283580_UGC-Cancelled-List.pdf
21	Schottky -Richardson mechanism in Oxalic acid doped (PVC-PMMA) blends	Dakre A. B, Lamdhade G.T	Physics	International Journal of Sci.& Research	2014-15	23197064	Not listed in present UGC approved list as well as in deleted approved UGC List
22	Application of Polypyrrole for CO_2 Gas Sensing at different Temperatures	Agrawal, R. M., G. T. Lamdhade, K.B.Raulkar, F.C.Raguwanshi	Physics	International Journal of Basic & Appl. Resech. Spe	2014-15	22493352	https://www.ugc.ac.in/pdfnews/5283580_UGC-Cancelled-List.pdf
23	Effect of Cypermethrin on the ovary of fresh water fish *Channa straitus*	V T Tantarpale SH Rathod	Zoology	Indian Journal of life Science 3(2) page 87-89	2014-15	22771743	Not listed in present UGC approved list as well as in deleted approved UGC List
24	Protein and amino acid modulation in fresh water fish *Ophiocephalus orientalis* exposed to Cypermethrin	Gijare Shruti Tantarpale VT	Zoology	Journal of Pharmascutical Scientific Innovation	2014-15	78972277	Not listed in present UGC approved list as well as in deleted approved UGC List

25	Effects of Cypermethrin on lipid and cholesterol contents of fresh water fish Channa orientalis	Gijare Shruti Tantarpale VT	Zoology	Indian journal of Sci. research	2014-15	22501991	Not listed in present UGC approved list as well as in deleted approved UGC List
26	Morhpometric and meristic variation in fins of Channa punctatus from fresh water habitats in Amravati Region.	V.T.Tantarpale, S.H. Rathod, P.S. Joshi, S.A.Tantarpale, S.R.	Zoology	Indian Journal of Sci. Research	2014-15	9762876	Not listed in present UGC approved list as well as in deleted approved UGC List
27	A review of Ophidian studies in Vidarbha Region (M.S)	Joshi P.S, V.T.Tantarpale & K.M. Kulkarni	Zoology	Sci. Research Reporter	2014-15	22492321	Not listed in present UGC approved list as well as in deleted approved UGC List
28	Synthesis and characterization of some New N, O and S containing chlorosubstituted heterocycles and their antimicrobial screening against some common causative organisms.	P.R.Rajput and N.G.Ghodile	Chemistry	International Journal of Engineering Science and Innovative Technology, (IJESIT), 3(4), 2014, 373-377.	2014-15	23195967	Not listed in present UGC approved list as well as in deleted approved UGC List
29	Wound Healing Activity of *Butea Monosperma* in Wistar Rats.	P.R.Rajput and M.O.Malpani	Chemistry	Am. J. PharmTech Res. 2014; 4(4), 560-570.	2014-15	22493387	Not listed in present UGC approved list as well as in deleted approved UGC List
30	Antimicrobial study of analogues prepared under microwave assistance of active ingredient isolated from *Butea monosperma* plant and their growth promoting impact on some flowering plants.	P.R.Rajput and M.O.Malpani	Chemistry	IJGHC, 2014; Sec. A; 3(4), 1378-1383.	2014-15	22783229	Not listed in present UGC approved list as well as in deleted approved UGC List
31	A Facile Solid Phase Microwave Induced Synthesis and Antifungal Activity of SomeSubstituted pyrazolines-N1-Carbaldehydes	P. R. Solanki and Sonal Boob	Chemistry	World J. of Phamacy and Pharmacetical Sciences	2014-15	22784357	Not listed in present UGC approved list as well as in deleted approved UGC List
32	QSAR models for anti-malarial activity of 4-aminoquinolines	V. H. Masand, A. A. Toropov, A. P. Toropova and D. T. Mahajan	Chemistry	Computer Aided Drug Designing, 2014, 10, 75-82	2014-15	18756697	Not listed in present UGC approved list as well as in deleted approved UGC List
33	Tautomerism and multiple modelling enhance the efficacy of QSAR: Anti-malarial activity of phosphoramidate and phosphorothioamidate analogues of amiprophos methyl	V. H. Masand, D. T. Mahajan, P. Gramatica and J. Barlow	Chemistry	Med. Chem. Res, 2014, 23, 4825-4835	2014-15	10542523	Not listed in present UGC approved list as well as in deleted approved UGC List
34	Synthesis of α, β-Unsaturated Carbonyl Based Compounds as Acetylcholinesterase and Butyrylcholinesterase Inhibitors: Characterization, Molecular Modeling, QSAR Studies and Effect Against Amyloid ß-Induced Cytotoxicity	S. N. A. Bukhari, I. Jantan, V. H. Masand, D. T. Mahajan, M. Sher, M. Naeem-ul-Hassan and M. W. Amjad	Chemistry	European Journal of Medicinal Chemistry, 2014, Volume 83, Pages 355–365	2014-15	2235234	Not listed in present UGC approved list as well as in deleted approved UGC List

35	Determination of Optimum Values of Descriptors to Set Filters for Synthetic Tri-Pyrrole Derivatives (Prodiginines) Against Multi Drug Resistant Strain of Plasmodium Falciparum	Vijay H. Masand, Devidas T. Mahajan,Eslam Pourbasheer, Taibi Ben Hadda, Harsh Chauhan,	Chemistry	Current Research in Drug Discovery, 2014, 1 (2), 51-59	2014-15	23333235	Not listed in present UGC approved list as well as in deleted approved UGC List
36	Studies of acoustic behavior of 3-(2-benzimidazol)-3-nitro-6-methyl-Chromen-4-one (bnmc) in a different solvents system by using ultrasonic Interferometer	S. Quazi, D. Mahajan, V. Masand, N. Mohammad and M. Ingle	Chemistry	International Journal of Research and Development in Pharmacy and Life Sciences, 2014, Vol. 3, No.5, pp 1206-1210	2014-15	22780238	Not listed in present UGC approved list as well as in deleted approved UGC List
37	Theoretical based studies of ultrasonic velocities in dioxane -water mixtures of 4-bromo-2-{(e)-[(4-chlorophenyl) imino] methyl}phenol at different temperatures	N. Mohammad, S. Quazi, D. Mahajan, V. H. Masand and M. Ingle	Chemistry	International Journal of Pharma Sciences and Research (IJPSR), 2014, Vol 5, No 12, 1045-1048	2014-15	9759492	Not listed in present UGC approved list as well as in deleted approved UGC List
38	Synthesis, X-ray Diffraction,Thermogravimetric and DFT Analyses of Pyrimidine Derivatives	A. Barakat, H. J. Al-Najjar, A. M. Al-Majid, S. F. Adil, M. Ali, V. H. Masand, H. A. Ghabbour	Chemistry	Molecules, 2014, 19, 17187-17201.	2014-15	14203049	Not listed in present UGC approved list as well as in deleted approved UGC List
39	QSAR of Antitrypanosomal Activities of Polyphenols and their Analogues Using Multiple Linear Regression and Artificial Neural Networks	V. Rastija and V. H. Masand	Chemistry	Combinatorial Chemistry & High Throughput Screening, 2014, 17 (8), 709-17	2014-15	13862073	Not listed in present UGC approved list as well as in deleted approved UGC List
40	Study of plant growth regulating antibiotic drugs - 3-(2-benzimidazol)-3-nitro-6-methyl-chromen-4-one with innertransition metal complexes on spinach (spinacia oleracea l.) at different ph	S. Quazi, D. Mahajan, N. Mohammad and V. Masand	Chemistry	Indian Journal of Research in Pharmacy and Biotechnology, 2014, 2(5), 1419-1421	2014-15	23215674	Not listed in present UGC approved list as well as in deleted approved UGC List
41	Study of seed germination activity (plant growth regulator) of 2[(Z)-(2-phenyl-4H-chromen-4-ylidene) aminophenol and its Ni(III) and Cu (III) complexes on vegetable plant Trigonella *foenum-graecum*	Noor Mohammad, S. Azhar Quazi, Devidas T. Mahajan, Vijay Masand	Chemistry	International Journal of Biosciences and Nanosciences, 1(5), 2014, 100-103	2014-15	23495251	Not listed in present UGC approved list as well as in deleted approved UGC List
42	Molecular Interactions in Substituted Pyrimidines – Acetonitrile Solutions at 298.15–318.15 K1	Dr Pravin S Bodkhe,M.L.Narwade,A. B.Naik and G.G.Muley	Chemistry	Russian Journal of Physical Chemistry A, 2014, Vol. 88, No. 1, pp. 37–41. © Pleiade s Publishing, Ltd., 2014.	2014-15	360244	Not listed in present UGC approved list as well as in deleted approved UGC List

43	Synthesis , Characterisation and in vitro antimicrobial evaluation of noval 2-mercapto-4,6-disubstituted phenyl pyrimidine derivatives.	Dr Pravin S Bodkhe ,S.S.Binani and R.V.Joat	Chemistry	International Journal of Pharmacy and Pharmaceutical Sciences	2014-15	9751491	Not listed in present UGC approved list as well as in deleted approved UGC List
44	Babarao Musale yanchya 'Zingu Lukhu Lukhu' madhil stri chitran	Prof. Dr. Gajanan Bansod	Marathi	Aksharvaidarbhi	2014-15	9760296	Not listed in present UGC approved list as well as in deleted approved UGC List
45	Characterization of Pure Nanostructure ZnO and its Application as Gas Sensor	S. D. Charpe, F. C. Raghuwanshi, V. S.	Physics	Journal of Pure Applied and Industrial Physics	2014-15	23198133	Not listed in present UGC approved list as well as in deleted approved UGC List
46	Synthesis and characterization of Magnesium oxide Nanoparticles with 1:1 molar ratio via liquid –Phase method	Agrawal R.M., Charpe S.D., Raghuwanshi F.C., Lamdhade G.T.	Physics	International J. of Applic. Or Innv in Engeen.& Manag. (IJAIEM)	2014-15	23194847	Not listed in present UGC approved list as well as in deleted approved UGC List
47	Synthesis of Nano structure Zinc Oxide by Spray Pyrolysis and its characterization for Gas Sensing Application.	S.D.Charpe, F.C.Raghuwanshi, G.T.Lamdhade, V.S.Kalymwar	Physics	IPASJ International J of Ele Engin.	2014-15	2321600X	Not listed in present UGC approved list as well as in deleted approved UGC List
48	SnO2 Nanoparticles synthesis via liquid –phase Co-precipitation technique	G.T.Lamdhade, F.C.Raghuwanshi, R.M.Agrawal, V.M.Balkhande,T.Shripat	Physics	Adv. Mater. Lett.6(8) pp738-742	2014-15	9763961	Not listed in present UGC approved list as well as in deleted approved UGC List
49	Tin Oxide and Titanium Dioxide based CO2 Gas Sensor	G.T.Lamdhade	Physics	J of EleDev	2014-15	16823427	Not listed in present UGC approved list as well as in deleted approved UGC List
50	Fabrication of multilayer SnO2–ZnO–PPy sensor for ammonia gas detection	G T Lamdhade, K B Raulkar, S S Yawale and S P Yawale	Physics	Indian Journal of Physics	2014-15	9749845	Not listed in present UGC approved list as well as in deleted approved UGC List
51	Preparation and Ethanol Sensing Behavior of Spinel-type Nanosized Mixed Ferrites Containing Zn	V. D. KAPSE, F.C. RAGHUWANSHI, V.S. SANGAWAR	Physics	International Journal of Chemical and Physical Sciences	2014-15	23196602	Not listed in present UGC approved list as well as in deleted approved UGC List
52	Synthesis, Characterisation and Antibacterial Activities of Some New Bromo/Nitro 1,3-Thiazenes.	Tejaswini S.Bante, Vandana V. Parhate, P. R. Rajput	Chemistry	Inter. Journal of Chemical and Physical Sciences, IJCPS 4 (NCSC) 2015, 218-	2014-15	23196602	Not listed in present UGC approved list as well as in deleted approved UGC List
53	Synthesis and characterization of some new chlorosubstituted thiazoles and thiazolo-imidazoles and their impact on pathogens damaging *Oyster Mushroom* cultivation.	P.R.Rajput and N.G.Ghodile	Chemistry	Inter. Journal of Chemical and Physical Sciences, IJCPS 4 (NCSC) 2015. 296-299.	2014-15	23196602	Not listed in present UGC approved list as well as in deleted approved UGC List
54	Effect of extracts of test plants, isolated ingredient and prepared analogues on serum inorganic ions (*Sodium, Potassium, Calcium, Magnesium and Phosphorous*) in *Albino Rats.*	M.O.Malpani and P.R.Rajput	Chemistry	Inter. Journal of Chemical and Physical Sciences, IJCPS 4 (NCSC) 2015. 387-396	2014-15	23196602	Not listed in present UGC approved list as well as in deleted approved UGC List

55	Study of *Phyllanthus amarus* Plant Extract and Newly Synthesized Analogue of *Pyllanthin* on Induced Hepatotoxicity in *Albino Rat.*	Vandana V. Parhate, M. M. Rathore, P. R. Rajput	Chemistry	Inter. Journal of Chemical and Physical Sciences, IJCPS 4 (NCSC) 2015. 417-423.	2014-15		23196602	Not listed in present UGC approved list as well as in deleted approved UGC List
56	Synthesis and antimicrobial activity of some chalcones and Flavones.	M. M. Rathore, Vandana V. Parhate, P. R. Rajput	Chemistry	Inter. Journal of Chemical and Physical Sciences, IJCPS 4 (NCSC) 2015, 473-	2014-15		23196602	Not listed in present UGC approved list as well as in deleted approved UGC List
57	Eco-friendly synthesis, characterization and antibacterial assay of some chlorosubstituted isoxazoles.	P.R.Rajput,M.W.Bhade,C.D.Badnakhe and A.V.Gajbhiye	Chemistry	Inter. Journal of Chemical and Physical Sciences, IJCPS 4 (NCSC) 2015 342-	2014-15		23196602	Not listed in present UGC approved list as well as in deleted approved UGC List
58	Studies in acoustic parameters of promethazine drug in dioxane-water solvent at different temperatures.	U.S.Wasnik,R.M.Jumle and P.R.Rajput	Chemistry	Inter. Journal of Chemical and Physical Sciences, IJCPS 4 (NCSC) 2015, 478-	2014-15		23196602	Not listed in present UGC approved list as well as in deleted approved UGC List
59	Synthesis, characterization and antimicrobial Screening of some pyrazoles.	V.D.Mane,D.T.Mahajan and P.R.Rajput	Chemistry	Int. J. Pharm. Bio. Sci. 2015, 6(1), 213-218	2014-15		9756299	Not listed in present UGC approved list as well as in deleted approved UGC List
60	Microwave Assisted Solvent Free Synthesis Of 2,7-(Substituted Phenyl)- -3-Phenyl-5,7,7a-Trihydro-2h-Thiazolo [4,5-D] [1,3] Thiazin-5-Amine Derivatives	Dr.P.R.Solanki and Sonal Boob	Chemistry	International journal of chemical and physical sciences,special issue ,64 ,2015	2014-15		23196602	Not listed in present UGC approved list as well as in deleted approved UGC List
61	Antimycobacterial activity and in silico study of highly functionalised dispiropyrrolidines	A. C. Wei, M. A. Ali, Y. K. Yoon, S. B. Choi, H. Osman, V. H. Masand	Chemistry	Med. Chem. Res, 2015, Volume 24, Issue 2, pp 818-828	2014-15		10542523	Not listed in present UGC approved list as well as in deleted approved UGC List
62	Effect of information leakage and method of splitting (rational and random) on external predictive ability and behavior of different statistical parameters of QSAR model	V. H. Masand, D. T. Mahajan, G. M. Nazeruddin, T. Ben Hadda, V. Rastija and A. M. Alfeefy	Chemistry	Med. Chem. Res, 2015, 24, 1241–1264.	2014-15		10542523	Not listed in present UGC approved list as well as in deleted approved UGC List
63	Molecular docking and QSAR analyses for understanding the antimalarial activity of some 7-substituted-4-aminoquinoline derivatives	I. Shibi, L. Aswathy, R. Jisha, V. Masand, A. Divyachandran and J. Gajbhiye	Chemistry	European Journal of Pharmaceutical Sciences, 2015, 77, 9–23	2014-15		9280987	Not listed in present UGC approved list as well as in deleted approved UGC List
64	Discovery of Rimonabant and its potential analogues as anti-TB drug candidates	J. Gajbhiye, N. More, M. D. Patil, R. Ummanni, S. Kotapalli, P. Yogeeswari, D. Sriram and V.	Chemistry	Medicinal Chemistry Research, 2015, Vol 24, Issue 7, 2960-2971	2014-15		10542523	Not listed in present UGC approved list as well as in deleted approved UGC List

65	Studies of ultrasonic and Viscometric behavior of Azithromycin with different Solvent systems dioxane-water And methanol-water mixture At 305.15K	S.A.Quazi, D.T.Mahajan, Noor Mohammad, M.L.Narwade, Vijay Masand, M.R. Ingle	Chemistry	International Journal of Pharma Sciences and Research (IJPSR), 2015, Vol 6, No 01, Jan 143-144	2014-15	9759492	Not listed in present UGC approved list as well as in deleted approved UGC List
66	Studies of relative and specific viscosities of Aceclofenacin 70% Dioxane water mixture at different temperature	S.A.Quazi, D.T.Mahajan, Noor Mohammad, M.L.Narwade, Vijay Masand, M.R. Ingle	Chemistry	Indian Journal of Research in Pharmacy and Biotechnology, 2015, 3(1), 13-14	2014-15	23215674	Not listed in present UGC approved list as well as in deleted approved UGC List
67	Computational POM and DFT Evaluation of Experimental in-vitro Cancer Inhibition	T. B. Hadda, Z. K. Genc, V. H. Masand, N. Nebbache, I. Warad, S. Jodeh, M. Genc, Y. N. Mabkhot, A. Barakat and	Chemistry	Acta Chimica Slovenica, 2015, 62,	2014-15	13180207	Not listed in present UGC approved list as well as in deleted approved UGC List
68	Phytochemical investigations of *Dioscorea bulbifera linn*	U. G. Malode, N. Mohammad, S. Quazi, D. Mahajan and V. Masand	Chemistry	Indian Journal of Research in Pharmacy and Biotechnology, 2015, 3(1),	2014-15	23215674	Not listed in present UGC approved list as well as in deleted approved UGC List
69	Synthesis of (E)-1-(5-chloro-2-hydroxy-4-methylphenyl)-3-(4-nitrophenyl)prop-2-en-1-one and 4-chloro-5-methyl-2-(5-(4-nitrophenyl)- 4,5-dihydro-1h-pyrazol-3-yl)phenol and its derivatives	Charita B. Patil, Vijay H. Masand	Chemistry	International Journal on Recent and Innovation Trends in Computing and Communication, 2015, 3(10), 5745-5747	2014-15	23218169	Not listed in present UGC approved list as well as in deleted approved UGC List
70	Effect of Adsorption of toxic metal ions on fruit skin	C.M Deshmukh, C.N Deshmukh	Chemistry	Journal of medicinal chemistry and drug	2014-15	23479027	Not listed in present UGC approved list as well as in deleted approved UGC List
71	Effect of metal ligand complex on germination of some vegetable plants	C.M Deshmukh, Rohit Kadam, Prachi Bharatiya, C.N Deshmukh	Chemistry	Journal of medicinal chemistry and drug discovery	2014-15	23479027	Not listed in present UGC approved list as well as in deleted approved UGC List
72	Synthesis, Molecular Modeling, and Biological Evaluation of Novel 1, 3-Diphenyl-2-propen-1-one Based Pyrazolines as Anti-inflammatory Agents	Bukhari,Xin Zhang, Ibrahim Jantan, Hai-Liang Zhu, Muhammad Wahab Amjad1 and Vijay H. Masand	Chemistry	Chem Biol Drug Des 2014; 888555, pg. 729-742	2014-15		Not listed in present UGC approved list as well as in deleted approved UGC List

Research Paper

PHYTOCHEMICAL SCREENING AND ASSESSMENT OF BIOMOLECULES COMPOUNDS IN *SCILLA HYACINTHINA* (Roth) Macbr. BULB

M. U. Ghurde[1] and Malode S.N.[2]

[1]Department of Botany Vidya Bharati Mahavidyalaya, Amravati.
[2]P.G. Department of Botany,
Govt. Vidarbh Institute of Science and Humanities,
Amravati- 444 601.

Abstract

In most of the developing countries drugs of herbal origin have been used in traditional systems of medicines since ancient times. Traditional systems of medicine continue to be widely practiced on many accounts. Population rise, inadequate supply of drugs, prohibitive cost of treatments, side effects of several allopathic drugs and development of resistance to currently used drugs for infectious diseases have led to increased emphasis on the use of plant materials as a source of medicines for a wide variety of human ailments. Ethno medicine represents one of the best avenues in searching new economic plants for medicine. Thus herbs are staging a comeback and herbal 'renaissance' is happening all over the Globe. The herbal products today symbolize safety in contrast to the synthetics that are regarded as unsafe to human and environment. The drugs are derived either from the whole plant or from different organs, like leaves, stem, bark, root, flower, seed, etc. Some drugs are prepared from excretory plant product such as gum, resins and latex. It is very much evident that plants have bio-active chemicals called Phytochemicals which have physiological effect on human body; these phytochemicals have formed the bases of modern drug industries. Hence, present investigation is carried out to establish the preliminary phytochemical screening of petroleum ether, chloroform, acetone and aqueous extracts of bulb of *Scilla hyacinthina* (Roth) Macbr. The phytochemical evaluation and quantification of various extracts revealed the presence of high carbohydrate (42.95 %), protein (%) and secondary metabolites such as alkaloid (1.34gm), flavonoids (0.99gm) and saponin (2.32gm). qualitatively in aqueous and acetone extract as compared to other solvent. These studies will be helpful in developing standards for quality, purity and secondary metabolites in preparations of herbal medicine.

Key words: *Scilla hyacinthina*, Herbal medicine, Phytochemicals, Secondary metabolites.

INTRODUCTION

Medicinal plants are of great importance to the health of individuals and communities. The medicinal value of these plants lies in some chemical substances that produce a definite physiological action on the human body and these chemical substances are called as phytochemicals. Phytochemical constituents are the basic source for the establishment of several pharmaceutical industries. The constituent presents in the plant play a significant role in the identification of crude drug. Phytohemical screening is very important in identifying the new sources of therapeutically and industrially important compounds like alkaloids, flavonoids, phenolic compounds, saponin, steroids, tannins, terpenoids etc (Akindele and Adeyemi, 2007). Previously the drugs were identified by comparison only with the standard description available but recently due to the advancement in the field of pharmacognosy various techniques have been following for the standardization of crude drugs (Savithramma *et al*, 2010).

Scilla hyacinthina(Roth) Macbr Family- Liliaceae common among grasses on the floor of scrub, found in India and some Asian countries (Mathew,1983). With the onset of pre-mansoon, clouds, the plant *Scilla hyacinthina* raise their heads above the ground and produce first flush of white -pink inflorescence. 10-15 cm herb with a perennial tunicated bulb. The largest size of bulb ranges from 10-14gm.Leaves are simple, oblong, succulent with purplish blotches on the upper surface of leaf is an identification feature. The leaves are acts as vegetative prapogative, the apex of leaf on touch with soil produces new plant from adventitious bud. Scape 5-10 cm tall, flowersin terminal receme, white-pink colour,perianth 6 lobes, persistant, stamens 6, anthers versatile, ovary sessile, three celled. Fruit is capsule, globose, thin walled. Seeds ovoid and black. Seed contains mucilage, calcium oxalate, dextrine, starch, albuminous bodies and volatile oil. It is medicinally important, since it is used as an expectorant, diuretic and cardiac stimulant. The present study deals with the preliminary phytochemical screening of Scilla bulb, by studying the presence of phytochemicals, the uses of this plant in traditional treatment can be explained scientifically.

MATERIALS AND METHODS

The fully matured healthy plant material (Bulb) of *Scilla hyacinthina* (Roth) Macbr. was collected from GVISH Campus, Amravati during the rainy season. The material was thoroughly washed; air dried under shade and powdered by the help of mechanical process. The coarse powder of bulb was stored in airtight container for further studies.

Preliminary Phytochemical Analysis: Qualitative screening of bulb was performed for the identification of various classes of active chemical constituents using the methods described by Kokate 2005, Raman, 2006 and Kandelwal.

Quantitative analysis:

Total Carbohydrate and Protein of bulb was measured by the methods described by Sadashivam and Manickam, 1997. The crude quantification of major phytochemicals was done by using precipitation method. Each sample was analyzed in triplicates. Only alkaloids, flavonoids and saponin from the plant under study were quantified.

RESULTS AND DISCUSSION

Qualitative Analysis:

Qualitative phytochemical studies of bulb was performed on its water, acetone, petroleum ether and chloroform extracts (1:10) to identify it's carbohydrate and glycosides, protein and amino acids, alkaloids and other secondary metabolites like phenolic compounds and flavonoids, phytosterol and terpenoid by using suitable chemicals and reagents (Table 1). The color intensity was shown as `+`, `++`, `+++` and ++++ for low/slight, moderate, good and high means positive tests respectively and `-` `for no change means negative test. The Test for all the phytoconstituents were mostly observed to be positive with different intensity (+, ++, +++, ++++). The result showed that the carbohydrates which constitute the major edible part of the plants were found to present in all the four extract but higher percentage were found to be in aqueous extract. Among all the test Fehling's test was found to be sensitive for the presence of the carbohydrate. Acetone extract showed negative test for Molisch, Seliwanoff's and Bradfords test. This may be due to insolubility of carbohydrates. Proteins which form the structural and functional basis of the cell were found to be present in all the four extract i.e. aqueous, acetone, petroleum ether and chloroform. Except ninhydrin test rests of the three tests viz Biuret, Millons and Xanthophorin test were showed the positive results in all the three extract except acetone extract. Amongst the above three tests Xanthophorin test showed good results, this indicated the presence of aromatic amino acids such as phenyl alanine, tyrosine and tryptophan in the extract. Ninhydrin is an oxidizing agent which reacts only with alpha amino group. As there was no change in the Ninhydrin test might be due to the absence of alpha amino group in the extract. However acetone extract of bulb showed negative in Biuret, Ninhydrin and Millons test. Petroleum ether extract showed slight present in Millon test, this might be due to insolubility of protein in ether and alcohol. The test for alkaloids showed their strong presence in aqueous extract for Dragendorff's test, Mayer's test and Wagner's test. The test showed good results in acetone extract also. Amongst all the test Dragendorff's test showed strong positivity in all four extract, this indicated the strong presence of tertiary amines in the extract or this may be due to the coupling of heavy metals in the reagent with the nitrogen in the alkaloid to form ion pairs that form an insoluble ppt, whereas Mayer and Wagner's test showed slight presence of alkaloid in Petroleum and chloroform extract. Flavonoids showed good response for the entire test in all the four extract except alkaline test showed slight presence in acetone extract and lead acetate showed negative test for petroleum ether and chloroform. Amongst all the test shinoda test showed abundant presence in all extract this indicate the presence of flavones in the test sample then they are reduced to anthocyanin under Shinoda test, dramatic change in colour indicate the presence of flavonoid. Glycosides and cardiac glycosides showed good characteristic colour and precipitate in all the tested extract. The presence of phenolic compounds and tannins were confirmed in aqueous, acetone and petroleum

ether extract and absent in chloroform extract. Gelatin test, Lead acetate, acetic acid test and ferric chloride test showed moderate to strong presence in aqueous extract. Acetone extract showed strong response to ferric chloride and gelatin test and good for lead acetate test, negative in acetic acid test. However ferric chloride and gelatin test showed good results in petroleum ether extract, whereas lead acetate and acetic acid test showed no change for the same. Phenolic compounds and tannins were found absent in chloroform extract. Salkowaski test showed strong presence of phytosterols. The strong presence of Phytosterols, triterpenoids and terpenoids has been seen in aqueous, acetone and chloroform extracts and found to be absent in petroleum ether extract.

Table 1: Qualitative Phytochemical analysis of *Scilla hycinthiana* bulb

Chemical constituent	Tests	Bulb			
		AQ	AC	PE	CH
Carbohydrates and Glycosides	Molisch's Test	+++	-	+++	+++
	Benedict's Test	+++	+	+++	++
	Fehlings test	++	++	+++	++++
	Seliwanoff's tests	+++	-	+++	+
	Bradfords tests	+++	-	-	-
	Borntrager's test	+++	+++	+++	+++
Proteins & amino acid	Biuret Test	+++	-	+++	+
	Ninhydrin Test	-	-	-	-
	Millon's Test	+++	-	+	++
	Xanthophorin Test	+++	+++	+++	+++
Alkaloids	Dragendorff's Test	++++	++	+++	++++
	Mayer's Test	+++	++	+	+
	Wagners Test	+++	++++	+	-
Cardiac Glycosides	Killer-Killiani Test	+++	+++	+++	+++
Flavonoids	Shinoda Test	++++	++++	++++	++++
	Alkalinereagent(NaOH)	+++	+	+++	+++
	Lead Acetate Test	+++	+++	-	-
Phenolic compounds & Tannins	Ferric Chloride Test	++++	++++	+++	-
	Lead Acetate Test	+++	+++	-	-
	Acetic Acid Test	+++	-	-	-
	Gelatin Test	++	++++	+++	-
Phytosterols & Triterpenods	Salkowaski Test	++++	++++	-	++++
	Libermann's BurchardT	+	++++		++++
	Libermann's test	++++	++++		-
Terpenoids		+++++ yellow orangecolor+ppt			

-, Negative; +, Slight' ++, Good; +++, Moderate; ++++, Strong

The above qualitative phytochemical screening showed the aqueous extract of *Scilla* bulb is rich source glycosides, proteins, alkaloids, flavonoids, phenolic compounds and tannins, phytosterols and terpenoid and triterpenoids. However, presence of all these compounds is limited in other extracts.

Quantitative analysis-

Carbohydrate, protein and the secondary metabolites in plant under study were found to present in appreciable concentration.

Table 2- Quantitative analysis of Phytochemical constituents

Plant Extract	Phytocostituents				
	Carbohydrate (%)	Proteins (%)	Alkaloids (g/100 gm)	Flavonoids (g/100gm)	Saponin (g/100gm)
Scilla Bulb	42.97	05.5	13.4± 0.05	9.9±0.04	23.2±0.04

Where, results are depicted as mean ± SD of three determinants

The quantitative findings showed bulb possesses higher amount of carbohydrates (42.97%).

Protein content of (5.5%), and the other secondary metabolites like alkaloids, flavonoids and saponin in Scilla bulb was showed the percentage of alkaloids 13.4± 0.05g/100g, flavonoids 09.9±0.04g/100g and saponin 23.2±0.04g/100g, the quantitative analysis showed maximum quantity of saponin in bulb.

Phytochemical analysis conducted on the plant extracts revealed the presence of constituents which are known to exhibit medicinal as well as physiological activities (Yadav & Agrawal 2011). Analysis of the plant extracts revealed the presence of phytochemicals such as alkaloids, flavonoids, saponins ,phenols, tannins, , glycosides, terpenoids, Alkaloids, have been associated with medicinal uses for centuries and one of their common biological properties is their cytotoxicity (Nobori,et.al.,1994). Flavonoids are hydroxylated phenolic substances known to be synthesized by plants in response to microbial infection and they have been found to be antimicrobial substances against wide array of microorganisms in vitro. Their activity is probably due to their ability to complex with extracellular and soluble proteins and to complex with bacterial cell wall (Marjorie. C. 1996). They also are effective antioxidant and show strong anticancer activities (Salah, et.al.,1995 and Del-Rio, et.al., 1997).The plant extracts were also revealed to contain saponins which are known to produce inhibitory effect on inflammation (Just, et.al., 1998), also has the property of precipitating and coagulating red blood cells. Some of the characteristics of saponins include formation of foams in aqueous solutions, hemolytic activity, cholesterol binding properties and bitterness (Sodipo,et.al.,2000). Glycosides are known to lower the blood pressure according to many reports(Nyarko, and Addy, 1990). The results obtained in this study thus suggest the identified phytochemical compounds may be the bioactive constituents and these plants are proving to be an increasingly valuable reservoir of bioactive compounds of substantial medicinal merit.

CONCLUSION

The results revealed the presence of medicinally important constituents in the plant studied. Many evidences gathered in earlier studies which confirmed the identified phytochemicals to be bioactive. Several studies confirmed the presence of these phytochemicals contribute medicinal as well as physiological properties to the plants

studied. Therefore the extract from the bulb could be seen as a good source for useful drugs. Further work should be carried out to isolate, purify and characterize the active constituents responsible for the activity of this plant.

ACKNOWLEDMENT

REFERENCES

1. Akindele, A.J. and O.O. Adeyemi,(2007). Antiinflammatory activity of the aqueous leaf extractofByrsocarpus coccineus. Fitoterapia, 78: 25-28.
2. Del-Rio, A., Obdululio, B.G., Casfillo, J., Main, F.G. and Ortuno, A. (1997). Uses and properties of citrus flavonoids. J. Agric. Food Chem., 45: 4505-4515.
3. Just, M.J., Recio, M.C., Giner, R.M., Cueller, M.U., Manez, S., Billia, A.R. and Rios, J.L. (1998). Antiinflammatory activity of unusual Lupine saponins from Bupleurum fruticescens, 64: 404-407.
4. Kokate, C.K.,Purohit, A.P. and Gokhale,S.B.(2005).Pharmacognosy, Nirali Prakashan, Pune.
5. Mathew, K.M.(1983). The Flora of Tamil Nadu Carnatic,part three, Monocotyledons, India, pp.1646-1647.
6. Mathew, K.M.1983. The Flora of Tamil Nadu Carnatic,part three, Monocotyledons, India, pp.1646-1647.
7. Nobori, T., Miurak, K., Wu, D.J., Takabayashik, L.A. and Carson, D.A. (1994). Deletion of cyclin-dependent kinase-4 inhibitor gene in multiple human cancers. Nature, 46: 753-756.
8. Nyarko, A.A.and Addy, M.E. (1990). Effects of aqueous extract of Adenia cissampeloides on blood pressure and serum analyte of hypertensive patients. Phytotherapy Res., 4(1): 25-28.
9. Raman N. (2006). Phytochemical technique. New Indian Publishing Agencies, NewDelhi, 19.
10. Sadashivan , S.and Manikam, A.(1997). Biochemical Methods. 2nd Edn., New Age International (P)Ltd., Publisher, New Delhi.
11. Salah, N., Miller, N.J., Pagange, G., Tijburg, L., Bolwell, G.P, Rice, E.,Evans, C. (1995). Polyphenolic flavonoids as scavenger of aqueous phase radicals as chai breaking antioxidant. Arc. Biochem. Broph., 2: 339-346.
12. Savithramma, N., P. Venkateswarlu, D. Suhrulatha,S.K.M. Basha and C.H. Venkataramanadevi (2010).Studies of Boswellia ovaliofoliolata Bal. andHenry– an endemic and endangered medicinal plant.The Bioscan., 5: 359-362.
13. Sodipo, O.A., Akiniyi, J.A.and Ogunbamosu, J.U. (2000). Studies on certain on certain characteristics of extracts of bark of Pansinystalia macruceras (K schemp) picrre Exbeille. Global J. Pure Appl. Sci., 6: 83-87.
14. Yadav and Munin Agarwala (2011). Phytochemical analysis of some medicinal plants Journal of Phytology 2011, 3(12): 10-14 ISSN: 2075-6240

RESEARCH ARTICLE

Cytogenetic effect of Systemic Fungicide Calixin on root meristem Cells of *Allium cepa* L.

Pulate PV¹ and Tarar JL²*

¹*Cytognetic Research Lab., P.G. Department of Botany, Vidya Bharati Mahavidyalaya Camp, Amravati 444602, Maharashtra, India.*

²*Department of Botany, Institute of Science, Nagpur 4440010, Maharashtra, India.*

Corresponding author, e-mail: pvpbot2005@rediffmail.com

ABSTRACT

The cytotoxic effect of Calixin, a fungicide was investigated in the mitotic cell division in root tip cells of *Allium cepa* L. The seeds of *Allium cepa* were treated with different concentrations (0.02%, 0.04%, 0.06% and 0.08%) of Calixin for 3, 6, 9, 12 h treatment periods. The obtained results indicate that Calixin had the ability to cause production of a large number of mitotic abnormalities. These abnormalities appeared in varying degrees depending on the dose. Various abnormalities on chromosomes like lagging early anaphase, chromosomal bridges, c-metaphase, sticky metaphase, multipolarity, fragment, vagrant etc were seen among mitotic divisions treated with Calixin.

Keywords : *Allium cepa*, mitotic index, chromosomal aberrations, cytotoxic effect, fungicides,

INTRODUCTION

Fungicides are most commonly used against diseases of agricultural crops in many countries of the world. Fungicides produce a diverse range of products with novel modes of action. The extensive use of fungicides in plant protection against fungal disease generates long term residues in food and in the environment (Petit et al., 2008).

Fungicides may also influence to change plant genetic system due to their mutagenicity and carcinogenicity. Constant use of these chemicals may result in changing the hereditary constitution of an organism (Wuu and Grant, 1967, Wuu and Grant, 1982). Cytogenetic studies have been carried out to detect harmful effects of different pesticides on different plant species (Rank et al., 2002, Marcano et al., 2004). Mutation breeding has become increasingly popular in present times as an effective tool for crop improvement (Siddiqui and Khan, 1999).

There are several studies aiming to explain and to understand the effects of fungicides in plant systems. Rayburn et al., (1993) stated out that amount of nuclear DNA is decreased by the fungicide, captan and this fungicide has been mutagenic, carcinogenic and teratogenic effects on many organisms. Celik (2006) used two fungicides in his experiment, Derosol and Korsikol and examined by cytogenetic effects on barley root tip meristem cells. The effect of these two fungicides effect on chromosome fragments, bridge, stickiness and polar deviation is evident.

Tridomorph are systemic fungicidal derivatives which are systemic and show eradiact action against powdery mildew of barley. Tridomorph is available under the commercial name Calixin as 25% E.C Syngenta and is used extensively in the agricultural area. The fungicide is also reported to be highly effective against Ascomycetes such as *Mycospaerella musicola* and *Erysiphae graminis.* It has also shown direct fungitoxic action against various phytopathogenic fungi including *Botrytis cinerea*, *Phomopsis citri, Diplodia hetalensis, Penicillum digitatum, Cladosporium cucumerinum.*

There is no literature available on the cytogenetic effects of this chemical in the plant systems. The aim of this study was to investigate the chromosomal aberration induced by fungicide Calixin in the root tips of *Allium cepa* L. and also to determine the relation between mitotic chromosomal aberrations with mitotic index.

MATERIAL AND METHODS

Healthy and dry seeds of untreated *Allium cepa* L var. N-53 were obtained from National Horticultural Research and Foundation (NHRDF) Chitegong, Nasik. Seeds (1,500) were pre-soaked in tap water for 12 hours and then treated with four different concentrations (0.02%, 0.04%, 0.06%, 0.08%) of tilt fungicide for 3, 6, 9 and 12 hours at room temperature (22+2°C). Conical flasks containing the seeds and solution were periodically shaken for 2-3 min. during the treatment. After treatment, the seeds were thoroughly washed with running tap water to remove the excess amount of fungicide from the seeds, if any. One set of seeds was kept untreated to act as control for comparison. Both the treated and controlled seeds were transferred to the petri dishes having moist filter papers for germination. Hundred seeds were used for each dose and control. The embryonic roots were reached 1.5 - 2 cm in length (both experimental and control) were excised and fixed with glacial acetic acid: ethanol (3:1) solution and kept for 24 hours. After 24 hours the root tips were transferred to 70% ethanol and stored in a refrigerator. The concentrations were chosen according to their dose of application in agricultural field to control different diseases. For mitotic studies, the root tips were hydrolyzed in 1 (N) HCl at 60^0C for 5 minutes, followed by staining with 2% aceto-orcein following the method described by Sharma and Sharma (1980). After staining, appropriate squash preparations were made for each of the treatment and control. Effect of chemical treatment and control on different chromosome plates were observed under light microscope. The mitotic index (MI) was calculated for each treatment as a number of dividing cells/100 cells. Cytological abnormalities were also observed and scored. Abnormalities were photographed using Carl Zeiss Axiostar Plus microscope mounted with Canon camera model, Power Shot G12. All experiments were conducted with five replicates and average results were taken

RESULTS AND DISCUSSION

Mitotic index is an acceptable measure of Cytotoxicity for all living organisms. The mitotic index of control set with a little reduction was noted as the time of treatment prolonged. The Cytotoxicity level can be determined by the decreased rate of mitotic index. The increase of mitotic abnormalities was dependent on the increasing treatment periods and concentrations. Careful screening in mitotic index was noticed in the root tip cells as concentration and duration of treatment. Mitotic index of control set was 15.23 ± 2.2 in 3h, 15.37 ± 1.6 in 6h, 15.42 ± 1.3 in 9h and 15.42 ± 1.3 in 12h. It declined to 9.70 ± 0.37 3h (0.02%) to 2.19 ± 0.16 12h (0.08%). The MI of the other concentration was sharply decreased as the time of treatment increased recording value of 2.19 ± 0.16 12h (0.08%) treatment (Table-1). The highest value was recorded at a higher concentration and longer exposure (40.58 ±1.59 at 0.08% concentration in 12 h treatment).

The most common abnormalities were Anaphase Bridge [Fig-1(a)], C-Metaphase [Fig-1(b)], Laggards [Fig-1(c)] Stickiness [Fig-1(d)], also observed.

Table 2: Mitotic Index (MI), type and percentage of mitotic abnormalities in the root tip cells of *Allium cepa* L. exposed to Calixin

| Treatment		Mitotic index (% ± SE)	No. of cells examined	Types and percentage of abnormalities.						Total aberration (% ± SE)
Time	Concentration			Stickiness	Bridge	Vagrant	C Anaphase	Multipolarity	Fragment	
	Control	15.23 ±2.2	500	0	1.8	0	2.72	0	0.04	4.56 ± 2.0
	0.02%	9.70 ± 0.37	500	0	11	3	2	0	0	3.20 ±0.37
3h	0.04%	8.09 ± 0.41	500	13	18	8	11	3	0	10.60 ±1.96
	0.06%	7.86 ± 0.33	500	23	16	20	9	1	1	13.60 ±0.75
	0.08%	3.48 ± 0.86	500	31	26	22	23	0	1	20.60 ±2.01
	Control	15.37 ±1.6	500	0	0	0	0	0	3.5	3.5 ± 1.52
	0.02%	7.27 ± 0.32	500	22	27	6	6	4	0	13.00 ±0.45
6h	0.04%	7.52 ± 0.36	500	25	19	7	17	1	0	13.80 ±1.39
	0.06%	7.01 ± 0.26	500	54	21	13	13	0	0	20.00 ±1.22
	0.08%	3.35 ± 0.51	500	68	6	11	2	0	1	27.16 ±1.35
	Control	15.42 ± 1.3	500	0	0	0	4.5	0	0	4.5 ± 2.03
	0.02%	9.12 ± 0.46	500	0	9	1	2	0	0	2.40 ±0.40
9h	0.04%	8.66 ± 0.43	500	23	12	12	7	3	0	11.40 ±0.51
	0.06%	5.15 ± 0.44	500	23	20	13	13	0	0	13.80 ±0.86
	0.08%	3.35 ± 0.51	500	68	6	11	2	0	1	27.16 ±1.35
	Control	15.42 ± 1.3	500	0	0	0	4.2	0	0	4.2 ± 2.03
	0.02%	8.43 ± 0.26	500	0	6	4	2	1	1	2.80 ±0.37
12 h	0.04%	5.84 ± 0.22	500	30	33	15	4	0	1	16.60 ±0.87
	0.06%	5.04 ± 0.47	500	25	32	21	16	1	0	19.00 ±1.14
	0.08%	2.19 ± 0.16	69	24	2	0	2	0	0	40.58 ±1.59

(a)   **(b)**   **(c)**   **(d)**
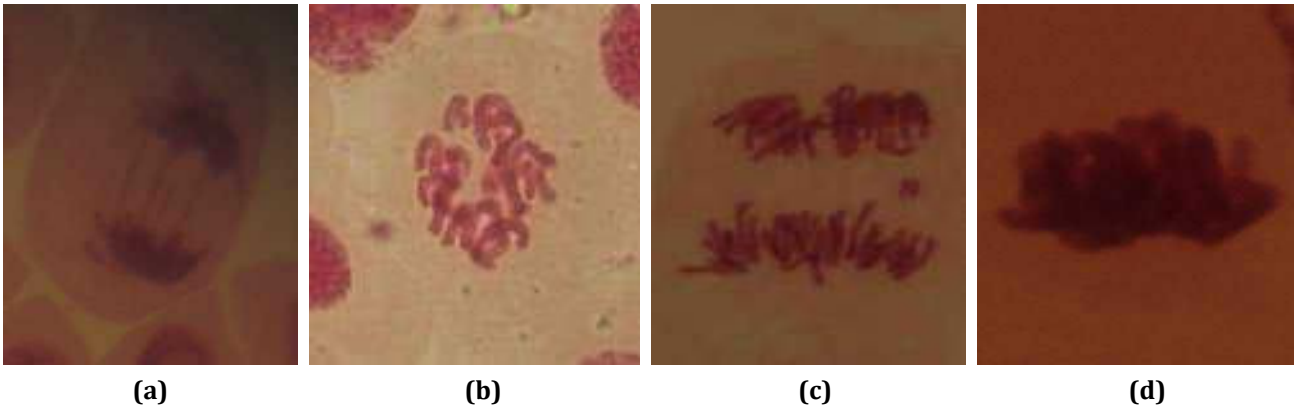
Fig. 1(a) Anaphase bridge (b): C- Metaphase (c): Laggards (d): Sticky Metaphase
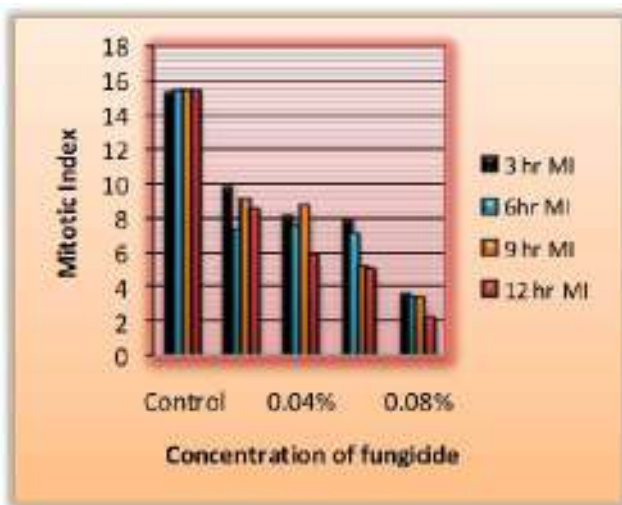

Fig. 2: Mitotic Index of *Allium cepa* L. root meristem cells treated with Calixin at different times and concentrations
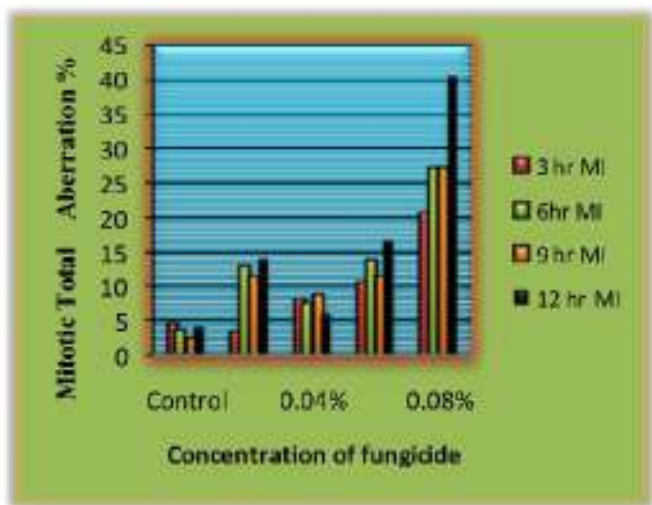

Fig. 3: Cytotoxic effects of Calixin at different times and concentrations in *Allium cepa* L. root tip cell

According to many investigators, abnormalities due to inhibition of spindle formation such as c-mitosis, multipolarity, stickiness reflects high toxicity of pollutants (Amer and Ali, 1974; Haliem, 1990; Lazareva et al., 2003). In the present study, Calixin decreased the mitotic index at all concentrations and at all treatment periods when compared with control. Similar type of result is also found by (Pulate and Tarar, 2014) on *Allium cepa* by using fungicide tilt.

The decrease of mitotic index was dose dependent. At all treatment periods, the highest concentration of Calixin decreased mitotic activity more than other used concentrations. The percentage of mitotic index decreased with the increase of cells with c-mitosis, stickiness, laggards, anaphase and telophase bridges, etc. Since it decreased the MI in root tip cells of *Allium cepa* L. Calixin can be accepted as a toxic agent in this

study. Calixin significantly increased the percentage of abnormal cells at all concentrations and treatment periods in mitotic cell divisions when compared with control. It has been shown by many investigators that several other fungicides induce chromosomal abnormalities in different plants (Behera et al., 1982; Badr, 1983; Armbruster et al., 1991; Pandy et al., 1994; Badr, 1998). In this study, the most common abnormalities were stickiness, laggards, c-mitosis, bridges, vagrant, Multi polarity telophase, clumping and fragmentations in cell division. Chromosomal stickiness is characterized by chromosomal clustering during any phase of the cell cycle. Stickiness and clumping may be caused by genetic and environmental factors. Several agents have been reported to cause chromosomal stickiness (Panneerselvam et al., 2012) C-mitosis is one of the consequences of inactivation of spindle apparatus connected with delay in the division

of centromere (Mann, 1977). Sıng (1992) mentioned that univalent and laggard formation may be due to the failure of pairing and lagging to the failure of moving apart. Bridges and fragments are clastogenic effects, both resulting from chromosomal and chromatid breaks (Kovalchuk et al., 1998). The induction of vagrant chromosomes leads to separation of unequal number of chromosomes in the daughter nuclei and subsequently formation of daughter cells with unequal sized or irregularly shaped nuclei at interphase (ElGhamery et al., 2003).

CONCLUSION

These results indicated that Calixin should be regarded as a mutagenic agent for plants. Hence, the use of this fungicide should be under control in agricultural fields.

REFERENCES

Amer SM and Ali EM (1974) Cytological effects of pesticides vs Effects of some herbicides on *Vicia faba*. *Cytologia*, 39: 633-643.

Armbruster BL Molin WT and Bugg MW (1991) Effects of the herbicide dithiopyr on cell division in wheat root tips. *Pesticide Biochemistry and Physiology*, 39(2): 110-120.

Badr A (1983) Mitodepressive and chromotoxic activities of two herbicides in *Allium cepa*. *Cytologia,* 48: 491-497.

Badr AA (1998) Cytogenetic activities of some fungicides. *Cytologia*, 53: 633-640.

Behera BN Sahu RK and Sharma CBSR (1982) Cytogenetic hazards from agricultural chemicals of sequential screening in the barley progeny test for cytogenetic activity of some systemic fungicides and a metabolite. *Toxicology Letters* 10(2-3): 195-203.

Celik TS (2006) Cytogenetic effects of some fungicides on Barley root tip meristem cells. *Pakistan Journal of Biological sciences*. 9(13): 2508-251.

Elghamery AA Elkholy MA and Elyousser A (2003) Evaluation of cytological effects of Zn^{2+} in relation to germination and root growth of *Nigella sativa* L. and *Triticum aestivum* L. *Mutation Research*, 537: 2941.

Haliem AS (1990) Cytological effects of the herbicide sencor on mitosis of *Allium cepa*. *Egyptian Journal of Botany*, 33:93-104.

Kovalchuk O Kovalchuk I Arkhipov A Telyuk P Hohn B and Kovalchuk L (1998) The *Allium cepa* chromosome aberration test reliable measures genotoxicity of soils of inhabited areas in the Ukraine contaminated by the Chernobyl accident. *Mutation Research*, 415:47-57.

Lazareva EM Polyakov VY Chentsov YS and Smirnova EA (2003) Time and cell cycle dependent formation of heterogeneous tubulin arrays induced by colchicines in *Triticum aestivum* root meristem cell. *Biology International*, 27:633-646.

Marcano I Carruyo I and Del Campo A (2004) Cytotoxicity and made of action of maleic hydrazide in root tips of *Allium cepa*. *Environmental Research*, 94:221-226.

Pandy RK Shukla R and Datta S (1994) Chromotoxic effects of one fungicide (Dithane M-45) and two insecticides (Aldrex-30 and Metacid-50). Cytologia, 59: 419-422.

Panneerselvam N Palanikumar L and Gopinathan S (2012) Chromosomal aberrations induced by Glycidol in *Allium cepa* L. root meristem cells. *International Journal of Pharma Sciences and Research,* 3(2): 300-304.

Petit AN Fontaine F Clément C and Vaillant-Gaveau N (2008) Photosynthesis limitations of grapevine after treatment with the fungicide fludioxonil. *Journal of Agricultural and Food Chemistry*, 56(15): 6761–6767.

Pulate PV and Tarar JL (2014) Cytogenetic effects of tilt on root tip meristem of onion *Allium cepa* L. *International Journal of Plant, Animal and Environmental Sciences,* 4(2): 53-57.

Rank J Lopez LC and Nielsen MH (2002) Genotoxicity of maleic hydrazide, acridine and DEHP in *Allium cepa* root cells performed by two different laboratories. *Hereditas*, 135:13.

Rayburn LA Wayne L and Pedersen L (1993) The fungicide Dithane M-45 reduce nuclear DNA content in maize seedling. *Pestic. Sci.,* 37:79-82.

Mann SK (1977) Cytological and genetical effects of dithane fungicides on *Allium cepa. Environmental and Experimental Botany*, 17(1): 7-12.

Sharma AK and Sharma A (1980) *Chromosome techniques*: Theory and practice. 3rd edition, Butterworths and Co. Ltd., London.

Siddiqui BA and Khan S (1999) *Breeding in crop plants*, Kalyani Publishers, 20-34.

Singh RN (1992) Chromosomal abnormalities and fertility in induced autotetraploid *Helianthus annuus* in C_1 and C_2 generation. *Cytologia*, 57: 277-281.

Wuu KD and Grant WF (1982) Chromosome aberration assays in *Allium.* A report of the U.S. EPA Gene Tox. Programme. *Mutation Research*, 99: 273-291.

Wuu KD and Grant WF (1967) Chromosomal aberrations induced by pesticides in meiotic cells of barley. *Cytologia,* 32(1): 31-41.

Journal of Research and Development

- A Multidisciplinary International Level Refereed Journal

Editor
Dr. R. V. Bhole

Liberalization of Indian Banking and Regulation

Dr. Sanjay B. Kadu

Associate Professor, Vidya Bharati Mahavidyalaya, Amravati.

Banking is an ancient business in India with some of oldest references in the writings of Manu. Bankers played an important role during the Mogul period. During the early part of the East India Company era, agency houses were involved in banking. Modern banking (i.e. in the form of joint-stock companies) may be said to have had its beginnings in India as far back as in 1786, with the establishment of the General Bank of India. Three Presidency Banks were established in Bengal, Bombay and Madras in the early 19th century. These banks functioned independently for about a century before they were merged into the newly formed Imperial Bank of India in 1921. The Imperial Bank was the forerunner of the present State Bank of India. The latter was established under the State Bank of India Act of 1955 and took over the Imperial Bank.

The Swadeshi movement witnessed the birth of several indigenous banks including the Punjab National Bank, Bank of Baroda and Canara Bank. In 1935, the Reserve Bank of India was established under the Reserve Bank of India Act as the central bank of India. In spite of all these developments, independent India inherited a rather weak banking and financial system marked by a multitude of small and unstable private banks whose failures frequently robbed their middle-class depositors of their life's savings. After independence, the Reserve Bank of India was nationalized in 1949 and given wide powers in the area of bank supervision through the Banking Companies Act (later renamed Banking Regulations Act). The nationalization of the Imperial bank through the formation of the State Bank of India and the subsequent acquisition of the state owned banks in eight princely states by the State Bank of India in 1959 made the government the dominant player in the banking industry. In keeping with the increasingly socialistic leanings of the Indian government, 14 major private banks, each with deposits exceeding Rs. 50 crores, were nationalized in 1969. This raised the proportion of scheduled bank branches in government control from 31% to about 84%. In 1980, six more private banks each with deposits exceeding Rs 200 crores , were privatized further raising the proportion of government controlled bank branches to about 90%. As in other areas of economic policy-making, the emphasis on government control began to weaken and even reverse in the mid-80s and liberalization set in firmly in the early 90's. The poor performance of the public sector banks, which accounted for about 90% of all commercial banking, was rapidly becoming an area of concern. The continuous escalation in non-performing assets (NPAs) in the portfolio of banks posed a significant threat to the very stability of the financial system. Banking reforms, therefore, became an integral part of the liberalization agenda.

The first Narasimham Committee set the stage for financial and bank reforms in India. Interest rates, previously fixed by the Reserve Bank of India, were liberalized in the 90's and directed lending through the use of instruments of the Statutory Liquidity Ratio was reduced. While several committees have looked into the ailments of commercial banking in India, but major work has been done according to the Narsimham committee reports.-the Narasimham committee I (1992) and II (1998)

Liberalization

Liberalization (or liberalization) refers to a relaxation of previous government restrictions, usually in areas of social or economic policy. In some contexts this process or concept is often, but not always, referred to as deregulation. In the arena of social policy it may refer to a relaxation of laws restricting. Most often, the term is used to refer to economic liberalization, especially trade liberalization or capital market liberalization.

Liberalization in Indian Banking Sector-

Liberalization in Indian banking sector was begun since 1992, following the Narsimham Committee Report (December 1991). The 1991 report of the Narasimham Committee served as the basis for the initial banking sector reforms .In the following years, reforms covered the areas of interest rate deregulation, directed credit rules, statutory pre-emptions and entry deregulation for both domestic and foreign banks. The objective of banking sector reforms was in line with the overall goals of the 1991 economic reform of opening the economy, giving a greater role to markets in setting prices and allocating resources, and increasing the role of the private sector. The Narsimhan Committee was first set up in 1991 under the chairmanship of Mr. M. Narasimham who was 13th governor of RBI. Only a few of its recommendations became banking reforms of India and others were not at all considered. Because of this a second committee was again set up in 1998. As far as recommendations regarding bank restructuring, management freedom, strengthening the regulation are concerned, the RBI has to play a major role. If the major recommendations of this committee are accepted, it will prove to be fruitful in making Indian banks more profitable and efficient.

Problems Identified By The Narasimham Committee

1. Directed Investment Program : The committee objected to the system of maintaining high liquid assets by commercial banks in the form of cash, gold and unencumbered government securities. It is also known as the Statutory Liquidity Ratio (SLR). In those days, in India, the SLR was as high as 38.5 percent. According to the M. Narasimha Committee it was one of the reasons for the poor profitability of banks. Similarly, Cash Reserve Ratio- (CRR) was as high as 15 percent. Taken together, banks needed to maintain 53.5 percent of their resources idle with the RBI.

2. Directed Credit Program : Since nationalization the government has encouraged lending to agriculture and small-scale industries at a confessional rate of interest. It is known as the directed credit programme. The committee opined that these sectors have

matured and thus do not need such financial support. This directed credit programme was successful from the government's point of view but it affected commercial banks in a bad manner. Basically it deteriorated the quality of loan, resulted in a shift from the security oriented loan to purpose oriented. Banks were given a huge target of priority sector lending, etc. ultimately leading to profit erosion of banks.

3. Interest Rate Structure: The committee found that the interest rate structure and rate of interest in India are highly regulated and controlled by the government. They also found that government used bank funds at a cheap rate under the SLR. At the same time the government advocated the philosophy of subsidized lending to certain sectors. The committee felt that there was no need for interest subsidy. It made banks handicapped in terms of building main strength and expanding credit supply.

4. Additional Suggestions: Committee also suggested that the determination of interest rate should be on grounds of market forces. It further suggested minimizing the slabs of interest.

Along with these major problem areas M. Narasimham's Committee also found various inconsistencies regarding the banking system in India.

Narasimham Committee Report I – 1991

The Narsimham Committee was set up in order to study the problems of the Indian financial system and to suggest some recommendations for improvement in the efficiency and productivity of the financial institution.

The committee has given the following major recommendations:-

1. Reduction in the SLR (Statutory Liquidity Ratio) and CRR(Cash Reserve Ratio) : The committee recommended the reduction of the higher proportion of the Statutory Liquidity Ratio (SLR) and the Cash Reserve Ratio (CRR). Both of these ratios were very high at that time. The SLR then was 38.5% and CRR was 15%. This high amount of SLR and CRR meant locking the bank resources for government uses. It was hindrance in the productivity of the bank thus the committee recommended their gradual reduction. SLR was recommended to reduce from 38.5% to 25% and CRR from 15% to 3 to 5%.

2. Phasing out Directed Credit Programme : In India, since nationalization, directed credit programmes were adopted by the government. The committee recommended phasing out of this programme. This programme compelled banks to earmark then financial resources for the needy and poor sectors at confessional rates of interest. It was reducing the profitability of banks and thus the committee recommended the stopping of this programme.

3. Interest Rate Determination : The committee felt that the interest rates in India are regulated and controlled by the authorities. The determination of the interest rate should be on the grounds of market forces such as the demand for and the supply of fund. Hence the committee recommended eliminating government controls on interest rate and phasing out the concessional interest rates for the priority sector.

4. Structural Reorganizations of the Banking sector : The committee recommended that the actual numbers of public sector banks need to be reduced. Three to four big banks including SBI should be developed as International banks. Eight to Ten Banks having nationwide presence should concentrate on the national and universal banking services. Local banks should concentrate on region specific banking. Regarding the RRBs (Regional Rural Banks), it recommended that they should focus on agriculture and rural financing. They recommended that the government should assure that henceforth there won't be any nationalization and private and foreign banks should be allowed liberal entry in India.

5. Establishment of the ARF Tribunal : The proportion of bad debts and Non-performing asset (NPA) of the public sector Banks and Development Financial Institute was very alarming in those days. The committee recommended the establishment of an Asset Reconstruction Fund (ARF). This fund will take over the proportion of the bad and doubtful debts from the banks and financial institutes. It would help banks to get rid of bad debts.

6. Removal of Dual control : Those days banks were under the dual control of the Reserve Bank of India (RBI) and the Banking Division of the Ministry of Finance (Government of India). The committee recommended the stepping of this system. It considered and recommended that the RBI should be the only main agency to regulate banking in India.

7. Banking Autonomy : The committee recommended that the public sector banks should be free and autonomous. In order to pursue competitiveness and efficiency, banks must enjoy autonomy so that they can reform the work culture and banking technology upgradation will thus be easy.

Some of these recommendations were later accepted by the Government of India and became banking reforms.

Narasimham Committee Report II – 1998

In 1998 the government appointed yet another committee under the chairmanship of Mr Narasimham. It is better known as the Banking Sector Committee. It was told to review the banking reform progress and design a programme for further strengthening the financial system of India. The committee focused on various areas such as capital adequacy, bank mergers, bank legislation, etc.

It submitted its report to the Government in April 1998 with the following recommendations.

1. Strengthening Banks in India: The committee considered the stronger banking system in the context of the Current Account Convertibility (CAC). It thought that Indian banks must be capable of handling problems regarding domestic liquidity and exchange rate management in the light of CAC. Thus, it recommended the merger of strong banks which will have 'multiplier effect' on the industry.

2. Narrow Banking: Those days many public sector banks were facing a problem of the Non-performing assets (NPAs). Some of them had NPAs were as high as 20 percent of

their assets. Thus for successful rehabilitation of these banks it recommended 'Narrow Banking Concept' where weak banks will be allowed to place their funds only in short term and risk free assets.

3. Capital Adequacy Ratio: In order to improve the inherent strength of the Indian banking system the committee recommended that the Government should raise the prescribed capital adequacy norms. This will further improve their absorption capacity also. Currently the capital adequacy ration for Indian banks is at 9 percent.

4. Bank ownership: As it had earlier mentioned the freedom for banks in its working and bank autonomy, it felt that the government control over the banks in the form of management and ownership and bank autonomy does not go hand in hand and thus it recommended a review of functions of boards and enabled them to adopt professional corporate strategy.

5. Review of banking laws: The committee considered that there was an urgent need for reviewing and amending main laws governing Indian Banking Industry like RBI Act, Banking Regulation Act, State Bank of India Act, Bank Nationalisation Act, etc. This upgradation will bring them in line with the present needs of the banking sector in India. Apart from these major recommendations, the committee has also recommended faster computerization, technology upgradation, training of staff, depoliticizing of banks, professionalism in banking, reviewing bank recruitment, etc.

Changes due to the recommendations made by the Narsimham committee are-

1. Statutory pre-emptions: The degree of financial regression in the Indian banking sector was significantly reduced with the lowering of the CRR and SLR, which were regarded as one of the main causes of the low profitability and high interest rate spreads in the banking system. During the 1960s and 1970s the CRR was around 5%, but until 1991 it increased to its maximum legal limit of 15%. The reduction of the CRR and SLR resulted in increase flexibility for banks in determining both the volume and terms of lending.

2. Priority sector lending: Besides the high level of statutory pre-emptions, the priority sector advances were identified as one of the major reasons for the below average profitability of Indian banks. The Narasimham Committee therefore recommended a reduction from 40% to 10%. However, this recommendation has not been implemented and the targets of 40% of net bank credit for domestic banks and 32% for foreign banks have remained the same.

3. Interest rate liberalization: Prior to the reforms, interest rates were a tool of cross-subsidization between different sectors of the economy. To achieve this objective, the interest rate structure had grown increasingly complex with both lending and deposit rates set by the RBI. The deregulation of interest rates was a major component of the banking sector reforms that aimed at promoting financial savings and growth of the organized financial system. The lending rate for loans in excess of Rs200,000 that account for over90% of total advances was abolished in October 1994. Banks were at the same

time required to announce a prime lending rate (PLR) which according to RBI guideline had to take the cost of funds and transaction costs into account.

4. Entry barriers: Before the start of the 1991 reforms, there was little effective competition in the Indian banking system for at least two reasons. First, the detailed prescriptions of the RBI concerning for example the setting of interest rates left the banks with limited degrees of freedom to differentiate themselves in the marketplace. Second, India had strict entry restrictions for new banks, which effectively shielded the incumbents from competition. Through the lowering of entry barriers, competition has significantly increased since the beginning of the1990s. Seven new private banks entered the market between 1994 and 2000. In addition, over 20 foreign banks started operations in India since 1994. By March 2004, the new private sector banks and the foreign banks had a combined share of almost 20% of total assets. Deregulating entry requirements and setting up new bank operations has benefited the Indian banking system from improved technology, specialized skills, better risk management practices and greater portfolio diversification.

5. Prudential norms: The report of the Narasimham Committee was the basis for the strengthening of prudential norms and the supervisory framework. Starting with the guidelines on income recognition, asset classification, provisioning and capital adequacy the RBI issued in 1992/93, there have been continuous efforts to enhance the transparency and accountability of the banking sector. The improvements of the prudential and supervisory framework were accompanied by a paradigm shift from micro-regulation of the banking sector to a strategy of macro-management.

6. Public Sector Banks : At the end of the 1980s, operational and allocative inefficiencies caused by the distorted market mechanism led to a deterioration of Public Sector Banks' profitability. Enhancing the profitability of PSBs became necessary to ensure the stability of the financial system. The restructuring measures for PSBs were threefold and included recapitalization, debt recovery and partial privatization.

Despite the suggestion of the Narasimham Committee to rationalize PSBs, the Government of India decided against liquidation, which would have involved significant losses accruing to either the government or depositors. It opted instead to maintain and improve operations to allow banks to create a good starting basis before a possible privatization.

Conclusion

Nevertheless, more than a decade since the beginning of economic reforms, the banking sector is still struggling under the burden of considerable NPAs and the poor performance of public sector banks continues to be a major issue. Liberalization has, however, had a predictable effect in the distribution of scheduled commercial banking in India. The reforms era growth in banking have focused on the more profitable urban and metro areas of the country. Between 1969 and 1991 for instance, the share of the rural branches increased from about 22% to over 58%. In 2004, the corresponding figure stood at a much lower

46%. The number of rural bank branches actually declined from the 1991 figure of over 35,000 branches by about 3000 branches. Between 1969 and 1991 the share of urban and metro branches fell from over 37% to less than 23%. In the years since it has crawled back up to over 31%.

Since India has decided to move toward a more market-based system, it is now important for policy makers to create the conditions for the well-functioning of a market based banking system. Among the necessary tasks are the building and strengthening of the necessary institutions like oversight bodies, accounting standards and regulations as well as the further restructuring and privatization of PSBs. If India continues on its current path of banking sector liberalization, it should be in a position to further strengthen its banking system, which will be vital to support its economic growth in the years to come. Thus Liberalisation has proved to be a great boon to the banking system as the structural changes which have been implemented due to the liberalisation has transformed the Indian banking system and moreover the recommendations of various committees has led to further strengthening banking system. Thus liberalisation has made banking from class banking to mass banking.

References :-

Available at http://en.wikipedia.org/wiki/Swadeshi_movement visited on September 15,2011.

Statutory Liquidity Ratio is the amount of liquid assets, such as cash, precious metals or other approved securities, that a financial institution must maintain as reserves other than the Cash with the Central Bank.

Rajesh Chakrabarti , Banking in India - Reforms and Reorganization

Sullivan, Arthur; Sheffrin, Steven M. (January 2002). Economics: Principles in Action. New Jersey: Pearson Prentice Hall. ISBN 0-13-063085-3.

Available at http://www.scribd.com/doc/53006431/Narasimham-Committee-on-Banking-Sector-Reforms visited on September 15,2011.

Arun, T.G./ Turner, J.D. (2002a): Financial liberalisation in India, in: Journal of International Banking Regulation, 4 (2),p.183;A brief overview of the most important reforms follows.

Available at http://kalyan-city.blogspot.com/2010/09/narasimham-committee-report-1991-1998.html visited on September 15,2011.

Statutory Liquidity Ratio

Ibid

Available at http://kalyan-city.blogspot.com/2010/09/narasimham-committee-report-1991-1998.html visited on September 15,2011.

Current account convertibility refers to freedom in respect of Payments and transfers for current international transactions.

A debt obligation where the borrower has not paid any previously agreed upon interest and principal repayments to the designated lender for an extended period of time. The nonperforming asset is therefore not yielding any income to the lender in the form of principal and interest payments.

Available at http://kalyan-city.blogspot.com/2010/09/narasimham-committee-report-1991-1998.html visited on September 15,2011.

Shirai, Sayuri (2002b): Road from State to Market - Assessing the Gradual Approach to Banking Sector Reforms in India, in: Asian Development Bank Institute Research Paper, No. 32, p. 12

Kamesam, Vepa (2002): Indian Economy - Financial Sector Reforms and Role of RBI, in: RBI Bulletin, May, p. 379

Ganesan, P . (2003): Impact of Priority Sector Advances on Profitability of Public Sector Banks in India, in: Journal of Financial Management and Analysis, 16 (2), p. 15

Arun, T.G./ Turner, J.D. (2002b): Financial Sector Reforms in Developing Countries: The Indian Experience, in: World Economy, 25 (3), p. 437

Deolalkar, G.H. (1999): The Indian Banking Sector: On the Road to Progress, in: (ed.): Rising to the Challenge in Asia: A Study of Financial Markets - India, Manila, p. 60

Arun, T.G./ Turner, J.D. (2002b): Financial Sector Reforms in Developing Countries: The Indian Experience, in: World Economy, 25 (3), p. 439;

Reserve Bank of India (2004a): Report on Trend and Progress of Banking in India 2003-04, p. 167

Ibid,p.24

Kamesam, Vepa (2002): Indian Economy - Financial Sector Reforms and Role of RBI, in: RBI Bulletin, May 2002, p. 377

Shirai, Sayuri (2002b): Road from State to Market - Assessing the Gradual Approach to Banking Sector Reforms in India, in: Asian Development Bank Institute Research Paper, No. 32, p. 26

GROWTH OF SERVICE SECTOR IN INDIAN ECONOMY

International Peer Reviewed Research Journal
Special Issue- Sept. 2014
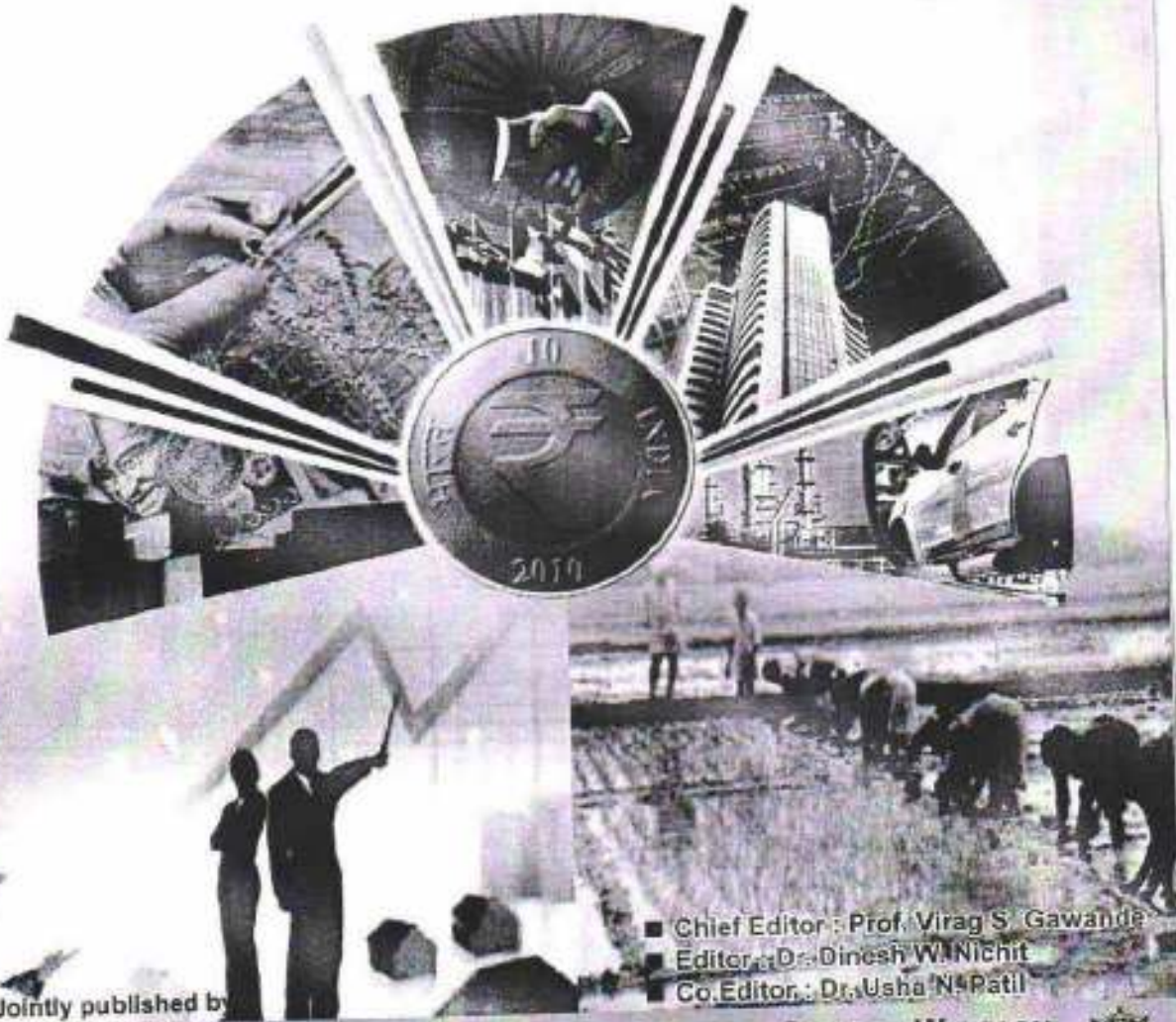
Priority Sector Lending for Agriculture in India
(11th plan 2008-2012)

Author
Dr. Sanjay B. Kadu
Associate Professor
Vidyabharti Mahavidyalaya
Camp, Amravati.

Research scholar
Praneeta Deshmukh
C/o Dr. H. N. Deshmukh
Opp NCC Bhavan, ZP Road,
Amravati.-444605

Introduction:

The concept of priority sector was evolved to ensure adequate credit facilities to certain neglected sectors of the economy particularly in the rural areas. The Priority Sector Lending is mainly intended to ensure that assistance from banking system should flow in an increasing manner to those sectors of the economy which though accounting for a significant proportion of the national product have not received adequate support or institutional finance in the past. The categories under priority sector include agriculture, micro & small enterprises, education, housing, export credit, and others.

An important role of regulator is being played by Reserve Bank of India (RBI) for evolving the concept of Priority Sector. It has recommended domestic/foreign banks to lend 32-40% of their adjusted net banking credit or credit equivalent of off-balance sheet exposure whichever is higher to the Priority Sectors. Of the total priority sector lending, 18% to be specifically utilized for agriculture purposes.

Objectives of the Study:

1. To study evolution of priority sector lending.
2. To study the contribution of scheduled commercial banks in financing agriculture, one of the priority sector for period 2008-2012
3. To analyze regionwise Priority Sector Lending for agricultural operations
4. To analyze distribution of advances for direct and indirect agricultural operations

Hypothesis:

1. There is significant increase over a period of time in willingness of the banks to lend for agricultural operations
2. There is a significant difference in the regionwise advances for agricultural operations
3. There is a significant difference in the direct and indirect financing utilized across regions of India.

Agriculture as Priority Sector:

Agriculture is the dominant sector of Indian economy because of its high share in employment and livelihood creation. It is also an important source of raw material and demands for many industrial products, particularly fertilizers, pesticides, agricultural implements and a variety of consumer goods.

The rapid growth of agriculture is essential not only for self-reliance but also for meeting the food and nutritional security of the people, to bring about equitable distribution of income and wealth in rural areas as well as to reduce poverty and improve the quality of life. Growth in agriculture has a maximum cascading impact on other sectors, leading to the spread of benefits over the entire economy and the largest segment of population.

Despite of contributing a substantial amount to the GDP, the sector faces huge demand supply gap to address needs of farmers for agricultural operations, for producing agriculture products and for land improvement. In order to address this financial exclusion problem, RBI adopted Priority Sector Lending policy and also defined compulsory lending to agriculture sector. RBI has given targets and sub targets to all domestic and foreign banks.

Categories	Domestic commercial banks / Foreign banks with 20 and above branches (As percent of ANBC or Credit Equivalent of Off-Balance Sheet Exposure, whichever is higher)	Foreign banks with less than 20 branches (As percent of ANBC or Credit Equivalent of Off-Balance Sheet Exposure, whichever is higher)
Total Priority Sector	40	32
Total agriculture	18	No specific target.

Agriculture loans are given to farmers on their need based credit. These loans are classified into following two categories:

Direct Agriculture Finance
> Loans to individual farmers (including Self Help Groups (SHGs) or Joint Liability Groups (JLGs)
> Loans to corporate including farmers' producer companies of individual farmers, partnership firms and co-operatives of farmers
> Loans to small and marginal farmers for purchase of land for agricultural purposes
> Loans to distressed farmers indebted to non-institutional lenders

Indirect Agriculture Finance
> Aggregate loan given to corporate of more than Rs 2 crore
> Loans upto Rs 5 crore to Producer Companies set up exclusively by only small and marginal farmers

The study is based on the Banking Operation reports published by RBI. Secondary source of data is considered for analyzing various parameters in Priority Sector Lending.

The Banking industry plays a dynamic role in the economic development of a country. The growth story of an economy depends on the robustness of its banking industry. India is backed by a wide population of banks but for this study only Scheduled Commercial Banks are considered as a sample of entire banking industry. Scheduled Commercial Banks have significant presence in rural regions of India so that it can reach the unbanked masses and avail them credit facilities.

Particulars	2008	2009	2010	2011	2012
Total Commercial Banks	175	170	169	169	173
Total no of Schedule Commercial Banks	171	166	165	165	169
Number of Offices of Scheduled Commercial Banks in India	76050	80547	85393	90263	98330
Number of Offices of Scheduled Commercial Banks in Rural India	31076	31667	32624	33683	36356
Total Priority Sector Advances amount outstanding (Rs. Million)	703759	874774	1138409	13722789	14909174
Total Priority Sector Advances to Agriculture amount outstanding (Rs. Million)	254693	308086	463323	5071757	5833433
Share of Priority Sector Advances towards Agriculture (per cent)	36%	37%	41%	37%	39%
Direct Agriculture Advances amount outstanding (Rs. Million)	172131	214644	317769	1602329	4407581
Share of Priority Sector Advances towards Direct financing for Agriculture (per cent)	24%	26%	28%	26%	30%
Indirect Agriculture Advances amount outstanding (Rs. Million)	82562	93443	145554	1469227	1425853
Share of Priority Sector Advances towards Indirect financing for Agriculture (per cent)	12%	11%	13%	11%	10%

Source: Reserve Bank of India website

It is been observed that over the period of 2008-2012, share of Priority Sector Advances (PSA) towards Agriculture has been more than 30% and had peaked to 41% in year 2010. These agricultural advances were further bifurcated into direct and indirect financing of which the former being the most preferred financing means. Share of PSA towards direct financing for agriculture has been growing since 2008 till 2010 after which it dipped for a year and reached a five year high of 30% in 2012. While share of PSA towards indirect financing for agriculture has been decreasing and has reached the lowest between the period of 10% in year 2012 with an exceptional high of 13% in year 2010.

The growth of credit to agriculture sector witnessed moderation during 2010 as compared to the previous year. The sharp decline in the growth of agricultural credit was partly on account of definitional changes affected during February- March 2011. It is pertinent to note that despite the enhancement of limit (From Rs 50,000 to Rs 1,00,000), for the waiver of

margin/security requirements for agricultural loans in June 2010, the credit flow to the agricultural sector decelerated in 2010-11 over the previous year[5]

Since these banks have existence across India, the sample is further divided into five regions i.e. Southern, Western, Central, Eastern and North Eastern regions. Following is the region-wise classification of states:

Region	States
Southern Region	Andhra Pradesh, Karnataka, Lakshadweep, Tamil Nadu, Kerala, Puducherry
Western Region	Gujarat, Maharashtra, Daman & Diu, Goa, Dadar & Nagar Haveli
Central Region	Uttar Pradesh, Uttarkhand, Madhya Pradesh, Chhattisgarh
Eastern Region	Bihar, Jharkhand, West Bengal, Odisha, Sikkim, Andaman & Nicobar
North Eastern Region	Assam, Meghalaya, Mizoram, Arunachal Pradesh, Nagaland, Manipur, Tripura
Northern Region	Delhi, Punjab, Haryana, Chandigarh, Jammu & Kashmir, Himachal Pradesh, Rajasthan

In Table 1 illustrates the region wise direct agriculture advances given by Scheduled Commercial Banks of India. There is a steep increase in the lending to the North Eastern and Eastern Regions for direct agriculture advances. The Southern region followed by Northern region has large amount of direct agriculture advances as compared to other regions which are Rs 17,84,927Million and Rs 8,15,622 Million respectively.

Table 1: Regionwise Direct Agriculture Advances

Direct Agriculture Advances amount outstanding (Rs. Million)	2008	2009	2010	2011	2012
Northern Region	32,052	41,102	61,616	6,91,777	8,15,622
North Eastern Region	1,180	2,225	2,467	29,868	47,114
Eastern Region	36,026	19,604	26,946	2,79,440	3,57,851
Central Region	31,054	38,736	54,733	5,86,742	7,57,242
Western Region	23,665	33,302	47,220	5,72,436	6,44,825
Southern Region	68,154	79,675	1,24,788	14,42,266	17,84,927
All India	1,72,131	2,14,644	3,17,769	36,02,529	44,07,561

In Table 1 illustrates the region wise Indirect agriculture advances given by Scheduled Commercial Banks of India. There is a steep increase in the indirect agriculture advance for North Eastern Region. Southern and Northern region are the leading regions for the indirect agriculture advances with advance amount of Rs 4,63,326 Million and Rs 3,67,659 Million.

Table 2: Regionwise Indirect Agriculture Advances

Indirect Agriculture Advances amount outstanding (Rs. Million)	2008	2009	2010	2011	2012
Northern Region	29,225	28,528	47,826	4,41,528	3,67,659
North Eastern Region	159	211	619	7,903	10,313
Eastern Region	4,023	7,156	13,657	1,58,113	1,55,519
Central Region	6,385	7,252	16,380	1,84,363	1,79,517
Western Region	24961	28,311	26,368	2,41,219	2,49,519
Southern Region	17,809	21,985	40,704	4,36,301	4,63,326
All India	82,562	93,443	1,45,554	14,69,227	14,25,553

It is observed that Southern Region has been the most preferred region under priority sector lending through both direct and indirect financing for agriculture. There is no significant difference in preference of regions for lending to agriculture through direct/indirect category by Scheduled Commercial Banks. According to the descending order namely Western, Central, Eastern, Northern and North Eastern Region are preferred for availing credit to carry agriculture and allied activities.

So it is observed that

1. There is significant increase over a period of time in willingness of the banks to lend for agricultural operations
2. There is a significant difference in the regionwise advances for agricultural operations
3. There is a significant difference in the direct and indirect financing utilized across regions of India

Conclusion:

The contribution of PSL in increasing the credit supply to priority sectors, primarily agriculture, MSEs and export in India is clear. However, imposing mandatory PSL restrictions on all types of SCBs uniformly, is not only an inefficient means of meeting the needs of the sectors, but is also costly for the banks. Further, the responsiveness of sectors to increase in PSL is governed by sector specific factors. Agriculture, in particular is characterized by factors such as dependence on monsoons, stagnating / lowering productivity, fragmentation of land holdings and the existence of an informal credit market that throttles the impact of increased PSL from reaching the intended beneficiaries, and contributing to the sector's growth.

There is an increase in the priority sector lending (direct and indirect financing) to agriculture by Scheduled Commercial Banks. Though lending to agriculture through indirect financing seems to be the most efficient in terms of cost and risk attached with small borrowers but it is not most widely used channel for credit in agriculture. Southern region of India evolves as the preferred PSL region for agriculture & allied activities.

It is observed that the scheduled commercial banks credit to GDP ratio has been increasing over the years while percentage of agriculture & allied activities to GDP has been decreasing over the years.

Scheduled Commercial Banks Credit as percentage of GDP

Agriculture and allied activities as percentage of GDP
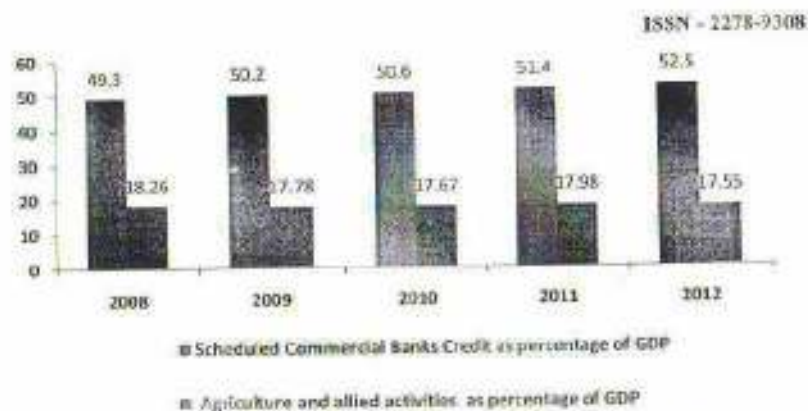
This indicates that increase in credit availability for agriculture and allied activities have not been increasing its contribution to GDP. The agricultural and allied activities suffers from several challenges, namely, fragmented and uneconomical size of landholding; seeds, fruits and vegetables are wasted every year; Significant dependence on monsoon and inadequacy of irrigation facilities; Low level of farm mechanization; Inadequacy of extension services in agriculture.

Though these reformative policies are adopted nationwide, mere increase in credit lending will not increase agricultural output contribution. Special focus is also required on developing the entire agriculture value chain.

References
- ing Group on the Modalities of Implementation of the Priority Sector Lending and 20-Point Economic Programme by Banks (Chairman: Dr K.S. Krishnaswamy), (1980)
- Working Group on the Role of Banks in Implementation of New 20-Point Programme (Chairman: Shri A. Ghosh), (1982)
- V.B. Angadi (1983), 'Bank's Advances to Priority Sector: an Enquiry in to the Causes of Concentration', *Economic & Political Weekly*, and XVIII (13):503-510, March 26.
- Yunus, Muhammad, (1988), 'The Poor as the Engine of Development', *Economic Impact*, 63:27-31.
- A.S. Chawala, K.K. Uppal, Keshav Malhotra (1988), 'Emerging issues in priority sector financing', *Indian Banking towards 21st century*, Deep and Deep Publication, Pp. 66-70.
- C. Rangarajan (1991), 'Banking Development since 1947; Achievement and Challenges', *Financial System in India*, II.
- Government of India (1991) Report of the Committee on Financial System, Ministry of Finance, (Narasimham Committee), December.
- S. Rajagopal, (1994), 'The Priority Sector', *IBA Bulletin*, XVI (): 52-54, January
- High Level Committee on Agricultural Credit through Commercial Banks (R.V.Gupta Committee), 1996.
- S.G. Patel, (1996), 'Role of Commercial Banks' Lending to Priority Sector in Gujarat - An Evaluation', *Finance India*, X (2): 389-393.
- R. Kohli, (1997), 'Directed Credit and Financial Reforms', *Economic and Political weekly*, XXXII (42):2267-2276 October 18.
- Ajit, D (1997), 'Poor Banking in India, some Issue', *Economic and Political weekly*, (October 18), XXXII (42).

- Govt of India (1998) Report of the Committee on Financial System, Ministry of Fina (Narasimham Committee-II), April.
- RBI, Department of Banking Supervision (1999), 'Some Aspects and Issues Relating to NPAs in Commercial Banks', *RBI Bulletin*, and LIII (7): 913-930.
- Technical Group on computation of Priority sector lending targets (chairman: Shri B.R. Verma), 2000
- Report of the Expert Committee on Rural Credit (V.S. Vyas Committee), 2001, NABARD, Mumbai, November 12.
- Y. V. Reddy, (2001), Address at the Conference of Indian Society of Agricultural Marketing at Vizag (A.P.) February.
- S. Niranjana and Anbumani, V. (2002), 'Social Objectives and Priority Sector Lending', *Banking and Financial Sector Reforms in India*, Deep and Deep Publications, PP- 231.
- N.B. Shete. (2002), 'Priority Sector Advances by Public Sector Banks during the Post Reform Period' (1992-93 to 2000-01), Working Paper, NIBM, Pune, March 2002.
- http://www.rbi.org.in/
- http://planningcommission.nic.in/data/datatable/index.php?data=datatab

The
HORIZON
द हॅराइझ्न

A- Bi-annual Interdisciplinary National Research Journal

Mahatma Gandhi National Rural Employment Guarantee Scheme: A Unique Scheme for Indian Rural Women

Dr. Sanjay B. Kadu
Associate Professor
Vidya Bharti Mahavidyalaya,Amravati

Prof. S. K. Hadde
Assistant Professor
Vidya Bharti Mahavidyalaya, Amravati.

Introduction

According to the United Nations Millennium Campaign the overwhelming majority of the labor that sustains life – growing food, cooking, raising children, caring for the elderly, maintaining a house, hauling water – is done by women, and universally this work is accorded low status and no pay. The role of women in protecting the family members from hunger and poverty had been highlighted by Rosi Braidotti (1994) and Caroline Moser (1988, 1989). According to them, in 1980's the international economic conditions and debt crisis led to increasing poverty of populations in the south and in what was termed a 'feminization of poverty'. An increasing number of women became providers of family subsistence, while men often migrated in search employment. In many societies around the world, women never belong wholly to themselves; they are the property of others throughout their lives. Their physical well-being – health, security and bodily integrity – is often beyond their own control. Where women have no control over money, they cannot choose to get health care for themselves or their children.

MNREGA and women

The Mahatma Gandhi National Rural Employment Guarantee Act (MNREGA) provides a legal Guarantee of 100 days of wage employment in a financial year to every rural household. The participation of women in the workforce has surpassed the statutory minimum requirement of 33 percent and through this it has protected the women justice and rights. The Act provides some explicit entitlements for women to facilitate their full participation.

These include: Equal wages for men and women – 'Equal wages shall be paid to both men and women workers and the provisions of Equal Remuneration Act, 1976 shall be complied with' (p.26)

Participation in Management and monitoring of the programme – 'The gram sabha will elect the members of the committee and ensure that SC/STs and women are represented on it' (p.44)

Participation is social audit – 'The timing of the forum must be such that it is convenient for people to attend – that is, it is convenient for REGS (Rural Employment Guarantee Scheme) workers, women and marginalized communities.' (p.56) Providing support for child care, and convenience to households – The guidelines mention the need for a crèche at the worksite, and for the works to be convenient for families. Ensuring that single women are eligible – By recognizing a single person as a 'household', the Act makes it possible for widows and other single women to access this work for widows and other single women to access work. (nrega.nic.in)

Relevance of the study

The explanation for relevance of a study may be given from the point of view of two major considerations. One, the 'women' is a major focus of the program in so far as the employment guarantee policy is seen as an instrument that can support job creation and bring about gender equality, essential for empowerment. And two, the program itself, in course of its implementation has brought into focus several issues concerning gender and poverty which should to be examined intensely for deriving planning lessons.

Research objectives

To know the relevance of MNREGS for women empowerment, the primary objective of the research is to study the impact of MNREGP on women empowerment and to identify major constraints, if any, on women's access to productive employment opportunities through MNREGP.

Research and sample design

The primary data source was household level data being collected through especially designed semi structured interviews/questionnaire, the job cards and the MIS reports/Monthly/quarterly progress reports of the District Program Coordinators and the district specific reports collected at the state level. On the whole, the basic method of data collection has been focus group discussions and few semi structured/ structured interviews with key informants besides information available through official statistics of the implementing agencies. A random sampling was also done to select women workers from worksites.

Empowerment impacts

The economic dependence of women on men in rural India plays a major role in the subjugation of women, and in this respect the MNREGA is an important tool of social change. (Drèze, J. and Oldiges, C.2007). But how has paid employment under MNREGS changed the position of rural women? Answer of this question can be finding out by knowing impact of this scheme on women workers. The main reason for their satisfaction is that; they are guaranteed 100 days of jobs. It means that no longer have they to fear the episode of seasonal unemployment and poverty and not only this MNREGS enabled them to participate effectively in society.

Major findings

* 95.5% of them believe that, the programme enhanced their credit worthiness and 78% women believe that, they could start saving some money only because of the MNREGS.

* Women's MNREGA earnings have increased their contribution to household income. A large majority (76 per cent) of the respondents said that they spent wages on regular food and consumer goods. The increased income locally available through NREGA work, they felt, is helping to ensure at least two regular meals in a day.

* According to most of the beneficiaries, the amount earned through MNREGA is insufficient to repay debts. Nevertheless, 49.1 per cent of the respondents said that they had spent their wages on repaying small debts. Not only this, it also helps them to keep themselves away from the grip of local moneylenders.

* Moreover the income from MNREGS helped them to increase the expenditure on education of their children (37.1%), medical expenses (62.7%). At the same time 92% of the women had the view that today, only because of the MNREGS, they are able to support their families and 71% opined that, the income from the MNREGS works provided economic independence to them. They are no longer dependent on the income earned by their husbands.

- 66.4% women asserted that MNREGS contributed much to the improvement of their social contact. In other words, the new wage employment programme succeeded ensuring freedom and equality for women in civil, economic and social areas of activity (Thomas, E.M. 2010)

- Participation in the scheme has meant that women (65%) are coming out of their homes, not only to work but also to visit banks which they have not done in the past. "Women can now be seen moving around in places like gram panchayat office, banks, schools, block office without anybody to accompany them.' (Sudarshan 2011)

Obstacles to women workers

However, MNREGS benefits have not come easily - their leisure time has misplaced with working hours for women and not only this have they to bear with physical and emotional strains. Some of the obstacles that we found during survey were as follows:

- While identifying the step of projects at Block level, very little was considered as regards suitability of women. In other words, hardly any project was selected in terms of providing direct benefit to women.

- The MNREGA guidelines provide certain positive action to encourage women participation in the program like facilities for creche, drinking water, shade and first aid are required to be provided at every worksite. The findings show that with the exception of provision for drinking water, other worksite facilities viz. creche, resting place, first-aid, recreational facility for children etc. and other facilities for the betterment of gender were generally absent in the worksites. As regards other household works, most respondents said, they don't get any support from their husbands and most of the domestic work like cooking, and care related works they used to do after return from work. This means, their working hours has been extended due to MNREGA.

- Delayed payments also come in the way of participation of poor women. Delays in wage payments make it difficult especially for single women, who cannot afford to wait as they are the only earners in the family. When they do not get wages in time, they are bound to return to previous, less preferred job. Delay in wages is due to the reason as the money is released only after submission of the completion report of every project by area engineer, which is a relatively long process.

Suggestions

Major suggestions by which effectiveness of this programme can be increased are:

- The Panchayat must create awareness among the local people about MNREGA. Awareness levels among the workers regarding rights, entitlements, provisions and procedures under MNREGS was found very low which shows poor performance of the officials.

- It is not sufficient to put some special facilities such as drinking water, shade for children, periods of rest and a first aid box care etc. on papers but implementation and maintenance must be done properly.

- However, overall in Haryana, only 11.08 per cent participating households completed 100 days of employment under MNREGS. It should be assured that participation days should be increased otherwise for few days nobody will give break in present job.

- Involvement of NGOs in MNREGS has been very low. This feature requires to be strengthened to make the rights-based MNREGS more successful and meaningful.

- It may be stressed here that effective information flows and dissemination about the various angles of this provision of the Scheme and also about the roles and responsibilities of the officials, Sarpanch and Gram Pradhans through all types of media and channels in the rural areas are essential. Then only this scheme can be performed in a meaningful sense and degree.

Conclusion

Viewed in a wider outlook, MNREGA signals a possible reshaping of priorities in India through a democratic determination to provide real livelihood opportunities for the rural poor. The MNREGA is a wage employment program, providing minimum wage employment to casual, unskilled labour, women, disabled especially during those days in which they are jobless or free from agriculture work. Gender has never been at the centre stage of the program as a policy. But still due to its provision for women, MNREGA has emerged as a very powerful tool for women empowerment. This programme of government has taken care of that corner which remained untouched from changes in society from last many years.

References:-

1) Bhuyan, Dasarathi, (2006) "Empowerment of Indian Women: A Challenge of 21st Century" Orissa Review Jan. 2006P 60

2) Dreze, Jean and Christian Oldiges (2007): "Commendable Act", Frontline, Vol 24, No 14, July.

3) Khera, Reetika and Nayak, Nandini (2009) "Women Workers and Perceptions of the National Rural Employment Guarantee Act", Economic & Political Weekly, xliv no 43 OCTOBER 24, www.nrega.nic.in

4) Ministry of Rural Development (2008): The National Rural Employment Guarantee Act 2005' Operation Guidelines 2008 3rd edition

5) Moser, Caroline O.N. (1989), "Gender Planning in the Third World: meeting Practical and Strategical Gender Needs" in World Development Vol. 17- 11

6) Pankaj, Ashok and Tankha, Rukmini (2010) " Empowerment Effects of the NREGS on Women Workers: A Study in Four States" Economic & Political Weekly EPW July 24

7) Sharma, A. (2012): "SC/ST Employment Guarantee Women's Empowerment in Rural India by MGNREGA"

8) International Journal of Human Development and Management Sciences Vol. 1 No. 1 (January-December, 2012) ISSN: 2250-8714 Mind Reader Publications

9) Singh, S.P. and Nauriyal, D.K. (2009) "System and Process Review and Impact Assessment of NREGS in the state of Uttarakhand" Professional Institutional Network, IIT Roorkee

10) Sudarshan, M. Ratna. (2011) "India's National Rural Employment Guarantee Act: women's participation and impacts in Himachal Pradesh, Kerala and Rajasthan" CSP Research Report 06 January

journal
of the
instrument
society
of india

Design of quick recovery heart beat sensor

R.A.Mishra*   and   N.B.Raut

Amolakchand Mahavidyalaya,Yavatmal-445001, India
Vidya Bhrati Mahavidyalaya, Amravati, India
* E-mail: mishrarammanohar@gmail.com

Abstract

Biomedical instruments are used in large scale for the purpose of diagnosis and research medical sciences. Electronic instruments are used in medical science and therefore it is necess improve the sensing of physiological parameter in biomedical instruments. The design technique quick recovery heart beat sensor (QRHBS), characteristics of this sensor and its comparison existing sensors in similar kind of biomedical instruments is discussed in this paper.

During the treatment to patient, body temperature and heart beats are quite often measure a physician for diagnosis of a patient. The researcher therefore decided to study those sensors used heart beat measurements. An attempt has been made by researcher to improve the performance of instruments by replacing the sensors in existing biomedical instruments. The heart beat detection existing sensor like electrode have a problem of interfacing with skin and skin preparation measurements of heart beat rate. In order to remove this problem paste-less electrodes may be

Many investigators had proposed concepts to measure the body temperature or heart be measurements in biomedical instruments. They have attempted to design transducers using prop of electronic components such as diode, photo emitters, photo detectors (photo diode and transistors), field effect devices(FET/MOSFET), laser based components (Laser-LED/diodes components(strain gauges), inductive components (LVDT/RVDT), capacitive components (pie crystal and diaphragm type), optical based components(optical fiber), thermal resistance (ph thermocouple metal oxides (thermistors), in biomedical instruments. The properties of these com are used to measure heart beat rate. The researcher has attempted to use some of these comp to develop the transducers for measurement of heart beat rate. QRHBS sensors are devel researcher by overcoming the limitations of electronic components.

1.Design technique of quick recovery heart beat sensor

The quick recovery heart beat sensor (QRHBS) is assembled by using tim oscillating circuit, LDR & LED. In the time base oscillating circuit, the frequency of output signal depends on series combination of resistor and capacitor connected to emitter of emitter resistor is replaced by LDR. The resistance of LDR is changed with intensity of ligh property of LDR is used to change the frequency of output sweep signals with intensity of ligh arrangement of QRHBS is shown in figure-1.

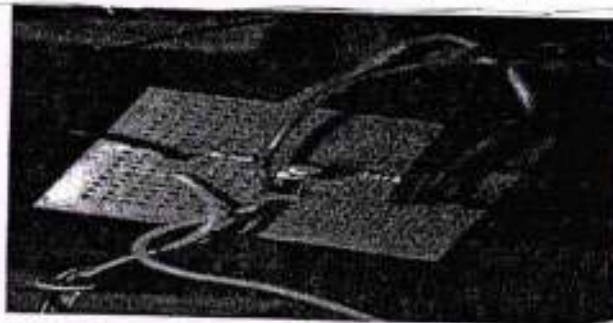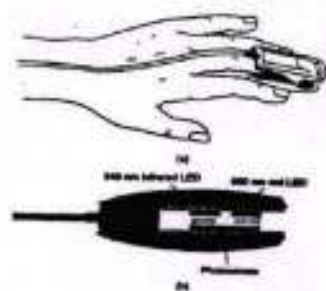**Fig. 1: Arrangement of QRHBS**   **Photograph showing QRHBS**

The QRHBS developed by researcher uses transmittance method. In this method a LED and phototransistor is mounted in an enclosure which is fitted over a tip of patient's finger. The light is then transmitted through the finger tip and the resistance of phototransistor is determined by the amount of intensity of light reaching it. With each contraction of heart, blood is forced to extremities and the amount of blood in the finger increase. The blood concentration in finger is altered to the optical density of the light transmitted through the finger and the resistance of phototransistor is also change accordingly. The output of phototransistor is connected to voltage divider circuit, which produces the variable voltage according to change in intensity of light transmitted through the finger. But the blood concentration is altered according to the expansion and contraction activity of the heart. This method has been used to measure the heart beat rate in terms of variable voltage.

In the time base oscillating circuit, emitter resistance is replaced by LDR and series resistance R. the emitter capacitor is chosen to the fixed value so that the frequency of output sweep signal is in the range from 50 Hz to 200Hz. The frequency of output sweep signal is noted in absence of the finger between LED & LDR and it is known as reference frequency. The frequency of output sweep signal in the time base oscillating circuit varies with change in the intensity of light focused on the surface of LDR from the LED source after transmitting through the finger. Under the dark condition, the frequency of QRHBS is reference frequency which is equal to 200Hz. The condition under which the finger is placed between LED & LDR, the frequency of output sweep signal is obtained in terms of two frequency values f1 and f2. The f1 is related to contraction of heart and f2 is related with expansion activity of heart. The frequency f1 & f2 is measured using digital frequency meter. The frequency difference between f1 & f2 indicates the variation in the frequency of output sweep signal due to expansion and contraction activity of heart. One heart beat is related to this frequency difference and the time required for one heart beat is calculated by knowing this difference ($T = 1/f$).

2. Experimental and characterization of QRHBS

The steps followed in present experimental study are as given below:

1 The reference frequency is adjusted to the values 200 Hz, 135 Hz, 100 Hz, and 50 Hz by selecting R and resistance of LDR and emitter capacitor is selected to fixed value of 0.1 micro farad. The reference frequency is noted in the absence of finger between LED & LDR.

2 The frequency values f1 and f2 are noted in the presence of finger between LED & LDR of sample (person) using digital frequency meter. The frequency difference (f1-f2) is calculated.

3 The time interval of heart beat cycle is calculated by taking reciprocal of this difference.

4 The heart beat rate of sample is calculated by beat to beat heart beat rate calculation method. The heart rate of sample is measured as 60/T.

5 Steps 2 to 5 are repeated for ten samples. The experimental observations have been repeated for three to four times to calculate the heart beat rate for ten samples each time.

Table – 2 Comparison of quick recovery heart beat sensor with existing sensor in heart beat monitoring biomedical instruments

Sr. No.	Parameter	Quick recovery heart beat sensor developed by researcher	Limb electrode	Floating electrode	Pre-gelled disposable electrode	Capacitive pasteless electrode	Air jet
1.	Heart beat	100-240 beats/min	50-300 beats/min	50-400 beats/min	6-400 beats/min	1-400 beats/min	1-400 beats/min
2.	Contact Impedance	1 - 30 GΩ at 10 Hz	2 - 5 KΩ at 10 Hz	50 KΩ at 10 Hz	564 Ω at 10 Hz	1000 - 30000 MΩ at 10 Hz	30000 MΩ at 10 Hz
3.	Shape	Round flat surface	Round flat surface	Round flat surface	Round shape	Round shape	Niddle shape
4.	Cost	Low	Low	Low	High	High	High
5.	Output	Frequency	Capacitance	Capacitance	Capacitance	Capacitance	Capacitance

3. Experimental analysis of QRHBS

1 QRHBS is developed to measure the heart beat rate by selecting reference frequency, and measuring the frequencies f1 and f2 and calculating the difference (df). The frequency change df indicates the heart beat rate by multiplying it by 60.

2 The QRHBS shows the result in the range of 60 to 300 beats per minute, which is the measuring range of heart beat rate observed from standard data. The df is easy to digitize in heart beat read-out using the counter circuit. The counter circuit counts the pulses in one second. These pulses are multiplied by 60 to indicate the heart beat rate.

3 There is no effect of environment or stray effect on the components used in fabrication of QRHBS during sensing of ECG signals. The power requirement of these components is quite low for their operation. Thus QRHBS can operate with dc source.

4 The output of QRHBS is low frequency. It is measured by low frequency meter. The skin contact impedance is not considered in this experiment.

5 Researcher has observed that the performance of QRHBS is fairly good as compared to the existing sensors used in heart beat measuring system to detect ECG signals. The comparison of QRHBS with other sensors is shown in table-2

4. Results

The work was initiated for development of new sensors/transducers of heart beat sensing using time base oscillating circuits. The results of present experimental study are given as under:

1 The output power consumption is comparatively low ac the nature of output signal is AC.

2 QRHBS uses LED & LDR arrangement for photo transmittance. The spectral response of LED is of unique wavelength for red light emission. Infrared LED was selected to give unique spectral response at 0.94 micrometer with peak bandwidth 0.707 micrometer. LDR is of round surface of 5mm diameter, which accepts almost all light transmitted from finger. This arrangement is sensitive to detect the heart activity.

3 The QRHBS measures the heart beat rate in the range of 60-300 beats/minute. The frequency range measured for heart beat activity is 2Hz to 5 Hz.

4 The QRHBS performance is similar to the performance of electrodes used in measurement of ECG signals.

5 Photoconductive cells CdSe has response time of about 10 ms and CdS is 100 ms. CdSe is more sensitive to change the resistance in an ambient temperature. CdS is best photo detector for LED light illumination.

6 The large response time of Photoconductive cell does not make much more effect in biomedical applications because the required frequency range in sensing of physiological parameters is less than 100 Hz.

5. CONCLUSIONS

The concept of QRS is used in designing QRHBS .The study of various concepts of sensors/transducers used for the measurement of heart beat rate in biomedical instruments is carried out during development of QRHBS. The limitations of existing sensors/transducers are also studied in their characteristics. The QRHBS is designed with detailed study of characteristics of quick recovery device (QRD as UJT 2646), characteristics of thermister & LDR. The properties of thermister, LED & LDR have been used in time based oscillating circuit to design QRHBS.

The measurement of heart beat rate with QRHBS is done in terms of frequency difference. This frequency difference is recorded by digital storage CRO for analysis of heart beat rate. The QRHBS is designed by using time base oscillating circuit and photo sensitive components like LED & LDR. The special arrangement is made to detect blood concentration in the part of body with LED & LDR. The direct read out of heart beat rate is possible in digital form by using counter circuit.

The researcher has developed the QRHBS to measure heart beat rate. The effectiveness of these transducers is compared with existing sensors/transducers such as thermal resistance, thermocouples, thermisters with NTC and PTC properties, optical sensors and LM35 used in biomedical instruments.

The QRHBS is used to measure the heart beat rate. The effectiveness of QRHBS was checked for various samples and observed it is that similar to existing sensors like limb electrode, floating electrode, pregelled disposable electrode, capacitive paste less electrode, air jet electrode used in biomedical instruments for heart beat measurements. The problem of skin impedance is not much effective in measurement of heart beat because there is no direct contact with the body part to detect heart beat as in existing sensors. The frequency obtained from heart beat action is quite low. Therefore proper filtering of heart beat signal is required to detect the heart beat signal at output without noise.

In case of QRHBS probable error is equal to 0.01 Hz. For effective measurement of heart beat rate by QRHBS the probable error should be minimized.

References

[1]   Anbar M, 1978, Clinical thermal imaging today, IEEE, Eng Med and Bio, 19, 4- 25.
[2]   Cohen a and N Wadsworth, 1972, Med and Biol Eng, 10, 385.
       ˀcek A and Pedrycz W, 2006, IEEE Trans on Bio Med Eng, 53(10), 1972.
[4]   ˌalvani et al, 2002, Handbook of biomedical instrumentation by R. S. Khandpur, 2nd Ed. TMH, 32, 66-112.
[5]   Ragheb T and L A Geddas, 1990, Med and Bio Eng and Comp, 182.
[6]   Raut N.B. & Mishra R.A.(2009): The study of some characteristics of sensors used in biomedical instruments.
[7]   Roy O Z, 1980, Med and Eng and Compute, 18,657.
[8]   Kandpur R S, 2003, Electronics Devices and Linear circuits, 17.

Indian Journal of Agricultural Library and Information Services

http//:www.

e-learning

Indian Journal of Agricultural Library and Information Services

EDITORIAL BOARD

CONTENTS

TOTAL QUALITY MANAGEMENT IN Dr. PANJABRAO DESHMUKH AGRICULTURAL UNIVERSITY LIBRARY, AKOLA, MAHARASHTRA: A USERS' STUDY

Vishal R. Shekawat* and Vaishali P. Gudadhe**

ABSTRACT

Since formation the State of Maharashtra has undoubtedly provided leadership at the national level in matters of economic growth and development. Moreover it has tried to retain the participation of agriculture and provided much needed research and development facilities by not only creating agricultural universities which are spread across the state in a balanced manner but taken them above record keeping and paper work to actually empower them to serve the purpose of transformation of conventional farming and agro practices into modern globalised one.

This research paper aims to bring about the use of total quality management techniques in managing the most essential support systems to any educational institutions, the libraries which pool up and arrange knowledge materials so as to be able to be used whenever needed. Naturally it becomes easy for all those who require using the services and smoothly continuing with their work whereas the library stays away from limelight playing a silent role.

India walks a new path to glory and being the only third world developing country which still relies on agriculture as its major source of national income a lot has to be done. But, not only at the top level but also at every juncture right from educating the next generation agro community members but also doing it in such a way that they are able to cope with the changes in the international environment. The paper reflects use of the following six attributes, which are: Reliability, Responsiveness, Assurance, Access, Communication, and Tangibility. The paper aims to put forth the benefits of use of Total Quality Management methods in getting better results making the path easy for overall development.

INTRODUCTION

Since the ancient times, it has been assured that libraries are the sources of knowledge and also the treasures of gentle culture. Their terminology is supposed to be the heart of a university and also in the form of soul and brain. There was also the occurrence of books by the Sardars' during the Mughal period. They used to keep their private libraries for learning. The then Sultans and Mughal monarchs were also book lovers. With this, are comes to know that libraries were in vogue during the Mughal period. Total Quality Management is not just a concept, rather an attitude that deals and touches every function, eliminating non-conformances with required objectives, identifying more suitable ways of handling and controlling operations so as to achieve desired results.

OBJECTIVES OF THE STUDY

The objectives of the research study were as following:

1. To understand the essentials of Total Quality Management (TQM) in Agricultural university libraries in Maharashtra.
2. To study the essence of TQM for library and information services.
3. To study quality techniques in Dr. Panjabrao Deshmukh Agricultural university library for sustainable library management.

---

* Assistant Librarian, Vidyabharti Mahavidyala, Amravati (MS).
** Associate Professor & Head, Department of Library & Information Science, Sant Gadge Baba Amravati University, Amravati (MS).

4. To identify internet resources and their quality for libraries.

5. To measure the users satisfaction using the different attributes of TQM.

SCOPE AND LIMITATION

The present research work was limited to the users of Dr. Panjabrao Deshmukh Agricultural University Library.

SAMPLE POPULATION

In order to satisfy the qualitative and quantitative information required for this research paper, the researcher selected 150 respondents i.e. the users of the Dr. Panjabrao Deshmukh Agricultural University library.

A standard structured questionnaire was designed to collect the required information where five point Likert type scale was used.

DESCRIPTION OF THE QUESTIONNAIRE USED

The questionnaire is essentially a skillful translation of objective into a set of questions intended to be answered in writing. It is a written list of questions requiring answers in writing.

USERS STUDY

Questionnaire was prepared to incur the data relating to the "Users" & to observe and record the actual reactions of the "Users" of Dr. Panjabrao Deshmukh Agricultural University library.

Dr. PANJABRAO DESHMUKH AGRICULTURAL UNIVERSITY LIBRARY

To study the performance of Dr. Panjabrao Deshmukh Agricultural University library on different attributes with regard to total quality management, the data was obtained on the following six attributes namely reliability, responsiveness, assurance, access, Communication, Tangibles and the respondents were asked to give their opinions on each attributes in the manner of 5 points scale.

Data was collected from 150 respondents from the University. These respondents were consisting of 100 students & 50 teachers. The score obtained for each point of the attributes was tabulated as under:

Note: The scoring pattern adopted by the researcher is as follows:

Option:	a	b	c	d	e
Score:	5	4	3	2	1

Note: 's' denotes Students, and 't' denotes Teachers

Reliability:

Table 1: Indicating Scores of Reliability

R12	s1	t1	s2	t2	s3	t3	s4	t4	s5	t5	total
1	36	13	16	19	15	7	13	5	11	4	150
2	43	32	24	8	13	4	9	1	16	1	150
3	49	24	24	1	7	3	10	1	9	1	150
4	52	23	22	11	12	8	10	4	4	4	150
5	44	23	27	14	13	1	9	4	7	4	150
6	47	20	26	14	10	7	4	8	9	1	150
7	41	15	17	11	9	5	9	8	13	8	150
8	47	24	31	12	12	6	10	4	10	4	150
9	26	13	16	18	17	4	11	1	10	5	130
10	52	10	27	13	15	9	16	1	14	5	140
11	32	14	20	13	21	11	9	3	12	1	130
12	32	16	11	16	12	9	17	1	12	4	130
Total	474	239	325	169	155	83	127	56	119	53	1809

From the Table no. 1, it was observed that, to study whether there is any similarity or discrepancy between the opinions of teachers & students with respect to scoring we calculated correlation co-efficient for each opinion. This co-relation between the opinion of teachers & students for each score is as follows:

Table 2: Correlation of Student & Teacher

Score	5	4	3	2	1
Correl	0.67444	0.66299	0.78846	0.58647	0.25763

From the Table no. 2, it was observed that for the score 5, 4, 3 & 2 there is consistency (positive co-relation between the opinions of teachers & students). As for as score 1 is concerned, no such conclusions can be drawn as the corresponding co-efficient of co-relation is very small (0.25763).

With respect to the total Scores for the reliability, we calculated total Scores for teachers & students separately & also calculated the means of score. The total score is calculated with the help of following formula:

Total score for the teachers = 5 x total number of teachers giving score 5 + 4 x total number of teachers giving score 4 + 3 x total number of teachers giving score 3 + 2 x total number of teachers giving score 2 + 1 x total number of teachers giving score 1, i.e.

Total score for teacher = 5 x 239 + 4 x 169 + 3 x 83 + 2 x 56 + 1 x 53 = 2285

The total score for the student is also obtained in the same manner.

Total score for student = 5 x 474 + 4 x 325 + 3 x 155 + 2 x 127 + 1 x 119 = 4508

Then the mean of scores for teachers is obtained as:

Mean score for teachers = total score for teachers/ total number of teachers & the same formula is used for calculating mean score for students. The total and means scores for teachers & students were given below:

Table 3: Means Score of Student & Teacher

Respondents	Total Score	Mean Score
Teachers	2285	45.7
Students	4508	45.8

From the Table no. 3, it was observed that, there was no significant difference between the mean score of teachers & students. The scores were so matching that no need of statistical tests for the same is needed.

Responsiveness

Table 4: Scores of Responsiveness

R12	s1	t1	s2	t2	s3	t3	s4	t4	s5	t5	Total
	59	22	19	13	10	5	7	6	5	4	150
1	59	22	19	13	11	4	9	4	7	3	150
2	51	27	22	12	11	7	9	4	8	4	150
3	54	25	18	10	7	3	6	5	9	1	150
4	52	23	26	18	7	3	14	5	4	5	150
5	53	24	13	12	16	4	11	7	8	4	150
6	51	24	18	10	12	5	9	4	11	3	150
7	41	31	27	10	12	2	13	7	4	5	150
8	36	52	28	11	14	5	11	3	8	1	150
9	44	27	27	18	10	4	13	6	10	6	170
10	44	23	22	12	9	3	9	2	9	2	150
11	37	13	13	11	23	4	9	6	3	6	150
12	47	19	21	13	15	6	9	6	3	6	1800
Total	569	293	263	150	150	52	122	69	96	40	1800

From the Table no.4, it was observed that, to study whether there is any similarity or discrepancy between the opinions of teachers & students with respect to scoring we calculated correlation co-efficient for each opinion. This co-relation between the opinion of teachers & students for each score is as follows:

Table 5: Correlation of Student & Teacher

Score	5	4	3	2	1
correl	-0.3271	0.36523	0.14325	0.28083	-0.182743471

From the Table no. 5, it was observed that for the score 4, 3, 2 & 1. As for as score is concerned, no such conclusions can be drawn as the corresponding co-efficient of co-relation is very small (0.36523), (0.14325), (0.28083) & (0.182743). For score 5, there is a negative co-efficient of co-relation (-03271), which indicates that, there is a difference between the opinions of teachers & students.

With respect to the total Scores for the responsiveness, we calculated total Scores for teachers & students separately & also calculated the means of scores. The total score is calculated with the help of following formula:

Total score for the teachers = 5 x total number of teachers giving score 5 + 4 x total number of teachers giving score 4 + 3 x total number of teachers giving score 3 + 2 x total number of teachers giving score 2 + 1 x total number of teachers giving score 1, i.e.

Total score for teacher = 5 x 293 + 4 x 150 + 3 x 52 + 2 x 59 + 1 x 46 = 2335

The total score for the student is also obtained in the same manner.

Total score for student = 5 x 569 + 4 x 263 + 3 x 150 + 2 x 122 + 1 x 96 = 4687

Then the mean of scores for teachers is obtained as:

Mean score for teachers = total score for teachers/total number of teachers & the same formula is used for calculating mean score for students. The total and means scores for teachers & students were given below:

Table 6: Means Score of Student & Teacher

Respondents	Total Score	Mean Score
Teachers	2385	47.7
Students	4687	46.86

From the Table no. 6, it was observed that, there is no significant difference between the mean score of teachers & students. The scores were so matching that no need of statistical tests for the same is needed.

Assurance

Table 7: Scores of Assurance

No	s1	t1	s2	t2	S3	t3	s4	t4	s5	t5	Total
1	58	28	13	10	13	7	8	3	8	2	150
2	62	33	15	7	8	3	9	3	6	4	150
3	61	28	14	7	12	5	7	5	6	5	150
4	59	23	16	8	13	9	7	3	3	8	150
5	52	26	25	12	10	4	7	5	6	3	150
6	52	31	24	12	11	1	7	3	6	3	150
Total	144	169	107	56	69	28	45	22	35	25	900

The Table no. 10 shows that, to study whether there is any similarity or discrepancy between the opinions of teachers & students with respect to scoring calculated correlation co-efficient for each opinion. This co-relation between the opinion of teachers & students for each score is as follows:

Table 11: Correlation of Student & Teacher

Score	5	4	3	2	1
correl	0.86491	0.46879	0.69908	0.32124	-0.5653

From the Table no. 11, it was observed that for the score 5 & 3 there is consistency (positive co-relation between the opinions of teachers & students). For score1, there is a negative co-efficient of co-relation (− 0.5653), which indicates that, there is a difference between the opinions of teachers & students. As for as score 4 & 2 is concerned, no such conclusions can be drawn as the corresponding co-efficient of co-relation is very small (0.46879) & (0.32124)

With respect to the total Scores for the access, we calculated total Scores for teachers & students separately & also calculated the means of score. The total score is calculated with the help of following formula:

Total score for the teachers = 5 x total number of teachers giving score 5 + 4 x total number of teachers giving score 4 + 3 x total number of teachers giving score 3 + 2 x total number of teachers giving score 2 + 1 x total number of teachers giving score 1, i.e.

Total score for teacher = 5 x 137 + 4 x 47 + 3 x23 + 2 x 21 + 1 x 22 = 1006

The total score for the student is also obtained in the same manner.

Total score for student = 5 x 239+ 4 x 100 + 3 x62 + 2 x 56 + 1 x 42 = 1936

Then the mean of scores for teachers is obtained as;

Mean score for teachers = total score for teachers/ total number of teachers & the same formula is used for calculating mean score for students. The total and means scores for teachers & students were given below:

Table 12: Means Score of Student & Teacher

Respondents	Total Score	Mean Score
Teachers	1006	20.12
Students	1936	19.36

From the Table no. 12, it was observed that, there is no significant difference between the mean score of teachers & students. The scores were so matching that no need of statistical tests for the same is needed.

Communication

Table 13: Scores of Communication

C6	s1	t1	s2	t2	s3	t3	s4	t4	s5	t5	Total
1	35	17	16	11	8	3	9	3	12	1	150
2	44	27	19	12	11	3	12	4	14	4	150
3	52	25	26	8	9	5	7	6	6	8	150
4	17	17	35	14	10	5	13	7	10	7	150
5	40	35	12	9	15	9	13	4	11	3	150
6	40	22	17	9	14	7	12	6	11	5	150
Total	258	149	145	63	67	32	66	30	64	26	900

From the Table no. 13, it was observed that, to study whether there is any similarity or discrepancy between the opinions of teachers & students with respect to scoring we calculated correlation co-efficient for each opinion. This co-relation between the opinion of teachers & students for each score is as follows:

Table 14: Correlation of Student & Teacher

Score	5	4	3	2	1
correl	0.14421	0.54299	0.8492	0.10541	-0.534

From the Table no. 14, it was observed that for the score 4 & 3 there is consistency (positive co-relation between the opinions of teachers & students). For score 1, there is a negative co-efficient of co-relation (-0.534), which indicates that, there is a difference between the opinions of teachers & students. As for as score 5 & 2 is concerned, no such conclusions can be drawn as the corresponding co-efficient of co-relation is very small (0.14421) & (0.10541)

With respect to the total Scores for the communication, we calculated total Scores for teachers & students separately & also calculated the means of score. The total score is calculated with the help of following formula:

Total score for the teachers = 5 x total number of teachers giving score 5 + 4 x total number of teachers giving score 4 + 3 x total number of teachers giving score 3 + 2 x total number of teachers giving score 2 + 1 x total number of teachers giving score 1, i.e.

Total score for teacher = 5 x 149 + 4 x 63 + 3 x 32 + 2 x 30 + 1 x 26 = 1179

The total score for the student is also obtained in the same manner.

Total score for student = 5 x 258 + 4 x 145 + 3 x 67 + 2 x 66 + 1 x 64 = 2267

Then the mean of scores for teachers is obtained as:

Mean score for teachers = total score for teachers/total number of teachers & the same formula is used for calculating mean score for students. The total and means scores for teachers & students were given below:

Table 15: Mean Score of Student & Teacher

Respondents	Total Score	Mean Score
Teachers	1179	23.58
Students	2267	22.67

From the Table no.15, it was observed that, there is no significant difference between the mean score of teachers & students. The scores were so matching that no need of statistical tests for the same is needed.

Tangibles

Table 16: Scores of Tangibles

T15	s1	t1	s2	t2	s3	t3	s4	t4	s5	t5	Total
1	32	26	19	17	20	5	14	2	15	0	150
2	43	22	26	21	8	3	12	2	11	2	150
3	54	26	19	9	8	5	7	5	12	5	150
4	48	22	21	13	11	6	11	4	9	5	150
5	48	23	17	9	12	5	14	6	9	7	150
6	35	19	30	13	14	8	10	5	11	5	150
7	39	22	24	17	16	9	12	1	9	1	150
8	37	23	24	12	14	7	14	2	11	6	150

T15	s1	t1	s2	t2	s3	t3	s4	t4	s5	t5	Total
9	38	21	20	11	17	8	12	8	13	4	150
10	38	19	20	12	15	9	15	4	12	6	150
11	38	17	25	9	14	8	11	7	12	9	150
12	41	22	22	12	10	6	14	7	13	3	150
13	50	24	11	5	13	8	12	5	14	8	150
14	39	22	17	10	27	9	6	5	11	4	150
15	31	15	17	9	21	10	18	9	13	7	150
Total	611	323	312	179	220	104	182	72	175	72	2250

From the Table no. 16, it was observed that, to study whether there is any similarity or discrepancy between the opinions of teachers & students with respect to scoring we calculated correlation co-efficient for each opinion. This co-relation between the opinion of teachers & students for each score is as follows:

Table 17: Correlation of Student & Teacher

Score	5	4	3	2	1
Correl	0.51395	0.60406	0.5993	0.1459	-0.0312

From the Table no. 17, it was observed that for the score 5, 4 & 3 there is consistency (positive co-relation between the opinions of teachers & students). For score 1, there is a negative co-efficient of co-relation (-0.0312), which indicates that, there is a difference between the opinions of teachers & students. As for as score 2 is concerned, no such conclusions can be drawn as the corresponding co-efficient of co-relation is very small (0.1439).

With respect to the total Scores for the tangibles, we calculated total Scores for teachers & students separately & also calculated the means of score. The total score is calculated with the help of following formula:

Total score for the teachers = 5 x total number of teachers giving score 5 + 4 x total number of teachers giving score 4 + 3 x total number of teachers giving score 3 + 2 x total number of teachers giving score 2 + 1 x total number of teacher- giving score 1, i.e.

Total score for teacher = 5 x 323 + 4 x 179 + 3 x104 + 2 x 72 + 1 x 72 = 2859

The total score for the student is also obtained in the same manner.

Total score for student = 5 x 611 + 4 x 312 + 3 x220 + 2 x 182 + 1 x 175 = 5502

Then the mean of scores for teachers is obtained as:

Mean score for teachers = total score for teachers/total number of teachers & the same formula is used for calculating mean score for students. The total and means scores for teachers & students were given below:

Table 18: Mean Score of Student & Teacher

Respondents	Total Score	Mean Score
Teachers	2859	57.18
Students	5502	55.02

From the Table no. 18, it was observed that, there is no significant difference between the mean score of teachers & students. The scores are so matching that no need of statistical tests for the same is needed.

Table 19: Means Score of Student & Teacher according to Attributes

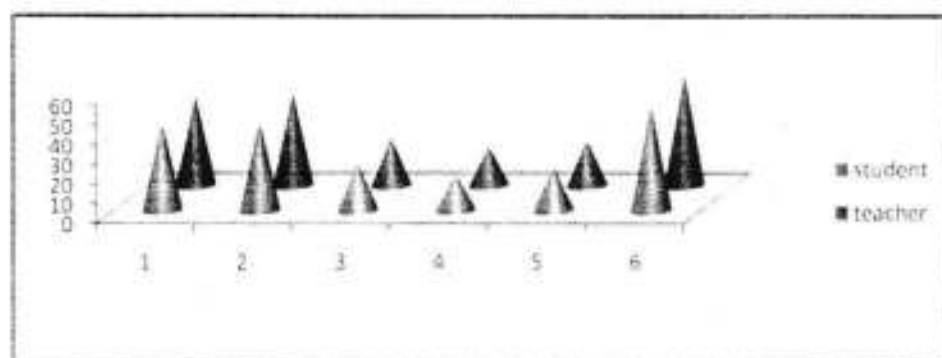| Student	teacher
45.8	45.7
46.86	47.7
24.8	24.44
19.36	20.12
22.67	23.56
55.02	57.18

Fig. 1: Means Score of Student & Teacher

CONCLUSION

The study concluded the following facts with reference to the first attribute i.e. "Reliability". These facts are as under:

The researcher concluded that, majority of the respondents i.e. "The Users of the Library", are able to find the reliable information to most of their queries in the reference of their collection and had not the experience of giving up a search due to finding difficulties in getting the relevant information. According to majority of the respondents, their university library is very consistent in making "Cataloging and Classifications" of their library materials, at the same time, the OPAC i.e. Online Public Access Catalogue in giving their required information is very reliable.

Majority of the respondents responded "Strongly Agree" on the "Accuracy" of the "Overdue and Fines" sent to them by their concerning library staff. Whenever they requested for any special service from their library, they got it "Very Consistently".

- Majority of the respondents are completely satisfied about the reliability in the references of "Inter – Library Loan Service", "CD-ROM/Database/Online Database Services", "Indexing and Abstracting Service", "Photo Copying Services" "Library Orientation Services" and "Information Literacy Programme"

- After applying the statistical tools i.e. Co-efficient of Co –relation, the researcher concluded that, there is positive co-relation between the opinions of teachers and students. At the same time, there is no significant difference between the mean score of teachers and students.

With reference to the second attribute i.e. "Responsiveness", the researcher concluded the following facts:

- Majority of the respondents got the latest and current published books in their subject area "very promptly i.e. within 3 minutes". Majority of them expected that, the books should be re-shelved within "Half – Day", as the inter library system in satisfying the information required by the users is

"Very effective". Majority of them are fully satisfied about the behaviour of the library staff while providing them OPAC service at the same time, they are highly satisfied about the availability of current newspapers and periodicals on the periodicals display shelves.

- Majority of the respondents are "Very Satisfied" about "Registration of User", "Duration of Books", "Compilation of reading list for users", "Prompt Bindery Services", "SDI Selection" and the "Answering user queries" provided to them by their library.

- After applying the statistical tools i.e. Co-efficient of Co- relation, in order to study, any similarity or discrepancy between the opinions of teachers and students with respect to scoring, the researcher concluded that, as for as score is concerned, no such conclusions can be drawn as the corresponding co-efficient of co-relation is very small. At the same time, there is no significant difference between the mean score of teachers and students.

With reference of the third attribute i.e. "Assurance", the researcher concluded the following facts

- The behaviour of the concerning library staff is very calm and co-operative while providing the relevant information from the collections, to the users. The library staff always take personal interest whenever any user approaches them for any requirement. Thus, majority of the respondents are very satisfied about the "quality based services" by their library at the same time, they are familiar with the CD ROM Database/Online Database system.

- After making applications of statistical tools, in order to study, any similarity or discrepancy between the opinions of teachers and students with respect to scoring, the researcher observed it that, for score 1 and 2 there is a negative co-efficient of co-relation and for the score 3 and 4 there is consistency (positive co-relation between the opinions of teachers and students). At the same time, there is no significant difference between the mean score of teachers and students.

In the reference of the fourth attribute i.e. "Access", the researcher concluded the following facts:

- The concerning library staff is "Always" available at the reference desk, photocopier machines available in sufficient quantity. The researcher further observed it that, majority of the respondents are not required to wait for using the computer terminal for accessing OPAC, Online Database, E-books, E- Journals, etc. at any time. Working hours of the library are convenient to the majority of the respondents, and they are not required to wait in the long queues at circulations counter.

- After making applications of statistical tools, in order to study, any similarity or discrepancy between the opinions of teachers and students with respect to scoring, the researcher observed it that, for score 1 there is a negative co efficient of co-relation (-0.5653), which indicates that, there is a difference between the opinions of teachers and students. For score 2 and 4 is concerned, no such conclusions can be drawn as the corresponding co-efficient of co-relation is very small and for the score 3 and 5 there is consistency (positive co-relation between the opinions of teachers and students). The researcher further observed it that, there is no significant difference between the mean score of teachers and students.

In the reference of the fifth attribute i.e. "Communication", the researcher concluded the following facts:

- Majority of the respondents are aware of the facilities and services available in the library and they learnt about its uses from the "Orientation of the Library". The researcher further observed that majority of the respondents got "OPAC user manuals", and "CD-ROM Database/ Online Database user manual" very easily and regularly. "E-learning modules available" are helpful to them to use library resources effectively and efficiently.

- After making applications of statistical tools, in order to study, any similarity or discrepancy between the opinions of teachers and students with respect to scoring. For score 1, there is a negative co-efficient of co-relation, i.e. there is a difference between the opinions of teachers and students. As for as score 2 and 5 is concerned, no such conclusions can be drawn as the corresponding co-efficient of co-relation is very small. For the score 3 and 4 there is consistency (positive co-relation between the opinions of teachers and students). The researcher further observed it that, there is no significant difference between the mean score of teachers and students.

In the reference of the sixth attribute i.e. "Tangible", the researcher concluded the following facts

- Majority of the respondents are "Very Satisfied" about the "Sitting Arrangements", "Maintenance of Lighting and Temperature in the Library", at the same time, all the staff members as well as the users have the cognizance to keep and maintain "Sufficient Silence" within the campus particularly in the library hall. The researcher further observed that majority of the respondents was satisfied towards the "Adequate and Comfortable Reading Rooms". At the same time, majority of them are satisfied about the various tangible facilities provided to them by their library. Thus, majority of them felt comfortable while using these facilities and services provided to them as per their requirements by their library.

- After making applications of statistical tools, in order to study, any similarity or discrepancy between the opinions of teachers and students with respect to scoring, For score 1, there is a negative co-efficient of co-relation, for score 2 is concerned, no such conclusions can be drawn as the corresponding co-efficient of co-relation is very small and for the score 3, 4 and 5 there is consistency (positive co-relation between the opinions of teachers and students). There is no significant difference between the mean score of teachers and students.

REFERENCES

1. Agarwal, J. N. (1954). Libraries in Ancient India. Delhi: Indian Librarian Association.

2. Bagade, S.D. (2000). Total Quality Management. Mumbai: Himalaya Publication.

3. Bhattachryya, D. (2006).). Research Methodology. New Delhi: Excel Books Publication.

4. Capezio, P. and Morehourse, D. (1995). Total Quality Management. New York: BBP Pub.

5. Dale, H. B. (2001). Total Quality Management. Delhi: Pearson Education Asia:

6. Deprospo, E. (1973). Performance Measures for public library. London: MCBUP Ltd.

7. Gun, A. M. (2005). Fundamentals of Statistics. Kolkata: World Press.

Synthesis and Characterization of Photoconductive CdS thin Semiconductor Film by Sillar Method

S.K. Karande*, F.C. Raghuwanshi**

*Vidnyan Mahavidyalaya, Malkapur Dist. Buldana,
**Principal, Department of Physics VidyaBharti Science college, Amravati

ABSTRACT : Glass substrate modified with ultrasonic cleaning were used to deposit CdS thin films in the process of successive ionic layer absorption and reaction [SILAR]. The films were characterized by X –ray diffraction, u. v. absorption ,and atomic force microscopy [AFM]. AFM showed that after ultrasonic cleaning substrate were in favor of the growth of films by comparison with the commercial glass slide. The deposition rate of the films was faster after the ultrasonification of glass substrate .

Key words : CdS ,thin films ,SILAR deposition

Introduction

CdS under thin film form is well known as an optoelectronic material for solar cell, photo detector and other optoelectronic devices [1-5]. Various chemical method have been used to grow CdS films, including electro deposition [6], chemical bath deposition [7,8] and SILAR deposing [9,10]. In comparison with other method, SILAR deposition has some advantages such as easy control, simple and less expensive. In the successive ionic layer absorption and reaction process the substrate are impressed into separated cationic and anionic precursor solution and rinsed with purified water after each immersion [11] many kinds of thin films have been prepared by SILAR technique [12]. However, because of weak interaction between ions and glass substrate, it is difficult to prepare the thin film on bare glass substrate. It is reported that the adhesion of the copper thin film to glass substrate was poor [13].

In this paper, we described how to improve interaction between ions and glass substrate. The glass substrate were modified with ultrasonification to anchor the cd^{2+} and s^{2-} ions to substrate. This work aimed to explore a way to improve the adhesion of the film to substrate. The structural and optical properties of CdS film were characterized.

Experimental:

The glass substrate were cleaned in boiling chromic acid for 1h, rinsed with double distilled water and dried in air .the glass substrate placed under the source of ultrasonic source of Radiology center. The treated glass substrate was first immersed into a 0.15 mol cadmium sulphate solution (pH-8) for 40s. The substrate was sufficiently rinsed with doubled distilled water for 25s. to remove superfluous cd^{2+} ions that interacted rather weakly with substrate. The substrate was then immersed into a 0.15 mol Thiourea solution (Ph -8) for 40s and rinsed with double distilled water for 25s. The temperature maintain at 75 0c with NH_3 complexing agent. The above deposition cycle were repeated to get desired film thickness.

The structural characterization of the film was carried out using XPERT-PRO X-ray diffractormeter with CuKa radiation (a = 1.5406 A') in 2θ range from 0 to 100'. The surface morphological study of CdS film was carried out by scanning electron microscopy using model JSM-7600F resolution 1 nm (15 KV). The optical absorption spectra of the film was recorded LAMBDA-25 (USA) spectrophotometer in the wavelength range 200 nm to 1100 nm. The grain morphology of thin

films was investigated using Atomic Force Microscopy (solver pro companies, model NT –MDT). It was operated in contact mode with the NS-01 cantilever.

RESULT AND DISCUSION

Utilizing ultrasonificated cleaned glass substrate cadmium ions were easily anchored to substrate. The pretreatment of the substrate accelerated the growth of CdS film. The substrate after formation of CdS film look like a yellow mirror. It can be concluded that average growth rates of CdS film were 0.30 nm/cycle on the modified substrate and 0.030 nm/cycle on the unmodified substrate as compare with growth rate reported for CdS film is 0.098 nm/cycle.[10]
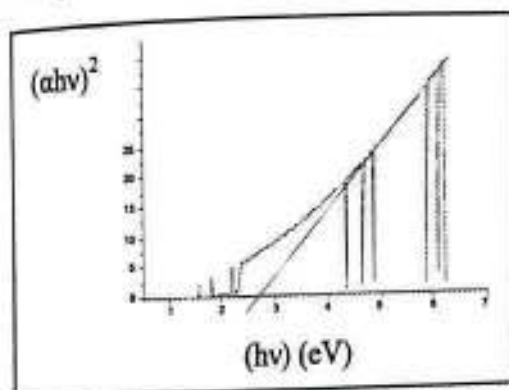

Figure 1: Plot shows the variation of $(ahv)^2$ verses (hv) of as deposited CdS thin film.

Figure 1 shows the spectra of the film were typical for those reported by many workers for polycrystalline CdS thin film. The band gap of the film were found to be 2.37 eV as compare with 2.4 eV.[8] The linear dependence of ahv^2 verses hv was indicative of direct band gap material.
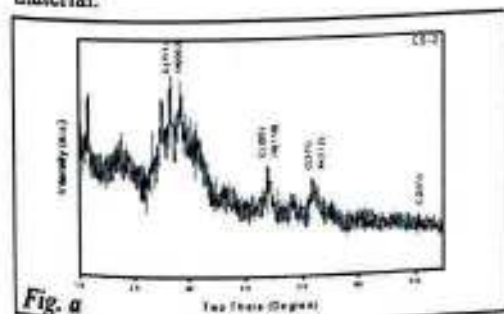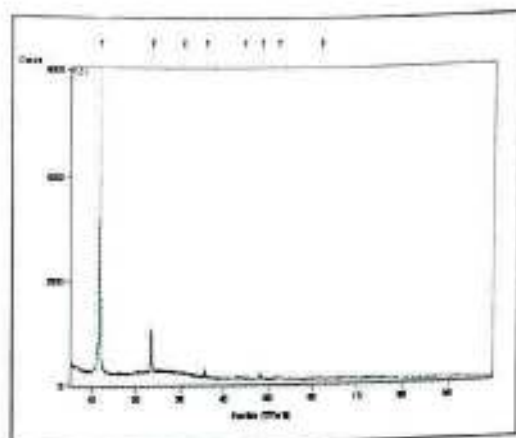

Fig. a

Fig. b

Figure 2 : X-ray diffraction pattern of CdS thin film with 27 cycles
a. Ultrasonified glass substrate
b. An un ultrasonified glass substrate

Figure 2 shows the x-ray diffraction pattern of CdS thin film. It was known that the CdS film on substrate without ultrasonification was amorphous while the film on the ultrasonified glass substrate was of both cubic an hexagonal crystal structure. The major peaks found for these two sets indicate the presence of both cubic and hexagonal phases. The peak of maximum broadening centered at 26.7 degree is suggestive of combination of many peaks including the dominant c(1 1 1)/h(0 0 2) at 26.6 degree.[14] Presence of CdO phase here is most likely in nano-CdS as it is very prone to oxidation when exposed to air. Also there are two characteristic peaks at 44.0 degree and 52.1 degree. A sharper peak at 44.0 degree also indicates either c(2 2 0)/h(1 1 0). Another peak of relatively large broadening at 51.8 degree can be associated with c(3 1 1) or h(1 1 2). However, a small intensity peak at 70.6 degree bears the signature of c(3 3 1)which is characteristic of cubic phase. The grain size is found to be 36 nm. JCPDF (80-0006 and 75-0581).

Figure 3 and Figure 4 shows the AFM images of CdS thin film on glass substrate. It can be seen from figure 3 that only some particles of microsize of CdS sparsely spread on the un
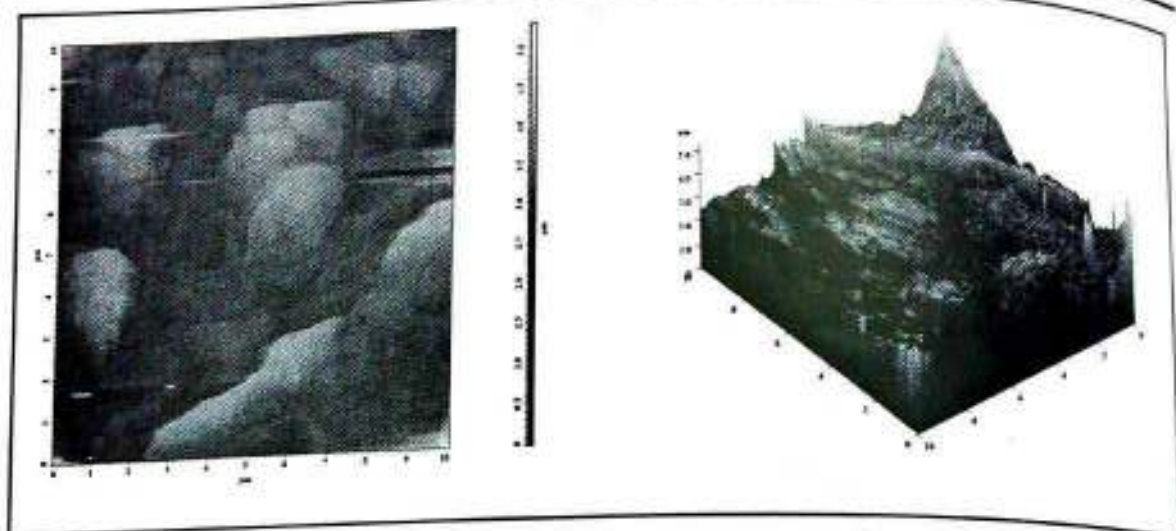
Figure 3: AFM image of CdS film with 150 cycles on un ultrasonificated glass substrate
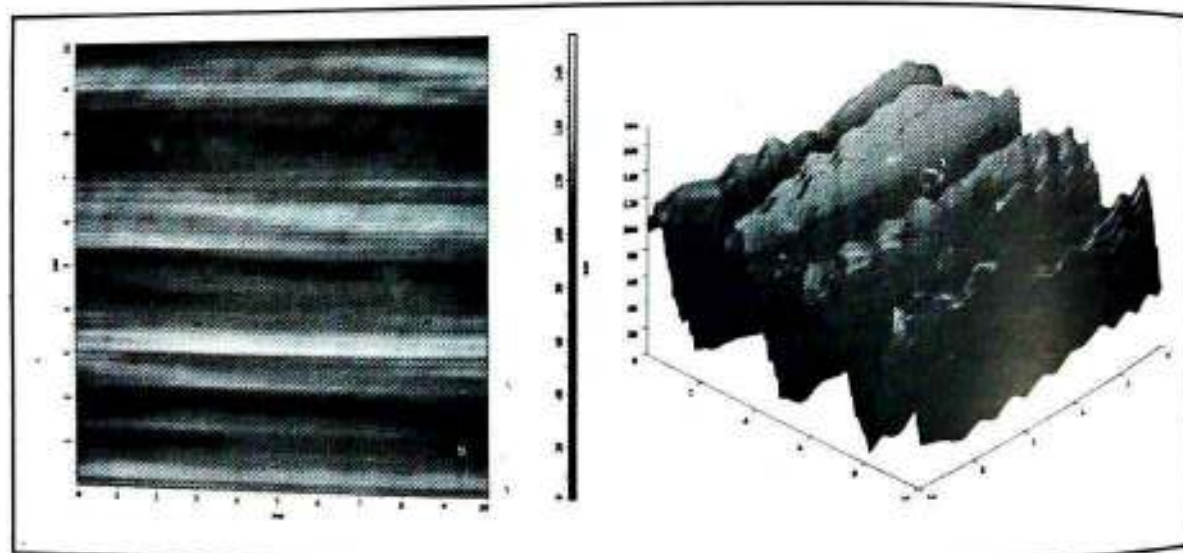

Figure 4 : AFM image of CdS film with 150 cycles on ultrasonificated glass substrate

ultrsonificated substrate however the dense of nanoparticle size film of CdS grew on the ultrasonificated substrate as shown in figure 4.

Conclusion :

The CdS film were successfully deposited on glass substrate treated with altrasonification. Such type of substrate was beneficial to the growth of nanostructure films during SILAR process. The experimental result confirms that the ultrasonification of the glass substrate was necessary for the growth of uniform and dense film of wide band gap II–VI semiconductors.

AKNOWLEDGEMENT

References:
[1] S. Ferekides, D. Marinsky, V. Viswanathan, B. Tetaly, V. Palekis, P. Selvaraj, D.L. Morel, *Thin Solid Films* 361-362,(2000) 520.

[2] M. Kobayashi, K. Kitamura, H. Umeya, A. W. Jia, A. Yoshikawa, M. Shimotomai, Y. Kato, K. Takahashi, *J. Vac. Sci. Technol* B 18 (2000) 1684.

[3] A. I. Oliva, O. Solis-Canto, R. Castro-Rod riguez, and Quintana, *Thin Solid Films* 391 (2001) 28.

[4] I. K. Battisha, H. H. Afify, G. Abd El Fattah, Y. Badr, *Fizika A 11* (2002) 31.

[5] Ph. Hoffmann, K. Horn, A.M. Bradshaw, R.L. Johson, D. Fuchs, M. Cardona, *Phys. Rev. B47* (1993) 1639.

[6] Kampmann, A., Lincot, D. (1996). J. Electroanal. Chem., 418:73–81.

[7] Lee, J.H., Yi, J.S., Yang, K.J., Park, J.H., and Oh, R.D. (2003) Thin Solid Films,431–432: 344–348.

[8] Ramaiah, K.S., Pilkington, R.D., Hill,A.E., Tomlinson, R.D.,Bhatnagar, A.K. (2001) Mater. Chem.Phys., 68: 22–30.

[9] Lokhande, C.D., Sankapal, B.R., Pathan, H.M., Muller, M.,Giersig, M., Tributsch, H. (2001). Appl. Surf. Sci., 181:277–282.

[10] Laukaitis, G., Lindroos, S., Tamulevicius, S., Leskela˝, M. (2001) Appl. Surf. Sci., 185:134–139.

[11] Nicolau, Y.F. (1985). Appl. Surf. Sci., 22–23: 1061–1074.

[12] Pathan, H.M., Salunkhe, P.V., Sankapal, B.R., Lokhande, C.D. (2001) Mater. Chem. Phys., 72: 105–108.

[13] Lindroos, S., Ruuskanen, T., Ritala, M., Leskela˝, M. (2004). Thin Solid Films, 460: 36–40.

[14] Sankapal, B.R., Mane, R.S., Lokhande, C.D. (2000) Mater. Res. Bull., 35: 177–184.

Synthesis and ammonia sensing properties of Bi_2O_3 nanoparticles

S. D. Kapse [*], F.C. Raghuwanshi [b], V. D. Kapse [c]

[*]Department of Physics, G.S. College, Khamgaon- 444303, Maharashtra State, India
[b]P.G. Department of Physics, Vidyabharati Mahavidyalaya, Amravati- 444602, Maharashtra State, India
[c]Department of Physics, Arts, Science and Commerce College, Chikhaldara- 444807, Maharashtra State, India

Abstract : Bismuth oxide (Bi_2O_3) nanoparticles were prepared by ethylene glycol mediated citrate sol-gel method followed by calcination at 600 °C for 4 h. The structure and crystal phase of the powders were characterized by X-ray diffraction (XRD) and microstructure by transmission electron microscopy (TEM). The responses of Bi_2O thick film to various reducing gases (hydrogen, hydrogen sulfide, ammonia and liquefied petroleum gas) were measured as function of operating temperature. The sensor element based on Bi_2O nanoparticles exhibited good response to 500 ppm NH_3 as compared with other tested reducing gases.

Keywords: Nanoparticles; Bi_2O_3; Reducing gases; Doping

1. Introduction

Gas sensors play vital role in detecting, monitoring and controlling the presence of hazardous and poisonous gases in the environment at very low concentrations. It is well known that the gas adsorption onto the semiconductor surface can influence its electrical conductivity. Actually, conductivity of semiconductor gas sensor changes by few orders of magnitude with regard to initial value in the presence of gas concentrations up to few ppm in air at ambient pressure. Metal oxides such as ZnO, SnO_2, In_2O_3, and WO_3 are extensively used as sensing materials in industry, such as environmental monitoring, security systems, biomedical instruments, and healthcare systems [1-5] The general sensing mechanism of these sensors is based on the change in the resistance of the functional sensing elements when they are expose to different environments such as different gases, humidity, and light.

Bismuth oxide (Bi_2O_3) has been extensively studied due to its useful features,

such as noteworthy energy band gap (2.85 and 2.58 eV for the monoclinic α- Bi_2O_3 and tetragonal β- Bi_2O_3 phases, respectively), high refractive index and high dielectric permittivity, as well as marked photoconductivity [6-8]. Consequently, it has a feasibility of practical applications, including optical coatings [9], microelectronics [10], ceramic glass manufacturing [11], and gas sensor technology [12-18]. In combination with other typically used metal oxide Bi_2O_3 was useful as sensitive materials for detecting CO, H_2, and NO gas, respectively [7-9]. In the present investigation, structural and gas sensing properties of Bi_2O_3 nanoparticles prepared by ethylene glycol mediated citrate sol-gel method were investigated.

2. Experimental

2.1. Synthesis of Bi_2O nanoparticles

Appropriate quantity of bismuth nitrate [Bi $(NO_3)_3 \cdot H_2O$] was grounded for 30 min. in an agate mortar pestle and then were dissolved in distilled water and then adding them to the warm solution of citric acid

monohydrate [C₆H₈O₇.H₂O] / Ethylene glycol. The resultant solution was stirred magnetically at 80 °C for 2 h to get homogeneous mixture. Then, this solution was subsequently transferred to Teflon lined stainless steel autoclave. The temperature of the autoclave was raised slowly to 125 °C and maintained for 12 hours to get gel precursor. Thereafter, the autoclave was allowed to cool naturally to room temperature and the resulting product further heated for 3 hours at 350 °C and subsequently calcined for 4 h at 600 °C to improve the crystallinity of the prepared materials.

2.2. Material characterization and gas sensing measurements

The phase constitution of as-prepared In_2O_3 powder was analyzed by X-ray diffractometer (Model: Philips X'pert) with a Cu Kα radiation (λ = 1.5406Å). The single phase was confirmed by comparison with JCPDS database. The average crystallite size (D) was calculated according to the Debye-Scherrer equation. The morphologies of the synthesized powder were observed through a transmission electron microscopy (TEM) (Model: Philips CM 200).

The sensing performance of the fabricated sensor elements was tested using a 'static gas-sensing system'. The description of the sensor element fabrication, schematic sensor assembly and the circuitry for the sensor characteristics measurement was reported in our earlier publication [30]. Sensor response (S) is defined as the ratio of change in conductance of the sensor on exposure to the target gas to the original conductance in air medium. The relation for S is as: $S = [G_g - G_a]/G_a$

where G_a and G_g are the conductance of a sensor in air and in gaseous medium, respectively.

3. Results and discussion

The X-ray diffraction pattern of Bi_2O_3 powder sample is illustrated in Fig. 1. The XRD pattern of as-prepared sample readily indexed Bi_2O_3 with monoclinic structure. The average crystallite size of the prepared Bi_2O_3

nanoparticles determined to be 35 nm from the XRD patterns. The average crystallite size estimated from XRD data corroborates with the TEM investigations. The TEM image of Bi_2O_3 powder calcinated at 600 °C is provided in Fig. 2. The significant amount of agglomeration was observed in the micrographs.
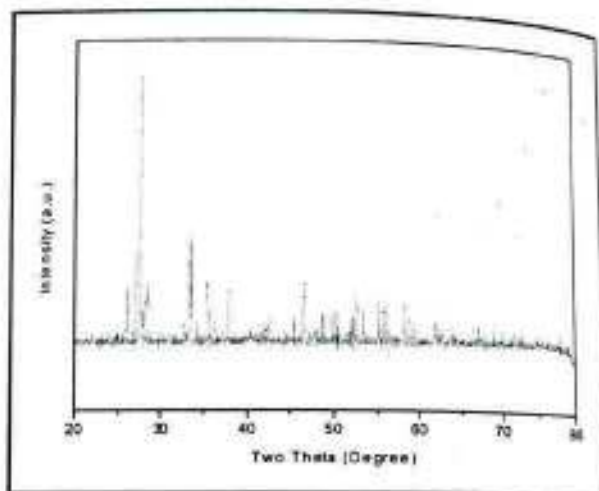

Fig. 1: X-ray diffraction pattern of Bi_2O_3 powder calcinated at 600 °C.

Fig. 2: TEM image of Bi_2O_3 calcinated at 600 °C.

The response of Bi_2O_3 towards various gases like hydrogen (H_2), hydrogen sulfide (H_2S), ammonia (NH_3) and liquefied petroleum gas (LPG) as a function of operating temperature is presented in Fig. 3. From the

figure it can be seen that the sensor element exhibited the superior response to 500 ppm NH_3 at 340 °C as compared to other tested reducing gases. The response of a semiconductor metal oxide based gas sensor to a particular gas depends on the speed of the chemical reaction on the surface of the grains and the speed of diffusion of the gas molecules into the surface. The conductance of the sample Bi_2O_3 in ammonia was obviously lower than that in air, indicating the p-type semiconducting properties of the samples. The result also demonstrates that Bi_2O_3 exhibited good selectivity towards 500 ppm NH_3. The stability of the sensor elements was also measured by repeating the tests up to the period of 90 days, at an interval of 10 days, from first measurement. During the tests, no considerable variations were observed indicating the good stability of the sensor.
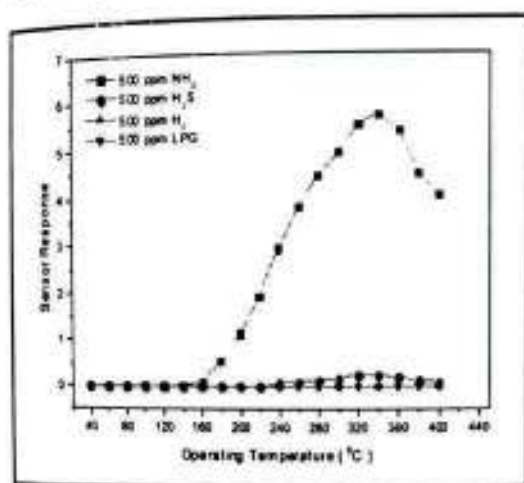

Fig. 3. Sensor response of pure Bi_2O_3 towards different reducing gases as a function of operating temperature

4. Conclusions

Bismuth oxide (Bi_2O_3) nanoparticles were successfully prepared by ethylene glycol mediated citrate sol-gel method followed by calcination at 600 °C for 4 h. The sensors based on Bi_2O_3 nanoparticles exhibited fair response to 500 ppm NH_3 gas as compared with other tested gases.

6. References

[1] Ansari, S. G.; Boroojerdian, P.; Sainkar, S. R.; Karekar, R. N.; Aiyer, R. C.; Kulkarni, S. K. Thin Solid Film 1997, 295, 271–276.

[2] Nayral, C.; Ould-Ely, T.; Maisonnat, A.; Chaudret, B.; Fau, P.;Lescouzeres, L.; Peyre-Lavigne, A. AdV. Mater. 1999, 11, 61–63.

[3] Martins, R.; Fortunato, E.; Nunes, P.; Ferreira, I.; Marques, A.; Bender, M.; Katsarakis, N.; Cimalla, V.; Kiriakidis, G. J. Appl. Phys. 1996, 96, 1398.

[4] Solis, J. L.; Heel, A.; Kish, L. B.; Granqvist, C. G.; Saukko, S.; Lantto, V. J. Am. Ceram. Soc. 2001, 84, 1504–1508.

[5] Gurlo, A.; Ivanovskaya, M.; Barsan, N.; Schweizer-Berberich, M.; Weimar, U.; Gopel, W.; Dieguez, A. Sens. Actuators, B 1997, 44, 327–333.

[6] H. Gobrecht, S. Seeck, H.E. Bergt, A. Martens, K. Kossmann, Phys. Status Solidi (b) 33 (1969) 599–606.

[7] V. Dolocan, F. Iova, Phys. Status Solidi (a) 64 (1981) 755–759.

[8] L. Leonite, M. Caraman, M. Alexe, C. Harnagea, Surf. Sci. 507–510 (2002) 480–485.

[9] M. Schuisky, A. H"arsta, Chem. Vap. Deposit. 2 (1996) 235–238.

[10] G. Bandoli, D. Barecca, E. Brescacin, G.A. Rizzi, E. Tondello, Chem. Vap. Deposit. 2 (1996) 238–242.

[11] A. Pan, A. Ghosh, J. Non-Cryst. Solids 271 (2000) 157–161.

[12] G.S. Devi, S.V. Manorama, V.J. Rao, Sens. Actuators B 56 (1999) 98–105.

[13] T. Hyodo, E. Kanazawa, Y. Takao, Y. Shimizu, M. Egashira, Electrochemistry 68 (2000) 24.

[14] A.A. Tomchenko, Sens. Actuators B 68 (2000) 48–52.

[15] E.L. Shoemaker, C.-U. Kim, M.C. Vogt, Sens. Actuators B 110 (2005) 89–100.

[16] A. Cabot, A. Marsal, J. Arbiol, J.R. Morante, Sens. Actuators B 99 (2004) 74–89. [17] G. Sakai, T. Jinkawa, N. Miura, M. Yamazoe, Transducers'99, Sendai, Japan, 1999, pp. 146–149.

Preparation techniques and applications of spinel ferrite nanoparticle: An overview

T.R.Tatte [a], V.D. Kapse [b], F.C. Raghuwanshi [c]

[a] Department of Physics, Government Vidarbha Institute of Science & Humanities, Amravati 444604, Maharashtra State, India
[b] Department of Physics, Arts, Science and Commerce College, Chikhaldara 444807, Maharashtra State, India
[c] Department of Physics, Vidyabharati Mahavidyalaya, Amravati 444602, Maharashtra State, India

Abstract : Nanostructured spinel ferrites are of *great interest for a wide variety of applications* like high density magnetic information storage, magnetic resonance imaging, targeted drug delivery, high density recording media etc. Spinel *ferrite nanomaterials are gaining importance due to its broad applications.* In order to meet the demands one must try to novel materials processing methods. This paper deals with the survey of the concept of ferrite nanoparticles, processing methods and application explored in gas sensing. Spinel ferrite powders can be fabricated by various methods such as hydrothermal method, sol-gel method, chemical co-precipitation method, citrate precursor method, combustion method, solid state high temperature reactions etc. In this article, various synthesis routes for the preparation of spinel ferrite nanomaterials and recent applications of nanostructured spinel ferrite have been discussed.

Key words: Spinel, Ferrites, Processing Methods, Nanoparticle

1. Introduction

Ferrites are one of the most significant materials giving useful magnetic, electrical, chemical, mechanical and structural properties [1-5]. These ferrites are classified as hard and soft on the basis of magnetic properties. Hard ferrites have properties such as high coercivity and high remanence after magnetization. eg. Permanent ferrite magnet and soft ferrites having properties like low coercivity. For this reason the magnetisation of the materials can reverse the direction easily without dissipating much energy. eg. Transformer, electromagnetic cores. Under soft ferrite there is a type of material called spinel ferrite which crystallizes in spinel structure, which is named after the mineral spinel, $MgAl_2O_4$. The unit cell of spinel corresponds to the space group O_h^7 (F3dm). The spinel crystaliline structure is determined firstly by the oxygen ion lattice and this oxygen anions are packed in a face centered cubic lattice. Metallic cations, magnetic and nonmagnetic, reside on the interstices of the close-packed oxygen lattice. Moreover, in the spinel structure these cations have four- or six-fold coordination and form tetrahedra (A) and octahedra (B) sub-lattices and then they are arranged in a close-packed arrangement.

Spinel ferrites in general have the chemical formulae MFe_2O_4 (molecular precursors, concentration, temperature and growth rate, types of surfactant and solvent. Spinel ferrite is again classified into two types such as normal spinel and inverse spinel. In normal spinel ferrite, M^{2+} cations occupy tetrahedral sites and Fe^{3+} cations occupy octahedral sites. eg. $ZnFe_2O_4$ & $CdFe_2O_4$. In *inverse* spinel ferrite, half cations occupy sites as Fe^{3+} in tetrahedral sites and remaining Fe^{3+} and all of M^{2+} cations occupy octahedral sites. eg.

$NiFe_2O_4$ and $CoFe_2O_4$.

The spinel ferrites are modified for its various applications by changing their physical and chemical properties. Spinel ferrites in general have the chemical formulae MFe_2O_4 (M = Mn, Fe, Co, Ni, Cu, Mg, Zn, etc.). The size and shape of spinel ferrite nanomaterial can be controlled by manipulating reaction variables such as properties is manipulated by changing the synthesis method, processing temperature and also substitution [6-8]. Nanoparticles of spinel ferrites are of growing interest for a wide range of applications like high density magnetic information storage, magnetic resonance imaging, targeted drug delivery etc. They also offer immense possibilities of tailoring its various properties for applications [9,10]. The review gives some general processing method and applications on spinel ferrite nanomaterial which is found to be useful due to their electronic, optical, electrical, magnetic and catalytic properties.

2. Preparation method of Ferrites

Ferrites are fabricated by using various methods. Some few methods such as sol-gel method [11,12], chemical co-precipitation [13], propagating high temperature synthesis (SHS) technique [14], citrate precursor method [15] etc. have been discussed.

2.1 Sol-Gel Method

The sol-gel process involves the transition of a solution of metal compounds from a liquid sol into a solid gel. In liquid, sol is a diffusion of the solid particles where only the Brownian motions suspend the particles and this sol is heated and then to form a homogenous gel which can achieved by the addition of base or acidic solutions. A gel is intermediate where both liquid and solid are dispersed in each other, which presents a solid network containing liquid components. Usually inorganic metal salts or metal organic compounds such as metal alkoxides are used as starting precursors in the preparation of the sol. The purpose of this precursor is to a series of hydrolysis and polymerization reactions to form a colloidal suspension, or a sol. By elimination of water, the hydroxide molecules get condensed and then formation of a metal hydroxide. When all metal hydroxides species are linked to one another in a network, and formation of dense porous gel is obtained. Further heating at higher temperature and then drying of the gel, the gel is converted into ultrafine powders of metal oxides.

2.2. Chemical Co-Precipitation

In the chemical co-precipitation method, an aqueous solution of suitable salts of iron, lithium, manganese and other desired, suitable materials is mixed under a fine control of pH by using a precipitating agent like NaOH or NH_4OH solutions which causes the precipitation of the other metals present in the solution. The precipitate represents a significantly uniform mixture of organic compounds of the ferrite metals on an atomic scale. In case of ferrite, it is important to prevent agglomeration; Ostwald ripening etc. Filtrated the precipitate and then dried. Then dried precipitate is heated at an high temperature to dehydrate the precipitate and to burn out carbonaceous matter leaving a residue of the oxides of the respective metals. After this, particles are sintered. The reaction and transport rates can be affected by the concentration of reactants, temperature, pH, the order in which the reagents are added to the solution and mixing. The particle structure and crystallinity can be influenced by reaction rates and impurities. This method doesn't work very well in cases where two reactants have very different solubilities in water and the reactants do not precipitate at the same rate. This method offers distinct advantages like simple, rapid preparation, easy control of particle size and composition.

2.3. Self Propagating High Temperature Synthesis Technique

In this method, organic acid is taken as precursur in aqueous solution. This solution containing all necessary cations and combustible anions in the desired product. After dehydration, the precursor becomes dry gel and this dry gel is amorphous in nature. Moreover, when calcinating this dry gel directly yields the required materials in presence of air/oxygen. In case of this process, the starting

materials are mixed in the atomic scale. The phase formation occurs at lower calcination temperature as compared to ceramic route and giving ultrafine powder. The overall process completes within 5 minutes.

2.4. Citrate Precursor Method

In this method, the starting materials such as nitrates are complexed in an aqueous solution with α–carboxylic acids such as citric acid. By adding ammonium hydroxide to the solution, the pH is controlled at 7. The solution is refluxed with continuous stirring using magnetic bar agitator and then dried. By the evaporation of the solution, a highly viscous mass is formed and resulting from metal nitrates and citric acid making a redox reaction to occur and then this metal nitrates react with water. The chelating agent citric acid is used for deprotonating with ammonium hydroxide and the metal hydroxide by removing protons. Then the formation of metal ions having a positive valency and carboxylic ions with negative valency together with water molecules. This co-ordinate bonds are used to form the metal and acid complex which is the ash-synthesized powder obtained. At last point auto-combustion process takes place. The powder is pressed into pellets and then given final sintering for densification.

3. Applications

There are various forms of application depending on the type like biomedical applications, permanent magnets, magnetic fluids, magnetic drug delivery, and high density recording media etc. Ferrites are primarily used for practical applications like sensor, power applications, EMI suppression, magnetic components, phase shifters, microwave devices etc. The application of ferrites like power are dominated by the power supplies for a large variety of devices such as TV, computers and video systems, and all types of small and medium instruments. A recent approach to increase efficiency of the ferrite cores is based on the decrease of eddy currents, by increasing resistivity and these ferrite cores are used for flyback transformers in television sets. This is to a great extent increase the energy received by a

receiving antenna. Since ferrites have high permeability, also make them suitable for filter inductor applications. Ferrites are mostly used in cores for magnetic memories [16,17]. Since, there is increasing interest in the amount of electronic equipment such as high-speed digital interfaces in notebooks and computers, digital cameras, scanners, and so forth, in small areas, has seriously enhanced the possibility of disturbing each other by electromagnetic interference (EMI). Hexaferrites can also be replaced by cubic ferrites as EMI suppressor components; they possess higher resonance frequencies, relatively high permeabilities (at microwave frequencies), and high electrical resistivities. The broad range of applications of nanostructured ferrite includes high density information storage, ferrofluid technology, magnetic resonance imaging enhancement, magnetically guided drug delivery and magnetocaloric refrigeration [18-21]. By using the combination of ferrite nanoparticles as contrast enhancement agents, harmless radio waves and computer technology, magnetic resonance imaging creates detailed images of the soft tissue morphology. Nanopowdered ferrites can also used for the design of magnetic storage and recording devices. Ferrofluids which is more stable colloidal suspensions composed of magnetic nanoparticles in organic or inorganic liquid carriers. The biocompatible ferrofluids which is based on ferrites are most promising for biomedical applications like cell separation and purification and magneto hyperthermia of tumour cells. Large number of biocompatible fluids are based on magnetitie and maghemite. Zinc ferrite nanoparticles gives enomorous potential applications in gas sensor and semiconductor photocatalysis [22, 23].

4. Conclusions

There is renewed interest in nanostructured spinel ferrite materials since many of the exhibit remarkable electrical and magnetic properties of these materials can be modified suitably and promising technological applications in different fields of life. There are various synthesis routes to prepare nanoparticles spinel ferrite. There are various

processing methods have been summarized for important ferrite systems along with some applications. The structural, magnetic, electrical and mechanical properties of spinel ferrites are found to be sensitive to their composition and microstructure, which in turn are dependent on the processing conditions.

References:

[1] L. Zhao, H. Yang, L. Yu, Y. Cui, X. Zhao, S. Feng, 305 (2006) 91.

[2] S.E. Jacobo, S. Duhalde, H.R. Bertorello, J. Magn. Magn. Mater., 272–276 (2004) 2253.

[3] D. Ravinder, B. Ravi Kumar, Mater. Lett., 57 (2003) 4471.

[4] M.H. Mahmoud, A.A. Sattar, J.Magn.Magn. Mater.,277 (2004)101.

[5] M.A. Ahmed, E. Ateia, S.I. El-Dek, Mater. Lett., 57 (2003) 4256.

[6] B.K. Kuanr, P. Kishan, N. Kumar, S.L.N. Rao, P.K. Singh and G.P. Srivastava, J.Appl. Phys, 8 (1986) 63.

[7] H.B Im, D.G Wickham, IEEE Trans.on magn., 8 (1972) 765.

[8] Z. Yue, Ji Zhou, X. Wang, Z. Gui and L. Li, J. European Cera. Soci., 23 189 (2003).

[9] R.D. McMichael, R.D. ShuU, L.J. Swartzendruber and L.H. Bennett, J. Magn. Magn. Mater., III (1992) 29.

[10] D.G. MitcheU, J. Magn. Reson. Imaging, 7 (1997) 1.

[11] J. Azadmanjiri , S.A. Seyyed Ebrahimi, H.K. Salehani, Ceramic International,1623–1625 (2007) 33.

[12] J. G. Lee, H. M. Lee, C. S. Kim, and Y. J. Oh, J. Magn. Magn. Mater., 900-902 (1998) 177.

[13] K. Maaz, A. Mumtaz, S. K. Hasanain, and A. Ceylan, J. Magn. Mater., 289-295 (2007)308.

[14] W.B. Cross, L. Affleck, M.V. Kuznetsov, et al. , J. Mater. Chem., 9 (1999) 2545.

[15] Ibetombi. Soibam ,S.Phanjoubam ,C.Prakash, J.Alloys Compd.,328-331 (2009)475.

[16] T. Nakamura, E. Hankui, J. Magn. Magn. Mater., 257 (2003) 158.

[17] S.A. Ghodake, U.R. Ghodake, S.R. Sawant, S.S. Suryavanshi and P.P. Bakare, 1. Magn. Magn. Mater., 305 (2006) 110.

[18] R.H. Kodama, A.E. Berkowitz, EJ. McNiff Jr. and S. Foner, Phys. Rev. Lett., 77 (1996) 394.

[19] S. Sun, C. B. Murray, D. Well er, L. Folks, A. Moser, Sci., 287 (2000) 1989.

[20] Q. A. Pankhurst, J. Connolly, S. K. Jones, J. Dobson, J.Physics D: Appl Phy. 36, (2003),RI67.

[21] M. H. Kryder, MRS Bull., 21 (1996) 17.

[22] C.C. Berry, A.S.G. Curtis, J. Phys. D :Appl. Phys.,36 (2003), R198.

[23] S. Gubbala, H. Nathani, K. Koizol and R.D.K. Misra, Physica B, 348 (2004) 317.

Miscibility studies of PVC/PMMA blends by FTIR analysis and measurements of AC electrical conductivity of PVC/PMMA blends.

A.B. Dakre[1*] , G.T.Lamdhade[1] , F.C. Raghuwanshi[2].

[1] Dept. of Physics, P.R. Pote (Patil) College of Engineering and Management, Amravati, M.S. 444602 India
[2]Dept. of Physics, Vidyabharati Mahavidyalaya, Camp, Amravati, M.S. 444602 India

E-mail: archana.dakre@rediffmail.com

Abstract : The polymer electrolytes composing of the blend of polyvinyl chloride–polymethyl methacrylate (PVC/PMMA) with oxalic acid as a dopant were prepared by isothermal evaporation technique. FTIR studies confirm the complexation between PVC/PMMA blends. The miscibility between PVC & PMMA is due to a specific interaction of hydrogen bonding type between carbonyl groups (C =O) of PMMA and hydrogen from (CHCl) groups of PVC, as evidenced by FTIR spectroscopy. AC electrical conductivity of PVC/PMMA blends was measured in the temperature range 303-363K. It is found that ac conductivity of thin film decreases with increase in temperature for all values of frequencies and it increases with increase in frequencies at constant temperature.
Keywords: PVC, PMMA, FTIR, Miscibility, AC conductivity

1. Introduction:

In recent years, studies on the electrical and optical properties of polymers have attracted much attention in view of their applications in electronic and optical devices [1, 2]. Blending of two or more polymers may generate new materials with a combination of properties not found in the pure polymers.

Blending is often a faster and more cost effective way of achieving the required properties than synthesizing new polymers. A blend of two components is classified [3] miscible, thermodynamically, if the Gibbs free energy of mixing is less than zero and the second derivative of the Gibbs free energy of mixing is zero or positive. Among the polymer electrolytes, PMMA-based electrolyte has special significance in view of its well-known chemistry and cheaper method of processing as laminates. To get PMMA amenable, choice of blending with PVC has been suggested [4].

Although there are many ,those containing PVC are among the most important from both scientific and commercial point of views [5, 6]. A relatively small number of studies have been reported on the development of PVC/PMMA-based polymer electrolyte systems [7–9].

Electrical and optical properties of the polymers can be suitably modified by the addition of dopant depending on their reactivity with the host matrix. It has been shown that carrier mobility can be greatly affected by impregnating the polymers with suitable dopants. The charge storage property of polymers can be considerably modified with the help of suitable dopants.

The present work aims to calculate the electrical conductivity of pure PVC, PMMA, blends & oxalic acid doped samples. The miscibility of PVC-PMMA is investigated by FTIR spectra. Polymer composite based on

charge transfer complex of PVC-PMMA with Oxalic Acid prepared in different weight ratios.

2. Experimental details:

The polymers PMMA (Otto Chemical, Mumbai) and PVC (Commercial Grade) in weight ratio were dissolved in 20ml solvent cyclohexanone (SD Fine Chemicals, Mumbai). For complete dissolution solution was kept in a stand for 3 days. After 3 days, the solution mixture was poured on perfectly plane and optically clean glass plate kept floating freely in a pool of mercury for perfect leveling. It was, thereafter, allowed to evaporate in air at room temperature. Further, it was dried for 48 hrs to remove any traces of solvent. The dry film was removed from the plate and cut into pieces (samples) of desired size, which were then coated on both sides with silver paint (Eltecks Corporation, Bangalore). The films of PVC-PMMA doped with 5%, 10% Oxalic acid were prepared by the same method given above. The thickness of the film was measured by DIGMATIC micrometer (Mitutoyo Corporation, Japan).

2.1. AC Electrical Conductivity :

The film was kept between the electrodes of a specially designed sample holder. The AC frequencies were applied (in the range 1 KHz –1 MHz) across the sample by using the 4284 A precision LCR meter (20 Hz –1 MHz) (Agilent Technologies, Singapore). The Corresponding dielectric constants were measured and AC conductivity of the samples was calculated by using the following relation given by equation 2.1 [10-12].

$$\sigma_{ac} = \frac{f \times \epsilon^{l} \times \tan\delta}{1.8 \times 10^{10}} \qquad (1)$$

Where, f = Frequency applied in Hz
  ϵ^{l} = Dielectric Constant at frequency f
  $\tan\delta$ = Dielectric loss tangent.

2.2. Fourier Transform Infrared Spectroscopy (FTIR) :

The freshly prepared samples are subjected to Fourier Transform Infrared Spectroscopy (FTIR) in the wave region between 4000-500cm^{-1}. The resolution of the spectra obtained at room temperature was 4 cm^{-1}. The FTIR data obtained were recorded in the transmission mode.

3.Results and Discussion:

3.1.Effect of Frequency on AC Conductivity:

The observed variation of AC electrical conductivity of pure PVC, pure PMMA and PVC–PMMA blend samples & PVC–PMMA doped samples, with frequency in the temperature range 313-363K is illustrated in figure (3.1.a,b,c.d,e). In all the samples it is found that A.C. conductivity increase with the frequency. The increasing of AC electrical conductivity in high frequency region can be related to the electronic polarization as well as to the hopping of charge carrier over a small barrier height [14]. The increasing of A.C electrical conductivity with angular frequency in the low frequency region can be attributed to the interfacial polarization [15].

At higher frequency, the mobility of charge carriers is higher and eventually contributes to higher electronic conductivity with respect to frequency [16]. It is due to the tremendous increase of the mobility of charge carriers in the composite film i.e. at higher frequencies blends of molecules starts vibrating with large amplitude within the polymeric chains hence the effect of increase in conductivity of blends[17].
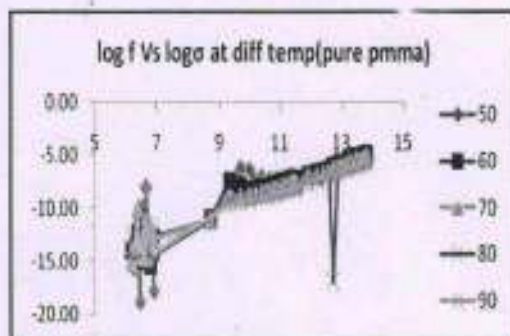

Fig.3.1. a
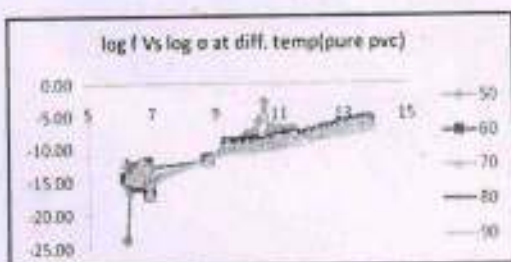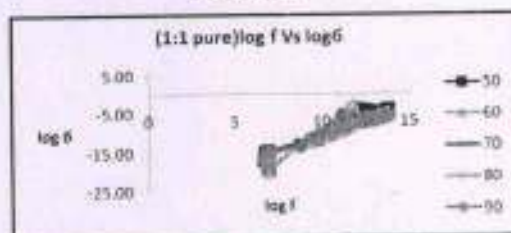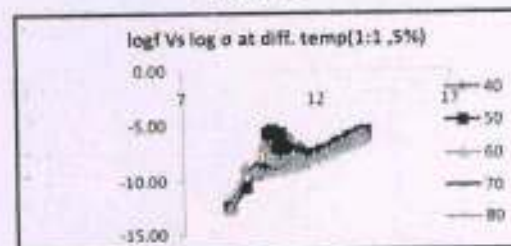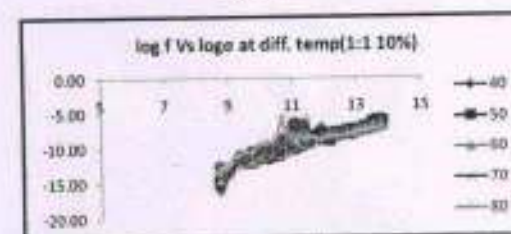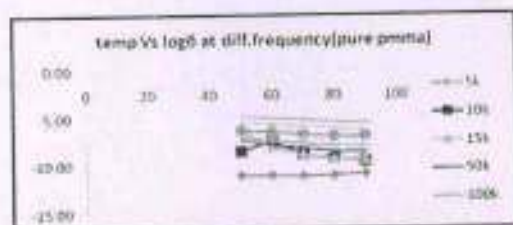
Fig.3.1. b

Fig.3.1. c

Fig.3.1. d

Fig.3.1. e

Fig.3.2 a

Fig.3.2 b

Fig.3.2 c

Fig.3.2 d

Fig.3.2 e

3.2. Effect of Temprature on A.C. Conductivity:

The following fig(.3.2a,b,c,d,e) shows the variation of electrical conductivity in the polymer blend (PVC-PMMA) with temprature in the frequncy range 5000Hz - 1MHz.
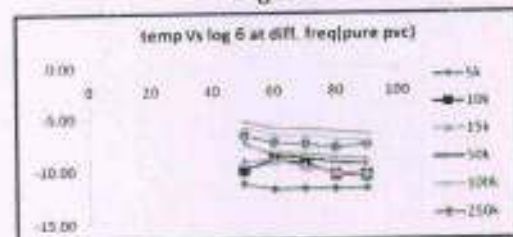
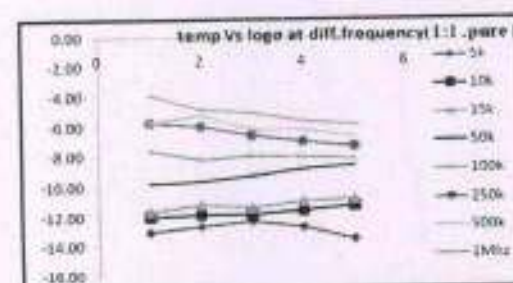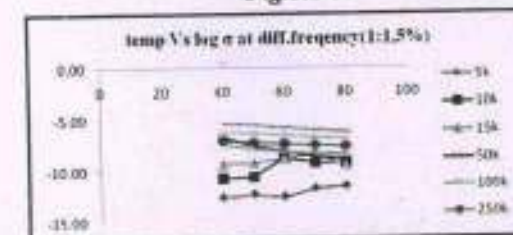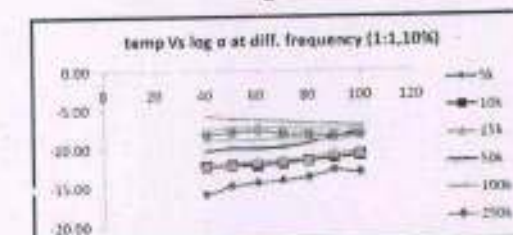A decrease of conductivity was observed with increasing temperature. These phenomena can be explained by the fact that, thermal lattice vibration perturbs the quasi-free movement of electrons, thus scattering between electrons and phonon may occur & so conductivity decreases [18].

From above fig. 3.2.a,b,c,d,e it can also be seen that the value of conductivity gets decreases with increase in percentage of doping as compared to undoped samples. We can explained this decrement of conductivity due to the addition of Oxalic Acid. This Oxalic Acid contribute to the over crowed of the ionic dopants thus reduces the number of charge carriers further gives limitation on the mobility of ions & so conductivity decreases [29].

3.3. Fourier Transform Infrared Spectroscopy (FTIR) Studies :

Infrared (IR) radiation refers broadly to the part of the electromagnetic spectrum between the visible and microwave regions.

FTIR spectroscopy is an important tool in the investigation of polymer structure. The IR spectra of these material vary according to their composition & may be able to show the occurrence of complection & interaction between the various constituents.

FTIR spectra were recorded in the transmittance mode. The FTIR spectra of pure PVC, pure PMMA and PVC–PMMA blend samples & PVC–PMMA doped with 10% oxalic acid are shown in Figs. 3.3a,b,c,d respectively. The band assignments for PVC and PMMA have already been reported in the literature [19–21] and are listed in Tables 1 and 2, respectively.

Table 1: Vibrational modes and wavenumbers exhibited by PVC

Description of vibrations	Wavenumbers (cm⁻¹)	References
C H stretching	2890–2958	[20]
CH₂ deformation	1339	[20,27]
CH rocking	1240–1257	[20,27]
trans CH wagging	961	[20]
C Cl stretching	844	[28]
cis CH wagging	600	[27]

Table 2: Vibrational modes and wavenumbers exhibited by PMMA

Description of vibrations	Wavenumbers (cm⁻¹)	References
C H stretching	2927–2986	[27,28]
C O stretching	1700–1744	[27,28]
CH₃ stretching	1439	[28]
OCH₃ stretching	1195	[28]

These bands can also be observed in Fig. 3.3 a (for PVC) and in fig. 3.3 b (for PMMA).

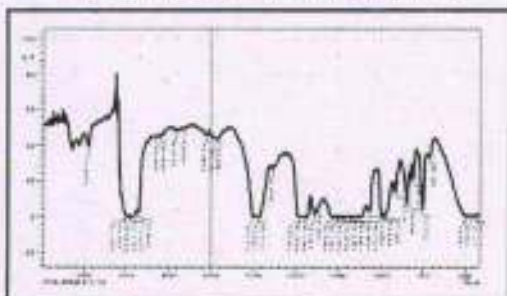*Fig.3.3 a. FTIR spectra of pure PVC*
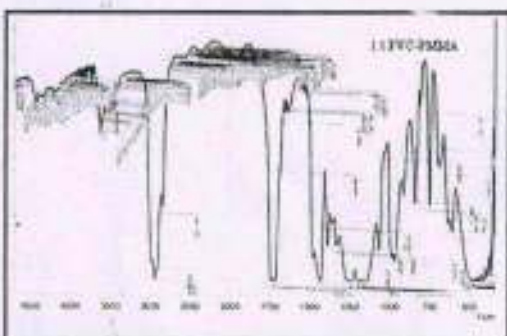

Fig.3.3 b FTIR spectra of pure PMMA

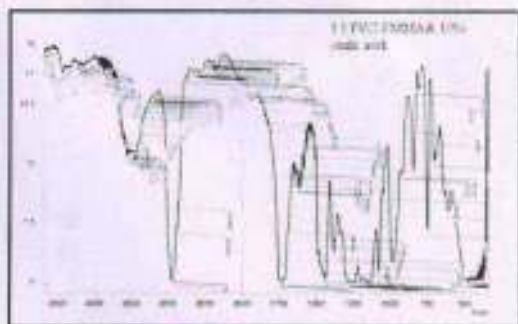*Fig.3.3 c FTIR spectra of pure PVC-PMMA blend*

Fig.3.3 d FTIR spectra of pure
PVC-PMMA blend with 10% doping

From fig.3.3 a, Vibrational bands of PVC are obtained at 2974 cm-1 (vC–H of CHCl), 2912.9 cm-1 (vas, C–H of CH2), 1435.9 cm-1 (w,CH2), 1334.1cm-1 (δ,C–H of CHCl), 1257.6 cm-1 (δ,C–H of CHCl), 1068 cm-1 (v(C–C)),966 cm-1 (r,CH2), 698 cm-1 (v,C–Cl), 638 cm-1 (v(C–Cl)) and 616 cm-1 (v ,C–Cl).

Figure 3.3 b which is FTIR spectrum of pure PMMA, it is observed from the spectrum reported by Saikia and Kumar [22] is similar to our spectrum. Peak at 749 cm-1 corresponds to out of plane C–H bending. Broader and stronger bands in the region 1300-1000 cm-1 correspond to C–O stretching vibrations, which usually consists of two asymmetric coupled vibrations. i.e.C–C (=O)–O and O–C–C. At approximate 1025 cm-1 ether lone pair peak is also present. The bands at 1387.2 and 1456.2 cm-1 correspond to symmetrical bending vibration (vsCH3) and asymmetrical bending vibration (vasCH3) of methyl group, respectively. Strong peak appearing in the region 1730.14cm-1 corresponds to C-O stretching vibrations. Two distinct bands appeared at 2978.4 and 2877.8 cm-1, the first band arises from the asymmetrical (as) stretching mode in which two C–H bonds of the methyl group are extending, while the third one is contracting (vasCH3) and the second band arises from symmetrical (s) stretching (vsCH3) in which all three of the C=H bonds extend and contract in phase.

Complexation may shift the polymer cage peak frequencies. FTIR would be sensitive both in situations where complexation has occurred in crystalline or amorphous phase [20].

Figure 3.3, c which is FTIR analysis of the 1:1 (PVC+PMMA) blends shows small shifting of the carbonyl bond of PMMA to lower wave numbers. The shift of the peak is about 4–6 cm within the domain of miscibility of the two polymers.

The miscibility of PVC/PMMA blends is due to a specific interaction of hydrogen bonding type between carbonyl (C=O) of PMMA and hydrogen from (CHCl) groups of PVC [23], [24], [25] and [26].

4. Conclusions:

AC electrical conductivity have been measured at different temperatures and at the different frequencies. It is found that,

i. AC conductivity of thin film decreases with increase in temperature for all values of frequencies

ii. AC conductivity of thin film increases with increase in frequencies at constant temperature.

iii. AC conductivity of thin film decreases with increasing doping percentage.

iv. The increasing AC electrical conductivity with frequency can be attributed to the interfacial polorisation.The polorisation effect is dependent on the frequency of applied A.C. electrical field.[30]

References:

[1] JL Acosta, E Morales Solid State Ion 85:85 (1996)

[2] JY Kim, SH Kim Solid State Ion 124(1–2):91 (1999)

[3] C. H. K. Douwel, W. E. J. R. Mass, W. S. Veeman,G. H. W. Buning, J. M. J. Vankan, Macromolecules23, 406 (1990).

[4] HJ Rhoo, HT Kim, JK Park, TS Hwang Electrochim Acta42 :1571 (1992)

[5]   K Pielichowski, I Hametron Eur Polym J 36:171 (2000)

[6]   SMS Neiro, DC Dragunski, AF Rubira, EC Muniz EurPolym J 36:583 (2000)

[7]   S. Ramesh, A.H. Yahaya, A.K. Arof, Solid State Ion152:291 (2002)

[8]   M Hamzah. , E Saion., A Kassim. and M Yousuf. , MPJ. Vol. 3, No. 2 ,p(24-31) , Malaysia (2008).

[9]   T Uma, T Mahalingam, U Stimmeng J Mater Sci 39:2897 (2004)

[10]   R. V. Waghmare, N. G. Belsare, F. C. Raghuwanshi and S. N. Shilaskar, Bull. Mater. Sci., 30, 167-172 (2007).

[11]   N. G Belsare. and V. S. Deogaonkar, Journal of Polymer Materials, 15, 157-170 (1998).

[12]   Vijayalakshmi Rao, P.V. Ashoakan and M. H. Shridhar Material Science and Eng., A281

[13]   N G Belsare and V S Deogaonkar b Indian J. Pure & Appl.Phys. 15 157(1998)

[14]   M. Hamzah, E. Saion,A. Kassim and M. Yousuf, MPJ. Vol. 3, No. 2 ,p(24-31) , Malaysia, 2008,

[15]   M. Hamzah , E. Saion, A. Kassim, E. Mahmud and I Shahrim, J. for the advancement of sci. Vol. 1, No. 1, P(9-14). 2009

[16]   S. Ramesh, A.K. Arof, Mater. Sci. Eng. B85 11–15(2001).

[17]   I.C. McNeill, Journal of Analytical and Applied Pyrolysis 43, 21-41(1997).

DC Conductivity of 2:1 (PVC:PMMA) Polyblends: Temperature Dependent

A.B. Dakare[1], F.C. Raghuwanshi[1], G.T.Lamdhade[1]

Department of Physics, Vidya Bharati Mahavidyalaya, Amravati (M.S.)- 444 602 India

Email : gtlamdhade@rediffmail.com, oumgajanan@gmail.com

Abstract: We have prepared the thin films of 2:1 (PVC: PMMA) Polyblends by using isothermal evaporation technique. The DC conductivity of 2:1 (PVC:PMMA) Polyblends thin films measured at different electric field (50V -650V) with respect to different constant temperatures ($50^{\circ}C$ to $125^{\circ}C$) were studied. It has been revealed that the electrical current increases with applied electric field at all the temperatures ,the conductivity of sample increases with temperature and the values of activation energy (E_a) have been found higher in high temperature region than those in low temperature region. The DC electrical conductivity of the sample has been found to increase with the increase in thickness of films.
Keywords: Polyblends thin films, 2:1 (PVC:PMMA), isothermal evaporation technique.

1. Introduction:

The polyblends are produced by the addition of small amount of a rubbery polymer to a polymeric glass. The impact strength of the glass is thus substantially increased .The rubbery polymer is not truly compatible and exist as a finely dispersed separate phase. Interpenetrating polymer networks, in which two different networks are intertwined constitutes on interesting special case of polyblends . Even though a large number of new polymers are synthesized it is still customary to use a mixture of two or more polymers in industry as a raw material for preparing various articles. The production of such mixture also helps in improving certain properties of individual polymer, like increase the strength of rubber by adding stronger plastic to them or improving the elastic properties of plastic by adding rubber to them. The enormous growth of synthetic polymers is due to the fact that they are lightweight materials, act as insulators for electricity and heat, cover a wide range of properties from soft packaging materials to fibers stronger than steel, and allow for relatively easy processing. The polymers are mainly divided into thermoplastics and

thermosets. The major thermoplastics include high-density polyethylene (HDPE), low-density polyethylene (LDPE), polyethylene terephthalate (PET), polypropylene (PP), polystyrene (PS and EPS), poly(vinyl chloride) (PVC), polyamide (PA), poly(methyl methacrylate) (PMMA) and styrene copolymers (ABS, SAN). Poly (vinyl chloride) (PVC) is an important commercial thermoplastic, which is widely used in industrial fields due to its good properties and low cost. However, its brittleness, low thermal stability and poor process ability limit its application. Poly (methyl methacrylate) (PMMA) is amorphous in nature due to presence of bulky side groups in molecules. It is colorless transparent plastic with an excellent outdoor life period, good strength and higher impact strength than glass.

The polyblends are certain to show the properties different from basic polymers. PVC, PMMA among the most extensively studied polymers having a great range of applications. The addition of methyl methacrylate and its polymer (PMMA) to improve the thermal and mechanical properties of PVC has been studied for over 35 years [1]. Khare *et al* [2], Belsare and

Deogaonkar [3] reported on the theory of electrical conduction and experimental findings have appeared in a number of such blends. The conductivity studies on PVC/PMMA polymer blend electrolytes have shown that the polymer component would render stability and they have many applications of blending [4].

2. Experimental:

In this work we have selected Polymethyl methacrylate (PMMA) as a base polymers which is in granule form obtained from Otto Kernl, Mumbai and PVC is prepared by the polymerization of vinyl chloride. The major role of Tetrahydrofuran (THF-E-Merck India Ltd., Mumbai) being as a solvent for polyblending process, which is a colorless, water-miscible organic liquid with low viscosity at standard temperature and pressure. The thin films of 2:1 (PVC: PMMA) Polyblends by weight ratio was prepared using isothermal evaporation technique [5]. The thin film was then sandwiched between two brass electrodes of the sample holder .The metal –insulator – metal system so formed was placed inside the furnace. The DC conductivity of Polyblends thin films measured by using two probe method at different electric field (50V - 650V) with respect to different constant temperatures (50°C to 125°C) were recorded. The same procedure was repeated for all the thin films of different thicknesses. In this present study, thickness of thin film is found to be in the range 20 to 50μm.

3. Results and Discussion:

The polymer films consist of both crystalline and amorphous regions [6,7]. Such polymers can exist in two states depending on temperature. At low temperature, they are glassy materials, while at high temperature (called their glass transition temperature T_g) they undergo transition from glassy to rubber like state. At this temperature gross molecular motion of polymer chains accompanies the transition from glassy to rubbery state .The

motion of the molecular chains enhance the freeing of charge carriers and thus there is an increase in conductivity. As a result of this, the conductivity–temperature plot shows that conductivity increases in accordance to the temperature as shown in fig. 1.
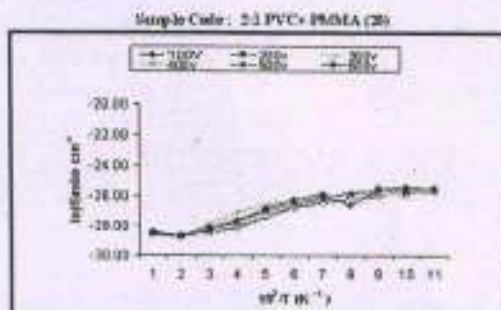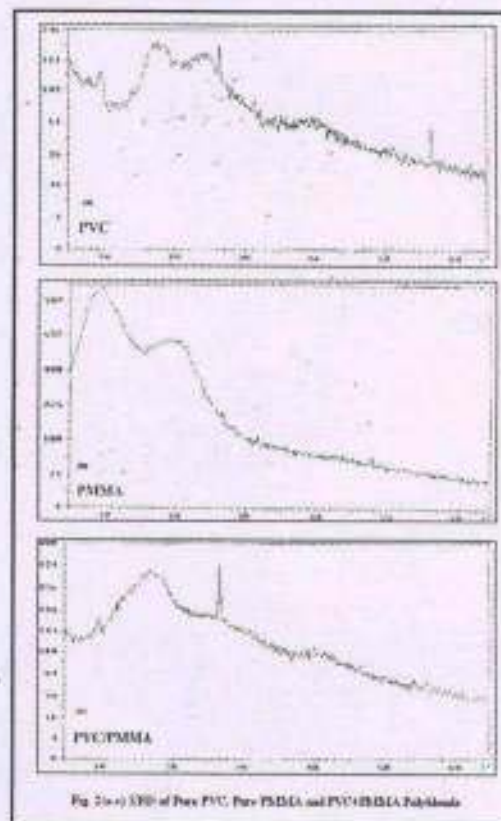

Fig. 1. Arrehnius Plot

Fig. 2(a-c) XRD of Pure PVC, Pure PMMA and PVC+PMMA Polyblends

Figures 2 (a), (b) and (c) illustrate the XRD diffractograms of pure PVC, pure PMMA and (PVC+PMMA) Polyblends respectively. From Figure 2(b), a broad characteristic peak of PMMA was obtained at angles of $2\theta = 11.4°$ with a shoulder at $2\theta = 21.5°$ which reveals the amorphous phase of PMMA. The intensity of these characteristic peaks is decreased after the impregnation of PVC. This implies that the addition of PVC disrupted the arrangement in the polymer backbone of PMMA [8]. The presence of interactions between PMMA and PVC, such as cross-linking, is attributed to complexation of PMMA and PVC. Apart from the peak intensity of these characteristic peaks, another evidence of complexation is observed by shifting of peaks. The blending of PMMA with PVC shifts the peaks at $2\theta = 18.5°$ and $2\theta = 28.1°$ revealing the change in crystallographic organization [9].

In case of polyblends having 30 ml, 25ml, 15ml and 10ml of cyclohexane (as a solvent) i.e. with increasing thickness of thin films it is found that the current linearly increases from 50V to 600V, hence indicates the ohmic conduction in higher as well as lower voltage region for all the samples. On application of step voltage across the specimen orientation of dipoles occur at low voltages as well as high voltages; the mobility of charge carriers increases resulting into the increase in current density with respect to applied voltages .Among the two polymers, PVC is strongly polar and high dielectric constant. Also it acts as an electron withdrawing group i.e. acceptor, which pulls electrons from neighboring atoms and hence tends to become a more reactive compound .While PMMA is weakly polar and it is a hard rigid, transparent thermoplastic. PMMA contains electrons releasing methyl group (CH,) i.e. it acts as an electron donor, which supplies electrons and tends to become a stronger bond. PMMA also contain acrylate group (−CH-CO-O-R), which is a bulky side group. Hence introduction of methyl constituent in the polymer decreases the C-C bond stability [10].

The electrical conductivity of PVC, as reported by standard literature is between 10^{-11} - 10^{-14} Ωcm^{-1} and of PMMA is in the range of 10^{-12} to 10^{-15} Ωcm^{-1}. This suggest that PVC is slightly better conducting material as compared to PMMA .The conductivity of PVC-PMMA polyblends as determined from our experimentation lies between 10^{-14} to 10^{-15} Ωcm^{-1}.This dc conductivity lies intermediate between that PVC & PMMA .Thus combination of PVC & PMMA slightly increases the conductivity of PMMA but decreases that of PVC.

4. Conclusions:

PVC-PMMA polyblends having different quantity of cyclohexane show semi conducting properties .The fact that the conductivity of sample increases with the increase of temperature (The rate of increase of conductivity with temperature is comparatively less than the conventional semiconductors such as Ge and Si). But this property is exhibited by the polyblends films. For all the samples, the conductivity increases with the increase in temperature. The conduction has been almost ohmic in low voltage region as well as in high voltage region. The conductivity of sample has also been found thickness dependent. The conductivity has been found to increase with the increase in thickness of sample films. The blending of PVC and PMMA retain the insulating properties quite intermediate between those two of component polymers.

References:

[1]   J.W. Shurer, A. de Boer, and G. Challa, Polymer, 16, 201 (1975).

[2]   Khare P K, Gaur M S and Srivastava A P (1994) Indian J. Pure & Appl. Phys. 32 14

[3]   Belsare N G and Deogaonkar V S (1998) Indian J. Pure & Appl. Phys. 36 280

[4]   V. Aravindan, C. Lakshmi, P. Vickraman, Current Applied Phys. 9 (2009) 1106-1111.

[5]   R. V. Waghmare, N. G. Belsare, F. C. Raghuwanshi and S. N. Shilaskar, Bull. Mater. Sci., Vol. 30, No. 2, April 2007, pp. 167–172.

[6]   N.G.Belsare ,Ph.D.Thesis, "Electrical
        conductivity in mixed polymers and
        their
        electrets"(1998),S.G.B. Amravati
        University, Amravati.

[7]   P.J.Harrop and D.S.Campbell (1970),
        "Handbook of Thin film technology
        (Edts.Maissel,L.I.and Glang.R.Mc
        Graw-Hill, New York) Chapter 16.

[8]   S. Ramesh, A. K. Arof, J. Power Sources
        99 (2001) 41-47.

[9]   R. Kumara, A. Subramania, N.T. K.
        Sundaram, G. V. Kumar, I. Baskaran,
        J.
        Membrane Sci 300 (2007) 104–110.

[10]   Y. Yang, C. H. Zhou, S. Xu, H. Hu, B.
        Lei Chen, J. Zhang, S. J. Wu, W. Liu,
        X. Z.

[11]   Zhao, J. Power Sources 185 (2008)
        1492-1498.

Zn_2SnO_4 modified ZnO thick film resistors as LPG sensor

V. S. Kalyamwar[*], N. S. Kadu[*], N. L. Jadhao[*],
S. D. Charpe[b], F. C. Raghuwanshi[b]

[*]Department of Physics, Bharatiya Mahavidyalaya, Amravati, India.
[b]Department of Physics, Vidyabharati Mahavidyalaya, Amravati, India.

Email: vinu_phy@rediffmail.com

Abstract : Zinc oxide nanostructures were synthesized by chemical route method. The XRD spectrum indicates that the sample is wurtezite (hexagonal) structured ZnO with lattice constants of $a = 3.249 A^0$, $c = 5.206 A^0$. Thick films of synthesized ZnO were prepared by screen printing technique. The Zn_2SnO_4 modified ZnO were obtained by dipping them into an aqueous solution of $SnCl_4.5H_2O$ for different interval of time. Gas sensing properties of pure and modified ZnO thick films were investigated. The Zn_2SnO_4 modified ZnO thick film dipped for 3 min was observed to be more sensitive to LPG as compared to other modified thick films at 240°C. The effect of surface microstructure and Zn_2SnO_4 concentrations on the sensitivity, selectivity, response and recovery of the sensor in the presence of LPG and other gases were studied and discussed.

Keywords : ZnO nanostructure, Zn_2SnO_4 modified ZnO thick films, LPG Sensor.

1.Introduction:

The detection of toxic and inflammable gases by a sensor was extremely important for human and environmental protection. Research on the gas sensors was aimed to obtaining new sensing materials to achieve highly sensitive and selective devices. ZnO has proven to be highly sensitive materials for the detection of both reducing and oxidizing gases [1-10]. Though, poor selectivity is one of its disadvantages.

Semiconductor gas sensors based on SnO_2 and ZnO have been studied for the detection of toxic or inflammable gases [11-14]. However, high operating temperature is one of their disadvantages. In order to modify the gas sensing properties, the use of metal additives such as Ag, Pt and Pd as catalysts were widely studied [15]. Another approach was the utilization of the interfaces between two different oxides such as hetero contact of p-n junction with new sensing mechanism was proposed to improve its sensing properties. However, the hetero contact type sensors have the poor reliability due to its pressed contact [16]. Composite type sensors were suggested to improve the reliability since they contain many heterogeneous interfaces between different phases. However, the composites make the study of the individual interface difficult. To overcome these problems, only surface of metal oxides were modified with other oxides by using dipping technology. In present work, the efforts were made to modify surface of ZnO thick film with Zn_2SnO_4 crystals nanostructure thick film with Zn_2SnO_4 crystals by using dipping technique to improve sensing properties.

2. Experimental

2.1 Synthesis of ZnO nanostructure

All chemicals were of analytical grade and used as purchased without further purification.

In present work, 2.974 g Zinc nitrate hexahydrate was dissolved in 100 ml distilled water and 2.0g of NaoH was dissolved in 100 ml distilled water. The zinc nitrate solution was added drop wise to the NaoH solution to form white solution. Then, white solution was subsequently kept at $75^\circ C$ for 12h. The resulting white precipitates were collected by centrifugation, washed with distilled water and ethanol several times and then dried at $80^\circ C$ in vacuum oven for 2h. The synthesized ZnO nanostructure was used for further study.

2.2 Preparation of thick films

Thick films of ZnO nanostructure were prepared by using screen printing technique. In present process, paste was formulated by mixing the ZnO nanostructure powder with ethyl cellulose in a mixture of organic solvents. The ratio of ZnO to ethyl cellulose was kept 93:07. The paste was screen printed on a glass substrate in desired patterns. The films were fired at $500^\circ C$ for 2h to remove temporary binder. Prepared thick films termed as pure ZnO thick films.

2.3 Zn_2SnO_4 modified ZnO thick films

Surface of pure ZnO thick film were modified by dipping them into a 0.01 M aqueous solution of $SnCl_4.5H_2O$ for different intervals of time (1, 3, 5 & 7 min). After dipping, thick films were dried under IR lamp for 45 min. and calcinated at $700^\circ C$ for 4h in air ambient. In calcination process, tin chlorides dispersed on the film surface were reacting with surface ZnO molecules and oxidized. Therefore sensor elements with different mass% of Zn_2SnO_4 on the surface of ZnO thick film were obtained. These surface activated films are termed as Zn_2SnO_4 modified thick films.

2.4 Characterization

The synthesized ZnO were characterized for structure and morphology by power X-ray diffraction (Philips PW 1710) and transmission electron microscopy (TecnaiG2 20 ultra-twin). The microstructure and chemical composition of the films were analyzed using a field emission scanning electron microscope (ZEISS SUPRA-55) coupled with an energy dispersive spectrometer. Thickness measurements were carried out using Marutek film Thickness Measurement System. Electrical and gas sensing characteristics were measured using a static gas sensing system.

2.5 Static gas sensing system
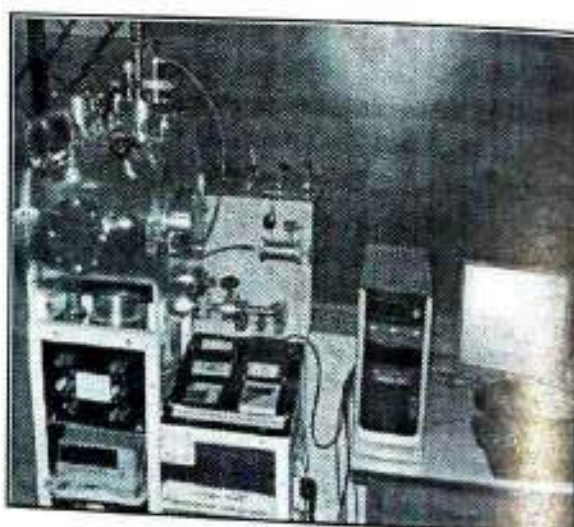
Fig. 1 Photograph of computerized gas sensing system

Fig. 1 represents photograph of computerized static gas sensing system to examine the sensing performance of the thick films. A constant voltage was applied to the sensor element and current was measured with the help of voltage source cum picoammeter (Keithley 6487). Heating element and thermocouple were connected to temperature controller (Nippon NC 2638). Sensor element and thermocouple were kept on the insulating surface of the heating element. The required gas concentration inside the static system was

achieved by injecting a known volume of test gas using a syringe. The vacuum pump is attached to chamber to create vacuum or to remove test gas.

3. Material Characterization:
3.1 X-ray diffraction

The recorded X-ray diffraction pattern (Fig. 2) confirmed that synthesized ZnO is highly crystalline in nature. The corresponding X-ray diffraction peak for (100), (002), (101) and (102) planes confirm the formation of hexagonal wurtzite structure of ZnO, which are in good agreement with the literature values (JCPDS card No. 36-1451). In this X-ray diffraction pattern, extra pick appear at $2\theta = 44°$. This peak was identified as surface hydroxyl groups, which can be related to the formation of water on the ZnO nanostructure surface [17]. The crystallite size was calculated by using Scherrer's formula [18] and found to be 16nm.
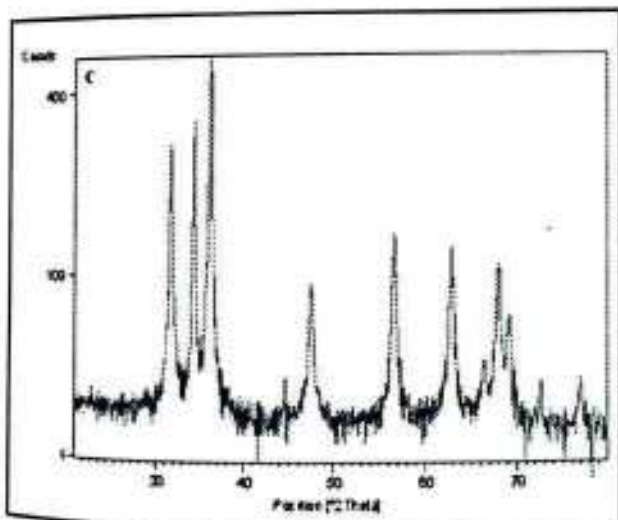

Fig. 3 TEM image of ZnO nanostructure synthesized by chemical route method

Fig. 2 powder XRD pattern of ZnO nanostructure synthesized by chemical route method

3.2 Transmission electron Microscope

Fig.3 illustrates the TEM image of the ZnO nanoparticles. TEM pattern shows that the particles are agglomerated up to some extent.
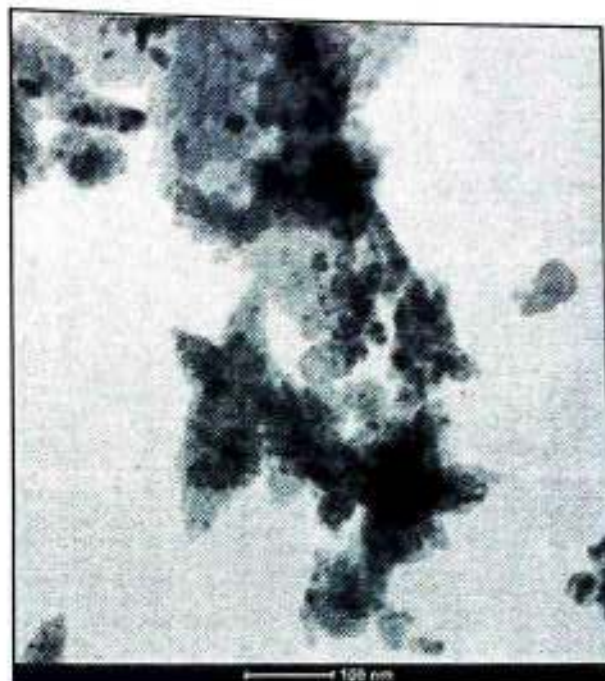
3.3 Scanning Electron Microscope:

The FE-SEM micrograph of the pure ZnO thick film prepared by screen printing technique is shown in Fig. 4a. Pure ZnO thick film consists of randomly distributed nanosheets. Fig. 4b corresponds to surface modified ZnO thick film with dipping time 1 min, clearly indicate that, growth of nanosize octahedral crystal began to occur on the surface of ZnO thick films. These nanosize octahedral crystals attributed to Zn_2SnO_4. Thus effective surface area of thick film gets increased. As dipping time increases to 3 min, growth of more and more Zn_2SnO_4 crystals on the surface of ZnO thick films occur (Fig. 4c). Further increasing in dipping time to 5min and 7min, these nanoscale Zn_2SnO_4 crystals start to disperse core of ZnO nanostructure as shown in Fig. 4d and 4e respectively. Fig. 4f shows high magnified FE-SEM image of Zn_2SnO_4 crystal created on the surface of modified ZnO thick film (dipped for 3 min.).

3.4 Elemental analysis

Fig. 5a-c represents the EDS patterns of pure and modified ZnO Thick films. These Figures illustrate that as the dipping time increases intensity of tin peak increases, which indicate the increasing in mass percentage of tin element on the surface of the ZnO thick film.

Fig. 4 FE-SEM images of a) pure ZnO thick film & modified ZnO thick film b) dipped for 1 min. c) dipped for 3 min. d) dipped for 5 min. e) dipped for 7 min. f) Highly magnified modified ZnO thick film (3 min dip.)
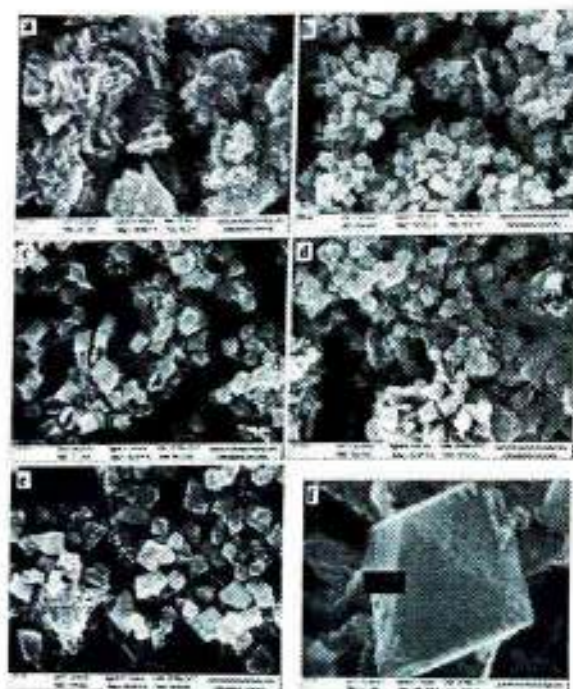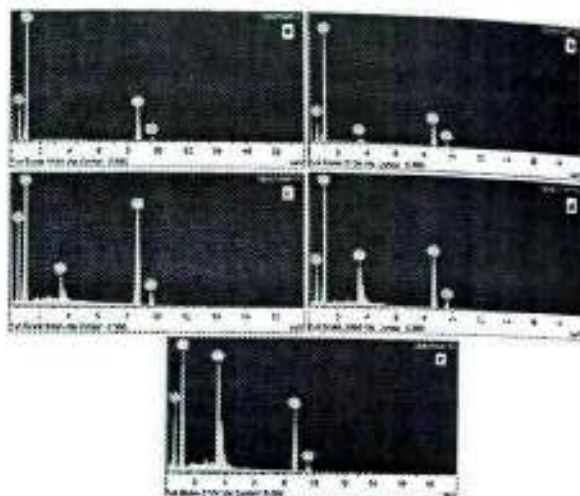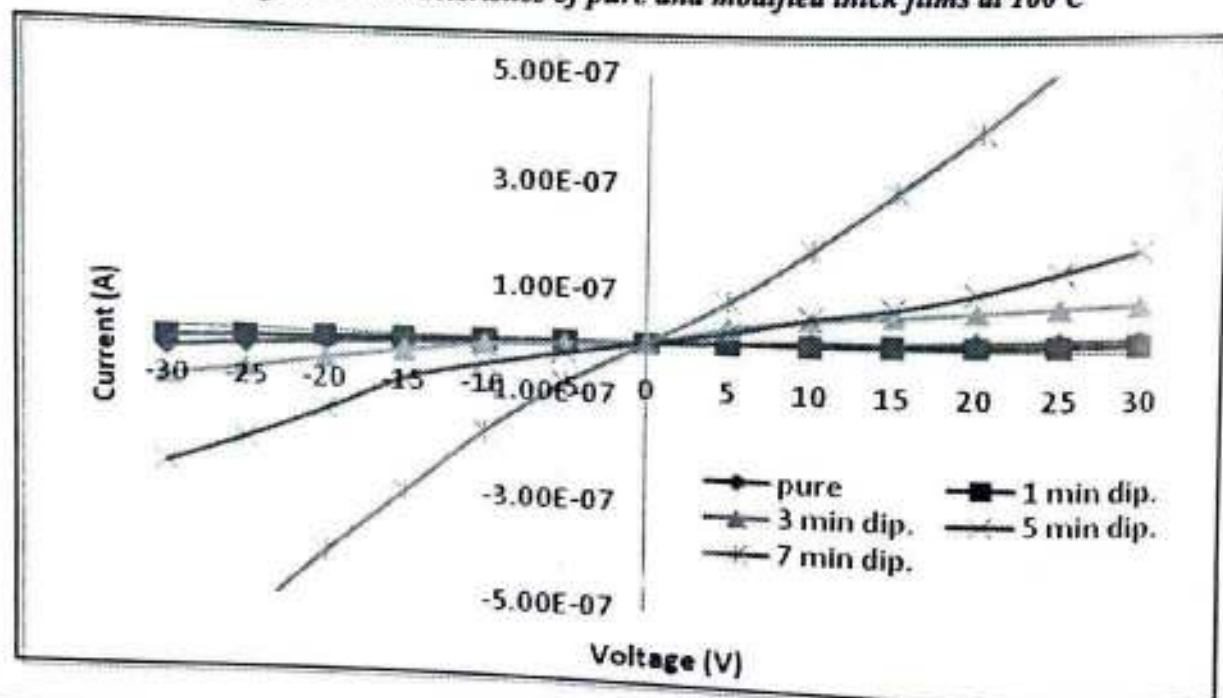

Fig. 5 EDS patterns of a) pure ZnO thick film & modified ZnO thick film b) dipped for 1 min. c) dipped for 3 min. d) dipped for 5 min. e) dipped for 7 min.

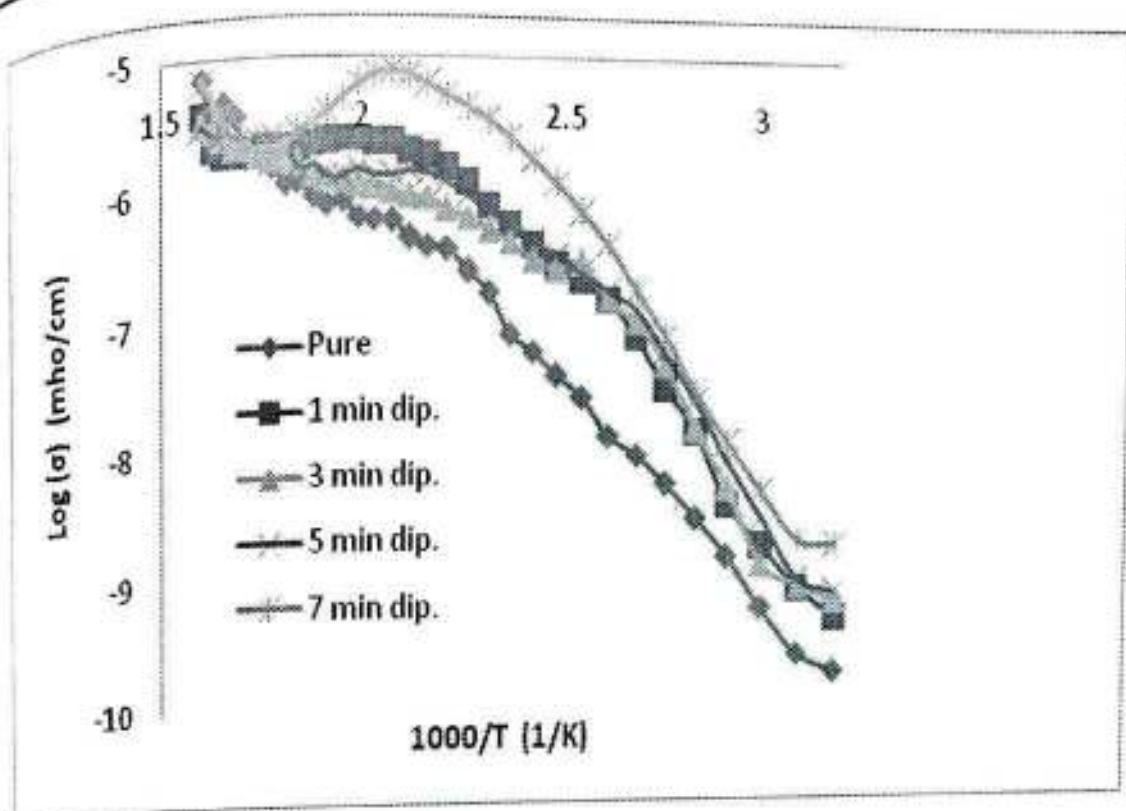*Fig. 6 I-V characteristics of pure and modified thick films at 100°C*

Fig. 7 *Variation of log σ with 1000/T of pure and Zn,SnO, modified thick films*

4.2 Electrical conductivity

Fig. 7 depicts that, for all the samples conductivity increases with increasing in temperature. It is observed that, the conductivity of pure ZnO thick film is less than Zn,SnO, modified ZnO thick films. Higher conductivity of Zn,SnO, modified ZnO thick films are attributed to growth of Zn,SnO, crystal over the surface of ZnO thick films. Zn,SnO, has high electronic mobility and thermal stability.

5. Sensing performance
5.1 Pure ZnO thick film

The gas response of the sensor was defied as the ratio of the change in conductance of a sample upon exposure to the target gas to the original conductance in air. The variation of gas response of ZnO thick film to 600ppm LPG with operating temperature is represented in Fig. 8. The response to LPG increases with increasing the operating temperature, reaches to the maximum (6.7) at 300°C and decreases with
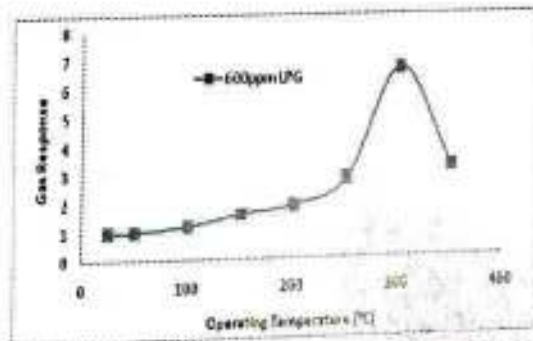
Fig. 8 *variation of gas response of pure ZnO thick film with temperature*

further increasing operating temperature. Response to a gas is due to the interaction between hydrocarbons (propane and butane present in LPG) and adsorbed oxygen ions present on the surface of the thick film. When hydrocarbons interact with the adsorbed oxygen ions on the surface of ZnO thick film they are converted to CO_2 and H_2O and releases the trapped electrons back to the conduction band of the zinc oxide thick film. As a result the
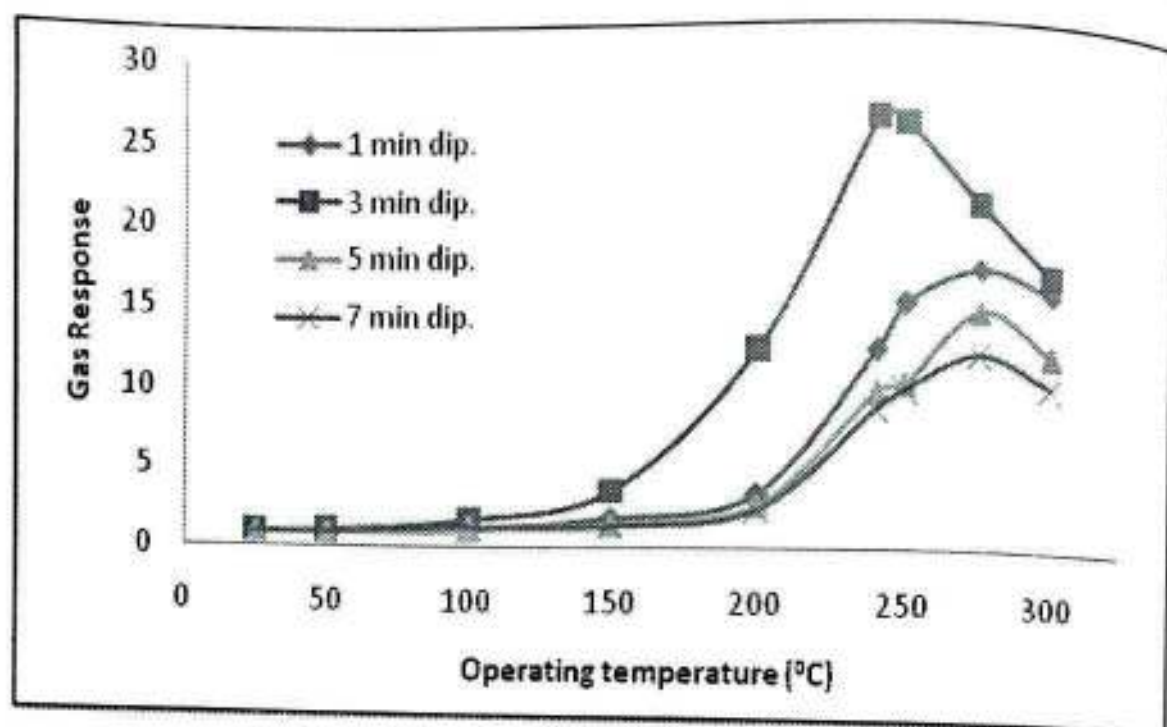
Fig. 9 variation of gas response of modified ZnO thick films with operating temperature.

conductance of ZnO thick film increases in existence of LPG.

5.2 Zn2SnO4 modified ZnO thick films
5.2.1 Gas response and operating temperature

The variation of gas response of modified ZnO thick films to LPG as a function of operating temperature is shown in Fig. 9. It represent that modified ZnO thick films with different dipping time are sensitive to 600 ppm LPG in the temperature range 200-300°C. The highest response of all thick films was observed around temperature 250°C.

5.2.2 Selectivity for LPG against various gases

Fig. 10 demonstrate the selectivity of all modified ZnO thick films for 600 ppm LPG, NH, and CO, gas at operating temperature 240°C. These modified thick films showed high selectivity to LPG among the gases such as CO, and NH,.

5.3.3 Response and recovery time of the sensor

Fig. 11 illustrates the response and recovery of the modified ZnO thick (3 min dip). It indicates that the response was quick (6 s) to 600 ppm of LPG, while the recovery is also fast (8 s) at operating temperature 240°C.

All modified ZnO thick films gives quick response to LPG at higher operating temperature and fast recovery when sensor element keeps in air atmosphere. Such quick response and fast recovery can be explained on basis of adsorption and desorption process of oxygen ions on surface of Zn,SnO, modified ZnO thick film.

6. Discussion

Enhancement of sensing performance of Zn,SnO, modified ZnO thick film to LPG

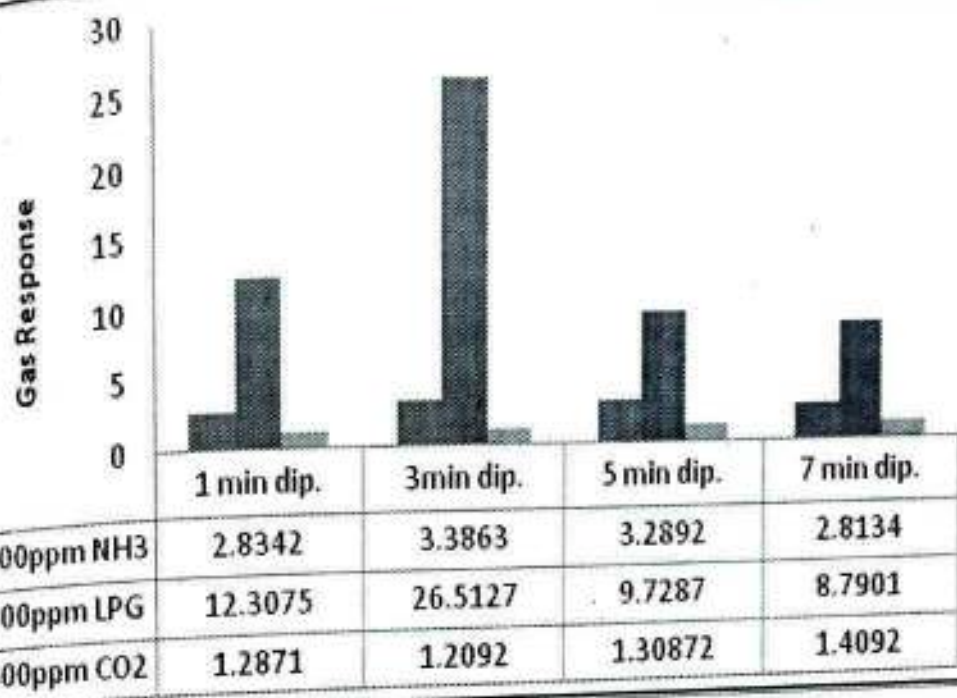|	1 min dip.	3min dip.	5 min dip.	7 min dip.
■600ppm NH3	2.8342	3.3863	3.2892	2.8134
■600ppm LPG	12.3075	26.5127	9.7287	8.7901
■600ppm CO2	1.2871	1.2092	1.30872	1.4092

Fig. 10 Selectivity of modified ZnO thick films to LPG from mixture of gases at operating temperature 240°C.
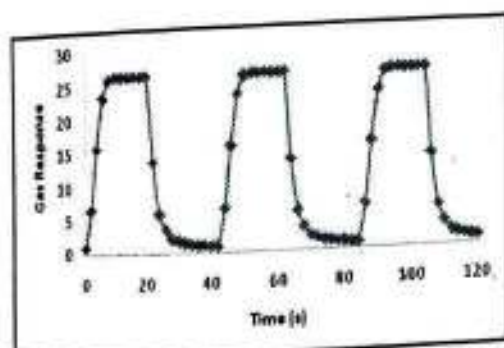
Fig. 11 variation of gas response of modified ZnO thick film (dipped for 3 min) to 600ppm LPG with time

[Fig. 9] as compared to pure ZnO thick films [Fig. 8] can be attributed to growth of zinc stanate crystals on the surface of ZnO thick film. This will increase the surface to volume ratio of the sensor material. The chemical composition and crystal morphology of Zn_2SnO_4 offers enhanced active sites for reactions of LPG molecules with adsorbed oxygen.

When Zn_2SnO_4 modified thick film

exposed to air, oxygen molecules were adsorbed on the Zn_2SnO_4 surface, which generate ionized oxygen species by trapping electrons from the conductance band of Zn_2SnO_4. These generated ionized oxygen species react with reducing gas such a LPG, which resulted in the release of electrons to the surface of Zn_2SnO_4 modified ZnO thick film. Thus the conductivity of Zn_2SnO_4 modified ZnO thick films were increases gradually.

Fig. 9 shows that the sensitivity of Zn_2SnO_4 modified ZnO thick film (dipped for 3 min) is highest among other thick films in the temperature region 200-300°C, it may be attributed to morphology of Zn_2SnO_4 crystals developed on the surface of ZnO thick film. The adsorption and desorption processes, which determine the sensor response mainly depends on the orientation and morphology of the crystals. As the size of the crystal domain becomes smaller, the ratio of edge and corner atoms increases and also the surface topology

becomes increasingly roughened [19]. Control of crystal size distributions and resulting changes in electronic and surface states provides an opportunity to tailor the interaction and adsorption of gas molecules on the exposed surfaces of Zn_2SnO_4 cubic structures and ZnO nanostructure resulting in enhanced sensor performance.

7. Summary

The sensing performance of pure and modified ZnO thick films can be summarized as

1. Zinc oxide power synthesized by chemical route method consists of nanoparticles and nanorods.
2. Pure ZnO thick films are less conductive as compared to modified ZnO thick films.
3. Pure ZnO thick films showed higher sensitivity and selectivity to 600 ppm LPG gas at 300^0C.
4. In case of surface modified thick films, thick film (dipped for 7 min.) shows higher conductivity.
5. All modified ZnO thick films shows sensitive to 600ppm of LPG in the temperature range 200-300^{0}C.
6. At 240^0C, modified ZnO thick film (dipped for 3 min.) shows higher sensitivity to 600 ppm of LPG as compared to other modified ZnO thick films.
7. Modified ZnO thick films showed very rapid response and fast recovery as compared to pure ZnO thick films.

References

[1] Shinde, V. R.; Gujar, T. P.; Lokhande, C. D., Sens. Actuators B, 2007, 120, 551.
[2] Hsueh, T. J.; Chen, Y. W.; Chang, S. J.; Wang, S. F.; Hsu, C. L.; Lin, Y. R.; Lin, T. S.; Chen, I. C., Sens. Actuators B, 2007, 125, 498.
[3] Chaikarn, L.; Sukon, P., Sensors, 2007, 7, 185.
[4] Mitra, P.; Halder, A., Sensor, Mat. Res. 2009, 12, 329.
[5] Kalyamwar, V. S.; Raghuwanshi, F. C.; Jadhao, N. L.; Gadewar, A. J., J. Sen. Tech. 2013, 3, 31.
[6] Patil, D. R.; Patil, L. A.; Patil, P. P., Sens. Actuators B, 2007, 126, 368.
[7] Trivikrama Rao, G. S.; Tarakarama Rao, D., Sens. Actuators B, 1999, 55, 166.
[8] Gnanasekar, K. I.; Prabhu, E.; Jayaraman, V.; Gnanasekaran, T., Adv. Mat. Lett. 2013, 4(6), 464.
[9] Gurav, K.V.; Patil, U.M.; Shin, S.W.; Pawar, S.M.; Kim, J.H.; Lokhande, C.D., J. Alloy. Comp., 2012, 525, 1-7.
[10] Mondal, S.; Kanta, K. P.; Mitra, P.; J. Phys. Sci. 2008, 12, 221.
[11] Zhang, W. H.; Zhang, W. D., Sens. Actuators B, 2008, 134, 403.
[12] Song, X.; Liu, L., Sens. Actuators A, 2009, 154, 175.
[13] Won Kim, K.; Cho, P. S.; Kim, S. J.; Lee, J. H.; Kang, C. Y.; Kim, J. S.; Yoon, S. J., Sens. Actuators B, 2007, 123, 318.
[14] Wagh, M. S.; Patil, L. A.; Seth, T.; Amalnerkar, D. P., Mat. Chem. Phys. 84 (2004) 228.
[15] Yamazoe, N.; Kurokawa, Y.; Seiyama, T., Sens. Actuators, 1983, 4, 283.
[16] Shin, B. C.; Miyayama, M.; Yanagida, H., J. Mat. Sci. Lett. 1994, 13, 719.
[17] Wong, K. W. J.; Field, M. R.; Ou, J. Z.; Latham, K.; Spencer, M. J. S.; Yarovsky, I.; Kalantar-zadeh, K., Nanotechnology, 2012, 23, 015705.
[18] Hilber, T.; Letonja, P.; Marr, R.; Polt, P.; Siebenhofer, M., Part. Part. Syst. Charact., 2002, 19, 342.
[19] Rioux, R. M.; Song, H.; Grass, M.; Habas, S.; Niesz, K.; Hoefelmeyer, J. D.; Yang, P.; Somorjai, G.A., Topics in Catalysis, 2006, 39, 167.

Electrical Conductivity of Surface Activated Nanostructure ZnO Thick Films

S.D.Charpe[1], F.C. Raghuwanshi[1], V.S. Kalymwar[2]

[1]Department of Physics, Vidya Bharati Mahavidyalaya, Amravati (M.S.) - 444 602, India.
2Department of Physics, Bharatiya Mahavidyalaya, Amravati (M.S.) - 444 601, India.

Email : sushildeo86@gmail.com

Abstract: Zinc Oxide particles were synthesized by Chemical Precipitation Method. The average particle size of ZnO is found to be 19 nm. Thick films of ZnO were prepared by screen printing technique and Al_2O_3 -surface activated ZnO films were prepared by dipping method. The variation of electrical conductivity of pure and surface activated films was studied with temperature. The results of electrical measurement at the room temperature show that, pure ZnO and surface activated thick films are semiconducting in nature. The decrease in conductivity of surface activated thick films may be due to presence of potential barrier at the intergrain boundaries of ZnO-Al_2O_3 and hence the grain boundary region becomes more resistive.

Keywords: ZnO, Chemical Precipitation Method, XRD, Surface activated thick film, Electrical conductivity.

1. Introduction

Today, when the world is prevailing on the roof of technology and electronics, mostly dominated by compatible electronic equipments and thereby creating the need for materials possessing useful properties. The world now demands a material that should possess inherent properties like larger band gap, higher electron mobility as well as higher breakdown field strength. So on making investigation about such a material the name of compound comes out is "Zinc Oxide" which is a wide gap semiconductor material very well satisfying the above required properties.Zinc oxide possessed many versatile properties for UV electronics, spintronic devices and sensor applications. This ignites many research minds all over the world and creates interest to develop proper growth and processing techniques for the synthesis of Zinc oxide.

The electrical, optical, magnetic, and chemical properties can be very well tuned by making permutation and combination of the two basic structural characteristics that is cations with mixed valence states, and anions with deficiencies(vacancies). Thus, making them suitable for several application fields such as semiconductor, superconductor, ferroelectrics, magnetic and gas sensing.

Nanostructured materials such as ZnO, SnO_2, and WO_3 have shown good electrical properties [1-12]. Among these nanostructure-semiconducting materials, ZnO has been studied extensively for electrical application. Due to its versatility and multifunctionality creates attention in the research field related to its electrical applications. A wide number of synthesis techniques also been developed by which ZnO can be grown in different nanoscale forms. Efforts were made to synthesize ZnO nanostructure with innovative morphology by chemical route method. The synthesized ZnO shows good electrical conductivity. In the present work, the efforts are made to study electrical conductivity with a low cost additive (Al_2O_3) using dipping technique which is a simplest method of surface modification.

2. Experimental
2.1. Synthesis of ZnO Nanostructure

All chemicals were of analytical grade and used as purchased without further purification. In present work, Zinc nitrate hexahydrate was dissolved in distilled water such that to make 0.15M solution. Subsequently, 0.5 M NaOH aqueous solution was introduced into the above aqueous solution drop by drop with constant stirring. The resultant white solution was subsequently kept at 75 °C For 12 hrs.and then cooled room temperature naturally and sonicated (Ultrasonic wave treatment) for 30 min. The resulting white precipitates were collected by centrifugation, washed with distilled water and ethanol several times and then dried at 80°C in vacuum oven for 2hr. Obtain ZnO nanostructure product were used for further study.

2.2. Preparation of Thick Films

Thick films of synthesized nanostructure ZnO were prepared by using screen printing technique. In present process, thixotropic paste was formulated by mixing the synthesized ZnO powder with ethyl cellulose (a temporary binder) in a mixture of organic solvents such as butyl cellulose, butyl carbitol acetate and turpineol. The ratio of ZnO to ethyl cellulose was kept at 95:05. The ratio of inorganic to organic part was kept as 75:25 in formulating the pastes. The thixotropic pastes were screen printed on a glass substrate in desired patterns. The films prepared were fired at 500°C for 12 hr. Prepared thick films were called as pure ZnO thick films.

3. Materials Characterization
3.1. Thickness Measurement

Thickness of all ZnO thick films were measured by using technique "Marutek film Thickness Measurement System" with the help of provided equipment. The thicknesses of all films were observed in the range from 31 to 35 μm. Thick films of approximately uniform thick-nesses were used for further characterization.

3.2. X-Ray Diffraction Studies

The crystallographic structure of the synthesized ZnO nanostructure was characterized by powder X-ray diffraction (Philips X-ray diffractometer) with Cu-α source and 2θ range of 10° - 70°. Fig 1shows the XRD pattern of the ZnO nanostructure. The recorded XRD pattern confirmed that synthesized ZnO are highly crystalline in nature. The corresponding X-ray diffraction peak for (100),
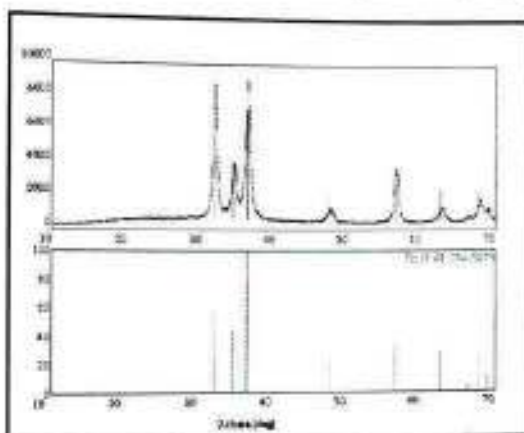
Fig1:XRD Pattern of Pure ZnONanostructure

(002), (101), (102) (110), (103) and (112) planes confirm the formation of hexagonal wurtzite structure of ZnO (JCPDS card no.-01-080-0075). The domain size of the crystal can be estimated from the full width at half maximum (FWHM) of the peaks by means of the Scherrer formula,

$$D = \frac{k\lambda}{\beta \sin\theta}$$

where λ is the wavelength of incident beam (1.5406 Å), β is the FWHM of the peak in radians, θ is the diffraction angle and K is Scherrer constant. The average particle size was calculated from (101) peak ZnO is found to be 19 nm.

Using X'pert High Score Plus software it is confirm that synthesized zinc oxide powder contains Zn and O elements only, not any impurity and another element.

Charpe et al.

4. Surface Modification of ZnO Thick Film

The pure ZnO thick film was surface activated by dipping it into a 0.01M aqueous solution of Aluminium chloride anhydrous [Al(H$_2$O)$_x$Cl$_y$] for 2 min and was dried at 90°C, followed by firing at 500°C for 12 h in ambient air. The particles of Aluminum chloride dispersed on the film would be transformed to Aluminum oxide (Al$_2$O$_3$) during firing process. This surface-activated filmis termed as Al$_2$O$_3$-activated film. Silver contacts were made by vacuum evaporation for electrical measurements

5. Electrical properties
5.1. I–V characteristics

Fig. 2 depicts the I–V characteristics of the pure and Al$_2$O$_3$-activated ZnO films at room temperature. The symmetricalnature of I–V characteristics shows that silver contacts on the film are ohmic in nature[13].
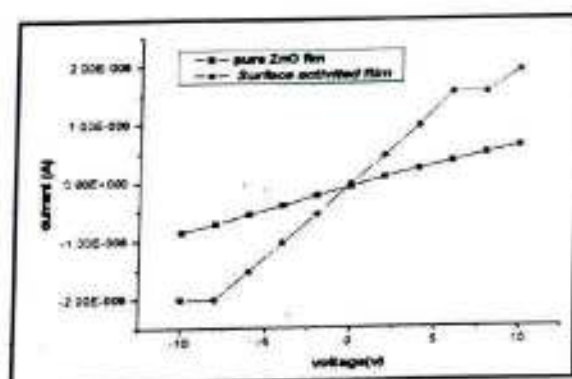
Fig 2: I-V Characteristics of pure ZnO and surface activatedthick film at room temperature

5.2. Effect of Temperature on Current

Fig. 3 shows the variation of current with temperature. The current values of all samples increase with operating temperature which shows good conduction in given samples.

5.3. Electrical conductivity

Fig. 4shows the variation of log σ
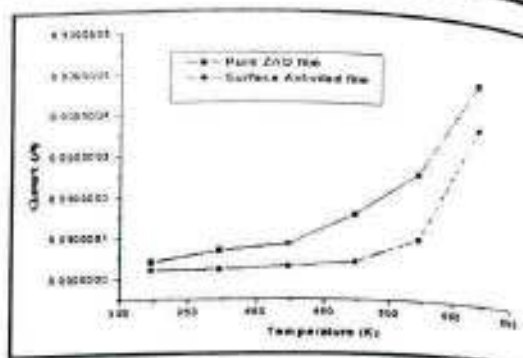
Fig 3: Variation of current with temperature

(conductivity) with reciprocal of temperature of pure and activated films. The conductivity values of all samples increase with increasingtemperature. They are nearly linear to 1000/T in the range from 100 to 250°C. The increase in conductivity with increasing temperature could be attributed to the negative temperature coefficient of resistance and semiconducting nature.
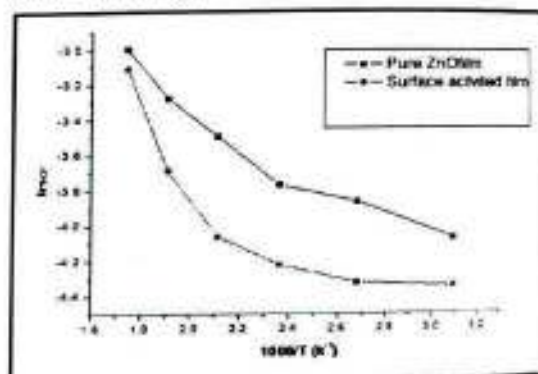
Fig 4: Variation of conductivity with reciprocal of temperature

6. Discussion:

Increasing in conductivity with temperature of ZnO may be due to large oxygen deficiency which could adsorb oxygen species at higher temperature. The adsorption phenomena of the Al$_2$O$_3$ modified ZnO thick film surface may be different form the pure ZnO thick films surface. The Al$_2$O$_3$ misfits on the surface are the places where the oxygen species adsorb. The Al$_2$O$_3$ misfits distributed evenly on the surface

would have made it possible to adsorb the oxygen ions even at low temperature. [14] Formfig 4 it is clear that conductivity of pure and Al_2O_3- modified ZnO films increases with an increase in temperature, indicating a positive temperature coefficient of conductance. This behavior confirmed the semiconducting nature of the pure and modified ZnO [15].

It is observed from fig 4 that the electrical conductivity of the pure ZnO film is higher than modified ZnO film in ambient air. It may be due to the intergranular potential barrier [14]. Pure ZnO has only one kind of grains arranged uniformly, where in the case of Al_2O_3 modified films the grains are of different natures such as Al_2O_3 and ZnO. The modification causes the formation of heterogeneous intergrain boundaries of the Al_2O_3-ZnO. Thus increased barrier heights of the intergranular regions of activated ZnO may be responsible to decrease the conductivity.

7. Summary :

Thick filmsof ZnO nanostructures were synthesized by a chemical precipitation method followed by sonication and their electrical properties were measured. The results demonstrated that the electrical conductivity of the pure ZnO film is higher than modified ZnO films in ambient air. Such nanomaterials with innovative structure can be used for future work such as gas sensing area.

References

[1] S. Pizzini, N. Butta, D. Narducci, M. Palladina, J. Electrochem. Soc., 136,(7), (1989), 1945-48.

[2] H.W. Ryu, B.S. Park, A.A. Sheikh, W.S. Lee, K.J. Hong, Y.J. Seo, D.C. Shin, J.S. Park, G.P. Choi, Sensors and Actuators B, 96, (2003), 717-722.

[3] S.T. Shishiyanu, T.S. Shishiyanu, 0.1. Lupan, Sensors and Actuators B, 107, (2005), 379-386.

[4] Can Li,Shunping Zhang, Mulin Hu, ChangeshengXie, Sensors and Actuators B, 153,(2011),415-420.

[5] M.C.Carotta,A.Cervi,v.di.Natale, Sensors and Actuators B, 137,(2009),164-169.

[6] M.Hubner, N.Barsan, U.Weimar, Sensorsand Actuators B,151,(2010),103-106.

[7] M.D.Rossell, AngewandteChemie-International Edition 50, (12), (2011) 2841-2844.

[8] Z. A. Ansari, Taegyung G. Ko, and Jae-Hee Oh, IEEE Sensor Journal, 5, (5), (2005), 817-824.

[9] G. Neri, A. Bonavita, G. Rizzo, S. Galvagno, N. Pinna, M. Niederberger, S. Capone, P. Siciliano, Sensor and Actuators B, 122 (2007) 564-571.

[10] M.D. Antonik, J.E. Schneider, E.L. Wittman, K. Snow, J.F. Vetelino, R.J. Lad, Thin Solid Films, 256 (1995) 247-252.

[11] V. Khatko, E. Llobet, X. Vilanova, J. Brezmes, J. Hubalek, K. Malysz, X. Correig, Sensor and Actuators B, 45 , (2005),111-112.

[12] W. Belkacem, A. Labidi, J. Guerin, N. Mliki, K. Aguir, Sensor and Actuators B, 132 (1),(2008), 196-201.

[13] G. H. Jain, M.S. Wagh, Sensors and Actuators B 123,(2007), 233-239.

[14] D. R. Patil, L.A. Patil , Sensors and Actuators B 123, (2007), 546- 553.

[15] KiCheol Park, Dae Young Ma, Kun Ho Kim, Thin solid films,305, (1997), 201-209.

Study of variation dielectric constant of 4:1 PS PMMA Polyblend thin films doped with Oxalic Acid in different weight proportions

A.S.Wadatkar[1*], T.S.Wasnik[1], S.G.Vidhale[1], N.G.Belsare [1]

[1]Department of Physics, Vidya Bharati Mahavidyalaya, Amravati (M.S.)- 444 602, India

Email : anantwadatkar@gmail.com

Abstract: The measurements of the dielectric constant (ε_r) of 4:1 PS PMMA polyblend systems doped with 0%, 5%, 10%, and 15%, Oxalic acid (OA) have been carried out in the temperature range 323 K – 373 K and at frequencies in the range 1 kHz – 1 MHz. The experimental results reveal that, dielectric constant (ε_r) increases with increase in temperature and concentration of dopant Oxalic acid (OA), whereas,, decreases with the increase of frequency.

Keywords: Polymethyl Methacrylate (PMMA),Polystyrene (PS), Oxalic Acid (OA), dielectric constant (ε_r).

Introduction:

We have used the polymers namely PS and PMMA. Among these PS is non-polar and PMMA is weakly polar. In the polar polymers, permanent dipoles can be assumed to be present. Such polymers can be treated as dielectrics. Such dielectrics have special properties of storing and dissipating electrical energy when subjected to electromagnetic fields. Studies of these materials particularly in a. c. fields provide an insight of the electrical nature of the molecular or atomic species which constitute the dielectric materials. This energy storing capacity of dielectric leads to the fabrication of capacitors (capacitance elements). In thin film capacitors, the dielectric materials are sandwiched between two electrodes. In our case, sample polyblend films had been sandwiched between two brass electrodes of the sample holder and as such the system constituted the capacitor. The presence of dielectric material between two electrodes increases the capacitance i.e. the storage capacity of electrical energy. The thin film capacitors are therefore extensively used in various devices such as in micro-miniature electronic circuits, memory devices, transducers in ultrasonic applications, etc. The study of a. c. field behaviour has been extensively carried out {Rajendran *et al.*(2002), Khaled *et al.* (2003), Raghavendra *et al.* (2003),} The behaviour of dielectrics in a.c. field gives us an idea about their polarization effects, dispersion of electromagnetic fields, both at audio and high frequency regions, relaxation phenomenon and a.c. conductivities.

Experimental Techniques

Sample Preparation:

Method of preparation of PS- PMMA Films without Dopant:

In the present work, Isothermal Evaporation Technique (Bahri and Sood 1983; Sangawar 1995) has been used, as it is best suited to the conditions in the laboratory. The two polymers PS and PMMA taken in the ratio 4:1 were dissolved in the common solvent Tetrahydrofuran (THF).The solution was kept for 3-4 days to allow polymers to dissolve completely to yield uniform solution. The solution mixture was then heated for 1 hour at 60°C to get completely homogeneous solution. A glass plate thoroughly cleaned with water and later with acetone was used as a substrate. To achieve perfect leveling a pool of mercury was

used in a plastic tray. The solution was poured on the glass plate and was allowed to spread uniformly in all directions on the substrate. The film on the glass substrate was then removed and cut into small pieces of suitable sizes. In this way the films were prepared by isothermal evaporation technique.

Method of preparation of PS PMMA Films Using dopant Oxalic Acid:

The 5 %, 10 %, and 15% of Oxalic acid (dopant) (means 0.125 gm, 0. 25 gm, 0.375 gm) were taken and dissolved in the mixture of 4:1 PS PMMA solution. After getting homogenous solution, the same procedure was repeated to prepare the films. The present study has been carried out with the following samples:

1) PS   PMMA + 0% Oxalic acid   [4:1 PSPMMA OA(0)]
2) PS   PMMA + 5% Oxalic acid   [4:1 PSPMMA OA(5)]
3) PS   PMMA +10% Oxalic acid [4:1 PSPMMA OA(10)]
4) PS   PMMA +15% Oxalic acid   [4:1 PSPMMA OA(15)]

Prominent Findings:

1.At constant frequency, Dielectric Constant (ε_r) increases with the increase of temperature. [Fig. 1 (a) to (d)]
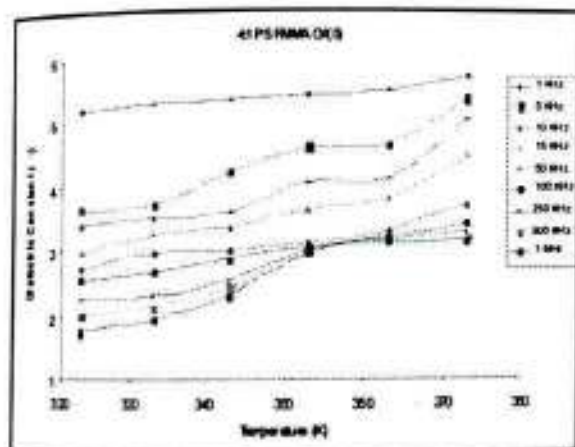
Fig. 1 (b)
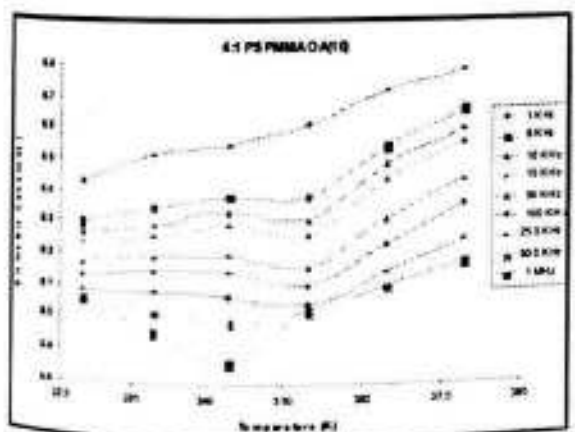
Fig. 1 (c)
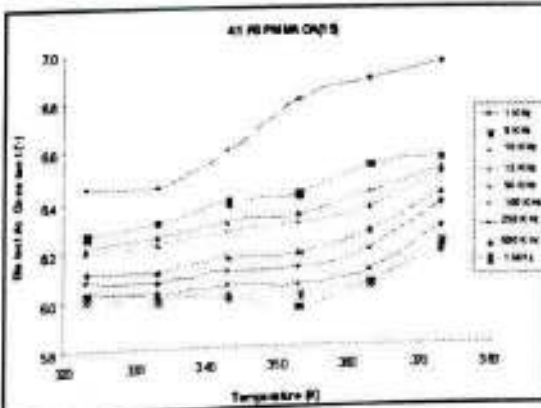
Fig. 1 (d)

Fig. 1 : Variation of Dielectric Constant (ε_r) with temperature at different frequencies for 4:1 PS PMMA OA system

2.At constant temperature, Dielectric Constant (ε_r) decreases with the increase of frequency. [Fig. 2 (a) to (d)]
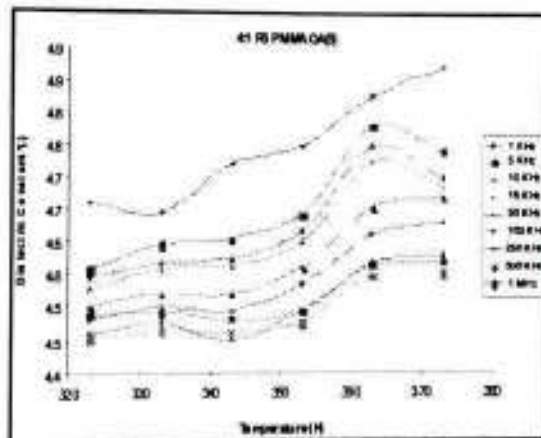

Fig. 2 (a)

Fig. 2 (b)

Fig. 2 (c)

Fig. 2 (d)

Fig. 2 : Variation of Dielectric Constant (ε_r) with frequency (Ln f) at different constant temperatures for 4:1 PS PMMA OA system

3.At constant temperature and frequency Dielectric Constant (ε_r) increases with the percentage of dopant. [Fig. 3 (a) to (c)]

Fig. 3 (a)

Fig. 3 (b)
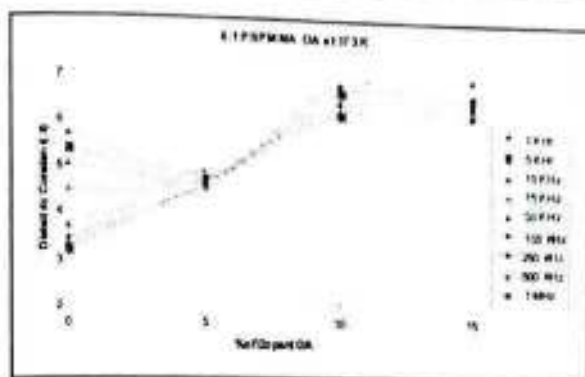
Fig. 3 (c)

Fig. 3 : Variation of Dielectric Constant (ε,) with Concentration of dopant at various frequencies at temperatures (333K, 353 K, 373K) for 4:1 PS PMMA OA system

Discussion of Results:
Effect of frequency and temperature on dielectric constant:

In the present study we have noticed that
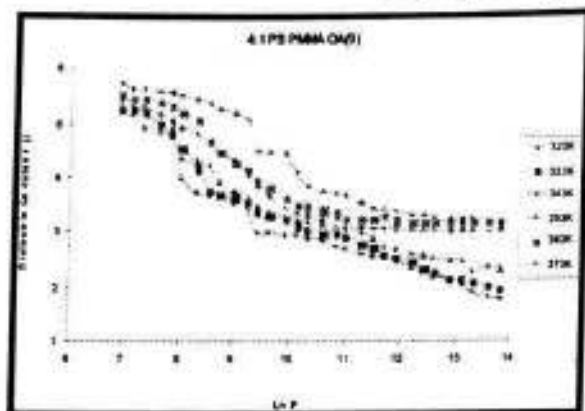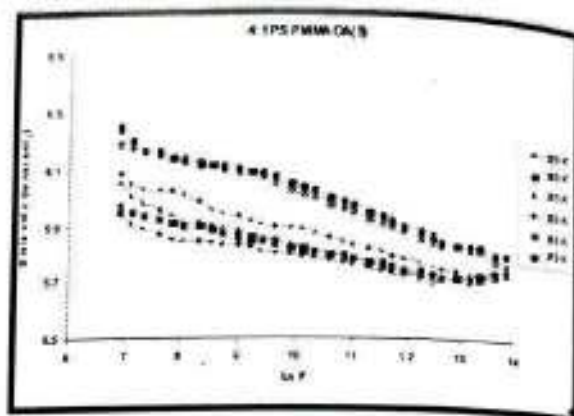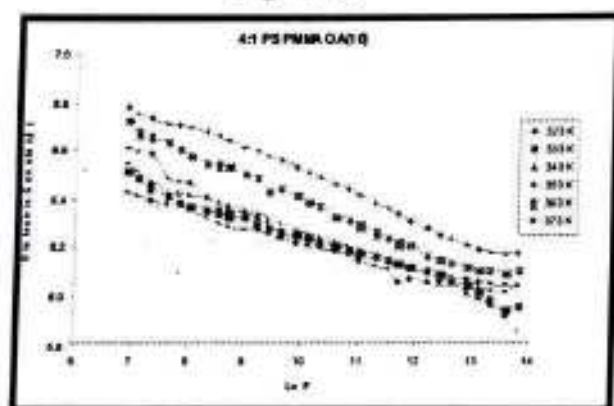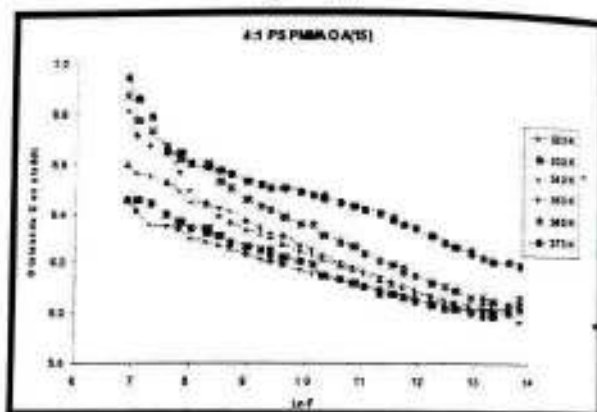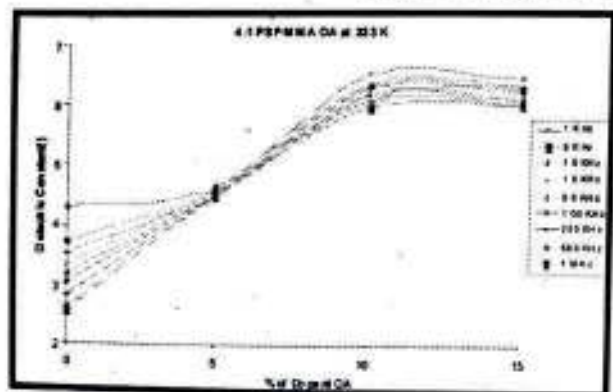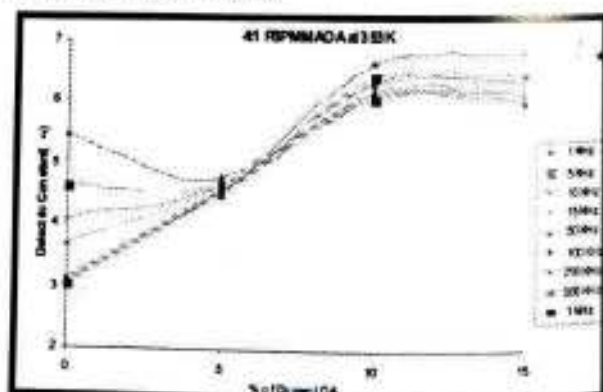1) At constant frequency, Dielectric Constant (ε,) increases with the increase of temperature.
2) At constant temperature, Dielectric Constant (ε,) decreases with the increase of frequency. 3) At constant temperature and frequency Dielectric Constant (ε,) increases with the percentage of dopant.

We have observed that the dielectric constant of our sample decreases with frequency and increases with temperature. This can be explained on the basis of the polarization and polarisability of the dielectric samples as follows:

When a dielectric is introduced in an electric field applied across two plates of a capacitor (two metal electrodes), the polarization of the dielectric takes place. This (polarization) is accompanied by the neutralization of some charges on the plates of the capacitor due to the induction resulting in the increase of the storing capacity of electric field. This arises from two main causes, namely:
a) aligning the polar species in conformity with the applied field.
b) altering the distribution of electric charges of the molecules constituting the dielectric.

The latter process (b) occurs for the

polar (PMMA) and non-polar (PS) species. The effect of high frequency field in (b) is less than that of the slow varying or static fields (except for cases where the field frequency is in resonance with the natural frequency of the molecules).

Thus the dielectric behavior of a macroscopic body is due to the dipolar nature of the constituent atoms or molecules. As such, there is a definite link between the macroscopic polarization and the molecular dipole moments.

The microscopic behaviour of a dielectric material such as the doped polyblends PS-PMMA under an electric field can be understood from the polarization phenomenon of the charged species which constitute a dielectric or which are introduced during its preparation. These may be extra-nuclear electrons and positively charged nuclei, anions and cat-ions, oppositely charged ionized impurities, charged molecular species, etc.

The oppositely charged species (i.e. having equal and opposite charges) with a reasonable bond (attractive force) between them will form a dipole. This dipole will behave as one unit. These dipoles under an electric field may undergo spatial translational or rotational displacement which will be reflected in the macroscopic behaviour of the dielectric. The polarization effect will also be dependent on the nature of the dipoles and the

frequency of applied electric field.

Dielectric constant or relative permittivity (ε_r) is the ratio of absolute magnitude of the permittivity (ε) of a medium to the permittivity (ε_0) of free space. Or it is also defined as the ratio of the capacitance (C) of the capacitor with dielectric to that of capacitance (C_0) without dielectric. (Keeping the plate dimensions and separation distance same).

$$\varepsilon_r = \frac{\varepsilon}{\varepsilon_0} = \frac{C}{C_0}$$

Thus the increase in dielectric constant is due to the greater freedom of moment of dipole molecular chains within the polymers blends. At lower temperatures as the dipoles are rigidly fixed in the dielectric, the field cannot change the condition of dipoles. As the temperature increases, the dipoles comparatively become free and they respond to the electric field. This causes the increase of polarization and hence the dielectric constant increases with temperature. {H. Frohlick, Theory of Dielectrics, University Press (Oxford 1956), p.13}.

Effect of dopant on Dielectric Constant:

It has been made clear that the addition of dopants Oxalic Acid impart polar character to PS PMMA polyblends. As a result the number of charge carriers and dipoles increases with the increase in the concentration of dopant. Consequently the dielectric constant increases with the dopant concentration.

Conclusions:

For the samples under investigation i.e. blends of 4:1 PSPMMA doped with 0%, 5%, 10% and 15% Oxalic acid:
1) At constant frequency, Dielectric Constant (ε_r) increases with the increase of temperature.
5) At constant temperature, Dielectric Constant (ε_r) decreases with the increase of frequency.
6) At constant temperature and frequency Dielectric Constant (ε_r) increases with the percentage of dopant.

REFERENCES

[1] Anderson J. C. (1964); *"Dielectrics"*, Chapman and Hall, London.

[2] Frohlich H., (1948); *"Theory of Dielectric"*, Oxford University Press, Oxford.

[3] Kaelble " Handbok of X-rays" (McGraw Hill Book Co. USA) Vol. 21,(1967) 61.

[4] McCurum N. G., Read B. E. and Williams A. (1967), *"An Elastic and Dielectric effects in Polymeric Solids"*, Wiley Sons, New York.

[5] Muhammad Akram, Athar Javed and Tasneem Zaher Rizvi (2005);Turk J. Phys.,29, 355-62.

[6] Raghavendra S. C., Syed Khasim, Revanasiddappa M., Ambika Prasad M. V. N. and Kulkarni A. B. (2003), Bulletin of Material Science, 26 (7), 733-39.39.

[7] Rajendran S., Mahendran O. and Kannan R. (2002); Materials Chem. and Physics, 74, 52-57.

[8] Rao Vijayalakshmi, Ashoakan P.V. and Shridhar M. H. (2000).; Material Science and Engg., (Elsevier), A281, 213-220.

[9] Reda S. M., Dyes and Pigments (Elsevier) Vol. XX. (2006), 1-7.

[10] Seanor D .A. (1982); *"Electrical[Properties of Polymers"*, Vol 15. 25,

[11] Seanor D.A.(1967); Proc 1957 NAS/NRC Conf. Insula Dielect Phenomenon, London. New York P 1-57.

[12] Sessler, G.M. and West, J.E. (1976); Journal of Applied Physics Vol 47, 3480-3484.

[13] Tager A., Physical Properties of Polymers (MIR Publication, Moscow), 2 ᵃ Ed. (1978) 306 -590.

Schottky -Richardson Mechanism in Oxalic acid Doped (PVC-PMMA) Blends

Dakre A. B[1], Lamdhade G.T [2]

[1]Department of Physics, P.R. Pote (Patil) College of Engineering & Management, Amravati (M.S.) India -444604

[2]Department of Physics, Vidya Bharati Mahavidyalaya, Camp, Amravati (M.S.) India -444602

Abstract: *We have measured the electrical conductivity of Oxalic acid doped Polyvinyl Chloride (PVC)- Polymethyl Methacryalate (PMMA) blends at temperatures (313K - 373K). The current voltage characteristic of blends does not obey the power law and there is absence of ohmic conduction. The electrical conduction mechanism discussed by various models such as Poole–Frenkel, Fowler– Nordheim, Schottky ln(J) Vs T plots, Richardson and Arrhenius Plots. Out of this, Schottky - Richardson mechanism is conscientious for the observed conduction mechanism in the Polyblends.*

Keywords: PVC, PMMA, Polyblends, Oxalic Acid

1. Introduction

The blending of two polymers is found to be new polymeric material which new materials may be promising candidate than indivisible polymer [1]. There are many investigations on polymer blending [2]. The conductivity study gives the origin of the charge carrying species, their number, and the way in which they move through the bulk of the material. These parameters are interlinked with the chemical composition of the microstructure and the morphology of the particular material.

The electrical conductivity of organic solid shows complex conduction behavior, while the conductivity due to electrons excited from valence band to conduction band is negligible [3,4]. The complex conduction behavior can be explained in terms of electron emission from cathode i.e. Schottky - Richardson mechanism [4] or by liberating electron from the traps in the bulk material, i.e. Poole–Frenkel mechanism [5]. In addition to there is also possibility of tunneling [6] or Fowler–Nordheim mechanism [7], space charge limited conduction [8], etc occurs. In case of polymer films space charge limited conduction, Poole-Frankel and Richardson-Schottky emission and tunneling mechanism generally discussed. When the applied field is sufficiently high and the electrode makes ohmic current with the polymer then the charge carriers are injected into the polymer by lowering of the barrier at the metal – insulator interface, this effect is known as Richardson-Schottky (RS) emission.

PVC is a polar molecule and one of the most important commercially available polymer due to its light, electrical & chemical resistant and it has the ability to get mixed with other to produce verity of compounds which has a wide range of physical & chemical properties.

PMMA is strongly polar and it is a hard, rigid and transparent polymer which has good outdoor weatherability and it has more impact resistance than glass. PMMA is a versatile polymer showing plenty of application. Blends of these two polymers are expected to yield strong and long lived electrets useful for industrial application. Both PVC-

PMMA are rigid polymers but by blending PVC with PMMA make the resultant blend soft & open to make useful applications. Many researchers reported the electrical conductivity and experimental observations in PS-PMMA [9], PVC-PMMA blends [10], [11], [12]. The conductivity studies on PVC-PMMA polymer blends electrolytes shows stability [10].

In the present study, the electrical conductivity of PVC-PMMA blends doped with Oxalic acid was measured to identify the mechanism of electrical conduction in the polyblends. The electrical conduction mechanism discussed by various models such as Poole–Frenkel, Fowler–Nordheim, Schottky ln(J) Vs T plots, Richardson and Arrhenius Plots.

2. Experimental

The polymers, PVC (Aldrich) and PMMA (Otto kemi, Mumbai) in 1:4 weight proportions were dissolved in 20 ml solvent cyclohexanone (SD Fine Chemicals, Mumbai) respectively. Oxalic acid used as a dopant in these selected polymers. The dopant & polymer mixture were mixed together and this mixed solution was kept in a stand for three days so as to get the complete homogenous dissolution of blends. After three days, the solution mixture was poured on perfectly plane and chemically clean glass plate, which is kept floating freely in a pool of mercury for perfect horizontal leveling. It was, thereafter, allowed to evaporate in air at room temperature. Further, it was dried for 48 hrs. to remove any traces of solvent.

The dried film was removed from the plate and cut into small pieces (samples) of desired size, which were then coated on both sides with silver paste (Eltecks Corporation, Bangalore) so that electrical contact hold very well. The polyblends films of PVC-PMMA doped with 5%, 10%, 15% Oxalic acid (wt. percentage) were prepared by the same method given above but the results are only interpreted for doping of 15% Oxalic acid due to the significant change in conduction of blends. The thickness of the polyblends film was measured

by using Digital Micrometer screw gauge (Mitutoyo Corporation, Japan, Least Count 0.001mm) is found to be 56 µm. These polyblends films were kept between the electrodes of a specially designed sample holder having gold plating. The variation between current and voltage measured by using Keithley 6487 Picoammeter / Voltage source meter instruments at various constant temperature.

3. Results & Discussion

3.1. I-V characteristics of Polyblends

The I-V characteristics of 1: 4 (PVC-PMMA) doped with 15% Oxalic acid is represented by lnI - lnV plots at various temperatures 313K, 323K, 333K, 343K, 353K, 363K and 373K are shown in figure 3.1. The current increases non-linearly with the applied voltage and does not follow a Power law $I = kV^m$ where, k and m are constant.
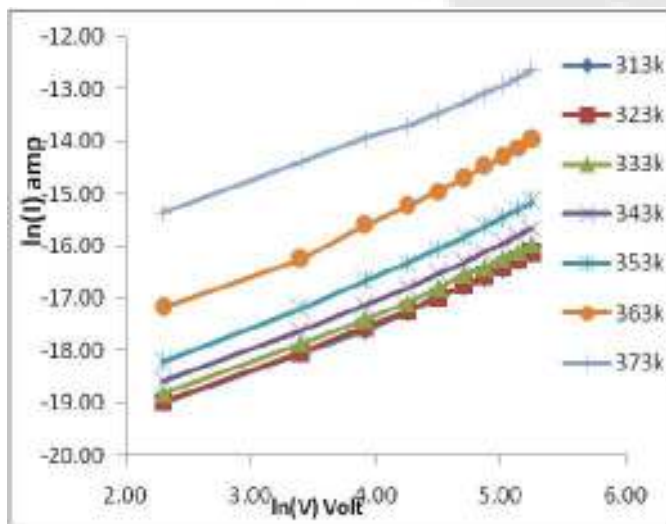
Figure 3.1: I-V characteristics

It is seen from the figure 3.1 that, the current increases nonlinearly with applied voltage at constant temperature and also the current increases with increase in temperature at constant applied voltage). The possibility of ohmic conductions as well as space charge limited conduction is ruled out from the observed behavior of *I–V* characteristics. As we know the compositions of blends are insulators and blends are almost non-crystalline, which give rise to wide scope for irregularities in the structure therefore there is absence of ohmic conduction.

3.2. Poole–Frenkel Mechanism

The Poole-Frenkel relation [5] for the current density is given by the equation 3.1 ,

$$J = B \exp\left(\frac{-\phi}{kT} + \beta_{PF} E^{\frac{1}{2}}\right) \tag{3.1}$$

Where, $\beta_{PF} = \frac{e}{2}\left(\frac{e}{\pi\varepsilon_0}\right)^{\frac{1}{2}} = $ constant

and e = electronic charge which predicts a field -dependent conductivity as,

$$\sigma = \sigma_0\, e^{\frac{\beta_{PF} E^{\frac{1}{2}}}{2kT}} \quad \text{or}$$

$$\log\sigma = \log\sigma_0 + \frac{\beta_{PF}}{2kT} E^{\frac{1}{2}} \tag{3.2}$$

So that, the Poole -Frenkl mechanism is characterized by linearity of $\log\sigma$ Vs $E^{\frac{1}{2}}$ plots with positive slope. In this present case of 1: 4 (PVC-PMMA) doped with 15% Oxalic acid the $\ln\sigma$ Vs $E^{\frac{1}{2}}$ plots are linear with negative slope (figure 3.2) indicating the absence of Poole-Frenkl mechanism.
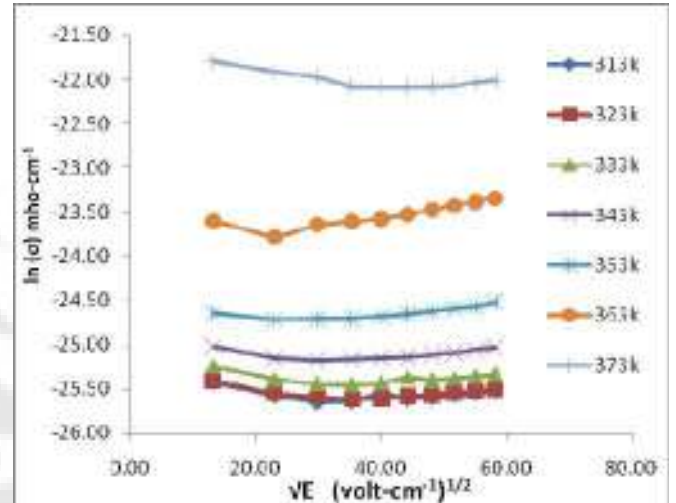
Figure 3.2: Poole-Frenkel Plot

3.3. Fowler– Nordheim Mechanism:

The Fowler -Nordheim Relation for [7] current density J can be expressed by equation 3.3.

$$\log \frac{J}{V^2} = \log A - \frac{\beta}{V} \tag{3.3}$$

and $\log \frac{J}{V^2}$ Vs $\frac{1}{V}$

Plots is expected to be a linear With a negative slope .

In this present case the $\log \frac{J}{V^2}$ Vs $\frac{1}{V}$ plots for 1: 4 (PVC-PMMA) doped with 15% Oxalic acid is represented by figure 3.3. Excepting few plots which have strayed away the graph are nearly straight lines with a positive slope indicates the absence of tunneling current as is suggested by Fowler -Nordheim mechanism.
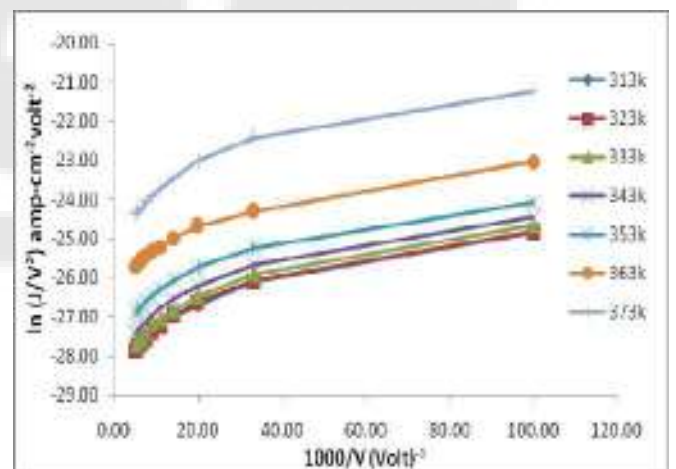
Figure 3.3: Fowler-Nordheim Plot

3.4. Schottky – Richardson Mechanism

2198

The Schottky – Richardson current voltage relationship is expressed by the equation 3.4.,

$$\log J = \log AT^{-4} - \frac{\phi_s}{KT} + \beta_{sn} E^{\frac{1}{2}} \qquad (3.4)$$

and that log J Vs $\sqrt{E}$ Plot referred to a Schottky Plots should be a straight line with positive slope.

For the present case, Schottky plot are shown in figure 3.4.1 below. The linear positive slope indicates that Schottky - Richardson mechanism is applicable to the process in 1:4 (PVC-PMMA) with 15% O.A.
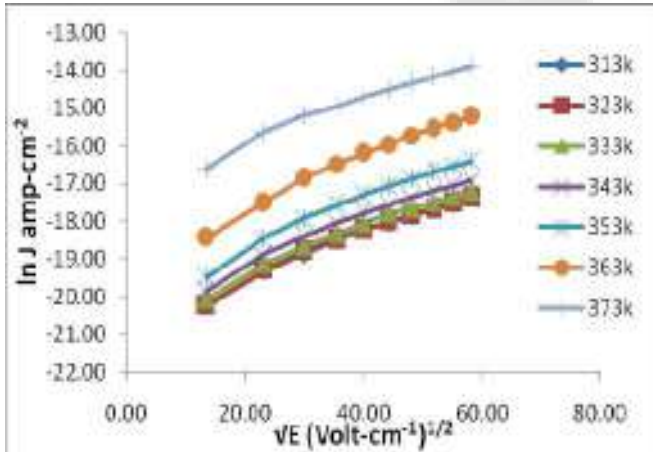
Figure 3.4.1: Schottky Plot

Further, in the case of Schottky – Richardson mechanism the current shows strong temperature dependence but not in case of Poole -Frenkel mechanism. The study of temperature dependence of current density is therefore of great importance.

The temperature dependence of current density is represented plot of ln (J) verses temperature shown in the figure 3.4.2, observed that ln (J) increases almost linearly with change in the temperature. The temperature dependence is great agreement with the Schottky -Richardson Mechanism. Further that the slopes of all the lines are nearly same for all the fields, shows that, no thermodynamic transition occurs in the temperature range studied.
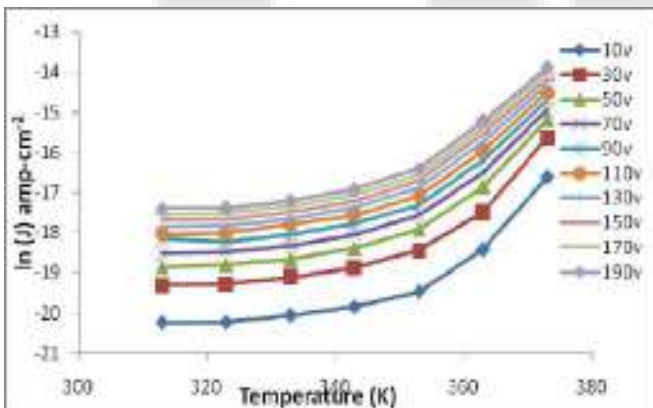
Figure 3.4.2: Current density Ln (J)Vs Temperature Plot
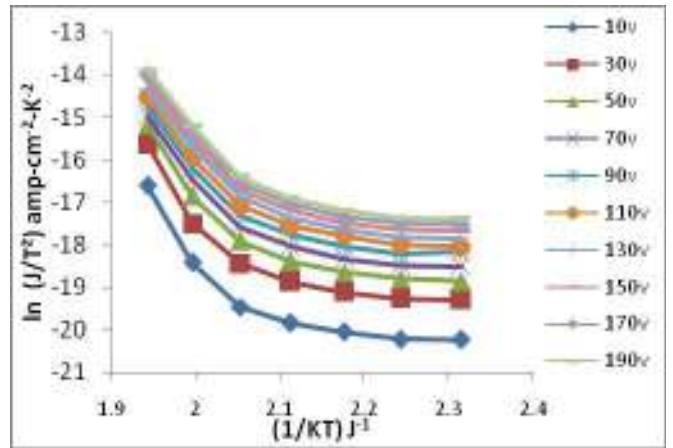
Figure 3.4.3: Richardson Plot

From the relation 3.4 we can plot the variation between Ln(J/T^2) versus (1/KT) shown in fig. 3.4.3 Richardson Plot, it is observed from plot, it should be a straight line with a negative slope. In our case such a straight line graph have been obtained with a negative slope. This shows the linearity of the plot which supports to Schottky- Richardson Mechanism.

3.5. Arrhenius Mechanism

The ln (σ) verses 1/T plots at all values of applied voltage is shown in figure 3.5., the conductivity of polymer is mostly dependent on the temperature. As the temperature increases polymer becomes soft and mobility of the main chain segment as well as the rotation of the side group becomes easier [13]. Thus at higher temperature more & more dipoles are oriented resulting in the higher equivalent surface charge density i,e. as the temperature increases conductivity also increases in accordance with the Arrhenius equation given by relation 3.5.

$$\sigma = \sigma_0 \ \exp\left(\frac{-E_a}{KT}\right) \qquad (3.5)$$

where , σ_0 - is the pre-exponential factor, E_a- is activation energy and K- Boltzmann constant
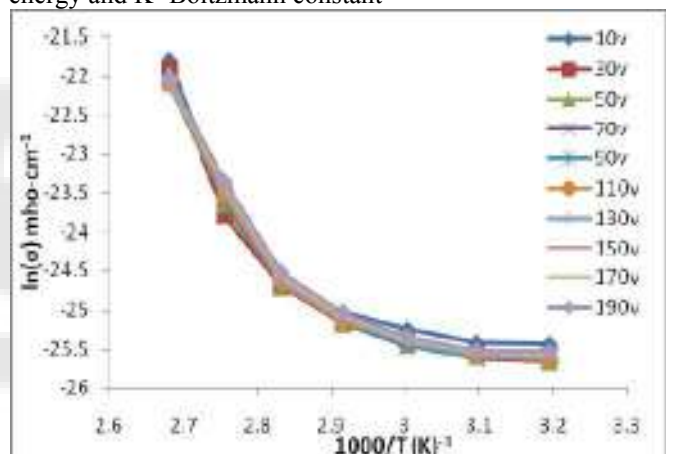
Figure 3.5: Arrhenius plot

From the slope of straight line the activation energy is calculated & is found to be in the neighbored of 0.1eV.This is in good agreement with the reported earlier.

4. Conclusions

The observed conduction nature at higher fields and temperatures is found to be Richardson-Schottky emission. Due to the formation of charge transfer complex, there exist a link between the dopant molecules and polymer molecules in amorphous region. Schottky and Richardson mechanism of conduction predominates over other mechanism in the doped sample. The applied field seems to be insufficient to liberate electrons from the trapping centers (dopant molecules) showing absence of the Poole–Frenkel mechanism.

References

[1] Utracki L.A., Polymer Alloys and Blends, Carl Hanser, Munich, FRG, (1990).
[2] Aravindan V., Lakshmi C., Vickraman P., Current Applied Phys. 9, PP1106-1111 (2009).
[3] Khare Pavan and Shrivastav A P, Indian J. Pure Appl. Phys. 29, pp1410 (1991)
[4] Schottky W Z, Phys. 15, pp872 (1914)
[5] Frenkel J, Phys. Rev. 54, pp647 (1938)
[6] Mann A T, J Appl Phys , 35, pp217 (1964)
[7] Fowler R H and Nordheim L, Proc. R. Soc. London 119, 173 (1928)
[8] Rose A, Phys. Rev. 97, pp1538 (1955).
[9] Belsare N. G., Deogaonkar V. S., Indian J. Pure & Appl. Phys. 36, pp280 (1998).
[10] Rajendran S., Uma T., Electrolytes Mater. Letts, 44, pp242-247 (2000).
[11] Waghmare R. V., Belsare N. G., Raghuwanshi F. C. and Shilaskar S. N., Bull. Mater. Sci., 30, pp167- 172 (2007).
[12] Belsare N.G, Wadatkar A.S., Joat R.V. Wasnik T.S., Raghuwanshi F.C.,Raulkar K.B. Lamdhade G. T. Journal of Electron Devices, Vol. 11, pp583-587, (2011).
[13] Sangawar V. S., Dhokne R.J., Ubale A.U., Chikhalikar P.S., , Meshram S.D., Bull. Mater. Sci., 30/2 , pp163–166, (2007).

Author Profile

**Ms. Archana B. Dakre** has received her B.Sc. degree in 1996, M.Sc. degree in 1998 from Sant Gadge Baba Amravati University, Amravati, Maharashtra State, India. Recently she is registered for Ph. D. degree in the Sant Gadge Baba Amravati University, Amrvati. Presently she is working as Assistant Professor at Department of Physics, P.R. Pote (Patil) College of Engineering & Management, Amravati since last four years and she has also ten years teaching experience in the UG and PG level. She has published two research papers in reputed international journals and two research papers presented in conference. Her current interests of research are synthesis and characterization of Polymers, polyblends, polymer electrolyte and gas sensors etc.

Dr. G. T. Lamdhade has received his B.Sc. and M. Sc. Degrees from Sant Gadge Baba Amravati University, Amravati, Maharashtra State, India. in the years 1996 and 1998 respectively. He obtained his Ph.D. degree in year 2003 from Sant Gadge Baba Amravati University, Amravati. Currently he is an Associate Professor in the Department of Physics, Vidya Bharati Mahavidyalaya, Amravati. He has fifteen years teaching experience at UG and PG Level classes, currently five students are working for Ph.D. Degree under his guidance and five students have been awarded by M.Phil. Degree under his guidance. He is also supervised fourteen M.Sc. Physics students for completion of dissertation/project. He is working as members on various committees of college administrative and university administrative also. He is working as a editorial board member, review members, referee, expert, members on many international/national journals and he has completed one research project sanctioned by UGC and one major research project is in progress. He has published more than thirty five research papers in reputed international journals and conferences. His current interests of research are in synthesis of metal oxides nanoparticles, Polymers, polyblends, polymer electrolyte, nanocomposites, Humidity sensors etc., characterizations and their applications as chemical gas sensors, thin and thick film sensors etc.

"Appliaction of Polypyrrole for CO₂ Gas Sensing at Different Tempetetures"

R.M.Agrawal*, G.T.Lamdhade , K.B. Raulkar , F C Raghuwanshi

Department of Physics ,Vidya Baharati Mahavidyalaya, Amravati.444602. India.

Email: rohit_agrawal1985@rediffmail.com

Abstract: In this paper we have prepared the Al_2O_3-ppy multilayer thin films sensor for the CO_2 gas detection. The sensor (Al_2O_3+PPY) shows the maximum sensitivity towards CO_2 gas detection at room temperature (303K). The plot showed the linear nature against concentration of CO_2 gas. The sensitivity of the different sample difference is due to the properties of metal oxide material and high porosity of materials. The sensitivity of the samples was found to be increasing with the change in the concentration of CO_2 gas.

The sensing mechanism is described as the surface oxygen atom absorbed when the sensor is exposed to the CO_2 gas. A p-n junction like structure is formed where at equilibrium flow of electron form lower work species to the higher work species. As the flow of electron increases there will be decrease in the electrical resistance with the increase in CO_2 gas concentration.

Key Words: Polypyrrole, Al_2O_3, CO_2 Gas.

1. Introduction: Recently, the solid state gas sensor based on the semiconducting metal oxides has becoming a promising alternative and have a good sensing properties. There have been several oxides tested Al_2O_3 doped with the polypyrrole has been reported. Electronic polymer has many excellent features: flexibility, functionality, processing and economics, etc.; among them, electronic function sensitive polymer, such as physical, chemical and biological, and their composites have been especially notable in the improvement of the modern electronic materials [1-4]. However, compression of the response of Al_2O_3 doped described in these studies gives discrepancies variation in the resistance. In the present study (Al_2O_3+PPY) multilayer thin films response only become applicable at CO_2 gas concentration so these sensor is more suitable for the high concentration application.

2. Experimental:

In the present work we have selected semiconducting metal oxides Al_2O_3 and Polypyrrole (AR grade).The chemicals in the powder formed are mixed with different stiochiometery in mol % as $(Al_2O_3$-ppy). The Polypyrrole (ppy) was prepared by taking 1.892 gm of Ferric chloride $(FeCl_3)$ which was added with the 7 ml of methanol. 0.84 ml of Polypyrrole monomer was taken in beaker. After that, these two solutions are combined with the constant string. This processes is done in the dark place and then it was allowed to kept it for 8 Hr. Then the above solution is washed with the methanol and dried it. After drying we get black colour precipitates as the ppy. The materials used for gas sensor are generally prepared in the form of multilayer thin films.

Initially, the material was calcinated at 700°C for 5 Hr by using the furnace in the air atmosphere, so as to remove the impurities. Then the material was crushed to make a fine powder by using moter pestel. This calcinated powder was weighted on monopan balance (K-Roy, India) with the proper mole % percent of Al_2O_3 and ppy. The Ethyl Cellulose (EC) and

Butyl Carbitol acetate (BCA) used as a binder for making multilayer thin film by using screen printing technique. After making these thin films the film were subjected to heating at 80°C for 1 hrs in the vacuum oven.

In the multilayer thin film for the surface conductance measurement the electrode was made on film by using silver paint which was formed on adjacent sides as shown in fig 1.
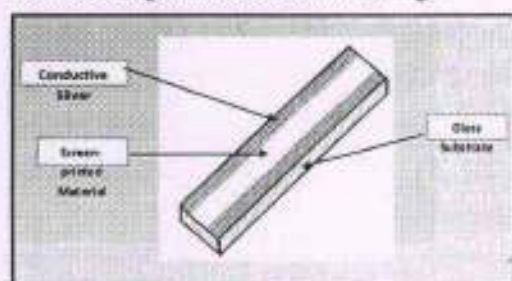
Fig 1. Screen- printed glass substrate (Sensor)

Again, these multilayers thin films were subjected to heating for 50°C for 15 min for drying the silver paint and the sample code surface area weight of film and thickness are listed in Table 1.

Sample code	Composition	Thickness of film(mm)
P1	Al_2O_3	1.38 mm
P2	Al_2O_3+Ppy	1.343 mm
P3	Ppy	1.313 mm

Table. 1

The crystalline size was calculated from the full width at hail maximum of the first peak using the Scherer's formula [5]. The electrical resistance of the thin films was measured by voltage drop method which was adopted by Yawale et al [6]. When CO_2 gas starts to flow via inlet to the chamber, then resistance of the thin film is change. We measured the output voltage by using voltage drop method at specific time instant with the help of stopwatch. With the help

if this voltage, study the variation of sensitivity with CO_2 gas concentration was done. The constant flow of CO_2 gas, a gas flow meter (FLOWTRAN make, India) was used. The sensitivity the device characteristics of perception a variation in electrical properties of the sensing material under gas exposure and it can be defined as in the equation

$$Sensitivity \ (S) = (Rg-Ra)/Ra \ If \ Rg > Ra \tag{1}$$

$$Sensitivity \ (S) = (Ra-Rg)/Ra \ If \ Ra > Rg \tag{2}$$

where, Rg is the change in resistance of the sensor in presence of gas /vapors and Ra is the original resistance of sensor in presence of air. Where Rg is the change in resistance of the sensor in the presence of gas vapors and Ra is the original resistance of sensor in the presence of air.

3. Result and Discursion:

In the present study the variation in CO_2, gas concentration with the electrical resistivity, conductivity and sensitivity have been studied. Figure (a,b,c) shows the variation of sensitivity with CO_2 gas concentration at room temperature for multilayer thin film P1,P2 and P3 respectively.
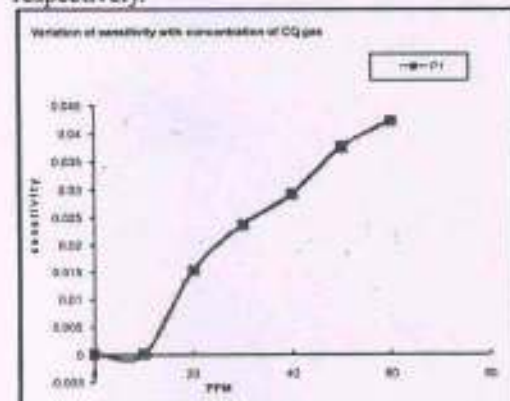
Figure (a)

From figure it is observed that; P2 sensor has maximum sensitivity and P1 and P3 sensor showed minimum sensitivity. Also change in sensitivity of P2 sensor is more as compare to P1 and P3 sensors. The Sensitivity
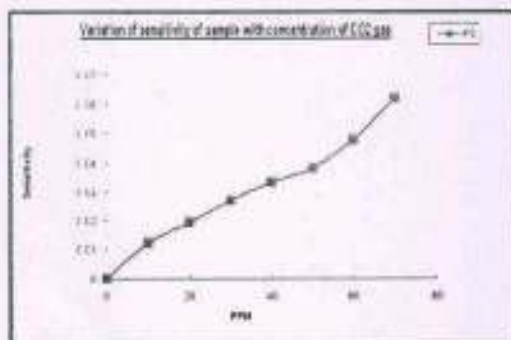
Figure (c)
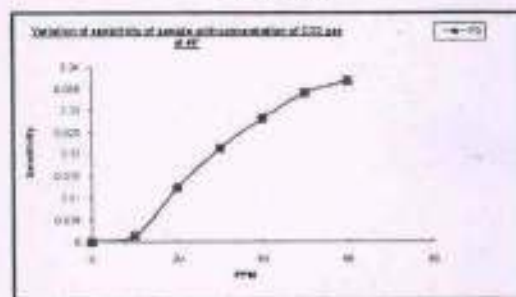
Figure (d)

The resistance of the sample decreases with increase in the concentration of CO_2 gas. The resistance of the P2 is more than the resistance of P1 and P2.As the resistance of the sample decreases the conductivity of sample increases.
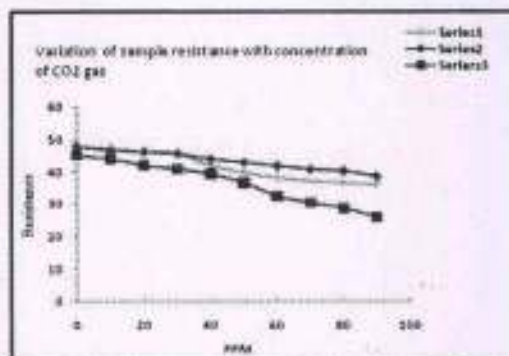
The surface morphology of polypyrrole material was studied by SEM and its picture is

shown in the Fig.
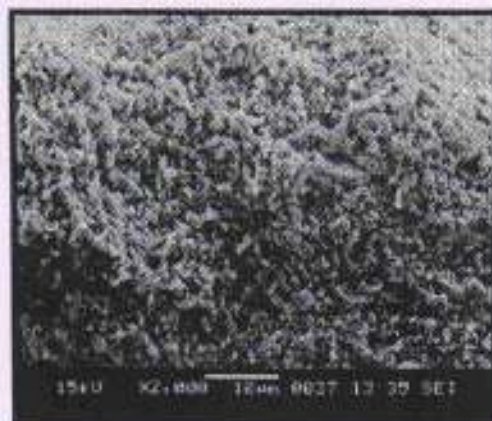
From SEM picture, it is observed that Ppy is more porous in nature and pore size varies from ~ 0.5 to 3 μm. Due to small pores size, its surface area is more and it shows more sensing nature. Some portion of SEM picture shows some rods with fine voids over them which helps to increase sensing properties.

Refrences:
[1]   M. Onoda, S. Morita et al., J. Appl. Phys. 32 _1993. 3534–3539.
[2]   E.M. Genies, M. Lapkowskc, Synth. Met. 24 _1998. 69.
[3] .   H. Shimehara, T. Chiba, M. Aizwa, Sens. Actuators 13 _1988. 79.
[4]   F. Selampthar, L. Toppare et al., Synth. Met. 68 _2. _1995. 109–116, January.
[5]   O.K. Tan, W. Zhu, Q. Yan, L.B. Kong, Sensors and Actuators B, 65,361-365,(2000).
[6]   S . P . Y a w a l e , S . S . Y a w a l e , G.TLamdhade, Sensors and Actuators , Article in press (2006).

EFFECT OF CYPERMETHERIN ON THE OVARY OF FRESHWATER FISH
Channa striatus

V. T. TANTARPALE[a1] AND S. H. RATHOD[b]

[ab]P. G. Deppartment of Zoology, Vidya Bharati Mahavidyalaya, Amravati, Maharashtra, India

ABSTRACT

Now day's enormous use of pesticides is the issue of increasing in pollution which affects the non targeted organisms. Animal living in the water are exposed to the pesticides are used in the agriculture field. The present study was carried to measure the impact of pesticide cypermethrin on the gonad that is ovary of freshwater fish *Channa striatus*. Alteration of ovary showed the structural, physiological and morphological changes in freshwater fish *Channa striatus*. Oocyte showed shrinkage and interfollicular oedema, as well as yolk of the oocyte cells showed damage and rupture membrane of the oocyte showed stromal hemorrahage was observed.

KEYWORDS : *Channa striatus*, ovary, cypermetherin, stromal hemorrahage

Pollution is the impairment of the quantity of some part of the environment of quality and by addition of harmful impurities. The increased use of insecticides in agriculture has contributed to the improvement of agriculture production. However many adverse effects have been recognized. The mode of action of these compounds has been subjected to intensive study. Like that pollutants the domestic sewage is also biggest harmful substances this sewage accumulates day by day and it is hazardous to environment not only in rural areas pollution it posed a threat for the survival of fish and other aquatic organisms in the estuarine ecosystem but also in urban area. The sewage is mixed with water sources and caused the, water quantity and even anesthetic quantity

Use of different pesticides in agriculture to prevent the crop from pest has increased especially in developing countries Santhakumar and Balaji, 2000. These pesticides, even when applied is restricted areas are washed and carried away by rains and flood to large water bodies like ponds and river and alter the physiochemical properties of water which are proved to be highly toxic, not only to fishes but also to other organisms, Madhav Prasad et al., 2002. The well documentary effect of pesticides on the physiology of fish includes its effect on reproductive organs. Cypermrthrin is a synthetic pyrethroid used widely to control a variety of insect pest, Crossdland, 1982 state that low concentration of cypermethrin is toxic to many species of aquatic organism. Increase use of pesticides not only helped in controlling insects and pests but also threaten to environmental contamination specially hazardous to aquatic fauna.

MATERIALS AND METHODS

The experimental fish of *Channa striatus* were collected from the local Wadali lake around Amravati region. They were washed with $KMnO_4$ solution to avoid dermal infection the fish were acclimatized to the laboratory condition for 15 days. During this period fish were fed on commercially available food .For experimental purpose the pesticide mixture was prepared by dissolving sufficient amount of pesticides in 1000 ml of water. A calculated quantity of stock solution was added to the water in the experimental aquarium. All fishes of average size that is (10-13cm) and weight (13-25gm) were used. After acclimatization of 10-15 days fishes has become divided into two groups:

GROUP I - Control fishes

GROUP II Experimental treated fishes

Group I fishes was kept in the cypermethrin free water and served as control and Group II freshwater fishes *Channa striatus* were treated to sub lethal concentration of synthetic parathyroid a cypermethrin. The LC_{50} values were calculated 0.00078 µl/lit at 96 hrs exposure period.

Then after the interval of 24, 48, 72, 96 hours from each group fish was taken out for the dissection and dissected out ovary of both controlled and treated fishes of different time interval. For observed the effect of cypermethrin an ovary of *Channa striatus*, after dissection proceed for the histological slide preparation and slides observed under the microscope.

---

[1]**Corresponding author**

Plate 1 : Ovary of control *Channa striatus*

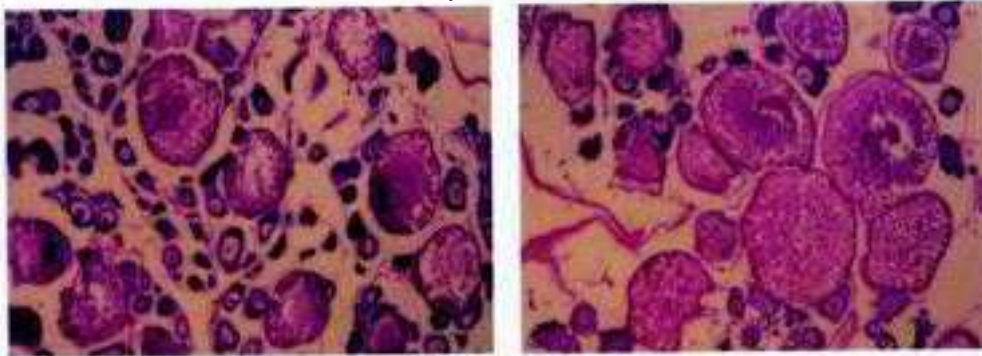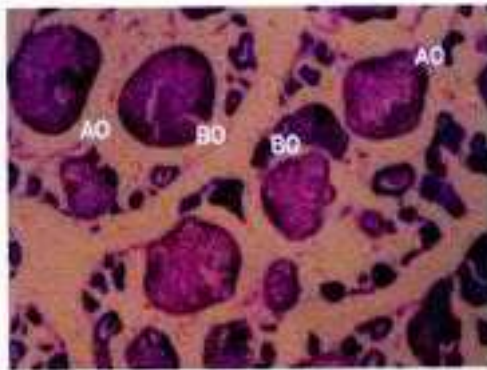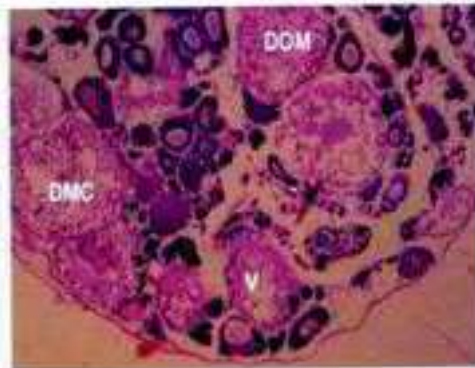**Plate 2 : Effect of sublethal concentration of Cypermethrin exposed to fresh water fish Channa striatus at different hours**
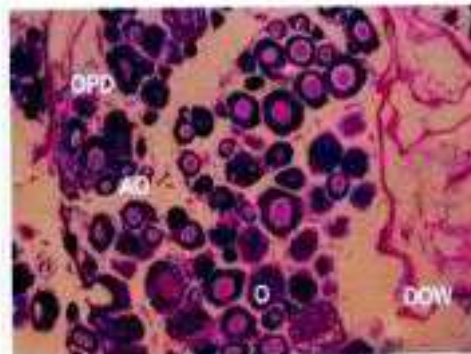

24 Hours

48 Hours

72 Hours

96 Hours

BO - Breakage Oocyte

YFO - Yolk Floats Outside

OPD - Ooplasam Disrupt

DMC - Disrupt of Matured Follicle

V - Vacuolation

AO- Atretic Oocyte

DOM - Disorganised Membrane

VF - Vacuole Formation

DOW - Disorganised Ovrianl Wall

O - Odema

OBSERVATIONS AND RESULTS

In the present study freshwater fish *Channa striatus* exposed to sub lethal concentration of cypermethrin showed the structural, physiological and morphological changes. The treated fish observed flabbyed and degenerative ovarian follicle. It showed degeneration and nacrosis in oocytic cells. Also showed shrinkage and interfollicular oedema in oocyte. The yolk of the oocyte cells showed damage and rupture membrane of the oocyte. Stromal hemorrahage were observed as compared to normal fish ovary. Treated fish ovary showed atretic oocyte, irregular shaped of oocyte. Also showed floating of contents due to rupture of cell membrane, so vacuole formed at the center of the oocyte. The Ovarian follicle rupture, ooplasm of the ovarian cells was disorganized. The stromal hemorrhage clearly observed .In this present investigation the ovary of fresh water fish *Channa striatus* exposed to cyermethrin were found to the disrupt, rupture and degenerate. Primary and secondary growth of oocyte was highly affected due to pesticide. Accumulated and forms vacuole. Atretic oocyte membranes of degenerated oocyte were observed prominently (Plate 1 and 2).

DISCUSSION

In the present study synthetic pyrethroid a cypermethrin was treated with fresh water fish *Channa straitus*. The Oocyte cell showed histological and morphological changes. Similar finding were observed by Dutta (1996) showed low concentration of fenetrothion and carbaryl arrested the vitallogenic growth of oocytes in *Channa punctatus*. Also observed in *G. giruris* exposed to sub lethal levels of malathion resulted in significant reduction in the ovarian weight and affected primary oocyte and impairment of vitellogenesis; Adityakumar et al., 2002, Chandra et al., 2004, Ghosh and Nath, 2005.

Similar findings by Khillare, 1992 observed oocyte maturation and arrest of oocyte development in tertiary yolk stage; Lee and Yang, 2002 observed at the dose of 100 ppm of sumithion, fragmented ova with abnormal shape and arrangement were observed in the experimental fish as compaired to normal. Jyothi and Narayan, 1999 reported the impact sub lethal concentration of carbaryl on the ovary of *Clarias batrachus* arrest of ovarian growth.

CONCLUSION

In the present study indicated that the pesticides cypermethrin exposed to fresh water fish *Channa straitus* at different time duration, Which affected the ovary of fishes, the disturb, rupture and degenerate ovary as compared to normal. So concluded that the very lower concentration of pesticides affect the physiology of fish , due to this it impact on yielding of the fishes.

REFERENCES

Aditya, Ajit Kumar, Sanjiv Chattopadhyay and Shyamal Mitra, 2002. Effect of mercury and Methyl parathion on the ovaries of *Laleo rohita* (Ham) J. Environ Biology **23(1)**: 61-64.

Chandra S., R.N. Ram and I. J. Singh, 2004. First ovarian maturity and recovery response in common carp, Cyprinus carpio after exposure to carbofuran J. Environ. Biol. **25(3)**: 239.

Crossdland N. O., 1982. Aquatic toxicology cypermethrin, Fate and biological effect in pond experiment. Aqua. Toxicol : 205-222.

Dutta H.M., 1996. A composite approach for evaluation of the effect of pesticides on fish, fish morphology, :249-277.

Ghosh J. and Panchanan Nath, 2005. Seasonal effect of melathion on ovary and plasma gonodotropin and vitellogenin levels in intract and pinealectomized catfish (Linn). India Journ. of exprim Biol. **43**: 224-225.

Jyothi B. and Narayan G., 1999. Toxic effect of carbaryl on gonads of fresh water fresh *Clarias batrachus* J. of Environ, Biol. **20(1)**: 73-76.

Khillare M., 1992. Effect of ammonium sulphate an oocyte development of fish *Barbus stigma* (Ham.) Adv. Biosci. **11**: 75-78.

Lee W. K. and S.W. Yang, 2002. Relationship between ovarian development and serum levels of gonadal steroid hormones, and induction of oocyte maturation and ovulation in the cultured female Koran spotted seabass lateola brax macutlatus (Jeom-nong-co.) Aquaculture 207:169-183.

Journal of Pharmaceutical and Scientific Innovation

www.jpsionline.com

Research Article

PROTEIN AND AMINO ACID MODULATION IN FRESH WATER FISH *OPHIOCEPHALUS ORIENTALIS* EXPOSED TO CYPERMETHRIN

Gijare Shruti S.* and V. T. Tantarpale

Vidya Bharati Mahavidyalaya Camp, Amravati, Maharashtra, India

*Corresponding Author Email: shruti_pande17@rediff.com

ABSTRACT

Cypermethrin, a synthetic pyrethroid showed non-target effects on the freshwater fish *Ophiocephalus orientalis*. The presents study showed the impact of sub lethal concentration (0.0007 μ/lit) of cypermethrin on the concentration of protein and amino acid in two tissues such as liver and muscle of freshwater fish *Ophiocephalis orientalis* at different time intervals. Decrease in protein level was observed in both tissues liver and muscle. But there was observed increase in amino acid level in both tissues muscle and liver of *Ophiocephalus orientalis* at different time intervals.

Keywords: Cypermethrin, liver, muscle, protein, amino acid.

INTRODUCTION

Water is main component of the environment which is dynamic entities. It has an effective means of transfer and transport of the waste and other materials. Soil on the other hand is stationary entities, which are indirectly affected by the contaminated water. Toxic waste dumped on a soil may cause harm to the animals and indirectly to human being. The structure and function of lotic ecosystems changed due to pollutants.[1] The toxic effect of contaminated water on non target organisms is observed by[2,3]. One among the environmental problems is the lack of proper management of domestic and industrial wastes which release hazardous chemicals. There is no doubt; these excessive levels of pollutants are causing a lot of damage observed in human and animal health. The organic pollutants may cause declines, deformity and death of autistic life, which in turn cause disease to humans[4-6]. The aquatic environment is very important because it is a store house of variety of fishery resource. Presently aquatic pollution a serious problem thought out the world. It has been estimated that about 70,000 manmade chemicals are used day to day. These chemical have contributed a lot to the green revolution but their deleterious effects on various ecosystems cannot be ignored[7].

MATERIALS AND METHODS

The freshwater fish *Ophiocephalus orientalis* were collected from Wadali lake around Amravati region, India. The fishes were acclimatized at laboratory condition for 1 week. The LC_{50} value was calculated by probity analysis method[8]. The LC_{50} value is 0.0007 μ/lit at 72 h. The acclimatized fishes were exposed to sub lethal concentration for 24 h, 48 h, 72 h and 96 h; simultaneously a control group of healthy fishes were maintained under identical conditions. The fishes were sacrificed at the end of exposure period and liver and muscle were processed for the biochemical estimation. Protein was estimated by the method of Lowry's[9] and amino acid was estimated by the method of Moor and Stein[10].

RESULT

The protein contents in the liver and muscle of the freshwater fish *Ophiocephalus orientalis* exposed to sublethal concentration of cypermethrin at different time intervals and it showed declined trend as compare to control values. Due to toxic effect of cypermethrin, the process of protein synthesis get altered and an increase in proteolysis activity and possible utilization of its products for metabolic purposes. The amino acid contents in the liver and muscle of the freshwater fish *Ophiocephalus orientalis* exposed to sublethal concentration of cypermethrin at different time intervals and it showed raised trend as compare to control value. Rised in amino acid level were the result of breakdown of protein for energy and impaired in association of amino acid in protein synthesis.

Figure 1: Changed in liver, protein of fish *Ophiocephalus orientalis* exposed to sub lethal concentration of cypermethrin at different time interval
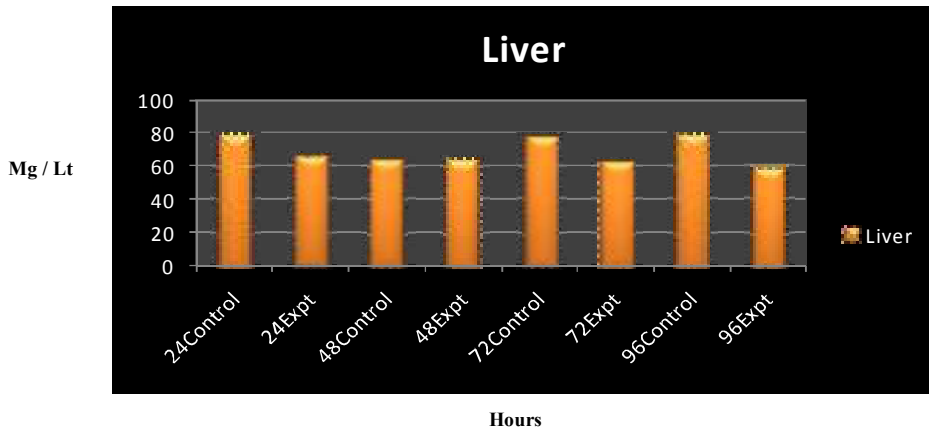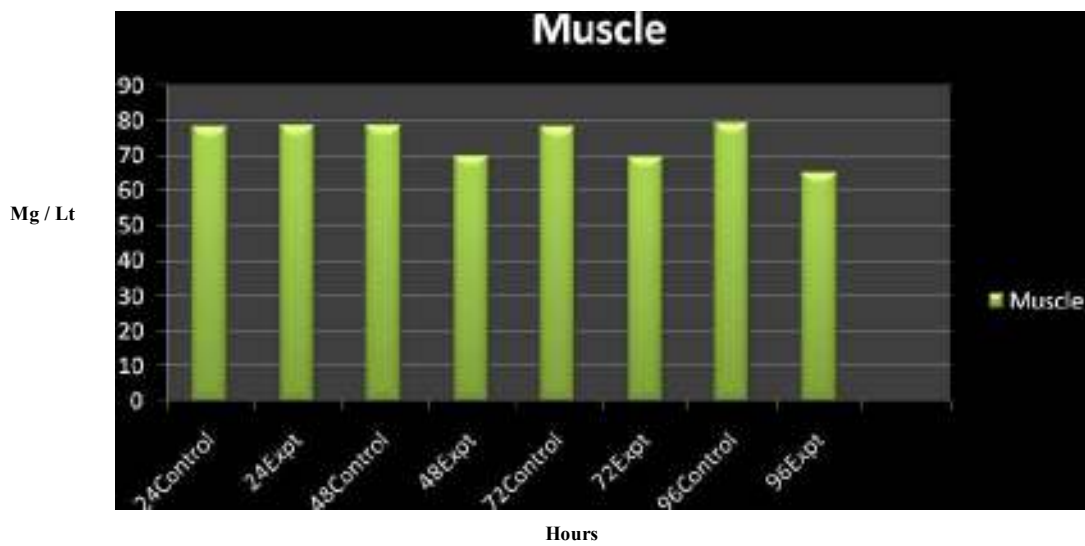

Figure 2: Changes in the Muscles, protein of fish *Ophiocephalus orientalis* exposed to sub lethal concentration of cypermethrin at different time interval
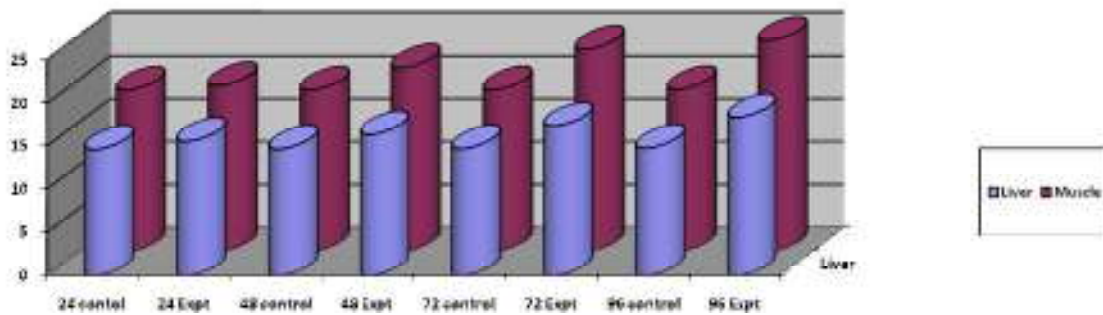

Figure 3: Changed in the Liver and muscle amino acid of the freshwater fish *Ophiocephalus orientalis* exposed to sublethal concentration of cypermethrin at different time interval

DISCUSSION

In the present study observed that there was significant decrease in total protein of muscle and liver tissues of freshwater fish *Ophiocephalus orientalis* at different time interval exposed to sublethal concentration of cypermethrin. The similar study is given by the[11] on the fresh water fish *Channa striatus* and found that there was toxic effect of cypermethrin on the liver and muscle protein level it decreases at different exposure period.

Also supported by[12], observed that there was effect of cypermethrin on protein content of rainbow trout *Oncarhynchus mykiss*. The depletion of protein fraction in liver, muscle and kidney may have been due to their degradation and possible utilization for metabolic processes. Similar results were also found by[13-17].

The protein level showed decreased trend in Nile Tilapia, *Oreochromis niloticus,* in response to the treatment of cypermethrin by[18]. In *Clarias gariepinus* exposed to cyhalothrin decreased protein observed by[19], in common carp. *Cyprinus carpio* by[20,21]; observed the decreased in protein level of due to effect of cypermethrin in freshwater teleost *Colisa fasciatus*. Also the increase in the amino acid level was observed under the toxic effect of a synthetic pyrethroid, cypermethrin exposed to freshwater fish *Ophiocephalus orientalis*.

Amino acids are considered one of the most reliable techniques for the detection of changes in protein synthesis in cell and therefore, the protein pattern can be used as a criterion for the differentiation between several organs exposed to some pollutants.

The similar study was also given by[22], on the freshwater fish *Cirrhinus mrigala*. The toxic effect of cypermethrin also showed increased trend in *Cirrihinus mrigala*[23], observed that there was increase in the amino acid level in the tissues of *Labeo rohita* and *Cirrhinus mrigala* exposed to fenvelerate. Similar increase of amino acid in *Labeo rohita* exposed to endosalfan was observed by[24].

The freshwater fish *Clarias batrachus* exposed to cypermethrin, showed increase level of amino acid in muscle and kidney of fish[25,26], observed that piscicidal activites of aqueous extract of *Euphorbia tirucalli* on freshwater fish *Chanaa punctatus* were altered the level of amino acid.[27] reported the effect of cypermethrin on gill, liver and muscle of freshwater fish *Tilapia mossambica* that increase in amino acid.

Similar study was also given by[28], observed that the increase in amino acid level in liver of *Channa maruius* when exposed to dimethoate and monocil.

Concluded that protein decreased because of more utilization due to pesticidal stress also which breakdown protein released amino acid in the tissue which was used in prolonged period.

REFERENCES

1. Schafer Ralf Bernhard, Thierry Caquet, Katri Siimes, Ralf Mueller, Laurent Lagadic and Matthias Liess. Effects of pesticides on community structure and ecosystem functions in agricultural streams of three biogeographical regions in Europe. Science of the total environment 2007; 382: 272-285. http://dx.doi.org/10.1016/j.scitotenv.2007.04.040
2. Burger J, F Mol and B Gerowitt. The necessary extent of pesticide use Thought about a key term in German pesticide policy Crop. Prot 2008; 27: 343-351. http://dx.doi.org/10.1016/j.cropro.2007.06.006
3. Mariyona J. Direct and Indirect impacts of integrated pest management on pesticide use. A case of rice agriculture in Javam Indonesia. Pest Manag. Sci 2008; 64: 1069-1073. http://dx.doi.org/10.1002/ps.1602
4. Diana TC and KS Ramulu. Observations of carbohydratelevels in liver and intestine of N. japonicus in relation to *Klebsiella* species infection. J. Pure and Appl. Microbiol 2009; 3(2): 715-718.
5. Diana TC and KS Ramulu. Changes in the protein content of liver and intestine in relation to *Klebsiella* infection in Nemipterus japonicus from the coast of Visakhapatnam, India. The Asian. J. of Animal Science 2010; 4(2): 143-145.
6. Rejomon G, Nair M and T Joseph. Trace metal dynamics in fishes from the southwest coast of India. Environ. Monit. Assess 2010; 167(1-4): 243-255. http://dx.doi.org/10.1007/s10661-009-1046-y
7. Hari P and P Neeraja. Ambient ammonia stress on certain metabolic aspects in liver tissue of fish, *Cyprinus carpio*. The Bioscan 2012; 7(11): 111-113.
8. Finney DJ. Probit Analysis. University Press Cambridge; p. 333.1971.
9. Lowry OH Rosenbrough, NJ Farr AL and RJ Randall. Protein measurement with folin phenol reagent. J. Biol. Chem 1951; 193: 265-267.
10. Moore S and GN Stein. A Modified rinhyain reagent for the photometric related compounds. J. Biol. Chem 1954; 211: 907-813.
11. Tantarpale SA. Cypermentrin impact on total protein in muscle and liver of the freshwater fish *Channa striatus*. Sci. Res. Repot 2011; 1(3): 155-158.
12. Atamanalp M, Keles MS Halilorglu HI and MS Aras. The effects of cypermethrin (A synthetic pyrethroid) on some biochemical parameters of (Ca, P, Na, and Tp) of Rainbow trout (*Oncorhynchus mykiss*). Turk. J. of Biol 2002; 26: 1157-1160.
13. Vutukuru SS. Acute effects of hexavalent chromium on survival oxygen consumption Hematological Parameters and some Biochemical's profiles of Indian major carp, *Labeo rohita*. Int. J. Environ Res. Public health 2005; 2(3): 456-462. http://dx.doi.org/10.3390/ijerph2005030010
14. Venktramana GV, Sadhya Rani PN and PS Murthy. Impact of malathion on the Biochemical parameters of gobid fish, *Glossogobius giurus* (Ham) J. Environ. Biol 2006; 27(1): 119-122.
15. Mamata Kumari. Biochemical changes induced by the pesticides abate in the liver of catfish *Heteropneutes fossilis* (Bloch). Environ and Eco 2007; 225(4): 1164-1166.
16. Muley DV, Karanijikar DM and SV Maske. Impact of industrial effluents on the biochemical composition of freshwater fish *Labeo rohita*. J. Environ.Biol 2007; 28 (2): 243-249.
17. Chezhian A, Kabilan N, Kumar St, Senthamilselvan D and K Sivakumari. Impact of common mixed Effluent of spicot industrial Estate on histopathological and biochemical changes in Estuatine fish *Lates calcorifer*. Curr. Res. J of Biol. Sci 2010; 2(3): 201-209.
18. Korkmaz NEL, Cengiz E Unlu, E Uysal and M Yanar. Cypermethrin-induced histopathological and biochemical changes in Nile tilapia (*Oreochromis niloticus*) and the protective and recuperative effect of ascorbic acid. Environ, Toxicol. and Pharmacol 2009; 28(2): 198-205. http://dx.doi.org/10.1016/j.etap.2009.04.004
19. Ogueji EO and J Auta. Investigation of Biochemical Effects of Acute Concentrations of Lambda- Cyhalothrin on African Catfish *Clarias gariepinus*-Teugels. J. of Fisheries Inten 2007; 2(1): 86-90.
20. Dobsikova R, Velisek J, Wlasow T, Gomulka P, Svobodova Z and L Novotny. Effects of cypermethrin on some haematological biochemical and histopathological parameters of common carp (*Cyprinus carpio* L.). Neuro Endocrinol Lett 2006; 2(27 Suppl.): 91-5.
21. Sing KS, Singh SKS and RP Yadav. Toxicological and biochemical alteration of cypermethrin (Synthetic Pyrethroids) against freshwater teleost *Colisa fasciatus* at different seasons. World J. Zool 2010; 5(7): 25-32.
22. Neelima PL, Cyril Arun Kumar J, Chandra Sekhara Rao and N Gopala Rao. Impact of cypermethrin 25 % EC on free amino acids and protease activity levels in the freshwater fish *Cirrhinus mrigala* (HAM). The Bioscan 2011; 6(3): 421-423.
23. Anita ST, K Sobha, K Veeraiah and KS Tilak. Studies on biochemical changes in the tissues of *Labeo rohita* and *Cirrhinus mrigala* exposed to fenvelerate technical grade. J. Toxicol. and Envi. Health. Sci 2010; 2(5): 53-62.
24. Sarvanan M Kumar, DV Malarvizhi A and M Ramesh. Bio safety of *Azadirachta indicia* (A. Juss) leave extracts on certain biochemical parameter of *Labeo rohita*. J. Bio pesticide 2010; 3(1): 227-231.
25. Begum Ghousia. Cypermethrin-Induced Biochemical perturbation in freshwater fish *Clarias batrachus* at sub lethal exposure and after released into freshwater. Drug. Chem. Toxicol 2007; 30(1): 55-65. http://dx.doi.org/10.1080/01480540601017686
26. Tiwari S and A Singh. Biochemical stress response in freshwater fish *Channa punctatus* induced by aqueous extracts of *Euporbia tirucalli* plant. Chemosphere 2006; 64(1): 36-42. http://dx.doi.org/10.1016/j.chemosphere.2005.11.049
27. Prashanth, Mahanthinamatha Shankaraiah Hiragond, Ningappa Changond Nikam and Kedari Nanasaheb. The effect of cypermethrin on

different tissues of freshwater fish *Tilapia mossambica* (Perters). J. of Basic Physiol. Pharmacol 2011; 22(4): 115-119.

28. Prasad BB, KM Singh and M Rani. Dimethoate and monocil toxicity on the concentration of protein and amino acid in the serum and liver of *Channa maruleus* (Ham). Nat Environ. Pollut. Tech 2002; 1: 147-150.

QUICK RESPONSE CODE	
	ISSN (Online) : 2277 –4572
	Website http://www.jpsionline.com

Effects of Cypermethrin on Lipid and Cholesterol Contents of Freshwater Fish *Channa Orientalis* (Bloch).

| **Shruti S, Gijare** | Vidyabharati Mahavidyalaya, Camp, Amravati.(MS) |
| **V.T. Tantarpale** | Vidyabharati Mahavidyalaya, Camp, Amravati.(MS) |

ABSTRACT

Water pollution is a major global problem that requires ongoing evaluation and revision of water resource policy at all levels. The water pollution is an acute problem in developing and industrialized countries. Fishes are very sensitive to a wide variety of toxicants in water and the deleterious effects of pesticides on fishes can be easily established. Ophiocephalus orientalis, freshwater fish exposed to sublethal concentration(0.0007μ/lit) of cypermethrin at different time intervals. Lipid and cholesterol contents were observed from liver and muscle after exposure period. There were decreased in lipid and cholesterol content at different time intervals.

KEYWORDS   Ophiocephalus orientalis, cypermethin, lipid, cholesterol.

INTRODUCTION:-

Pesticides are an integral part of present day agricultural technology. They are greatly contributing towards increasing world food supply by protecting the crop yield. Due to intensive development of agriculture in recent years and rapid growth of industrialization in our country, there has been a great increase in manufacture and utilization of fertilizers, pesticides, petrochemical products, detergents and other synthetic chemicals and pose a serious threats to the water ecosystem. Pesticides and related chemicals destroys the delicate balance between species and a functioning ecosystem (Khan and Francis,2005).

Pesticides are not highly selective but are generally toxic to many macrophytes, non-target organisms such as fish (Ayoola,2008; Franklin et al.,2010). Acute exposures of fish to pesticides result in some biochemical changes, causing some interference. Every living organism has its own so called detoxification mechanism to get rid of foreign substances in the body, however if toxic substances are encountered in higher concentration, they are bound to bring severe adverse effects (Satyavardhan 2010).

Some of the biochemical alteration occurring in the body gives the first indication of the stress in the organism and hence effect on the part of the pollution (Venkataramana et al.,2006; Rathod et al.,2009). The biochemical studies are good parameters which help to see the effects of toxicants on metabolism of fish (Kajare et al.,2000). In present investigation, an attempt has made to find out effect of cypermethrin on lipid and cholesterol constituents from liver and muscles of experimental fish, Ophiocephalus orientalis.

MATERIALS AND METHODS

The freshwater fish Ophiocephalus orientalis were collected from Wadali lake around Amravati region. The fishes were acclimatized at laboratory condition for 1 week. The LC_{50} value was calculated by probit analysis method (Finey,1971) . The LC_{50} value is 0.0007μ/lit. at 72hrs. The acclimatized fishes were exposed to sub lethal concentration for 24hr, 48hr, 72hr and 96hrs. Simultaneously a control group of healthy fishes were maintained under identical conditions. The fishes were sacrificed at the end of exposure period and liver and muscle were processed for the biochemical estimation. Lipids were estimated according to the method of Floch et al., (1957) . and cholesterol content was estimated with the help of Leiberman Burchad method by King and Wolten (1959).

RESULTS:-

The sublethal concentration of cypermethrin treated with Ophiocephalus orientalis at different time interval and observed that in the liver and muscle lipid showed declined trend. The lipid level declined in liver that is, 19.85±1.58, 18.67±1.68, 16.32±1.78, 15.66±1.79 as compared to control value 20.30±2.00 and in muscles that is, 9.89±1.58, 8.88±1.78, 7.45±1.68, 6.96±1.48 as compared to control value 10.30±3.00.

Lipids in liver and muscles of fish Ophiocephalus orientalis were decreased due to exposure to cypermethrin. Lipids constitute very rich energy reserve, it showed decrease trend indicates the changes in energy demand of fish during exposure to cypermethrin.

The sublethal concentration of cypermethrin treated with Ophiocephalus orientalis at different time interval and observed that in the liver and muscle cholesterol showed declined trend. The cholesterol level after exposure to cypermethrin was declined in liver that is, 10.38±0.07, 10.38±0.07, 10.36±0.02, 10.15±0.03 as compared to control value 11.45±0.70, 10.97±0.50, 10.96±0.50, 10.30±1.02 respectively. The cholesterol level declined in muscle that is, 0.89±0.06, 0.62±0.02, 0.51±0.03, 0.47±0.02 as compared to control value 1.35±0.93,1.24±1.00, 1.11±0.1, 1.00±0.5. The reduced cholesterol level due to the inhibition of cholesterol biosynthesis in the liver and reduced absorption of dietary cholesterol.
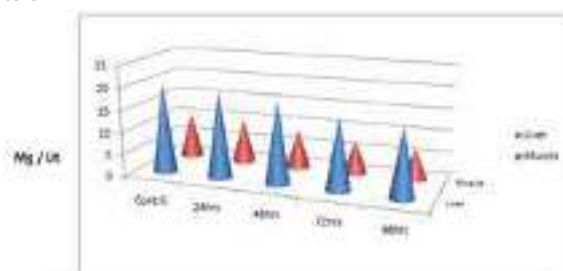

Fig.No.1Changed in the Liver and muscle lipid of the freshwater fish Ophiocephalus orientalis exposed to sublethal concentration of cypermethrin at different time interval. (Mg/lit).
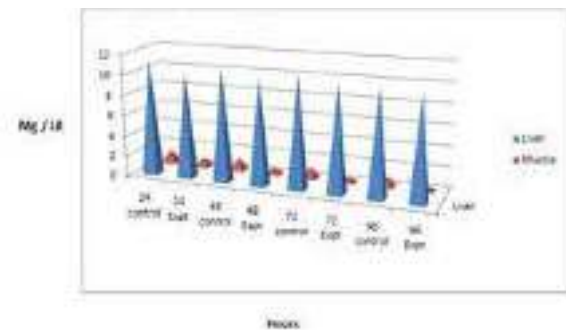
Fig.No.2 Changed in the Liver and muscle cholesterol of the freshwater fish Ophiocephalus orientalis exposed to sublethal concentration of cypermethrin at different time interval.(Mg/lit).

DISCUSSION:-

In the present investigation, cypermethrin exposed to freshwater fish Ophiocephalus orientalis. The level of lipid content decreased in liver and muscle tissues. Lipid plays an important role in energy metabolism and provide energy to metabolic processes. They are also important for cellular and sub-cellular membrane. It is used as energy reservoir, stored and transported in the form of glycerol ester. These decreased in lipid content in tissues suggested that the lipid have been channelized to meet the metabolic demand for extra energy needed to mitigated the toxic stress. Similar finding was given by Patil and Patole,(2012) that the effect of malathion and cypermethrin on lipid constituents of freshwater fish Lepidocephalicchthys guntea. They observed that, the level of lipid content decreased significantly in all treated groups,.

Lipid level decreases significantly because liver is the principle site of detoxification in fishes (Dixith, 2005). Stalin and Das, (2012) were observed the decrease in lipid levels in the liver tissues of Cirrhina mrigala exposed to fenthion.

The level of cholesterol content decreased in liver and muscle tissues. The reduced cholesterol level due to the inhibition of cholesterol biosynthesis in the liver and due to reduced absorption of dietary cholesterol. There was also depletion in the lipid content of fish Tilapia mossambica exposed to monocrotophos reported by Remia et al., (2008).

Ganeshwade (2012), reported that there was decrease in cholesterol content in the liver and muscle tissues of freshwater fish Punctius ticto. Due to dimethoate toxicity stress which suppressed lipid metabolism and leads decrease value of cholesterol Choudhary and Gaur (2001); Shindhe et al., (2002). Cholesterol is an important normal body constituent used in the structure of cell membrane synthesis of bile acid and synthesis of steroid hormones. Significant decrease in cholesterol content is studied in fish Oreochromis niloticus by Kahtani, (2011).

REFERENCES

Ayoola S.O. (2008): Toxicity of glyphosate herbicide on Nile tilapia (Oreochromis niloticus) juvenile. Afr. J. Agric . Res. Vol.3(12) : pp. 825-834. | Chodhary, A. and Gaur S. (2001): Effect of sodium fluoride on the muscle and liver of a freshwater fish I. J. Aqua. Biol.Vol. 16(2) :pp. 67-68. | Dixit Y.B. (2005): Biochemical changes in the liver of a freshwater teleost, Heteropneustes fossilis (Bloch) exposed to rogor J. Zool Vol.25:pp.51-53. | Finney,D.J. (1971) : Probit Analysis. University Press Cambridge. pp.333. | Folch, J.N. Leer and Sloane, G. Stanley (1957) : Simplified method for isolation and purification of total lipids from animal tissues, J. Bio. Chem 226- 497. | Franklin R.K., H.S.Loo and H.A. Osu.anu, (2010): Incorporation of Bentazone with Exrerohilum rostratum for Controlling Cyperus iria A.M. J. Agri. Biol.Sci., Vol.5: pp.210-214. | Ganeshwade R.M. (2012): Effect of Dimethoate on the level of cholesterol in freshwater Puntius ticto (Ham). Sci. Res. Report. Vol. 2(1) :pp. 26-29. | Kahtani Mohammed A. Al (2011) : Effect of an Insecticide Abamectin on Some Biochemical Characteristics of Tilapia fish (Oreochromis Niloticus) American Journal of Agricultural and Biological Sciences Vol.6(1) : pp.62-68. | Kajare,A., S. Singh and K. Shrivastava (2000): Malathion induced biochemical changes in kidney of freshwater fish Clarias batrachus. J. Ecotoxicol. Environ. Monit. Vol.10, pp. 11-14. | Khan Zaheer M. and Francis C.P. Law (2005): Adverse effects of pesticides and related chemicals on enzyme and hormone systems of fish, amphibians and reptiles. Proc. Pakistan Acad. Sci. Vol. 42(4),pp. 315-323. | Libermann Buchard (1959) : Giuen by King E.J. and Wolten I.D.P. micra analysis in method biochemistry, Churchill, London P. 42. | Patil M.U. Dr. Patole S.S. (2012): Effect of Malathion and Cypermethrin on Biochemical Constituents of Freshwater Fish, Lepidocephalichthys guntea (Ham-bach) International Indexed & Referred Research Journal Vol. IV (39). | Patole S.S. Patil M. and Mahajan R.T. (2008): Studies on metabolic changes during intoxication by phytotoxicants in fish Nemacheilus evizardy (Day) int. J. Pharmacol. Bio Sci. Vol.2:pp.63-68. | Rathod , D.S. M.V. Lokhunde and V.S. Shembekar (2009) : Toxic impact of dimethoate on the Biochemical composition of vital tissues of Fish Arias dussumieri. Shodh, Samiksha and Muyankan. Vol. 2, pp. 147-149. | Remia , K.M., S. Loguswamy , K. Logankumar and D. Rajmohan (2008) : Effect of an insecticide (Monocrotophos) on some biochemical constituents of the fish Tilapla massambica poll. Res . Vol.27(3) pp. 529-526. | Satyavardhan, K. (2010): Effect of fenvalerate TM on various tissues of Channa punctatus (Bloch). World Appl. Sci.J. Vol.10, pp 70-74.. | Shinde V.R. Veeresh M.U., and Kulkarni R.S. (2002): Ovarian changes in response to heavy metals exposure to the fish Notoperus notopterus (Pallas) J. Environ.Biol. Vol.23(2): pp.137-141. | Stalin Israel S, Sam Manohar Das. S. (2012): Biochemical changes in certain tissues of Cirrhina mrigala (Hamilaton (Cyprinidae :Cyprniformes) exposed to fenthion. Inter. J. of Environ. Sci. Vol.2, (3). | Venkataraman G.V. Sandhya P.N. and Murthy P.S. (2006): Impact of malathion on the biochemical parameter of gobiid fish Glossogobius giuris(Ham).J. Envi. Bio. Vol.27(1):pp. 119-122. |

MORPHOMETRIC AND MERISTIC VARIATIONS IN FINS OF *CHANNA PUNCTATUS* FROM FRESH WATER HABITATS IN AMRAVATI REGION (M.S.)

V. T. TANTARPALE[a1], S. H. RATHOD[b], P. S. JOSHI[c], S. A. TANTARPALE[d] AND S. R. KAPIL[e]

[abcde]P.G. Department of Zoology, Vidya Bharati Mahavidyalaya, Amravati, Maharashtra, India

ABSTRACT

The freshwater fish which has been selected for present study were *Channa punctatus* which is locally called as dhok. Fishes were collected from the local wadali lake of Amravati region. Morphometric study of fins were done by the measured as different fins their characterstics such as fin length, fin width and number of fin rays. Fin variables relationship were observed with standard lengths of fish *Channa punctatus*. The meristic characters are the countable structure useful for differentiation and identification of species and populatiom. Channa *punctatus* showed L/W ratio and also gave phenotypic differences between different fins regarding its length, width and number of fin rays and growth pattern with their increasing body length.

KEYWORDS: Morphometric, Meristic, variation, fin, *Channa punctatus*

The success of fishery industry largely depends on the growth and reproductive potential of the concerned fish species. The development and improvement of the species mostly depends on the knowledge of the biology. Majority of the people need fish throughout the year as a necessary food, its demands the wide aquaculture resources are utilized widely. The shape and structure of fins and fin rays of fishes show modifications due to varied swimming habits, habitat, sex, growth factors, age and size of the fishes, **Ugwumba and Adebbisi (1992)**, **Ugwumba and Ugwumba (1993), Weisel (1995), Oyekanmi (2000),**. It is also known that the morphometric and meristic parameters are influenced by environmental factors, **Dynes *et. al.,* (1999).** Information on the morphometric and meristic characterstic of fins of fishes are useful in marking sex determination, species identification and in ascertaining the suitability of cultivable species.

Channa punctatus, locally known as Dhok, were found in rivers, canals, lakes and other aquatic habitats along with other species of same genus **Wee (1982)**. The fish belonging to genus *Channa* contribute a lot to the commercial fishery of inland waters of India high market price, tolerance to a variety of habitats and carnivorous food habitat make them an important element of fish farming which demands an understanding of their biology and ecological requirements **Omnoniyi and Agborn (2008)**. These fishes contain high protein, substantive iron and low fat content which is beneficial for human health.

It is not easy to identify the different species through colour and marking as it is with other fish. Nearly all snakeheads have different colours and making as juveniles compared to an adult species. Also some snakeheads can change their colour and marking within seconds depending on the situation. Thus in present investigation morphometric and meristic study such as fins length, width and finrays numbers were studied to give clear idea and identification of *Channa punctatus* fish from other species of same genus.

MATERIAL AND METHODS

The *Channa punctatus* which is locally called as dhok were collected from the local wadali lake of Amravati region. After collection healthy fishes were selected (size 30-150mm in length and 30-60gm in weight) and washed with dilute solution of potassium paramagnet (KMno4, 1.0mg/l) to remove dermal infection and acclimatized in laboratory condition for 10 days.
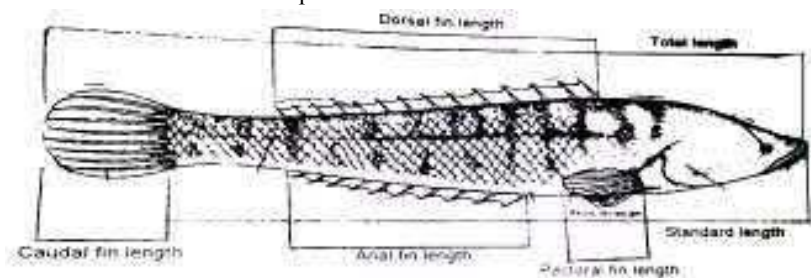
Figure 1: Measurement of *Channa Punctatus*

Morphometric and meristic study of fins was done by the measurement of different fins their characterstics such as fin length, fin width and number of fin rays. Fin variables relationship is observed between standard length of fish *Channa punctatus*.

OBSERVATION AND RESULTS

Morphometrically dorsal fin length measured as 4.28 + 2.36, width 0.46 + 0.19, and fin rays were 24.48 + 4.89, anal fin length 3.2 + 2.36, width 0.3 + 0.005, fin rays were 18.8 + 2.77, caudal fin length 1.58 + 1.14, width 0.66 + 0.42 and finrays was 13.18 + 5.26, pectoral fin 1.56 + 0.82, width 0.66 + 0.42, and fin rays were 13.18 + 5.26, pectoral fin 1.56 + 0.82, width of fin 0.56 + 0.36 and fin rays were 12.22 + 3.50. Pelvic fin length 0.94 + 0.01, width 0.31 + 0.12, and fin rays were 6.02 + 0.33 observed in fish length of *Channa punctatus* were ranges 30-130 mm respectively (Table 1) were found in between 18-30; mean 24.48 respectively. While relationship between body length of fish and dorsal fin length of *Channa punctatus* fish was found to be Y= -0.2179 + 0.49X

The coefficient of correlation of the fish *Channa punctatus* was r = 0.63 showed Substantial degree of co-relation. The relationship between body length and dorsal fin width were found to be Y= -0.7916 + 0.04X. The coefficient correlation r=0.64 showed substantial degree of correlation. While the relationship between body length and dorsal fin rays was found to be Y= -14.366 + 1.22X

The coefficient correlation r= 0.76 showed substantial degree of correlation. The relationship between body length and anal fin length was found to be Y = -0.8621 + 0.49X.

Table 1: Morphometric and Meristic study of different fins with their fin length, width and fin rays numbers of freshwater fish *Channa punctatus*

Fins	Fish length (Ranges)	Length	Width	Fin Rays
Dorsal Fin		4.28 ±2.36	0.46 ± 0.19	24.48 ± 4.84
Anal Fin		3.2 ± 2.36	0.3 ±0.005	18.8 ±2.77
Caudal Fin	30-130 mm	1.58 ± 1.14	0.66 ± 0.42	13.18 ± 5.26
Pectoral Fin		1.56 ± 0.82	0.56 ± 0.36	12.22 ± 3.50
Pelvic Fin		0.94 ± 0.00	0.3 ± 0.12	6.02 ± 0.00

Table 2: Relationship between fish length and Morphometric and Meristic study of different fins of freshwater fish *Channa punctatus*

Fins	Fin length	Fin Width	Fin Rays
Dorsal Fin	y = -0.2179+0.49X r= 0.63	y = -07916+0.04x r = 0.64	y = -14.366+1.22x r = 0.76
Anal Fin	y = 0.8621+ 0.49x r = 0.63	y = 0.183+0.014x r = 0.60	y = -12.997+0.70x r = 0.76
Caudal Fin	y = - 0.5754+ 0.26x r = 0.69	y = -0.0382+0.07x r = 0.54	y = -6.548+0.80 r = 0.46
Pectoral Fin	y = 0.0151+0.19x r = 0.70	y = 0.708+0.059x r = 0.49	y = -4.759+0.90x r = 0.77
Pelvic Fin	y = 0.6351+0.19X r = 0.66	y = 0.151+0.017x r = 0.43	y = -6+0x r = 0.0

The coefficient of correlation r = 0.63 showed substantial degree of correlation. The relationship between body length and anal fin width was found to be Y = -0.183+0.014x. The coefficient of correlation r = 0.60 showed substantial correlation between body length Anal width. The relation between body length and Anal fin rays was found to be Y= -12.997+0.70x. The coefficient of correlation r = 0.76 showed substantial degree of correlation between body length anal fin rays. The relation between fish length and

pectoral fin length was found to be Y= 0.0151+0.19x. The coefficient of correlation r = 0.70 showed substantial degree of correlation. The relation between body length and pectoral fin width of *Channa punctatus* was found to be Y = -0.708+0.059x. The coefficient correlation r = 0.49 showed moderate degree of correlation. The relation between body length and pectoral fin rays was found to be Y = -4.759+0.90x. The coefficient correlation r = 0.77 showed moderate degree of correlation.

In the relationship between body length of fish *Channa punctatus and* different fin length was found that regression coefficient of dorsal fin length and Anal fin length was more than caudal fin length, pelvic fin length and pectoral fin length while coefficient correlation was near about same that was 0.63, 0.63, 0.69, 0.66, and 0.70 respectively. The relationship between body length of *Channa punctatus* fish and different fin width was found that regression coefficient of caudal fin width and dorsal fin width was observed larger as compared to fin width of pectoral fin, pelvic fin and anal fin. While coefficient correlation in dorsal fin width and anal fin width was observed more that is 0.64 and 0.60 and coefficient correlation of caudal fin width, pectoral fin width, pelvic fin width was seen as 0.54, 0.49, and 0.43, respectively. While the relationship between body length of fish and number of fin rays of different fins was found that regression coefficient as dorsal fin rays were more following pectoral, caudal and anal fin rays. But pelvic fin rays showed regression coefficient as 0. Same way coefficient correlation of pelvic fin rays was also found to be 0.The coefficient correlation of dorsal fin rays, Anal fin rays, pectoral fin rays and caudal fin rays was found to be 0.76, 0.76, 0.77, 0.46 respectively; (table no.**2**).

The above values showed that increase in body length; fin length, width and fin rays also changes and showed increase in them with substantial, moderate degree of correlation respectively .In case of pelvic fin, even with increase in body length of the fish *Channa punctatus* there is no increase in number of fin rays thus showed coefficient correlation as r=0.00

DISCUSSION

The present morphometric analysis of different fins of *Channa punctatus* showed variation in length, width and number of fin rays'. It was observed that with the growth of fish, body length, fin length and fin width and fin rays number also increase with high degree of correlation was also shown in fin rays such as 0.76,

0.76, 0.77, 0.46 for dorsal fin, anal fin, pectoral fin and caudal fin respectively. But pelvic fin showed no change or increase in number of fin rays r =0.

According to **Turan *et.al*., (2005)** and **Omoniyi and Agbon (2008)** distinct environmental structure causes the high morphometric variation and plasticity which response to differences in environmental condition such as food abundance and temperature. **Usha (2000)** reported that anal, caudal, pectoral, and pelvic fins of *Catla catla* were longer than *Cyprinus carpio* and *Labeo rohita* due to its surface feeding suited ecologically which is rich in vegetation and species of *Clarias gariepinus*. They belong to benthic habitat and have robust bodies and large pectoral fins which allow them to withstand current on smaller, smoother substratum. **Dynes *et.al.*, (1999)** found that dorsal and pectoral fin lengths of pelagic fish were shorter than littoral ones in brooke chart, *Salvelias fountinalis*. The morphometric study of fins of *Channa punctatus* were seen broadly by their location, shape and size. In *Channa punctatus* species long dorsal fin, anal fin, lobed shaped caudal fin, two pectoral fin, two pelvic fins.and varying number of fin rays were also noticed.

The increase in size of the fins was accompanied by branching and segmentation of fin rays. Such increase was noticed in number of fin rays once these were formed because a constant number of rays are characteristic of a particular species, genus or family **(Lagler 1962, Usha and Prakasam 2005).** The sequential development of pectoral fin followed by caudal and dorsal fins appeared to be related to the timely uses of these fins as suggested by **(Whitehead 1975, Devenport 1993).** In the present analysis of fresh water fish *Channa punctatus* showed the phenotypic differences between different fins regarding its length, width and number of fin rays and growth pattern with their increasing body length.

REFERENCES

Barlow, G.W. (1961): Causes and significance of morphological variation in fishering *syst. Zool*. **10**: 105-117.

Dynes, P. Magnan, L. Bernatchez and M.A. Rodrinquez (1999): Genetic and morphological variation between two forms of Lacustrine brook charr. *J. Fish. Biol.* **54**: 955-972.

Devenport, J. (1995): Ventilation of the gills by the pectoral fins in the long tooth (Anoplogaster cornutum). How to breath with a full mouth. *J. Fish. Biol.*, **22**(2): 105-111.

Lagler, K., J.E. Bardach and R.R. Miller (1962) : Ichthyology. Wiley, New York, U.S.A.

Ominiyi I. T. and A. O. Agbon (2008): Morphometric variation in *Sarotherodon melanotheron* from brackish and fresh water habitat in south wwestern Nigeria. *W, Afr. J. Appl. Ecol.* **12**: 01-05

Turan Cemal, Sukran Yalcin, Funda Turan, Emel Okur and Ihsan Akyurt (2005): Morphometric comparision of African catfish, *Clarias gariepinus* population in Turkey. Folia Zool. **54** (1-2): 165-172.

Ugwumba A.A. and A.A. Adebisi (1992): Food and feeding ecology of *Sarotherodon melanotheron* in a small fresh water reservoir in Ibadam, Nigeria. *Hydrobiol.* **124** (3): 367-382.

Ugwumba A.O. and A.A. Ugwumba (1993): On the biology of black jaw tilapia *Sarotherodon melanotheronin* a tropical fresh water lake Niger. *J. Res. Rev. Sci.* **1**: 12-25

Usha. S. (2000): Studies on the fins of carp fishes (*Cyprinus carpio, Labeo rohita, catla catla*) used in polyculture. Doctoral thesis. Univ. Kerala. India.

Usha, S. and V.R. Prakasam (2005) : Fins of carp fish, Catla catla in relation to Ecology, Morphology composition and Development *J. Enviroment Ecology,* **23**(1) : 106-112.

Weisel, G.F. (1995): Variation in number of fin rays of two Cyprinid fishes correlated with natural water temperatures. *Ecology* **36**: 1-6.

Whitehead (1975): How fishes Live. Elsevierphalden, London, U.K.

Wee, K.L. (1982): Snakeheads-the biology and culture. In. Recent Advances in Aquaculture (Eds: J. F. Muir and R.J. Roberts). Croom. Helm Ltd., London *PP*- 179-213.

Full Length Article

A review of ophidian studies in Vidarbha region (M.S.) India

Joshi PS[1], Tantarpale VT[2] and KM Kulkarni[3]

[1]Research Student, Dept. of Zoology, Jijamata Mahavidyalaya, Buldhana (M.S.) India
[2]Associate Professor, P. G. Dept. of Zoology, Vidya-Bharti Mahavidyalaya, Amravati (M.S.) India
[3]Former Director of Higher Education, Government of Maharashtra, Pune (M.S.) India
Former Vice- Chancellor, S. R. T. M University, Nanded (M.S.) India

ABSTRACT

Through literature survey and current knowledge on the ophidian fauna, this paper deals with a review of ophidian studies in the Vidarbha Region (M.S.) India. A complete bibliography with respect to ophidian taxonomy, distribution, range extension, status reports and conservation is listed. These studies cleared that thirty five ophidian species belonging to six families were common in Vidarbha region in which Colubridae family contributes more number of species.

Key word: Ophidian fauna, Vidarbha Region, Bibliography, Overview.

INTRODUCTION

The biological diversity of the earth and its origins has long been a source of amazement and curiosity. Vidarbha is one of the most diversified Regions in Maharashtra State of India, with respect to biodiversity. Its healthy climate, mountainous terrain, rugged configuration and sudden fall in elevation are phenomenal and have received notable interest that provides favourable environment for ophidian fauna (Joshi and Tantarpale, 2014).

Studies on ophidian fauna of Vidarbha Region comparatively better than amphibian and fishes but has not equaled the progress made on birds and mammalian fauna. Literature survey shows that a few naturalists and scientists have attempted to study this ophidian fauna. The first appreciable study was carried out by D'Abreu (1928), he made a comprehensive collection of snakes for the Central museum, Nagpur, which provides information on reptiles of Vidarbha in general and Amravati in particular.

The scattered but detailed information about ophidian fauna of Vidarbha Region is available in some of the mention studies. Wadatkar (2003) documented 12 ophidian species from Amravati University Campus. Captain *et al.* (2005) was reported *Elaschitodon westermanni* from Wardha district which is adjacent to Amravati District. Nande and Deshmukh (2007) recorded 32 species from Amravati district including Melghat. Harney *et al.* (2009) and Harney (2011) reported 17 ophidian species from Bhadravati of District Chandrapur. Joshi (2009) studied the diversity and population dynamics of reported 24 species of snakes in Yavatmal district. A preliminary survey of Joshi (2011) reveals occurrence of 22 ophidian species in Buldhana District. Narayanan (2012) gave record of Indian Egg Eater Snake *Elaschitodon westermanni* from the localities of Shegaon, Dist. Buldhana. Uke *et al.* (2013) studied eco-diversity, distribution and conservation strategy of *Amphiesma stolatum* in Nagpur city. Recently Joshi *et al.* (2013 a) studied the Ecology and behaviour of *Coelognathus helena montecolaris*. Joshi *et al.* (2013 b) studied Sexual dimorphism in *Xenochrophis piscator* in Buldhana District. Gore and Joshi (2013) studied the dicephalic *Naja naja* from Washim District. Joshi and Tantarpale (2014) studied diversity and population dynamics of 33 ophidian species in Buldhana District of Vidarbha Region (M.S.) India.

Sr.No.	Taxa*	Common Name*	Type*	Status[#]
	Family: Typhlopidae			
1.	*Grypotyphlops acutus* (Dumeril and Bibron, 1844)	Beaked worm snake	NV	Frequent
2.	*Ramphotyphlops braminus* (Daudin, 1803)	Common worm snake	NV	Common
	Family: Pythonidae			
3.	*Python molurus molurus* (Linnaeus, 1758)	Indian rock python	NV	Occasional
	Family: Boidae			
4.	*Gongylophis conicus* (Schneider, 1801)	Common sand boa	NV	Frequent
5.	*Eryx johnii* (Russell, 1801)	Red sand boa	NV	Rare
	Family: Colubridae			
6.	*Ahaetulla nasuta* (Lacepede, 1789)	Common vine snake	SV	Occasional
7.	*Amphiesma stolatum* (Linnaeus, 1758)	Striped keelback	NV	Frequent
8.	*Argyrogena fasciolata* (Shaw, 1802)	Banded racer	NV	Abundant
9.	*Boiga forsteni* (Dumeril, 1854)	Forsten's cat snake	SV	Uncommon
10.	*Boiga trigonata* (Bechstein, 1802)	Indian cat snake	SV	Abundant
11.	*Coelognathus helena helena* (Daudin, 1803)	Common trinket snake	NV	Abundant
12.	*Coelognathus helena monticollaris* (Schulz, 1992)	Montane trinket snake	NV	Occasional
13.	*Coronella branchyura* (Gunther, 1866)	Indian smooth snake	NV	Occasional
14.	*Dendrelaphis tristis* (Daudin, 1803)	Bronzback tree snake	NV	Frequent
15.	*Elachistodon westermanni* (Reinhardt, 1863)	Indian egg eater	SV	Rare
16.	*Lycodon aulicus* (Linnaeus, 1758)	Common wolf snake	NV	Abundant
17.	*Lycodon flavomaculatus* (Wall, 1907)	Yellow spotted wolf snake	NV	Common
18.	*Lycodon striatus* (Shaw, 1802)	Barred wolf snake	NV	Abundant
19.	*Macropisthodon plumbicolour* (Cantor, 1839)	Green keelback	NV	Common
20.	*Oligodon arnesis* (Shaw, 1802)	Common kukri snake	NV	Abundant
21.	*Oligodon taeniolatus* (Jerdon, 1853)	Russell's kukri snake	NV	Occasional
22.	*Psammophis condanarus* (Merrem, 1820)	Condanarus sand snake	SV	Frequent
23.	*Psammophis leithii* (Gunther, 1869)	Leith's sand snake	SV	Occasional
24.	*Psammophis longifrons* (Boulenger, 1897)	Stout sand snake	SV	Occasional
25.	*Ptyas mucosa* (Linnaeus, 1758)	Indian rat snake	NV	Abundant
26.	*Sibynophis subpunctatus* (Dumeril, 1854)	Black headed snake	NV	Occasional
27.	*Xenochrophis piscator* (Schneider, 1799)	Checkered keelback	NV	Abundant
	Family: Elapidae			
28.	*Bungarus caeruleus* (Schneider, 1801)	Common krait	V	Common
29.	*Bungarus fasciatus* (Schneider, 1801)	Banded krait	V	Rare
30.	*Bungarus sindanus walli* (Wall, 1908)	Wall's sind krait	V	Rare
31.	*Calliophis melanurus* (Shaw, 1802)	Slender coral snake	V	Rare
32.	*Naja naja* (Linnaeus, 1758)	India spectacled cobra	V	Abundant
	Family: Viperidae			
33.	*Daboia russelii* (Shaw and Nodder, 1797)	Russell's viper	V	Abundant
34.	*Echis carinatus* (Schneider, 1801)	Saw-scaled viper	V	Frequent
35.	*Trimeresurus gramineus* (Shaw, 1802)	Green pit viper	V	Rare

Table 1. Systematic list of Ophidian species reported from Vidarbha Region (M.S.) India

* According to Whitaker and Captain (2008) / # Summary of Review
Type: NV- Non-Venomous; SV- Semi- venomous; V- Venomous

Conservation and protected areas

Vidarbha region has lush green deciduous forests with large protected areas which are home to variety of flora and fauna. It has approximately 37,251 km^2 forest cover. Vidarbha has many popular wildlife sanctuaries and parks *viz.* Melghat in Amravti, Amba-barwa and Nalganga in Buldhana, Tadoba-Andhari in Chandrapur, Nagzira and Navegaon Bandh in Gondia, etc. These Protected Area networks are managed by Forest departments with the prime objectives to conserve entire biodiversity of Region. But it raises a question; whether the present management practices really supports the conservation of entire biodiversity? It does not because the present management practices and plans of protected areas focus only on mega wildlife projects. The different wildlife and forest conservation acts also provides legislative protection to biodiversity.

Present status and threats to ophidian fauna

Snakes are part of our ecosystems and they play a vital role in pest-control. Along with that, they form a vital part of the food chain as a prey as well as a predator. These important animals are always threatened by anthropogenic and environmental factors. The diverse habitats of the Vidarbha Region are rapidly changing due to new irrigation projects and industrialization. Forest areas are being de-notified for implementing development projects such as mining, industry, communication and tourism. This has resulted in alternating climate as well shrinkage, fragmentation, degradation and destruction of natural habitats. Road accidental killing on highways across wildlife refuges are an intrusion and affect the wildlife and its habitats adversely. Misconceptions and fear about snakes are also threatening this important creature of the ecosystem.

Species account

The literature survey shows that total 35 ophidian species belonging to six families have been reported from Vidarbha Region (M.S.) India (Table 1). These families are namely Typhlopidae (2 Species), Pythonidae (1 Species), Boidae (2 Species), Colubridae (22 Species), Elapidae (5 Species) and Viperidae (3 Species). Out of these thirty five ophidian species, 8 species are venomous, 7 species are semi venomous, and (20) species are non-venomous. There are, in future, chances of more species being reported because few pockets and habitats in the Region required extensive exploration.

REFERENCES

Captain A, F Tillack, A Gumprechet and P Dandage, 2005. First record of *Elachistodon westermanni* from Wardha District of Maharashtra, India. *Russian J. Herp.* **12** (2): 323-324

D'Abreu AE, 1928. *Records of the Nagpur museum No.VI. A list of reptiles of the Central Province.* Government Press, Nagpur. 1-13

Gore AM and PS Joshi, 2013. Record of dicephalic *Naja naja* (Lin.1758) from Washim District (M.S.) India. *NCEIOR* 2013- *J. Aqua. Biol.* 114-115.

Harney NV, Sitre SR, Wadhave NS and PN Nasare, 2009. Biodiversity of snake during monsoon months in Bhadrawati tahsil of Chandrapur district, Maharashtra. *J. of Ecol. and Fish.,* **2**(2): 103-106.

Harney NV, 2011. Studies on snakes of Bhadravati, District Chandrapur (M.S.) India. *Online Intern. Interd. Res. J.* **1**(1): 12-17.

Joshi P, 2009, Studies on the diversity and populattion dynamics of snakes in Yavatmal district of Maharashtra, India. *Bios. Biot. Res. Com.* **2** (1): 99-105.

Joshi PS, 2011. A preliminary survey on snake of Buldhana District, Maharashtra. *Gold. Res. Tho.* **1**(2): 73-74.

Joshi PS and VT Tantarpale, 2014. Diversity and population dynamics of ophidian fauna from Buldhana District, Maharashtra (India), Thesis Submitted to S. G. B. Amravati University, Amaravati. 260 pp.

Joshi PS, Tantarpale SA, Tantarpale VT and KM Kulkarni, 2013 a. Ecology and behaviour of *Coelognathus Helena montecolaris* (Schulz 1992) from Buldhana District (M.S.) India. *NCEIOR* 2013- *J. Aqua. Biol.* 24-25.

Joshi PS, Tantarpale VT and KM Kulkarni, 2013 b. Sexual dimorphism in *Xenochrophis piscator* (Schneider 1799). *AILSPF*- 244-246.

Nande R and S Deshnukh, 2007. Snakes of Amravti district including melghat, Maharshtra. With important record of the Indian egg-eater, Montane trinket snake and Indian smooth snake. *Zoos Print J.* **22**(2): 2920-2974.

Narayanan A, 2012. Records of Indian Egg Eater Snake *Elaschitodon westermanni* in the localities of Shegaon, Maharashtra, India. *Reptiles Rap*. **14** (6): 09-12.

Uke SB, Shende VA and KG Patil, 2013. Eco-diversity, distribution and conservation strategy of *Amphiesma stolatum* in Nagpur city. *Asian J. Biol. and Biotech.* 2 (2) 212:001-005.

Wadatkar JS, 2003. Herpetofauna of the Amravati university campus. Maharashtra. *Zoos Print J.* **19(2):** 1381-1382.

Whitaker R and A Captain, 2004. *Snakes of India. The Field Guide*. Draco Books. Chengalpattu, Tamil Nadu. xiv+479 pp, pls, text-figs.

How to Cite this Article:

Joshi PS, Tantarpale VT and KM Kulkarni, 2014. A review of ophidian studies in Vidarbha region (M.S.) India. *Science Research Reporter,* **4**(2):167-170.

Synthesis and Characterization of Some New N, O and S Containing Chlorosubstituted Heterocycles and Their Antimicrobial Screening against Some Common Causative Organisms

N. G. Ghodile[1*] & P. R. Rajput[2]

[1]Department of Chemistry, S.S.S.K.R. Innani MV, Karanja (Lad), [2]Department of Chemistry, Vidya Bharati MV, C. K. Naidu Road, Camp, Amravati-444602.

Abstract—Some new nitrogen, oxygen and sulfur containing heterocyclic systems such as pyrazoles, isoxazoles and 1,3-thiazoles were synthesized via cyclization of 1-(2-hydroxy-3,5-dichlorophenyl)-3'-ethyl-1,3-dione and 1-(2-hydroxy-3,5-dichlorophenyl)-4-bromo-3-ethyl-1,3-dione by using suitable reagents. Structures of the newly synthesized compounds were established by molecular weight determinations, elemental analysis and spectral data. All the products were also screened in vitro for their antimicrobial activity against the bacteria P. vulgaris and B. subtilis spp. and antifungal activity against Aspergillusn niger , Curvularia lunata by disc diffusion method.

Index Terms—Antimicrobial activity, Isoxazoles, Pyrazoles and 1, 3-Thiazoles..

I. INTRODUCTION

The N, O and S containing chlorosubstituted heterocycles viz. pyrazoles, isoxazoles and 1, 3-thiazoles, is an important class of heterocyclic compounds. These are reported to have a broad spectrum of biological and medicinal activities, such as Anticonvalsant [1], cytotoxic, herbicidal [2], antiinflammatory [3], antifungal [4], antimicrobial [5], antioxidant [6] activities.

Pyrazole ring is incorporated into many of the commercially available pharmaceuticals, agrochemicals [7]. Isoxazole derivatives [8] have been in commercial use for many years. Thiazole being an integral part of many potent biologically active molecules [9] plays an important role as antifungal and antibacterial agent.

In view of the above mentioned findings, we decided to synthesize some new pyrazoles, isoxazoles and 1,3-thiazoles and investigate their antimicrobial activities.

II. EXPERIMENTAL

Preparation of 2-hydroxy-3,5-dichloro-4'-ethylchalcone (3a):

To the boiling solution of the 2-hydroxy-3,5-dichloroacetophenone (2b) (0.01 mol) and propanaldehyde (0.01 mol) in ethanol (20ml), 40% solution of NaOH was added gradually. The reaction mixture was stirred mechanically at room temperature for 1 hr. and kept it at room temperature for 6 to 8 h. followed by decomposition with ice-cold HCl (1:1). The yellow granules thus obtained were filtered and washed with 10% NaHCO$_3$ solution and then crystallized from ethanol to obtain compound (3a) m.p.94°C, yield: 75%**.**

Preparation of Chalconedibromide (3b)

2-Hydroxy-3,5-dichlorophenyl-4'-ethylchalcone (3a) was suspended in bromine-glacial acetic acid reagent. The reagent was added drop by drop with constant stirring and reaction mixture was kept at room temperature for about 30 minutes. The solid product thus separated was filtered and washed with a little petroleum ether to get the compound (3b). M.P. 75°C, Yield 82%.

Preparation of 6,8-dicloroflavone (4a).

Compound (3b) was dissolved in ethanol (25ml) containing a little piperidine. To this aqueous KOH solution (25 ml) was added. The reaction mixture was then refluxed for 1 hour, cooled and diluted with water. The product thus separated was filtered and crystallized from ethanol to get the compound (4a). M.P. 147°C, Yield 60 %.

Preparation of 1-(2-hydroxy-3,5-dichlorophenyl)-3'-ethyl-1,3-dione (5a).

1-Ethyl-6,8-dichloroflavone (4a) was dissolved in ethanol containing a little piperidine. To this aqueous HCl solution (25 ml) was added. The reaction mixture was then refluxed for 1 hour, cooled and diluted with water. The product thus separated was filtered and crystallized from ethanol to get the compound (5a). M.P. 110°C, Yield 65 %.

Preparation of 1-(2-hydroxy-3,5-dichlorophenyl)-4-bromo-3-ethyl-1,3-dione (5b).

1-(2-Hydroxy-5-chlorophenyl)-3-ethyl-1,3-dione(5a) was dissolved in ethanol (10 ml) containing a little piperidine. To this, liquid bromine (0.5 ml) was added and allowed it to stand for 1 hour. It was then diluted and washed several times with water and finally extracted with ether to get the compound (5b), M.P. 78°C, Yield 60 %.

Preparation of pyrazole 3-(2-hydroxy-3,5-dichlorophenyl)-5 –ethylpyrazole (6a).

1-(2-Hydroxy-3,5-chlorophenyl)-3'-ethyl-1,3-dione (5a) and phenylhydrazine hydrochloride were dissolved in ethanol (25 ml) containing a little piperidine refluxed for 1.5 hours, cooled and diluted with water and acidified with conc. HCl. The product thus separated was filtered and crystallized from ethanol to get the compound (6a). M.P. 167°C, Yield 75 %. Elemental analysis: % **C** 60.21/ 61.23; % **H** 4.39/ 5.40; % **O** 7.75/ 8.16; % **Cl** 17.86/ 18.07; % **N** 6.82/ 7.14; UV spectrum (dioxane) λ_{max}, 395.0 nm (n—›π*). IR (KBr,): 3600 (-OH stret.), 3038 (Aromatic stret.), 3200 (-NH stret.), 2850 (Ali. C-CH stret.), 1431 (-CH$_2$ bend.), 1304 (-CH$_3$ bend.), 825.57(C-Cl Stret.), ^{1}H NMR: δ 1.28 (t, 3H, -CH$_2$-**CH$_3$**), δ 2.05 (q, 2H, -**CH$_2$**-CH$_3$), δ 6.91 to 8.11 (m, 3H, Ar-H), 11.2 (s, H, -O**H**), 4.6 (s, 1H, -N**H**).

Preparation of isoxazole 3-(2-hydroxy-3,5-dichlorophenyl)-5-ethylisoxazole (6b).

1-(2-Hydroxy-3,5-chlorophenyl)-3'-ethyl-1,3-dione (5a) and hydroxylamine hydrochloride were dissolved in ethanol (25 ml) contains few drops of piperidine refluxed for 2.5 hours, cooled and diluted with water and acidified with conc. HCl. The product thus separated was filtered and crystallized from ethanol to get the compound (6a). M.P. 185°C, Yield 75 %. Elemental analysis: % **C** 52.00/ 52.02; % **H** 3.59/ 3.69; % **O** 15.66/ 15.99 % **Cl** 23.44/ 23.62 % **N** 4.55/ 4.67; UV spectrum (dioxane) λ_{max}, 402.0 nm (n—›π*). IR (KBr): 3500 (-OH stret.), 3084 (Aromatic stret.), 3359 (-NH stret.), 2861(Ali. C-CH stret.), 1451(-CH$_2$ bending), 1338, (CH$_3$ bending), 819 (C-Cl Stret.), ^{1}H NMR: δ 1.26 (t, 3H, -CH$_2$-**CH$_3$**), δ 2.4, (s, 2H, -**CH$_2$**-CH$_3$), δ 6.67 to 7.83 (m, 3H, Ar-H), 11.3 (s, H, -O**H**).

Preparation of 5-(2-hydroxy-3,5-dichlorophenyl)-4'-ethyl-2'-amino-1,3-thiazole (6c).

1-(2-Hydroxy-3,5-chlorophenyl)-2-bromo-3-ethyl-1,3-dione (5b) and thiourea were dissolved in ethanol (25 ml) contains few drops of piperidine. To this reaction mixture aqueous KOH solution (10ml) was added and refluxed for 2.5 hours, cooled and diluted with water and acidified with conc. HCl. The product thus separated was filtered and crystallized from ethanol to get the compound (6a). M.P. 102°C, Yield 64 %. Elemental analysis: %**C** 46.79/ 46.89; %**H** 2.39/ 2.46; %**O** 7.75/ 7.82; %**Cl** 8.56/ 8.65; %**N** 6.82/ 6.89; %**S** 7.73/ 7.82.; UV spectrum (dioxane) λ_{max}, 401.0 nm (n—›π*). IR (KBr): 3500, (-OH stret.), 3038 (Aromatic stret.), 3300 (-NH stret.), 2850 (Ali. C-CH stret.), 1434 (-CH$_2$ bend.), 1338, (-CH$_3$ bend.) 1022 (C-S stret.), 829.39 (C-Cl Stret.), ^{1}H NMR: δ 2.7 (s, 3H, -**CH$_3$**), δ 7-8 (m, 12H, Ar-**H**), δ 6.2 (s, 1H, -N**H**), δ 12.5 (s, 2H, Ar-O**H**), 11.2 (s, H, -O**H**), 4.7 (s, 1H, -N**H**).

Preparation of 5-(2-hydroxy-3,5-dichlorophenyl)-4'-ethyl-2'-aminophenyl-1,3-thiazole (6d).

1-(2-Hydroxy-3,5-chlorophenyl)-4'-bromo-3'-ethyl-1,3-dione (5b)and phenylthiourea were dissolved in ethanol

(25 ml) contains few drops of piperidine. To this reaction mixture aqueous KOH solution (10ml) was added and refluxed for 2.5 hours, cooled and diluted with water and acidified with conc. HCl. The product thus separated was filtered and crystallized from ethanol to get the compound (6b). M.P. 130°C, Yield 70 %. Elemental analysis: %**C** 56.02/ 56.74; %**H** 3.98/ 4.76 %**O** 15.78/ 16.75 %**Cl** 6.09/ 6.62; %**N** 7.12/ 7.56; %**S** 6.98/ 7.57.; UV spectrum (dioxane) $\lambda_{max,}$ 395 nm (n—›π*). IR (KBr): 3300, (-OH stret.), 3035 (Aromatic stret.), 3300 (-NH stret.), 2839 (Ali. C-CH stret.), 1431 (-CH$_2$ bend.), 1338, (-CH$_3$ bend.) 1022 (C-S stret.), 830 (C-Cl Stret.), ^{1}H NMR: δ 2.7 (s, 3H, -C**H**$_3$), δ 7-8 (m, 12H, Ar-**H**), δ 6.2 (s, 1H, -N**H**), δ 12.75, (s, 8H, Ar-O**H**), 11.5 (s, H, -O**H**), 5.0 (s, 1H, -N**H**).

SCHEME
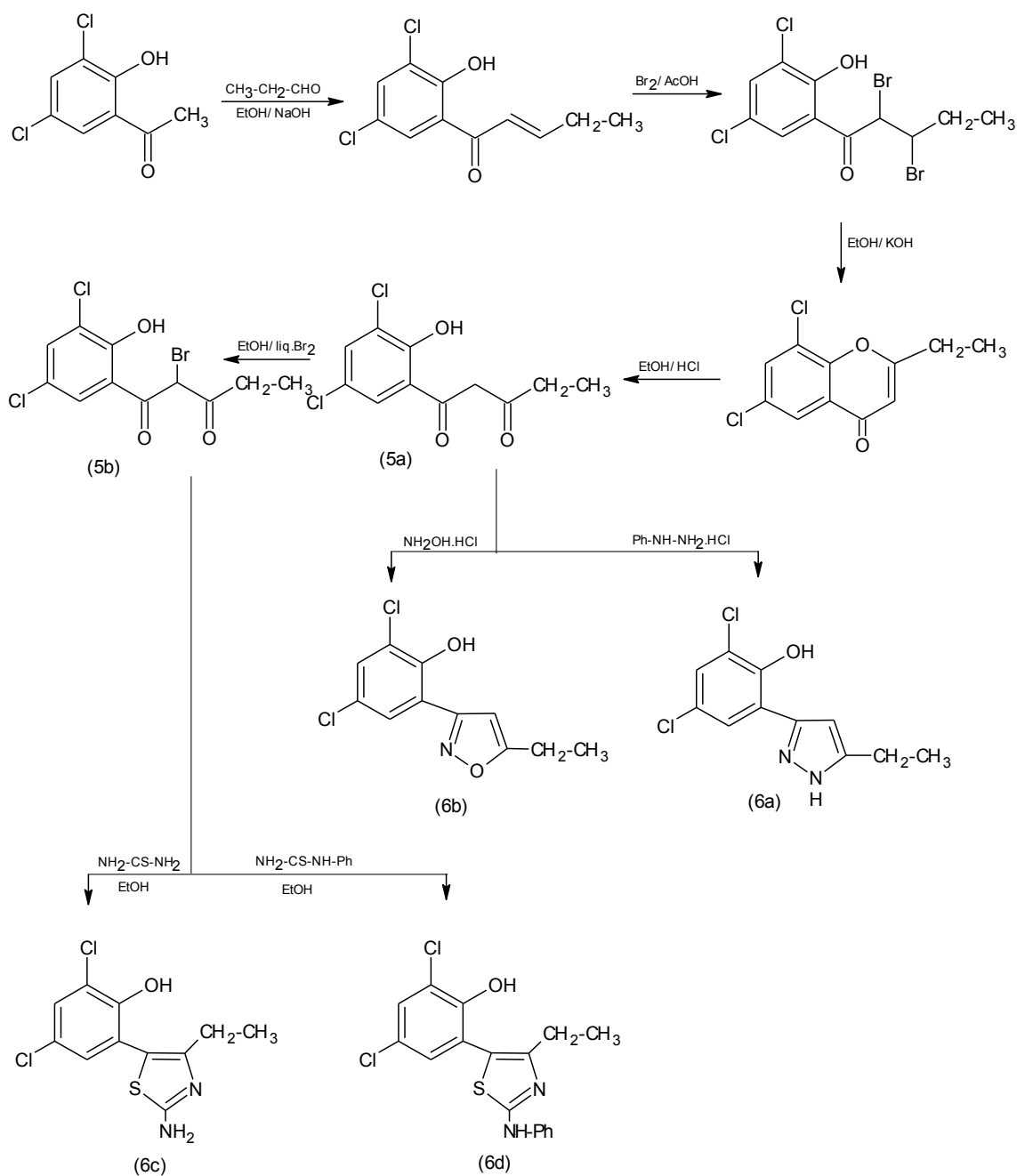
III. ANTIMICROBIAL ACTIVITY

All the compounds synthesized in the first part of the study were screened *in vitro* for their antibacterial activity against the bacteria *P. vulgaris* and *B. subtilis spp.* and antifungal activity against *Aspergillus niger*, *Curvularia lunata* by disc diffusion method.

The efficacy of the test compounds were determined by measuring the visible clear area of growth free zones i.e. *zone of inhibition* produced by diffusion of the antibiotics in to media from the discs by callipers in mm. The results are tabulated in the table given below:

Table I: Antimicrobial activity of test compounds

Test compounds	Zone of inhibition (mm)							
	P. vulgaris		*B. subtilis spp.*		*Aspergillus niger*		*Curvularia lunata*	
	10 ug/ disc	500 ug/ disc	10 ug/ Disc	500 ug/ disc	10 ug/ disc	500 ug/ disc	10 ug/ disc	500 ug/ disc
3a	4	18	2.4-2.3	16	3.3-4.0	12	3-5	13
5a	3	20	2-3	19	4	16	4.0-4.3	17
5b	3	17	2-3	18	5	15	8	17
6a	5	22	6	20	7	23	6	21
6b	5	21	8	23	4	24	7	18
6c	3	19	2-3	16	3.4-3.7	19	5.9-6.5	25
6d	5	21	8	22	6	16	5	22
Gentamicine	-	-	-	-	-	-	-	-

The results depicted in Table-I revealed that most of the synthesized compounds were found to possess various antimicrobial activities towards the test organisms. In general, most of the synthesized compounds have better activities against the microbial strains in comparison with the starting material (3a). Compounds **6a, 6b, 6c** and **6d** were found to possess high inhibitory activities at 500 ug/disc concentration against the test organisms. In this context it has also been observed that the antimicrobial activities of newly synthesized heterocycles increases with increased structural complexity.

REFERENCES

[1] A. Kalusalingam, I. Arumugam, R. Velayutham, U. Natarajan, A. J. S. Johnsamuel., and P. Promwichit, "Synthesis, characterization and anticonvulsant activity of some pyrazole derivatives," Journal of Global Pharma Technology., vol. 3, no. 3, pp. 25-30, 2011.

[2] N. Kudo, S. Furuta, M. Taniguchi, T. Endo, and K. Sato, "Synthesis and herbicidal activity of 1, 5-diarylpyrazole derivatives." Chem. Pharm. Bull., vol. 47, pp. 857–868, 1999.

[3] A. A. Bekhit, H.M.A. Ashour, Y.S.A. Ghany, A.E.A. Bekhit, and A. Baraka, "Synthesis and biological evaluation of some thiazolyl and thiadiazolyl derivatives of 1*H*-pyrazole as antinflammatory antimicrobial agents." Eur. J. Med. Chem., vol. 43, 456–463, 2008.

[4] B. Sadek, "Antimicrobial prospect of newly synthesized 1,3-thiazole derivatives." Molecules, vol. 16, pp. 9386-9396, 2011.

[5] T.E.S. Ali, and A.M. El-Kazak, "Synthesis and antimicrobial activity of some new 1,3-thiazoles, 1,3,4-thiadiazoles, 1,2,4-triazoles and 1,3-thiazines incorporating acridine and 1,2,3,4-tetrahydroacridine moieties." European Journal of Chemistry vol. 1, no. 1, pp. 6-11, 2010.

[6] H. Osman, "Microwave-assisted synthesis and antioxidant properties of hydrazinyl thiazolyl coumarin derivatives." Chemistry Central Journal, vol. 6, no. 32, pp. 1-10. 2012.

[7]   M. A. Salem, H. K. H. Thabet, M. H. Helal, A. S. Abdelaal, and Y. A. Ammar, "Synthesis and pharmacological evaluation of some Pyrazoles, Thiazolopyrimidine, Triazolopyrimidine, Pyridone and 2-Iminochromene containing naproxenoyl moiety as NSAIDs," Chemical Sciences Journal, vol. CSJ-32, pp. 1-12, 2011.

[8]   M. Shailaja, A. Manjula, and B.V. Rao, "Synthesis of novel 3, 5-disubstituted-4, 5-dihydroisoxazole and 3, 4, 5-trisubstituted isoxazole and their biological activity." Indian journal of chemistry, vol.50B, pp. 214-222, 2011.

[9]   Heterocyclic Chemistry-II, Five-membered heterocycles, R. R. Gupta, M. Kumar, V. Gupta, Springer publication. ISBN 81-8128-221-3.

Wound Healing Activity of *Butea Monosperma* in Wistar Rats

Malpani M. O.[1]*, Rajput P. R.[2]

1. Department of Chemistry, Shankarlal Khandelwal College, Akola,
2. Department of Chemistry, Vidya Bharati Mahavidyalaya, Amravati

ABSTRACT

Wound is a physical injury that causes breakdown in the protective function of the skin and the loss of continuity of epithelium with or without loss of underlying connective tissues. Proper healing of wound is essential for the restoration of normalcy in disrupted anatomical continuity and altered functional status of the skin. Wound healing is a complex and dynamic process of restoring cellular structures and tissue layers. It can be divided into 3 distinct phases: an immediate haemostatic phase, an early phase of re-epithelialization, a later phase of dermal repair and remodelling. The present investigation was undertaken to determine the efficacy of *Butea monosperma* leaves aqueous extract, isolated acidic ingredient and its newly synthesized amide analogue along with silver sulphadiazine as control on burn wound in *Wistar albino rats*. The histopathological examinations confirmed that the treated animals showed improved rate of epithelialization and wound contraction. On comparison among the impact of test compounds; it was further revealed that, the *Butea monosperma* leaves aqueous extract and synthesized amide analogue showed significant wound healing activity than isolated acidic ingredient.

Keywords: *Butea monosperma*, isolated ingredient, amide analogue, burn wound.

INTRODUCTION

The physical injury that results breakdown in the protective function of the skin and the loss of continuity of epithelium with or without loss of underlying connective tissue is called wound. Proper healing of wound is essential for the restoration of disrupted anatomical continuity and also altered functional status of the skin. Wound healing is a complex and fundamental activity of all damaged body structures. The same principle underlines the healing of cuts, abrasions, ulcers and areas damaged by chemical attack, invasion by microorganisms or immune reactions. Healing of the skin damaged by a physical assault may be divided into following three aspects[1],

     i.   An immediate haemostatic phase,

     ii.   An early phase of re-epithelialization,

     iii.   A later phase of dermal repair and remodelling.

Research on wound healing agents is one of the developing areas in modern biomedical sciences. Recently there has been a shift in universal trend from synthetic to herbal medicine, which we can say 'Return to Nature'. Medicinal plants have been known for 'millennia' and are highly esteemed all over the world as a rich source of therapeutic agents for treating wounds, cuts and burns. The herbal drugs are popular for wound healing among rural and urban communities of India. The one reason for the popularity and acceptability is the belief that all natural products are safe. The demand for plant-based medicines, health products, pharmaceuticals, food supplements, cosmetics, etc., are increasing in both developing and developed countries due to the growing recognition that the natural products are nontoxic, have less side effects and are easily available at affordable prices[2].

In the literature, *B. monosperma* is ascribed to have many medicinal properties. The flowers and leaves are reported to possess astringent, diuretic, depurative, aphrodisiac and tonic properties. They are also effective in leprosy, leucorrhoea and gout. The leaves are also used to cure boils, pimples and tumorous hemorrhoids and are internally given in flatulent colic, worms and piles. The leaves are reported to contain alkaloids, protein, fibre and minerals. The bark is useful in tumors, bleeding piles and ulcers[3]. Topical administration of an alcoholic bark extract was found to improve the different phases of wound repair, including collagen synthesis and maturation, wound contraction and epithelialization[4].

The present study was undertaken to explore the efficacy of aqueous extract of *Butea monosperma* leaves, isolated acidic ingredient and newly synthesized amide analogue along with silver sulphadiazine as control on burn wound healing in *Wistar albino rats*.

MATERIALS AND METHODS

Plant material:

The leaves of *Butea monosperma* plant were collected seasonally from the Melghat region of Amravati, District of Maharashtra, India. It was authenticated by the taxonomist Dr. S. P. Rothe with Voucher specimen (ML – 101) and was deposited in the herbarium of Department of Botany, Shri Shivaji College, Akola.

Extraction and Isolation:

The leaves of *Butea monosperma* plant were shade dried at room temperature and ground in a manual mill to get coarse powder. The powder was kept in the airtight polythene bag and stored at dry place. This powder was extracted with water as a solvent by using soxhlet apparatus. The extract was concentrated at 40 ^{o}C using rotary evaporator. Finally it was dried, crushed and stored in air tight bottle at 4 ^{o}C for further study. The aqueous test extract (100g) was dissolved in $NaHCO_3$ till there was no effervescence then filter and crude acidic ingredients were re-appeared from filtrate using 10% HCl.

The crude acidic ingredients (35g) adsorbed on to a silica gel (s d fine 60-120 mesh) and subjected to column chromatography over silica gel (100-200 mesh) and eluted with n-hexane followed by petroleum ether-benzene-acetic acid gradient system (20:40:40, 40:20:40, 40:40:20). The fractions were collected in 100ml conical flasks. The eluted fractions were combined to give major fractions by comparing their R_f values, when run on TLC Aluminium sheets Silica Gel 60 F_{254} 0.2 mm thickness with similar solvent systems. The separated components on the silica plate were visualized in UV light and then to Iodine, methyl red, bromophenol blue, vanillin sulphuric acid. After developing TLC profile, similar TLC pattern fractions were mixed together to get major fractions. Total seven fractions were collected (F1-F7). Fraction F-5 was subjected to repeated chromatographic purification over silica gel using elution with petroleum ether-benzene-acetic acid (40:40:20) to give compound 1 (100 mg)[5&6] .

Characterization of compound 1:

M.P.: 245 °C, **Elemental analysis:** Found C =49.40,

H = 3.52, O = 47.00, Calculated C = 49.42, H = 3.55, O = 47.02 %. **UV spectrum:** λmax283 nm (n $\rightarrow$π*). **IR spectrum, v, cm^{-1}:** 3367.61, 3289.24, 3064.85, 3011.46 (-OH stretching), 3064.85 (Ar-H stretching), 1702.93, 1618.06 (two C=O absorptions), 1600-1450 (aromatic ring), 1300-1000 (C-O). **^{1}H NMR spectrum (400 MHz):**δ ppm 4.801 (3H, s, aromatic C-O**H**), 7.087-7.221 (2H, s, Ar-**H**).

From the characterization it was found that isolated compound 1 was Gallic acid. The major ingredient i.e. Gallic acid (Compound 1) thus separated from test extracts was then used for the preparation of its amide analogue (Compound 2).
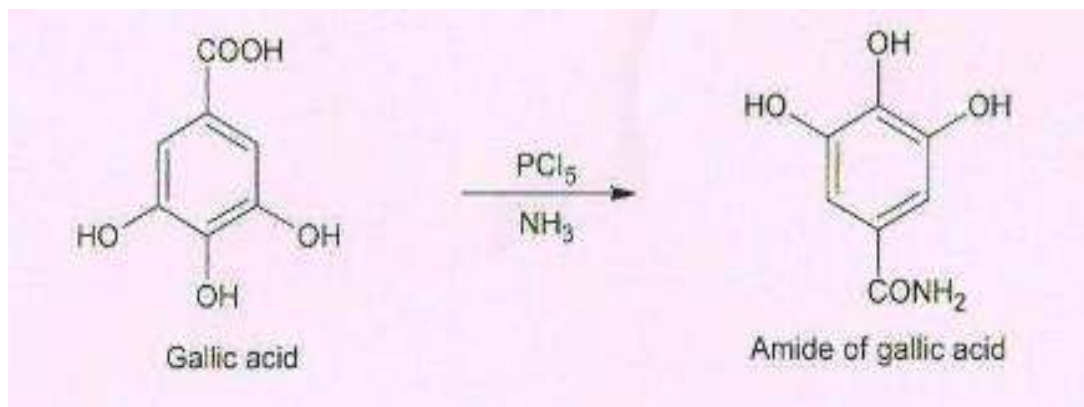
Characterization of compound 2: **M.P.:** 240 °C, **Elemental analysis for $C_7H_8N_2O_4$:**

Found C = 45.40, H = 4.32, O = 34.73, Calculated C = 45.66, H = 4.38, N = 15.21, O = 34.75 %.

UV spectrum: λmax283 nm (n $\to \pi^*$). **IR spectrum v, cm^{-1}:** 3754 (-NH$_2$ stretching), 3714(overtone of 1658), 3273 (-NH stretching/-OH stretching), 2375, 2341(-CH stretching) 1658 (-NH bending, primaryamine), 1614 (C-O stretching), 1541(NH bending, secondary amine), 769 (-NH oop). **^{1}H NMR spectrum(400 MHz):** δ ppm 1.902 (2H, s, primary amine), 2.007(1H, s, secondary amine), 4.800 (3H, s, aromatic C-O**H**), 7.015 (2H, s, Ar-**H**).

Animals:

The interdisciplinary part of proposed study was carried out after getting permission from the Institutional Animal Ethical Committee, Pusad (CPCSEA/IAEC/CP_PL/07-2012). The care of laboratory animals was taken according to the guidelines of CPCSEA, Ministry of Forests and Environment, Government of India (registration number 729/02/a/ CPCSEA).

All the experiments were carried out using adult *albino Wistar male rats* weighing about 130-150 gm. The animals had free access to food and water and they were housed in cages in a natural (12 hrs each) light–dark cycle. The animals were acclimatized to the laboratory conditions for at least 5 days before behavioral experiments which were carried out between 0900 h and 1800 h.

Burn wound healing activity[7]:

Dorsal skin of the *Wistar rats* were shaved at full thickness. The animals were anesthetized by ketamine injection and burn wound of approximate 2 cm in diameter were created (circular area) by the brass probe which was immersed in boiling (100 °C) water until thermal equilibrium was reached. The probe was then placed on the back of the rats for 20 s without applying pressure. They were then housed individually in separate cages after complete recovery from anaesthesia.

Rats were randomly divided into five groups of ten animals each:

Control group:

Immediately after burning, burn areas were covered with propylene glycol solution once a day for 20 days.

Standard Silver Sulphadiazine group:

Immediately after burning, burn areas were covered with Silver Sulphadiazine cream once a day for 20 days.

Crude extract group:

Immediately after burning, burn areas were covered with crude extract of leaves sample which was prepared in propylene glycol once a day for 20 days.

Isolated acid group:

Immediately after burning, burn areas were covered with isolated acid sample prepared in propylene glycol, once a day for 20 days.

Prepared analogue group:

Immediately after burning, burn areas were covered with the prepared analogue sample also prepared in propylene glycol once a day for 20 days.

The wounds were clinically observed in all groups every day. After 10th and 20th days later, the rats were sacrificed after being anesthetized.

BIOPHYSICAL PARAMETERS

Measurement of wound contraction:

The animals were inspected daily and the observations of percentage wound closure were made on 10th, 15th and 20th post wounding days and the photographs were taken. The wound closure was monitored by planimetric measurement of the wound area which was achieved by tracing the wound on a graph paper. The healed area was calculated by subtracting it from the original wound area (2nd day). The percentage of wound contraction was determined using the following formula:

Percept wound contraction = Healed area/Total wound area x 100

To apply this equation, the wound margins were traced and measured to calculate the non-healed area which was then subtracted from the original wound area[8].

Measurement of thickness of epithelial:

The thickness of granulation tissues (epithelial) was measured by planimetric measurement of center of wound[9]. The thickness of granulation tissue was measured on the isolated burn wound sample of skin at 10th day and at 20th day of sacrification of respective group of animals. The thickness was measured by planimetric, by simply placing the sample of wound area between the

plane surfaces of two slides. The gap between the two slides after placing the skin sample between them was measured. This was considered as thickness (cm) of granulation tissue.

Histopathological examination:

At the end of 10th day and 20th day's trial, the rats were sacrificed and the burned skin tissue samples were collected for histopathological examination. The tissue samples were fixed in 10% formalin solution and then dehydrated through dehydrated alcohol series, cleared in xylene and embedded in paraffin wax. The series of sections were cut and stained with Hematoxylin and Eosin. The sections were examined under light microscope and the photographs were taken.

Statistical analysis:

The results were expressed as mean ± SD of 5 rats in each group. One way ANOVA followed by Tukey's test and Newman-keuls multiple comparison test were carried out to determine the significant difference on rate of percentage contraction and thickness of granulation tissue of wound area between the control group and the test samples at different trial periods ($p<0.05$).

RESULTS AND DISCUSSION:
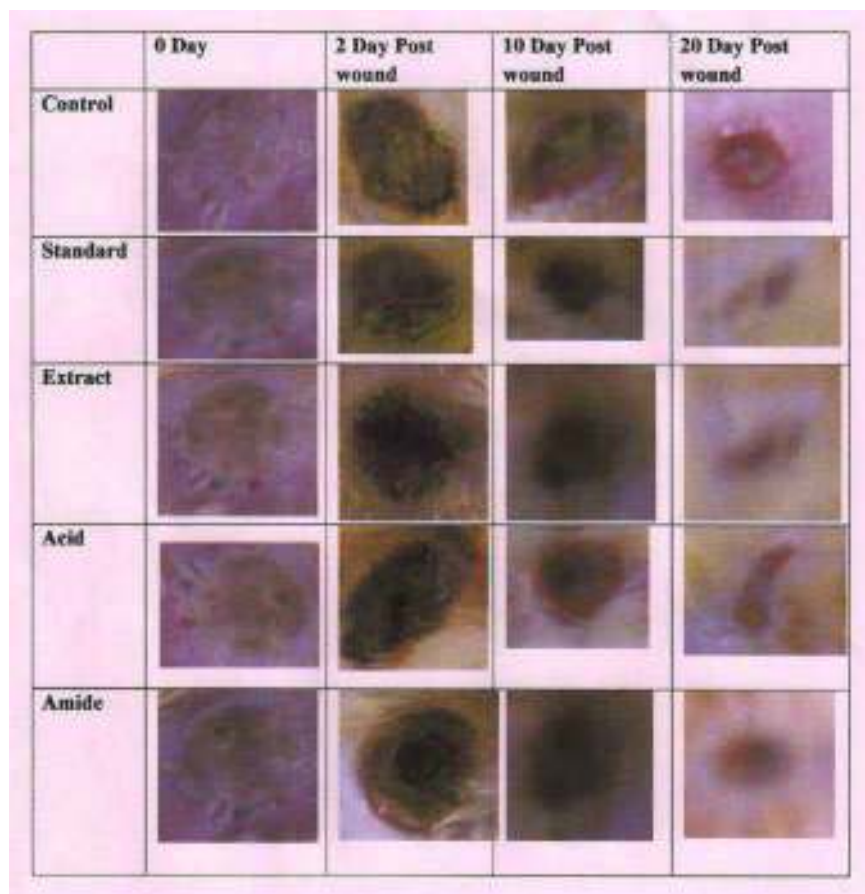
Figure 1: Photographic representation of contraction rate on different days of control and experimental wounds

No mortality was observed in animals during the study period. The wounds in the controlled group of animals displayed a greater degree of inflammation on the basis of three clinical sign of the inflammation process i.e. heat, redness and swelling which appeared to be lessened in wounds treated with test samples. Up to 5 days, the degree of redness was found to remain comparatively same in all animals including treated group of animals. At the end of 10th day of trial period, the redness was still present on the surface of wound in control and isolated acid treated group of animals, while in silver sulphadiazine, crude extract and amide treated group, the degree of redness on the surface of wound appeared to be lessened. On 20th day of trial period there was complete disappearance of redness in all treated groups as shown in figure 1.

Table 1: Percent wise effect of treatments on wound contraction

Treatments	On 2 Day	After 10 Days	After 15 Days	After 20 Days
Control	1.84±0.101 (100)	1.24 ±0.12 (32.6)[a]	0.82±0.103 (55.44)[b]	0.51±0.13 (72.29)[c]
Standard (SSD)	1.88±0.231 (100)	0.887±0.24 (52.8)[a, 1]	0.425±0.13 (77.4)[b, 1]	0.13±0.047 (92.91)[c, 1]
Extract (2%)	1.84±0.102 (100)	0.69±0.058 (62.5)[a, 3]	0.36±0.06 (80.44)[b, 3]	0.15±0.05 (91.85)[c, 3]
Acid (2%)	2.02±0.132 (100)	0.83±0.13 (58.91)[a, 2]	0.46±0.04 (77.1)[b, 2]	0.24±0.096 (88.25)[c, 2]
Amide (2%)	1.825±0.227 (100)	0.725±0.075 (60.28)[a, 4]	0.33±0.047 (81.74)[b, 4]	0.13±0.047 (92.7)[c, 4]

All the readings were in mean of centimeter (N=5) ± S.D. Values in parenthesis were given in percent of wound contraction considering their 2nd day reading as 100 %. [abc] The Values in row shown significant different as compared to their 2nd day values; [1234] The Values in column indicated significant different as compared to their corresponding control readings (One way ANOVA followed by post hoc Newman-keuls multiple comparison test)

The rate of contraction of control and experimental wounds are represented in Table 1 and Figure 1 & 2. The treated wounds were found to contract much faster. At the end of 20th day after burn wound creation, the control rats showed 72.29 % of wound contraction indicating the natural healing property of skin. The acid demonstrated 88.25%, extract represented 91.85 % while amide derivative indicated 92.7 % wound contraction. These results demonstrated the treatment increased the healing property of burn wound. Statistically, the percentage of wound contraction showed that, there was significant difference between the different groups (p<0.01). The wound healing potential for the aqueous extract and amide analogue demonstrated excellent activity as compared to isolated acid of *Butea monosperma*.
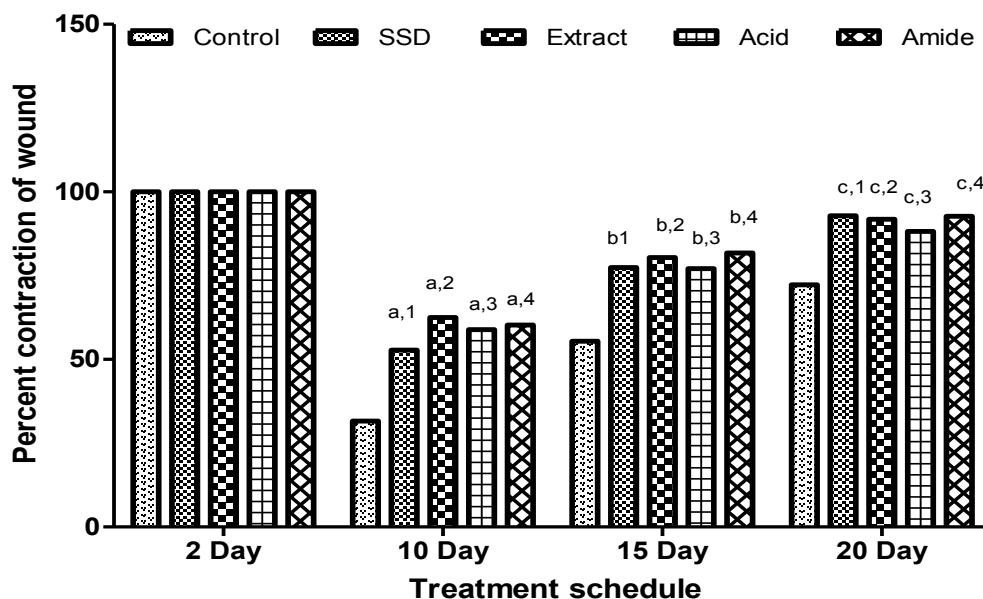
Figure. 2.The periodical rate of contraction in control and treated group rats.

The wound healing activity in treated group animals indicated significant ($p < 0.05$) increase in the thickness of granulation tissue which were measured among the groups at 10th and 20th day. On the 10th day of the trial period, the thickness of the granulation tissue was on higher side in all treated group animals as compared to control group animals. The statistical difference was observed on 20th day of the trial period. The thickness of the granulation tissue was statistically different ($p < 0.05$) among all treated groups except the isolated acid treated group animals. The mean values of thickness of granulation tissues in the center of wound are shown in table 2.
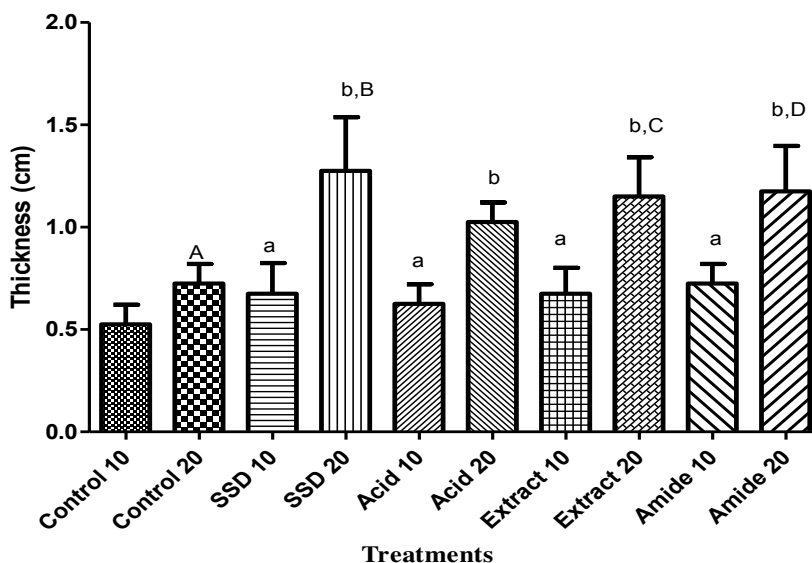
Figure 3:Effect of different treatment on thickness of granulation tissue of wound

Table 2:Thickness of granulation tissues in the center of the wound

| Days | Groups | | | | |
	Control	SSD	Extract	Acid	Amide
10th Days	0.525±0.083	0.725±0.109^a	0.675±0.109^a	0.625±0.083^a	0.725±0.083^a
20th Days	0.77±0.083^A	1.27±0.23^{bB}	1.15±0.165^{bC}	1.02±0.083^b	1.175±0.192^{bD}

(SSD=Silver Sulphadiazine); All the reading were in mean of centimeter ±S.D (N=5); ^{ab} values in same column were significantly different ($p<0.05$); ^{ABCD} values in same row were significantly different ($p<0.05$); One way ANOVA followed by post hoc Tukey's test.
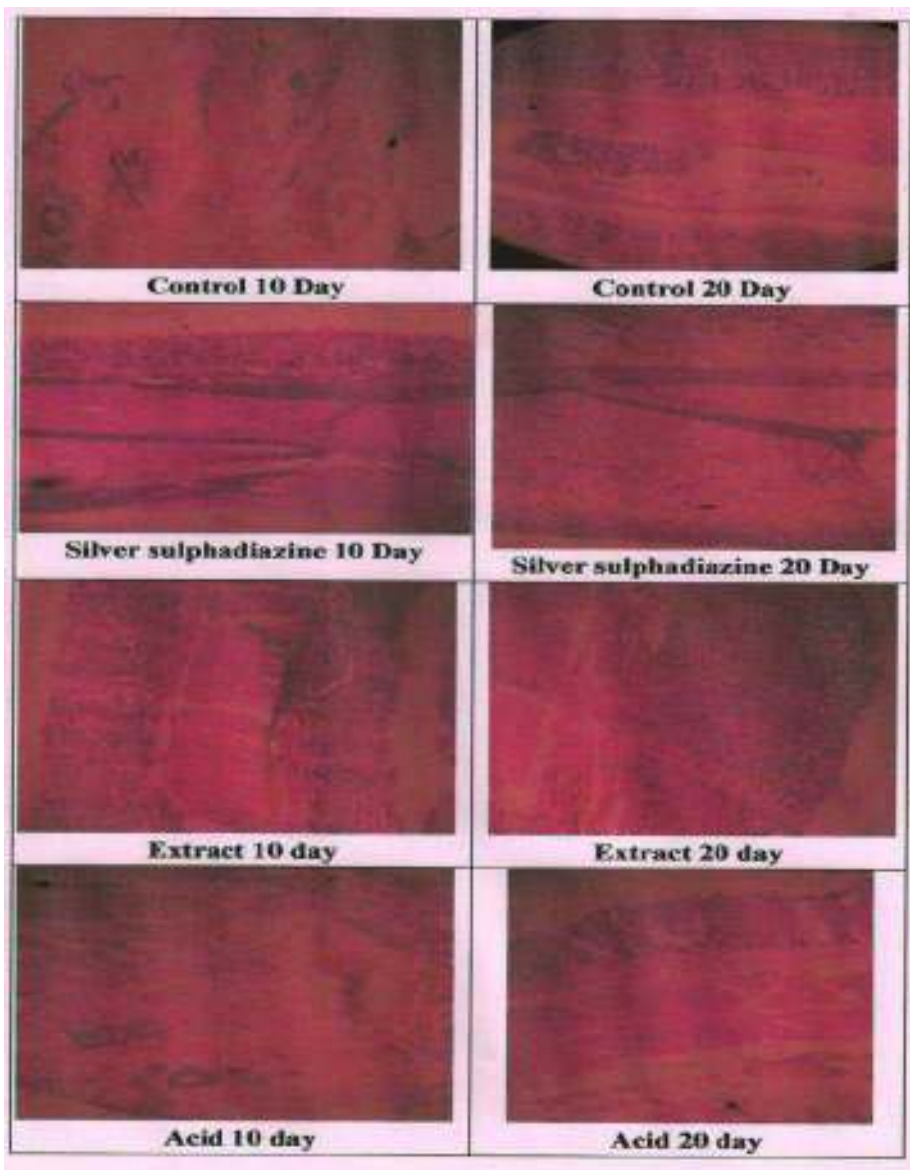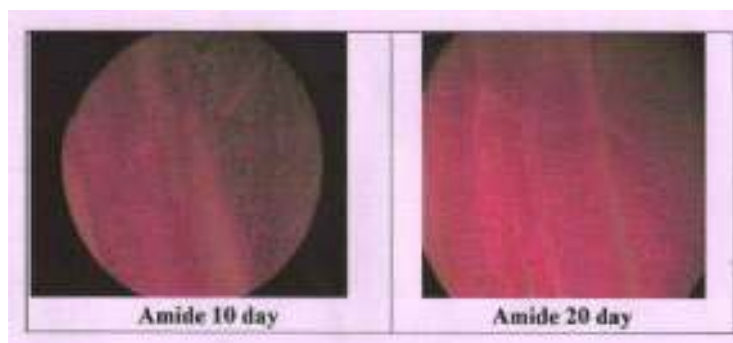
Figure 4: Photographs of Histopathological study

At the end of each 10th and 20th day's trial period, the experiment of histological examination was carried out for treated and untreated wound samples. At 10th day of histological examination in control group animals, the collagen fibers were found loosely packed with irregular arrangement and incomplete epithelialization with less fibrous tissues at wound site. Whereas in treated animals at 10th day the collagen fibres were found orderly packed and keratinocytes were easily differentiated from epidermis. After 20th day of histological examination, there was lessened inflammation in treated group wounds as compared to control group wounds. Granulation tissues in dermis and epithelial layers had better appearance in treated animals as compared to control group animals.

CONCLUSION

On the basis of the results obtained in the present investigations, it can be concluded that the 2% w/w of isolated acid ingredient had significant burn wound healing activity. While the results of extract and synthesized amide analogue (2% w/w) had excellent wound healing activity than the isolated acid treated group. These results were supported by the folklore reflecting the use of plant and its analogues in the management of burns.

ACKNOWLEDGEMENT

REFERENCES

1. Marks R. Roxburgh's Common Skin Diseases. 17th Ed., International Students Edition; 2003.

2. Shah B, Seth AK. Text Book of Pharmacognosy and Phytochemistry. Elseveir publications; 2010.

3. The Wealth of India: A Dictionary of Indian Raw materials and Industrial products. First supplement series Volume 1: A-Ci; National Institute of Science Communication and Information Resources, CSIR, New Delhi; 2004.

4. Lochin S, Miriyala S, Panchatcharam M. Efficacy of *Butea monosperma* on dermal wound healing in rats. The International Journal of Biochemistry & Cell Biology 2005; 37:566-573.

5. Egon Stahl. Thin-Layer Chromatography. 3rd Indian Reprint, Springer International Edition; 2009.

6. Harborne JB.Phytochemical Methods: A guide to modern techniques of plant analysis. 6th Indian reprint, Springer International Edition; 2010.

7. Nilugal KC, Perumal K, Ugander RE, Chittor A. Evaluation of Wound Healing Activity of *Piper Betle* Leaves and Stem Extract in Experimental *Wistar* Rats. Am. J. Pharm Tech Res. 2014; 4 (3): 443-452.

8. Yaman AS, Durmus S, Ceribasi M, Yaman M. Effects of *Nigella sativa* and silver sulfadiazine on burn wound healing in rats. Veterinarni Medicina 2010; 55 (12): 619–624.

9. Somboonwong J, Kankaisre M, Tantisira B, Tantisira MH. Wound healing activities of different extracts of *Centella asiatica* in incision and burn wound models: an experimental animal study. BMC Complementary and Alternative Medicine 2012; 12:103.

10. Karodi R, Jadhav M, Rub R, Bafna A. Evaluation of the wound healing activity of a crude extract of *Rubia cordifolia* L. (Indian madder) in mice. International Journal of Applied Research in Natural Products 2009; 2(2):12-18.

11. Avula M, Sudhakar Babu K, Ravi sankar T, Reddanna P, Latha J. Evaluation of wound healing properties of bioactive fractions from the extract of *Butea monosperma* (lam) stem bark. International Journal of Phytomedicine 2011; 3:41-49.

12. Manoj GS, Murugan K. Wound healing activity of methanolic and aqueous extracts of *plagiochila beddomei* Steph. Thallus in rat model. Indian Journal of Experimental Biology 2012; 50: 551-558.

International Journal of Green and Herbal Chemistry

Research Article
CODEN (USA): IJGHAY

Antimicrobial study of analogues prepared under microwave assistance of active ingredient isolated from *Buteamonosperma* plant and their growth promoting impact on some flowering plants

M. O. Malpani[1*], P. R. Rajput[2]

[1]Department of Chemistry, Shankarlal Khandelwal College, Akola 444-002,

[2]Department of Chemistry, Vidya Bharati Mahavidyalaya, Amravati 444-602.

Abstract: *Buteamonosperma*is one of the medicinally potential plants found in Melghat region which is frequently used for the eradication of skin diseases. In the present study we have undertaken microwave assisted synthesis the analogues of active ingredient isolated from leaves of *Buteamonosperma*plant extract and screened for their antibacterial activity against pathogens responsible for skin diseases viz. *Streptococcus pyogenes, Nocardiacalcarea, Trichosporoncutaneum, Rhodotorularubra.* The synthesized compounds were screened for their growth promoting impacts on some flowering plants viz. *Papaverrhoeas, Gladiola tristis, Dianthus chinensis, Candy tuft, Gaillardia, Calendula officinalise.*

Key words: *Buteamonosperma*, microwave assisted synthesis of analogues, skin diseases, *Streptococcus pyogenes, Nocardiacalcarea, Trichosporoncutaneum, RhodotorularubraPapaverrhoeas, Gladiola tristis, Dianthus chinensis, Candy tuft, Gaillardia, Calendula officinalise.*

INTRODUCTION

The forest of Melghat Tiger reserve is of deciduous nature and has been categorized as "Dry deciduous forest". The geological formation of the soil largely determines the type of vegetation it is going to support. The most of the area has the soil of trap origin which is rich in minerals and having a high water holding capacity. The soil strata has a remarkable rate of exchangeable

calcium and pH varying from 6.5 to 7.5 thus supporting the best form of teak and its associate flora.This is the main reason that to make *Tectonagrandis* (teak) is the most dominant species of Melghat forest. This region is also determined as a unique blend of multiple high hills and deep valleys with terrains and vegetations changing at close intervals.

More than 750 plant species have been enlisted in the Flora of Melghat[1]. These species belong to 400 genera representing as many as 97 families. There are 91 trees, 109 shrubs, 450 herbs, 38 climbers, 23 sedges and 84 grass species.

In the literature, *B. monosperma*is ascribed to have many medicinal properties such as astringent, diuretic, depurative, aphrodisiac, rubefacient, tonic, and anthelmintic. They are effective in leprosy, leucorrhoea, gout, diarrhoea, puerperal women, elephantiasis, night blindness and other defects of sight, dysentery, phthisis and haemorrhage from stomach and bladder, inflammations, ringworm, ulcers and sore – throats[2, 3].

MATERIALS AND METHODS

The leaves of *Buteamonosperma* plant was collected from the Melghat region of Amravati, District of Maharashtra, India seasonally and authenticated by the taxonomists Dr. S. P. Rothe from the Department of Botany, Shri Shivaji College Akola. Voucher specimen (ML – 101) was deposited in the herbarium of Department of Botany, Shri Shivaji College, Akola.

Chemicals: All the chemicals used in the study were obtained commercially and of analytical grade.

Microorganisms: The microorganisms which were used viz: *Streptococcus pyogenes, Nocardiacalcarea, Trichosporoncutaneum,* and *Rhodotorularubra*procured from National Collection of Industrial Microorganisms (NCIM), National Chemical Laboratory, Pune 411 008.

Experimental: The leaves of *Buteamonosperma* plant was shade dried at room temperature and ground in a manual mill to get coarse powder. It was kept in the air tight polythene bag and stored at a dry place. The powdered material was extracted with water as a solvent by using soxhlet apparatus. The extract was concentrated for further studies at 40 ºC in water bath. The test extract then dried, crushed and stored in air tight bottle for further study. The acidic ingredients present in the extracts were separated by conventional as well as sophisticated chromatographic methods. The major active acidic ingredient i.e. Gallic acid (1a) separated from acidic ingredients was then used for the preparation of analogues under Microwave irradiation.

Synthesis of 3, 4, 5-trihydroxy benzohydrazide (2a): Gallic acid (0.01 mol), methanol (0.03 mol) and hydrazine hydrate (0.02 mol) were mixed and stirred for five minutes. The reaction mixture was exposed to microwave irradiation at low frequency for 45 seconds. The product thus obtained was crystallized by using ethanol.

Synthesis of 5-(4-amino-5-sulfanyl-4H-1, 2, 4-triazole-3-yl) benzene-1, 2, 3-triol (3a):3, 4, 5-Trihydroxy benzohydrazide (II) (0.01 mol), carbon disulphide (0.03 mol), potassium hydroxide (0.02 mol) and hydrazine hydrate (0.03 mol) were mixed together and exposed to microwave irradiation at low frequency for 45 seconds. The yellow colour product thus separated was crystallized by ethanol.
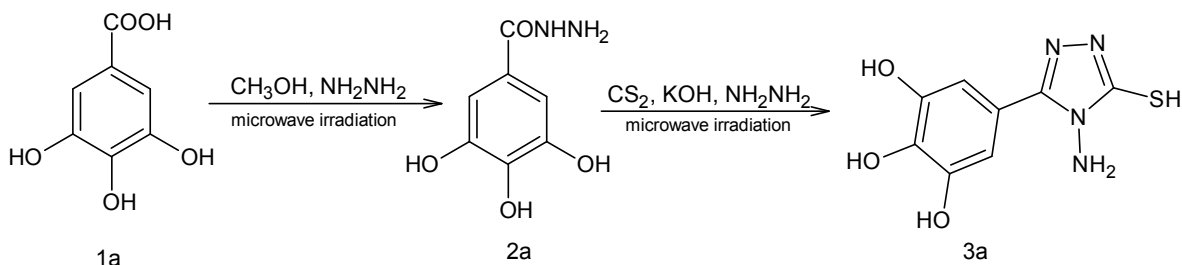
The isolated active ingredient and synthesized analogues were characterized on the basis of elemental analysis, molecular weight determination, and spectral data: The details thereof are as:

COMPOUND (1A):

Yield: 40%, *M.P.:* 250 °C, *Elemental analysis for $C_7H_6O_5$:* Found C =49.40, H = 3.52, O = 47.00, Calculated C = 49.42, H = 3.55, O = 47.02 %. *UV spectrum (EtOH):*λmax283 nm (n→π*).

IR spectrum, v, cm^{-1}: 3367.61, 3289.24, 3064.85, 3011.46 (-OH stretching), 3064.85 (Ar-H stretching), 1702.93, 1618.06 (two C=O absorptions), 1600-1450 (aromatic ring), 1300-1000 (C-O). *^{1}H NMR spectrum (400 MHz, CDCl$_3$):*δ ppm 4.801 (3H, s, aromatic C-O**H**), 7.087-7.221 (2H, s, Ar-**H**).

COMPOUND (2A):

*Yield:*75%, *M.P.:* 192 °C, *Elemental analysis for $C_7H_8 N_2O_4$:*Found C = 45.40, H = 4.32, O = 34.73, Calculated C = 45.66, H = 4.38, N = 15.21, O = 34.75 %.

*UV spectrum (EtOH):*λmax283 nm (n →π*);*IR spectrum v, cm^{-1}:* 3754 (-NH$_2$ stretching), 3714 (overtone of 1658), 3273 (-NH stretching/-OH stretching), 2375, 2341(-CH stretching) 1658 (-NH bending, primary amine), 1614 (C-O stretching), 1541(NH bending, secondaryamine), 769 (-NH oop). *^{1}H NMR spectrum (400 MHz, CDCl$_3$):* δ ppm 1.902 (2H, s, primary amine), 2.007(1H, s, secondary amine), 4.800 (3H, s, aromatic C-O**H**),7.015 (2H, s,Ar-**H**).

COMPOUND (3A):

Yield: 70%, **M.P.:** 166 °C, **Elemental analysis for $C_8H_8N_4O_3S$:** Found C =40.00, H = 3.30, N= 23.30, O = 19.92, S = 13.29, Calculated C = 40.00, H = 3.36, N= 23.32, O =19.98, S = 13.35 %.

UV spectrum (EtOH):λmax366 nm (n →π*). **IR spectrum, v,cm^{-1}:** 3273 (-OH stretching), 3178 (-NH$_2$ stretching) 2956 (Ar-H stretching), 2380 (-SH stretching), 1638, 1527 (Ar C=C stretching), 1487 (-CN stretching), 1527 (-NH bending, primary amine), 753-678 (monosubstituted oop).**^{1}H NMR spectrum (400 MHz, CDCl$_3$):**δ ppm1.943 (2H, s,primary amine), 2.054 (1H, s, aromatic C-S**H**), 4.525-5.192 (3H, s, aromatic C-O**H**) 7.033 (2H, s, Ar-**H**).

Antimicrobial Assay: The crude acidic ingredients, major acidic ingredient (1a), analogues prepared (2a & 3a) along with whole extract of leaves were screened for their antibacterial potency

by cup plate agar method[4,5] against bacterial species *viz.,Streptococcus pyogenes, Nocardiacalcarea, Trichosporoncutaneum,* and *Rhodotorularubra*. The petriplates were prepared with 25ml sterile Mueller Hinton Agar. A sterile cork borer (8 mm) was used to make wells in each plate.1 ml inoculums' suspension was swabbed uniformly over the agar medium to get uniform distribution of bacteria. After labelling the plates 100 l of each test compound (at concentration of 0.01 mol) was added aseptically into the wells. The petriplates were then incubated at 37°C for 24 hrs during which the activity was evidenced by the presence of zone of inhibition surrounding the well. The negative control was prepared using respective solvent. *Ampicilin disc* (10 mcg/disc) and *Vancomycin disc* (30 mcg/disc) were used as positive control. The zones of inhibition were recorded in millimetres by using Himedia Zone Reader Scale.

Table- 1: Antibacterial activity of test compounds:

Extracts & analogues	Concentration	Inhibitory zones in mm			
		S. pyogenes	*N. calcarea*	*T. cutaneum*	*R. rubra*
1) Crude acidic ingredients	0.01 mol	18	22	18	20
2) Active acidic ingredient (1a)	0.01 mol	24	24	20	22
3) Analogue (2a)	0.01 mol	30	26	22	24
4) Analogue (3a)	0.01 mol	28	28	26	25
5) Whole extract of leaves	0.01 mol	16	14	18	17
6) *Ampicilin*disc	10 mcg/disc	16	20	18	18
7) *Vancomycin*disc	30 mcg/disc	16	20	22	18

Physiological Activity: The analogues prepared (2a & 3a) were screened for their growth promoting impacts on some flowering plants viz. *Papaverrhoeas, Gladiola tristis, Dianthus chinensis, Candy tuft, Gaillardia, Calendula officinalise.*The experimental set up of the study was divided into seed treatment and field experiment.

Seed treatment: With a view to safeguard dormant seed's potential from harmful external agencies, the seed of the test plants were treated by test compounds before sowing.

Field experiment: Pre-germinated quality seeds of *Papaverrhoeas, Gladiola tristis, Dianthus chinensis, Candy tuft, Gaillardia, Calendula officinalise* were procured from genuine agricultural agencies. The beds of black cotton soil, 2.5 x 2.5m size were prepared on an open field. The sowing of seeds of all six flowering plants under examination were done in beds and in earthen pots separately by conventional methods and irrigated as and when required. The plants from each bed and pot were divided into two groups, i.e. A and B which were designated as *'control'* and *'treated'* group plants respectively. The plants from group B were sprayed with the solution of synthesized compounds at fortnightly intervals. The field experiments were conducted to compare the treated plants of group B with untreated plants of controlled group A. In this context, the observation were recorded on 15, 30, 45, 60, 75 and 90 days after sowing; corresponding to early vegetative, late vegetative, flowering, pod filling and pod maturation stages, with special reference to number of leaves and height of shoots. The results of field's experiments with synthesized compounds are tabulated in **Table 1.**

Table-1: Activity of the synthesized compounds (2a), (3a)

Periodicity of the observation (in days)	Poppy (*Papaver rhoeas*)				Calendula (*Calendula officinalise*)				Gladiolus (*Gladiola tristis*)				*Gaillardia* (*Gaillardia aristata*)				Pink (*Dianthus chinensis*)				Candytuft (*Iberis* sp)			
	Shoot height		No of leaves		Shoot height		No of leaves		Shoot height		No of leaves		Shoot height		No of leaves		Shoot height		No of leaves		Shoot height		No of leaves	
	C	T	C	T	C	T	C	T	C	T	C	T	C	T	C	T	C	T	C	T	C	T	C	T
Activity of the synthesized compound 3, 4, 5-trihydroxy benzohydrazide (2a)																								
15	3	3	10	10	1	1	8	7	2	2	1	2	4	3	4	5	2	2	4	4	3	2	9	5
30	6	7	14	15	3	7	17	18	6	7	2	3	6	8	15	8	5	4	10	8	6	4	15	20
45	9	10	21	25	9	10	28	30	8	9	4	5	8	15	30	20	7	8	15	16	8	7	45	40
60	11	12	22	30	10	16	52	55	15	16	5	6	12	17	50	38	10	12	25	29	12	11	60	70
75	16	17	31	47	14	20	78	85	18	20	6	8	16	20	60	70	13	17	34	41	15	15	100	105
90	20	23	52	78	16	21	98	115	20	21	6	10	20	21	95	105	18	20	50	63	18	19	130	150
Activity of the synthesized compound 5-(4-amino-5-sulfanyl-4H-1, 2, 4-triazole-3-yl) benzene-1, 2, 3-triol (3a)																								
15	3	4	9	7	2	4	9	12	2	3	1	1	4	2	4	5	2	2	4	2	3	4	9	10
30	7	7	15	15	4	5	18	28	6	7	2	2	6	5	15	8	5	4	10	6	6	8	15	27
45	10	12	20	21	8	11	30	40	10	11	4	5	8	8	30	20	7	7	15	15	8	12	45	62
60	12	18	22	25	10	15	55	60	15	16	5	6	12	14	50	38	10	11	25	25	12	15	60	100
75	16	22	30	38	13	20	80	100	20	21	6	8	16	18	70	80	13	14	34	34	15	19	100	145
90	20	25	47	50	15	22	100	130	22	25	6	10	20	22	100	100	18	19	50	50	18	24	130	150

Note: C= Control, T= Treated

RESULTS AND DISCUSSION

The results obtained for the antibacterial test performed with analogues prepared from isolated acidic ingredient along with mixture of acidic ingredients and whole extract of *Buteamonosperma* leaves presented in Table 1. The analogues prepared were found to be most effective against all pathogenic bacteria. The isolated active acidic ingredient was found to be more effective as compared with the mixture of crude acidic ingredients. The whole extract of leaves found to be moderately active. The results obtained were assessed on their comparison with the activities of standard antibacterial agent like *Ampicilin* and *Vancomycin* as control.

The analogues prepared (2a & 3a) were screened for their growth promoting impacts on some flowering plants viz. *Papaverrhoeas, Gladiola tristis, Dianthus chinensis, Candy tuft, Gaillardia, Calendula officinalise.* The efforts have been made to examine and analyze the morphology of treated plants. When the comparison of morphological characters was made between those of treated and control groups plants, it was interesting to note that all the plants exhibited significant shoot growth, and considerable increase in the number of leaves as compared to those of untreated ones.

ACKNOWLEDGEMENT

The authors are thankful to SAIF, CDRI, Lucknow for providing the spectral data. The authors are also thankful to the Dr. S. P. Rothe, Department of Botany, Shri Shivaji College, Akola for the authentification of leaves of *Buteamonosperma* plants.

REFERENCES

1. Official web site of Melghat Tiger Project, Amravati.
2. The Wealth of India, Raw materials Volume – 2: B; Council of Scientific & Industrial Research, New Delhi, **1988,** pp. 341 – 346.
3. K.R. Kirtikar, B.D. Basu; Indian Medicinal Plants, International Book distributors, Dehradun, 2005**,** Vol. I.
4. F. Kavanagh. Analytical microbiology, Part II. Academic Press; New York: **1972**.pp. 126.
5. V.D. Mane, P.R. Rajput, *et al*., phytochemical investigation and antibacterial activity of various extract of *cassia fistula* plant:*International Journal of Chemistry Research*, 2012: 3(1).
6. V.J. Hushare, P.R. Rajput, *etal.,* Synthesis, characterization and physiological activity of some novel isoxazoles: Bioscience, 2012:4(2), 81-85.
7. V.J. Hushare, P.R. Rajput, et.al., Synthesis, characterization of some novel pyrazoles and their growth promoting activity on some flowring plants: *International research journal of pharmacy*, 2013:4(1), 205-208.

Corresponding author: Dr. M.O.Malpani,

Department of Chemistry, ShankarlalKhandelwal College, Akola
momalpani@gmail.com

Effect of UV Radiation Exposure on The Dielectric Constant of Salicylic Acid Doped Polymer Thin Film of PMMA.

S.G.Vidhale[1*], N.G. Belsare[2], A.S.Wadatkar[2]

[1*]Dr Sau.Kamaltai Gawai Institute of Engineering and Technology, Darapur
2Department of Physics, Vidyabharati Mahavidyalaya, Amravati (M.S.) 444602 India

Email: shilpavidhale20@gmail.com

Abstract : The thin films of PMMA, pure and doped with 1%, 3%, 5%, 7%, 9% salicylic acid (SA) were prepared by using isothermal evaporation technique .The measurement of dielectric constant (ε_r) for all above samples have been carried out within the temperature range 323k-363k and at frequencies in the range 1KHz-1MHz.The results reveal that the dielectric constant decreases with the increase in the exposure time of UV radiations. The samples were characterized by XRD, SEM and FTIR

Keywords : PMMA-Polymethylmethacrylate, SA-Salicylic acid, UV- Ultraviolet Radiation.

Introduction:

Low dielectric materials have been intensively researched by ceramic and polymer scientists [1-3] . However, these materials posses a vast myriad of electrical, thermal, chemical and mechanical properties. Therefore, in many cases, the application of low dielectric constant materials are dictated by these other properties and the choice of low dielectric material may have a tremendous effect on a device's performance and lifetime.

Modern ultra-large scale integration (UWI) devices contain 10^8-10^9 transistors in an area smaller than 1 cm² and operate at a clock frequency approaching several GHz. As device dimensions shrink, the switching speed of its basic element increases as a consequence of the decrease in carrier's transit time across the length of a transitory channel, Of course, these basic elements must be interconnected to make the ULSI device functional.

As the functional complexity of devices increases, the number of interconnections levels and metal length continue to increase to the extent that an advanced ULSI device may consist of 8-10 levels of metal lines. For this reason, the effective speed of the device is becoming ever more dominated by the signal propagation through the horizontal and vertical metal interconnects of components with various functions. It is here that the resistance (R) and capacity (C) characteristics of the interconnect materials become important. In fact, the rapid increase in RC delay time is one of the main bottlenecks in deep submicron devices. The RC delay is given by

$$RC = 2\rho k \varepsilon_0 = (4L^2/P^2 + L^2/T^2) \dots \dots \dots (1)$$

ρ – is the metal resistivity, ε_0 is the vacuum permittivity, k is the relative dielectric constant of interlayer dielectric (ILD), P is the metal line pitch (Sum of the line width and line spacing), T is the metal thickness and L is the metal line length. This equation demonstrates that RC delay can be reduced using metals with

low resistivity and dielectric materials with a low dielectric constant. The introduction of copper and low dielectric const materials has improved the situation as compared with the conventional Al/SiO$_2$ technology by reducing both the resistivity and capacitance between wires.

Copper is becoming the common metallization material. Further lowering of the signal delay by introducing low-k dielectrics is one of the main challenges today (Maex et al, 2003). A description of all the problems related to the introduction of copper and low-k dielectrics is beyond the scope of this paper and hence we have limited our discussion to approaches to decreasing the dielectric constant of polymer thin film of PMMA, So that it will act as interlayer dielectric (ILD).

Classically, the dielectric constant of materials is described by Clausius- Mossoti Equation

$$(k-1)/(k+2) = 4\pi N\alpha \ldots\ldots\ldots\ldots (2)$$

Where, $k = \varepsilon/\varepsilon_0$

ε And ε_0 are the dielectric constants of material and vacuum, N is the number of molecules per unit volume (Molecular density) and α is total polarizability, including electronic (α_0), distortion (α_d) and orientation (α_o) polarizabilities. According to equation (2), the dielectric constant of materials can be reduced by decreasing the total polarizability and density. Early generations of low-k dielectrics were obtained by doping the traditional SiO$_2$ with fluorine and carbon during the chemical vapor deposition (CVD) of the dielectrics which typically have a k value in the range of 3-3.5. Other types of low-k dielectrics are based on organic polymers. Saturated hydrocarbons have a lower polarizability than unsaturated conjugated and aromatic hydrocarbons. Most of the organic low-k films with sufficient thermal stability have dielectric constant close to or in the range of 2.6-3.0. Decreasing the density produces a further reduction in the dielectric

constant. Therefore, ultra low k dielectrics with k less than 2.6 must be porous[4].

In this paper, we have discussed the effect of UV radiation on dielectric constant of salicylic acid doped polymer thin films of PMMA. Especially we have focused on lowering dielectric constant of thin films for the development of microelectronic devices based on low dielectric constant polymer films. For this purpose weight of PMMA in all sample remains fixed and salicylic acid doped at different weight percentage, so that we can find the optimum percentage ratio of SA that exhibits lowest dielectric constant value.

2. Experimental Procedure:
2.1 Materials:
In this study, PMMA (Sigma Aldrich), dopant salicylic acid (SA), and solvent THF (J.T. Baker) were used without further purification. Isothermal evaporation technique [5-8] was used to prepare the thin films of polymer.

2.2 Preparation of thin films:
1gm. PMMA was dissolved in THF (Tetrahydrofuran), and doped with salicylic acid in different weight percentage (1%, 3%, 6%, 7%, and 9%). The solution was cast on a glass plate and was allowed to evaporate slowly. This process has produced a mechanically stable and a free standing thin film.

2.3 UV Irradiation
A low pressure mercury vapor lamp (TUV 30W, Philips, Holland), which emits radiation at 254 nm, was used. The intensity of the incident light was 24 W m^{-2}. Films of the same thickness and surface area were placed at 15 cm distance from the light source. Irradiation times were for 0, 5, and 10 minutes. All irradiations were performed at room temperature in air.

2.4. Thickness Measurement:
The thickness of the film was measured by digital micrometer (Mitutago Corporation, Japan)
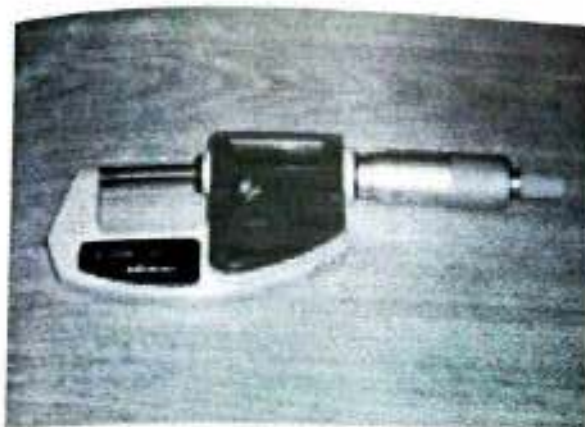
2.5 Dielectric constant measurement:

The AC conductivity of the samples was determined by 4284 A precision LCR meter over the frequency range 20 H$_z$ to 1MH$_z$ supplied by Agilent Technology, Singapore and corresponding dielectric constant (ε_r) was measured in the temperature range 323 K- 363K.

2.6 Characterization
2.6.1 X-ray diffraction (XRD)

The amorphousity of polymer thin films was investigated using XRD. The XRD pattern were recorded on Siemens D 5000 diffractometer with Cu-K α radiation (λ=1.54060A) over the range of 2θ=10°-60° at ambient temperature.

2.6.2 Scanning Electron Microscopy (SEM)

The morphology of polymer thin films at room temperature was studied by SEM.

2.6.3 FTIR Study:

To study the structural changes including the alteration in position and intensity of the characteristic bands Fourier Transform Infrared (FTIR) spectroscopy using Shimazu FTIR spectrophotometer 8300) over the range 400- 4000 cm-1 was used.

2.7. Prominent findings
Dielectric constant

i) decreases with increase in frequency at different constant temperatures.

ii) increases with increase in temperature at different constant frequencies

iii) decreases with increase in dopant percentage at constant temperature and constant frequency

iv) decreases with increase in time of exposure to UV radiation at constant temperature, frequency and dopant percentage.

3. Results and Discussion
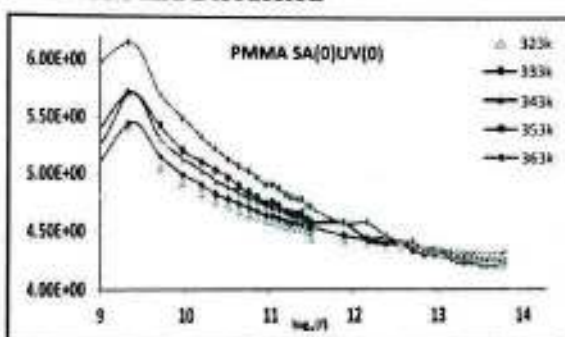
Fig 1: Variation of dielectric constant with log f at different constant temperatures
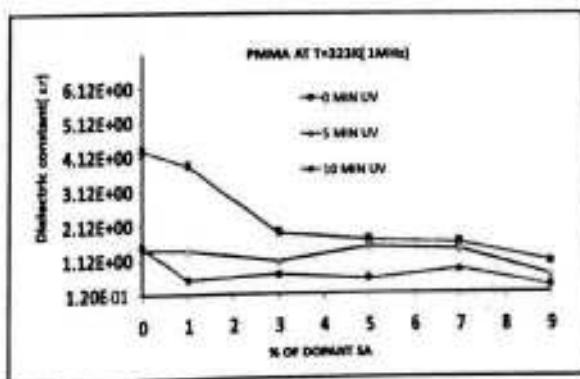
Fig 2: Variation of dielectric constant with percentage of dopant at increasing time of exposure to UV radiation

From fig.1 it is clear that dielectric constant decreases with the increase in frequency and increases with the increase in temperature. This can be explained as PMMA is weakly polar polymer[9] under alternating electric field, polar polymers require some time to align the dipoles. At very low frequencies the dipoles have sufficient time to align with the field before it changes direction. At very high frequencies the dipoles do not have time to align before the field changes direction. At intermediate frequencies the dipoles move but have not completed their movement before the field changes direction and they must realign with the changed field. The electronic polarization and to some extent atomic polarization, is instantaneous, at high or low frequency for both polar and non polar polymers. Therefore, polar polymers at low frequencies (e.g. 60 Hz) generally have dielectric constants of between 3 and 9, and at high frequencies (eg 1MHz) generally have dielectric constants of between 3 and 5. So as frequency increases, the orientational polarization decreases since it takes more time than electronic and atomic polarization .This decreases the value of dielectric constant with frequency reaching a nearly constant value at high frequency. The motion possibly occurring in amorphous material in the order of increasing temperature are: side chain motion, motion of two four moieties in the main chain (The Schatzki Cruck shaft effect), motion of moieties containing hetero atoms in polymer chain, motion of segments containing 50-100 backbone atoms (corresponding to Tg) and motion of the entire chain as a unit (Seanor1982). These motions are responsible for the freeing of change carriers and assisting the orientation of polar species as per the variation in the direction of applied AC electric field of constant frequency. The total polarization of the sample arises from the electronic polarization, atomic or ionic polarization and orientation polarization. Among these three contributions; orientation polarization is greatly assisted by the increase of temperature. This result is in agreement with

those reported in the literature [10-12]. The dielectric polarization results from molecular dipoles [13,14] ,which remain frozen at lower temperature and attains rotational freedom at higher temperature ,when the effect of molecular interaction energy becomes weaker than that of the thermal energy [13] .Therefore dielectric constant increases with temperature.
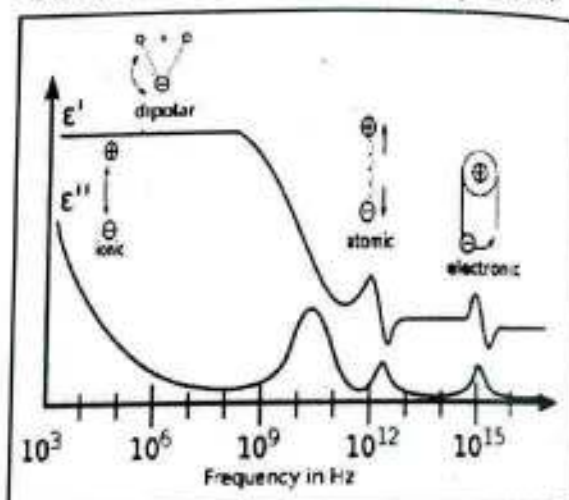
Fig 3 Dielectric constant and loss dispersion of dielectric materials against frequency.

The dielectric constant gets decreased with the increase in dopant percentage (Fig 2). As the dopant salicylic acid has –OH and –COOH groups ortho to each other, both these groups have tendency to release their hydrogen atoms as H^+ ions and the –COO group is electron hungry segment of PMMA that attracts the electrons present in C-CH and O-CH,bonds towards itself. As a result of this, a drift of electrons from nearby bonds starts flowing towards the COO group that imparts polarity in the parent molecule. But due to proximity and availability of electron rich centers within the molecule, the H^+ ions of Salicylic acid tend to form intramolecular hydrogen bonding. As a consequence of this, dopant salicylic acid remains unmoved. Under vigorous conditions, these H' ions may get departed partially but it is difficult to break their association completely from parent molecule. In this situation if we go on increasing the percentage of doping that may

enhance the complexity due to which the dielectric constant gets decreased with the increase in dopant percentage.

From fig 2 it is clear that, before irradiation value of dielectric constant is in the range of 4.3-1.03. After irradiation the value of dielectric constant is in range 1.5-0.64 for 5 min irradiation and for 10 min irradiation value is in the range of 1.5- 0.30.This means the dielectric constant gets decreased with the increase in time of exposure and the rate at which the dielectric constant decreases also becomes higher with the increase in time of exposure. This can be explained as; the bonds between the atoms in many polymers have dissociation energies that are very similar to the quantum energy present in UV radiation which is capable of breaking the bonds in the polymer chain to generate a cascade of reaction, oxygen radicals, hydro peroxide unit's carbonyl group formation, chain cleavage. As a result, the polarization group may get reduced and dielectric constant gets decreased as shown in fig (2)[15].Also the evaporation of THF solvent during the preparation of thin film may have led to the formation of pores in the thin film[16]. It should be emphasized that the formation of porous film follows the principle of phase separation. In this principle one phase is induced to create the matrix and the other (i.e. solvent) to create convex surface shapes, which can be removed to leave free space by evaporation. Decreasing the density produces a further reduction in the dielectric constant. Therefore, ultra low k dielectrics with k less than 2.6 must be porous [17]. So from above explanation, we can say that after exposure the porosity in film gets increased [18] .But lowest value of dielectric constant observed for PMMA SA (9) at 5 and 10 min exposure is 0.60 and 0.30 which is very less than dielectric constant of air .As reported by Mikaail Ballanov et al, the material with dielectric constant less than 2.6 must be porous and materials with dielectric constant less than one is called metamaterials (Dixon 2012). These materials are made with high dielectric inclusions with specific shapes and sizes in a lower dielectric matrix.

So here we conclude that, the dielectric constant of material can be reduced by doping with salicylic acid and increasing time of exposure to UV radiation and with increase in time of irradiation the porous material becomes to metamaterials.

The FTIR spectra of PMMA shows the presence of C=O stretching at 1064cm confirms the presence of ester moiety. The bend for CH_2 is observed at 1442cm $^{-1}$ also for CH' at 1367cm'.The sp' C-H stretching has been observed at 2854cm $^{-1}$ .The IR spectrum of PMMA SA (3) and PMMA SA (9) shows the C=O stretching at 1612.49 cm'.The SEM photographs (Fig 5) shows the amorphous nature of PMMA SA (0), PMMA SA (3), PMMASA (9) which is in agreement with XRD results (Fig 6)
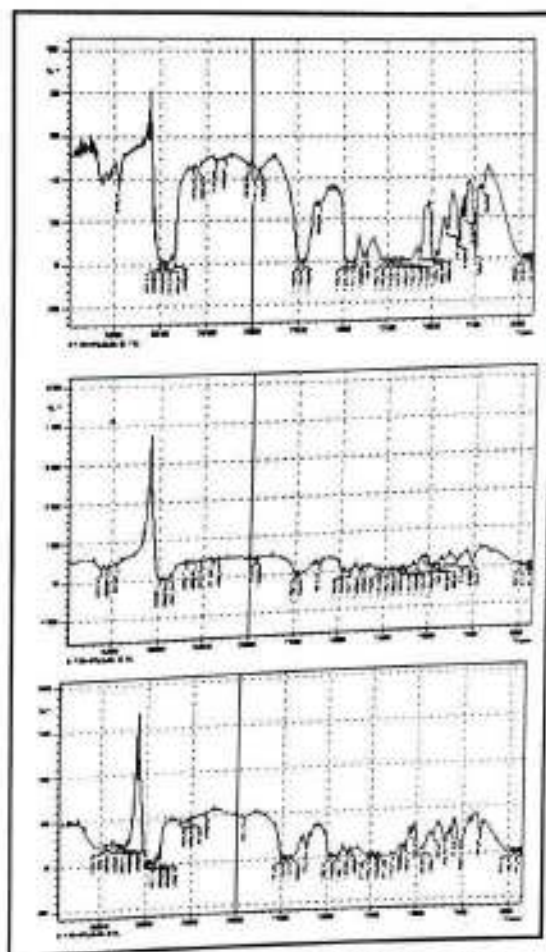
Fig 4: FTIR spectra of a) PMMA SA (0) b) PMMA SA (3) c) PMMA SA (9)

Fig 6: XRD spectra of a) PMMA SA (0)
b) PMMA SA (3) c) PMMA SA (9)

radiation so that it can be used as interlayer dielectrics in microelectronic devices.

Acknowledgements

References:

[1]   Shen J., Luo A. , Yao L. and Lin X., Materials Science and Engineering C, Elsevier, 2007, Vol. 27, 1145–1148.

[2]   Jousseaume V., Rolland G., Bubonneau D., Simon J.P., Applied Surface Science, 2007, Vol. 254, 473–479.

[3]   Singh S. K., Kumbhar A.A., Dusane R.O.,Materials Letters, 2006, Vol. 60, 1579–158.

[4]   Maex K, Baklanov M.R, Shamiryan D, Iacopi F, Brongersma S.H, Yanovitskaya Z.S., *Appl. Phys. Rev.*, 2003, Vol 93, 8793–8841

[5]   Bahri R.and Seth R.K., Indian Journal of Pure and Applied Physics, 1997, Vol 35, 104-108.

[6]   Belsare N.G.and Deogaokar V.S., Journal of Polymer Materials (Oxford and IBM Pub.Co.Pvt.Ltd.), 1998, Vol 15,157-70.

Fig 5: SEM images for a) PMMA SA (0)
b) PMMA SA (3) c) PMMA SA (9)

4. Conclusion:

The dielectric constant of thin films of PMMA, pure and doped with salicylic acid at different weight percentage, can be reduced by doping with salicylic acid and by exposure to UV

[7] Narayan A. and Singh H.P., Indian Journal of Pure and Applied Physics, 1991, Vol 29, 814-816.

[8] Sangawar V. And Adgaonkar C.S., Indian Journal of Pure and Applied Physics, 1995, Vol 33, 401-11.

[9] Tager A., Physical Chemistry of Polymers (MIR Publication; Moscow), 1972,151.

[10] Muhammad Akram, Athar Javed and Tasneem Zaher Rizvi, Turk J. Phys, 2005, Vol 29,355-62.

[11] Rao Vijayalakshmi, Ashokan P.V. and Sridhar M.H. Mater.Sci.and Engg. (Elsevier), 2000,A281,213-220.

[12] Reda S.M., Dyes and Pigments (Elsevier), 2006, 1-7.

[13] Goel D.G., Singh C.P., ShuklaR.K.Kumar A., J.Mater.Sci. 2000,Vol 35,1017.

[14] Srivastava K.K.,Goyal D.R., Kumar A.,Lakshinarayan K.N.,Panwar O.S.,Krishan I.,Phys. Status Solidi,1977,A 41,323.

[15] Scierka Stephni and Forster Amanda, 81st annual meeting technical Program of FSCT, 2003

[16] Stephan A. M., Kumar T. P, Renganathan N. G., Pitchumani S., Thirunakaran R., Muniyandi N., J. Power Sources, 2000, Vol 89, 80-87.

[17] Mikhail R. Baklanov, Karen Macx, Phil. Trans. R. Soc.,2006, Vol. 364 ,No. 1838, 201-15.

[18] Kohl P.A., Jassem Abdallah, Marshall Silver, Sue Ann Bidstrup Allen, J. Mater. Chem., 2007, Vol 17, 873–885

Temperature and Electric Field Dependence of DC Electrical Conductivity of 4:1 PVC-PMMA Polyblend thin films doped with Cinnamic Acid.

A.S.Wadatkar[1*], R.V.Waghmare[1], S.G.Vidhale[1],V.B. Gawali[1] , N.G.Belsare[1]

Department of Physics, Vidya Bharati Mahavidyalaya, Amravati (M.S.)- 444 602, India

E-mail : anantwadatkar@gmail.com

Abstract : DC electrical Conductivity of Cinnamic Acid doped 4:1 PVC- PMMA has been investigated as a function of i) Electric Field ii) Temperature and iii) Concentration of Cinnamic Acid (CA) used as a dopant. The Current – Voltage (I-V) measurements were carried out by applying the voltages ranging from 50V to 800V at various constant temperatures viz. 323 K, 333 K ,373 K. Films prepared by using Isothermal Evaporation Technique consisted of two commercial grade polymers PS and PMMA in the weight ratio 1:1. The weight percentage of dopant was 0%, 5%, 10 %, 15 %. The conductivity has been found to increase with electric field, temperature and also the concentration of dopant.

Keywords: Polymethyl Methacrylate (PMMA), Polystyrene (PS), Tetrahydrofuran (THF), Cinnamic Acid(CA)

1. Introduction

The d.c. electrical conductivity studies are aimed at understanding the origin of the charge carrying species, their numbers and ways in which they move through the bulk materials. These parameters are related with the morphology, microstructure and chemical compositions of the materials (Seanor, 1982). For thin films, the mechanisms generally discussed are tunnelling (Ochiai, Maeda, Ogawa et al.,1993), Schottky (Thomas, Pillai and Jayalakshmi, 1988: Mujairi and Kondo, 1991), Poole-Frenkel emission (Rao, Rao KVS, Reddy et al., 1991: Bahri and Seth, 1997) and Space Charge Limited Conduction (SCLC) (Sessle, Hahn and Yoon, 1986). The depolarising current increases with the increase in the percentage of PMMA (Keller, Dubey and Datt, 1991).

The electrical properties of thermoplastics are measured to determine performance capability in electrical properties (Mark et al,1985). Materials such as polyethylene, polystyrene find an extensive usage as an electrical insulator (Goosey, 1985). PS is a non-polar, low loss polymer and hence has desirable electric properties for the use in the insulation (Chutia and Baru, 1981). PMMA is hard, rigid, transparent thermoplastic, which has good weatherability. PMMA is weakly polar (Blythe, 1979). The blends PS/PMMA doped with iodine (Belsare and Deogaonkar, 1998) and PNA (Waghmare et al., 2007) have been studied earlier. The present study is aimed at finding the effect of percentage of dopant Cinnamic Acid (CA) on the dc electrical conductivity of PVC-PMMA polyblend thin films by applying electrical field in the range 50V-700V at various thermostatically controlled temperatures in the range 323 K -373 K.

2. Experimental:
2.1 Sample Preparation:

The Polyvinylchloride (PVC) of commercial grade and Poly Methylmethacrylate (PMMA) were used for the present study. The two polymers were taken in the ratio 4:1, were dissolved in the common solvent Tetrahydrofuran (THF). The solution was kept for 3-4 days to allow polymers to dissolve completely to yield uniform solution. The solution mixture was poured on a perfectly plane glass plate kept floating freely in a pool of mercury for perfect levelling. Then the solvent was allowed to evaporate in air at room temperature. In this way the films were prepared by isothermal evaporation technique (Narayan and Singh, 1987: Bahri and Sood, 1983). Further it was dried for 3 days to remove any trace of solvent. The dry film was removed from the plate and then it was coated with silver paint. The Cinnamic Acid doped blend films have been prepared by taking CA in the percentage weights 5%, 10%, 15%. The films were prepared by using the same technique and were subjected to outgassing described above. The present study has been carried out with the following samples:

1) PVC PMMA + 0% Cinnamic acid [4:1 PVC-PMMA CA(0)]
2) PVC PMMA + 5% Cinnamic acid [4:1 PVC-PMMA CA(5)]
3) PVC PMMA +10% Cinnamic acid [4:1 PVC-PMMA CA(10)]
4) PVC PMMA +15% Cinnamic acid [4:1 PVC-PMMA CA(15)]

2.2. Measurement of DC Electrical Conductivity:

The thin film sample prepared by using isothermal evaporation technique, was coated with the silver paint and then loaded into the sample holder(Fig.) which was kept in thermostatically controlled oven. The DC voltage was applied (in the range 50 V-800 V) across the sample by using highly regulated DC power supply (model EHT-111). The corresponding DC current was measured by using digital pico-ammeter (model DPM-111). Such current – voltage (I-V) measurements were taken at different constant temperatures (323 K, 333 K, 343 K, 353 K, 363 K, 373 K.) From these measurements the DC conductivity for all the samples was calculated.

Results and Discussion:

As stated earlier, the DC Conductivities of each of these Samples have been investigated by carrying out current- voltage (I -V) measurements at various constant temperatures: 323 K, 333 K, 343 K, 353 K, 363 K, 373 K.

The DC currents were recorded at each of above constant temperatures by applying the DC voltages: 50 V, 100 V, 150 V,800 V.
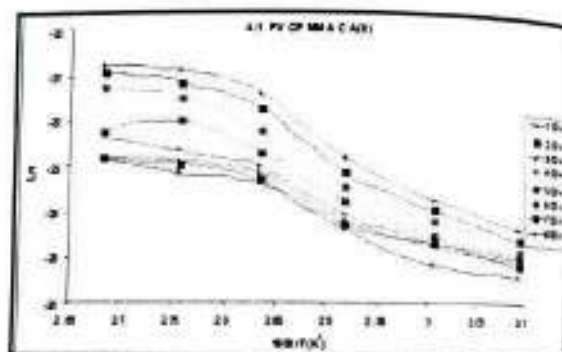
Fig.1 (a)
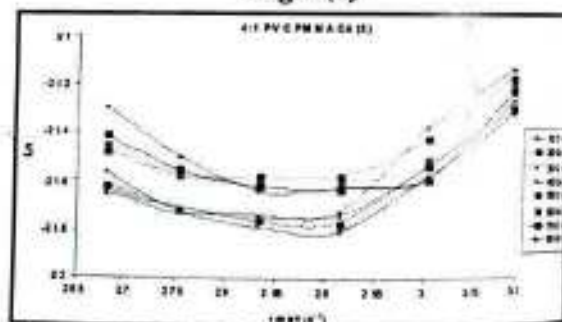
Fig.1 (b)
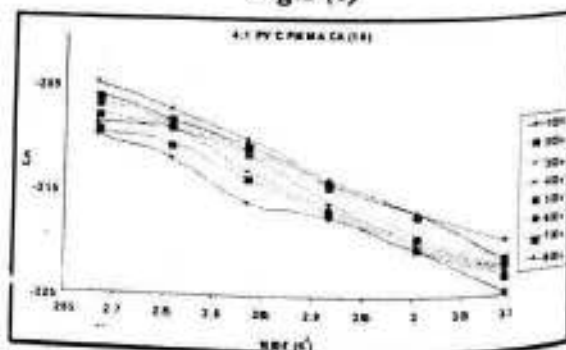
Fig.1 (c)
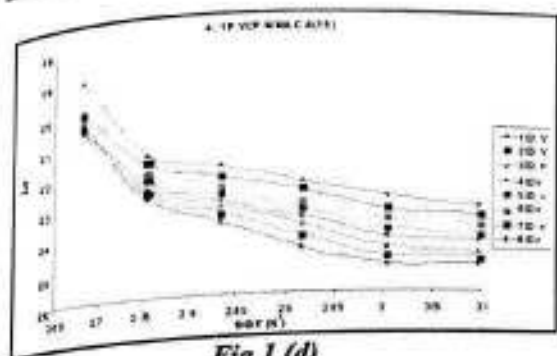
Fig.1 (d)

Fig. 1: Variation of Conductivity with Temperature at different constant voltages for 4:1 PVCPMMA CA system{Arrhenius Plot}
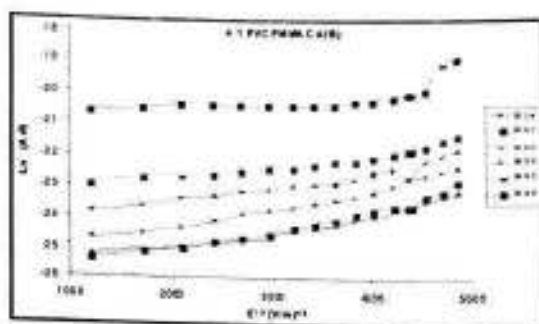
Fig.2 (d)

Fig. 2:Variation of Conductivity with $(E)^{1/3}$ at different constant Temperature for 4:1 PVCPMMA CA system {Poole- Frenkel mechanism}

Fig.2 (a)

Fig.2 (b)

Fig.2 (c)
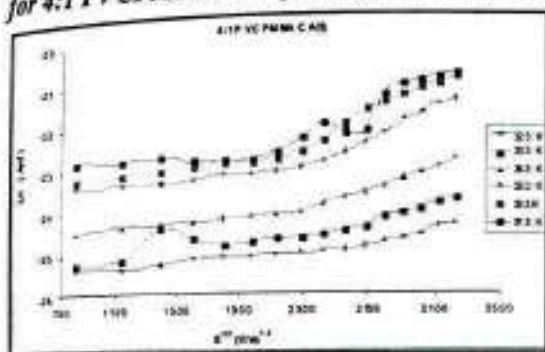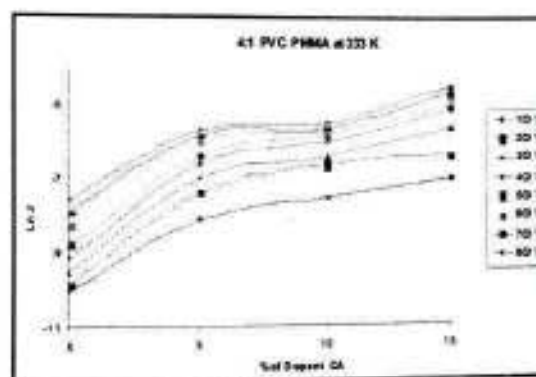
Fig.3 (a)
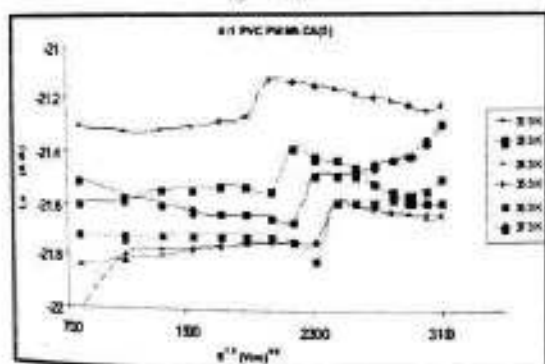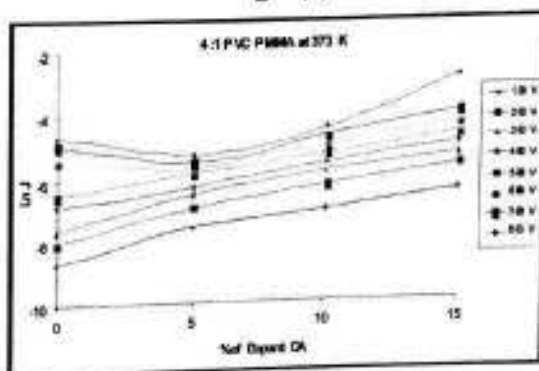
Fig.3 (b)

Fig. 3: Variation of Current density (Ln J) with Concentration of dopant CA at various voltages at temperatures(333K,373K) for 4:1 PVC PMMA CA system

Prominent Findings:

On the basis of the analysis of the results, the prominent findings of this part of the study can
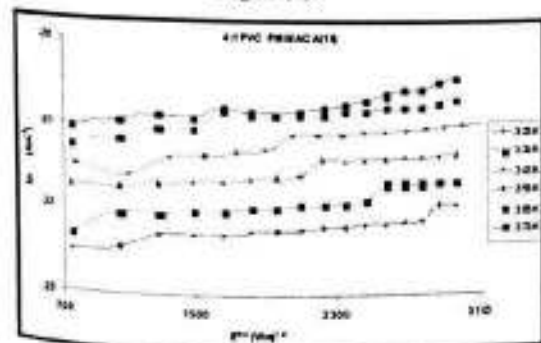
be summarized as under:

1) The electrical conductivity (σ) increases with the increase in temperature at every applied voltage. Fig 1:(a) to (d)

2) The Increase in electrical conductivity (σ), shown in the following results from 1) Increase in Electric Field, 2) Increase in Temperature, 3) Increase in percentage of Dopants Cinnamic Acid. Fig 2:(a) to (d) Fig 3:(a) and (b)

Discussion of Results:

In case of PVC PMMA polyblend, the conductivity undergoes almost similar variations with respect to temperature, voltage and dopant (Cinnamic Acid) concentration.

Cinnamic Acid
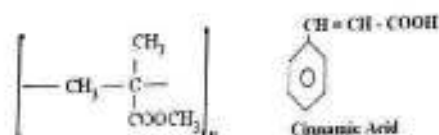
Structurally Polyvinyl Chloride (PVC) molecule is syndiotaetic so it has low Crystallinity. It is relatively unstable to heat and light. Thermal initiation involves loss of chlorine atom adjacent to some structural abnormality which reduces the stability of C-Cl bond. A hydrogen atom forms HCl. The resulting chain radical then reacts to form chain unsaturation with regeneration of chlorine radical.

PVC PMMA is commercial copolymer combination having more solubility and workability. The addition of Cinnamic acid as a dopant in the PVC PMMA polymer blend may provide a new site for chlorine exchange. An unsaturated substituent of Cinnamic acid easily add-up to PVC which liberate chlorine. Similarly the carboxylic proton with its natural affinity reacts with chlorine radical to form HCl molecule which, under the influence of heat or UV light, regenerates chlorine radical. This process of formation of HCl molecule and regeneration of chlorine radical continues till the removal of external energy disturbances.

Liberated chlorine and hydrogen from PVC and Cinnamic acid respectively have natural fascination towards carbonyl group of PMMA molecule. With this interaction, several reactive sites come into force to create new oppositely charged associations. As a result of this, there is a great possibility of increase in conductivity with temperature.

Khan *et al.* (2008) carried out the Viscometric Study of PSPMMA and PVC PMMA systems. Their Study reveled immiscibility for PS PMMA miscibility for PVC PMMA. Their findings from FTIR spectroscopy suggested specific interaction between PVC and PMMA. The results of FTIR spectroscopy carried out in the present work are in agreement with the above findings.

REFERENCES

1. Aziz M. S.. and Aggour Y. A., Polymer Testing, Vol. 18,(1999) 511-521.

2. Belsare N. G. and Deogaonkar V. S., Indian Journal of Pure and applied Physics, Vol. 36, (1998) 280-289.

3. Billmeyer F. W. (Jr.), "Text Book of Polymer Science", 3rd Ed., (Wiley Inter science Publication, New York), (1984) 229-53.

4. Burghate D. K., Deshmukh S. H., Lakmi Joshi, Deogaonkar V. S.and Deshmukh P. T. (2004); Indian Journal Pure and Applied Physics, Vol. 42, 533-38.

5. Goswami A., Thin Flim Fundamentals, (New Age International Publisher, India) (1996), 360-61, 377-78.

6. Gulalkari R. S., Bakale Y. G., Burghate D. K. And Deogaonkar V. S., Pramana-Journal of Physics, Vol. 69, (2007)485-490.

7. Khare P. K.; Indian Journal of Pure and Applied Physics, Vol. 32, (1994) 160-65.

8. Muhammad Akram, Athar Javed and Tasneem Zaher Rizvi (2005);Turk J. Phys.,29, 355-62.

9. Pollock M. and Geballe T H. (1961); Phy, Rev., Vol. 122. 1742.

10. Raghavendra S. C., Syed Khasim, Revanasiddappa M., Ambika Prasad M. V. N. and Kulkarni

11. A. B. (2003), Bulletin of Material Science, 26 (7), 733-39.

12. Rajendran S., Mahendran O. and Kannan R. (2002); Materials Chem. and Physics, 74, 52-57.

Investigation of Temperature Dependence of Electrical Conductivity of PVAC-PPy-CrCl3 Composite Polymer Film

R. Joat[1], S. Joshi[1], S. Bakde[1], T. Wasnik[1], A. Wadatkar[1], P. Bodkhe[2]

[1]Department of Physics, Vidyabharati Mahavidyalaya, Amravati
[2]Department of Chemistry, Vidyabharati Mahavidyalaya, Amravati

e-mail: sjoshi.swapnil@gmail.com

Abstract : PVAC-PPy-CrCl$_3$ composite polymer thin film prepared by using isothermal evaporation technique. The electrical conductivity measurements were taken at different constant temperatures (313K, 323 K, 333 K, 343 K, 353 K, and 363 K). The current density, electrical conductivity was increases with temperature. The enhancement in electrical conductivity is due to mobility of free charge carriers. The current- voltage relation obeys the Ohm's law.

Keywords: Polypyrrole, Polyvinyl acetate, electrical conductivity.

1. Introduction:

In this present work our aim is to determine electrical conductivity of PVAC+PPy and to study variation of conductivity with the doping of CrCl3.

Over the years, electrical application of polymers has been extensively explored. Traditionally the electrical applications of polymers have been as an electrical insulation and therefore major emphasis has been placed on the study of properties which help polymers act as passive electrical elements. But in recent times highly conducting polymers materials have been discovered. There are polymeric materials, which exhibit piezoelectric and pyroelectric properties too. Such materials have the potential to act as active elements. There has been the major stress worldwide to explore non-conventional energy sources, and finding ways of exploring solar energy has been major feature of human endeavour to meet the growing energy requirements of the mankind. Consequently there has been a developing need for large area photoactive materials that converts the solar energy into the usable electrical energy. Polymers, being disordered materials, have some unique properties that are based upon them. The capability is being utilized as active electrical elements.

Among all of them, polypyrrole (PPy) has obtained much interest due to its properties such as good processability, relatively high conductivity, cheap and commercially available. One of the approaches that have been used by global researchers to improve the limitation of PPy is by introducing PPy in polymer matrix making as composite polymer. The examples of well- known matrices that have been studied include polyvinyl acetate (PVAc), polyvinyl alcohol (PVA), Polymethyl methacrylate (PMMA) and Polyvinyl chloride (PVC). Polypyrrole is a heterocyclic polymer (-C4H4NH-) n which has attracted great attention due to its high electrical conductivity and good environment stability and relative ease of synthesis. During the last two decades there have been a lot of research works in the literature - about the preparation of the polypyrrole (PPy)-polymer composite or blend coatings by chemically repared [1]. In general, electrochemically deposited PPy composite "lms show a high electrical conductivity, whereas the chemically prepared PPy blends are less conductive and more transparent. As for the

host polymers, several well-known polymers have been used in the chemically prepared PPy composite materials, such as polymethyl methacrylate [2], rubber [3], poly(styrenebutyl acrylate- hydroxyethyl acrylate) [4], polyvinyl alcohol [5], polyvinyl acetate [6] and polyethylene oxide [7]. Polypyrrole (PPy) is a poly conjugated polymer that is one of the most frequently used and studied polymers owing to its suitable properties and easy preparation. PPy can be prepared by chemical or electrochemical oxidation of pyrrole in various organic solvent and in aqueous Media [8-12]. The preparation conditions and various additives introduced into reaction mixture influence the properties of final conducting polymer [13-14]. The properties of fabricated conducting polymers are strongly dependent on the preparation conditions and various additives introduced into reaction mixture [14,15].

The incorporation of polymer matrices significantly changes their physical properties, which make the samples more resistive to chemicals, ambient and physical action. PVAc has been the main focus to be used as matrix because it is water soluble, good polarity and good mechanical strength. However, the transport properties in which related to free charges become more complicated as the system becomes disordered. Polarons is a defect as a result of doping encompasses reaction between pyrrole monomer and dopant whereas free ions come from dopant which does not take place upon polymerization of polypyrrole. Therefore, it is recognized to use dc conductivity for quantifying and investigating the disordered composites system. The ariation of temperature can provide more detail on the behaviour of charges and ability to enhance the electrical conductivity. In this paper, the dc electrical conductivity of the blend of polypyrrole doped with chromium (III) chloride in PVAc matrix at different temperatures has been studied. The results cover direct current (dc).

2. Method of preparation of pure film:
A solution containing 0.6g of PVAC in 100ml distilled water was prepared by constant

stirring and heating the mixture up to 95°C for an hour. Then the mixture was left to cool down to laboratory temperature while the stirring of the mixture was carried out to ensure a homogenous composition.

3. Method of preparation of doped film:
PVAC and polypyrrole (PPy), supplied by Fluka, were used and pyrrole was distilled for purification prior to use. Reagent Chromium (III) Chloride (CrCl3) (99% purity) supplied by Riedel de Haen was used as received. The sampling process was carried out at room temperature (27°C).

A solution containing 0.6g of PVAC in 100 ml distilled water was prepared by constant stirring and heating the mixture up to 95°C for an hour. Then the mixture was left to cool down to laboratory temperature while the stirring of the mixture was carried out to ensure a homogenous composition. From the cooled mixture, 30 ml was taken and was mixed with 0.67 ml polypyrrole in 15 ml of distilled water and stirred for 5 minutes at the room temperature in order to get homogenous solution. Finally, 4.8gm of CrCl3 was added in the mixture and stirred for 10 minutes. The concentration of dopant is 0.01 mol. concentrations.

The solution was then poured into a casting glass plate 14cm×14cm and dried at the room temperature for ca.120 hours. After drying, the composite polymer films were stripped from the plate and cut into 4cm × 4cm pieces for electrical conductivity. The reaction mechanism to form PVAC-PPy-CrCl3 composite is shown below (this mechanism is proposed by Benseddik and his co-workers in 1995):

$nC_4H_4NH(PVAC)+2.25nCrCl_3$ $C_4H_3N^{0.25}+Cl^{0.25}]$
$n(PVAC)+2nHCl+2.25nCrCl_2(H_2O)$
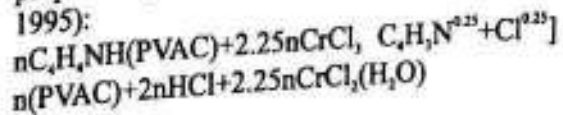
4. Results:
1. V- (Voltage) V
2. I- (Current) Amp.
3. R- (Resistance) Ohm
4. E- (Electric field) = V/d, Volts/cm
5. P- (Specific resistivity) $\sigma = AR/d$ (Ωcm)

Joat et al.

6. σ- conductivity (Mho cm^{-3})
7. J- current density (J) = I/A (Amp cm^{-2})

In order to present the result we should consider the nature of graph.
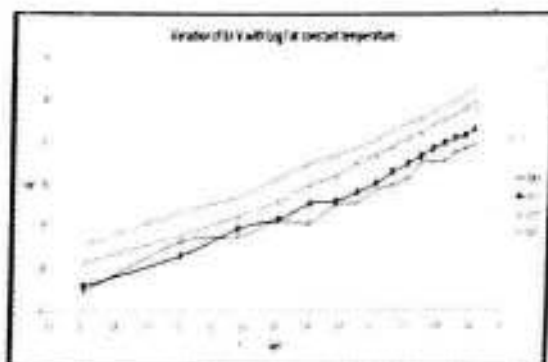
Fig. A.1
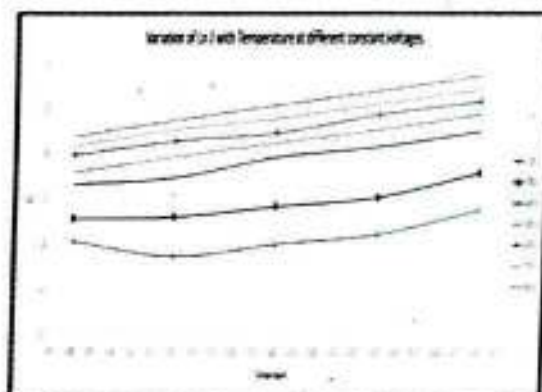
Fig. A.2
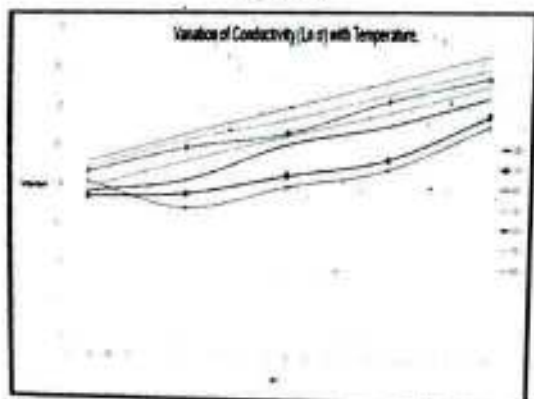
Fig. A.3

Fig. B.1

Fig. B.2

Fig. B.3

Fig. A.1, Fig. A.2, Fig. A.3 shows the results of pure material i.e. (PVAC+PPy).
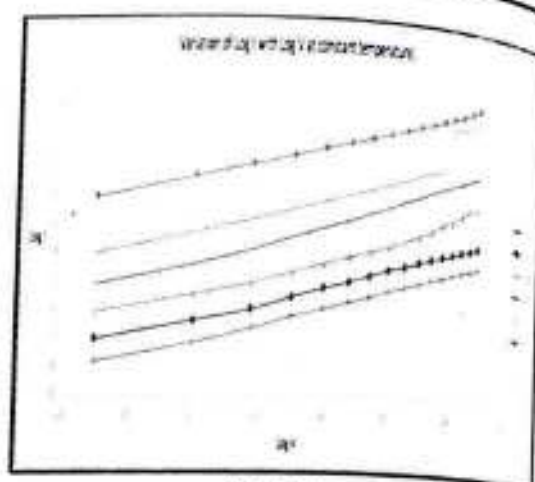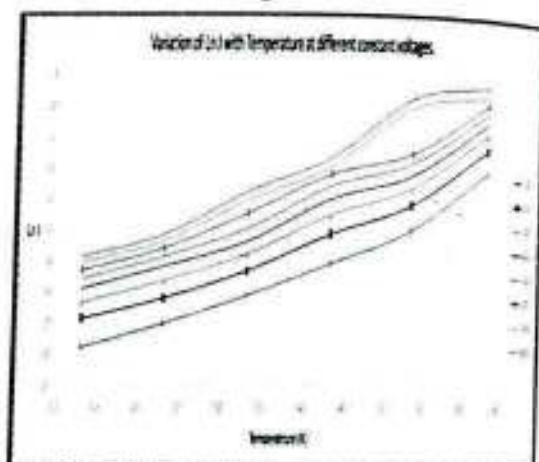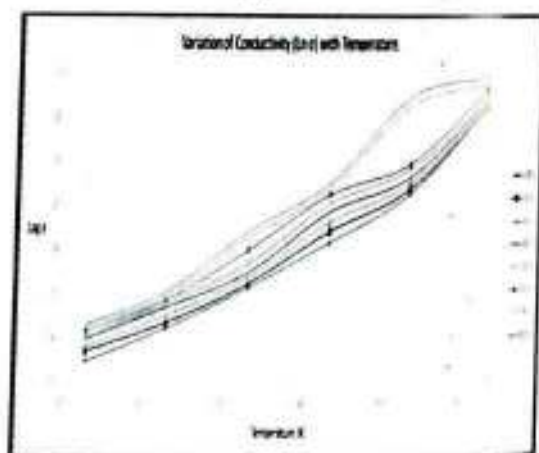
Fig. B.1, Fig. B.2, Fig. B.3 shows the results of doped material i.e. (PVAC+PPy+CrCl$_3$).

5. Discussion:

From Fig. A.1 and Fig. B.1 it is revealed that as we increase the voltage, current I also increase linearly at constant temperature i.e. it obeys Ohm's law.

From Fig. A.2 and Fig. B.2 it is revealed that current density of material increases with increasing temperature.

From Fig. A.3 and Fig. B.3 it is revealed at high temperature conductivity of PVAC bearing high value due to negative temperature coefficient of resistance while as temperature goes on decreasing then conductivity also decreases.

6. Conclusion:

Extensive study on temperature dependence of dc electrical conductivity of PVAC+PPy+CrCl3 had been carried out. The dc conductivity increases with the increment of temperature. An increase of the values of the dc electrical conductivity is driven by mobility of free charges (i.e. polarons and free ions) as temperature is increased. It becomes more conductive as the temperature applied was increased. This finding is confirmed with the gradual increment of values of the dc electrical conductivity obtained from different temperatures.

7. References:

[1] H.-L. Wang, J.E. Fernandez, Macromolecules 25, 6179(1992).

[2] T. Ojio, S. Miyata, Polym. J. 18, 95(1986).

[3] M.E. Nicho, H. Hu, Solar Energy Materials & Solar Cells, 63,423- 435 (2000).

[4] J.H. Han, T. , Y.E. Wang, S. Miyata, Synth. Met., 45, 261 (1991).

[5] J.F. Rabek, J. Lucki, H. Kereszti, B. Krische, B.J. Qu, W.F. Shi, Synth. Met. 45, 335 (1991).

[6] M. Morita, I. Hashida, M. Nishimura, J. Appl. Polym. Sci. 36 ,1639 (1988).

[7] Y. Sun, E. Ruckenstein, Synth. Met., 72, 261(1995).

[8] M. Omastova, S. Kosina, J. Pionteck, A. Janke, J. Pavlinec, Synth. Met. 81, 49 (1996).

[9] J. Yang, Y. Yang, J. Hou, X. Zhang, W. Zhu, M. Xu, M. Wan, Polymer. 37,793 (1996).

[10] W. Yin, H. Liu, J. Li, Y. Li, T. Gu, J. Appl. Polym. Sci. 64, 2293 (1996).

[11] H.C. Kang, K.E. Geckeler, Polymer 41, 6931(2000).

[12] L.-X. Wang, X.-G. Li, Y.-L, Yang, React. Funct. Polym. 47 (2001).

[13] C. DeArmitt, S.P. Armes, Langmuir 9 ,652 (1993).

[14] Bukowska, J. Jackowska, K Synth. Met. 35, 143-150 (1990).

[15] Zarbin A. J. G., De Paoli M. A., Alves O. L., Synth. Met. 99, 227-235 (1999).

The Study of Molecular Interaction of Proton Polymer Electrolytes Using Ultrasonic Technique

R. Joat[1], S. Bakde[1], S. Jadhao[1], S. Joshi[1], P. Bodkhe[2], S. Binani[2]

[1]*Department of Physics, Vidya Bharati Mahavidyalaya, Amravati.*
[2]*Department of Chemistry, Vidya Bharati Mahavidyalaya, Amravati*

ABSTRACT : The Ultrasonic velocity, density and viscosity have been measured for aqueous electrolyte solution of ammonium acetate. The samples were prepared by using different concentration of ammonium acetate doped with polyvinyl alcohol. These experimental data have been used to estimate the physical parameter such as adiabatic compressibility, free path length, internal pressure, relaxation time, acoustic impedance, Gibb's free energy for the aqueous electrolyte solution. The strength of intermolecular interaction between component of liquid have been successfully investigated by ultrasonic method.

KEYWORDS: PVA solution, ultrasonic velocity, Acoustic parameters.

INTRODUCTION

Polyvinyl alcohol is a water soluble polymer. It is used to study the physical parameter of polymer polyvinyl alcohol in solvent distiled water. Ultrasonic is a versatile nondestructive technique and powerful tool for characterization of various acoustic parameters of solution of different concentration [1, 2, 3]. Acoustic parameters provide the information to understand the solute-solvent interaction in proton conducting polymer electrolyte solution [4]. The development of molecular sciences with the help of intermolecular interaction. In this work, we have studied important acoustic parameter like adiabatic compressibility, free length, internal pressure, relaxation time, acoustic impedance, Gibb's free energy of proton conductor PVA solution at different concentration. The ultrasonic velocity and their related acoustic parameters were provides information to understand the molecular interaction in proton conductor polymer blend.

Materials and methods:

Polyvinyl alcohol was procurred from merck and the Aq. Polyvinyl alcohol mixture were made with masses weigh by analytical balance. Distilled water was use as a solvent. Similarly the aq. Solution of ammonium acetate was prepared. As polyvinyl alcohol has remarkably slow rate of dissolution in water at room temperature. Therefore it is warming up with continuous stirring and obtained one phase solution. After cooling solution were weighed again and evaporated water in the process of warming up were compensated by adding the distilled water similarly the Aq. solution of ammonium acetate was prepared. As per weight percentage sample were mixed and prepared the sample of 10%, 20% and 30% concentrated of ammonium acetate with polyvinyl alcohol. In the present study the physical parameter of polymer electrolyte solution were studied by using ultrasonic technique.

Result and Discussion

The experimental value of ultrasonic velocity, density and viscosity for the binary solution of polyvinyl alcohol and ammonium acetate are given in Graph 1, 2, 3.

Graph-1

Ultrasonic velocity
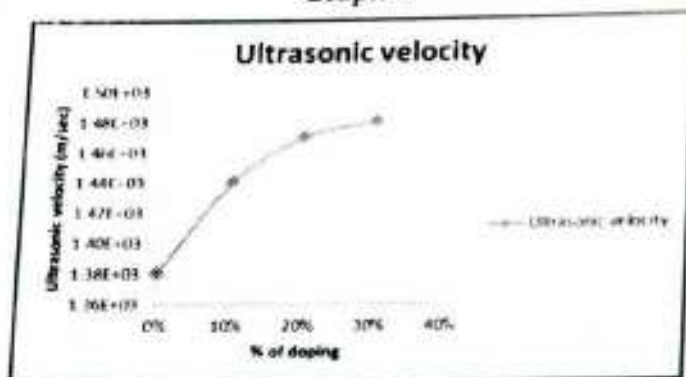
*Variation of ultrasonic velocity
with % of doping*

The graph of the adiabatic compressibility, Intermolecular free path length, Free volume, Acoustic Impedence , Relaxation time , and Internal pressure are given

Graph-4

Adiabatic compressibility
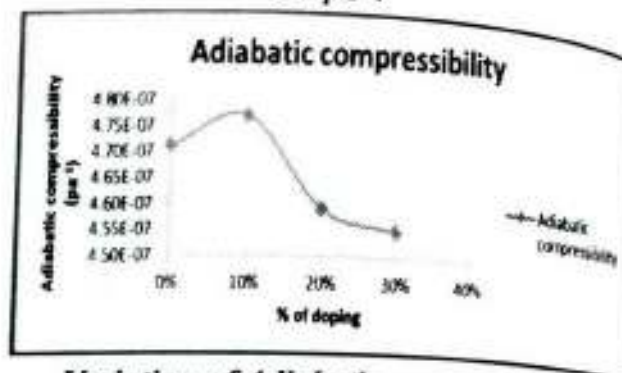
*Variation of Adiabatic compressibility
with % of doping*

Graph-2

Density

*Variation of density
with % of doping*

Graph-5

Intermolecular freepath length
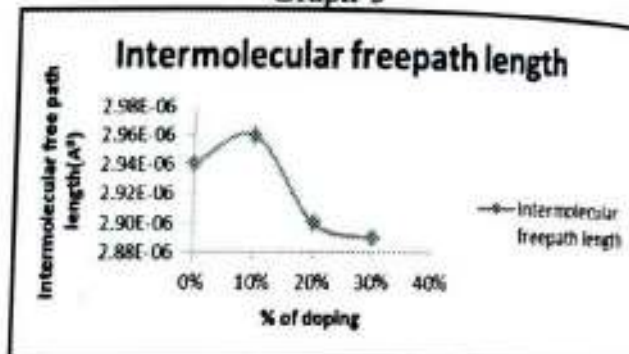
*Variation of intermolecular free path length
with % of doping*

Graph-3

Viscosity

*Variation of viscosity
with % of doping*
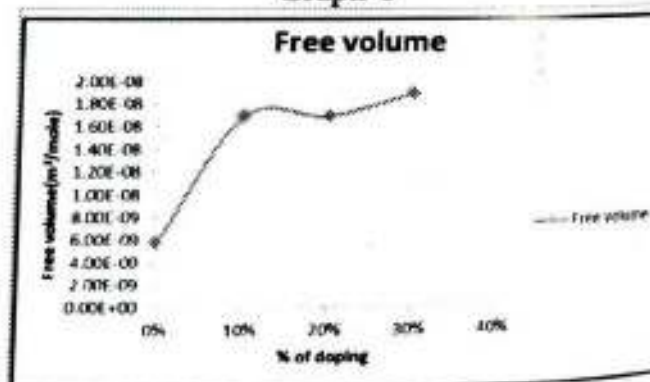
Graph-6

Free volume

*Variation of Free Voluma
with % of doping*

Graph-7

Acoustic impedance
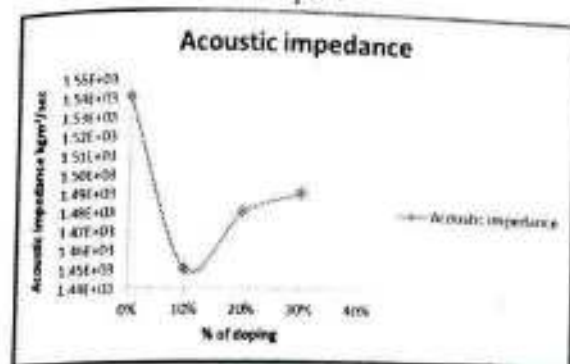
Variation of Acoustic impedance
with % of doping

Graph-8
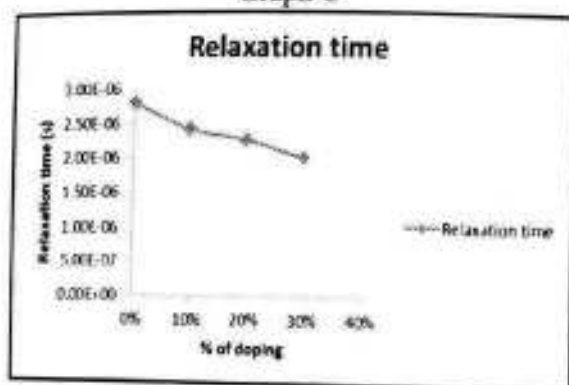
Relaxation time

Variation of Relaxation time
with % of doping

Graph-9
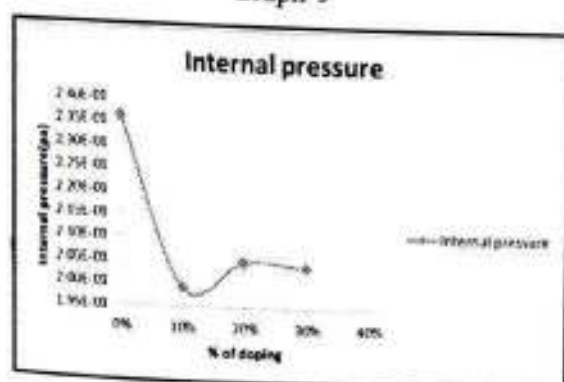
Internal pressure

Variation of Internal pressure
with % of doping

From graph-1, 2 and 3 it is noted that density and ultrasonic velocity increases with increasing percentage of doping and viscosity decreases. The increase in velocity is due to the decrease in intermolecular free length and adiabatic compressibility of the liquid solution. The adiabatic compressibility and intermolecular free length are the deciding factor of the ultrasonic velocity in the liquid solution. The interdependences of intermolecular free path length and ultrasonic velocity has been evolved. The internal pressure decreases and free volume increases with increasing percentage of doping. The internal pressure may give information regarding the nature and strength of force existing between the molecules. The increase in free volume shows that the strength of interaction decreases gradually with the increase in ammonium acetate. The relaxation time decreases with increase in percentage of doping. The dispersion of ultrasonic velocity is the system should contain information about characteristic time T of the relaxation process that causes dispersion. The relaxation time which is in the order of 10^{-6} sec is due to the structural relaxation process and such situation it is suggested that the molecules get arranged due to co-operative process.

Conclusion

From the data of ultrasonic velocity, density and viscosity, computed acoustical parameters and their values point to the presence of specific molecular interaction in the electrolyte solution. The increase in free volume show that strength of interaction decreases gradually hence it is conclude that there exist weak interaction between molecules of electrolyte solution of polyvinyl alcohol and ammonium acetate with distilled water at room temperature. Molecules in the electrolyte solution get arranged due to co-operative process as relaxation time is in the order of 10^{-6} sec. From it is conclude that, a very less attenssion is paid to the study of physical parameter of protonic electrolyte PVA and ammonium acetate and which is useful for to study of protonic electrolyte use as a fuel cell in various devices.

References

[1] Dash UN, Sahu R, Acoustic letters, 17, (1994), 157.

[2] Dash UN, Pasupalak NN, Indian journal of chemistry 36A ,(1997), 834.

[3] Praharaj MK, Satapathy A, Mishra PR, Mishra S, Golden Research thought, 2 (8), (2013), 1-10.

[4] Pankaj K. Singh, S. C. Bhatt J. Appl. Phys. (2010) 1916-9647.

[5] S. panda, G. C. Mohanty, G. S. Roy, S. Kalia, R. N. Samal Golden Research Thoughts (2013) 2231-5063.

[6] S. panda, G. C. Mohanty, G. S. Roy, S. Kalia, R. N. Samal J. Chemical and Pharmaceutical Research 81-89 (2013) 0975-7384

[7] M. K. Praharaj, Abhiram Satapathy, P. R. Mishra, S. Mishra Archives of Applied Science Research 837-845 (2012) 0975-508X.

[8] V. D. Bhandakkar Journal of Applied Physics 38-48 (2012) 2278-4861.

[9] P. Tabhane, O. P. Chimanker, C. M. Dudhe, V. A. Tabhane Pelagia Research Library 944-947 (2012) 0976-8505

[10] P. Tabhane, O. P. Chimanker, C. M. Dudhe, V. A. Tabhane J. Chemical and Pharmaceutical Research 3051-3056 (2012) 0975-7384.

[11] M. Talukdar, D. Moharatha, G. S. Roy, U. N. Das J. Pure and Applied Physics 202-206 (2013).

Stannic Oxide Doped with Zinc Oxide based for CO_2 gas Sensing

R.M.Agrawal, G.T.Lamdhade , K.B. Raulkar

Department of Physics ,Vidya Baharati Mahavidyalaya, Amravati.444602, India.

Email : rohit_agrawal1985@rediffmail.com

Abstract: Metal Oxide (SnO_2–ZnO) thick films have been prepared by screen printing technique. Sensitivity of these sensors to CO_2 gas was examined found to be better sensitive to CO_2 gas than pure SnO_2 films may be due to porosity created by ZnO into SnO_2 matrix.

CO_2 gas sensor the p-n junction like structure is formed of (SnO_2–ZnO) film where at equilibrium flow of electron form lower work species to the higher work species. As the CO_2 gas concentration increases the flow of electron increases and there will be decrease in the electrical resistance of the sensor with respect to CO_2 gas.

Keywords: SnO_2–ZnO; CO_2 gas sensor

1.Introduction:

Recently various materials are used to sense for various gases. These semiconducting materials include electronics ceramic and often a combination of various metals oxides. The SnO_2 based gas sensor are widely used for the detection of CO_2, H_2S, NOx, LPG,C_2H_5OH, H_2 etc[1]. There are many conducting polymers such as polypyrrole, polyacetylene, polyaniline and polythiophene are recently useful for the gas detection [2,3]. K. Suri *et al* [4] reported that iron oxide polypyrrole nanocomposite sensors showed the maximum response to CO_2 gas compared to N_2 and CH_4 gases. ZnO, TiO_2 , SnO_2 are the n-type semiconductor materials , which are most promising candidates for the gas sensors [5]. The metal oxide doped with different semiconducting metals is good sensing materials for gas detection.

The sensors shows the parameter such as response magnitude and dynamic response were studies at the room temperature (303K) for different concentrations of CO_2 gas with an aim to know the behaviors of electrical properties of ZnO-SnO_2 under concentration of CO_2 gas.

2. Experimental

The ($60SnO_2$ - $40ZnO$) sensor was prepared by using screen printing technique, followed by an adequate heat treatment. The binder was prepared by thoroughly mixed 8 wt.% of butyl carbitol with 92 wt. % of ethyl cellulose. The material ZnO and SnO_2 was calcinated at 700°C for 4 Hr. in air atmosphere in furnace to remove the impurities. After calcinations the fine powder was formed by using agated motor pestle. The calcinated chemicals are of (A R grade) are weighted on monopan balance (K-Roy, India) with proper wt.% of ZnO and SnO_2. The two components are mixed together to form a homogeneous mixture. The mixture is then placed in porcelain crucible and subjected to heating at 700°C for 1Hr. The paste for screen printing was prepared by taking materials in different ratios of wt.% with a binder in a moter pestel for mixing it. The paste thus prepared was screen printed on a chemically cleaned glass substrate of size 75x25 mm^2 and dried at room temperature at (303K). The prepared film was subjected to for heating at 373-403K for again 1Hr. During this stage,

Table 2.1. Composition of sample.

Sample code	Composition	Thickness of film(mm)
P1	$100\ SnO_2 + Al_2O_3$	1.383 mm
P2	$80SnO_2 + 20ZnO + Al_2O_3$	1.381 mm
P3	$60SnO_2 + 40ZnO + Al_2O_3$	1.939 mm

the volatile organic solvent was removed via decomposition and the prints adhered to the glass substrate of basic layer of Al_2O_3. For the surface resistance measurement the electrodes of conducting silver paint were formed on adjacent sides of the films and then films were subjected to heating at 80°C for again 15 min. for drying the silver paste and the sample code and thickness of the film are listed in table. The electrical resistance of the films was measured by using a voltage drop method adopted by Yawale et al. [6]. We have compared the various sample with composition given in the table 2.1.

3.Results and Discussion:

In the present study the variation of

CO_2 gas concentration with the sensitivity have been studied. Figure (3.1a, 3.1b, 3.1c) shows the variation of sensitivity with CO_2 gas concentration at the room temperature for the multilayer thin films of samples with different ratios P1,P2 and P3 respectively.

From figure it is observed that, P3 sensor has maximum sensitivity and P1 and P2 sensor showed minimum sensitivity. Also change in sensitivity of P3 sensor is more as compare to P1 and P3 sensors. The Sensitivity linearly increases with the increase in CO_2 gas concentration for P3 sample be after 20 ppm of CO_2 gas. It is found that sensitivity of P3 sensor in more than P1 and P3 sensors. Sensitivity is nearly constant i.e. it is goes in saturation region after the range 100 ppm of CO_2 gas.
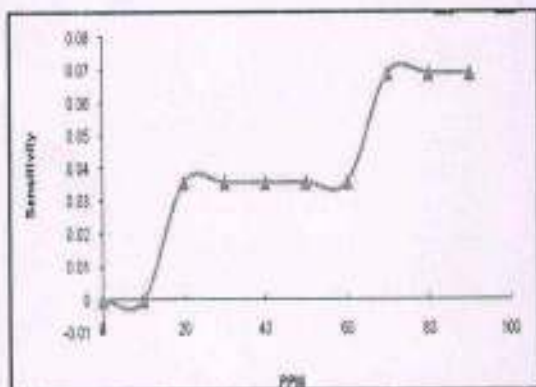
Fig. (3.1a)
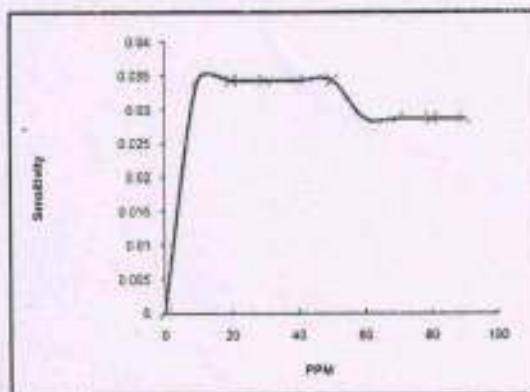
Fig. (3.1b)
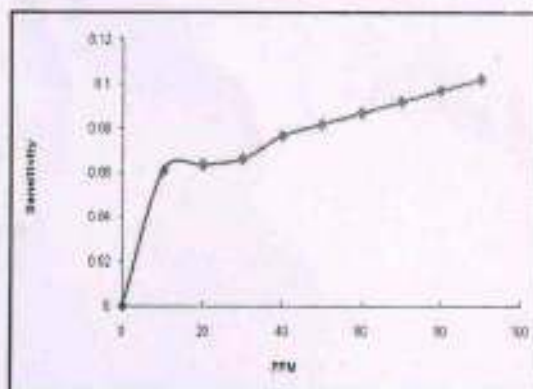
Fig. (3.1c)

The surface morphology of polypyrrole material was studied by SEM and its picture is shown in the Figure (3.2a, 3.2b, 3.2c)
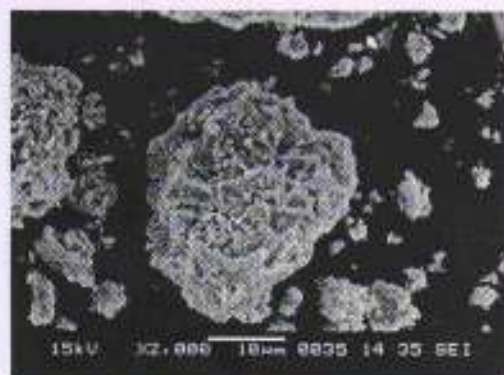
Fig.3.2a SEM pictures of pure SnO_2
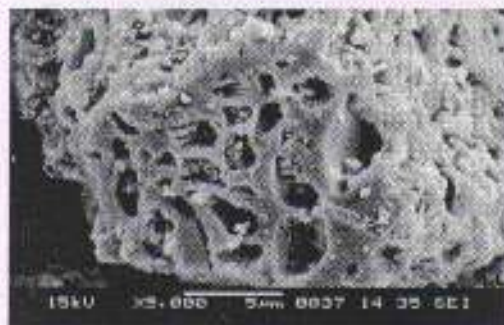
Fig. 3.2b SEM picture of ZnO
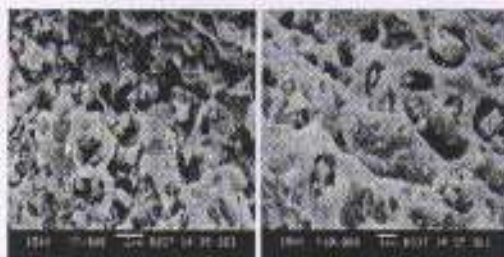
Fig. 3.2c SEM pictures of ($60SnO_2$-$40ZnO$) at different magnifications.

From SEM picture, it is observed that ($60SnO_2$-$40ZnO$) is more porous in nature and average diameter pore size found to be 360nm. Due to small pores size, its surface area is more and it shows more sensing nature. Some portion of SEM picture shows some rods with fine voids over them which helps to increase sensing properties.

Table 3.2. Shows the average diameter of pore and number of pores per inch of pure samples and their compositions.

Sr. No.	Pure sample and their compositions (mole %)	Average diameter of pore (nm)	Number of pores per inch (in x 2000 magnification)
	SnO_2 (Pure)	590	65
	ZnO (Pure)	760	62
	$60SnO_2$:$40ZnO$	360	109

It was concluded that the Sensitivity linearly increases with the increase in CO_2 gas concentration for P3 sample be after 20 ppm of CO_2 gas. From SEM picture, it is observed that $60SnO_2:40ZnO$ is more porous in nature and average diameter pore size found to be 360nm. In CO_2 gas sensor the p-n junction like structure is formed of (SnO_2-ZnO) film where at equilibrium flow of electron form lower work species to the higher work species. As the CO_2 gas concentration increases the flow of electron increases and there will be decrease in the electrical resistance of the sensor with respect to CO_2 gas.

4. References:

1] N.Yamozoe, J. Tamaki,N.Mirua,Mat. Sci. Eng.B.41(1996)178.

2] E.Ruckenstein, J.S.Park, J. Appl.Poly. Sci. 42 (1991) 925-934.

3] A.B.Kaiser,Rep.Porg.phys.64(2001) 1-49.

4] K. Suri, S.Annapoorni, A.K.Sarkar, R.P.tondon, Sen.ActuatorB, Chem 81 (2002) 277-282.

5] C,N.R.Rao,A.R.Raju,K.Vijayamohanan. Gas-Sensor Materials, Discussion meeting on new materials: Bangalore, New Mater_1992.1-37

6] S.P.Yawale, S.V. Pakade, J.Mater. Sci.28 (1993) 5451-5455.

A FACILE SOLID PHASE MICROWAVE INDUCED SYNTHESIS AND ANTIFUNGAL ACTIVITY OF SOME SUBSTITUTED PYRAZOLINES-N1-CARBALDEHYDES.

Sonal D. Boob* and P.R. Solanki

Vidyabharti Mahavidyalaya, Camp Amravati, (MS) India 444601

*Correspondence for
Author
Sonal D.Boob
Vidyabharti
Mahavidyalaya, Camp
Amravati, (MS) India

ABSTRACT

A novel one pot formylation of substituted pyrazolines has been carried out using K_2CO_3 as solid phase catalyst under microwave irradiation. The solvent free reaction afforded title compounds in 80-90% yield with high purity. All synthesized compounds were tested for their antifungal activity using standard drug.

KEYWORDS:- N-Formylation, Pyrazoline, Microwave Irradiation, Antifungal Activity.

INTRODUCTION

Pyrazolines and their derivatives are known to possess impressive biological activities. They have been reported to have bactericidal[1,2], acarcidal[3,4], anti-inflammatory[5], antidepressant[6], antipyretic[7], antibacterial[8] and antifungal[9] properties. Certain pyrazolines due to their non-toxic properties have been used as local anesthetics also. [10] Recently reported studies on the microwave irradiation for the synthesis of heterocyclic compound revealed that it is safe, rapid, economic and convenient, eco-friendly method for chemical synthesis. Pollution free synthesis, lesser reaction time, easy workup and minimum use of solvent are the major advantages of this technique.[11-13] A serious constrain of this method is selection of appropriate solvent, which can be avoided by synthesis under solid phase solvent free condition[14].These facts have promoted us to synthesize some new pyrazolines carboxyaldehydes using microwave irradiation under solvent free condition.

MATERIALS AND METHODS

All chemicals used were of analytical grade. All the synthesized compounds have been characterized on the basis of chemical properties, elemental and spectral analysis. The

melting points were measured in a open glass capillary and are uncorrected .IR spectra in KBr were recorded on instrument Perkin Elmer - Spectrum RX-IFTIR. ^{1}H-NMR spectra were recorded on FT NMR Spectrometer model Advance-II (Bruker) Its ^{1}H frequency is 400 MHz. All reactions were monitored by TLC using silica gel 60-f-254plates. All reactions were carried out in scientific microwave oven (Scientific microwave system model RG31lL1,700w, 2450MHz).satisfactory C,H,N analysis were carried out for most of the compounds on Thermo Scientific (FLASH 2000) CHN Elemental Analyzer at RSIC, Punjab university, Chandigarh

Table I: Physical data of 7-(substituted benzylidiene)-3-(substituted phenyl)-3,3a,4,5,6,-pentahydrocyclo-hexa(c) pyrazoline-2-carbaldehyde & (6-(substituted benzylidiene)-3-(substitutedphenyl)-3,3a,4,5,-tetrahydrocyclo-penta(c)-pyrazoline-2-carbaldehyde

Compound no.	Compound	R	Molecular formula	M.P. °C	Reaction Time (min.)	Yield (%)
5a	7- benzylidiene-3- phenyl-3,3a,4,5,6-pentahydrocyclo-hexa(c) pyrazoline-2-carbaldehyde	-C6H5	$C_{21}H_{20}N_2O$	156	6	84
5b	7-(4-chloro benzylidiene)-3-(4-chloro phenyl)-3,3a,4,5,6 -pentahydrocyclo-hexa(c) pyrazoline-2-carbaldehyde	$-C_6H_4Cl$	$C_{21}H_{18}N_2Cl_2O$	182	6	89
5c	7-(4-bromo benzylidiene)-3-(4-bromo phenyl)-3,3a,4,5,6 -pentahydrocyclo-hexa(c) pyrazoline-2-carbaldehyde	$-C_6H_4Br$	$C_{21}H_{18}N_2OBr_2$	134	5	87
5d	7-(2,4 dichloro benzylidiene)-3-(2,4 dichloro phenyl)-3,3a,4,5,6 -pentahydrocyclo-hexa(c) pyrazoline-2-carbaldehyde	$-C_6H_3Cl_2$	$C_{21}H_{16}N_2Cl_4O$	174	7	85
5e	6-(benzylidiene-3-(4-phenyl)3,3a,4,5-tetrahydro cyclopenta(c)pyrazoline-2-carbaldehyde	$-C_6H_5$	$C_{20}H_{18}N_2O$	147	5	90

5f	6-(4- chlorobenzylidiene-3-(2,4-chlorophenyl)3,3a,4,5 tetrahydro cyclopenta(c)pyrazoline-2-carbaldehyde	-C_6H_4Cl	$C_{20}H_{16}Cl_2N_2O$	181	6	87
5g	6-(4- bromobenzylidiene-3-(2,4-bromophenyl)3,3a,4,5tetrahydro cyclopenta(c)pyrazoline-2-carbaldehyde	-C_6H_4Br	$C_{20}H_{16}Br_2N_2O$	128	6	89
5h	6-(2,4 dichloro benzylidiene)-3-(2,4 dichlorophenyl)-3,3a,4,5,-tetrahydrocyclo-penta(c)-pyrazoline-2-carbaldehyde (Vh)	-$C_6H_3Cl_2$	$C_{20}H_{14}Cl_4N_2O$	164	6	91

Synthesis of 7-(substituted benzylidiene)- 3- (substituted phenyl) -3, 3a, 4, 5, 6,-pentahydrocyclo-hexa(c) pyrazoline-2-carbaldehyde & (6-(substituted benzylidiene)-3-(substitutedphenyl)-3,3a,4,5,-tetrahydrocyclo-penta(c)-pyrazoline-2-carbaldehyde

N-substituted pyrazoline were prepared by the reaction of 7-(substitutedbezylidiene)-3-(substituted phenyl)-3,3a,4,5,6,-pentahydrocyclo-hexa(c)-2H-Pyrazoline(Iva-d) and 6-(substituted bezylidiene)-3-(substitutedphenyl)-3,3a,4,5,-tetrahydrocyclo-penta(c)-2H-pyrazoline (IVe − IVh) (0.01M) with formic acid(0.01M) in presence of K_2CO_3 as a solid phase catalyst.. The reaction mixture was thoroughly mixed and irradiated under microwave at 750Wfor 5-6 minutes. After completion of reaction as indicated by TLC, the reaction mixture was cooled to room temperature and extracted with ethyl acetate. After concentration under reduced pressure it was left at room temperature .The solid separated was filtered, dried, and recrystalized to afford compounds(Va-Vh).

RESULT AND DISCUSSION

Eight substituted pyrazoline(Va-h) have ben synthesized from bisbenzylidiene derivative (IIIa-h) using literature method resulting in synthesis of pyrazoline(IVa-h) treated with K_2CO_3 /formic acid (0.01M) to get the target molecule (Va-h) and are characterized by spectral analysis. . Singlet at 10.1 δ,1H confirms CHOwhereas NH- singlet disappear of comound (IV). Double doublet at 5.6 δ,1H confirms= CH due to the allylic coupling the range is shifted in the higher region.1.2-2.4 δ,6H,Confirms 3-CH_2 fragment and quintet at 2.5 δ,1H confirms presence of –CH bond whereas doublet at4.8 δ,1H confirms presence of –CH

bond. and multiplet in aromatic region (7.2- 9.1 δ,6H) confirms the presence of two phenyl rings.IR absorption frequency at 1710cm^{-1} corrspondsa to carbonyl group. 1,2,4 trisubstituted combination band can be observed at 1878 cm^{-1} and its oop bending is at 823 cm^{-1},3188 cm^{-1} shows CH- aromatic stretching whereas 2924 cm^{-1} confirms the CH aliphatic stretch ,1303 cm^{-1} shows C-N stretch.
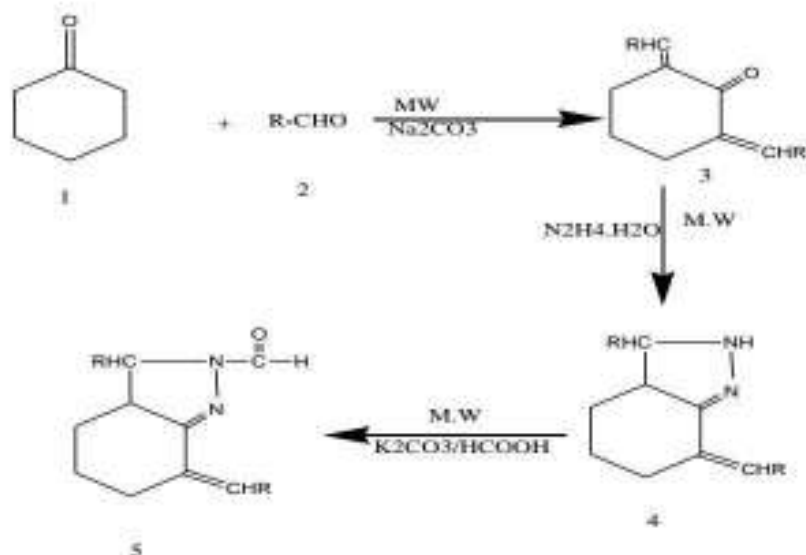
SCHEME – I: Experimental scheme for the synthesis of pyrazoline – N^1 – carbaldehydes (5a-h)
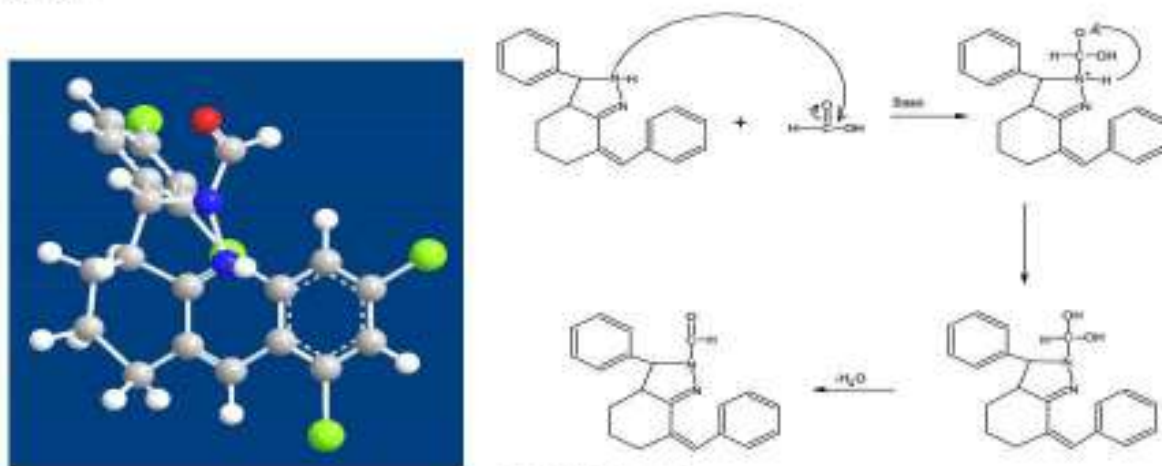
SCHEME – II

In continuation of our interest in the development of new green protocol using K_2CO_3 as a base catalyst helps in the activation of formic acid as an N-formylating agent under solvent free condition in microwave. K_2CO_3 also enhance the nucelophilicity of pyrazoline moiety and also functions as a desiccant in the reaction.

Scanned by CamScanner

Nucleophlic attack of nitrogen of pyrazoline moiety on +ve electrophilic carbon of formic acid due to inductive effect of C=O group followed by shifting of proton and dehydration leads to formyl derivative.

Spectral data for all the compounds

1) **7- benzylidiene-3- phenyl-3, 3a, 4, 5, 6-pentahydrocyclo-hexa(c) pyrazoline-2-carbaldehyde**

M.wt:-316.4 gm, M.P:-156^{0}C, greyish crystalline solid

H^{1}NMR:-400 MHz (CDCl3): 1.7-2.52[m, 6H, 3(CH$_2$)], 2.6[q,1H,-CH], 3.8[d,1H,-CH],5.6[dd,1H,=CH],7.2-8.82[m,10H,Ar-H],10.1[s,1H,CHO].

IR(cm-1): 3105[C-H st (aromatic)], 2849[C-Hst (aliphatic)], 1907[Combination band(monosubstituted)], 1630(C=O), 1595[C=N]1593,1573,1497 [C=C], 1400 [CH$_2$bend], 747,725[monosubstituted OOP bending].

2) **7-(4-chloro benzylidiene)-3-(4-chloro phenyl)-3, 3a, 4, 5, 6 -pentahydrocyclo-hexa(c) pyrazoline-2-carbaldehyde**

M.wt:-384 gm, M.P:-182^{0}C, brownish crystalline solid

H^{1}NMR:-400 MHz (CDCl3): 1.2-2.4[m, 6H, 3(CH$_2$)], 2.5[t,1H,-CH], 2.7[m,1H,-CH],6.9[m,1H,=CH],7.0-8.9[m,8H,Ar-H],10.1[s,1H,CHO].

IR(cm-1): 3044[C-H st (aromatic)], 2943[C-Hst (aliphatic)], 1900[Combination band(parasubstituted)], 1624(C=O), 1624[C=N(overlapping)], 1585,1489,1470 [C=C], 1403 [CH$_2$bend], 1318 [C-N], 1090,1053 [C-Cl(aryl halide)], 827[parasubstituted OOP bending]

3) **7-(4-bromo benzylidiene)-3-(4-bromo phenyl)-3, 3a, 4, 5, 6 -pentahydrocyclo-hexa(c) pyrazoline-2-carbaldehyde**

M.wt:-474.19 gm, M.P:-134^{0}C , white solid

H^{1}NMR:-400 MHz (CDCl3): 1.1-2.5 [m, 6H, 3(CH$_2$)], 2.6[t,1H,-CH], 4.93[dd,1H,-CH],5.1-5.2[d,1H,=CH],7.2-8.5[m,8H,Ar-H],10.1[s,1H,CHO]

IR(cm-1): 2943[C-H st (aromatic)], 2857[C-Hst (aliphatic)], 1912-1791[Combination band(parasubstituted)], 1688(C=O), 1688[C=N(overlapping)], 1593,1485,1448 [C=C], 1409 [CH$_2$bend], 1311 [C-N], 1067,1042 [C-Br(aryl halide)], 827[parasubstituted OOP bending]

4) **7-(2,4-dichloro benzylidiene)-3-(2,4-dichloro phenyl)-3, 3a, 4, 5, 6,-pentahydrocyclo-hexa(c) pyrazoline-2-carbaldehyde (Vd)**

M.wt:- 452 gm, M.P:-174^{0}C . faint yellow colour solid

H^{1}NMR:-400 MHz (CDCl3): 1.2-2.4[m, 6H, 3(CH$_2$)], 2.5[q,1H,-CH], 4.8[d,1H,-CH],5.6[dd,1H,=CH],7.2-9.1[m,6H,Ar-H],10.1[s,1H,CHO]

IR(cm-1): 3188[C-H st (aromatic)], 2924[C-Hst (aliphatic)], 1878[Combination band(1,2,4 trisubstituted)], 1710(C=O), 1710[C=N(overlapping)], 1600,1585,1548 [C=C], 1467 [CH$_2$bend], 1303 [C-N], 1101,1049 [C-Cl(aryl halide)], 831,[2,4 trisubstituted OOP bending]

5) 6-(2,4 dichloro benzylidiene)-3-(2,4 dicholorophenyl)-3,3a,4,5,tetrahydrocyclo-penta(c) - pyrazoline-2-carbaldehyde (Vh)

M.wt:- 440.15 gm, M.P:-164^{0}C . grayish crystalline solid.

H^{1}NMR:-400 MHz (CDCl3): 1.2-2.4[m, 4H, 2(CH$_2$)], 2.5[q,1H,-CH], 4.8[d,1H,-CH],5.6[dd,1H,=CH],7.2-9.1[m,6H,Ar-H],10.1[s,1H,CHO]

IR(cm-1): 3089[C-H st (aromatic)], 2951[C-Hst (aliphatic)], 1921[Combination band(1,2,4 trisubstituted)], 1616(C=O), 1616[C=N(overlapping)], 1583,1544,1469 [C=C], 1469 [CH$_2$bend], 1384 [C-N], 1103,1053 [C-Cl(aryl halide)], 866,[2,4 trisubstituted OOP bending]

ANTIFUNGAL ACTIVITY

All the synthesized compounds were screened for their antifungal activity viz. *fusarium oxysporum, Rhizoctonia solani* by using disc diffusion method for their antifungal activity.The punch discs of 6.25 mm diameter of Whatman filter paper no. 1 were prepared and dispensed in the batches of 100 each in screw capped bottles. These were sterilized by dry heat at 140^{0}C for 60 minutes. The solutions of 1000 ppm and 100 ppm concentrations of test compounds were prepared in dimethyl formamide (DMF) solvent separately. The discs were soaked, assuming that each disc will contain approximately 0.01 ml of test solution.

Table 2 - In vitro antifungal screening of above tested compounds

Sr.No.	Tested Compounds	Fungus (zone of inhibition in mm)			
		Fusarium oxysporum		Rhizoctonia solani	
		100 ppm	1000 ppm	100 ppm	1000 ppm
1	Va	13	14	16	19
2	Vb	15	17	14	18
3	Vc	20	21	22	24
4	**Vd**	**29**	**32**	**28**	**31**
5	Ve	20	21	16	18
6	Vf	21	22	12	13
7	Vg	17	18	21	26
8	Vh	16	19	18	20

The observations show that activity of compound Vd is maximum against both the fungi . Almost all the compounds were active against all the test pathogens. The compound 5d is the most dominant among all the test compounds. Their inhibitory impact on the bacterial growth is remarkable.

CONCLUSIONS

This was an attempt to synthesize biologically potential heterocyclic moiety in solid phase and solvent free reaction condition that leads to considerable saving in the reaction time and energetically profitable. The solvent free condition contributes to saving in cost, time and diminishes the waste disposal problem and environmental pollution this work may bring research fraternity towards sustainable development.

ACKNOWLEDGEMENT

REFERENCES

1. Khali H Z and Yanni, S A, J. Indian Chem. Soc., 1981; 58:168.

2. Patel P, Koregaokar S, Shad M, and Parekh H, I L Pharmaco, 1955, 50.

3. Singh G, Deb B, Ila H and Junjappa H, Synthesis, 1987; 286.

4. Anderson. and Brianard A G, Chem. Abstr, 1982; 96:104235d.

5. George H G and Prakash C, J. Pharma., Sci, 1971; 14: 649.

6. Rangari V, Gupta V N and Atal C K, Indian J. Pharma. Sci, 1990; 52: 158.

7. Vornin V G, Sharmova Z I, Shachilova S Y, Kulikova L D, and Zakas A S, Khim-Pharma. Zh., 1985;19:1208.

8. Barr A L, Biol. Abstr, 1997; 64:25,183.

9. Thorn G D, phytopathology, 1961; 51:77.

10. Rao K S and Subbaraju G V, Indian J. Heterocyclic Chem., 1994; 56: 6948

11. Bose A K, Minhas M, Ghosh M and Shah M, J. Org. Chem., 1991;56: 6948

12. Gelna S, Chem. Soc. Rev, 1997; 26:233.

13. Caddick S, Tetrahedron, 1995; 51: 373.

14. Langa P, Delacruz and Delacruz A, Contemporary Org Synth. 1997; 373.

QSAR Models for Anti-Malarial Activity of 4-Aminoquinolines

Vijay H. Masand[*,1], Andrey A. Toropov[*,2], Alla P. Toropova[2] and Devidas T. Mahajan[1]

[1]*Department of Chemistry, Vidya Bharati College, Camp, Amravati, Maharashtra, 444 602, India*

[2]*IRCCS, Istituto di Ricerche Farmacologiche Mario Negri, 20156, Via La Masa 19, Milano, Italy*

Abstract: In the present study, predictive quantitative structure – activity relationship (QSAR) models for anti-malarial activity of 4-aminoquinolines have been developed. CORAL, which is freely available on internet (http://www.insilico.eu/coral), has been used as a tool of QSAR analysis to establish statistically robust QSAR model of anti-malarial activity of 4-aminoquinolines. Six random splits into the visible sub-system of the training and invisible sub-system of validation were examined. Statistical qualities for these splits vary, but in all these cases, statistical quality of prediction for anti-malarial activity was quite good. The optimal SMILES-based descriptor was used to derive the single descriptor based QSAR model for a data set of 112 aminoquinolones. All the splits had $r^2 > 0.85$ and $r^2 > 0.78$ for sub-training and validation sets, respectively. The three parametric multilinear regression (MLR) QSAR model has $Q^2 = 0.83$, $R^2 = 0.84$ and $F = 190.39$. The anti-malarial activity has strong correlation with presence/absence of nitrogen and oxygen at a topological distance of six.

Keywords: Anti-malarial activity, 4-aminoquinolines, QSAR, optimal descriptor, CORAL software.

1. INTRODUCTION

Malaria, with high occurrence in tropical and sub-tropical regions, is responsible for more than 2 million deaths each year. This vector-borne deadly disease is becoming a major challenge to medicinal chemists due to the emergence of multi drug resistant strains of causative agent in different parts of world. Therefore, search for anti-malarial agents is an important task of modern medicinal chemistry. Different compounds like xanthones, prodiginines, and aminoquinolines have been synthesized and tested to develop new remedies for malaria [1-3].

Aminoquinolines, the quinoline derivatives, which show anti-malarial activity at very low concentration, considerable parasite clearance against wild and multi drug resistant strains of *Plasmodium falciparum* (*P. falciparum*) has gained considerable attention [2]. However, search for aminoquinolines with better ADMET (Absorption, Distribution, metabolism, Excretion and Toxicity) and activity profile still persists. Quantitative structure – activity relationships (QSARs) is a modern thriving chemometric technique under the umbrella of computer aided drug design (CADD) that could be a possible tool to select promising compounds against malaria [4-14].

QSAR studies are routinely performed to determine the factors that influence the activity and to predict the activity of a molecule prior to its actual synthesis and biological screening [4-14]. This considerably reduces time, efforts and chemicals, thereby making the process of drug designing

more cost effective and efficient. In the present study, we performed extensive QSAR analysis to determine the factors that govern the anti-malarial activity of 4-aminoquinolines and to develop highly predictive models. Two different approaches viz. CORAL (Correlation and Logic) [15-34] and GA-MLR QSAR were utilized to develop the models that satisfy OECD principles.

2. MATERIALS AND METHODS

2.1. Dataset

The dataset selected from literature [2], for the present study, comprised of one hundred and twelve 4-aminoquinoline derivatives with a variety of susbstituents at different positions (see Fig. **1**). The anti-malarial activity reported as EC_{50} was converted to pEC_{50} for smoother statistical calculations using the standard protocol mentioned in the literature [4-8,11,12]. The data set was splitted six times into sub-training, calibration, test, and validation sets. These splits obey the following principles; (i) they are various; and (ii) they are random.
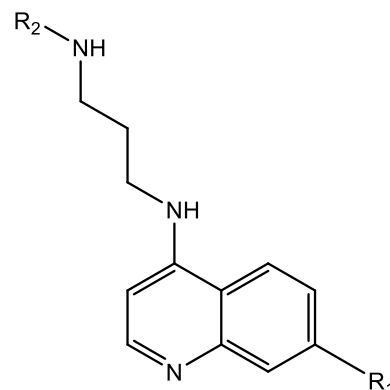
Fig. (1). 4-aminoquinolines used in present study.

*Address correspondence to these authors at the (Vijay H. Masand) Department of Chemistry, Vidya Bharati College, Camp, Amravati, Maharashtra, 444 602, India; Tel: +91-9403312628; Fax: +91-721-2662740; E-mail: vijaymasand@gmail.com and (Andrey A. Toropov) Istituto di Ricerche Farmacologiche Mario Negri, 20156, Via La Masa 19, Milano, Italy; Tel: +39-02-39014595; Fax: +39-02-39014735; E-mail: toropov@marionegri.it

2.2. Coral Approach

CORAL is a well established alignment independent technique for the development of predictive QSAR models that uses its unique approach of using optimal SMILES-based descriptors. The optimal SMILES-based descriptor is calculated using CORAL software [11] as follows:

$$DCW(Threshold, N_{epoch}) =$$
$$\sum CW(S_k) + \sum CW(SS_k) + \sum CW(SSS_k) \qquad (1)$$

If SMILES is represented by symbols of ABCDE, then examples of S_k, SS_k, and SSS_k can be illustrated as

ABCDE → A + B + C + D + E (S_k)

ABCDE → AB + BC + CD + DE (SS_k)

ABCDE → ABC+BCD+CDE (SSS_k)
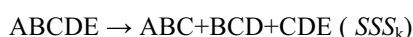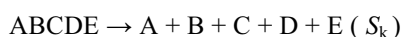
Table **1** contains more realistic example of SMILES attributes Sk, SSk, and SSSk. CW(x) is the correlation weight for a SMILES attribute x. The values of CWs are calculated by the Monte Carlo method. The numerical data on the CWs should be providers of maximal value of the target function (TF):

TF = (R+R') – abs(R-R')

(2)

where R and R' are correlation coefficient between experimental and calculated pEC_{50} values for the sub-training and calibration sets. The calculated values of the pEC50 are calculated with equation

pEC_{50} = C0 + C1* DCW (Threshold, Nepoch) (3)
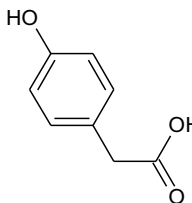
Statistical quality of the model calculated with Eq. 3 for test set is a mathematical function of the threshold and the number of epochs of the Monte Carlo optimization for the TF. For each split, the threshold and the number of epochs which give maximal correlation coefficient between experimental and calculated pEC_{50} were defined by scheme described in [17, 23, 24, 29-31, 35]. The threshold is the criterion for classification of SMILES attributes into rare and not rare. The attributes which are rare, are characterized by CW= 0. In this study, the threshold range is from 1 to 5. The maximal number of epochs of the Monte Carlo optimization is 50. Preferable values of the threshold (T*) and the number of epochs (N*) are represented below.

2.3. Calculation and Selection of Descriptors

To cover different aspects of the molecules in the data set, myriad numbers of descriptors available in e-Dragon

Table 1. Example of Representation of SMILES by the S_k, SS_k, and SSS_k

SMILES="c1(CC(=O)O)ccc(O)cc1" CAS= 156-38-7

	S_k zone 1 zone 2 zone 3	SS_k zone 1 zone 2 zone 3	SSS_k zone 1 zone 2 zone 3
	c..........		
	1..........	c...1.......	
	(..........	1...(.......	c...1...(...
	C..........	C...(.......	C...(...1...
	C..........	C...C.......	C...C...(...
	(..........	C...(.......	C...C...(...
	=..........	=...(.......	C...(...=...
	O..........	O...=.......	O...=...(...
	(..........	O...(.......	=...O...(...
	O..........	O...(.......	O...(...O...
	(..........	O...(.......	(...O...(...
	c..........	c...(.......	c...(...O...
	c..........	c...c.......	c...c...(...
	c..........	c...c.......	c...c...c...
	(..........	c...(.......	c...c...(...
	O..........	O...(.......	c...(...O...
	(..........	O...(.......	(...O...(...
	c..........	c...(.......	c...(...O...
	c..........	c...c.......	c...c...(...
	1..........	c...1.......	c...c...1...

Note: It is to be noted that ')' is changed by '(', because these symbols are indicators of the same phenomenon (branching).

Table 2.   4-Aminoquinolines Used in Present Study Along with EC$_{50}$ and *p*EC$_{50}$
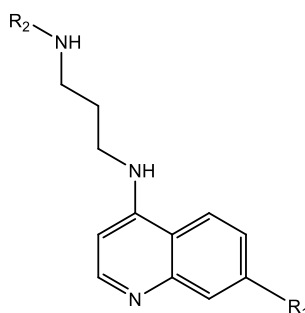
Sr. No.	R$_1$	R$_2$	3D7 EC$_{50}$ (μM)	*p*EC$_{50}$(M)	Status	Pred. *p*IC$_{50}$	Residuals	HAT i/i
1	PhO	Furfuryl	0.314	6.503	Training	6.5587	0.0557	0.0453
2	PhO	2-HO-3-MeO-Bn	0.015	7.824	Training	7.6864	-0.1376	0.0363
3	PhO	Piperonyl	0.018	7.745	Training	7.725	-0.0200	0.0207
4	PhO	3-F-6-MeO-Bn	0.162	6.790	Training	6.4476	-0.3424	0.0607
5	2-MeO-PhO	Furfuryl	0.001	9.000	Training	8.3393	-0.6607	0.2011
6	2-MeO-PhO	2-HO-3-MeO-Bn	0.009	8.046	Training	7.9729	-0.0731	0.0726
7	2-MeO-PhO	Piperonyl	0.014	7.854	Prediction	7.936	0.08200	0.0463
8	2-MeO-PhO	3-F-6-MeO-Bn	0.022	7.658	Training	7.5623	-0.0957	0.0525
9	3-MeO-PhO	Furfuryl	0.009	8.046	Training	7.9969	-0.0491	0.0534
10	3-MeO-PhO	2-HO-3-MeO-Bn	0.018	7.745	Prediction	7.7924	0.0474	0.0386
11	3-MeO-PhO	Piperonyl	0.162	6.790	Training	6.5545	-0.2355	0.0370
12	3-MeO-PhO	3-F-6-MeO-Bn	2.4	5.620	Training	5.6397	0.0197	0.2015
13	4-MeO-PhO	Furfuryl	0.004	8.398	Prediction	7.8083	-0.5897	0.0358
14	4-MeO-PhO	2-HO-3-MeO-Bn	0.004	8.398	Training	7.9151	-0.4829	0.0335
15	4-MeO-PhO	Piperonyl	0.046	7.337	Training	7.4219	0.0849	0.0420
16	4-MeO-PhO	3-F-6-MeO-Bn	0.054	7.268	Prediction	7.326	0.0580	0.0533
17	4-F-PhO	Furfuryl	0.026	7.585	Training	7.6565	0.0715	0.0273
18	4-F-PhO	2-HO-3-MeO-Bn	0.011	7.959	Prediction	8.1661	0.2071	0.0763
19	4-F-PhO	Piperonyl	0.015	7.824	Prediction	7.8573	0.0333	0.0292
20	4-F-PhO	3-F-6-MeO-Bn	0.297	6.527	Training	6.6567	0.1297	0.0433
21	4-Cl-PhO	Furfuryl	0.040	7.398	Training	7.4217	0.0237	0.0371
22	4-Cl-PhO	Furfuryl	0.011	7.959	Prediction	8.2714	0.3124	0.1033
23	4-Cl-PhO	Piperonyl	0.038	7.42	Prediction	7.3794	-0.0406	0.0414
24	4-Cl-PhO	3-F-6-MeO-Bn	0.031	7.509	Training	7.8902	0.3812	0.0323
25	3-Me2N-PhO	Furfuryl	0.027	7.569	Training	7.5835	0.0145	0.0235
26	3-Me2N-PhO	2-HO-3-MeO-Bn	0.010	8.000	Training	7.793	-0.2070	0.0311
27	3-Me2N-PhO	Piperonyl	1.4	5.854	Training	6.4909	0.6369	0.0400
28	3-Me2N-PhO	3-F-6-MeO-Bn	0.007	8.155	Prediction	7.9951	-0.1599	0.053
29	4-tertBu-PhO	Furfuryl	1.1	5.959	Training	6.5236	0.5646	0.0422
30	4-tertBu-PhO	2-HO-3-MeO-Bn	0.054	7.268	Training	7.249	-0.0190	0.0803
31	4-tertBu-PhO	Piperonyl	0.137	6.863	Prediction	6.6961	-0.1669	0.0376
32	4-tertBu-PhO	3-F-6-MeO-Bn	0.106	6.975	Training	6.5679	-0.4071	0.0400
33	4-F-Ph	Furfuryl	0.032	7.495	Prediction	7.5361	0.0411	0.0401

(Table 2) contd…..

Sr. No.	R_1	R_2	3D7 EC$_{50}$ (μM)	pEC$_{50}$(M)	Status	Pred. pIC$_{50}$	Residuals	HAT i/i
34	4-F-Ph	2-HO-3-MeO- Bn	0.009	8.046	Training	7.7829	-0.2631	0.0240
35	4-F-Ph	Piperonyl	0.018	7.745	Training	7.6162	-0.1288	0.0222
36	4-F-Ph	3-F-6-MeO-Bn	0.018	7.745	Prediction	7.672	-0.0730	0.0272
37	3,5-CF3- Ph	Furfuryl	0.285	6.545	Training	6.569	0.0240	0.0506
38	3,5-CF3-Ph	2-HO-3-MeO- Bn	0.029	7.538	Training	7.4902	-0.0478	0.0312
39	3,5-CF3-Ph	Piperonyl	0.284	6.547	Training	6.6903	0.1433	0.0428
40	3,5-CF3- Ph	3-F-6-MeO-Bn	0.092	7.036	Training	6.8562	-0.1798	0.0684
41	1-Naphtyl	Furfuryl	0.031	7.509	Training	7.4197	-0.0893	0.0820
42	1-Naphtyl	2-HO-3-MeO- Bn	0.033	7.481	Training	7.7499	0.2689	0.0214
43	1-Naphtyl	Piperonyl	0.598	6.223	Training	6.4839	0.2609	0.0680
44	1-Naphtyl	3-F-6-MeO-Bn	1.2	5.921	Training	6.5033	0.5823	0.0455
45	4-CF3-Ph	Furfuryl	0.020	7.699	Training	7.9595	0.2605	0.0794
46	4-CF3-Ph	2-HO-3-MeO- Bn	0.013	7.886	Prediction	7.9446	0.0586	0.0551
47	4-CF3-Ph	Piperonyl	0.025	7.602	Training	7.6892	0.0872	0.0203
48	4-CF3-Ph	3-F-6-MeO-Bn	0.054	7.268	Prediction	7.3932	0.1252	0.051
49	Ph	Furfuryl	0.020	7.699	Training	8.029	0.3300	0.068
50	Ph	2-HO-3-MeO- Bn	0.009	8.046	Training	7.695	-0.351	0.0313
51	Ph	Piperonyl	0.017	7.770	Training	7.7075	-0.0625	0.0205
52	Ph	3-F-6-MeO-Bn	0.011	7.959	Training	7.848	-0.1110	0.0359
53	4-tertBu- Ph	Furfuryl	0.704	6.152	Training	6.5031	0.3511	0.0701
54	4-tertBu- Ph	2-HO-3-MeO- Bn	0.251	6.600	Prediction	6.5959	-0.0041	0.0438
55	4-tertBu- Ph	Piperonyl	0.223	6.652	Training	6.6766	0.0246	0.0512
56	4-tertBu- Ph	3-F-6-MeO-Bn	0.144	6.842	Training	6.5327	-0.3093	0.0388
57	Piperonyl	Furfuryl	0.019	7.721	Training	7.8579	0.1369	0.0792
58	Piperonyl	2-HO-3-MeO- Bn	0.008	8.097	Prediction	8.1051	0.0081	0.0729
59	Piperonyl	Piperonyl	0.026	7.585	Training	7.8584	0.2734	0.0554
60	Piperonyl	3-F-6-MeO-Bn	0.031	7.509	Prediction	7.4455	-0.0635	0.0353
61	4-MeO- Ph	Furfuryl	0.011	7.959	Training	8.1777	0.2187	0.0939
62	4-MeO- Ph	2-HO-3-MeO- Bn	0.013	7.886	Prediction	7.4777	-0.4083	0.0369
63	4-MeO- Ph	Piperonyl	0.029	7.538	Prediction	7.572	0.0340	0.0245
64	4-MeO-Ph	3-F-6-MeO-Bn	0.096	7.018	Training	6.6431	-0.3749	0.0405
65	4-F-Bn	Furfuryl	0.057	7.244	Training	7.2843	0.0403	0.0584
66	4-F-Bn	2-HO-3-MeO-Bn	0.015	7.824	Prediction	7.9019	0.0779	0.0327
67	4-F-Bn	Piperonyl	0.127	6.896	Prediction	6.7672	-0.1288	0.0561
68	4-F-Bn	3-F-6-MeO-Bn	0.075	7.125	Training	7.2232	0.0982	0.0779
69	iso-butyl	Furfuryl	0.581	6.236	Prediction	6.75	0.5140	0.0465
70	iso-butyl	2-HO-3-MeO-Bn	0.020	7.699	Training	8.0767	0.3777	0.0643
71	iso-butyl	Piperonyl	0.066	7.180	Prediction	7.292	0.1120	0.0555
72	iso-butyl	3-F-6-MeO-Bn	0.089	7.051	Training	6.9244	-0.1266	0.0572
73	cHex	Furfuryl	0.118	6.928	Training	6.6176	-0.3104	0.0539
74	cHex	2-HO-3-MeO-Bn	0.019	7.721	Prediction	7.789	0.0680	0.0302
75	cHex	Piperonyl	0.128	6.893	Prediction	6.7434	-0.1496	0.0587

(Table 2) contd…..

Sr. No.	R_1	R_2	3D7 EC$_{50}$ (µM)	pEC$_{50}$(M)	Status	Pred. pIC$_{50}$	Residuals	HAT i/i
76	cHex	3-F-6-MeO-Bn	0.090	7.046	Training	7.1	0.0540	0.1009
77	1-Et-Pr	Furfuryl	0.086	7.066	Prediction	6.807	-0.259	0.0500
78	1-Et-Pr	2-HO-3-MeO-Bn	0.004	8.398	Prediction	7.6897	-0.7083	0.0223
79	1-Et-Pr	Piperonyl	0.027	7.569	Training	7.529	-0.0400	0.0328
80	1-Et-Pr	3-F-6-MeO-Bn	0.040	7.398	Training	7.34	-0.0580	0.0507
81	3-CF3-Bn	Furfuryl	0.056	7.252	Training	7.2848	0.0328	0.0621
82	3-CF3-Bn	2-HO-3-MeO-Bn	0.025	7.602	Training	7.8598	0.2578	0.0928
83	3-CF3-Bn	Piperonyl	0.039	7.409	Prediction	7.3914	-0.0176	0.0410
84	3-CF3-Bn	3-F-6-MeO-Bn	0.040	7.398	Training	7.4129	0.0149	0.0372
85	4-CN-Bn	Furfuryl	0.039	7.409	Training	7.3337	-0.0753	0.0488
86	4-CN-Bn	2-HO-3-MeO-Bn	0.011	7.959	Training	7.6393	-0.3197	0.0400
87	4-CN-Bn	Piperonyl	0.023	7.638	Training	7.9179	0.2799	0.0344
88	4-CN-Bn	3-F-6-MeO-Bn	0.028	7.553	Training	7.6046	0.0516	0.0455
89	Bn	Furfuryl	0.040	7.398	Prediction	7.2629	-0.1351	0.0720
90	Bn	2-HO-3-MeO-Bn	0.017	7.770	Prediction	7.7643	-0.0057	0.0222
91	Bn	Piperonyl	0.720	6.143	Training	6.56	0.4170	0.0371
92	Bn	3-F-6-MeO-Bn	0.011	7.959	Training	7.7384	-0.2206	0.0480
93	3,5-Me-Bn	Furfuryl	0.009	8.046	Training	8.0201	-0.0259	0.0612
94	3,5-Me-Bn	2-HO-3-MeO-Bn	0.009	8.046	Training	8.0978	0.0518	0.0626
95	3,5-Me-Bn	Piperonyl	0.041	7.387	Prediction	7.5476	0.1606	0.0348
96	3,5-Me-Bn	3-F-6-MeO-Bn	0.034	7.469	Training	7.5174	0.0484	0.0277
97	2-Cl-4-F-Bn	Furfuryl	0.020	7.699	Training	7.9236	0.2246	0.0342
98	2-Cl-4-F-Bn	2-HO-3-MeO-Bn	0.013	7.886	Prediction	7.9517	0.0657	0.0431
99	2-Cl-4-F-Bn	Piperonyl	0.027	7.569	Prediction	7.5924	0.0234	0.0219
100	2-Cl-4-F-Bn	3-F-6-MeO-Bn	0.208	6.682	Training	6.6133	-0.0687	0.0527
101	iso-pentyl	Furfuryl	0.176	6.754	Prediction	6.714	-0.0400	0.0384
102	iso-pentyl	2-HO-3-MeO-Bn	0.022	7.658	Prediction	7.8368	0.1788	0.0369
103	iso-pentyl	Piperonyl	0.027	7.569	Training	7.6044	0.0354	0.0934
104	iso-pentyl	3-F-6-MeO-Bn	0.116	6.936	Training	6.5859	-0.3501	0.0374
105	cHexmethyl	Furfuryl	0.055	7.260	Training	7.2364	-0.0236	0.0687
106	cHexmethyl	2-HO-3-MeO-Bn	0.050	7.301	Prediction	7.3529	0.0519	0.0456
107	cHexmethyl	Piperonyl	0.041	7.387	Training	7.235	-0.1520	0.0736
108	cHexmethyl	3-F-6-MeO-Bn	0.138	6.860	Training	6.4918	-0.3682	0.0411
109	PhEt	Furfuryl	0.046	7.337	Training	7.4056	0.0686	0.0649
110	PhEt	2-HO-3-MeO-Bn	0.017	7.770	Prediction	8.0022	0.2322	0.0640
111	PhEt	Piperonyl	0.013	7.886	Prediction	7.8166	-0.0694	0.0949
112	PhEt	3-F-6-MeO-Bn	0.132	6.879	Training	6.6684	-0.2106	0.0463

were calculated. The descriptors with nearly constant values or with a high correlation coefficient ($R > 0.50$) with other descriptors were considered as redundant descriptors and eliminated subsequently. Genetic Algorithm (GA) as implemented in QSARINS [36] was used to select optimum number and set of descriptors using the default settings, except for Lack of Fit (LOF) which was set to a value of 0.5.

The selected fitness function used to maximize in GA was Q^2, which is essential to avoid naive Q^2.

Literature survey reveals that a QSAR model is more useful if it is appropriately validated by internal and external validation [4-14]. For proper validation of GA-MLR model, different measures like R^2, R^2_{adj}, F, p, R^2_{LMO}, Q^2, etc. were

calculated to check the robustness of the developed Multi Linear Regression (MLR) equations. In addition, the data set was divided into training and test set for better validation.

3. RESULTS AND DISCUSSION

The CORAL software gave the following models for pEC_{50} for different splits:

Split 1

pEC_{50} = 0.0017 (± 0.0843) + 0.1179 (± 0.0013) * DCW(2,56)

n=32, r^2=0.92, r^2_{LOO} =0.91, s=0.18, F=362 (sub-training set)

n=18, r^2=0.88, r^2_{LOO}= 0.83, s=0.26 (calibration set)

n=24, r^2=0.79, r^2_{LOO}= 0.72, s=0.30, R_m^2=0.77 (test set)

n=38, r^2=0.78, s=0.27 (validation set, CORAL)

n=38, r^2=0.80, s=0.22 (validation set, GA-MLR)

Split 2

pEC_{50}= 1.1222 (± 0.1225) + 0.1153 (± 0.0022) * DCW(1,87)

n=26, r^2=0.89, r^2_{LOO} = 0.86, s=0.23, F=190 (sub-training set)

n=27, r^2=0.89, r^2_{LOO}=0.86, s=0.27 (calibration set)

n=20, r^2=0.73, r^2_{LOO}= 0.67, s=0.24, R_m^2=0.71 (test set)

n=39, r^2=0.85, s=0.25 (validation set, CORAL)

n=39, r^2=0.82, s=0.25 (validation set, GA-MLR)

Split 3

pEC_{50}= 0.0201(± 0.1951) + 0.1459(± 0.0038) * DCW(3,38)

n=23, r^2=0.88, r^2_{LOO} =0.84, s=0.26, F=152 (sub-training set)

n=31, r^2=0.87, r^2_{LOO}=0.85, s=0.28 (calibration set)

n=36, r^2=0.78, r^2_{LOO}=0.76, s=0.27, R_m^2=0.76 (test set)

n=22, r^2=0.85, s=0.22 (validation set, CORAL)

n=22, r^2=0.86, s=0.18 (validation set, GA-MLR)

Split 4

pEC_{50}= -0.0002 (± 0.2056) + 0.1184 (± 0.0033) * DCW(1,61)

n=23, r^2=0.85, r^2_{LOO} = 0.81, s=0.24, F=121 (sub-training set)

n=35, r^2=0.85, r^2_{LOO}=0.83, s=0.27 (calibration set)

n=34, r^2=0.86, r^2_{LOO}= 0.83, s=0.24, R_m^2=0.81 (test set)

n=20, r^2=0.89, s= 0.19 (validation set, CORAL)

n=20, r^2=0.88, s= 0.19 (validation set, GA-MLR)

Split 5

pEC_{50}= 0.0124 (± 0.1549) + 0.1437 (± 0.0029) * DCW(3,66)

n=25, r^2=0.91, r^2_{LOO} =0.88, s=0.19, F=235 (sub-training set)

n=32, r^2=0.87, r^2_{LOO}=0.84, s=0.26 (calibration set)

n=27, r^2=0.84, r^2_{LOO}= 0.81, s=0.22, R_m^2=0.81(test set)

n=28, r^2=0.83, s=0.25 (validation set, CORAL)

n=28, r^2=0.88, s=0.20 (validation set, GA-MLR)

Split 6

pEC_{50}= 1.5518 (± 0.1145) + 0.1211 (± 0.0023) * DCW(3,96)

n=25, r^2=0.91, r^2_{LOO} =0.89, s=0.18, F=245 (sub-training set)

n=28, r^2=0.91, r^2_{LOO}=0.89, s=0.30 (calibration set)

n=39, r^2=0.83, r^2_{LOO}= 0.81, s=0.25, R_m^2=0.69 (test set)

n=20, r^2=0.69, s=0.21 (validation set, CORAL)

n=20, r^2=0.53, s=0.26 (validation set, GA-MLR)

One can see that each split is characterized by various statistical qualities of the prediction. However, in all the cases, the statistical characteristics are quite good. The supplementary materials section contains splits into the training (i.e. the sub-training, calibration and test sets) and validation sets. In addition, the section contains examples of theoretical promising anti-malarial agents. These agents were selected according to their correlation weights: if a SMILES-attribute X has only positive correlation weights in a group of runs of the Monte Carlo optimization then the X should be interpreted as a promoter of increase of the pEC_{50}; if the X has only negative correlation weights then the X should be interpreted as a promoter of decrease of the pEC_{50}[17, 23, 24, 29-31, 35].

For GA-MLR model, the descriptors were selected using first split and validated the model using the same descriptors. The three parametric GA-MLR equation along with statistical parameters and its interpretation in terms of structural features is as follows:

$pEC_{50} = C_0 + C_1 RDF040v + C_2 F06[N-O] + C_3 Mor13e$

N_{tr} = 74, N_{ex} = 38, R^2_{tr}= 0.85, R^2_{adj} = 0.84, Q^2 = 0.82, Q^2_{LMO} = 0.83, K_{xx} = 0.23, ΔK = 0.21, $RMSE_{tr}$ = 0.25, $RMSE_{cv}$ = 0.26, $RMSE_{ex}$ = 0.22, S = 0.25, F = 128.52, Q^2_{F1} = 0.83, Q^2_{F2}= 0.79, Q^2_{F3}= 0.88, CCC_{tr} = 0.92, CCC_{cv} = 0.90, CCC_{ex} = 0.89, MAE_{tr} = 0.19, MAE_{cv} = 0.20, MAE_{ex} = 0.14, $PRESS_{cv}$ = 5.25, $PRESS_{ex}$ = 1.79, R^2_{LMO} = 0.85,

The symbols depicted here have usual meaning. The high value of R^2, R^2_{adj}, F, R^2_{LMO}, Q^2, Q^2_{Fn},Q^2_{LMO}, CCC_{tr} and CCC_{ex} confirmed that the model is statistically robust and also possesses high external productivity. The positive coefficient (C_1 = 0.092, for split 1) of $RDF040v$, a 3D descriptor belonging to Radial Distribution Function (RDF), indicates that it plays a positive role in deciding the anti-malarial activity of 4-aminoquinolines, same is true for $Mor13e$ (C_3 = 0.234, for split 1), a 3D-descriptor. The RDF selected here is in general used for the explanation of the diffraction patterns obtained in powder X-ray diffraction experiments. RDF descriptors can be used in different tasks to fit the requirements of the information to be represented. These atomic properties enable the discrimination of the atoms of a molecule for almost any property that can be attributed to an atom. $RDF040v$ stands for RDF-4.0/weighted by atomic van der Waal's volume. The dependence of activity on this descriptor indicates that these molecules adapt a very different conformation during interaction with the receptor, such that the atoms with high

van der Waal's volume come closer and lie within a distance of $4A^o$, though it results in internal repulsion, however, with augmentation in activity [13]. This looks fairly reasonable due to the presence of a good number of single bonds in the molecules. The circle (in Fig. **2**) with a diameter of $4A^o$ has been drawn to represent *RDF040v* [37]. The radius corresponds to the inner part of the compounds and can be roughly assigned to the Nitrogen atom connected to the quinoline ring. Thus, the activity depends on the presence of heavy atoms at the internal atmosphere of the compounds.

The negative coefficient ($C_2 = -0.926$, for split 1) of *F06[N-O]*, a 3D cum indicator variable, points out that the anti-malarial activity has strong correlation with the presence/absence of nitrogen and oxygen at topological distance of six. This observation is supported when the activities of following molecules are compared: **1-4** ($EC_{50} =$ 0.018 to 0.314μM) with **33-36** ($EC_{50} =$ 0.009 to 0.032 μM) and with **49-52** ($EC_{50} =$ 0.009 to 0.020 μM). To elucidate this, we have highlighted (in bold) the topological distance of six between N and O in a molecule in Fig. (**2**).
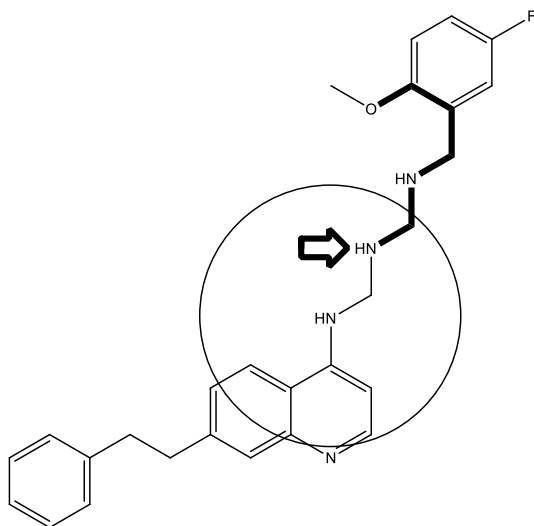
Fig. (2). Graphical representation of *RDF040v* and *F06[N-O]*.

It is a typical approach during the QSAR analysis to divide the available data into single split of training set (compounds which are "visible" during building up a model) and test set (compounds which are "invisible" during building up a model). However, the split has significant influence to the statistical quality of the prediction [38-40]. The split can be "lucky", thereby an approach gives excellent statistics also for external test set; reverse is true if the split is "unlucky". Under such circumstances, the validation [41-43] of an approach with a group of splits becomes source of robust estimation of the approach. Our computational experiments have shown that there is a significant influence of the split upon predictability of two examined approaches; hence, this influence can take place for cases of other approaches.

CONCLUSIONS

Statistically robust and highly predictive QSAR models (for six random various splits into the training and test sets) for anti-malarial activity have been built up by means of GA-MLR and optimal SMILES-based descriptors (CORAL

software). In three cases (Split 1,Split 3, and Split 5) preferable models have been built by GA-MLR and in three cases (Split 2,Split 4, and Split 6) preferable models have been obtained by optimal descriptors. The models clearify that the topological distance of six between N and O has significant correlation with activity. The anti-malarial activity depends on the presence of heavy atoms in the internal environment of the compounds. Using these models, promising anti-malarial agents could be developed.

CONFLICT OF INTEREST

The authors confirm that this article content has no conflict of interest.

ACKNOWLEDGEMENTS

SUPPLEMENTARY DATA

Supplementary material is available on the publisher's web site along with the published article.

REFERENCES

[1]   Papireddy, K.; Smilkstein, M.; Kelly, J.X.; Shweta; Salem, S.M.; Alhamadsheh, M.; Haynes, S.W.; Challis, G.L.; Reynolds, K.A. Antimalarial activity of natural and synthetic prodiginines. *J. Med. Chem.*, **2011**, *54*, 5296-5306.

[2]   Hwang, J.Y.; Kawasuji, T.; Lowes, D.J.; Clark, J.A.; Connelly, M.C.; Zhu, F.; Guiguemde, W.A.; Sigal, M.S.; Wilson, E.B.; DeRisi, J.L.; Guy, R.K. Synthesis and evaluation of 7-substituted 4-aminoquinoline analogues for antimalarial activity. *J. Med. Chem.*, **2011**, *54*, 7084-7093.

[3]   M.M.M. Pinto; M.E. Sousa; Nascimento, M.S.J. Xanthone derivatives: new insights in biological activities. *Curr. Med. Chem.*, **2005**, *12*, 2517-2538.

[4]   Jawarkar, R.D.; Masand, V.H.; Patil, K.N.; Mahajan, D.T.; Youssoufi, M.H.; Ben Hadda, T.; Kumbhare, S.L. 3D-QSAR study on coumarin analogues as potent inhibitors of MAO-B using a COMFA approach. *Der. Pharma. Chemica.*, **2010**, *2*, 302-310.

[5]   Mahajan, D.T.; Jawarkar, R.D.; Patil, K.N.; Masand, V.H.; Nazerruddin, G.M. 3D-QSAR studies on xanthone derivatives to understand pharmacological activities as MAO inhibitors. *Der. Pharma. Chemica.*, **2010**, *2*, 298-308.

[6]   Masand, V.H.; Jawarkar, R.D.; Patil, K.N.; Mahajan, D.T.; Ben Hadda, T.; Kurhade, G.H. COMFA analysis and toxicity risk assessment of coumarin analogues as MAO-A Inhibitors: Attempting better insight in drug design. *Der. Pharm. Lettre.*, **2010**, *2*, 350-357.

[7]   Masand, V.H.; Jawarkar, R.D.; Patil, K.N.; Nazerruddin, G.M.; Bajaj, S.O. Correlation potential of Wiener index vis-à-vis molecular refractivity: Antimalarial activity of xanthone derivatives. *Organic Chem. Indian J.*, **2010**, *6*, 30-38.

[8]   Masand, V.H.; Jawarkar, R.D.; Mahajan, D.T.; Ben Hadda, T.; Manikrao, A.M.; Khatale, P.N.; Vyas, J.V. Presuming the probable anti-inflammatory mechanism of ursolic acid: a plant derived pentacyclic triterpenoid, using molecular docking. *J. Comput. Method Mol. Des.*, **2011**, *1*, 9-13.

[9]   Mahajan, D.T.; Masand, V.H.; Patil, K.N.; Ben Hadda, T.; Jawarkar, R.D.; Thakur, S.D.; Rastija, V. CoMSIA and POM

analyses of anti-malarial activity of synthetic prodiginines. *Bioorg. Med. Chem. Lett.*, **2012**, *22*, 4827-4835.

[10] Masand, V.H.; Jawarkar, R.D.; Mahajan, D.T.; Hadda, T.B.; Sheikh, J.; Patil, K.N. QSAR and CoMFA studies of biphenyl analogs of the anti-tuberculosis drug (6S)-2-nitro-6-{[4-(trifluoromethoxy) benzyl]oxy}-6,7-dihydro-5H-imidazo[2,1-b][1,3]oxazine(PA-824). *Med. Chem. Res.*, **2012**, *21*, 2624-2629.

[11] Masand, V.H.; Mahajan, D.T.; Patil, K.N.; Chinchkhede, K.D.; Jawarkar, R.D.; Hadda, T.B.; Alafeefy, A.A.; Shibi, I.G. k-NN, quantum mechanical and field similarity based analysis of xanthone derivatives as α-glucosidase inhibitors. *Med. Chem. Res.*, **2012**, *21*, 4523-4534.

[12] Mahajan, D.T.; Masand, V.H.; Patil, K.N.; Hadda, T.B.; Rastija, V. Integrating GUSAR and QSAR analyses for antimalarial activity of synthetic prodiginines against multi drug resistant strain. *Med. Chem. Res.*, **2013**, *22*, 2284-2292.

[13] Masand, V.H.; Mahajan, D.T.; Ben Hadda, T.; Jawarkar, R.D.; Chavan, H.; Bandgar, B.P.; Chauhan, H. Molecular docking and quantitative structure activity relationship (QSAR) analyses of indolylarylsulfones as HIV-1 non-nucleoside reverse transcriptase inhibitors. *Med. Chem. Res.*, **2014**, 23, 417-425.

[14] Masand, V.H.; Mahajan, D.T.; Patil, K.N.; Hadda, T.B.; Youssoufi, M.H.; Jawarkar, R.D.; Shibi, I.G. Optimization of antimalarial activity of synthetic prodiginines: QSAR, GUSAR, and CoMFA analyses. *Chem. Biol. Drug Des.*, **2013**, *81*, 527-536.

[15] Benfenati, E.; Toropov, A.A.; Toropova, A.P.; Manganaro, A.; Gonella Diaza, R. Coral software: QSAR for anticancer agents. *Chem. Biol. Drug Des.*, **2011**, *77*, 471-476.

[16] Toropov, A.A.; Toropova, A.P.; Lombardo, A.; Roncaglioni, A.; Benfenati, E.; Gini, G. CORAL: building up the model for bioconcentration factor and defining it's applicability domain. *Eur. J. Med. Chem.*, **2011**, *46*, 1400-1403.

[17] Toropova, A.P.; Toropov, A.A.; Benfenati, E.; Gini, G.; Leszczynska, D.; Leszczynski, J. CORAL: quantitative structure-activity relationship models for estimating toxicity of organic compounds in rats. *J. Comput. Chem.*, **2011**, *32*, 2727-2733.

[18] Toropova, A.P.; Toropov, A.A.; Benfenati, E.; Gini, G.; Leszczynska, D.; Leszczynski, J. CORAL: QSPR models for solubility of [C60] and [C70] fullerene derivatives. *Mol. Divers.*, **2011**, *15*, 249-256.

[19] Milekhin, A.; Yeryukov, N.; Toropov, A.; Dmitriev, D.; Sheremet, E.; Zahn, D.R. Raman scattering of InAs/AlAs quantum dot superlattices grown on (001) and (311)B GaAs surfaces. *Nanoscale. Res. Lett.*, **2012**, *7*, 476.

[20] Stvolinsky, S.; Toropova, K.; Gordeeva, M.; Kazey, V.; Sato, T.; Meguro, K.; Boldyrev, A. Carnosine and its (S)-Trolox derivative protect animals against oxidative stress. *Amino Acids*, **2012**, *43*, 165-170.

[21] Tiunova, A.A.; Toropova, K.A.; Konovalova, E.V.; Anokhin, K.V. Effects of systemic administration of histone deacetylase inhibitor on memory formation and immediate early gene expression in chick brain. *Bull Exp. Biol. Med.*, **2012**, *153*, 742-745.

[22] Toropov, A.A.; Toropova, A.P.; Benfenati, E.; Gini, G.; Leszczynska, D.; Leszczynski, J. Calculation of molecular features with apparent impact on both activity of mutagens and activity of anticancer agents. *Anticancer Agents Med. Chem.*, **2012**, *12*, 807-817.

[23] Toropov, A.A.; Toropova, A.P.; Benfenati, E.; Gini, G.; Puzyn, T.; Leszczynska, D.; Leszczynski, J. Novel application of the CORAL software to model cytotoxicity of metal oxide nanoparticles to bacteria Escherichia coli. *Chemosphere*, **2012**, *89*, 1098-1102.

[24] Toropov, A.A.; Toropova, A.P.; Rasulev, B.F.; Benfenati, E.; Gini, G.; Leszczynska, D.; Leszczynski, J. CORAL: binary classifications (active/inactive) for liver-related adverse effects of drugs. *Curr. Drug Saf.*, **2012**, *7*, 257-261.

[25] Toropov, A.A.; Toropova, A.P.; Rasulev, B.F.; Benfenati, E.; Gini, G.; Leszczynska, D.; Leszczynski, J. CORAL: QSPR modeling of rate constants of reactions between organic aromatic pollutants and hydroxyl radical. *J. Comput. Chem.*, **2012**, *33*, 1902-1906.

[26] Toropova, A.P.; Toropov, A.A.; Benfenati, E.; Gini, G. QSAR models for toxicity of organic substances to Daphnia magna built up by using the CORAL freeware. *Chem. Biol. Drug. Des.*, **2012**, *79*, 332-338.

[27] Toropova, A.P.; Toropov, A.A.; Lombardo, A.; Roncaglioni, A.; Benfenati, E.; Gini, G. Coral: QSAR models for acute toxicity in fathead minnow (Pimephales promelas). *J. Comput. Chem.*, **2012**.

[28] Veselinovic, A.M.; Milosavljevic, J.B.; Toropov, A.A.; Nikolic, G.M. SMILES-based QSAR model for arylpiperazines as high-affinity 5-HT(1A) receptor ligands using CORAL. *Eur. J. Pharm. Sci.*, **2012**, *48*, 532-541.

[29] Toropov, A.A.; Toropova, A.P.; Benfenati, E.; Gini, G.; Leszczynska, D.; Leszczynski, J. CORAL: Classification model for predictions of anti-sarcoma activity. *Curr. Top. Med. Chem.*, **2012**, *12*, 2741-2744.

[30] Toropov, A.A.; Toropova, A.P.; Benfenati, E.; Gini, G.; Leszczynska, D.; Leszczynski, J. CORAL: QSPR model of water solubility based on local and global SMILES attributes. *Chemosphere*, **2013**, *90*, 877-880.

[31] Toropov, A.A.; Toropova, A.P.; Benfenati, E.; Gini, G.; Leszczynska, D.; Leszczynski, J.; De Nucci, G. QSAR models for inhibitors of physiological impact of *Escherichia coli* that leads to diarrhea. *Biochem. Biophys. Res. Commun.*, **2013**, *432*, 214-225.

[32] Toropov, A.A.; Toropova, A.P.; Puzyn, T.; Benfenati, E.; Gini, G.; Leszczynska, D.; Leszczynski, J. QSAR as a random event: Modeling of nanoparticles uptake in PaCa2 cancer cells. *Chemosphere*, **2013**, *92*, 31-37.

[33] Veselinovic, A.M.; Milosavljevic, J.B.; Toropov, A.A.; Nikolic, G.M. SMILES-based QSAR models for the calcium channel-antagonistic effect of 1,4-dihydropyridines. *Arch. Pharm. (Weinheim)*, **2013**, *346*, 134-139.

[34] Toropov, A.A.; Rasulev, B.F.; Leszczynski, J. QSAR modeling of acute toxicity for nitrobenzene derivatives towards rats: Comparative analysis by MLRA and optimal descriptors. *QSAR Combin. Sci.*, **2007**, *26*, 686-693.

[35] Toropov, A.A.; Toropova, A.P.; Benfenati, E.; Gini, G.; Leszczynska, D.; Leszczynski, J. CORAL: classification model for predictions of anti-sarcoma activity. *Curr. Top. Med. Chem.*, **2012**, *12*, 2741-2744.

[36] Chirico, N.; Papa, E.; Kovarich, S.; Cassani, S.; Gramatica, P. QSARINS, software for QSAR MLR model development and validation. 2012, QSAR Res. Unit in Environ. Chem. and Ecotox., University of Insubria, Varese, Italy. http://www.qsar.it. **2012**.

[37] Abreu, R.M.; Ferreira, I.C.; Queiroz, M.J. QSAR model for predicting radical scavenging activity of di(hetero)arylamines derivatives of benzo[b]thiophenes. *Eur. J. Med. Chem.*, **2009**, *44*, 1952-1958.

[38] Golbraikh, A.; Shen, M.; Xiao, Z.; Xiao, Y.D.; Lee, K.H.; Tropsha, A. Rational selection of training and test sets for the development of validated QSAR models. *J. Comput. Aided Mol. Des.*, **2003**, *17*, 241-253.

[39] Roy, K.; Mitra, I. On the use of the metric rm(2) as an effective tool for validation of QSAR models in computational drug design and predictive toxicology. *Mini Rev. Med. Chem.*, **2012**, *12*, 491-504.

[40] Roy, P.P.; Leonard, J.T.; Roy, K. Exploring the impact of size of training sets for the development of predictive QSAR models. *Chemo. Intell. Lab. Sys.*, **2008**, *90*, 31-42.

[41] Chirico, N.; Gramatica, P. Real external predictivity of qsar models: how to evaluate it? Comparison of different validation criteria and proposal of using the concordance correlation coefficient. *J. Chem. Inf. Model*, **2011**, *51*, 2320-2335.

[42] Chirico, N.; Gramatica, P. Real external predictivity of QSAR models. Part 2. New intercomparable thresholds for different validation criteria and the need for scatter plot inspection. *J. Chem. Inf. Model.*, **2012**, *52*, 2044-2058.

[43] Benigni, R.; Bossa, C. Predictivity and reliability of QSAR models: the case of mutagens and carcinogens. *Toxicol. Mech. Meth.*, **2008**, *18*, 137-147.

Tautomerism and multiple modelling enhance the efficacy of QSAR: antimalarial activity of phosphoramidate and phosphorothioamidate analogues of amiprophos methyl

Vijay H. Masand, Devidas T. Mahajan, Paola Gramatica & James Barlow

Springer

Springer

ORIGINAL RESEARCH

Tautomerism and multiple modelling enhance the efficacy of QSAR: antimalarial activity of phosphoramidate and phosphorothioamidate analogues of amiprophos methyl

**Vijay H. Masand · Devidas T. Mahajan ·
Paola Gramatica · James Barlow**

Abstract In the present study, sixty phosphoramidate and phosphorothioamidate analogues of amiprophos methyl (APM) previously reported as potential antimalarial agents were selected to build GA-MLR QSAR models to determine the features that govern the antimalarial activity. In addition, field similarity analysis was performed to determine the molecular fields that are responsible for the difference in the activity. The two tautomeric forms, possible for the molecules in the present study, were considered to determine the effect of tautomerism on QSAR modelling. In the present analysis, a simplistic approach was employed with the assumption that all the molecules either exist in keto-type tautomeric form or in enol-type form. To get more results from QSAR analysis, multiple models were developed. All the models have been thoroughly validated according to the OECD principles. The best four-parametric GA-MLR QSAR model is with $R^2 = 0.787$ and $R^2_{ex} = 0.806$ for the keto form, and $R^2 = 0.785$ and $R^2_{ex} = 0.770$ for the enol form. In addition, optimum values for more easily interpretable descriptors like molecular weight (MW), lipophilicity ($ALogP$), etc., have been determined. The analysis reveals that consideration of tautomerism and multiple models development enhance the efficiency of QSAR analysis for lead optimization and for prediction of the activities of as-yet untested molecules.

Abbreviations
GA   Genetic algorithm
MLR   Multiple linear regression
QSAR   Quantitative structure–activity analysis
WHO   World Health Organization
ADMET   Absorption, distribution, metabolism,
          excretion and toxicity
OLS   Ordinary least square
QSARINS   QSAR Insubria

V. H. Masand (✉) · D. T. Mahajan
Department of Chemistry, Vidya Bharati College, Camp,
Amravati 444 602, Maharashtra, India
e-mail: vijaymasand@gmail.com; vijaymasand@rediffmail.com

P. Gramatica
QSAR Research Unit in Environmental Chemistry and
Ecotoxicology, Department of Theoretical and Applied Sciences,
University of Insubria, Via Dunant 3, 21100 Varese, Italy

J. Barlow
Department of Pharmaceutical & Medicinal Chemistry, Royal
College of Surgeons in Ireland, Stephens Green, Dublin 2,
Ireland

Introduction

The recent WHO report on malaria (http://www.who.int/malaria/en/2013) clearly indicates that though malaria has its major presence in undeveloped and developing countries from Africa, Asia and South America, yet, its ill-effects are global. This vector-borne disease is responsible for more than 2 million cases every year (http://www.who.

int/malaria/en/2013; Mahajan *et al.,* 2012; Masand *et al.,* 2013c). Recently, many researchers have reported the emergence of multidrug-resistant strain of *Plasmodium falciparum* (*P. falciparum*), the main etiological agent of malaria, thereby, making the complete eradication of malaria a more difficult task. To curb this deadly disease, established antimalarial classes like artemisinins, amino-quinolines, etc., and largely unexplored many new compounds such as prodiginines, xanthones, amiprophos methyl derivatives, etc., have been tested in last decade (Hwang *et al.,* 2011; Mahajan *et al.,* 2012; Mara *et al.,* 2011; Mara *et al.,* 2013; Masand *et al.,* 2010b; Masand *et al.,* 2013c; Ojha and Roy, 2012).

Amiprophos methyl derivatives have received considerable attention in the last decade because of their insecticidal, antimicrobial and herbicidal properties, and ease of synthesis with the possibility to vary the structure relatively easy (Mara *et al.,* 2011; Mara *et al.,* 2013). Despite these advantages and the efforts executed, search for amiprophos methyl derivatives with high activity and better ADMET profile still persists.

Computer-assisted drug designing (CADD) has secured a unique place in modern drug designing because of quicker, cheaper and result-oriented analysis. Quantitative structure–activity relationship (QSAR), a thriving branch of CADD technique, is useful to determine the structural and pharmacophoric patterns that govern the activity of congeneric molecules (Scior *et al.,* 2009; Yuriev *et al.,* 2011). Tautomerism is an import molecular phenomenon that has significant influence on the different aspects of molecules, like pKa, LogP, solubility and other properties (Pospisil *et al.,* 2003a). Recently, a minor tautomer (in solution) of barbiturate analogue was found to be the active form in a 1.8 Å crystal structure of matrix metalloproteinase 8. Another example is that of pterin tautomer bound to the 2.3 Å structure of ricin toxin A-chain (Martin, 2010). Thus, a thermodynamically favoured tautomeric form in the solution may not be the 'bioactive tautomeric form' during the course of mechanism. Moreover, a molecule may interact in different tautomeric forms with different receptors (Martin, 2009, 2010; Masand *et al.,* 2013a; Oellien *et al.,* 2006; Pospisil *et al.,* 2003b; Thalheim *et al.,* 2010; Zou *et al.,* 2007). Herein, we have considered the influence of tautomerism on QSAR model development and multiple QSAR modelling with the determination of optimum values for some of the more easily interpretable descriptors for phosphoramidate and phosphorothioamidate analogues of amiprophos methyl. In the present study, we have performed integrated QSAR and field similarity analysis to determine the structural features that steer the antimalarial activity of amiprophos methyl derivatives.

Materials and methods

Dataset

The dataset consists of sixty phosphoramidate and phosphorothioamidate analogues of amiprophos methyl previously reported as potential antimalarial agents (Mara *et al.,* 2011; Mara *et al.,* 2013). The compounds were tested for inhibitory activity against *P. falciparum*. The experimental antimalarial activities reported as IC_{50} (μM) were converted to pIC_{50} (M) for QSAR analysis (Jawarkar *et al.,* 2010; Mahajan *et al.,* 2010, 2012; Masand *et al.,* 2010a; Masand *et al.,* 2010b; Masand *et al.,* 2013b; Masand *et al.,* 2012, 2013c). The compounds possess varying substituents at different positions, cyclic and non-cyclic derivatives and tautomerism also. For the present analysis, both the tautomeric forms were considered. The structures were drawn using ChemDraw 2008 with default settings followed by energy optimization with MMFF94 field. The general structures for both the tautomers are depicted in Table 1 along with the experimental data [IC_{50} (μM) and pIC_{50} (M)].

Descriptor calculation and model development

In the present analysis, a simplistic approach was employed with the assumption that all the molecules exist either in first tautomeric (keto-type) form or in other (enol-type) form. Therefore, the first set (Set 1) consists of 60 molecules in keto-type tautomeric form only, while the second set (Set 2) consists of 59 molecules but in enol-type of tautomeric form only. For one of the molecules, **44**, M and Y are oxygen and sulphur, respectively (see Table 1); therefore, enolization was not possible for it, and hence it was excluded from set 2. For both the tautomeric forms, a good number of descriptors were generated for the lowest energy conformer using e-Dragon followed by the removal of highly collinear ($|R| > 0.70$) and constant (>75 %) descriptors to avoid the inclusion of multi-collinear and spurious variables in GA-MLR model, using objective feature selection in QSARINS v1.2 (Gramatica *et al.,* 2013, 2014). This substantially decreased the total set of descriptors from 3,224 to 224 and 334 for sets 1 and 2, respectively. The reduced descriptors pool consists of zero-, one-, two- and three-dimensional descriptors, charge descriptors and molecular properties. Subjective feature selection was used to build the statistically robust OLS QSAR models using genetic algorithm (GA) in QSARINS. Thorough statistical validation of all the models for the two sets was performed according to OECD principles; only models with high internal and external predictivities were considered (Chavan *et al.,* 2013). To develop simple and informative QSAR models, the heuristic search was limited to four variables per model.

Table 1 Experimental data. IC_{50} and pIC_{50} for phosphoramidate and phosphorothioamidate analogues of amiprophos methyl

S. no.	R^1	R^2	X	IC_{50} (μM)	pIC_{50} (M)
1.	4-CH$_3$-2-NO$_2$	*i*-Propyl	S	4	5.398
2.	4-CH$_3$-2-NO$_2$	*i*-Propyl	O	126	3.900
3.	2-CH$_3$-4-NO$_2$	*i*-Propyl	O	128	3.893
4.	2-CH$_3$-5-NO$_2$	*i*-Propyl	O	128	3.893
5.	3-CH$_3$-4-NO$_2$	*i*-Propyl	O	79	4.102
6.	2-CH$_3$-3-NO$_2$	*i*-Propyl	O	128	3.893
7.	2-CN-4-CH$_3$	*i*-Propyl	O	128	3.893
8.	2-Br-4-CH$_3$	*i*-Propyl	O	39	4.409
9.	2-CH$_3$O-4-CH$_3$	*i*-Propyl	O	128	3.893
10.	2-Cl-4-CH$_3$	*i*-Propyl	O	39	4.409
11.	2-CF$_3$	*i*-Propyl	O	87	4.060
12.	3-CF$_3$	*i*-Propyl	O	50	4.301
13.	4-CF$_3$	*i*-Propyl	O	50	4.301
14.	2-Naphthol	*i*-Propyl	O	72	4.143
15.	1-NO$_2$-2-Naphthol	*i*-Propyl	O	87	4.060
16.	4-CH$_3$-2-NO$_2$	*n*-Butyl	O	28	4.553
17.	4-CH$_3$-2-NO$_2$	*i*-Butyl	O	75	4.125
18.	4-CH$_3$-2-NO$_2$	*n*-Pentyl	O	51	4.292
19.	4-CH$_3$-2-NO$_2$	Cyclopentyl	O	47	4.328
20.	5-CH$_3$-2-NO$_2$	*n*-Propyl	O	102	3.991
21.	4-CF$_3$	NH$_2$	O	79	4.102
22.	4-CF$_3$	*n*-Butyl	O	32	4.495
23.	4-CF$_3$	sec-Butyl	O	40	4.398
24.	4-CF$_3$	Cyclobutyl	O	45	4.347
25.	4-CF$_3$	*n*-Pentyl	S	4.5	5.347
26.	4-CF$_3$	Cyclopentyl	O	26	4.585
27.	4-CF$_3$	Cyclopentyl	S	8.6	5.066
28.	4-CF$_3$	Cyclohexyl	O	43	4.367
29.	4-CF$_3$	*n*-Heptyl	O	44	4.357
30.	4-CF$_3$	Piperidino	O	84	4.076
31.	4-CF$_3$	Pyrrolidino	O	56	4.252
32.	4-CF$_3$	Morpholino	O	98	4.009
33.	2-CH$_3$-4-NO$_2$	*n*-Pentyl	S	6.9	5.161
34.	2-CH$_3$-4-NO$_2$	Cyclopentyl	S	1.6	5.796
35.	4-Br	Cyclopentyl	O	17	4.770
36.	4-Br	Cyclopentyl	S	23	4.638
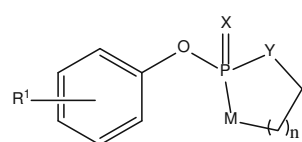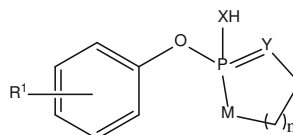
Table 1 continued

S. no.	R^1	R^2	X	IC$_{50}$ (μM)	pIC$_{50}$ (M)
37.	4-CH$_3$-2-NO$_2$	–	S	77	4.114
38.	2-CH$_3$-4-NO$_2$	–	S	51	4.292
39.	2-CH$_3$-4-NO$_2$	–	S	128	3.893
40.	2-CH$_3$-5-NO$_2$	–	S	24	4.620
41.	2-CH$_3$-5-NO$_2$	–	S	108	3.967
42.	4-CF$_3$	–	S	108	3.967
43.	4-CF$_3$	–	S	62	4.208
44.	4-CF$_3$	–	S	64	4.194

Tautomer-1   Tautomer-2
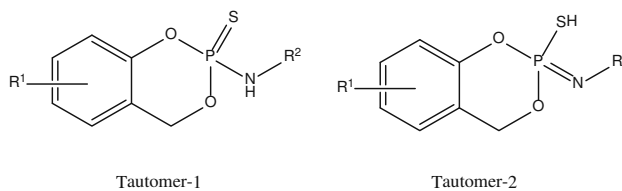
S. no.	R^1	R^2	X	IC$_{50}$ (μM)	pIC$_{50}$ (M)
45.	H	*i*-Pr	S	62	4.208
46.	H	*n*-Pr	S	95	4.022
47.	H	*i*-Bu	S	58	4.237
48.	4-NO$_2$	*i*-Pr	S	108	3.967
49	4-NO$_2$	*i*-Bu	S	118	3.928
50.	Naphtal-2-ol	*i*-Propyl	O	128	3.893
51.	2-OH-4-CH$_3$-3-NO$_2$pyridine	*i*-Propyl	O	128	3.893
52.	2-OH-5-CF$_3$pyridine	*i*-Propyl	O	25	4.602
53.	2-OH-5-CF$_3$pyridine	*i*-Propyl	S	29	4.538
54.	2-OH-5-CF$_3$pyridine	Cyclopentyl	O	23	4.638
55.	2-OH-4-CH$_3$-5-NO$_2$pyridine	*i*-Propyl	O	25	4.602
56.	4-OH pyridine	i-Propyl	O	128	3.893
57.	8-OH quinoline	Cyclopentyl	S	25	4.602
58.	6-OH quinoline	Cyclopentyl	S	19	4.721
59.	4-CF$_3$ phenyl		S	0.038	7.420
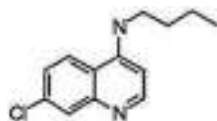
S. no.	R^1	R^2	X	IC$_{50}$ (μM)	pIC$_{50}$ (M)
60.	4-CH$_3$-2-NO$_2$		S	0.64	6.194
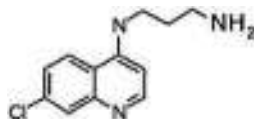
The general procedure (employed on both the tautomeric forms) for building the GA-MLR QSAR models is as follows:

(1) The set was divided randomly, using random splitting option in QSARINS (Gramatica *et al.,* 2013, 2014), into training and prediction sets of 48 (i.e. 80 % training set) and 12 (i.e. 20 % prediction set), respectively. The training set was used for model development, and the prediction set for the evaluation of predictivity on new chemicals, with the condition that the molecules which constitute the prediction set for set 1 also constitute the prediction set of set 2. In short, prediction sets of both the sets are identical. This was done for the appropriate comparison.

(2) QSARINS was used to build mono-parametric to tetra-parametric OLS models for both the sets (for sets 1 and 2) using default settings, except that Lack of Fit (LOF) was set to a value of 0.5. The selected fitness function to maximize in GA was Q^2. The descriptors that have been selected in models 1–4 are available in the supplementary information.

(3) All the models were subjected to internal as well as external validation along with Y-scrambling using QSARINS. The various parameters for internal validation include determination coefficient R^2, leave-one-out (LOO) cross-validation Q^2, leave-many-out (LMO) Q^2_{LMO}, coefficient of determination for Y-scrambling R^2_{Yscr}, and root mean squared error (RMSE). The LMO was repeated 500 times with 30 % of the objects left out randomly from the training set each time, and then the mean value of Q^2_{LMO} has been reported. The external validation parameters are $RMSE_{ex}$, MAE_{ex}, R^2_{ex}, Q^2_{F1}, Q^2_{F2}, Q^2_{F3} and CCC_{ex} (Chirico and Gramatica 2011, 2012; Consonni et al., 2009; Schuurmann et al., 2008).

(4) Another important step carried out for the model's validation was to check the model applicability domain (AD) and has been represented by Williams plots in Fig. 2. It is a theoretical region defined by the descriptors used in the modelling. It is evaluated by leverage (or hat) analysis using the formula: $h_i = x_i (X^T X)^{-1} x_i^T$, where $(i = 1, …, m)$, x_i is the descriptor row vector of the query compound i, m is the number of query compounds and X is the $n \times p$ matrix of the training set (p is the number of descriptors in the model and n is the number of training set compounds). The limit of the model domain is quantitatively defined by the leverage cutoff h^*, set as $3(p + 1)/n$. A leverage bigger than h^* for the training set means that the compound is very dominant in determining the model, while for the test set (X outlier), it means that the prediction is the substantial extrapolation of the model and could be unreliable. Meanwhile, a compound with a standardized residual greater than 3σ (3 standard deviation units) is recognized as a Y outlier (Masand et al., 2013d; Tropsha and Golbraikh, 2007; Yoona et al., 2013).

Results and discussion

For both the sets, the GA analysis provided a good number of MLR models with almost similar statistical characters comprising different descriptors. Generally, in such a situation, the QSAR modellers choose only one MLR model on the basis of its statistical performance. The drawbacks,

however, of this 'first among equals' approach are (1) for a QSAR model comprising esoteric descriptors only, appropriate and feasible interpretation in terms of structural features is more tricky and exigent; (2) a single QSAR model may be influenced by (i) the composition of training and test sets and (ii) some molecules in the dataset. Thus, it seems rational that building and reporting multiple models or consensus modelling (Yoon et al., 2013) are the feasible and appropriate solutions to overcome the drawbacks of 'first among equals' approach. Therefore, in the present study, multiple models have been built for both the sets. The models that do not satisfy the OECD principles were rejected. The GA-MLR QSAR models for both the sets along with their physical interpretation are as follows:

Set 1 (Keto form)

Model 1 $pIC_{50} = 2.3367 (\pm 0.7641) + 1.5695 (\pm 1.7697)$ $R6p -0.0306 (\pm 0.0254) nBT + 0.4084 (\pm 0.1941) nN + 0.6338 (\pm 0.1605) ALogP$.

Model 2 $pIC_{50} = 2.3499 (\pm 0.8363) + 0.4006 (\pm 0.2031) nN + 0.6195 (\pm 0.1657) AlogP - 0.0273 (\pm 0.0260) Se + 1.3502 (\pm 1.8907) R6p$.

The above models, with usual meaning of the symbols, are statistically robust and predictive with satisfactory values of the various parameters for internal and external validation (see Table 2). The high values of R^2, Q^2, R^2_{ex}, Q^2_{Fn} and CCC_{ex} indicate that the models are statistically acceptable and also have good external predictivity (Chirico and Gramatica 2011, 2012). These parameters, additionally vindicated by the low correlation among the descriptors, point out that these models are not fortuitous (see supplementary information). A QSAR model is primarily build for the following two reasons: (1) to predict the activity of as-yet untested molecules and (2) to get the relevant information useful for the lead optimization i.e. interpretation of the model for mechanistic details.

The positive coefficients for $ALogP$ (Ghose/Crippen octanol/water partition coefficient, represents lipophilicity of molecule), nN (number of nitrogen atoms) and $R6p$ (R autocorrelation of lag 6/weighted by atomic polarizabilities) indicate that these descriptors have positive correlation with the activity, whereas the reverse is true for nBT (number of bonds) and Se (Sum of atomic Sanderson electronegativities). The relatively low value of std. coeff. 0.1491 and -0.2659 for $R6p$ and Se, respectively, indicates that these descriptors have relatively low influence on the activity profile of the molecules. For lipophilicity ($ALogP$), the standardized coefficient (std. coeff.) is 1.0005 and 0.9780 in models 1 and 2, respectively. However, for the descriptor nN, the std. coeff. is 0.4249 and 0.4168 in models 1 and -2, respectively. Thus, these two descriptors play a crucial role in deciding the activity. Of these two descriptors,

Table 2 Statistical parameters for different GA-MLR models 1–4 and combined set model

S. no.	Statistical parameter	Model 1 Keto form	Model 2 Keto form	Model 3 Enol form	Model 4 Enol form	Combined set model
1.	N_{tr}	48	48	47	47	96
2.	N_{ex}	12	12	12	12	23
3.	Number of descriptors	4	4	4	4	4
Fitting criteria						
4.	R^2_{tr}	0.79	0.78	0.78	0.78	0.72
5.	$R^2_{adj.}$	0.77	0.76	0.76	0.76	0.71
6.	$RMSE_{tr}$	0.28	0.29	0.29	0.29	0.32
7.	MAE_{tr}	0.23	0.23	0.22	0.21	0.26
8.	CCC_{tr}	0.88	0.88	0.88	0.88	0.84
9.	s	0.30	0.30	0.30	0.30	0.33
10.	F	39.69	38.20	37.81	38.09	59.33
Internal validation criteria						
11.	R^2_{cv} (Q^2loo)	0.72	0.71	0.70	0.70	0.68
12.	$RMSE_{cv}$	0.32	0.33	0.34	0.34	0.34
13.	MAE_{cv}	0.27	0.27	0.26	0.25	0.28
14.	Q^2_{LMO}	0.54	0.54	0.58	0.60	0.58
15.	CCC_{cv}	0.83	0.83	0.82	0.82	0.81
16.	R^2_{Yscr}	0.08	0.08	0.09	0.09	0.04
External validation criteria						
17.	$RMSE_{ex}$	0.30	0.30	0.30	0.30	0.27
18.	MAE_{ex}	0.25	0.24	0.27	0.27	0.23
19.	R^2_{ex}	0.81	0.81	0.85	0.85	0.88
20.	Q^2_{F1}	0.78	0.78	0.76	0.77	0.82
21.	Q^2_{F2}	0.77	0.77	0.76	0.76	0.82
22.	Q^2_{F3}	0.76	0.76	0.76	0.77	0.80
23.	CCC_{ex}	0.89	0.89	0.90	0.90	0.92

lipophilicity has more influence on the activity than *nN*, as evident by its higher std. coeff. in models 1 and 2 and difference in the activity of molecules **21–32**. The negative influence of *nBT* is further vindicated by the negative std. coeff. of −0.2988 in model 1. A comparison of the following pairs of molecules **50** with **52**, **51** with **53** and **54** with **55** reveals that the values of *nN*, *nBT* and *ALogP* are either same or very close for molecules in these pairs, yet there is good difference in the activity; thus, the descriptor which influences the activity of these molecules is *R6p*. *R6p*, a GET-AWAY 3D descriptor, is a type of spatial autocorrelation descriptor. The autocorrelation is weighted by different physicochemical properties such as Sanderson's electronegativities, atomic polarizabilities, etc., at a certain topological distance. It considers the leverage of the atoms and their inter-atomic distance within the molecule relative to each other. For *R6p*, the topological distance is 6 and the weight has been made by atomic polarizabilities as stated above. Thus, it signifies the presence of polar atoms at a relative topological distance of 6 in the molecule, i.e. representing the polar environment within the molecule. A

largest value of *R6p* is expected when more number of highly polar atoms are distant from the centre of the molecule at a topological distance of 6 and at the same time close to each other in the molecular space which has, besides, a significant favourable effect on the activity of the molecule. For better clarification, the topological distance of 6, in turn *R6p*, has been highlighted (with pink colour) between the polar atoms for molecules **38** and **40**, as representatives (see Fig. 1).

Set 2 (Enol form)

Model 3 pIC_{50} = 2.1974 (±0.5893) + 1.3098 (±1.2403) $E3m$ + 0.4230 (±0.2207) nN − 0.1044 (±0.1144) nO + 0.4600 (±0.1019) $ALogP$.

Model 4 pIC_{50} = 1.8452 (±0.4747) + 1.6878 (±1.1720) $E3m$ + 0.4117 (±0.2111) nN − 0.2181 (±0.2303) $nArNO_2$ + 0.4701 (±0.0991) $ALogP$.

The symbols have their usual meaning (Chirico and Gramatica, 2011, 2012; Gramatica *et al.*, 2013; Yoon *et al.*, 2013). All the above-mentioned models satisfy most of the statistical parameters, i.e. they are statistically acceptable.
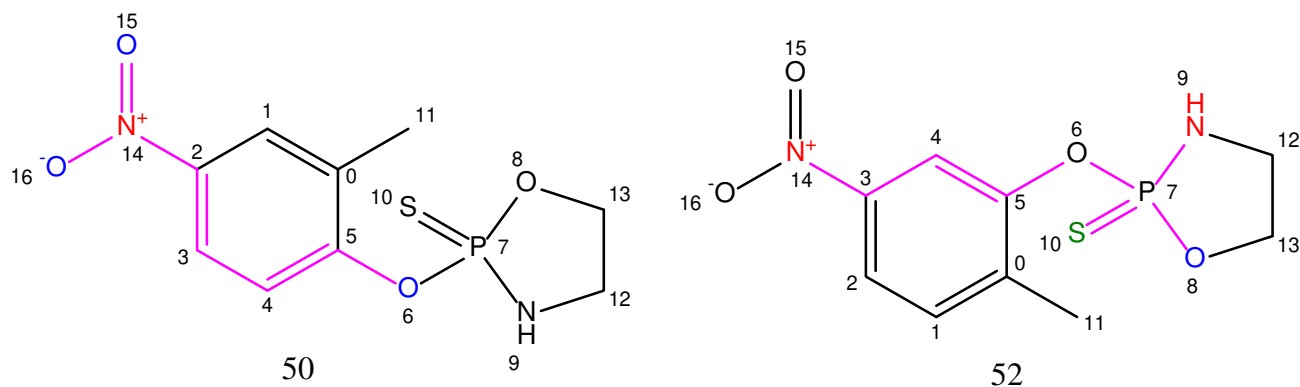
IC$_{50}$ = 51 μM, *R6p* = 0.431

IC$_{50}$ = 24 μM *R6p* = 0.465

Fig. 1 Physical interpretation of *R6p* using molecule numbers **50** and **52** as representatives

It is clear that lipophilicity (*ALogP*) (Std. Coeff. 0.7246 and 0.7405 in models 3 and 4, respectively) has significant positive role in deciding the activity; the same is acceptable for *nN* (Std. Coeff. 0.3848 and 0.3745 in model 3 and 4, respectively) and *E3m* (Std. Coeff. 0.1837 and 0.2367 in model 3 and 4, respectively). However, *nO* (Std. Coeff. −0.1762 in model 3) and *nArNO$_2$* (Std. Coeff. −0.1762 in model 4) have negative influence on activity. The predicted residuals, statistical parameters and correlation matrices for descriptors used for different GA-MLR models 1–4 have been listed in tables 3–5 in supplementary information.

A four-parametric QSAR model based on a dataset comprising both tautomeric forms has also been developed.

Combined set model $pIC_{50} = 2.2298\ (\pm 0.3391) + 0.3463\ (\pm 0.1126)\ nN + 0.2501\ (\pm 0.1349)\ nS + 0.3910\ (\pm 0.2538)\ nArX + 0.4279\ (\pm 0.0775)\ ALogP.$

The graphs for correlation, residuals and Y-randomization have been depicted in Figs. 1 and 2 of supporting information. Further, the Williams plot has been used to represent the AD of the models. From Fig. 2, it is evident that some molecules lie outside the AD of the entire reported model.

It appears that the QSAR models for both the tautomeric forms are statistically significant and independent of tautomerism. The plausible reasons for negligible influence of the tautomerism on QSAR models could the insensitivity of the descriptors in recognition and discrimination of tautomers. Moreover, tautomerization is a natural, rapid and dynamic phenomenon, resulting in rapid equilibrium among the tautomers.

Determination of optimum values of different descriptors

Even though many QSAR modellers report properly validated QSAR equations, which are efficient to guide for the development of novel drugs or modification of existing drugs, they are not practised due to the following reasons: (i) complexity in understanding and interpretation of QSAR equation in terms of structural or pharmacophoric features; (ii) the accurate and reproducible computation or estimation of descriptors is either very complex or resource consuming; (iii) computational facilities/resources like sophisticated and particular softwares may not be accessible to organic chemist to compute the reported descriptors in the QSAR equation; (iv) in addition, some other descriptors may have good correlation with the activity but are not included in QSAR equation due to some reasons; and (v) the organic chemist may not be well skilled or trained in QSAR.

Therefore, in the present study, we have determined the optimum values for more easily interpretable different descriptors to gauge the discovery of novel small molecules with the specified chemical properties. A very simple yet effective method to establish the optimal value of any descriptor is to develop either parabolic (quadratic) or bilinear equation (Pinto *et al.,* 2005; Abreu *et al.,* 2009). These functions presume that the correlation between the descriptor and the activity is non-linear in nature with the peak of the curve representing the optimum value. *R*, R^2, R^2_{adj}, *F*, *Spress*, *SDEP* and *s* were calculated to check the robustness of the bilinear/parabolic equations. Though we have compared the activities of the molecules of the dataset in terms of descriptors like lipophilicity/hydrophobicity, number of bonds, molecular weight, etc., for which we have determined the optimum value, we make it clear that the combined or converse effect of confounding factors/descriptors do have additional influence on the activity profile of the compounds. The optimum values will be the handy tool for medicinal chemists in developing novel amiprophos methyl analogues with improved antimalarial activity profile.
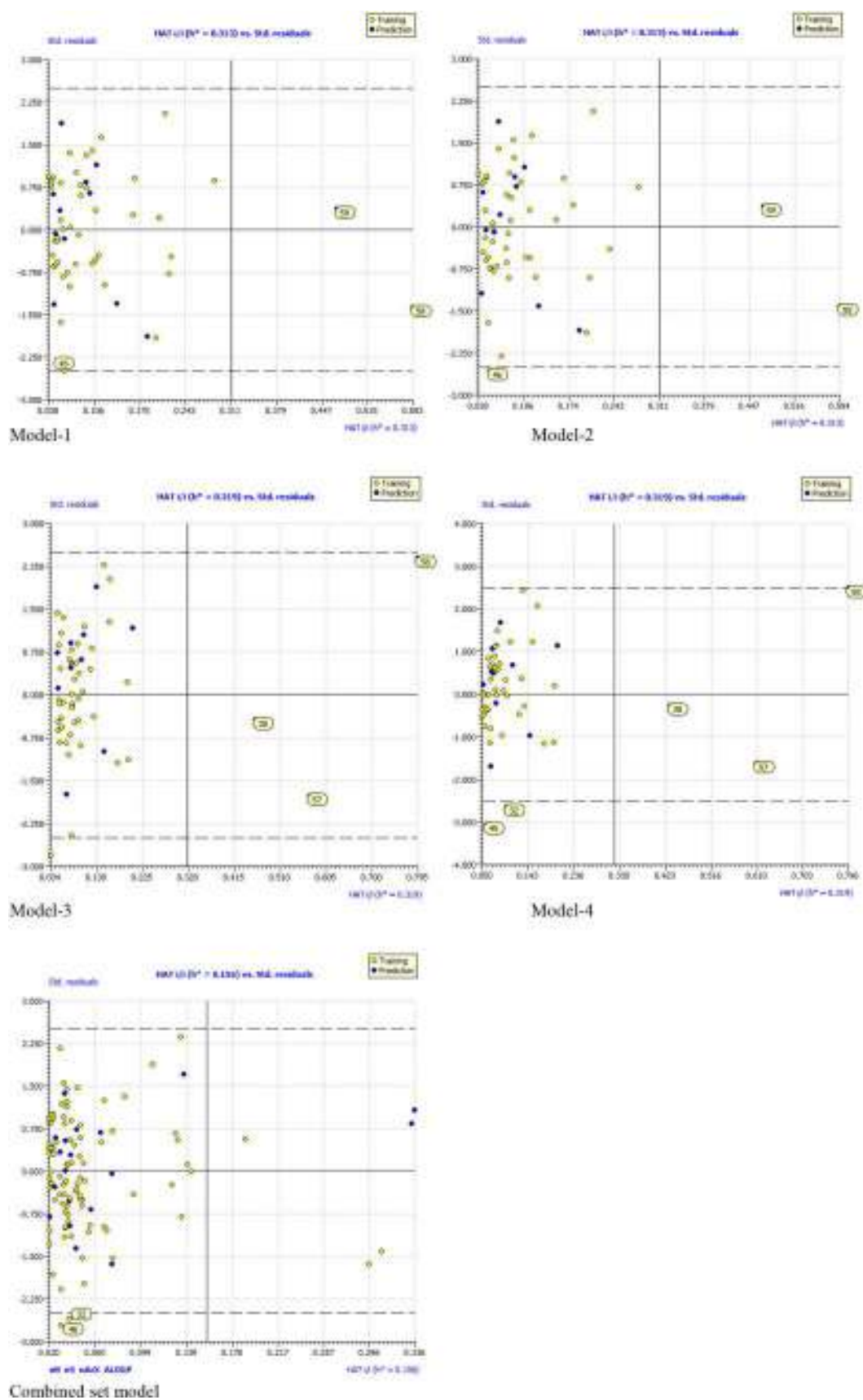
Fig. 2 Applicability domain representation using Williams plot for models 1–4 and combined set model

Molecular weight (MW)

Model 5 $pIC_{50} = + 0.0002$ (± 0.0070) $MW + 0.0117$ (± 0.0081) Log $(\beta\ 10^{MW} + 1) + 4.0275\ (\pm 2.0353)$.

Ntr $= 60$, $R = 0.808$, $R^2 = 0.6522$, $R^2_{adj.} = 0.634$, $Q^2 = 0.573$, $s = 0.375$, $F = 34.997$, $p < 0.0001$, $SPress = 0.415$, $SDEP = 0.408$, $Log\ \beta = -299.441$, MW-$Optimum = 297.777$, Outliers $=$ compound numbers **32** and **46**.

Number of carbon atoms (nC)

Model 6 $pIC_{50} = +0.0763$ (± 0.0550) $nC + 1.1983$ (± 0.4840) Log $(\beta\ 10^{nC} + 1) + 3.3909\ (\pm 0.6794)$.

Ntr $= 60$, $R = 0.783$, $R^2 = 0.613$, $R^2_{adj.} = 0.593$, $s = 0.395$, $F = 29.607$, $p < 0.0001$, $Q^2 = 0.588$, $SPress = 0.407$, $SDEP = 0.400$, $Log\ \beta = -20.043$, nC-$Optimum = 18.875$, Outliers $=$ compound numbers **23**, **32** and **46**.

Lipophilicity (ALogP)

Model 7 $pIC_{50} = +0.2074$ (± 0.1638) ALogP $+ 0.7029$ (± 0.3499) Log $(\beta\ 10^{ALogP} + 1) + 3.6044\ (\pm 0.4805)$.

Ntr $= 60$, $R = 0.836$, $R^2 = 0.699$, $R^2_{adj.} = 0.683$, $s = 0.349$, $F = 43.270$, $p < 0.0001$, $Q^2 = 0.664$, $SPress = 0.368$, $SDEP = 0.362$, $Log\ \beta = -4.123$, $ALogP$-$Optimum = 3.745$, Comment: No outlier.

Sum of atomic polarizabilities (Sp)

Model 8 $pIC_{50} = 0.0186$ (± 0.0502) $Sp + 0.1706$ (± 0.0774) Log $(\beta\ 10^{Sp} + 1) + 3.7687\ (\pm 1.2016)$.

Ntr $= 60$, $R = 0.796$, $R^2 = 0.634$, $R^2_{adj.} = 0.614$, $s = 0.384$, $F = 32.298$, $p < 0.0001$, $Q^2 = 0.554$, $SPress = 0.424$, $SDEP = 0.417$, $Log\ \beta = -26.248$, Sp-$Optimum = 25.337$, Outliers $=$ compound numbers **32** and **46**.

In the above models, the symbols have their usual meanings. A better statistics is possible if the number of congener compounds in the dataset and also the range of the biological data are augmented. In many cases, the acceptable fitting of the equation ($R^2 > 0.60$), though statistically not outstanding, indicates that there prevails optimum value of lipophilicity, molecular weight (MW), Sum of atomic polarizabilities (Sp) and Number of carbon atoms (nC).
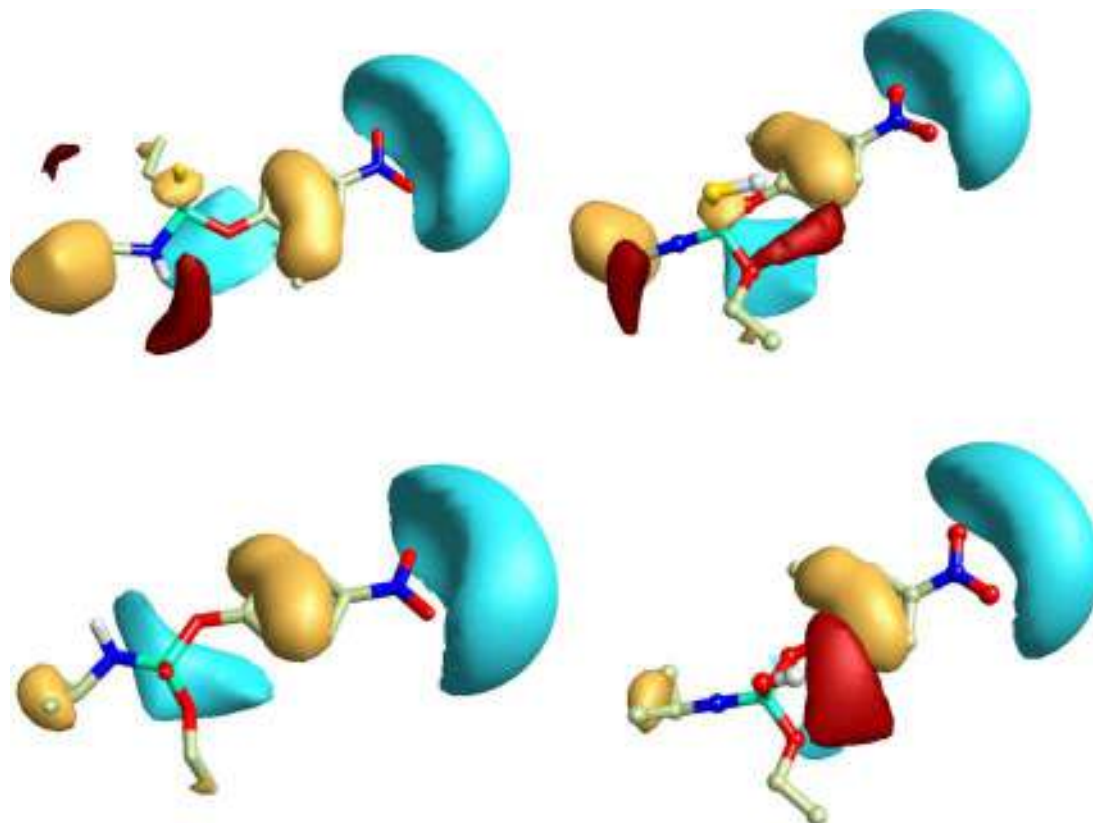
Fig. 3 Field similarity analysis of Mol id **34** (Most active) and Mol id **3** (least active) **34** (Most active) with side view of Keto form (*left*) and enol form (*right*) (*red* positive field, *blue* negative field and *yellow* hydrophobic region) **3** (least active) Side view of Keto form (*left*) and enol form (*right*) (Color figure online)

Fig. 4 Summary of SAR, QSAR and field similarity analysis

presence of =S/-SH is good

presence of this N is good

-NH₂ is favourable

presence of lipophilic group like n-butyl, cyclopentyl is favourable

presence of n-propyl or n-butyl is good as R₃

replace these Oxygen atoms by N/S/C
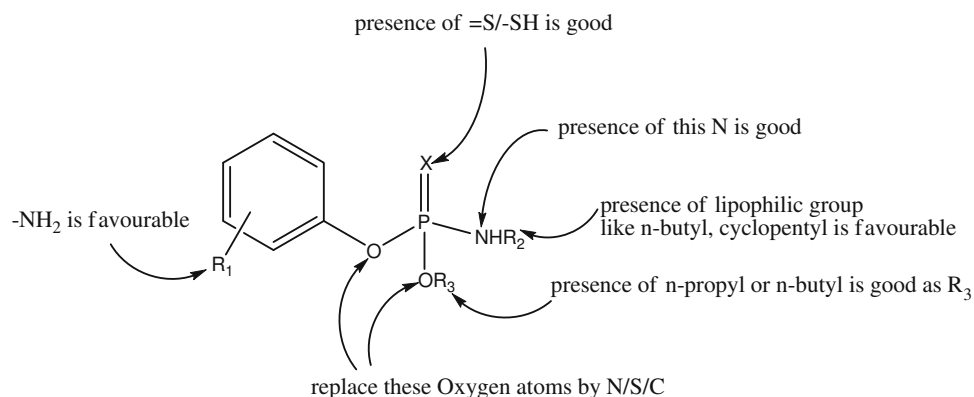
Field similarity analysis

Field similarity analysis was performed to compare the fields of tautomeric forms of the most active and least active compounds, as representatives, to identify the key features that control the biological activity. The results are as shown below in Fig. 3.

From Fig. 3, it is clear that sulphur is very important for enhancing the activity due to its lipophilicity. The presence of red contour near N reveals that the presence of this positive field is very important for activity. This positive field is also present in the enol form of the least active molecule (compound **3**). This positive field could be a possible reason for the lesser activity of the primary amido **21** (IC$_{50}$ = 79 μM) than the tertiary amides **30–32**. In their previous publication, Mara *et al.* (2011) obtained a modest relation (R^2 = 0.504) between activity and *clogP* (represents lipophilicity). It is evident from the above figure that the pharmacophoric pattern consists of not only lipophilic region, but also positive and negative fields. Another observation is that a possible reason for the difference in the activities of **34** and **3** could be the presence of bigger lipophilic region due to cyclopentyl ring in **34** (depicted by the yellow-coloured contour) than a relatively small lipophilic region in **3** due to iso-propyl group.

The summary of SAR, QSAR and field similarity analysis are depicted in Figs. 4 and 5.

Conclusions

In the present study, we have investigated the influence of tautomerism on the predictive QSAR model development for antimalarial activity of phosphoramidate and phosphorothioamidate analogues of amiprophos methyl. The four-parametric models satisfy the threshold values for many statistical parameters like R^2_{ex}, Q^2_{F1}, Q^2_{F2}, Q^2_{F3} and CCC$_{ex}$, which are essential to judge the real external predictivity. The analysis indicates that tautomerism has no
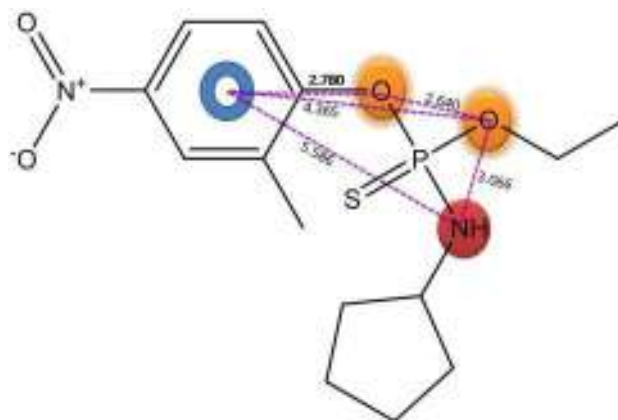
Fig. 5 Summary of SAR, QSAR and field similarity analysis in terms of pharmacophoric pattern. *Blue*, *golden* and *red circles* represent aromatic, H-bond acceptor and H-bond donor, respectively. All the values are in Å (Color figure online)

influence on the statistical performance of QSAR models built using different tautomeric forms. However, important information in terms of structural and pharmacophoric patterns that affect the activity can be extracted when multiple models are built for the different tautomeric forms for the congeners. Thus, tautomerism and multiple modelling improve the efficacy of QSAR for lead optimization and to predict the activities of as-yet untested molecules.

Disclosure The authors have no other relevant affiliations or involvement with any organization or entity with a financial interest in or financial conflict with the subject matter or materials discussed in the manuscript apart from those disclosed.

References

Abreu Rui MV, Ferreira Isabel CFR, Queiroz MJRP (2009) QSAR model for predicting radical scavenging activity of di(hetero)arylamines derivatives of benzo[*b*]thiophenes Eur. J Med Chem 44:1952–1958

Chavan HV, Bandgar BP, Adsul LK, Dhakane VD, Bhale PS, Thakare VN, Masand V (2013) Design, synthesis, characterization and anti-inflammatory evaluation of novel pyrazole amalgamated flavones. Bioorg Med Chem Lett 23(5):1315–1321

Chirico N, Gramatica P (2011) Real external predictivity of QSAR models: how to evaluate it? Comparison of different validation criteria and proposal of using the concordance correlation coefficient. J Chem Inf Model 51(9):2320–2335

Chirico N, Gramatica P (2012) Real external predictivity of QSAR models. Part 2. New intercomparable thresholds for different validation criteria and the need for scatter plot inspection. J Chem Inf Model 52(8):2044–2058

Consonni V, Ballabio D, Todeschini R (2009) Comments on the definition of the Q2 parameter for QSAR validation. J Chem Inf Model 49(7):1669–1678

Gramatica P, Cassani S, Chirico N (2014) QSARINS-chem: insubria datasets and new QSAR/QSPR models for environmental pollutants in QSARINS. J Comput Chem 35(13):1036–1044

Gramatica P, Chirico N, Papa E, Cassani S, Kovarich S (2013) QSARINS: a new software for the development, analysis, and validation of QSAR MLR models. J Comput Chem 34(24):2121–2132

Hwang JY, Kawasuji T, Lowes DJ, Clark JA, Connelly MC, Zhu F, Guiguemde WA, Sigal MS, Wilson EB, DeRisi JL, Guy RK (2011) Synthesis and evaluation of 7-substituted 4-aminoquinoline analogues for antimalarial activity. J Med Chem 54(20):7084–7093

Jawarkar RD, Masand VH, Patil KN, Mahajan DT, Youssoufi MH, Ben Hadda T, Kumbhare SL (2010) 3D-QSAR study on coumarin analogues as potent inhibitors of MAO-B using a COMFA approach. Der Pharma Chemica 2(6):302–310

Mahajan DT, Jawarkar RD, Patil KN, Masand VH, Nazerruddin GM (2010) 3D-QSAR studies on xanthone derivatives to understand pharmacological activities as MAO inhibitors. Der Pharma Chemica 2(4):298–308

Mahajan DT, Masand VH, Patil KN, Ben Hadda T, Jawarkar RD, Thakur SD, Rastija V (2012) CoMSIA and POM analyses of anti-malarial activity of synthetic prodiginines. Bioorg Med Chem Lett 22(14):4827–4835

Mara C, Dempsey E, Bell A, Barlow JW (2011) Synthesis and evaluation of phosphoramidate and phosphorothioamidate analogues of amiprophos methyl as potential antimalarial agents. Bioorg Med Chem Lett 21(20):6180–6183

Mara C, Dempsey E, Bell A, Barlow JW (2013) Synthesis and evaluation of phenoxyoxazaphospholidine, phenoxyoxazaphosphinane, and benzodioxaphosphininamine sulfides and related compounds as potential anti-malarial agents. Bioorg Med Chem Lett 23(12):3580–3583

Martin YC (2009) Let's not forget tautomers. J Comput Aided Mol Des 23(10):693–704

Martin YC (2010) Tautomerism, Hammett sigma, and QSAR. J Comput Aided Mol Des 24(6–7):613–616

Masand VH, Jawarkar RD, Patil KN, Mahajan DT, Ben Hadda T, Kurhade GH (2010a) COMFA Analysis and toxicity risk assessment of coumarin analogues as MAO-A inhibitors: attempting better insight in drug design. Der Pharm Lettre 2(6):350–357

Masand VH, Jawarkar RD, Patil KN, Nazerruddin GM, Bajaj SO (2010b) Correlation potential of Wiener index vis-à-vis molecular refractivity: antimalarial activity of xanthone derivatives. Org Chem Indian J 6(1):30–38

Masand VH, Mahajan DT, Patil KN, Chinchkhede KD, Jawarkar RD, Hadda TB, Alafeefy AA, Shibi IG (2012) k-NN, quantum mechanical and field similarity based analysis of xanthone derivatives as α-glucosidase inhibitors. Med Chem Res 21(12):4523–4534

Masand VH, Mahajan DT, Ben Hadda T, Jawarkar RD, Alafeefy AM, Rastija V, Ali MA (2013a) Does tautomerism influence the outcome of QSAR modeling? Med Chem Res 23(4):1742–1757

Masand VH, Mahajan DT, Patil KN, Hadda TB, Youssoufi MH, Jawarkar RD, Shibi IG (2013b) Optimization of antimalarial activity of synthetic prodiginines: QSAR, GUSAR, and CoMFA analyses. Chem Biol Drug Des 81(4):527–536

Masand VH, Mahajan DT, Hadda TB, Jawarkar RD, Chavan H, Bandgar BP, Chauhan H (2013b) Molecular docking and quantitative structure–activity relationship (QSAR) analyses of indolylarylsulfones as HIV-1 non-nucleoside reverse transcriptase inhibitors. Med Chem Res 23(1): 417–425

Masand VH, Mahajan DT, Patil KN, Hadda TB, Youssoufi MH, Jawarkar RD, Shibi IG (2013d) Optimization of antimalarial activity of synthetic prodiginines: QSAR, GUSAR, and CoMFA analyses. Chem Biol Drug Des 81(4):527–536

Oellien F, Cramer J, Beyer C, Ihlenfeldt WD, Selzer PM (2006) The impact of tautomer forms on pharmacophore-based virtual screening. J Chem Inf Model 46(6):2342–2354

Ojha PK, Roy K (2012) First report on exploring structural requirements of 1,2,3,4-tetrahydroacridin-9(10H)-one analogs as antimalarials using multiple QSAR approaches: descriptor-based QSAR, CoMFA-CoMSIA 3D-QSAR, HQSAR and G-QSAR approaches. Comb Chem High Throughput Screen 16(1):7–21

Pinto MMM, Sousa ME, Nascimento MSJ (2005) Xanthone derivatives: new insights in biological activities. Curr Med Chem 12:2517–2538

Pospisil P, Ballmer P, Scapozza L, Folkers G (2003a) Tautomerism in computer-aided drug design. J Recept Signal Transduct 23(4): 361–371

Pospisil P, Ballmer P, Scapozza L, Folkers G (2003b) Tautomerism in computer-aided drug design. J Recept Signal Transduct Res 23(4):361–371

Schuurmann G, Ebert RU, Chen J, Wang B, Kuhne R (2008) External validation and prediction employing the predictive squared correlation coefficient test set activity mean vs training set activity mean. J Chem Inf Model 48(11):2140–2145

Scior T, Medina-Franco JL, Do QT, Martinez-Mayorga K, Yunes Rojas JA, Bernard P (2009) How to recognize and workaround pitfalls in QSAR studies: a critical review. Curr Med Chem 16(32):4297–4313

Thalheim T, Vollmer A, Ebert R-U, Kühne R, Schüürmann G (2010) Tautomer identification and tautomer structure generation based on the InChI code. J Chem Inf Model 50(7):1223–1232

Tropsha A, Golbraikh A (2007) Predictive QSAR modeling workflow, model applicability domains, and virtual screening. Curr Pharm Des 13(34):3494–3504

Yoon YK, Ali MA, Wei AC, Choon TS, Khaw KY, Murugaiyah V, Osman H, Masand VH (2013) Synthesis, characterization, and molecular docking analysis of novel benzimidazole derivatives as cholinesterase inhibitors. Bioorg Chem 49:33–39

Yoona YK, Ali MA, Wei AC, Choon TS, Khaw K-Y, Murugaiyah V, Osman H, Masand VH (2013) Synthesis, characterization, and molecular docking analysis of novel benzimidazole derivatives as cholinesterase inhibitors. Bioorg Chem 49:33–39

Yuriev E, Agostino M, Ramsland PA (2011) Challenges and advances in computational docking: 2009 in review. J Mol Recognit 24(2):149–164

Zou JW, Luo CC, Zhang HX, Liu HC, Jiang YJ, Yu QS (2007) Three-dimensional QSAR of HPPD inhibitors, PSA inhibitors, and anxiolytic agents: effect of tautomerism on the CoMFA models. J Mol Graph Model 26(2):494–504

Original article

Synthesis of α, β-unsaturated carbonyl based compounds as acetylcholinesterase and butyrylcholinesterase inhibitors: Characterization, molecular modeling, QSAR studies and effect against amyloid β-induced cytotoxicity

Syed Nasir Abbas Bukhari [a, *], Ibrahim Jantan [a, *], Vijay H. Masand [b], Devidas T. Mahajan [b], Muhammad Sher [c], M. Naeem-ul-Hassan [c], Muhammad Wahab Amjad [a]

[a] Drug and Herbal Research Centre, Faculty of Pharmacy, Universiti Kebangsaan Malaysia, Jalan Raja Muda Abdul Aziz, 50300 Kuala Lumpur, Malaysia
[b] Department of Chemistry, Vidya Bharati Mahavidyalaya, Amravati, Maharashtra 444 602, India
[c] Department of Chemistry, University of Sargodha, Sargodha 40100, Pakistan

ARTICLE INFO

ABSTRACT

A series of novel carbonyl compounds was synthesized by a simple, eco-friendly and efficient method. These compounds were screened for anti-oxidant activity, *in vitro* cytotoxicity and for inhibitory activity for acetylcholinesterase and butyrylcholinesterase. The effect of these compounds against amyloid β-induced cytotoxicity was also investigated. Among them, compound **14** exhibited strong free radical scavenging activity (18.39 μM) while six compounds (**1**, **3**, **4**, **13**, **14**, and **19**) were found to be the most protective against Aβ-induced neuronal cell death in PC12 cells. Compounds **4** and **14**, containing *N*-methyl-4-piperidone linker, showed high acetylcholinesterase inhibitory activity as compared to reference drug donepezil. Molecular docking and QSAR (Quantitative Structure–Activity Relationship) studies were also carried out to determine the structural features that are responsible for the acetylcholinesterase and butyrylcholinesterase inhibitory activity.

© 2014 Elsevier Masson SAS. All rights reserved.

1. Introduction

According to the World Alzheimer Report 2013, Alzheimer's disease and other forms of dementia are among the biggest global public health issues facing our generation. Currently, over 35 million people around the world live with these conditions and this number is likely to increase threefold by 2050, to 115 million people [1]. Alzheimer's disease (AD), the most common form of dementia amongst the aged, is a deadly neurodegenerative disease categorized by the loss of mental abilities and a diversity of neuropsychiatric symptoms and behavioral disorders [2,3]. Neurofibrillary tangles and amyloid β (Aβ) plaques are found in the brain. The cholinergic system is predominantly vulnerable to synapse loss, particularly in cortical regions related with memory and executive function [4]. Most treatment approaches to date have been based on the cholinergic hypothesis which assumes that memory loss in patients suffering from this disease result from a loss of cholinergic function in brain for cholinergic neurotransmission is specifically affected in patients suffering from Alzheimer's disease.

For the treatment of AD, one of the most common methods is to increase the acetylcholine levels in brain with acetylcholinesterase inhibitors [5]. The best characterized therapeutic effect of cholinesterase inhibitors (ChE) in Alzheimer disease patients is to maintain cognitive function for a 1-year period in about 50% of the patients [6]. Two kinds of cholinesterase enzymes are found in the central nervous system; acetylcholinesterase (AChE) and butyrylcholinesterase (BuChE). Both enzymes are capable of hydrolyzing acetylcholine, but AChE has a 10^{13}-fold higher hydrolytic acetylcholine activity than BuChE, at the similar temperature and pH [7]. In the healthy brain, BuChE is thought to play a trivial role in regulating brain acetylcholine levels. In the AD brain, BuChE activity rises while AChE activity remains unchanged or declines. Hence, both enzymes may contribute to regulating acetylcholine levels and are appropriate therapeutic targets to enhance the cholinergic deficit. The two enzymes vary in location, substrate specificity and kinetics. The most recent studies suggest that

BuChE might also have a part in the etiology and development of AD beyond the regulation of synaptic acetylcholine levels. Experimental evidence from the use of agents with improved selectivity for BuChE and ChE, such as rivastigmine (having dual inhibitory action on both AChE and BuChE), shows that there are possible therapeutic benefits of inhibiting both AChE and BuChE in AD and associated dementias. The development of specific small molecule drugs BuChE inhibitors with the capability to inhibit BuChE together with AChE should lead to better clinical outcomes [8].

In our previous studies, we synthesized and screened the series of novel chalcone derivatives and curcumin analogues with α, β-carbonyl linkers for their activity against phagocytic chemotaxis and the production of reactive oxygen species (ROS) from zymosan stimulated human phagocytes. On the basis of these findings and a those of other scientists, it was determined that chalcone derivatives and curcumin-like compounds bearing α, β-carbonyl group have a wide diversity of pharmacological activities [9–14]. Our latest studies showed that a range of compounds with a α, β-unsaturated moiety are capable of inhibiting both AChE and BuChE and can be possible candidates for the treatment of Alzheimer's disease [15,16].

Numerous studies have documented increased protein oxidation [17] and reactive oxygen species (ROS) formation [18] in the brain tissue of AD patients. Aβ is considered to be a cause of lipid peroxidation in brain cell membranes that may contribute to neurodegeneration [19,20]. Encouraged by these results, we continued our work in this area, and in the current study we synthesized thirty novel compounds bearing the α, β-carbonyl moiety and have screened them for their effects on the AChE/BuChE activities in addition to amyloid β-induced cytotoxicity in PC12 cells. Lastly, molecular modeling calculations and QSAR studies were performed to understand the structural basis for the biological activity of compounds.

2. Results and discussion

2.1. Chemistry

Thirty novel compounds of ten different types were synthesized in the current study as reported previously [21,22]. To synthesize the desired α, β-unsaturated carbonyl based compounds, Claisen–Schmidt condensation was used [23] between different ketones and suitable aryl aldehydes at a molar ratio 1:2, (twenty one compounds, **1–7**; **11–17**; **21–27**) in the presence of NaOH in ethanol. Some compounds were synthesized in acetic acid in the presence of dry HCl gas. Nine compounds (**8–10**; **18–20**; **28–30**) resembling chalcone analogues were synthesized by same Claisen–Schmidt condensation using molar ratio 1:1 of ketone and aldehyde (Scheme 1). Eight compounds (**7**, **8**, **10**, **17**, **18**, **20**, **27**, **28**) were synthesized using both types of catalytic systems comprising NaOH and the dry HCl gas mixture. As compared to NaOH, the catalytic system with HCl gas mixture produced compounds more efficiently with a higher yield. When using NaOH, a mixture of numerous unidentified products was obtained requiring extensive purification by column chromatography.

All synthesized new compounds were characterized by spectrophotometric techniques as well as elemental analysis of C, H, and N, and melting points. Carbon nuclear magnetic resonance spectra were also obtained. For compounds **3**, **13** and **23**, the NH absorption peaks were not seen in the ^{1}H NMR spectra of the compounds. Absence of NH absorption peaks is also reported previously by other researchers [24,25].

2.2. Antioxidant activity of α, β-unsaturated carbonyl based compounds

The DPPH (1,1-diphenyl-1-picrylhydrazyl) assay was performed to assess the compounds for their antioxidant activity. The data of the antioxidant assay is summarized in Table 1. According to the data, five compounds (**1**, **3**, **4**, **14** and **19**) were found to possess potent DPPH radical scavenging activity with IC_{50} in the range of 18.39–22.99 μM. Compound **14**, having a N-methyl-4-piperidone linker and diethoxymethyl substitution at position 4 of aromatic rings, showed the strongest antioxidant activity (18.39 μM), even more than the positive control (ascorbic acid; 19.36 μM). Among all thirty compounds, only eleven compounds have poor antioxidant activities, exhibiting IC_{50} values greater than 50 μM.

2.3. Cytotoxicity of synthetic compounds in PC12 cells

To investigate the effect of the new compounds on cell viability, the MTT assay was conducted on PC12 cells. The cells were incubated with varying concentrations (0.01–100 μM) of the test compounds for 24 h and under these conditions the α, β-unsaturated carbonyl based compounds were nontoxic to PC12 cells at any of the concentrations tested.

2.4. Neuroprotective effect of synthetic compounds against Aβ-induced cell cytotoxicity

The MTT assay was performed to evaluate the effect of novel synthetic compounds on Aβ-induced PC12 cell toxicity. The cells treated with Aβ exhibited significantly reduced cell viability as compared to control cells (decreased cell viability by 48%). Pretreatment of cells with the synthetic compounds protected against Aβ-induced cell death up to 87%, at a concentration of 100 μM. Six compounds (**1**, **3**, **4**, **13**, **14**, **19**) were the most protective against Aβ-induced PC12 cell toxicity (Fig. 1). As compared to the positive control selegiline, the protective effect of the synthetic compounds was significantly higher with compound (**14**) being the best. Amongst the tested compounds, all those possessing 2-nitro and 4-dimethylamine groups (**11–20**) had extremely high protective activities, while a diethoxymethyl group at position 4 of the rings (**1–10**) lead to significantly less protective activity. The presence of pyrolidine at position 4 of compounds (**21–30**) decreased the protective activity against Aβ-induced cytotoxicity. Compounds having a 4-piperidone (**3**, **13**) and those possessing N-methyl-4-piperidone (**4**, **14**) linker exhibited somewhat more protection as compared to all other compounds. These results suggest that a few of the novel α, β-unsaturated carbonyl based compounds may reduce cell damage caused by Aβ-induced cytotoxicity.

2.5. Acetylcholinesterase and butyrylcholinesterase inhibition activity

Evaluation of new compounds for their inhibitory effects on AChE and BChE was done by Ellman's method. The screening of novel α, β-unsaturated carbonyl based compounds against AChE and BChE demonstrated that nearly all these were moderate to strongly active against AChE (Table 1). The compounds were found to be less active on BChE but most inhibited AChE to various extents. The IC_{50} values of the compounds **8**, **9**, **15–18**, **21**, **22**, **25**, **26**, and **28–30** could not be calculated owing to their weak inhibition potency, which did not surpass 50% at the highest concentration (100 μM). In contrast, the compounds **3**, **4**, **12–14**, **23** and **24** exhibited IC_{50} values ranging from 0.042 to 9.52 μM for inhibition of AChE. In addition, the compounds **3**, **4**, **13** and **14** showed substantial AChE inhibitory activity below 1 μM, which is similar to

	R	R$_1$
1	4-Diethoxymethyl-benzene	CH$_2$
2	4-Diethoxymethyl-benzene	O
3	4-Diethoxymethyl-benzene	NH
4	4-Diethoxymethyl-benzene	NCH$_3$
5	4-Diethoxymethyl-benzene	NCH$_2$-benzene
11	Phenyl-2-nitro-4-dimethylamine	CH$_2$
12	Phenyl-2-nitro-4-dimethylamine	O
13	Phenyl-2-nitro-4-dimethylamine	NH
14	Phenyl-2-nitro-4-dimethylamine	NCH$_3$
15	Phenyl-2-nitro-4-dimethylamine	NCH$_2$-benzene
21	Phenyl-4-pyrrolidine	CH$_2$
22	Phenyl-4-pyrrolidine	O
23	Phenyl-4-pyrrolidine	NH
24	Phenyl-4-pyrrolidine	NCH$_3$
25	Phenyl-4-pyrrolidine	NCH$_2$-benzene

	R
6	4-Diethoxymethyl-benzene
16	Phenyl-2-nitro-4-dimethylamine
26	Phenyl-4-pyrrolidine
7	4-Diethoxymethyl-benzene
17	Phenyl-2-nitro-4-dimethylamine
27	Phenyl-4-pyrrolidine
8	4-Diethoxymethyl-benzene
18	Phenyl-2-nitro-4-dimethylamine
28	Phenyl-4-pyrrolidine
9	4-Diethoxymethyl-benzene
19	Phenyl-2-nitro-4-dimethylamine
29	Phenyl-4-pyrrolidine
10	4-Diethoxymethyl-benzene
20	Phenyl-2-nitro-4-dimethylamine
30	Phenyl-4-pyrrolidine

Scheme 1. Structures and synthesis scheme of α, β-unsaturated carbonyl based compounds. Reagents and conditions: (i) NaOH, EtOH, Room temperature.

that of donepezil (0.062 μM). The compounds **4** and **14**, having *N*-methyl-4-piperidone linker, had a better inhibitory potency than the reference drug donepezil. For the inhibition of BuChE, compounds **3**, **7** and **12** displayed IC$_{50}$ below 20 μM, but none was found more active than donepezil (6.92 μM).

These findings encouraged us to explore the relationship between AChE inhibitory activity and the chemical structures of the compounds. Ten varying types of ketones were used as linkers, but only three types of linkers present in compounds (**3**, **4**, **12**, **13**, **14**, **23**, and **24**) were found to be the most effective. The presence of tetrahydropyran-4-one linker displayed good inhibition but only in the presence of 2-nitro and 4-dimethylamine substitution patterns (compound **12**). Table 1 shows that the compounds (**4**, **14**, and **24**) having *N*-methyl-4-piperidone linker were strong inhibitors of AChE. Synthetic α, β-unsaturated carbonyl based compounds possessing the 4-piperidone moiety (**3**, **13**, and **23**) were also good inhibitors but relatively weaker than those with 4-piperidone linker. In an earlier study, Yalda et al. reported the synthesis of piperidone-grafted novel mono- and bisspiro heterocyclic hybrids containing functionalized piperidine, pyrrolizine and oxindole rings. The cholinesterase inhibitory activity of those cycloadducts revealed that monospiripyrrolizines were more active with IC$_{50}$ in

the range of 3.36–20.07 μM than dipolarophiles or bisspiropyrrolizines [26]. The current investigation shows that the increased activity is the result of specific linkers, whereas substitution patterns on the linked aromatic rings participated to lesser extent. The comparison amongst the three active compounds with same linker (**4**, **14**, **24**) revealed that compound **4** with diethoxymethyl group at position 4 of the aromatic rings showed more activity than compound **14** possessing a 2-nitro and 4-dimethylamine substitution pattern. The introduction of pyrrolidine at position 4 of compound **24** reduced the inhibition of AChE. A similar like activity relationship was also observed amongst compounds (**3**, **13** and **23**), having 4-piperidone groups on the aromatic rings. The activities of these compounds showed that the linkers derived from ketones during synthesis play key roles in terms of inhibitory activity. Compounds (**1**–**10**) have similar substitution pattern, but only two compounds (**3**, **4**) with 4-piperidone and *N*-methyl-4-piperidone moieties are potent inhibitors. Similar results were seen amongst other two series of synthetic compounds (**11**–**20** and **21**–**30**). Contreras et al. reported the synthesis of novel compounds by using 1-benzyl-4-piperidone and a conventional structure–activity relationship examination proposed that the presence of a central pyridazine ring is vital for high AChE

Table 1
Antioxidant activity and inhibitory effects of synthetic α, β-unsaturated carbonyl based compounds against AChE and BChE.

Compounds	IC$_{50}$ AChE (μM)	IC$_{50}$ BuChE (μM)	Selectivity for AChE[a]	IC$_{50}$ DPPH (μM)
1	12.43 ± 1.22	43.66 ± 1.93	3.51	20.12 ± 1.20
2	41.22 ± 2.20	38.53 ± 1.64	0.93	29.30 ± 1.83
3	0.92 ± 0.73	12.34 ± 0.67	13.41	19.29 ± 3.20
4	0.042 ± 0.01	>100	−	20.40 ± 1.93
5	27.54 ± 2.21	65.27 ± 0.52	2.37	28.22 ± 0.96
6	55.34 ± 1.76	88.93 ± 2.37	1.61	>50
7	76.64 ± 3.21	14.66 ± 0.68	0.19	>50
8	>100	>100	−	37.22 ± 2.54
9	>100	>100	−	39.45 ± 5.44
10	76.93 ± 1.89	>100	−	>50
11	45.29 ± 2.71	>100	−	32.46 ± 2.16
12	1.54 ± 0.02	19.74 ± 1.22	12.82	29.22 ± 1.34
13	0.88 ± 0.04	22.65 ± 1.28	25.74	25.67 ± 0.45
14	0.057 ± 0.05	>100	−	18.39 ± 1.75
15	>100	>100	−	>50
16	>100	>100	−	>50
17	>100	>100	−	47.77 ± 4.27
18	>100	>100	−	>50
19	79.31 ± 2.84	>100	−	22.99 ± 2.14
20	39.44 ± 1.73	>100	−	49.10 ± 1.76
21	>100	>100	−	31.29 ± 2.43
22	>100	>100	−	>50
23	9.52 ± 0.45	>100	−	26.94 ± 0.85
24	2.78 ± 0.55	66.75 ± 5.76	24.01	43.28 ± 1.48
25	>100	56.92 ± 2.87	−	>50
26	>100	>100	−	>50
27	66.43 ± 2.91	>100	−	>50
28	>100	>100	−	>50
29	>100	>100	−	29.22 ± 1.67
30	>100	>100	−	27.87 ± 2.51
Donepezil	0.062 ± 0.08	6.92 ± 0.21	111.61	−
Ascorbic acid	−	−	−	19.36 ± 1.55

[a] AChE selectivity index defined as IC$_{50}$ BChE/IC$_{50}$ AChE affinity ratio.

inhibition [27]. The data in our current investigation support the significance of the piperidone moiety for the inhibition of AChE.

2.6. Docking and QSAR analyses

Molecular docking analysis was performed to obtain better insight into mechanism of action of the AChE inhibitors. The active site of AChE is located at the base of ~20 A° deep and narrow gorge, from the surface of the enzyme and is composed by two subsites [28,29]: (1) catalytic esteratic site (CES) and (2) peripheral anionic site (PAS). The active site consists of Gln71-Tyr-Val-Asp-Thr-Leu76, Gly82-Thr-Glu84, Trp86-Asn-Pro88, Tyr121, Leu130, Tyr133, Glu199, Ser200, Glu202-Ser-Ala204, Trp279, Trp286, Phe295, Phe297, Glu327, Phe330, Tyr334, Tyr337-Phe338, Tyr341, Trp439, His447-Gly-Tyr449, and Ile451. The mechanism of acetylcholine (ACh) hydrolysis involves trapping of ACh to PAS, followed by the transfer of ACh to the active site.

From Figs. 2 and 3, it is clear that the most active AChE inhibitor (compound **4**) interacts with the receptor mainly due to hydrophobic and mild polar interactions. The close proximity of compound **4** with Tyr334 and Trp279 is due to mild polar interactions, indicating that it binds reversibly with the receptor (see Fig. 3).

QSAR analysis: For QSAR analysis, a myriad number of descriptors were calculated followed by elimination of redundant descriptors using QSARINS. Then, GA–MLR (Genetic Algorithm–Multilinear Regression) was performed to develop robust QSAR model. The best two parametric QSAR model along with its statistical parameters is as following:

pIC$_{50}$ = 126.3811 (±28.0863) −7.2606 (±2.3866) RDF090m −4.8896 (±2.0119) F01[C−N].

N_{tr} = 14, N_{ex} = 3, R^2 = 0.8558, R^2_{adj} = 0.8296, CCC$_{tr}$ = 0.9223, F = 32.6359, Q^2_{LOO} = 0.7924, CCC$_{cv}$ = 0.8897, R^2_{ex} = 0.7718, CCC$_{ex}$ = 0.8578.

The symbols have the usual meaning [30–33]. The high value of R^2, R^2_{adj}, CCC$_{tr}$, F, Q^2_{LOO}, CCC$_{cv}$ and R^2_{ex} indicates that the QSAR model is not only robust but also possesses good predictive ability (see Fig. 4) [30–35]. Since the model is based on a data set of seventeen molecules only, further improvements in the external predictive ability are also possible. From the QSAR model, it is clear that activity has correlation with RDF090m (Radial Distribution Function − 9.0/weighted by atomic masses, RDF descriptors) and F01[C−N] (frequency of C−N at topological distance of 01, a 2D frequency fingerprints descriptor). It is quite clear that the docking and the QSAR analyses not only support each other but are complementary to each other also.

3. Conclusion

In the work described above, we report the synthesis, pharmacological evaluation and molecular modeling of thirty novel α, β-unsaturated carbonyl based compounds. From docking and QSAR analyses, it can be stated that lipophilicity steers the AChE activity which is additionally supported by the hydrophobic interactions between the ligand and the receptor. We propose that the free radical scavenging activity of these novel compounds is responsible for their neuroprotective effects as it was seen that all strong antioxidant compounds possess more protective effect against Aβ-induced PC12 cell death. The most potent AChE inhibitors in this series correspond to N-methyl-4-piperidone and 4-piperidone moieties. The type of the substituent at the aromatic rings in compounds does not appear to have a strong influence on the inhibitory activity. Overall, the substitution of benzene rings by diethoxymethyl group at position 4 and presence of piperidone moiety imparts strong acetylcholinesterase inhibition. The multiple activities of these compounds suggest that they may be useful for the treatment of neurodegenerative diseases such as AD that involve a loss of cholinergic neurons.

4. Experimental

4.1. Materials

All chemicals and reagents were purchased from Sigma−Aldrich, Merck and Acros Organics (above 98% purity) and were used without additional purification. MTT [3-(4,5-dimethylthiazol-2-yl)-2,5-diphenyltetrazolium bromide] was procured from Sigma−Aldrich (St. Louis, MO, USA). AChE, (E.C.3.1.1.7 from Electric Eel, 500 units), BChE, (E.C. 3.1.1.8, from horse serum, 1000 units) and donepezil hydrochloride were also purchased from Sigma−Aldrich. Aβ$_{1−42}$ was purchased from Bachem (Bubendorf, Switzerland). Potassium dihydrogen phosphate, 5,5′-dithiobis-(2-nitrobenzoic acid) (DTNB), potassium hydroxide, sodium hydrogen carbonate, gelatine, acetylthiocholine iodide (ATC) and butrylthiocholine iodide (BTC) were supplied by Fluka (Buchs, Switzerland). Spectrophotometric analyses were performed using a Shimadzu UV-1700, UV−Vis spectrophotometer. Phosphate buffer (100 mM, pH 8.0) at 25 °C was used to measure cholinesterase activity of the compounds, using ATC and BTC (75 mM) as substrates. In both cases, DTNB (10 mM) was used to observe absorbance changes at 412 nm. Donepezil hydrochloride was used as a positive control [36].

4.2. General procedures

^{1}H and ^{13}C NMR spectra were recorded on a JEOL ECP spectrometer operating at 500 MHz, with Me4Si as internal standard
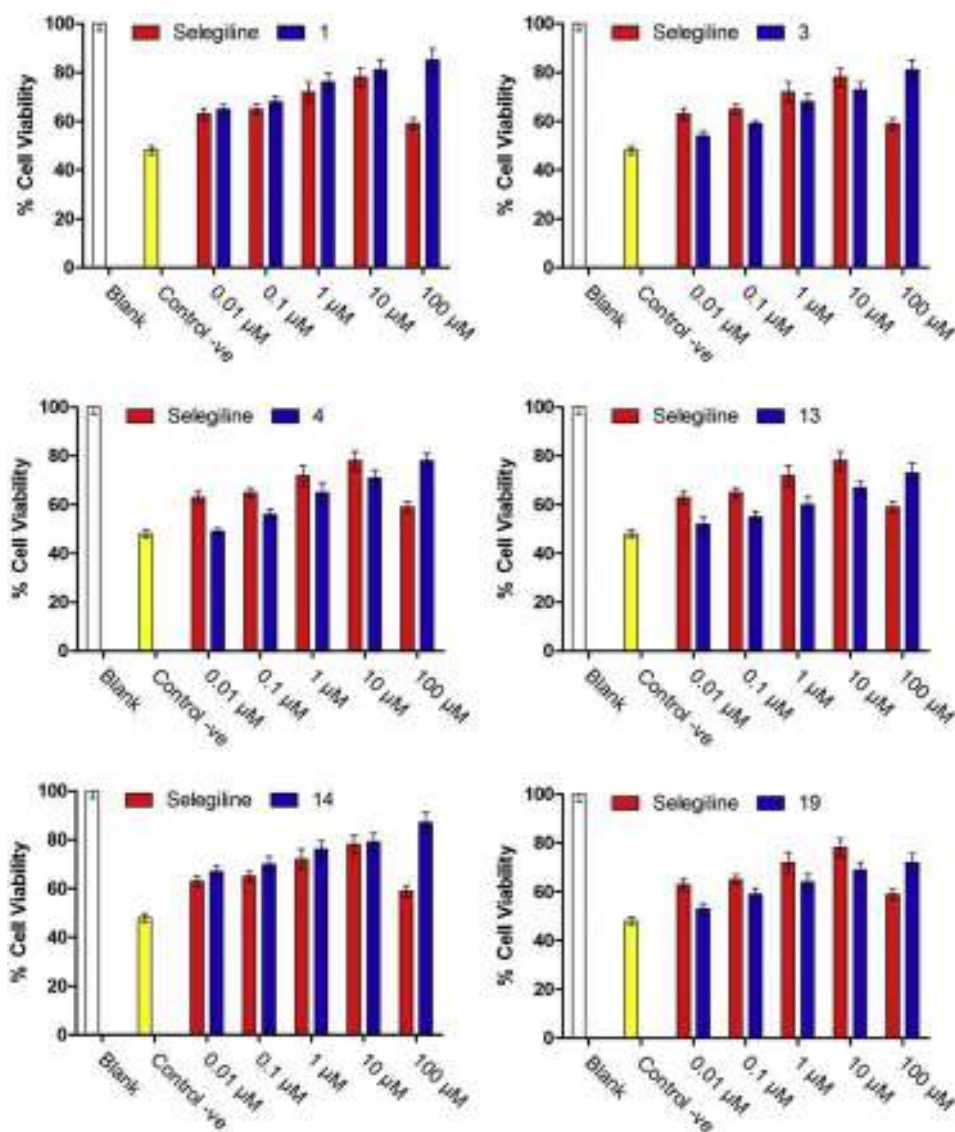
Fig. 1. Protective effects of the most active synthetic compounds against $A\beta_{1-42}$-induced cell damage. Cell viability of compounds was evaluated using the MTT assay. All groups were treated with 25 μM $A\beta_{1-42}$ except for the control group. Selegiline was used as a positive control at the same concentrations. Synthetic compounds and selegiline were pre-incubated at various concentrations (0.01–100 μM) in serum-free media for 24 h before the addition of Aβ peptide. Cell viability is expressed as the mean percentage of viable cells compared with the untreated cells. The data are the mean ± SE ($n = 5$).

and $CDCl_3$ or DMSO-d^6 as the solvent. Electrospray ionization mass spectrometry (ESI-MS) on MicroTOF-Q mass spectrometer (Bruker) was used to obtain high resolution mass spectra (HRMS). Micro-analyses data was obtained using Fison EA 1108 elemental analyzer. Infrared spectra using KBr disc were recorded on a Perkin Elmer 400 (FTIR) spectrometer. Flash column chromatography was carried out with silica gel 60 (230–400 mesh) (Merck) and thin layer chromatography (TLC) was performed on pre-coated silica plates (Kiesel gel 60 F_{254}, BDH). Melting points were determined using an electrothermal instrument and are uncorrected. The compounds were visualized by illumination under ultraviolet (UV) light (254 nm) or by vanillin stain followed by charring on a hotplate.

4.3. Synthesis of α, β-unsaturated carbonyl based compounds

Twenty one α, β-unsaturated carbonyl based compounds (**1**–**7**; **11**–**17**; **21**–**27**) were synthesized by direct coupling of the appropriate aromatic aldehyde with the ten different types of ketones at a molar ratio of 1:2, and the compounds (**8**–**10**; **18**–**20**; **28**–**30**)

were synthesized at a molar ratio of 1:1 under base catalyzed Claisen–Schmidt condensation reaction conditions. Scheme 1 demonstrates the general synthesis of α, β-unsaturated carbonyl based compounds d. Concisely, the appropriate aromatic aldehyde (20 mmol, 2 equivalent) and the suitable ketone (10 mmol, 1 equivalent) were mixed and dissolved in 15 ml of ethanol in single necked round bottomed flask, and stirred at 5 °C for a couple of minutes. Afterwards, a 40% NaOH solution in ethanol was then added drop wise for several minutes. The mixture was left stirring at room temperature (27 °C) for 1–24 h. The precipitate formation and color changes of the reaction mixture served as an indication of product formation. The reaction was monitored by TLC and upon completion; the reaction was quenched by the addition of acidified ice to the mixture. The α, β-unsaturated carbonyl based compounds were isolated by column chromatography or by recrystallization.

4.3.1. 2,6-Bis[4-(diethoxymethyl)benzylidene]cyclohexanone (*1*)

Yellow crystals (2.59 g, 54%). mp: 112–114 °C; ^{1}H NMR (500 MHz, $CDCl_3$) δ: 7.89 (s, 2H), 7.29 (d, $J = 8$ Hz, 4H), 6.82 (d,
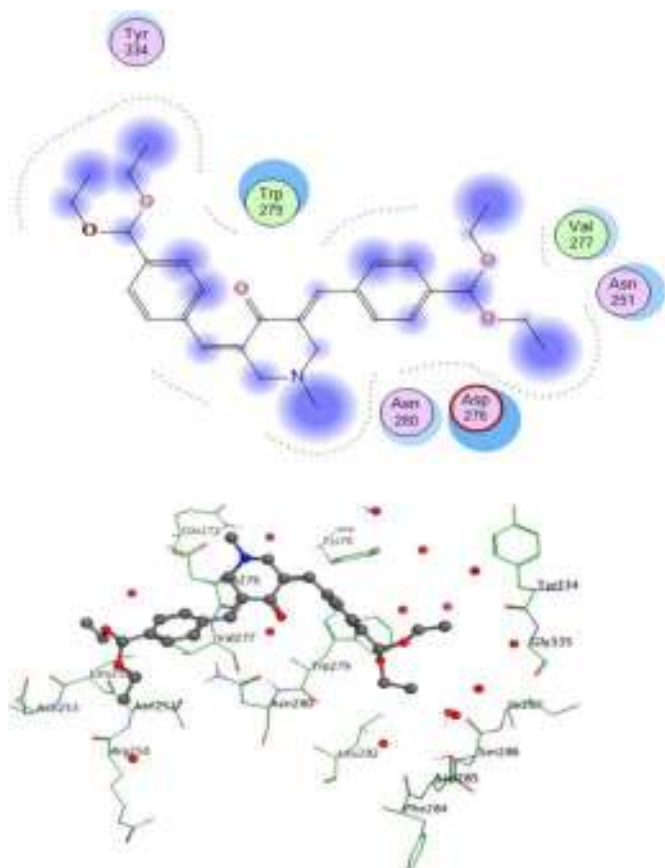
Fig. 2. Docking pose for most active molecule **4** in the active site of AChE.

J = 8 Hz, 4H), 5.89 (s, 2H), 3.42 (q, J = 7.5, 8H), 2.32 (t, J = 12.0 Hz, 4H), 1.82 (m, 2H), 1.24 (t, J = 7.5, 12H); ^{13}C NMR (500 MHz, CDCl$_3$) δ: 186.4, 152.9, 144.4, 136.5, 132.5, 127.3, 126.5, 101.1, 55.0, 28.3, 27.8, 16.2; HRMS (ESI) *m/z*: 479.68 [M+H]$^+$, Microanalysis calculated for C$_{30}$H$_{38}$O$_5$ (478.62), C: 75.28%, H: 8.00%. Found C: 75.42%, H: 8.12%.

4.3.2. 3,5-Bis-(4-diethoxymethyl-benzylidene)-tetrahydro-pyran-4-one (2)

Pale yellow crystals (3.06 g, 64%). mp: 106–108 °C; ^{1}H NMR (500 MHz, CDCl$_3$) δ: 7.85 (s, 2H), 7.32 (d, J = 8 Hz, 4H), 6.95 (d, J = 8 Hz, 4H), 5.52 (s, 2H), 3.62 (q, J = 7.5, 8H), 2.69 (s, 4H), 1.18 (t, J = 8, 12H); ^{13}C NMR (500 MHz, CDCl$_3$) δ: 187.2, 152.7, 143.8, 136.7, 131.9, 126.2, 125.2, 101.5, 62.4, 55.2, 16.1; HRMS (ESI) *m/z*: 481.65 [M+H]$^+$, Microanalysis calculated for C$_{29}$H$_{36}$O$_6$ (480.59), C: 72.48%, H: 7.55%. Found C: 72.62%, H: 7.72%.

4.3.3. 3,5-Bis[4-(diethoxymethyl)benzylidene]piperidin-4-one (3)

Yellow solid (2.89 g, 60%). mp: 101–102 °C; ^{1}H NMR (500 MHz, CDCl$_3$) δ: 7.68 (s, 2H), 7.12 (d, J = 7.5 Hz, 4H), 6.93 (d, J = 7.5 Hz, 4H), 5.65 (s, 2H), 3.36 (q, J = 7.5, 8H), 2.65 (s, 4H), 1.27 (t, J = 7.0, 12H); ^{13}C NMR (500 MHz, CDCl$_3$) δ: 185.2, 145.1, 144.5, 138.5, 136.2, 128.1, 127.8, 102.1, 55.1, 48.7, 16.4; HRMS (ESI) *m/z*: 480.71 [M+H]$^+$, Microanalysis calculated for C$_{29}$H$_{37}$NO$_5$ (479.61), C: 72.62%, H: 7.78%, N: 2.92%. Found C: 72.71%, H: 7.86%, N: 3.10%.

4.3.4. 3,5-Bis[4-(diethoxymethyl)benzylidene]-1-methyl-piperidin-4-one (4)

Light yellow solid (2.12 g, 43%). mp: 142–144 °C; ^{1}H NMR (500 MHz, CDCl$_3$) δ: 7.63 (s, 2H), 7.32 (d, J = 8 Hz, 4H), 7.15 (d, J = 8 Hz, 4H), 5.59 (s, 2H), 3.29 (q, J = 7.5, 8H), 2.71 (s, 4H), 2.12 (s, 3H), 1.20 (t, J = 7.0, 12H); ^{13}C NMR (500 MHz, CDCl$_3$) δ: 189.7, 148.2,
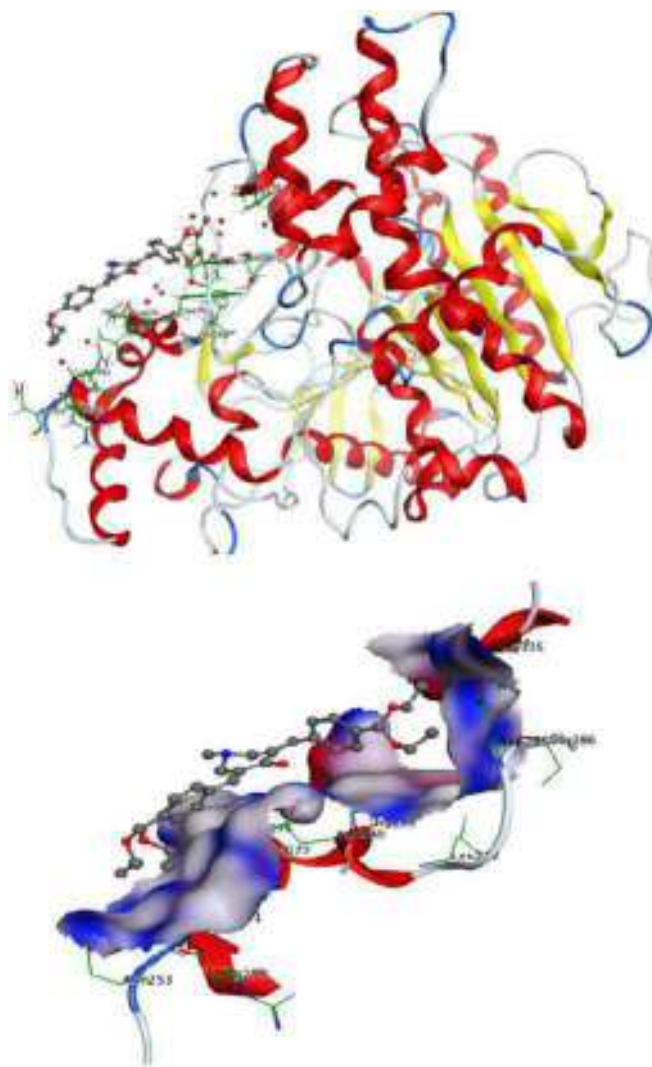
Fig. 3. Docking pose for most active molecule **4** with surface area of active site of AChE (Blue: H-Bonding, White: Hydrophobic and Red: Mild Polar regions). (For interpretation of the references to colour in this figure legend, the reader is referred to the web version of this article.)

147.5, 139.8, 135.1, 128.4, 127.1, 101.4, 56.6, 51.2, 40.1, 16.7; HRMS (ESI) *m/z*: 494.65 [M+H]$^+$, Microanalysis calculated for C$_{30}$H$_{39}$NO$_5$ (493.63), C: 72.99%, H: 7.96%, N: 2.84%. Found C: 72.95%, H: 7.99%, N: 2.87%.

4.3.5. 1-Benzyl-3,5-bis[4-(diethoxymethyl)benzylidene]piperidin-4-one (5)

Brown semisolid (2.76 g, 48%). mp: 112–114 °C; ^{1}H NMR (500 MHz, CDCl$_3$) δ: 7.89 (d, J = 8 Hz, 2H), 7.65 (s, 2H), 7.52 (d, J = 8 Hz, 2H), 7.22 (d, J = 7 Hz, 4H), 7.12 (d, J = 7 Hz, 4H), 6.69 (t, J = 6.5 Hz, H), 5.17 (s, 2H), 4.17 (s, 2H), 3.38 (q, J = 7.5, 8H), 2.95 (s, 4H), 1.14 (t, J = 7.0, 12H); ^{13}C NMR (500 MHz, CDCl$_3$) δ: 191.5, 148.2, 147.9, 139.5, 139.1, 132.5, 128.4, 127.6, 127.0, 125.2, 124.9, 101.8, 64.3, 56.2, 50.92, 17.1; HRMS (ESI) *m/z*: 570.84 [M+H]$^+$, Microanalysis calculated for C$_{36}$H$_{43}$NO$_5$ (569.73), C: 75.89%, H: 7.61%, N: 2.46%. Found C: 75.92%, H: 7.64%, N: 2.44%.

4.3.6. 1,5-Bis-(4-diethoxymethyl-phenyl)-penta-1,4-dien-3-one (6)

Pale brownish solid (1.96 g, 45%). mp: 98–100 °C; ^{1}H NMR (500 MHz, CDCl$_3$) δ: 7.82 (d, J = 6.5 Hz, 4H), 7.71 (d, J = 8 Hz, 2H), 7.49 (d, J = 6.5 Hz, 2H), 7.16 (d, J = 7 Hz, 4H), 5.25 (s, 2H), 3.52 (q, J = 7 Hz, 8H), 1.17 (t, J = 7.0, 12H); ^{13}C NMR (500 MHz, CDCl$_3$) δ:
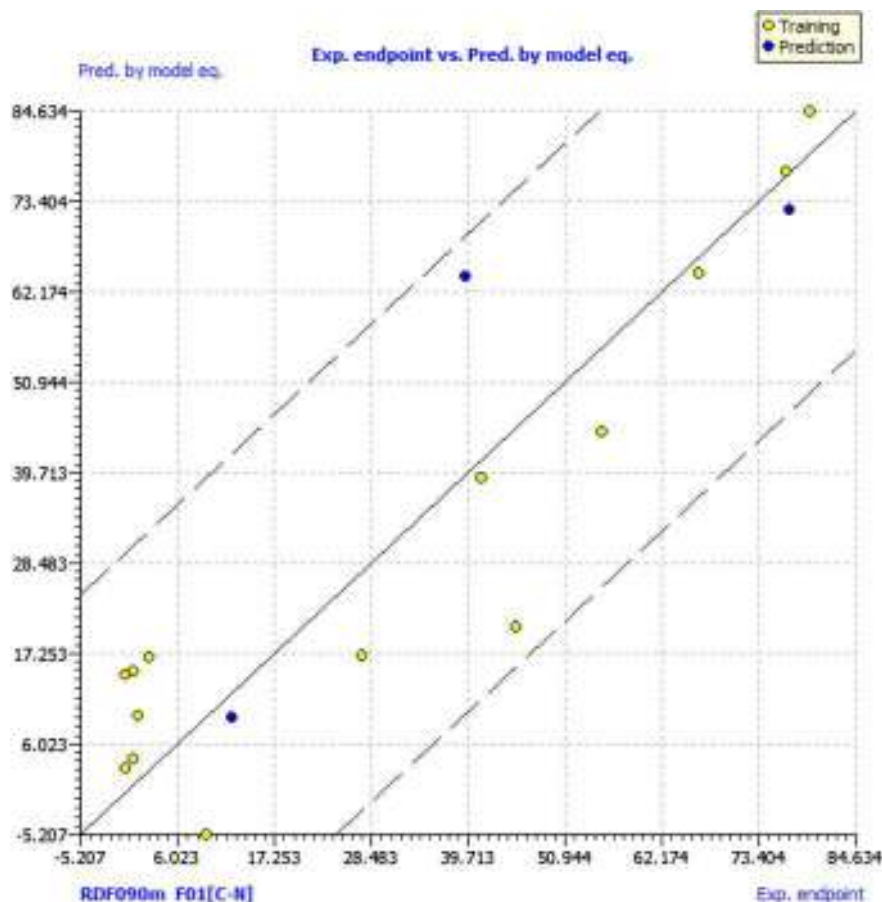
Fig. 4. Correlation between experimental and predicted pIC$_{50}$.

190.5, 152.2, 148.6, 139.7, 136.4, 135.2, 132.8, 102.2, 55.5, 16.9; HRMS (ESI) m/z: 439.62 [M+H]$^+$, Microanalysis calculated for C$_{27}$H$_{34}$O$_5$ (438.56), C: 73.94%, H: 7.81%. Found C: 74.12%, H: 7.89%.

4.3.7. 2,5-Bis-(4-diethoxymethyl-benzylidene)-cyclopentanone (7)
Light yellow crystals (3.12 g, 67%). mp: 88–89 °C; ^{1}H NMR (500 MHz, CDCl$_3$) δ: 7.69 (d, J = 6.5 Hz, 4H), 7.42 (s, 2H), 7.21 (d, J = 6.5 Hz, 4H), 5.45 (s, 2H), 3.62 (q, J = 7 Hz, 8H), 2.38 (t, J = 7 Hz, 4H), 1.22 (t, J = 7.0, 12H); ^{13}C NMR (500 MHz, CDCl$_3$) δ: 189.7, 149.4, 145.5, 138.7, 136.4, 133.9, 129.1, 100.9, 56.2, 32.5, 16.1; HRMS (ESI) m/z: 465.72 [M+H]$^+$, Microanalysis calculated for C$_{29}$H$_{36}$O$_5$ (464.59), C: 74.97%, H: 7.81%. Found C: 75.18%, H: 7.87%.

4.3.8. 2-(4-Diethoxymethyl-benzylidene)-indan-1-one (8)
White powder (2.52 g, 78%). mp: 152–154 °C; ^{1}H NMR (500 MHz, CDCl$_3$) δ: 7.80 (d, J = 8 Hz, 2H), 7.69 (s, H), 7.48 (d, J = 8 Hz, 2H), 7.25 (d, J = 7.5 Hz, H), 7.20 (d, J = 7.5 Hz, H), 7.05 (t, J = 7.5 Hz, H), 6.94 (t, J = 7 Hz, H), 5.34 (s, H), 3.49 (q, J = 7 Hz, 4H), 2.75 (s, 2H), 1.29 (t, J = 6 Hz, 6H); ^{13}C NMR (500 MHz, CDCl$_3$) δ: 193.2, 144.5, 142.2, 140.1, 139.2, 138.8, 136.5, 130.4, 129.6, 128.1, 125.6, 125.1, 124.2, 102.2, 56.3, 29.9, 16.4; HRMS (ESI) m/z: 323.67 [M+H]$^+$, Microanalysis calculated for C$_{21}$H$_{22}$O$_3$ (322.40), C: 78.23%, H: 6.88%. Found C: 78.44%, H: 6.92%.

4.3.9. 2-(4-Diethoxymethyl-benzylidene)-3,4-dihydro-2H-naphthalen-1-one (9)
Light yellow solid (2.67 g, 80%). mp: 94–95 °C; ^{1}H NMR (500 MHz, CDCl$_3$) δ: 7.84 (d, J = 8 Hz, 2H), 7.59 (s, H), 7.47 (d, J = 8.5 Hz, 2H), 7.29 (d, J = 7.5 Hz, H), 7.22 (d, J = 7.5 Hz, H), 7.12 (t, J = 7.5 Hz, H), 7.02 (t, J = 7 Hz, H), 5.49 (s, H), 3.35 (q, J = 7 Hz, 4H), 2.29 (t, J = 7 Hz, 2H), 2.05 (t, J = 7 Hz, 2H), 1.17 (t, J = 6 Hz, 6H); ^{13}C NMR (500 MHz, CDCl$_3$) δ: 188.3, 152.2, 150.1, 148.5, 146.2, 143.9, 137.5, 134.4, 129.2, 127.2, 126.2, 124.8, 117.2, 101.7, 56.2, 29.5, 28.2, 16.0; HRMS (ESI) m/z: 337.51 [M+H]$^+$, Microanalysis calculated for C$_{22}$H$_{24}$O$_3$ (336.42), C: 78.54%, H: 7.19%. Found C: 78.33%, H: 7.12%.

4.3.10. 2-[3-(4-Diethoxymethyl-phenyl)-acryloyl]-3,4-dihydro-2H-naphthalen-1-one (10)
Yellow solid (3.16 g, 83%). mp: 121–122 °C; ^{1}H NMR (500 MHz, CDCl$_3$) δ: 7.75 (d, J = 6 Hz, H), 7.52 (d, J = 6 Hz, H), 7.42 (d, J = 8 Hz, 2H), 7.39 (d, J = 8 Hz, 2H), 7.32 (d, J = 7 Hz, H), 7.29 (d, J = 7 Hz, H), 7.17 (t, J = 7 Hz, H), 6.89 (t, J = 7 Hz, H), 5.29 (s, H), 3.47 (q, J = 7 Hz, 4H), 3.29 (t, J = 8.5 Hz, H), 2.12 (t, J = 8 Hz, 2H), 1.95 (t, J = 7 Hz, 2H), 1.24 (t, J = 6.5 Hz, 6H); ^{13}C NMR (500 MHz, CDCl$_3$) δ: 194.6, 151.1, 148.9, 144.6, 142.3, 139.2, 138.4, 136.2, 135.5, 132.4, 130.6, 129.1, 125.2, 124.2, 103.1, 66.1, 55.7, 30.2, 28.6, 16.7; HRMS (ESI) m/z: 379.52 [M+H]$^+$, Microanalysis calculated for C$_{24}$H$_{26}$O$_4$ (378.46), C: 76.17%, H: 6.92%. Found C: 76.21%, H: 6.91%.

4.3.11. 2,6-Bis-(4-dimethylamino-2-nitro-benzylidene)-cyclohexanone (11)
White powder (2.78 g, 62%). mp: 139–140 °C; δ: 7.94 (s, 2H), 7.55 (d, J = 8 Hz, 2H), 7.41 (d, J = 8 Hz, 2H), 7.13 (s, 2H), 3.15 (s, 12H), 2.35 (t, J = 12.0 Hz, 4H), 1.87 (m, 2H); ^{13}C NMR (500 MHz, CDCl$_3$) δ: 190.7, 149.5, 145.7, 145.6, 140.1, 128.2, 118.6, 117.6, 106.5, 46.8, 29.1, 27.5; HRMS (ESI) m/z: 451.64 [M+H]$^+$, Microanalysis calculated for C$_{24}$H$_{26}$N$_4$O$_5$ (450.49), C: 63.99%, H: 5.82%, N: 12.44%. Found C: 64.12%, H: 5.72%, N: 12.42%.

4.3.12. 3,5-Bis[4-(dimethylamino)2-nitro-benzylidene]tetrahydro-pyran-4-one (12)

White powder (2.92 g, 65%). mp: 188–190 °C; ^{1}H NMR (500 MHz, CDCl$_3$) δ: 7.89 (s, 2H), 7.46 (d, J = 8 Hz, 2H), 7.14 (d, J = 8 Hz, 2H), 7.05 (s, 2H), 3.13 (s, 12H), 2.93 (s, 4H); ^{13}C NMR (500 MHz, CDCl$_3$) δ: 190.5, 149.2, 146.9, 145.1, 139.9, 128.4, 118.9, 118.1, 107.8, 65.5, 46.2; HRMS (ESI) m/z: 475.52 [M+Na]$^+$, Micro-analysis calculated for C$_{23}$H$_{24}$N$_4$O$_6$ (452.46), C: 61.05%, H: 5.35%, N: 12.38%. Found C: 61.24%, H: 5.59%, N: 12.42%.

4.3.13. 3,5-Bis[4-(dimethylamino)2-nitro-benzylidene]piperidin-4-one (13)

Light yellow solid (2.28 g, 51%). mp: 192–194 °C; ^{1}H NMR (500 MHz, CDCl$_3$) δ: 7.82 (s, 2H), 7.72 (d, J = 8 Hz, 2H), 7.21 (d, J = 8 Hz, 2H), 6.92 (s, 2H), 3.17 (s, 12H), 3.13 (s, 4H); ^{13}C NMR (500 MHz, CDCl$_3$) δ: 189.4, 149.7, 148.6, 142.5, 140.7, 127.3, 118.8, 118.1, 106.5, 49.4, 46.9; HRMS (ESI) m/z: 452.52 [M+H]$^+$, Micro-analysis calculated for C$_{23}$H$_{25}$N$_5$O$_5$ (451.48), C: 61.19%, H: 5.58%, N: 15.51%. Found C: 61.42%, H: 5.62%, N: 15.89%.

4.3.14. 3,5-Bis[4-(dimethylamino)2-nitro-benzylidene]-1-methyl-piperidin-4-one (14)

White powder (2.56 g, 55%). mp: 181–182 °C; ^{1}H NMR (500 MHz, CDCl$_3$) δ: 7.76 (s, 2H), 7.45 (d, J = 8 Hz, 2H), 7.23 (d, J = 8 Hz, 2H), 7.13 (s, 2H), 3.21 (s, 12H), 3.03 (s, 4H), 2.19 (s, 3H); ^{13}C NMR (500 MHz, CDCl$_3$) δ: 187.5, 148.9, 148.2, 143.2, 141.8, 126.7, 119.6, 118.9, 106.2, 44.5, 46.1, 38.8; HRMS (ESI) m/z: 466.72 [M+H]$^+$, Microanalysis calculated for C$_{24}$H$_{27}$N$_5$O$_5$ (465.50), C: 61.92%, H: 5.85%, N: 15.04%. Found C: 61.99%, H: 5.91%, N: 15.19%.

4.3.15. 1-Benzyl-3,5-bis-(4-dimethylamino-2-nitro-benzylidene)-piperidin-4-one (15)

White crystals (3.22 g, 60%). mp: 165–166 °C; ^{1}H NMR (500 MHz, CDCl$_3$) δ: 7.82 (d, J = 8 Hz, 2H), 7.72 (s, 2H), 7.59 (d, J = 8 Hz, 2H), 7.32 (d, J = 7 Hz, 2H), 7.25 (t, J = 7 Hz, 2H), 7.02 (s, 2H), 6.92 (t, J = 6.5 Hz, H), 4.22 (s, 2H), 3.19 (s, 12H), 2.72 (s, 4H); ^{13}C NMR (500 MHz, CDCl$_3$) δ: 189.6, 148.9, 147.2, 139.5, 139.0, 131.9, 128.6, 126.5, 126.0, 125.3, 124.5, 119.2, 104.9, 64.8, 53.8, 45.9; HRMS (ESI) m/z: 542.65 [M+H]$^+$, Microanalysis calculated for C$_{30}$H$_{31}$N$_5$O$_5$ (541.60), C: 66.53%, H: 5.77%, N: 12.93%. Found C: 66.48%, H: 5.79%, N: 12.54%.

4.3.16. 1,5-Bis-(4-dimethylamino-2-nitro-phenyl)-penta-1,4-dien-3-one (16)

Pale yellow solid (2.97 g, 68%). mp: 177–179 °C; ^{1}H NMR (500 MHz, CDCl$_3$) δ: 7.70 (d, J = 6 Hz, 2H), 7.68 (d, J = 8 Hz, 2H), 7.44 (d, J = 6 Hz, 2H), 7.25 (d, J = 8 Hz, 2H), 7.12 (s, 2H), 3.15 (s, 12H); ^{13}C NMR (500 MHz, CDCl$_3$) δ: 187.5, 150.9, 148.6, 144.4, 132.8, 128.1, 117.5, 113.8, 107.9, 46.7; HRMS (ESI) m/z: 409.45 [M−H]$^+$, Micro-analysis calculated for C$_{21}$H$_{22}$N$_4$O$_5$ (410.42), C: 61.45%, H: 5.40%, N: 13.65%. Found C: 61.48%, H: 5.62%, N: 13.77%.

4.3.17. 2,5-Bis-(4-dimethylamino-2-nitro-benzylidene)-cyclopentanone (17)

White powder (2.41 g, 55%). mp: 156–157 °C; ^{1}H NMR (500 MHz, CDCl$_3$) δ: 7.92 (d, J = 6.5 Hz, 2H), 7.88 (d, J = 6 Hz, 2H), 7.75 (d, J = 6.5 Hz, 2H), 7.44 (s, 2H), 3.10 (s, 12H), 2.45 (t, J = 7 Hz, 4H); ^{13}C NMR (500 MHz, CDCl$_3$) δ: 188.9, 153.2, 149.9, 144.2, 143.8, 125.8, 118.1, 116.4, 108.3, 46.9, 32.6; HRMS (ESI) m/z: 437.72 [M+H]$^+$, Microanalysis calculated for C$_{23}$H$_{24}$N$_4$O$_5$ (436.46), C: 63.29%, H: 5.54%, N: 12.84%. Found C: 63.42%, H: 5.48%, N: 12.72%.

4.3.18. 2-(4-Dimethylamino-2-nitro-benzylidene)-indan-1-one (18)

Yellow semisolid (1.95 g, 63%). mp: 169–171 °C; ^{1}H NMR (500 MHz, CDCl$_3$) δ: 7.56 (d, J = 8 Hz, H), 7.48 (s, H), 7.32 (d, J = 8 Hz, H), 7.12 (s, H), 6.98 (d, J = 7.5 Hz, H), 6.91 (d, J = 7.5 Hz, H), 6.74 (t, J = 7.5 Hz, H), 6.65 (t, J = 7 Hz, H), 3.22 (s, 6H), 2.81 (s, 2H); ^{13}C NMR (500 MHz, CDCl$_3$) δ: 192.8, 145.6, 142.6, 141.3, 139.8, 138.2, 137.4, 130.9, 128.7, 128.0, 125.9, 123.8, 119.5, 117.6, 108.6, 46.8, 28.3; HRMS (ESI) m/z: 309.55 [M+H]$^+$, Microanalysis calculated for C$_{18}$H$_{16}$N$_2$O$_3$ (308.33), C: 70.12%, H: 5.23%, N: 9.09%. Found C: 70.18%, H: 5.59%, N: 9.18%.

4.3.19. 2-(4-Dimethylamino-2-nitro-benzylidene)-3,4-dihydro-2H-naphthalen-1-one (19)

White powder (2.50 g, 78%). mp: 138–139 °C; ^{1}H NMR (500 MHz, CDCl$_3$) δ: 7.82 (d, J = 6.5 Hz, H), 7.57 (s, H), 7.42 (d, J = 6.5 Hz, H), 7.35 (s, H), 7.28 (d, J = 7 Hz, H), 7.20 (d, J = 7 Hz, H), 7.19 (t, J = 7.5 Hz, H), 6.92 (t, J = 8 Hz, H), 3.14 (s, 6H), 2.47 (t, J = 7 Hz, 2H), 2.14 (t, J = 7 Hz, 2H); ^{13}C NMR (500 MHz, CDCl$_3$) δ: 188.7, 152.8, 151.3, 148.9, 146.8, 144.2, 136.8, 134.6, 129.9, 127.6, 126.1, 125.3, 124.2, 107.8, 46.2, 29.9, 27.9; HRMS (ESI) m/z: 323.45 [M+H]$^+$, Microanalysis calculated for C$_{19}$H$_{18}$N$_2$O$_3$ (322.36), C: 70.79%, H: 5.63%, N: 8.69%. Found C: 71.12%, H: 5.52%, N: 8.72%.

4.3.20. 2-[3-(4-Dimethylamino-2-nitro-phenyl)-acryloyl]-3,4-dihydro-2H-naphthalen-1-one (20)

Pale yellow powder (2.93 g, 80%). mp: 102–103 °C; ^{1}H NMR (500 MHz, CDCl$_3$) δ: 7.79 (d, J = 6.5 Hz, H), 7.62 (d, J = 6.5 Hz, H), 7.45 (d, J = 7.5 Hz, H), 7.32 (s, H), 7.29 (d, J = 7.5 Hz, H), 7.21 (d, J = 7.5 Hz, H), 7.14 (d, J = 7.5 Hz, H), 7.02 (t, J = 7.5 Hz, H), 6.94 (t, J = 7.5 Hz, H), 3.45 (t, J = 8.5 Hz, H), 3.10 (s, 6H), 2.22 (t, J = 8 Hz, 2H), 2.15 (t, J = 8 Hz, 2H); ^{13}C NMR (500 MHz, CDCl$_3$) δ: 193.8, 152.2, 148.7, 145.2, 142.8, 139.6, 137.1, 136.8, 135.6, 131.9, 130.5, 129.4, 124.8, 123.5, 116.5, 106.2, 65.8, 46.8, 31.3, 28.7; HRMS (ESI) m/z: 365.55 [M+H]$^+$, Microanalysis calculated for C$_{21}$H$_{20}$N$_2$O$_4$ (364.39), C: 69.22%, H: 5.53%, N: 7.69%. Found C: 69.34%, H: 5.59%, N: 7.81%.

4.3.21. 2,6-Bis-(4-pyrrolidin-1-yl-benzylidene)-cyclohexanone (21)

Brownish powder (3.12 g, 76%). mp: 105–107 °C; ^{1}H NMR (500 MHz, CDCl$_3$) δ: 7.92 (s, 2H), 7.45 (d, J = 8 Hz, 4H), 6.99 (d, J = 8 Hz, 4H), 2.37 (t, J = 10.0 Hz, 4H), 2.10 (m, J = 6.5 Hz, 8H), 1.84 (m, J = 5.5, 2H); ^{13}C NMR (500 MHz, CDCl$_3$) δ: 188.9, 152.2, 145.2, 136.7, 131.9, 127.5, 126.9, 58.1, 28.8, 27.2, 25.6; HRMS (ESI) m/z: 413.62 [M+H]$^+$, Microanalysis calculated for C$_{28}$H$_{32}$N$_2$O (412.57), C: 81.51%, H: 7.82%, N: 6.79%. Found C: 81.67%, H: 7.99%, N: 6.95%.

4.3.22. 3,5-Bis-(4-pyrrolidin-1-yl-benzylidene)-tetrahydro-pyran-4-one (22)

Light brown solid (2.40 g, 58%). mp: 99–101 °C; ^{1}H NMR (500 MHz, CDCl$_3$) δ: 7.81 (s, 2H), 7.37 (d, J = 6.5 Hz, 4H), 7.17 (d, J = 6.5 Hz, 4H), 2.94 (s, 4H), 1.92 (m, J = 6.5 Hz, 8H); ^{13}C NMR (500 MHz, CDCl$_3$) δ: 189.0, 150.3, 144.7, 136.8, 130.1, 126.8, 125.6, 62.9, 57.1, 25.5; HRMS (ESI) m/z: 415.49 [M+H]$^+$, Microanalysis calculated for C$_{27}$H$_{30}$N$_2$O$_2$ (414.54), C: 78.23%, H: 7.29%, N: 6.76%. Found C: 78.45%, H: 7.52%, N: 6.72%.

4.3.23. 3,5-Bis-(4-pyrrolidin-1-yl-benzylidene)-piperidin-4-one (23)

Pale yellow powder (2.83 g, 69%). mp: 92–93 °C; ^{1}H NMR (500 MHz, CDCl$_3$) δ: 7.72 (s, 2H), 7.17 (d, J = 7.5 Hz, 4H), 6.81 (d, J = 7.5 Hz, 4H), 2.88 (s, 4H), 1.74 (m, J = 6 Hz, 8H); ^{13}C NMR (500 MHz, CDCl$_3$) δ: 185.7, 145.9, 143.4, 137.1, 136.5, 128.7, 119.9, 56.4, 48.2, 24.9; HRMS (ESI) m/z: 436.62 [M+Na]$^+$, Microanalysis calculated for C$_{27}$H$_{31}$N$_3$O (413.55), C: 78.42%, H: 7.56%, N: 10.16%. Found C: 78.44%, H: 7.60%, N: 10.25%.

4.3.24. 1-Methyl-3,5-bis[4-(pyrrolidinyl)benzylidene]piperidin-4-one (24)

Yellow powder (1.99 g, 47%). mp: 122–124 °C; ^{1}H NMR (500 MHz, CDCl$_3$) δ: 7.89 (d, $J = 8.5$ Hz, 4H), 7.65 (s, 2H), 7.52 (d, $J = 8.5$ Hz, 4H), 2.99 (s, 4H), 2.43 (s, 3H), 1.96 (m, $J = 6$ Hz, 8H); ^{13}C NMR (500 MHz, CDCl$_3$) δ: 190.1, 146.4, 144.7, 141.9, 131.8, 128.2, 109.6, 57.4, 56.5, 38.2, 25.5; HRMS (ESI) m/z: 428.71 [M+H]$^+$, Microanalysis calculated for C$_{28}$H$_{33}$N$_3$O (427.58), C: 78.65%, H: 7.78%, N: 9.83%. Found C: 78.82%, H: 7.95%, N: 10.12%.

4.3.25. 1-Benzyl-3,5-Bis-(4-pyrrolidin-1-yl-benzylidene)-piperidin-4-one (25)

Light yellow crystals (2.16 g, 43%). mp: 88–89 °C; ^{1}H NMR (500 MHz, CDCl$_3$) δ: 7.71 (d, $J = 8$ Hz, 2H), 7.45 (s, 2H), 7.31 (d, $J = 8$ Hz, 2H), 7.25 (d, $J = 7$ Hz, 4H), 7.19 (d, $J = 7$ Hz, 4H), 6.81 (t, $J = 6.5$ Hz, H), 4.19 (s, 2H), 2.92 (s, 4H), 1.78 (m, $J = 6$ Hz, 8H); ^{13}C NMR (500 MHz, CDCl$_3$) δ: 192.2, 148.8, 146.3, 138.2, 137.7, 132.7, 128.5, 126.2, 125.4, 124.9, 118.9, 65.1, 58.1, 50.2, 25.7; HRMS (ESI) m/z: 504.69 [M+H]$^+$, Microanalysis calculated for C$_{34}$H$_{37}$N$_3$O (503.68), C: 81.08%, H: 7.40%, N: 8.34%. Found C: 81.25%, H: 7.69%, N: 8.17%.

4.3.26. 1,5-Bis-(4-pyrrolidin-1-yl-phenyl)-penta-1,4-dien-3-one (26)

Light brownish solid (2.02 g, 54%). mp: 111–113 °C; ^{1}H NMR (500 MHz, CDCl$_3$) δ: 7.76 (d, $J = 6$ Hz, 4H), 7.52 (d, $J = 6$ Hz, 2H), 7.12 (d, $J = 8$ Hz, 2H), 7.05 (d, $J = 8$ Hz, 4H), 1.85 (m, $J = 6$ Hz, 8H); ^{13}C NMR (500 MHz, CDCl$_3$) δ: 190.0, 151.8, 148.2, 138.2, 136.5, 134.9, 131.2, 56.9, 26.6; HRMS (ESI) m/z: 373.82 [M+H]$^+$, Microanalysis calculated for C$_{25}$H$_{28}$N$_2$O (372.50), C: 80.61%, H: 7.58%, N: 7.52%. Found C: 80.88%, H: 7.74%, N: 7.85%.

4.3.27. 2,5-Bis-(4-pyrrolidin-1-yl-benzylidene)-cyclopentanone (27)

Yellow powder (2.96 g, 74%). mp: 94–95 °C; ^{1}H NMR (500 MHz, CDCl$_3$) δ: 7.87 (d, $J = 8$ Hz, 4H), 7.59 (s, 2H), 7.12 (d, $J = 8$ Hz, 4H), 2.42 (t, $J = 7$ Hz, 4H), 1.91 (m, $J = 6$ Hz, 8H); ^{13}C NMR (500 MHz, CDCl$_3$) δ: 190.1, 149.5, 145.8, 139.1, 136.8, 134.5, 129.8, 58.1, 32.9, 26.2; HRMS (ESI) m/z: 399.51 [M+H]$^+$, Microanalysis calculated for C$_{27}$H$_{30}$N$_2$O (398.54), C: 81.37%, H: 7.59%, N: 7.03%. Found C: 81.42%, H: 7.62%, N: 7.12%.

4.3.28. 2-(4-Pyrrolidin-1-yl-benzylidene)-indan-1-one (28)

White powder (1.94 g, 67%). mp: 136–137 °C; ^{1}H NMR (500 MHz, CDCl$_3$) δ: 7.94 (d, $J = 8$ Hz, 2H), 7.81 (s, H), 7.43 (d, $J = 8$ Hz, 2H), 7.37 (d, $J = 7.5$ Hz, H), 7.01 (d, $J = 7.5$ Hz, H), 6.92 (t, $J = 7.5$ Hz, H), 6.79 (t, $J = 7$ Hz, H), 2.82 (s, 2H), 1.84 (m, $J = 6$ Hz, 4H); ^{13}C NMR (500 MHz, CDCl$_3$) δ: 192.8, 144.7, 142.9, 141.2, 139.5, 137.9, 136.6, 130.8, 129.8, 128.6, 125.2, 124.5, 122.9, 57.7, 28.5, 27.4; HRMS (ESI) m/z: 290.40 [M+H]$^+$, Microanalysis calculated for C$_{20}$H$_{19}$NO (289.37), C: 83.01%, H: 6.62%, N: 4.84%. Found C: 83.25%, H: 6.75%, N: 4.82%.

4.3.29. 2-(4-Pyrrolidin-1-yl-benzylidene)-3,4-dihydro-2H-naphthalen-1-one (29)

Brown solid (2.41 g, 80%). mp: 123–125 °C; ^{1}H NMR (500 MHz, CDCl$_3$) δ: 7.76 (d, $J = 8$ Hz, 2H), 7.52 (s, H), 7.42 (d, $J = 8$ Hz, 2H), 7.21 (d, $J = 7.5$ Hz, H), 7.15 (d, $J = 7.5$ Hz, H), 7.02 (t, $J = 7.5$ Hz, H), 6.99 (t, $J = 7$ Hz, H), 2.24 (t, $J = 7$ Hz, 2H), 1.97 (t, $J = 7$ Hz, 2H), 1.81 (m, $J = 6$ Hz, 4H); ^{13}C NMR (500 MHz, CDCl$_3$) δ: 188.8, 150.5, 149.2, 148.7, 147.4, 142.6, 135.1, 132.4, 129.8, 128.9, 125.5, 124.2, 117.5, 58.9, 29.7, 27.9, 25.9; HRMS (ESI) m/z: 304.56 [M+H]$^+$, Microanalysis calculated for C$_{21}$H$_{21}$NO (303.40), C: 83.13%, H: 6.98%, N: 4.62%. Found C: 83.06%, H: 6.91%, N: 4.89%.

4.3.30. 2-[3-(4-Pyrrolidin-1-yl-phenyl)-acryloyl]-3,4-dihydro-2H-naphthalen-1-one (30)

Pale yellow solid (2.52 g, 73%). mp: 118–120 °C; ^{1}H NMR (500 MHz, CDCl$_3$) δ: 7.70 (d, $J = 6$ Hz, H), 7.48 (d, $J = 6$ Hz, H), 7.33 (d, $J = 6.5$ Hz, 2H), 7.21 (d, $J = 6.5$ Hz, 2H), 7.17 (d, $J = 6.5$ Hz, H), 7.02 (d, $J = 6.5$ Hz, H), 6.98 (t, $J = 6.5$ Hz, H), 6.81 (t, $J = 6$ Hz, H), 3.24 (t, $J = 6$ Hz, H), 2.29 (t, $J = 8$ Hz, 2H), 1.98 (t, $J = 7$ Hz, 2H), 1.94 (m, $J = 6$ Hz, 4H); ^{13}C NMR (500 MHz, CDCl$_3$) δ: 192.5, 151.8, 149.1, 145.7, 142.5, 140.4, 138.7, 136.9, 135.6, 131.9, 130.8, 129.5, 126.1, 119.1, 65.5, 58.2, 32.5, 28.7, 25.9; HRMS (ESI) m/z: 346.57 [M+H]$^+$, Microanalysis calculated for C$_{23}$H$_{23}$NO$_2$ (345.43), C: 79.97%, H: 6.71%, N: 4.05%. Found C: 80.19%, H: 6.55%, N: 4.09%.

4.4. DPPH (1,1-diphenyl-2-picrylhydrazyl) assay

The reported DPPH method was applied to assess the scavenging ability of the compounds [37]. The compounds were tested in the range of 0–25 μg/mL in methanol. To 2.5 ml of compound in 5 different concentrations, 1 ml of 0.3 mM DPPH ethanol solution was added. Then 1 ml of methanol was added to the solution and allowed to react for 30 min in the dark at room temperature. The change in the absorbance was read at 518 nm. The blank was comprised of 2.5 ml of test compound and 1 ml methanol, while the mixture of 1 ml DPPH and 2.5 ml of methanol served as negative control. The percentage antioxidant activity was calculated as follows:

$$\% \text{ Inhibition} = \frac{A_A - A_B}{A_B} \times 100$$

where: A_B: absorption of blank sample, A_A: absorption of test samples. The IC$_{50}$ value was calculated and compared with that of ascorbic acid as a reference.

4.5. Cell culture

The rat pheochromocytoma (PC12) cell line was purchased from the ATCC. The cells were maintained in RPMI-1640 medium consisting of 10% heat-inactivated FBS and 1% penicillin–streptomycin. The cells were incubated at 37 °C in a 5% CO$_2$ atmosphere with 95% humidity.

4.6. Cell viability assay

To investigate the cytotoxicity or neuroprotective effects of synthetic compounds in PC12 cells, the MTT assay was performed. The cells (1 × 10^4 cells/well) were seeded in 96-well cell culture plates and treated with different concentrations of compounds for 24 h. The cell viability was expressed as a relative percentage against control cultures. To assess the Aβ-induced neuroprotective activity, different concentrations of all compounds were individually added to cells for 24 h, before treatment with Aβ. The positive control drug selegiline was also evaluated in the same manner for comparison. 2.0 mg/ml MTT solution was added to each well and incubated for 4 h at 37 °C. The medium was removed and the formazan crystals were solubilized in 100 μL dimethyl sulfoxide (DMSO). A microplate reader was used to determine the optical density (excitation at 570 nm, emission at 630 nm) and data are plotted as percent of control.

4.7. AChE and BuChE inhibition assay

To evaluate the potency of compounds to inhibit AChE and BuChE, all compounds were subjected to a slightly modified method of Ellman's test [38]. The reaction of released thiocholine to

give a colored product with a chromogenic reagent 5,5-dithio-bis (2-nitrobenzoic) acid (DTNB) is the basis of the spectrophotometric method. The measurements were performed on a 1700 Shimadzu UV-1700, UV–Vis spectrophotometer. At a concentration of 2.5 units/mL, the enzyme solutions were prepared in gelatin solution (1%). AChE or BChE solution (50 μL) and compound solution (50 μL), prepared in 2% DMSO at a concentration range of 10^{-1}–10^{-6} mM, were added to 3.0 ml phosphate buffer (pH 8 ± 0.1) and were incubated at 25 °C for 5 min. DTNB (50 μL) and ATC (10 μL) were added to the enzyme-inhibitor mixture to start the reaction. For 10 min, the production of the yellow anion was recorded at 412 nm. Serving as a control, an identical solution of the enzyme without the inhibitor was processed using the same protocol. The blank reading consisted of 3.0 ml buffer, 50 μL 2% DMSO, 50 μL DTNB and 10 μL substrate. All the processes were assayed in triplicate. The percentage inhibition rate was calculated by the following equation:

$$\% \text{ Inhibition} = \frac{A_C - A_I}{A_C} \times 100$$

where A_I is the absorbance in the presence of the inhibitor, A_C is the absorbance of the control and A_B is the absorbance of blank. Both values were corrected with blank-reading value. The data was expressed as Mean ± SD.

4.8. Molecular docking and QSAR analysis

For docking, the molecules were drawn using ACD Chemsketch 12 freeware followed by energy optimization using MMFF94 force field in TINKER [32]. The protein was first subjected to energy minimization, protonation followed by detection of site detection. The receptor and the drug candidates were optimized before actual docking followed by docking in MOE using the standard procedure found in the manual of software. The molecules were docked in the active site using 'force field' as a refinement technique with default settings in MOE [29]. All of the newly synthesized molecules were docked in the active site of AChE (pdb-1GQR, X-ray resolution = 2.20 A°). For the sake of convenience and comparison, as a representative, we report the docking poses for the most active compound of the series. For QSAR analysis, e-Dragon was used to calculate myriad number of descriptors, followed by random splitting of data set into training set (80%) and test set (20%). QSARINS v1.2 was used to eliminate redundant descriptors and for building GA–MLR (Genetic Algorithm–Multilinear regression) model [31,32].

Acknowledgments

Appendix A. Supplementary data

Supplementary data related to this article can be found at http://dx.doi.org/10.1016/j.ejmech.2014.06.034.

References

[1] World Alzheimer Report 2013, Alzheimer's Disease International, 2013, p. 1.
[2] D.K. Lahiri, M.R. Farlow, N.H. Greig, K. Sambamurti, Current drug targets for Alzheimer's disease treatment, Drug Dev. Res. 56 (2002) 267–281.
[3] J.L. Cummings, Alzheimer's disease, N. Engl. J. Med. 351 (2004) 56–67.
[4] J.A. Bailey, D.K. Lahiri, A novel effect of rivastigmine on pre-synaptic proteins and neuronal viability in a neurodegeneration model of fetal rat primary cortical cultures and its implication in Alzheimer's disease, J. Neurochem. 112 (2010) 843–853.
[5] A. Enz, R. Amstutz, H. Boddeke, G. Gmelin, J. Malanowski, Brain selective inhibition of acetylcholinesterase: a novel approach to therapy for Alzheimer's disease, Prog. Brain Res. 98 (1993) 431–438.
[6] E. Giacobini, Cholinesterase inhibitors: new roles and therapeutic alternatives, Pharmacol. Res. 50 (2004) 433–440.
[7] P.J. Houghton, Y. Ren, M.-J. Howes, Acetylcholinesterase inhibitors from plants and fungi, Nat. Prod. Rep. 23 (2006) 181–199.
[8] N.H. Greig, T. Utsuki, Q.-S. Yu, X. Zhu, H.W. Holloway, T. Perry, B. Lee, D.K. Ingram, D.K. Lahiri, A new therapeutic target in Alzheimer's disease treatment: attention to butyrylcholinesterase, Curr. Med. Res. Opin. 17 (2001) 159–165.
[9] J. Lal, S.K. Gupta, D. Thavaselvam, D.D. Agarwal, Design, synthesis, synergistic antimicrobial activity and cytotoxicity of 4-aryl substituted 3,4-dihydropyrimidinones of curcumin, Bioorg. Med. Chem. Lett. 22 (2012) 2872–2876.
[10] A.M. Magerramov, M.M. Kurbanova, R.T. Abdinbekova, I.A. Rzaeva, V.M. Farzaliev, M.A. Allakhverdiev, Synthesis and antioxidative properties of some 3,4-dihydropyrimidin-2(1H)ones (-thiones), Russ. J. Appl. Chem. 79 (2006) 787–790.
[11] R. Feng, Y. Lu, L.L. Bowman, Y. Qian, V. Castranova, M. Ding, Inhibition of activator protein-1, NF-κB, and MAPKs and induction of phase 2 detoxifying enzyme activity by chlorogenic acid, J. Biol. Chem. 280 (2005) 27888–27895.
[12] S.N.A. Bukhari, Y. Tajuddin, V.J. Benedict, K.W. Lam, I. Jantan, J. Jalil, M. Jasamai, Synthesis and evaluation of chalcone derivatives as inhibitors of neutrophils' chemotaxis, phagocytosis and production of reactive oxygen species, Chem. Biol. Drug Des. 83 (2014) 198–206.
[13] S.N. Bukhari, I. Jantan, M. Jasamai, Anti-inflammatory trends of 1, 3-diphenyl-2-propen-1-one derivatives, Mini Rev. Med. Chem. 13 (2013) 87–94.
[14] S.N. Bukhari, M. Jasamai, I. Jantan, Synthesis and biological evaluation of chalcone derivatives (mini review), Mini Rev. Med. Chem. 12 (2012) 1394–1403.
[15] S. Bag, S. Ghosh, R. Tulsan, A. Sood, W. Zhou, C. Schifone, M. Foster, H. LeVine Iii, B. Török, M. Török, Design, synthesis and biological activity of multifunctional α,β-unsaturated carbonyl scaffolds for Alzheimer's disease, Bioorg. Med. Chem. Lett. 23 (2013) 2614–2618.
[16] D. Silva, M. Chioua, A. Samadi, P. Agostinho, P. Garção, R. Lajarín-Cuesta, C. de los Ríos, I. Iriepa, I. Moraleda, L. Gonzalez-Lafuente, E. Mendes, C. Pérez, M.I. Rodríguez-Franco, J. Marco-Contelles, M. Carmo Carreiras, Synthesis, pharmacological assessment, and molecular modeling of acetylcholinesterase/butyrylcholinesterase inhibitors: effect against amyloid-β-induced neurotoxicity, ACS Chem. Neurosci. 4 (2013) 547–565.
[17] R. Sultana, M. Perluigi, D.A. Butterfield, Oxidatively modified proteins in Alzheimer's disease (AD), mild cognitive impairment and animal models of AD: role of Abeta in pathogenesis, Acta Neuropathol. 118 (2009) 131–150.
[18] X. Zhu, B. Su, X. Wang, M.A. Smith, G. Perry, Causes of oxidative stress in Alzheimer disease, Experientia 64 (2007) 2202–2210.
[19] R.J. Mark, M.A. Lovell, W.R. Markesbery, K. Uchida, M.P. Mattson, A role for 4-hydroxynonenal, an aldehydic product of lipid peroxidation, in disruption of ion homeostasis and neuronal death induced by amyloid β-peptide, J. Neurochem. 68 (1997) 255–264.
[20] D.A. Butterfield, K. Hensley, M. Harris, M. Mattson, J. Carney, β-Amyloid peptide free radical fragments initiate synaptosomal lipoperoxidation in a sequence-specific fashion: implications to Alzheimer's disease, Biochem. Biophys. Res. Commun. 200 (1994) 710–715.
[21] S.N. Bukhari, I. Jantan, O.U. Tan, M. Sher, N.U. Hassan, H.L. Qin, Biological activity and molecular docking studies of curcumin related alpha, beta-unsaturated carbonyl based synthetic compounds as anticancer agents and mushroom tyrosinase inhibitors, J. Agric. Food Chem. (2014), http://dx.doi.org/10.1021/jf501145b.
[22] S.N.A. Bukhari, G. Lauro, I. Jantan, G. Bifulco, M.W. Amjad, Pharmacological evaluation and docking studies of α, β-unsaturated carbonyl based synthetic compounds as inhibitors of secretory phospholipase A2, cyclooxygenases, lipoxygenase and proinflammatory cytokines, Bioorg. Med. Chem. (2014), http://dx.doi.org/10.1016/j.bmc.2014.05.052.
[23] J.R. Dimmock, M.P. Padmanilayam, R.N. Puthucode, A.J. Nazarali, N.L. Motaganahalli, G.A. Zello, J.W. Quail, E.O. Oloo, H.-B. Kraatz, J.S. Prisciak, T.M. Allen, C.L. Santos, J. Balzarini, E. De Clercq, E.K. Manavathu, A conformational and structure–activity relationship study of cytotoxic 3,5-bis(arylidene)-4-piperidones and related n-acryloyl analogues, J. Med. Chem. 44 (2001) 586–593.
[24] U. Das, M. Kawase, H. Sakagami, A. Ideo, J. Shimada, J. Molnár, Z. Baráth, Z. Bata, J.R. Dimmock, 3-(3,4,5-Trimethoxyphenyl)-1-oxo-2-propene: a novel pharmacophore displaying potent multidrug resistance reversal and selective cytotoxicity, Bioorg. Med. Chem. 15 (2007) 3373–3380.
[25] U. Das, J. Alcorn, A. Shrivastav, R.K. Sharma, E. De Clercq, J. Balzarini, J.R. Dimmock, Design, synthesis and cytotoxic properties of novel 1-[4-(2-

alkylaminoethoxy)phenylcarbonyl]-3,5-bis(arylidene)-4-piperidones and related compounds, Eur. J. Med. Chem. 42 (2007) 71—80.

[26] Y. Kia, H. Osman, R.S. Kumar, V. Murugaiyah, A. Basiri, S. Perumal, H.A. Wahab, C.S. Bing, Synthesis and discovery of novel piperidone-grafted mono- and bis-spirooxindole-hexahydropyrrolizines as potent cholinesterase inhibitors, Bioorg. Med. Chem. 21 (2013) 1696—1707.

[27] J.-M. Contreras, Y.M. Rival, S. Chayer, J.-J. Bourguignon, C.G. Wermuth, Aminopyridazines as acetylcholinesterase inhibitors, J. Med. Chem. 42 (1999) 730—741.

[28] K.K. Roy, A. Dixit, A.K. Saxena, An investigation of structurally diverse carbamates for acetylcholinesterase (AChE) inhibition using 3D-QSAR analysis, J. Mol. Gr. Model. 27 (2008) 197—208.

[29] Y.K. Yoon, M.A. Ali, A.C. Wei, T.S. Choon, K.-Y. Khaw, V. Murugaiyah, H. Osman, V.H. Masand, Synthesis, characterization, and molecular docking analysis of novel benzimidazole derivatives as cholinesterase inhibitors, Bioorg. Chem. 49 (2013) 33—39.

[30] D. Mahajan, V. Masand, K. Patil, T. Hadda, V. Rastija, Integrating GUSAR and QSAR analyses for antimalarial activity of synthetic prodiginines against multi drug resistant strain, Med. Chem. Res. 22 (2013) 2284—2292.

[31] V.H. Masand, D.T. Mahajan, K.N. Patil, T.B. Hadda, M.H. Youssoufi, R.D. Jawarkar, I.G. Shibi, Optimization of antimalarial activity of synthetic prodiginines: QSAR, GUSAR, and CoMFA analyses, Chem. Biol. Drug Des. 81 (2013) 527—536.

[32] V. Masand, D. Mahajan, T. Hadda, R. Jawarkar, H. Chavan, B.P. Bandgar, H. Chauhan, Molecular docking and quantitative structure—activity relationship (QSAR) analyses of indolylarylsulfones as HIV-1 non-nucleoside reverse transcriptase inhibitors, Med. Chem. Res. 23 (2014) 417—425.

[33] D.T. Mahajan, V.H. Masand, K.N. Patil, T. Ben Hadda, R.D. Jawarkar, S.D. Thakur, V. Rastija, CoMSIA and POM analyses of anti-malarial activity of synthetic prodiginines, Bioorg. Med. Chem. Lett. 22 (2012) 4827—4835.

[34] P. Gramatica, On the development and validation of QSAR models, Methods Mol. Biol. 930 (2013) 499—526.

[35] P. Gramatica, N. Chirico, E. Papa, S. Cassani, S. Kovarich, QSARINS: a new software for the development, analysis, and validation of QSAR MLR models, J. Comput. Chem. 34 (2013) 2121—2132.

[36] G.L. Ellman, K.D. Courtney, V. Andres jr, R.M. Featherstone, A new and rapid colorimetric determination of acetylcholinesterase activity, Biochem. Pharmacol. 7 (1961) 88—95.

[37] C.W. Choi, S.C. Kim, S.S. Hwang, B.K. Choi, H.J. Ahn, M.Y. Lee, S.H. Park, S.K. Kim, Antioxidant activity and free radical scavenging capacity between Korean medicinal plants and flavonoids by assay-guided comparison, Plant Sci. 163 (2002) 1161—1168.

[38] N.S. Perry, P.J. Houghton, A. Theobald, P. Jenner, E.K. Perry, In-vitro inhibition of human erythrocyte acetylcholinesterase by salvia lavandulaefolia essential oil and constituent terpenes, J. Pharm. Pharmacol. 52 (2000) 895—902.

Original Research Paper

Determination of Optimum Values of Descriptors to Set Filters for Synthetic Tri-Pyrrole Derivatives (Prodiginines) Against Multi Drug Resistant Strain of *Plasmodium Falciparum*

[1]**Vijay H. Masand,** [1]**Devidas T. Mahajan,** [2]**Eslam Pourbasheer,**
[3]**Taibi Ben Hadda,** [4]**Harsh Chauhan**, [5]**J.M. Gajbhiye and** [6]**A.M. Alafeefy**

[1]*Department of Chemistry, Vidya Bharati College, Camp, Amravati, Maharashtra, India*
[2]*Department of Chemistry, Faculty of Science, University of Qom, Qom, Iran*
[3]*Laboratoire Chimie des Matériaux, Université Mohammed Premier, Oujda-60000, Morocco*
[4]*Creighton University, Omaha, NE, USA*
[5]*Division of Organic Chemistry, CSIR-National Chemical Laboratory, Pune 411008, India*
[6]*Department of Pharmaceutical Chemistry, Kind Saud University, Alkharj, Saudi Arabia*

Abstract: In the present study, we have carried out extensive non-linear Quantitative-Structure Activity Relationship (QSAR) analysis to correlate *in vitro* anti-malarial activity against multi drug resistant strain of *Plasmodium falciparum*. Forty-three synthetic prodiginines with different structural features were used for their potential antimalarial activity. Linear, bilinear, biexponential and parabolic equations were developed. These equations were compared to determine the optimum values of descriptors for very useful and easily interpretable descriptors. The optimum values of these descriptors could be helpful in finding and optimizing a good lead compound. Obtained correlations reveal that various factors like lipophilicity, molecular weight and number of bonds have non-linear relation with the anti-malarial activity.

Keywords: Prodiginines, Anti-Malarial Activity, Optimum/Desirability Values, Hybrid Inverse-QSAR

Introduction

Malaria, a dreadful vector-borne protozoal disease is responsible for more than two million deaths every year (WHO, 2012; http://www.who.int/malaria/en/). Developing a potent antimalarial compound is still a major challenge for the medicinal chemists (Biamonte *et al*., 2013). The situation is worsening with the rapid spread of multi drug resistant strains of causative agent (Biamonte *et al*., 2013; Mahajan *et al*., 2012; 2013; Mara *et al*., 2013; Masand *et al*., 2013b; Murugesan *et al*., 2013; Ojha and Roy, 2012; Papireddy *et al*., 2011). Therefore, there is essential need to curb this deadly disease either by modifying the existing marketed drugs or developing new therapeutic molecules. Different compounds like xanthones, artemisinins, prodiginines have been synthesized and tested to develop new potential remedies for malaria (Biamonte *et al*., 2013; Mahajan *et al*., 2012; 2013; Mara *et al*., 2013; Masand *et al*., 2013b; Murugesan *et al*., 2013; Ojha and Roy, 2012; Papireddy *et al*., 2011).

Prodiginines (Mahajan *et al*., 2012; 2013; Masand *et al*., 2013b; Papireddy *et al*., 2011), the oligopyrrole derivatives with a characteristic conjugated system, are promising anti-malarial agents (Fig. 1). These compounds have the ability to inhibit *Plasmodium falciparum* (*P. falciparum*) at very low concentrations. They show marked clearance of the protozoa parasite and can be effectively administered orally. Despite these advantages, search for a potent prodiginines with good Absorption, Distribution, Metabolism, Excretion and Toxicity (ADMET) profile and improved ease of synthesis has resulted in limited success (Mahajan *et al*., 2012; 2013; Masand *et al*., 2013b; Papireddy *et al*., 2011). The progress can be expedited using the contemporary method of drug designing like QSAR, Molecular docking and Pharmacophore modelling. Of the above mentioned methods, QSAR is an established technique with good success in last few decades and is utilized in our research (Huang *et al*., 2011; Myint *et al*., 2010; Scior *et al*., 2009; Tropsha, 2010).
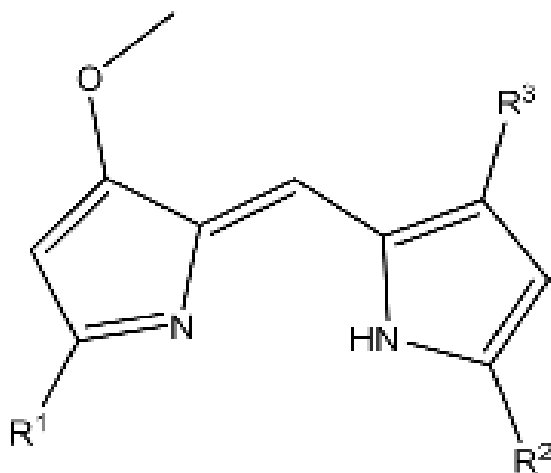
Fig. 1. Synthetic prodiginines used in present study

A typical QSAR study involves establishment of correlation between structure and activity (Mahajan *et al.*, 2012; 2013; Masand *et al.*, 2012a; Masand *et al.*, 2013a; 2012b; 2013b; Rastija *et al.*, 2013). Different characteristics or attributes of chemical structure are expressed in terms of numerical entities termed as molecular descriptors (also known as parameters or features). One or more molecular descriptors are used to build statistically robust linear regression equation. A properly validated QSAR equation is considered more useful if it is derived using descriptors that represent maximum useful information with minimum overlap and are interpretable in terms of structural features (Chirico and Gramatica, 2011; 2012a; Chirico *et al.*, 2012b; Gramatica, 2013; Gramatica *et al.*, 2012; Gramatica *et al.*, 2013; Martin *et al.*, 2012; Mitra *et al.*, 2010; Roy *et al.*, 2012; Saha *et al.*, 2012; Tropsha, 2010). Unfortunately, limited number of validated QSAR equations with the ability to guide for the development of new drugs or modification of existing drugs are utilized, due to the following reasons (Chirico and Gramatica, 2011; 2012a; Chirico *et al.*, 2012b; Doweyko, 2008; Gramatica, 2013; Gramatica *et al.*, 2012; Gramatica *et al.*, 2013; Martin *et al.*, 2012; Mitra *et al.*, 2010; Roy *et al.*, 2012; Saha *et al.*, 2012; Tropsha, 2010) (i) Difficulty in interpretation of QSAR equation in terms of structural features; (ii) The calculation or estimation of descriptors is very complex or resource consuming; (iii) computational facilities/resources like advanced and specific softwares may not be available to organic chemist to calculate descriptors that are mentioned in QSAR equation. (iv) The organic chemist may not be well skilled or trained in QSAR; (v) In addition, important descriptors having good correlation with activity might get missed in QSAR equations due to some reasons.

To overcome the difficulties, many researchers use inverse-QSAR (*i*-QSAR). In *i*-QSAR, the molecules are optimised using a set of physico-chemical properties or theoretical descriptors, which are obtained or derived using a well known marketed drug as 'reference' (Brown *et al.*, 2006; Faulon *et al.*, 2005). This approach has certain limitations like (i) proper selection of drug is an exigent and tricky process (ii) the drug should have similarity in structural or shape with the molecules of data set in hand (iii) For some diseases, no marketed drugs are available whereas for some diseases, a lot of marketed drugs are available. (iv) The physico-chemical properties or theoretical descriptors which are associated with one chemo-type of drug may not be possible to calculate or estimate for other chemo-type of molecule. (iv) The physico-chemical properties or theoretical descriptors associated with one chemo-type of drug may not be possible to calculate or estimate for other chemo-type molecules. After determining the values of different descriptors, the problem then lies in constructing a viable molecule from these descriptors. This is the real limiting factor of most inverse-QSAR methods, because most of the descriptors are not reversible.

A good solution is to determine the optimum value of useful and information rich descriptors, during the QSAR equation development. The most striking advantage in determining optimal values of different descriptors is that the 'most active' compound in the given data set may or may not fit to optimum values of all the descriptors. This optimization is not based on single 'reference' drug as in *i*-QSAR. In this case a data set is used to derive a set of physico-chemical properties or theoretical descriptors to optimize the molecules. Thereby, increasing the chances of finding better alternatives to visible 'most active' and potential compounds outside the present data set. This approach can be viewed as 'Hybrid-inverse QSAR'. It could significantly accelerate the discovery of novel small molecules with specified chemical properties.

Literature survey reveals (Buchwald *et al.*, 2014; Gidskehaug *et al.*, 2008; Hansch *et al.*, 2004; Jager *et al.*, 2009; Kubinyi, 2002) that a well established method to determine the optimum value of any descriptor is to derive non-linear equation, especially bilinear or biexponential or parabolic equation. These functions assume that the relationship between descriptor and the activity is non-linear with the vertex of curve representing the optimum value.

In our previous work, we successfully performed CoMSIA, GUSAR and QSAR analyses for antimalarial activity of synthetic prodiginines. The objectives of the present study are (i) to determine optimum value of easily interpretable descriptors used in the QSAR equation (ii) to determine optimum value of some other useful descriptors having good correlation with activity but not included in the reported QSAR equations and (iii) to compare the performance and ability of linear, parabolic, bilinear and biexponential QSAR models to determine the optimum values of descriptors.

Methodology

Data Set

The experimental *in vitro* Inhibitory Concentrations (IC_{50}) expressed in nanomolar units of forty three synthetic prodiginines against the Chloroquine (CQ) resistant strain Dd2 are selected from a recent publication (Papireddy *et al.*, 2011). The data set includes prodiginines with different substituents like varying length of alkyl chain, substituents at different positions of benzene ring etc. Table 1, provides the experimental data. The values were converted into the logarithm units, (-log $_{10}$ IC_{50} = pIC_{50}) for molecular modelling purpose.

The structures were drawn using ACD Chemsketch 12 freeware and were converted into 3D structures. This was followed by geometry optimization using a molecular mechanics method implemented in the program VegaZZ, using Gasteiger partial charges and Tripos force field

(Mahajan *et al.*, 2012; 2013; Masand *et al.*, 2013b). The optimized structures (β-isomer) were uploaded onto the e-DRAGON server to calculate myriad number of 1D-, 2D- and 3D- molecular descriptors (Fig. 2). Before QSAR model development, descriptors with constant or nearly constant (for 80% molecules) values were discarded. Genetic Algorithm (GA) available in QSARINS (Chirico and Gramatica, 2011; 2012a; Chirico *et al.*, 2012b; Gramatica *et al.*, 2013; Chirico and Gramatica, 2011; 2012a; Chirico *et al.*, 2012b; Gramatica *et al.*, 2013) was used to select optimum number and set of descriptors to build statistically sound multi linear regression equation. Matlab and BuildQSAR were used to build bilinear, biexponential and parabolic equations. In addition, Microsoft excel was used for different statistical functions.

A good number of statistical parameters like R, R^2, R^2_{adj}, S and F were calculated along with R^2_{cv} (R^2_{LOO}) for internal validation and to check the robustness of the model.
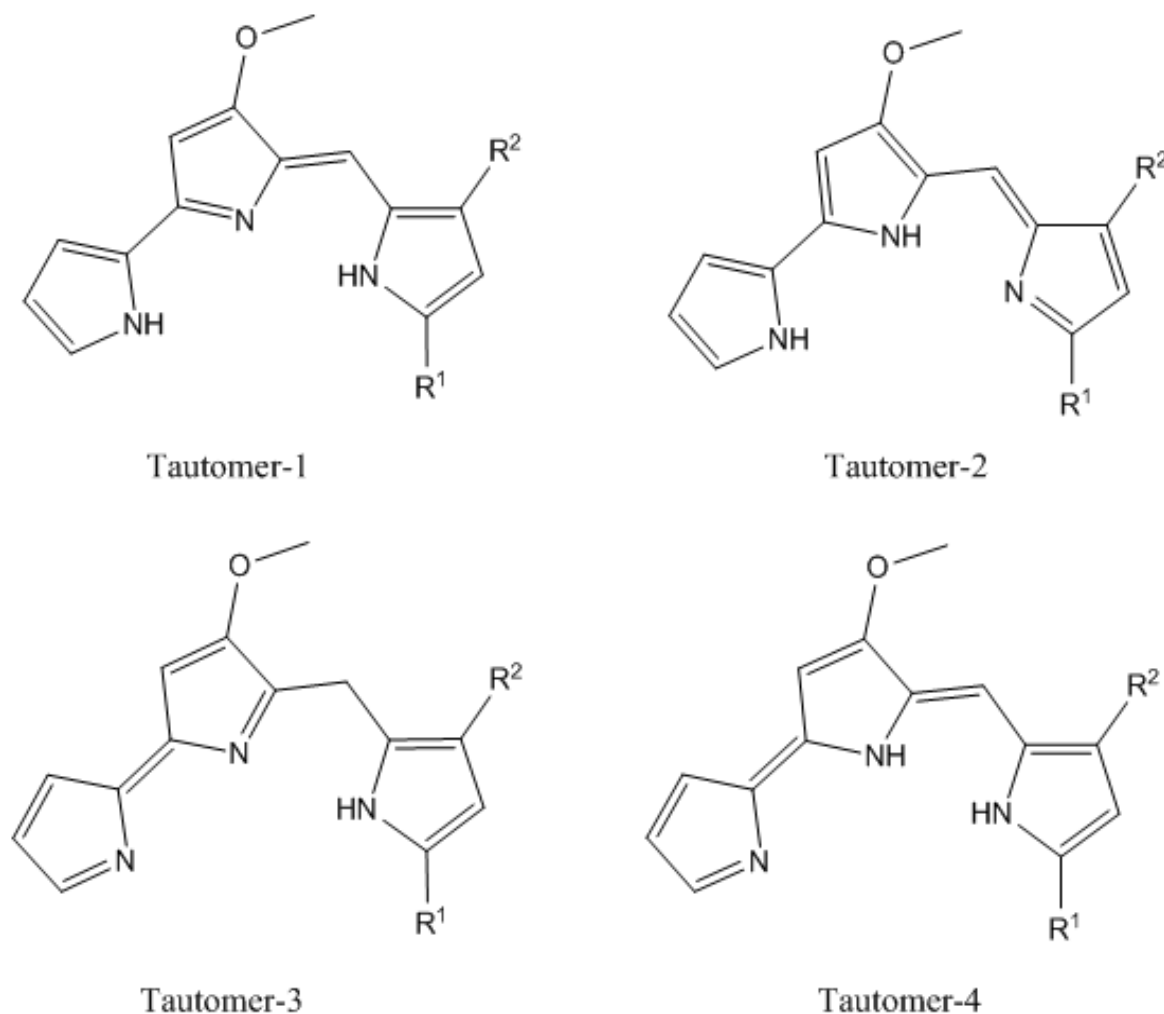

Fig. 2. Tautomeric forms of synthetic prodiginines (β-isomer) used in present study

Table 1. Different synthetic prodiginines along with experimental data IC_{50} (nM) and pIC_{50}

S. No.	R^1	R^2	R^3	IC_{50}(nM) Dd2	pIC_{50} expt.
1	2-pyrolyl	n-C_4H_9	H	1590.0	5.799
2	2-pyrolyl	n-C_6H_{13}	H	450.0	6.347
3	2-pyrolyl	n-C_8H_{17}	H	130.0	6.886
4	2-pyrolyl	n-$C_{16}H_{33}$	H	400.0	6.398
5	2-pyrolyl	H	$CH_2CH(CH_3)_2$	230.0	6.638
6	2-pyrolyl	H	n-C_4H_9	18.0	7.745
7	2-pyrolyl	H	n-C_6H_{13}	7.0	8.155
8	2-pyrolyl	H	n-C_8H_{17}	1.8	8.745
9	2-pyrolyl	H	n-$C_{10}H_{21}$	10.0	8.000[a]
10	2-pyrolyl	H	$C_6H_5CH_2$	86.0	7.066
11	2-pyrolyl	H	4-$OCH_3C_6H_4CH_2$	156.0	6.807
12	2-pyrolyl	H	4-$ClC_6H_4CH_2$	81.0	7.092
13	2-pyrolyl	H	4-$BrC_6H_4CH_2$	108.0	6.967
14	2-pyrolyl	CH_3	CH_3	8130.0	5.090
15	2-pyrolyl	n-C_6H_{13}	n-C_3H_7	4.0	8.398
16	2-pyrolyl	n-C_8H_{17}	n-C_3H_7	2.7	8.569
17	2-pyrolyl	n-C_3H_7	⌇⌇	1.3	8.886
18	2-pyrolyl	n-C_6H_{13}	n-C_6H_{13}	1.1	8.959
19	2-pyrolyl	n-C_7H_{15}	n-C_6H_{13}	1.2	8.921
20	2-pyrolyl	n-C_6H_{13}	n-C_8H_{17}	2.0	8.699
21	2-pyrolyl	n-C_7H_{15}	n-C_8H_{17}	2.9	8.538
22	2-pyrolyl	n-C_8H_{17}	n-C_8H_{17}	129.0	6.889
23	2-pyrolyl	⌇⌇	⌇⌇	3.5	8.456
24	2-pyrolyl	C_2H_5	4-$ClC_6H_4CH_2$	6.2	8.208
25	2-pyrolyl	n-C_3H_7	4-$ClC_6H_4CH_2$	2.6	8.585
26	2-pyrolyl	n-C_6H_{13}	4-$ClC_6H_4CH_2$	1.8	8.745
27	2-pyrolyl	n-C_7H_{15}	4-$ClC_6H_4CH_2$	2.2	8.658
28	2-pyrolyl	n-C_8H_{17}	4-$ClC_6H_4CH_2$	12.0	7.921
29	2-pyrolyl	4-$ClC_6H_4CH_2$	⌇⌇	2.9	8.538
30	2-pyrolyl	n-C_6H_{13}	4-$FC_6H_4CH_2$	0.9	9.046
31	2-pyrolyl	n-C_8H_{17}	4-$FC_6H_4CH_2$	1.2	8.921
32	2-pyrolyl	n-C_6H_{13}	4-$BrC_6H_4CH_2$	2.8	8.553
33	2-pyrolyl	n-C_8H_{17}	4-$BrC_6H_4CH_2$	2.9	8.538
34	2-pyrolyl	4-$ClC_6H_4CH_2$	4-$ClC_6H_4CH_2$	4.8	8.319
35	2-pyrolyl	4-$FC_6H_4CH_2$	4-$FC_6H_4CH_2$	5.7	8.244
36	2-pyrolyl	4-$BrC_6H_4CH_2$	4-$BrC_6H_4CH_2$	11.0	7.959
37	2-pyrolyl	4-$FC_6H_4CH_2$	4-$ClC_6H_4CH_2$	6.1	8.215
38	2-pyrolyl	4-$BrC_6H_4CH_2$	4-$ClC_6H_4CH_2$	7.7	8.114
39	2-pyrolyl	4-$BrC_6H_4CH_2$	4-$FC_6H_4CH_2$	5.1	8.292
40	2-pyrolyl	2,4-$Cl_2C_6H_3CH_2$	2,4-$Cl_2C_6H_3CH_2$	11.0	7.959
41	2-pyrolyl	2,4-$F_2C_6H_3CH_2$	2,4-$F_2C_6H_3CH_2$	18.3	7.738
42	2-pyrolyl	3-$FC_6H_4CH_2$	3-$FC_6H_4CH_2$	6.7	8.174
43	2-pyrolyl	2-$ClC_6H_4CH_2$	2-$ClC_6H_4CH_2$	4.9	8.310

Results and Discussion

In the present study, we derived and compared the linear, biexponential, bilinear (two equations) and parabolic equations. These equations are listed in Table 2 and 3. The equations provide useful correlation between activity and many easily interpretable useful descriptors like *Sv* (Sum of atomic van der Waal's volumes), *Sp* (Sum of atomic polarizabilities), *X1v* (first order valence connectivity index, to represent the steric factor), ALOG*P* (Ghose-Crippen Octanol-water coefficient) and *nAT* (number of atoms).

The linear model cannot be used for the determination of optimum value of any descriptor. The general form of the parabolic, bilinear Equation 1 (proposed by Kubinyi), bilinear Equation 2 and biexponential model is as following:

$$Y = aX + bX^2 + c \tag{1}$$

$$Y = aX + b \log(cX + 1) + d \tag{2}$$

$$Y = aX + b \, Log(\beta \, 10^X + 1) + c \tag{3}$$

$$Y = -b \, (\log((e^{(-c(x-a)/b)}) + (e^{(e(x-a)/b)}))) + d \tag{4}$$

Comparison of Different Models

For some descriptors viz. *nAT*, *Sv*, *Sp* and *ALOGP*, non-linear models are either superior or equivalent to the linear model. Whereas, for rest of the descriptors, the fitting of the non-linear models is better than the linear model. This indicates that the relation between the activity and the selected descriptors is non-linear in nature. In other words, non-linear model can better explain the variation of activity. Among non-linear models, bilinear Equation 1 (based on Kubinyi formula) fits better than the rest, with biexponential models being least fit in nature for many descriptors. None of the model satisfies the recommended threshold value (>0.85) of *CCC*, though for some models, it is close to it.

In the above models, the symbols have their usual meanings. Increasing the number of congeneric compounds in the data set as well as the range of biological data might result in better statistical fitting. In many cases, the substantial fitting of the equation ($R^2 > 0.60$), though not outstanding, is satisfactory. This proves that there prevails the optimum value of

lipophilicity, number of atoms, number of bonds and *X1v* (to represent steric factor). Thus, the selected descriptors, for which the optimum values are determined, represent the overall descriptor space.

A comparison of values of descriptors for four most active (highlighted as bold and italic) and four least active (highlighted as bold and italic) compounds justify the importance of optimum values of descriptors (Table 3). The value for selected descriptors for four most active molecules selected as representatives are close to optimum values whereas reverse is true for the four least active molecules. Thus, the optimum values of these descriptors could be helpful in finding a good "lead prodiginine" for anti-malarial activity.

Interestingly, the values of descriptors for the 'most active' compound 30 in the present data set are close to optimum values of many descriptors. However, it does not match with the optimum values of all the descriptors. This confirms that the appropriate lead/drug optimization using only most active or single drug as 'reference' is not a perfect method.

Table 2. Different linear and non-linear equations along with their statistical parameters

Descriptor	Statistical parameter	Linear	Parabolic	Bilinear Equation 1	Bilinear Equation 2	Biexponential
nAT	R^2	0.242	0.685	0.640	0.664	0.242
	R^2_{adj}	0.224	0.669	0.612	0.638	0.162
	RMSE	0.800	0.516	0.565	0.533	0.800
	SSE	27.517	11.442	13.073	12.211	27.517
	F	13.099	43.465	23.105	25.349	3.035
	CCC	0.389	0.813	0.781	0.796	0.390
nBT	R^2	0.267	0.676	0.657	0.654	0.713
	R^2_{adj}	0.249	0.660	0.631	0.628	0.683
	RMSE	0.786	0.523	0.565	0.540	0.492
	SSE	26.613	11.758	12.443	12.548	10.407
	F	14.935	41.756	24.933	24.354	23.629
	CCC	0.421	0.807	0.793	0.790	0.833
Sv	R^2	0.331	0.633	0.673	0.612	0.331
	R^2_{adj}	0.314	0.614	0.648	0.582	0.260
	RMSE	0.752	0.557	0.551	0.573	0.752
	SSE	24.302	13.339	11.857	14.093	24.302
	F	20.254	34.438	26.808	20.279	4.693
	CCC	0.497	0.775	0.805	0.758	0.497
Sp	R^2	0.320	0.647	0.679	0.624	0.320
	R^2_{adj}	0.304	0.629	0.654	0.596	0.249
	RMSE	0.758	0.546	0.547	0.563	0.758
	SSE	24.679	12.819	11.652	13.639	24.679
	F	19.317	36.648	27.508	21.377	4.475
	CCC	0.485	0.786	0.809	0.767	0.485
X1v	R^2	0.329	0.625	0.641	0.605	NC
	R^2_{adj}	0.313	0.607	0.614	0.574	NC
	RMSE	0.752	0.562	0.578	0.578	NC
	SSE	24.336	13.601	13.022	14.351	NC
	F	20.169	33.388	23.245	19.717	NC
	CCC	0.496	0.769	0.782	0.753	NC
ALOGP	R^2	0.323	0.683	0.711	0.650	0.232
	R^2_{adj}	0.307	0.667	0.688	0.623	0.151
	RMSE	0.756	0.517	0.519	0.543	0.805
	SSE	24.573	11.506	10.511	12.701	27.875
	F	19.579	43.112	31.906	23.576	9.349
	CCC	0.488	0.812	0.831	0.786	0.065

SSE- Sum of Squared Errors, RMSE-Root Mean Square Error, CCC- Concordance Correlation Coefficient

In present case, a plausible reason for this could be the ability of the molecules (prodiginines in present case) to attain different conformations and tautomeric forms. Prodiginines possess azafulvene-pyrrole tautomerism due to the three pyrrole rings joined by -CH= link. As prodiginines can form four different tautomeric forms, the tautomeric form, which is energetically favoured in solution, may not be the 'bioactive tautomeric form' which shows interaction with the specific receptor and is responsible for the pharmacologic activity of this group.

Prodiginine may interact with different receptors in different tautomeric forms. In addition, prodiginines can exist in two conformations viz. α and β isomer, which have been discussed in our previous work (Reference). Another possible reason is satisfactory fitting ($R^2 \sim 0.60$) for most of the developed models.

Variation of Activity with Various Parameters

Herein, the activities of some more active and less active molecules from the dataset in terms of various descriptors like lipophilicity/hydrophobicity, number of rotatable bonds, steric factor etc. for which the optimum value, determined using bilinear Equation 2, has been derived and discussed. For optimum value determination, parabolic and bilinear Equation 1 can also be use, but, these have some serious drawbacks, like (1) the parabolic approach forces the data into a symmetrical parabola, resulting in deviations between the experimental and parabola-calculated data. (2) The ascending slope is curved and conflicts with the observed linear data. (3) The bilinear equation provides better optimum value only if the dataset is large in size with wide spread variation in activity value. The bilinear Equation 2 does not confined to such limitations. Therefore, in the present work, it has been used for optimum value determination.

We here clarify that we have though discussed the effect of individual descriptor, but the combined or converse effect of other factors/descriptors do have additional influence on the activity profile of these compounds.

nBT (Number of Bonds)

The optimum value for the number of bonds from the bilinear equation (Table 2) is 66.076. This suggests that the compounds that have number of bonds closer to this value should have good activity compared tothe rest of the compounds. This observation is supported by the lower activity of the following compounds which possess either very low or very high *nBT*: 1 (*nBT* = 45, IC_{50} = 1590 nM), 2 (*nBT* = 51, IC_{50} = 450 nM), 4 (*nBT* = 81, IC_{50} = 400 nM), 11 (*nBT* = 51, IC_{50} = 156 nM), 14 (*nBT* = 39, IC_{50} = 8130 nM) and 22 (*nBT* = 81, IC_{50} = 129 nM). A comparison of following pairs of compounds further confirms this observation: 15 (*nBT* = 60, IC_{50} = 4.0 nM) with 16 (*nBT* = 66, IC_{50} = 2.7 nM), 6

(*nBT* = 45, IC_{50} = 18 nM) with 7 (*nBT* = 51, IC_{50} = 7 nM) with 8 (*nBT* = 57, IC_{50} = 1.8 nM). Though, compound number 10 possess *nBT* = 63 (close to optimum value) but its activity is very low with IC_{50} = 129 nM. This could be attributed to high value of *F10[C-C]*, which has negative contribution towards the activity profile. Another examples are 20 (*nBT* = 75, IC_{50} = 2.0 nM), 21 (*nBT* = 78, IC_{50} = 2.9 nM) and 22 (*nBT* = 81, IC_{50} = 129 nM). In addition, similar trend is observed for 24 (*nBT* = 53, IC_{50} = 6.2 nM), 25 (*nBT* = 56, IC_{50} = 2.6 nM), 26 (*nBT* = 65, IC_{50} = 1.8 nM), 27 (*nBT* = 68, IC_{50} = 2.2 nM) and 28 (*nBT* = 71, IC_{50} = 12.0 nM). The most active compound 30 (IC_{50} = 0.9 nM) is with *nBT*= 65, which is very close to optimum value.

Sv (Sum of Atomic Van Der Waal's Volumes)

The optimum value for *Sv* is 41.753. The two most active and two least active compounds 30 (IC_{50} = 0.9 nM), 31(IC_{50} = 1.2 nM), 1(IC_{50} = 1590 nM) and 2 (IC_{50} = 450 nM) have *Sv* = 38.97, 42.17, 26.87 and 30.07, respectively. For the active compounds the value of *Sv* is close to the optimum value, while reverse is true for the least active molecules. This observation is further supported by low activity of 14 (*Sv* = 23.68, IC_{50} = 8130 nM), 4 (*Sv* = 46.05, IC_{50} = 400 nM), 22 (*Sv* = 46.05, IC_{50} = 129 nM) and 5 (*Sv* = 26.87, IC_{50} = 230 nM).

Sp (Sum of Atomic Polarizabilities)

For this descriptor *Sp*, the optimum value obtained from the bi-linear equation is 44.281. The most active compounds 30 (IC_{50} = 0.9 nM), 31(IC_{50} = 1.2 nM) and the least active compounds 1(IC_{50} = 1590 nM) and 2 (IC_{50} = 450 nM) have *Sp* = 41.07, 44.59, 28.32 and 31.85, respectively. In addition, compounds4 and 14 have *Sp* = 49.46 and 24.80 with IC_{50} = 400 and 8130 nM, respectively.

X1v (First Order Valence Connectivity Index, to Represent the Steric Factor)

For *X1v*, the optimum value obtained from the bi-linear equation is 11.790. The most active compounds 30 (IC_{50} = 0.9 nM), 31(IC_{50} = 1.2 nM) and the least active compounds 1(IC_{50} = 1590 nM) and 2 (IC_{50} = 450 nM) have *X1v* = 11.314, 12.314, 7.680 and 8.680, respectively. In addition, compound 4 and 14 possess *X1v* = 13.680 and 6.536 with IC_{50} = 400 and 8130 nM, respectively.

Lipophilicity/Hydrophobicity (in Terms of ALOGP)

In modern drug designing, lipophilicity is considered as one of the most important factors. For the present data set, the optimum value of ALOGP is 7.112 from a parabolic equation. Similar to other descriptors, the most active compounds 30 (IC_{50} = 0.9 nM), 31(IC_{50} = 1.2 nM) and the least active compounds 1(IC_{50} = 1590 nM) and 2

(IC$_{50}$ = 450 nM) have *ALOGP* = 6.970, 7.882, 3.878 and 4.790, respectively. In addition, compound 4 and 14 have *ALOGP* = 9.352 and 2.785 with IC$_{50}$ = 400 and 8130 nM, respectively. This means, the compounds that posses number of bonds closer to this value should have good activity than the rest of the compounds. This observation is supported by the lower activity of following compounds which possess either very low or very high *ALOGP*: 11 (*ALOGP* = 4.111, IC$_{50}$ = 156 nM) and 22 (*ALOGP* = 9.382, IC$_{50}$ = 129 nM). A comparison of following pairs of compounds further confirms this observation: 15 (*ALOGP* = 6.189, IC$_{50}$ = 4.0 nM) with 16 (*ALOGP* = 7.101, IC$_{50}$ = 2.7 nM), 6 (*ALOGP* = 4.008, IC$_{50}$ = 18 nM) with 7 (*ALOGP* = 4.920, IC$_{50}$ = 7 nM) with 8 (*ALOGP* = 5.832, IC$_{50}$ = 1.8 nM). Another example is 3 (*ALOGP* = 5.702, IC$_{50}$ = 130 nM), 16 (*ALOGP* = 7.101, IC$_{50}$ = 2.7 nM) and 22 (*ALOGP* = 9.382, IC$_{50}$ = 129 nM). In addition, similar trend is observed for 24 (*ALOGP* = 5.604, IC$_{50}$ = 6.2 nM), 25 (*ALOGP* = 6.060, IC$_{50}$ = 2.6 nM), 26 (*ALOGP* = 7.429, IC$_{50}$ = 1.8 nM), 27 (*ALOGP* = 7.885, IC$_{50}$ = 2.2 nM) and 28 (*ALOGP* = 8.341, IC$_{50}$ = 12.0 nM).

nAT (Number of Atoms)

Similar to *nBT*, this is a very easily interpretable and a useful descriptor for synthetic chemists. From parabolic equation, the optimum value obtained is 63.031. The active molecules possess *nAT* close to the optimum value, whereas opposite is true for the less active molecules. Examples are 1 (*nAT* = 43, IC$_{50}$ = 1590 nM), 2 (*nAT* = 49, IC$_{50}$ = 450 nM), 4 (*nAT* = 79, IC$_{50}$ = 400 nM), 11 (*nAT* = 48, IC$_{50}$ = 156 nM), 14 (*nAT* = 37, IC$_{50}$ = 8130 nM) and 22 (*nAT* = 79, IC$_{50}$ = 129 nM). A comparison of following pairs of compounds further confirms this observation: 15 (*nAT* = 58, IC$_{50}$ = 4.0 nM) with 16 (*nAT* = 64, IC$_{50}$ = 2.7 nM), 6 (*nAT* = 44, IC$_{50}$ = 18 nM) with 7 (*nAT* = 49, IC$_{50}$ = 7 nM) with 8 (*nAT* = 55, IC$_{50}$ = 1.8 nM). Other examples are 20 (*nAT* = 73, IC$_{50}$ = 2.0 nM), 21 (*nAT* = 76, IC$_{50}$ = 2.9 nM) and 22 (*nAT* = 79, IC$_{50}$ = 129 nM). In addition, similar trend is observed for 24 (*nAT* = 50, IC$_{50}$ = 6.2 nM), 25 (*nAT* = 53, IC$_{50}$ = 2.6 nM), 26 (*nAT* = 62, IC$_{50}$ = 1.8 nM), 27 (*nAT* = 65, IC$_{50}$ = 2.2 nM) and 28 (*nAT* = 68, IC$_{50}$ = 12.0 nM). To add further, the most active compound 30 (IC$_{50}$ = 0.9 nM) is with *nAT* = 62, which is very close to the optimum value.

Conclusion

In summary, the present study reveals that the non-linear models should be developed to determine optimum values of the descriptors. A good lead compound (prodiginine in the present work) can be identified and optimized if the optimum value of lipophilicity, sum of atomic van der Waal's volumes, sum of atomic polarizabilities, first order valence connectivity index, number of atoms, number of benzene-like rings and number of rotatable bond are used correctly and efficiently. The "ready to use" optimum/desirability values will be useful to the medicinal chemists in developing novel prodiginines with good anti-malarial activity profile.

Author's Contributions

Vijay H. Masand: Performed QSAR analysis and designed the research plan and organized the study.

Devidas T. Mahajan: Performed QSAR analysis and manuscript writing.

Eslam Pourbasheer: Performed QSAR analysis and manuscript writing.

Taibi Ben Hadda: Structure drawing and contributed in writing the results and discussion section.

Harsh Chauhan: Calculation of Descriptors and revised English of the manuscript.

J.M. Gajbhiye: Contributed in writing the manuscript.

A.M. Alafeefy: Contributed in writing the results and discussion section and designed the research plan and organized the study.

Ethics

This article is original and contains unpublished material. The corresponding author confirms that all of the other authors have read and approved the manuscript and no ethical issues involved.

References

Biamonte, M.A., J. Wanner, K.G. Le Roch, 2013. Recent advances in malaria drug discovery. Bioorg. Med. Chem. Lett., 23: 2829-2843. DOI: 10.1016/j.bmcl.2013.03.067

Brown, N., B. McKay and J. Gasteiger, 2006. A novel workflow for the inverse QSPR problem using multiobjective optimization. J. Comp. Aided Mol. Des., 20: 333-341. DOI: 10.1007/s10822-006-9063-1

Buchwald, P. and F. Yamashita, 2014. Bilinear model for the size-dependency of the CYP3A4 inhibitory activity of structurally diverse compounds. Mol. Inf., 33: 8-14. DOI: 10.1002/minf.201300132

Chirico, N. and P. Gramatica, 2011. Real external predictivity of QSAR models: How to evaluate it? Comparison of different validation criteria and proposal of using the concordance correlation coefficient. J. Chem. Inf. Model., 51: 2320-2335.

Chirico, N. and P. Gramatica, 2012a. Real external predictivity of QSAR models. Part 2. New intercomparable thresholds for different validation criteria and the need for scatter plot inspection. J. Chem. Inf. Model., 52: 2044-2058.

Chirico, N., E. Papa, S. Kovarich, S. Cassani and P. Gramatica, 2012b. QSARINS, software for QSAR MLR model development and validation. University of Insubria, Varese, Italy.

Doweyko, A.M., 2008. QSAR: Dead or alive? J. Comput. Aided Mol. Des., 22: 81-89. DOI: 10.1007/s10822-007-9162-7

Faulon, J.L., W. Brown and S. Martin, 2005. Reverse engineering chemical structures from molecular descriptors: How many solutions? J. Comp. Aided Mol. Des., 19: 637-650. DOI: 10.1007/s10822-005-9007-1

Gidskehaug, L., E. Anderssen and B.K. Alsberg, 2008. Cross model validation and optimisation of bilinear regression models. Chemo. Intell. Lab. Syst., 93: 1-10. DOI: 10.1016/j.chemolab.2008.01.005

Gramatica, P., 2013. On the development and validation of QSAR models. Methods Mol. Biol., 930: 499-526. DOI: 10.1007/978-1-62703-059-5_21

Gramatica, P., N. Chirico, E. Papa, S. Cassani and S. Kovarich, 2013. QSARINS: A new software for the development, analysis and validation of QSAR MLR models. J. Comput. Chem., 34: 2121-2132. DOI: 10.1002/jcc.23361

Gramatica, P., S. Cassani, P.P. Roy, S. Kovarich and C.W. Yap *et al.*, 2012. QSAR modeling is not "Push a Button and Find a Correlation": A case study of toxicity of (Benzo-)triazoles on Algae. Mol. Inf., 31: 817-835. DOI: 10.1002/minf.201200075

Hansch, C., A. Leo, S.B. Mekapati and A. Kurup, 2004. QSAR and ADME. Bioorg. Med. Chem. Lett., 12: 3391-3400. DOI: 10.1016/j.bmc.2003.11.037

Huang, J. and X. Fan, 2011. Why QSAR fails: An empirical evaluation using conventional computational approach. Mol. Pharm., 8: 600-608. DOI: 10.1021/mp100423u

Jager, T. and S.A.L.M. Kooijman, 2009. A biology-based approach for Quantitative Structure-Activity Relationships (QSARs) in ecotoxicity. Ecotoxicology, 18: 187-196. DOI: 10.1007/s10646-008-0271-4

Kubinyi, H., 2002. From narcosis to hyperspace: The history of QSAR. Quant. Struct. Act. Rel., 21: 348-356. DOI: 10.1002/1521-3838(200210)21:4<348::AID-QSAR348>3.0.CO;2-D

Mahajan, D.T., V.H. Masand, K.N. Patil, T. Ben Hadda and R.D. Jawarkar *et al.*, 2012. CoMSIA and POM analyses of anti-malarial activity of synthetic prodiginines. Bioorg. Med. Chem. Lett., 22: 4827-4835. DOI: 10.1016/j.bmcl.2012.05.115

Mahajan, D.T., V.H. Masand, K.N. Patil, T.B. Hadda and V. Rastija, 2013. Integrating GUSAR and QSAR analyses for antimalarial activity of synthetic prodiginines against multi drug resistant strain. Med. Chem. Res., 22: 2284-2292. DOI: 10.1007/s00044-012-0223-7

Mara, C., E. Dempsey, A. Bell and J.W. Barlow, 2013. Synthesis and evaluation of phenoxyoxazaphospholidine, phenoxyoxazaphosphinane and benzodioxaphosphininamine sulfides and related compounds as potential anti-malarial agents. Bioorg. Med. Chem. Lett., 23: 3580-3583. DOI: 10.1016/j.bmcl.2013.04.026

Martin, T.M., P. Harten, D.M. Young, E.N. Muratov and A. Golbraikh *et al.*, 2012. Does rational selection of training and test sets improve the outcome of QSAR modeling? J. Chem. Inf. Model., 52: 2570-2578.

Masand, V.H., D.T. Mahajan, K.N. Patil, K.D. Chinchkhede and R.D. Jawarkar *et al.*, 2012b. k-NN, quantum mechanical and field similarity based analysis of xanthone derivatives as α-glucosidase inhibitors. Med. Chem. Res., 21: 4523-4534. DOI: 10.1007/s00044-012-9995-z

Masand, V.H., D.T. Mahajan, K.N. Patil, T.B. Hadda and M.H. Youssoufi *et al.*, 2013b. Optimization of antimalarial activity of synthetic prodiginines: QSAR, GUSAR and CoMFA analyses. Chem. Biol. Drug. Des., 81: 527-536. DOI: 10.1111/cbdd.12099

Masand, V.H., D.T. Mahajan, T. Ben Hadda, R.D. Jawarkar and H. Chavan, 2013a. Molecular Docking and Quantitative Structure Activity Relationship (QSAR) analyses of indolylarylsulfones as HIV-1 non-nucleoside reverse transcriptase inhibitors. Med. Chem. Res. DOI: 10.1007/s00044-013-0647-8

Masand, V.H., R.D. Jawarkar, D.T. Mahajan, T.B. Hadda and J. Sheikh *et al.*, 2012a. QSAR and CoMFA studies of biphenyl analogs of the anti-tuberculosis drug (6S)-2-nitro-6-{[4-(trifluoromethoxy)benzyl]oxy}-6,7-dihydro-5H-imidazo [2,1-b][1,3]oxazine (PA-824). Med. Chem. Res., 21: 2624-2629. DOI: 10.1007/s00044-011-9787-x

Mitra, I., P.P. Roy, S. Kar, P.K. Ojha and K. Roy, 2010. On further application of r_m^2 as a metric for validation of QSAR models. J. Chemomem., 24: 22-33. DOI: 10.1002/cem.1268

Murugesan, D., A. Mital, M. Kaiser, D.M. Shackleford and J. Morizzi *et al.*, 2013. Discovery and structure-activity relationships of pyrrolone antimalarials. J. Med. Chem., 56: 2975-2990. DOI: 10.1021/jm400009c

Myint, K.Z. and X.Q. Xie, 2010. Recent advances in fragment-based QSAR and multi-dimensional QSAR methods. Int. J. Mol. Sci., 11: 3846-3866. DOI: 10.3390/ijms11103846

Ojha, P.K. and K. Roy, 2012. First report on exploring structural requirements of 1,2,3,4-Tetrahydroacridin-9(10H)-one analogs as antimalarials using multiple QSAR approaches: Descriptor-based QSAR, CoMFA-CoMSIA 3DQSAR, HQSAR and G-QSAR approaches. Comb. Chem. High Throughput Screen, 16: 7-21.

Papireddy, K., M. Smilkstein, J.X. Kelly S.M. Salem and M. Alhamadsheh *et al.*, 2011. Antimalarial activity of natural and synthetic prodiginines. J. Med. Chem., 54: 5296-5306.
DOI: 10.1021/jm200543y

Rastija, V., S. Nikolic and V.H. Masand, 2013. Quantitative relationships between structure and lipophilicity of naturally occurring polyphenols. Acta Chim. Slov., 60: 781-789.

Roy, K. and I. Mitra, 2012. On the use of the metric rm 2 as an effective tool for validation of QSAR models in computational drug design and predictive toxicology. Mini. Rev. Med. Chem., 12: 491-504.
DOI: 10.2174/138955712800493861

Saha, A. and K. Roy, 2012. In silico modeling for prediction of drug-induced adverse reactions and environmental hazards using QSAR tools. Curr. Drug Saf., 7: 255-256.
DOI: 10.2174/157488612804096560

Scior, T., J.L. Medina-Franco, Q.T. Do, K. Martinez-Mayorga and J.A. Yunes Rojas *et al.*, 2009. How to recognize and workaround pitfalls in QSAR studies: A critical review. Curr. Med. Chem., 16: 4297-4313.
DOI: 10.2174/092986709789578213

Tropsha, A., 2010. Best practices for QSAR model development, validation and exploitation. Mol. Inform., 29: 476-488. DOI: 10.1002/minf.201000061

Research Article

STUDIES OF ACOUSTIC BEHAVIOR OF 3-(2-BENZIMIDAZOL)-3-NITRO-6-METHYL-CHROMEN-4-ONE (BNMC) IN A DIFFERENT SOLVENTS SYSTEM BY USING ULTRASONIC INTERFEROMETER

S.A.Quazi[1], D.T.Mahajan[2], Vijay Masand[3], Noor Mohammad[4], M.R. Ingle[5]

1.   Department of chemistry, VidyaBhartiMahavidyalaya, Camp, Amravati (M.S) India

2.   Department of chemistry, Govt.Vidarbha Institute of Sci. and Humanities, Amravati (M.S) India

3.   Department of chemistry, G.S college, Khamgaon

*Corresponding Author: Email: quazi.azhar@rediffmail.com

ABSTRACT

By using various acoustic parameters ultrasonic velocity of3-(2-benzimidazol)-3-nitro-6-methyl-chromen-4 one (BNMC) in different solvent mixtures has been investigated to understand the effect of (BNMC) in interaction with water and organic solvent.

Keywords: Apparent molal adiabatic compressibility, Hydration numbers, 3-(2-benzimidazol)-3-nitro-6-methyl-chromen-4-one(BNMC),dioxane-water mixture, Interferometer.

INTRODUCTION

Vibrational waves of frequency above hearing range of normal ear are referred as Ultrasonic waves. All waves of frequencies more than 20 KHz are Ultrasonic waves. The waves are being used for detected of flaws of materials, mechanical cleaning of surface etc,in the field of technology. In medicinal science too, the waves are being used to detect cancer tumors, bone fractures, cardiology etc. In present day applications of Ultrasonic are emerging in the field of forensic sciences, space research and in wars.Studies of stability constants and thermodynamically parameters (ΔH, ΔG, ΔS) of inner transition metal ions complexes with substituted chromoneschiff bases 70% dioxane – water solvent1.Studies of some acoustic parameters of cu (No3)2 in water-dioxane mixture at 298.150k by physico -chemical

method2.Adiabatic molal Compressibility and apparent molal volumes of many electrolytes in mixed organic solvent are found out earlier3-8. Recently some co-workers have investigated acoustic parameters of some binary liquids mixture at different temperatures 9-15.Narwade et a16have studied the adiabatic compressibility and apparent molar volume of substitute pyrazoles in water-dioxane mixture.Deosarkar17have investigated the adiabaticcompressibility, apparent molar compressibility and other parameters of pyrazoles in aqueous acetone-mixture. Hydration numbers are calculated using partial molal volume and adiabatic compressibility data.Pawar18have studied the apparent molal adiabatic compressibility andhydration numbers of some peptides. Khobragadeet al19have investigated apparent molal compressibility for isoxazoline

in 70% dioxane-water mixture.This paper is in continuation to our research work on ultrasonic investigation of adiabatic molalcompressibilities and apparent molal volume of 3-(2-benzimidazol)-3-nitro-6-methyl-chromen-4-one(BNMC), dioxane- water mixture.

EXPERIMENTAL SECTION

Instruments

Pyknometer:

Pyknometer (Borosil make) are used in the present investigation for measuring the densities. Pyknometer were standardized by the standard procedure[20].

Balance

Weighing was made on MechanikiZaktadyPrecyzyjnej Gdansk balance, made in Poland (± 0.001 gm).

Ultrasonic Interferometer:

An ultrasonic interferometer MX-3 model (Mittal Enterprises, Delhi) having frequency 2MHz and accuracy ± 0.03% was used for the measurement of ultrasonic velocity in solutions.

Thermostat

A special thermostatic arrangement was done for density and ultrasonic velocity measurements. Elite Thermostatic water bath was used, in which continuous stirring of water was carried out with the help of electric stirrer and temperature variation was maintain within ± 0.1°C.

Solvents and chemicals

All chemicals are analytical reagent (AR) grade with were obtained from SdFine chemicals, India which is used as such without further purification. Water used in the experiment was demonized, distilled and degassed prior to making solutions. The cell of ultrasonic interferometer was filled fully with the solution and needle of ammeter was adjusted in the range of 20 to 60 with the help of "Adj" knob. It was warmed for 10 minutes so that the range should remain steady. Micrometer reading was noted. Screw was moved anticlockwise to get the maximum deflections of needle. To movement of screw was co untied to gate 5 deflection. After retuning back to its original position, Micrometer screw was noted. The difference between these two readings gave the distance travelled by screw for getting five maxima. From this distance required though which micrometer screw should move for one maximum was calculated by dividing it by 5. Same procedure repeated many times. The apparent molal volume (Φv) and apparent molar adiabatic compressibility (Φ K(s)) of (BNMC) in solution are determined from density (dS) and adiabatic compressibility (βs) of solution calculated by using following equations.

$$\Phi K(s) = ((\square sdo-\square ods) \llbracket 10 \rrbracket ^3)/(m \times ds \times do) + \square sM/ds \quad \ldots\ldots\ldots\ldots (1)$$

Table – 1 Ultrasonic Velocity in Distilled Water; Ultrasonic Frequency = 2 MHZ; Temp. 27± 0.1°C

Sr. No.	Number of rotation of Screw	Micrometer Reading (mm)	Difference between Reading (mm)	Distance traveled by Screw for one maxima [(D)mm]	Ultrasonic Velocity [(U)msec-1]
1	5	25.15		0.392	1649
2	10	23.17	1.86	0.393	1645
3	15	21.21	1.8	0.393	1645
4	20	19.25	1.84	0.392	1641
5	25	17.34	1.83	0.391	1637
6	30	15.32	1.82	0.3905	1633

Table - 2 Ultrasonic Velocity In 20% of ethanol-water, acetone-water & Dioxane-water mixtures

| | System - (BNMC) | | | Ultrasonic Frequency = 2 MHz | |
| | Temp. 27± 0.1°C | | | Molality = 0.0091 | |

Ultrasonic Velocity In 20% Ethanol-Water Mixture

Sr. No.	Number of rotation of Screw	Micrometer Reading (mm)	Difference between Reading (mm)	Distance traveled by Screw for one maxima [(D)mm]	Ultrasonic Velocity [(U)msec-1]
1	5	22.75		0.3840	1650
2	10	21.50	1.96	0.3825	1645
3	15	21.20	1.92	0.3878	1635
4	20	18.90	1.90	0.3844	1630
5	25	17.85	1.87	0.3851	1627
6	30	17.20	1.84	0.3867	1622
		Average		0.3850	1634

Ultrasonic Velocity In 20% Acetone- Water Mixture

1	5	27.15		0.3750	1540
2	10	26.90	1.98	0.3720	1535
3	15	25.21	1.94	0.3770	1535
4	20	23.95	1.92	0.3740	1531
5	25	22.34	1.90	0.3750	1527
6	30	21.30	1.87	0.3760	1523
		Average		0.3748	1531

Contd.

Ultrasonic Velocity In 20% Ethanol-Water Mixture				
Number of rotation of Screw	Micrometer Reading (mm)	Difference between Reading (mm)	Distance traveled by Screw for one maxima [(D)mm]	Ultrasonic Velocity [(U)msec-1]
Ultrasonic Velocity In 20% Dioxane- Water Mixture				
1	5	26.10		0.3950	1544
2	10	25.90	1.99	0.3920	1552
3	15	24.25	1.97	0.3970	1536
4	20	22.91	1.96	0.3940	1539
5	25	21.30	1.93	0.3950	1528
7	30	20.35	1.89	0.3960	1526
		Average		0.3944	1537.5

Table 3 Φ K(s) & Φ v values along with other parameters in 20% of ethanol-water, acetone-water & dioxane-water mixtures of ligand (BMNC)   Ultrasonic frequency : 2MHz   Temp 27+ 0.1°C

Parameters	Solvent percentage (v/ v) 20		
	Ethanol-Water	Dioxane- Water	Acetone- Water
Molality	0.0091	0.0091	0.0091
D_0	0.4680	0.4623	0.4666
d_0	1.0651	0.0398	0.0365
U_0	1570.0	1592.0	1559.0
B_0	46.5551	44.8001	48.6050
D_S	0.4850	0.4948	0.4632
d_S	1.0743	1.0203	1.0091
U_s msec^{-1}	1610.0	1657.0	1582.0
$\beta s \times 10^8$	44.30	40.91	48.23
$\beta s\ d_s \times 10^8$	47.5213	45.6740	45.8760
$\beta s\ d_0 \times 10^8$	45.2543	43.4876	49.5678
$\Phi K(s) \times 10^4$	0.8932	-26.4237	49.76521
Φv	540.87	2457.32	7321.10

Φ v = ((do-ds) 〖 10 〗 ^3)/(m× ds× do) + M/ds
……………….. (2)

Where, do is the density of pure solvent.

M is the molecular weight of solute

β o is adiabatic compressibility of pure solvent & βs is adiabatic compressibility of solution.

The adiabatic compressibility is calculated from ultrasonic velocity using the equation

β o= 1/ 〖 〖U0〗 ^2〗 _d0 …………for solvent

β s= 1/ 〖 〖Us〗 ^2〗 _ds …………for solution

Velocity of ultrasonic wave in solvent is represented by UO & in solution by US.

RESULTS & DISCUSSION

After the study of following observation table 1, 2 & 3 the values of ΦK(s) Φv is higher in case of acetone-water mixture than ethanol water of methanol water mixture due to electron releasing group present in acetone and difference in functional group and hydration numbers. The values of Φvis in the order as follows,

Acetone-Water > Dioxane-water > Ethanol-water at 20% solutions. After the investigation it is to be concluded that there is no regular order of ΦK(s) and Φv values for all the system.

Acknowledgement

I would like to thanks to the Principal, Vidyabharati Mahavidyalaya, Amravati and Dr. D. T. Mahajan, Dr. M. L Narwade, for providing necessary laboratory facilities.

REFERENCES

1. Noor,S.A.Quazi, Mahajan, Masand, Recent Trends in Material Preparation &Characterization, National ConferenceISBN - 978-81-929395-2-0,24th February (2014), pp86-89
2. S.A.Quazi, Mahajan, Masand, Noor,National Conference ISBN – 978-93-82588-41-2, Recent application mathematical tools in science May 8-3(2014),pp76-80
3. Kaulugud M.V., Patil K.J., Ind J. Pure and applPhys, 13,322 (1975).
4. Singh S., Singh. R, Prasald N, Prakash S,Ind. J. Pure and Appl. Phys., 15 629, (1977)
5. Reddy K.S., Sreenivasulam, Naidu P.R, Zeir. PhysicsChemic NeveFolge, 124,149 (1981)
6. Prakash O., Pandey S.P., Prakash S,Ind. J. Pure and appl. Phys, 20, 8 (1982)
7. Ragouramane D., Shrinivasrao A., Ind J. Chem, 37, 659 (1998)
8. Khobragade B.G., Ph.D Thesis in Chemistry, Amravati University Amravati (1999)
9. Pankanti S. U., Ph.D. Thesis in Chemistry, Marathwada University, Aurangabad (1986)
10. Sawalakhe P.D., Narwade M.N., Acoustica, 82, 1 (1996)
11. Mistry A.A,Bhandarkar V.D and Chimankar O.P.,J.Chem.& Pharm.Research,4(1),170-174(2012)
12. RamtekeJ.N,Adv.In appl.Sci.Res,3(3),1832-1835(2012)
13. PalanniappanL,Asian J.Mat.Sci.,4(1),21-27(2012).
14. Fakruddinsk,srivasa .c and Kolla.N. Int.J.Res.Chem.Env.2 (3), 164-167(2012)
15. Santhi.N,Alamelumangai.G,Madhumitha.J.andEmayava ambanM.Int.Lett.of Chem.Phy.&Ast.5(1),59-71(2012)
16. Narwade M.L and RamtekeA,Arch of Appl.Sci.Res.4(1),254-261(2012)
17. DeosarkarS.D,RussianJ.Phy.Chem.(A),86(10),1507-1511(2012)
18. Pawar R.B, Int.Res.J.2 (2), 281-291(2012)
19. Khobragade B.G., Meshram U.P, Der. Pharm. Chemica, 3(2), 376-382(2012)
20. Jaines,A.M,Practical Physical Chemistry,J and A.Churchill Ltd,London,88 (1961)

Theoretical based studies of ultrasonic velocities in dioxane -water mixtures of 4-bromo-2-{(e)-[(4-chlorophenyl) imino] methyl}phenol at different temperatures

Noor Mohammad[1], S.A.Quazi[2], D.T.Mahajan[2], Vijay.H.Masand[2], M.R.Ingle[3]

1)Department of Chemistry, Govt.Vidarbha Institute of Sci. and Humanities, Amravati (M.S) India
2)Department of Chemistry, Vidya Bharti Mahavidyalaya, Amravati (M.S.) India
3)Department of Chemistry, G.S.College, Khamgaon(M.S) India

ABSTRACT

Ultrasonic velocity examined from Nomoto's relation, Van Dael ideal mixing relation, impedance relation, Rao's specific velocity relation and Junjie's theory has been compared in the mixtures of 4-bromo-2-{(e)-[(4-chlorophenyl)imino]methyl}phenol as a common component with different percentage of dioxane- water mixture at 305.15, 310.15, 315.15 and 320.15 K . A good agreement has been justified between experimental and theoretical ultrasonic velocities.U^2_{exp}/U^2_{mix} has also been evaluated for non-ideality in the mixtures. The relative applicability of above theories to the present systems has been compared and discussed. The results are highlighted on the basis of molecular interactions occurring in these liquid mixtures.

Key words: Ultrasonic velocity, 4-bromo-2-{(e)-[(4-chlorophenyl) imino] methyl} phenol, dioxane- water mixture.

INTRODUCTION

Acoustics parameter like ultrasonic dealing with sound above the audible range and frequencies are higher than 20,000 Hz and their wavelengths are small. The results was showed in terms of molecular interactions, ultrasonic investigations on liquid mixtures and compared the experimental results of ultrasonic velocity with theoretical relations of Nomoto [1], Van dael and Vangeel [2],impedence relation [3], Rao's specific velocity [4] and Junjie [5] carried out by some scholars[6-10].Ultrasonic velocities in dioxane- water mixtures of 4-bromo-2-{(e)-[(4-chlorophenyl)imino]methyl}phenol(L) by using the above theoretical relations are compared with the experimental values of ultrasonic velocities at different temperatures 305.15, 310.15and 315.15 K and study the molecular interaction from the deviation in the values of U^2_{exp}/U^2_{mix} on the basis of earlier studies. Studies of acoustic behavior of 3-(2-benzimidazol)-3-nitro-6-methylchromen-4-one (BNMC) in a different solvents system by using ultrasonic interferometer[11].

EXPERIMENTAL PROCEDURE

All chemicals are analytical reagent (AR) grade with were obtained from Sd Fine chemicals, India which is used as such without further purification. After literature survey [12,13]the purity of samples was checked. The mixtures were prepared of required proportions by Job's method of continuous variation. Weighing was made on Mechaniki Zaktady Precyzyjnej Gdansk Balance, made in Poland (± 0.001 gm). The speed of sound waves was obtained by using variable path, single crystal interferometer (Mittal Enterprises, Model MX-3) with accuracy of ± 0.03% and frequency 1 MHz A special thermostatic arrangement was done for density and ultrasonic velocity measurements. Elite thermostatic water bath was used; in which continuous stirring of water was carried out with the help of electric stirrer and temperature variation was maintained within ± 0.1°C.

THEOROTICAL RELATION FOR ULTRASONIC VELOCITY

1. **Nomoto relation**

    $$U_N = [(x_1R_1+x_2R_2) / (x_1V_1+x_2V_2)]^3 \ldots\ldots\ldots\ldots\ldots\ldots..1$$

    Where, R- molar sound velocity

    $x_1$and x_2 - mole fractions of liquid mixture

    V- is molar volume.

2. **Van Dael and Vangeel relation**

    $$U_{mix} = [(x_1/M_1U^2_1 + x_2/M_2U^2_2) (x_1M_1+x_2M_2)]^{-1/2} \ldots\ldots\ldots..2$$

    Where, U_{mix}- mixing ultrasonic velocity in liquid mixture

    U_1 and U_2 -ultrasonic velocities of individual compounds.

3. Impedance relation

$$U_{Imp} = \sum x_i Z_i / \sum x_i \rho_i \dots\dots\dots\dots\dots 3$$

Where, x_i - mole fraction,

ρ_i - density of the mixture

Z_i -acoustic impedance

4. Rao's velocity

$$U_R = (\sum x_i \, r_i \, \rho_i)^3 \dots\dots\dots\dots\dots 4$$

Where, x_i - mole fraction

U_i -ultrasonic velocity,

ρi - density of the mixture

r_i -Rao's specific sound velocity = $U^{1/3}_i / \rho_i$

Z_i -acoustic impedance

5. Jungie equation

$$U_J = (x_1 M_1/\rho_1 + x_2 M_2/\rho_2)/ [\{x_1 M_1 + x_2 M_2\}^{1/2} \times \{x_1 M_1/\rho_1 U^2_1 + x_2 M_2/\rho_2 U^2_2\}]^{1/2} \dots 5$$

Where, M_1, M_2 - molecular weights of constituent components,

ρ_1 and ρ_2 -densities of constituent components.

RESULTS AND DISCUSSION

Comparative study of theoretical values of ultrasonic velocities and which obtained experimentally in the present liquid mixtures is explained the nature of interaction between the component molecules in the mixture. Theoretical study is useful in building the comprehensive theoretical model for the liquid mixtures. The theoretical values of ultrasonic velocities calculated by using the above all equations i.e. 1-5. and the experimental values for mixtures at different temperatures of 305.15, 310.15 and 315.15 K are given in below table. From table it is clear that the theoretical values of ultrasonic velocity calculated by using various theories show deviation from experimental values. Due to the limitations and approximation of these theories are responsible for the deviations of theoretical values from experimental values.

In Nomoto's theory, it is supposed that the volume does not change on mixing. On mixing of liquids, the interaction between the molecules of liquids takes place due to the presence of various factors such as dispersive forces, charge transfer, hydrogen bonding, dipole-dipole and dipole-induced dipole interactions. The deviations of experimental values from theoretical values calculated using van Dael and Vangeel equation might be due to the compressibility of the component liquids in the present mixtures. The deviations of experimental values and calculated values from impedance relation and Rao's relation simply non-additively of acoustic impedance and Rao's velocity in the liquid mixtures. In case of Junjie's relation large deviations are observed. It is reveals that, the observed deviation of theoretical values of velocity from the experimental values shows that there are molecular interactions takes place. On rising the temperature, the ultrasonic velocity values decrease in the liquid mixtures.

Theoretical results of ultrasonic velocities in liquid mixtures are showed, it is observed that out of all five theories Nomoto's theory gives best results followed by Impedance dependence relation in all the systems studied.

Table-A : Experimental and theoretical values of velocities (m.s^{-1}) in L + water- dioxane system at 305.15K

X_1	U_{exp}	U_N	U_{mix}	U_{Imp}	U_R	U_J
0.0000	1585.27	1585.27	1585.27	1585.27	1585.27	1559.10
0.0889	1600.01	1592.02	1590.08	1591.61	1591.26	1561.95
0.1799	1609.48	1598.79	1595.24	1598.05	1597.42	1564.88
0.2733	1615.80	1605.58	1600.79	1604.60	1603.76	1567.89
0.3691	1625.27	1612.39	1606.75	1611.26	1610.28	1570.98
0.4673	1631.59	1619.23	1613.17	1618.03	1616.98	1574.16
0.5682	1634.22	1626.08	1620.08	1624.92	1623.89	1577.41
0.6718	1637.90	1632.95	1627.54	1631.93	1631.01	1580.75
0.7783	1644.22	1639.84	1635.59	1639.06	1638.34	1584.17
0.8877	1650.54	1646.76	1644.28	1646.31	1645.90	1587.68
1.0002	1653.69	1653.69	1653.69	1653.69	1653.69	1591.29

Table-B: Experimental and theoretical values of velocities (m.s^{-1}) in L + Water- dioxane system at 310.15 K

X_1	U_{exp}	U_N	U_{mix}	U_{Imp}	U_R	U_J
0.0000	1465.27	1565.27	1465.27	1465.27	1465.27	1439.10
0.0889	1580.08	1572.09	1570.15	1571.68	1571.34	1542.02
0.1799	1589.59	1578.88	1575.36	1578.15	1577.54	1544.98
0.2733	1575.87	1565.65	1560.84	1564.67	1563.83	1527.97
0.3691	1605.34	1592.41	1596.75	1591.28	1590.30	1550.98
0.4673	1611.59	1599.25	1593.17	1598.05	1596.98	1554.19
0.5682	1614.24	1606.08	1600.10	1604.92	1603.89	1557.43
0.6718	1617.90	1612.97	1617.56	1611.95	1611.04	1560.78
0.7783	1624.24	1619.84	1615.63	1619.08	1618.34	1564.19
0.8877	1630.56	1626.78	1624.29	1626.31	1625.92	1567.70
1.0002	1633.69	1633.69	1633.68	1633.70	1633.69	1571.31

Table-C: Experimental and theoretical values of velocities (m.s^{-1}) in L + Water- dioxane system at 315.15 K

X_1	U_{exp}	U_N	U_{mix}	U_{Imp}	U_R	U_J
0.0000	1460.25	1560.25	1460.25	1460.25	1460.25	1434.10
0.0889	1575.08	1567.04	1570.14	1566.66	1555.34	1546.06
0.1799	1584.57	1573.88	1570.36	1578.10	1572.55	1540.99
0.2733	1555.87	1545.65	1540.84	1544.67	1543.83	1507.99
0.3691	1585.34	1572.41	1576.75	1571.28	1570.30	1530.99
0.4673	1591.59	1579.25	1573.17	1578.05	1576.98	1534.21
0.5682	1594.24	1586.08	1580.10	1584.92	1583.89	1537.45
0.6718	1597.90	1592.97	1597.56	1591.95	1591.04	1540.79
0.7783	1604.24	1599.84	1595.63	1599.08	1598.34	1544.19
0.8877	1610.56	1606.78	1604.29	1606.31	1605.92	1547.72
1.0002	1613.69	1613.69	1613.68	1613.70	1613.69	1551.33

REFERENCES
[1] O Nomoto. J. Phys. Soc. Jpn., 1958, 13, 1528.
[2] C Subhash Bhatia; Rachana Bhatia; Gyan P Dubey. J. Mol. Liq., 2010, 152, 39.
[3] S Baluja; P H Parsania. Asian J. Chem., 1995, 7, 417.
[4] D Sravan kumar; D Krishna Rao. Indian J. Pure Appl. Phys., 2007, 45, 210.
[5] S Azhagiri; S Jayakumar; R Padmanaban; S Gunasekaran; S Srinivasan. J. Sol. Chem., 2009, 38, 441.
[6] S R Aswale; S S Aswale; A B Dhote; D T Tayade. J. Chem. Pharm. Res., 2011, 3(6), 233.
[7] K Narendra; P Narayanamurthy; Ch Srinivasu. IJCMI, 2010, 2, 55.
[8] R Uvarani; S Punitha. E J. Chem., 2009, 6, 235.
[9] M Aravinthraj; S Venkatesan; D meera. J. Chem. Pharm. Res., 2011, 3(2), 623.
[10] K Narendra; K B B Tulasi; K Babu Rao; S S J Srinivas; M Sarath Babu. RJPBCS, 2011, 2(4), 916.
[11] Quazi S. A. Mahajan, Vijay Masand, Noor Mohammad,Ingle, Int. J. Res. Dev. Pharm. L. Sci , August - September, 2014, 3(5), 1206-1210
[12] Jagan Nath. Fluid Phase Equi., 1995, 109, 39.
[13] K Narendra; Ch Srinivasu; Sk Fakruddin; P Narayana Murthy. J. Chem. Pharm. Res., 2012, 4(1), 686.

Article

Synthesis, X-ray Diffraction, Thermogravimetric and DFT Analyses of Pyrimidine Derivatives

Assem Barakat [1,2,†,*], **Hany J. Al-Najjar** [1,†]**, Abdullah M. Al-Majid** [1,†]**, Syed F. Adil** [1,†]**, Mohamed Ali** [3,†]**, Vijay H. Masand** [4,†]**, Hazem A Ghabbour** [5,†] **and Hoong-Kun Fun** [5,6,†]

[1] Department of Chemistry, College of Science, King Saud University, P.O. Box 2455, Riyadh 11451, Saudi Arabia

[2] Department of Chemistry, Faculty of Science, Alexandria University, P.O. Box 426, Ibrahimia, Alexandria 21321, Egypt

[3] Petrochemical Research Chair, Department of Chemistry, College of Science, King Saud University, B.O. 2455, Riaydh 11451, Saudi Arabia

[4] Department of Chemistry, Vidya Bharati College, Amravati, Maharashtra 444602, India

[5] Department of Pharmaceutical Chemistry, College of Pharmacy, King Saud University, P.O. Box 2457, Riyadh 11451, Saudi Arabia

[6] X-ray Crystallography Unit, School of Physics, Universiti Sains Malaysia, 11800 USM, Penang, Malaysia

[†] These authors contributed equally to this work.

[*] Author to whom correspondence should be addressed; E-Mail: ambarakat@ksu.edu.sa; Tel.: +96-6146-75884; Fax: +96-6146-75992.

External Editor: Derek J. McPhee

Abstract: An eco-benign synthesis of pyrimidine derivatives **2a**,**b** containing different functional groups with different electronic character starting from nitroalkenes **1a** and **2b** has been described. The structures for **1a** and **2a**,**b** have been characterized by single crystal X-ray diffraction analysis. The thermal data of the molecules pointed towards important structural aspects of their stability. The mechanism of their thermal decomposition is discussed. The thermodynamic parameters of the dissociation steps were evaluated and discussed. DFT calculations reveal that the compound **1a** possesses a high calculated dipole moment value (8.28 D) which indicates its high reactivity towards its surrounding molecules.

---

1. Introduction

Pyrimidine and its derivatives, which are important *N*-heterocyclic molecules, have received the consideration of researchers due to their significant biological and pharmaceutical properties. Pyrimidine and its derivatives have immense importance as antibiotics, and as crucial parts of many vitamins, and coenzymes. Indeed, some of them are the basic constituents of DNA and RNA, and play an important role in the constitutional properties of nucleic acids. Pyrimidine-derived biomolecules have received much attention from spectroscopists, drug, clinical, and industrial researchers because of their therapeutic importance [1–9]. Barbiturates (barbituric acid derivatives) are a class of central nervous system depressants, [10] utilized as sedatives, sleeping agents, hypnotics, anxiolytics, anticonvulsants, and anesthetics [7]. In addition, they have additional pharmacological activities as antioxidant anxiolitics, analeptics, anti-AIDA, immunomodulatory, anticancer agents and in other psychiatric disorders, and possess effects on motor and sensory functions [11–15] For example, phenobarbital, a 5-alkylated barbituric acid, was reported to exhibit sedative and hypnotic properties, and most importantly is an anticonvulsant [16].

In continuation of our research program [17–23], in the present work, the structures of some pyrimidine derivatives were characterized for the first time by single-crystal crystallography and TGA studies. DFT calculations were undertaken to study the optimized molecular structural parameters, vibrational frequencies, thermodynamic parameters, total dipole moment and HOMO-LUMO energy gap for the synthesized molecules using B3LYP/6-311G(d,p) basis set. The findings of these spectroscopic and theoretical studies are reported herein.

2. Results and Discussion

2.1. Synthesis of the Pyrimidine Derivatives

Green chemistry is being increasingly exploited as a powerful tool for the generation of privileged medicinal scaffolds and fine chemicals due to its numerous advantages, such as providing high enantio- and regioselectivity and more environmentally friendliness.

Recently, research groups have become involved in using green chemistry as a synthetic tool for the generation of valuable scaffolds to achieve new biological knowledge. The chemistry used in this paper involves an aqueous diethylamine catalyzed Michael addition of 1,3-dimethylbarbituric acid to nitro-olefins at room temperature for less than 1 h [16] (Scheme 1).

2.2. X-ray Crystal Structures

The structures of **1a** and **2a**,**b** were confirmed by single crystal X-ray analysis (Figure 1). Tables 1–7 display the crystal data and main geometrical parameters of the compounds.

X-ray analysis was performed using a Bruker Apex II D8 Venture diffractometer (Bruker AXS GmbH, Karlsruhe, Germany). The data were processed with SAINT and corrected for absorption using

SADABS [24]. The structure was solved by direct method using the program SHELXTL [25] and were refined by full-matrix least squares technique on F^2 using anisotropic displacement parameters. The non-hydrogen atoms were refined anisotropically. In these compounds, all the H atoms were calculated geometrically with isotropic displacement parameters set to 1.2 times the equivalent isotropic U values of the parent carbon atoms.

Scheme 1. Synthesis of pyrimidine derivatives **2a** and **2b**.
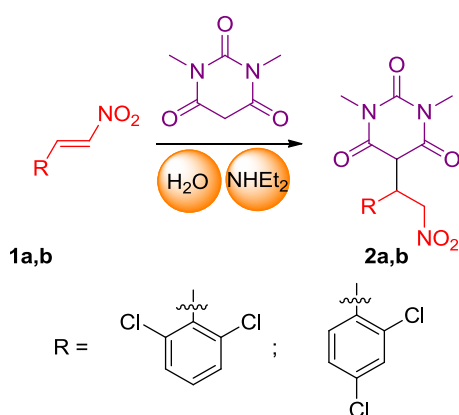
Figure 1. ORTEP diagrams of the structures of **1a** and **2a**,**b**.

| (1a) | (2a) | (2b) |
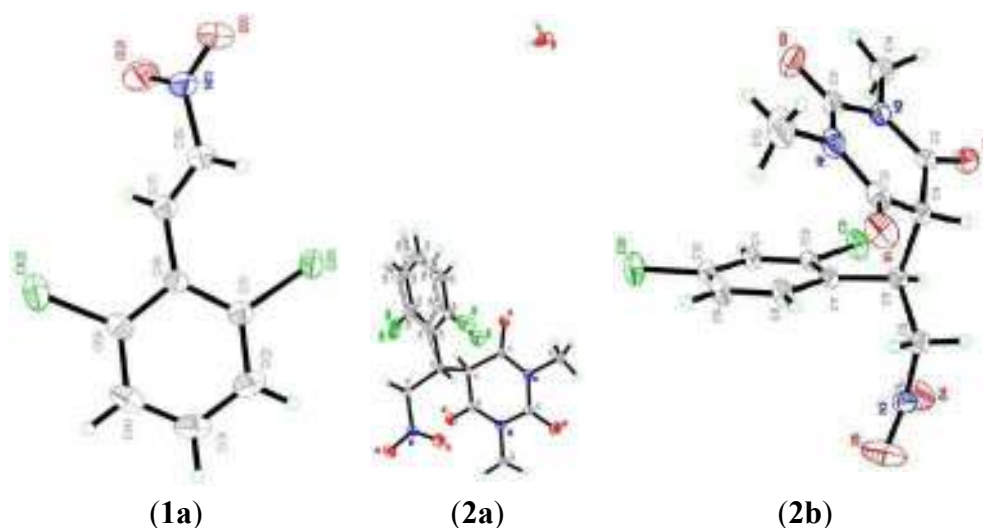
The title compound **1a**, $C_8H_5Cl_2NO_2$, which crystallizes in the monoclinic space group P 21/c comprises one crystallographically independent molecule in its asymmetric unit, as depicted in Figure 1. In the crystal structure (Figure 2A), there is an intramolecular C7-H7A···O2 hydrogen bond. The crystal is essentially consolidated by Van Der Waals interactions. The crystal data and parameters for structure refinement of the title compound are given in Table 1. Selected geometric parameters are given in Table 2. H-bonding interactions are listed in Table 3.

The title compound **2a**, $C_{14}H_{13}Cl_2N_3O_5 \cdot H_2O$, which crystallizes in the trigonal space group R-3 comprises one crystallographically independent molecule with disorder in the phenyl ring and a water molecule in its asymmetric unitas shown in Figure 1. Figure 2B shows the crystal packing for the major and minor components of **2a** respectively with occupancy ratio 0.755:0.245. There are two intermolecular C6-H6A···O2 and C9-H9A···O3 hydrogen bonds (Table 5). The crystal structure is

further consolidated by Van Der Waals interactions. The crystal data and parameters for structure refinement of the title compound are given in Table 1. Selected geometric parameters are given in Table 4. H-bonding interactions are listed in Table 5.

Figure 2. Crystal packings of (**A**) **1a**, (**B**) **2a** and (**C**) **2b**.

(**A**)

(**B**)

Packing of major component of disorder   Packing of minor component of disorder

(**C**)
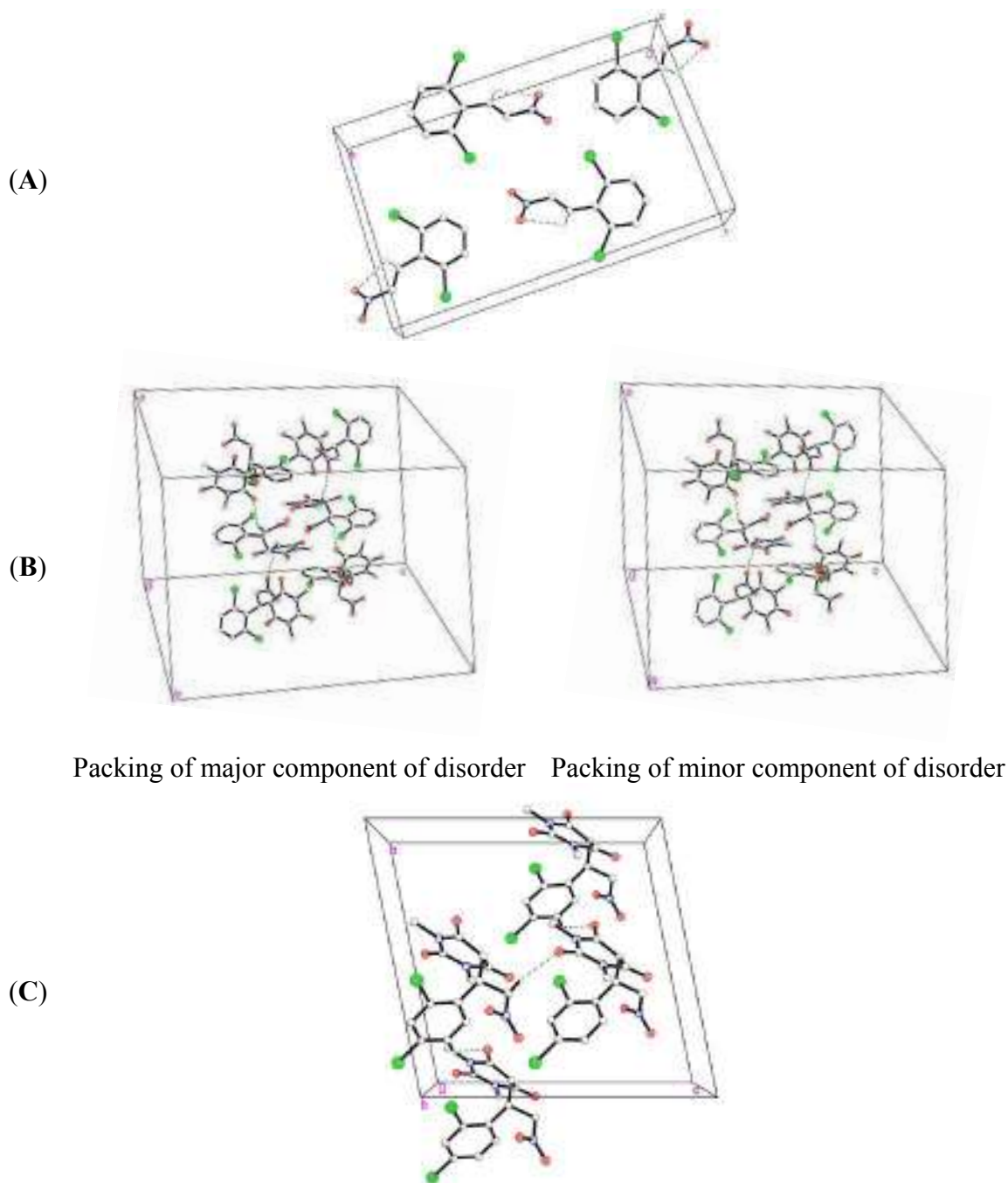
The title compound **2b**, $C_{14}H_{13}Cl_2N_3O_5$, which crystallizes in the monoclinic space group Cc comprises one crystallographically independent molecule in its asymmetric as shown in Figure 1. In the crystal structure (Figure 2C), there are two intermolecular C6-H6A⋯O1 and C13-H13C⋯O5 hydrogen bonds (Table 7). The crystal is further consolidated by Van Der Waals interactions. The crystal data and parameters for structure refinement of the title compound are given in Table 1. Selected geometric parameters are given in Table 6. H-bonding interactions are listed in Table 7.

Table 1. Crystal and experimental data of compounds **1a**, **2a** and **2b**.

Parameters	Compound 1a	Compound 2a	Compound 2b
Empirical formula	$C_8H_5Cl_2NO_2$	$C_{14}H_{13}Cl_2N_3O_5 \cdot H_2O$	$C_{14}H_{13}Cl_2N_3O_5$
Formula weight	218.03	391.02	374.17
Temperature	293(2) K	293(2) K	293(2) K
Wavelength (Mo $K\alpha$ radiation, λ)	0.71073 Å	0.71073 Å	0.71073 Å
Crystal system	monoclinic	trigonal	Monoclinic
Space group	P 21/c	R-3	Cc
Unit cell dimensions	a = 3.8395 (1) Å, α = 90.00° b = 19.8653 (7) Å β = 90.6258 (10)° c = 11.9619 (4) Å, γ = 90.00°	a = 18.0177(7) Å, α = 90.00° b = 18.0177(7) Å, β = 90.00° c = 26.6558(9) Å, γ = 120.00°	a = 12.9432 (4) Å, α = 90.00° b = 9.3084 (4) Å, β = 101.3572 (16)° c = 13.4650 (5) Å, γ = 90.00°
Volume	912.31 (5)Å^3	7494.1(6) Å^3	1590.51 (11) Å^3
Z	4	6	4
Density (calculated)	1.587 Mg/m^3	1.535 Mg/m^3	1.563 Mg/m^3
Absorption coefficient	0.67 mm^{-1}	0.424 mm^{-1}	0.439 mm^{-1}
F(000)	440	3564	768
Crystal size	0.58 × 0.35 × 0.27 mm	0.33 × 0.21 × 0.09 mm	0.57 × 0.35 × 0.26 mm
Theta range for data collection	2.7 to 30.5°.	2.3 to 30.6°.	2.7 to 30.6°.
Index ranges	−5 ≤ h ≤ 5, −28 ≤ k ≤ 28, −17 ≤ l ≤ 17	−25 ≤ h ≤ 25, −25 ≤ k ≤ 25, −38 ≤ l ≤ 38	−18 ≤ h ≤ 18, −13 ≤ k ≤ 13, −19 ≤ l ≤ 19
Reflections collected/ unique	41303/2404 [R(int) = 0.042]	107278/5130 [R(int) = 0.059]	35961/4754 [R(int) = 0.024]
Completeness to theta = 30.57°	99.8%	99.6%	99.6%
Absorption correction	multi-scan	multi-scan	multi-scan
Refinement	method Full-matrix least-squares on F^2	method Full-matrix least-squares on F^2	method Full-matrix least-squares on F^2
Goodness-of-fit on F^2	1.04	1.03	1.27
Largest diff. peak and hole	0.28 and −0.22 e.Å^{-3}	0.72 and −0.26 e.Å^{-3}	0.22 and −0.25 e.Å^{-3}

Table 2. Selected geometric parameters (Å, °) of compound **1a**.

Bond	Experimental	Calculated
Cl1-C1	1.7320 (13)	1.7314
Cl2-C5	1.7295 (14)	1.7405
O1-N1	1.222 (2)	1.2370
O2-N1	1.211 (2)	1.2372
N1-C8	1.4563 (18)	1.4511
Atom Angle	**Experimental**	**Calculated**
O1-N1-O2	124.37 (14)	125.1111
O1-N1-C8	115.73 (14)	115.6492
O2-N1-C8	119.90 (14)	119.2397
Cl1-C1-C2	117.62 (11)	124.7209
Cl1-C1-C6	120.34 (9)	113.6358
Cl2-C5-C4	118.18 (11)	114.3525
Cl2-C5-C6	119.58 (10)	123.4094
N1-C8-C7	120.57 (13)	119.8515

Table 3. Hydrogen-bond geometry (Å, °) of compound **1a**.

D-H···*A*	*D*-H	H···*A*	*D*···*A*	*D*-H···*A*
C7-H7A···O2	0.9300	2.4000	2.7323 (18)	101.00

Table 4. Selected geometric parameters (Å, °) of compound **2a**.

Bond	Experimental	Calculated
Cl1A-C8A	1.738 (4)	1.7277
Cl1B-C8B	1.721 (14)	NC
Cl2A-C12A	1.751 (6)	1.7365
Cl2B-C12B	1.715 (14)	NC
O1-C1	1.204 (2)	1.2278
O2-C2	1.205 (2)	1.2325
O3-C3	1.212 (2)	1.2276
O4-N3	1.196 (3)	1.2362
O5-N3	1.215 (3)	1.2378
O1W-O1W [i]	0.969 (19)	NC
O1W-O1W [ii]	0.97 (2)	NC
N1-C1	1.378 (2)	1.3855
N1-C13	1.473 (3)	1.4513
N1-C2	1.382 (2)	1.3724
N2-C2	1.387 (3)	1.3925
N2-C14	1.463 (3)	1.4515
N2-C3	1.370 (2)	1.3881
N3-C6	1.500 (2)	1.4962
Atom Angle	**Experimental**	**Calculated**
O1W [ii]-O1W-O1W [i]	60.0 (18)	NC
C1-N1-C2	124.36 (15)	122.9525

Table 4. *Cont.*

Atom Angle	Experimental	Calculated
C2-N1-C13	117.61 (15)	117.6313
C1-N1-C13	117.39 (15)	117.0595
C2-N2-C3	124.74 (15)	123.0628
C3-N2-C14	117.62 (17)	116.9594
C2-N2-C14	117.50 (16)	117.4505
O4-N3-C6	121.03 (18)	117.2445
O4-N3-O5	123.45 (19)	125.7819
O5-N3-C6	115.53 (16)	116.9697
O1-C1-N1	121.69 (16)	123.7575
O1-C1-C4	121.91 (15)	122.9936
N1-C1-C4	116.24 (15)	113.2488
O2-C2-N2	120.68 (18)	123.3871
N1-C2-N2	117.42 (14)	116.2983
O2-C2-N1	121.9 (2)	121.7454
O3-C3-C4	121.55 (15)	123.7560
O3-C3-N2	121.13 (15)	121.7802
N2-C3-C4	117.24 (14)	112.8565
N3-C6-C5	112.43 (14)	111.9825
Cl1A-C8A-C7A	119.7 (3)	124.0885
Cl1A-C8A-C9A	117.4 (3)	114.4806
Cl1B-C8B-C9B	116.7 (10)	NC
Cl1B-C8B-C7B	121.7 (9)	NC
Cl2A-C12A-C7A	120.8 (3)	122.7008
Cl2A-C12A-C11A	114.7 (4)	115.2511
Cl2B-C12B-C7B	122.5 (8)	NC
Cl2B-C12B-C11B	114.4 (10)	NC

Symmetry codes: (i) $-x + y + 1$, $-x + 1$, z; (ii) $-y + 1$, $x - y$, z. NC: Not calculated.

Table 5. Hydrogen-bond geometry (Å, °) of compound **2a**.

D-H⋯*A*	*D*-H	H⋯*A*	*D*⋯*A*	*D*-H⋯*A*
O1W-H2W1⋯O1W [iii]	0.9100	2.1000	2.859 (6)	140.00
O1W-H2W1⋯O1W [iv]	0.9100	1.8500	2.689 (6)	152.00
O1W-H2W1⋯O1W [v]	0.9100	2.0500	2.689 (7)	125.00
C5-H5A⋯O4	0.9800	2.2700	2.741 (3)	108.00
C6-H6A⋯O1 [vi]	0.9700	2.5300	3.337 (3)	141.00
C6-H6B⋯Cl2A	0.9700	2.6800	3.125 (4)	109.00
C6-H6B⋯O3	0.9700	2.5800	2.979 (2)	105.00
C13-H13A⋯O2	0.9600	2.2900	2.716 (3)	106.00
C13-H13C⋯O5 [vii]	0.9600	2.5100	3.425 (3)	159.00
C14-H14B⋯O2	0.9600	2.2400	2.690 (4)	108.00

Symmetry codes: (iii) $-x + 4/3$, $-y + 2/3$, $-z + 2/3$; (iv) $y + 1/3$, $-x + y + 2/3$, $-z + 2/3$; (v) $x - y + 1/3$, $x - 1/3$, $-z + 2/3$; (vi) $y - 1/3$, $-x + y + 1/3$, $-z + 4/3$; (vii) $-x + y$, $-x$, z.

Table 6. Selected geometric parameters (Å, °) of compound **2b**.

Bond	Experimental	Calculated
Cl1-C12	1.7310 (11)	1.7247
Cl2-C10	1.7338 (13)	1.7195
O1-C1	1.2101 (19)	1.2276
O2-C2	1.219 (2)	1.2325
O3-C3	1.2148 (16)	1.2278
O4-N3	1.212 (2)	1.2362
O5-N3	1.204 (3)	1.2378
N1-C1	1.376 (2)	1.3881
N1-C2	1.386 (2)	1.3925
N1-C13	1.469 (2)	1.4515
N2-C2	1.3947 (19)	1.4071
N2-C3	1.3661 (16)	1.3855
N2-C14	1.471 (2)	1.4513
N3-C6	1.496 (2)	1.4962
Atom Angle	**Experimental**	**Calculated**
C1-N1-C2	124.73 (12)	122.7743
C1-N1-C13	117.37 (15)	117.4505
C2-N1-C13	117.89 (15)	117.0006
C2-N2-C3	124.33 (11)	122.9525
C2-N2-C14	117.89 (12)	117.0593
C3-N2-C14	117.64 (12)	117.6313
O4-N3-O5	122.4 (2)	125.7819
O4-N3-C6	118.79 (15)	116.9697
O5-N3-C6	118.86 (17)	117.2445
O1-C1-N1	122.31 (14)	123.3871
O1-C1-C4	120.81 (13)	123.7560
N1-C1-C4	116.80 (12)	112.8565
O2-C2-N1	121.70 (15)	121.7802
O2-C2-N2	120.54 (14)	121.7454
N1-C2-N2	117.74 (12)	116.2983
O3-C3-N2	121.68 (12)	123.7575
O3-C3-C4	121.06 (11)	122.9936
N2-C3-C4	117.18 (10)	113.2488
N3-C6-C5	109.74 (11)	111.9825
Cl2-C10-C9	118.98 (10)	119.8634
Cl2-C10-C11	119.27 (9)	119.9545
Cl1-C12-C7	121.01 (8)	123.6597
Cl1-C12-C11	116.44 (9)	115.4596

Table 7. Hydrogen-bond geometry (Å, °) of compound **2b**.

D-H⋯*A*	*D*-H	H⋯*A*	*D*⋯*A*	*D*-H⋯*A*
C6-H6A⋯O2 ^i	0.9700	2.3900	3.222 (2)	144.00
C6-H6B⋯O1	0.9700	2.5500	3.118 (2)	117.00
C9-H9A⋯O3 ^ii	0.9300	2.5100	3.2290 (18)	134.00
C13-H13B⋯O2	0.9600	2.3100	2.727 (3)	105.00
C14-H14C⋯O2	0.9600	2.2700	2.715 (2)	107.00

Symmetry codes: (i) *x*, −*y* + 1, *z*+1/2; (ii) *x* − 1/2, *y* + 1/2, *z*.

2.3. Optimized Molecular Geometry

From the XRD data, it is clear that the compounds **1a** and **2b** possess monoclinic, whereas, **2a** has trigonal crystal structures. The cell dimensions and other data are tabulated in Table 1. Selected values of experimental and DFT calculated geometric parameters for the compounds are listed in Tables 2, 4, 6 and 8. Figure 3 shows the optimized structures for **1a** and **2a**,**b**.

Table 8. Optimized calculations of various parameters for **1a** and **2a**,**b** using B3LYP/6-311G basis set.

Parameter	1a	2a	2b
Heat of Formation (kcal/mol)	22.075	−100.903	−99.472
Total Energy (kcal/mol)	−896424.216	−1244859.443	−102495.469
Dipole (Debye)	8.281	4.116	3.848
HOMO energy (eV)	−10.019	−10.575	−10.813
LUMO energy (eV)	−4.320	−2.278	−2.383
HOMO–LUMO energy gap (eV)	5.699	8.297	8.430

Figure 3. The optimized structures for **1a** and **2a**,**b**.

| 1a | 2a | 2b |
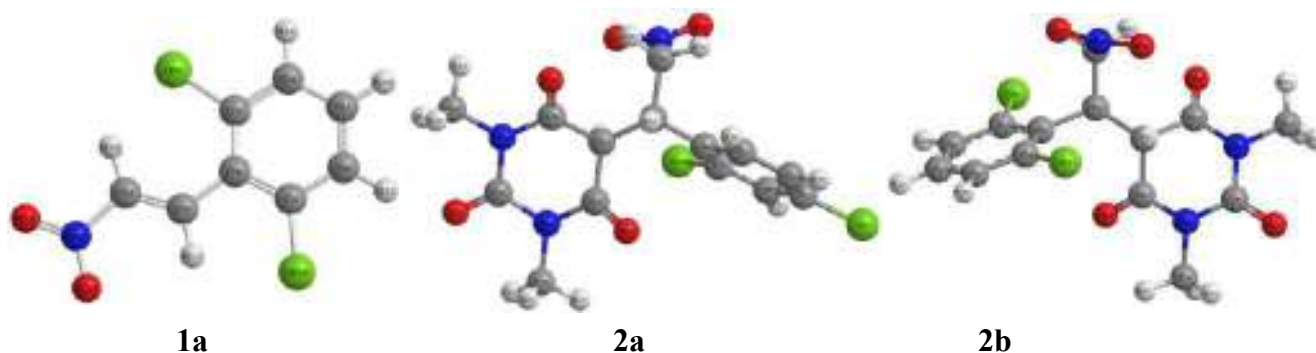
Figure 4 shows the experimental and calculated (B3LYP/6-311G) IR spectrum for **1a** and **2a**,**b**. A comparison of predicted (B3LYP/6-311G) with experimental IR reveals that B3LYP/6-311G basis set gives reasonable deviations from the experimental values. The discrepancies observed between the calculated and the experimental vibrational frequencies may be attributable to the fact that the calculations have been actually performed on a single molecule in the gaseous state contrary to the experimental values recorded in the solid state in the presence of intermolecular interactions.

Figure 4. Experimental and calculated IR spectra for **1a** and **2a**,**b**.

| **1a** | Calculated | Experimental |

| **2a** | Calculated | Experimental |

| **2b** | Calculated | Experimental |
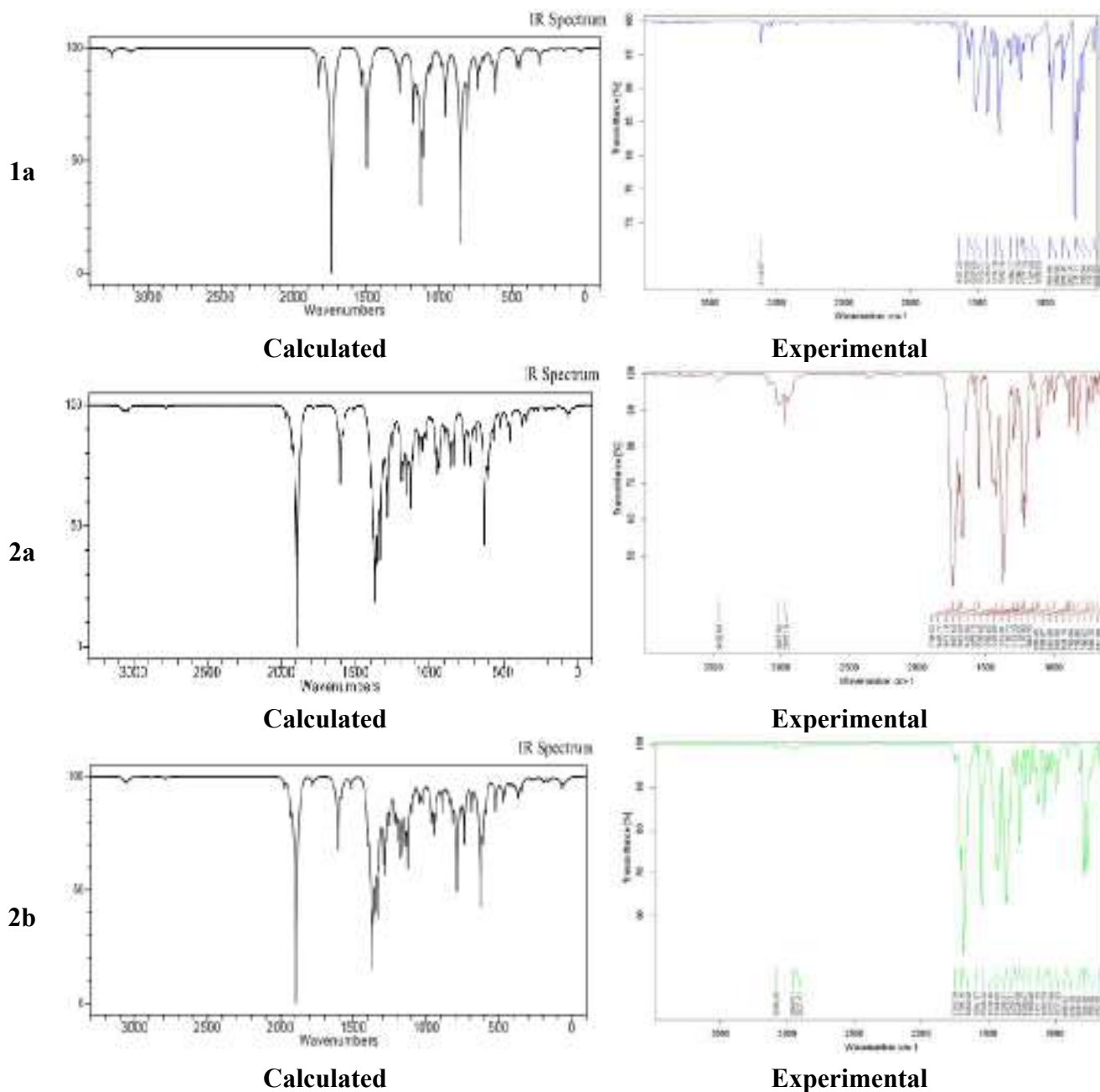
2.4. Experimental and Calculated IR Vibrations

The calculated (B3LYP/6-311G) and experimental C-H, C-Cl, N=O, C=O, and C=C vibration values for all the molecules have good agreement, except for C=O for **2a**. For **2a**, the computed C=O stretching vibrations at 1894 cm^{-1} deviated substantially from the experimental result. A plausible reason for this could be the intermolecular interactions present in solid state whereas during DFT calculations the molecule is assumed to be in isolated gaseous state.

2.5. Geometric Parameters

The solid state X-ray structure analysis revealed disorder in the phenyl moiety for **2a** (see Figure 2). This incongruity noted between the calculated and the experimental vibrational frequencies may be due

to the fact that the calculations have been actually performed on a single molecule in the gaseous state contrary to the experimental values recorded in the solid state. In DFT calculations, bond lengths and angles have been reported only for the major component of the phenyl moiety of **2a** (designated by the suffix "A"). The selected calculated and experimental geometric parameters for **1a** and **2a**,**b** have been tabulated in Tables 2, 4 and 6.

2.6. Thermal Gravimetric Analysis (TGA)

The synthesized novel compounds were subjected to thermogravimetric analysis (TGA) to evaluate their thermal stability and degradation patterns (Table 9) and the TGA and DTG patterns are shown in Figure 5. All samples were subjected to analysis in a nitrogen atmosphere in the temperature range from 30 °C to 800 °C with a heating ramp rate of 10 °C per min. It was observed that the different nitrostyrene derivatives displayed different thermal stabilities and degradation patterns. The pyrolysis processes of the materials are characterized by single-stage degradation, with an exception of **2a**, which displays two-stage degradation. Interestingly, it was detected that upon the incorporation of the barbituric acid ring into the styrene, the resulting molecule was slightly more thermally stable than its precursor. The weight loss pattern of all the compounds was found to be different at different intervals with **1a**,**b** displaying a weight loss of 70% and 98% respectively at 200 °C, but at the same temperature the weight loss percentage for the barbituric acid derivatives **2a**,**b** were found to be 48% and 18 % respectively. When a comparison of thermal degradation pattern between **1a** and **2a** was made it was found that **1a** undergoes single stage degradation with decomposition range of 100–190 °C (90 °C), while **2a** displays two stage degradation with decomposition taking place in the range of 105–195 °C (90 °C) and 200–275 °C (75 °C). The degradation temperature range of **1b** and **2b** was found to take place at a 162–262 °C (100 °C) and 125–230 °C (105 °C), respectively. The peak temperature of **2b** (220.02 °C) was higher than that of **1b** (199.38 °C), while the decomposition intensity of **1b** was found to be high with 2.35 wt %/°C compared to 1.99 wt %/°C **2b**. This behaviour can be attributed to the presence of barbituric acid. However, when the temperature was increased further all the compounds followed similar weight loss patterns with varying percentages of residue at the final temperature of 800 °C. From the residual weight values obtained at ~800 °C it can be concluded that there is no significant thermal stability among any of the four compounds tested, however it can be said that thermal stability of the barbituric acid derivative of the styrene molecule is slightly improved compared to that of its precursor. The weight loss percentage at different temperatures is mentioned in the table below and a comparative graphical representation of the compounds is given in Figure 5. A detailed study into the thermal behaviour of the synthesized compounds shall be carried out the thermal kinetics will be reported separately.

Table 9. Weight loss percentage at different temperatures for **1a**,**b** and **2a**,**b**.

Temperature	Weight Loss (%)			
	1a	**2a**	**1b**	**2b**
100	0.33	0.63	1.42	0.44
200	70.85	48.06	98.37	18.45
300	98.72	91.07	98.46	84.73

Table 9. *Cont.*

Temperature	Weight Loss (%)			
	1a	**2a**	**1b**	**2b**
400	98.98	93.95	98.40	88.19
500	99.11	95.67	98.29	92.93
600	99.56	96.47	98.08	96.10
700	99.77	97.14	97.87	98.52
800	99.66	97.47	97.55	99.81

Figure 5. TGA and DTG curves of the synthesized compounds.
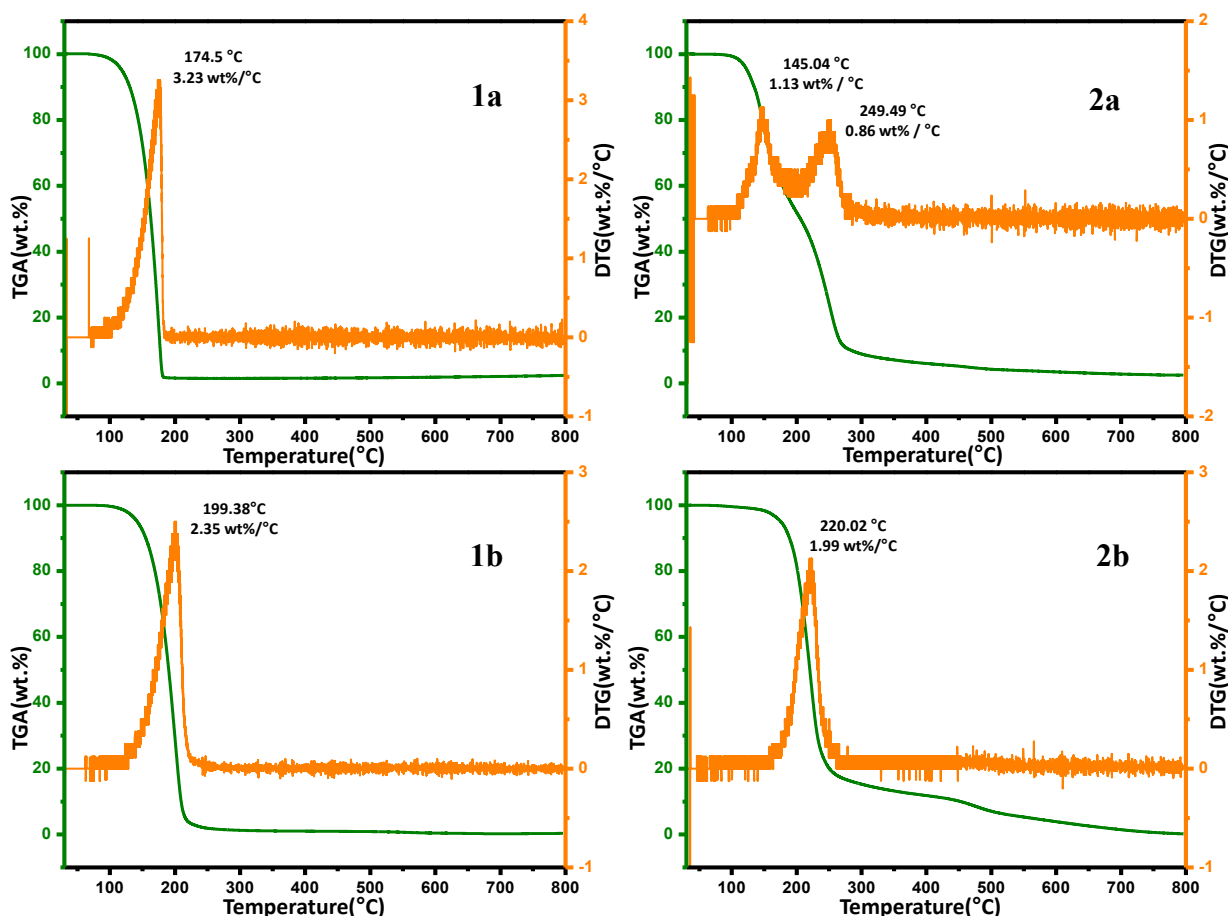
3. Experimental Section

3.1. General

All the chemicals were purchased from Aldrich (Riedstraße, Germany), Sigma-Aldrich (St. Louis, MO, USA), Fluka (Buchs, Switzerland), and used without further purification, unless otherwise stated. The structure of **1a** was confirmed by X-ray crystal structure analysis (Bruker AXS GmbH, Karlsruhe, Germany). The crystallographic data for **1a** (CCDC-992700), **2a** (CCDC-992327) and **2b** (CCDC-992701) have been submitted to the Cambridge Crystallographic Data Centre (www.ccdc.cam.ac.uk/data_request/cif). Compound **1a** was prepared from 2,6-dicholorobenzaldehyde and nitromethane as white crystals according to the reported procedure [16]. Colorless block-shaped

crystals of the compound suitable for X-ray analysis were formed in isopropanol/heptane at room temperature after 3 days.

3.2. 5-(1-(2,6-Dichlorophenyl)-2-nitroethyl)-1,3-dimethylpyrimidine-2,4,6(1H,3H,5H)-trione (**2a**)

According to the reported procedure [16], **2a** was prepared from 1,3-dimethylbarbituric acid (**1a**) and (*E*)-2,6-dichloro-1-(2-nitrovinyl)benzene (**1a**) as white crystals. Colorless block-shaped crystals of the compound suitable for X-ray analysis were formed in $CHCl_3/Et_2O$ at room temperature after 2 days.

3.3. 5-(1-(2,4-Dichlorophenyl)-2-nitroethyl)-1,3-dimethylpyrimidine-2,4,6(1H,3H,5H)-trione (**2b**)

According to the reported procedure [16], **2b** was prepared from 1,3-dimethylbarbituric acid and (*E*)-2,4-dichloro-1-(2-nitrovinyl)benzene (**1a**) as yellow crystals. Colorless block-shaped crystals of the compound suitable for X-ray analysis were formed in DCM/Pet. ether at room temperature after 1 day.

3.4. DFT Calculations

The DFT calculations were performed using the GAMESS package. The input geometry of the synthesized molecules were optimized without imposing any external constraint on the potential energy surfaces generated by the B3LYP/6-311G(d,p) basis set for C, O, N and H atoms. The resulting optimized geometry was used as an input for vibrational frequencies calculations, with inclusion of polarization functions to handle the polar bonds such as N=O, C=O, *etc.*

4. Conclusions

In a summary, pyrimidine derivatives **2a**,**b** were prepared starting from nitroalkenes **1a**,**b** using an eco-benign method. The structures for **1a** and **2a**,**b** have been characterized by their single crystal X-ray diffraction analysis. DFT/TGA/IR analyses were performed and discussed.

Supplementary Materials

Supplementary materials can be accessed at: http://www.mdpi.com/1420-3049/19/10/17187/s1.

Acknowledgments

Author Contributions

Hany J. Al-Najjar and Mohamed Ali carried out the experimental part; Syed F. Adil carried out thermo-analysis; Vijay H. Masand carried out computational studies; Hazem A Ghabbour and Hoong-Kun Fun carried out X-ray part; Abdullah M. Al-Majid helped in the results and discussion and writing the manuscript; Assem Barakat: proposed the subject and designed the study. All the authors read and approved the final manuscript.

Conflicts of Interest

The authors declare no conflict of interest.

References

1. Rastogi, V.K.; Mittal, H.P.; Sharma, Y.C.; Sharma, S.N. *Spectroscopy of Biological Molecules*; Hester, R.E., Girling, R.B., Eds.; Royal Society of Chemistry: London, UK, 1991; pp. 403–404.
2. Bandekar, J.; Zundel, G. Normal coordinate analysis treatment on uracil in solid state. *Spectrochim. Acta A* **1983**, *39*, 343–355.
3. Aruna, S.; Shanmugam, G. Vibrational assignments of six-membered heterocyclic compounds: Normal vibrations of 6-amino uracil and 6-amino 2-thio uracil. *Spectrochim. Acta A* **1985**, *41*, 531–536.
4. Portalone, G.; Ballirano, P.; Maras, A. The crystal structure of 3-methyluracil from X-ray powder diffraction data. *J. Mol. Struct.* **2002**, *608*, 35–39.
5. Grosmaire, L.; Delabre, J.L. Vibrational spectra of 6-methyluracil, 6-methyl-2-thiouracil and their deuterated analogues. *J. Mol. Struct*. **2012**, *1011*, 42–49.
6. Yaniv, M.; Folk, W.R. The nucleotide sequences of the two glutamine transfer ribonucleic acids from *Escherichia coli*. *J. Biol. Chem.* **1975**, *250*, 3243–3253.
7. Amir, M.; Javed, S.A.; Kumar, H. Pyrimidine as antiinflammatory agent: A review. *Indian J. Pharm. Sci.* **2007**, *69*, 337–343.
8. Çırak Ç.; Sert, Y.; Ucun, F. Experimental and computational study on molecular structure and vibrational analysis of a modified biomolecule: 5-Bromo-2'-deoxyuridine. *Spectrochim. Acta A* **2012**, *92*, 406–414.
9. Demirbaş N, Uğurluoğlu R, Demirbaş A Synthesis of 3-alkyl(aryl)-4-alkylidenamino-4,5-dihydro-1H-1,2,4-triazol-5-ones and 3-alkyl-4-alkylamino-4,5-dihydro-1H-1,2,4-triazol-5-ones as antitumor agents. *Bioorg. Med. Chem.* **2002**, *10*, 3717–3723.
10. Elinson, M.N.; Vereshchagin, A.N.; Stepanov, N.O.; Zaimovskaya, T.A.; Merkulova, V.M.; Nikishin, G.I. The first example of the cascade assembly of a spirocyclopropane structure: Direct transformation of benzylidenemalononitriles and *N,N*-dialkylbarbituric acids into substituted 2-aryl-4,6,8-trioxo-5,7-diazaspiro[2.5]octane-1,1-dicarbonitriles. *Tetrahedron Lett.* **2010**, *51*, 428–431.
11. Barakat, A.; Al-Majid, A.M.; Al-Najjar, H.J.; Mabkhot ,Y.N.; Javaid, S.; Yousuf, S.; Choudhary, M.I. Zwitterionic pyrimidinium adducts as antioxidants with therapeutic potential as nitric oxide scavenger. *Eur. J. Med. Chem.* **2014**, *84*, 146–154.
12. Ray, R.; Krishna, S.H.; Sharma, J.D.; Limaye, S.N. Variations in the Physico-Chemical Parameters of Some 5a and 5b Substituted Barbiturate Derivatives. *Asian J. Chem.* **2007**, *19*, 2497–2501.
13. Brunton, L.L.; Lazo, J.S.; Lazo, P.; Keith, L. *Goodman & Gilman's The Pharmacological Basis of Therapeutics*, 11th ed.; McGraw-Hill: New York, NY, USA, 2006.
14. Fillaut, J.L.; de Los Rios, I.; Masi, D.; Romerosa, A.; Zanobini, F.; Peruzzini, M. Synthesis and Structural Characterization of (Carbene)ruthenium Complexes Binding Nucleobases. *Eur. J. Inorg. Chem*. **2002**, 935–942.

15. Temiz-Arpaci, O.; Ozdemir, A.; Yalcin, I.; Yildiz, I.; Aki-Sener, E.; Altanlar, N. Synthesis and antimicrobial activity of some 5-[2-(morpholin-4-yl)acetamido] and/or 5-[2-(4-substituted piperazin-1-yl)acetamido]-2-(p-substituted phenyl)benzoxazoles. *Arch. Pharm.* **2005**, *338*, 105–111.

16. Kwan, P.; Brodie, M.J. Phenobarbital for the treatment of epilepsy in the 21st century: A critical review. *Epilepsia* **2004**, *45*, 1141–1149.

17. Al-Najjar, H.J.; Barakat, A.; Al-Majid, A.M.; Mabkhot, Y.N.; Weber, M.; Ghabbour, H.A.; Fun, H.-K. A greener and efficient approach to Michael addition of barbituric acid to nitroalkene in aqueous diethylamine mediu. *Molecules* **2014**, *19*, 1150–1162.

18. Al-Majid, A.M.; Barakat, A.; Al-Najjar, H.J.; Mabkhot, Y.N.; Ghabbour, H.A.; Fun, H-K. Tandem Aldol-Michael reactions in aqueous diethylamine medium: A greener and efficient approach to bis-pyrimidine derivatives. *Int. J. Mol. Sci.* **2013**, *14*, 23762–23773.

19. Barakat, A.; Al-Majid, A.M.; Al-Ghamdi, A.M.; Mabkhot, Y.N.; Siddiqui, M.R.; Ghabbour, H.A.; Fun, H-K. Tandem Aldol-Michael reactions in aqueous diethylamine medium: A greener and efficient approach to dimedone-barbituric acid derivatives. *Chem. Cent. J.* **2014**, *8*, doi:10.1186/1752-153X-8-9.

20. Barakat, A.; Al-Majid, A.M.; Al-Najjar, H.J.; Mabkhot, Y.N.; Ghabbour, H.A.; Fun, H-K. An efficient and green procedure for synthesis of rhodanine derivatives by Aldol-thia-Michael protocol using aqueous diethylamine. *RSC Adv*. **2014**, *4*, 4909–4916.

21. Barakat, A.; Al Majid, A.M.A.; Islam, M.S.; Al-Othman, Z.A. Highly enantioselective Friedel-Crafts alkylations of indoles with α,β-unsaturated ketones under Cu(II)-simple oxazoline-imidazoline catalysts. *Tetrahedron* **2013**, *69*, 5185–5192.

22. Al-Majid, A.M.; Islam, M.S. Barakat, A.; Elkahatany, N.; Yousuf, S.S.; Choudhary, M.I. Tandem Knoevenagel-Michael reactions in aqueous diethylamine medium: A greener and efficient approach to *bis*-Dimedone derivatives. *Arab. J. Chem.* **2014**, doi:10.1016/j.arabjc.2014.04.008.

23. Islam, M.S.; Al-Majid, A.M.A.; Al-Othman, Z.A.; Barakat, A. Highly Enantioselective Friedel-Crafts Alkylation of Indole with electron deficient trans-β-Nitroalkenes under simple Zn(II)-Oxazoline-Imidazoline Catalysts. *Tetrahedron: Asymmetry* **2014**, *25*, 245–251.

24. *Bruker, APEX2, SAINT and SADABS*; Bruker AXS Inc.: Madison, WI, USA, 2009.

25. Sheldrick, G.M. A short history of SHELX. *Acta Crystallogr*. **2008**, A64, 112–122.

Sample Availability: Samples of the compounds **1a**,**b** and **2a**,**b** are available from the authors.

QSAR of Antitrypanosomal Activities of Polyphenols and their Analogues Using Multiple Linear Regression and Artificial Neural Networks

Vesna Rastija[*,1] and Vijay H. Masand[2]

[1]*Faculty of Agriculture, J. J. Strossmayer University of Osijek, P. Svačića 1d, Osijek, 31 000, Croatia*

[2]*Department of Chemistry, Vidya Bharati College, Camp, Amravati, Maharashtra, 444 602, India*

Abstract: In order to find a thriving quantitative structure-activity relationship for antitrypanosomal activities (against *Trypanosma brucei rhodesiense*) of polyphenols that belong to different structural groups, multiple linear regression (MLR) and artificial neural networks (ANN) were employed. The analysis was performed on two different-sized training sets (59% and 78% molecules in the training set), resulting in relatively successful MLR and ANN models for the data set containing the smaller training set. The best MLR model obtained using the five descriptors ($R3m^{+}$, *GAP*, *DISPv*, *HATS2m*, *JGI2*) was able to account only for 74% of the variance of antitrypanosomal activities of the training set and achieved a high internal, but low external prediction. Nonlinearities of the best ANN model compared with the linear model improved the coefficient of determination to 98.6%, and showed a better external predictive ability. The obtained models displayed relevance of the distance between oxygen atoms in molecules of polyphenols, as well as stability of molecules, measured by the difference between the energy of the highest occupied molecular orbital and the energy of the lowest unoccupied molecular orbital (GAP) for their activity.

Keywords: Antitrypanosomal activity, genetic algorithm, multiple linear regression, neural networks, polyphenols, QSAR.

INTRODUCTION

Polyphenols are natural compounds that are common constituents of plant food, beverages and medicinal plants. These compounds manifest a wide range of beneficial effects on human health, such as antibacterial, antiviral, anti-carcinogenic activities and effects on cardiovascular diseases [1-4]. They also act as prophylactic agents against trypanosomiasis, human tropical parasitic disease, also know as sleeping sickness, caused by *Trypanosoma brucei rhodesiense* and *Trypanosoma cruzi* [5]. Recent studies have revealed that several fruit and medicinal plants possess trypanocidal compounds, such as: papaya (*Carica papaya*) [6]; black pepper [7]; *Khaya senegalensis* [8]; *Senna occidentalis* [9]; *Cassia fistula* [10]; *Grewia erythraea*, *Lavandula dentata* and *Vernonia leopoldii* [11].

Due to a restricted number of drugs available and their serious side effects, polyphenols are promising new molecules for cheap and safe treatment of these diseases.

In the study of Tasdemir *et al.* [5], a large number of flavonoids and their analogues were tested against *Trypanosma brucei rhodesiense* and *Trypanosoma cruzi*, but a clear quantitative structure-activity relationship (QSAR) was not established. QSAR model for the activity against *T. brucei rhodesiense*, which is based on the binding affinity of each compound towards the receptor, was not statistically significant. Authors concluded that compounds in the presented data set do not follow a common structure-activity relationship or that the structures of the molecules are not represented by adequate molecular descriptors.

However, the above-mentioned study [5] and another structure-activity study [12] identified significant chemical features for the most active trypanocidal compounds: C2,3-double bound, C4-keto group and 3`,4`,5`-trihydroxy-B-ring (7,8-dihydroxyflavone, 3-hydroxyflavone, rhamnetin, 7,8,3`,4`-tetrahydroxyflavone and catechol). A possible mechanism for antitrypanosomal activity of flavonoids is an inhibition of *Trypanosma brucei* hexokinase 1 (TbKH1), the enzyme that catalyzes the glycolysis for ATP production during mammalian infection [13]. In the present study, the main goal was to build QSAR models for the description and prediction of antitrypanosomal activity of polyphenols and their analogues against *Trypanosma brucei rhodesiense* using multiple linear regression (MLR) and artificial neural networks (ANN). The relevance of the best QSAR model should also be to provide a chemical and structural explanation of antitrypanosomal activity of the most active compounds.

The MLR method was applied in order to select a suitable descriptor using the best subset method. This approach can only capture the linear relationship between the molecular structure and the activity.

Subsequently, the descriptor subset used in the best multiple linear regression model was used to build neural networks models. ANN is usually performed if there is an assumption about a nonlinear and a highly complex relationship between the structure and the observed activity. This kind of relation occurs very often when the data set contains molecules with very diverse chemical structures [14]. Therefore, we propose the application of neural networks to develop models with enhanced predictive capabilities relative to multiple linear regression.

*Address correspondence to this author at the Faculty of Agriculture, J. J. Strossmayer University of Osijek, P. Svačića 1d, Osijek, 31 000, Croatia; Tel: +385 31 554 903; Fax: +385 31 554 803; E-mail: vrastija@pfos.hr

MATERIALS AND METHODS

Data Set

A data set of 102 polyphenols and their derivates with antitrypanosomal *in vitro* activities against *Trypanosma brucei rhodesiense* were taken from the literature [5]. General structures of the analysed groups of polyphenols are presented in Fig. (**1**). Structural details of 102 polyphenols and their derivates with antitrypanosomal activities (50% inhibitory concentrations, $IC_{50}/\mu g\ mL^{-1}$) are shown in Table **1**. Typanocidal activities (IC_{50}) were converted in the form of the negative logarithm (pIC_{50}). Compounds were classified into several structural groups: flavones, biflavones, flavon-3-ols, flavanones, isoflavones, coumarines, simple phenolic and cinnamic acid derivates.

Descriptor Calculation

The 3D structures of 102 polyphenols and their derivates were optimized applying the HyperChem 7.0 (HyperCube, Inc., Gainesville, FL) using the molecular mechanics force field (MM+) [15]. Subsequently, all structures were submitted to geometry optimization using the semiempirical AM1 method [16].

After geometry optimization, several physico-chemical parameters were calculated with HyperChem: the energy of the highest occupied molecular orbital (E_{HOMO}), the energy of the lowest unoccupied molecular orbital (E_{LUMO}), the difference between E_{HOMO} and E_{LUMO} (GAP), the heat of formation (H_f),

hydration energy (E_{HYDR}), and volume (V) of the molecule. The 2D and 3D molecular descriptors used in this study were calculated by applying the online software Parameter Client (Virtual Computational Chemistry Labo-ratory, http://146.107.217.178/lab/pclient/) an electronic remote version of the Dragon program [17]. 17 groups of Dragon's descriptors were used to generate QSAR models: constitutional, topological, walk and path counts, connect-ivity, information, 2D autocorrelations, edge adjacency, BCUT (Burden eigenvalues), topological charge, eigenvalue-based, geometrical, RDF (Radial Distribution Function), 3D-MoRSE (3D-molecular representation of structures based on electron diffraction), WHIM (WeigHted Covariance Matrices), GETAWAY (Geometry, Topology, and Atom-Weights AssemblY) descriptors, functional group counts, and molecular properties [18].

Descriptor Selection and Training and Test Set Compounds Selection

Prior to splitting a data set on a training and a test set, the initial number of 1210 calculated molecular descriptors and physicochemical properties were reduced to 33 descriptors. The procedure started with the elimination of variables that are weakly correlated with pIC_{50} ($R = 0.30$). Further selection of predictor variables was preceded by the best-subset method using STATISTICA 8.0 (StatSoft, Inc., Tulsa, OK, USA, 2007).

Best-subset regression is a model-building technique that finds subsets of predictor variables that best predict the
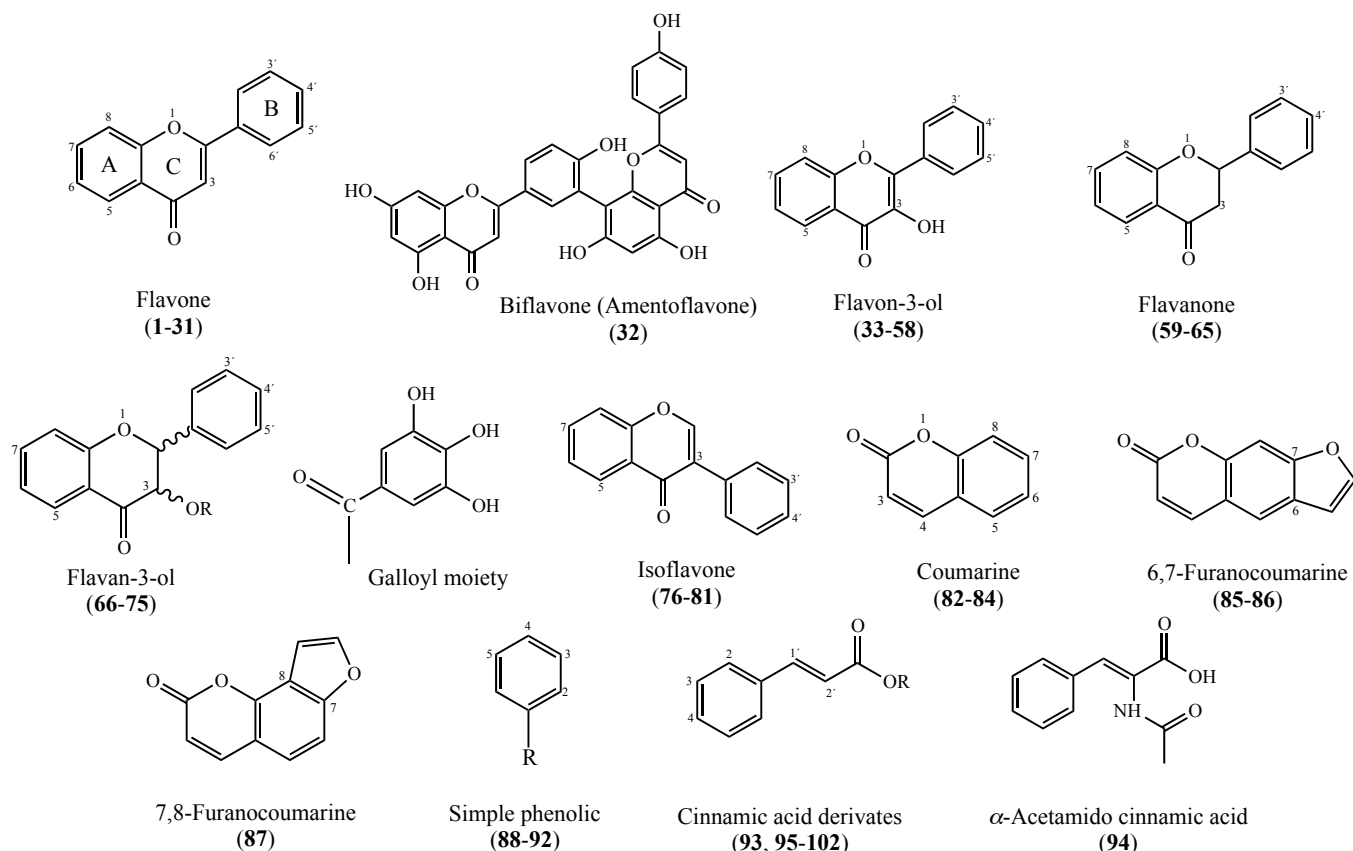
Fig. (1). Structures of analysed groups of polyphenols.

Table 1.   Structures of analysed polyphenols.

Class	No.	Compound	CAS	Position(s) of OH	Position(s) of OMe or Me	R
Flavone Aglycone	1	Flavone	525-82-6			
	2	5-Hydroxyflavone (primuletin)	491-78-1	5		
	3	5-Methoxyflavone	42079-78-7		5	
	4	6-Hydroxyflavone	6665-83-4	6		
	5	6-Methoxyflavone	26964-24-9		6	
	6	7-Hydroxyflavone	666-86-7	7		
	7	7-Methoxyflavone	22395-22-8		7	
	8	Chrysin	480-40-0	5,7		
	9	Tectochrysin	520-28-5	5	7	
	10	Chrysin dimethylether	21392-57-4		5,7	
	11	6,7-Dihydroxyflavone	38183-04-9	6,7		
	12	7,8-Dihydroxyflavone	38183-03-8	7,8		
	13	7,8-Dimethoxyflavone	65548-54-1		7,8	
	14	7,4´- Dihydroxyflavone	2196-14-7	7,4´		
	15	Apigenin	520-36-5	5,7, 4´		
	16	Genkwanin	437-64-9	5,4´	7	
	17	Ladanein	10176-71-3	5,6	7, 4´	
	18	Cirsimaritin	6601-62-3	5,4´	6,7	
	19	Scutellarein	529-53-3	5,6, 7,4´		
	20	3´,4´-Dihydroxyflavone	14919-49-4	3´,4´		
	21	7, 3´,4´-Trihydroxyflavone	2150-11-0	7, 3´,4´		
	22	Luteolin	491-70-3	5,7, 3´,4´		
	23	Diosmetin	520-34-3	5,7, 3´	4´	
	24	Luteolin tetramethylether	855-97-0		5,7, 3´,4´	
	25	7,8, 3´,4´-Tetrahydroxyflavone	3440-24-2	7,8, 3´,4´		
	26	7,8, 3´,4´-Tetramethoxyflavone	65548-55-2		7,8, 3´,4´	
Flavone Glycoside	27	Apigenin-7-*O*-glucoside	578-74-5	5,4´;7-*O*-Glu		
	28	Luteolin-5-*O*-glucoside	20344-46-1	7, 3´,4´;5-*O*-Glu		
	29	Luteolin-7-*O*- glucoside	5373-11-5	7, 3´,4´;7-*O*-Glu		
	30	Luteolin-7-*O*- rutinoside	20633-84-5	7, 3´,4´;7-*O*-Rut		
	31	Vitexin	3681-93-4	5,7, 4´	8-C-Glu	
Biflavone	32	Amentoflavone	1617-53-4	The structure is in Fig. (**1**)		
Flavon-3-ol Aglycone	33	3-Hydroxyflavone	577-85-5	3		
	34	3-Methoxyflavone	7245-02-5		3	
	35	3,6-Dihydroxyflavone	108238-41-1	3,6		
	36	3,7-Dihydroxyflavone	492-00-2	3,7		
	37	7-Methoxyflavonol	7478-60-6	3	7	
	38	Galangin	548-83-4	3,5,7		
	39	Kaempferol	520-18-3	3,5,7, 4´		
	40	Kaempferide	491-54-3	3,5,7	4´	
	41	Morin	654055-01-3	3,5,7, 2´,4´		

(Table 1) contd…..

Class	No.	Compound	CAS	Position(s) of OH	Position(s) of OMe or Me	R
Flavon-3-ol Aglycone	42	Fisetin	528-48-3	3,7, 3´,4´		
	43	Quercetin	117-39-5	3,5,7, 3´,4´		
	44	Tamarixetin	603-61-2	3,5,7, 3´	4´	
	45	Isorhamnetin	480-19-3	3,5,7, 4´	3´	
	46	Rhamnetin	90-19-7	3,5, 3´,4´	7	
	47	3,4´-Dimethylquercetin	33429-83-**3**	5,7, 3´	3,4´	
	48	Quercetin-3,7, 3´,4´-tetramethylether	1245-15-4	5	3,7, 3´,4´	
	49	Quercetagetin	90-18-6	3,5,6,7,3´,4´		
	50	Robinetin	490-31-3	3,7, 3´,4´,5´		
	51	Myricetin	529-44-2	3,5,7,	3´,4´,5´	
	52	Syringetin	4423-37-4	3,5,7, 4´	3´,5´	
	53	Myricetin trimethylether	146132-95-8	3,5,7	3´,4´,5´	
Flavon-3-ol Glycoside	54	Kaemferol-3-*O*-glucoside	480-10-4	5,7, 4´;3-*O*-Glu		
	55	Kaemferol-3-*O*-rutinoside	31921-42-3	5,7, 4´;3-*O*-Rut		
	56	Hyperoside	482-36-0	5,7, 3´,4´;3-*O*-Gal		
	57	Quercitrin	522-12-3	5,7, 3´,4´;5-*O*-Rha		
	58	Rutin	153-18-4	5,7, 3´,4´;3-*O*-Rut		
Flavanone	59	Naringenin (2*S*)	480-41-1	5,7,4´		
	60	5,7-Dimethoxy-8-methylflavanone	-		5,7,8-Me	
	61	5,4´-Dyhidroxy-6,7-dimethoxyflavanone	6601-62-3	5,4´	6,7	
	62	Eriodictyol (2*S*)	552-58-9	5,7, 3´,4´		
	63	(+)-Taxifolin (2*R*,3 *R*)	480-18-2	3,5,7, 3´,4´		
Flavanone Glycoside	64	Hesperidine (2*S*)	520-26-3	5,3´,7-*O*-Rut	4´	
	65	Neohesperidine	13241-33-3	5,3´,7-*O*-Glu-Rha	4´	
Flavan-3-ol	66	(+)-Catechin (2*R*,3*S*)	154-23-4	3,5,7,3´,4´		H
	67	(-)-Catechin (2*S*,3*R*)	154-23-4	3,5,7,3´,4´		H
	68	(+)-Epicatechin (2*S*,3*S*)	35323-91-2	3,5,7,3´,4´		H
	69	(-)-Epicatechin (2*R*,3*R*)	35323-91-2	3,5,7,3´,4´		H
	70	(-)-Gallocatechin (2*S*,3*R*)	3371-27-5	3,5,7,3´,4´,5´		H
	71	(-)-Epigallocatechin (2*R*,3*R*)	970-74-1	3,5,7,3´,4´,5´		H
	72	(-)-Catechingallate (2*S*,3*R*)	130405-40-2	3,5,7,3´,4´		Galloyl
	73	(-)-Epicatechingallate (2*R*,3*R*)	1257-08-5	3,5,7,3´,4´		Galloyl
	74	(-)-Gallocatechingallate (2*S*,3*R*)	4233-96-9	3,5,7,3´,4´,5´		Galloyl
	75	(-)-Epigallocatechingallate (2*R*,3*R*)	989-51-5	3,5,7,3´,4´,5´		Galloyl
Isoflavone	76	Daidzein	486-66-8	7,4´		
	77	Genistein	446-72-0	5,7,4´		
	78	Demethyltexasin	17817-31-1	6,7,4´		
	79	3´-Hydroxydaidzein	485-63-2	7,3´,4´		
	80	Prunetin	552-59-0	5,4´	7	
	81	Biochanin A	491-80-5	5,7	4´	
Coumarine	82	Scopoletin	92-61-5	7	6	
	83	Umbelliferone	93-35-6	7		
	84	4-Methylumbeliferone	90-33-5	7	4-Me	

(Table 1) contd…..

Class	No.	Compound	CAS	Position(s) of OH	Position(s) of OMe or Me	R
6,7-Furanocoumarine	85	Bergapten	484-20-8		5	
	86	Bergaptol	486-60-2	5		
7,8-Furanocoumarine	87	Angelicin	523-50-2	The structure is in Fig. (**1**)		
Simple phenolics	88	Catechol	120-80-9	3,4,5		H
	89	Pyrogallol	87-66-1	3,4,5		COOH
	90	Gallic acid	149-91-7	2,3		COOH
	91	2,3-Dihydroxybenzoic acid	303-38-8	3,4		COOH
	92	3,4-Dihydroxybenzoic acid	99-50-3			
Cinnamic acid and derivates	93	*trans*-Cinnamic acid	140-10-3			H
	94	α-Acetamido cinnamic acid	5469-45-4	The structure is in Fig. (**1**)		
	95	*o*-Coumaric acid	5469-45-4	2		H
	96	*m*-Coumaric acid	1262776-19-1	3		H
	97	*p*-Coumaric acid	501-98-4	4		H
	98	3-Methoxycinnamic acid	6099-04-3		3	H
	99	4-Methoxycinnamic acid	830-09-1		4	H
	100	Caffeic acid	331-39-5	3,4		H
	101	Hydrocaffeic acid ($\Delta^{1',2'}$ saturated)	1078-61-1	3,4		H
	102	Ferulic acid	1135-24-6	4	3	H

Abbreviations: Glu, glucose; Rut, rutinose; Gal, galactose; Rha, rhamnose; OMe, methoxyl; Me, methyl.

response on a dependent variable by linear regression. The criterion for the best model is based on the R^2 values of the obtained models. Descriptors involved in the 20 best triparametric, diparametric, and monoparametric models were used as the set of 33 independent variables for further analysis. In order to avoid overfitting, the terminal selection of the models was based on the inter-correlation study between variables included in the equation. Models with highly inter-correlated ($|R| \geq 0.70$) descriptors were discarded.

The sphere exclusion algorithm was used for creating the training and test sets. The sphere-exclusion algorithm is based on the similarities between molecules. Each selected molecule generates a hyper-sphere around itself, so that any molecule inside the sphere is excluded from the selection in the training and driven toward the test set [19]. Two data sets with different training sets and test set sizes were generated from the initial data set: data set I contains 60 molecules in the training set and 42 molecules in the test set, while data set II contains 80 molecules in the training set and 22 molecules in the test set.

Regression Analysis and Validation of Models

The best QSAR models were obtained using a Genetic Algorithm (GA) available in QSARINS [20]. The number of descriptors (*I*) in the multiple regression equation was limited to five.

In QSARINS, CV (cross validation) techniques are used as the optimization parameter for the GA-based variable selection and also to verify the model robustness. Internal validation included the following criteria: the coefficient of

determination of the training set (R^2_{tr}), adjusted (R^2_{adj}), cross-validate R^2 using leave-one-out method (Q^2_{LOO}), global correlation among descriptors (Kxx), difference between global correlation between molecular descriptors and *y* the response variable, and global correlation among descriptors (ΔK), and Fisher ratio (*F*) [21-23].

Internal and external validations also included the following parameters: root-mean-square error of the training set ($RMSE_{tr}$); root-mean-square error of the training set determined through cross validated LOO method ($RMSE_{cv}$), root-mean-square error of the external validation set ($RMSE_{ex}$), concordance correlation coefficient of the training set (CCC_{tr}), test set using LOO cross validation (CCC_{cv}), and of the external validation set (CCC_{ex}) [24], mean absolute error of the training set (MAE_{tr}), internal validation set (MAE_{cv}) and external validation set (MAE_{ex}) [22], predictive residual sum of squares determined through cross-validated LOO method ($PRESS_{cv}$) in the training set and in the external prediction set ($PRESS_{ex}$). The analysed external validation parameters also included the predictive squared correlation coefficients Q^2_{F1}, Q^2_{F2} and Q^2_{F3} [25] and parameters based on the r^2_m metrics $(\overline{r^2_m})$ and (Δr^2_m) [26].

Neural Networks

In an attempt to improve the prediction of antitrypanosomal activity obtained by the multiple linear regression analysis, the neural networks analysis was performed using STATISTICA 7.0. In this study, the back-propagation algorithm, which may be considered as the

outcome of an error correction process was performed [14]. A three-layer neural network, which consists of an input layer, a hidden layer and an output layer, was developed. Five molecular descriptors, included in the best MLR models, were selected as the network input nodes. The maximal number of hidden neurons was limited to 4-8, while the outputs were values of pIC$_{50}$. Input and output data were normalized between −1 and 1. The Broyden-Fletcher-Goldfarb-Shanno (BFGS) or quasi-Newton method of back-propagation algorithm was used as a training network function [27] and a multilayer perceptron (MLP) was chosen as a network architecture [28]. The types of activation functions used were: identity, logistic sigmoid, and exponential. All neural networks obtained on the training set were performed on the test set. The best neural network has the highest R^2 for the training and test set, the lowest training error and the smallest hidden unit size.

RESULTS AND DISCUSSSION

Multiple Linear Regression Models

Multiple linear regression was performed on two different data sets. The first data set consisted of 59% compounds in the training set. The second data set had a larger training set (78% molecules).

The best multiple linear regression model for data set I is:

pIC$_{50}$ = 1.589 − 1.147 *HATS7u* − 10.942 *R2m$^+$* +11.216 *R3m$^+$* - 0.100 *F04[O-O]* − 0.244 *GAP* (1)

N (training) = 60; *N* (test) = 42

R^2_{tr} = 0.7384; R^2_{adj} = 0.7142; Q^2_{LOO} = 0.6677; *Kxx* = 0.2884; ΔK = 0.0124; *F* = 30.4885; *RMSE$_{tr}$* = 0.2112; *RMSE$_{cv}$* = 0.2380; *RMSE$_{ex}$* = 0.7567; *CCC$_{tr}$* = 0.8495; *CCC$_{cv}$* = 0.8091; *CCC$_{ex}$* = 0.4384; *MAE$_{tr}$* = 0.1632; *MAE$_{cv}$* = 0.1822; *MAE$_{ex}$* = 0.6799; *PRESS$_{cv}$* = 3.4000; *PRESS$_{ex}$* = 24.0468; Q^2_{F1} = 0.3127; Q^2_{F2} = -0.6758; Q^2_{F3} = -2.3574; $\overline{r^2_m}$ = 0.0759; Δr^2_m = 0.6218

For data set II, the best QSAR model obtained is:

pIC$_{50}$ = -0.5827 + 1.183 *R3m$^+$* − 0.774 *GAP* − 0.789 *DISPv* − 1.297 *HATS2m* + 0.474 *JGI2* (2)

N (training) = 80; *N* (test) = 22

R^2_{tr} = 0.4573; R^2_{adj} = 0.4206; Q^2_{LOO} = 0.3488; *Kxx* = 0.2839; ΔK = 0.0251; *F* = 12.4689; *RMSE$_{tr}$* = 0.4507; *RMSE$_{cv}$* = 0.49360; *RMSE$_{ex}$* = 0.4776; *CCC$_{tr}$* = 0.6276; *CCC$_{cv}$* = 0.5584; *CCC$_{ex}$* = 0.5128; *MAE$_{tr}$* = 0.3359; *MAE$_{cv}$* = 0.3654; *MAE$_{ex}$* = 0.3378; *PRESS$_{cv}$* = 19.4948; *PRESS$_{ex}$* = 5.0186; Q^2_{F1} = 0.2637; Q^2_{F2} = 0.2473; Q^2_{F3} = 0.3904; $\overline{r^2_m}$ = 0.1664; Δr^2_m = 0.1310

Experimental (pIC$_{50}$) and predicted values, calculated by Eqs. 1 and 2 are given in **S1** with related residuals. As shown in Table **2**, descriptors included in Eq. 1 and Eq. 2 are not mutually correlated. Low collinearity is also verified by the low values of *Kxx* (0.2884 for model 1, and 0.2839 for model 2).

The min/max absolute values of residuals are 0.014/1.546 for model 1, and 0.001/1.608 for model 2. The prediction error sum of squares (PRESS), a sum of squares of residuals between the experimental and predicted values for the molecules included in the training set, is smaller (3.4) for model 1, than for model 2 (19.49).

Also, the first model developed for a smaller training set, shows a better performance in the internal validation (higher R^2_{tr}, R^2_{adj}, Q^2_{LOO}, *CCC$_{tr}$*, *CCC$_{cv}$*, and *F* values, as well as smaller *RMSE$_{tr}$*, *RMSE$_{cv}$*, *MAE$_{tr}$*, *MAE$_{cv}$*) than the second model. In spite of a good fitting performance and good internal validation, unfortunately, the real predictive power of model I has failed, according to the external validation parameters. The concordance correlation coefficient of the external validation set (*CCC$_{ex}$*) is significantly lower (0.4384) compared to the fitting (*CCC$_{tr}$* = 0.8495) and LOO correlation coefficient (*CCC$_{cv}$* = 0.8091). Furthermore, although the difference between the mean absolute error of the training set (*MAE$_{tr}$* = 0.1632) and the internal validation set (*MAE$_{cv}$* = 0.1822) is negligible, *MAE* of the external validation set is much greater (*MAE$_{ex}$* = 0.6799), as well as *RMSE$_{ex}$* (0.7567). In addition, low values of Q^2_{F1} (0.3127), as well as negative values of Q^2_{F2} and Q^2_{F3} (-0.6758 and -2.5574, respectively), including the very low value of $\overline{r^2_m}$ (0.0759) and very high value of Δr^2_m (0.6218) indicate that the model is useless for external predictivity.

Table 2. Correlation matrix for the descriptors included in Eqs. 1 and 2.

	HATS7u	*HATS2m*	*R2m+*	*R3m+*	*F04[O-O]*	*GAP*	*JGI2*	*DISPv*
HATS7u	1.00							
HATS2m	0.29	1.00						
R2m+	-0.12	0.26	1.00					
R3m+	0.07	0.43	0.01	1.00				
F04[O-O]	-0.02	0.08	-0.55	-0.14	1.00			
GAP	-0.10	0.06	0.25	0.23	-0.30	1.00		
JGI2	-0.21	0.19	-0.11	0.64	0.19	0.17	1.00	
DISPv	0.03	-0.18	-0.30	-0.21	0.60	-0.15	0.09	1.00

The quality of the internal validation for the second model, which is developed for the 80 compounds in the training sets, is not acceptable considering the low values of R^2_{tr}, R^2_{adj}, Q^2_{LOO}, CCC_{tr}, CCC_{cv}, and F, as well as high values of $RMSE_{tr}$, $RMSE_{cv}$, MAE_{tr}, MAE_{cv}. However, the quality of external validation of model 2 is more acceptable than for model 1. Values of $RMSE_{tr}$, $RMSE_{cv}$, $RMSE_{ex}$ have approximately equal values (0.4507, 0.49360, 0.4776, respectively, as well as MAE_{tr}, MAE_{cv}, MAE_{ex} (0.3359, 0.3654, 0.3378, respectively). Although values obtained for parameters Q^2_{F1}, and Q^2_{F3} are not even close to the threshold (0.70), they are higher than for model 1. The value of $\overline{r^2_m}$ is unacceptably low (0.1664) since that parameter may attain a maximum value of 1. On the other hand, Δr^2_m has an acceptable value lower than 0.2 (0.131). However, a reduced size of the test set, compared to model 1, may be the potential reason for better external validation results.

Considering the fact that both models do not satisfy criteria of the internal and external validation to be "predictive" QSAR models [21], we may conclude that the linear relationship between the antitrypanosomal activity and the structures of observed polyphenols does not exist. A possible reason for this occurrence lies in the great diversity of the chemical structure of molecules. Therefore, a complex nonlinear relationship between structures and observed activities of polyphenols was examined by neural networks using descriptors involved in the best MLR equations.

The majority of descriptors involved in models 1 and 2 belong to the GETAWAY group of descriptors. Two of them, *HATS7u* and *HATS2m* leverage-weighted autocorrelation indices, unweighted and weighted by atomic masses [29], respectively, exert a negative influence on pIC_{50}. Thus, the enhanced values of the descriptor *HATS2m*, or heavier atoms than carbon or hydrogen (oxygen atoms) located at topological distance 2, affect the lower antitrypanosomal activity. Therefore, compounds with two oxygen atoms at topological distance 2 possess higher *HATS2m* values, e.g. coumarines and furanocoumarines because of their 2-pyrone structure, as well as flavonoid glucosides as a result of *O*-glycosidic bond.

Other two GETAWAY descriptors (*R2m*+, *R3m*+) are autocorrelation R-GETAWAY descriptors that are based on the influence/distance matrix **R**. Descriptors *R2m*+ and *R3m*+ represent a maximal contribution to the autocorrelation at topological distance 2 and 3, respectively. As in the case with *HATS2m*, the negative coefficient of *R2m*+ implies that oxygen atoms at topological distance 2 affect the reduction of antitrypanosomal activity. On the other hand, higher values of *R3m*+ are favourable for the exhibition of inhibitory activity of polyphenols. The given descriptor reflects the relevance of the catechol functional group for higher trypanocidal activities at the A and B ring of flavonoids, as in 7,8,3′,4′-tetrahydroxyflavone (**25**) ($pIC_{50} = 0.301$) and 3′,4′-dihydroxyflavone (**20**) ($pIC_{50} = -0.0041$). An equal effect is exhibited by two OH groups at C-7 and C-8 of flavones, as in the most active compound, 7,8-dihydroxyflavone (**12**) ($pIC_{50} = 1.167$), or two OH groups at C-6 and C-7 of 6,7-dihydroxyflavone (**11**) ($pIC_{50} = -0.279$).

Eq. 2 also reveals that higher values of 2nd order mean topological charge index (*JGI2*) enhance the activity. Negative signs of the other three descriptors in Eqs. 1 and 2 (*DISPv*, *F04[O-O]*, *GAP*) indicate that higher values of those descriptors are unfavourable for the activity. *DISPv* is a geometrical descriptor weighted by atomic van der Waals volumes. *F04[O-O]* is a 2D frequency fingerprint descriptor, which corresponds to the frequency of occurrence of two oxygen atoms at topological distance 4. This occurrence is most evident for glycosides, which are, at the same time, the most inactive compounds. Another descriptor that negatively affects the antitrypanosomal activity is the quantum-chemical descriptor, energy gap (*GAP*), the measure of the molecular stability [30]. A large HOMO-LUMO gap implies high stability for the molecules in the sense of its lower reactivity, which is proved by the negative coefficient of this descriptor in Eqs. 1 and 2.

Neural Networks Models

In order to find a nonlinear relationship between antitrypanosomal activity and polyphenols, and possibly improve the prediction, the neural networks (NN) models were obtained using five descriptors appearing in MLR models 1 and 2. Neural networks were performed on the same training and test set as the MLR analysis.

The best network for data set I (*N* (training) = 60; *N* (test) = 42) (NN I) was obtained with five inputs (*HATS7u*, *R2m*+, *R3m*+, *F04[O-O]*, *GAP*). The networks consist of six hidden units while the outputs were pIC_{50} values. The neuron hidden activation function was logistic, while the output activation was identity. The correlation coefficients of networks (5-6-1) are:

$R^2_{train} = 0.986$, training error = 0.000961, $R^2_{test} = 0.758$

For data set II (*N* (training) = 80; *N* (test) = 22), the best neural network (NN II) was obtained with the five descriptors (*R3m*+, *GAP*, *DISPv*, *HATS2m*, *JGI2*). The architecture of the obtained network is 5-5-1 (5 inputs, 5 hidden units and 1 output). The hidden activation function was logistic, while the output function was exponential function. The correlation coefficients of networks are:

$R^2_{train} = 0.913$, training error = 0.003251, $R^2_{test} = 0.673$

Prediction results for both neural networks are presented in the Supplementary data (S1). The plot of the observed versus calculated pIC_{50} for the training set of compounds derived by NN I is shown in Fig. (**2**), and for the test set in Fig. (**3**).

Comparing the results of both networks, it is evident that NN created for data set I has better statistical parameters than NN for data set II, as well as in case of MLR models. Therefore, the correlation coefficients of NN I are higher than of NN II, while the training error and difference between R^2_{train} and R^2_{test} is smaller. Moreover, ANN applied to the same data set shows a better predictive ability than MLR. Thus, the NN I model is able to account for 98.6% of the variance of antitrypanosomal activity of the training set, while model 1 obtained by MLR accounts only for 73.84%. However, better statistical results of model 1 and NN I compared with the results of model 2 and NN II indicate that pIC_{50} significantly correlated with the five descriptors

included in the models (*HATS7u*, *R2m*$^+$, *R3m*$^+$, *F04[O-O]*, *GAP*).
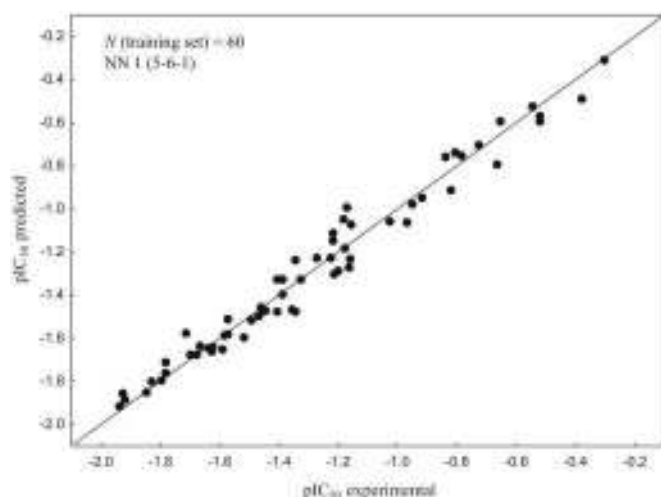

Fig. (2). Observed versus predicted pIC$_{50}$ for the 60 compounds of the training set (data set I) derived by neural network I (5-6-1).
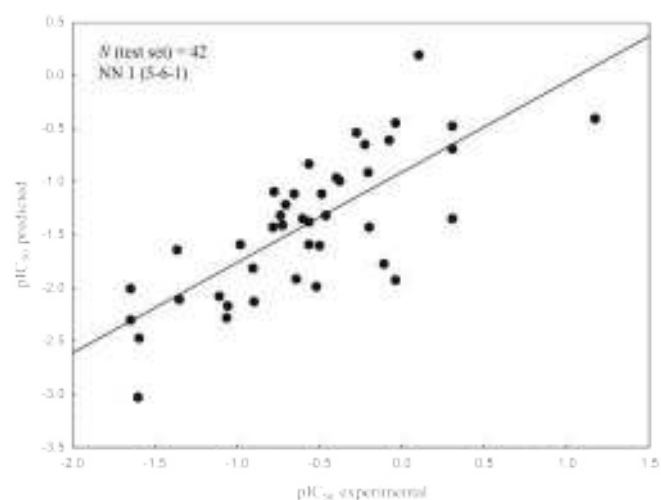

Fig. (3). Observed versus predicted pIC$_{50}$ for the 42 compounds of the test set (data set I) derived by neural network I (5-6-1).

CONCLUSION

In this study, we compared linear QSAR models obtained by multiple regression and nonlinear models obtained by neural networks. It was demonstrated that artificial neural network methods were superior to the multiple regression analysis for the given data set. The improved predictive performance observed through ANN approaches reflects a nonlinear relationship between descriptors and antitrypano-somal activity of polyphenols. However, the multiple linear regression analysis that utilizes best-subset regression as a model-building technique is successful in selecting descriptors prior to ANN analysis. Moreover, the obtained MLR models are suitable for the purpose of qualitative interpretation of the QSAR models. Although ANN models gave accurate results, it is not possible to determine the influence of each descriptor in the model. Therefore, we propose the application of neural networks to develop

models with enhanced predictive capabilities in combination with linear regression as a complement method.

Evaluation of the descriptors relevance in the obtained models shed new light on the comprehension of antiparasitic potential of the most active compounds. The obtained models show relevance of the distance of adjacent hydroxyl groups in molecules of polyphenols, as well as stability of molecules, measured by the difference between the energy of the highest occupied molecular orbital and the energy of the lowest unoccupied molecular orbital (GAP) for their activity. The results obtained will be useful for further research of more effective plant-derived agents against the *Trypanosoma*.

ABBREVIATIONS

QSAR   =   Quantitative structure activity relationship

MLR   =   Multiple linear regression

ANN   =   Artificial neural networks

CONFLICT OF INTEREST

The authors confirm that the manuscript has no conflict of interest.

ACKNOWLEDGEMENTS

SUPPLEMENTARY DATA

Supplementary material is available on the publisher's web site along with the published article.

REFERENCES

[1]   Katalinić, V.; Smole Možina, S, Skroza D.; Generalić, I.; Abramović, H.; Miloš, M,; Ljubenkov, I.; Piskernik, S.; Pezo, I.; Terpinc, P.; Boban, M. Polyphenolic profile, antioxidant properties and antimicrobial activity of grape skin extracts of 14 *Vitis vinifera* varieties grown in Dalmatia (Croatia). *Food Chem.*, **2010**, *119*(2), 715-723.

[2]   Sithisarn, P.; Michaelis, M.; Schubert-Zsilavecz, M.; Cinatl, Jr. J. Differential antiviral and anti-inflammatory mechanism of the flavonoids biochanin A and baicalein in H5N1 influenza A virus-infected cells. *Antiviral Res.*, **2013**, *97*(1), 41-48.

[3]   Chen, A.Y.; Chen, Y.C. A review of the dietary flavonoid, kaempferol on human health and cancer chemoprevention, *Food Chem.*, **2013**, *138*(4), 2099-2107.

[4]   Al-Awwadi, N.; Azay, J.; Poucheret, P.; Cassanas, G.; Krosniak, M.; Auger, C.; Gasc, F.; Rouanet, J.-M.; Cros, G.; Teissedre, P.L. Red wine polyphenols alone or in association with ethanol prevent hypertension, cardiac hypertrophy, and production of reactive oxygen species in the insulin-resistant fructose-fed. *J. Agric. Food Chem.*, **2004**, *52*(18), 1008-1016.

[5]   Tasdemir, D.; Kaiser, M.; Brun, R.; Yardley, V.; Schmidt, T.J.; Tosun, F.; Rüedi, P. Antitrypanosomal and antileishmanial activities of flavonoids and their analogues: *In vitro*, *in vivo*, structure-activity relationship, and quantitative structure-activity relationship studies. *Antimicrob. Agents Chemother.*, **2006**, *50*(4), 1352-1364.

[6]   Jiménez-Coello, M.; Guzman-Marín, E.; Ortega-Pacheco, A.; Perez-Gutiérrez, S.; Acosta-Viana, K.Y. Assessment of the anti-protozoal activity of crude *Carica papaya* seed extract against *Trypanosoma cruzi. Molecules*, **2013**, *18*(10), 12621-12632.

[7]　Shaba, P.; Pandey, N.N.; Sharma, O.P.; Singh, R.K. Antitrypanosomal activity of *Piper nigrum* L. (black pepper) against *Trypanosoma evansi*. *J. Vet. Adv.*, **2012**, *2*(4), 161-167.

[8]　Shaba, P.; Pandey, N.N.; Sharma, O.P.; Rao, J.R.; Mishra, A.K.; Singh, R.K. Antitrypanosomal activity of methanolic extract of *Khaya senegalensis* tree bark against *Trypanosoma evansi*. *Int. J. Food Agr. Vet. Sc.*, **2011**, *1*(1), 21-26.

[9]　Ibrahim, M.A.; Aliyu, A.B.; Sallau, A.B.; Yunusu, I.; Umar, T.S. *Senna occidentalis* leaf extract possesses antitrypanosomal activity and ameliorates the trypanosome-induced anemia and organ damage. *Pharmacognosy Res.,* **2010**, *2*(3), 175-180.

[10]　Sartorelli, P.; Carvalho, C.S.; Reimão, J.Q.; Ferreira, M.J.P.; Tempone, A.G. Antiparasitic activity of biochanin A, an isolated isoflavone from fruits of *Cassia fistula* (Leguminosae). *Parasitol. Res.*, **2009**, *10*(2), 311-314.

[11]　Al-Musayeib, N.M.; Mothana, R.A.; Matheeussen, A.; Cos, P.; Maes, L. *In vitro* antiplasmodial, antileishmanial and antitrypanosomal activities of selected medicinal plants used in the traditional Arabian Peninsular region. *BMC Complement Altern Med.* **2012**, *12*, 49-49.

[12]　Scotti, L.; Ferreira, E.I.; da Silva, M.S.; Scotti, M.T. Chemometric studies on natural products as potential inhibitors of the NADH oxidase from *Trypanosoma cruzi* using the VolSurf approach. *Molecules*, **2010**, *15*(10), 7363-7377.

[13]　Dodson, H.C.; Lyda, T.A.; Chambers, J.W.; Morris, M.T.; Christensen, K.A.; Morris, J.C. Quercetin, a fluorescent bioflavonoid, inhibits *Trypanosoma brucei* hexokinase 1. *Exp. Parasitol.*, **2011**, *127*(2), 423-428.

[14]　Niculescu, S.P. Artificial neural networks and genetic algorithms in QSAR. *J. Mol. Struct. (Theochem)*, **2003**, *622*(1-2), 71-83.

[15]　Hocquet. A.; Langgård, M. An evaluation of the MM+ force field. **1998**, *J. Mol. Model*, *4*(3), 94-112.

[16]　Dewar, M.J.S.; Zoebisch, E.G.; Healy, E.F.; Stewart, J.J.P. AM1: A new general purpose quantum mechanical model. *J. Am. Chem. Soc.*, **1985**, *107*(13), 3902-3909.

[17]　Tetko, I.V.; Gasteiger, J.; Todeschini, R.; Mauri, A.; Livingstone, D.; Ertl, P.; Palyulin, V.A.; Radchenko, E.V.; Zefirov, N.S.; Makarenko, A.S.; Tanchuk, V.Y.; Prokopenko, V.V. Virtual computational chemistry laboratory – design and description. *J. Comput. Aided Mol. Des.*, **2005**, *19*(6), 453-463.

[18]　Todeschini, R.; Consonni, V. *Handbook of molecular descriptors*, Wiley-VCH: Weinheim, **2000**.

[19]　Hudson, B.D.; Hyde, R.M.; Rahr, E.; Wood, J. Parameter based methods for compound selection from chemical database. *Quantitative Structure-Activity Relationships*, **1996**, *15*(4), 285-289.

[20]　Gramatica, P.; Chirico, N.; Papa, N.; Cassani, S.; Kovarich, S. QSARINS: A new software for the development, analysis, and validation of QSAR MLR models. *J. Comput. Chem.,* **2013**, *34*(24), 2121-2132.

[21]　Gramatica, P. Principles of QSAR models validation: internal and external. *QSAR Comb. Sci.*, **2007**, *26*(5), 694-701.

[22]　Tropsha, A. Best practices for QSAR model development, validation, and exploitation. *Molecular Informatics* **2010**, *29*(6-7), 476-488.

[23]　Todeschini, R.; Consonni, V.; Maiocchi, A. The K correlation index: theory development and its application in chemometrics. *Chemom. Intell. Lab. Syst.*, **1999**, *46*(1), 13-29.

[24]　Chirico, N.; Gramatica, P. Real external predictivity of QSAR models: how to evaluate it? Comparison of different validation criteria and proposal of using the concordance correlation coefficient. *J. Chem. Inf. Model*, **2011**, *51*(9), 2320-2335.

[25]　Schüürmann, G.; Ebert, R.; Chen, J.; Wang, B.; Kühne, R. External validation and prediction employing the predictive squared correlation coefficients test set activity mean *vs* training set activity mean, *J. Chem. Inf. Model*, **2008**, *48*(11), 2140–2145.

[26]　Ojha, P.K.; Mitra, I.; Das, R.N.; Roy, K. Further exploring r_m^2 metrics for validation of QSPR models dataset. *Chemom. Intell. Lab. Syst.*, **2011**, *107*(1), 194-205.

[27]　Anastasiadis, A.D.; Magoulas, G.D.; Vrahatis, M.N. New globally convergent training scheme based on the resilient propagation algorithm. *Neurocomputing*, **2005**, *64*, 253-270.

[28]　Rumelhart, D.E.; McClelland, J. *Parallel distributed processing;* MIT Press: Cambridge, **1986**, Vol. *1*, pp. 305-314.

[29]　Consonni, V.; Todeschini, R.; Pavan, M. Structure/response correlations and similarity/diversity analysis by GETAWAY descriptors. 1. Theory of the novel 3D molecular descriptors. *J. Chem. Inf. Comput. Sci.*, **2002**, *42*(3), 682-692.

[30]　Zhou, Z.; Parr, R.G. New measures of aromaticity: absolute hardness and relative hardness. *J. Am. Chem. Soc.*, **1989**, *111*(19), 7371-7379.

Study of plant growth regulating antibiotic drugs - 3-(2-benzimidazol)-3-nitro-6-methyl-chromen-4-one with innertransition metal complexes on spinach (*spinacia oleracea* l.) at different p[h]

S.A.Quazi[1*], D.T.Mahajan[2], Noor Mohammad[3,] Vijay Masand[4]
Department of chemistry, VidyaBhartiMahavidyalaya, Camp, Amravati (M.S) India
Department of chemistry, Govt.Vidarbha Institute of Sci. and Humanities, Amravati (M.S) India
*Corresponding author: E.Mail:quazi.azhar@rediffmail.com

ABSTRACT
Antibiotic drugs - 3-(2-benzimidazol)-3-nitro-6-methyl chromen-4-one (Chromone derivatives) with inner transition metal complexes at different pH on plant growth of spinach were studied. Plant growth was decided by measurement of different growth parameters.
Keywords: plant growth, germination, antibiotic drugs, metal complexes.

INTRODUCTION

Chromone derivatives having great attention for their applications, plants make plant growth regulators, often called phytohormones, to regulate growth, development, and responses to stimuli. Each of these small organic molecules has pleiotropic effects. The balance between them shifts constantly. Changes in phytohormone levels result in gene activation shifts. In tissue culture the concentration of growth regulators in the medium must be optimized and may change according to the desired result. Cytokines promote shoot formation, but need auxins as well to promote mitosis. We offer the naturally occurring hormones as well as potent synthetic substitutes. We also offer antagonists, useful as tools for investigating hormonal mechanisms of action. These compounds exhibit a wide spectrum of biological activities including antimicrobial (Goker, 2005; Nawort, 2006), antibacterial (Harborne, 2000; Guz, 2001), antitumor (Yakut, 2004), antifungal (Ali, 2008; Ali 2007, Uher, 1994), anti-allergic (Ohata, 1991), antiviral (Desideri, 2003), anti-inflammatory (Jerzy, 1995) and anticancer (Denis, 1999) activities. Plant growth regulating activities of various organic ligands and their transition metal ion complexes for various plants were studied by many workers (AB Patil, 2007; Adams, 2009; Meshram, 2011; SKumar, 2010; Magar, 2011; Mane, 2010). Germination is an economical and simple method for improving the nutritive value and several studies have reported (King, 1981; Frias, 1995; Honke, 1998) higher levels of nutrients and lower levels of antinutrients in sprouts compared to the ingeminated seeds. studies of acoustic behavior of 3-(2-benzimidazol)-3-nitro-6-methylchromen-4-one (bnmc) in a different solvents system by using ultrasonicinterferometer(Quazi, 2014).Studies ofstability constants and thermodynamically parameters (ΔH,ΔG, ΔS) of inner transition metal ions complexes with substituted chromone Schiff bases 70% dioxane – water(Noor, 2014). Studies of some acoustic parameters of cu (No3)2 inwater-dioxane mixture at 298.150k by physico -chemical method (Quazi, 2014).

3-(2-benzimidazol)-3-nitro-6-methyl chromen-4-one (Chromone derivatives) with inner transition metal complexes. Spinach have rich source of vit-A, vit-C, vit-E, vit-K, Mg, Mn, Foliate, Betaine, Fe, vit-B_{12}, Ca, K, vit-B_6, Folic acid, Cu,Protein, P, Zn, Niacin, Se and omega $_3$ fatty acids since no work is reported on the biological applications of metal complexes with chromone derivatives, present work is carried out with metal complexes of Ce (III) and Sm(III) with 3-(2-benzimidazol)-3-nitro-6-methyl chromen-4-one to study the effect of these complexes on germination, survival, seedling height action spinach plant.

MATERIALS AND METHODS

All metal nitrates available from Sigma Aldrich Chem. Co., U.S.A. Metal nitrate was prepared in triply distill water and concentration was estimated by standard method. Solutions of Ce (III) and Sm (III) metal nitrates of 0.01 mol/dm^3 concentration were prepared by adding accurate amounts of metal salts in distilled water. The solution of 3-(2-benzimidazol)-3-nitro-6-methyl chromen-4-one of 0.01 mol/dm^{3}concentration was prepared in distilled water. The biological applications were studied at pH 4.5, 7.5 and 9.0 at 0.1 mol/dm^3 ionic strength of KNO$_3$ solution.

The basic requirement for this experiment was soil fertilized soil, which collected from agricultural land. Stones and other hard material removed from it. It was then grind and filtered. Two parts of this finely powdered soil was mixed with one part of filtered pink stone sand. This soil was then filled in two wooden trays having compartments of equal size. The soil in the tray was moistened with water. Sowing of seeds was done in this soil after one hour.*Spinacia oleracea*

(spinach) are selected, healthy seeds of spinach [*Spinacia oleracea* L.] of equal size were selected for same germination were taken and thoroughly washed using doubly distilled water. 100 seeds from these healthy seeds of equal size immersed in tested solution of pH 4.5, 7.5 and 9.0. These seeds soaked were taken out of each solution. The seeds were sowed in the wooden trays in a row. Effect of the ligand, metal ion, complex solution on growth of plants was studied at different pH 4.5, 7.5 and 9.0 the seeds being immersed in the solution at about 6 hours. A controlled set was similarly run using double distilled water. Plant growth is decided on the basis of measured average value of parameters such as percentage of germinations, survival, seedling height, shoot length, root length and leaf area of young leaves compared with control system. The germination and Survival was noted after 4 and 10 days. After noting the survival of the plants, they were taken out of the soil. The seedling height (root length/shoot length) and leaf area (width & length) of young leaf of survived plants were measured. Table 1, 2 and 3 represents the average values of growth parameters.

Table.1.Effect of ligand, metal ion and complex on Germination, Survival, seeding height etc. on *Spinacia oleracea* (L.) at 4.5 pH

Parameters	Effect				Order of plant Growth regulators
	Control	Ligand	Metal-Complex		
			Ce (III)	Sm (III)	
%germination after 4 days	51.00	66.00	54.00	52.00	L>complex>metal>control
% survival after10days	66.00	82.00	76.00	74.00	
Seedling height (cm)	2.30	2.45	2.40	2.39	
Root length (cm)	4.03	4.10	4.08	4.05	
Shoot length (cm)	4.30	4.50	4.45	4.42	
Root/Shoot ratio	0.9369	0.9106	0.9164	0.9158	
Width length of young leaf (cm)	0.9607	0.9684	0.9606	0.9558	

Table.2.Effect of ligand, metal ion and complex on Germination, Survival, seeding height etc. on *Spinacia oleracea* (L.) at 7.5 pH

Parameters	Effect				Order of plant Growth regulators
	Control	Ligand	Metal-Complex		
			Ce(III)	Sm(III)	
%germination after 4 days	54.00	68.00	58.00	57.00	L>complex>metal>control
% survival after10days	68.00	84.00	78.00	76.00	
Seedling height (cm)	2.40	2.48	2.43	2.41	
Root length (cm)	4.05	4.12	4.08	4.07	
Shoot length (cm)	4.32	4.55	4.51	4.42	
Root/Shoot ratio	0.9372	0.9049	0.9040	0.9100	
Width length of young leaf (cm)	0.9652	0.9699	0.9642	0.9594	

Table.3.Effect of ligand, metal ion and complex on Germination, Survival, seeding height etc. on *Spinacia oleracea* (L.) at 9.0 pH

Parameters	Effect				Order of plant Growth regulators
	Control	Ligand	Metal-Complex		L>complex>metal>control
			Ce (III)	Sm (III)	
%germination after 4 days	55.00	71.00	63.00	58.00	
% survival after10days	71.00	86.00	79.00	77.00	
Seedling height (cm)	2.41	2.50	2.47	2.43	
Root length (cm)	4.07	4.14	4.09	4.07	
Shoot length (cm)	4.35	4.59	4.53	4.50	
Root/Shoot ratio	0.9353	0.9011	0.9000	0.9059	
Width length of young leaf (cm)	0.9729	0.9737	0.9230	0.9640	

RESULTS AND DISCUSSION

The parameter of plant growth was considered on the basis of percentage of germination, survival, seedling height, soot length, root length, root/shoot ratio, and thickness of young leaf. The average values of these parameters are reported in Table (2).Seed Germination is one of the main feature of plant physiology. It was cleared from table 1, 2 & 3 that, the percent germination in all the treatments showed increase than that of control (distilled water).

The seedling height (root length/shoot length) and leaf area (width & length) of young leaf of plants were measured. The average values of these parameters are showed in table 1, 2 & 3. In the present investigation, effect of the ligand, complex and metal ion on percentage seed germination, root length, shoot length (root /shoot ratio) and seedling height etc. have been studied. The ligand-L has found high value for all these parameters at different pH. Thus, at pH 4.5, 7.5 and 9.0 Ligand (L) can functions as plant growth regulators. The percent germination in all the treatments showed increase than that of control (distilled water). The root and shoot lengths differ. It clearly show in the Table 1, 2 & 3, the average root length in ligand, complex, Ce (III) at all pH increases over control and complex of Sm (III) with L showed decrease in shoot length but increase as compared to control. It is also examined that Root/ Shoot ratio is decrease in complex (Sm (III)-L) and ligand, but it is increases for control.

ACKNOWLEDGEMENT

REFERENCES

AB Patil, Ph. D. Thesis, Chemistry, S. G. B, Amravati University, INDIA, 2007.

Ali, Phosphorous, Sulfur, and Silicon, 182(8), 2007, 1717-1726.

Ali; S.A. Ghfaar; H.M. El-Shaaer; F.I. Hanafy and A.Z. El-Fauomy, Turk. J. Chem., 2008, 32(3), 365-374.

AV Mane, RR Sankpal, LA Mane, MS Ambawade, J. Chem. Pharm. Res., 2010, 2 (5), 206-215.

BK Magar, AS Kirdant, VA Shelke, SG Shankarwar and T K Chondhekar, J. Chem. Pharm. Res., 2011, 3(5),11 , 6-123.

CM Adams, Orient. J. Chem., 2009, 25 (2), 459-460.

Guz; F.R. Stermitz; J.B. Johnson; T.D. Beeson; S. Willen; J.F. Hastang and K. Lewis, J. Med. Chem., 2001, 44(2), 261-268.

H. Goker; D.W. Boykin and S. Yildiz, Bioorg. Med. Chem., 2005, 13(5), 1707-1714.

J Frias; M Prodanov; I Sierra; C Vidal-Valerie. Journal of Food Protection., 1995, 58, 692–695.

J Honke; H Kozłowska; C Vidal-Valverde; J Frias; R Go. Recki Zeitschrift f €ur Lebensmittel-Untersuchungund -Forschung A., 1998, 206, 279–283.

J.B. Harborne and C.A. Williams, Photochemistry, 2000, 55(6), 481-504.

K. Jerzy and Z. Teodor, Chem. Abstr., 1995, 123, 339629.

L. Denis; M.S. Morton and K. Griffith, Eur. Urol., 1999, 35(5-6), 377-387.

M. J. Nawort; E. Nawrot and J. Graczyk, Eur. J. Med. Chem., 2006, 41(11), 1301-1309.

M. Ohata; K. Watanabe; K. Kumata; K. Hisamichi; S. Suzuki and H. Ito, Annu. Rep. Tohoku Coll. Pharm., 1991, 38, 35.

M. Uher;V. Konecny and O. Rajniakova, Chem. Pap., 1994, 48(4), 282-284.

N. Desideri; P. Mastromarino and C. Conti, Antiviral Chem. And Chemotherapy, Chem.Abstr., 2003, 14(4), 195-203.

Noor,S.A.Quazi, Mahajan, Masand, Recent Trends in Material Preparation & Characterization , National Conference ISBN - 978-81-929395-2-0,24th February 2014, pp86-89

RD King; P Perwastien. J. of Food Science., 1987, 52, 106–108.

S Kumar, A Kumar Singh, J. Chem. Pharm. Res., 2010, 2(6), 118-124.

S.A.Quazi, Mahajan, Masand, Noor Mohammad,M.R. Ingle., August - September, 2014, Vol. 3, No.5, pp 1206-1210.,ISSN: 2278-0238

S.A.Quazi, Mahajan, Masand, Noor,NationalConference ISBN – 978-93-82588-41-2, Recent application mathematical tools in science May 8- 3,2014,pp76-80

UP Meshram, BG Khobragade, ML Narwade, VB Khobragade, Der Pharma Chemica, 2011, 3 (2), 376-382.

Study of seed germination activity (plant growth regulator) of 2[(Z)-(2-phenyl-4H-chromen-4-ylidene) aminophenol and its Ni (III) and Cu (III) complexes on vegetable plant Trigonella *foenum-graecum*

Noor Mohammad[1], S. Azhar Quazi[2], Devidas t. mahajan[2,] Vijay Masand[2]

[1]Department of Chemistry, Govt.Vidarbha Institute of Sci. and Humanities, Amravati (M.S) India
[2]Department of Chemistry, Vidya Bharti Mahavidyalaya, Camp, Amravati (M.S) India
*Corresponding author: **quazi.azhar@rediffmail.com**

Abstract

The seed germination activity of 2-[(Z)-(2-phenyl-4H-chromen-4-ylidene)aminophenol and its Ni(III) and Cu (III) complexes on *Trigonella foenum-graecum* (Methi) have been studied at pH 4.5 and 9.5 in order to justify whether this ligand and its ternary complexes of can be used as seed germination activity by measurement of parameters like percentage of germination, survival, seedling height, soot length, root length, root/soot ratio and width of young leaf. The average values of these parameters have been used to make a justification about seed germination activity of ligand and its ternary complexes.

Keyword: Seed germination, Ligand metal, Soot length, Root length, Root/Soot ratio.

INTRODUCTION

Plants are autotrophic in nature, they produce their own food. But we are completely and absolutely dependent on plants for the necessities of life. A plant-based diet – mainly on vegetables, fruits and whole grains – has become one of the most important guidelines for lowering the risk of human diseases. Therefore, need to improve the nutritive value of the final products of vegetables plant. So that it is necessary to do agricultural research is the production of new and better qualities and varieties of crop plants, the improvement of plant growth, protection against insects, diseases and weeds, the control of soil fertility. Chromone have immersed biological properties reported (Noor Mohammad, 2014). Plant growth regulating activity of complexes of transition metal ions reported by different co-workers,

(Sharma et al., 1981; Patil, 2009; Thakare, 2007 ; Adams and Bernays, 1978;

Meshram et al., 2011 ; Singh, et al., 2011 ; Mane et al., 2010). Germination is an economical and simple method for improving the nutritive value of plants studies has reported, King- Ramteke, et al [9-12]. As we move among several economical plants, *Trigonella* (Methi) is selected as a plant system because this plant is in ideal system to study the germination and growth pattern. Further, economical importance of this plant is highlighted by its wide use for the vegetable purposes. The seed germination activity of 2-[(Z)-(2-phenyl-4H-chromen-4-ylidene) aminophenol and its Ni (III) and Cu (III) complexes on *Trigonella foenum-graecum* (Methi) is still lacking. So that the present work is carried out to study the plant

100

growth regulating activity of this ligand and its complexes on methi plant.

EXPERIMENTAL SECTION

Solutions of Ni (III) and Cu (III) metal nitrates of 0.01 mol/dm^3 concentration were prepared by adding accurate amounts of metal salts in distilled water. The solution of 2- [(Z)-(2-phenyl - 4H- chromen -4 -ylidene) aminophenol ligand of 0.01 mol/dm3 concentration was prepared in distilled water. The biological applications were studied at pH 4.5 and 9.5 and at 0.1mol/dm^3 ionic strength of KNO$_3$ solution. Fertilized soil was collected from agricultural land. Stones and other materials were sorted out and discarded. Two parts of this finely powdered soil was mixed with one part of filtered pink-stone-sand. This soil was filled in wooden trays having compartments of equal size. The soil in the tray was moistened with water. Sowing of seeds was done in this soil after one hour.

Healthy seeds of Methi of equal size were selected. 600 seeds were soaked in water and kept in refrigerator for 6 hours. From these, healthy seeds of equal size were chosen out of which 50 seeds each were soaked in distilled water, ligand solution, and ternary complex solution with Ni (III) and Cu (III) of pH 4.5 and 9.50 for 6 hours. The pH of test solutions was maintained using ELICO-pH meter-L1-10 (accuracy ±0.05 units). The seeds soaked were taken out of each solution and washed with distilled water. The seeds were sowed in the wooden trays in a row. Effect of ternary complexes of Ni (III) and Cu (III) studied at different pH (5.0 and 8.00), the seeds being immersed in experimental solution for 6 hours. Germination and survival were noted after12 days and 14 days respectively. By noting survival of the plants after 12 days, they were taken out of the soil. The seedling height, shoot length, root length, root/shoot ratio, and thickness (width length) of young leaf of survived plant were measured.

RESULTS AND DISCUSSION

Seed germination or plant growth was justified on the basis of parameters such as percentage of germination, survival, seedling height, shoot length, root length, root/shoot ratio, and thickness of young leaf. The average values of these parameters are shown in Table. The root/shoot ratio is one of the measures of overall health of the plants and it was determined .root/shoot ratio dry weight for roots/dry weight for top of plant. The dry weight was measured by keeping 50 fresh plantlets in oven first at 70°C and later at 100°C to obtain a constant weight. It can be seen from Table that there is change in the root: shoot ratio over control (water) which shows change in overall growth of the plant. In this presentation the root: shoot ratio has increased for both Ni(III) and Cu (III) complex at pH 4.5 and 9.5 as compared to control treatment, this increase is a sign of a healthier plant compared to other treatments.

Increase in this ratio came from greater root size and not from a decrease in shoot weight. Vigor index was determined using equation Vigour index % germination (root length in mm),(shoot length in mm). The higher value of vigor index at pH 4.5 and 9.5 are shown for the treatment of Cu (III) complex solutions. The vigor index values for various treatments are increased compared to control.

The order of plant growth regulators found at different pH is shown below: At pH 4.5 and 9.5, Cu (III)-Ligand complex solution > Ni (III)-Ligand complex solution > Ligand > Control (water).The Cu (III) - of 2-[(Z)-(2-phenyl-4H-chromen-4-ylidene) aminophenol complex solution is proposed as a plant growth regulator at pH 9.50 for *Trigonella foenum-graecum* (Methi) plant.

Table: Effect of ligand and its complexes with Ni (III) and Cu (III) on growth parameters of Methi plant (I=0.1 mol/dm^3 KNO$_3$)

Parameters	Effect of following solutions on different growth parameters			
	Control	Ligand	Ni (III)-Ligand complex	Cu (III)-Ligand complex
pH 4.5				
Germination seed number	50	50	50	50
% Germination after 12days	61	66	79	72
% Survival after 14 days	71	77	84	95
Seedling height (cm)	6.6	6.9	7.4	8.0
Root length (cm)	2.2	2.5	3.2	3.2
Shoot length (cm)	4.7	5.0	5.7	6.1
Root/shoot	0.35	0.45	0.57	0.63
Vigor index	4022	4747	6786	6463
Width of young leaf (cm)	0.5	0.6	0.7	0.7
pH 9.5				
Germination seed number	50	50	50	50
% Germination after 12days	62	61	68	76
% Survival after 14 days	73	79	83	90
Seedling height (cm)	7.8	8.0	8.3	8.4
Root length (cm)	2.7	3.1	3.5	3.8
Shoot length (cm)	4.7	5.1	5.8	6.2
Root/shoot	0.49	0.54	0.65	0.70
Vigor index	4333	4742	6032	7278
Width of young leaf (cm)	0.6	0.4	0.7	0.8

REFERENCES

Noor Mohammad *Ph.D. Thesis*, *Chemistry*, 2014, S. G. B. Amravati University, (MS) India.

Sharma, R.C, Tripathi, S.P and Khann, S and RS Sharma. *Curr. Sci.*, 1981, 50, 748-750.

Patiln, AB, *Orient. J. Chem.*, **2009**, 25(2), 459-460.

Thakare, V.J, *Ph.D. Thesis*, *Chemistry*, 2007, S. G. B. Amravati University, (MS) India.

Adams, C.M and Bernays, E.A. *Entomol. Exp. Appl.*, **1978**, 23, 101-109.

Meshram, U.P, Khobragade, B.G, Narwade, M.L, and Khobragade, V.B. *Der Pharma Chemica*, **2011**, 3(2), 376-382.

Singh, V.P.,Yashovardhan and Bhati, S.K. *Int. J. ChemTech Res.,* **2011**, 3 (2), 892-900.

Mane, A.V., Sankpal, R.R., Mane, L.A and Ambawade, M.S. *J. Chem. Pharm. Res.,* **2010**, 2(5), 206-215.

King, R.D and P. Perwastien, *J. of Food Science*. **1987,** 52, 106–108.

Frias, J and M. Prodanov and I. Sierra and C. Vidal-Valerie, *Journal of Food Protection*. **1995,** 58, 692–695.

Honke, J and H. Kozłowska and C.Vidal-Valverd and J. Frias, R Go, *Recki Zeitschrift ƒ Єur Lebensmittel- Untersuchung und - Forschung A*., **1998**, 206, 279–283.

Ramteke, A and M. L. Narwade and P. D. Shirgave, *Journal of Chemical and Pharmaceutical Research,* **2012**, 4(4):1889 1894.

103

Molecular Interactions in Substituted Pyrimidines—Acetonitrile Solutions at 298.15—318.15 K[1]

A. B. Naik[a], M. L. Narwade[b], P. S. Bodakhe[b], and G. G. Muley[c]

[a] *Physical Chemistry Laboratory, Department of Chemical Technology, SGB Amravati University,
Amravati-444602 (M.S.) India*
[b] *Vidyabharati Mahavidyalaya, Amravati-444602 (M.S.) India*
[c] *Department of Physics, SGB Amravati University, Amravati-444602 (M.S.) India*
e-mail: anilnaik@sgbau.ac.in; naikabn@gmail.com

Abstract—Density, ultrasonic speed in pure solvent acetonitrile (AN) and ligand solution of substituted pyrimidine in pure AN were measured at different temperatures (298.15, 303.15, 308.15, 313.15, and 318.15 K). Acoustical parameters such as adiabatic compressibility, intermolecular free length, acoustical impedance and relative association were determined from the experimental data of density and ultrasonic speed. The effect of temperature variations on the strength of molecular interaction has been studied. An excellent correlation represents in terms of solute—solvent interaction at all temperatures.

Keywords: density, ultrasonic velocity, acoustical parameter, molecular interaction, pyrimidine, acetonitrile.

INTRODUCTION

Ultrasonic methods have established an important place in science and new applications are found for the solution of many theoretical and practical problems [1]. Most important features of ultrasonic systems are robustness, non-invasiveness, precision, low cost, rapidity, and easy automation. Investigation of changes in thermodynamical properties of mixtures and the degree of their deviations from ideal mixing behavior are an excellent qualitative way to elicit information about molecular structure and intermolecular forces in liquid mixture. This has given impetus to the theoretical and experimental investigation of excess thermodynamic properties of liquid mixtures [2—5].The measurements of physicochemical properties such as density, viscosity, ultrasonic velocity and refractive indices of pure components and their mixtures are being increasingly used as tools for investigations of the properties of pure and the nature intermolecular interaction between components of liquid mixtures [6, 7]. The knowledge of fluid properties is important for many industrial applications. Among these properties density plays an important role in many industrial processes [8].

Ultrasonic studies have found wide applications owing to their ability to characterize the physicochemical behavior of solutions. The measurements of ultrasonic velocity in solutions thus provide useful information regarding the degree of deviation from ideality, molecular association in solution and important correlation with various acoustical parameters [9—11]. Ultrasonic speed measurements are useful when dealing with the problems of structure and molecular interaction in liquids because of their accuracy. The concentration and temperature dependence of acoustic properties has proved to be a significant observation of intermolecular interaction in liquids and liquid mixtures [12, 13].

The thermodynamical functions like adiabatic compressibility, acoustic impedance, intermolecular free length, molar sound velocity have proved to be of immense value in predicting nature and strength of molecular association in liquid medium [14]. Bachu et al. [15] have reported the densities, viscosities and speed of sound of binary mixtures of phenylacetonitrile with some aliphatic alcohols at 308.15 K. This result reveals that the position of hydroxyl group, alkyl chain length and branching of alkyl chain have significant effects on thermodynamic properties of the system investigated. The substantial work also has been reported on the excess properties of acetonitrile + alkanols [16], acrylonitrile + alkanols [17], and benzonitrile + alkanols [18]. Abraham et al. [19] reported densities and sound speeds of AN + toluene mixture and observed negative variations in deviations of isentropic compressibility thereby suggesting strong interactions between AN—toluene molecules. These considerations prompted us to assess the densities, ultrasonic velocities and acoustical parameters of the mixture of AN with L_1, L_2, L_3, and L_4 mixtures at different tem-
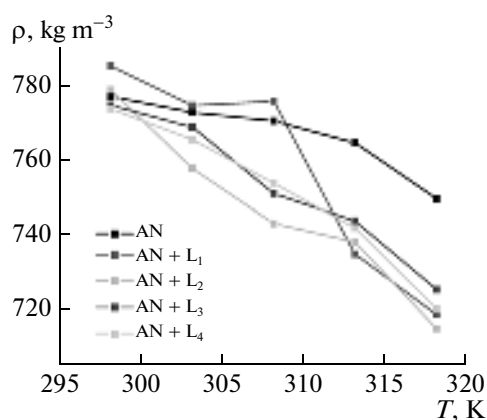
Fig. 1. The temperature dependences of experimental density of solutions of AN, L_1, L_2, L_3, and L_4 in AN with solute concentration of 1×10^{-3} M.

peratures (298.15, 303.15, 308.15, 313.15, and 318.15 K).

Heterocyclic compounds are of a great synthetic and structural versatility because they have a number of potential substitution positions. Furthermore heteroatoms offer the possibility of several modes of coordination. Heterocycle containing pyrimidine moiety possesses pharmaceutical, medicinal, agricultural, industrial and biotechnological significances. AN belong to nitrile series having functional group ($-C\equiv N$). It is a part of several biologically important molecules such as proteins, lipids and hormones. AN molecules are highly polar with their dipoles arranged in antiparallal pairs and this strongly ordered structure is stabilized by dipole−dipole interactions. AN is used mainly as a solvent in the purification of butadiene [20] in battery applications and also in the manufacture of DNA oligonucleotides from monomers. Industrially, it is used as a solvent for the manufacture of pharmaceuticals and photographic film. The great potential along with their interesting molecular structure promoted us to study molecular interaction in non aqueous media.

In the view of applications of these solvents and solutes in chemistry and modern technology for four binary mixtures they have been studied at different temperatures (297.15, 303.15, 308.15, 313.15, and 318.15 K).

EXPERIMENTAL

The ligands L_1, L_2, L_3, and L_4 were synthesized in the laboratory by known literature method [21]. The concentrated solutions of ligands were prepared by dissolving an accurate amount in AN solvent in standard flasks with airtight caps and the mass measurements were performed using high precision digital balance (Adair Datta of accuracy ±0.01 mg). The ultrasonic velocity in pure components and their mixtures were measured by ultrasonic interferometer (Mittal

enterprises, model F-81s) at 2 MHz with frequency tolerance ±0.03%. It consists of high frequency generator and a measuring cell. The densities of AN and ligands were measured by the specific gravity bottle with capacity 10 mL (Fig. 1). The accuracy of instrument was examined with pure distilled water and AN.

THEORY

Numerous methods are available in the literature for measuring ultrasonic velocity in solids and liquids. The ultrasonic interferometer is considered as more reliable and precise instrument. The expression used to determine ultrasonic velocity using ultrasonic interferometer is;

$$u = \nu\lambda, \qquad (1)$$

where u is ultrasonic velocity, and λ is wavelength. The adiabatic compressibility (β_s) was calculated from Newton−Laplace equation. It is extensively applicable in understanding physicochemical behavior of liquid mixtures such as molecular association, dissociation and formation. The adiabatic compressibility is given by equation:

$$\beta_s = 1/\rho_s u^2, \qquad (2)$$

where ρ_s is density of solution, and u is speed of ultrasonic velocity. The intermolecular free length between molecules in the liquid state is an essential and characteristic feature for interaction. Intermolecular force is one way or another to determine the properties of liquids of attractive and repulsive forces [22]. The intermolecular free length (L_f) is calculated by using the standard expression;

$$L_f = K\beta_s^{1/2}, \qquad (3)$$

where K is a temperature dependent constant known as Jacobson constant. The acoustic impedance (Z) of a wave can be mathematically defined as the product of the wave velocity in the medium and its density. As the waves encounter the interface between the liquid and solid, they sense a change in acoustic impedance and are obtained by equation:

$$Z = u\rho. \qquad (4)$$

The relative association (R_A) was calculated by the following equation;

$$R_A = (\rho_s/\rho_0)(u_0/u_s)^{1/3}, \qquad (5)$$

where ρ_0 is density of solvent, and u_0 is velocity of solvent.

RESULTS AND DISCUSSION

The calibration of the ultrasonic interferometer and specific gravity bottle were done by measuring the ultrasonic velocities and densities of pure AN and distilled water respectively. The measured values reported in Table 1 are good concordance with literature values. Small difference may result from differences in the

Table 1. Comparison of densities (ρ) and ultrasonic velocities (u) of distilled water and AN along with their literature values at different temperatures

Liquid	T, K	ρ, g cm^{-3}		u, m s^{-1}	
		exptl.	lit.	exptl.	lit.
Water	298.15	0.9962	0.9900 [23], 0.9970 [24]	1497	1480 [23], 1520 [24],
	293.15		0.9982 [26]		1496.9 [25], 1483.1 [26]
AN	298.15	0.7771	0.7765 [27], 0.775 [28]	1268	1271.3 [28]
	303.15	0.7728	0.7699 [27]	1252	1250 [27]
	308.15	0.7705	0.7652 [26]	1234	—
	313.15	0.7646	—	1218	—
	318.15	0.7496	—	1206	—

Table 2. Experimental density and ultrasonic velocity of L_1, L_2, L_3, and L_4 in AN at different temperatures with solute concentration of 1×10^{-3} M

T, K	ρ, kg m^{-3}					u, m s^{-1}				
	AN	AN + L_1	AN + L_2	AN + L_3	AN + L_4	AN	AN + L_1	AN + L_2	AN + L_3	AN + L_4
298.15	777.1	785.3	778.9	774.7	773.7	1268	1288	1296	1292	1289
303.15	772.8	774.6	757.7	768.8	765.5	1252	1260	1260	1262	1262
308.15	770.5	775.8	743.0	751.0	753.8	1234	1248	1245	1247	1253
313.15	764.6	734.8	738.1	743.7	741.8	1218	1232	1224	1220	1232
318.15	749.6	718.6	714.8	725.3	720.2	1206	1212	1184	1192	1208

purity of chemicals, measurements, techniques and calibrations. The values of densities and ultrasonic velocities of L_1, L_2, L_3, and L_4 listed in Table 2 showed that decreases with increase in temperature [29, 30]. As the temperature increased available thermal energy facilitates the breaking of the bonds between the associated molecules into their monomers. Moreover, increases of thermal energy weaken the molecular forces which tend the decrease the ultrasonic velocity. Figure 2 shows the variation of ultrasonic velocity with substituted pyrimidine in AN at different temperatures. The thermodynamic parameters, adiabatic compressibility, free length, acoustic impedance and relative association are presented in Tables 3 and 4. Figure 3, it can be seen that the values of adiabatic compressibility increase by increasing temperature
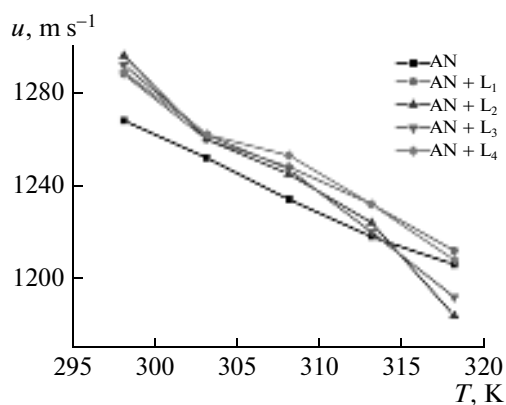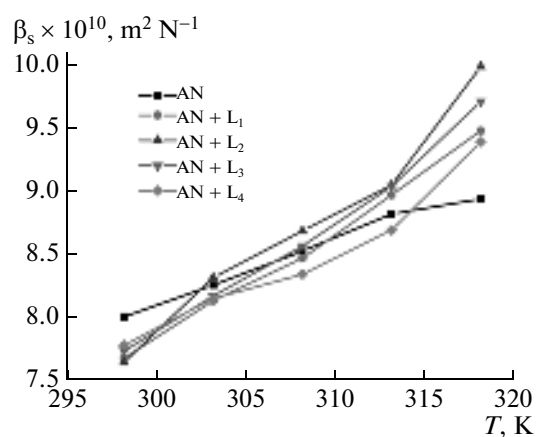

Fig. 2. The temperature dependences of ultrasonic velocity in solutions of AN, L_1, L_2, L_3, and L_4 in AN with solute concentration of 1×10^{-3} M.

Fig. 3. The temperature dependences of adiabatic compressibility (β_s) of solutions of AN, L_1, L_2, L_3 and L_4 in AN with solute concentration of 1×10^{-3} M.

Table 3. Variation of adiabatic compressibility (β_s) and linear free length (L_f) and acoustic impedance (Z) of L_1, L_2, L_3, and L_4 in AN at different temperatures with solute concentration of 1×10^{-3} M

T, K	AN	AN + L_1	AN + L_2	AN + L_3	AN + L_4
			$\beta_s \times 10^{10}$, m^2 N^{-1}		
298.15	8.0035	7.6759	7.6437	7.7328	7.7789
303.15	8.2551	8.1317	8.3130	8.1671	8.1490
308.15	8.5230	8.4670	8.6830	8.5630	8.3390
313.15	8.8159	8.9662	9.0431	9.0341	8.6883
318.15	8.9338	9.4734	9.9795	9.7035	9.3847
			$L_f \times 10^{10}$, m		
298.15	5.6182	5.4845	5.4730	5.5048	5.5211
303.15	5.7331	5.6901	5.7258	5.7024	5.6961
308.15	5.8715	5.8522	5.8798	5.8853	5.8078
313.15	6.0279	6.0790	6.1051	6.1021	5.9841
318.15	6.1153	6.3168	6.4833	6.3930	6.2871
			Z, N s m^{-5}		
298.15	985.36	1011.46	1009.45	1000.91	997.29
303.15	967.54	975.99	954.70	970.22	972.37
308.15	950.79	946.35	925.03	936.49	957.63
313.15	931.28	905.27	903.43	907.31	934.22
318.15	904.01	870.94	846.32	864.55	882.08

this is because at higher temperature ion–solvent interactions are weakened and therefore the number of AN molecules affected by the ions decreases with increasing temperature [31]. In the system the interaction becomes weak due to the thermal agitation of component molecules and this is indicated by the decrease in velocity values [32].

Figure 4 shows the variation of free length at different temperatures. The adiabatic compressibility and free length show an opposite trend to that of velocity. The decreased compressibility brings the molecules to a closer packing resulting a decrease in intermolecular free length. This may be due to presence of solvent molecules around the ions. According to a model proposed by Erying and Kinkaid [11], ultrasonic velocity decreases with increase in free length and vice versa. Increase in compressibility and free length with temperature for all system suggests breaking of hetero and homo association of molecules at higher temperature [33]. Acoustic impedance (Z) is dependent on both material and its geometry. It is seen from Fig. 5 the acoustic impedance decreases with increasing temperature in all the system [34]. The relative association (R_A) is influenced by two factors (i) the breaking up of
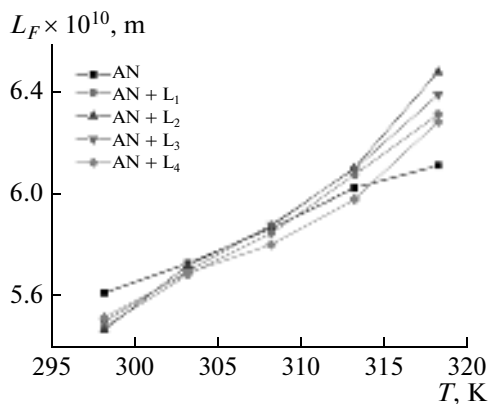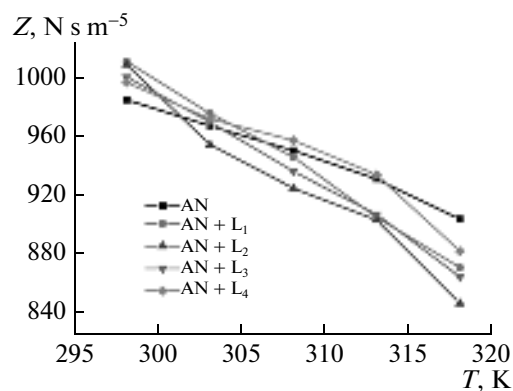

Fig. 4. Variation of linear free length (L_f) of L_1, L_2, L_3, and L_4 in AN at different temperatures T (K) with solute concentration of 1×10^{-3} M.

Fig. 5. The temperature dependences of acoustic impedance (Z) of L_1, L_2, L_3, and L_4 in AN different temperatures T (K) with solute concentration of 1×10^{-3} M.

Table 4. Variation of relative association (R_A) of L_1, L_2, L_3, and L_4 in AN at different temperatures with solute concentration of 1×10^{-3} M

T, K	AN + L_1	AN + L_2	AN + L_3	AN + L_4
298.15	1.0052	0.9950	0.9907	0.9901
303.15	1.0002	0.9783	0.9921	0.9943
308.15	0.9804	0.9614	0.9712	0.9862
313.15	0.9573	0.9637	0.9721	0.9879
318.15	0.9570	0.9594	0.9713	0.9735

the solvent molecules on addition of solute to it and (ii) the solvation of solute that are simultaneously present [35].

CONCLUSIONS

Ultrasonic method is a powerful tool for characterizing physicochemical properties and existence of molecular interaction in the mixture. The result reveals that the density and ultrasonic velocity of pure acetonitrile and ligand solutions increases with decreased with temperature. It is also seen that the formation of linear plot between temperature and respective parameters indicated that the stronger solute−solvent interaction. The plot between temperature and relative association are found to be nonlinear showed that the weaker solute−solvent interaction.

REFERENCES

1. A. M. E. Raj, L. B. Rasmi, V. B. Jothy, M. Jayachandran, and C. Sanjeeviraja, Fluid Phase Equlib. **281**, 78 (2009).
2. S. Singh, S. Parveen, D. V. Shukla, M. Yasmin, M. Gupta, and J. P. Shukla, J. Solution Chem. **40**, 889 (2011).
3. D. Shukla, S. Singh, S. Parveen, M. Gupta, and J. Shukla, Chin. J. Chem. **28**, 371 (2010).
4. N. G. Tsierkezos, M. M. Palaiologou, and I. E. Molinou, J. Chem. Eng. Data **45**, 272 (2000).
5. A. Ali, A. K. Nain, V. K. Sharma, and S. Ahamad, Ind. J. Phys. B **75**, 519 (2001).
6. D. V. Jahagirdar, B. R. Arbad, A. A. Walvekar, A. G. Shankarwar, and M. K. Lande, J. Mol. Liq. **85**, 361 (2000).
7. B. R. Arbad, M. K. Lande, M. K. Wankhede, and N. N. Wankhede, J. Chem. Eng. Data **51**, 68 (2006).
8. M. R. Francisca, Mesquita, X. Fillipe, Feitosa, R. S. Santiago, and H. B. S. Ana, J. Chem. Eng. Data **56**, 153 (2011).
9. R. Palani and S. Balakrishna, Ind. J. Pure Appl. Phys. **48**, 644 (2010).
10. R. Palani and K. Meenakshi, Ind. J. Chem. A **46**, 252 (2007).
11. J. F. Kincaid and H. Eyring, J. Chem. Phys. **6**, 587 (1938).
12. S. L. Oswal and N. B. Patel, J. Chem. Eng. Data **45**, 225 (2000).
13. K. Tumura, T. Sonada, and S. Murakami, J. Solution Chem. **28**, 777 (1999).
14. D. Bhatnagar, D. Joshi, Ashok Kumar, and C. L. Jain, Ind. J. Pure Appl. Phys. **48**, 31 (2010).
15. R. K. Bachu, M. K. Patwari, S. Boodida, S. J. Tangeda, and S. Nallani, Ind. J. Chem. A **47**, 1026 (2008).
16. P. S. Nikam, L. N. Sirsat, and M. Hasan, J. Chem. Eng. Data **43**, 732 (1998).
17. M. I. Aralguppi, C. V. Jadar, and T. M. Aminabhavi, J. Chem. Eng. Data **44**, 216 (1999).
18. P. S. Nikam, B. S. Jagdale, A. B. Sawant, and M. Hasan, J. Chem. Eng. Data **45**, 214 (2000).
19. R. Abraham, M. Abdul Khader, and C. V. Asokan, J. Chem. Thermodyn. **32**, 1 (2000).
20. K. Sarojini and T. Thenappan, J. Mol. Liq. **151**, 39 (2010).
21. P. S. Bodkhe, PhD Thesis (Amravati Univ., India, 2002).
22. B. Jacobson, Acta Chem. Scand. **6**, 1485 (1952).
23. M. Vatandas, A. B. Koe, and C. Koe, Eur. Food Res. Technol. **225**, 525 (2007).
24. V. K. Sharma and Satishkumar, J. Sol. Chem. **34**, 387 (2005).
25. J. M. Resa, C. Goensalez, J. M. Goenaga, and M. Iglesias, J. Therm. Anal. Calorim. **87**, 237 (2007).
26. M. M. Palaiologou, G. K. Arianas, and N. Tsierkezos, J. Solution Chem. **35**, 1551 (2006).
27. N. Sharma, S. Rana, and A. Sharma, Iron. J. Energy Environ. **1**, 280 (2010).
28. K. Rajgopal, S. Chenthilnath, and A. K. Nain, J. Mol. Liq. **151**, 23 (2010).
29. F. M. R. Mesquita, F. X. Feitosa, R. S. Santiago, and H. B. Ana, J. Chem. Eng. Data **56**, 153 (2011).
30. M. Hasan, A. P. Hiray, U. B. Kadam, D. F. Shinde, K. J. Kurhe, and A. B. Sawant, J. Chem. Eng. Data **55**, 535 (2010).
31. R. Sadeghi, R. Golabiazar, and M. Zialii, J. Chem. Eng. Data **55**, 125 (2010).
32. J. D. Pandey, S. Shukla, R. D. Rai, and K. Misra, J. Chem. Eng. Data **34**, 29 (1989).
33. T. Sumathi, S. Priyatharshini, and S. Punithasri, Ind. J. Pure Appl. Phys. **49**, 328 (2011).
34. A. N. Kannappan, R. Kesavasamy, and V. Ponnuswamy, ARPN J. Eng. Appl. Sci. **3** (4), 41 (2008).
35. P. B. Agrawal and M. L. Narwade, Ind. J. Chem. A **42**, 1047 (2003).

SYNTHESIS, CHARACTERIZATION AND IN VITRO ANTIMICROBIAL EVALUATION OF NOVEL 2-MERCAPTO-4,6-DISUBSTITUTED PHENYL PYRIMIDINE DERIVATIVES

SHRADHA. S. BINANI*, P. S. BODKE, R.V.JOAT[1].

Department of chemistry, [1]Department of Physics, Vidyabharati Mahavidyalaya, Amravati 444602. Email: Shradhabinani88@gmail.com

ABSTRACT

Objective: Synthesis and antimicrobial evaluation of a novel 2-mercapto-4,6-disubstituted phenyl pyrimidine derivatives.

Methods: A series of novel 2-mercapto-4,6-disubstituted phenyl pyrimidine derivatives(5a-d) were synthesized by refluxing 1-(2'hydroxy aryl)-3-(substituted aryl) prop-1,3-dione(4a-d) with thiourea in DMF solvent and obtained in good yield. 1-(2'-hydroxy aryl)-3-(substituted aryl) prop-1,3-dione(4a-d) were obtained by BVT rearrangement in pyridine medium from corresponding 2-benzoyloxy acetophenone (3a-d). The newly synthesized compounds are characterized by IR, H[1]NMR mass spectral studies and elemental analysis. These compounds were also screened for their In-vitro antibacterial and antifungal activities.

Results and conclusion: Preliminary results reveal that some of the synthesized compounds are showing promising antibacterial and antifungal activity.

Keywords: 2-mercapto-4,6-disubstituted pyrimidines, prop-1,3-dione, thiourea, antibacterial, antifungal activity.

INTRODUCTION

Recent decades have witnessed an exponential growth in the applications of heterocyclic compounds containing nitrogen, oxygen and sulphur due to their wide range of pharmacological activities. Pyrimidine based heterocyclic compounds are of interest as potential bioactive molecules and exhibit analgesic, (1)antihypertensive(2), antipyretic(3), antiviral(4) and anti-inflammatory(5) activities. These are also associated with nucleic acid, antibiotic, antimalarial, anticancer drugs(6).Many of the pyrimidine derivatives are reported to possess potential CNS depressant properties(7).

Fig. 1: Experimental scheme for the synthesis of 2-mercapto-4,6-disubstituted phenyl pyrimidines (5a-d)

There are few reports concerning with pyrimidine ring containing mercapto groups (8).The mercapto derivatives have been shown to exhibit cytotoxic activity (9) and various derivatives of mercapto fused with pyrimidine ring were synthesized and evaluated for antibacterial, antifungal activities in our laboratory (10, 11).hence it was thought of interest to synthesize new derivatives of mercapto pyrimidines by simple method and investigate them for biological and pharmacological activities.

From the above facts it was contemplated to synthesize a novel series of 2-mercapto-4,6-disubstituted phenyl pyrimidines. The final synthesized compounds were screened for their in-vitro antibacterial,antifungal activities.

The key starting materials 2-benzoyloxy acetophenone (3a-d) were prepared by condensation of 5-chloro-2-hydroxy-4-methyl acetophenone (1) in pyridine medium using appropriate aromatic acids(3-OCH$_3$ benzoic acid/4-OCH$_3$ benzoic acid/Para chloro benzoic acid/2,4-dichloro benzoic acid)(2)in presence of POCl$_3$.1-(2'-hydroxy aryl)-3-(substituted aryl) prop-1,3-dione(4a-d) were obtained by BVT(12) of corresponding 2-benzoyloxy acetophenone as per known procedures. A mixture of diketone and thiourea in DMF solvent was refluxed to yield the title compounds 2-mercapto-4,6-disubstituted phenyl pyrimidines(5a-d).The synthetic strategies adopted to obtain the target compounds are depicted as **Scheme-01.**

MATERIAL AND METHODS

The IR spectrum is recorded by using Alpha Bruker IR spectrometer using a thin film on KBr pellets and frequencies are expressed in cm^{-1}.The H^{1}NMR spectra were recorded on bruker advance ii 400 MHz NMR spectrometer. All spectra were obtained in CDCl3 and DMSO d$_6$ as a solvent. Chemical shifts values are reported as values in ppm relative to TMS as internal standard. Mass spectra were recorded on ESI. Melting point were determined by open capillary method and are uncorrected. All the synthesized compounds were purified by recrystallization. Elemental analysis was also performed. Purity of the compound was checked by TLC.

Synthesis

A mixture of diketone (0.01 mole) and thiourea (0.01 mole) in DMF(50 ml) solvent was refluxed on water bath at 75-90 ^{0}C for 1hr and mixture was cooled and pour in ice cold aqueous solution. The solid separated was washed with water and crystallized from aq. alcohol to give mercapto pyrimidines. The progress of the reaction was monitored by TLC (benzene: chloroform 8:2).The physical data is as follows.
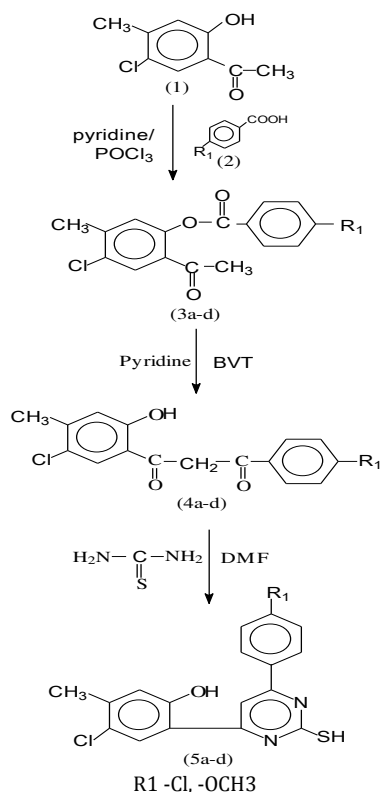
Spectral data for all the compounds

1) 2-mercapto-4-(3-OCH3 phenyl)-6-(2' hydroxy-4' methyl-5' chloro phenyl) pyrimidine:

M.wt:-358.5gm, M.P:-142 ⁰C, yellow solid coloured compound.

H¹Nmr:-400 MHz (CDCl₃): 10.37(s, 1H, SH), 6.68-8.07(m, 7H, Ar-H)

IR(cm⁻¹):3526(Ar-OH),3026(CH),1577(C=N),1427(C=C),1265(-OCH3),773(C-Cl),2559(S-H).

Mass :359 (M⁺)

2) 2-mercpto-4-(4-OCH3 phenyl)-6-(2' hydroxyl -4' methyl-5' chloro phenyl) pyrimidine:

M.wt:- 358.5gm,M.P:-150 ⁰C,yellow solid coloured compound.

H¹NMR:-400 MHz (CDCl₃):12.4(s,1H,SH),6.8-7.4(m,7H,Ar-H)

IR(cm⁻¹):3448(Ar-OH),   2983(CH),1605(C=N),1428(C=C),1263(-OCH3),772(C-Cl),2554(S-H).

Mass :359 (M⁺)

3) 2-mercpto-4-(4-chloro phenyl)-6-(2' hydroxyl -4' methyl-5' chloro phenyl) pyrimidine:

M.wt:- 363 gm, M.P:-179 ⁰C, white solid coloured compound.

H¹NMR:-400 MHz (CDCl₃):11.9 (s,1H,SH),6.15-8.4 (m,7H,Ar-H)

IR(cm⁻¹):3448(Ar-OH),   2982(CH),1612(C=N),1424(C=C),761(C-Cl),2557(S-H).

Mass :364 (M⁺)

4)2-mercapto-4-(2,4-dichloro phenyl)-6-(2' hydroxyl-4'methyl-5' chloro phenyl) pyrimidine:

M.wt:- 397.5 gm, M.P:-152 ⁰C, white solid coloured compound.

H¹NMR:-400 MHz (CDCl₃):11.9 (s,1H,SH),7.4-8.2 (m,7H,Ar-H)

IR(cm⁻¹):3431(Ar-OH),   2962(CH),1624(C=N),1408(C=C),771(C-Cl),2544(S-H).

Mass: 398 (M⁺)

Antimicrobial activity

The in-vitro anti microbial screening of newly synthesized 2-mercapto-4,6-disubstituted pyrimidine was carried out against gram +ve organisms (staphylococcus aureus), Gram –ve organisms(Salmonella typhus, pseudomonas aeruginosa and E.coli) and fungi(Candida albicans and aspergillus niger) by disc diffusion method(13) and compared with that of the standard drugs Oxacillin and Fluconazole respectively.MIC of each drug was defined as the lowest concentration of an antimicrobial that will inhibit the visible growth of micro organism after incubation time. Muller Hinton Agar was used as basal medium for test of bacteria and fungi respectively. The compounds tested at a concentration of 50ug/ml for bacterial 500ug/ml for fungal growth in DMF solution was added to the wells made on culture medium. After 24hr of incubation at 25⁰C for antibacterial activity and 48hrs at 30⁰C for antifungal activity, the zone of inhibition was compared with the standard drug Oxacillin (sensitivity at 13mm or more) and Fluconozole (sensitivity at 11mm or more).The antibacterial activity results revealed that compounds showed significant activity against gram +ve organisms. The compound 5a, 5b, 5c, 5d showed good activity against E. coli and most of the compounds displayed significant activity against S. aureus. However the compounds showed only moderate activity against the gram –ve organisms when compared to the standard drug.

In the antifungal activity, compounds showed moderate to weak activity against A. niger. The compounds 5a, 5b, 5c, 5d showed significant activity against C. albicans when compared to the standard drug.

RESULTS AND DISCUSSION

A novel series of 2-mercapto-4,6-disubstituted phenyl pyrimidine (5a-d) derivatives have been synthesized and screened for their in-vitro antibacterial and antifungal activities. The physical data of the final synthesized compounds are as follows:-

Table 1: Physical data of 2-mercapto-4,6-disubstituted phenyl pyrimidine derivatives (5a-d)

Compound	Ar-COOH	M.W.	M.P(⁰C)	Elemental Analysis			Yield (%)
				C (%)	H (%)	N (%)	
5a.	3-OCH₃	358.5 gm	142-144⁰C	60.3	4.18	7.82	53
5b.	4-OCH₃	358.5 gm	148-150⁰C	60.3	4.18	7.82	76
5c.	4-Cl	363 gm	177-179⁰C	56.19	3.30	7.79	65
5d.	2,4-Cl	397.5 gm	152-155⁰C	51.3	2.76	7.04	75

M.W: Molecular Weight; **M.P**: Melting point in ⁰C

Table 2: Antimicrobial activity of 2-mercapto-4,6-disubstituted phenyl pyrimidine (5a-d) by disc diffusion method

S. No.	Tested compounds	Bacterial(zone of inhibition in mm) at 50µg/ml				Fungal(zone of inhibition in mm) at 500µg/ml	
		E.coli	P.aeruginosa	S.typhi	S.aureus	A.niger	C. albicans
1.	5a	11 mm	_	12 mm	18 mm	_	18 mm
2.	5b	13 mm	12 mm	14 mm	16 mm	15 mm	16 mm
3.	5c	15 mm	11 mm	13 mm	17 mm	16 mm	12 mm
4.	5d	14 mm	12 mm	13 mm	19 mm	_	10 mm

Oxacillin sensitivity -13mm or more, **Fluconazole** sensitivity -12mm or more.

'‒' No inhibition

The structures of the newly synthesized compounds were established on the basis of spectral data and elemental analysis. The compounds were purified by recrystallization from appropriate solvents. The completion of the reaction is monitored by TLC.

The antimicrobial activity of the compounds showed good activity against the gram +ve organism most of the synthesized compounds showed significant activity against staphylococcus aureus.

The compounds also displayed good activity against fungal organism C. albicans.

CONCLUSIONS

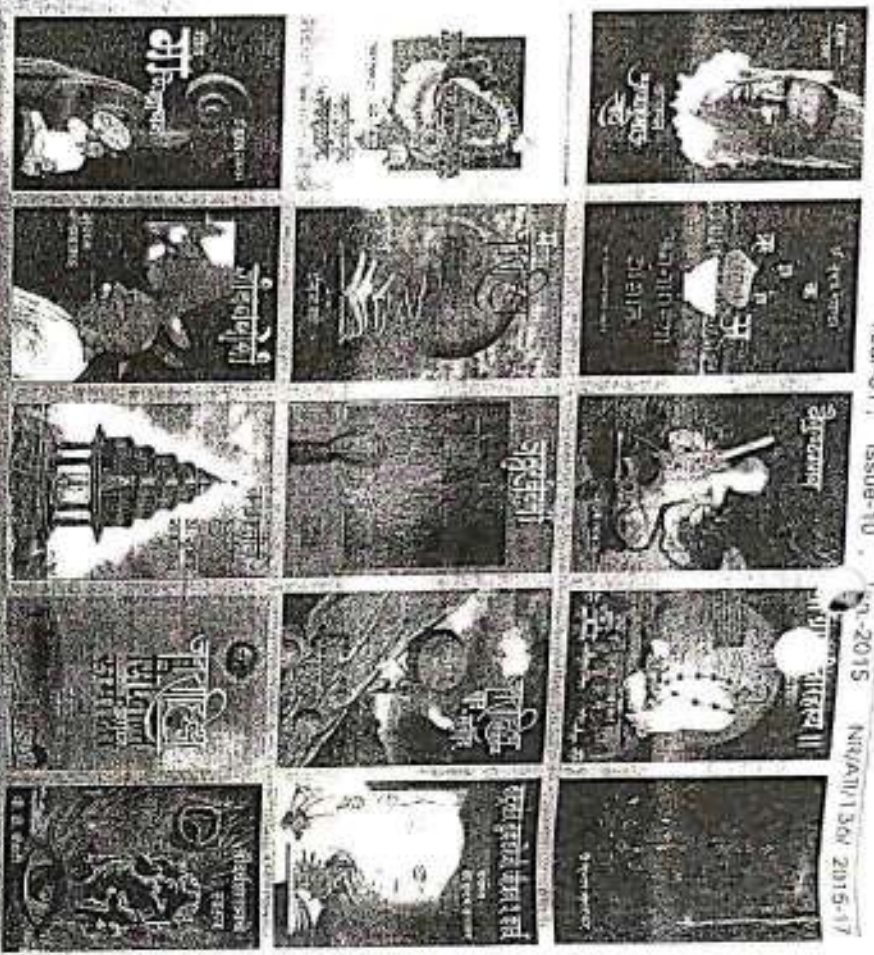From the above results it can be concluded that the compound having electron releasing group (C₆H₅) exhibit more activity. Further introduction of chlorine atom and hydroxyl group in benzene ring increases anti-microbial activity of compounds. Among the compounds (5a-d) disubstituted halogens (5d) are more active than mono substituted halogens (5c) against antimicrobial activity and the rest compound (5a, 5b) show moderate activity.

ACKNOWLEDGEMENT

REFERENCES

1. Anshu chaudhary, pramod Kumar Sharma, prabhakar verma, Nitin Kumar, Rupesh dudhe.Microwave assisted synthesis of novel pyrimidine derivatives and investigation of their analgesic and ulcerogenic activity. Medicinal chemistry research 2012; 21(11):3629-45.
2. Sekiya T, Hiranuma H, Hata S, Mizogami S, Hanazuka M, Yamada S. Synthesis and hypertensive activity of 4-amino-2-(4-cinnamoylpiperazino)-6,7-dimethoxyquinazoline derivatives. J.Med chem.1983 26(3):411-6.
3. Makino H, Kuzuna S, Naka T, Saijo T, Maki Y. Anti-inflammatory, analgesic, and antipyretic activities of methyl 7-butyl-4, 5, 6, 7-tetrahydro-3-methylamino-4, 6-dioxo-5-propyl-2H-pyrazol o [3, 4-d] pyrimidine-2-carboxylate (AA-2379), a novel non-acidic agent. Agents Actions. 1988 Dec; 25(3-4):385-93.
4. Ajitha.M, Rajnarayana K. Synthesis and evaluation of new-3-substituted – [3, 4-dihydropyrimidinones-Indolin-2-ones for cytotoxic activity. Int J pharmacy and pharmaceutical Sciences. 2011;3(4):89-93.
5. M Amir, SA Javed, Harish Kumar Pyrimidine as anti-inflammatory agent: A review 2007; 69(3): 337-343.
6. V.N.Ingle, S.T.Kharche and U.G.Upadhyay. Synthesis of some new 4-0-(-β-D-glucopyranosyloxy)-4,6–diaryl –tetra hydro pyrimidine -2-thianes and their biological activities. Indian journal of chemistry. 2004, pp 2027-2031.
7. Abdellatif M. Salaheldin and Ligia M.Rodrigues. Synthesis of some novel pyrazolo [3, 4-d] pyrimidine derivatives. Arikvoc 2007; 16: 92-100.
8. M.P.V.Boarland and J. F. W. McOmie. Pyrimidine part III.The ultra-violet adsorption spectra of some polysubstituted pyrimidines**. J. Chem. Soc.,** 1952, 3722-3728
9. Xanthopoulou MN, Hadjikakou SK, Hadjiliadis N, Schumann M, Jurkschat K, Michaelides A, Skoulika S, Bakas T, Binolis J, Karkabounas S, Charalabopoulos K.Synthesis,structural characterization and in vitro cytoxicity of organotin (IV) derivatives of heterocyclic thioamides,2-mercaptobenzothiazole,5-chloro-2-mercaptobenzothiazole,3-methyl-2-mercaptobenzothiazole and 2-mercaptonicotinic acid. J Inorg Biochem. 2003 Aug 1; 96(2-3):425-34.
10. MN Kumaraswamy, DA Prathima Mathias, C Chandrashekhar, VP Vaidya. Synthesis and pharmacological evaluation of 2-mercapto-4-substituted-naphtho [2, 1-b] furo [3, 2-d] pyrimidines, Indian journal of pharmaceutical sciences. 2006 ; 68 (6): 731-736
11. Gertrude B. Elion, Elizabeth Burgi, George H. Hitchings. Studies on Condensed Pyrimidine Systems.IX. The Synthesis of some 6-Substituted Purines J. Am. Chem. Soc., 1952, 74 (2): 411–414
12. George A. Kraus, Brian S. Fulton, Soon Hyung Wood. Aliphatic acyl transfer in the Baker-Venkataraman reaction J. Org. Chem., 1984, 49 (17): 3212–3214
13. Murray P.R, Baron E.J, Pfaller M.A, Tenover F.C, Yolken R, American Society for Microbiology, Washington DC, 1995, 1342-1349.

प्रा. मनिष चोपडे

प्रति,

वर्ष-३१ | अंक-१० | नोव्हेंबर-२०१५

बाबाराव मुसळे यांच्या 'झिंगू लिंगू लिंगू' मधील स्त्री चित्रण

डॉ. गजानन बनसोड
सहयक्षक प्राध्यापक, मराठी विभाग, विदाभारती महाविद्यालय, अमरावती

प्रास्ताविक-

ग्रामीण वास्तवाचे सूक्ष्मदर्शी चित्रण करणारे बाबाराव मुसळे हे कथाकार व कादंबरीकार म्हणून मराठी साहित्यविश्वात परिचित आहेत. त्यांच्या 'पखाल' या कादंबरीला महाराष्ट्र शासनाचा अनुदूक वाड्मय निर्मितीचा पुरस्कार मिळाला आहे. त्यांच्या 'मोहरलेला चंद्र' या कथासंग्रह प्रसिद्ध आहे. मेहता पब्लिशिंग हाऊसने 'झिंगू लिंगू लिंगू' या शीर्षकाचा कथासंग्रह १९९२ मध्ये प्रकाशित केला. या संग्रहात एकूण १३ कथा आहेत. यातील कथा वाचनीय असून ग्रामजीवनातील पात्रे चांगून रेखाटली...

(१) **'झिंगू लिंगू लिंगू' मधील ग्रामजीवन-**

...

(२) **चित्रांच्या जीवनजाणिवेचा आविष्कार-**

...

लग्याशी बोलताना अतिशय कडवट प्रतिक्रिया देते. 'त्याले मनाव आंधी तुझ्या मायचं काळंपांढरं कर, तव्हा मले नेयाले ये. तसं मनशिल तं तुहं तोंड पाह्याची इच्छा नाही मनाव.'१

मायच्या चोरून बायकोला भेटणारा देवकीचा नवरा वरील प्रसंगात आहे. सासूच्या अत्याचारापासून सोडवून तिला माहेरी पोहोचवून देणारा देवकीचा सासरा, 'कॅन्सर' या कथेत आंजूबयला लूटणारा जावई सुब्रिद्रीचा नवरा लक्षात राहातो. घरातले भांडे-कुंडे विकणारा, मायेचे से चोरणारा, 'म्या पैसे घेतले हे का तुवा मायले सांगतलं तं तुही खाटच पाडीन' असं बायकोला धमकावणारा सुरेखाचा नवराही लक्षात राहातो. नळावरचं पाणी आणल म्हणून गिरजाला मारणारा 'पूजा' बदल स्वीकारीत नाही. 'पखाल' कोणी घेत नाही म्हणून खजील होतो. 'बनाव' कथेत दारू पिण्यासाठी रघु लहाने बायकोला घेऊन दारुच्या दुकानात जातो. त्याच्या दारात बायकोला उभं करतो व म्हणतो, 'वामन, ही रांड रातभर तुझ्या घरात ठेव. खाऊ खाऊ माजली. इच्या बदल्यात मले आजूक दारु पियाले दे.'१० भोवतालचे लोक तमाशा पाहातात. सीता संतापते व दारू पिण्याचा 'बनाव' जेव्हा ती करते तेव्हा नवऱ्याची ती पुरती जिरवते. आपल्या व्यसनापायी बायकोचे हाल होतात हे त्यांच्या लक्षात येत नाही. ग्रामीण भागातल्या छंदीफंदी लोकांचे वर्णनही बाबाराव मुसळे कथेत करतात.

निष्कर्ष-

(१) बाबाराव मुसळे यांनी ग्रामीण भागातील स्त्रियांचे प्रभावी चित्रण 'झिंगु लुखू लुखू' या कथासंग्रहात केले आहे. (२) परंपरा जपणारी रूढिप्रिय 'स्त्री' कथेतील नायिकेच्या रूपात व्यक्त झाली. (३) 'झिंगू लुखू लुखू' मधील स्त्री परिवर्तनाचा पुरस्कार करणारी नाही. (४) सासूचा छळ निमूटपणे सोसणारी सून 'खेळवण', 'रुखवत' या कथांत व्यक्त होते. (५) तेराही कथांतील स्त्रियांचे चित्रण लेखकांनी जिव्हाळ्याने केलेले जाणवते. (६) शेतामध्ये काबाडकष्ट करणारी, श्रमणारी, तरीही शोषणाला बळी पडलेल्या स्त्रियांचे 'कॅन्सर', 'रुखवत', 'खेळवण', 'झिंगु लुखू लुखू' मध्ये उठावदार चित्रण आहे.(७) सुनेची बाजू घेणारा सासरा 'रुखवत' व 'झिंगू लुखू लुखू' या कथांत आहे.

संदर्भ टीपा-

(१) मराठी कथा : वाटा आणि वळणे - प्रा. जयंतकुमार बंड, मराठी जनसाहित्य परिषद, अमरावती, प्रथमावृत्ती १९८८, पृ.१०६-१०७. (२) १९८० नंतरची ग्रामीण कथा- डॉ.मनोहर सुरवाडे, बळीवंश प्रकाशन, नांदेड, प्र.आ.१७ सप्टेंबर २०१०, पृ.१८७. (३) झिंगु लुखू लुखू- बाबाराव मुसळे, मेहता पब्लिशिंग हाऊस, पुणे, प्र.आ.१९९२, पृ.६१. (४) उ.नि., दावणीचा बैल, पृ.६. (५) उ.नि., दावणीचा बैल, पृ.९ (६) उ.नि., तंबाखू, पृ.१३. (७) उ.नि. रुखवत, पृ.२५. (८) उ.नि.,१९८० नंतरची ग्रामीण कथा, पृ. २७८. (९) उ.नि., रुखवत, पृ.२९. (१०) उ.नि., बनाव, पृ.१२०.

Characterization of Pure Nanostructure ZnO and its Application as Gas Sensor

S. D. Charpe[1], F. C. Raghuwanshi[2] and V. S. Kalymwar[3]

[1]Department of Physics,
Vidya Bharati Mahavidyalaya, Amravati, INDIA.
sushildeo86@gmail.com
[2]The Principal,
Department of Physics,
Vidya Bharati Mahavidyalaya, Amravati, INDIA.
[3]Department of Physics,
Bharatiya Mahavidyalaya, Amravati, INDIA.

ABSTRACT

The ZnO nanostructures have been synthesized and studied as the sensing element for the detection of H_2S gas. The ZnO nanostructures were synthesized by Sol-gel method followed by sonication. By using screen printing method, thick films of synthesized ZnO nanostructure were deposited on glass substrate. Gas sensing properties of ZnO nanostructure thick films were studied for low concentration H_2S gas at different temperature. ZnO nanostructure synthesized by this method can be used as a promising material for semiconductor gas sensor to detect gas like H_2S at room temperature with high sensitivity and selectivity.

Keywords: Nanostructure ZnO, Characterization; UV, FTIR, XRD, TEM, SEM and H_2S Sensor.

1. INTRODUCTION

Sensor science and engineering is relevant to virtually all aspects of life including safety, security, surveillance, monitoring, and awareness in general. Owing to recent consciousness in environmental pollution, there is a growing need for reliable and inexpensive gas sensors and monitoring systems for industrial process and production areas. The modern industrial monitoring is based on the capability of measuring and controlling physical and chemical parameters such as temperature, pressure and chemical composition. Hence, the development of specific and efficient sensors is a necessity. Recently, sensors has

been using for a variety of purposes such as detection of smoke, radiation, hazardous gases. This demand has been created by an increasing concern for pollution monitoring and improved safety in various environments, both industrial and domestic. In addition, these sensors could have an important role in the intelligent automatic control of a large number of processes, ranging from microwave cooking to the efficient combustion of motor engines[1]. Sensors are also central to medicines being used for diagnostics, monitoring, critical care, and public health.

Gas sensors play an important role in our everyday life in which we gather information, process it and perform some task. Yet, the successful application of a sensor is determined by its performance, cost and reliability. Recent technological developments both in the knowledge of the sensing principles and enabling technologies have led to the design of superior sensors with linear outputs. These sensors, which analyze or identify atmospheric gases, are useful in many fields of human activity including detection of toxic and explosive gases inside mines, gas leak inside residences and the control of atmospheric pollution. Aside from other applications, gas sensors are heavily used in areas like environmental monitoring, biotechnology, chemical analysis, and on-line detection of products. Thus, sensors open a wide range of applications from home to factory floor. They were first developed in Japan for devices such as gas leak alarms and measuring instruments. In addition, gas sensors make a major impact on many other different applications in areas like automotive industries, oil industries etc.

Nanostructured materials such as ZnO, SnO_2, and WO_3 have shown good electrical properties[2-13]. Among these nanostructure-semiconducting materials, ZnO has been studied extensively for electrical application and gas sensing. Due to its versatility and multifunctionality creates attention in the research field related to its electrical applicationsand gas sensing. A wide number of synthesis techniques also been developed by which ZnO can be grown in different nanoscale forms. Efforts were made to synthesize ZnO nanostructure with innovative morphology by Sol-gel method. The synthesized ZnO shows good electrical conductivity. In the present work, the efforts are made to study Characterizationand gas sensing of low cost (ZnO).

H_2S is a toxic gas produced from the coal, oil and natural gas industries. In order to enhance the sensitivity and selectivity of H_2S, many attempts were made to synthesized nanostructure ZnO with different morphologies[14-18].

2. EXPERIMENTAL

2.1. Synthesis of ZnO Nanostructure

All chemicals were of analytical grade and used as purchased without further purification. In present work, Zinc nitrate hexahydrate was dissolved in distilled water such that to make 0.15 M solution. Subsequently, 0.5 M NaOH aqueous solutionswere introduced into the above aqueous solution drop by drop with constant stirring. The resultant white solution was subsequently kept at 75 ^{0}C For 12 hrs and then cooled room temperature

naturally and sonicated (Ultrasonic wave treatment) for 30 min. The resulting white precipitates were collected by centrifugation, washed with distilled water and ethanol several times and then dried at 80^0C in vacuum oven for 2hr. Obtain ZnO nanostructure product were used for further study.

2.2. Preparation of Thick Films

Thick films of synthesized nanostructure ZnO were prepared by using screen printing technique. In present process, thixotropic paste was formulated by mixing the synthesized ZnO powder with ethyl cellulose (a temporary binder) in a mixture of organic solvents such as butylcellulose, butyl carbitol acetate and turpineol. The ratio of ZnO to ethyl cellulose was kept at 95:05. The ratio of inorganic to organic part was kept as 75:25 in formulating the pastes. The thixotropic pastes were screen printed on a glass substrate in desired patterns. The films pre-pared were fired at 500°C for 12 hr. Prepared thick films were called as pure ZnO thick films.

3. MATERIALS CHARACTERIZATION

3.1. Thickness Measurement

Thickness of all ZnO thick films were measured by using technique "Marutek film Thickness Measurement System" with the help of provided equipment. The thicknesses of all films were observed in the range from 35 μm. Thick films of approximately uniform thick-nesses were used for further characterization.

3.2 UV-visible absorption spectrum

UV-visible absorption spectroscopyis widely used tool for checking the opticalproperties of nanosized particles. Figure 3.2 shows the UV-visible absorption spectrum of ZnO nanoparticles calcined at temperature 800°C for 6 Hrs. From the spectrum four peaks are observed at 362nm, 318nm, 344nm and 296nm, out of this at 318 nm wavelength has been found maximum absorption, if we calculate band gap for this wavelength it is 3.30eV, which is very close to the band gap of ZnO 1s–1s electron transition (3.37eV)[19].

3.3 FTIR analysis

FTIR analysis spectrum shown in figure 3.6, indicating significant absorption peaks at wave numbers 4350, 4200, 3900, 3850, 1700, 1550 and 600, 510 cm^{-1}. The absorption band at 600 and 510 cm^{-1} is obtained due existence of Zn-O bond stretching vibration[20]. The peaks at 1700 and 1550 cm^{-1} shows H-O-H bending vibration due to the adsorption of moisture, when FTIR sample disks were prepared in an open air atmosphere. The remaining peaks between 4350 to 3850 cm^{-1} are corresponding to O-H stretching vibrations[21].
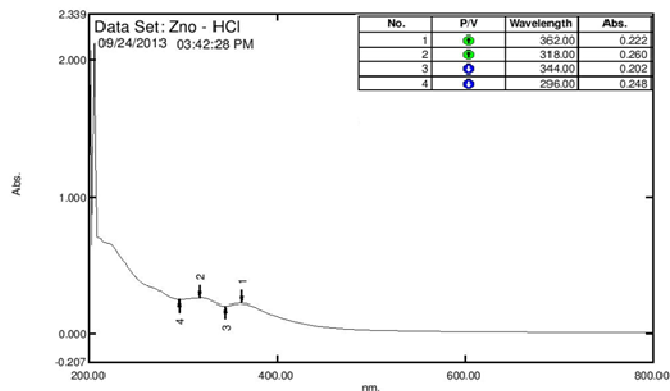
Figure 3.2UV-visible absorption spectrum of Pure ZnO
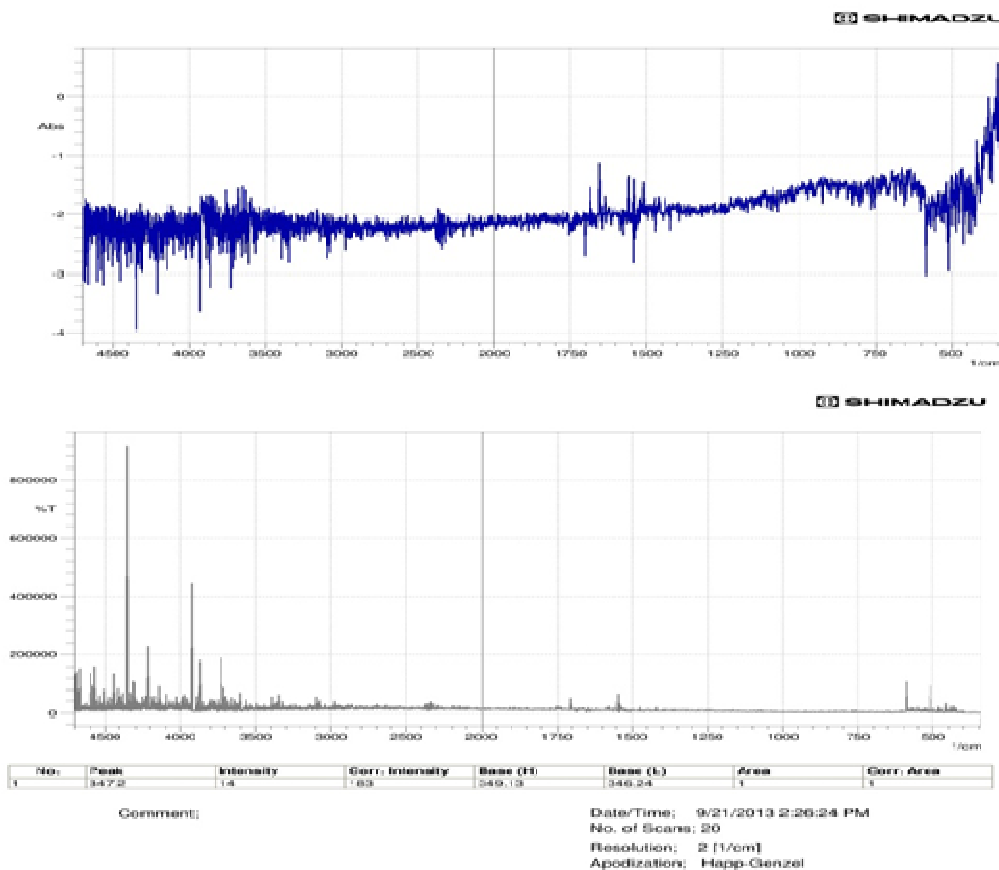
Figure 3.3FTIR absorption/transmission spectrum of Pure ZnO

3.4 X-Ray Diffraction Studies

The crystallographic structure of the synthesized ZnO nanostructure was characterized by powder X-ray diffraction (Philips X-ray diffractometer) with Cu-α source and 2θ range of 10° - 70°. Fig 1shows the XRD pattern of the ZnO nanostructure. The recorded XRD pattern confirmed that synthesized ZnO are highly crystalline in nature. The corresponding X-ray diffraction peak for (100), (002), (101), (102) (110), (103) and (112) planes confirm the formation of hexagonal wurtzite structure of ZnO (JCPDS card no.-01-080-0075). The domain size of the crystal can be estimated from the full width at half maximum (FWHM) of the peaks by means of the Scherrer formula,

$$D = \frac{k\lambda}{\beta sin\theta}$$

whereλ is the wavelength of incident beam (1.5406 Å), β is the FWHM of the peak in radians, θ is the diffraction angle and K is Scherrer constant. The average particle size was calculated from (101) peak ZnO is found to be 78 nm.

Using X'pert High Score Plus software it is confirm that synthesized zinc oxide powder contains Zn and O elements only, not any impurity and another element.
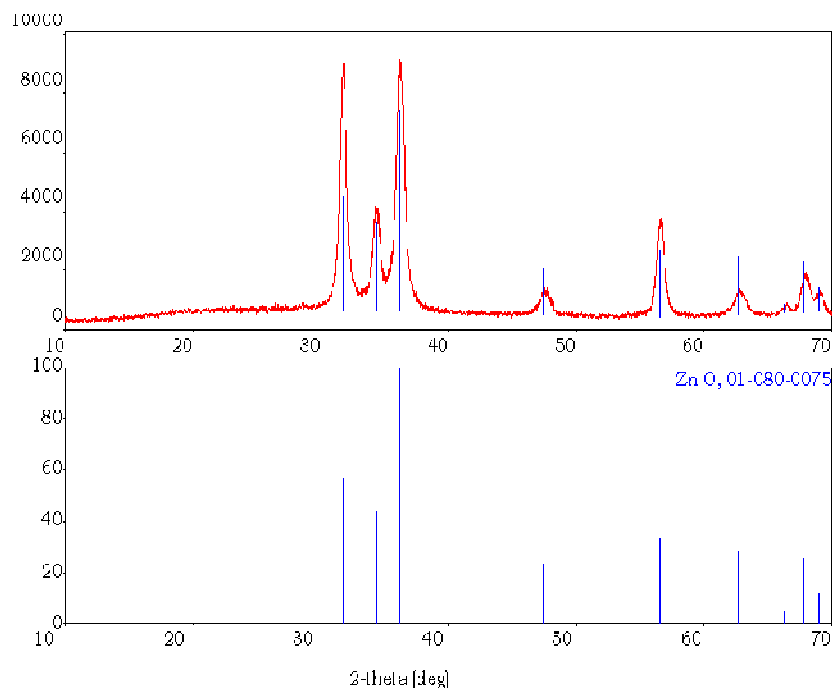
Figure 3.4 X- Ray diffraction Pattern of Pure Zinc Oxide (ZnO)

3.5 Transmission electron microscope

Figure 3.5shows transmission electron microscope image of ZnO nanostructure synthesized by Sol-gel method. It is clearly seen from the TEM image that the ZnO powders consist of large number of nanosphere which were cumulated to form superior size crystal.
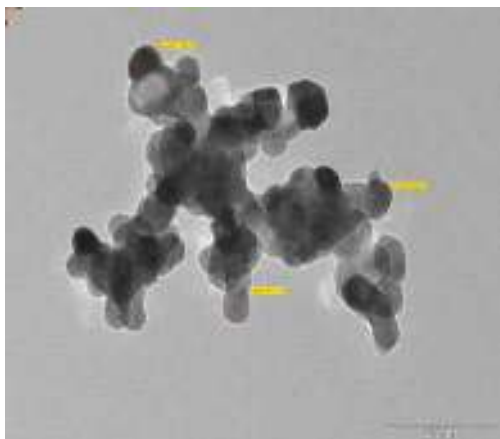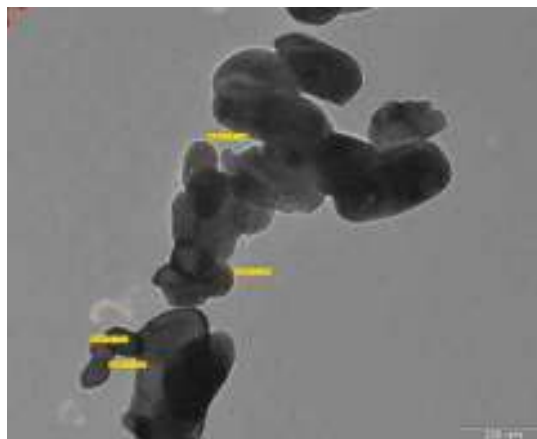
| Fig 3.5 (a) | Fig 3.5 (b) |

3.6 Scanning Electron Microscopic Study

Figure 3.6 shows typical SEM images of the pure ZnO thick film prepared by screen printing technique. The ZnO synthesized by the Sol- gel method consist of randomly distributed nanosphere as shown in Figure 3.6(a),(b) Due to such a deposition of nanosphere, surface to volume ratio of the ZnO may be increase.
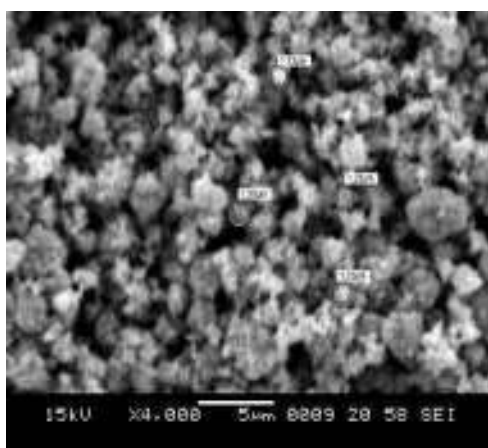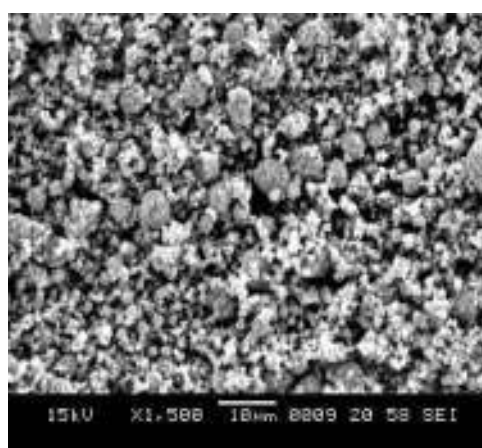
| Fig 3.6 (a) | Fig 3.6 (b) |

4. ELECTRICAL PROPERTIES

4.1. I–V characteristics

Figure 4.1depicts the I–V characteristics of the pure ZnO films at room temperature. The symmetrical nature of I–V characteristics shows that silver contacts on the film are ohmic in nature[22].
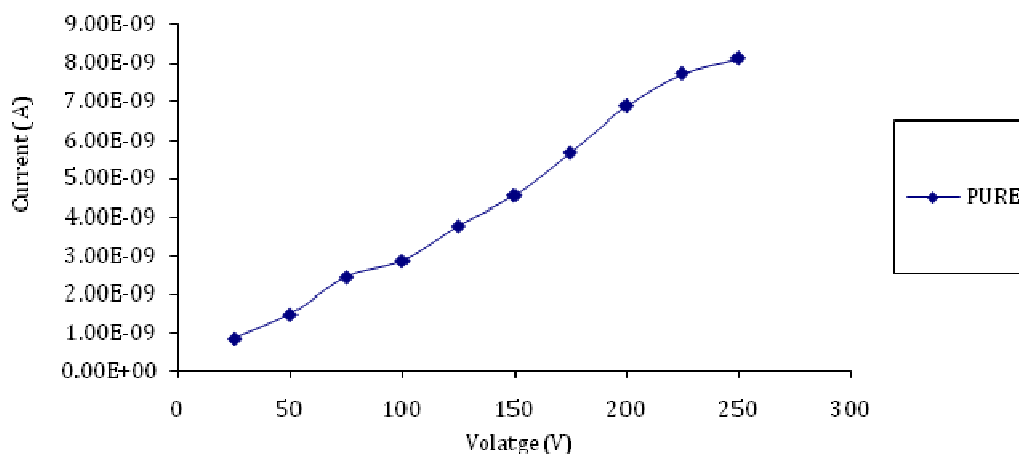
Figure 4.1 I-V Characteristics of Pure ZnO Thick Films
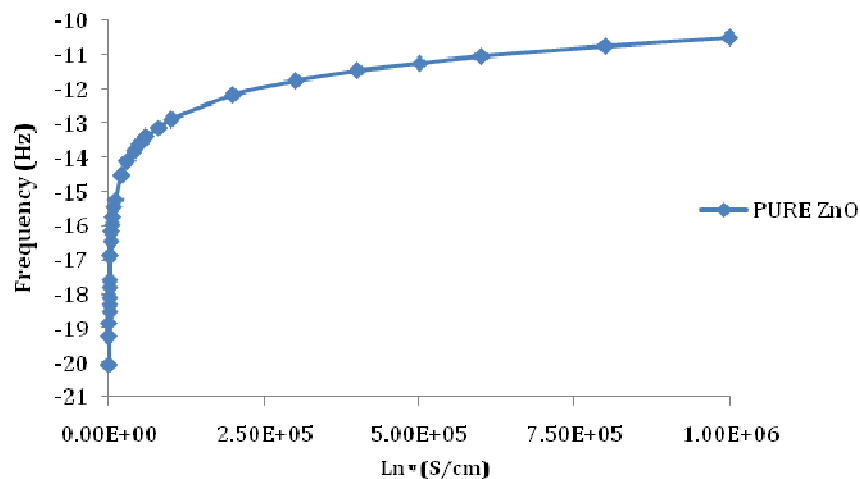
Figure 4.2 A.C. Conductivity of Pure ZnO Thick Film

4.2 For Measurement of A.C. Conductivity

A.C. electrical conductivity of the thick films was measured by using Agilent 4284A LRC meter. Variation of electrical conductivity with the frequency was observed in the frequency range 100- 1MHz at room temperature.

The A.C. conductivity of pure ZnO thick films measured in the frequency range of 100Hz to 1MHz at room temperature. The experimental data reveal that ac conductivity increases with frequency (Figure 4.2)Variation of A.C. conductivity with frequency can be explained with the help of barrier hopping mode[23].

4.3 Gas Sensing Properties

The gas response of the sensor was defied as the ratio of the change in conductance of a sample upon exposure to the target gas to the original conductance in air. Figure 4.3shows the gas responses of ZnO thick films to H_2S at operating temperature. This high response of ZnO thick film to H_2S may be due to the interaction of ZnO with H_2S, forming ZnS[24]. ZnS exhibits higher electronic conductivity as compared to pure ZnO.
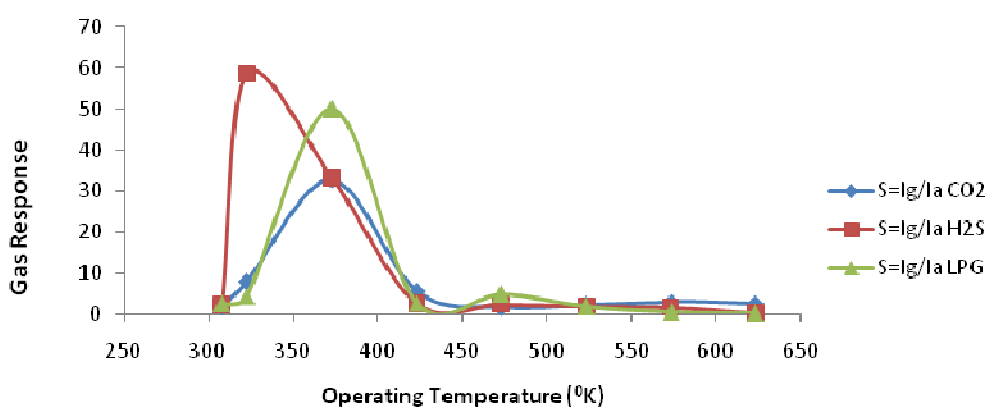
Figure 4.3 sensitivity of gas from mixture of gases

Figure 4.3also indicates the pure ZnO have maximum gas response to low concentration H_2S. The higher response ZnO nanostructure upon exposure to H_2S may be attributed to the decrease in con- centration of oxygen adsorbents (O^{2-}_{ad}) and a resulting increase in concentration of electron.

The gas response was mainly dependent upon two factors. The first was the amount of active sites for oxygen and the reducing gases on the surface of the sensor materials. It is seen form TEM images Figure 3.6 (a),(b).The surfaces pure ZnO contain more active sites. This could explain why the response of pure ZnO thick films was higher than other thick films.

5. CONCLUSION

In summary, sensors were fabricated with ZnO nanostructures, which were synthesized by a sol-gel method followed by sonication, and their gas sensing properties were measured. The results demonstrated that pure ZnO is very sensitive to low concentration H_2S. Such nanomaterials with innovative structure can be used for gas sensors to monitor hazards gas like H_2S.

ACKNOWLEDGEMENT

REFERENCES

1. L. Morawska' , Z. Ristovski, E.R. Jayaratne, D.U. Keogh, X. Ling, *Atmospheric Environment*, Volume 42, Issue 35, pp. 8113–8138 (November 2008).
2. S. Pizzini, N. Butta, D. Narducci, M. Palladina, *J. Electrochem. Soc.*, 136, (7), 48 (1945).
3. H.W. Ryu, B.S. Park, A.A. Sheikh, W.S. Lee, K.J. Hong, Y.J. Seo, D.C. Shin, J.S. Park, G.P. Choi, *Sensors and Actuators B*, 96, pp.717-722 (2003).
4. S.T. Shishiyanu, T.S. Shishiyanu, 0.1. Lupan, *Sensors and Actuators B*, 107, pp.379-386 (2005).
5. Can Li,Shunping Zhang, Mulin Hu, Changesheng Xie, *Sensors and Actuators B*, 153,pp.415-420 (2011).
6. M.C.Carotta, A.Cervi,v.di.Natale, *Sensors and Actuators B*, 137,pp.164-169 (2009).
7. M.Hubner, N.Barsan, U.Weimar, *Sensors and Actuators B*, 151,pp.103-106 (2010).
8. M. Hubner, D. Koziej, M. Bauer, M.D. Rossell, Angewandte Chemie-International Edition 50, (12), pp. 2841-2844 (2011).
9. Z. A. Ansari, Taegyung G. Ko, and Jae-Hee Oh, *IEEE Sensor Journal*, 5, (5), pp. 817-824 (2005).
10. G. Neri, A. Bonavita, G. Rizzo, S. Galvagno, N. Pinna, M. Niederberger, S. Capone, P. Siciliano, *Sensor and Actuators B*, 122,pp.564-571 (2007).
11. M.D. Antonik, J.E. Schneider, E.L. Wittman, K. Snow, J.F. Vetelino, R.J. Lad, *Thin Solid Films*, 256, pp.247-252 (1995).
12. V. Khatko, E. Llobet, X. Vilanova, J. Brezmes, J. Hubalek, K. Malysz, X. Correig, *Sensor and Actuators B*, 45, pp.111-112 (2005).
13. W. Belkacem, A. Labidi, J. Guerin, N. Mliki, K. Aguir, *Sensor and Actuators B*, 132 (1), pp.196-201(2008).
14. T. Brousse and D. M. Schleich, *Sensors and Actuators B: Chemical*, Vol. 31, No. 1-2, pp. 77-79 (1996).

15. A. P. Chatterjee, P. Mitra and A. K. Mukhopadhyay, *Journal of Materials Science*, Vol. 34, No. 17, pp. 4225-4231 (1999).
16. L. Liao, H. B. Lu, J. C. Li, H. He, D. F. Wang, D. J. Fu, C. Liu and W. F. Zhang, *The Journal of Physical Chemistry C*, Vol. 111, No. 5, pp. 1900-1903 (2007).
17. S. S. Badadhe and I. S. Mulla, "CO_2 Gas Sensitive Indium-Doped ZnO Thin Films: Preparation and Characterization," *Sensors and Actuators B: Chemical*, Vol. 143, No. 1, pp. 164-170 (2009).
18. Z. T. Liu, T. X. Fan, D. Zhang, X. L. Gong and J. Q. Xu, "Hierarchically Porous ZnO with High Sensitivity and Selectivity to CO_2 Derived from Biotemplates," *Sensors and Actuators B: Chemical*, Vol. 136, No. 2, pp. 499-509 (2009).
19. Hsieh P.T., Chen Y.C., Kao K.S., Lee M.S., Cheng C.C., *Journal of the European Ceramic Society*, Vol. 27, 13-15, pp. 3815-3818 (2007).
20. Wang J.,Gao L., *Inorg. Chem. Commun*. 6, pp.877–881 (2003).
21. Hong R Y, Li J H, Chen L L, Liu D Q, Li H Z, Zheng Y and Ding J, *Powder Technology*, 189(3), pp.426-432 (2009).
22. G. H. Jain, M.S. Wagh, *Sensors and Actuators B* 12, pp. 233-239 (2007).
23. K. Lal, S. K. Chattopadhyay, A. K. Meikap, S. K. Chatterjee , *Czechoslovak Journal of Physics*, Vol. 53,No. 3 (2003).
24. D. Wang, X. F. Chu and M. L. Gong, *Nanotechnology*, Vol. 18, No. 18, (2007).

Synthesis and Characterization of Magnesium oxide Nanoparticles with 1:1 molar ratio via Liquid-Phase Method

Agrawal R.M., Charpe S.D., Raghuwanshi F.C. and *Lamdhade G.T.

Department of Physics, Vidya Bharati Mahavidyalaya, CK Naidu Road, Camp, Amravati Maharshtra State- 444602 India

ABSTRACT

Magnesium nitrate and Sodium hydroxide are used as a starting material for the preparation of nanoparticles of Magnesium oxide (MgO) via liquid phase method.   The XRD analysis shows that nanocrystalline size of MgO remarkably with the 1:1 molar ratio. The respective average crystalline size is found to be 25.91nm. The resistance of MgO nanoparticles is temperature dependent and decreases exponentially (from 10^{11} Ω to 10^7 Ω). The activation energy of the MgO nanoparticles is found to be 0.49eV or 48.196 KJ/mol by using Arrhenius plot. The I/V characteristics of MgO nanoparticles is found to be linear in nature and obey the Ohms law in the operating temperature range (50-350 ^oC).
Keywords: [Mg(NO$_2$)(H$_2$O)$_6$] , (NaOH), Ethanol, Activation Energy

1. INTRODUCTION

Now-a-days one dimensional nanomaterial such as nanowires, nanorods, nanofibers of various metal oxides materials has been growing an interest due to their potential applications in various functional devices and their fundamental scientific interest [1-4]. The synthesis of nanomaterials can be broadly categories; Liquid-phase, Gas-phase and Vapour-phase . Under liquid phase the techniques used for synthesis are: co-precipitation, sol-gel processing, micro-emulsions, hydrothermal /solvo-thermal , microwave , sono-chemical , Template and biomimetic . The MgO has a good additive properties in heavy fuel oil because of high oil dispersion ability and large specific surface area and also bactericidal performance in the aqueous environments due to the formation of super oxide [5-7]. As the Magnesium hydroxide is eco-friendly, non toxic, thermally stable flame retardant and suppressing fumes under fire conditions. There are various kinds of techniques which are used to synthesize the MgO nano-particles by using different methods such as pulse laser deposition (PLD) [8], Laser ablation [9], hydrothermal method [10], sol-gel method [10-11], thermal decomposition of hydroxide or carbonate [12-13] etc. Out of above all the synthesis technique, sol-gel method has synthesis and large scale production of MgO nanoparticles [14].

The nanosize oxide particles with narrow size distribution can be prepared by using various techniques as given above. The oxide particle size and morphology can be controlled by various parameters such as preparation conditions as the pH, temperature of precipitation, different molar concentration or ionic strength, and different calcinations temperature or time [15].

In the present study is to synthesize and structural characterisation of MgO nanoparticles by using liquid phase method with large surface area in short reaction time at room temperature and this method is the simplest, cost effective, eco-friendly method. It is also probed for its effect on nanocrystalline size structure via XRD studies and also reported I/V characteristics, the activation energy of MgO nanoparticles.

2. EXPERIMENTAL

2.1 Synthesis of MgO Nanoparticles

The synthesis of MgO nanoparticles is divided into various steps, such as mixing, stirring, filtering, drying and calcination [16]. Finally by the calcinating the powder at 400 ^oC for 3 h, the MgO is obtained in the nanoparticles form, the flow chart of procedure is as shown in figure 1.

International Journal of Application or Innovation in Engineering & Management (IJAIEM)
Web Site: www.ijaiem.org Email: editor@ijaiem.org

Volume 4, Issue 2, February 2015   **ISSN 2319 - 4847**
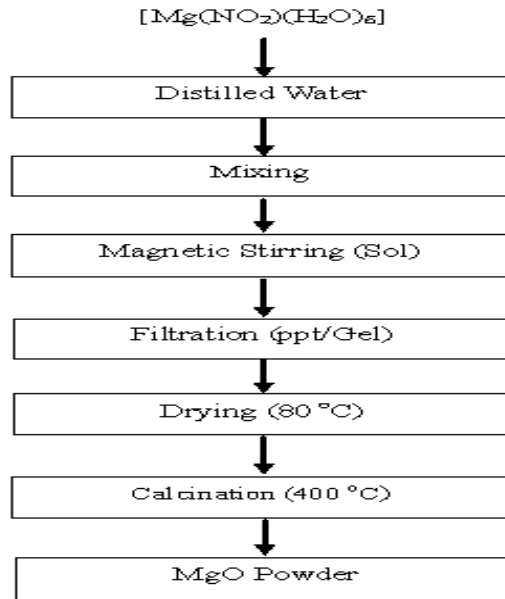
Figure 1. Flow Chart of Preparation

Magnesium Nitrate Hexahydrade [$Mg(NO_2)(H_2O)_6$] and Sodium Hydroxide (NaOH) powder of AR grade of high purity (LOBA Chemicals) used in this work. The distilled water and Ethanol (AR grade 99.9% purity) used as a solvent and washing reagent in the chemical reaction respectively.

Initially the Magnesium Nitrate Hexahydrade of wt. 5.21 gm (0.2 M) and dissolved in 200ml of distilled water. The 0.8 gm (0.2 M) of NaOH in 200ml distilled water. Then 200ml of NaOH solution is added in solution of [$Mg(NO_2)(H_2O)_6$] drop-wise by using glass rod. After that, solution kept under magnetic stirring for 2 h after stirring the solution was kept on table at rest for 2 h so that, the precipitation is formed at the bottom of beaker. This precipitation was filtered and washed several times by using distilled water and Ethanol so as to get the final products. The final product is kept in vacuum oven (Quality Make, India) at 80 °C for 4 h for drying product and removing the moisture. This dried powder is then crush and make it very fine powder by using mortal pestle. Finally the fine powder of MgO is calcinated at 400 °C for 3 h for the removal of impurities present in the powder. So that we will get synthesized MgO possessed high crystallinity with the particle size in nanosized range.

3. RESULTS AND DISCUSSION

3.1 Characterization of MgO materials
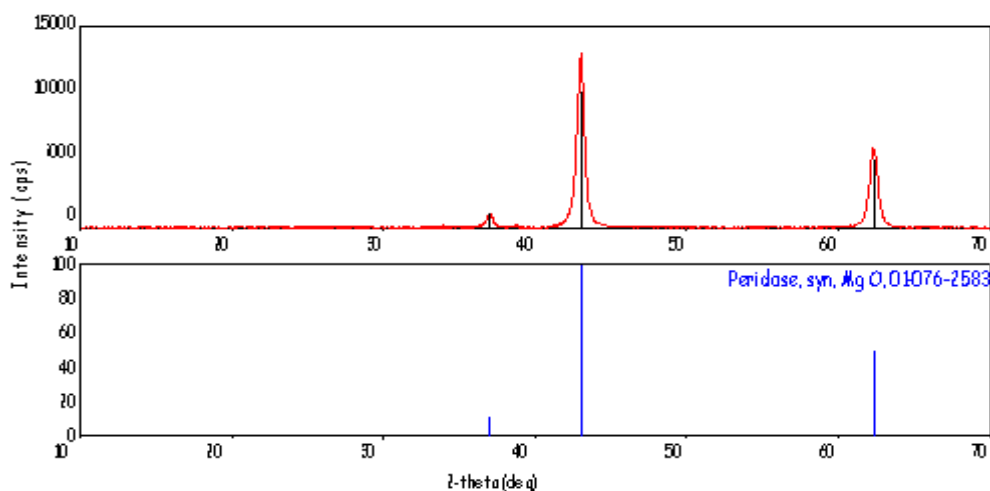
Figure 2. XRD of Magnesium Oxide

Figure 2. shows the XRD of the MgO calcinated at 400 °C, it is clearly observed that the highest intensity peak is obtained at (200) crystal planes of MgO with FCC phase (lattice constant a of cubic unit cell: 0.421 nm), owing to diffraction peaks assigned to (111), (200) and (220) crystal planes (JCPDS Card No. 87-0653) [17]. The sharp

International Journal of Application or Innovation in Engineering & Management (IJAIEM)
Web Site: www.ijaiem.org Email: editor@ijaiem.org
Volume 4, Issue 2, February 2015   **ISSN 2319 - 4847**

diffraction peaks were clearly seen and they are perfectly matches with crystal structure of MgO, therefore, we get clear crystallinity of MgO particles having average crystalline size in nano order. The estimated crystallite size of the synthesized MgO from the line broadening of (200) diffraction peak, which is the most preferentially oriented crystal plane, using Debye Scherrer equation [18] is approximately 25.91 nm. The Debye-Scherrer equation is as under eq. 3.1,

$$D = \frac{0.94\,\lambda}{\beta\,\cos\theta}$$

(3.1)

Where, D – is the average crystalline size, 0.94 – is the particle shape factor which was depend on the shape and size of the particle, λ- is the CuKα radiation (1.54A$^\circ$), β–is full width at half maximum (FWHM) of the selected diffraction peaks (β=0.545), θ– is the Braggs angle obtained from 2θ values which was corresponding to the maximum intensity peak in XRD pattern. (θ =0.7501rad)

3.2 Temperature Dependence of MgO Nanoparticles

We have recorded the change in resistance of MgO nanoparticles by using Keithley picoammeter (Model No. 6487, Keithley Instruments Inc. USA) with increasing temperature from 50 $^\circ$C to 350 $^\circ$C by using digital temperature controlled furnace (Tempo Make, Mumbai).
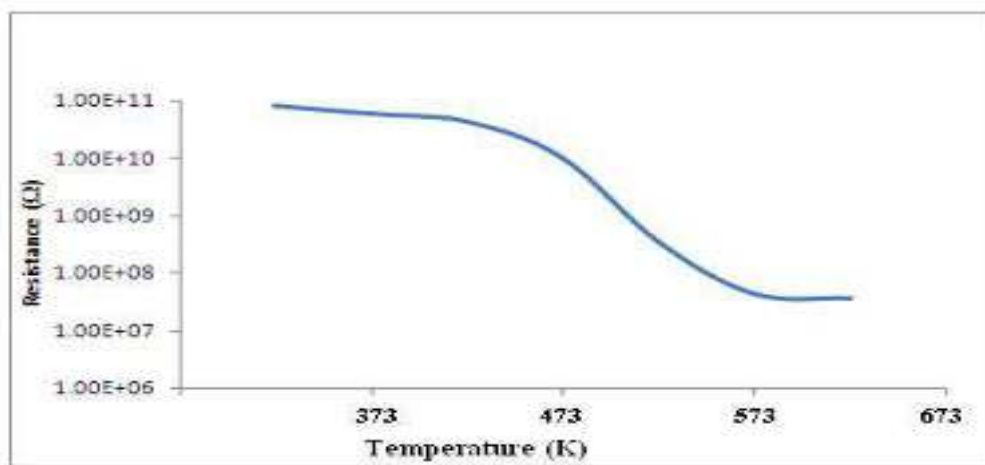
Figure 3. The variation of the resistance of MgO nanoparticles with temperature.

Figure 3 shows the variation of the resistance of MgO nanoparticles with temperature, it is seen that the resistance of MgO nanoparticles varies exponentially decrease (from 10^{11} Ω to 10^7 Ω) with increase in the temperature of sample. i.e. the resistance of MgO nanoparticles is temperature dependent.

We have calculated dc conductivity of MgO nanoparticles by using formula given by equation 3.2.1

$$\sigma_{dc} = (1/R_s) \times (t/A)$$

(3.2.1)

Where, R_s is sample resistance, t is the thickness and A is the area of the sample

The Arrhenius equation gives the relation between dc conductivity and absolute temperature (reciprocal) (1/T) is given by equation 3.2.2

$$\sigma_{dc}(T) = \sigma_o e^{-\,E_a/K_B T}$$

(3.2.2)

Where, σ_o is a pre exponential factor, E_a is the activation energy, K_B is the Boltzmann constant, and T is the temperature (K).

Figure 4. Arrhenius plot

International Journal of Application or Innovation in Engineering & Management (IJAIEM)
Web Site: www.ijaiem.org Email: editor@ijaiem.org
Volume 4, Issue 2, February 2015   **ISSN 2319 - 4847**
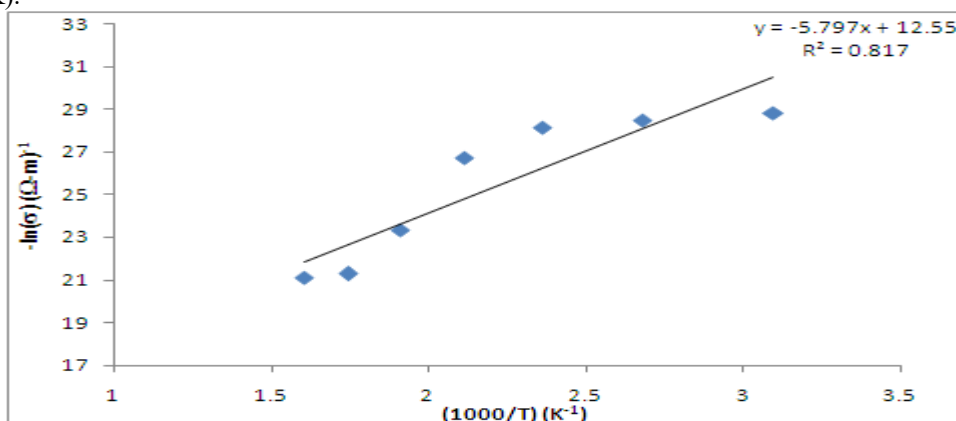
Figure 4 represents Arrhenius plot between logarithmic of DC conductivity $\ln(\sigma_{dc})$ and $1000/T$. The Arrhenius behavior (linear relations) is exist between $\ln(\sigma dc)$ and $1000/T$ for MgO nanoparticles, which indicate the temperature dependence of dc conductivity satisfies the Arrhenius relation. The activation energy of the MgO nano particles, calculated from $\ln(\sigma_{dc})$ - 1000/T plot, is found to be 0.49eV [19] or 48.196 KJ/mol [20]. The value of activation energy is less than 1eV, so that our sample shows the predominance of electronic conductivity.
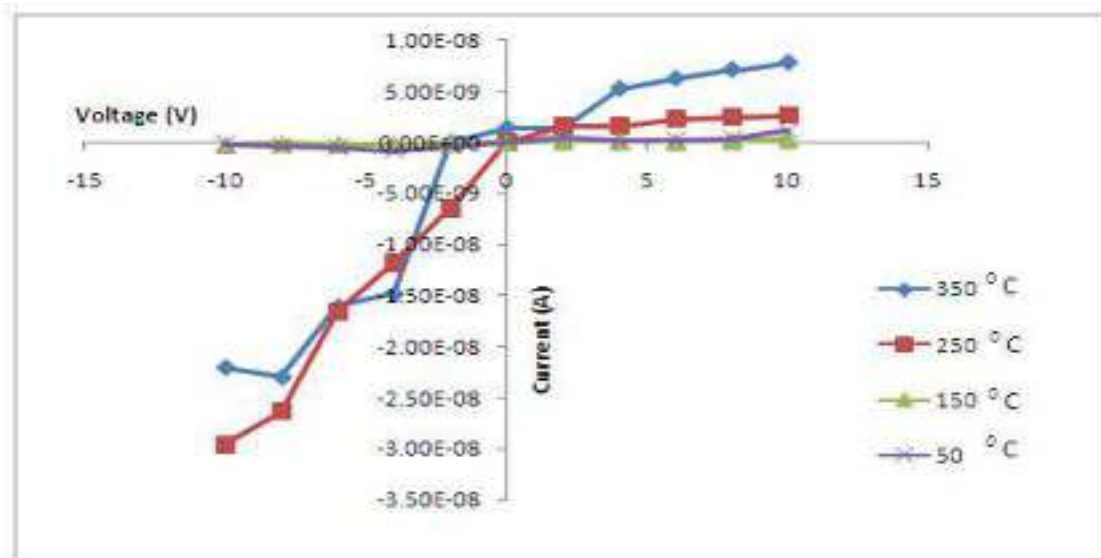
Figure 5. I/V Characteristics of MgO at various constant temperatures

I/V characteristics of MgO nanoparticles recorded by using Keithley voltage source (Model No. 2400, Keithley Instruments Inc. USA) in the (+10 to 0 V) and (0 to -10 V) voltage interval in the temperature range $50^{\circ}C$ to $350^{\circ}C$. Fig.5 represents the I/V characteristics of MgO nanoparticles found to be linear in nature and obey Ohms law in the entire operating temperature range and I/V characteristics is also temperature dependents [19].

4. CONCLUSIONS

The major conclusions of this work can be summarized as follows;
  i) We are succeed to synthesize Nano-crystalline size MgO via liquid phase method i.e. sol-gel technique so as this technique is simple, fast and effective.
  ii) The activation energy is found to be equal obtained from literature survey.
  iii) The current-voltage characteristic is found to be linear and temperature dependence.

REFERENCES

[1] G.Yu, A.Cao, C.M.Liber. Nat. Nanotech. (2).pp 372,2007.
[2] B.Tian, X.Zheng, T.J.Kempa, Y.fang, N.Yu, G.Yu. J.Huang, C.M.liber., Nature (449), pp.885,2007.
[3] W.Lu,C.M.Liber, Nat.Mater.(6),pp.841,2007.
[4] M. Fernández-García, A. Rodriguez.. Metal Oxide Nanoparticles, Encyclopedia of Inorganic Chemistry, 2009.
[5] Y. R. Li, Z. Liang, Y. Zhang, J. Zhu, S. W. Jiang, and X. H. Wei, Thin Solid Films, (489), pp. 245,2005.
[6] J. Davies, J. W. Laxton, and M. J. Owers, J. Inst. Energy, (14), pp. 21,1981.
[7] J. Sawai, H. Kojima, H. Igarashi, A. Hashimoto, S. Shoji, T. Sawaki, A. Hakoda, E. Kawada, V. Kokugan,M Shimizu, World J. Microb. Biotechnol. (16), pp.187-194, 2000.
[8] W. Rizwan, S. Absari, M. Dar, Y . Kim, H .Shin, Mater sci. forum (558-559),pp. 983-986, 2007.
[9] P .Tran, H. Bret., M. Donald, Y. Soong , C. Minking, Opt. Laser. Eng. (46),pp. 829-834, 2008.
[10]J. Wang, O. Novaro, X. Bokhimi, T. Lopez, R. Gomez, J. Navarrete, M. Llanos , E. Lopez-Salinas, Mater. Lett. (35), pp. 317-323, 1998.
[11] S. Utamapanya, K. Klabunde, J. Schlup, Chem. Mater. (3), pp. 175-180, 1991.
[12] D. Lide, CRC Handbook of Chemistry and Physics, CRC Press, Boca Raton - New York, 2004.
[13] M. Aramendia, V. Borau , C. Jimenez, J. Mater. Chem. 6(12), pp. 1943-1949, 1996.
[14] T. Lopez, R. Gomez, Journal of Solid State Chemistry (115), pp. 411–415, 1995.
[15] M. Laska, J. Valtyni, P. Fellner, Cryst. Res. Tech., (28), pp. 931, 1993.
[16] G. Moussavi, M. Mahmoudi, Journal of Hazardous Materials (168), pp. 806–812, 2009.

[17] V. Smith, X-ray Powder Data File, American Society for Testing Materials, 1960.
[18] B. Cullity, Elements of X-ray Diffraction. Massachusetts, Addison-Wesley Publication   Company, 1978.
[19] N. Kilincl, L. Arda, S. Ozturk, Z. Ozturk, Cryst. Res. Technol. 45, (5), pp. 529 – 538, 2010.
[20] T. Jeffrey, M. Simone, P. Ivan, J. Am. Ceram. Soc., 97 (1), pp. 275– 282,2014.

Synthesis of Nano structure Zinc Oxide by Spray Pyrolysis and itsCharacterizationfor Gas Sensing Application

S.D.Charpe[1]*, F.C. Raghuwanshi[2]*, G.T. Lamdhade *, V.S. Kalymwar[†]

* Department of Physics, Vidya Bharati Mahavidyalaya, Amravati, India.

[†] Department of Physics, Bharatiya Mahavidyalaya, Amravati, India.

ABSTRACT

Thin film of Zinc Oxide (ZnO) nanostructure has been deposited on glass substrate by using spray pyrolysis method. This method can be used as a promising material for semiconductor gas sensor to detect gas like H_2S at above room temperature with high sensitivity and selectivity. Characterizations of Zinc Oxide (ZnO) using UV, FTIR, XRD, SEM, EDS has been done.
Keywords: ZnO, Spray Pyrolysis, XRD, SEM, EDS and H_2S Sensor.

1. INTRODUCTION

Metal oxide is a very important material which exhibits electric, magnetic and structural ordering has attracted great interest in the past few years resulting in concurrent applications like gas sensors, microelectronics, optoelectronic devices and solar cells. These materials offer a wide opportunity for possible applications spintronic devices and sensors where both structural and electricproperties giving enough opportunity for manipulating devices. These nanocrystalline materials have interesting physical and chemical properties prepared using new man-made routes for the production of special nanoparticles which have new applications in material science and nanotechnology.

Zinc Oxide (ZnO) has been extensively studied for various applications in sensing, acoustic wave resonator, acoustic optic modulator [1], [2]. The origin of various applications the lies in its crystal structure, in which the oxygen atoms and zinc atoms are tetrahedral, bonded. In such a non-Centro symmetric structure, the center of positive charge and negative charge can be displaced due to external pressure induced lattice distortion. In fact, among the tetrahedrally bonded semiconductors, ZnO has the highest wide band gap semiconductor with a band gap ~3.3 eV at room temperaturewhich provides a large electro-mechanical coupling. This property of ZnO nanostructures was also investigated for their potential applications in nano systems [3].

Pure and doped ZnO thin films have been deposited using various techniques such as Liquid-phase synthesis [4]-[6]and secondly by using liquid or vapor precursorssuch as Chemical Vapour Synthesis [7], Spray Pyrolysis [8], [9], Laser Pyrolysis [10], Flame Spray Pyrolysis [11].Spray pyrolysis (SP) technique is a very easy, low cost, safe, and non-vacuum system of deposition for preparing transparent conducting oxides as compared with the other techniques. The other advantage of the Spray pyrolysis technique is that it can be adapted easily for production of large area uniform film coatings. The aim of this work is to study the structural, and gas sensing properties of Pure ZnO thin film.

2. EXPERIMENTAL DETAILS

Synthesis of NanostructureZnO by using Spray Pyrolysis

All substrates were thoroughly cleaned by the following sequence: cleaned by labolene detergent and then rinsed with double-distilled (DD) water; then boiled with dilute chromic acid for 15 minutes and thoroughly rinsed with DD water; after that, ultrasonicated for 10min in acetone and then in methanol, and finally all substrates were dried in an oven.

Zinc acetate dehydrate [Zn $(CH_3COO)_2 2H_2O$], sodium hydroxide (NaOH) pallet and ethanol used for the sprayed pure ZnO thin films were analytical reagent grade (99.5 %purity, Sigma Aldrich). The spray pyrolysis experimental set-up and the details of the procedure for the pure ZnO thin films deposition have been described elsewhere [12]. 0.1M zinc acetate was dissolved in 25 ml of de-ionized water then mixed with ethanol in the ratio 1:3 and stirred for 10 minutes using a magnetic stirrer. Similarly, 1 M sodium hydroxide solution was also prepared. The NaOH solution was slowly added from a burette held vertically with zinc acetate dehydrate solution until the pH value reached 7. Cleaned glass slides were used as substrates to form pure ZnO films. The prepared solution was sprayed on glass substrates, kept at 500^0C temperatures.

3. MATERIAL CHARACTERIZATIONS

The crystalline natures of nanoparticles were investigated using XRD. The XRD patterns were recorded on a Siemens D 5000 diffractometer with Cu-Kα radiation (λ=1.54060Å), over the range of 2θ = 5-80° at ambient temperature. Using UV-visible absorption spectrum of nanoparticlesrecorded on Shimadzu 1800 spectrophotometer at room temperature was studied. Measurements of FTIR (Shimadzu FTIR IR Affinity-spectrometer -Japan Make) are recorded from 400 cm^{-1} to 4000 cm^{-1} wave number. . Using Leica's SEM (model S440) at 10kV, the morphology of nanoparticles at room temperature was studied.

4. RESULTS AND DISCUSSION

4.1. Thickness Measurement

Thickness of pure ZnO thin film was measured by using technique "Marutek film Thickness Measurement System" with the help of provided equipment. The thickness of film was observed in the range from 200-350 nm. Thin film of approximately uniform thicknesses was used for further characterization.

4.2 UV-visible absorption spectrum

UV-visible absorption spectroscopy is widely used tool for checking the optical properties of nanosized particles. Figure 1shows the UV-visible absorption spectrum of ZnO nanoparticles. From the spectrum four peaks are observed at 362nm, 318nm, 344nm and 296nm, out of this at 318 nm wavelength has been found maximum absorption and for this wavelength band gap is 3.30eV, which is very close to the band gap of ZnO 1s–1s electron transition (3.37eV) [13].
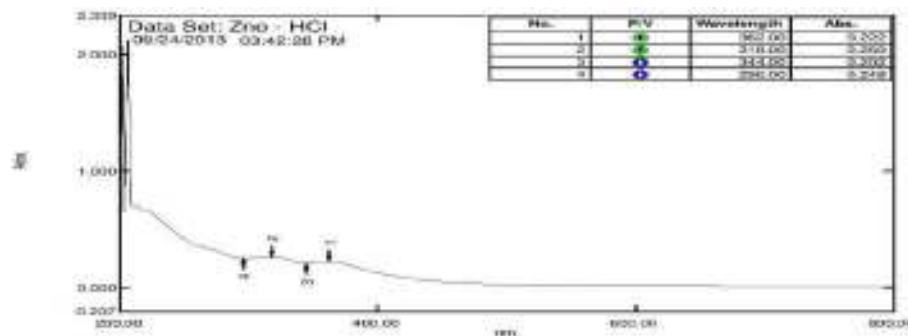
Figure1. UV-visible absorption spectrum of Pure ZnO

4.3 FTIR analysis

FTIR analysis spectrum shown in figure 2 , indicating significant absorption peaks at wave numbers 4350, 4200, 3900, 3850, 1700, 1550, 600 and 510 cm^{-1}. The absorption band at 600 and 510 cm^{-1} is obtained due to existence of Zn-O bond stretching vibration [14]. The peaks at 1700 and 1550 cm^{-1} shows H-O-H bending vibration due to the adsorption of moisture, when FTIR sample disks were prepared in an open air atmosphere. The remaining peaks between 4350 to 3850 cm^{-1} are corresponding to O-H stretching vibrations [15].
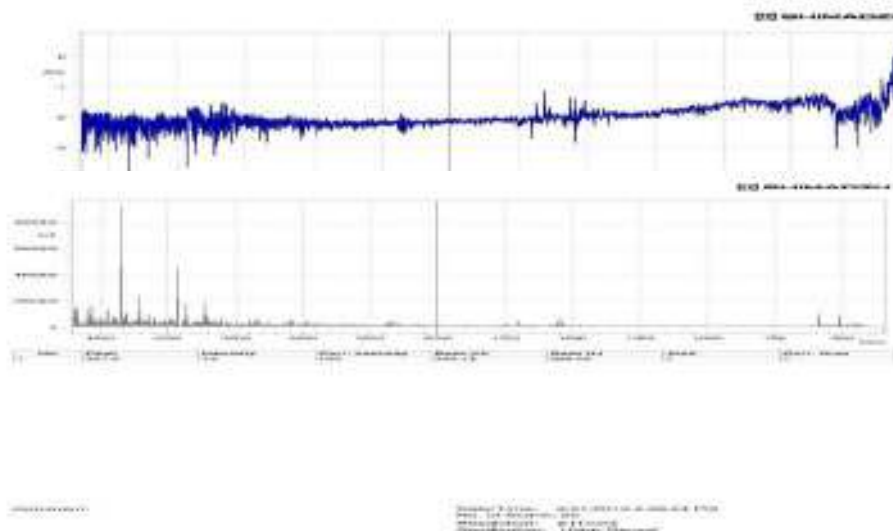
Figure 2. FTIR absorption/transmission spectrum of Pure ZnO

IPASJ International Journal of Electrical Engineering (IIJEE)

Web Site: http://www.ipasj.org/IIJEE/IIJEE.htm

A Publisher for Research Motivation........

Email: editoriijee@ipasj.org

Volume 3, Issue 2, February 2015

ISSN 2321-600X

4.4 X-Ray Diffraction Studies

The crystallographic structure of the synthesized ZnO nanostructure was analyzed by powder X-ray diffraction (Philips X-ray diffractometer) with Cu-α source and 2θ range of = 5-80^0. Figure 3 shows the XRD pattern of the ZnO nanostructure. The recorded XRD pattern confirmed that synthesized ZnO are highly crystalline in nature. The corresponding X-ray diffraction peak for (100), (002), (101), (102) (110), (103) and (112) planes confirm the formation of hexagonal wurtzite structure of ZnO (JCPDS card no.-01-080-0075). The domain size of the crystal has been estimated from the full width at half maximum (FWHM) of the peaks by means of the Scherrer formula,

$$D = \frac{k\lambda}{\beta sin\theta}$$

where λ is the wavelength of incident beam (1.5406 Å), β is the FWHM of the peak in radians, θ is the diffraction angle and K is Scherrer constant. The average particle size was calculated from (101) peak ZnO is found to be 19 nm. Using X'pert High Score Plus software it is confirm that synthesized zinc oxide powder contains Zn and O elements only, not any impurity and another element.
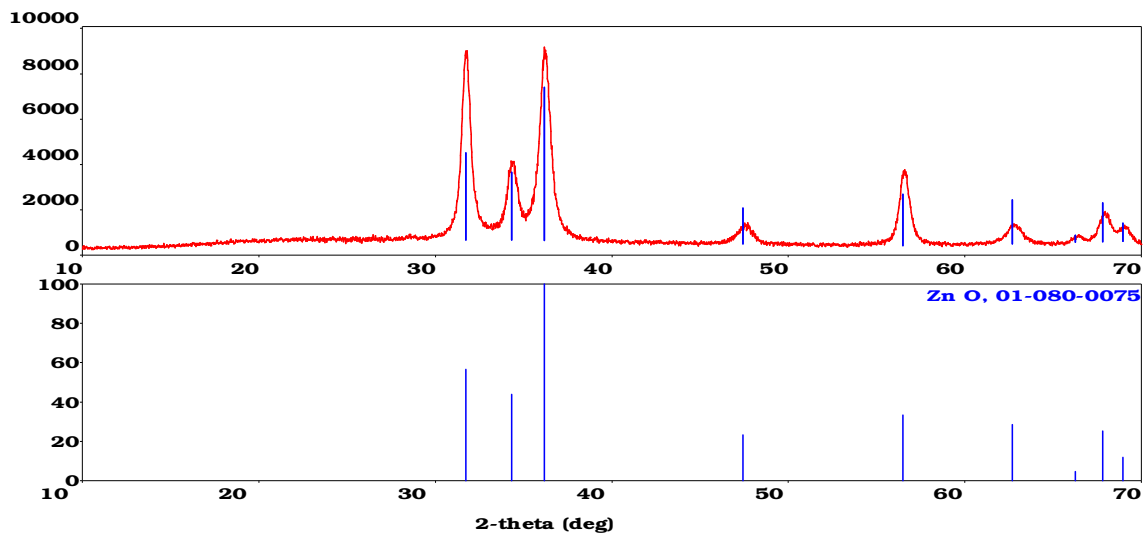
Figure 3. XRD Pattern of Pure ZnONanostructure

4.5 Surface Topography Using SEM

Scanning electron micrograph is shown in figure 4 (a, b) by using topography of the film surface. Scanning electron microscope could not resolve nanoparticles associated with the film even at very high magnification. It may be due to very small nanocrystalline particles associated with the film. The ZnO Spray Pyrolysissynthesized by method consist of randomly distributed nano particles as shown in figure 4(a),(b) such distribution of particles increase such a deposition of nan particles, surface to volume ratio of the ZnO..
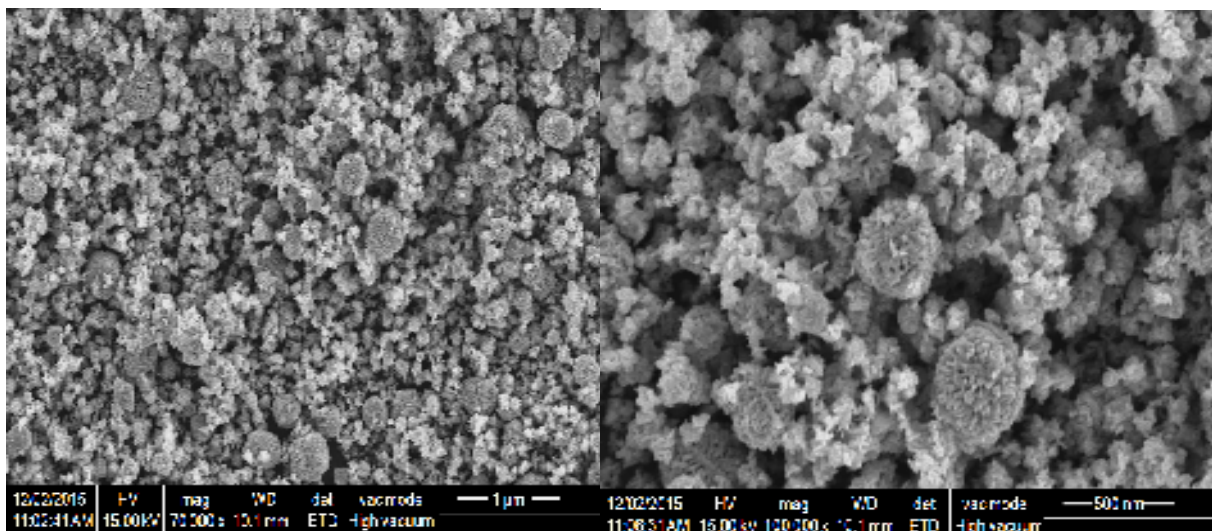
Figure 4 (a) SEM of ZnO at x 70000   **Figure 4** (b) SEM of ZnO at x 100000

IPASJ International Journal of Electrical Engineering (IIJEE)

Web Site: http://www.ipasj.org/IIJEE/IIJEE.htm

A Publisher for Research Motivation........

Email: editoriijee@ipasj.org

Volume 3, Issue 2, February 2015

ISSN 2321-600X

4.6 Quantitative Elemental Analysis

From figure 5quantitative elemental composition of the ZnO was analyzed using an energy dispersive spectrometer (EDS). Observed At% of Zn and O is 42.12 and 57.88 respectively [16].
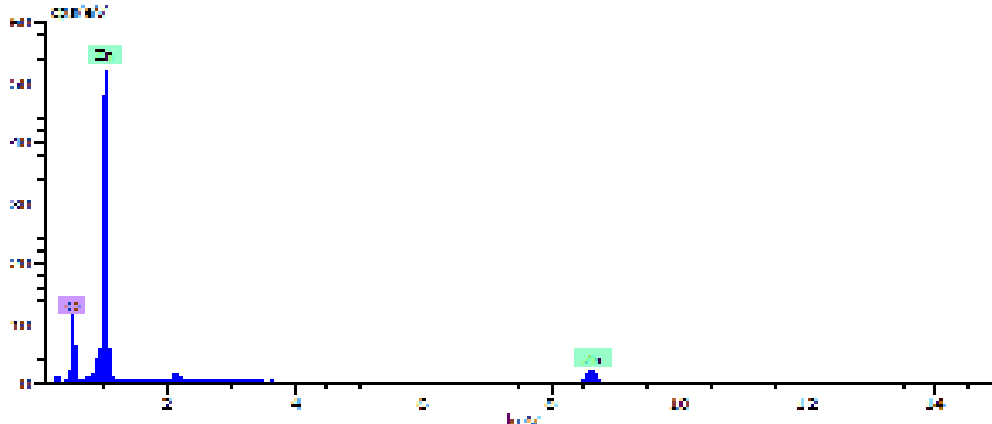
Figure 5. EDS of Pure Zinc Oxide

4.7 Gas Sensing Properties

i. Gas Response.

The sensing performance of the sensors was examined using a "static gas sensing system'. The gas response (S) is defined as the ratio of the change in the conductance of the sensor on exposure to the target gas to the original conductance in air and is given by the following relation [17].

$$S = Gg - Ga/ Ga \qquad .... (1)$$

where Ga is the conductance of sensor in air and Gg is the conductance of sensor in a target gas.

Figure 6 depicts the variation of gas response with operating temperature of the nanocrystalline ZnO sensor for 600 ppm CO_2, H_2S, and LPG. It is clear from the figure that the sensor response for each test gas increase in operating temperature reaches maximum corresponding to optimum operating temperature and decreases further [18][19]. In present study the sensor element exhibited highest response towards H_2S at an operating temperature of 50^0C as compared to other tested gases at the same temperature. These sensors show reasonably better sensitivity at lower operating temperatures. The enhancement of sensitivity at a relatively lower operating temperature may be due to the nanocrystalline nature of ZnOthin film employed to fabricate the sensors.
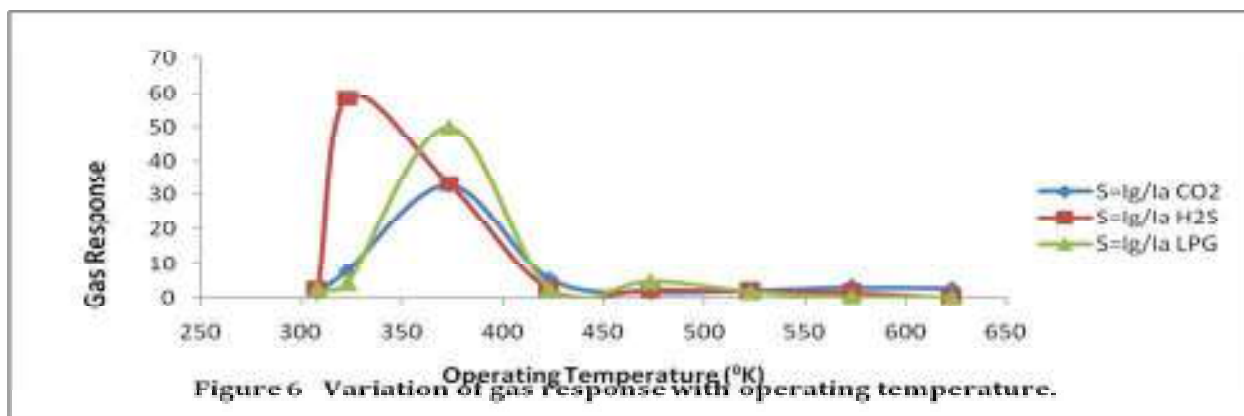
Figure 6 Variation of gas response with operating temperature.

ii. Selectivity of Sensor

Selectivity can be defined as the ability of a sensor to respond to a certain gas in the presence of different gases [20]. It is observed that the ZnO thick film sensor gives maximum response to H_2S (600 ppm) at 50^0C. The sensor showed highest selectivity for H_2S against all other tested gases: LPG and CO_2.

iii. Response Time and Recovery Time

The response/ recovery time is an important parameter used for characterizing a sensor. It is defined as the time required to reach 90 % of the final change in current, when the gas is turned on /off respectively [21], [22]. The response was quick (8 s) while the recovery was fast (< 18 s). The quick response may be due to faster oxidation of gas.

5. CONCLUSION

A Spray pyrolysis method is used to prepare ZnO nanocrystalline thin film. XRD analysis confirmed that the synthesized thin film to be that of the ZnO. The average grain size calculated from XRD was 19 nm. The band-gap energy calculated from an absorption spectrum was 3.37 eV. This value matches exactly with the reported value. The response of the nanocrystalline ZnO -based sensor was observed to be the largest to H_2S gas. The sensor showed good selectivity to H_2S gas against LPG, CO_2 gases.

Scope for Future Research

Crystalline ZnO has been studied for more than three decades and is one of the most closely investigated compound semiconductors. Due to the complexity of both the structure and the behavior of the material and also the great number of parameters affecting the final product there are though still many question marks left to be straightened. The most fundamental question of all why are ZnO resistors so special? – is still open.

Acknowledgements

REFERENCES

[1] A. Ashour, M.A. Kaid, N.Z. El-sayed, A.A. Ibrahim, Physical properties of ZnO thin films deposited by spray pyrolysis technique, Applied surface Science 252,pp.7844- 7848, 2006.

[2] M.T. Mohammad, A.A. Hashim, M.H. Al-Maamory, Highly conductive and transparent ZnO thin films prepared by spray pyrolysis technique, Materials Chemistry and Physics 99,pp.382-387, 2006.

[3] A. Chakraborty, T. Mondal, S.K. Bera, S.K. Sen, R. Ghosh, G.K. Paul, Effects of Al and In incorporation on the structural and optical properties of ZnO thin films synthesized by spray pyrolysis technique, Materials Chemistry and Physics 112 ,pp.162-168, 2008.

[4] Grieve K, Mulvaney P, Grieser F., Synthesis and electronic properties of semiconductor nano particles and quantum dots, Curr Opin Colloid Interf Sci 5, pp.168 –72, 2000.

[5] Trindade T, O'Brien P, Pickett NL., Nanocrystalline semiconductors, synthesis, properties, and perspectives, Chem Mater 13, pp.3843 –58,2001.

[6] Murray CB, Kagan CR, Bawendi MG., Synthesis and characterization of mono disperse nano crystals and close-packed nano crystal assemblies, Annu Rev Mater Sci 30,pp.545 – 610, 2000

[7] Ostraat ML, De Blauwe JW, Green ML, Bell LD, Atwater HA, Flagan RC. Ultraclean two-stage aerosol reactor for production of oxide-passivated silicon nanoparticles for novel memory devices J, Electrochem Soc, 148,pp.G265 – G270, 2001.

[8] Ahonen PP, Joutsensaari J, Richard O, Mobility size development and the crystallization path during aerosol decomposition synthesis of TiO_2 particles,J Aerosol Sci 32, pp.615–30. 2001.

[9] C.S. Prajapati, S. N. Pandey, P.P. Sahay, Sensing of LPG with nanostructured zinc oxide thin films grown by spray pyrolysis technique, Physica B 406, pp.2684-2688, 2011.

[10] Borsella E, Botti S, Cesile MC, Martelli S, Nesterenko A, Zappelli PG., Mo_2S nanoparticles produced by laser induced synthesis fromgaseous precursors, J Mater Sci Lett 20, pp.187–91, 2001.

[11] Ma¨dler L, Kammler HK, Mueller R, Pratsinis SE. Controlled synthesis of nanostructured particles by flame spray pyrolysis, J Aerosol Sci 33,pp. 369 –89, 2002.

[12] R. Mariappan, V. Ponnuswamy, P. Suresh, Effect of doping concentration on the structural and optical properties of pure and Sn doped ZnO thin films by spray pyrolysis technique, Superlattices and Microstructures, 52, pp.500-513, 2012.

[13] Hsieh P.T., Chen Y.C., Kao K.S., Lee M.S., Cheng C.C., The ultraviolet emission mechanism of ZnO thin film fabricated by sol–gel technology, Journal of the European ceramic Society, Vol. 27, 13-15, pp.3815-3818, 2007.

[14] Wang J., Gao L., Synthesis and characterization of ZnO nanoparticles assembled in one-dimensional order, Inorg. Chem. Commun. 6, pp.877–881, 2003.

[15] Hong R Y, Li J H, Chen L L, Liu D Q, Li H Z, Zheng Y and Ding J, Synthesis, surface modification and photocatalytic property of ZnO nanoparticles, Powder Technology, 189(3), pp.426-432, 2009.

[16] Patil, Pratap , G. Kajale, D .D Patil, V. P. Patil, G .E. Jain, Synthesis of nanostructured ZrO_2 for gas sensing application, International journal on smart sensing and intelligent systems, Vol. 5, No. 3, pp.673-684, 2012.

[17] Ganesh E. Patil D. D. Kajale, P. T. Ahire, D. N. Chavan, N. K. Pawar, S. D. Shinde, V. B. Gaikwad, G. H. Jain, "Synthesis,characterization and gas sensing performance of SnO2 thin films prepared by spray pyrolysis", Bulletin of Material Science ,Vol. 34, No. 1, pp. 1–9, 2011.

[18] V. S. Kalyamwar, F. C. Raghuwanshi,TiO2 modified ZnO thick film resistors as ammonia gas sensor, Adv. Mat. Letter,Vol. 4,Issue 12, pp .895-898,2013.

[19] F.C. Raghuwanshi, N.G. Belsare,G.T. Lamdhade, International Journal of Advanced Engineering Technology, Vol. II,Issue IV, pp. 226-230, Oct- Dec 2011.

[20] S. D. Shinde, G. E. Patil, D. D. Kajale, V. B. Gaikwad and G. H. Jain, Synthesis of ZnO nanorods by spray pyrolysis for H2S gas sensor, Journal of Alloys and Compounds, Vol. 528, pp.109-114, 2012.

[21] Ganesh E. Patil, D. D. Kajale, V. B. Gaikwad, N. K. Pawar and G. H. Jain, "Properties and Gas Sensing Mechanism Study of CTO Thin Films as Ethanol Sensor", Sensors &Transducers Journal, Vol. 137, Issue2, pp. 47-58, 2012.

[22] Patil, P. G., Kajale, D. D., Patil, V. P., Patil, G. E., & Jain, G. H., Synthesis Of Nanostructured ZnO for Gas Sensing, 5(3), pp.673–684, 2012.

AUTHOR

Mr. Sushil Charpe post graduated in physics from Vidya Bharati Mahavidyalaya Amravati which isaffiliated to S.G.B.A.U. Amravati. He is Ph.D. student at this University, studying structural and gassensing properties of metal oxide Nano materials for applications in gas-sensor devices.

Dr. F. C. Raghuwanshi received his Ph.D. in Physics from Rashtrasant Tukadoji Maharaj Nagpur University, presently working as a Principal of Vidya Bharati Mahavidyalaya, Amravati and Deanof Faculty of Science in S.G.B.A.U. Amravati. His field of interest is solid state ionics andsemiconductor metal oxide gas sensor.

SnO$_2$ nanoparticles synthesis via liquid-phase co-precipitation technique

G. T. Lamdhade[1*], F. C. Raghuwanshi[1], R. M. Agrawal[1], V. M. Balkhande[1], T. Shripathi[2]

[1]*Department of Physics, Vidya Bharati Mahavidyalaya Camp, C.K. Naidu Road, Amravati, Maharashtra 444602, India*
[2]*ESCA Lab and Molecular Spectroscopy Lab, UGC-DAE Consortium for Scientific Research, University Campus, Khandwa Road, Indore, Madhya Pradesh 452001, India*

[*]Corresponding author. Tel: (+91) 9404518185; E-mail: gtlamdhade@rediffmail.com

ABSTRACT

The samples have been prepared in the form of pellets of SnO$_2$ nanoparticles and synthesized via the liquid-phase co-precipitation technique. The ac electrical conductivity of samples is found to be frequency dependent. The dielectric constant increases with temperature and decreases with frequency of applied field. The semiconducting behavior of SnO$_2$ nanoparticles have been studied from I-V characteristics. The characterization of samples has been studied by XRD, FESEM, UV-spectra and TG-DTA plot. Copyright © 2015 VBRI Press.

Keywords: SnO$_2$ nanoparticles; liquid-phase synthesis; ac conductivity; dielectric constant; dielectric loss.

Introduction

Stannic oxide (SnO$_2$) is a wideband gap n-type semiconductor exhibiting rutile structure [1]. SnO$_2$ is applicable to the large number of field such as sensors, humidity sensors, optoelectronic devices, transparent electrodes, Li-ion batteries, etc [2-6].

Single SnO$_2$ nanowire have been synthesized by thermal evaporation method and its I-V characteristics show semiconducting behavior , these nanowires would be a promising candidate for gas sensing applications due to its structural and electrical properties [7]. Nanocrystalline composites of Zinc oxide and Tin oxide synthesize by using chemical route and the sensing response characteristics for NO$_2$ gas has been studied and compared with corresponding results obtained for pure SnO$_2$ and ZnO thin film based sensor structure [8]. Thick film resistors of nano-phase SnO$_2$ powder have been prepared by using screen printing method and their surfaces were modified by dip coating in platinum chloride solution different time periods. The sensors were found to be extremely stable and repeatable [9]. Tin oxide quantum dots have been synthesized by solution-combustion method and there is formation of a rutile SnO$_2$ phase with a tetragonal lattice structure. The origin of the blue emission in the SnO$_2$ quantum dots is studied with reference to the energy band diagram [10].

The properties of nanostructure material can be oriented as per requirements can be achieve by using the various experimental process for synthesis of nanoparticles such as chemical precipitation, sol–gel, hydrothermal, microwave technique, spray pyrolysis, CVD, etc [11, 12].

Bueno *et al.* [13] investigated the AC electrical properties of tin oxide found that the two time constants with different activation energies, one at low frequencies and the other at high frequencies. AC transport properties of nanocrystalline tin oxide were studied by Sahay *et al*. [14, 15], show that it is frequency dependent and obey the power law. The AC electrical conductivity of nanocrystalline tin oxide is found to be frequency dependent at a temperature of 200 °C and the result are interpreted in terms of the random potential barrier model [16]. As per the literature survey, there is less attention towards AC electrical, dielectric properties of nanocrystalline tin oxide as compared to DC conductivities mechanism [17]. This paper is devoted to effective method for the synthesis of nanocrystalline tin oxide using liquid phase co-precipitation method and AC electrical, dielectric measurements in the temperature range (313-473 K) were carried out in the frequency range (20 Hz - 1 MHz) , I-V characteristics, crystallographic structural (X-RD), morphological behavior (FESEM) and UV-vis absorbance spectrum are reported.

Experimental

Materials

All the chemicals used in this present work were of GR grade purchased from Sd-fine chemicals, India having purity 99.99% except conducting silver paint purchased from Sigma Aldrich Chemical, USA. Stannous chloride dehydrates (SnCl$_2$.2H$_2$O), ammonia solution and deionised water were used during reaction. The conducting silver paint is used to form electrodes during the experimental work.

Method of Preparation

In preparation of SnO_2, 2 g (0.1 M) of stannous chloride dihydrate ($SnCl_2.2H_2O$) is dissolved in 100 ml water. After complete dissolution, about 4 ml ammonia solution is added to above aqueous solution with magnetic stirring. Stirring is continued for 20 minutes. White gel precipitate is immediately formed. It is allowed to settle for 12 hours. Then it is filtered and washed with water 2-3 times by using deionised water. The obtain precipitate were mixed with 0.27 g carbon black powder (charcoal activated). The obtained mixer is kept in vacuum oven at 70°C for 24 hours so that the mixer gets completely in to dried powder. Then this dry product was crushed into a find powder by grinder. Now obtained product of fine nanopowder of SnO_2 was calcinated at 700°C up-to 6 hours in the auto controlled muffle furnace (Gayatri Scientific, Mumbai, India.) so that the impurities from product will be completely removed. The pellets of SnO_2 nanopowder were prepared by using electrically operated automatic press machine (Kbr Press) at load of 5 tons / cm^2 for half an hour. All the pellets were sintered at 150°C for half an hour. The sintered pellets were polished and the electrodes were formed by painting conductive silver paint on the opposite faces. Again pellets were sintered for the drying the silver paint at 100°C for half an hour.

Measurement of AC electrical conductivity and dielectric constant

The pellets of SnO_2 nanoparticles having diameter 12 mm and thickness 1.19 mm are placed in the silver electrodes sample holder (Pusha Scientific, Hyderabad, India) kept in electric oven to attained desired temperature. The samples is interlink to a precision LCR meter (20 Hz –1 MHz) (Model No. 4284 A, Agilent Technologies, Singapore), the corresponding effective capacitance (C_p) and effective resistance (R_p) measure at different environment of temperature recorded, finally the dielectric constants and ac electrical conductivity of the samples was calculated using expression [18],

$$\sigma_{ac} = (f \, \varepsilon' \, \tan(\delta)) / (1.8 \times 10^{10}) \qquad (1)$$

where, f is the frequency applied field in Hz, (ε') is the dielectric constant or relative permittivity and $\tan(\delta)$ is the dielectric loss tangent or loss factor.

The values of the real part of the dielectric constant (ε') at different frequencies and temperatures were derived from the measured capacitance (C_p) and knowing the geometrical dimensions of the pellets using the expression,

$$\varepsilon' = (C_p \, L) / (\varepsilon_o \, A) \qquad (2)$$

where, C_p is the measured capacitance, L is the thickness of the sample, A is the electrode area and (ε_o) is the permittivity of free space (8.854 X 10^{-12} F/m).

The dielectric loss tangent or dielectric loss factor i.e. $\tan(\delta)$ can be expressed by relation,

$$\tan(\delta) = \omega \cdot C_p \cdot R_p \qquad (3)$$

where, C_p is the measured capacitance, R_p is the measured resistance and f is the frequency applied field in Hz.

Measurement of current voltage characteristics

The current voltage (I-V) characteristics of SnO_2 nanoparticles were measured by using Source meter (Keithey Model No. 2400) in the temperature range (313 - 473 K). The samples are in the form of bulk pellets having diameter 12 mm and thickness 1.19 mm.

Characterization of SnO_2 nanoparticles

The crystalline nature of (SnO_2) nanoparticles was investigated using XRD. The XRD patterns were recorded on a Siemens D 5000 diffractometer with Cu-Kα radiation (λ=1.54060Å), over the range of 2θ = 5 - 80° at ambient temperature. Using Leica's SEM (Model S440) at 10kV, the morphology of (SnO_2) nanoparticles at room temperature was studied. Using UV-visible absorption spectrum of (SnO_2) nanoparticles are recorded on Shimadzu 1800 spectrophotometer at room temperature was studied.

Results and discussion

XRD pattern of the SnO_2 nanoparticles

The crystalline nature of the SnO_2 can be confirmed by the XRD pattern as shown in the **Fig. 1**. We observed the all peaks are perfectly matches with the JCPDS Data Card No. 77-0452, which indicating the present structure is found to be of SnO_2, which exist in the tetragonal rutile crystalline phase. The lattice parameters of the crystal were calculated as a = 0.4739 nm and c = 0.3221 nm which matches well with the standard values of SnO_2. The average crystalline size calculated by using Debye–Scherrer formula is found to be 21 nm for the three major peaks at (110), (101), (211) the crystal planes from the XRD pattern [19]. The average crystalline size was calculated by using Scherrer's formula given by equation (**4**),
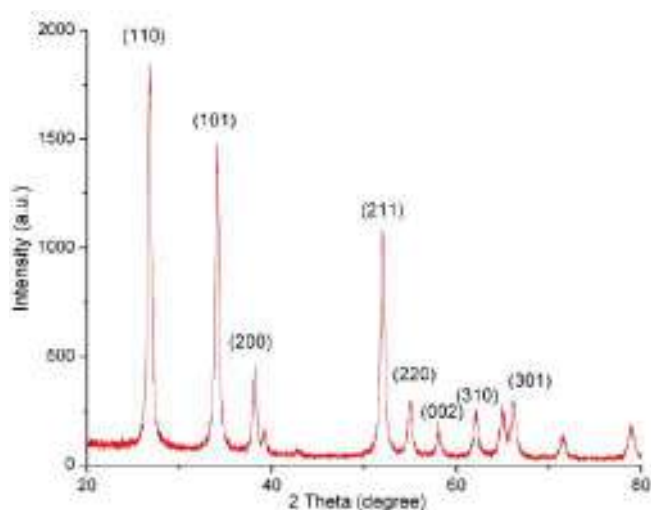
Fig. 1. XRD pattern of the SnO_2 nanoparticles.

$$D = \frac{K\lambda}{\beta \cos\theta} \qquad (4)$$

where, D is the crystalline size, K is the shape factor and β is the full width at half maximum of diffraction angle in radians.

AC electrical conductivity and dielectric constant

The **Fig. 2** shows the variation between log of ac conductivity and applied frequency (20 Hz - 1 MHz) at different temperature (313 K, 353 K, 393 K, 433 K and 473 K) of the samples. The ac electrical conductivity of SnO_2 nanoparticles found to be frequency dependence which increases sharply from 20 Hz to 1 KHz frequency but beyond that it increase linearly with applied frequency. The frequency dependence of ac conductivity also obeys the power law relation [20]. The frequency dependence of ac conductivity of SnO_2 nanoparticles can be explained on the basis of Jonscher's classical equation [21] which shows the real part of ac conductivity has been frequency dependence. The another mechanism can also be explain on the basis of quantum-mechanical tunneling (QMT) through the barrier and classical hopping over the barrier [22]. It is also noted that due to increase in the temperature of samples, mobility of hopping ions increases which causing the increase in the conductivity with increase in the temperature.
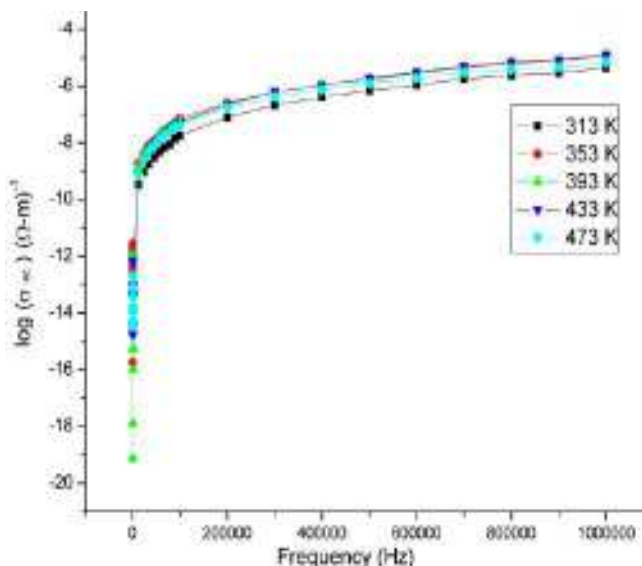
Fig. 2. Variation between log of ac conductivity and applied frequency.

The values of the real part of the dielectric constant (ε') at different frequencies and temperatures were derived from the **Eq.** (**2**). The variation of real part of the dielectric constant (ε') of SnO_2 nanoparticles with frequency of the applied field is plotted in the **Fig. 3** at constant temperature. These values can be obtained from the **Eq.** (**2**). It is clearly observed that the dielectric constant is found to decrease very rapidly from 20 Hz to 1 KHz frequency, but after 200 KHz frequency dielectric constant decreases very slowly up to 1 MHz frequency at all the constant temperature. In a dielectric study, the real part of dielectric constant (ε') represents the polarizability of the material while the imaginary part (ε'') represents the energy loss due to polarization and ionic conduction [23].
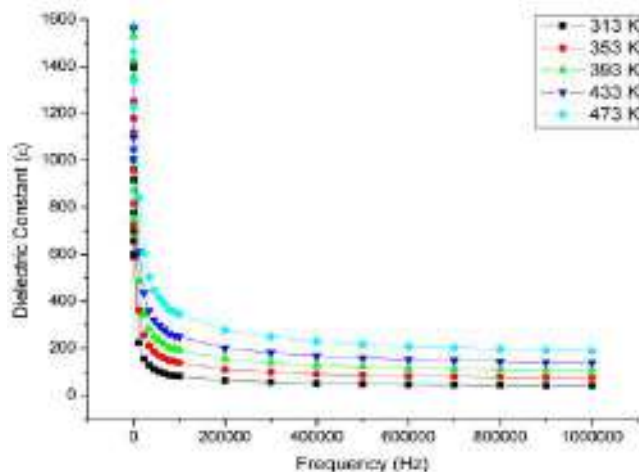
Fig. 3. Variation of dielectric constant (ε') with frequency of the applied field.

Dielectric loss factor (tan δ)

The **Fig. 4** shows the variation of dielectric loss factor (tan δ) of SnO_2 nanoparticles with applied field frequency (from 20 Hz to 1 MHz) at the different constant temperature. The values of the dielectric loss factor (tan δ) were derived from the eq. (3) which measures a part of polarization, which is out of phase with the applied field. Goldstone Mode (GM) relaxation and Soft Mode (SM) relaxation [24] are two types of rotational fluctuations of molecular dipoles. In the present study, the Goldstone Mode (GM) relaxation fluctuation are found be near the 200 Hz frequency while Soft Mode (SM) relaxation fluctuation are said to be absent.

It is also seen that dielectric constant and Dielectric loss factor (tan δ) increases with the increase in temperature for all the frequencies. When the temperature of samples increases, then its dipoles are more free accessible and easily react to the applied electric field, result of this the polarization will be increased, therefore the dielectric constant also increases with the increase in temperature [25].
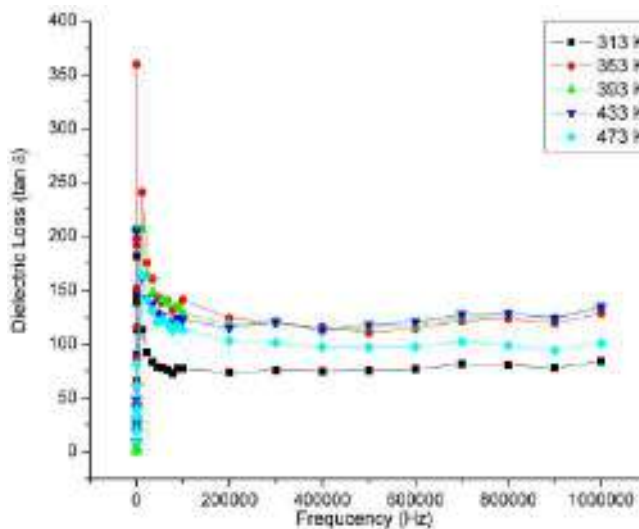
Fig. 4. Variation of dielectric loss factor (tan δ) with applied field frequency.

Current voltage characteristics

The **Fig. 5** shows I-V characteristics of SnO_2 nanoparticles at temperature range 313 - 473 K. The nature of plot shows the semiconducting behavior and obeys Ohms Law at temperature range 313 - 473 K. The semiconducting behavior of SnO_2 nanoparticles plays very important role in the gas sensing characteristics [26]. Therefore SnO_2 is said to be an promising candidate for the chemical gas sensors. The resistance of SnO_2 nanoparticles is found to be 2.29 MΩ at 473 K temperature.
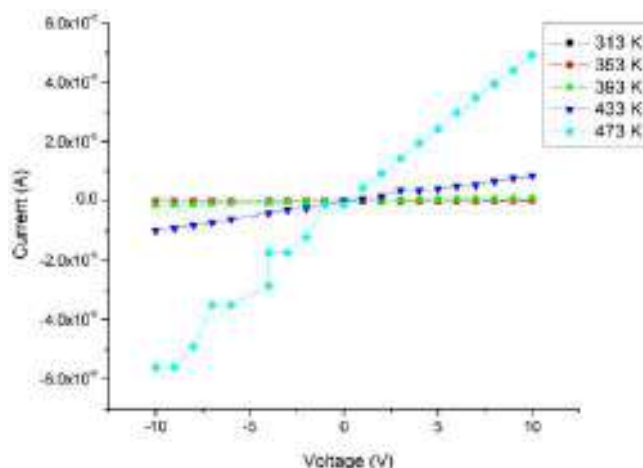
Fig. 5. I-V characteristics of the SnO_2 nanoparticles at temperature range (313-473 K).

Field emission scanning electron microscopy (FESEM)

The morphology and particle size of the prepared SnO_2 samples were determined by FESEM analysis as shown in **Fig. 6** which shows the FESEM picture of SnO_2 nanoparticles synthesized by using Liquid-phase method via co-precipitation. It is observed from micrographs, particles are found to be in the tetragonal shape within the particle size in the range about 15 - 31.2 nm. The average particle size observed in both FESEM and XRD measurement were found to be nearly equal.
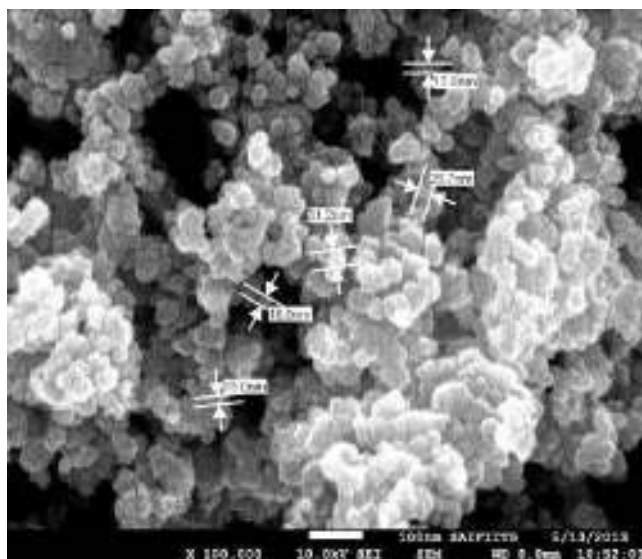
Fig. 6. FESEM picture of the SnO_2 nanoparticles.

UV-visible absorption spectrum

UV-visible absorption spectroscopy is widely used tool for checking the optical properties of nanosized particles. **Fig. 7** shows the UV-visible absorption spectrum of SnO_2 nanoparticles calcinated at temperature 700°C for 6 hours. From the spectrum four peaks are observed at 225 nm, 306 nm, 731 nm and 761 nm, out of this at 306 nm wavelength has been found maximum absorption, optical band gap for this wavelength found to be 4.05 eV, which is higher than the reported value of the bulk SnO_2, i.e. 3.6 eV [27]. This small difference in the optical band gap may be indicating that some impurity bands are developed near conduction bands [28].
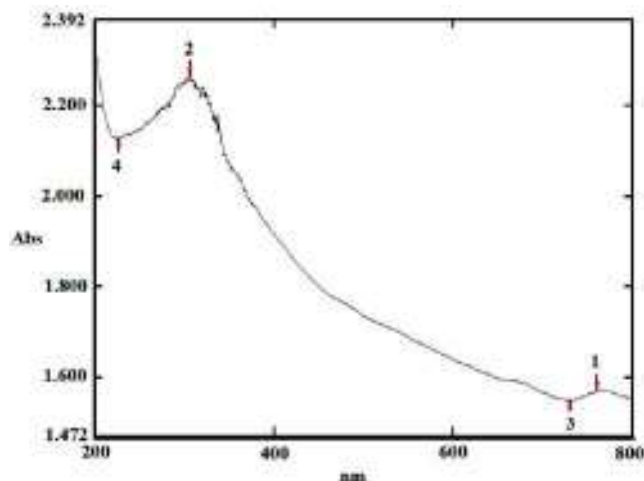
Fig. 7. UV-visible absorption spectrum of the SnO_2 nanoparticles.

TG-DTA plots

As shown in **Fig. 8**, show TG-DTA plots for pure SnO_2, which shows significant loss of weight is observed from room temperature to 500°C without plateau. The total rate of decomposition is found to be 0.52 mg/°C and total loss is 6 %. The endothermic peak on DTA curve is observed at 39°C which is associated with surface water loss. The small exothermic peak is observed at 490°C which may be attributed to phase change.
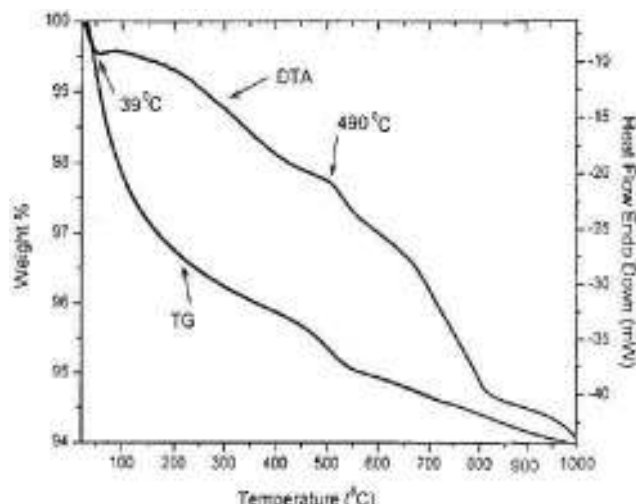
Fig. 8. TG-DTA plots for pure SnO_2.

From TG-DTA curves, upto 100^0C, loss of weight is due to loss of water contents in the sample. Weight loss is in the range ~0.5 to 4%. Onwards 100^0C upto 800^0C, the weight loss observed upto 12 %. During this temperature range the samples are found to be stable. After 800^0C, a sudden weight loss observed upto 6% which is due to transformation of $SnO \rightarrow Sn_3O_4$ during heating of the powder sample [29].

Conclusion

Preparation of SnO_2 nanostructures by using liquid-phase co-precipitation method is fast and easy. The ac electrical conductivity and dielectric constant has been frequency dependent. Tetragonal rutile crystalline phase, morphology of SnO_2 has been identified by XRD and FESEM respectively. The optical band gap is found to be 4.05eV. The significant loss of weight is observed from room temperature to 500 ^{0}C without plateau.

Reference

1. Rockenberger, J.; Felde, U.; M. Tischer, L.; Troger, M.; Haase, H.; Weller; *J. Chem. Phys.,* **2000**, *112,* 4296.
   DOI: 10.1063/1.480975
2. Seiyama, T.; Kato A.; Fujiishi, K.; Nagatani, M.; *Anal. Chem.*, **1962**, *34,* 1502.
   DOI: 10.1021/ac60191a001
3. Shukla, S.K.; Mishra, A.K.; Arotiba, O.A.; Mamba, B.B.; *Enzymes Microb. Technol.* **2014**, *66,* 48.
   DOI: 10.1016/j.enzmictec.2014.08.003
4. Zhang, J.; Gao, L.J.; *Solid State Chem*. **2004**, *177*, 1425.
   DOI: 10.1016/j.jssc.2003.11.024
5. Wang, Y.; Lee, J.Y.; *J. Phys. Chem.* B **2004,** *108,* 13589.
   DOI: 10.1021/jp048454w
6. Bhagwat. M.; Shah, P.; Ramaswamy, V.; *Mater. Lett.* **2003,** *57*, 1604.
   DOI: 10.1016/s0167-577x(02)01040-6
7. Johari A.; Bhatnagar, M.C.; Rana, V.; *Adv. Mat. Lett*. **2012**, *3(6)***,** 515.
   DOI: 10.5185/amlett.2012.icnano.251
8. Sonker, R.K.; Sharma, A.; Shahabuddin, Md.; Tomar, M.; Gupta, V.*; Adv. Mat. Lett*. **2013**, *4(3)*, 196.
   DOI: 10.5185/amlett.2012.7390
9. Garje, A.D.; Sadakale S.N.; *Adv. Mat. Lett*. **2013**, *4(1)*, 58.
   DOI: 10.5185/amlett.2013.icnano.228
10. Kumar, V.; Kumar, V.; Som, S.; Neethling, J.H.; Lee, M.; Ntwaeaborwa, O.M.; Swart, H.C.; *Nanotechnology*. **2014**, *25(13)*, 135701.
    DOI: 10.1088/0957-4484/25/13/135701
11. Ristic, M.; Ivanda, M.; Popovic, S.; Music, S.; *J. Non-Cryst. Solids*, **2002**, *303*, 270.
    DOI: 10.1016/s0022-3093(02)00944-4
12. Liu, Y.; Koep, E.; Liu, M.; *Chem. Mater*. **2005**, *17*, 3997.
    DOI: 10.1021/cm050451o
13. Bueno, P. R .; Pianaro, S.A.; Pereira, E.C.; Bulhoes, L.O.S.; Longo, E.; Varela, J.A.; *J. Appl.Phys.,* **1998**, *84*, 3700.
    DOI: 10.1063/1.368587
14. Sahay, P.P.; Mishra, R.K.; Pandey, S.N.; Jha, S.; Shamsuddin, M.; *Ceramics Int.* **2012**, *38(2)* , 1281.
    DOI: 10.1016/j.ceramint.2011.08.062
15. Sahay, P. P.; Mishra, R.K.; Pandey, S.N.; Jha, S.; Shamsuddin, M.; Current *Appl. Phys.* **2013**, *13(3),* 479.
    DOI: 10.1016/j.cap.2012.09.010
16. Chizhov, A.; Rumyantseva, M.; Gaskov, A.*; Inorg. Mat.* **2013**, *49(10)*, 1000.
    DOI: 10.1134/s0020168513100014
17. Ni, J.; Zhao, X.; Zheng, X.; Zhao, J.; Liu, B. ; *Acta Mater.* **2009**, *57*, 278.
    DOI: 10.1016/j.actamat.2008.09.013
18. Vijayalakshmi, R.; Ashokan, P.V.; Shridhar, M.H. ; *Mat. Sci. Eng. A* **2000**, *281,* 213.
    DOI: 10.1016/s0921-5093(99)00723-6
19. Cullity, B.D.; *Elements of X-ray diffraction* (Addison-Wesley), **1970,** 102.
    DOI: 10.1119/1.1934486
20. Butcher, P.N.; Morys, P.L.; *J. Phys. C, Solid State Phys*., **1973**, *6*, 2147.
    DOI: 10.1088/0022-3719/6/13/014
21. Ce-Wen, N.; Holten, S.; Birringer, R.; Haibin, G. ; Kliem, H.; Gleiter, H.; *Phys. stat. sol.* **1997**, *(a) 164 No.1 ,* R1-R2.
    DOI: 10.1002/1521-396x(199711)164:13.0.co;2-#
22. Elliot, S.R.; *Adv. Phys.* **1987**, *36,* 135.
23. Saltas, V.; Vallianatos, F.; Soupios, P.; Makris, J.P.; Triantis, D.; *J. Hazard. Mater.* , **2007**, *142*, 520.
    DOI: 10.1016/j.jhazmat.2006.08.051
24. Singh, D.P.; Gupta, S.K.; Pandey, A.C.; Manohar, R.; *Adv. Mat. Lett.* , **2013**, *4(7)*, 556.
    DOI: 10.5185/amlett.2012.11463.
25. Frohlick, H.; Theory of Dielectrics; Oxford University press, **1956**.
26. Johari A.; Rana V.; Bhatnagar M. C.; *Nanomater; nanotechnol.,* **2011**, *1(2)* ,49.
    DOI : 10.1109/inec.2011.5991739
27. Fang, L.M.; Zu, X.T.; Li, Z.J.; Zhu, S.; Liu, C.M.; Wang, L.M.; Gao, F.; *J. Mater. Sci: Mater. Electron*, **2008**, *19* , 868.
    DOI: 10.1007/s10854-007-9543-7
28. Terrier, C.; Chatelon, J.P.; Roger, J.A.; *Thin Solid Films*, **1997**, *295,* 95.
    DOI: 10.1016/s0040-6090(96)09324-8
29. Madhusudhana Reddy, M.H.; Jawalekar, S.R; Chandorkar A.N.; *Thin solid films*, **1989**, *169,* 117.
    DOI: 10.1016/s0040-6090(89)80010-0

TIN OXIDE AND TITANIUM DIOXIDE BASED CO₂ GAS SENSOR

Gajanan Trymbakappa Lamdhade

Department of Physics, Vidya Bharati Mahavidyalaya, CK Naidu Road, Camp, Amravati Maharashtra State 444 602, INDIA
gtlamdhade@rediffmail.com, oumgajanan@gmail.com

ABSTRACT

The influence of CO_2 gas concentration on the transport properties of SnO_2-$10Al_2O_3$-$10TiO_2$ oxide thick films has been studied. From the X-RD spectra the average crystallite size of the samples is found to be of the order of 10.80 nm to 56.05 nm and shows polycrystalline and granular nature. For a fixed concentration of gas the sensitivity decreases with increase in temperature, but increases with increasing concentration of CO_2 gas. Transient response of the samples was studied. The resistance of all the samples increases by increasing the concentration of CO_2 gas, due to oxidization process on the surface of the material.

Keywords: Metal oxide thin films, electrical conductivity, transient response, CO_2 gas Sensor.

I. INTRODUCTION

The hetero-structure mechanism and the amorphous nature of the samples are important for the sensing devices. Ceramic and amorphous materials may be the best sensors for sensing the present gases. Most of the research workers have studied the electrical resistance of the material in presence of CO_2 gas environment. Today multi–functioning sensors are available in the market but now there is a need to develop the best sensor for sensing the single gas only. The semiconductor metal oxide materials are generally used in the form of wafer (thin pellet) or film (thin or thick) deposited on a substrate (glass, silica, silicon, alumina, steatite etc.). Gas sensors in the form of thin or thick films seems to be more promising detectors over the pellet form, because they are potentially of low cost, rugged and have low consumption of electric power and more active surface area.

A sensor array comprising of three chemical gas sensors was evaluated to predict the concentrations of O_2, CO and CO_2 in a gas stream at 600^oC [1]. The sensors in the array included a resistance-based 2% CuO/10% La_2O_3/TiO_2 material and yttrium stabilized zirconium (YSZ) sensor with a metal/metal oxide internal reference electrode and a lithium phosphate-based sensor. Electrochemical impedance spectroscopy (EIS) was used to study the electrical properties of heat treated electrochemical gas sensors [2]. In the present paper solid solution of metal oxides SnO_2-$10TiO_2$-$10Al_2O_3$ in the form of thick films is selected. The pure TiO_2 and Al_2O_3 are mixed with SnO_2 for the improvement of temperature characteristic and stability respectively.

II. EXPERIMENTAL DETAILS

The thick films of tin oxide (SnO_2), titanium oxide (TiO_2) and alumina (Al_2O_3) were prepared by screen-printing technique on chemically clean optically plane glass substrate. The X-ray diffraction (XRD, Rigaku X-ray diffractometer, Japan) analyses of thick films was conducted using Cu Kα radiation to determine the different phases and the grain size. The crystallite size was calculated from the full width at half maximum of the first peak using the Scherrer's formula [3].

The thickness of the sensor films was measured by Digimatic Outside Micrometer (Series-293, Japan) having a resolution of ±0.001mm and found to be 7.45, 40.09 and 73.34 μm for (SnO_2-$10TiO_2$-$10Al_2O_3$) solid solution, pure SnO_2 and pure TiO_2 sensors respectively. The resistance of the sensor was measured by voltage drop method adopted by Yawale *et al* [4, 5]. By knowing sensor resistance the sensitivity was calculated.

III. RESULTS AND DISCUSSION:

Tin oxide (SnO_2) is a wide energy gap n-type semiconductor. It is used as sensor because of its chemical and mechanical stability. The fig.1 shows the XRD spectra of (SnO_2-$10TiO_2$-$10Al_2O_3$) solid solution and shows polycrystalline and granular nature of the selected oxides. From fig. 1 it is observed that XRD spectra contains 10–15 peaks which are due to SnO_2 and TiO_2. The (h, k, l) values are obtained by using 2θ and d-values. Tin dioxide has one stable state called as rutile. Anatase phase of TiO_2 changes to rutile when heated above temperature 500 ^oC along with SnO_2 and Al_2O_3 [6, 7]. So the structure of TiO_2 and SnO_2 is same. The lattice parameter values obtained for SnO_2 and TiO_2 are $a = b = 4.7382$ ^oA and $c = 3.1871$ $^\circ A$ with c/a ratio of 0.6726 and $a = 4.5933$ $^\circ A$ and $c = 2.9595$ $^\circ A$ with c/a ratio of 0.6442, respectively. These values are in agreement with the values reported in references [8, 9]. The rutile phase is stable and because of the same structure of SnO_2 and TiO_2, the space group and atom location sites changes the Ti^{4+} by Sn^{4+} metallic cation. Similarly the Al_2O_3 which is added as stabilizer to SnO_2–TiO_2 material, forms hexagonal phase with $a = 4.758$ $^\circ A$ and $c = 12.925$ A$^\circ$. These phases are playing very important role for sensing the CO_2 gas [10, 11].
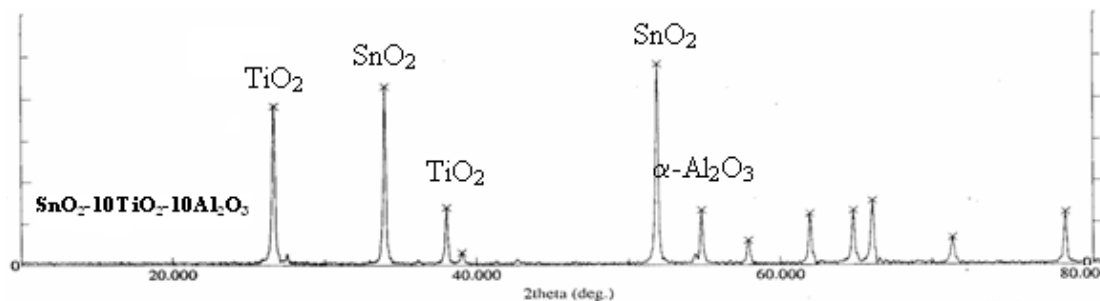
Figure 1: X-RD spectra of $(SnO_2-10TiO_2-10Al_2O_3)$ thick film

The average crystallite size calculated using FWHM and ON time and OFF time of various sensor parameters are reported in the table 1.

Table 1: Crystallite size and response time of sensors.

SN	Composition (mol %)	crystallite size (nm)	Sensitivity (s) at 500ppm at 313K	Response Time (sec)	
				ON time	OFF time
1	Pure SnO_2	56.05	10.19	90	105
2	Pure TiO_2	10.80	5.57	75	105
3	$SnO_2-10TiO_2-10Al_2O_3$	10.80	26.07	60	105

Fig. 2 shows the variation of sensitivity with change in concentration of CO_2 gas at different temperatures 313K, 323K, 333K and 343K for sensor $(SnO_2-10TiO_2-10Al_2O_3)$. From figure 2, it appears that the sensitivity decreases by increasing temperature of thick films. At lower concentration of gas a linear behavior is observed whereas at higher concentration, the plot deviates from linearity. At higher temperature range the change in the sensitivity with concentration is small. The sensor sensitivity (S) is proportional to the number of active centers on the surface of sensor. The number of active centers is the product of surface area and surface density of the active centers. The specific surface is a ratio of surface area to mass of the sensor therefore; the sensor sensitivity is proportional to the product of specific surface, density of active centers and the sensor mass. So if the specific surface is more, the number of active centers will be more and therefore the higher sensitivity of the material [12]. The TiO_2 doped polycrystalline SnO_2 sensor shows higher sensitivity just as in metal oxide $(SnO_2-10TiO_2-10Al_2O_3)$ thick film.
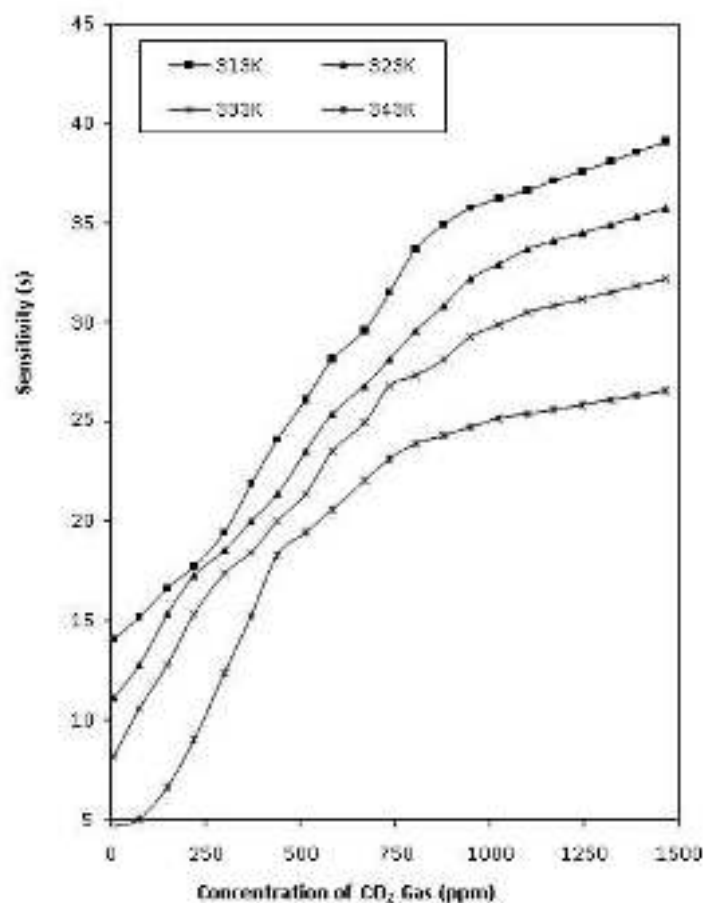
Figure 2: Variation of sensitivity with concentration of CO_2 gas at different temperatures for $SnO_2-10TiO_2-10Al_2O_3$ thick film.

Fig. 3 shows the variation of sensitivity with temperature at constant concentration of CO_2 gas (1465ppm) for the thick film (SnO_2-$10TiO_2$-$10Al_2O_3$), pure SnO_2 and pure TiO_2. These plots are found to be linear. It is seen that the sensitivity of solid solution is more than the pure SnO_2 and pure TiO_2 at higher and lower concentration of CO_2 gas.
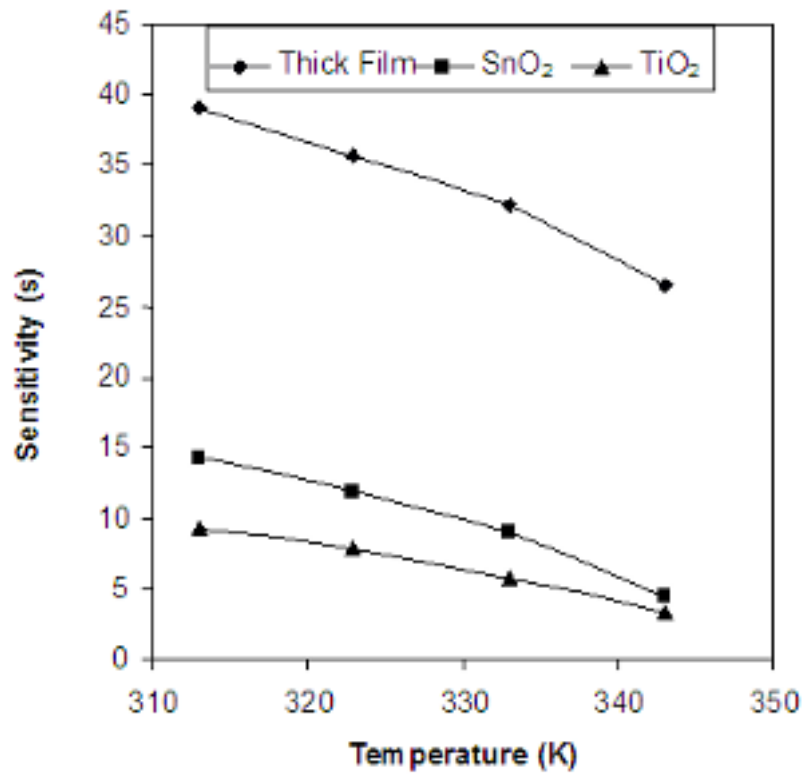
Figure 3: Variation of sensitivity with temperature at constant concentration of CO_2 gas (1465ppm)

Fig.4: shows the variation of sensitivity with change in concentration of CO_2 gas for the solid solution, SnO_2 and TiO_2 thick films at constant temperature (313K). In all the films the sensitivity increases linearly for the lower concentration range but for higher concentration range it deviates from linearity. It is also observed that the sensitivity change in solid solution thick film is more than SnO_2 and TiO_2 films.
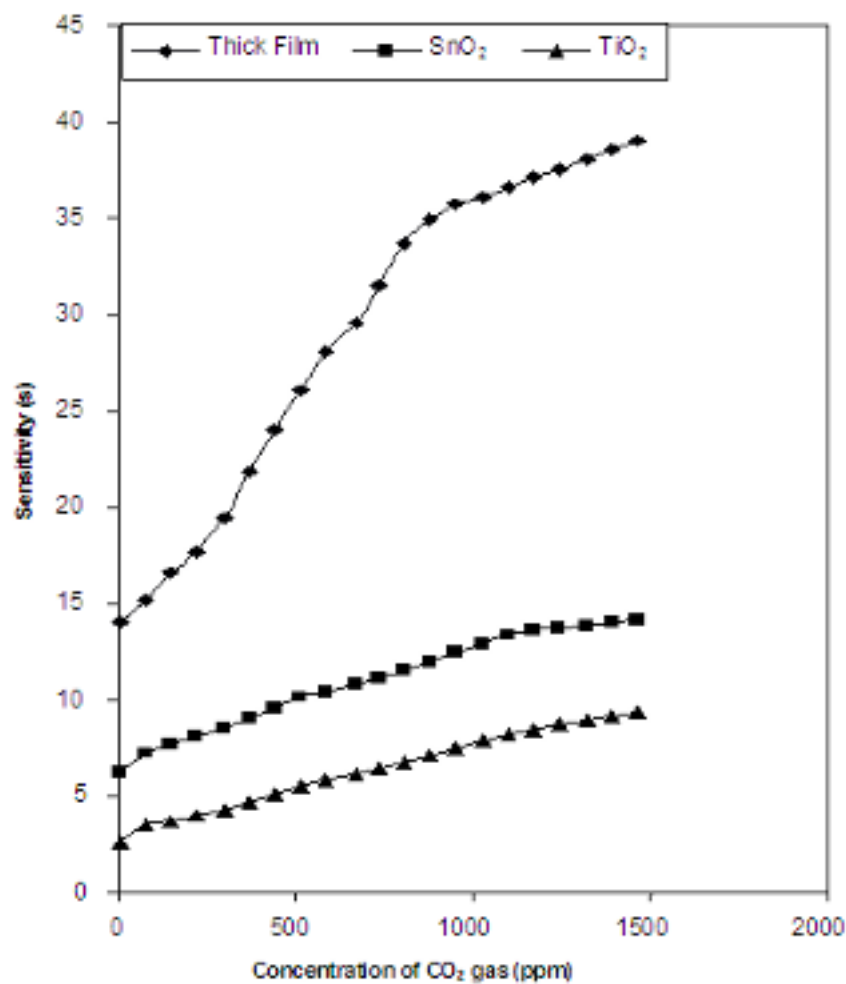
Figure 4: Variation of sensitivity with concentration of CO_2 gas at constant temperature (313K)

Fig. 5 shows the transient response of the solid solution thick film, SnO_2 and TiO_2 at 500-ppm concentration of CO_2 gas. It is observed that the solid solution has 75 s ON time and 105 s OFF time whereas for the pure SnO_2 film the ON time and OFF time is 90 and 105 s respectively. But it is also noted that, pure TiO_2 has minimum OFF time and higher ON time. This shows that the addition of TiO_2 in SnO_2 reduces the ON time of the sensors.
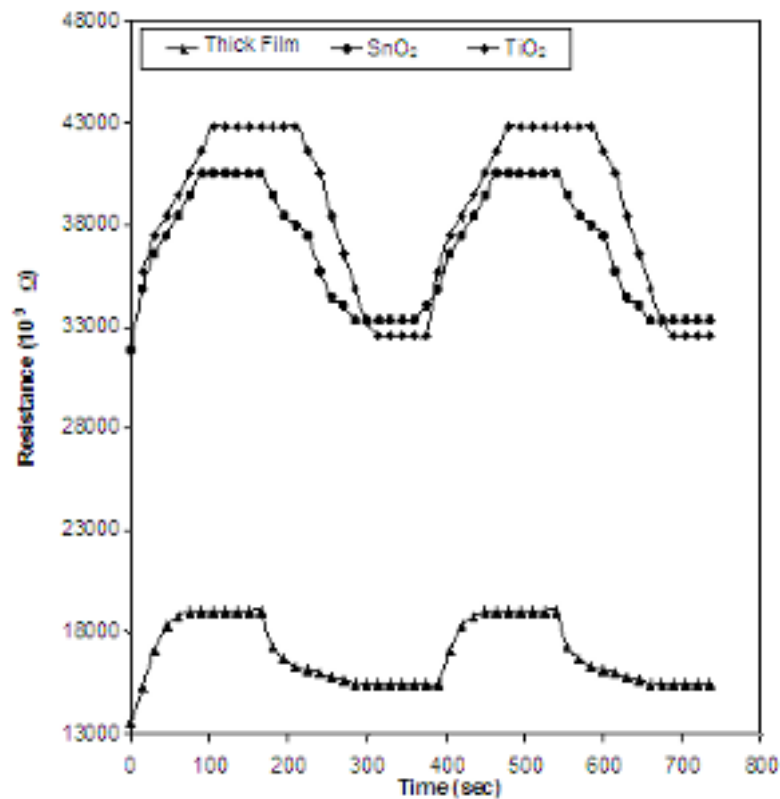
Figure 5: The transient response of CO_2 gas at constant concentration (500ppm)

At temperature 313 K, the change in resistance in presence of CO_2 gas is found to be small, whereas at 343 K the resistance change is appreciable. Addition of Al_2O_3 and TiO_2 in pure SnO_2 never affect the nature of the curves, only the resistance change is observed. The sensitivity of the (SnO_2-$10TiO_2$-$10Al_2O_3$) thick film increases by increasing the concentration of CO_2 gas. The surface conductance effects are dominant in sensing the gases. The electrical conductivity (σ) depends on the electron concentration 'n' and this concentration is related to the equilibrium constant and the partial pressure of the gases. The CO_2 gas has oxidizing properties and it leads to an oxidization of material therefore, the conductivity of the material reduces [12-14]. The possible mechanism for CO_2 gas detection in SnO_2 material is based on reactions that occur at the sensor surface, resulting in a change in concentration of adsorbed oxygen. At lower temperature (<150°C), oxygen adsorption at the surface is mainly in the form of O^{2-}. Oxygen ions adsorb onto the surface of material removes electrons from the bulk and create a potential barrier that limits electron movement and resistivity. When exposed to an oxidizing gas such as CO_2 then it is chemisorbed on bridging oxygen atoms with the formation of a surface carbonate [15], subsequently increasing the barrier height and the resistivity. Under the presence of O_2 atmosphere, the sensing material chemisorbs gas on its surface. Oxygen can be adsorbed in the several forms such as O^-_2, O^-, O^{2-} while, CO absorbs O atom from the surface becoming CO_2.

The small amount of Ti can be disperse at grain boundaries, directly or indirectly affected the density of centers which are active for gas adsorption. The grain size effect i.e. average crystalline size is also important for the sensing mechanism. It has been reported [16-19], that the sensitivity decreases with crystallite size in case of hydrogen and carbon monoxide. The granular and polycrystalline structure plays very important role in the electrical properties. The films, which have a grain size of nanometer order, they facilitated the adsorption process of gas like water molecule in the humidity sensors [7]. In this way the adsorption of CO_2 gas on the surface of thin film takes place through chemisorptions process.

IV. CONCLUSION

The solid solution has been polycrystalline nature and crystallite size found to be order of 10.80 nm. The sensitivity of solid solution is higher than the pure SnO_2 and pure TiO_2. This shows that by the addition of TiO_2 and Al_2O_3 temperature characteristic and stability of the sensor improved. The ON time for this sensor is 60s and OFF time is 105s at 500ppm of CO_2 gas. The resistance of the film increases in presence of CO_2 gas due to decrease in the electron concentration at the surface of the sensor because of oxidization of the material.

References

[1] Zhang B. Pengbei, Lee C.Chonghoon, Verweij C. Henk, A.Sheikh, C. Akbar, Hunter D. Gary, K. Prabir, A.Dutta, "High temperature sensor array for simultaneous determination of O_2, CO, and CO_2 with kernel ridge regression data analysis", Sensors and Actuators B, **123**, 950-963 (2007).

[2] M. Wierzbicka, P. Pasierb, M. Rekas, "CO_2 sensor studied by impedance spectroscopy", Physica B, **387**, 302-312 (2007).

[3] B. D. Cullity, "Elements of X-Ray Diffraction", Addison-Wesley Publishing Company Inc., London (1978).

[4] G. T. Lamdhade, S. S. Yawale, S. P. Yawale, "Tin oxide and zinc oxide based doped humidity sensors", Sensors and Actuators A, **135**, 388-393 (2007).

[5] S. P. Yawale, S. V. Pakade, "D.C. conductivity and hopping mechanism in Bi_2O_3-B_2O_3 glasses", J. Mater. Sci. **28**, 5451-5455 (1993).

[6] Seng-Lu ,Yang, Wu Jenn-Ming, "ZrO_2–TiO_2 ceramic humidity sensors", J. Mater. Sci., **26**, 631-636 (1991).

[7] Radecka Marta, Zokrzewska Katavzyna, Rekas Mieczyslaw, "SnO_2-TiO_2 solid solutions for gas sensors"**,** Sensors and Actuators B, **47**, 194-204 (1998).

[8] A. Dieguez, "Structural analysis for the improvement of SnO_2 based gas sensor", Ph.D. Thesis, Universitat de Barcelona, Barcelona, (1999).

[9] J. Robertson, "Defect levels of SnO_2", Phys. Rev. B, **30** 3520–3522 (1984).

[10] K. D. Schierbaum, S. Vaihinger, W. Gopel, H. H. Van Den, V. Lekkert, B. Kloeck, N.F. Rooij, "Prototype structure for systematic investigations of thin-film gas sensors", Sensors and Actuators B, **1**, 171-175 (1990).

[11] H. Nanto, T. Morita , H. Habara , K. Kondo, Y. Douguchi, T. Minami, "Properties and sensor performance of zinc oxide thin films", Sensors and Actuators B, **35**, 384-387 (1996).

[12] Marc J. Madou. and Roy S. Morrison, "Chemical Sensing with Solid State Devices", Academic Press Inc., London, (1989).

[13] Waghuley S.A., Yenorkar S.M., Yawale S.S., Yawale S.P., "Application of chemically synthesized conducting polymer-polypyrrole as a carbon dioxide gas sensor", Sensors and Actuators B, **128** 366-373 (2008).

[14] Waghuley S.A. , Yenorkar S.M., Yawale S.S., Yawale S.P., "SnO_2/PPy Screen-Printed Multilayer CO_2 Gas Sensor", Sensors and Transducers, **79**, 1180-1185 (2007).

[15] Matthias Batzill, U. Diebold, "The surface and materials science of tin oxide", Progress in Surface Science, **79**, 47-154 (2005).

[16] Yamazoe Noboru, "New approaches for improving semiconductor gas sensors", Sensors and Actuators B, **5**, 7-19 (1991).

[17] R.M. Agrawal, "H_2S sensing properties of metal oxide (SnO_2-CuO-TiO_2) thin films at room temperature", Journal of Electron Devices, **12**, 730-733 (2012).

[18] AK Yewale, KB Raulkar, AS Wadatkar, GT Lamdhade, "Application of metal oxide thick film as a NH_3 gas sensor", Journal of Electron Devices, **11**, 544-550 (2011).

[19] GT Lamdhade, KB Raulkar, SS Yawale, SP Yawale, "Fabrication of multilayer SnO_2–ZnO–PPy sensor for ammonia gas detection", Indian Journal of Physics, (2015) 1-6, (DOI 10.1007/s12648-015-0676-x).

Fabrication of multilayer SnO$_2$–ZnO–PPy sensor for ammonia gas detection

G. T. Lamdhade, K. B. Raulkar, S. S. Yawale & S. P. Yawale

ONLINE FIRST

Indian Journal of Physics

Official Publication of the Indian Association for the Cultivation of Science

Indian Association for the Cultivation of Science

Springer

Springer

ORIGINAL PAPER

Fabrication of multilayer SnO_2–ZnO–PPy sensor for ammonia gas detection

G T Lamdhade[1]*, K B Raulkar[1], S S Yawale[2] and S P Yawale[2]

[1]Department of Physics, Vidya Bharati Mahavidyalaya, Amravati 444 602, Maharashtra, India

[2]Department of Physics, Government Vidarbha Institute of Science and Humanities, Amravati 444 604, Maharashtra, India

Abstract: The sensitivity of SnO_2–ZnO composites in multilayer with PPy and Al_2O_3 has been studied. Composites of SnO_2–ZnO have been prepared and multilayer sensor has been fabricated using screen printing technique with Al_2O_3 as substrate on glass plate and PPy in multilayer with SnO_2–ZnO. The morphologies of composites of SnO_2–ZnO and PPy have been studied by scanning electron microscopy and crystallite size by X-ray diffraction. Sensitivity has been found to be more for $70SnO_2$:$30ZnO$/PPy/Al_2O_3 multilayer sensor, which is supported by scanning electron microscopy and X-ray diffraction studies. It has been found that with the increase in concentration of NH_3 gas, the response of multilayer sensor increases.

1. Introduction

Gas sensors based on semiconductor metal oxides are the most investigated devices. They have attracted the attention of many researchers due to their low cost, ease of fabrication, simplicity of use and large number of detectable gases [1]. Most of the companies provide metal oxide-based gas sensors due to their applications ranging from detection of combustible or toxic gas to air intake control in automobile and glucose biosensors [2]. Tin oxide (SnO_2) is the most used sensing material among commercially sensor devices for toxic gas detection [3]. It is well known that the sensing properties of SnO_2-based materials depend on their chemical and physical characteristics, which are strongly dependent on the preparation conditions, dopant and grain size. This implies that the synthesis of the sensing materials is a key step in the preparation of high-performance metal oxide semiconductor (MOS) gas sensors. SnO_2 powders and films can be prepared by a variety of methods [4–7]. DC-electrical resistance of SnO_2 doped with ZnO and TiO_2 sensors is measured in the presence of humidity. SnO_2–$5Al_2O_3$ and ZnO–$5Al_2O_3$ sensors are found to be good sensing materials for humidity.

Due to various applications in organic light-emitting diodes (OLEDs) [8], lithography [9], electrode material [10], electromagnetic shielding [11] and sensing [12, 13], conducting polymers have attracted considerable interest. Sensors constructed from conducting polymers such as polypyrrole, polyhexylthiophene, polymethylthiophene, polyethylene and polyaniline have been investigated [14–19] to study their potential applications in detecting gases, like nitrogen dioxide, carbon monoxide, carbon dioxide, ammonia and hydrogen besides moisture and a number of organic volatile compounds [20].

The present paper mainly deals with the preparation of NH_3 gas sensor in multilayer pattern with SnO_2 doped as ZnO and polypyrrole layer. It is found that SnO_2–ZnO system in multilayer with polypyrrole shows sensitivity to 70 ppm of ammonia gas concentration even at room temperature.

2. Experimental details

Powder polypyrrole was prepared from 4.290 (high) weight ratio of pyrrole (Py) monomer and oxidant ($FeCl_3$). During

*Corresponding author, E-mail: gtlamdhade@rediffmail.com; oumgajanan@gmail.com

the synthesis, concentration of $FeCl_3$ was kept constant and methanol was used as a solvent. The Py-monomer, anhydrous iron(III) chloride ($FeCl_3$) and methanol were used for synthesis of PPy. The solution of 7 ml methanol and 1.892 g $FeCl_3$ was first prepared in round-bottom flask and 8.4 ml Py-monomer was added to ($FeCl_3$ + methanol) solution with constant stirring in absence of light. The amount of Py-monomer was added to the solution (1/2.33 times of $FeCl_3$) in such a way to get maximum yield [21]. The polymerization of Py, which was suppressed in a solution, progressed rapidly due to an increase of oxidation potential caused by evaporation of solvent. In the polymerization reaction of Py, it was observed that as soon as the Py-monomer was added to the solution, the colour changed to dark green/black. There was an increase in temperature of the solution during the start of reaction, indicated that it was an exothermic reaction [22] and it was carried out at room temperature for 4 h. The final precipitated polymer was filtered by a conventional method. The polymer was washed with distilled water several times till the filtrate obtained was colourless. To remove last traces of un-reacted pyrrole and remaining ferric and fer-

rous chloride formed due to polymerization, it was then washed with methanol. The polymer, obtained in powder forms, was dried first at room temperature for a few hours and then finally dried in an oven (Gallenkamp, British Made) kept at 80 °C for 5–6 h. This polypyrrole was then used for active layers of semiconductor gas sensors.

SnO_2, ZnO and Al_2O_3 powders (AR grade) were calcinated at about 800 °C for 4–5 h and were crushed to get fine powder of the samples. XRD patterns of the samples were obtained using diffractometer system XPERT-PRO (CuKα radiation $\lambda = 1.54$ Å) at continuous scan type at step size $2\theta = 0.017°$.

The ink or paste of the sample was prepared by using screen printing (thick film technique) technique [23, 24]. The binder for screen printing was prepared by thoroughly mixing 8 wt% butyl carbitol with 92 wt% ethyl cellulose. On chemically cleaned glass plate, paste of Al_2O_3 was screen-printed and it was kept for 24 h to dry it at room temperature and then heated at 140 °C for 2.5 h to remove
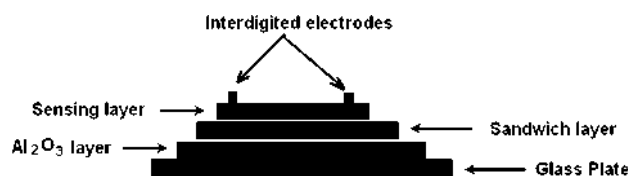
Fig. 1 Design of multilayer sensor
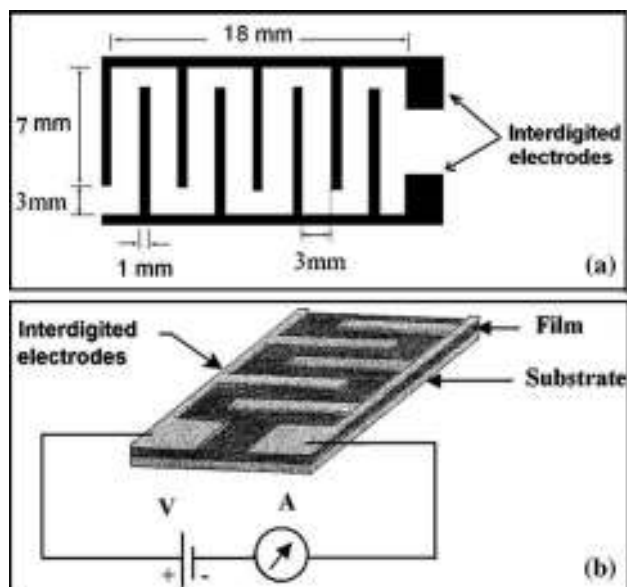
Fig. 2 (a) Fabrication of interdigited electrodes, (b) circuit of resistance measurement using interdigited electrodes
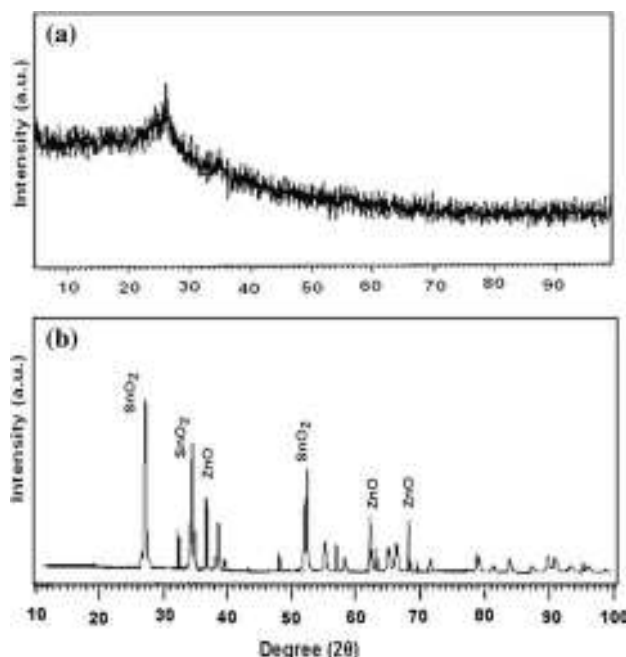
Fig. 3 (a) XRD of polypyrrole and (b) XRD of $70SnO_2:30ZnO$

Table 1 Crystallite size, sensitivity and response time of sensors

S. no.	Composition (mol%)	Crystallite size (nm)	Sensitivity (S) at 70 ppm at 313 K	Response time (s)	
				On time	Off time
1	$70SnO_2–30ZnO$	96.01	0.67	67	106
2	Pure SnO_2	120.68	0.48	114	145
3	Pure ZnO	162.09	0.35	125	168

the binder. The Al_2O_3 layer provided mechanical support as well as high thermal conductivity. Paste of SnO_2 and ZnO mixed in proper stoichiometry was then screen-printed on Al_2O_3 layer. Again plate was dried at room temperature for 24 h and binder was removed by heating it at 150 °C for 2.5 h. Finally, polypyrrole layer was deposited on SnO_2 doped with ZnO layer by screen printing, whole plate was dried and again binder was removed as
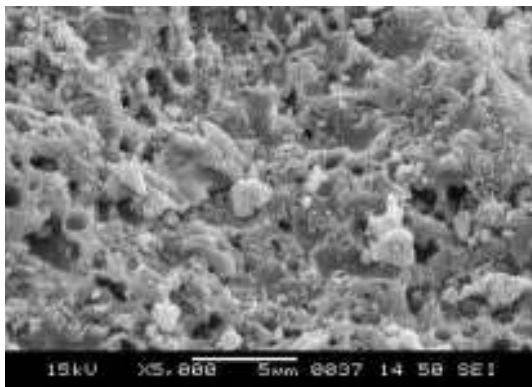
Fig. 4 SEM picture of polypyrrole

above. Polypyrrole was selected as one of the layers during the fabrication of sensors, but it did not act as interdigited electrodes. Fabrication of multilayer sensor was done, as shown in Fig. 1.

Finally on the top surface of the sensor, interdigited electrodes [25–27] were fabricated using conducting silver paste, as shown in Fig. 2(a). Thickness of SnO_2 doped with ZnO layer and PPy layers was recorded with the help of digital micrometre (series 293, Japan) having resolution of ±0.001 mm and was found to be 10 and 7 μm, respectively. To measure the sensitivity, electrical resistance was measured with the help of voltage drop method [28]. The circuit of resistance measurement using interdigited electrodes was shown in Fig. 2(b).

3. Results and discussion

XRD of PPy is shown in Fig. 3(a), which indicates amorphous nature of polypyrrole. Figure 3(b) indicates crystalline nature of ($70SnO_2$:$30ZnO$) composition sample. The average crystalline size has been calculated by using Scherrer's formula given by Eq. (1),
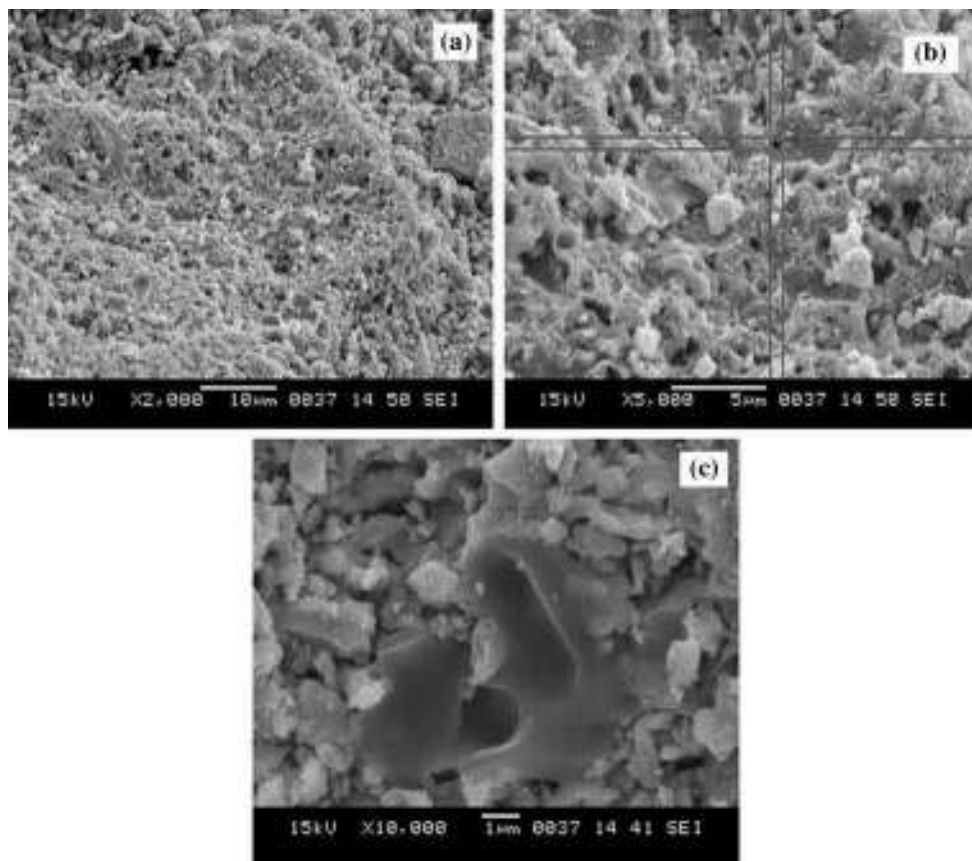
Fig. 5 SEM pictures of $70SnO_2$:$30ZnO$ at magnification (**a**) ×2000, (**b**) ×5000 and (**c**) ×10,000

$$D = \frac{K\lambda}{\beta\cos\theta} \qquad (1)$$

where D is the crystalline size, K is the shape factor and β is the full width at half maximum of diffraction angle in radians. The sensor parameters are listed in the Table 1.

The surface morphology of polypyrrole material has been studied by SEM as shown in Fig. 4.

From SEM picture, it is observed that PPY is porous in nature and pore size varies from $\sim$0.5 to 3 μm. The active surface area is found to be large due to their small pores size and hence, it shows more sensitivity. Some portion of SEM picture shows some rods with fine voids over them which helps to increase sensing properties.

SEM pictures of 70SnO$_2$:30ZnO at different magnifications are shown in Fig. 5(a)–5(c). It has been found that 70SnO$_2$:30ZnO composition has more pores per unit area than SnO$_2$ and ZnO individual and also the surface is rough because of pores and small granules of SnO$_2$ and ZnO. The pore size is found to be of the order of 0.8 μm. Thus,

Fig. 6 Variation of sensitivity with of NH$_3$ gas concentration at room temperature
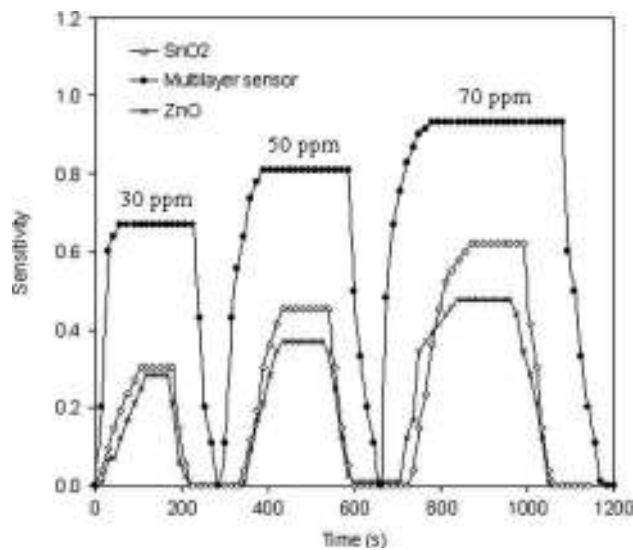
Fig. 8 Static response of pure SnO$_2$, pure ZnO and multilayer sensor at room temperature

Fig. 7 Dynamic response of pure SnO$_2$, pure ZnO and multilayer sensor at room temperature
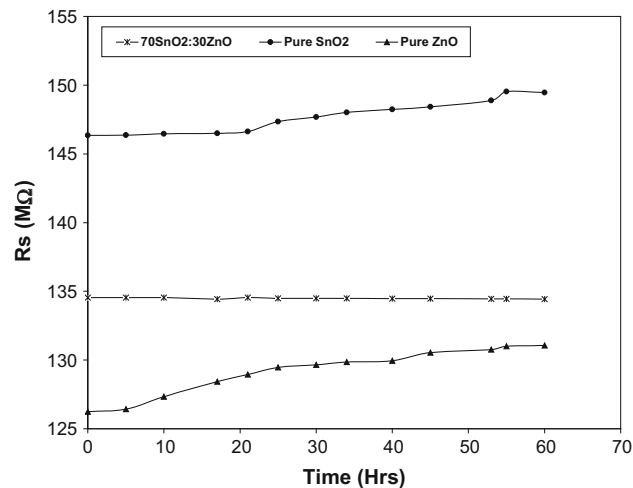
Fig. 9 Dependence of response on time for pure SnO$_2$, pure ZnO and multilayer sensor

70SnO$_2$:30ZnO composition has more active surface area and exhibits more sensitivity to NH$_3$ gas.

The sensitivity of the sensor is given by Eq. (2) shown below,

$$S = \left(\frac{R_{air} - R_{gas}}{R_{air}}\right) = \left(\frac{\Delta R}{R_{air}}\right) \qquad (2)$$

where R_{air} and R_{gas} are the resistances of sensors in air and gas, respectively.

From Fig. 6, it is observed that the multilayer structure of the sensor shows more sensitivity to ammonia gas than that for pure ZnO and pure SnO$_2$. Resistance of multilayer sensor is found to be decreasing with the increase of ammonia gas concentration and thereby sensitivity increases. Maximum sensitivity has been recorded for multilayer sensor at 70 ppm concentration of NH$_3$. The sensing mechanism is explained on the basis of NH$_3$ heats of adsorption [29, 30]. Four-coordinate Sn^{2+} cations at bridging oxygen vacancies on the reduced surface appear to be more acidic than five-coordinate Sn^{4+} cations. The stronger interactions with Sn^{2+} cations are attributed to a predominant covalent contribution to the NH$_3$–Sn bond. The Lewis acidity of the Sn cations based on NH$_3$ heats of adsorption goes through a maximum for the formation of a reduced surface as the surface becomes more oxygen deficient, and a similar trend is seen in the extent of dissociation of methanol. Four-coordinate Sn^{2+} cations form stronger covalent bonds with NH$_3$ and methanol due to greater molecular overlap with lone pairs available on both molecules. The introduction of in-plane oxygen vacancies on the defective surface reduces the heats of adsorption of the associated cations possibly due to a higher electronic charge density around the cations associated with in-plane oxygen vacancies.

Dynamic and static responses for pure SnO$_2$, pure ZnO and multilayer sensor for 30, 50 and 70 ppm are shown in Figs. 7 and 8, respectively. The time taken to reach 90 % of the response when ppm of gas is changed is known as response time and time taken to reach 90 % of recovery when gas is turned off is known as recovery time. The response time (t_{res}) and recovery time (t_{rec}) are the two important parameters of the sensor. It is found that response time is 67.2 s and recovery time is 106.2 s for multilayer sensor at 70 ppm of NH$_3$. Recovery time is found to be longer than response time, also t_{res} and $t_{rec.}$ for multilayer sensor are found to be smaller than that for pure SnO$_2$ and pure ZnO, i.e. multilayer sensor is fast. The selected PPy has major component due to his high porosity nature and it has more sensitivity at room temperature with SnO$_2$ and sensing conditions are improved.

The rate of change of resistance of the sensor with respect to time defines the stability of the sensor. A sensor should be more stable for its better response. The changes in the resistance for multilayer sensor (70SnO$_2$:30ZnO) and pure samples are shown in the Fig. 9. It is observed that resistance of multilayer sensor does not change drastically as that in case of pure samples. This shows that multilayer sensor is more stable than the other. Figure 10 shows the TG–DTA curve of PPy, plotted as a function of temperature. It is observed from Fig. 10 that the weight loss decreases continuously, i.e. PPy goes on decomposition on heating. At about 70 °C, an endothermic peak is observed and it may be due to the combined loss of water and PPy [31]. The total rate of decomposition is found to be 2.9 mg/°C and total loss is nearly 42 % up to 900 °C.

Fig. 10 TG-DTA curve of polypyrrole (PPy)
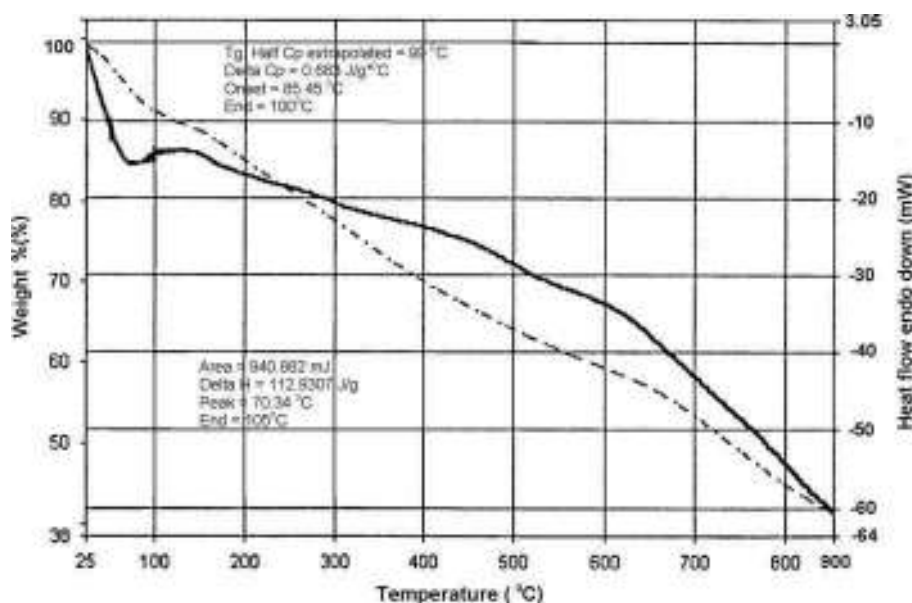
4. Conclusions

From XRD and SEM analysis, it is concluded that the crystallite size of $70SnO_2:30ZnO$ multilayer is smaller and it is more porus and hence has greater surface area and therefore shows greater response to ammonia gas. $70SnO_2:30ZnO$ multilayer sensor shows better stability than pure samples and dynamic response is also fast.

References

[1] P T Moselicy *Solid state gas sensor. Meas. Sci. Technol.* **8** 223 (1997)

[2] S P Yawale, S S Yawale and G T Lamdhade *Sens. Actuators A* **135** 388 (2007)

[3] Z Han, N Guo, F Li, W Zhang, H Zhao and Y Qian *Mater. Lett.* **48** 99 (2001)

[4] K C Song and J H Kim *Powder Technol.* **107** 268 (2000)

[5] C H Shek, JK L Lai and G M Lin *Nanostruct. Mater.* **11** 887 (1999)

[6] D Briand, M Labeau, J F Currie and G Delabouglise *Sens. Actuators B* **48** 395 (1998)

[7] N. Pinna and M Niederberger *Angew. Chem. Int. Ed.* **47** 5292 (2008)

[8] J W Schultze and H Karabulut *Electrochim. Acta* **50** 1739 (2005)

[9] T Asmus and G K Wolf *Nucl. Instr. Meth. Phy. Res. B*. **166** 732 (2000)

[10] M Mastragostino, C Arbizzani and F Soavi *Solid State Ionics* **148** 493 (2002)

[11] S K Dhawan, N Singh and D Rodrigues *Sci. Technol. Adv. Mater.* **4** 105 (2003)

[12] S Koul, R Chandra and S K Dhawan *Sens. Actuators B* **75,** 151 (2001)

[13] S Jain, S Chakane, A B Samui, V N Krishnamurthy and S V Bhoraskar *Sens. Actuators B* **96** 124 (2003)

[14] Y Joon-Boo, B Hyung-Gi, S Myung-Suk and H Jeung-Soo *Sens. Actuators B* **108** 305 (2005)

[15] R Gangopadhay and A De *Sens. Actuators B* **77** 326 (2001)

[16] M E H Amrani, R M Dowdeswell, P A Payne and K C Persaud *Sens. Actuators B* **44** 512 (1997)

[17] C Jouve, D Jullien and B Remaki *Sens. Actuators B* **28** 75 (1995)

[18] S Dogan, U Akbulut, T Yalcin, S Suzer and L Toppare *Synth. Metal* **60** 27 (1993)

[19] M K Ram, O Yavuz and M Aldissi *Synth. Metal* **151** 77 (2005)

[20] S A Waghuley, S M Yenorkar, S S Yawale and S P Yawale *Sens. Actuators B* **128** 366 (2008)

[21] S Machida, S Miyata and A Techagumpuch *Synth. Metals* **31** 311 (1989)

[22] S H Hahn *PhD Thesis* University of Tubingen (2002)

[23] T Ishihara, K Kometani, Y Mizuhara and Y Takita *J. Am. Ceram. Soc.* **75** 3 (1992)

[24] C A Harper *Inorg. Chem. Acta* **34** 175 (1979)

[25] Y Shimizu and M Egashira *MRS Bull.* **24** 18 (1999)

[26] V Jayaram *New Materials* (India: Narosa Publishing House) (eds.) S K Joshi, T Tsurata, C N R Rao and S Nagakura (1992)

[27] A Salomonsson *PhD Thesis* University of Linkopings (2005)

[28] S P Yawale and S V Pakade *J. Mater. Sci.* **28** 5451 (1993)

[29] J Y Ouyang and Y F Li *Polymer* **38** 27 (1997)

[30] W M Abee and D F *Cox Surf. Sci.* **77** 520 (2002)

[31] H P Wong, B C Dave, F Lenoux, J Harreld, B Dunn and L F Nazar *J. Mater. Chem.* **8** 1019 (1998)

Preparation and Ethanol Sensing Behavior of Spinel-type Nanosized Mixed Ferrites Containing Zn

V. D. KAPSE [1,*], F.C. RAGHUWANSHI [2], V.S. SANGAWAR [3]

[1] Department of Physics, Arts, Science and Commerce College, Chikhaldara 444807, Maharashtra, India
[2] Department of Physics, Vidyabharati Mahavidyalaya, Amravati 444602, Maharashtra, India
[3] Department of Physics, Government Vidarbha Institute of Science & Humanities, Amravati 444604, Maharashtra, India, Corresponding author: vdk.nano@gmail.com

Abstract

Nanocrystalline $Ni_{1-x}Zn_xFe_2O_4$ (x = 0, 0.2, 0.3 and 0.4) mixed ferrite with cubic spinel structure was successfully prepared by the citrated sol-gel method followed by calcinations at 600 ^0C. Characterization of the materials was performed by XRD. Indirect-heating sensors using as-prepared powders of mixed ferrite as sensitive materials were fabricated on an alumina tube with Au electrodes and Platinum wires. The gas response of $Ni_{1-x}Zn_xFe_2O_4$ based thick film sensor to C_2H_5OH, was measured. $Ni_{0.6}Zn_{0.4}Fe_2O_4$ based thick film sensor showed better response to ethanol gas at 300 ^0C as compared with other tested reducing gases. The observed gas sensing potential is explained by using the reducer nature of the gaseous species that react on the surface of the heated semi-conducting mixed oxide. The sensor exhibited a fast response and a good recovery.

Keywords: X-ray diffraction; Mixed ferrites; Gas sensor; Sensor response.

1. Introduction

Metal oxides based semiconductor gas sensors are commonly used in the monitoring of toxic pollutants and can provide the necessary sensitivity, selectivity and stability required by such systems [1]. Gas-sensing properties of semiconducting materials based on SnO_2, ZnO, WO_3, TiO_2, In_2O_3, Fe_2O_3, mixed oxides, ferrites and complex metal oxides have been extensively studied to detect explosive, inflammable, toxic and hazardous gases. In the last decade there is growing interest to investigate the gas sensing properties of ferrites [2-4]. $NiFe_2O_4$ (AB_2O_4) is a well-known inverse spinel with all Ni^{2+} ions on the B-sites and Fe^{3+} ions equally distributed between A and B-sites [5]. $NiFe_2O_4$ exhibit high sensitivity for the reducing gases like chlorine and liquefied petroleum gas [6, 7]. However, to our knowledge the ethanol gas-sensing properties of $NiFe_2O_4$ and Zn doped $NiFe_2O_4$ are still not so widely available.

The gas sensing mechanism involves surface reaction of the oxide surface with the test gas [8]. The ability to control the surface of the nanocrystals by adopting different synthesis routes has opened-up a new dimension to modify material for specific property applications. Also, nano sized materials, which have high surface activity due to their small particle size and enormous surface area, can increase the

efficiency of the chemical sensor [9, 10]. There are several routes to obtain nanosized ferrites such as hydrothermal synthesis, sol–gel, microemulsion techniques, etc.

The aim of the present investigation is to prepare nanocrystalline Zn modified Ni ferrite by citrated sol-gel method with a low calcination temperature involving low cost metal nitrates as raw materials and characterize them for ethanol gas sensing.

2. Experimental details

The stoichiometric molar amounts of Ferric nitrate [$Fe(NO_3)_3.9H_2O$], Nickel nitrate [$Ni(NO_3)_2.6H_2O$], Zinc nitrate [$Zn(NO_3)_2.6H_2O$] and citric acid monohydrate [$C_6H_8O_7.H_2O$] were weighed and mixed with ethylene glycol. The prepared mixture was stirred magnetically at 80 ^{0}C for 2 h. A transparent solution was obtained after 2 h. Then, this solution was consequently transferred to Teflon-lined stainless steel autoclave. The temperature of the autoclave was raised slowly to 125 ^{0}C and maintained for 10 h to get gel precursor. Afterward, the autoclave was allowed to cool naturally to room temperature and the resulting product further heated for 3 h at 350 ^{0}C in muffle furnace and then milled to a fine powder. The obtained powder was then calcined at 600 for 5 h ^{0}C to improve the crystallinity of the prepared materials. Fig. 1 shows the flowchart to prepare nanosized $Ni_{1-x}Zn_xFe_2O_4$ powder samples.
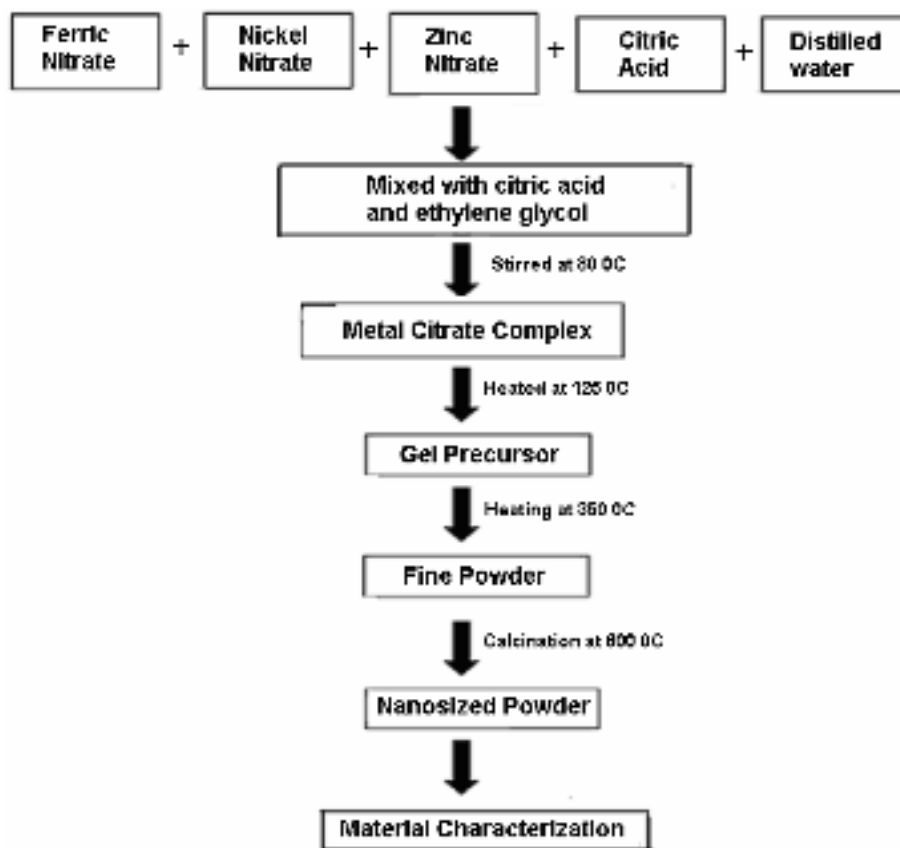
Figure 1. Flow chart for synthesis of $Ni_{1-x}Zn_xFe_2O_4$ powders

The structure and constituents of the products were determined on an X-ray diffractometer (Model: Philips X'pert) with a Cu Kα radiation (λ = 1.5406Å). The crystallite size (D_{hkl}) of the powder sample was calculated using Scherrer relation, which is given by,

$$D = \frac{K\lambda}{B.Cos\theta}$$

Where B is the full width at half-maximum intensity (in radians) of a peak at an angle θ; K is a constant, depending on the line shape profile; λ is the wavelength of the X-ray source. The crystallite size was determined by taking the average of the strongest peaks D_{220}, D_{311}, D_{400}, D_{511} and D_{440}.

The description of the sensor fabrication and gas sensing measurements has been already depicted in one of earlier reports [4]. Gas sensing properties were investigated at various operating temperatures from 50 to 350 ^{0}C. The experiments were performed with four test gases: liquefied petroleum gas (LPG), ammonia (NH_3), hydrogen (H_2), and ethanol gas (C_2H_5OH). The concentration of test gases was 500 ppm for NH_3, H_2 and LPG whereas it is 100 ppm for C_2H_5OH. The sensor response (S) is defined as the ratio $\Delta R/R_a$, i.e. change in resistance of the sensor (R_a) in air and in the gas (R_g), normalized to the sensor resistance in air.

$$S = \frac{\Delta R}{R_a} = \frac{|R_a - R_g|}{R_a}$$

3. Results and Discussion

3.1. Materials characterizations

The X-ray diffraction patterns of $Ni_{1-x}Zn_xFe_2O_4$ (x = 0, 0.2, 0.3 and 0.4) calcinated at 600 ^{0}C are displayed in Fig. 2. The XRD peaks and their positions with the calculated lattice parameters confirm that all the compositions exhibit single-phase cubic spinel structure with Fd3m space group. No peaks corresponding to any additional crystalline component are observed in the obtained patterns. The average crystallite size has been calculated from the XRD peaks using Debye−Scherrer formula and was found in the range of 23-38 nm for all the investigated samples. The lattice parameters estimated from XRD peaks are presented in Table 1. It is observed that the average crystallite size is minimum for $Ni_{0.6}Zn_{0.4}Fe_2O_4$ composition. Also, it is seen that the lattice parameter increases with an increase of Zn content. The increase in the value of the lattice constant with Zn ion substitution can be explained on the basis of ionic radius, where the ionic radius of Zn ion (0.82 Å) is smaller than that of Ni ion (0.78 Å).

3.2. Ethanol sensing characteristics

To reveal the potential use of the nanocrystalline spinel $Ni_{1-x}Zn_xFe_2O_4$ (x = 0, 0.2, 0.3 and 0.4) synthesized in the present investigation to chemical sensors, its ethanol sensing properties were studied. The response of $Ni_{1-x}Zn_xFe_2O_4$ to ethanol was measured at different operating temperatures to find out the optimal operating temperature for ethanol detection. The response of the nanocrystalline spinel Ni_{1-}

$_x$Zn$_x$Fe$_2$O$_4$ to 100 ppm ethanol as a function of operating temperature is illustrated in Fig. 3. It can be seen that the composition Ni$_{0.6}$Zn$_{0.4}$Fe$_2$O$_4$ exhibited the maximum response to 100 ppm C$_2$H$_5$OH at 300 ^{0}C. At lower operating temperatures, the sensor response is relatively low, but it increases gradually with an increase in the operating temperature. The sensor response to ethanol attains a maximum at ~300 ^{0}C and subsequently it decreases with a further increase of the operating temperature. Thus, the optimal operating temperature for the Ni$_{0.6}$Zn$_{0.4}$Fe$_2$O$_4$ spinel to detect ethanol was at 300 ^{0}C, which is the modest from the perspective of semiconducting oxide gas sensors. Hence, the optimal operating temperature of 300 ^{0}C was chosen to investigate further ethanol sensing properties such as response and recovery times, reproducibility and selectivity.
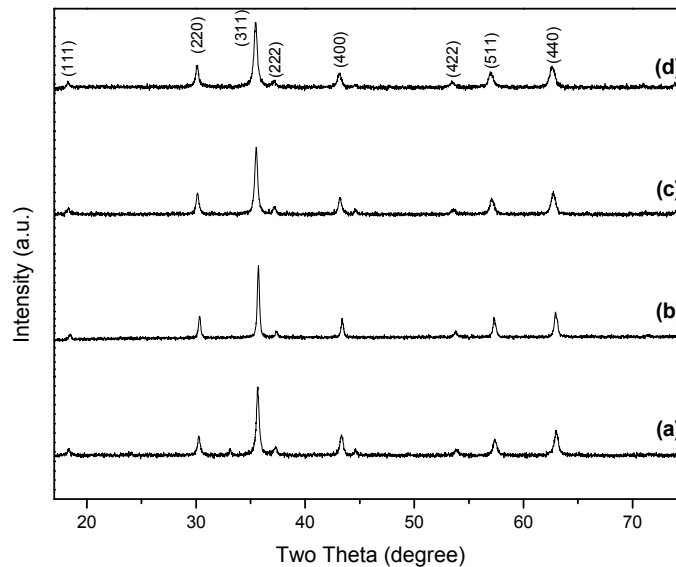
Figure 2. XRD pattern of Ni$_{1-x}$Zn$_x$Fe$_2$O$_4$ (x = 0, 0.2, 0.3 and 0.4) powder samples calcinated at 600 ^{0}C.
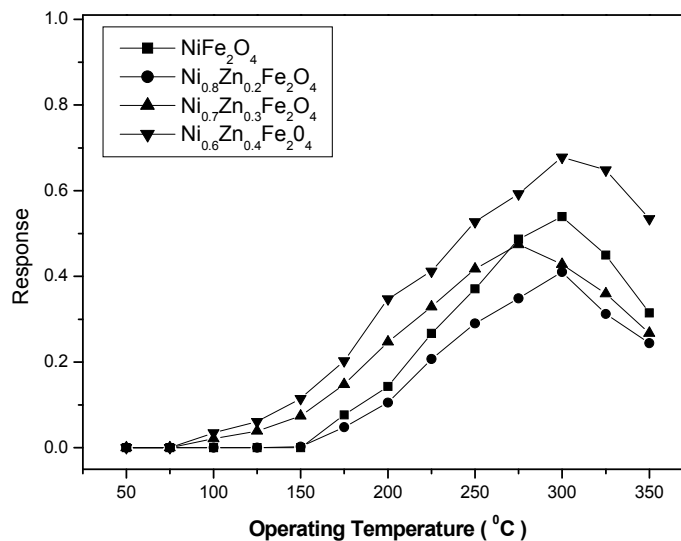
Figure 3. Sensor response of Ni$_{1-x}$Zn$_x$Fe$_2$O$_4$ (x = 0, 0.2, 0.3 and 0.4) to 100 ppm ethanol as a function of operating temperature.

Table 1: Calculated lattice parameters of $Ni_{1-x}Zn_xFe_2O_4$ (x = 0, 0.2, 0.3 and 0.4)

Sample $Ni_{1-x}Zn_xFe_2O_4$	Lattice parameters (Å) a=b=c
x = 0	8.343 ± 0.002
x = 0.2	8.348 ± 0.001
x = 0.3	8.379 ± 0.007
x = 0.4	8.393 ± 0.002

For practical application of sensor, not only the sensor response but the response and recovery times are also vital parameters for evaluating the performance of gas sensors. The response and recovery times are defined as the time required for the sensor-resistance to change by 90% of the final resistance. It was found that the nanocrystalline $Ni_{0.6}Zn_{0.4}Fe_2O_4$ based sensor element responds rapidly after introduction of 100 ppm ethanol and recovers immediately when it is exposed to air. The $Ni_{0.6}Zn_{0.4}Fe_2O_4$ has response time of ~70–75 s and the recovery time of ~180–190 s. Furthermore, it was observed that the resistance of the sensing element decreases when exposed to ethanol (reducing gas), which suggests that $Ni_{0.6}Zn_{0.4}Fe_2O_4$ behaves as a n-type semiconductor.

The variation of the response of nanocrystalline $Ni_{0.6}Zn_{0.4}Fe_2O_4$ based sensor element with respect to the ethanol concentration at the optimal operating temperature of 300 ^{0}C is shown in Fig. 4. The $Ni_{0.6}Zn_{0.4}Fe_2O_4$ spinel is able to detect up to 25 ppm for ethanol with good response at the optimal operating temperature of 300 ^{0}C.
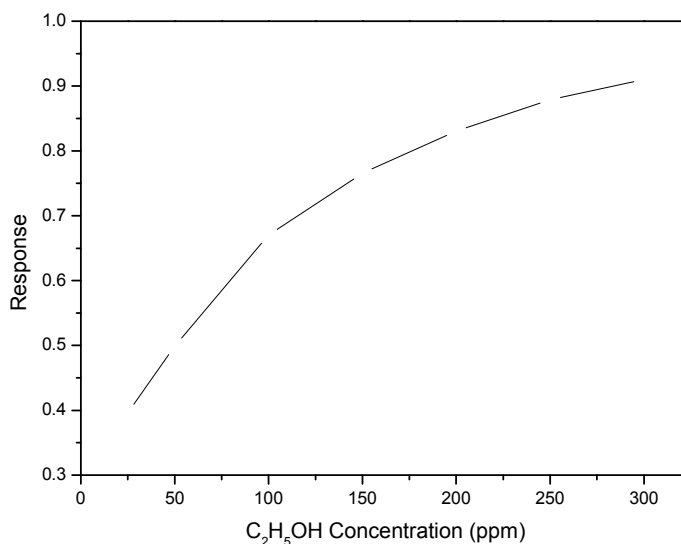
Figure 4. Variation in the response of $Ni_{0.6}Zn_{0.4}Fe_2O_4$ sensor element at 300 ^{0}C against ethanol concentration.

Selectivity is an important parameter of gas sensors and the sensor response toward a specific gas needs to be markedly higher than those to other gases for selective gas detection. To study the selective

behavior of the nanocrystalline $Ni_{0.6}Zn_{0.4}Fe_2O_4$ to ethanol at the optimal operating temperature of 300 ^0C, the sensor responses towards H_2, NH_3 and LPG were also measured. The corresponding results are demonstrated in Fig. 5. The $Ni_{0.6}Zn_{0.4}Fe_2O_4$ exhibits higher response to ethanol, whereas it shows a considerably lower response to H_2, NH_3 and LPG. Taking into account the results of gas sensing experiments, it is concluded that the nanocrystalline $Ni_{0.6}Zn_{0.4}Fe_2O_4$ has good ethanol sensing properties such as higher gas response, good selectivity, quick response and recovery, excellent repeatability and relatively lower operating temperature.
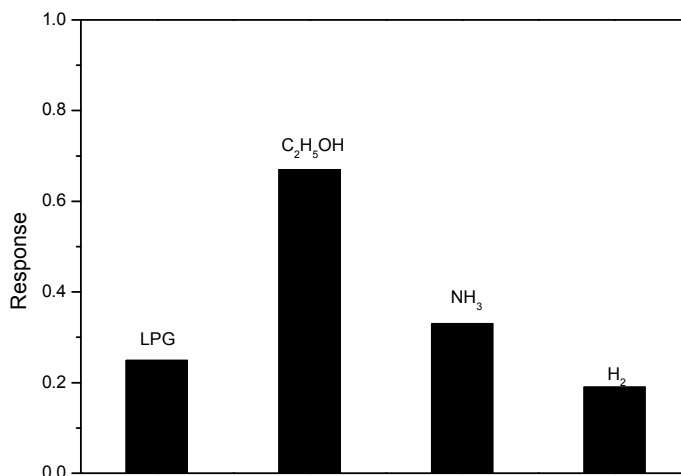
Figure 5. Response of $Ni_{0.6}Zn_{0.4}Fe_2O_4$ towards 100 ppm C_2H_5OH, 500 ppm NH_3, 500 ppm H_2 and 500 ppm LPG at 300 ^0C.

3.3. Ethanol sensing mechanism

The oxygen is adsorbed on the surface of the sensor in air and adsorbed oxygen is transformed into chemisorbed oxygen at a definite temperature. The reaction between C_2H_5OH gas and the chemisorbed oxygen ion can take place as [11]:

$$C_2H_5OH_{gas} + O_{ad}^{2-} \rightarrow C_2H_5O_{ad}^- + OH_{ad}^-$$

$$C_2H_5O_{ad}^- \rightarrow (C_2H_5)_2O_{ad} + O_{ad}^- + e^-$$

$$C_2H_5OH_{gas} + Oad^{2-} + hole \rightarrow CO_2 + H_2O + V_O^-$$
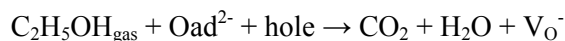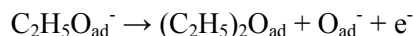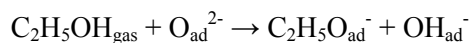
Where V_O^- is a doubly charged oxygen vacancy. These reactions impart electrons into the sensing material, leading to an increase in electron concentration, and a decrease in resistance of the $Ni_{0.6}Zn_{0.4}Fe_2O_4$-based sensor.

The concentration of chemisorbed oxygen increased and reached optimum value with the increasing operating temperature. When the absorption–desorption of chemisorbed oxygen attained a dynamic equilibrium, the sensor exhibited maximum response towards ethanol gas at 300 ^0C. Difference in gas-sensing response to different gases might be due to differences in the adsorption and the reaction processes.

4. Conclusions

In conclusion, $Ni_{1-x}Zn_xFe_2O_4$ (x = 0, 0.2, 0.3 and 0.4) mixed ferrite powder samples with cubic spinel structure were successfully synthesized by citrate sol-gel route. The response of $Ni_{0.6}Zn_{0.4}Fe_2O_4$ based sensor element to 100 ppm ethanol was found maximum at an optimal operating temperature 300 ^{0}C. The response time was ~70–75 s and the recovery time was found to be ~180–190 s. Furthermore, $Ni_{0.6}Zn_{0.4}Fe_2O_4$ sensor exhibited good selectivity to C_2H_5OH when operating at 300 ^{0}C. This means that $Ni_{0.6}Zn_{0.4}Fe_2O_4$ sensor can be a good candidate for practical application in detecting C_2H_5OH because of the good characteristics mentioned.

Acknowledgement

References

[1]   R.D. McMichael, R.D. Shull, L.J. Swartzendruber, L.H. Bennett, R.E.Watson, *J. Magn. Magn. Mater.*, 1992, **111**, 29-33.

[2]   C.V. Gopal Reddy, S.V. Manorama, V.J. Rao, *J. Mater. Sci. Lett.*, 2000, **9**, 775-778.

[3]   Y.-L. Liu, Z.-M. Liu, Y.Yang, H.F.Yang, G.-L. Shen, R.-Q.Yu, *Sens. Actuators B*, 2005, **107**, 600-604.

[4]   V. D. Kapse, S. A. Ghosh, F. C. Raghuwanshi and S. D. Kapse, *Mater. Chem. Phys.*, 2009, **113**, 638–644.

[5]   C.N. Chinnasamy, A. Narayanasamy, N. Ponpandian, K. Chattopadhyay, K. Shinoda, B. Jeyadevan, *Phys. Rev. B*, 2001, **63**, 184108–184116.

[6]   R.C.V. Gopal, S.V. Manorama, V.J. Rao, *Sensor. Actuat. B* 1999, **55**, 90–95.

[7]   L. Satyanarayana, R.K. Madhusudan, S.V. Manorama. *Mater. Chem. Phys.*, 2003, **82**, 21–26.

[8]   M.J. Madou, S.R. Morrison, Chemical Sensing in Solid State Devices, Academic Press, San Diago, 1989.

[9]   K.N.P. Kumar, K. Keizer, A.J. Burggraaf, T. Okubo, H. Nagamoto, S. Morooka, *Nature*, 1992, **358**, 48-51.

[10] G. Sberveglieri, L.E. Depero, M. Ferroni, V. Guidi, G. Martinelli, P. Nelli, C. Perego, L. Sangletti, *Adv. Mater.*, 1996, **8**, 334-337.

[11] Z.P. Sun, L. Liu, D.Z. Jia, W.Y. Pan, *Sens. Actuators B*, 2007, **125**, 144-148.

Synthesis, Charecterisation and Antibacterial Activities of Some New Bromo/Nitro 1,3-Thiazenes

TEJASWINI S.BANTE, V. V. PARHATE AND P.R.RAJPUT

Department of Chemistry, VidyabhartiMahavidyalaya, Amravati. (MS) 444602.India
Corresponding author: bantetejaswini12@gmail.com

Abstract

1,3-thiazines were prepared by refluxing the mixture of 2-hydroxy-3-bromo/nitro -5-chlorochalcone and diphenylthiourea in alcohol and aq.KOH medium. The newly synthesized 1,3-thiazenes were characterized on the basis of elemental analysis and spectroscopic data of IR,NMR. The melting points were taken in an open capillary tube. All compounds have been evaluated for their in vitro growth of inhibitory activity against Escherichia coli, Staphylococcus aureaus, Bacillus subtilis and Phaseolusargenosa.

Keywords: 1, 3-Thiazines, Antibacterial Activity, pathogenic bacteria.

Introduction

Thiazine is a six membered heterocyclic compound which contains two hetero atoms (N and S) placed at 1,3 positions. 1,3-thiazines have a very broad spectrum of fungicides, insecticides, growth promoting hormonal effect etc. Thiazines are very useful units in the fields of medicinal and pharmaceutical chemistry and have been reported to exhibit a variety of biological activities[1-2].The reaction of thiourea with α,β-unsaturated ketones results in 1, 3 thiazines[3-4] .Some chloro-substituted-1, 3-thiazines have been reported for antimicrobial activity[5]

Thiazine reported to exhibit antitubercular, antibacterial used as cannabinoid receptor against[6] 1,3-thiazine derivatives and their evaluation as potential antimycobacterial agents[7].The synthesis of 2,4-dihydro-1H-benzo[d] [1,3] thiazines via silver catalyzed addition-cyclization reactions are reported[8]. Synthesize of new chromene base heterocyclic like thiazine from 2-Amino-5-hydroxy-4-phenyl-7-methyl-4H[1-chromeno-3-carbonitrile which may show a good biological activity[9].Some 1,3-thiazines are reported for its antimicrobial activity.[10]

Experimental

The synthesis of 1,3-thiazines from 3-bromo-5-chlorochalcone and 3-nitro-5-chlorochalcone on treatment with diphenylthiourea in presence of alcoholic KOH. The melting points of these compounds were recorded on 'Tempo' melting point apparatus and are uncorrected. The carbon, nitrogen, sulphur and hydrogen analysis was carried out on 'Carlo Ebra 1106' analyzer. The IR spectra were recorded on 'Perkin-Elmer Infra Red spectrophotometer. The PMR spectra were recorded on DRX 300 spectrometer in CDCl3. Purity of the compound was tested by TLC. The study were treated for their antibacterial

International Journal of Chemical and Physical Sciences, ISSN:2319-6602
IJCPS Vol. 4 Special Issue – NCSC Jan-2015
www.ijcps.org

impact against some common pathogenic bacteria viz. *E. Coli, S. aureus, B. Subtilis, P. argenosa.* The solutions of 0.01 mol dilution of test compounds were prepared in dioxane solvent separately. The discs were soaked, assuming that each disc will contain approximately 0.01 ml of test solution. The culture media was prepared by using following composition for one liter distilled water-

Peptone	:	5.0 g./litre
Sodium chloride	:	5.0 g./litre
Beef extract	:	1.5 g./litre
Yeast extract	:	1.5 g./litre
Agar	:	15.0 g./litre
pH (approximately)	:	7.4 ± 0.2.

The culture medium thus prepared was sterilized in autoclave at 15 lbs/inch pressure and 121^0C temperature for 15 minutes. After sterilization, it was cooled down to about 50^0C and poured into presterilized petriplates of 8.5 cm in diameter each and allowed to solidify the nutrient agar medium of about 14 mm depth. The petriplates were kept with nutrient broth at 37^0C for2 4 hr. in an incubator.

(a) **Preparation of 4-(2-hydroxy-3-bromo/nitro-5-chlorophenyl)-6-(1'-propene)-2-iminophenyl-3,6- dihydro-1, 3-thiazine (IIa/b)**

2-Hydroxy-3-bromo/nitro-5-chlorochalcone and diphenylthiourea were dissolved in ethanol. To this aqueous KOH solution was added and this reaction mixture was refluxed for three hours, after cooling, diluted with water and acidified with 1:1 HCl. The product thus obtained was 4-(2-hydroxy-3-bromo/nitro-5-chlorophenyl)-6-(1'-propene)-2-iminophenyl-3,6-dihydro-1,3-thiazine.
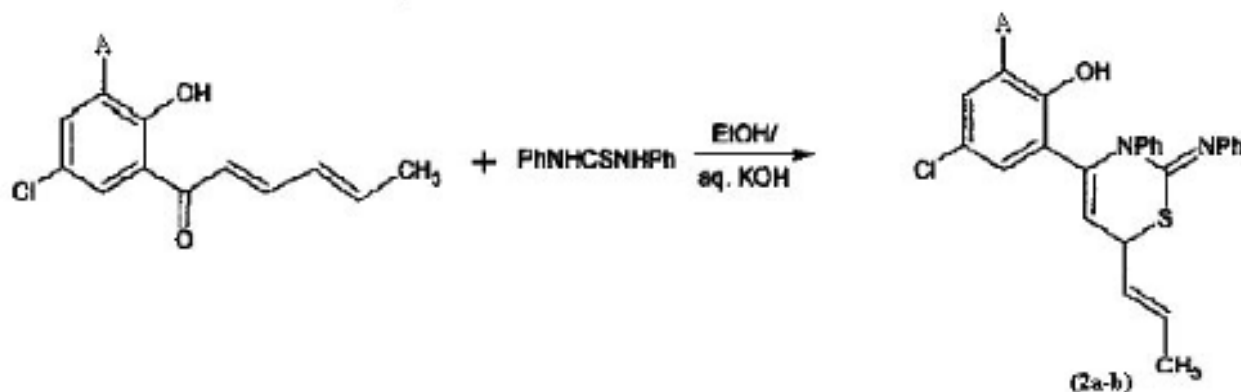
A=Br/NO$_2$Scheme-1

Compound	Molecular Formula	M.P.	Yield	Rf
1a	$C_{12}H_{10}BrO_2Cl$	85^0C	78%	0.76
1b	$C_{12}H_{10}NO_4Cl$	110^0C	70%	0.61
2a	$C_{13}H_{10}N_2(Ph)_2BrOCl$	138^0C	70%	0.67
2b	$C_{13}H_{10}N_3(PH)_2SO_3Cl$	127^0C	70%	0.28

International Journal of Chemical and Physical Sciences, ISSN:2319-6602
IJCPS Vol. 4 Special Issue – NCSC Jan-2015
www.ijcps.org

Spectral interpretation of (IIb)

(a) The important frequencies observed in the IR spectrum recorded in KBr are correlated as

Follows-IR **(υmax)** cm-1:3423υ (-OH Stretching); 2320 υ (-C=N Stretching); 1444 υ (Ar-NO2); 1230 υ (C=OStretching); 1313 υ (C-N Stretching)

(b) The PMR spectrum of the compound (IIb) was recorded in CDCl3 with TMS as an internal standard. The observed chemical shifts and their correlations are as follows-

NMR : 2.5 (d,3H , C=CH-CH3); 4.17 (d,1H , C=C-C-H); 5.5 (d,1H, -CH=CH); 6.5 (d,1H , =C-H); 6.9-7.8 (m,12H ,Ar-H); 11.99 (s, 1H ,Ar-OH);

Results And Discussion

The 1,3-thiazines when screened in vitro against some common bacteria viz. *E. coli,S. aureaus*, *B. subtilis, P. argenosa* it was noticed that most of all these compounds have shown remarkable inhibitory activity. An assay of newly synthesized 1,3-thiazines revels that, almost all the compounds were strongly active against all the test pathogensE. coli, S. aureaus, B. subtilis, P. argenosa. Their inhibitory impact on the bacterial growth is remarkable.

Table-2: Antibacterial activities of test compounds

S.No.	Test Compound	Zone of inhibition (mm)			
		E. coli	*S. aureus*	*B.subtilis*	*P. argenosa*
1	IIa	27	25	25	26
2	IIb	25	24	25	25

References

[1]   R.Vyas, P.Choudhary, H. Sharma and B. L. Varma, Indian J. Heterocyclic Chem., 17(1), 237(2008).

[2]   Y. S. Jhala, Pradhuman, S. Ranawat, S. S. Dulawat and B. L. Varma, Indian J. Heterocyclic Chem.,14, 357(2005).

[3]   A. C. Jain and A. K. Prasad, Indian J. Chem., 34 B, 496 (1995).

[4]   Yoshiu, Chem. Soc. Jpn., 93(2) 1016 (2004).

[5]   S.P.Rathod, A.P.Charjanand P. R.Rajput, Rasayan J.Chem., 3, (2) 363(2010),

[6]   V.V.Dabholkar; S.D. Parab, Heterolett.Org. 1, 176(2011).

[7]   M.Koketsu, K.Tanaka, Y.Takenaka, C.D.Kwong, H.Ishihara, Eur.J. of Pharm. Sci.,15, (3),307(2002).

[8]   D.Qiuping and W.Jie, J. Comb. Chem., 10(4), and 541(2008), DOI: 10.1021/cc800043r.

[9]   F.K.Mohammed, A.Y.Soliman, A.Ssawy, M.G.Badre, J. Chem. Pharm. Res, 1 (1), 213(2009).

[10] F. H. Z. Haider, J. Pharm. Res., 4(4), 2263(2012).

Synthesis and Characterization of Some New Chlorosubstituted Thiazoles and Thiazolo-Imidazoles and their Impact on Pathogens Damaging Oyster Mushroom Cultivation

N. G. GHODILE AND P. R. RAJPUT

Department of Chemistry, S.S.S.K.R. Innani Mahavidyalaya, Karanja (Lad), Washim.
Department of Chemistry, Vidya Bharati Mahavidyalaya, Amravati, India. 444 602
Corresponding author*: nitinghodile@gmail.com*

Abstract

The mushroom growers in and around Vidarbha region of Central India have been engaged in the cultivation of one of the edible and highly profiTable varieties of mushroom crop ie. Oyster mushroom spp. But now a days farmers of this region facing the most alarming problem related to the susceptibility of this variety that easily falls prey to the pathogenic attack. As a result of this the efforts and investment that farmers put in the cultivation of this crop would not commensurate with the yield. Literature survey reveals that the paucity of data in the field of protection of mushroom cultivation from the attack of causative organism, creates a considerable amount of scope to undertake a systematic research of synthesis of some eco-friendly heterocycles and study of their curative impact on edible mushroom varieties with special reference to Oyster mushroom spp. In this context, in the present study, we have synthesized some new chlorosubstituted thiazoles and thiazolo-imidazole from chlorosubstituted diketones, chromones and chromanones in benign solvents.
The newly synthesized titled compounds were screened for their antipathogenic activities against the causative organisms responsible for the damage of mushroom cultivation in the tropical belt of Vidarbha region. It was encouraging to note that the titled compounds not only inhibit the growth of all the pathogens under examination (C. verticillatum, G. deliquescene, Cladobotryum apiculatum, Velricillium fungicola, Gliocladium vireus, Sibirina fungicola, P. agarici, Arthrobotrys pleuroli and Pseudomonas stulzeri.) to a considerable extent but also exerted a positive impact on the phytotic growth of the test variety of mushroom.

Key words: chlorosubstituted thiazoles, thiazolo-imidazoles, diketones, chromones and chromanones, *Oyster mushroom* crop pathogens like *C. verticillatum, G. deliquescene, C. apiculatum, V. fungicola, G. vireus, S. fungicola, P. agarici. A. pleuroli, P. stulzeri.*

Introduction:

Pleurotus commonly called as *Oyster mushroom* is one of the most widely eaten mushrooms[1] appreciated for its culinary properties[2]. *Oyster spp.* can be successfully cultivated at temperatures of around 30°C and hence it is becoming increasingly popular in both tropical and sub-tropical countries. Being a tropical country, India has been bestowed with bountiful crops. In India, the cultivation of this variety of mushroom is picking up at an alarmingly high rate due to ease of its cultivation.

International Journal of Chemical and Physical Sciences, ISSN:2319-6602
IJCPS Vol. 4 Special Issue – NCSC Jan-2015
www.ijcps.org

After *Agaricus spp.* (Button mushrooms), *Pleurotus species* are the second most populer mushrooms growing in India. Though cultivation of *Oyster mushroom* in Vidarbha region is increasing gradualy but the major constraint in its speedy popularization is the susceptibility of this crop towards pathogenic attack. As a consequence, initial investment incurred on the cultivation of *Oyster mushroom* crop could not be recovered. The pathogens inhibit the growth of mushrooms and hinders the production of fruiting bodies. The disease and pasts happen to be devastating and perpeturate easily from one season to another. Shah and Nasreen reported[3] that some growers hardly use the fungicides for the treatment of this havoc of disease. They often found fungicidal treatment as non-economical. Chitra[4] *et al* reported that the 60% concentration of potassium humate influence the mushroom growth as well as nutritional value and recommended to use this for the increase of production.

Literature survey reveals that, nitrogen and oxygen containing chlorosubstituted heterocycles such as pyrazolines, pyrazoles, isoxazolines, and isoxazoles were found to be very useful in controlling the diseases in the field of agriculture. This series of compounds reported to have antibacterial[5], antifungal[6], analgesic[7], anesthetic[8] and antinflammatory activities.

The present study has been carried out to develop ecofriendly and economically viable management of mushroom crop disease by synthesizing some new chlorosubstituted thiazoles and thiazolo-imidazoles from chlorosubstituted diketones, chromones and chromanones and applying them to inhibit the growth of causative organisms.

Experimental:

The synthetic route for obtaining the final products is presented in scheme I. 1-(2-Hydroxy-5-chlorophenyl)-3-phenyl-1,3-propanedione (1a) was suspended in bromine-glacial acetic acid reagent to get the compound 1-(2-hydroxy-5-chlorophenyl)-2-bromo-3-phenyl-1,3-propanedione (2a). The bromosubstituted-1,3-propanedione (2a) refluxed with thiourea for about 2.5 hrs. using aqueous KOH solution and ethanol as a solvent. Finally on acidification with conc. HCl yield the product substituted thiazole (3a).

The reaction of substituted thiazole(3a) with 2-bromo-1-(2-chloro-5-hydroxy phenyl) ethanone in absolute ethanol lead to the formation of substituted α- amino ketone (4a) which on treatment with KSCN in glacial acetic acid for 4 hrs. gave substituted thiazolo-imidazole (5a). which on acetylation give its acetyl derivative (6a).

Melting points of all the synthesized compounds were determined in open capillaries and are uncorrected. The homogeneity of all compounds was checked by TLC using benzene-CCl₄ as developing solvent. IR spectra were recorded on Perkin-Elmer 1000 spectrophotometer in KBr. The ¹H NMR spectra were recorded on Bruker advance II 400 NMR spectrophotometer using TMS as an internal standard and chemical shifts are expressed in δ (ppm).

International Journal of Chemical and Physical Sciences, ISSN:2319-6602
IJCPS Vol. 4 Special Issue – NCSC Jan-2015
www.ijcps.org

Scheme-I:
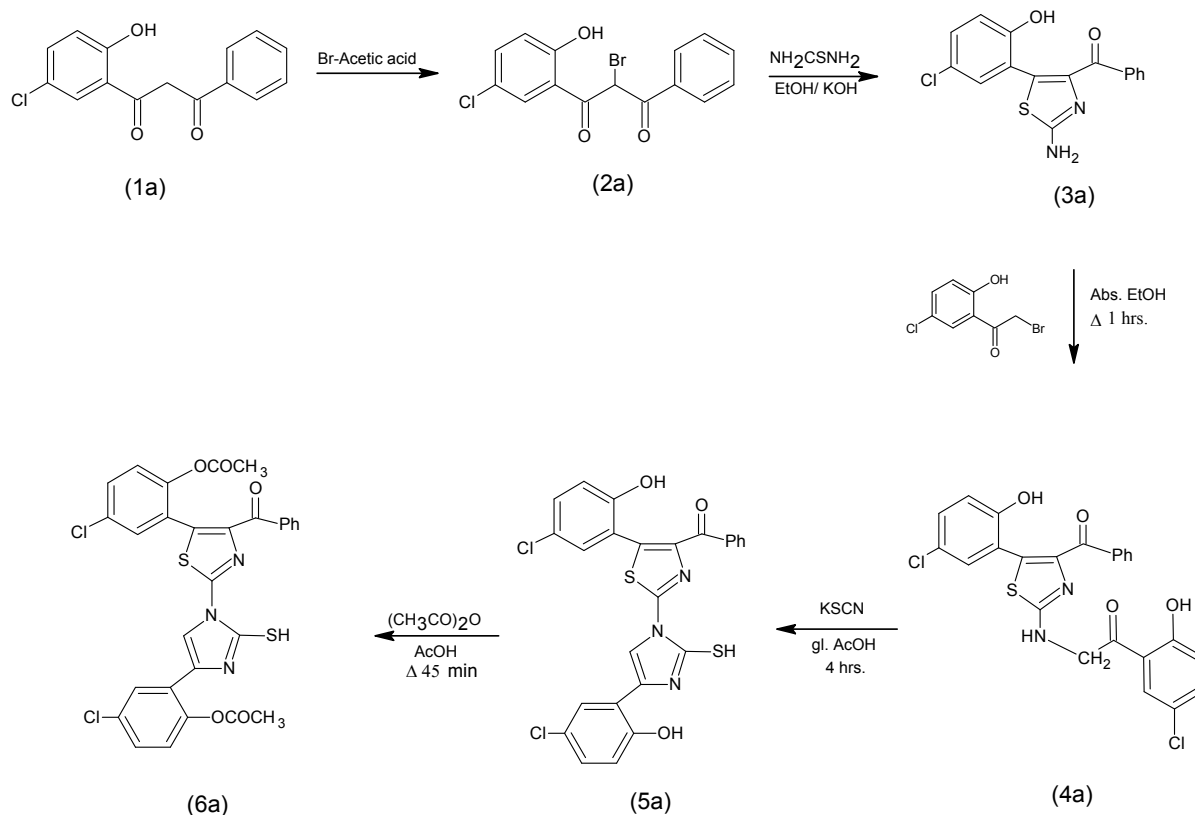
Antifungal and antibacterial assays of the newly synthesized compounds (3a, 4a, 5a, and 6a):

The titled compounds were assayed for their antifungal and antibacterial activities against the pathogens responsible for *Oyster mushroom* diseases.

DMF was used as a solvent control using agar-agar plate techniques. The zones of inhibition formed were measured in mm and are shown in the following Table:

Entry	*C. verticillatum*	*G. deliquescene*	*C. apiculatum*	*V. fungicola*	*G. vireus*	*S. fungicola*	*P. agarici*	*A. pleuroli*	*P. stulzeri*
3a	10	05	08	07	08	08	08	07	06
4a	10	09	10	09	08	09	10	08	09
5a	11	11	12	10	10	11	12	11	10
6a	12	09	14	12	11	13	13	11	12

The compounds synthesized were found to be detrimental to the growth of the pathogens. From the Table it can be noticed that antifungal and antibacterial properties gradually increase as the complexity of the molecular structures increases.

References:

[1]. Shah S., Nasreen S. and Munshi N.A., *International Journal of botany,* 7(3), **2011**, 209-215.

[2]. Baysal, E., Peker H., Yalinkilic M.K. and Temiz A., *Bioresour. Technol.,* 89, **2003**, 95-97.

[3]. Shah S. and S. Nasreen, *Int. J. Plant Pathol.,* 2, **2011,** 81-88.

[4]. Prakash. P, Samundeeswari. R, Vivek. C and Chitra D.A, *World Journal of Science and Technology* 1(7), **2011**, 28-31.

[5]. Hans N. Swiss Patent, 592103, 1977, *Chem. Abstra.,* 88, **1978**, 22886.

[6]. Borthakur S. K., Boruah P. and Goswami B. N., *J. Chemical Research*, 128, *2007*, 127.

[7]. Narayan B., Raj Vijaya K.K., Ashalata, B.V. and Sucheta N.K., *Indian J. Chem.* 45B, **2006**, 1704.

[8]. Altintes H, and Birteksoz S., *Indian J. Chem*. 44B, **2005**, 585.

Effect of Extracts of Test Plants, Isolated Ingredient and Prepared Analogues on Serum Inorganic Ions (*Sodium, Potassium, Calcium, Magnesium and Phosphorous*) in *Albino Rats*

M. O. MALPANI [1*], P. R. RAJPUT [2]

[1]Department of Chemistry, Shankarlal Khandelwal College, Akola, 444-002
[2]Department of Chemistry, Vidya Bharati Mahavidyalaya, Amravati 444 - 602.
Corresponding author: momalpani@gmail.com

Abstract

Medicinal plants are of great value in the field of treatment and cure of diseases. Over the years, scientific research has expanded our knowledge of the chemical effects and composition of the active constituents, which determine the medicinal properties of the plants. It has now been universally accepted fact that the plant drugs and remedies are far safer than that of synthetic medicines for curing the complex diseases like cancer and AIDS. Melghat region is a rich source of medicinal flora. Near about 772 naturalized species found in Melghat region which are used for the cure of various diseases. Butea monosperma, Cassia fistula, Ceasalpinina bonduc, Cassine glauca, and Cassia absus, plants are found in Melghat region. All these plants are frequently used for the eradication of various diseases. In case of serum inorganic ions, the four cations, Na^+, K^+, Mg^{2+} and Ca^{2+}, are widely distributed in all living organisms. These cations play a tremendous variety of roles such as in the transmission of nerves impulses, in muscle contraction, and as enzyme activators and structural factors. In the present study we have undertaken this task to explore the impact of test plants whole extracts; some isolated ingredients and prepared analogues on serum composition of test animals with special reference to inorganic ions.

Keywords: Test plants, isolated ingredient, prepared analogue, serum inorganic ions.

Introduction

Primarily it may be stated that cutaneous lesions are due to influences of source outside the body or which exist or arise within the body. To the former class may be assigned such as depend on temperature and climate, such as are due to traumatism of various kind, such as result from various parasitic invasions, etc. this is in reality but a limited class, on other hand, the etiological factors which arise within the body itself are very numerous. The external causes like excessive heat direct exposure to the Sun may exhibit undue activity of the sudoriferous gland and result in the production of *sudamina* or Sunburn. The excessive cold may result in absolute, congelation of exposed portion of the integument. On the other hand internal causes of skin diseases, however, are far more frequently in operation. In this class we may place those affections of the skin which are due to pre-existing lesions of some part of the nervous system. The nervous system acts as a medium for the transmission of some internal irritation to the surface, thus, the gastric irritation resulting from the ingestion of shell-fish may manifest itself on the skin till another

International Journal of Chemical and Physical Sciences, ISSN:2319-6602
IJCPS Vol. 4 Special Issue – NCSC Jan-2015
www.ijcps.org

internal cause of cutaneous lesions is found in ill nutrition or imperfect assimilation. Finally we may have external lesions resulting from the accumulation in the blood of certain infectious material. Sometimes such materials may be generated within the body itself through imperfections in the digestive, assimilative or excretory functions.

In order that nutrition may be healthily carried on in any part there must be a proper state of the blood, a proper condition and behaviour of the tissues to be nourished and a right exercise of the controlling influence exerted by the nerves. These three must work harmoniously together. The theoretical origin, therefore, of diseased changes in the skin may be especially in the blood and here the skin affection is only symptomatic.

The four cations, Na^+, K^+, Mg^{2+} and Ca^{2+}, are widely distributed in all living organisms These cations play a tremendous variety of roles such as in the transmission of nerves impulses, in muscle contraction, and as enzyme activators and structural factors. The extra- and intracellular concentrations of Na^+, K^+, Mg^{2+} are very different (the values for Ca^{2+} being quite similar). This observation raises the questions about the establishment, maintenance and distribution of dissymmetry[1-4].

In the present study we have undertaken this task to explore the impact of test plants whole extracts, some isolated ingredients and prepared analogues on serum composition of test animals with special reference to inorganic ions.

Materials And Methods

Plant material: The test plant materials of *Butea monosperma, Cassia fistula, Ceasalpinina bonduc, Cassine glauca,* and *Cassia absus,* plants were collected seasonally from the Melghat region of Amravati, District of Maharashtra, India. They were authenticated by the taxonomist Dr. S. P. Rothe with Voucher specimens (ML – 101, ML – 102, ML – 103, ML – 104, ML – 105) and were deposited in the herbarium of Department of Botany, Shri Shivaji College, Akola.

Extraction and Isolation: The test plant materials of *Butea monosperma, Cassia fistula, Ceasalpinina bonduc, Cassine glauca,* and *Cassia absus,* plants were shade dried at room temperature and ground in a manual mill to get coarse powder. The powders were kept in the airtight polythene bags and stored at dry place. These powders were extracted with water as a solvent by using soxhlet apparatus. The extracts were concentrated at 40 ^{o}C using rotary evaporator. Finally it was dried, crushed and stored in air tight bottle at 4 ^{o}C for further study. Again by using thin layer and column chromatography techniques, we have isolated the acidic ingredient from Butea monosperma test plant extracts and from the characterization it was found that isolated compound 1 was Gallic acid. The Gallic acid (Compound 1) thus separated from test extracts of Butea monosperma plant was then used for the preparation of its amide analogue (Compound 2) and ester analogue (Compound 3).
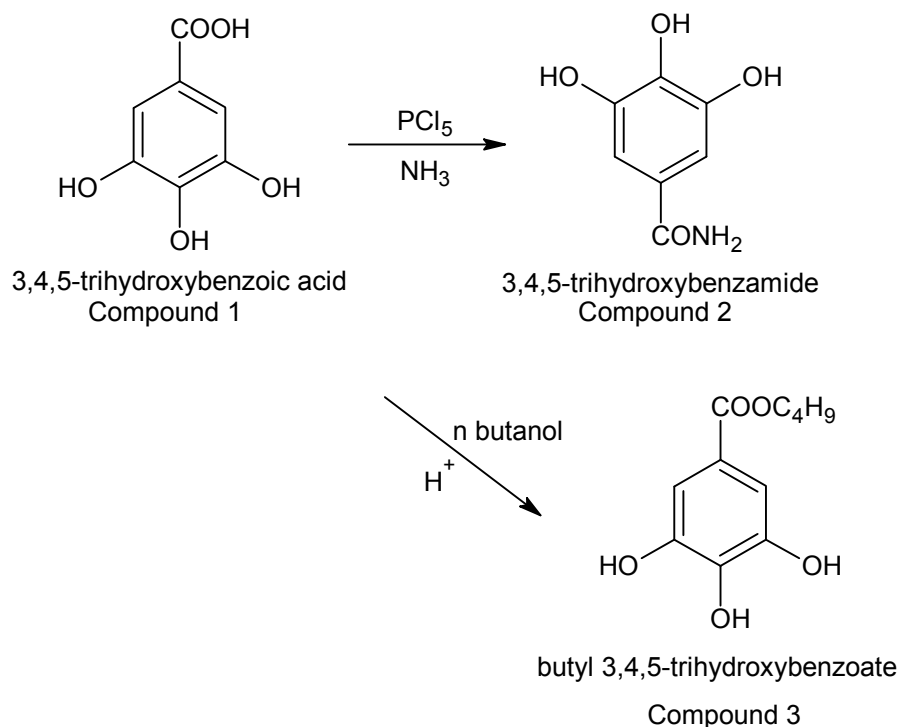
International Journal of Chemical and Physical Sciences, ISSN:2319-6602
IJCPS Vol. 4 Special Issue – NCSC Jan-2015
www.ijcps.org

3,4,5-trihydroxybenzoic acid
Compound 1

3,4,5-trihydroxybenzamide
Compound 2

butyl 3,4,5-trihydroxybenzoate
Compound 3

Animals: The interdisciplinary part of proposed study was carried out after getting permission from the Institutional Animal Ethical Committee, Pusad (CPCSEA/IAEC/CP_PL/07-2012). The care of laboratory animals was taken according to the guidelines of CPCSEA, Ministry of Forests and Environment, Government of India (registration number 729/02/a/ CPCSEA). All the experiments were carried out using adult *albino Wistar male rats* weighing about 130-150 gm. The animals had free access to food and water and they were housed in cages in a natural (12 hrs each) light–dark cycle. The animals were acclimatized to the laboratory conditions for at least 5 days before behavioural experiments which were carried out between 0900 h and 1800 h.

Creation of Burn wound: Dorsal skins of the Wistar rats were shaved at full thickness. The animals were anesthetized by ketamine injection and burn wound of approximate 2 cm in diameter were created (circular area) by the brass probe which was immersed in boiling (100 °C) water until thermal equilibrium was reached. The probe was then placed on the back of the rats for 20 s without applying pressure. They were then housed individually in separate cages after complete recovery from anaesthesia.

Rats were randomly divided into following groups of five animals each:

Control group: Immediately after burning, burn areas were covered with propylene glycol solution once a day for 20 days.

International Journal of Chemical and Physical Sciences, ISSN:2319-6602
IJCPS Vol. 4 Special Issue – NCSC Jan-2015
www.ijcps.org

Whole extract of *Butea Monosperma* group: Immediately after burning, burn areas were covered with whole extract of *Butea Monosperma* sample which was prepared in propylene glycol once a day for 20 days.

Whole extract of *Cassia fistula* group: Immediately after burning, burn areas were covered with whole extract of *Cassia fistula* sample which was prepared in propylene glycol once a day for 20 days.

Whole extract of *Ceasalpinina bonduc* group: Immediately after burning, burn areas were covered with whole extract of *Ceasalpinina bonduc* sample which was prepared in propylene glycol once a day for 20 days.

Whole extract of *Cassine glauca* group: Immediately after burning, burn areas were covered with whole extract of *Cassine glauca* sample which was prepared in propylene glycol once a day for 20 days.

Whole extract of *Cassia absus* group: Immediately after burning, burn areas were covered with whole extract of *Cassia absus* sample which was prepared in propylene glycol once a day for 20 days.

Isolated acid group: Immediately after burning, burn areas were covered with isolated acid sample (Gallic acid) prepared in propylene glycol, once a day for 20 days.

Prepared amide analogue group: Immediately after burning, burn areas were covered with the prepared amide analogue sample prepared in propylene glycol once a day for 20 days.

Prepared ester analogue group: Immediately after burning, burn areas were covered with the prepared ester analogue sample also prepared in propylene glycol once a day for 20 days.

Blood samples were collected from control and treated group test animals and left to clot at room temperature for at least 30 minutes. They were centrifuged at 2000rpm for a minute to remove clot and cell debris. Equal amount of serum from Experimental and control animals were pulled in order to have sufficient material to perform the estimations.

The serum samples were analyzed for their *sodium* and *potassium* contents by flam photometric method, *calcium* and *magnesium* by titration method and *phosphorus* by photo colorimetric method the values were expressed as MEq/lit[5-9].

Observation And Results

Data obtain about composition of serum inorganic ions in *control* and *treated* group test animals are shown in the Tables (Table No. 1.1-1.5) along with their graphical presentations (Fig. No. 1.1-1.5).

During cutaneous infection the concentration of *sodium, potassium* and *calcium* get significantly increased. It may be due to histopathological changes in kidneys of test animal. Increased potassium concentration may be due to cellular necrosis which has already been reported in many tissues during cutaneous infections. So also dehydration in such cases has been reported. Increased *calcium* in serum could be ascertained due to its release from bones. The level of *calcium* and *phosphorous* in extra cellular

International Journal of Chemical and Physical Sciences, ISSN:2319-6602
IJCPS Vol. 4 Special Issue – NCSC Jan-2015
www.ijcps.org

fluids rise markedly because kidney cannot excrete them rapidly. As a consequence of this excessive phosphorous is reabsorbed by bones.

Table 1.1: Serum *sodium ion* change on exposure to burn and
exogenous pharmacological drugs in *Albino rats.*

Day	Control	Induced	Treated							
			1	2	3	4	5	6	7	8
2	1.38 ± 0.17	1.41 ± 0.17	1.37 ± 0.17	1.36 ± 0.17	1.34 ± 0.17	1.35 ± 0.17	1.33 ± 0.17	1.37 ± 0.17	1.35 ± 0.17	1.36 ± 0.17
10	1.35 ± 0.17	1.38 ± 0.17	1.32 ± 0.18	1.34 ± 0.18	1.33 ± 0.18	1.34 ± 0.18	1.31 ± 0.18	1.34 ± 0.18	1.35 ± 0.18	1.35 ± 0.18
15	1.33 ± 0.18	1.47 ± 0.18	1.32 ± 0.18	1.30 ± 0.18	1.32 ± 0.18	1.31 ± 0.18	1.29 ± 0.18	1.32 ± 0.18	1.30 ± 0.18	1.31 ± 0.18
20	1.35 ± 0.18	1.56 ± 0.18	1.35 ± 0.18	1.32 ± 0.18	1.34 ± 0.18	1.33 ± 0.18	1.32 ± 0.18	1.33 ± 0.17	1.34 ± 0.17	1.34 ± 0.17

1= *Butea monosperma*, 2= *Cassia fistula*, 3= *Caesalpinia bonduc*, 4= *Cassine glauca*, 5= *Cassia absus*, 6= Gallic acid, 7= Amide and 8= Ester analogues of gallic acid.

Fig. 1.1:   Serum *sodium ion* change: *Wistar Albino rat*

International Journal of Chemical and Physical Sciences, ISSN:2319-6602
IJCPS Vol. 4 Special Issue – NCSC Jan-2015
www.ijcps.org

Table 1.2: Serum *potassium ion* change on exposure to burn and exogenous pharmacological drugs in *Albino rats*.

Day	Control	Induced	Treated							
			1	2	3	4	5	6	7	8
2	6.08 ± 0.20	6.07 ± 0.20	6.01 ± 0.20	6.05 ± 0.20	6.03 ± 0.20	6.01 ± 0.20	6.02 ± 0.20	6.05 ± 0.20	6.07 ± 0.20	6.06 ± 0.20
10	5.96 ± 0.17	7.39 ± 0.22	5.88 ± 0.18	5.86 ± 0.17	5.88 ± 0.17	5.89 ± 0.17	5.87 ± 0.17	5.90 ± 0.18	5.92 ± 0.18	5.93 ± 0.18
15	6.18 ± 0.17	8.29 ± 0.23	6.12 ± 0.18	6.09 ± 0.17	6.13 ± 0.17	6.11 ± 0.17	6.14 ± 0.17	6.13 ± 0.18	6.17 ± 0.18	6.17 ± 0.18
20	6.08 ± 0.18	9.39 ± 0.22	6.03 ± 0.18	6.02 ± 0.18	6.04 ± 0.18	6.01 ± 0.18	6.02 ± 0.18	6.08 ± 0.17	6.06 ± 0.17	6.05 ± 0.17

1= *Butea monosperma*, 2= *Cassia fistula*, 3= *Caesalpinia bonduc*, 4= *Cassine glauca*, 5= *Cassia absus*, 6= Gallic acid, 7= Amide and 8= Ester analogues of gallic acid.

Fig. 1.2: Serum *potassium ion* change: *Wistar Albino rat*

International Journal of Chemical and Physical Sciences, ISSN:2319-6602
IJCPS Vol. 4 Special Issue – NCSC Jan-2015
www.ijcps.org
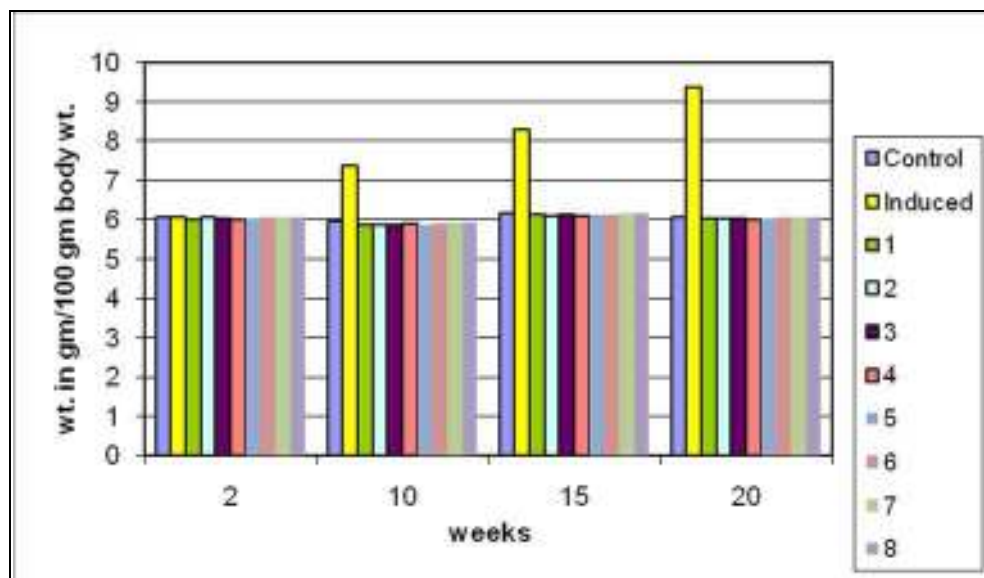
Table 1.3: Serum *calcium ion* change on exposure to burn and exogenous pharmacological drugs in *Albino rats.*

Day	Control	Induced	Treated							
			1	2	3	4	5	6	7	8
2	6.5 ± 0.21	8.9 ± 0.18	6.0 ± 0.21	5.9 ± 0.21	6.3 ± 0.21	6.1 ± 0.21	6.3 ± 0.21	6.4 ± 0.21	6.3 ± 0.21	6.3 ± 0.21
10	6.0 ± 0.21	8.36 ± 0.20	5.8 ± 0.34	5.8 ± 0.34	5.9 ± 0.34	5.7 ± 0.34	5.8 ± 0.34	5.7 ± 0.34	5.9 ± 0.34	5.9 ± 0.34
15	6.4 ± 0.39	9.20 ± 0.37	6.0 ± 0.38	6.2 ± 0.38	6.0 ± 0.38	6.1 ± 0.38	6.1 ± 0.38	6.3 ± 0.34	6.2 ± 0.38	6.2 ± 0.38
20	6.1 ± 0.20	9.42 ± 0.29	5.8 ± 0.34	5.9 ± 0.34	5.8 ± 0.34	6.0 ± 0.34	5.8 ± 0.34	5.9 ± 0.34	6.0 ± 0.34	6.0 ± 0.34

1= *Butea monosperma,* 2= *Cassia fistula,* 3= *Caesalpinia bonduc,* 4= *Cassine glauca,* 5= *Cassia absus,* 6= Gallic acid, 7= Amide and 8= Ester analogues of gallic acid.
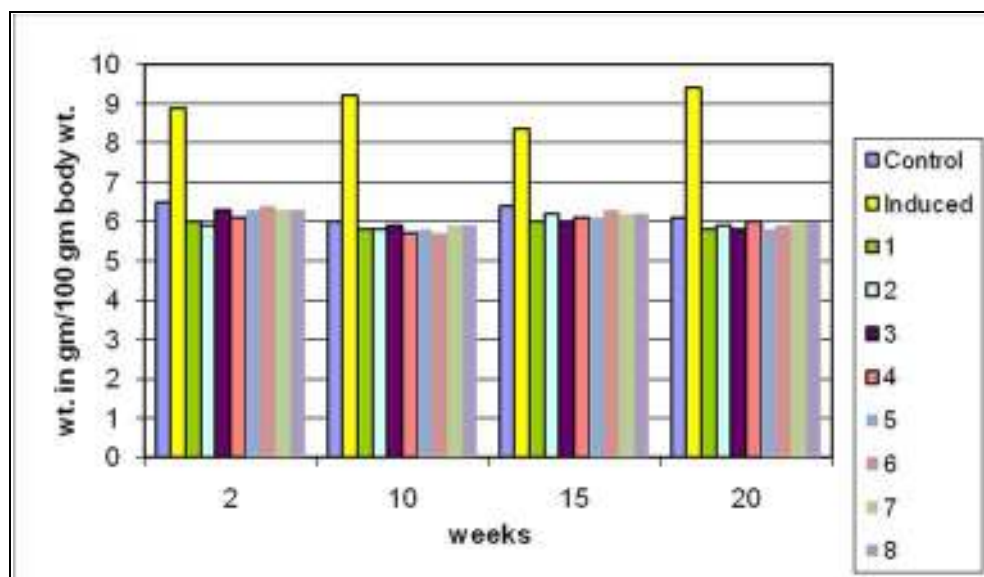
Fig. 1.3:   Serum *calcium ion* change: *Wistar Albino rat*

International Journal of Chemical and Physical Sciences, ISSN:2319-6602
IJCPS Vol. 4 Special Issue – NCSC Jan-2015
www.ijcps.org

Table 1.4: Serum *magnesium ion* change on exposure to burn and
exogenous pharmacological drugs in *Albino rats*.

Day	Control	Induced	Treated							
			1	2	3	4	5	6	7	8
2	3.4 ± 0.18	3.6 ± 0.19	3.0 ± 0.18	3.2 ± 0.18	3.0 ± 0.18	3.1 ± 0.18	3.3 ± 0.18	3.3 ± 0.18	3.2 ± 0.18	3.2 ± 0.18
10	3.4 ± 0.18	4.8 ± 0.18	3.1 ± 0.17	3.1 ± 0.17	3.3 ± 0.17	3.2 ± 0.17	3.0 ± 0.17	3.1 ± 0.17	3.2 ± 0.18	3.3 ± 0.18
15	3.2 ± 0.18	3.7 ± 0.18	3.1 ± 0.18	3.0 ± 0.18	3.0 ± 0.18	2.9 ± 0.18	3.1 ± 0.18	3.0 ± 0.17	3.1 ± 0.17	3.1 ± 0.17
20	3.2 ± 0.18	3.8 ± 0.18	3.0 ± 0.17	3.1 ± 0.17	2.9 ± 0.17	3.2 ± 0.17	3.0 ± 0.17	3.0 ± 0.18	3.1 ± 0.18	3.2 ± 0.18
1= *Butea monosperma*, 2= *Cassia fistula*, 3= *Caesalpinia bonduc*, 4= *Cassine glauca*, 5= *Cassia absus*, 6= Gallic acid, 7= Amide and 8= Ester analogues of gallic acid.										

Fig. 1.4:   Serum *magnesium ion* change: *Wistar Albino rat*

International Journal of Chemical and Physical Sciences, ISSN:2319-6602
IJCPS Vol. 4 Special Issue – NCSC Jan-2015
www.ijcps.org

Table 1.5: Serum *phosphate ion* change on exposure to burn and
exogenous pharmacological drugs in *Albino rats*.

Day	Control	Induced	Treated							
			1	2	3	4	5	6	7	8
2	6.0 ± 0.20	4.2 ± 0.18	5.9 ± 0.17	5.7 ± 0.17	5.9 ± 0.17	5.6 ± 0.17	5.6 ± 0.17	5.9 ± 0.18	5.8 ± 0.18	5.8 ± 0.18
10	6.3 ± 0.20	4.8 ± 0.18	6.0 ± 0.18	5.9 ± 0.18	5.8 ± 0.18	6.21 ± 0.18	6.1 ± 0.18	6.2 ± 0.18	6.0 ± 0.18	6.1 ± 0.18
15	6.20 ± 0.20	7.20 ± 0.20	6.15 ± 0.18	6.17 ± 0.18	6.16 ± 0.18	6.18 ± 0.18	6.17 ± 0.18	6.19 ± 0.17	6.17 ± 0.18	6.18 ± 0.18
20	6.5 ± 0.20	8.3 ± 0.20	6.3 ± 0.20	6.0 ± 0.20	6.2 ± 0.20	6.2 ± 0.20	6.3 ± 0.20	6.4 ± 0.20	6.2 ± 0.20	6.3 ± 0.20

1= *Butea monosperma*, 2= *Cassia fistula*, 3= *Caesalpinia bonduc*, 4= *Cassine glauca*, 5= *Cassia absus*, 6= Gallic acid, 7= Amide and 8= Ester analogues of gallic acid.
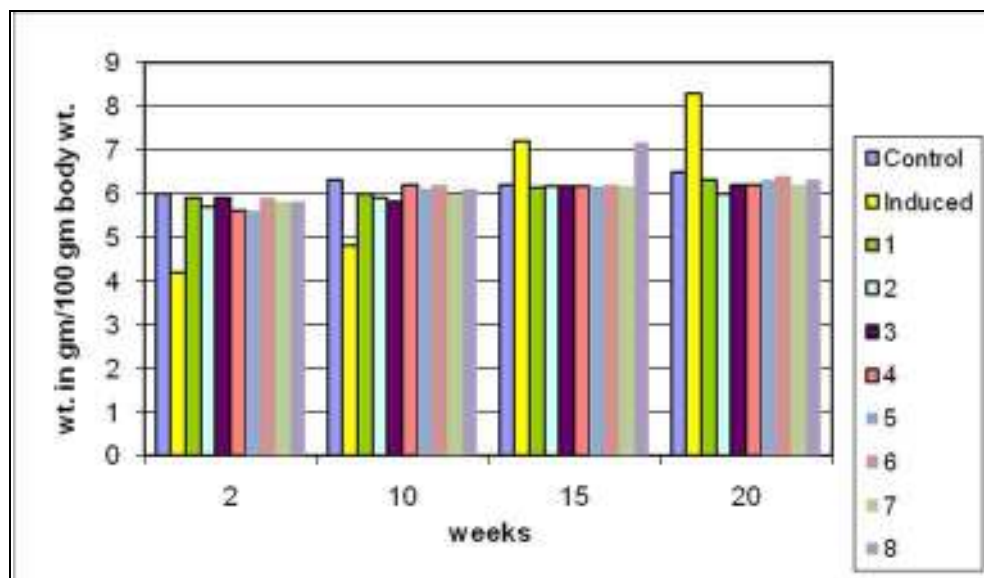
Fig. 1.5:   Serum *phosphate ion* change: *Wistar Albino rat*

International Journal of Chemical and Physical Sciences, ISSN:2319-6602
IJCPS Vol. 4 Special Issue – NCSC Jan-2015
www.ijcps.org

Conclusion:

Cutaneous infections adversely influence the ion exchange permeability of the skin. This leads to creating barriers in the supply of vital materials (ingredients) to the infected sites resulting into the deterioration of the natural composition and also the texture of the skin. Since the infected part of the skin becomes more susceptible to bacterial infections, the proportion of metal ions present in serum gets abnormally altered. From the above data it was very obvious that the concentration of the *sodium*, *potassium*, *calcium*, *magnesium* and *phosphate* ions for treated animals restored almost to the state of normalcy. It has also been revealed that isolated ingredients of the plant extracts and their chemical analogues are more effective in restoring the normalcy of the skin as compared whole plant extracts. However the author would like to mention that further extensive and systematic study in this field can lead to revealing many more life saving properties and potentials of these herbal preparations.

Acknowledgement

References

[1]. I. Bertini, H. B. Gray, S. J. Lippard and J. S. Valentine, Bioinorganic Chemistry, Viva Books Pvt. Lmt., 1998.

[2]. R. J. P. Williams, Calcium in Biological Systems, Cambridge University Press, 1976.

[3]. J. David Rawn, Biochemistry, first Indian reprint, Panima Publishing Corporation, New Delhi / Bangalore, 2004.

[4]. G. P. Talwar, L. M. Srivastava, Textbook of Biochemistry and Human biology, third ed., Prentice-Hall of India, New Delhi, 2002.

[5]. Temkitthawon, P., Viyoch, J., Limpeanchob, N., et al., 2008. Screening for phosphodiesterase inhibitory activity of Thai medicinal plants. Journal of Ethnopharmacology 119, 214–217.

[6]. Ansari, T.M., Ikram, N., Khalid, N., et al., 2004. Essential trace metal (Zinc, Manganese, Copper and Iron) levels in plants of medicinal importance, J. Biol. Sci. 4(2), 95-99.

[7]. Duggal, A. K., Yadav, P, Agarwal, A. K., Rewan, B. B, 2006. Clinical Approach to Altered Serum Sodium levels. JIACM 7(2), 91-103.

[8]. Noordzij, M., Boeschoten, E. W., Bos., W. J., et al., 2007. Disturbed mineral metabolism is associated with muscle and skin complaints in a prospective cohort of dialysis patients. Nephrol Dial Transplant 22, 2944–2949.

[9]. Alan B. G. Lansdown, 1995. Physiological and toxicological changes in the skin resulting from the action and interaction of metal ions, Critical Reviews in Toxicology 25(5), 397-4

Study of *Phyllanthus Amarus* Plant Extract and Newly Synthesized Analogue of *Pyllanthin* on Induced Hepatotoxicity in *Albino Rat*

VANDANA V.PARHATE, M.M.RATHORE AND P.R.RAJPUT

Department of Chemistry, Vidya Bharti Mahavidyalaya, Camp, Amravati-444602, India
Corresponding author: vandanaparhate@gmail.com

Abstract

Phyphyllanhtus amarus (Bhuiamala) is medicinally important plant. The literature survey reveals that this plant controls the adverse effect of hepatitis in human being. The extracts isolated from various parts of phyllonthus amarus and newly synthesized analogue of active ingredient i.e. phyllanthin were tested for their curative impact on cythion induced activities in albino rats with special reference to blood serum (VLDL, LDL and HDL) hepatotoxicity. The effects of intraperitonial administration of test plant extract and snewly synthesized analogue were studied on cythion induced blood serum hepato-toxicity. The blood serum VLDL, LDL and HDL were estimated in order to assess the liver functions by established procedures. Biochemical observations were supplemented with histological examination of liver section. It is evident from the results that levels of various serum lipoproteins were altered in cythion treated animals than control group animals. There was small but significant decrease in the concentration of total serum lipids which may largely due to the reduction of the total lipid concentration in the VLDL, LDL and HDL. However the altered lipoprotein concentration levels were restored almost to the level of their normalcy in Phyphyllanhtus amarus (Bhuiamala) and newly synthesized analogou of active ingredient i.e. phyllanthin treated animals.

Keywords:- Phyphyllanhtus amarus (Bhuiamala), albino rats.

Introduction

Hepatic diseases is a major public health problem in the developed as well as developing countries. This is due to a wide spread use of pesticides in every field of life that become alarmingly hazardous to human health. Most of the pesticides cause metabolic transformations in the body of higher animals and the main site of metabolism is the liver[1,2]. Any metabolic disturbance in the liver produces characteristic hepatic disease.[3-8] These metabolic disturbances are mainly responsible for physiological and chemical alterations in the liver functions. In fact the use of pesticides and their interactions with liver and its most important bio-constituent lipoprotein is the root cause of many diseases and fatty liver. The major form in which triglycerides released by the liver is very low density lipoproteins (VLDL)[9]. In the circulation of low density lipoprotein (LDL), such release was found in a considerable amount.

Phyphyllanhtus amarus (Bhuiamala): Phyllanthin is one of the active ingredients of *Phyphyllanhtus amarus spp*. It has been reported that the heterocyclic compounds have a broad spectrum of biological activity with special references to curing impact on hepatotxicity.[10] The paucity of data in the study of

International Journal of Chemical and Physical Sciences, ISSN:2319-6602
IJCPS Vol. 4 Special Issue – NCSC Jan-2015
www.ijcps.org

hepatoprotective effects of *Phyphyllanhtus* motivated us to undertake the study of test plant extract and analogue prepared on cythion induced hepatic malfunctioning in *albino rats*. We report herewith the synthesis of bromosubstituted phyllanthin as an analogue on its reaction with bromine in acetic acid. The effects of this compound and crude extract of test plant have been studied on cythion induced activities in *albino rats*.

Experimental:-

Phyllanthin (0.01 mol) ingredient extracted from test plant Phyllanthus amarus was dissolved in Glacial acetic acid (2 ml). To this solution bromine in acetic acid reagent was added drop by drop with constant starring. After complete addition of reagent, the reaction mixture was allowed to stand for half an hour. The solid product thus obtained was filtered and washed with a little petroleum ether to get the analogue. It gives yellowish brown layer test with CCl_4 and yellow precipitate with $AgNO_3$ solution thereby confirming the presence of bromine in the product.

Phyllanthin   Br₂ in acetic acid

Bromo derivative of phyllanthin
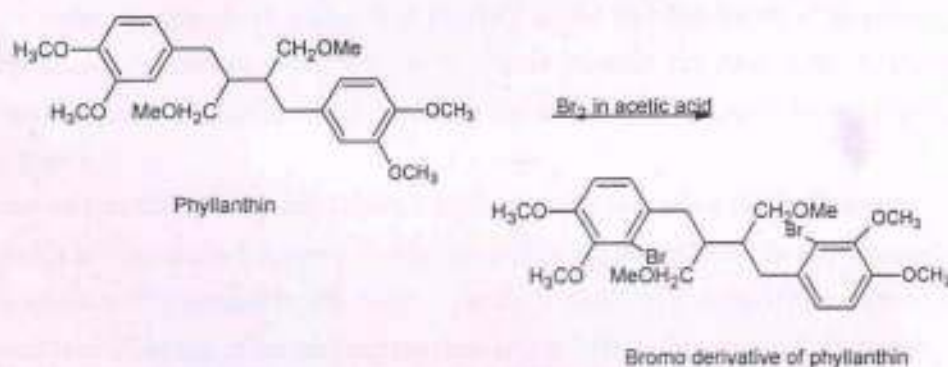
The spectral analysis of bromo derivative of phyllanthin : **IR (nujol) in cm^{-1}** :- 2916(C-H stre.), 2850.6 (C-H stre.),1168.8 (C-O-C stre.),723.3(C-Br stre.);**UV-VIS (CHCl₃)** λ_{max} 370 nm corresponding to n→π*transition; **PMR(CDCl₃)**:-δ6.8-7.4(m,4H,Ar-H),δ4.5(s,6H,-OCH₃),δ3.5(s,6H,-OCH₃),δ2.5(s,6H,C-OCH₃),δ2.1(d,4H,-CH₂), δ1.5(s,4H,Ar-CH₂-),δ1.4 (m,2H,-CH-). Melting points recorded are uncorrected and their purity was tested by TLC on microscopic slides with silica gel- G layers in benzene. From elemental analysis, chemical properties and spectral data, the compound (2b) assigned the structure bromo-phyllanthin.

Materials and Methods

The healthy *albino rats* of 6-8 weeks of age and 100-200 gm body weight were obtained from Dr. Punjabrao Deshmukh Medical College, Amravati and maintained in suiTable environment. They were supplied commercial pelleted diet and water ad libitum. The animals were divided into four groups (ABCD). The animals of group A were fed on stock diet and used as control species. Animals of group B

were given cythion pesticide intraperitionially (40SD/Kg body wt/day) for one week. Animals of groups C were given newly synthesised crude extract separately. Animals of group D were given analouge (bromo phyllanthin) in conjugation with cythion. The total period of observation was ten weeks.

The blood samples were collected from animals of group ABCD and left to clot at room temperature for at least 30 minutes to remove the clot and cell debries to perform following analysis.

i) Isolation of LDL and VLDL by precipitation with heparin and $MnCl_2$:

To 5ml of serum were added 0.2ml of 5% heparin solution and 0.25 ml of $MnCl_2$ solution. A ppt. appeared immediately. The reaction mixture was centrifuged for 10 minutes at 600 r.p.m. The precipitated lipoprotein sedimented at the bottom. The supernatant liquid was decanted and precipitate was dissolved in 10% sodium bicarbonate solution. The manganese associated with lipoproteins as bicarbonate salt was removed by concentration. 5 ml of Tris-HCl buffer was added to the clear yellow supernatant and lipoproteins were completely precipitated by the addition of 2ml $MgCl_2$. The ppt was separated by centrifugation and redissolved in 5% NaCl. In order to remove contaminating serum protein, the lipoproteins were precipitated by adding 5ml Tris-HCl buffer and 2ml $MgCl_2$. The solution was then dialysed for 24 hrs. against the tris-HCl buffer to remove heparin. The dialysis bag was transferred to another flask containing 5% $BaCl_2$ solution. After 24 hrs. the insoluble Heparin-Barium salt was removed by centrifugation.

The supernatant was dialysed against Tris-HCl buffer in order to remove $BaCl_2$. This resulted in a clear yellow solution of concentrated lipoprotein. The lipoprotein isolated in this way was the mixture of LDL and VLDL which were separated by ultra centrifugation. After 24 hr. at 1,00,00 r.p.m. the VLDL formed an opalescent band at the top of the tube and the clear yellow LDL sedimented at the bottom.

ii) Isolation of HDL by precipitation with sodium Phosphatungstate and $MgCl_2$:

To 5 ml of serum were added 5ml of 4% sodium phosphotungstate. (NaPhT) and 2 ml $MgCl_2$. The ppt of LDL and VLDL were removed by centrifugation. 4.5 ml of NaPhT was added to the clear supernatant (I). The ppt which appeared immediately was free of lipids and content mostly V-globulins which was removed by centrifugation. To supernatant (II) was added 0.0875 ml of 2ml $MgCl_2$. The precipitation was completed after 2hrs. and the mixture was centrifuged for 30 minutes at 20,000 r.p.m. The clear supernatant (III) (pH 7.1) was decanted and the ppt was dissolved in 2.5 ml of solution of the following composition (1% NaCl + 0.4%, NaPhT + 0.1 M $MgCl_2$). After washing ppt was recovered by centrifugation and was suspended in 1% NaCl, and 10% Na_2CO_3 solution was added dropwise with stirring until redissolution was achieved. This concentrated neutral solution of HDL, contaminated by small amount of serum protein was further purified by ultra centrifugation.

The serum concentration of the VLDL, LDL and HDL were determined by measuring their proteins and total lipid concentrations.

International Journal of Chemical and Physical Sciences, ISSN:2319-6602
IJCPS Vol. 4 Special Issue – NCSC Jan-2015
www.ijcps.org

iii) **Protein** : The protein contents were estimated by Lowry et al. method[11] and values were expressed as mg/100ml of serum.

iv) **Total lipids** : They were estimated gravimetrically by Folch et al. method.[12]

v) **Lipoproteirs** :

A suiTable aliquot of the isolated fraction was estimated according to Folch et al.[12] method by using chloroform-methanol (2:1) mixture. These extracts were evaporated and taken in a known valume of chloroform and stored in sealed stopper tubes at 20°C. until required for further estimations.

Observations and Results:

Serum VLDL, LDL and HDL

It is evident from the Tables 1 to 3 and figures 1_f to 3_f the level of serum lipoproteins was altered in animal treated with cythion than controls. There was small but significant decrease in the concentration of serum total lipids which was largely or solely due to a reduction of the total lipid concentration in the VLDL, LDL and HDL.

Tables 1 to 3 and figures $1f$ to $3f$ showed total lipid changes in serum VLDL,LDL and HDL.

Table 1: Serum total lipid changes in very low density lipoprotein (VLDL) on exposure to cythion,plant extrac and analogue of phyllanthin (2b) in *albino rat*.

Weeks	Control	Induced	Plant extract	Analogue
2	61.35 ± 6.25	59.60 ± 5.50	59.82 ± 5.49	59.80 ± 5.39
4	60.95 ± 6.35	58.90 ± 5.80	59.15 ± 5.85	59.35 ± 5.37
6	60.60 ± 6.20	58.65 ± 5.00	58.75 ± 5.33	58.79 ± 5.22
8	61.25 ± 6.35	57.55 ± 5.25	57.90 ± 5.29	57.99 ± 5.32
10	60.90 ± 6.26	57.33 ± 5.4	57.85 ± 5.10	57.90 ± 5.21
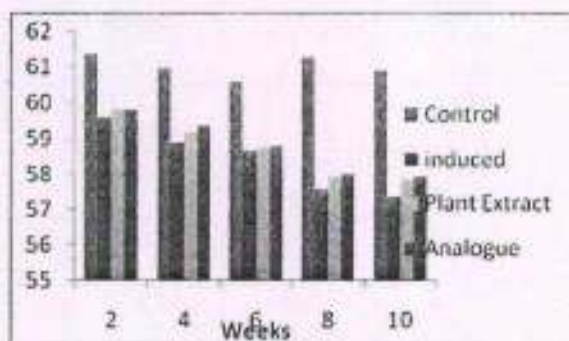
Fig. $1f$: Serum total lipids : *Albino rat.*

Study of Phyllanthus Amarus Plant Extract and Newly Synthesized
Analogue of Pyllanthin on Induced Hepatotoxicity in Albino Rat

VANDANA V.PARHATE,
M.M.RATHORE AND P.R.RAJPUT

- 420 -

International Journal of Chemical and Physical Sciences, ISSN:2319-6602
IJCPS Vol. 4 Special Issue – NCSC Jan-2015
www.ijcps.org

Table 2: Serum total lipid changes in low density lipoprotein (LDL) on exposure to cythion, plant extract and analogue of phyllanthin (2b) in *albino rat.*

Weeks	Control	Induced	Plant Extract	Analogue
2	71.80 ± 10.37	63.27 ± 10.45	64.11 ± 10.39	64.80 ± 10.56
4	70.85 ± 10.69	53.02 ± 10.15	54.25 ± 10.35	54.85 ± 10.38
6	70.95 ± 10.27	41.25 ± 10.90	42.65 ± 10.25	43.85 ± 10.01
8	71.10 ± 10.61	39.05 ± 10.05	40.25 ± 10.05	41.39 ± 10.22
10	71.05 ± 10.26	30.25 ± 10.4	30.75 ± 10.21	31.85 ± 10.11
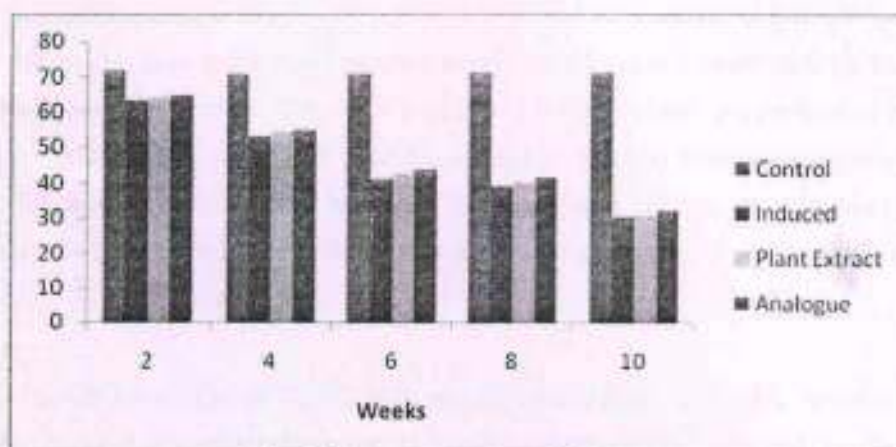
Fig. 2f : Serum protein : *Albino rat.*

Table No. 3 : Serum total lipid changes in high density lipoprotein (HDL) on exposure to cythion, plant extract and analogue of phyllanthin (2b) in *albino rat.*

Weeks	Control	Induced	Plant Extract	Analogue
2	113.21 ± 3.00	111.16 ± 7.6	111.79 ± 9.1	112.65 ± 2.5
4	113.22 ± 3.22	110.01 ± 7.23	111.29 ± 9.02	112.10 ± 2.56
6	113.10 ± 3.21	109.00 ± 7.33	110.90 ± 9.10	112.00 ± 2.29
8	121.97 ± 2.99	106.29 ± 6.75	109.29 ± 8.99	111.21 ± 2.10
10	113.29 ± 2.55	105.01 ± 6.59	30.75 ± 8.65	31.85 ± 2.22

International Journal of Chemical and Physical Sciences, ISSN:2319-6602
IJCPS Vol. 4 Special Issue – NCSC Jan-2015
www.ijcps.org
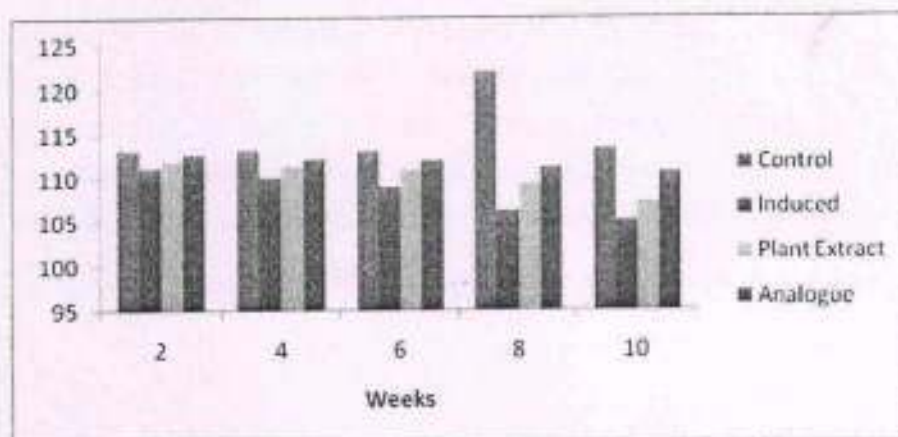
Fig. 3 *f* : Serum lipoprotein : *Albino rat*

Result

In cyhtinon treated rats there was a significant decrease in the total lipid concentration i.e.VLDL,LDL and HDL. Whereas a remarkable rie in HDL level is observed in blood serum as compared to that of control group rats.The plant extract and newly synthesised analogues under examination showed significant increase in the levels of VLDL,LDL and HDL.The study also reveled that the newly synthesised analogues have slight curative age over the crude plant extract in HDL level as compared that of VLDL and LDL.

Conclusion

The results of serum estimations in VLDL, LDL and HDL containing total lipids reveals that there is a declining trend in the values of these constituents in cythion treated *albino rats*. And the administration of phyllanthin and analogue of phyllanthin showed remarkable curative effect.

References

[1].   Traiger, G. J., G. Plaa, *Toxicol App. Pharmacol* 1971, **20**, 105-112.

[2].   Mailing, H. M., Stripp, B., Sipes, I.G., Higman, B., Saul, W. and M.A. Willams, *Toxicol Appl. Pharmacol,* 1975, **33**, 291-308.

[3].   Hall, P.M., Plummer, J.L., Iisley, A.H., and M. Cousins, *J. Hepatology,* 1991, **13**, 815-119.

[4].   Grochowski, J., Bilinska, M., and D. Stankiewiez, *Biuletyn Apipol* 1987, **7/8**, 25-26.

[5].   Zeilonka, E., Zaborski, W., Dymarczyk, M., and G. Kuziemska, *Biuletyn Apipol* 1987, **7/8**, 29-32.

[6].   Scheller, S, Stojko A., Szwarnowiecka, I., Tustanowski and J. Shani, *J., eitschrift, fur Naturforchung* 1989, 44c, 1063-1065.

[7].   Scheller, S., Stajko, A., Szwarnowiecka, I., Tustanowaski and J, Obszko, Z., *Arzneinmittel, Forchung / Drug Research* 1977, **27**, 2138-2140.

[8].   Alcaraz, M.J. and M. Jimenez .J., *Fitoterapia*, 1988, **59**, 25-38.

[9].   Kay, R.E. and C. Entenman, *J.Biol. Chem* 1961, **236**, 1006.

[10].   Shivakumar, B., Nurgund, H.V.G. *Indian J. Hetro. Chem.* (1998) **Vol. 8**, 27.

[11].   Lowry, O.H., Rosenbrough, N.H., Forr A.L., and R.J. Randall, *J. Biol. Chem.* 1951, **193**, 265.

[12].   Folch, J., Less, M. and Sloone, G.H. Staley, J.-Boil. Chem. 1957, 226, 497

Synthesis and Antimicrobial Activity of Some Chalcones and Flavones

M.M.RATHORE, P. R. RAJPUT ,V.V.PARHATE

Vidya Bharati Mahavidyalaya, Amravati Maharastra 444602.
Corresponding author: mithsrathore@gmail.com

Abstract

The chalcones (3a-e) were obtained by Claisen-Schimdt condensation of aromatic aldehydes with o-hydroxy acetophenone. Chalcones (3a-e) on reaction with catalytic amount of I2 in DMSO gave Flavones (4a-e) in high yields. All the synthesized flavones were evaluated in vitro for antifungal screening. It is observed that all flavones showed moderate to good inhibitory activity.

Keywords: 2-Hydroxy acetophenone, 2-Hydroxy chalcones, Flavones, Antifungal activity.

Introduction

Flavones constitute one of the major classes of naturally occurring products. Synthesis of flavones and their derivatives have attracted considerable attention due to their significant biocidal[1-3],pharmaceutical[4-7] and antioxidant[8-10] activities. Chalcones and its derivatives have attracted particular interest during the last few decades . Chalcones are the α,β-unsaturated carbonyl compounds.Chalcones exhibits various biological activities such as antimalerial[11], antiviral[12], anticancer[13] and other activities[14-15]. . In addition to these features chalcones are also acting as anintermediate for the synthesis of various biologically active heterocycles such as pyrimidines[16-17], pyrazolines [18-19], isoxazolines[20-21], flavonoids[22-23], benzodiazepines[24]. Here we describe the syntheses flavones (4a-d) from their corresponding chalcones (3a-d) by usingDMSO/I 2 as an oxidizing agent.

Materials and Methods

General procedure for the preparation of chalcones (3a-e)

To the boiling solution of 2-hydroxy-5-chloro acetophenone (1 mole), aromatic aldehydes(1 mole) and ethanol 20 (ml) were added. Then an aqueous solution of NaOH (40%) was added gradually with constant stirring and the reaction mixture was kept for overnight . It was poured in ice cold water and neutralised with dilute HCl (1:1). Yellow granules thus obtained were filtered, washed with NaHCO3 and finally crystallized from ethanol-acetic mixture..

(3a)-1-(2-Hydroxy-5-chlorophenyl)-3-(4-phenyl)chalcone

Yellow solid; m.p. =80°C; yield= 78%;Elemental analysis: C 74.00/73.09, O6.11/6.58,

International Journal of Chemical and Physical Sciences, ISSN:2319-6602
IJCPS Vol. 4 Special Issue – NCSC Jan-2015
www.ijcps.org

H 4.01/4.93 Cl 14.22/14.60, IR (KBr) in cm^{-1}:-16801.63(C=O stret.), 1635.55 (C=C stret.) 2934.83 (C-H stret.), 3733.17(-OH stret.), 1H NMR-: δ 7.9(m,10H, Ar-H), δ 6..5 (s, 1H, =CH), δ 6..1(d, 1H, =CH),

Scheme 1

a: R = H
b: R = OH
c: R = Cl
d: R = NO$_2$

3(a-d)

I$_2$/DMSO

4(a-d)
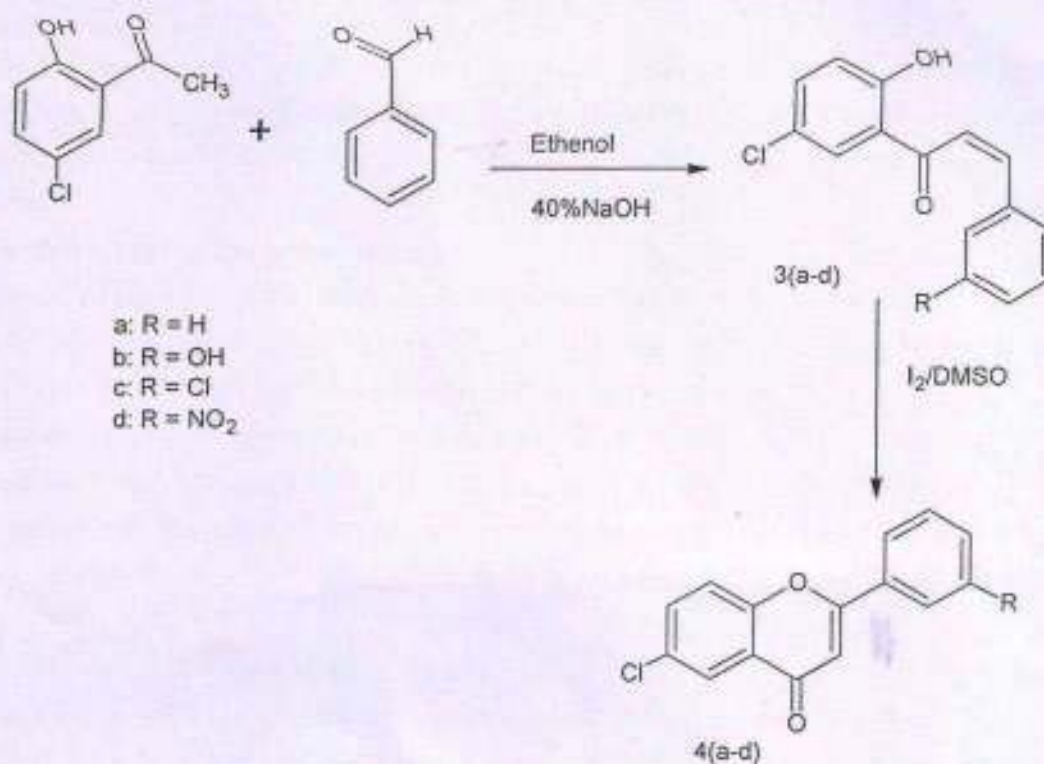
(3b)-1-(2-Hydroxy-5-chlorophenyl)-3-(4-hydrooxyphenyl)chalcone

Yellow solid; m.p. =134^{0}C; yield= 72% ;Elemental analysis: C 69.11/69.49, O12.22/12.35
H 4.22/4.63; Cl14.22/14.60 ; IR (KBr): in cm^{-1} 456.59 (C=Cstret.),1766.78(C=O stret.),
2922.48(C-H stret.), 3733.53(-OH stret.), 1H NMR: δ7.9 (m 10 H Ar-H), δ 5.6 (d 1H =CH), δ 6.3 (d,1H =CH) ,δ 11.12 (s,1H,Ar-OH (H-bonded),

(3c)-1-(2-Hydroxy-5-chlorophenyl)-3-(4-chlorophenyl)chalcone

Red solid; m.p. =170^{0}C; yield= 70% ;Elemental analysis: C 64.44 /64.74, O5.61/5.77
H 3.5/3.95; Cl 25.33/25.53; IR (KBr) in cm^{-1} : 1454.59 (C=C stret.),1511.31(C=O stret.), 2913 (C-H stret.)3439(-OH stret.), 1H NMR: δ 8.1(m, 9 H, Ar-H), δ 5.8 (d, 1H, =CH), δ6.6 (d,1H, =CH) ,

(3d)-1-(2-Hydroxy-5-chlorophenyl)-3-(4nitrophenyl)chalcone

Brown solid; mp=130^{0}C; yield= 71% ;Elemental analysis: C 62.12/62.28, O16.58/16.60,

International Journal of Chemical and Physical Sciences, ISSN:2319-6602
IJCPS Vol. 4 Special Issue – NCSC Jan-2015
www.ijcps.org

H 3.89/3.95N 4.94/4.89; Cl .09/.12, ; IR(KBr in cm⁻¹) : 1379 (-NO2 stret.); 1445.45 (C=Cstret.), 1691 (C=O stret.), 2944 (C-H stret.), 3479 (-OH stret.), 1H NMR: δ 8.0(m, 9 H, Ar-H), δ 5.6 (d ,1H =CH), δ 6.5(d,1H, =CH) .

General procedure for the preparation of flavones (4a-e):

Chalcones 3a-d (1 mole) were refluxed separately with catalytic amount of I2 (0.1 mole) in DMSO for 20-40 minutes to get flavones (4a-d) .The products thus obtained were filtered, washed with 20% Sodium thiosulphate solution to remove the colour of Iodine and finally crystallized from ehanol-acetic mixture.

(4a)6-chloro-2-phenyl-4Hchromen-4-one

Yellow solid; mp=670C; yield= 63% ; Elemental analysis: C 70.21/70.31, O11.99/12.55, H 3.00/3.51; ,Cl 0.11/0.13 .,IR (KBr) in cm⁻¹ : 1119 (C-OCstret.); 1609 (C=C stret.), 1639(C=O stret.), 2864(CH stret.),2979 , 1H NMR: δ 8.1 (m,8 H, Ar-H), δ 6.5 (s, 1H,=CH),

(4b)6-chloro-2-(2-hydroxypheny)l-4Hchromen-4-one

Yellow solid; mp=95°C; yield= 62% ; Elemental analysis: C 62.11/66.17, O15.55/17.64, H 2.08/3.30; IR (KBr) in cm⁻¹: 784.05 (mono substitutedbenzene), 1132 (C-O-C stret.); 1559.25 (C=C stret.), 1686(C=O stret.), 2914.47(CH)stret.), 1H NMR δ 8.4 (m,8 H, Ar-H), δ 6.5(s,1H ,=CH), δ 11.3 (s ,1H ,Ar-OH)

(4c)6-chloro-2-(4-chlorophenyl)-4Hchromen-4-one

Brown solid; mp=48°C; yield= 60% ;Elemental analysis: C 60.11/61.85, O9.04/1O.99, H 2.06/2.7; Cl .22.1/.24.39 ; IR (KBr) in cm⁻¹: 1118.75 (C-O-C stret.); 1642 (C=C stret.), 1719 (C=O stret.), 2860 (-CH)stret1HNMR: δ 8.6 (m,7 H ,Ar-H), δ 6.7(s,1H,=CH),

(4d)6-chloro-2-(4-nitroophenyl)-4Hchromen-4-one

Black solid; mp=92°C; yield= 63% ; Elemental analysis: C 65.32/67.66, O 22.77/24.06, H 2.91/3.09; N 4.98/5.26.; Cl 12.55.1/.13.39   IR (KBr) in cm⁻¹ : 1181.40 (C-O-C stret.); 1526.60 (-NO2 stret.) , 1644 (C=C stret.),1689 (C=Ostret 2862 (-CH stret.), 1H NMR δ 8.8 (m,7 H, Ar-H), δ 6.8(s,1H,=CH),

Table 1 *Antifungal activity of flavones*

S.N	Name of Compound	Zone of inhabitation in mm			
		Curvularia Eryostides	Drecheslera tetrameda	Fusarium cicerg	Bipolaris sorokenia
1	4a	09	12	14	08
2	4b	08	09	10	06
3	4c	10	12	11	14
4	4d	07	06	09	07

International Journal of Chemical and Physical Sciences, ISSN:2319-6602
IJCPS Vol. 4 Special Issue – NCSC Jan-2015
www.ijcps.org

Antimicrobial Screening

The antifungal activities of compounds 4(a-d)have been assayed at the concentration of 200 µg/disc assays against four plants pathogenic and moulds fungi. The inhibitory effects of compounds 4 a-d against these organisms are given in Table 1.The screening results indicate that the compound 4a-e shows good to moderate antifungal activities to the tested fungi against *Curvulariaeryostides, Drecheslera tetrameda, Fusariumcicerg, and Bipolaris sorokenia.*

Results And Discussion

The substituted 2-hydroxy 5-chloro acetophenone was condensed with aromatic aldehydes to obtain corresponding 2-hydroxy5-chloro chalcones (3a-d).the structure of this compound were established from their physical and spectral data. The IR spectrum of 3a-d shows absorption band in the region 1630-1650 cm-1(C=O) and 3295-3480 cm-1 ('-OH).

The flavones (4a-e) were obtained by oxidative cyclization of 2-hydroxy-5-chlorochalcone

(3a-d). .All synthesised flavone were evaluated for in vitro antifungal screening. It is observed that the all flavone shows good to moderate antifungal activity. The results are shown in (Table 1).

Conclusion

In summary, we have synthesised some chalcones having 2-hydroxy-5-chloroacetophenone and convert them into flavones. The antifungal screening of flavones (4a-d) were found to be active and due to presence of chlorine on phenyl ring increases the activity of the compound.

References

[1]. Rao, K. V.; Chattopadhyay, S. K.; Reddy, G. C. Flavonoids with mosquito larval toxicity.J. Agric. Food. Chem. 1990, 38, 1427-1430.

[2]. Weidenborner, M.; Jha, H. C. Antifungal activity of flavonoids and their mixtures against differentfungi occurring on grain. Pestic. Sci. 1993, 38, 347-351.

[3]. Silva, A. M.; Weidenbörner, M.; Cavaleiro, J. A. S. Growth control of different fusarium speciesby selected flavones and flavonoid mixtures. Mycol. Res. 1998, 102, 638-640.

[4]. Wu, E. S. C.; Loch, J. T.; Toder, B. H.; Borrelli, A. R.; Gawlak, D.; Radov, L. A.; Gensmantel, N.P. Flavones. 3. Synthesis, biological activities, and conformational analysis of isoflavone derivatives and related compounds. J. Med. Chem. 1992, 35, 3519-3525.

[5]. Wolfman, C.; Viola, H.; Marder, M.; Wasowski, C.; Ardenghi, P.; Izquierdo, I.; Paladini, A. C.;Medina, J. H. Anxioselective properties of 6,3'-dinitroflavone, a high-affinity benzodiazepine receptor ligand. Eur. J. Pharmacol. 1996, 318, 23-30.

[6]. Akama, T.; Ishida, H.; Kimura, U.; Gomi, K.; Saito, H.; Fuse, E.; Kobayashi, S.; Yoda, N.; Kasai,M. Design and synthesis of potent antitumor 5,4'-diaminoflavone derivatives based on metabolic considerations. J. Med. Chem. 1997, 40, 1894-1900.

International Journal of Chemical and Physical Sciences, ISSN:2319-6602
IJCPS Vol. 4 Special Issue – NCSC Jan-2015
www.ijcps.org

[7]. Gee, J. M.; Johnson, I. T. Polyphenolic compounds: interactions with the gut and implications for human health. Curr. Med. Chem. 2001, 8, 1245-1255.

[8]. Rice-Evans, C. A.; Miller, N. J.; Paganga, G. Structure antioxidant activity relationships of flavonoids and phenolic acids. Free. Rad. Biol. Med. 1996, 20, 933-956.

[9]. Rice-Evans, C. Flavonoid antioxidants. Curr. Med. Chem. 2001, 8, 797-807.

[10]. Pietta, P. G. Flavonoids as antioxidant. J. Nat. Prod. 2000, 63, 1035-1042. resistance. J. Med. Chem. 1998, 41, 4161-4164.

[11]. Liu M, Wilairat P and Mei- LMG. J. Med. Chem; 2001, 44(25): 4443-4452.

[12]. W. J. Ebenezer & P. Weight, Comprehensive organic function group transformation. A. R.Katriziky, Meth-Cohn O & Ress CW (Eds), (Pergmon Press, Oxfod), 1995, 3, 206.

[13]. V. K. Ahluwalia, L. Nayal, N. Kalia, S. Bala & A. K. Tehim, Indian J Chem 26B;1987,384;Chem Abstr.; 1988: 108, 150237.

[14]. Y. Ninomiya, N. Shimma & H. Ishitsuka, Antiviral Res, 13, 1990, 61; Chem Abtsr,13,34387.

[15]. Anjani Solanki, Smruti Lad, Sejal Solankee & Ghanshyam Patel, Indian J. Chem, 2009,48B, 1442-1446.

[16]. Moni Sharma, Vinita Chaturvedi, Y. K. Manju, Shalini Bhatnagar, Kumkum Srivastava, S.

[17]. K. Puri and Prem M. S. Chauhan, Europ. J. Med. Chem.2009, 44, 5, 2081-2091.

[18]. Rita Bamnela, S. P. Shrivastava, E-Journal of Chem., 2010, 7, 3, 935-941.

[19]. Shyam S. Mokle, Archana Y. Vibhute, Sandeep V. Khansole, Sainath B. Zangade, YeshwantB Vibhute, RJPBCS, 2010, 1, 3, 631.

[20]. Ji-Tai Li, Xiao-Hui Zhang and Zhi-Ping Lin, Beilstein Journal of OrganicChemistry,2007,3,13.

[21]. Tejaskumar Shah, Vikas Desai, J. Serb. Chem.. Soc., 2007, 72, 5, 443-449.

[22]. J. T. Desai, C. K. Desai and K. R. Desai, J. Iran. Chem. Soc., 2008, 5, 1, 67-73.

[23]. Swapnil R. Sarda, Wamanrao. N. Jadhav, Rajendra P Pawar. International Journal of chem. tech research, 2009, 1, 3, 539-543.

[24]. Maurizio Cabrera, Macarena Simoen, Gabriela Falchi, M. Laura Lavaggi, Ocar E. Pivo,

[25]. Eduardo E. Castellano, Anabel Vidal, Amaia Azqueta, Antonio Monge, Adela Lopes de Cerain,Gabriel Sagrera, Gutavo Sedane, Hugo Cerecetto and Mercedes Gonzalez, Bioorg. Med. Chem, 2007, 15, 3356-3367

[26]. 24. S. R. Sarda, W. N. Jadhav, N. B. Kolhe, M. G. landge and R. P. Pawar, J. Iran. Chem. Soc., 2009, 6, 3, 477-482.

Ecofriendly Synthesis, Characterization and Antibacterial Assay of Some Chlorosubstituted Isoxazoles

P. R. RAJPUT[1], M. W. BHADE[2], C. D. BADNAKHE[3], A. V. GAJBHIYE[4]

[1] Department of Chemistry, Vidyabharati Mahavidyalaya, Camp Amravati
[2] Department of Chemistry, Amolakchand Mahavidyalaya, Yavatmal
[3] Department of Chemistry, Dr. Manorama & Prof. H.S. Pundkar Arts, Commerce & Science College, Balapur
[4]. Department of Chemistry, MGV's A.S.C. College, Nampur
Corresponding author: madhuri.bhade@gmail.com

Abstract

The concept of green chemistry is now widely adopted to meet the scientific challenges in order to protect the human health and environment. Nowadays researchers are working extensively to synthesize new compounds using ecofriendly solvents and other conditions. Literature survey reveals that isoxazoles are very useful units in the fields of medicinal, pharmaceutical and agriculture. Isoxazoles have been reported to exhibit a broad spectrum of biological activities. In this regard, in the present study, we have undertaken synthesis and characterization of new chlorosubstitutedisoxazole derivatives by the action of chlorosubstituted flavones, which were prepared from chalcones in a ecofriendly single step, with hydroxylamine hydrochloride in good yields. The newly synthesized compounds are screened against some bacteria with special reference to study antipathogenic activities.

Keywords: *Chlorosubstitutedisoxazoles, flavones, chalcones, antibacterial assay, antipathogenic activities.*

Introduction

Literature survey shows that the chlorosubstituted heterocycles[1] have antifungal[2], antimicrobial[3], antitubercular[4], antiviral[5], and antibacterial[6] activity. Taking into account the widespread applications of chlorosubstituted heterocycles such as pyrazoles, thiazoles, isoxazoles[7] in the fields of pharmaceutical, medicine and agriculture, it was thought interesting to synthesize some new chlrosubstituted isoxazoles and study their impact on plant pathogens especially bacteria. The isoxazoles are the compounds having five membered ring containing both oxygen & nitrogen atoms in the 1,2 positions. It has been observed that flavones are the best starting compounds for the preparation of isoxazole derivatives. These flavones are prepared from chalcones in a ecofriendly single step.

Experimental

Scheme-I

Preparation of 2,4-dichloro phenyl acetate(*1a*): 2,4-dichlorophenol (10gm) was mixed with acetic anhydride (12ml) and anhydrous sodium acetate (1gm). The mixture was refluxed for about an hour. The

International Journal of Chemical and Physical Sciences, ISSN:2319-6602
IJCPS Vol. 4 Special Issue – NCSC Jan-2015
www.ijcps.org

mixture was cooled and poured into cold water. Acetate layer was separated and then washed with water several times. It was finally collected by distillation.

Preparation of 1-(3,5-dichloro-2-hydroxyphenyl)ethanone(2a): 2,4-dichlorophenol (10ml) was mixed with anhydrous $AlCl_3$(24gm) and heated at 120^0C for 45 minutes. The reaction mixture was decomposed with ice cold water containing a little HCl. A greenish solid thus separated was recrystallised by ethanol to get compound 2a.

IR(KBr ν_{max})(cm^{-1}) 3050cm^{-1}(-OH phenolic str),1665(C=Ostr), 1300(C-Ostr), 730(C-Clstr)

NMR: δ12.73(s,1H,Ar-H) , δ7.25-7.63(m,2H,Ar-H) , δ2.60,(s,3H,-CH₃).

Preparation of 1-(3,5-dichloro-2-hydroxyphenyl)-3-(2,3-dichlorophenyl)prop-2-en-1-one(3a): 1-(3,5-dichloro-2-hydroxyphenyl) ethanone (0.01M) and 2,3-dichlorobenzaldehyde(0.01M) were added to ethanol(20ml). To this mixture KOH solution(40%,10ml) was added drop wise . The reaction mixture was kept for overnight, then poured on ice containing little HCl. The product was filtered and recyrstallised from ethanol to obtain the compound 3a.

IR(KBr ν_{max})(cm^{-1}) 3417cm^{-1}(O-Hstr),1645(C=Ostr),308cm^{-1}(ArC-Hstr),1648cm^{-1} (C=Cstr),738cm^{-1}(C-Clstr).

NMR: δ8.17(d,1H,CH=CH) , δ7.39(d,1H,CH=CH), δ6.7-7.5(m,5H,Ar-H), δ5.0(s,1H,Ar-OH).
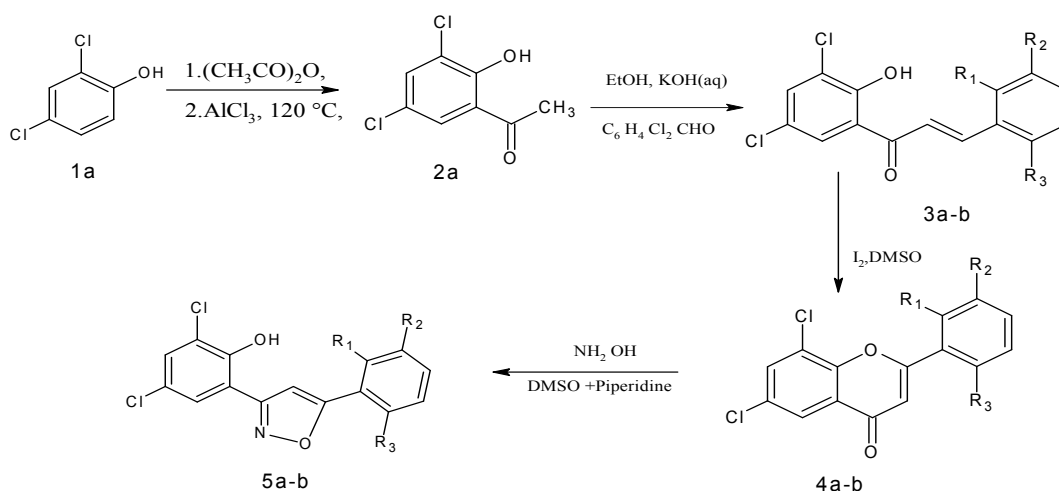
where a; R₁=Cl, R₂=H,R₃=Cl and b ; R₁=Cl, R₂=Cl,R₃=H

Preparation of 6,8-dichloro-2-(2,3-dichlorophenyl)-4*H*-chromen-4-one (4a) -

1-(3,5-dichloro-2-hydroxyphenyl)-3-(2,3-dichlorophenyl)prop-2-en-1-one (0.01M) was dissolved in 20ml DMSO, To this few crystals of Iodine were added. The mixture was refluxed for 10 min. Then the

International Journal of Chemical and Physical Sciences, ISSN:2319-6602
IJCPS Vol. 4 Special Issue – NCSC Jan-2015
www.ijcps.org

mixture was poured on the crushed ice. The product was filtered and recrystallised from chloroform to get compound 4a.

IR(KBr ν_{max})(cm^{-1}):3400cm^{-1}(O-Hstr), 1650cm(C=Ostr),1310cm^{-1}(C-Osrt),730cm^{-1}(C-Clstr).

NMR: δ9.1(m,2H,Ar-H) , δ7.9(m,2H,Ar-H),δ7.3(s,1H,Ar-H),δ7.1(m,4H,Ar-H), δ5.1(s,1H,Ar-OH), δ4.8(m,1H,CH), δ2.0(d,1H,-CH$_2$), δ1.8(d,1H,-CH$_2$).

Preparation of 2,4-dichloro-6-[5-(2,3-dichlorophenyl)-1,2-oxazol-3-yl]phenol (5a) : 6,8-dichloro-2-(2,3-dichlorophenyl)-4*H*-chromen-4-one (0.01M) and hydroxylamine hydrochloride(0.01) dissolved in 20ml DMSO with a few drops of pipyridine. The mixture was refluxed for 1.5 hrs. The product was filtered and recrystallised from chloroform to get compound 5a.

IR(KBr ν_{max})(cm^{-1}) :3400cm^{-1}(O-Hstr),1584cm^{-1} (C=Nstr),1310cm^{-1}(C-Osrt), ,730cm-1(C-Clstr).

NMR: δ8.3(s,1H,C-H),δ7.1-7.3(m,5H,Ar-H),δ5.2(s,1H,Ar-H).

Antibacterial Study

The newly synthesized compounds(5a and 5b) were screened for their antibacterial activity against some *Gram positive* pathogens viz. *Staphylococcus aureas* and *Streptococcus sp.* and some *Gram negative* pathogens viz. *Pseudomonas sp.* and *Solmonella Typhi.* at conc.of 1000 μm gentamycine as a standard. DMF was used as solvent control using agar plate techniques. The chlorosubstituted isoxazoles synthesized when screened for antibacterial activity, it was noticed that all these compounds had shown remarkable inhibitory activity.

Results And Discution

Physical characterization data of all the compounds are given in Table-1.

TABLE-1

CHARACTERIZATION DATA OF NEWLY SYNTHESIZED COMPOUNDS

Compound	Mol. Formula	M.P.(^{0}C)	Yield(%)	R_f
1a	$C_8 H_6 Cl_2O_2$	214(B.P.)	85	0.75
2a	$C_8 H_6 Cl_2O_2$	91-92	70	0.80
3a	$C_{15} H_8Cl_4O_2$	84-86	80	0.77
3b	$C_{15} H_8Cl_4O_2$	95-97	82	0.73
4a	$C_{15} H_7 Cl_4 O_2$	160-162	59	0.74
4b	$C_{15} H_7Cl_4 O_2$	183-185	57	0.82
5a	$C_{15} H_7Cl_4NO_2$	195-197	63	0.72
5b	$C_{15} H_7Cl_4NO_2$	186-188	61	0.81

International Journal of Chemical and Physical Sciences, ISSN:2319-6602
IJCPS Vol. 4 Special Issue – NCSC Jan-2015
www.ijcps.org

The synthetic routes which furnished the target compounds are shown below along with their IR and NMR data. The newly synthesized compounds (5a and 5b) were found to be active against test pathogens. A further detailed study in the light of Medical sciences is advised.

Acknowledgements

References

[1]. Vinata V. Mulwad, Bhushan P Langi and Atul C Chaskar, *Acta Polo. Pharma.Drug Research, 68(1),39-47,(2011).*

[2]. D. D. Guy, P. M. Carabates, (Sterling Drug Inc.) U.S. 4,268,678 (C1. 548-247; C07D261/08), 19 May (1981), Appl. 72,134, 04 Sep (1979); 4 pp; *Chem. Abstr.,* 1981, 95,203923n

[3]. M. T. Shreenivas, B. E. Kumara Swamy, J. G. Manjunatha, Umesh Chandra, G. R.Srinivasa and B. S. Sherigara *Der Pharma Chemica*, 2011, 3 (6),224-234

[4]. Caradonna, C.and Stein,M.L.,*Farmoco. Edn. Sci*, 15, (1960), 674

[5]. Stelger, N., *Chem Abstr*., 45 (1951), 10259.

[6]. Okuda, T., Kitamura, J. and azika, *Proc. Gifu. Coll. Pharm*., K.A.,No.5 (1955), 208.

[7]. B Veeraswamy, C.Kurumurthy, G Santosh Kumar, P Sambsiva Rao, Kavya Thelekkal, Srigiridhar Kotamraju and B Narsaiah, *Indian J. Chemistry*, 51B,(2012), 1369-75.

Studies in Acoustic Parameters of Promethazine Drug in Dioxane-Water Solvent at Different Temperatures

U.S. WASNIK[1], R.M.JUMLE[2] AND P.R. RAJPUT[3]

1-Department of Chemistry, Arts Science and Commerce College, Chikhaldara Dist : Amravati (M.S.)
2-Department of Chemistry , Shivaji College, AkotDist : Akola (M.S.) India
3-Department of Chemistry, VBMV, Amravati (M.S.) India
Corresponding author: us.wasnik@gmail.com

Abstract

Measurements of ultrasonic velocity have been carried out for Promethazine hudrochloride (PM) at three different temperatures. Viscosities and densities of present system have been measured at 303K, 308K & 313K. From this data various acoustic parameters such as apparent molar compressibility (ϕ_k), apparent molar volume (ϕ_v), adiabatic compressibility (β_s), specific acoustic impendence (Z), intermolecular free length (L_f), molar compressibility (W) & relative association (R_A) have been determined. From these derived parameters limiting apparent molal volume (ϕ^0_v), limiting apparent molal compressibility (ϕ^0_k) and Experimental slopes (S^0_V & S^0_K) have calculated by using Massons equation. The viscosity data are analysed using Jones – Dole equation. The results are interpreted on the basis of solute-solvent and solute-solute interactions.

Keywords: Promethazine hydrochloride, acoustic parameters.

Introduction

The studies on volumetric, ultrasonic and viscometric properties of liquid mixtures and their dependence on composition and temperature are of importance in many fields of applied research and find applications in many important chemical, textile, leather, industrial and biological process. Ultrasonic waves provide valuable information about the molecular interaction in pure liquids, aqueous solutions, liquid mixtures and also provide valuable information about the structure of solids[1-4].

Ultrasonic velocity measurements have been successfully employed to detect and assess weak and strong molecular interactions, present in binary liquid mixtures [5, 6]. Ultrasonic studies have found wide applications owing to their ability to characterize the physico-chemical behaviour of solutions. The excess properties have been claimed to be an aid in the characterization of the molecular interactions that are present in solutions and liquid mixtures. This is achieved through elevation of ideal quantities. In recent years, considerable efforts have been given for the elevation of ideal and excess thermodynamic quantities of binary and ternary liquid mixtures [7, 8].The study of molecular interaction in the liquid mixtures is of considerable in the elucidation of the structural properties of the molecules.

The nature and degree of molecular interactions in different solutions depend upon the nature of the medium, the structure of the solute molecule and also the extent of solvation taking place in solution.For

International Journal of Chemical and Physical Sciences, ISSN:2319-6602
IJCPS Vol. 4 Special Issue – NCSC Jan-2015
www.ijcps.org

the present study drug *[Dimethy1 (1-(10-H phenothiazin-10-y1) propan-2-y1] amine)* is selected. This drug is used as antihistaminic, sedative. Acoustic parameters provide a better insight into molecular environment to liquid mixtures, it seemed important to study molecular interactions, which motivated theauthors to carry out the present investigation in the binary liquid mixtures of Promethazine hydrochloride (PM) with dioxane-water solvent at different temperatures using ultrasonic technique.

Materials and Methods

Solventdioxane used in the present work was of AR grade, purified and dried by the usual procedure. Densities, viscosities and ultrasonic velocities were measured at different temperatures over a wide range of composition. Densities were determined by using bicapillarypyknometer. The Viscosities (η) of pure compounds and their mixtures were determined using Oswald's Viscometer calibrated with double distilled water [8,9]. Ultrasonic velocity measurements were made by using an ultrasonic interferometer (Mittal Enterprises, New Delhi) at a frequency of 2MHz with a tolerance of $\pm$ 0.005%. All the measurements were carried out at different temperatures.

Acoustic parameters such as apparent molar compressibility (ϕ_k), apparent molar volume (ϕ_v), adiabatic compressibility (β_s), specific acoustic impendence (Z), intermolecular free length (L_f),molar compressibility (W) & relative association (R_A)were determined using following relationsLimiting apparent molar volume (ϕ^0_v), limiting apparent molar compressibility(ϕ^0_k)and Experimental slopes (S^0_V&S^0_K) have calculated by using Massons equation.

Ultrasonic velocity	$u = \lambda \upsilon$	1
Adiabatic compressibility	$\beta_s = 1/ u^2_s \rho_s$	2
Apparent molar compressibility	$\phi_k = 10^3(\rho_0\beta_s-\rho_s\beta_0)/m-\rho_s \rho_0 + \beta_sM/\rho_s$	3
Apparent molar volume	$\phi_v = 10^3(\rho_0-\rho_s)/m-\rho_0 \rho_s + M/\rho_0$	4
Specific acoustic impendence	$Z = \rho.u$	5
Intermolecular free length	$L_f = K (\beta_s)^{1/2}$	6
Molar compressibility	$W = M \times (\beta_s)^{-1/7}\rho_s$	7
Relative association	$R_A = (\rho/\rho_0) \times (u_0/u)^{1/3}$	8
Limiting apparent molar volume	$\phi_v = \phi^0_v + S_vC^{1/2}$	9
Limiting apparent molar compressibility	$\phi_k = \phi^0_k + S_k^{1/2}$	10

In the present paper, we report densities (ρ) and Ultrasonic velocities of binary mixtures of Promethazine hydrochloride (PM) withdioxane-water solvent at different temperatures, over the entire composition range.

International Journal of Chemical and Physical Sciences, ISSN:2319-6602
IJCPS Vol. 4 Special Issue – NCSC Jan-2015
www.ijcps.org

Table 1: The Experimental values Density, Ultrasonic Velocity and related Parameters at different temperatures System- PM in 20% Dioxane-Water medium

Temp T(K)	Conc. mol. dm^{-3}	Density ρs Kgm^{-3}	Ultrasonic Velocity (u) m/s	β_s x10^{-10} Pa^{-1}	Φv x10^{-5} m^{3}mol^{-1}	Φk x10^{-14} m^{3}mol^{-1} Pa^{-1}	L_f x10^{-11} (m)	Z x10^5 Kg m^{-2} sec^{-1}	Relative association R$_A$ X10^{-3}
298K	0.02	1025.45	1621.1	3.7108	-11.454	-152.81	3.9723	16.6235	996.42
	0.04	1025.74	1622.8	3.7020	7.7182	-73.593	3.9675	16.6457	996.36
	0.06	1026.06	1625.4	3.6890	14.506	-47.909	3.9606	16.6775	996.13
	0.08	1026.19	1628.5	3.6745	17.451	-35.190	3.9528	16.7115	995.63
	0.1	1026.41	1631.5	3.6602	19.399	-27.586	3.9451	16.7458	995.23
303K	0.02	1024.45	1625.3	3.6952	-21.937	-176.235	3.9972	16.6503	997.24
	0.04	1024.77	1627.6	3.6836	2.4168	-86.030	3.9909	16.6791	997.08
	0.06	1024.91	1629.9	3.6728	10.820	-55.763	3.9850	16.7050	996.75
	0.08	1025.12	1632.1	3.6621	14.937	-40.646	3.9792	16.7309	996.65
	0.1	1025.31	1634.6	3.6502	17.420	-31.704	3.9728	16.7597	996.18
308K	0.02	1020.96	1629.2	3.6901	-7.9301	-179.43	4.0273	16.6334	993.22
	0.04	1021.12	1631.1	3.6810	9.8516	-86.888	4.0223	16.6554	992.99
	0.06	1021.84	1633.3	3.6685	14.866	-56.945	4.0154	16.6897	993.24
	0.08	1022.06	1635.1	3.6596	17.976	-41.313	4.0106	16.7117	993.09
	0.1	1022.21	1637.5	3.6484	19.909	-32.160	4.0044	16.7386	992.75

Table 2.   Limiting values of ϕ_v and ϕ_k along with slope (S$_V$&S$_K$) for PM indioxane-water medium at different temperatures

Temp.T (K)	Medium	Parameters			
		ϕ_v^0x10^{-5} m^{3}mol^{-1}	ϕ_k^0 x10^{-14} m^{3}mol^{-1}pa^{-1}	S$_v$x10^{-5} m^{3}mol$^{-3/2}$dm$^{3/2}$	S$_k$ x10^{-14} m^{3}mol$^{-3/2}$dm$^{3/2}$pa^{-1}
298K	20%D-W	-31.28	-232.3	171.7	695.7
303K	20%D-W	-40.29	-273.3	194.1	820.8
308K	20%D-W	-40.09	-274.3	205.9	818.5

Results and Discussion

Table 1 shows that density (ρ), ultrasonic velocity (u) and viscosity (η) increases with increase in concentration for all three systems. The increase in ultrasonic velocity is due to decrease in intermolecular free length (L$_f$) as shown in Table. This suggests that there is a strong interaction between promethazine hydrochloride and solvent molecule. Adiabatic compressibility (β_s) is a measure of intermolecular association or repulsion calculated from the measured ultrasonic velocity (u) and density (ρ). Adiabatic compressibility is found to decrease with increase in concentration[10]. Since adiabatic compressibility is inversely related to the product of density and ultrasonic velocity based on this the compressibility is expected to decrease which has observed in the present case.

International Journal of Chemical and Physical Sciences, ISSN:2319-6602
IJCPS Vol. 4 Special Issue – NCSC Jan-2015
www.ijcps.org

Fig-System-PM in 20% D -Water
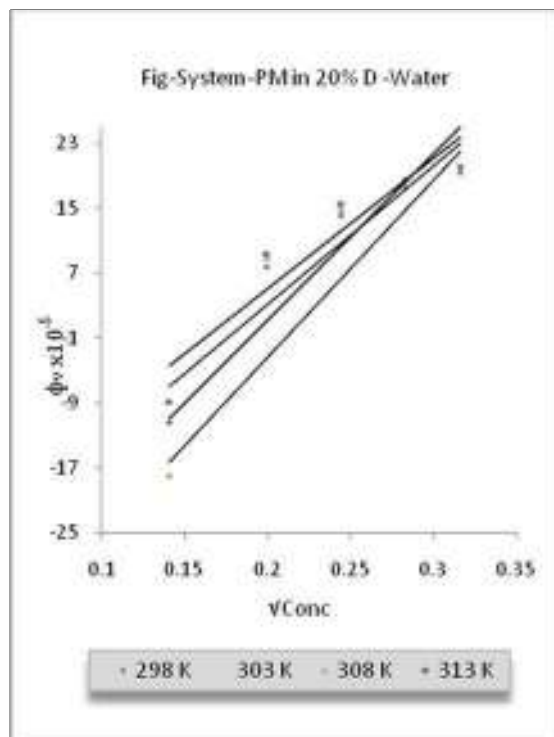
When the sound waves travels through the solution, certain part of it travels through the medium and rest gets reflected by the ion[11] i.e. restriction for flow of sound velocity by the ions. The character that determines the restriction movement of sound waves is known as acoustic impendence (Z). It has been found that acoustic impendence increases with increase in concentration. The apparent molar compressibility (ϕ_k) explains the solute-solvent and solute- solute interactions in solution and was calculated by using the equation 3. The apparent molar volume (ϕ_v) is defined as the change in volume of solution for the added one mole of a particular component at constant temperature and pressure. It is thermodynamic property which helps in elucidating solvation behavior of electrolyte in solution. Apparent molar volume was evaluated from the density of solution and solvent. It is evident from the Table 2 that ϕ^0_k values are negative for 20% Dioxane-water. The negative ϕ^0_k values are suggest solute-solvent interaction whereas positive values are due to solute- solute interaction. S_v is a measure of solute - solvent interaction. It is observed from the Table 2 that The decreasing values of ϕ^0_v and increasing values of S_v clearly indicates the decrease in solute-solvent and increase in solute-solute interactions with the rise of temperature which indicates the solute-solute interactions are stronger than solute-solvent interactions.

References

[1]. R P Verma and S Kumar, Ind J Pure and apply Phy 2000; 312:59.

[2]. S Kamila, S jena and B Bihari. J ChemThermodyn 2005; 37:820.

[3]. R Abraham, M Abdulkhadar and CV Asokan. J ChemThermodyn 2001; 32:1.

[4].   S Mukharjee, C Basu and US Ghosh. J Non-Cryst Solids.1992; 144:159.

[5].   Kannappan V and Jaya SanthiR Indian J pure &applPhy 2005;43, 750.

[6].   Kannappan V, Xavier Jesu Raja and JayasanthiR Indian J pure &apply 2003;41,690.

[7].   Jayakumar S, Karunanithi N, Kannappan V andGunasekaran S Asian Chem Lett1999;3, 224.

[8].   YonzhanLuo and Robert L Bldwin J MolBiology 1998; 49, 279.

[9].   Kannappan V and Jaya Santhi R Indian J pure & apply 2005; 43,167.

[10]. Owen B.B and Kronick P K, J Phys Chem,1961; 65:81.

[11]. Sumathi T & Uma Maheshwari, Indian J Pure and Applied phys., 2009; 47:782

INTERNATIONAL JOURNAL
OF PHARMA AND BIO SCIENCES

IJPBS

Internationally indexed journal

Indexed in Chemical Abstract Services (USA), Index coppernicus, Ulrichs Directory of Periodicals, Google scholar, CABI ,DOAJ , PSOAR, EBSCO , Open J gate , Proquest , SCOPUS , EMBASE ,etc.

Rapid and Easy Publishing

The "International Journal of Pharma and Bio Sciences" (IJPBS) is an international journal in English published quarterly. The aim of IJPBS is to publish peer reviewed research and review articles rapidly without delay in the developing field of pharmaceutical and biological sciences

Pharmaceutical Sciences

- Pharmaceutics
- Novel drug delivery system
- Nanotechnology
- Pharmacology
- Pharmacognosy
- Analytical chemistry
- Pharmacy practice
- Pharmacogenomics

- Polymer sciences
- Biomaterial sciences
- Medicinal chemistry
- Natural chemistry
- Biotechnology
- Pharmacoinformatics
- Biopharmaceutics

Biological Sciences

- Biochemistry
- Biotechnology
- Bioinformatics
- Cell biology
- Microbiology

- Molecular biology
- Neurobiology
- Cytology
- Pathology
- Immunobiology

Indexed in Elsevier Bibliographic Database

(Scopus and EMBASE)

SCImago Journal Rank 0.288

Impact factor 2.958*

Chemical Abstracts Service (www.cas.org)

A division of the American Chemical Society

CODEN IJPBJ2

Google Scholar BETA

Elsevier Bibliographic databases (Scopus & Embase)

SNIP value – 0.77

SJR - 0.288

IPP - 0.479

SNIP – Source normalised impact per paper
SJR – SCImago Journal rank
IPP –Impact per publication
Source –www.journalmetrics.com
(Powered by scopus (ELSEVIER)

International Journal of Pharma and Bio Sciences

Indicator	2006-2013	Value
SJR		0.29
Cites per doc		0.51
Total cites		852

www.scimagojr.com

ProQuest

INDEX COPERNICUS
INTERNATIONAL
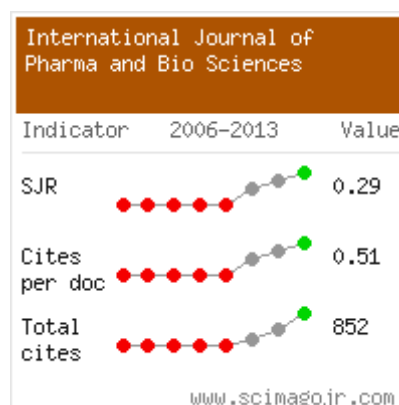
LUND UNIVERSITY

JSU
Jacksonville State University
Houston Cole Library
USA (Alabama)

UNIVERSITY OF OXFORD
Oxford, United Kingdom

And indexed/catalogued in many more university

*Instruction to Authors visit **www.ijpbs.net***

For any Queries, visit "contact" of www.ijpbs.net

International Journal of Pharma and Bio Sciences

SYNTHESIS, CHARACTERIZATION AND ANTIMICROBIAL SCREENING OF SOME PYRAZOLES.

V. D. MANE[*1], D. T. MAHAJAN[2] AND P. R. RAJPUT[2]

[1]*Department of Chemistry, S. K. College, Akola, India.*
[2]*Department of Chemistry, Vidyabharti Mahavidyalaya Amravati, India.*

ABSTRACT

In the present study the pyrazole have been synthesized by the reaction of chalcone dibromide with phenyl hydrazine hydrochloride to afford the yellow solids of pyrazoles. The synthesized compounds have been confirmed by their chemical, analytical and spectral study and these synthesized compounds have been screened for their antimicrobial activity against some kharip plant pathogens viz *Xanthomonas Campestris, Alternari Macrospora, Fusarium Spp.Pseudomonas syringae.*

KEYWORDS:*Pyrazole, chalconedibromide, antimicrobial activity, plant pathogen, chalcone.*

*Corresponding author

V. D. MANE
Department of Chemistry, S. K. College, Akola, India.

INTRODUCTION

The great majority of the known compounds with two hetero atoms in the five membered ring are aromatic and can be derived formally from pyrrole by the replacement of one of the methine (-CH=) by a nitrogen atom in case of pyrazole. As early as 1884 Knorr discovered the antipyretic action of pyrazole derivatives in the man, knorr named the compound antipyrine. This stimulated interest in pyrazole chemistry a number of pharmaceuticals and dyestuffs contain the pyrazole ring[1]. The literature survey shows that pyrazole and its derivatives are an important class of compounds and attracted vide spread attention due to their pharmacological properties, being reported to have a large spectrum of biological effects[2], especially analgesic[3] and anti-inflammatory[4], antibacterial[5], antiparasitic[6], antiamoebic[7], antifungal[8] and antiaggregating[9], properties.

MATERIALS AND METHODS

Preparation of 2-hydroxy 3, 5-dichloroacetophenone (2a)

2-hydroxy 3, 5-dichloroacetate (50 ml) was mixed with anhydrous $AlCl_3$ (120 gm) and heated at 120^oC for 45 minutes on the parafine oil bath. The reaction mixture was decomposed by taking ice cold water containing a few amount of HCl acid and allowing the solution to fall drop by drop into cold water with constant stirring . A greenish white solid of compound (2a) was obtained.

Preparation of 2-hydroxy-3, 5-dichlorophenyl-4-p-chlorochalcone (3a, 3b)

2-Hydroxy-3,5-dichloroacetophenone(2a) (0.01mol) and p-chlorobenzaldehyde and p, m-dichlorobenzaldehyde (0.01mol), were dissolved in ethanol (25ml). after that in this solution the 40% 30 ml NaOH solution is added drop wise with constant stirring getting the saffron color solid kept it overnight after that

acidify this solid by 50% HCL solution, affords a yellow solid was filtered, washed with sodium bicarbonate (10%) followed by water. The crude product was crystallized from ethanol acetic acid.

Synthesis of 2-hydroxy 3, 5-dichlorophenylchalconedibromide (6a, 6b)

2-hydroxy 3, 5-dichlorophenyl chalcone (3a) and chalcone (3b) (0.01 mol 3.26, 3.65gm respectively) was dissolved in bromine -acetic acid reagent (25%, w/v) (6.4 ml). The reagent was added drop wise with constant stirring. After complete addition of reagent, the reaction mixture was kept at room temperature for about 30 minutes. The solid product thus separated was filtered and washed with a little petroleum ether to get the compound (6a) and (6b).

Synthesis of 2-hydroxy-3, 5-dichlorophenyl pyrazole (7a, 7b)

A mixture of chalconedibromide (6a) and (6b) (0.01 mol, 4.84 and 5.18 gm, respectively) and Ph.NH.NH$_2$.HCl (0.02 mol, 2.78gm) was refluxed in ethanol (20 ml) and piperidine (1ml) for about 3.5 hours. After cooling the reaction mixture was acidified with dil. HCl (1:1). The solid product separated was filtered, washed with sodium bicarbonate solution (5 %) and water. The product was finally crystallized from ethanol-acetic acid mixture to get the compound (7a) and (7b).

Characterization of the compounds

Melting points of all synthesized compounds were determined in open capillaries and are uncorrected. IR spectra were recorded on Perkin-Elmer 1000 Spectrophotometer in KBr. NMR spectra were recorded on Bruker advance 400 NMR spectrometer using TMS as internal standard and chemical shift were expressed in δ ppm.

1. Compound: Chalcone (3a)

I.R. (KBr): cm – 3400 (-OH phenolic), 3065 (=CH str. in alkene), 1720 (>C=O str. in ketone), 1324 (-OH bending in phenol), 650 (C-Cl stretching).
PMR: δ 2.75; (s, 3H, -COCH3); 7.35 -7.73 (m, 2H, Ar H); 12.61 (s, 1H, Ar-OH). U. V.:- λ max 344 nm. corresponding to n →π*

2. Compound: Chalcone (3b)

I.R. (KBr): cm-3455 (-OH phenolic), 2990 (aliphatic –CH stretching). 1705 (>C=O str.in ketone), 1314 (-OH bending in phenol), (C-Cl stretching).
PMR: δ 3.75(d, 1H, -CH=CH); 4.23(d, 1H, - CH=CH) 7.0-8.0 (dd, 2H, Ar-H); 12.7(s, 1H, Ar-OH) U. V.:- λ max 344 nm. Corresponding to n →π* shows conjugation in aromatic molecule

3. Compound: Dibromide (6a)

I.R. (KBr): cm – 3500 (-OH phenolic), 2981 (aromatic str.), 2857 (aliphatic CH str.), 1654(-C=O str.), 1319 (O-H bending).
PMR: δ 2.5 (d, 1H, -CO-CH-Br); 3.5 (d, 1H,-CHBr-CHBr); 7.4-8.4 (m, 6H, Ar-H).12.04(s, 1H, Ar-OH), U. V.:- λ max 314 nm. Corresponding to n →π*

4. Compound: Dibromide (6b)

I.R. (KBr): cm – 3580 (-OH phenolic), 3074 (aromatic str.), 3007 (aliphatic CH str.), 1640(-C=O str.), 1313 (O-H bending).
PMR: δ 3.9 (d, 1H, -CO-CH-Br); 3.5 (d,1H,-CHBr-CHBr); 7.1-8.4 (m, 5H, Ar-H).11.90(s, 1H, Ar-OH), U. V.:- λ max 300- 400 nm. Corresponding to n →π*

5. Compound: Pyrazole (7a)

I.R. (KBr): cm – 3580 (w, -OH phenolic), 3070 (s, aromatic str.), 1496 (-C-N str.), 1261(s,- N=N- str.).
PMR: δ 6-81-8.07 (m, 12H, Ar-H).11.36(s, 1H, Ar-OH), U. V.:- λ max 400 nm. Corresponding to n →π*

6. Compound: Pyrazole (7b)

I.R. (KBr): cm – 3600 (w, -OH phenolic), 3076 (s, aromatic str.), 1465(-C-N str.), 1269(s,- N=N- str.).
PMR: δ 6-76-8.13 (m, 11H, Ar-H), 11.17(s, 1H, Ar-OH), U. V.:- λ max 410 nm. Corresponding to n →π*
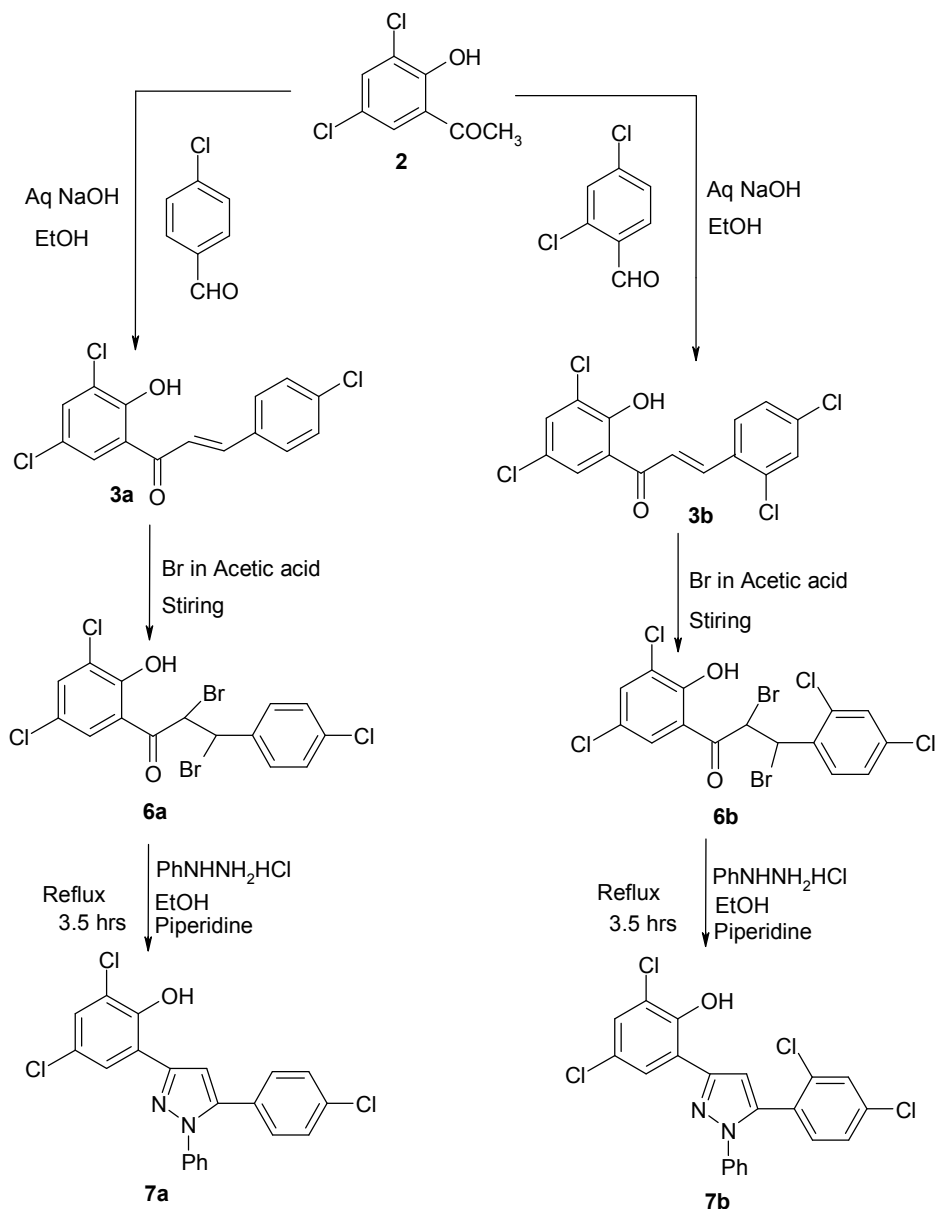
Figure
The flow diagram of the pyrazole synthesis

Table 1
Physical data of the synthesized compounds

Sr. No.	Name of the compounds	M.P. °C	R f value (solvent CCl$_4$)
1	2	93	0.84
2	3a	215	0.62
3	3b	176	0.66
4	6a	190	0.71
5	6b	170	0.78
6	7a	170	0.70
7	7b	270	0.75

Antimicrobial activity
Antimicrobial activities of all synthesized compounds were determined by cup plate method. All plant pathogens were purchased from NCIM, Pune, Institute of Microbial Technology, Chandigarh and Plant pathology department ICAR New Delhi. The agar medium and PDA were purchased from Hi- media lab. Mumbai. The stock solution of test 1000µg/ml were prepared by dissolving appropriate quantities of test compounds in DMSO, The stock inoculums of the microbes was prepared by the inoculation the 5o ml nutrient broth with test organisms and incubating it at 37 ± 2^0C for 24 hrs. The sterilized nutrient agar medium was pour into the petridishes an allowed to solidify. The lawn of the culture was prepared spreading the microbial suspension on the surface of the medium with the help of sterilized triangular loop. Petri dishes were allowed to remain for 10 min, after which excess of nutrient broth cultures was taken out aseptically using pasture pipettes. Standard 8 mm size cup was then prepared in the solidified medium with the help of pre sterilized steel cylinder of 8 mm diameter. The wells were then filled with the 0.5ml stock solution of the test compounds, controls were run using DMSO solvent. All the plates were then incubated at 37±20C for 24, and 48 hrs. The zones of inhibition were recorded by using Himedia scale[10-12].

Table 2
Antimicrobial screening of the synthesized compounds.

S. No.	Name of the compounds	Zone of Inhibition (mm)			
		Xanthomonas Campestris	*Alternaria Macrospora*	*Fusarium Spp.*	*Pseudomonas syringae*
1	2	17	12	22	23
2	3a	---	12	15	15
3	3b	12	15	15	19
4	6a	33	26	25	13
5	6b	30	30	18	16
6	7a	---	25	17	14
7	7b	16	18	11	11

RESULTS AND DISCUSSIONS

The structures of synthesized heterocyclic compounds were confirmed by UV, IR and NMR data. The synthesized heterocyclic compounds have tested for their antimicrobial activity against some plant pathogens. Viz. *Xanthomonas Campestris, Alternari Macrospora, Fusarium Spp.Pseudomonas syringae.*The result from table no.2 shows that the synthesized pyrazoles have varying degree of inhibition against the entire three microorganisms but showed the excellent activity against *Alternaria Macrospora.*

CONCLUSION

We have synthesized some chalcones, possessing one –OH group and convert them into chalcone dibromides. Finaly pyrazoles were prepared from these chalcone dibromides. The antimicrobial screening of pyrazoles were found to be effective against some plant pathoges.

ACKNOWLEDGMENT

REFERENCES

1. Bansal R. K, Heterocyclic Chemistry, 4th edition.New age international publishers, New Delhi, 443, (2005).
2. Cheng C.C., Edward F., Elslager L. M., Werbel W. R., Leopold III, Synthesis and antineoplastic activity of 3-(2-chloroethyl)-3,4-dihydro-4-oxopyrazole [5 1-d] -1, 2, 3, 5- tetrazine-8-carboxamide and rerlated compounds: *J Med Chem*, 12, (545), (1969).
3. Kedar R. M, Vidhale N. N, Chincholkar M. M ,Synthesis of new heterocycles and their antimicrobial activity*: Orient J Chem*, 13, 143, (1997).
4. Sahu S. K., Banarjee M., Samantray A., Behera, C. and Azam M. A., Synthesis, analgesic, Anti-inflammatory and antimicrobial Activities of Some Novel Pyrazoline derivatives: *Trop J Pharm Res,* 7, 2, (2008).
5. Lee K. Y., Kimand J. M., Kim J. N., synthesis of heterocyclic compounds by using the Baylis-Hillman adducts: *Tetrahedron Lett.,* 44, 6737,(2003).
6. Singh A., Rathod S., Berad B. N., Patil S. D., Doshi, Synthesis and structural studies of some mixed ligand transition metal complexes of histidine and adenine or guanine: *A. J. Orient J Chem.,*16, 315, (2000).
7. Abidand M., Azam A., Synthesis, characterization and antiamoebic activity of 1-(thiazolo[4,5-b]quinoxaline-2-yl)-3-phenyl-2-pyrazoline derivatives: *Biorg Med Chem Lett.,* 16, (10), 2812,(2006).
8. Yan Li, Zang, H. Q, Liu J, Yang X. P, Liu Z. J, Stereoselective synthesis and antifungal activity of E-α-(methoxyimina) benzeneacetate derivatives containing 1, 3, 5- substituted pyrazole ring: *J. Agric. Food. Chem,* 54, (10), 3636-3640, (2006)
9. Lee K. Y., Kim J. M, Regioselective synthesis of 1, 2, 3, 5- tetrasubstituted pyrazoles from baylis-Hillman adducts. *Tetrahedron Lett.,* 44, 6737, (2003).
10. Li JX, Xub B, Chai Q, Liu ZX, Zhao APand Chan LB., Antihypertansive Effect of Total Flavonoid fraction of Astragalus complanatus in Hypertensive Rats: *Chin. J. Physiol.*, 48, 101-106,(2005).
11. Inoue T, Sugimoto Y, Masuda H and Kamei C., Antiallergic Effect of Flavonoid Glycosides obtained from *Mentha piperita L.: Biol. Pharm. Bull,.*25: 256-259, (2002).
12. Malpani M. O. and Rajput P.R., Phytochemical screening ,characterization and in vitro antimicrobial activity of beutea monosperma flower, leaves and gum: methanolic and aquous extract. *Int. J. Pharm. Bio. Sci.*, 4, (2): 427 – 430, 2013.

Microwave Assisted Solvent Free Synthesis of 2,7-(Substituted Phenyl)- 3-Phenyl-5,7,7A-Trihydro-2H-Thiazolo [4,5-D] [1,3] Thiazin-5-Amine Derivatives

SONAL D.BOOB AND P.R. SOLANKI

Vidyabharti Mahavidyalaya, Camp Amravati, (MS) India 444601
Corresponding author: sonal.mundhada@gmail.com

Abstract

Synthesis of Novel 2,7-(substituted phenyl)- -3-phenyl-5,7,7a-trihydro-2H-thiazolo [4,5-d] [1,3] thiazin-5-amine(Va-Vh) by condensation of 2-(substituted phenyl)-3-phenyl thiazolidin-4-one (IVa-IVh) with excess of aromatic aldehyde and thiourea dissolved in polar solvent. In vitro assay of newly synthesized compound were carried out to test antifungal activity by disc diffusion method against Fusarium oxysporum and Rhizoctonia solani. All synthesized compounds were characterized by UV.IR, ^{1}HNMR, ^{13}C NMR, spectral and elemental analysis.

Keywords- Thiazolidione, Thiazolo-Thiazine, Antifungal Activity

Introduction-:

Chemistry nowadays is at fore front of the development of clean production processes and products. Chemistry is no doubt determinant to understand and protect our environment, as the world's future is strongly dependant on the chemical processes adopted. Chemistry plays an integral part of our lives. Sustainability, eco-friendly and green chemistry are new principles that are guiding the development of next generation of products and processes[1,2]. "Green chemistry is considered an essential piece of a comprehensive program to protect human health and the environment." In its essence green chemistry[3-8] is a science based non-regulatory and economically driven approach to achieving the goals of environmental protection and sustainable development. Thiazoles are a familiar group of heterocyclic compounds possessing wide variety of biological activities, and their usefulness as medicines are well established. Thiazole nucleus is also an integral part of all the available penicillin's, which have revolutionized the therapy of bacterial diseases[9]. Thiazoles have attracted continuing interest because of their varied biologicalactivities[10], which have found applications in the treatment of allergies[11], hypertension[12], inflammation[13], schizophrenia[14]microbial infections[15-16], HIV infections[17], hypnotics[18]and for the treatment of pain[19]. They have been also used asfibrinogen receptor antagonists with antithrombotic activity[20]and as new inhibitors of bacterial DNA gyrase B[21]. Aldo Andreani reported the synthesis and antitubercular activity of imidazo(2,1-b) thiazoles, Raghav Mishra, Synthesized and studied antimicrobial evaluation of some novel thiazole –pyrazoline derivatives. This has been prompted us to synthesize fused thiazo-thiazine derivatives.

International Journal of Chemical and Physical Sciences, ISSN:2319-6602
IJCPS Vol. 4 Special Issue – NCSC Jan-2015
www.ijcps.org

Material and methods-: All chemicals used were of analytical grade. All the synthesized compounds have been characterized on the basis of chemical properties, elemental and spectral analysis. The melting points were measured in a open glass capillary and are uncorrected **.**IR spectra in KBr were recorded on instrument Perkin Elmer - Spectrum RX-IFTIR. ^{1}H-NMR spectra were recorded on FT NMR Spectrometer model Advance-II (Bruker) Its ^{1}H frequency is 400 MHz. ^{13}C the frequency is 100 MHz. (CDCl$_3$ and DMSO-d$_6$) using TMS as an internal standard All reactions were monitored by TLC using silica gel 60-f-254plates. All reactions were carried out in scientific microwave oven (Scientific microwave system model RG31lL1,700w, 2450MHz).satisfactory C,H,N analysis were carried out for most of the compounds on Thermo Scientific (FLASH 2000) CHN Elemental Analyzer at RSIC, Punjab university, Chandigarh

Synthesis Of 2,7-(Substituted Phenyl)- -3-Phenyl-5,7,7a-Trihydro-2h-Thiazolo [4,5-D] [1,3] Thiazin-5-Amine(Va-h)

The reaction is completed in following two steps.

1)**Synthesis of 2-(substituted phenyl)-3-phenylthiazolidin-4-one(IVa-IVh)**-:A neat rection technology for one pot synthesis of the starting material 2-(substituted phenyl)-3-phenylthiazolidin)-4-one by condensation of aromatic aldehyde(0.01M), aniline(0.01M), and thioglycolic acid(0.01M). carried out under scientific microwave oven. The irradiation time is 1-1.5 min. The reaction mixture was cooled at room temperature and poured in ice-cold water. The product thus separated out was filtered and crystallized from ethanol to get fine crystals of 2-(substituted phenyl)-3-phenylthiazolidin-4-one . (IVa-IVh).

II) Synthesis of 2,7-(substituted phenyl)-3-phenyl-5,7,7a-trihydro-2H-thiazolo [4,5-d] [1,3] thiazin-5 –amine(Va-Vh)-: The synthesis of Novel 2,7-(substituted phenyl)- -3-phenyl-5,7,7a-trihydro-2H-thiazolo [4,5-d] [1,3] thiazin-5-amine(Va-Vh) by condensation of 2-(substituted phenyl)-3-phenyl thiazolidin-4-one.(0.01M) (IVa-IVh) with excess of aromatic aldehyde and thiourea dissolved in polar solvent under microwave mode (1.5 min) followed by filtration, washing with water and recrystallize from ethanol to get the product

Mechanism

Thiazolidione are the potential synthons in the synthesis of heterocyclic compounds. It is noteworthy that the reactivity of thiazolidione is due to inductive effect of carbonyl group. Thiourea is a weak base ,the reason is that the lone pair of electrons on nitrogen are removed in the formation of ∏- molecular orbital. In this mechanism the first step concern with Knoevengel condensation of thiozalidione and aldehyde through carbonium ion intermediate in situ results in the formation of α-β unsaturated ketone and second step involve nucleophilic addition of thiourea followed by cyclodehydration to lead target molecule.
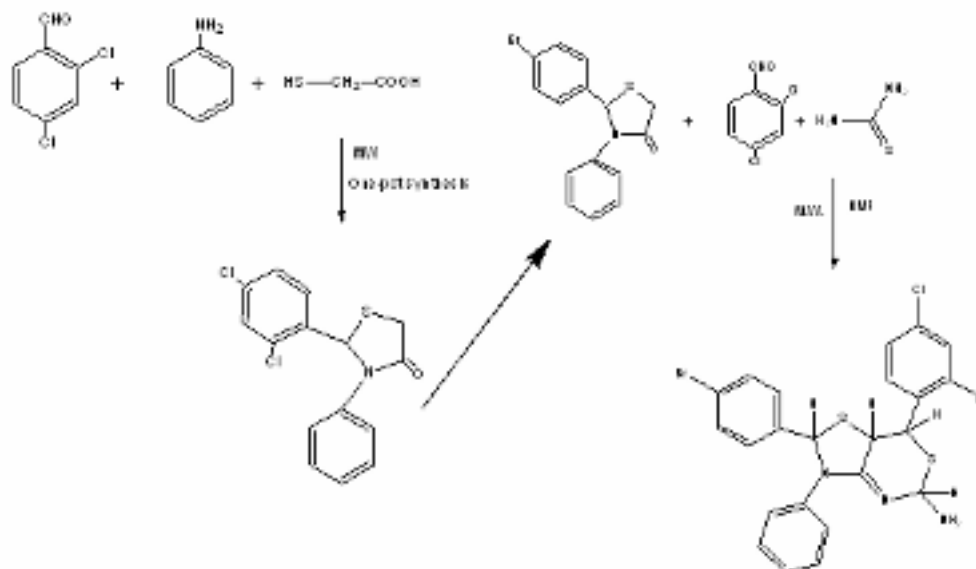
International Journal of Chemical and Physical Sciences, ISSN:2319-6602
IJCPS Vol. 4 Special Issue – NCSC Jan-2015
www.ijcps.org

SCHEME – I Experimental scheme for the synthesis of2,7-(substituted phenyl)-3-phenyl-5,7,7a-trihydro-2H-thiazolo [4,5-d] [1,3] thiazin-5 –amine(Va-Vh) (IVa-h)

SCHEME – II

International Journal of Chemical and Physical Sciences, ISSN:2319-6602
IJCPS Vol. 4 Special Issue – NCSC Jan-2015
www.ijcps.org
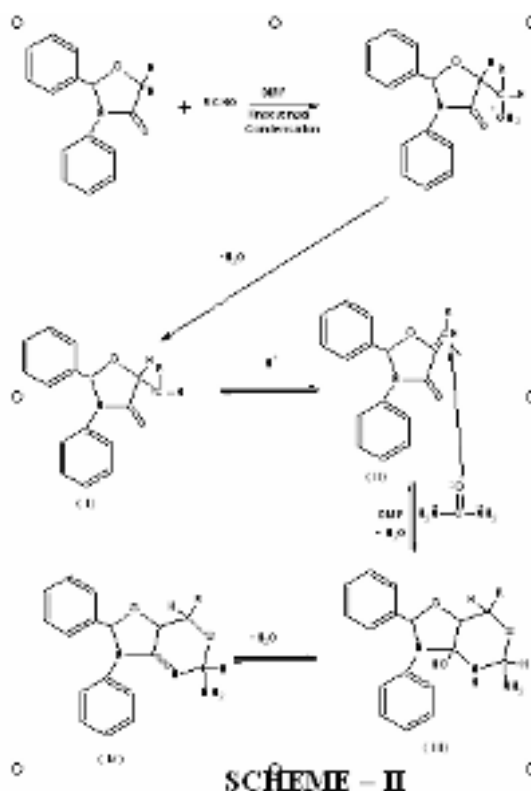
Table I: Physical data of of2,7-(substituted phenyl)-3-phenyl-5,7,7a-trihydro
-2H-thiazolo [4,5-d] [1,3] thiazin-5 –amine(Va-Vh

Compound (Va-Vh)	R	R_1	R_2	*Molecular Formula*	*Melting Point*
a	$-C_6H_5$	$-C_6H_4Cl$	$C_6H_3Cl_2$	$C_{23}H_{18}Cl_3N_3S_2$	265^0C
b	$-C_6H_5$	$-C_6H_4OH$	C_6H_4Br	$C_{23}H_{20}BrN_3OS_2$	270^0C
c	$-C_6H_5$	$-C_6H_4Br$	$C_6H_3Cl_2$	$C_{23}H_{18}BrCl_2N_3S_2$	284^0C
d	$-C_6H_5$	$-C_6H_4-OCH_3$	C_6H_4Br	$C_{24}H_{22}BrN_3OS_2$	264^0C
e	$-C_6H_5$	$-C_6H_4Cl$	$-C_6H_5$	$C_{23}H_{20}ClN_3S_2$	274^0C
f	$-C_6H_5$	$-C_6H_5$	$-C_6H_3Cl_2$	$C_{23}H_{19}Cl_2N_3S_2$	283^0C
g	$-C_6H_5$	$-C_6H_4Br$	$-C_6H_5$	$C_{23}H_{20}BrN_3S_2$	254^0C
h	-C6H5	$-C_6H_5$	$-C_6H_5$	$C_{23}H_{21}N_3S_2$	263^0C

Spectral data

1)2-(4-bromophenyl)- 7-(2,4-dichlorphenyl)3-phenyl-5,7,7a-trihydro-2H-thiazolo [4,5-d] [1,3] thiazin-5 –amine(V c)

M.wt:-551.35 gm, M.P:-284^{0}C, brownish crystalline solid **IR(cm-1):** 3303(-NH$_2$) ,3058[C-H st (aromatic)], 2900[C-Hst (aliphatic)], 1693(C=N), 1618 (N-H bend), 1597 [C=C], 1490 [C-N], 1100 [C-Cl(aryl halide)], 692[N-H wagging] ;**^{1}HNMR:**-400 MHz (CDCl3): 3.3[(s,1H,-CH(W-coupling)],3.5(d,2H,NH2) ,3.6[(S,1H, ,-CH(W-coupling)], 3.8(d,1H,-CH ,J^3-15.7Hz) ,3.9(d,1H,-CH ,J^3-15.7Hz)6.4-8.0(m,12H,Ar-H);^{13}CNMR-100 MHz. (CDCl$_3$ and DMSO-d$_6$) 63.48(C-N,62.79(-CH),32.71(CH)121.07(CNH2),127.97,170.36,130.97,131.35,126.47,137.17,147.7,125.46,128.22,121.37, 139.54,128.67,131.55,137.42,188.74(C=N) calculated %C= 50.10 %N=7.62 %S =11.63 % Br=14.49 % Cl=3.29 % H= 12.86 observed %C= 50.02 %N= 7.12 %S =11.06 % Br= 14.11 % Cl =2.45 % H=12.21

2) **2-(methoxyphenyl)-7-(4-bromophenyl)3-phenyl-5,7,7a-trihydro-2H-thiazolo [4,5-d] [1,3] thiazin-5 –amine(V d)**

M.wt:-511.04 gm, M.P:-264^{0}C, brownish crystalline solid **IR(cm-1):** 3400(-NH assym) ,3258 (NH sym),3058[C-H st (aromatic)], 2940[C-Hst (aliphatic)], 1723(C=N), 1600 (N-H bend), 1625 [C=C], 1444 [C-N], 1067 [C-Br(aryl halide)], 960[N-H wagging] ;**^{1}HNMR:**-400 MHz (CDCl3): 1.28(s,3H,OCH$_3$), 3.6[(s,1H,-CH(W-coupling)],3.37(Br,2H,NH2) ,3.7[(d,1H, ,-CH(W-coupling)], 4.2(d,1H,-CH ,J^3-7.2Hz) ,4.3(d,1H,-CH ,J^3-7.2Hz),7.0-7.7(m,12H,Ar-H);^{13}CNMR-100 MHz.(CDCl$_3$andDMSOd$_6$)63.22(CN),61.29(OCH3),43.14(CH)113.86(CNH2),13.8(CH) ,130.18,128.62,131.99,159.16,138.74,119.23,128.75,123.34,138.83,131.46,131.65,123.52(Ar-CH),167.03(C=N) calculated %C= 56.25 %N=8.20 %S =12.51 % Br=15.59 % O=3.12 % H= 4.33 observed %C= 56.12 %N= 7.98 %S =12.01 % Br= 15.21 % O =2.94 % H=4.33

International Journal of Chemical and Physical Sciences, ISSN:2319-6602
IJCPS Vol. 4 Special Issue – NCSC Jan-2015
www.ijcps.org

Antifungal Activity-: All the synthesized compounds were screened for their antifungal activity viz. *fusarium oxysporum, Rhizoctonia solani* by using disc diffusion method for their antifungal activity.The punch discs of 6.25 mm diameter of Whatman filter paper no. 1 were prepared and dispensed in the batches of 100 each in screw capped bottles. These were sterilized by dry heat at 140^0C for 60 minutes. The solutions of 1000 ppm and 100 ppm concentrations of test compounds were prepared in dimethyl formamide (DMF) solvent separately. The discs were soaked, assuming that each disc will contain approximately 0.01 ml of test solution

Table   2 - In vitro antifungal screening of above tested compounds

Sr.No.	Tested Compounds	Fungus (zone of inhibition in mm)			
		Fusarium oxysporum		*Rhizoctonia solani*	
		100 ppm	1000 ppm	100ppm	1000ppm
1	Va	6	7	-	12
2	Vb	15	17	14	18
3	**Vc**	**32**	**34**	**31**	**34**
4	Vd	26	28	18	20
5	Ve	20	21	16	18
6	Vf	11	12	9	11
7	Vg	17	18	21	26
8	Vh	9	13	8	10

The observations show that activity of compound Vc is maximum against both the fungi . Almost all the compounds were active against all the test pathogens. The compound 5c is the most dominant among all the test compounds. Their inhibitory impact on the bacterial growth is remarkable.

Conclusion

 This was an attempt to synthesize biologically potential heterocyclic moiety in solvent free reaction condition that leads to considerable saving in the reaction time and energetically profiTable. The solvent free condition contributes to saving in cost, time and diminishes the waste disposal problem and environmental pollution this work may bring research fraternity towards sustainable development.

Acknowledgement

References-

[1]. F. Smith, B. Cousins, J. Bozic and W. Flora, Anal-chim-Acta, 177, 243,6,1985.

[2]. J.A. Hesek and R.C. Wilson, Anal. Chem,. 46,1160,1974

[3]. R.A. Nadkarni, Anal. Chem., 56,2233,1984

[4]. M. Bacci, M.Bini, A.Checcucci, A.Ignesti, L. Millanta, N. Rubino and R. Vanni, J. Chem. Soc. Faraday Trans.,1, 77, 1503, 1981

[5]. R.S. Verma, Green Chem., 1,43,1999

[6]. L. Perreux, A. Loupy, Tetrahedron 57,9199,2001

[7]. D. Mathe, Synthesis, 1213, 1998

[8]. R.S. Verma, D. Kumar, Synth. Commun., 29,1333,1999

[9]. S. Onca, M. Punar, H. Erakosy, Chemotherapy 50 (2004) 98e100.

[10]. S.J. Kashyap, V.K. Garg, P.K. Sharma, N. Kumar, R. Dudhe, J.K. Gupta, Med.Chem. Res. 21 (2012) 2123e2132.

[11]. K.D. Hargrave, F.K. Hess, J.T. Oliver, J. Med. Chem. 26 (1983) 1158e1163.

[12]. W.C. Patt, H.W. Hamilton, M.D. Taylor, M.J. Ryan, D.G. Taylor Jr., C.J.C. Connolly, A.M. Doherty, S.R. Klutchko, I. Sircar, B.A. Steinbaugh, B.L. Batley, C.A. Painchaud, S.T. Rapundalo, B.M. Michniewicz, S.C.J. Olso, J. Med. Chem. 35 (1992) 2562e2572.

[13]. R.N. Sharma, F.P. Xavier, K.K. Vasu, S.C. Chaturvedi, S.S. Pancholi, J. Enzym. Inhib.Med. Chem. 24 (2009) 890e897.

[14]. J.C. Jaen, L.D. Wise, B.W. Caprathe, H. Tecle, S. Bergmeier, C.C. Humblet, T.G. Heffner, L.T. Meltzner, T.A. Pugsley, J. Med. Chem. 33 (1990) 311e317.

[15]. K. Omar, A. Geronikoki, P. Zoumpoulakis, C. Camoutsis, M. Sokovic, A. Ciric, J. Glamoclija, Bioorg. Med. Chem. 18 (2010) 426e432.

[16]. K. Liaras, A. Geronikoki, J. Glamoclija, A. Ciric, M. Sokovic, Bioorg. Med. Chem. 9 (2011) 3135e3140.

[17]. F.W. Bell, A.S. Cantrell, M. Hogberg, S.R. Jaskunas, N.G. Johansson, C.L. Jordon,

[18]. M.D. Kinnick, P. Lind, J.M. Morin Jr., R. Noreen, B. Oberg, J.A. Palkowitz,

[19]. C.A. Parrish, P. Pranc, C. Sahlberg, R.J. Ternansky, R.T. Vasileff, L. Vrang,

[20]. S.J. West, H. Zhang, X.X. Zhou, J. Med. Chem. 38 (1995) 4929e4936.

[21]. N. Ergenc, G. Capan, N.S. Gunay, S. Ozkirimli, M. Gungor, S. Ozbey, E. Kendi,

[22]. Arch. Pharm. Pharm. Med. Chem. 332 (1999) 343e347.

[23]. J.S. Carter, S. Kramer, J.J. Talley, T. Penning, P. Collins, M.J. Graneto, K. Seibert,

[24]. C. Koboldt, J.Masferrer, B. Zweifel, Bioorg.Med. Chem. Lett. 9 (1999) 1171e1174.

[25]. A. Badorc, M.F. Bordes, P. De Cointet, P. Savi, A. Bernat, A. Lale, M. Petitou,

[26]. J.P. Maffrand, J.M. Herbert, J. Med. Chem. 40 (1997) 3393e3401.

[27]. J. Rudolph, H. Theis, R. Hanke, R. Endermann, L. Johannsen, F.U. Geschke,J. Med. Chem. 44 (2001) 619e626

ORIGINAL RESEARCH

Antimycobacterial activity and in silico study of highly functionalised dispiropyrrolidines

Ang Chee Wei · Mohamed Ashraf Ali · Yeong Keng Yoon ·
Sy Bing Choi · Hasnah Osman · Vijay H. Masand ·
Tan Soo Choon

Abstract Two series of novel and highly functionalised dispiropyrrolidines were synthesized using 1,3-dipolar cycloaddition reaction. The synthesized compounds were screened for their antimycobacterial activity against *M. tuberculosis* $H_{37}Rv$ using the Promega reagent BacTiter-Glo^{TM} Microbial Cell Viability (BTG). Molecular docking analysis was carried out for the active compounds against the target enzyme enoyl-ACP reductase (InhA) to understand the possible binding mode. Of the 24 novel synthesized compounds, seven dispiropyrrolidines revealed inhibition with EC_{50} <25 μM. Compound **5b** 7′-(4-chlorophenyl)-5′,6′,7′,7a′-tetrahydrodispiro[indan-2,5′-pyrrolo [1,2-*c*]-[1,3]thiazole-6′,2″-indan]-1,3,1″-trione was found to be the most active with EC_{50} of 10.52 μM, and was 2.2-fold more active than cycloserine. The docking result revealed that **5b** had good affinity with the catalytic residues in InhA, forming hydrophobic and mild polar interactions with the important amino acids in the active site.

Keywords Dispiropyrrolidines · 1,3-Dipolar cycloaddition · Antimycobacterial · Enoyl-ACP-reductase · Molecular docking

A. C. Wei (✉) · M. A. Ali · Y. K. Yoon · T. S. Choon
Institute for Research in Molecular Medicine, Universiti Sains
Malaysia, 11800 Minden, Penang, Malaysia
e-mail: cwei_ang@hotmail.com

M. A. Ali
New Drug Discovery Research, Department of Medicinal
Chemistry, Alwar Pharmacy College, Alwar 301030, Rajasthan,
India

M. A. Ali
New Drug Discovery Research, Department of Medicinal
Chemistry, Sunrise University, Alwar 301030, Rajasthan, India

S. B. Choi
School of Industrial Technology, Universiti Sains Malaysia,
11800 Minden, Penang, Malaysia

H. Osman
School of Chemical Sciences, Universiti Sains Malaysia,
11800 Minden, Penang, Malaysia

V. H. Masand
Department of Chemistry, Vidya Bharati College,
Amravati 444 602, Maharashtra, India

Introduction

Tuberculosis (TB) is an airborne disease caused by various strains of mycobacterium, typically *Mycobacterium tuberculosis*. According to the World Health Organization, one-third of the world's population harbors a latent form of TB which is asymptomatic and 10 % of those infected people will develop active TB in their lifetime (Introduction 2008). Despite half of a century of anti-TB chemotherapy, TB still remains the leading infectious disease, especially in the third world countries (Zhang, 2005; Lawn and Zumla, 2011). In 2012, the total number of TB cases worldwide was approximately 8.6 million, causing 1.3 million deaths. India and China alone had accounted for 26 and 12 % of the global burden, respectively (WHO, 2013). The pandemic of AIDS and the emergence of drug-resistant strains in recent years have further complicated this situation (Chiang *et al.*, 2010; Pawlowski *et al.*, 2012). Therefore, it is of utmost importance to discover a new drug candidate to combat this disease.

The current front line TB treatment regimen relies mostly on isoniazid (INH), one of the most effective anti-TB agents that was discovered in 1950s (Mitchison, 2000). INH is a prodrug that requires activation step by KatG, the mycobacterial catalase-peroxidase enzyme, to form a tight INH-NAD covalent adduct (Zhang et al., 1992; Timmins and Deretic, 2006). This active adduct inhibits the biosynthesis of mycolic acids by targeting InhA, the enoyl acyl carrier protein (ACP) reductase in type II fatty acid biosynthesis pathway (Banerjee et al., 1994). Recent studies on drug-resistant strains suggest that the predominant mechanism of INH resistance arises from the mutations in KatG (Musser et al., 1996; Cade et al., 2010). Therefore, compounds that can inhibit the ultimate target of INH by by-passing the KatG activation would have great potential for combating ING-resistant as well as other drug-resistant TB (Kuo et al., 2003).

Pyrrolidines have drawn considerable attention lately due to their highly pronounced biological activities (Crooks and Rosenberg, 1978; Bellina and Rossi, 2006; Stylianakis et al., 2003). They make the central skeleton of many natural products, such as Tryprostatin A, (Usui et al., 1998), elacomine (Pellegrini et al., 1996), and broussonetine H (Brimble et al., 2003). Construction of the substituted pyrrolidines with spiro moiety was achieved through 1,3-dipolar cycloaddition. This reaction, also known as the Huisgen cycloaddition, is a classical method to build various highly substituted five-membered heterocycles (Tsuge and Kanemasa, 1989). Our previous studies have utilized the chemistry of this cycloaddition between azomethine ylides with cyclic ketones to form different series of dispiropyrrolidines (Wei et al., 2012b, 2013). Since the previous results shown promising antimycobacterial activity, herein our group further investigated the potential of a new series of dispiropyrrolidines using in vitro and in silico studies.

Materials and methods

Chemistry

All the chemicals and reagents were purchased from Sigma-Aldrich Chemical Co. and E.Merck (Germany). Thin layer chromatography (TLC) was performed on pre-coated silica gel aluminum plates (Kieselgel 60, 254, E. Merck, Germany). ^{1}H and ^{13}C NMR were performed on Bruker Avance 300 (^{1}H: 300 MHz, ^{13}C: 75 MHz) spectrometer in CDCl$_3$, using TMS as internal standard. Mass spectra were recorded on Varian 320-MS TQ LC/MS using ESI. Elemental analyses were performed on Perkin Elmer 2400 Series II CHN Elemental Analyzer. X-ray structural

analysis was carried out using Bruker SMART APEXII CCD area-detector diffractometer.

General procedure for synthesis of 2-[(E)-1-(substituted aryl) methylidene]-1-indanone

An equimolar mixture of 1-indanone and various aromatic aldehydes was dissolved in ethanol (10 mL), and 30 % of sodium hydroxide solution (5 mL) was added and stirred at room temperature for 4 h. The mixture was then poured into crushed ice and neutralized with concentrated HCl. The precipitated solid was filtered, washed with water, and re-crystallized from methanol to reveal the titled compounds.

Synthesis of substituted dispiropyrrolidine analogs (5a–5j and 6a–6j)

A mixture of substituted 2-[(E)-1-arylmethylidene]-1-indanone (0.001 mol), ninhydrin or acenaphthenequinone (0.001 mol), and thiazolidine-4-carboxylic acid (0.002 mol) (1:1:2) was dissolved in methanol (10 mL) and refluxed for 4–8 h. After completion of the reaction as evident from TLC, the mixture was poured into iced water (50 mL). The precipitated solid was filtered, washed with water, and purified by either recrystallization or silica gel column chromatography to give the desired products.

7′-Phenyl-5′,6′,7′,7a′-tetrahydrodispiro[indan-2,5′-pyrrolo [1,2-c]-[1,3]thiazole-6′,2″-indan]-1,3,1″-trione (5a) ^{1}H NMR (CDCl$_3$) δ$_H$: 3.09 (d, 1H, J = 18.5 Hz, H-3″), 3.12 (t, J = 5.5 Hz, 1H, H-1′), 3.42 (t, J = 9.5 Hz, 1H, H-1′), 3.67 (d, J = 7.0 Hz, 1H, H-3′), 3.91 (d, J = 17.5 Hz, 1H, H-3″), 4.08 (d, J = 7.0 Hz, 1H, H-3′), 4.51 (d, J = 9.0 Hz, 1H, H-7′), 4.70–4.74 (m, 1H, H-7a′), 7.09–8.02 (m, 13H, Ar–H); ^{13}C NMR (CDCl$_3$) δ$_C$: 30.9 (CH$_2$, C-3″), 36.3 (CH$_2$, C-1′), 50.9 (CH, C-7′), 51.8 (CH$_2$, C-2″), 71.5 (CH$_2$, C-3′), 73.2 (CH, C-7a′), 81.5 (C, C-5′), 122.5 (CH, Ar), 123.9 (CH, Ar), 126.1 (CH, Ar), 126.3 (CH, Ar), 126.4 (CH, Ar), 127.5 (CH, Ar), 128.8 (CH, Ar), 129.1 (CH, Ar), 129.2 (CH, Ar), 133.5 (CH, Ar), 133.6 (CH, Ar), 135.6 (CH, Ar), 135.7 (CH, Ar), 135.9 (C, Ar), 140.1 (C, Ar), 140.4 (C, Ar), 140.7 (C, Ar), 152.5 (C, Ar), 197.6 (C, C=O), 199.8 (C, C=O), 201.6 (C, C=O). ESI–MS: m/z 452 (M+H)$^+$. Anal. calcd. C$_{28}$H$_{21}$NO$_3$S: C, 74.48; H, 4.69; N, 3.10. Found: C, 74.49; H, 4.75; N, 3.06.

7′-(4-Chlorophenyl)-5′,6′,7′,7a′-tetrahydrodispiro[indan-2,5′-pyrrolo[1,2-c]-[1,3]thiazole-6′,2″-indan]-1,3,1″-trione (5b) ^{1}H NMR (CDCl$_3$) δ$_H$: 3.07 (d, 1H, J = 18.5 Hz, H-3″), 3.11 (t, J = 5.0 Hz, 1H, H-1′), 3.41 (t, J = 9.5 Hz, 1H, H-1′), 3.65 (d, J = 7.5 Hz, 1H, H-3′), 3.91 (d, J = 17.5 Hz, 1H, H-3″), 4.07 (d, J = 7.5 Hz, 1H, H-3′), 4.52

(d, $J = 9.0$ Hz, 1H, H-7′), 4.70–4.73 (m, 1H, H-7a′), 7.08–8.01 (m, 12H, Ar–H); ^{13}C NMR (CDCl$_3$) δ_C: 30.9 (CH$_2$, C-3″), 36.2 (CH$_2$, C-1′), 50.8 (CH, C-7′), 51.8 (C, C-2″), 71.5 (CH$_2$, C-3′), 73.1 (CH, C-7a′), 81.5 (C, C-5′), 122.5 (CH, Ar), 123.1 (CH, Ar), 123.5 (CH, Ar), 126.5 (CH, Ar), 127.5 (CH, Ar), 128.6 (CH, Ar), 128.8 (CH, Ar), 130.0 (CH, Ar), 130.0 (CH, Ar), 133.5 (CH, Ar), 133.7 (CH, Ar), 135.6 (C, Ar), 135.7 (CH, Ar), 135.7 (C, Ar), 136.7 (C, Ar), 140.4 (C, Ar), 140.7 (C, Ar), 152.5 (C, Ar), 197.6 (C, C=O), 199.8 (C, C=O), 201.5 (C, C=O). ESI–MS: m/z 486 (M+H)$^+$. Anal. calcd. C$_{28}$H$_{20}$ClNO$_3$S: C, 69.20; H, 4.15; N, 2.88. Found: C, 69.26; H, 4.20; N, 2.79.

7′-(4-Bromophenyl)-5′,6′,7′,7a′-tetrahydrodispiro[indan-2,5′-pyrrolo[1,2-c]-[1,3]thiazole-6′,2″-indan]-1,3,1″-trione (5c) ^{1}H NMR (CDCl$_3$) δ_H: 3.06 (d, 1H, $J = 18.5$ Hz, H-3″), 3.11 (t, $J = 5.0$ Hz, 1H, H-1′), 3.42 (t, $J = 9.5$ Hz, 1H, H-1′), 3.60 (d, $J = 7.5$ Hz, 1H, H-3′), 3.91 (d, $J = 17.5$ Hz, 1H, H-3″), 4.06 (d, $J = 7.5$ Hz, 1H, H-3′), 4.52 (d, $J = 9.5$ Hz, 1H, H-7′), 4.69–4.73 (m, 1H, H-7a′), 7.09–8.01 (m, 12H, Ar–H); ^{13}C NMR (CDCl$_3$) δ_C: 30.9 (CH$_2$, C-3″), 36.2 (CH$_2$, C-1′), 50.8 (CH, C-7′), 51.8 (C, C-2″), 71.6 (CH$_2$, C-3′), 76.8 (CH, C7a′), 81.5 (C, C-5′), 119.6 (C, Ar), 122.5 (CH, Ar), 126.5 (CH, Ar), 127.5 (CH, Ar), 128.6 (CH, Ar), 128.8 (CH, Ar), 130.3 (CH, Ar), 130.4 (CH, Ar), 130.4 (CH, Ar), 130.6 (CH, Ar), 133.5 (CH, Ar), 133.7 (CH, Ar), 135.7 (CH, Ar), 136.7 (C, Ar), 139.9 (C, Ar), 140.4 (C, Ar), 140.7 (C, Ar), 152.5 (C, Ar), 197.6 (C, C=O), 199.8 (C, C=O), 201.5 (C, C=O). ESI–MS: m/z 531 (M+H)$^+$. Anal. calcd. C$_{28}$H$_{20}$BrNO$_3$S: C, 63.40; H, 3.80; N, 2.64. Found: C, 63.31; H, 3.82; N, 2.60.

7′-(4-Trifluoromethylphenyl)-5′,6′,7′,7a′-tetrahydrodispiro [indan-2,5′-pyrrolo[1,2-c]-[1,3]thiazole-6′,2″-indan]-1,3,1″-trione (5d) ^{1}H NMR (CDCl$_3$) δ_H: 3.05 (d, 1H, $J = 18.0$ Hz, H-3″), 3.12 (t, $J = 5.0$ Hz, 1H, H-1′), 3.42 (t, $J = 9.5$ Hz, 1H, H-1′), 3.60 (d, $J = 7.5$ Hz, 1H, H-3′), 3.91 (d, $J = 17.5$ Hz, 1H, H-3″), 4.06 (d, $J = 7.5$ Hz, 1H, H-3′), 4.52 (d, $J = 9.5$ Hz, 1H, H-7′), 4.69–4.74 (m, 1H, H-7a′), 7.07–8.01 (m, 12H, Ar–H); ^{13}C NMR (CDCl$_3$) δ_C: 30.9 (CH$_2$, C-3″), 36.2 (CH$_2$, C-1′), 50.8 (CH, C-7′), 51.9 (C, C-2″), 71.5 (CH$_2$, C-3′), 76.8 (CH, C-7a′), 81.5 (C, C-5′), 122.5 (CH, Ar), 123.2 (CF$_3$, Ar), 123.7 (CH, Ar), 123.9 (CH, Ar), 125.1 (C, Ar), 126.5 (CH, Ar), 127.5 (CH, Ar), 127.6 (CH, Ar), 128.8 (CH, Ar), 129.1 (CH, Ar), 129.1 (CH, Ar), 133.5 (CH, Ar), 133.6 (CH, Ar), 135.7 (CH, Ar), 136.7 (C, Ar), 140.4 (C, Ar), 140.7 (C, Ar), 144.1 (C, Ar), 152.6 (C, Ar), 197.6 (C, C=O), 199.9 (C, C=O), 201.5 (C, C=O). ESI–MS: m/z 520 (M+H)$^+$. Anal. calcd. C$_{29}$H$_{20}$F$_3$NO$_3$S: C, 67.04; H, 3.88; N, 2.70. Found: C, 67.01; H, 3.82; N, 2.66.

7′-(4-Trifluoromethoxylphenyl)-5′,6′,7′,7a′-tetrahydrodispiro[indan-2,5′-pyrrolo[1,2-c]-[1,3]thiazole-6′,2″-indan]-1,3,1″-trione (5e) ^{1}H NMR (CDCl$_3$) δ_H: 3.06 (d, 1H, $J = 17.9$ Hz, H-3″), 3.10 (t, $J = 5.2$ Hz, 1H, H-1′), 3.40 (t, $J = 9.8$ Hz, 1H, H-1′), 3.65 (d, $J = 7.6$ Hz, 1H, H-3′), 3.88 (d, $J = 17.5$ Hz, 1H, H-3″), 4.05 (d, $J = 7.6$ Hz, 1H, H-3′), 4.51 (d, $J = 9.0$ Hz, 1H, H-7′), 4.69–4.74 (m, 1H, H-7a′), 7.01–8.00 (m, 12H, Ar–H); ^{13}C NMR (CDCl$_3$) δ_C: 30.9 (CH$_2$, C-3″), 36.2 (CH$_2$, C-1′), 50.8 (CH, C-7′), 51.9 (C, C-2″), 71.5 (CH$_2$, C-3′), 76.8 (CH, C-7a′), 81.5 (C, C-5′), 114.2 (CH, Ar), 114.3 (CH, Ar), 122.1 (CH, Ar), 122.1 (CH, Ar), 122.5 (CH, Ar), 126.6 (CH, Ar), 127.5 (OCF$_3$, Ar), 128.9 (CH, Ar), 129.4 (CH, Ar), 129.5 (CH, Ar), 133.5 (CH, Ar), 133.6 (CH, Ar), 135.2 (C, Ar), 135.7 (CH, Ar), 136.5 (C, Ar), 140.4 (C, Ar), 140.7 (C, Ar), 146.1 (C, Ar), 152.5 (C, Ar), 197.6 (C, C=O), 199.9 (C, C=O), 201.5 (C, C=O). ESI–MS: m/z 536 (M+H)$^+$. Anal. calcd. C$_{29}$H$_{20}$F$_3$NO$_4$S: C, 65.04; H, 3.76; N, 2.62. Found: C, 65.07; H, 3.81; N, 2.60.

7′-(3-Nitrophenyl)-5′,6′,7′,7a′-tetrahydrodispiro[indan-2,5′-pyrrolo[1,2-c]-[1,3]thiazole-6′,2″-indan]-1,3,1″-trione (5f) ^{1}H NMR (CDCl$_3$) δ_H: 3.07 (d, 1H, $J = 18.5$ Hz, H-3″), 3.11 (t, $J = 5.5$ Hz, 1H, H-1′), 3.41 (t, $J = 9.5$ Hz, 1H, H-1′), 3.65 (d, $J = 7.5$ Hz, 1H, H-3′), 3.91 (d, $J = 17.5$ Hz, 1H, H-3″), 4.07 (d, $J = 7.5$ Hz, 1H, H-3′), 4.52 (d, $J = 9.0$ Hz, 1H, H-7′), 4.70–4.73 (m, 1H, H-7a′), 7.06–8.11 (m, 12H, Ar–H); ^{13}C NMR (CDCl$_3$) δ_C: 30.1 (CH$_2$, C-3″), 36.2 (CH$_2$, C-1′), 50.9 (CH, C-7′), 51.8 (C, C-2″), 71.5 (CH$_2$, C-3′), 76.5 (CH, C-7a′), 81.5 (C, C-5′), 117.9 (CH, Ar), 122.5 (CH, Ar), 122.6 (CH, Ar), 123.1 (CH, Ar), 123.2 (CH, Ar), 126.5 (CH, Ar), 127.5 (CH, Ar), 128.8 (CH, Ar), 133.5 (CH, Ar), 133.7 (CH, Ar), 135.7 (CH, Ar), 135.7 (CH, Ar), 136.2 (C, Ar), 140.4 (C, Ar), 140.7 (C, Ar), 141.5 (C, Ar), 146.7 (C, Ar), 152.5 (C, Ar), 197.6 (C, C=O), 199.8 (C, C=O), 201.5 (C, C=O). ESI–MS: m/z 497 (M+H)$^+$. Anal. calcd. C$_{28}$H$_{20}$N$_2$O$_5$S: C, 67.73; H, 4.06; N, 5.64. Found: C, 67.76; H, 4.10; N, 5.69.

7′-(4-Methoxyphenyl)-5′,6′,7′,7a′-tetrahydrodispiro[indan-2,5′-pyrrolo[1,2-c]-[1,3]thiazole-6′,2″-indan]-1,3,1″-trione (5g) ^{1}H NMR (CDCl$_3$) δ_H: 3.07 (d, 1H, $J = 18.5$ Hz, H-3″), 3.11 (t, $J = 5.5$ Hz, 1H, H-1′), 3.41 (t, $J = 9.5$ Hz, 1H, H-1′), 3.65 (d, $J = 7.5$ Hz, 1H, H-3′), 3.69 (s, 3H, OCH$_3$), 3.91 (d, $J = 17.5$ Hz, 1H, H-3″), 4.07 (d, $J = 7.5$ Hz, 1H, H-3′), 4.52 (d, $J = 9.0$ Hz, 1H, H-7′), 4.70–4.73 (m, 1H, H-7a′), 6.67–8.00 (m, 12H, aromatic); ^{13}C NMR (CDCl$_3$) δ_C: 30.9 (CH$_2$, C-3″), 36.2 (CH$_2$, C-1′), 50.9 (CH, C-7′), 51.9 (C, C-2″), 54.3 (CH$_3$, OCH$_3$), 71.8, (CH$_2$, C-3′), 73.4 (CH, C-7a′), 81.7 (C, C-5′), 112.2 (CH, Ar), 112.3 (CH, Ar), 122.5 (CH, Ar), 123.7 (CH, Ar), 126.4 (CH, Ar), 127.5 (CH, Ar), 128.9 (CH, Ar), 129.4 (CH, Ar), 129.4 (CH, Ar), 133.5 (CH, Ar), 133.7 (CH, Ar), 135.6 (C, Ar),

135.7 (CH, Ar), 136.0 (C, Ar), 140.4 (C, Ar), 140.7 (C, Ar), 152.5 (C, Ar), 156.7 (C, Ar), 197.6 (C, C=O), 199.8 (C, C=O) 201.5 (C, C=O). ESI–MS: m/z 482 (M+H)$^+$. Anal. calcd. $C_{29}H_{23}NO_4S$: C, 72.33; H, 4.81; N, 2.91. Found: C, 72.36; H, 4.81; N, 2.95.

7′-(4-Benzo[d][1,3]dioxole)-5′,6′,7′,7a′-tetrahydrodispiro [indan-2,5′-pyrrolo[1,2-c]-[1,3]thiazole-6′,2″-indan]-1,3,1″-trione (5h) ^{1}H NMR (CDCl$_3$) δ$_H$: 3.04–3.07 (m, 1H, H-1′), 3.09 (d, J = 18.0 Hz, 1H, H-3″), 3.43 (t, J = 9.0 Hz, 1H, H-1′), 3.67–3.71 (m, 2H, H-3′, H-3″), 4.07 (d, J = 7.5 Hz, 1H, H-3′), 4.53 (d, J = 8.5 Hz, 1H, H-7′), 4.79–4.84 (m, 1H, H-7a′), 5.95 (s, 2H, CH$_2$), 7.05–8.00 (m, 11H, H–Ar); ^{13}C NMR (CDCl$_3$) δ$_C$: 32.1 (CH$_2$, C-3″), 36.2 (CH$_2$, C-1′), 50.9 (CH, C-7′), 51.8 (C, C-2″), 71.2 (CH$_2$, C-3′), 73.6 (CH, C-7a′), 81.5 (C, C-5′), 101.4 (CH$_2$, OCH$_2$O), 109.3 (CH, Ar), 119.2 (CH, Ar), 121.2 (CH, Ar), 122.5 (CH, Ar), 123.0 (CH, Ar), 123.1 (CH, Ar), 126.5 (CH, Ar), 127.5 (CH, Ar), 134.9 (C, Ar), 135.2 (CH, Ar), 135.2 (CH, Ar), 135.7 (CH, Ar), 136.7 (C, Ar), 140.5 (C, Ar), 140.7 (C, Ar), 145.7 (C, Ar), 147.0 (C, Ar), 153.1 (C, Ar), 197.9 (C, C=O), 199.2 (C, C=O), 201.5 (C, C=O). ESI–MS: m/z 496 (M+H)$^+$. Anal. calcd. $C_{29}H_{21}NO_5S$: C, 70.29; H, 4.27; N, 2.83. Found: C, 70.41; H, 4.31; N, 2.85.

7′-(4-(Dimethylamino)phenyl)-5′,6′,7′,7a′-tetrahydrodispiro[indan-2,5′-pyrrolo[1,2-c]-[1,3]thiazole-6′,2″-indan]-1,3,1″-trione (5i) ^{1}H NMR (CDCl$_3$) δ$_H$: 2.90 (s, 6H), 3.07 (d, 1H, J = 18.0 Hz, H-3″), 3.09 (t, J = 5.5 Hz, 1H, H-1′), 3.43 (t, J = 9.5 Hz, 1H, H-1′), 3.67 (d, J = 7.5 Hz, 1H, H-3′), 3.91 (d, J = 17.5 Hz, 1H, H-3″), 4.07 (d, J = 7.5 Hz, 1H, H-3′), 4.53 (d, J = 8.5 Hz, 1H, H-7′), 4.84–4.90 (m, 1H, H-7a′), 6.62–8.19 (m, 12H, H–Ar); ^{13}C NMR (CDCl$_3$) δ$_C$: 31.9 (CH$_2$, C-3″), 36.2 (CH$_2$, C-1′), 40.2 (CH$_3$, N(CH$_3$)$_2$), 40.4 (CH$_3$, N(CH$_3$)$_2$), 50.9 (CH, C-7′), 51.8 (C, C-2″), 71.2 (CH$_2$, C-3′), 73.1 (CH, C-7a′), 81.5 (C, C-5′), 111.9 (CH, Ar), 112.1 (CH, Ar), 123.0 (CH, Ar), 123.4 (CH, Ar), 123.6 (CH, Ar), 126.5 (CH, Ar), 127.5 (CH, Ar), 130.2 (CH, Ar), 130.3 (CH, Ar), 131.2 (C, Ar), 135.4 (CH, Ar), 135.5 (CH, Ar), 135.7 (CH, Ar), 136.7 (C, Ar), 140.5 (C, Ar), 140.7 (C, Ar), 147.5 (C, Ar), 152.9 (C, Ar), 197.9 (C, C=O), 199.7 (C, C=O), 201.5 (C, C=O). ESI–MS: m/z 495 (M+H)$^+$. Anal. calcd. $C_{30}H_{26}N_2O_3S$: C, 72.85; H, 5.30; N, 5.66. Found: C, 72.97; H, 5.31; N, 5.65.

7′-(4-(Morpholine-1-yl)phenyl)-5′,6′,7′,7a′-tetrahydrodispiro[indan-2,5′-pyrrolo[1,2-c]-[1,3]thiazole-6′,2″-indan]-1,3,1″-trione (5j) ^{1}H NMR (CDCl$_3$) δ$_H$: 3.05 (d, 1H, J = 17.5 Hz, H-3″), 3.10 (t, J = 5.5 Hz, 1H, H-1′), 3.12 (t, J = 9.0 Hz, 4H, CH$_2$), 3.43 (t, J = 9.5 Hz, 1H, H-1′), 3.67 (d, J = 7.5 Hz, 1H, H-3′), 3.87 (t, J = 9.0 Hz, 4H, CH$_2$), 3.90 (d, J = 17.5 Hz, 1H, H-3″), 4.07 (d, J = 7.5 Hz, 1H, H-3′), 4.53 (d, J = 8.5 Hz, 1H, H-7′), 4.79–4.82 (m, 1H,

H-7a′), 6.69–8.19 (m, 12H, H–Ar); ^{13}C NMR (CDCl$_3$) δ$_C$: 31.9 (CH$_2$, C-3″), 36.3 (CH$_2$, C-1′), 49.2 (CH$_2$, NCH$_2$), 49.3 (CH$_2$, NCH$_2$), 50.9 (CH, C-7′), 51.8 (C, C-2″), 69.5 (CH$_2$, OCH$_2$), 69.5 (CH$_2$, OCH$_2$), 71.2 (CH$_2$, C-3′), 73.1 (CH, C-7a′), 81.5 (C, C-5′), 116.7 (CH, Ar), 116.9 (CH, Ar), 123.0 (CH, Ar), 123.5 (CH, Ar), 124.1 (CH, Ar), 126.1 (CH, Ar), 127.0 (CH, Ar), 130.0 (CH, Ar), 130.1 (CH, Ar), 131.2 (C, Ar), 135.4 (CH, Ar), 135.5 (CH, Ar), 135.7 (CH, Ar), 136.7 (C, Ar), 140.6 (C, Ar), 140.7 (C, Ar), 146.1 (C, Ar), 152.9 (C, Ar), 197.9 (C, C=O), 199.7 (C, C=O), 201.5 (C, C=O). ESI–MS: m/z 537 (M+H)$^+$. Anal. calcd. $C_{32}H_{28}N_2O_4S$: C, 71.62; H, 5.26; N, 5.22. Found: C, 71.70; H, 5.31; N, 5.25.

7′-(2,5-Dimethoxylphenyl)-5′,6′,7′,7a′-tetrahydrodispiro[indan-2,5′-pyrrolo[1,2-c]-[1,3]thiazole-6′,2″-indan]-1,3,1″-trione (5k) ^{1}H NMR (CDCl$_3$) δ$_H$: 3.04–3.07 (m, 1H, H-1′), 3.21 (d, J = 17.5 Hz, 1H, H-3″), 3.38 (s, 3H, OCH$_3$), 3.45 (t, J = 9.5 Hz, 1H, H-1′), 3.64–3.70 (m, 2H, H-3′), 3.70 (s, 3H, OCH$_3$), 4.08 (d, J = 7.5 Hz, 1H, H-3″), 4.69 (d, J = 8.5 Hz, 1H, H-7′), 4.81–4.86 (m, 1H, H-7a′), 7.00–8.13 (m, 11H, Ar–H); ^{13}C NMR (CDCl$_3$) δ$_C$: 32.1 (CH$_2$, C-3″), 36.6 (CH$_2$, C-1′), 49.4 (CH, C-7′), 50.9 (C, C-2″), 54.5 (CH$_3$, OCH$_3$), 55.8 (CH$_3$, OCH$_3$), 71.5 (CH$_2$, C-3′), 73.0 (CH, C-7a′), 80.2 (C, C-5′), 110.1 (CH, Ar), 112.5 (CH, Ar), 115.8 (CH, Ar), 122.9 (CH, Ar), 123.0 (CH, Ar), 123.0 (CH, Ar), 124.2 (CH, Ar), 125.9 (C, Ar), 126.8 (CH, Ar), 134.8 (CH, Ar), 135.2 (CH, Ar), 135.9 (CH, Ar), 136.8 (C, Ar), 140.5 (C, Ar), 142.6 (C, Ar), 151.5 (C, Ar), 152.0 (C, Ar), 153.1 (C, Ar), 197.9 (C, C=O), 199.0 (C, C=O), 200.9 (C, C=O). ESI–MS: m/z 512 (M+H)$^+$. Anal. calcd. $C_{30}H_{25}NO_5S$: C, 70.43; H, 4.93; N, 2.74. Found: C, 70.49; H, 5.01; N, 2.77.

7′-(4-(Piperidin-1-yl)phenyl)-5′,6′,7′,7a′-tetrahydrodispiro [indan-2,5′-pyrrolo[1,2-c]-[1,3]thiazole-6′,2″-indan]-1,3,1″-trione (5l) ^{1}H NMR (CDCl$_3$): 1.52–1.63 (m, 6H, CH$_2$), 2.67 (t, J = 9.0 Hz, 4H, CH$_2$), 3.07 (d, 1H, J = 18.5 Hz, H-3″), 3.11 (t, J = 5.0 Hz, 1H, H-1′), 3.43 (t, J = 9.0 Hz, 1H, H-1′), 3.67 (d, J = 7.5 Hz, 1H, H-3′), 3.91 (d, J = 17.5 Hz, 1H, H-3″), 4.03 (d, J = 7.5 Hz, 1H, H-3″), 4.51 (d, J = 9.5 Hz, 1H, H-7′), 4.69–4.73 (m, 1H, H-7a′), 7.08–8.01 (m, 12H, Ar–H); ^{13}C NMR (CDCl$_3$) δ$_C$: 23.9 (CH$_2$), 24.4 (CH$_2$), 24.6 (CH$_2$), 32.1 (CH$_2$, C-3″), 36.7 (CH$_2$, C-1′), 49.3 (CH, C-7′), 50.4 (CH$_2$, NCH$_2$), 50.9 (CH$_2$, NCH$_2$), 52.9 (C, C-2″), 71.4 (CH$_2$, C-3′), 73.0 (CH, C-7a′), 80.3 (C, C-5′), 112.7 (CH, Ar), 112.8 (CH, Ar), 122.9 (CH, Ar), 123.0 (CH, Ar), 123.0 (CH, Ar), 124.3 (CH, Ar), 126.5 (CH, Ar), 128.4 (CH, Ar), 129.0 (CH, Ar), 130.7 (C, Ar), 134.1 (CH, Ar), 134.7 (CH, Ar), 135.4 (CH, Ar), 136.8 (C, Ar), 140.5 (C, Ar), 141.7 (C, Ar), 149.1 (C, Ar), 152.9 (C, Ar), 197.9 (C, C=O), 199.0 (C, C=O), 200.9 (C, C=O). ESI–MS: m/z 535 (M+H)$^+$. Anal. calcd. $C_{33}H_{30}N_2O_3S$:

C, 74.13; H, 5.66; N, 5.24. Found: C, 74.16; H, 5.72; N, 5.25.

7′-Phenyl-1′,3′,5′,6′,7′,7a′-hexahydrodispiro[acenaphthyl-ene-1,5′-pyrrolo-[1,2-c]thiazole-6′,2″-indane]-2,1″(1H)-dione (6a) ^{1}H NMR (CDCl$_3$) δ$_H$: 2.91 (d, $J = 16.5$ Hz, 1H, H-3″), 3.13 (dd, $J = 11.4$, 3.0 Hz, 1H, H-1′), 3.34–3.37 (m, 1H, H-1′), 3.67 (d, $J = 10.2$ Hz, 1H, H-3′), 4.03 (d, $J = 16.6$ Hz, 1H, H-3″), 4.06 (d, $J = 10.2$ Hz, 1H, H-3′), 4.27 (d, $J = 10.6$ Hz, 1H, H-7′), 4.73–4.76 (m, 1H, H-7a′), 6.75–8.10 (m, 15H, H–Ar); ^{13}C NMR (CDCl$_3$) δ$_C$: 32.0 (CH$_2$, C-3″), 36.5 (CH$_2$, C-1′), 53.0 (CH, C-7′), 53.9 (CH$_2$, C-3′), 71.4 (CH, C-7a′), 71.9 (C, C-2″), 83.0 (C, C-5′), 120.9 (CH, Ar), 123.1 (CH, Ar), 125.1 (CH, Ar), 125.9 (CH, Ar), 126.3 (CH, Ar), 126.4 (CH, Ar), 126.5 (CH, Ar), 126.6 (CH, Ar), 127.7 (CH, Ar), 127.9 (CH, Ar), 128.0 (CH, Ar), 128.2 (C, Ar), 128.4 (CH, Ar), 130.6 (CH, Ar), 131.5 (CH, Ar), 132.1 (C, Ar), 134.1 (C, Ar), 134.9 (CH, Ar), 136.7 (C, Ar), 137.9 (C, Ar), 142.0 (C, Ar), 151.2 (C, Ar), 202.4 (C, C=O), 204.3 (C, C=O). ESI–MS: *m/z* 474 (M+H)$^+$. Anal. calcd. C$_{31}$H$_{23}$NO$_2$S: C, 78.62; H, 4.90; N, 2.96. Found: C, 78.66; H, 4.89; N, 2.91.

7′-(4-Chlorophenyl)-1′,3′,5′,6′,7′,7a′-hexahydrodispiro[ace-naphthylene-1,5′-pyrrolo-[1,2-c]thiazole-6′,2″-indane]-2,1″(1H)-dione (6b) ^{1}H NMR (CDCl$_3$) δ$_H$: 3.01 (d, $J = 16.5$ Hz, 1H, H-3″), 3.08 (dd, $J = 11.4$, 3.0 Hz, 1H, H-1′), 3.34–3.37 (m, 1H, H-1′), 3.67 (d, $J = 10.2$ Hz, 1H, H-3′), 4.03 (d, $J = 16.6$ Hz, 1H, H-3″), 4.06 (d, $J = 10.2$ Hz, 1H, H-3′), 4.27 (d, $J = 10.6$ Hz, 1H, H-7′), 4.73–4.76 (m, 1H, H-7a′), 6.84–8.12 (m, 14H, H–Ar); ^{13}C NMR (75 MHz, CDCl$_3$): ^{13}C NMR (CDCl$_3$) δ$_C$: 31.9 (CH$_2$, C-3″), 36.1 (CH$_2$, C-1′), 52.1 (CH, C-7′), 53.9 (CH$_2$, C-3′), 71.4 (CH, C-7a′), 71.9 (C, C-2″), 83.0 (C, C-5′), 122.5 (CH, Ar), 123.0 (CH, Ar), 123.4 (CH, Ar), 123.5 (CH, Ar), 123.5 (CH, Ar), 123.9 (CH, Ar), 124.9 (CH, Ar), 126.2 (CH, Ar), 127.1 (CH, Ar), 127.7 (CH, Ar), 130.0 (CH, Ar), 130.1 (C, Ar), 130.6 (CH, Ar), 131.3 (CH, Ar), 132.7 (CH, Ar), 133.6 (C, Ar), 135.4 (C, Ar), 135.6 (C, Ar), 135.7 (C, Ar), 136.7 (C, Ar), 141.0 (C, Ar), 152.0 (C, Ar), 202.4 (C, C=O), 204.3 (C, C=O). ESI–MS: *m/z* 508 (M+H)$^+$. Anal. calcd. C$_{31}$H$_{22}$ClNO$_2$S: C, 73.29; H, 4.36; N, 2.76. Found: C, 73.26; H, 4.41; N, 2.72.

7′-(4-Bromophenyl)-1′,3′,5′,6′,7′,7a′-hexahydrodispiro[ace-naphthylene-1,5′-pyrrolo-[1,2-c]thiazole-6′,2″-indane]-2,1″(1H)-dione (6c) ^{1}H NMR (CDCl$_3$) δ$_H$: 2.88 (d, $J = 16.5$ Hz, 1H, H-3″), 3.08 (dd, $J = 11.5$, 3.0 Hz, 1H, H-1′), 3.30–3.34 (m, 1H, H-1′), 3.67 (d, $J = 9.9$ Hz, 1H, H-3′), 4.00 (d, $J = 16.7$ Hz, 1H, H-3″), 4.05 (d, $J = 10.0$ Hz, 1H, H-3′), 4.28 (d, $J = 10.5$ Hz, 1H, H-7′), 4.88–4.90 (m, 1H, H-7a′), 6.79–8.30 (m, 14H, H–Ar); ^{13}C NMR (CDCl$_3$) δ$_C$: 31.5 (CH$_2$, C-3″), 36.2 (CH$_2$, C-1′), 52.6 (CH, C-7′), 53.6

(CH$_2$, C-3′), 70.9 (CH, C-7a′), 71.3 (C, C-2″), 82.7 (C, C-5′), 120.5 (CH, Ar), 121.5 (C, Ar), 122.8 (CH, Ar), 123.4 (CH, Ar), 123.9 (C, Ar), 125.7 (CH, Ar), 125.7 (CH, Ar), 126.3 (CH, Ar), 127.3 (CH, Ar), 127.6 (CH, Ar), 128.2 (CH, Ar), 130.4 (C, Ar), 131.0 (CH, Ar), 131.2 (CH, Ar), 131.8 (CH, Ar), 131.9 (CH, Ar), 133.5 (C, Ar), 134.8 (CH, Ar), 135.3 (C, Ar), 136.1 (C, Ar), 140.5 (C, Ar), 151.2 (C, Ar), 202.1 (C, C=O), 204.2 (C, C=O). ESI–MS: *m/z* 553 (M+H)$^+$. Anal. calcd. C$_{31}$H$_{22}$BrNO$_2$S: C, 67.39; H, 4.01; N, 2.54. Found: C, 67.36; H, 4.05; N, 2.55.

7′-(4-Trifluoromethylphenyl)-1′,3′,5′,6′,7′,7a′-hexahydrodi-spiro[acenaphthylene-1,5′-pyrrolo-[1,2-c]thiazole-6′,2″-indane]-2,1″(1H)-dione (6d) ^{1}H NMR (CDCl$_3$) δ$_H$: 2.89 (d, 1H, $J = 16.6$ Hz, H-1′), 3.10 (dd, $J = 11.4$, 3.0 Hz, 1H, H-3″), 3.31–3.35 (m, 1H, H-1′), 3.67 (d, $J = 10.0$ Hz, 1H, H-3″), 4.00 (d, $J = 16.6$ Hz, 1H, H-3′), 4.06 (d, $J = 10.0$ Hz, 1H, H-3′), 4.33 (d, $J = 10.6$ Hz, 1H, H-7′), 4.87–4.95 (m, 1H, H-7a′), 7.01–8.30 (m, 14H, H–Ar); ^{13}C NMR (CDCl$_3$) δ$_C$: 32.0 (CH$_2$, C-3″), 36.5 (CH$_2$, C-1′), 53.2 (CH, C-7′), 53.9 (CH$_2$, C-3′), 71.4 (CH, C-7a′), 71.8 (C, C-2″), 82.7 (C, C-5′), 123.5 (CH, Ar), 123.7 (C, CF$_3$), 124.1 (CH, Ar), 126.0 (CH, Ar), 126.2 (CH, Ar), 126.7 (CH, Ar), 127.1 (C, Ar), 127.7 (CH, Ar), 127.9 (CH, Ar), 128.1 (CH, Ar), 128.5 (CH, Ar), 128.6 (CH, Ar), 130.6 (C, Ar), 131.0 (C, Ar), 132.3 (CH, Ar), 133.5 (CH, Ar), 133.7 (CH, Ar), 133.9 (C, Ar), 135.4 (CH, Ar), 136.4 (C, Ar), 141.0 (C, Ar), 144.2 (C, Ar), 151.3 (C, Ar), 202.4 (C, C=O), 204.4 (C, C=O). ESI–MS: *m/z* 542 (M+H)$^+$. Anal. calcd. C$_{32}$H$_{22}$F$_3$NO$_2$S: C, 70.97; H, 4.09; N, 2.59. Found: C, 71.00; H, 4.10; N, 2.55.

7′-(4-Trifluoromethoxyphenyl)-1′,3′,5′,6′,7′,7a′-hexahydro-dispiro[acenaphthylene-1,5′-pyrrolo-[1,2-c]thiazole-6′,2″-indane]-2,1″(1H)-dione (6e) ^{1}H NMR (CDCl$_3$) δ$_H$: 2.88 (d, 1H, $J = 16.6$ Hz, H-3″), 3.10 (dd, $J = 11.4$, 3.0 Hz, 1H, H-1′), 3.32–3.35 (m, 1H, H-1′), 3.67 (d, $J = 10.0$ Hz, 1H, H-3′), 4.00 (d, $J = 16.6$ Hz, 1H, H-3″), 4.06 (d, $J = 10.0$ Hz, 1H, H-3′), 4.32 (d, $J = 10.4$ Hz, 1H, H-7′), 4.87–4.95 (m, 1H, H-7a′), 6.79–8.30 (m, 14H, H–Ar); ^{13}C NMR (CDCl$_3$) δ$_C$: 32.1 (CH$_2$, C-3″), 36.6 (CH$_2$, C-1′), 53.2 (CH, C-7′), 53.9 (CH$_2$, C-3′), 71.4 (CH, C-7a′), 71.8 (C, C-2″), 82.5 (C, C-5′), 114.2 (CH, Ar). 114.3 (CH, Ar), 123.5 (CH, Ar), 124.1 (CH, Ar), 126.0 (CH, Ar), 126.2 (CH, Ar), 126.7 (CH, Ar), 127.9 (CH, Ar), 127.9 (CH, Ar), 128.5 (CH, Ar), 128.9 (C, OCF$_3$), 129.4 (CH, Ar), 129.5 (CH, Ar), 130.6 (C, Ar), 131.0 (C, Ar), 132.3 (CH, Ar), 133.5 (C, Ar), 135.4 (C, Ar), 135.7 (CH, Ar), 136.4 (C, Ar), 141.0 (C, Ar), 146.7 (C, Ar), 151.2 (C, Ar), 202.4 (C, C=O), 204.4 (C, C=O). ESI–MS: *m/z* 558 (M+H)$^+$. Anal. calcd. C$_{32}$H$_{22}$F$_3$NO$_3$S: C, 68.93; H, 3.98; N, 2.51. Found: C, 68.91; H, 4.03; N, 2.53.

7′-(3-Nitrophenyl)-1′,3′,5′,6′,7′,7a′-hexahydrodispiro[ace-naphthylene-1,5′-pyrrolo-[1,2-c]thiazole-6′,2″-indane]-2,1″ (1H)-dione (6f) ^{1}H NMR (CDCl$_3$) δ$_H$: 2.83 (d, 1H, J = 16.8 Hz, H-1′), 3.11 (dd, J = 11.4, 3.3 Hz, 1H, H-3″), 3.34–3.40 (m, 1H, H-1′), 3.71 (d, J = 9.6 Hz, 1H, H-3″), 4.01–4.08 (m, 2H, H-3′), 4.43 (d, J = 10.5 Hz, 1H, H-7′), 4.96–5.02 (m, 1H, H-7a′), 6.82–8.31 (m, 14H, H–Ar); ^{13}C NMR (CDCl$_3$) δ$_C$: 32.1 (CH$_2$, C-3″), 36.5 (CH$_2$, C-1′), 53.1 (CH, C-7′), 53.8 (CH$_2$, C-3′), 71.4 (CH, C-7a′), 71.8 (C, C-2″), 82.8 (C, C-5′), 121.0 (CH, Ar), 123.0 (CH, Ar), 123.4 (CH, Ar), 124.6 (CH, Ar), 126.0 (CH, Ar), 126.2 (CH, Ar), 126.7 (CH, Ar), 127.9 (CH, Ar), 128.0 (CH, Ar), 128.6 (CH, Ar), 130.1 (C, Ar), 130.8 (C, Ar), 131.3 (CH, Ar), 132.4 (CH, Ar), 133.6 (C, Ar), 135.3 (CH, Ar), 136.3 (C, Ar), 136.6 (C, Ar), 139.1 (CH, Ar), 141.0 (C, Ar), 148.8 (C, Ar), 151.2 (C, Ar), 202.4 (C, C=O), 204.4 (C, C=O). ESI–MS: m/z 519 (M+H)$^+$. Anal. calcd. C$_{31}$H$_{22}$N$_2$O$_4$S: C, 71.80; H, 4.28; N, 5.40. Found: C, 71.76; H, 4.32; N, 5.41.

7′-(4-Methoxyphenyl)-1′,3′,5′,6′,7′,7a′-hexahydrodispiro [acenaphthylene-1,5′-pyrrolo-[1,2-c]thiazole-6′,2″-indane]-2,1″(1H)-dione (6g) ^{1}H NMR (CDCl$_3$) δ$_H$: 3.03 (d, 1H, J = 16.8 Hz, H-1′), 3.11 (dd, J = 11.4, 3.3 Hz, 1H, H-3″), 3.34–3.36 (m, 1H, H-1′), 3.69 (s, 3H, OCH$_3$), 3.71 (d, J = 9.6 Hz, 1H, H-3″), 4.01–4.08 (m, 2H, H-3′), 4.26 (d, J = 10.5 Hz, 1H, H-7′), 4.86–4.93 (m, 1H, H-7a′), 6.82–8.31 (m, 14H, H–Ar); ^{13}C NMR (CDCl$_3$) δ$_C$: 31.9 (CH$_2$, C-3″), 36.6 (CH$_2$, C-1′), 51.9 (CH, C-7′), 54.0 (CH$_2$, C-3′), 55.1 (C, OCH$_3$) 71.1 (CH, C-7a′), 71.7 (C, C-2″), 83.0 (C, C-5′), 112.2 (CH, Ar), 112.6 (CH, Ar), 120.9 (CH, Ar), 123.0 (CH, Ar), 123.5 (CH, Ar), 125.7 (CH, Ar), 126.0 (CH, Ar), 126.4 (CH, Ar), 126.7 (CH, Ar), 127.9 (CH, Ar), 129.9 (CH, Ar), 130.1 (CH, Ar), 130.7 (CH, Ar), 131.0 (CH, Ar), 131.9 (C, Ar), 132.1 (C, Ar), 133.9 (C, Ar), 135.4 (C, Ar), 136.3 (C, Ar), 140.4 (C, Ar), 151.5 (C, Ar), 151.9 (C, Ar), 202.4 (C, C=O), 204.5 (C, C=O). ESI–MS: m/z 504 (M+H)$^+$. Anal. calcd. C$_{32}$H$_{25}$NO$_3$S: C, 76.32; H, 5.00; N, 2.78. Found: C, 76.21; H, 5.03; N, 2.79.

7′-(4-Benzo[d][1,3]dioxole)-1′,3′,5′,6′,7′,7a′-hexahydrodi-spiro[acenaphthylene-1,5′-pyrrolo-[1,2-c]thiazole-6′,2″-indane]-2,1″(1H)-dione (6h) ^{1}H NMR (CDCl$_3$) δ$_H$: 3.04 (d, J = 16.8 Hz, 1H, H-3″), 3.13 (dd, J = 11.5, 2.8 Hz, 1H, H-1′), 3.32–3.35 (m, 1H, H-1′), 3.64 (d, J = 10.2 Hz, 1H, H-3′), 4.04 (d, J = 16.6 Hz, 1H, H-3″), 4.09 (d, J = 10.2 Hz, 1H, H-3′), 4.26 (d, J = 10.6 Hz, 1H, H-7′), 4.83–4.87 (m, 1H, H-7a′), 5.95 (s, 2H, CH$_2$), 6.80–8.29 (m, 13H, H–Ar); ^{13}C NMR (CDCl$_3$) δ$_C$: 31.9 (CH$_2$, C-3″), 36.6 (CH$_2$, C-1′), 52.6 (CH, C-7′), 54.1 (CH$_2$, C-3′), 71.4 (CH, C-7a′), 71.7 (C, C-2″), 83.1 (C, C-5′), 101.4 (CH$_2$, OCH$_2$O), 109.3 (CH, Ar), 119.2 (CH, Ar), 120.3 (CH, Ar), 121.0 (CH, Ar), 122.6 (CH, Ar), 123.4 (CH, Ar), 125.5

(CH, Ar), 125.9 (CH, Ar), 126.4 (CH, Ar), 128.1 (CH, Ar), 130.2 (CH, Ar), 130.3 (CH, Ar), 131.8 (C, Ar), 132.8 (CH, Ar), 133.7 (C, Ar), 134.5 (C, Ar), 134.9 (C, Ar), 136.3 (C, Ar), 140.4 (C, Ar), 145.7 (C, Ar), 147.0 (C, Ar), 151.8 (C, Ar), 202.4 (C, C=O), 204.5 (C, C=O). ESI–MS: m/z 518 (M+H)$^+$. Anal. calcd. C$_{32}$H$_{23}$NO$_4$S: C, 74.26; H, 4.48; N, 2.71. Found: C, 74.23; H, 4.53; N, 2.74.

7′-(4-(Dimethylamino)phenyl)-1′,3′,5′,6′,7′,7a′-hexahydro-dispiro[acenaphthylene-1,5′-pyrrolo-[1,2-c]thiazole-6′,2″-indane]-2,1″(1H)-dione (6i) ^{1}H NMR (CDCl$_3$) δ$_H$: 2.87 (s, 6H), 3.04 (d, J = 16.8 Hz, 1H, H-3″), 3.13 (dd, J = 11.5, 2.8 Hz, 1H, H-1′), 3.32–3.35 (m, 1H, H-1′), 3.64 (d, J = 10.2 Hz, 1H, H-3′), 4.04 (d, J = 16.6 Hz, 1H, H-3″), 4.09 (d, J = 10.2 Hz, 1H, H-3′), 4.26 (d, J = 10.6 Hz, 1H, H-7′), 4.87–4.91 (m, 1H, H-7a′), 6.60–8.36 (m, 14H, H–Ar); ^{13}C NMR (CDCl$_3$) δ$_C$: 31.3 (CH$_2$, C-3″) 36.6 (CH$_2$, C-1′), 40.1 (CH$_3$, N(CH$_3$)$_2$), 40.4 (CH$_3$, N(CH$_3$)$_2$), 52.6 (CH, C-7′), 54.1 (CH$_2$, C-3′), 71.1 (CH, C-7a′), 71.7 (C, C-2″), 83.1 (C, C-5′), 111.9 (CH, Ar), 112.4 (CH, Ar), 120.3 (CH, Ar), 122.6 (CH, Ar), 123.4 (CH, Ar), 125.5 (CH, Ar), 125.9 (CH, Ar), 126.4 (CH, Ar), 127.0 (CH, Ar), 127.4 (CH, Ar), 128.1 (CH, Ar), 130.2 (CH, Ar), 130.3 (CH, Ar), 131.1 (C, Ar), 131.8 (C, Ar), 132.8 (CH, Ar), 133.7 (C, Ar), 134.5 (C, Ar), 136.3 (C, Ar), 140.4 (C, Ar), 149.6 (C, Ar), 151.8 (C, Ar), 202.3 (C, C=O), 204.5 (C, C=O). ESI–MS: m/z 517 (M+H)$^+$. Anal. calcd. C$_{33}$H$_{28}$N$_2$O$_2$S: C, 76.72; H, 5.46; N, 5.42. Found: C, 76.66; H, 5.49; N, 5.41.

7′-(4-(Morpholine-1-yl)phenyl)-1′,3′,5′,6′,7′,7a′-hexahyd-rodispiro[acenaphthylene-1,5′-pyrrolo-[1,2-c]thiazole-6′, 2″-indane]-2,1″(1H)-dione (6j) ^{1}H NMR (CDCl$_3$) δ$_H$: 3. 05 (d, 1H, J = 16.6 Hz, H-3″), 3.10 (dd, J = 11.5, 2.8 Hz, 1H, H-1′), 3.15 (t, J = 9.0 Hz, 4H, CH$_2$), 3.32–3.35 (m, 1H, H-1′), 3.67 (d, J = 10.5 Hz, 1H, H-3′), 3.87 (t, J = 9.0 Hz, 4H, CH$_2$), 4.01 (d, J = 16.6 Hz, 1H, H-3″), 4.07 (d, J = 10.0 Hz, 1H, H-3′), 4.26 (d, J = 10.6 Hz, 1H, H-7′), 4.82–4.90 (m, 1H, H-7a′), 6.69–8.21 (m, 14H, H–Ar); ^{13}C NMR (CDCl$_3$) δ$_C$: 31.6 (CH$_2$, C-3″), 36.9 (CH$_2$, C-1′), 49.7 (CH$_2$, NCH$_2$), 49.9 (CH$_2$, NCH$_2$), 53.1 (CH, C-7′), 54.4 (CH$_2$, C-3′), 69.4 (CH$_2$, OCH$_2$), 69.6 (CH$_2$, OCH$_2$), 71.2 (CH, C-7a′), 72.0 (C, C-2″), 82.9 (C, C-5′), 116.7 (CH, Ar), 116.9 (CH, Ar), 120.7 (CH, Ar), 123.1 (CH, Ar), 125.9 (CH, Ar), 126.3 (CH, Ar), 126.3 (CH, Ar), 126.7 (CH, Ar), 127.3 (CH, Ar), 127.4 (CH, Ar), 127.8 (CH, Ar), 128.5 (CH, Ar), 130.5 (CH, Ar), 130.7 (C, Ar), 131.5 (C, Ar), 132.2 (CH, Ar), 134.1 (C, Ar), 134.9 (C, Ar), 136.7 (C, Ar), 141.9 (C, Ar), 151.5 (C, Ar), 151.9 (C, Ar), 202.4 (C, C=O), 204.4 (C, C=O). ESI–MS: m/z 559 (M+H)$^+$. Anal. calcd. C$_{35}$H$_{30}$N$_2$O$_3$S: C, 75.24; H, 5.41; N, 5.01. Found: C, 75.35; H, 5.49; N, 4.97.

7′-(2,5-Dimethoxyphenyl)-1′,3′,5′,6′,7′,7a′-hexahydrodispiro [acenaphthylene-1,5′-pyrrolo-[1,2-c]thiazole-6′,2″-indane]-2,1″(1H)-dione (6k) ^{1}H NMR (CDCl$_3$) δ$_H$: 3.04 (d, J = 16.6 Hz, 1H, H-3″), 3.12 (dd, J = 11.5, 2.8 Hz, 1H, H-1′), 3.33–3.35 (m, 1H, H-1′), 3.38 (s, 3H, OCH$_3$), 3.65 (d, J = 10.2 Hz, 1H, H-3′), 3.70 (s, 3H, OCH$_3$), 4.04 (d, J = 16.6 Hz, 1H, H-3″), 4.09 (d, J = 10.2 Hz, 1H, H-3′), 4.26 (d, J = 10.6 Hz, 1H, H-7′), 4.86–4.90 (m, 1H, H-7a′), 6.90–8.20 (m, 13H, H–Ar); ^{13}C NMR (CDCl$_3$) δ$_C$: 31.4 (CH$_2$, C-3″), 36.6 (CH$_2$, C-1′), 51.9 (CH, C-7′), 54.1 (CH$_2$, C-3′), 54.5 (CH$_3$, OCH$_3$), 55.8 (CH$_3$, OCH$_3$), 71.1 (CH, C-7a′), 71.7 (C, C-2″), 83.0 (C, C-5′), 110.2 (CH, Ar), 112.6 (CH, Ar), 115.8 (CH, Ar), 120.9 (CH, Ar), 123.0 (CH, Ar), 123.5 (CH, Ar), 125.7 (CH, Ar), 126.0 (CH, Ar), 126.4 (CH, Ar), 126.7 (CH, Ar), 127.9 (CH, Ar), 130.2 (CH, Ar), 130.7 (C, Ar), 131.0 (C, Ar), 131.9 (CH, Ar), 133.9 (C, Ar), 135.4 (C, Ar), 136.3 (C, Ar), 140.4 (C, Ar), 151.5 (C, Ar), 151.9 (C, Ar), 152.0 (C, Ar), 202.3 (C, C=O), 204.5 (C, C=O). ESI–MS: m/z 534 (M+H)$^{+}$. Anal. calcd. C$_{33}$H$_{27}$NO$_4$S: C, 74.27; H, 5.10; N, 2.62. Found: C, 74.16; H, 5.13; N, 2.61.

7′-(4-(Piperidin-1-yl)phenyl)-1′,3′,5′,6′,7′,7a′-hexahydrodispiro[acenaphthylene-1,5′-pyrrolo-[1,2-c]thiazole-6′,2″-indane]-2,1″(1H)-dione (6l) ^{1}H NMR (CDCl$_3$) δ$_H$: 1.54–1.66 (m, 6H, CH$_2$), 2.83–3.16 (m, 6H, H-3″), 3.32–3.39 (m, 1H, H-1′), 3.66 (d, J = 9.9 Hz, 1H, H-3″), 4.08–4.19 (m, 2H, H-3′), 4.28 (d, J = 10.5 Hz, 1H, H-7′), 4.88–4.93 (m, 1H, H-7a′), 6.79–8.38 (m, 14H, H–Ar); ^{13}C NMR (CDCl$_3$) δ$_C$: 23.9 (CH$_2$), 24.4 (CH$_2$), 24.6 (CH$_2$), 31.7 (CH$_2$, C-3″), 36.9 (CH$_2$, C-1′), 50.4 (CH$_2$, NCH$_2$), 50.9 (CH$_2$, NCH$_2$), 53.1 (CH, C-7′), 54.4 (CH$_2$, C-3′), 71.4 (CH, C-7a′), 72.0 (C, C-2″), 82.9 (C, C-5′), 116.4 (CH, Ar), 116.7 (CH, Ar), 120.7 (CH, Ar), 123.1 (CH, Ar), 125.9 (CH, Ar), 126.3 (CH, Ar), 126.3 (CH, Ar), 126.7 (CH, Ar), 127.3 (CH, Ar), 127.4 (CH, Ar), 127.8 (CH, Ar), 128.5 (CH, Ar), 130.5 (CH, Ar), 130.7 (C, Ar), 131.5 (C, Ar), 132.2 (CH, Ar), 134.1 (C, Ar), 134.9 (C, Ar), 136.7 (C, Ar), 141.9 (C, Ar), 151.5 (C, Ar), 152.1 (C, Ar), 202.4 (C, C=O), 204.4 (C, C=O). ESI–MS: m/z 557 (M+H)$^{+}$. Anal. calcd. C$_{36}$H$_{32}$N$_2$O$_2$S: C, 77.67; H, 5.79; N, 5.03. Found: C, 77.50; H, 5.83; N, 5.09.

Biological evaluation

All the synthesized compounds 5a–5l and 6a–6l were tested for their antimycobacterial activity in vitro against M. tuberculosis H$_{37}$R$_V$ (MTB-H$_{37}$Rv) using a modified high throughput screen assay (Collins and Franzblau, 1997), and the end-point detection was assessed by the Promega reagent BacTiter-Glo^{TM} Microbial Cell Viability (BTG). Compounds screened in dose response were tested in ten twofold dilutions from 100 μM to 0.195 μM. Three standard drugs (isoniazid, ethambutol, and cycloserine) were used as references for the assay. Concurrent with the activity screening,

cytotoxicity test was also performed in VERO cells at concentrations of 62.5 μg/mL. After 72 h of exposure, viability was assessed on the basis of cellular conversion of MTT into a formazan product using the Promega CellTiter 96 nonradioactive cell proliferation assay.

Molecular docking studies

To investigate the binding interactions of the target compounds, docking studies were performed on the lead compound 5b against M. tuberculosis enoyl reductase, InhA (PDB ID: 2H7M, Resolution = 1.62 Å). Two different programs, Autodock 4.2 and Glide 5.7 were used in order to identify the proper docking protocol. The receptor and drug candidates were structurally optimized prior to the actual docking simulation. Control dock of InhA was performed against the bounded ligand, and the root mean square deviation (RMSD) between the crystal geometry and the docked pose was investigated. Since Glide pose showed a lower rmsd value (rmsd = 0.228 Å) compared to Autodock (rmsd = 1.929 Å), Glide XP protocol was used for the rest of the studies to dock the target compounds.

Results and discussion

2-[(E)-1-(substituted aryl) methylidene]-1-indanones were synthesized by Claisen-Schmidt condensation according to the literature method (Ali et al., 2009), followed by synthesis of dispiropyrrolidines via 1,3-dipolar cycloaddition of azomethine ylides generated in situ from the decarboxylative condensation of ninhydrin or acenaphthenequinone and thiazolidine-4-carboxylic acid with appropriate dipolarophiles, 2-[(E)-1-arylmethylidene]-1-indanones (Schemes 1, 2). Purity of the newly synthesized dispiropyrrolidines was checked using NMR, CHN, and mass spectrometry. All the analytical and spectral data showed that the synthesized compounds were in full agreement with the proposed structures. The regio and stereochemical outcome of the cycloaddition reaction of compounds 5a (Wei et al., 2011) was ascertained by single crystal X-ray analysis (Figs. 1, 2). The molecular structure was stabilized by the intramolecular C–H···O and C–H···N hydrogen bonds.

BacTiter-Glo^{TM} Microbial Cell Viability was used to screen the activity of the newly synthesized compounds. This method was based on the measurement of ATP content as an indicator of the metabolically active cells. The luminescence signal generated by luciferase reaction was proportional to the amount of viable cells present (Yuroff et al., 2008). From the 24 new compounds, six of them showed better activity than cycloserine. Compound 5b 7′-(4-chlorophenyl)-5′,6′,7′,7a′-tetrahydrospiro[indan-2,5′-pyrrolo[1,2-c]-[1,3]thiazole-6′,2″-indan]-1,3,1″-trione was found to be the most active with EC$_{50}$ of 10.52 μM.

Scheme 1 Protocol for synthesis of titled compounds **5a–5l** and **6a–6l**. (*i*) Ethanol, NaOH, reflux 4 h. (*ii*) Methanol, reflux 4–8 h
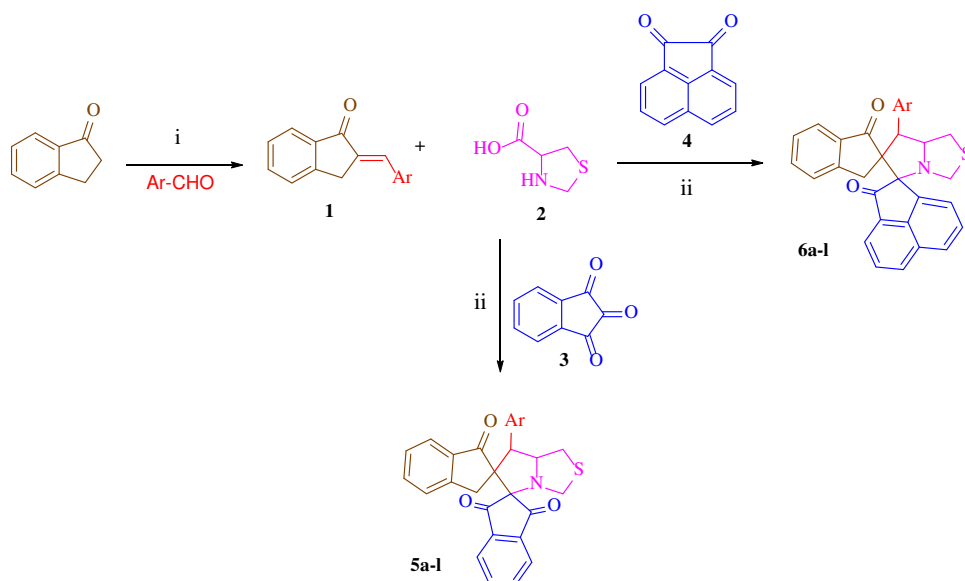
Scheme 2 Plausible mechanism for the formation of dispiropyrrolidine
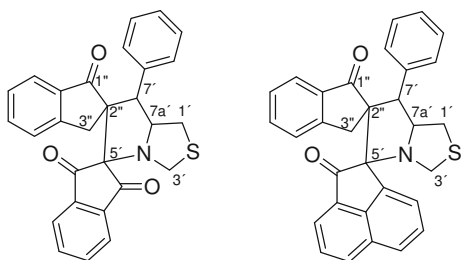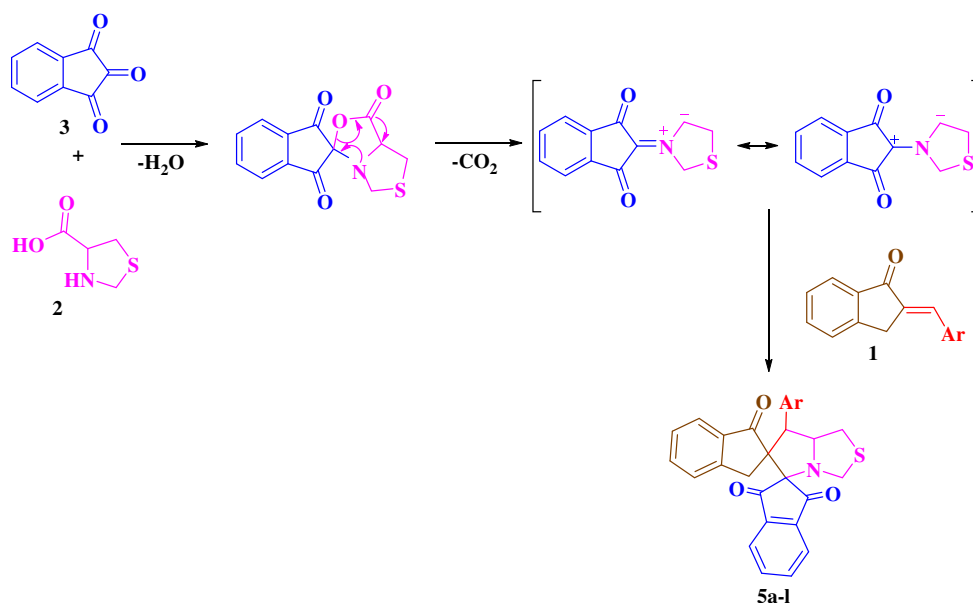
Fig. 1 Structure of compound **5a** and **6a** with atomic numbering

and **6**, derivatives with ninhydrin showed better activity than derivatives with acenaphthenequinone. Among the twelve compounds from series **5**, eleven showed EC_{50} of less than 100 μM, whereas for series **6**, only two out of twelve showed the similar inhibition. The biological evaluation results also showed that derivatives with electron-withdrawing groups have exhibited comparatively higher antimycobacterial activity. It is noted that the halogen substituent in the phenyl ring enhanced the activity remarkably. However, none of the screened compounds is more potent than ethambutol and isoniazid. Cytotoxicity test was also performed in VERO cells, and all of the compounds were found to be non-toxic up to 62.5 μg/mL. All the data are shown in Table 1.

It was followed by compound **5e** (11.07 μM), **6e** (14.76 μM) and **5g** (18.37 μM) that showed EC_{50} of less than 20 μM. By comparing the compounds of two series **5**
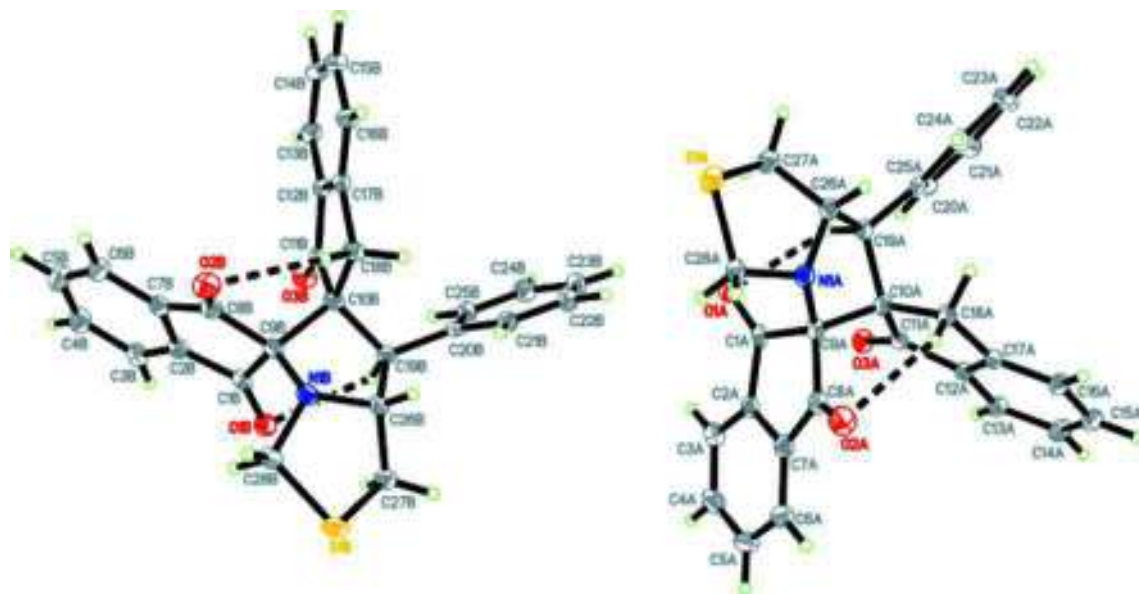
Fig. 2 ORTEP diagram of compound **5a** (from different views). Intramolecular hydrogen bonds are shown in *dashed lines*

Table 1 Antimycobacterial activity of pyrrolidine derivatives **5a–5l** and **6a–6l** against MTB-H$_{37}$Rv strains

Com	Ar	Entries 5			Entries 6		
		EC$_{50}$ (μM) BTG	MIC (μM) BTG	Cytotoxicity VERO cells (μg/ml)	EC$_{50}$ (μM) BTG	MIC (μM) BTG	Cytotoxicity VERO cells (μg/ml)
a	Phenyl	84.24	NA	>62.5	>100.00	NA	>62.5
b	4-Chlorophenyl	10.52	NA	>62.5	>100.00	NA	>62.5
c	4-Bromophenyl	30.15	NA	>62.5	>100.00	NA	>62.5
d	4-Trifluoromethylphenyl	21.14	NA	>62.5	81.71	NA	>62.5
e	4-Trifluoromethoxyphenyl	11.07	NA	>62.5	14.76	NA	>62.5
f	3-Nitrophenyl	>100.00	NA	>62.5	>100.00	NA	>62.5
g	4-Methoxyphenyl	18.37	NA	>62.5	>100.00	NA	>62.5
h	Benzo[d][1,3]dioxole	24.07	NA	>62.5	>100.00	NA	>62.5
i	4-Dimethylaminophenyl	n.d.	NA	>62.5	>100.00	NA	>62.5
j	1-(4-(Morpholine-1-yl)phenyl)	n.d.	NA	>62.5	>100.00	NA	>62.5
k	2,5-Dimethoxyphenyl	63.35	NA	>62.5	>100.00	NA	>62.5
l	1-(4-(Piperidine-1-yl)phenyl)	23.36	NA	>62.5	>100.00	NA	>62.5
	Cycloserine	23.55	100.00	>62.5			
	Ethambutol	1.50	6.25	>62.5			
	Isoniazid	0.18	0.31	>62.5			

Molecular docking analysis was performed to study the possible binding mode between the synthesized compounds and the target protein. The active pocket was determined based on the consideration where the native ligand, 1-cyclohexyl-N-(3,5-dichlorophenyl)-5-oxopyrrolidine-3-carboxamide was complexed with InhA in 2H7M. It consists of Gly 96, Phe 97, Met 98, Met 103, Phe 149, Met 155, Pro 156, Ala 157, Tyr 158, Met 161, Pro 193, Met 199, Gln 214, Ile 215, Leu 218, Glu 219, and Trp 222 (He

et al., 2006). The interaction analysis reveals that the native ligand and synthesized dispiropyrrolidines interact with receptor primarily by hydrophobic and mild polar interactions (He *et al.,* 2007).

From the docking results, compounds **5b** occupied essentially the same pocket as the native ligand (Figs. 3, 4), by retaining some of the interactions mentioned above such as hydrophobic and polar interaction. Besides, some additional interactions were found as well. The two oxygen
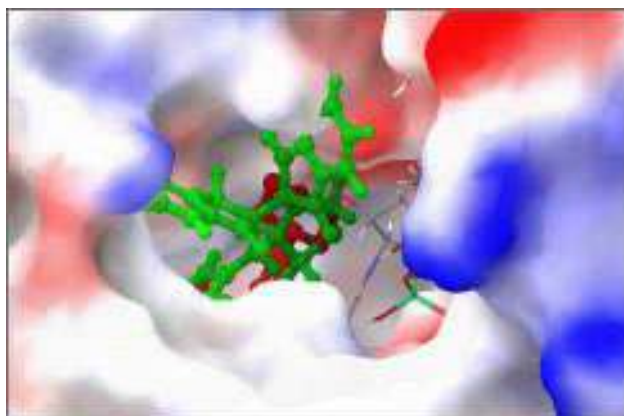
Fig. 3 Overlay of lead compound **5b** (*green*) with the bound ligand (*red*) in crystal geometry at the active site (PDB id: 2H7M) (Color figure online)

atoms of indandione of compound **5b** formed hydrogen bonding with catalytic residue Met 98 backbone amide "NH" (at distance of 1.922 Å) and phosphoryl group of

cofactor NADH (at 2.362 Å), respectively. The phenyl moiety of indandione also formed π–π stacking with Phe 97 which further stabilized the conformation of compound **5b** in the active site. Most importantly, **5b** was found to be docked near the substrate-binding loop (residues 195–210) that covered the entrance of active site. It formed hydrophobic interactions with Ala 198, Ile 202, and Leu 207.

Conclusion

Twenty-four of highly functionalised dispiropyrrolidines were designed and synthesized using 1,3-dipolar cycloaddition. This reaction was proved to be highly efficient and selective, affording exclusively one stereoisomer (Wei *et al.,* 2011, 2012a). The synthesized compounds were screened for antimycobacterial activity, and cytotoxicity test was also performed using VERO cells. It is conceivable that derivatives showing more potency and low toxicity make them excellent leads as potential antitubercular agent.
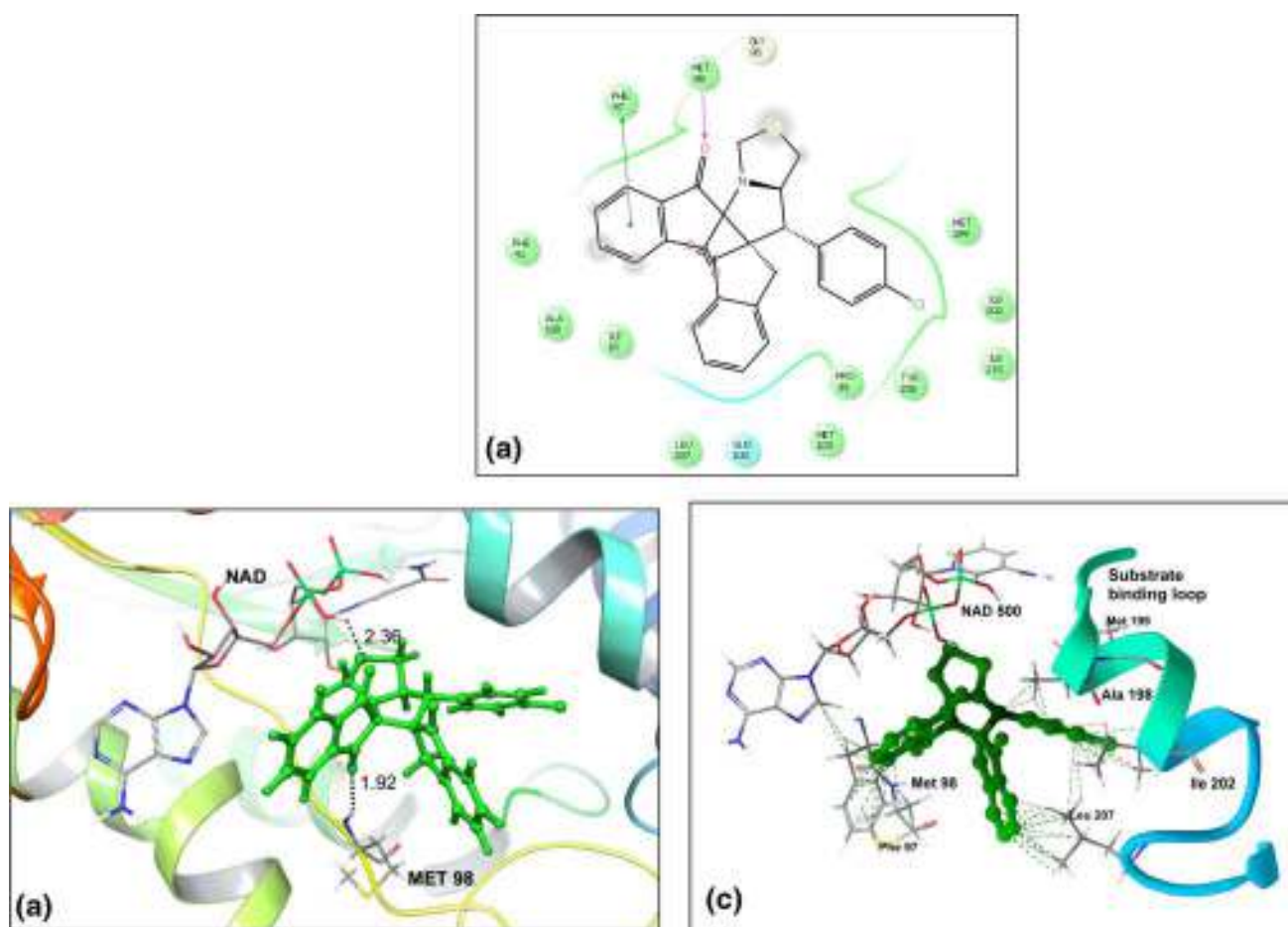
Fig. 4 **a** 2D interaction diagram of lead compound **5b** with the target protein InhA (*Green solid line* represents π–π stacking; *red line* represents hydrogen bonding). *Panel* **b** shows the hydrogen bonding between **5b** (in *green*, *ball* and *stick*) and Met 98 as well as NADH

within the active site. *Panel* **c** represents the substrate-binding loop of InhA (in *blue* cartoon) and the hydrophobic contacts of **5b** with residues within 4 Å cut-off distance (Color figure online)

Molecular docking results reveal that the binding mode of the most active compound, **5b** is similar with pyrrolidine carboxamides, the known direct InhA inhibitor. It is encouraging to see that dispiropyrrolidines display potential as direct InhA inhibitor as it is docked near the substrate-binding loop. Further modification on the novel scaffolds is ongoing in our laboratory to exhibit better potency than standard drugs.

Conflict of interest The authors confirm that this article content has no conflicts of interest.

References

Ali MA, Samy JG, Manogaran E, Sellappan V, Hasan MZ, Ahsan MJ, Pandian S, ShaharYar M (2009) Synthesis and antimycobacterial evaluation of novel 5,6-dimethoxy-1-oxo-2,5-dihydro-1*H*-2-indenyl-5,4-substituted phenyl methanone analogues. Bioorg Med Chem Lett 19(24):7000–7002

Banerjee A, Dubnau E, Quemard A, Balasubramanian V, Um KS, Wilson T, Collins D, de Lisle G, Jacobs WR Jr (1994) inhA, a gene encoding a target for isoniazid and ethionamide in *Mycobacterium tuberculosis*. Science 263(5144):227–230

Bellina F, Rossi R (2006) Synthesis and biological activity of pyrrole, pyrroline and pyrrolidine derivatives with two aryl groups on adjacent positions. Tetrahedron 62(31):7213–7256

Brimble MA, Park JH, Taylor CM (2003) Synthesis of the spiroacetal fragment of broussonetine H. Tetrahedron 59(31):5861–5868

Cade CE, Dlouhy AC, Medzihradszky KF, Salas-Castillo SP, Ghiladi RA (2010) Isoniazid-resistance conferring mutations in *Mycobacterium tuberculosis* KatG: catalase, peroxidase, and INH-NADH adduct formation activities. Protein Sci 19(3):458–474

Chiang C-Y, Centis R, Migliori GB (2010) Drug-resistant tuberculosis: past, present, future. Respirology 15(3):413–432

Collins L, Franzblau SG (1997) Microplate alamar blue assay versus BACTEC 460 system for high-throughput screening of compounds against *Mycobacterium tuberculosis* and *Mycobacterium avium*. Antimicrob Agents Chemother 41(5):1004–1009

Crooks PA, Rosenberg HE (1978) Synthesis of spiro[tetralin-2,2′-pyrrolidine] and spiro[indan-2,2′-pyrrolidine] derivatives as potential analgesics. J Med Chem 21(6):585–587

He X, Alian A, Stroud R, Ortiz de Montellano PR (2006) Pyrrolidine carboxamides as a novel class of inhibitors of enoyl acyl carrier protein reductase from *Mycobacterium tuberculosis*. J Med Chem 49(21):6308–6323

He X, Alian A, Ortiz de Montellano PR (2007) Inhibition of the *Mycobacterium tuberculosis* enoyl acyl carrier protein reductase InhA by arylamides. Bioorg Med Chem 15(21):6649–6658

Introduction (2008). Tuberculosis 88 (2):85–86

Kuo MR, Morbidoni HR, Alland D, Sneddon SF, Gourlie BB, Staveski MM, Leonard M, Gregory JS, Janjigian AD, Yee C, Musser JM, Kreiswirth B, Iwamoto H, Perozzo R, Jacobs WR, Sacchettini JC, Fidock DA (2003) Targeting tuberculosis and malaria through inhibition of enoyl reductase: compound activity and structural data. J Biol Chem 278(23):20851–20859

Lawn SD, Zumla AI (2011) Tuberculosis. Lancet 378(9785):57–72

Mitchison DA (2000) Role of individual drugs in the chemotherapy of tuberculosis. Int J Tuberc Lung Dis 4(9):796–806

Musser JM, Kapur V, Williams DL, Kreiswirth BN, van Soolingen D, van Embden JDA (1996) Characterization of the catalase-peroxidase gene (katG) and inhA locus in isoniazid-resistant and -susceptible strains of *Mycobacterium tuberculosis* by automated DNA sequencing: restricted array of mutations associated with drug resistance. J Infect Dis 173(1):196–202

Pawlowski A, Jansson M, Sköld M, Rottenberg ME, Källenius G (2012) Tuberculosis and HIV co-infection. PLoS Pathog 8(2): e1002464

Pellegrini C, Weber M, Borschberg H-J (1996) Total synthesis of (+)-elacomine and (−)-isoelacomine, two hitherto unnamed oxindole alkaloids from *Elaeagnus commutata*. Helv Chim Acta 79(1):151–168

Stylianakis I, Kolocouris A, Kolocouris N, Fytas G, Foscolos GB, Padalko E, Neyts J, De Clercq E (2003) Spiro[pyrrolidine-2,2′-adamantanes]: synthesis, anti-influenza virus activity and conformational properties. Bioorg Med Chem Lett 13(10): 1699–1703

Timmins GS, Deretic V (2006) Mechanisms of action of isoniazid. Mol Microbiol 62(5):1220–1227

Tsuge O, Kanemasa S (1989) Recent advances in azomethine ylide chemistry. In: Alan RK (ed) Advances in heterocyclic chemistry, vol 45. Academic Press, New York, pp 231–349

Usui T, Kondoh M, Cui CB, Mayumi T, Osada H (1998) Tryprostatin A, a specific and novel inhibitor of microtubule assembly. Biochem J 333(3):543–548

Wei AC, Ali MA, Choon TS, Quah CK, Fun H-K (2011) 7′-Phenyl-5′,6′,7′,7a′-tetrahydrodipiro[indan-2,5′-pyrrolo[1,2-*c*][1,3]thia-zole-6′,2″-indan]-1,3,1″-trione. Acta Crystallographica Section E 67(12):o3218–o3219

Wei AC, Ali MA, Choon TS, Arshad S, Razak IA (2012a) 7′-Phenyl-1′,3′,5′,6′,7′,7a′-hexahydrodipiro[acenaphthylene-1,5′-pyrrolo[1,2-*c*]thiazole-6′,2″-indane]-2,1″(1*H*)-dione. Acta Crystallogr Sect E 68(4):o1265–o1266

Wei AC, Ali MA, Yoon YK, Ismail R, Choon TS, Kumar RS, Arumugam N, Almansour AI, Osman H (2012b) Antimycobacterial activity: a facile three-component [3 + 2]-cycloaddition for the regioselective synthesis of highly functionalised dispiropyrrolidines. Bioorg Med Chem Lett 22(15):4930–4933

Wei AC, Ali MA, Yoon YK, Ismail R, Choon TS, Kumar RS (2013) A facile three-component [3 + 2]-cycloaddition for the regioselective synthesis of highly functionalised dispiropyrrolidines acting as antimycobacterial agents. Bioorg Med Chem Lett 23(5):1383–1386

WHO (2013) Global tuberculosis report

Yuroff A, Fan F, Butler B, Collins M (2008) Application of the BacTiter-Glo^TM assay for rapid enumeration and screening of antimicrobial compounds for mycobacterium avium complex bacteria. Promega Notes 98:8–10

Zhang Y (2005) The magic bullets and tuberculosis drug targets. Annu Rev Pharmacol Toxicol 45:529–564

Zhang Y, Heym B, Allen B, Young D, Cole S (1992) The catalase-peroxidase gene and isoniazid resistance of *Mycobacterium tuberculosis*. Nature 358(6387):591–593

Effect of information leakage and method of splitting (rational and random) on external predictive ability and behavior of different statistical parameters of QSAR model

Vijay H. Masand, Devidas T. Mahajan, Gulam M. Nazeruddin, Taibi Ben Hadda, Vesna Rastija & Ahmed M. Alfeefy

Springer

Springer

ORIGINAL RESEARCH

Effect of information leakage and method of splitting (rational and random) on external predictive ability and behavior of different statistical parameters of QSAR model

Vijay H. Masand · Devidas T. Mahajan · Gulam M. Nazeruddin · Taibi Ben Hadda · Vesna Rastija · Ahmed M. Alfeefy

Abstract Quantitative Structure–Activity Relationship not only provides guidelines regarding structural features responsible for biological activity but it can be used also for prediction of desired activity prior to synthesis of untested chemicals. Therefore, an appropriate validation of any QSAR is of utmost importance to judge its external predictive ability. Generally, internal and external validations (preferred by many) are used in the absence of a true external dataset. The model developed using external method may not be reliable as it may not capture all essential features required for the particular SAR due to omission of some compounds, especially for small datasets. In external validation, the splitting is done either rationally or in random manner before descriptor selection. In the present study, rational splitting of dataset was performed using a novel method and its effect on statistical parameters was analyzed. The analysis reveals that the predictive ability of a QSAR model is sensitive toward (1) the method of splitting and (2) distribution of the training and the prediction sets. In addition, purposeful selection can be used to influence the statistical parameters; therefore, external validation based on single split is insufficient to guarantee the true predictive ability of a QSAR model. Besides, it appears that the selection of descriptors prior to splitting (information leakage) has little role to play in deciding external predictivity of the model. The present study reveals that as many as possible statistical parameters should be examined along with boot-strapping instead of single external validation.

Keywords QSAR · External validation · Statistical parameters · Splitting methods · Predictivity

V. H. Masand (✉) · D. T. Mahajan
Department of Chemistry, Vidya Bharati College, Camp, Amravati, Maharashtra, India
e-mail: vijaymasand@gmail.com; vijaymasand@rediffmail.com

G. M. Nazeruddin
Department of Chemistry, Poona College, Pune, Maharashtra, India

T. B. Hadda
Laboratoire Chimie des Matériaux, Université Mohammed Premier, 60000 Oujda, Morocco

V. Rastija
Department of Chemistry, Faculty of Agriculture, Josip Juraj Strossmayer University of P. Svacica 1d, Osijek, Croatia

A. M. Alfeefy
Department of Pharmaceutical Chemistry, College of Pharmacy, Salman Bin Abdulaziz University, P.O. Box 173, Alkharj 11942, Saudi Arabia

Introduction

Under the umbrella of modern drug designing, Computer Assisted Drug Designing (CADD) is the method of choice due to faster, cheaper, and result-oriented analysis (Kubinyi, 2002; Van Drie, 2007; Yuriev et al., 2011). Over the years, CADD has matured with the advent of new techniques, algorithms, and software programs. Quantitative Structure–Activity Relationship (QSAR), molecular docking, pharmacophore modeling, etc. are thriving techniques from the tenant of CADD. Of these, QSAR has gained much attention because of its applicability in risk assessment, toxicity prediction, and regulatory decisions apart from drug discovery and lead optimization. Further
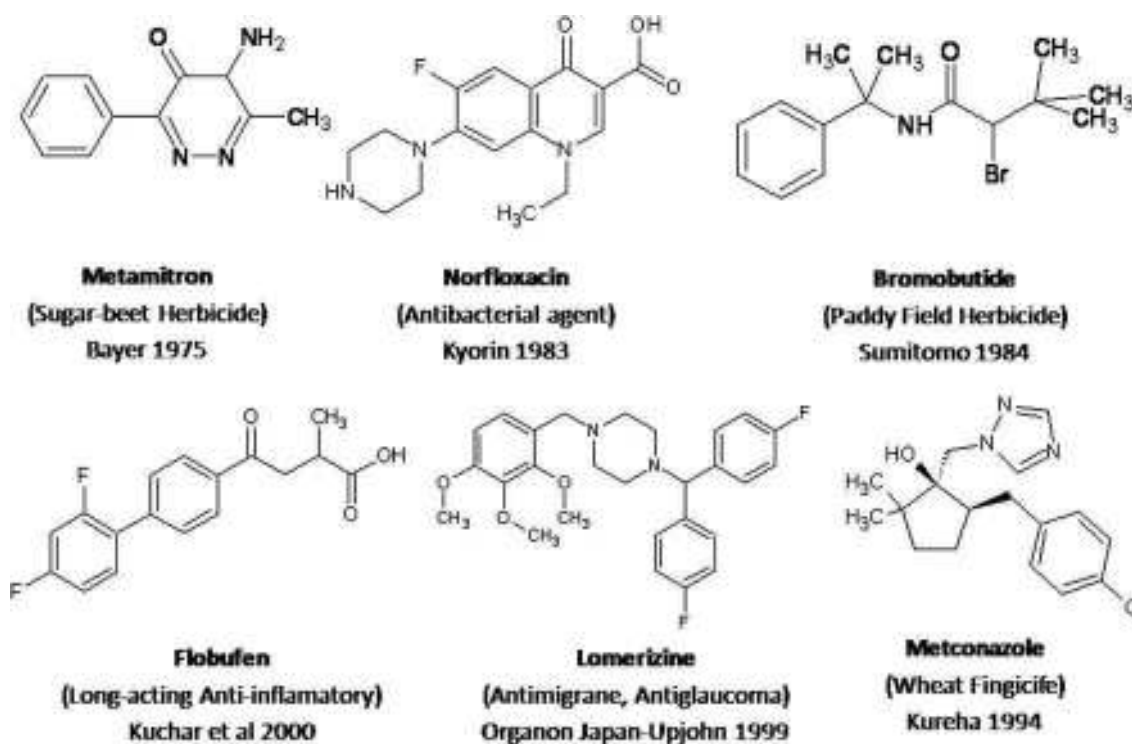
Fig. 1 Some of the commercial drugs developed with the aid of QSAR

application of QSAR models includes prediction of desired activity/property for a molecule before its synthesis and testing (Mahajan *et al.*, 2012, 2013; Masand *et al.*, 2012, 2010, 2013). In last decades, QSAR has contributed significantly in bringing many successful drugs in the market (see Fig. 1) (Selassie, 2003).

Therefore, QSAR models are routinely built to establish the statistical correlation between structural features (independent or predictor variables) that govern the biological activity or a physico-chemical property (dependent variable) (Scior *et al.*, 2009). The four main steps involved in QSAR model building are (1) Structure drawing and geometry optimization, (2) calculation of myriad number of descriptors, (3) generation of model using least (optimal) number of descriptors, and (4) appropriate validation of mathematical model (Tropsha, 2010). The success of any QSAR model depends on various factors like accuracy of the experimental (input) data, selection of appropriate number and type of descriptors, statistical method (or algorithms), and most significantly on apposite validation of the developed model (see Fig. 2) (Huang and Fan, 2011). The utility of a QSAR model depends on its ability to predict accurately for unknown chemicals with some known degree of certainty (Roy *et al.*, 2008). The prediction ability is a crucial aspect related to appropriate validation of the QSAR models. A QSAR model is considered appropriately statistically validated if it possesses good internal and external predictive ability, such models are successful in predicting the activity/property of unknown chemical (Scior *et al.*, 2009; Tropsha, 2010).

Recently, appropriate validation of QSAR model is under hot debate. For thriving QSAR models, validation must be primarily for statistical robustness, prediction abilities, and applicability domain of the models (Sahigara *et al.*, 2012, 2010). There are two standard ways of doing this (1) internal validation (2) external validation (Hawkins *et al.*, 2003). These are performed in five different ways: leave-one-out cross-validation, leave-many-out cross-validation, Y-randomization, bootstrapping (least known among the five), and external validation (Hawkins *et al.*, 2003; Kiralj and Ferreira, 2009).

The widely accepted parameter Q^2 (also symbolized as R^2_{cv}, r^2_{cv}, q^2, and Q^2_{LOO}) for internal validation is calculated by the formula (Consonni *et al.*, 2010; Todeschini *et al.*, 2004):

$$Q^2 = 1 - \frac{\sum\limits_{i=1}^{n} (\hat{y}i - yi)^2}{\sum\limits_{i=1}^{n} (yi - \bar{y})^2}.$$

Internal validation, a statistical method regularly performed using leave-one-out or by leave-many-out cross-validation, leads to an overestimation of predictive
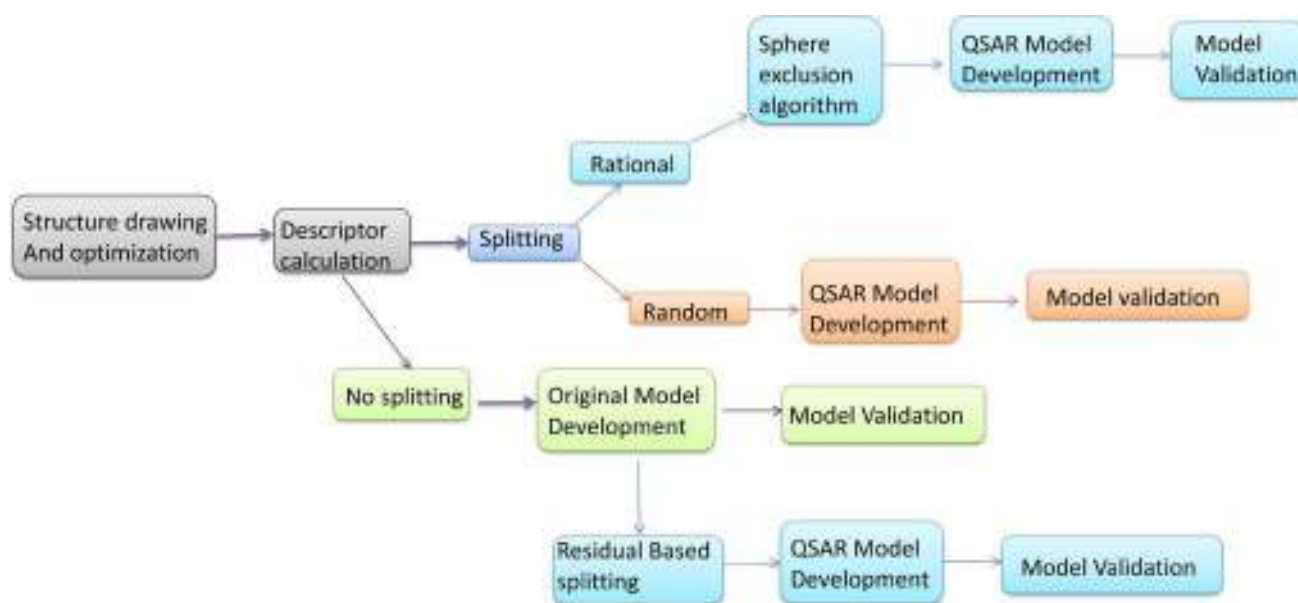
Fig. 2 Flowchart diagram for the methodology used in present study

capacity in many instances. But, it is useful for verification of robustness of the model. Therefore, internal validation may not be sufficient for validation, but it is essential (Consonni *et al.*, 2010; Golbraikh and Tropsha, 2002; Gramatica, 2013; Tropsha, 2010). It is still useful, especially, when the dataset is small or of modest size (Hawkins *et al.*, 2003).

On the other hand, external validation involves splitting the available data into training (or learning) and test (or prediction) sets. For external validation, selection of proper size of training and prediction sets is very crucial (Kiralj and Ferreira, 2009; Roy *et al.*, 2008). Generally, this splitting is performed using random division, but purposeful or rational splitting for selection of compounds whose chemistry covers the whole (or maximum) population, but does not introduce any bias is a good idea (Hawkins *et al.*, 2003). Rational or purposeful splitting methods can divide datasets into training and prediction sets in an intelligent fashion (Martin *et al.*, 2012). Different algorithms like Kennard-Stone, minimal prediction set dissimilarity, and sphere exclusion algorithms have been developed for smarter way of dividing the datasets into training and prediction sets with the aim of producing more predictive models (Chirico and Gramatica, 2012; Consonni *et al.*, 2010; Gramatica 2013; Huang and Fan 2011; Kiralj and Ferreira 2009; Martin *et al.*, 2012; Scior *et al.*, 2009). Even though, earlier studies have pointed out the superiority of rational division algorithms over the simple random splitting and activity sorting methods. Yet, appropriate selection of rational division method is still unclear because of the conflicting results (Huang and Fan 2011). Recent literature survey indicates that the method/

algorithm of choice for splitting has little influence on the statistical performance of a QSAR model. Recently, Martin and co-workers reported the influence of rational selection of training and prediction sets on the model's predictivity (Martin *et al.*, 2012). However, if the prediction set is small, unknowingly, the researcher may get a prediction set for which the developed model might show a high predictive ability (Baumann and Stiefl, 2004; Chirico and Gramatica, 2012; Consonni *et al.*, 2009; Consonni *et al.*, 2010; Hawkins, 2004; Huang and Fan, 2011; Martin *et al.*, 2012; Scior *et al.*, 2009; Todeschini *et al.*, 2004; Tropsha, 2010).

The aim of the present study is to compare the statistical performance of different algorithms of rational selection, and to study the effect of descriptors selection prior to splitting (information leakage) on the external predictive ability of the model. In addition, the aim of the present study is to devise, evaluate, and compare a novel non-algorithmic method for rational splitting that influences the statistical parameters of QSAR model.

Experimental section

Datasets

For the present study, three datasets of varying size are used. The first dataset consists of forty-four N-Phenyl Ureidobenzenesulfonate Derivatives (N-PUSs) with wide variety of substituents present at different positions, as shown in Table 1, was selected from the literature (Turcotte *et al.*, 2012). The activities of these compounds

Table 1 Substituted N-Phenyl Ureidobenzenesulfonate derivatives along with $-\log IC_{50}$ (pIC_{50}) and descriptor values

S. no.	X	R_1	R_2	pIC_{50} (M) (HT-29)	F07 [C–N]	F05 [C–C]	Mor29e	Mor03m	RDF095v
1	O	4-OH	4-CEU	5.824	1	12	0.728	−3.81	1.503
2	O	2-Me	3-CEU	4.481	2	13	0.04	−5.025	5.266
3	O	2-CH$_2$-CH$_3$	3-CEU	5.367	2	14	0.283	−5.342	3.314
4	O	2-(CH$_2$)$_2$-CH$_3$	3-CEU	4.824	2	16	0.04	−4.293	5.093
5	O	4-OH	3-CEU	3.921	2	12	0.408	−4.627	4.138
6	O	2-CH$_2$-CH$_3$	4-CEU	4.770	1	14	0.246	−2.51	1.679
7	O	2-(CH$_2$)$_2$-CH$_3$	4-CEU	5.602	1	16	0.249	−4.542	3.791
8	NH	2-Me	3-CEU	4.149	2	13	0.044	−5.776	5.265
9	NH	2-CH$_2$-CH$_3$	3-CEU	4.319	2	14	0.003	−4.2	3.792
10	NH	2-(CH$_2$)$_2$-CH$_3$	3-CEU	4.824	2	16	−0.015	−5.66	6.562
11	NH	2-Me	4-CEU	4.260	2	13	−0.056	−4.842	4.379
12	NH	2-CH$_2$-CH$_3$	4-CEU	4.398	2	14	−0.199	−4.036	3.316
13	NH	2-(CH$_2$)$_2$-CH$_3$	4-CEU	4.678	2	16	−0.109	−5.379	4.276
14	O	2-Me	3-CPU	4.678	2	13	−0.099	−4.91	4.18
15	O	2-CH$_2$-CH$_3$	3-CPU	4.638	2	14	0.057	−5.709	3.351
16	O	2-(CH$_2$)$_2$-CH$_3$	3-CPU	4.854	2	16	0.09	−4.777	5.737
17	O	4-OH	3-CPU	4.292	2	12	0.371	−3.81	3.557
18	O	2-Me	4-CPU	4.585	1	13	0.026	−3.933	2.952
19	O	2-CH$_2$-CH$_3$	4-CPU	4.824	1	14	0.1	−4.001	2.835
20	O	2-(CH$_2$)$_2$-CH$_3$	4-CPU	4.886	1	16	−0.033	−4.132	4.372
21	O	4-OH	4-CPU	4.301	1	12	0.137	−3.322	2.426
22	NH	2-Me	3-CPU	4.377	2	13	0.144	−4.557	4.698
23	NH	2-CH$_2$-CH$_3$	3-CPU	4.018	2	14	−0.233	−5.079	4.639
24	NH	2-(CH$_2$)$_2$-CH$_3$	3-CPU	4.824	2	16	−0.265	−5.077	5.298
25	NH	2-Me	4-CPU	4.194	2	13	−0.247	−2.874	2.342
26	NH	2-(CH$_2$)$_2$-CH$_3$	4-CPU	4.585	2	16	−0.199	−5.308	4.241
27	O	2-Me	4-CEU	5.328	1	13	0.182	−4.774	3.14
28	O	2-Me	3-EU	4.357	2	13	0.048	−3.826	3.679
29	O	2-CH$_2$-CH$_3$	3-EU	4.481	2	14	0.123	−3.92	3.658
30	O	2-(CH$_2$)$_2$-CH$_3$	3-EU	4.602	2	16	0.064	−4.152	5.884
31	O	4-OH	3-EU	4.125	2	12	0.245	−3.361	3.747
32	O	2-Me	4-EU	4.921	1	13	0.226	−3.517	2.458
33	O	2-CH$_2$-CH$_3$	4-EU	4.921	1	14	0.289	−3.603	2.334
34	O	2-(CH$_2$)$_2$-CH$_3$	4-EU	5.620	1	16	0.179	−3.78	3.85
35	O	4-OH	4-EU	4.921	1	12	0.275	−2.822	2.042
36	O	3-Me	4-CEU	5.143	1	12	0.179	−5.158	2.729
37	NH	2-Me	3-EU	3.991	2	13	0.114	−4.003	5.481
38	NH	2-CH$_2$-CH$_3$	3-EU	4.824	2	14	−0.077	−3.948	3.99
39	NH	2-(CH$_2$)$_2$-CH$_3$	3-EU	4.387	2	16	−0.121	−3.772	4.862
40	NH	2-CH$_2$-CH$_3$	4-EU	4.066	2	14	−0.106	−3.638	2.681
41	NH	2-(CH$_2$)$_2$-CH$_3$	4-EU	4.495	2	16	−0.179	−3.383	3.517
42	O	4-Me	4-CEU	4.523	1	12	0.411	−2.191	3.995
43	O	4-OMe	4-CEU	4.745	1	13	0.579	−3.646	2.832
44	O	4-N(Me)$_2$	4-CEU	4.409	2	14	0.274	−3.852	5.562

CEU 2-chloroethylurea, *CPU* 3-chloropropylurea, *EU* ethylurea

reported as IC_{50} (μM) against HT-29 colon carcinoma cells were converted to pIC_{50} (M). These derivatives of N-PUS, their corresponding $-logIC_{50}$ (pIC_{50}) values along with the values of descriptor are presented in Table 1.

The second data consists of one hundred and twelve 4-aminoquinoline derivatives (Hwang *et al.*, 2011) with a variety of substituents at different positions (see Table 2). The anti-malarial activity tested against chloroquine (CQ) sensitive (3D7) strain of *P. falciparum* reported as EC_{50} (μM) values were converted to pEC_{50} (M) for smoother statistical calculations. These derivatives of 4-aminoquinolines, their corresponding $-logEC_{50}$ (pEC_{50}) values and values of descriptor are presented in Table 2.

The third dataset, which is a subset of the dataset 2, comprises cytotoxicity data of one hundred 4-aminoquinolines (Hwang *et al.*, 2011) tested against HepG2 cell lines (see Table 3). For convenience, EC_{50} (μM) values were converted to pEC_{50} (M).

Calculation and selection of descriptors

The structures were drawn using Chemsketch 12 freeware, optimized using MMFF94 force field in TINKER, and then subjected to calculation of a large number of descriptors using e-Dragon, and PowerMV. Objective feature selection was performed to eliminate highly correlated and constant variables using QSARINS v1.2 and RapidMiner 5.0. Redundant descriptors were identified and eliminated using objective feature selection (Chirico and Gramatica, 2012; Gramatica, 2013; Mahajan *et al.*, 2013; Masand *et al.*, 2012, 2010, 2013). The procedure reported in the literature was employed for objective feature selection (Chirico and Gramatica 2012; Gramatica, 2013; Mahajan *et al.*, 2013; Masand *et al.*, 2012, 2010, 2013). As a general rule, constant for >80 % molecules, low-variance and correlated ($|R| \geq 0.6$) descriptors were excluded prior to modeling.

Methodology

The general procedure of external validation involves selection of descriptor on the basis of training set after splitting. It is well established that a QSAR model well predicts for a prediction molecule that is structurally very similar to the training set molecules because the descriptor (hence, the model) has captured common features of the training set molecules and is proficient to detect them in the new molecule (Consonni *et al.*, 2009, 2010; Huang and Fan, 2011; Schuurmann *et al.*, 2008; Todeschini *et al.*, 2004), reverse is true for a new molecule which has very little in common with the training set data. That is, the confidence in its prediction should be low. Recently, Roy et al. proposed a new approach to overcome this critical issue, in which they used undivided dataset for selection of

variables and performed internal validation (LOO cross-validation) in two different ways to ensure external predictivity of the developed model (Mitra *et al.*, 2010). In the present work, descriptor selection was performed for the whole data set prior to splitting (information leakage) to determine the effect of selection of descriptors on external predictivity and behavior of different statistical parameters of the model. Genetic Algorithm (GA) available in QSA-RINS v1.2 was employed for the selection of optimum number and the set of descriptors applying the default settings (Chirico and Gramatica, 2011, 2012). Though, this step contravenes the basic rule that prediction set compounds should be excluded from the model development procedure, that is, they should be unknown to the developed model. But, this ensures that the selected descriptors capture the essential features that control the biological activity. In addition, it allows determining the effect of early descriptor selection (that is, prior to splitting or information leakage) on external predictivity of the models. Ferreira and Kiralj have termed such models as 'Auxiliary models' (Kiralj and Ferreira, 2009).

In QSARINS (Gramatica *et al.*, 2014, 2013), CV (cross-validation) techniques are used as the optimization parameter (fitness function) for GA-based variable selection and also to verify model robustness and to avoid naïve Q^2 (Chirico and Gramatica, 2011, (2012). The novel methodology for splitting (first time reported in this work, termed as residual-based method (RBM)) begins with the creation of an original model on the basis of undivided dataset followed by splitting of dataset into training and prediction sets on the basis of sign of residuals (difference between the actual and predicted value by original model) for each sample. In short, for the whole undivided dataset, a statistically robust GA-MLR model (Original Model) was built. For some molecules, this original model resulted in positive residuals and negative for the rest. Now, for the novel methodology of splitting i.e., RBM, the whole dataset was divided rationally into training and prediction sets on the basis of sign of the residuals (obtained in the original model with the condition that the bigger set as training set). A GA-MLR QSAR model was built for the training and the prediction sets created by RBM method. For comparison purpose, the whole dataset was again divided randomly (random splitting model, termed as RSM) and rationally (using sphere exclusion model, termed a SEM method) into the training and the prediction sets with number of compounds similar to training and prediction sets as in RBM, that is, during these various splitting, the number of molecules in training and prediction set is identical in RBM, RSM, and SEM. A molecule in the training set of one method (RBM or RSM or SEM) may or may not be in the training set of other method (RBM or RSM or SEM). The identical data split with

Table 2 4-aminoquinolines used in present study along with pEC$_{50}$ and descriptors

Sr. no.	R$_1$	R$_2$	pEC$_{50}$ (M)	Mor13e	RDF040v	F06 [N–O]
1	PhO	Furfuryl	5.620	−0.218	7.086	2
2	PhO	2-HO-3-MeO-Bn	5.854	−0.81	7.784	1
3	PhO	Piperonyl	5.921	−1.085	8.62	1
4	PhO	3-F-6-MeO-Bn	5.959	−0.506	7.366	1
5	2-MeO-PhO	Furfuryl	6.143	−0.729	8.331	1
6	2-MeO-PhO	2-HO-3-MeO-Bn	6.152	−1.446	9.537	1
7	2-MeO-PhO	Piperonyl	6.223	−1.455	9.351	1
8	2-MeO-PhO	3-F-6-MeO-Bn	6.236	−0.523	9.875	1
9	3-MeO-PhO	Furfuryl	6.503	−0.319	7.272	1
10	3-MeO-PhO	2-HO-3-MeO-Bn	6.527	−0.748	9.432	1
11	3-MeO-PhO	Piperonyl	6.545	−1.079	9.32	1
12	3-MeO-PhO	3-F-6-MeO-Bn	6.547	−0.64	9.523	1
13	4-MeO-PhO	Furfuryl	6.600	−0.245	7.489	1
14	4-MeO-PhO	2-HO-3-MeO-Bn	6.652	−0.838	9.878	1
15	4-MeO-PhO	Piperonyl	6.682	−1.017	9.645	1
16	4-MeO-PhO	3-F-6-MeO-Bn	6.754	−0.392	9.149	1
17	4-F-PhO	Furfuryl	6.790	−0.428	6.34	1
18	4-F-PhO	2-HO-3-MeO-Bn	6.790	−0.651	8.072	1
19	4-F-PhO	Piperonyl	6.842	−0.842	8.321	1
20	4-F-PhO	3-F-6-MeO-Bn	6.860	−0.691	7.491	1
21	4-Cl-PhO	Furfuryl	6.863	−0.252	8.598	1
22	4-Cl-PhO	Furfuryl	6.879	−0.778	9.636	1
23	4-Cl-PhO	Piperonyl	6.893	−0.749	10.379	1
24	4-Cl-PhO	3-F-6-MeO-Bn	6.896	−0.636	10.35	1
25	3-Me2 N-PhO	Furfuryl	6.928	−0.024	7.162	1
26	3-Me2 N-PhO	2-HO-3-MeO-Bn	6.936	−0.727	8.607	1
27	3-Me2 N-PhO	Piperonyl	6.975	−0.858	8.745	1
28	3-Me2 N-PhO	3-F-6-MeO-Bn	7.018	−0.212	7.919	1
29	4-tertBu-PhO	Furfuryl	7.036	0.559	8.276	1
30	4-tertBu-PhO	2-HO-3-MeO-Bn	7.046	1.005	9.795	1
31	4-tertBu-PhO	Piperonyl	7.051	0.206	9.918	1
32	4-tertBu-PhO	3-F-6-MeO-Bn	7.066	−0.375	10.119	1
33	4-F-Ph	Furfuryl	7.125	−0.585	5.107	0
34	4-F-Ph	2-HO-3-MeO-Bn	7.180	−0.77	6.327	0
35	4-F-Ph	Piperonyl	7.244	−0.931	6.653	0
36	4-F-Ph	3-F-6-MeO-Bn	7.252	−1.058	6.982	0
37	3,5-CF3-Ph	Furfuryl	7.260	−0.722	5.599	0
38	3,5-CF3-Ph	2-HO-3-MeO-Bn	7.268	−0.92	7.079	0
39	3,5-CF3-Ph	Piperonyl	7.268	−1.35	7.336	0
40	3,5-CF3-Ph	3-F-6-MeO-Bn	7.268	−0.935	7.85	0
41	1-Naphtyl	Furfuryl	7.301	−0.703	6.82	0
42	1-Naphtyl	2-HO-3-MeO-Bn	7.337	−0.761	7.719	0
43	1-Naphtyl	Piperonyl	7.337	−1.118	8.451	0
44	1-Naphtyl	3-F-6-MeO-Bn	7.387	−0.556	8.566	0
45	4-CF3-Ph	Furfuryl	7.387	−0.594	5.258	0
46	4-CF3-Ph	2-HO-3-MeO-Bn	7.398	−0.331	6.622	0
47	4-CF3-Ph	Piperonyl	7.398	−0.877	7.122	0
48	4-CF3-Ph	3-F-6-MeO-Bn	7.398	−0.562	7.114	0

Table 2 continued

Sr. no.	R_1	R_2	pEC$_{50}$ (M)	Mor13e	RDF040v	F06 [N–O]
49	Ph	Furfuryl	7.398	−0.449	5.193	0
50	Ph	2-HO-3-MeO-Bn	7.409	−0.4	6.467	0
51	Ph	Piperonyl	7.409	−0.754	6.74	0
52	Ph	3-F-6-MeO-Bn	7.420	−0.588	6.815	0
53	4-tertBu-Ph	Furfuryl	7.469	−0.104	7.086	0
54	4-tertBu-Ph	2-HO-3-MeO-Bn	7.481	0.348	8.467	0
55	4-tertBu-Ph	Piperonyl	7.495	−0.658	8.7	0
56	4-tertBu-Ph	3-F-6-MeO-Bn	7.509	0.472	9.679	0
57	Piperonyl	Furfuryl	7.509	0.326	4.927	0
58	Piperonyl	2-HO-3-MeO-Bn	7.509	−0.592	7.546	0
59	Piperonyl	Piperonyl	7.538	−0.501	7.801	0
60	Piperonyl	3-F-6-MeO-Bn	7.538	−0.268	8.098	0
61	4-MeO-Ph	Furfuryl	7.553	0.539	6.398	0
62	4-MeO-Ph	2-HO-3-MeO-Bn	7.569	−0.221	8.104	0
63	4-MeO-Ph	Piperonyl	7.569	−0.536	8.312	0
64	4-MeO-Ph	3-F-6-MeO-Bn	7.569	−0.071	7.819	0
65	4-F-Bn	Furfuryl	7.569	0.959	5.326	0
66	4-F-Bn	2-HO-3-MeO-Bn	7.585	−0.233	8.929	0
67	4-F-Bn	Piperonyl	7.585	−0.067	10.705	0
68	4-F-Bn	3-F-6-MeO-Bn	7.602	0.219	8.134	0
69	iso-butyl	Furfuryl	7.602	1.507	6.712	0
70	iso-butyl	2-HO-3-MeO-Bn	7.638	0.808	9.125	0
71	iso-butyl	Piperonyl	7.658	0.497	6.044	0
72	iso-butyl	3-F-6-MeO-Bn	7.658	0.112	10.014	0
73	cHex	Furfuryl	7.699	1.544	7.704	0
74	cHex	2-HO-3-MeO-Bn	7.699	0.438	11.277	0
75	cHex	Piperonyl	7.699	0.752	10.997	0
76	cHex	3-F-6-MeO-Bn	7.699	0.756	9.319	0
77	1-Et-Pr	Furfuryl	7.721	1.399	6.966	0
78	1-Et-Pr	2-HO-3-MeO-Bn	7.721	0.074	9.59	0
79	1-Et-Pr	Piperonyl	7.745	0.193	8.59	0
80	1-Et-Pr	3-F-6-MeO-Bn	7.745	0.864	7.615	0
81	3-CF3-Bn	Furfuryl	7.745	0.117	7.599	0
82	3-CF3-Bn	2-HO-3-MeO-Bn	7.745	−0.196	9.004	0
83	3-CF3-Bn	Piperonyl	7.770	0.261	8.227	0
84	3-CF3-Bn	3-F-6-MeO-Bn	7.770	0.413	8.458	0
85	4-CN-Bn	Furfuryl	7.770	1.409	8.512	0
86	4-CN-Bn	2-HO-3-MeO-Bn	7.824	−0.322	9.482	0
87	4-CN-Bn	Piperonyl	7.824	0.399	9.507	0
88	4-CN-Bn	3-F-6-MeO-Bn	7.824	0.776	9.032	0
89	Bn	Furfuryl	7.854	1.122	8.522	0
90	Bn	2-HO-3-MeO-Bn	7.886	0.25	10.837	0
91	Bn	Piperonyl	7.886	−0.019	6.437	0
92	Bn	3-F-6-MeO-Bn	7.886	0.494	10.293	0
93	3,5-Me-Bn	Furfuryl	7.886	1.444	6.402	0
94	3,5-Me-Bn	2-HO-3-MeO-Bn	7.959	1.194	10.845	0
95	3,5-Me-Bn	Piperonyl	7.959	1.419	11.419	0
96	3,5-Me-Bn	3-F-6-MeO-Bn	7.959	0.887	8.162	0

Table 2 continued

Sr. no.	R$_1$	R$_2$	pEC$_{50}$ (M)	Mor13e	RDF040v	F06 [N–O]
97	2-Cl-4-F-Bn	Furfuryl	7.959	0.839	11.876	0
98	2-Cl-4-F-Bn	2-HO-3-MeO-Bn	7.959	−0.479	9.369	0
99	2-Cl-4-F-Bn	Piperonyl	7.959	−0.34	10.094	0
100	2-Cl-4-F-Bn	3-F-6-MeO-Bn	8.000	0.067	9.652	0
101	iso-pentyl	Furfuryl	8.046	1.491	7.984	0
102	iso-pentyl	2-HO-3-MeO-Bn	8.046	1.243	8.878	0
103	iso-pentyl	Piperonyl	8.046	0.237	9.109	0
104	iso-pentyl	3-F-6-MeO-Bn	8.046	0.566	7.314	0
105	cHexmethyl	Furfuryl	8.046	1.37	8.807	0
106	cHexmethyl	2-HO-3-MeO-Bn	8.046	0.976	10.656	0
107	cHexmethyl	Piperonyl	8.097	0.756	11.296	0
108	cHexmethyl	3-F-6-MeO-Bn	8.155	1.236	8.876	0
109	PhEt	Furfuryl	8.398	0.843	7.842	0
110	PhEt	2-HO-3-MeO-Bn	8.398	0.615	9.586	0
111	PhEt	Piperonyl	8.398	0.336	7.842	0
112	PhEt	3-F-6-MeO-Bn	9.000	0.636	14.152	0

respect to number of compounds in the training and the prediction sets was used in external validation for all models of a dataset to allow better comparison between the respective statistics (Kiralj and Ferreira, 2009). GA-MLR models were built also for the RSM and SEM. Briefly, four models were generated for each dataset.

Results and discussion

For small- and moderate-sized datasets, which is the realistic situation for a QSAR modeler, a very serious problem in developing QSAR models with reduced sets of data (splitting the sets) is the loss of considerable amount of information due to holding out of some compounds for validation purpose (Chirico and Gramatica, 2011, 2012; Consonni et al., 2009, 2010; Hawkins, 2004; Hawkins et al., 2008; Huang and Fan, 2011; Mitra et al., 2010; Roy et al., 2008; Schuurmann et al., 2008; Scior et al., 2009). Other confines associated in using small datasets include fortuitous correlation, poor regression statistics, failure of carrying out various statistical tests, and abnormal behavior in performed tests (Kiralj and Ferreira, 2009). This may lead to spurious conclusions in model interpretation and incorrect proposals for the mechanism of action of the compounds.

In the present study, the main emphasis is on various methods for splitting the dataset. For external validation, random as well as rational splitting methods were adopted to create training and prediction sets. For the rational splitting, a special method RBM was also evaluated.

Interestingly, for all the datasets, the residual-based method resulted in radical splitting with ∼55–60 % and ∼40–45 % compounds in the training and the prediction sets, respectively. GA-MLR models were rebuilt for training and prediction sets using the same descriptors that were used for building the original model. In addition to RBM, sphere exclusion algorithm (SEM) and random (RSM) methods were also used for creating training and prediction sets, keeping the number of compounds the same as in residual-based method in the training and prediction sets. This ensures better comparison of various statistical parameters.

The analysis of Tables S1–S3 and 4, 5, 6 indicates that (i) the training and prediction sets used in RBM, RSM, and SEM models cover the diversity of the datasets and (ii) many compounds in the training and the prediction sets are close to each other (see supplementary figure S1, S2, and S3).

The statistical results for the original model for the three datasets are presented in Table 7. The minimum acceptable statistics (or recommended threshold values of statistical parameters) (Chirico and Gramatica, 2011, 2012; Huang and Fan, 2011; Kiralj and Ferreira, 2009; Martin et al., 2012) for regression models in QSAR include following conditions: $R^2 > Q^2$, $Q^2 \geq 0.5$, $R^2_{tr} \geq 0.6$, $R^2_{ex} \geq 0.6$, $RMSE_{tr} < RMSE_{cv}$, $\Delta K \geq 0.05$, $CCC \geq 0.85$, Q^2-$F^n \geq 0.70$, and $r^2_m \geq 0.6$ with $RMSE$, and MAE should be close to zero. In addition, the chance correlation of a QSAR model is validated on following criteria: $R^2_{Yrand} > Q^2_{Yrand}$,

$Q^2_{Yrand} < 0.2$ and $R^2_{Yrand} < 0.2 \rightarrow$ no chance correlation;

Table 3 4-aminoquinolines used in present study along with pEC_{50} and descriptors

Sr. no.	R₁	R₂	pEC₅₀	GATS1p	E3u	E1 m	H6u	R2e
1	PhO	2-HO-3-MeO-Bn	5.046	0.959	0.41	0.552	1.306	1.88
2	PhO	Piperonyl	5.886	1.052	0.383	0.578	1.446	2.004
3	PhO	3-F-6-MeO-Bn	6.097	0.907	0.396	0.576	1.404	1.952
4	2-MeO-PhO	Furfuryl	5.538	1.089	0.309	0.483	1.1	1.988
5	2-MeO-PhO	2-HO-3-MeO-Bn	4.812	1.011	0.279	0.572	1.212	2
6	2-MeO-PhO	Piperonyl	5.215	1.085	0.288	0.595	1.355	2.133
7	2-MeO-PhO	3-F-6-MeO-Bn	5.076	0.964	0.353	0.586	1.485	2.008
8	3-MeO-PhO	Furfuryl	5.086	1.089	0.447	0.507	1.073	1.934
9	3-MeO-PhO	3-F-6-MeO-Bn	5.161	0.964	0.316	0.602	1.42	1.983
10	4-MeO-PhO	Furfuryl	5.553	1.089	0.45	0.507	1.07	1.935
11	4-MeO-PhO	2-HO-3-MeO-Bn	5.367	1.011	0.364	0.523	1.445	1.925
12	4-MeO-PhO	Piperonyl	5.066	1.085	0.429	0.607	1.096	2.03
13	4-MeO-PhO	3-F-6-MeO-Bn	5.041	0.964	0.375	0.602	1.402	1.959
14	4-F-PhO	2-HO-3-MeO-Bn	4.857	0.875	0.435	0.657	1.331	1.906
15	4-F-PhO	3-F-6-MeO-Bn	5.066	0.845	0.395	0.683	1.402	1.974
16	4-Cl-PhO	Furfuryl	4.996	0.974	0.471	0.686	1.21	1.89
17	4-Cl-PhO	Furfuryl	5.167	0.901	0.395	0.771	1.293	1.88
18	4-Cl-PhO	Piperonyl	5.056	0.986	0.389	0.786	1.446	1.997
19	4-Cl-PhO	3-F-6-MeO-Bn	5.215	0.858	0.389	0.798	1.264	1.899
20	3-Me2 N-PhO	2-HO-3-MeO-Bn	4.963	1.049	0.361	0.55	1.153	1.948
21	3-Me2 N-PhO	3-F-6-MeO-Bn	5.699	0.993	0.382	0.581	1.17	1.965
22	4-tertBu-PhO	Furfuryl	5.409	1.043	0.446	0.427	1.59	1.972
23	4-tertBu-PhO	2-HO-3-MeO-Bn	5.921	0.949	0.413	0.482	1.646	1.957
24	4-tertBu-PhO	Piperonyl	5.921	1.043	0.404	0.501	1.858	2.096
25	4-tertBu-PhO	3-F-6-MeO-Bn	5.056	0.898	0.389	0.505	1.617	1.977
26	4-F-Ph	Furfuryl	5.013	0.84	0.332	0.592	0.974	1.888
27	4-F-Ph	2-HO-3-MeO-Bn	5.027	0.799	0.393	0.665	1.252	1.91
28	4-F-Ph	Piperonyl	4.921	0.882	0.281	0.706	1.214	2.013
29	4-F-Ph	3-F-6-MeO-Bn	6	0.77	0.424	0.69	1.269	1.955
30	3,5-CF3-Ph	Furfuryl	5.523	0.739	0.262	0.663	0.878	2.48
31	3,5-CF3-Ph	2-HO-3-MeO-Bn	5.921	0.735	0.353	0.759	1.538	2.267
32	3,5-CF3-Ph	Piperonyl	5.854	0.765	0.307	0.762	1.322	2.519
33	3,5-CF3-Ph	3-F-6-MeO-Bn	6	0.73	0.347	0.783	1.441	2.283
34	1-Naphtyl	Furfuryl	5.092	0.98	0.452	0.48	1.156	1.903
35	1-Naphtyl	2-HO-3-MeO-Bn	5.432	0.863	0.367	0.575	1.259	1.918
36	1-Naphtyl	Piperonyl	5.161	0.986	0.4	0.582	1.469	2.008
37	4-CF3-Ph	Furfuryl	5.167	0.749	0.34	0.688	0.919	2.109
38	4-CF3-Ph	2-HO-3-MeO-Bn	5.377	0.74	0.414	0.756	1.279	2.107
39	4-CF3-Ph	Piperonyl	5.481	0.79	0.406	0.77	1.306	2.245
40	4-CF3-Ph	3-F-6-MeO-Bn	5.092	0.728	0.381	0.775	1.169	2.136
41	Ph	Furfuryl	5.092	1.012	0.33	0.51	0.975	1.854
42	Ph	2-HO-3-MeO-Bn	5.409	0.892	0.354	0.566	1.181	1.883
43	Ph	Piperonyl	5.328	1.015	0.279	0.637	1.21	1.979
44	Ph	3-F-6-MeO-Bn	5.456	0.835	0.374	0.603	1.165	1.919
45	4-tertBu-Ph	Furfuryl	5.409	1.009	0.353	0.447	1.453	2.019
46	4-tertBu-Ph	2-HO-3-MeO-Bn	6.155	0.886	0.377	0.497	1.569	2.037
47	4-tertBu-Ph	Piperonyl	5.796	1.011	0.415	0.528	1.756	2.163
48	4-tertBu-Ph	3-F-6-MeO-Bn	6	0.83	0.357	0.528	1.577	2.061

Table 3 continued

Sr. no.	R$_1$	R$_2$	pEC$_{50}$	GATS1p	E3u	E1 m	H6u	R2e
49	Piperonyl	Furfuryl	5.076	1.057	0.255	0.582	1.033	2.073
50	Piperonyl	2-HO-3-MeO-Bn	5.721	0.985	0.213	0.589	1.608	2.026
51	Piperonyl	Piperonyl	5.119	1.057	0.218	0.604	1.474	2.155
52	Piperonyl	3-F-6-MeO-Bn	5.046	0.939	0.208	0.688	1.718	2.084
53	4-MeO-Ph	Furfuryl	5.119	1.05	0.197	0.532	1.306	1.908
54	4-MeO-Ph	2-HO-3-MeO-Bn	5.602	0.956	0.354	0.504	1.68	1.96
55	4-MeO-Ph	Piperonyl	5.187	1.049	0.225	0.502	1.641	2.051
56	4-MeO-Ph	3-F-6-MeO-Bn	5.041	0.905	0.32	0.497	1.551	1.963
57	4-F-Bn	Furfuryl	5.215	0.838	0.35	0.597	0.765	1.941
58	4-F-Bn	2-HO-3-MeO-Bn	5.027	0.797	0.28	0.605	1.016	1.945
59	4-F-Bn	Piperonyl	5.155	0.88	0.433	0.663	0.961	1.977
60	4-F-Bn	3-F-6-MeO-Bn	5.538	0.768	0.407	0.645	1.403	1.874
61	iso-butyl	2-HO-3-MeO-Bn	5.409	0.925	0.286	0.395	1.138	2.053
62	iso-butyl	Piperonyl	5.569	1.05	0.423	0.438	1.042	2.107
63	iso-butyl	3-F-6-MeO-Bn	5.444	0.865	0.303	0.373	1.305	2.041
64	cHex	Furfuryl	5.18	1.012	0.312	0.476	1.052	2.075
65	cHex	2-HO-3-MeO-Bn	5.77	0.892	0.353	0.464	1.251	2.082
66	cHex	Piperonyl	5.268	1.015	0.256	0.541	1.231	2.129
67	cHex	3-F-6-MeO-Bn	5.495	0.835	0.228	0.517	1.377	2.031
68	1-Et-Pr	Furfuryl	4.987	1.049	0.299	0.484	1.331	1.969
69	1-Et-Pr	2-HO-3-MeO-Bn	6.959	0.925	0.361	0.444	1.619	2.021
70	1-Et-Pr	Piperonyl	5.131	1.05	0.304	0.527	1.334	2.121
71	1-Et-Pr	3-F-6-MeO-Bn	5.032	0.863	0.271	0.584	1.882	1.973
72	3-CF3-Bn	Furfuryl	5.409	0.746	0.369	0.722	1.296	2.168
73	3-CF3-Bn	2-HO-3-MeO-Bn	5.678	0.737	0.356	0.499	1.701	2.132
74	3-CF3-Bn	Piperonyl	5.602	0.787	0.337	0.732	1.565	2.246
75	3-CF3-Bn	3-F-6-MeO-Bn	6.398	0.725	0.311	0.525	1.738	2.205
76	4-CN-Bn	Furfuryl	4.943	0.963	0.23	0.602	0.981	1.931
77	4-CN-Bn	2-HO-3-MeO-Bn	5.066	0.872	0.32	0.566	1.335	1.853
78	4-CN-Bn	Piperonyl	5.066	0.983	0.152	0.578	1.257	1.97
79	4-CN-Bn	3-F-6-MeO-Bn	5.119	0.824	0.157	0.581	1.388	1.802
80	Bn	2-HO-3-MeO-Bn	5.092	0.891	0.14	0.491	1.554	1.792
81	Bn	Piperonyl	5.086	1.014	0.436	0.481	1.119	2.066
82	Bn	3-F-6-MeO-Bn	5.081	0.834	0.211	0.508	1.435	1.787
83	3,5-Me-Bn	Furfuryl	5.143	1.009	0.355	0.494	1.25	1.983
84	3,5-Me-Bn	2-HO-3-MeO-Bn	5.602	0.887	0.176	0.473	1.993	1.875
85	3,5-Me-Bn	Piperonyl	5.523	1.012	0.189	0.49	1.639	1.991
86	3,5-Me-Bn	3-F-6-MeO-Bn	6.046	0.831	0.318	0.499	1.465	2.046
87	2-Cl-4-F-Bn	Furfuryl	5.06	0.789	0.385	0.674	1.245	1.82
88	2-Cl-4-F-Bn	2-HO-3-MeO-Bn	5.538	0.757	0.266	0.597	1.555	1.975
89	2-Cl-4-F-Bn	Piperonyl	5.276	0.834	0.273	0.744	1.297	2.003
90	2-Cl-4-F-Bn	3-F-6-MeO-Bn	5.495	0.733	0.403	0.624	1.312	1.957
91	iso-pentyl	2-HO-3-MeO-Bn	5.194	0.922	0.332	0.625	1.365	2.086
92	iso-pentyl	Piperonyl	5.538	1.047	0.3	0.689	1.134	2.228
93	iso-pentyl	3-F-6-MeO-Bn	6	0.865	0.306	0.451	1.106	2.031
94	cHexmethyl	Furfuryl	5.658	1.011	0.33	0.478	1.266	2.051
95	cHexmethyl	2-HO-3-MeO-Bn	5.921	0.891	0.278	0.473	1.733	2.079
96	cHexmethyl	Piperonyl	5.027	1.014	0.234	0.553	1.335	2.27

Table 3 continued

Sr. no.	R_1	R_2	pEC_{50}	GATS1p	E3u	E1 m	H6u	R2e
97	cHexmethyl	3-F-6-MeO-Bn	5.553	0.834	0.293	0.476	1.355	2.082
98	PhEt	2-HO-3-MeO-Bn	5.119	0.799	0.278	0.535	1.744	1.963
99	PhEt	Piperonyl	5.229	0.832	0.204	0.554	1.546	1.854
100	PhEt	3-F-6-MeO-Bn	5.252	1.013	0.317	0.542	1.794	1.96

Any Q^2_{Yrand} and $0.2 < R^2_{Yrand} < 0.3 \rightarrow$ negligible chance correlation;

Any Q^2_{Yrand} and $0.3 < R^2_{Yrand} < 0.4 \rightarrow$ tolerable chance correlation;

Any Q^2_{Yrand} and $R^2_{Yrand} > 0.4 \rightarrow$ recognized chance correlation.

$(1-r^2/r_o^2) < 0.1$, $0.9 \le k \le 1.1$ or $(1-r^2/r_o'^2) < 0.1$, $0.9 \le k' \le 1.1$ with $| r_o^2 - r_o'^2| < 0.3$

Except for the dataset-3, the statistical parameters point out that the GA-MLR original models for the dataset-1 and 2 are statistically robust with statistically acceptable values of R^2_{tr}, $R^2_{adj.}$, R^2_{cv}, R^2_{LMO}, R^2_{Yrand}, s, Kxx, ΔK, $RMSE_{tr}$, $RMSE_{cv}$, CCC_{tr}, CCC_{cv}, MAE_{tr}, MAE_{cv}, and F. Thus, from the internal validation point of view, the original models for the dataset 1 and 2 are satisfying all the essential conditions and criteria. The positive or negative contribution of a descriptor to activity remains the same during the data split and building original model indicating self-consistency of data(Kiralj and Ferreira, 2009), which is useful for model interpretation and mechanism of action.

Since, for a dataset, the same descriptors that cover the diversity of training and prediction sets are used to build models for different types of training and prediction sets, the statistical performance of residual based, random splitting and sphere exclusion should be comparable with each other for all the datasets. But, the statistical performance of each model is different (see Tables 7, 8, 9, 10). This indicates that the method of splitting has significant effect on the behavior of statistical parameters. Additionally, since the descriptors have been selected prior to splitting, the built models have captured common features of training and prediction set molecules, therefore, the models are capable to detect them in the test molecules, also. Consequently, the external predictivity of models should be high and comparable to each other for a dataset. However, the analysis of Tables 8, 9, and 10 indicates that the external predictivity of different models is different. Thus, it appears that the selection of descriptors prior to splitting has little role to play in deciding external predictivity of model. In fact, it is the diversity of training and prediction set that decides the external predictivity of any QSAR model. In other words, if the compounds in prediction set resemble the training set compounds, high

predictive ability is observed for the developed model. Therefore, more number of model based on different training and prediction sets for a dataset must be developed, else, boot-strapping is an attractive option.

Results for the dataset-1

A comparison of various statistical parameters viz. R^2_{tr}, $R^2_{adj.}$, R^2_{cv}, R^2_{LMO}, R^2_{Yrand}, s, R^2_{ex}, Kxx, ΔK, $RMSE_{tr}$, $RMSE_{cv}$, CCC_{tr}, CCC_{cv}, MAE_{tr}, MAE_{cv}, $r^2_m av$, and F reveals that the performance of RBM model is better than the other models, which suggests that the model is statistically soundful and has good predictive ability. The r^2_m statistic, which penalizes the model profoundly for large difference between predicted and the corresponding experimental response, is higher for residual-based model indicating good external predictivity (Mitra et al., 2010; Roy and Mitra, 2012). A plausible reason for this could be the distribution of the training and the prediction sets in the chemical space because both the sets used in RBM model covers diversity of the dataset. Though RBM model appears statistically robust but apropos of many statistical parameters, everything is not rosy-red for it.

For a good predictive ability $RMSE_{ex}$ and MAE_{ex} should be as low as possible (Chirico and Gramatica, 2011), but for RBM model, the values for these parameters are higher than the rest of the models. The large difference between $RMSE_{tr}$ (=0.118) and $RMSE_{ex}$ (=0.441) as well as between MAE_{tr} (=0.089) and MAE_{ex} (=0.394) raises question on residual-based model's generalizability (Chirico and Gramatica, 2011, 2012). In addition, the lower values of CCC_{ex}, Q^2-F^1, Q^2-F^2, and Q^2-F^3 for RBM model than RSM and SEM models indicate low external predictivity of this model (Chirico and Gramatica 2011, 2012; Consonni et al., 2009, 2010; Schuurmann et al., 2008). Thus, the RBM model is appearing statistically soundful on the basis of many parameters, but some parameters raise doubts on its external predictivity. A possible reason could be the sensitivity of Q^2-F^1 and Q^2-F^2 toward the presence of outliers in the prediction set (Consonni et al., 2010). That is, the presence of more number of outliers in the prediction set of RBM model than the other models is responsible for its low external predictivity. Therefore, it can be stated

Table 4 Experimental and predicted pIC_{50} by different models for dataset-1

ID	pIC_{50}	Status	Pred. pIC_{50} (Originalmodel)	Status	Pred. pIC_{50} RBM	Status	Pred. pIC_{50} RSM	Status	Pred. pIC_{50} SEM
1	5.8240	Training	5.2945	Prediction	4.9468	Training	5.5246	Training	5.2338
2	4.4810	Training	4.1434	Prediction	4.0651	Prediction	4.3532	Prediction	4.0669
3	5.3670	Training	5.1114	Prediction	4.6446	Training	5.1312	Prediction	5.0960
4	4.8240	Training	4.6201	Prediction	4.5856	Prediction	4.6241	Training	4.7066
5	3.9210	Training	4.3456	Training	4.2006	Prediction	4.7011	Training	4.2484
6	4.7700	Training	4.9528	Training	4.8453	Training	4.7697	Training	5.0715
7	5.6020	Training	5.4692	Prediction	5.2327	Training	5.4758	Prediction	5.5231
8	4.1490	Training	4.4768	Training	4.1421	Prediction	4.5794	Training	4.3759
9	4.3190	Training	4.4971	Training	4.2888	Training	4.3606	Prediction	4.5313
10	4.8240	Training	4.8351	Prediction	4.5429	Prediction	4.8050	Training	4.8310
11	4.2600	Training	4.2126	Prediction	4.0629	Prediction	4.2534	Prediction	4.1652
12	4.3980	Training	4.3672	Prediction	4.1746	Prediction	4.0790	Prediction	4.4456
13	4.6780	Training	4.8172	Training	4.6643	Prediction	4.8165	Prediction	4.8690
14	4.6780	Training	4.2410	Prediction	4.0579	Training	4.2332	Training	4.2110
15	4.6380	Training	4.8594	Training	4.5173	Training	4.9219	Training	4.8445
16	4.8540	Training	4.7210	Prediction	4.6080	Prediction	4.7724	Prediction	4.7689
17	4.2920	Training	4.3798	Training	4.1487	Training	4.4670	Prediction	4.3226
18	4.5850	Training	4.6987	Training	4.5177	Training	4.6012	Training	4.6975
19	4.8240	Training	4.9861	Training	4.7799	Training	4.8915	Prediction	5.0179
20	4.8860	Training	5.0662	Training	4.9380	Prediction	4.9073	Prediction	5.1382
21	4.3010	Training	4.5949	Training	4.3935	Training	4.4711	Training	4.5774
22	4.3770	Training	4.3227	Prediction	4.1462	Training	4.4158	Prediction	4.2844
23	4.0180	Training	4.2580	Training	4.1286	Training	4.2083	Training	4.2826
24	4.8240	Training	4.5794	Prediction	4.4278	Prediction	4.4112	Training	4.6660
25	4.1940	Training	3.8950	Prediction	3.9259	Prediction	3.6105	Training	3.9953
26	4.5850	Training	4.6599	Training	4.5970	Training	4.6743	Prediction	4.7344
27	5.3280	Training	5.0269	Prediction	4.6933	Prediction	5.0460	Training	4.9675
28	4.3570	Training	4.3042	Prediction	4.1023	Training	4.1680	Training	4.3111
29	4.4810	Training	4.5794	Training	4.3587	Prediction	4.4580	Prediction	4.6178
30	4.6020	Training	4.6885	Training	4.5141	Training	4.5384	Prediction	4.7488
31	4.1250	Training	4.2266	Training	3.9974	Prediction	4.1417	Training	4.1867
32	4.9210	Training	4.9349	Training	4.6648	Training	4.8049	Prediction	4.9387
33	4.9210	Training	5.2090	Training	4.9217	Prediction	5.0860	Training	5.2472
34	5.6200	Training	5.3283	Prediction	5.1025	Prediction	5.1492	Training	5.4025
35	4.9210	Training	4.7116	Prediction	4.4781	Prediction	4.5533	Prediction	4.7109
36	4.9590	Training	4.9578	Prediction	4.5756	Training	5.0387	Prediction	4.8530
37	3.9910	Training	4.1116	Training	3.9965	Training	4.1346	Training	4.0684
38	4.8240	Training	4.3522	Prediction	4.1887	Prediction	4.1562	Training	4.4158
39	4.3870	Training	4.5814	Training	4.4422	Training	4.2705	Prediction	4.7137
40	4.0660	Training	4.3520	Training	4.2611	Training	4.1534	Prediction	4.4426
41	4.4950	Training	4.5532	Training	4.4897	Prediction	4.2078	Training	4.7186
42	4.5230	Training	4.3868	Prediction	4.3279	Training	4.3650	Training	4.3516
43	4.7450	Training	5.1121	Training	4.8920	Training	5.2956	Training	5.0681
44	4.4090	Training	4.3261	Prediction	4.2793	Prediction	4.4605	Prediction	4.3016

RBM Residual-based model, *RBM* Random splitting model, *SEM* Sphere exclusion model

Table 5 Experimental and predicted pEC_{50} by different models for dataset-2

ID	pEC_{50}(M)	Status	Pred. pEC_{50} (Original model)	Status	Pred. pEC_{50} RBM	Status	Pred. pEC_{50} RSM	Status	Pred. pEC_{50} SEM
1	5.620	Training	5.6830	Training	5.3535	Prediction	5.8460	Training	5.6082
2	5.854	Training	6.5075	Training	6.2924	Prediction	6.5813	Training	6.4897
3	5.921	Training	6.5065	Training	6.2847	Training	6.5663	Prediction	6.4877
4	5.959	Training	6.5481	Training	6.3330	Prediction	6.6285	Training	6.5248
5	6.143	Training	6.5698	Training	6.3449	Prediction	6.6337	Training	6.5420
6	6.152	Training	6.4911	Training	6.2631	Training	6.5357	Prediction	6.4734
7	6.223	Training	6.4744	Training	6.2494	Training	6.5223	Training	6.4594
8	6.236	Training	6.7401	Training	6.4880	Prediction	6.7765	Prediction	6.6853
9	6.503	Training	6.5859	Training	6.3683	Training	6.6674	Prediction	6.5571
10	6.527	Training	6.6512	Training	6.4103	Prediction	6.6959	Prediction	6.6101
11	6.545	Training	6.5626	Training	6.3303	Prediction	6.6101	Prediction	6.5347
12	6.547	Training	6.6844	Training	6.4399	Training	6.7272	Prediction	6.6382
13	6.600	Training	6.6207	Training	6.3983	Training	6.6982	Prediction	6.5865
14	6.652	Training	6.6644	Training	6.4187	Training	6.7015	Prediction	6.6207
15	6.682	Training	6.6030	Prediction	6.3645	Training	6.6446	Prediction	6.5687
16	6.754	Training	6.7149	Prediction	6.4709	Prediction	6.7637	Training	6.6648
17	6.790	Training	6.4868	Prediction	6.2853	Training	6.5849	Training	6.4738
18	6.790	Training	6.5683	Prediction	6.3457	Training	6.6367	Prediction	6.5412
19	6.842	Training	6.5417	Prediction	6.3193	Training	6.6062	Training	6.5182
20	6.860	Training	6.5133	Prediction	6.3001	Training	6.5919	Prediction	6.4950
21	6.863	Training	6.7057	Prediction	6.4669	Prediction	6.7638	Prediction	6.6576
22	6.879	Training	6.6599	Prediction	6.4166	Prediction	6.7011	Prediction	6.6172
23	6.893	Training	6.7250	Prediction	6.4700	Prediction	6.7531	Training	6.6718
24	6.896	Training	6.7500	Prediction	6.4931	Training	6.7783	Training	6.6931
25	6.928	Training	6.6484	Prediction	6.4264	Prediction	6.7312	Prediction	6.6106
26	6.936	Training	6.5918	Prediction	6.3628	Training	6.6509	Training	6.5605
27	6.975	Training	6.5710	Prediction	6.3426	Training	6.6280	Prediction	6.5426
28	7.018	Training	6.6622	Prediction	6.4328	Training	6.7322	Prediction	6.6214
29	7.036	Training	6.8761	Prediction	6.6254	Prediction	6.9378	Training	6.8033
30	7.046	Training	7.1023	Training	6.8198	Prediction	7.1363	Training	6.9942
31	7.051	Training	6.9193	Prediction	6.6514	Training	6.9531	Prediction	6.8380
32	7.066	Training	6.7948	Prediction	6.5360	Training	6.8266	Prediction	6.7317
33	7.125	Training	7.2652	Training	7.1980	Training	7.3070	Prediction	7.3185
34	7.180	Training	7.3159	Training	7.2344	Training	7.3368	Prediction	7.3602
35	7.244	Training	7.3026	Training	7.2195	Prediction	7.3181	Prediction	7.3484
36	7.252	Training	7.2977	Training	7.2123	Prediction	7.3078	Training	7.3438
37	7.260	Training	7.2706	Training	7.1989	Training	7.3042	Training	7.3225
38	7.268	Training	7.3385	Training	7.2489	Training	7.3466	Training	7.3785
39	7.268	Training	7.2549	Prediction	7.1703	Training	7.2595	Prediction	7.3069
40	7.268	Training	7.3952	Training	7.2943	Prediction	7.3897	Prediction	7.4258
41	7.301	Training	7.3706	Training	7.2803	Prediction	7.3827	Training	7.4062
42	7.337	Training	7.4269	Training	7.3244	Training	7.4233	Training	7.4530
43	7.337	Training	7.3980	Training	7.2920	Prediction	7.3824	Prediction	7.4275
44	7.387	Training	7.5425	Training	7.4232	Prediction	7.5236	Prediction	7.5505
45	7.387	Training	7.2748	Prediction	7.2056	Prediction	7.3140	Training	7.3265
46	7.398	Training	7.4449	Training	7.3498	Prediction	7.4595	Prediction	7.4697
47	7.398	Training	7.3523	Prediction	7.2611	Prediction	7.3594	Prediction	7.3902

Table 5 continued

ID	pEC_{50}(M)	Status	Pred. pEC_{50} (Original model)	Status	Pred. pEC_{50} RBM	Status	Pred. pEC_{50} RSM	Status	Pred. pEC_{50} SEM
48	7.398	Training	7.4276	Training	7.3300	Prediction	7.4341	Training	7.4544
49	7.398	Training	7.3047	Prediction	7.2334	Training	7.3447	Training	7.3521
50	7.409	Training	7.4161	Training	7.3248	Prediction	7.4336	Prediction	7.4454
51	7.409	Training	7.3521	Prediction	7.2640	Training	7.3657	Training	7.3905
52	7.420	Training	7.3980	Prediction	7.3054	Training	7.4098	Prediction	7.4295
53	7.469	Training	7.5359	Training	7.4292	Prediction	7.5418	Training	7.5467
54	7.481	Training	7.7528	Training	7.6162	Training	7.7333	Prediction	7.7299
55	7.495	Training	7.5284	Training	7.4092	Training	7.5073	Prediction	7.5383
56	7.509	Training	7.8774	Training	7.7202	Prediction	7.8364	Training	7.8346
57	7.509	Training	7.4709	Prediction	7.3874	Training	7.5136	Training	7.4941
58	7.509	Training	7.4541	Prediction	7.3507	Training	7.4532	Training	7.4765
59	7.538	Training	7.4960	Prediction	7.3869	Training	7.4903	Prediction	7.5118
60	7.538	Training	7.5754	Training	7.4571	Training	7.5639	Prediction	7.5791
61	7.553	Training	7.6372	Training	7.5275	Prediction	7.6535	Training	7.6340
62	7.569	Training	7.5872	Training	7.4678	Prediction	7.5755	Training	7.5892
63	7.569	Training	7.5275	Prediction	7.4115	Training	7.5129	Prediction	7.5380
64	7.569	Training	7.6011	Training	7.4829	Prediction	7.5941	Prediction	7.6014
65	7.569	Training	7.6547	Training	7.5522	Training	7.6888	Prediction	7.6503
66	7.585	Training	7.6488	Training	7.5174	Training	7.6226	Training	7.6406
67	7.585	Training	7.8276	Training	7.6663	Prediction	7.7699	Training	7.7908
68	7.602	Training	7.6956	Training	7.5667	Training	7.6824	Training	7.6816
69	7.602	Training	7.8951	Training	7.7607	Prediction	7.9036	Training	7.8535
70	7.638	Training	7.9151	Training	7.7593	Prediction	7.8830	Training	7.8675
71	7.658	Training	7.5994	Prediction	7.4958	Prediction	7.6221	Training	7.6022
72	7.658	Training	7.8168	Training	7.6621	Training	7.7707	Prediction	7.7825
73	7.699	Training	7.9816	Training	7.8316	Training	7.9726	Training	7.9259
74	7.699	Training	7.9941	Training	7.8138	Training	7.9251	Training	7.9320
75	7.699	Training	8.0479	Training	7.8653	Prediction	7.9831	Training	7.9783
76	7.699	Training	7.9178	Training	7.7601	Training	7.8823	Training	7.8694
77	7.721	Training	7.8890	Training	7.7530	Training	7.8932	Training	7.8479
78	7.721	Training	7.7745	Training	7.6269	Prediction	7.7360	Training	7.7469
79	7.745	Training	7.7250	Prediction	7.5898	Prediction	7.7038	Training	7.7061
80	7.745	Training	7.8106	Training	7.6761	Prediction	7.8049	Training	7.7803
81	7.745	Training	7.6292	Prediction	7.5104	Training	7.6256	Prediction	7.6257
82	7.745	Training	7.6636	Prediction	7.5303	Training	7.6360	Training	7.6531
83	7.770	Training	7.7130	Prediction	7.5819	Training	7.6980	Prediction	7.6963
84	7.770	Training	7.7678	Prediction	7.6300	Training	7.7483	Prediction	7.7427
85	7.770	Training	8.0122	Training	7.8530	Training	7.9893	Prediction	7.9510
86	7.824	Training	7.6705	Prediction	7.5327	Prediction	7.6349	Training	7.6585
87	7.824	Training	7.8463	Training	7.6933	Training	7.8085	Training	7.8083
88	7.824	Training	7.9001	Training	7.7463	Training	7.8697	Training	7.8548
89	7.854	Training	7.9437	Training	7.7903	Prediction	7.9214	Training	7.8926
90	7.886	Training	7.9143	Training	7.7445	Training	7.8535	Prediction	7.8646
91	7.886	Training	7.5056	Prediction	7.4069	Prediction	7.5227	Training	7.5218
92	7.886	Training	7.9307	Training	7.7639	Training	7.8788	Prediction	7.8792
93	7.886	Training	7.8557	Prediction	7.7272	Training	7.8698	Training	7.8203
94	7.959	Training	8.1426	Training	7.9532	Training	8.0793	Training	8.0592

Table 5 continued

ID	pEC_{50}(M)	Status	Pred. pEC_{50} (Original model)	Status	Pred. pEC_{50} RBM	Status	Pred. pEC_{50} RSM	Status	Pred. pEC_{50} SEM
95	7.959	Training	8.2417	Training	8.0391	Training	8.1678	Prediction	8.1430
96	7.959	Training	7.8589	Prediction	7.7158	Training	7.8435	Training	7.8208
97	7.959	Training	8.1376	Training	7.9401	Prediction	8.0571	Training	8.0536
98	7.959	Training	7.6238	Prediction	7.4910	Training	7.5906	Training	7.6188
99	7.959	Training	7.7140	Prediction	7.5675	Prediction	7.6677	Prediction	7.6948
100	8.000	Training	7.7776	Prediction	7.6292	Prediction	7.7381	Training	7.7496
101	8.046	Training	7.9907	Prediction	7.8377	Training	7.9769	Training	7.9333
102	8.046	Training	8.0007	Prediction	7.8395	Prediction	7.9719	Training	7.9408
103	8.046	Training	7.7762	Prediction	7.6324	Prediction	7.7457	Training	7.7490
104	8.046	Training	7.7153	Prediction	7.5914	Prediction	7.7155	Training	7.6994
105	8.046	Training	8.0258	Prediction	7.8630	Training	7.9979	Prediction	7.9622
106	8.046	Training	8.0753	Training	7.8931	Training	8.0159	Training	8.0020
107	8.097	Training	8.0722	Prediction	7.8851	Prediction	8.0021	Training	7.9986
108	8.155	Training	7.9989	Prediction	7.8379	Prediction	7.9701	Prediction	7.9392
109	8.398	Training	7.8233	Prediction	7.6858	Training	7.8136	Prediction	7.7908
110	8.398	Training	7.9046	Prediction	7.7459	Training	7.8649	Training	7.8579
111	8.398	Training	7.7010	Prediction	7.5740	Prediction	7.6926	Prediction	7.6866
112	9.000	Training	8.2665	Prediction	8.0393	Prediction	8.1465	Prediction	8.1606

that residual-based model possesses poor external predictivity, hence should not be adopted to create QSAR models. In addition, as many as possible parameters should be reported for a QSAR model developed using single splitting method. Because, the true predictive ability of residual-based model was captured, only when many statistical parameters were calculated.

For some parameters viz. R_{tr}^2, $R_{adj.}^2$, R_{cv}^2, R_{LMO}^2, R_{Yrand}^2, s, Kxx, ΔK, $RMSE_{tr}$, $RMSE_{cv}$, CCC_{tr}, CCC_{cv}, MAE_{tr}, MAE_{cv}, and F, the performance of random splitting model is either statistically satisfactory or comparable with the other models. But, for some parameters viz. CCC_{ex}, $r_m^2 av$, and r_m^2, the performance of the model is questionable. A large difference of 0.309 between R_{tr}^2 (=0.674), and R_{cv}^2 (=0.365) for sphere exclusion model reflects large inaccuracy of the model (Schuurmann et al., 2008) or overfitting (Kiralj and Ferreira, 2009). A probable reason could be either the small size of dataset-1 or size of training and prediction sets. But, the problem of large inaccuracy of model or overfitting is not visible for other models. Similarly, the very low value of F (=7.023) indicates low statistical reliability of the sphere exclusion model. A very surprising and rare observation for sphere exclusion model is the higher values of $Q^2 - F^1$ (=0.706), $Q^2 - F^2$ (=0.705), and $Q^2 - F^3$ (=0.828) than R^2 (=0.674), leading to the contrasting conclusion that the model is able to predict new data better than fitting available ones (Chirico and Gramatica, 2011; 2012).

For residual-based and random splitting models, $RMSE_{tr}$ and MAE_{tr} are lower than $RMSE_{ex}$ and MAE_{ex},

respectively. This indicates that the samples for which the models fit very well are present in the training set. Exactly reverse is true for the sphere exclusion model, for which $RMSE_{tr}$ and MAE_{tr} are higher than $RMSE_{ex}$ and MAE_{ex}, respectively. This observation points out one serious drawback of common practice followed in external validation, in which single split is performed to validate the model. If a researcher purposely selects training and prediction sets such that $RMSE_{tr}$ and MAE_{tr} are higher than $RMSE_{ex}$ and MAE_{ex}, respectively then, the model will be with lower internal predictivity but with high external predictivity. In such case, many parameters will give false positive results because of the purposeful selection of training and prediction sets. Therefore, one cannot merely rely on external validation based on single split; instead, boot-strap or multiple modeling (Masand et al., 2014) must be followed to develop a good number of statistically robust QSAR models with good external predictive ability.

As the number of compounds is same in the training and the prediction sets for the three models, the difference between R^2 and Q^2 should be comparable for all the models. But, different models have different variation indicating that the method of splitting has good influence on many statistical parameters.

Results for the dataset-2

Similar to the dataset-1, different statistical parameters viz. R_{tr}^2, $R_{adj.}^2$, R_{cv}^2, R_{LMO}^2, R_{Yrand}^2, s, R_{ex}^2, Kxx, ΔK, $RMSE_{tr}$,

Table 6 Experimental and predicted pEC_{50} by different models for dataset-3

ID	pEC_{50} (M)	Status	Pred. pEC_{50} (Original model)	Status	Pred. pEC_{50} RBM	Status	Pred. pEC_{50} RSM	Status	Pred. pEC_{50} SEM
1	5.0460	Training	5.2880	Training	5.0711	Prediction	5.2655	Training	5.2987
2	5.8860	Training	5.3162	Prediction	5.1067	Prediction	5.1656	Training	5.3758
3	6.0970	Training	5.4203	Prediction	5.1851	Training	5.4203	Prediction	5.4266
4	5.5380	Training	5.1536	Prediction	5.0015	Prediction	5.0639	Training	5.2397
5	4.8120	Training	5.1292	Training	4.9953	Prediction	5.0477	Prediction	5.1723
6	5.2150	Training	5.2416	Training	5.0927	Prediction	5.0486	Training	5.3319
7	5.0760	Training	5.3873	Training	5.1679	Prediction	5.3175	Training	5.4200
8	5.0860	Training	5.2170	Training	5.0278	Training	5.1048	Prediction	5.2875
9	5.1610	Training	5.2564	Training	5.0749	Training	5.1851	Training	5.2775
10	5.5530	Training	5.2207	Prediction	5.0306	Training	5.1083	Training	5.2915
11	5.3670	Training	5.3308	Prediction	5.1010	Prediction	5.2687	Training	5.3750
12	5.0660	Training	5.1657	Training	5.0194	Prediction	4.9778	Prediction	5.2299
13	5.0410	Training	5.2956	Training	5.0944	Training	5.2224	Training	5.3125
14	4.8570	Training	5.2932	Training	5.0920	Training	5.2728	Training	5.2583
15	5.0660	Training	5.3473	Training	5.1502	Prediction	5.3307	Prediction	5.3120
16	4.9960	Training	5.1086	Training	4.9515	Prediction	4.9761	Training	5.0904
17	5.1670	Training	4.9870	Prediction	4.8743	Prediction	4.8687	Prediction	4.9219
18	5.0560	Training	5.0659	Training	4.9428	Prediction	4.8331	Training	5.0495
19	5.2150	Training	4.9953	Prediction	4.8925	Prediction	4.9007	Training	4.9143
20	4.9630	Training	5.1377	Training	4.9818	Training	5.0357	Prediction	5.1872
21	5.6990	Training	5.2073	Prediction	5.0408	Training	5.1339	Training	5.2368
22	5.4090	Training	5.6696	Training	5.3335	Training	5.6231	Training	5.7631
23	5.9210	Training	5.6557	Prediction	5.3315	Training	5.6635	Training	5.7037
24	5.9210	Training	5.7666	Prediction	5.4245	Training	5.6428	Training	5.8705
25	5.0560	Training	5.6574	Training	5.3471	Training	5.7013	Prediction	5.6881
26	5.0130	Training	5.1211	Training	4.9909	Prediction	5.2146	Prediction	5.0824
27	5.0270	Training	5.2824	Training	5.1005	Training	5.3394	Prediction	5.2222
28	4.9210	Training	5.0851	Training	4.9867	Training	5.0342	Prediction	5.0581
29	6.0000	Training	5.3765	Prediction	5.1800	Training	5.4363	Prediction	5.3123
30	5.5230	Training	5.6885	Training	5.5625	Prediction	5.7878	Training	5.7320
31	5.9210	Training	5.7055	Prediction	5.4872	Prediction	5.7108	Prediction	5.6846
32	5.8540	Training	5.8074	Prediction	5.6322	Training	5.7752	Training	5.8473
33	6.0000	Training	5.6413	Prediction	5.4524	Prediction	5.6397	Training	5.6148
34	5.0920	Training	5.3899	Training	5.1492	Training	5.4014	Training	5.4303
35	5.4320	Training	5.3296	Prediction	5.1263	Prediction	5.3885	Prediction	5.3132
36	5.1610	Training	5.4215	Training	5.1878	Training	5.3298	Prediction	5.4626
37	5.1670	Training	5.3199	Training	5.2029	Prediction	5.4170	Training	5.2786
38	5.3770	Training	5.4780	Training	5.2955	Training	5.5066	Prediction	5.4217
39	5.4810	Training	5.5637	Training	5.3845	Prediction	5.5192	Training	5.5493
40	5.0920	Training	5.4044	Training	5.2601	Prediction	5.4386	Training	5.3439
41	5.0920	Training	5.0119	Prediction	4.8827	Training	4.9975	Training	5.0372
42	5.4090	Training	5.2179	Prediction	5.0396	Training	5.2640	Prediction	5.2032
43	5.3280	Training	4.9977	Prediction	4.8990	Prediction	4.8683	Prediction	5.0198
44	5.4560	Training	5.2855	Prediction	5.1040	Training	5.3574	Prediction	5.2528
45	5.4090	Training	5.5518	Training	5.2783	Training	5.5371	Training	5.6367
46	6.1550	Training	5.7172	Prediction	5.4084	Training	5.7770	Prediction	5.7592
47	5.7960	Training	5.8079	Training	5.4795	Prediction	5.6956	Prediction	5.9094
48	6.0000	Training	5.7385	Prediction	5.4377	Training	5.8305	Training	5.7611

Table 6 continued

ID	pEC_{50} (M)	Status	Pred. pEC_{50} (Original model)	Status	Pred. pEC_{50} RBM	Status	Pred. pEC_{50} RSM	Status	Pred. pEC_{50} SEM
49	5.0760	Training	5.0362	Prediction	4.9532	Prediction	4.9090	Training	5.1036
50	5.7210	Training	5.2562	Prediction	5.0786	Prediction	5.1665	Prediction	5.2963
51	5.1190	Training	5.2491	Training	5.1047	Training	5.0739	Prediction	5.3336
52	5.0460	Training	5.2651	Training	5.1029	Training	5.1386	Training	5.2798
53	5.1190	Training	4.9765	Prediction	4.8580	Training	4.8949	Prediction	5.0200
54	5.6020	Training	5.5567	Prediction	5.2637	Training	5.5449	Prediction	5.6006
55	5.1870	Training	5.3790	Training	5.1589	Prediction	5.2824	Prediction	5.4672
56	5.0410	Training	5.5276	Training	5.2577	Training	5.5819	Training	5.5568
57	5.2150	Training	5.1070	Prediction	5.0042	Training	5.2056	Training	5.0763
58	5.0270	Training	5.1689	Training	5.0449	Training	5.2921	Training	5.1264
59	5.1550	Training	5.1929	Training	5.0573	Training	5.1803	Training	5.1693
60	5.5380	Training	5.3921	Prediction	5.1635	Prediction	5.4864	Prediction	5.3224
61	5.4090	Training	5.5410	Training	5.3063	Prediction	5.6685	Prediction	5.6176
62	5.5690	Training	5.5278	Prediction	5.2954	Training	5.4907	Training	5.6434
63	5.4440	Training	5.7260	Training	5.4307	Prediction	5.9172	Training	5.7908
64	5.1800	Training	5.3365	Training	5.1632	Training	5.3221	Prediction	5.4211
65	5.7700	Training	5.6413	Prediction	5.3814	Prediction	5.7366	Training	5.6995
66	5.2680	Training	5.3039	Training	5.1497	Training	5.2291	Prediction	5.3851
67	5.4950	Training	5.4599	Prediction	5.2491	Training	5.5817	Training	5.4745
68	4.9870	Training	5.2660	Training	5.0696	Training	5.2030	Prediction	5.3385
69	6.9590	Training	5.7388	Prediction	5.4117	Prediction	5.7975	Training	5.8029
70	5.1310	Training	5.3843	Training	5.1923	Prediction	5.2749	Prediction	5.4800
71	5.0320	Training	5.5372	Training	5.2608	Prediction	5.5536	Training	5.5362
72	5.4090	Training	5.5461	Training	5.3585	Prediction	5.5900	Prediction	5.5134
73	5.6780	Training	6.0272	Training	5.6627	Prediction	6.2168	Prediction	6.0480
74	5.6020	Training	5.6556	Training	5.4393	Training	5.6306	Prediction	5.6522
75	6.3980	Training	6.0451	Prediction	5.6965	Training	6.2229	Training	6.0713
76	4.9430	Training	4.8893	Prediction	4.8292	Training	4.8592	Training	4.8908
77	5.0660	Training	5.2310	Training	5.0376	Prediction	5.2929	Training	5.2048
78	5.0660	Training	4.9741	Prediction	4.8859	Training	4.9271	Training	4.9982
79	5.1190	Training	5.0173	Prediction	4.8858	Training	5.1317	Training	4.9584
80	5.0920	Training	5.1228	Training	4.9395	Prediction	5.2270	Training	5.1068
81	5.0860	Training	5.5045	Training	5.2698	Training	5.4702	Prediction	5.5902
82	5.0810	Training	5.1924	Training	4.9968	Prediction	5.3423	Prediction	5.1544
83	5.1430	Training	5.3475	Training	5.1368	Training	5.3156	Prediction	5.4093
84	5.6020	Training	5.4963	Prediction	5.2000	Training	5.5783	Training	5.5088
85	5.5230	Training	5.3221	Prediction	5.1095	Training	5.2794	Training	5.3884
86	6.0460	Training	5.6648	Prediction	5.3883	Training	5.7883	Prediction	5.6897
87	5.0600	Training	5.1604	Training	4.9940	Prediction	5.2306	Training	5.0745
88	5.5380	Training	5.4862	Prediction	5.2545	Training	5.6187	Training	5.4473
89	5.2760	Training	5.0955	Prediction	4.9946	Prediction	5.0613	Training	5.0430
90	5.4950	Training	5.5162	Training	5.2800	Prediction	5.6582	Training	5.4595
91	5.1940	Training	5.3851	Training	5.1992	Prediction	5.3311	Prediction	5.4108
92	5.5380	Training	5.1659	Prediction	5.0812	Prediction	4.9477	Training	5.2390
93	6.0000	Training	5.5070	Prediction	5.2861	Training	5.6562	Prediction	5.5464
94	5.6580	Training	5.4254	Prediction	5.2085	Prediction	5.3977	Training	5.5069
95	5.9210	Training	5.7454	Prediction	5.4344	Training	5.8117	Training	5.8043
96	5.0270	Training	5.4707	Training	5.2993	Training	5.3705	Training	5.5809

Table 6 continued

ID	pEC$_{50}$ (M)	Status	Pred. pEC$_{50}$ (Original model)	Status	Pred. pEC$_{50}$ RBM	Status	Pred. pEC$_{50}$ RSM	Status	Pred. pEC$_{50}$ SEM
97	5.5530	Training	5.6583	Training	5.3984	Training	5.8009	Prediction	5.6963
98	5.1190	Training	5.6214	Training	5.3299	Prediction	5.7446	Prediction	5.6112
99	5.2290	Training	5.2426	Training	5.0457	Training	5.3492	Prediction	5.2081
100	5.2520	Training	5.4367	Training	5.1699	Training	5.3379	Training	5.4874

Table 7 Comparison of statistical parameters for original model for dataset-1, 2 and 3

Statistical Parameter	DataSet-1	DataSet-2	DataSet-3
R^2_{tr}	0.709	0.841	0.410
$R^2_{adj.}$	0.670	0.837	0.378
R^2_{cv}	0.597	0.827	0.344
R^2_{LMO}	0.723	0.843	0.419
R^2_{Yrand}	0.120	0.242	0.050
Q^2_{Yrand}	−0.185	−0.488	−0.076
s	0.250	0.242	0.300
Kxx	0.425	0.245	0.208
ΔK	0.025	0.209	0.027
$RMSE_{tr}$	0.233	0.238	0.291
$RMSE_{cv}$	0.274	0.248	0.307
CCC_{tr}	0.830	0.914	0.581
CCC_{cv}	0.763	0.906	0.537
MAE_{tr}	0.193	0.172	0.226
MAE_{cv}	0.226	0.179	0.239
F	18.50	190.388	13.047
r^2	0.601	0.827	0.347
r^2_o	0.429	0.793	−0.574
$1-(r^2/r^2_o)$	0.285	0.040	2.653
r'^2_o	0.597	0.827	0.344
$1-(r^2/r'^2_o)$	0.007	0.000	0.009
k	0.996	0.999	0.997
k'	1.001	1.000	0.999

$RMSE_{cv}$, CCC_{tr}, CCC_{cv}, MAE_{tr}, MAE_{cv}, and r^2_m av indicate good predictive ability and robust statistical performance of the residual-based model than the other models. The high value of r^2_m (=0.744) for residual model, though lower than sphere exclusion model (=0.804), indicates good external predictivity. A very high F (=328.459) value for residual-based model than the other models (=112.835 for random splitting and 111.362 for sphere exclusion model) indicates very high statistical significance of regression model. Similar to dataset-1, a large difference between $RMSE_{tr}$ (=0.143) and $RMSE_{ex}$ (=0.405) as well as between MAE_{tr} (=0.109) and MAE_{ex} (=0.353) suggests low

Table 8 Comparison of statistical parameters for original, residual-based rational, random splitting, and sphere exclusion models for dataset-1

Statistical Parameter	Original model	Residual-based model	Random splitting Model	Sphere exclusion model
R^2_{tr}	0.709	0.855	0.801	0.674
$R^2_{adj.}$	0.670	0.813	0.743	0.578
R^2_{cv}	0.597	0.732	0.640	0.365
R^2_{LMO}	0.723	0.871	0.815	0.709
s	0.250	0.137	0.241	0.320
R^2_{ex}	–	0.845	0.418	0.722
R^2_{Yrand}	0.120	0.223	0.238	0.231
Q^2_{Yrand}	−0.185	−0.443	−0.421	−0.433
Kxx	0.425	0.457	0.452	0.446
ΔK	0.025	0.036	0.015	0.017
$RMSE_{tr}$	0.233	0.118	0.207	0.275
$RMSE_{cv}$	0.274	0.159	0.279	0.384
$RMSE_{ex}$	–	0.441	0.344	0.200
CCC_{tr}	0.830	0.922	0.890	0.805
CCC_{cv}	0.763	0.859	0.795	0.621
CCC_{ex}	–	0.606	0.611	0.845
MAE_{tr}	0.193	0.089	0.161	0.238
MAE_{cv}	0.226	0.122	0.220	0.325
MAE_{ex}	–	0.394	0.260	0.169
Q^2-F^1	–	0.443	0.266	0.706
Q^2-F^2	–	0.097	0.266	0.705
Q^2-F^3	–	−1.039	0.451	0.828
r^2m	–	0.762	0.290	0.655
r^2m av	–	0.678	0.270	0.612
r^2m de	–	0.168	0.040	0.085
F	18.50	20.120	13.714	7.023
r^2	0.601	0.845	0.418	0.722
r^2_o	0.429	0.757	0.256	0.677
$1-(r^2/r^2_o)$	0.285	0.105	0.386	0.062
r'^2_o	0.597	0.836	0.324	0.713
$1-(r^2/r'^2_o)$	0.007	0.011	0.223	0.012
k	0.996	0.916	0.974	1.005
k'	1.001	1.089	1.021	0.993

Table 9 Comparison of statistical parameters for original, residual-based rational, random splitting, and sphere exclusion models for dataset-2

Statistical Parameter	Original model	Residual-based model	Random splitting Model	Sphere exclusion model
R^2_{tr}	0.841	0.945	0.856	0.854
$R^2_{adj.}$	0.837	0.942	0.848	0.847
R^2_{cv}	0.827	0.934	0.836	0.834
R^2_{LMO}	0.843	0.947	0.859	0.855
s	0.242	0.148	0.212	0.227
R^2_{ex}	–	0.877	0.842	0.816
R^2_{Yrand}	0.242	0.052	0.053	0.051
Q^2_{Yrand}	−0.488	−0.087	−0.086	−0.089
Kxx	0.245	0.246	0.293	0.220
ΔK	0.209	0.231	0.201	0.219
$RMSE_{tr}$	0.238	0.143	0.205	0.220
$RMSE_{cv}$	0.248	0.157	0.219	0.234
$RMSE_{ex}$	–	0.405	0.287	0.266
CCC_{tr}	0.914	0.972	0.922	0.921
CCC_{cv}	0.906	0.967	0.912	0.911
CCC_{ex}	–	0.777	0.876	0.893
MAE_{tr}	0.172	0.109	0.149	0.166
MAE_{cv}	0.179	0.119	0.160	0.177
MAE_{ex}	–	0.353	0.197	0.187
Q^2-F^1	–	0.553	0.809	0.822
Q^2-F^2	–	0.442	0.809	0.810
Q^2-F^3	–	0.561	0.717	0.788
r^2m	–	0.744	0.689	0.804
$r^2m\ av$	–	0.803	0.581	0.720
$r^2m\ de$	–	0.118	0.217	0.168
F	190.388	328.459	112.835	111.362
r^2	0.827	0.877	0.842	0.816
r^2_o	0.793	0.877	0.649	0.768
$1-(r^2/r^2_o)$	0.040	0.000	0.229	0.060
r'^2_o	0.827	0.854	0.809	0.816
$1-(r^2/r'^2_o)$	0.000	0.026	0.039	0.000
k	0.999	0.953	1.000	0.992
k'	1.000	1.048	0.998	1.007

Table 10 Comparison of statistical parameters for original, residual-based rational, random splitting, and sphere exclusion models for dataset-3

Statistical parameter	Original model	Residual-based model	Random splitting Model	Sphere exclusion model
R^2_{tr}	0.410	0.621	0.527	0.478
$R^2_{adj.}$	0.378	0.583	0.478	0.426
R^2_{cv}	0.344	0.516	0.430	0.365
R^2_{LMO}	0.419	0.634	0.537	0.495
s	0.300	0.134	0.279	0.305
R^2_{ex}	–	0.662	0.237	0.280
R^2_{Yrand}	0.050	0.093	0.090	0.092
Q^2_{Yrand}	−0.076	−0.144	−0.153	−0.142
Kxx	0.208	0.176	0.232	0.203
ΔK	0.027	0.084	0.028	0.079
$RMSE_{tr}$	0.291	0.127	0.263	0.288
$RMSE_{cv}$	0.307	0.143	0.289	0.318
$RMSE_{ex}$	–	0.524	0.353	0.306
CCC_{tr}	0.581	0.766	0.690	0.647
CCC_{cv}	0.537	0.704	0.625	0.575
CCC_{ex}	–	0.339	0.480	0.488
MAE_{tr}	0.226	0.099	0.203	0.212
MAE_{cv}	0.239	0.112	0.225	0.236
MAE_{ex}	–	0.458	0.280	0.257
Q^2-F^1	–	0.239	0.112	0.246
Q^2-F^2	–	−0.728	0.105	0.238
Q^2-F^3	–	−5.512	0.145	0.414
r^2m	–	0.516	0.151	0.238
$r^2m\ av$	–	0.302	0.113	0.127
$r^2m\ de$	–	0.430	0.077	0.220
F	13.047	16.382	10.909	9.158
r^2	0.347	0.662	0.237	0.280
r^2_o	−0.574	−0.093	−0.235	−0.602
$1-(r^2/r^2_o)$	2.653	1.141	1.991	3.150
r'^2_o	0.344	0.614	0.106	0.257
$1-(r^2/r'^2_o)$	0.009	0.073	0.554	0.082
k	0.997	0.916	0.995	1.006
k'	0.999	1.089	1.001	0.257

generalizability of the residual-based model. In addition, the lower value of CCC_{ex}, Q^2-F^1, Q^2-F^2, and Q^2-F^3 for residual-based model than random splitting model, and sphere exclusion model points out low true external predictivity of this model.

A conceivable reason for the lower values of Q^2-F^1, Q^2-F^2, and Q^2-F^3 could be the presence of prediction set objects near the boundary of the training set (Chirico and Gramatica, 2011, 2012; Consonni *et al.*, 2009, 2010; Schuurmann *et al.*, 2008). Again, these statistical

parameters are sensitive to mean of training and prediction sets, a simple analysis of Table 11 reveals that the mean of the test and the training sets of residual-based model have higher difference than the rest (Chirico and Gramatica 2011, 2012; Consonni *et al.*, 2009, 2010; Schuurmann *et al.*, 2008). This observation once again confirms that the distribution of the test and the training set has important impact on performance of many statistical parameters. Thus, the residual-based model is scoring high for many parameters suggesting statistical robustness of this model,

Table 11 Mean of experimental pIC_{50} for prediction and training sets of various models for datasets 1–3

DataSet	Set	Original	Residual-based model	Random splitting Model	Sphere exclusion model
1	Prediction	–	4.8308	4.6389	4.6509
	Training	4.6397	4.4652	4.6404	4.6295
2	Prediction	–	7.5342	7.3803	7.3017
	Training	7.3867	7.2633	7.3921	7.4577
3	Prediction	–	5.6296	5.3598	5.3570
	Training	5.3778	5.1799	5.3925	5.3941

but some parameters raise doubts on its external predictivity.

Results for the dataset-3

Various statistical parameters viz. R^2_{tr}, $R^2_{adj.}$, R^2_{cv}, R^2_{LMO}, R^2_{Yrand}, s, R^2_{ex}, Kxx, ΔK, $RMSE_{tr}$, $RMSE_{cv}$, CCC_{tr}, CCC_{cv}, MAE_{tr}, MAE_{cv}, r^2_m av, and F (see Table 10) indicate low predictive ability and poor statistical performance of all the models. But, a closer inspection of various models indicates that the performance of residual-based model is better than the other models. Some of the statistical parameters like R^2_{tr}, R^2_{LMO}, s, R^2_{ex}, $RMSE_{tr}$, $RMSE_{cv}$, MAE_{tr}, and MAE_{cv} are with acceptable values. However, the model possesses low internal and external predictivity. As stated earlier, it is not a useful model at all for the prediction and pattern recognition. The Q^2-F^2 and Q^2-F^3 are negative which indicates that the model is useless for external predictivity.

Comparison of performance of splitting methodologies and statistical behavior of statistical parameters

In the present analysis, information leakage was purposely performed for RBM. The descriptors were selected using the whole dataset, therefore, due to the information leakage, the selected descriptors must have captured the common structural features that influence the activity, and consequently, after splitting in any pattern/composition, the performance of RBM model for the all the datasets must be superior than SEM and RSM with respect to internal and external cross-validation parameters, i.e., must show high level of external predictivity with high validation score. Surprisingly, for RBM model, various validation parameters do not show expected behavior and values for all the datasets.

The random splitting models, for all the datasets, have varying performance; this could be due to the fact that during splitting the training or prediction set may not be

covering the diversity of the whole dataset or the compounds are not close to each other. Repeating the random splitting several times is a good solution to arrive at best random splitting (Huang and Fan, 2011; Kiralj and Ferreira, 2009). Yet, as pointed out in a recent study, a QSAR model with high external predictivity for one prediction set does not necessarily indicate high accuracy for another external set (Huang and Fan, 2011). Therefore, precautions must be taken in using single random splitting.

Since, the performance of the RBM, RSM, and SEM models is varying, but by luck or due to rational splitting, the researcher may arrive at the training and prediction sets that indicate high external predictive ability, such situation, though, leads to a statistically robust but a misguiding QSAR model as observed in RBM. An easy and handy solution to this problem is to develop a model using undivided dataset and compare its performance with the other models. Herein, in all the datasets, the performance of original model, though not better than residual based and sphere exclusion models, is still statistically satisfactory. It is expected that a model developed with no prediction set will be most accurate and possess the highest coverage for external evaluation set. But, a recent study reports exactly opposite results in certain situations (Martin *et al.*, 2012). Therefore, we recommend and accentuate reporting of a statistically robust QSAR model that is developed using undivided whole dataset and same set of descriptors, which were selected and used in splitting-based model. Then, such a model tells the true effect of inclusion of compounds in the dataset. That is, it is useful in understanding the effect of increase/decrease in size of dataset as well as for capturing less privileged yet useful structural features that govern the activity.

A higher value of R^2_{tr} for residual-based model in all the datasets than the rest of the models indicates a better fitting or explanation of variance (see Tables 8–10). Similar trend for R^2_{ex} for residual-based model for different datasets confers as if the residual based splitting is better method of splitting. Therefore, a QSAR modeler may consider the residual-based model superior than others. This apparent superiority can be attributed to the purposeful selection of the training and the prediction sets, that is, the method of splitting has significant impact on many statistical parameters. Moreover, a careful comparison of residual values for all the models (see Fig. 3) reveals that the difference between the experimental and predicted in many instances is large in case of residual-based model than the others. But, during the calculation of various statistical parameters either sum or average is used. Therefore, the statistical parameters are unable to recognize this serious pitfall. In fact, a QSAR model based on splitting method with an unusually robust training set R^2_{tr} of 0.8 or greater than R^2_{tr} of undivided set

Fig. 3 Difference between experimental and predicted pIC$_{50}$ by various models for dataset-1, 2, and 3 (*X-axis*: Compound number and *Y-axis*: pIC$_{50}$/pEC$_{50}$; *X-axis*: Serial number of compound, *Y-axis*: pIC$_{50}$ value)

For Data set-1

For Data set-2

For Data set-3
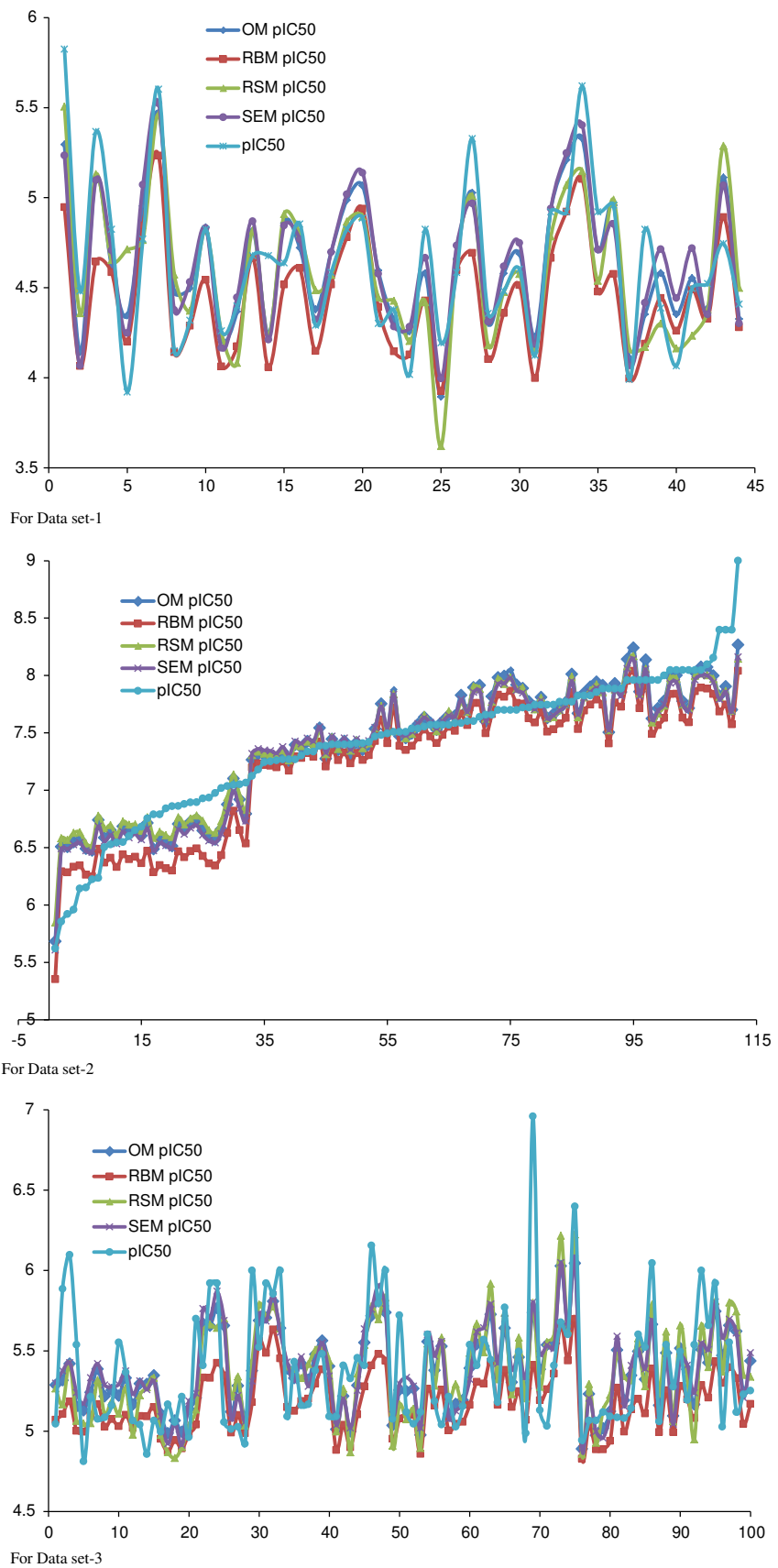
should be viewed with suspicion. Some parameters like CCC_{ex}, Q^2-F^1, Q^2-F^2, Q^2-F^3, and r_m^2 are more successful in identifying this crucial aspect. This can be ascribed to the method of calculation of these parameters (Chirico and Gramatica, 2011, 2012); (Consonni *et al.*, 2009, 2010; Schuurmann *et al.*, 2008).

$$Q^2 - F^1 = 1 - \frac{\sum_{i=1}^{n_{ext}} (\widehat{y}i - yi)^2}{\sum_{i=1}^{n_{ext}} (yi - \bar{y}_{tr})^2}$$

$$Q^2 - F^3 = 1 - \frac{\sum_{i=1}^{n_{ext}} (\widehat{y}i - yi)^2 / n_{ext}}{\sum_{i=1}^{n_{tr}} (yi - \bar{y}_{tr})^2 / n_{tr}}.$$

$$Q^2 - F^2 = 1 - \frac{\sum_{i=1}^{n_{ext}} (\widehat{y}i - yi)^2}{\sum_{i=1}^{n_{ext}} (yi - \bar{y}_{ext})^2}$$

$$r_m^2 = r^2(1 - \sqrt{r^2 + r_o^2})$$

Thus, r_m^2 considers agreement between the actual and the predicted values as an essential factor to establish the true predictivity (Mitra *et al.*, 2010; Roy and Mitra, 2012). Thence, the statistical parameters viz. CCC_{ex}, Q^2-F^1, Q^2-F^2, Q^2-F^3, and r_m^2 reflect the factual performance of model regarding true external predictivity of a QSAR model. Therefore, these parameters should be used as criteria for selection of a consensus model, as in QSARINS v1.2. In QSARINS v1.2, MAE_{tr}, MAE_{ex}, $RMSE_{tr}$, $RMSE_{ex}$, CCC_{tr}, CCC_{ex}, Q^2-F^1, Q^2-F^2, Q^2-F^3, and some other parameters are used to find a consensus model.

In agreement with the previous reports, the trend of lower CCC with higher RMSE value is true for all the datasets (Chirico and Gramatica, 2011, 2012). However, the claim that the smaller the dataset size, the better the performances of r_m^2-EyPx and CCC compared to the other external validation measures was not observed for any of the dataset (Chirico and Gramatica, 2011, 2012). The similar values of Q^2-F^1 and Q^2-F^2 for random splitting model for dataset 1 and 2 can be attributed to the fact that these parameters depend on agreement between the mean of the training and the prediction set values (Consonni *et al.*, 2009, 2010). For dataset 1 and 2, the mean of test and training sets values is very close to each other (see Table 11). A good difference between the mean of the undivided set and the training set values of the residual-based model for all the datasets indicates that the prediction set was not selected properly. Such a noticeable difference is absent in case of other models. This again indicates that residual-based method of

splitting cannot be functionalised for splitting the dataset for external validation.

Since the whole dataset is involved in descriptor selection and model development, another point view toward the present approach is to consider it as a methodology to develop a model with good external predictivity using advantages of internal validation method. A model with good internal predictivity may or may not be good at external predictivity (Chirico and Gramatica, 2011, 2012; Consonni *et al.*, 2009, 2010; Gramatica 2013, Schuurmann *et al.*, 2008). In the present analysis, sphere exclusion model with higher values of Q^2-F^3, CCC_{ex}, and lower values of $RMSE_{ex}$, MAE_{ex} indicate good external predictivity of model.

Consonni et al. argued that increasing the mean of training set values increases Q^2 artificially (Consonni *et al.*, 2009). From Table 11, it is observed that the mean of the training set values for the random (for dataset- 1 and 2) and the sphere exclusion models (for dataset-1) is very close to mean of undivided set values; therefore, the value of Q^2 for these models should be close to Q^2 of the original model. However, for random splitting model, $Q^2 = 0.640$ for dataset-1, and $Q^2 = 0.836$ for dataset-2 are higher than that of the original model ($Q^2 = 0.597$). In addition, lower $Q^2 = 0.365$ for sphere exclusion model for dataset-1 than $Q^2 = 0.597$ for original model conflicts the finding of Consonni et al. The mean of the training set for residual model (=4.4652) is lower than mean of training set of undivided set (=4.6397). Therefore, for the sphere exclusion model, Q^2 should be lower than the Q^2 for original model, but the results are exactly opposite. Therefore, further studies are required to understand the effect of mean of training set on Q^2.

Conclusions

In conclusion, external validation based on single splitting is neither perfect nor absolutely accurate method of QSAR model validation as the statistical parameters can be influenced easily due to the biased and purposeful selection of the training and prediction sets. Moreover, the predictive ability of a QSAR model is sensitive toward the method of splitting and its manipulation is feasible. Thus, it is still insufficient to guarantee the true predictability of a QSAR model. The true external predictivity of any QSAR model cannot be decided on the basis of one or two parameters, that is, as many as possible statistical parameters should be calculated to judge the external predictivity. A good number of statistical parameters need to be calculated and presented to identify the true external predictivity of any QSAR model. We

suggest and emphasize reporting of at least one statistically robust QSAR model that is developed using undivided whole dataset with appropriate cross validation.

In the present study, we presented a novel method for splitting the dataset for external validation. The residual method, though, generates statistically robust model but with low external predictivity. Further studies are in progress for the improvement of this method.

References

Baumann K, Stiefl N (2004) Validation tools for variable subset regression. J Comput Aided Mol Des 18(7–9):549–562

Chirico N, Gramatica P (2011) Real external predictivity of qsar models: how to evaluate it? comparison of different validation criteria and proposal of using the concordance correlation coefficient. J Chem Inf Model 51(9):2320–2335

Chirico N, Gramatica P (2012) Real external predictivity of QSAR models. Part 2. New intercomparable thresholds for different validation criteria and the need for scatter plot inspection. J Chem Inf Model 52(8):2044–2058

Consonni V, Ballabio D, Todeschini R (2009) Comments on the definition of the Q2 parameter for QSAR validation. J Chem Inf Model 49(7):1669–1678

Consonni V, Ballabio D, Todeschini R (2010) Evaluation of model predictive ability by external validation techniques. J Chemomet 24:194–201

Golbraikh A, Tropsha A (2002) Beware of q2! J Mol Graph Model 20(4):269–276

Gramatica P (2013) On the development and validation of QSAR models. Methods Mol Biol 930:499–526

Gramatica P, Chirico N, Papa E, Cassani S, Kovarich S (2013) QSARINS: a new software for the development, analysis, and validation of QSAR MLR models. J Comput Chem 34(24):2121–2132

Gramatica P, Cassani S, Chirico N (2014) QSARINS-chem: insubria datasets and new QSAR/QSPR models for environmental pollutants in QSARINS. J Comput Chem 35(13):1036–1044

Hawkins DM (2004) The problem of overfitting. J Chem Inf Comput Sci 44(1):1–12

Hawkins DM, Basak SC, Mills D (2003) Assessing model fit by cross-validation. J Chem Inf Comput Sci 43:579–586

Hawkins DM, Kraker JJ, Basak SC, Mills D (2008) QSPR checking and validation: a case study with hydroxy radical reaction rate constant. SAR QSAR Environ Res 19(5–6):525–539

Huang J, Fan X (2011) Why QSAR fails: an empirical evaluation using conventional computational approach. Mol Pharm 8(2):600–608

Hwang JY, Kawasuji T, Lowes DJ, Clark JA, Connelly MC, Zhu F, Guiguemde WA, Sigal MS, Wilson EB, DeRisi JL, Guy RK (2011) Synthesis and evaluation of 7-substituted 4-aminoquinoline analogues for antimalarial activity. J Med Chem 54(20):7084–7093

Kiralj R, Ferreira MMC (2009) Basic validation procedures for regression models in QSAR and QSPR studies: theory and application. J Braz Chem Soc 20:770–787

Kubinyi H (2002) From narcosis to hyperspace: the history of QSAR. Quant Struct Act Relat 21:348–356

Mahajan DT, Masand VH, Patil KN, Ben Hadda T, Jawarkar RD, Thakur SD, Rastija V (2012) CoMSIA and POM analyses of anti-malarial activity of synthetic prodiginines. Bioorg Med Chem Lett 22(14):4827–4835

Mahajan DT, Masand VH, Patil KN, Hadda TB, Rastija V (2013) Integrating GUSAR and QSAR analyses for antimalarial activity of synthetic prodiginines against multi drug resistant strain. Med Chem Res 22:2284–2292

Martin TM, Harten P, Young DM, Muratov EN, Golbraikh A, Zhu H, Tropsha A (2012) Does rational selection of training and test sets improve the outcome of QSAR modeling? J Chem Inf Model 52(10):2570–2578

Masand VH, Jawarkar RD, Patil KN, Nazerruddin GM, Bajaj SO (2010) Correlation potential of Wiener index and molecular refractivity vis-a'-vis Antimalarial activity of xanthone derivatives. Org Chem 6(1):30–38

Masand VH, Jawarkar RD, Mahajan DT, Hadda TB, Sheikh J, Patil KN (2012) QSAR and CoMFA studies of biphenyl analogs of the anti-tuberculosis drug (6S)-2-nitro-6-{[4-(trifluoromethoxy)benzyl]oxy}-6,7-dihydro-5H-imidazo[2,1-b][1,3]oxazine(PA-824). Med Chem Res 21:2624–2629

Masand VH, Mahajan DT, Patil KN, Hadda TB, Youssoufi MH, Jawarkar RD, Shibi IG (2013) Optimization of antimalarial activity of synthetic prodiginines: QSAR, GUSAR, and CoMFA analyses. Chem Biol Drug Des 81(4):527–536

Masand VH, Mahajan DT, Gramatica P, Barlow J (2014) Tautomerism and multiple modelling enhance the efficacy of QSAR: antimalarial activity of phosphoramidate and phosphorothioamidate analogues of amiprophos methyl. Med Chem Res

Mitra I, Roy PP, Kar S, Ojha PK, Roy K (2010) On further application of r m2 as a metric for validation of QSAR models. J Chemomet 24(1):22–33

Roy K, Mitra I (2012) On the use of the metric rm(2) as an effective tool for validation of QSAR models in computational drug design and predictive toxicology. Mini Rev Med Chem 12(6):491–504

Roy K, Roy PP, Leonard JT (2008) Exploring the impact of size of training sets for the development of predictive QSAR models. Chemomet Intel Lab Sys 90:31–42

Sahigara F, Mansouri K, Ballabio D, Mauri A, Consonni V, Todeschini R (2012) Comparison of different approaches to define the applicability domain of QSAR models. Molecules 17(5):4791–4810

Schuurmann G, Ebert RU, Chen J, Wang B, Kuhne R (2008) External validation and prediction employing the predictive squared correlation coefficient test set activity mean vs training set activity mean. J Chem Inf Model 48(11):2140–2145

Scior T, Medina-Franco JL, Do QT, Martinez-Mayorga K, Yunes Rojas JA, Bernard P (2009) How to recognize and workaround pitfalls in QSAR studies: a critical review. Curr Med Chem 16(32):4297–4313

Selassie CD (2003) History of Quantitative Structure-Activity Relationships. In *Burger's Medicinal Chemistry and Drug Discovery*, 6 ed.; Abraham, D. J., Ed. JohnWiley&Sons, Inc.: 2003; Vol. 1

Sushko I, Novotarskyi S, Korner R, Pandey AK, Cherkasov A, Li J, Gramatica P, Hansen K, Schroeter T, Muller KR, Xi L, Liu H, Yao X, Oberg T, Hormozdiari F, Dao P, Sahinalp C, Todeschini R, Polishchuk P, Artemenko A, Kuz'min V, Martin TM, Young DM, Fourches D, Muratov E, Tropsha A, Baskin I, Horvath D, Marcou G, Muller C, Varnek A, Prokopenko VV, Tetko IV (2010) Applicability domains for classification problems: benchmarking of distance to models for Ames mutagenicity set. J Chem Inf Model 50(12):2094–2111

Todeschini R, Consonni V, Mauri A, Pavan M (2004) Detecting "bad" regression models: multicriteria fitness functions in regression analysis. Anal Chim Acta 515(1):199–208

Tropsha A (2010) Best practices for QSAR model development, validation, and exploitation. Mol Inform 29:476–488

Turcotte V, Fortin S, Vevey F, Coulombe Y, Lacroix J, Cote MF, Masson JY, R CG (2012) Synthesis, biological evaluation, and structure-activity relationships of novel substituted N-phenyl ureidobenzenesulfonate derivatives blocking cell cycle progression in S-phase and inducing DNA double-strand breaks. J Med Chem 55(13):6194–6208

Van Drie JH (2007) Computer-aided drug design: the next 20 years. J Comput Aided Mol Des 21(10–11):591–601

Yuriev E, Agostino M, Ramsland PA (2011) Challenges and advances in computational docking: 2009 in review. J Mol Recognit 24(2):149–164

CrossMark

Molecular docking and QSAR analyses for understanding the antimalarial activity of some 7-substituted-4-aminoquinoline derivatives

I.G. Shibi [a,*], L. Aswathy [a], R.S. Jisha [a], V.H. Masand [b], A. Divyachandran [a], J.M. Gajbhiye [c]

[a] Department of Chemistry, Sree Narayana College, Chempazhanthy, Kerala, India
[b] Department of Chemistry, Vidya Bharati College, Camp, Amravati, Maharashtra, India
[c] Division of Organic Chemistry, CSIR-National Chemical Laboratory, Pune, India

A R T I C L E   I N F O

A B S T R A C T

The quinoline moiety is one of the widely studied scaffolds for generating derivatives with various pharmacophoric groups due to its potential antimalarial activities. In the present study, a series of 7-substituted-4-aminoquinoline derivatives were selected to understand their antimalarial properties computationally by molecular modeling techniques including 2D QSAR, comparative molecular field analysis (CoMFA), comparative molecular similarity indices analysis (CoMSIA) and molecular docking. The 2D-QSAR model built with four descriptors selected by genetic algorithm technique and CoMFA model showed satisfactory statistical results ($Q^2 = 0.540$, $R^2_{ncv} = 0.881$, F value = 157.09). A reliable CoMSIA model out of the fourteen different combinations has a Q^2 value of 0.638. The molecular docking studies of the compounds for 1CET as the protein target revealed that ten compounds showed maximum interactions with the binding site of the protein. The present study highlights the unique binding signatures of the ligands within the active site groove of the target and it explains the subtle differences in their EC_{50} values and their mechanism of inhibition.

© 2015 Elsevier B.V. All rights reserved.

* Corresponding author at: PG & Research Department of Chemistry, Sree Narayana College, Chempazhanthy, Thiruvananthapuram 695 587, Kerala, India.
    E-mail address: shibiig@gmail.com (I.G. Shibi).

1. Introduction

Malaria is a severe and infectious disease caused mainly by *Plasmodium falciparum* (*P. falciparum*) (White et al., 2014). About 207 million cases and 627,000 deaths are reported annually, mainly in African sub-Saharan countries (Sonin et al., 2013). Recent reports show that *P. falciparum* has become resistant to all chemotherapeutic agents that are currently in use (O'Brien et al., 2011). Consequently World Health Organization (WHO) has recommended the use of Artemisinin-based combination therapy (ACT) for the treatment of *P. falciparum* related uncomplicated and severe malarial infection. But it has been reported that parasite shows resistance to Artemisinin, compounding an urgent requirement for additional therapeutic agents targeting *Plasmodium* parasites (Kyaw et al., 2013).

The quinoline moiety has attracted much consideration of medicinal chemists, as it is one of the imperative pharmacophores accountable for imparting antimalarial action (Boechat et al., 2014; Videnović et al., 2014; Mishra et al., 2014). Quinoline based drugs exert antimalarial activity by interfering with hemoglobin (Hb) degradation in the parasitic food vacuole. One of the waste products of the parasite's hemoglobin diet is ferriprotoporphyrin IX (FP); a toxic iron-containing molecule (O'Neill et al., 1998). The parasite detoxifies this molecule by means of a crystallization reaction that converts FP into non-toxic hemozoin or malaria pigment while the globin is hydrolyzed into individual amino acids (Ridley, 1996). The most accepted hypothesis is that antimalarial drugs form a complex with FP that inhibits the formation of hemozoin and result in an accumulation of toxic molecules in the parasite, which eventually kills it (Dorn et al., 1998).

In drug discovery process Quantitative Structure–Activity Relationships (QSAR) have great importance (Pourbasheer et al., 2013; Pourbasheer et al., 2010; Riahi et al., 2008, 2009). Molecular descriptors can be 2D as well as 3D. The 3D-QSAR models can be employed for the identification of regions in space which correlate with the biological activities (Du et al., 2012). The 3D QSAR models can be generated using Comparative Molecular Field Analysis (CoMFA) (Cramer et al., 1988) and the Comparative Molecular Similarity Indices Analysis (CoMSIA) (Klebe et al., 1994). CoMFA works out the steric and electrostatic fields surrounding the molecules and correlates the differences in these fields with biological activity. CoMSIA works out three more molecular descriptors than CoMFA: hydrophobic fields, H-bond donor fields and H-bond acceptor fields.

In the present work, the application of CoMFA, CoMSIA methods and molecular docking studies have been employed to generate quantitative models, to predict and determine the pharmacophoric features that govern the activity of 7-substituted 4-aminoquinoline analogs synthesized by Hwang et al. with antimalarial activity against the chloroquine (CQ) – resistant *Plasmodium* strains (Hwang et al., 2011), and to specify regions in space where interactive fields might enhance their activity. QSAR studies of these compounds have already been carried out by Masand et al. (2014). The objective of their study was to determine the factors that influence the activity of the selected compounds and generate QSAR models to predict the activity of molecules prior to actual synthesis and biological screening. They used GA-MLR and optimal SMILES-based descriptors to build QSAR models. The models elucidate that anti-malarial activity has high correlation with the topological distance of six between N and O. Also the models predicted that, the antimalarial activity depends on the presence of heavy atoms in the internal environment of the compounds. We have used *Plasmodium* lactate dehydrogenase (pLDH) in our *in silico* studies as it is an important enzyme of glycolysis and is essential for energy production in the Plasmodia. Moreover, Plasmodia lack

functional Krebs cycle during some erythrocytic stages (Lang Unnasch and Murphy, 1998). Lactate dehydrogenase (LDH) is an essential enzyme that catalyses the interconversion of pyruvate and lactate with concomitant conversion of NADH and NAD$^+$ (Wiwanitkit, 2007). The parasite lactate dehydrogenase is a tetrameric enzyme containing 316 amino acids and present in all four human parasitic *Plasmodium* species. It is known that pLDH has notable structural and kinetic properties making it different from mammalian and bacterial LDH. The predictive ability of the generated model was tested by an external validation technique using 22 test set compounds. The obtained model was further used to generate contour maps for explaining the interaction of the compounds and to study SAR. Molecular docking studies were carried out to understand the important structural features required for binding at the active sites of the protein 1CET (Read et al., 1999).

2. Materials and methods

A series of 112 analogs of 7-substituted-4-aminoquinoline were taken to perform the present study. Table 1 describes the structures and EC$_{50}$ values of the data set. The three-dimensional chemical structures of the compounds were drawn by ChemDraw (version 64-1.5.3). The optimization of the cleaned compounds was done through MOE (MOE Version 2007.09, Chemical Computing Group, Inc.).

2.1. 2D-QSAR modeling and dataset

EC$_{50}$ (μM) data was converted to pEC$_{50}$ (M) for all the QSAR analyses.

$$pEC_{50} = -\log EC_{50} \tag{1}$$

2.1.1. Descriptor calculation

A total of 251 descriptors were calculated which included 2D and 3D molecular descriptors (Lin, 2000). 2D descriptors which describe notation and terminology, physical properties, subdivided surface areas, atom counts and bond counts, Kier & Hall connectivity and Kappa shape indices, adjacency and distance, matrix, pharmacophore features and partial charges. 3D descriptors are classified into internal 3D descriptors (i3D) and external 3D descriptors (×3D) which describe potential energy, surface area, volume and shape and conformation-dependent charge. After objective feature selection filtering, finally a total of 37 descriptors were selected to build the 2D-QSAR model.

2.2. 3D-QSAR method

For the development of 3D-QSAR models the complete set of these compounds (112 compounds) were divided into a training set (90 compounds) to generate the models and a test set (22 compounds) to evaluate the predictive ability of the resulting models. The steric and electrostatic CoMFA potential fields were performed using Open3DQSAR (Tosco and Balle, 2011). MOE 2007.09 was used to explore the results and graphical visualization. The CoMSIA method was performed with the same parameters used in CoMFA analysis so as to evaluate the similarity indices among the compounds.

2.2.1. Partial least-squares analysis

The predictive ability of the 3D-QSAR models is assessed by applying partial least squares (PLS) analysis (Bush and Nachbar, 1993) as well as the leave-one-out (LOO) (Wold et al., 1984) cross-validation method. In the cross-validation analysis, LOO method was used, in which one compound was removed from

Table 1
Structures and antimalarial activities values of a series of 7-substituted-4-aminoquinline analogs.
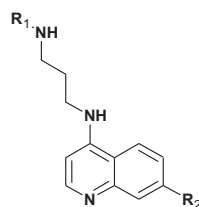
Compounds	R_1	R_2	EC_{50} (µM)	pEC_{50} (M)
1	Furfuryl	PhO	0.314	6.5031
2[a]	2-HO-3-MeO-Bn	PhO	0.015	7.8239
3	Piperonyl	PhO	0.018	7.7447
4[a]	3-F-6-MeO-Bn	PhO	0.162	6.7905
5	Furfuryl	2-MeO-PhO	0.092	9.0000
6	2-HO-3-MeO-Bn	2-MeO-PhO	0.001	8.0458
7	Piperonyl	2-MeO-PhO	0.009	7.8539
8	3-F-6-MeO-Bn	2-MeO-PhO	0.009	7.6576
9	Furfuryl	3-MeO-PhO	0.014	8.0458
10	2-HO-3-MeO-Bn	3-MeO-PhO	0.022	7.7447
11	Piperonyl	3-MeO-PhO	0.023	6.7905
12	3-F-6-MeO-Bn	3-MeO-PhO	0.009	5.6198
13	Furfuryl	4-MeO-PhO	0.018	8.3979
14	2-HO-3-MeO-Bn	4-MeO-PhO	0.162	8.3979
15[a]	Piperonyl	4-MeO-PhO	2.400	7.3372
16	3-F-6-MeO-Bn	4-MeO-PhO	0.004	7.2676
17	Furfuryl	4-F-PhO	0.004	7.5850
18	2-HO-3-MeO-Bn	4-F-PhO	0.046	7.9586
19	Piperonyl	4-F-PhO	0.054	7.8239
20	3-F-6-MeO-Bn	4-F-PhO	0.026	6.5272
21	Furfuryl	4-Cl-PhO	0.011	7.3979
22[a]	2-HO-3-MeO-Bn	4-Cl-PhO	0.015	7.9586
23	Piperonyl	4-Cl-PhO	0.297	7.4202
24[a]	3-F-6-MeO-Bn	4-Cl-PhO	0.040	7.5086
25	Furfuryl	3-Me$_2$N-PhO	0.011	7.5686
26	2-HO-3-MeO-Bn	3-Me$_2$N-PhO	0.038	8.0000
27	Piperonyl	3-Me$_2$N-PhO	0.031	5.8539
28[a]	3-F-6-MeO-Bn	3-Me$_2$N-PhO	0.027	8.1549
29	Furfuryl	4-tertBu-PhO	0.010	5.9586
30	2-HO-3-MeO-Bn	4-tertBu-PhO	1.400	7.2676
31	Piperonyl	4-tertBu-PhO	0.007	6.8633
32	3-F-6-MeO-Bn	4-tertBu-PhO	1.100	6.9747
33	Furfuryl	4-F-Ph	0.054	7.4949
34	2-HO-3-MeO-Bn	4-F-Ph	0.137	8.0458
35	Piperonyl	4-F-Ph	0.106	7.7447
36	3-F-6-MeO-Bn	4-F-Ph	0.032	7.7447
37	Furfuryl	4-F-Bn	0.096	7.2441
38	2-HO-3-MeO-Bn	4-F-Bn	0.057	7.8239
39	Piperonyl	4-F-Bn	0.015	6.8962
40[a]	3-F-6-MeO-Bn	4-F-Bn	0.127	7.1249
41	Furfuryl	iso-pentyl	0.176	6.7545
42	2-HO-3-MeO-Bn	iso-pentyl	0.022	7.6576
43	Piperonyl	iso-pentyl	0.027	7.5686
44	3-F-6-MeO-Bn	iso-pentyl	0.116	6.9355
45	Furfuryl	cHexmethyl	0.055	7.2596
46	2-HO-3-MeO-Bn	cHexmethyl	0.050	7.3010
47	Piperonyl	cHexmethyl	0.041	7.3872
48	3-F-6-MeO-Bn	cHexmethyl	0.138	6.8601
49	Furfuryl	PhEt	0.046	7.3372
50	2-HO-3-MeO-Bn	PhEt	0.017	7.7696
51[a]	Piperonyl	PhEt	0.013	7.8861
52	3-F-6-MeO-Bn	PhEt	0.132	6.8794
53[a]	Furfuryl	iso-butyl	0.075	6.2358
54	2-HO-3-MeO-Bn	iso-butyl	0.581	7.6990
55	Piperonyl	iso-butyl	0.020	7.1805
56	3-F-6-MeO-Bn	iso-butyl	0.066	7.0506
57	Furfuryl	cHex	0.089	6.9281
58[a]	2-HO-3-MeO-Bn	cHex	0.118	7.7212
59[a]	Piperonyl	cHex	0.019	6.8928
60	3-F-6-MeO-Bn	cHex	0.128	7.0458
61	Furfuryl	1-Et-Pr	0.090	7.0655
62	2-HO-3-MeO-Bn	1-Et-Pr	0.086	8.3979
63[a]	Piperonyl	1-Et-Pr	0.004	7.5686

(continued on next page)

Table 1 (continued)

Compounds	R_1	R_2	EC_{50} (μM)	pEC_{50} (M)
64[a]	3-F-6-MeO-Bn	1-Et-Pr	0.027	7.3979
65	Furfuryl	3,5-CF_3-Ph	0.009	6.5452
66	2-HO-3-MeO-Bn	3,5-CF_3- Ph	0.018	7.5376
67	Piperonyl	3,5-CF_3-Ph	0.018	6.5467
68	3-F-6-MeO-Bn	3,5-CF_3-Ph	0.285	7.0362
69	Furfuryl	1-Naphtyl	0.029	7.5086
70	2-HO-3-MeO-Bn	1-Naphtyl	0.284	7.4815
71	Piperonyl	1-Naphtyl	0.031	6.2233
72[a]	3-F-6-MeO-Bn	1-Naphtyl	0.033	5.9208
73	Furfuryl	4-CF_3-Ph	0.598	7.6990
74	2-HO-3-MeO-Bn	4-CF_3-Ph	1.200	7.8861
75	Piperonyl	4-CF_3-Ph	0.020	7.6021
76[a]	3-F-6-MeO-Bn	4-CF_3-Ph	0.013	7.2676
77	Furfuryl	Ph	0.025	7.6990
78[a]	2-HO-3-MeO-Bn	Ph	0.054	8.0458
79	Piperonyl	Ph	0.020	7.7696
80	3-F-6-MeO-Bn	Ph	0.017	7.9586
81	Furfuryl	4-tertBu-Ph	0.011	6.1524
82[a]	2-HO-3-MeO-Bn	4-tertBu-Ph	0.704	6.6003
83	Piperonyl	4-tertBu-Ph	0.251	6.6517
84	3-F-6-MeO-Bn	4-tertBu-Ph	0.223	6.8416
85	Furfuryl	Piperonyl	0.144	7.7212
86	2-HO-3-MeO-Bn	Piperonyl	0.019	8.0969
87	Piperonyl	Piperonyl	0.008	7.5850
88	3-F-6-MeO-Bn	Piperonyl	0.026	7.5086
89	Furfuryl	4-MeO-Ph	0.031	7.9586
90	2-HO-3-MeO-Bn	4-MeO-Ph	0.011	7.8861
91	Piperonyl	4-MeO-Ph	0.013	7.5376
92[a]	3-F-6-MeO-Bn	4-MeO-Ph	0.029	7.0177
93	Furfuryl	3-CF_3-Bn	0.040	7.2518
94[a]	2-HO-3-MeO-Bn	3-CF_3-Bn	0.056	7.6021
95	Piperonyl	3-CF_3-Bn	0.025	7.4089
96	3-F-6-MeO-Bn	3-CF_3-Bn	0.039	7.3979
97	Furfuryl	4-CN-Bn	0.040	7.4089
98	2-HO-3-MeO-Bn	4-CN-Bn	0.039	7.9586
99	Piperonyl	4-CN-Bn	0.011	7.6383
100	3-F-6-MeO-Bn	4-CN-Bn	0.028	7.5528
101	Furfuryl	Bn	0.040	7.3979
102[a]	2-HO-3-MeO-Bn	Bn	0.017	7.7696
103	Piperonyl	Bn	0.720	6.1427
104	3-F-6-MeO-Bn	Bn	0.011	7.9586
105	Furfuryl	3,5-Me-Bn	0.009	8.0458
106	2-HO-3-MeO-Bn	3,5-Me-Bn	0.009	8.0458
107	Piperonyl	3,5-Me-Bn	0.041	7.3872
108[a]	3-F-6-MeO-Bn	3,5-Me-Bn	0.034	7.4685
109[a]	Furfuryl	2-Cl-4-F-Bn	0.020	7.6990
110	2-HO-3-MeO-Bn	2-Cl-4-F-Bn	0.013	7.8861
111	Piperonyl	2-Cl-4-F-Bn	0.027	7.5686
112	3-F-6-MeO-Bn	2-Cl-4-F-Bn	0.208	6.6819

[a] Test set compounds.

the data set and its activity was predicted using the model derived from the rest of the data set (Podlogar and Ferguson, 2000). The optimum number of components (ONC) and the highest cross-validated coefficient Q^2 were determined using the cross-validation method on the basis of the first minimum cross-validated standard error of prediction. The final non-cross-validated model was developed using ONC by producing the standard error of the estimate (SEE), the non-cross-validated correlation coefficient (R^2_{ncv}) and the F-test value.

Also, the CoMFA and CoMSIA models were assessed by predicting the activity of 22 external test set compounds. The predictive R^2 (R^2_{pred}) of test set compounds is computed using the following equation.

$$R^2_{pred} = \frac{(SD - PRESS)}{SD} \qquad (2)$$

where SD is the sum of the squared deviations between the biological activity of compounds in the test set snd the mean biological activity of the same, and the predictive sum of squares (PRESS) is

the sum of the squared deviations between predicted and actual activity values of test set compounds. The model is said to be healthy and predictive if the statistical parameters $R^2_{ncv} > 0.6$, $R^2_{pred} > 0.5$, and $Q^2 > 0.6$. (Afantitis et al., 2009; Golbraikh and Tropsha, 2002).

To further validate the predictive ability of the constructed models, the following equation was used (Rännar et al., 1994):

$$R^2_{m(overall)} = R^2 \times (1 - \sqrt{R^2 - R_0^2}) \qquad (3)$$

where R^2 is squared correlation coefficient between observed and predicted pEC_{50} values of 112 analogs of 7-substituted-4-aminoquinoline and R_0^2 is squared correlation coefficient with intercept set to zero. The parameter determines whether the range of predicted activity values for the whole dataset is really close to the observed activity or not. The value of $R^2_{m(overall)}$ should be greater than 0.5 for a satisfactory model.

2.3. Molecular docking

2.3.1. Target analysis

An X-ray crystallography structure of *P. falciparum* lactate dehydrogenase (PDB ID: 1CET) was obtained from the RCSB Protein Data Bank (Rose et al., 2015). The structure has a resolution of 2.05 Å.

2.3.2. Structure prediction and validation of the target

Primary structure prediction was carried out using the Expasy ProtParam server (Gasteiger et al., 2005). Physiochemical properties like theoretical isoelectric point (pI), molecular weight, total number of positive and negative residues, extinction coefficient, instability index, aliphatic index and Grand Average Value of Hydropathicity (GRAVY) are computed.

Secondary structure prediction has been carried out using Self-Optimized Prediction Method with Alignment (SOPMA) (Geourjon and Deléage, 1995). The protein sequence was submitted to the server and was analyzed for secondary structure.

The stereochemical quality of the protein was evaluated by Ramachandran plot using MOE 2007.09.

2.3.3. Energy minimization and molecular docking

Molecular docking studies are carried out using MOE (MOE Version 2007.09, Chemical Computing Group, Inc.), in order to explore the interaction mechanism and probable binding mode of 7-substituted-4-aminoquinoline derivatives at the active site of the protein 1CET. The energy of the protein molecule is minimized using the Energy minimization algorithm of MOE tool. The initial and final energy of protein are calculated (in kcal/mol) by GizMOE using MMFF94x force field with conjugant gradient method (Gill et al., 1981). In this molecular docking program, the flexibility of ligands is considered while the protein or biomolecule is considered as a rigid structure. A maximum of 30 conformations was allowed to be saved for each ligand using the default parameters of MOE. At the end of molecular docking, the best conformations of the ligands were analyzed for their binding interactions. The resulted binding interactions between these ligands and protein were observed.

3. Results and discussion

3.1. 2D-QSAR

The subjective feature selection was performed using Genetic Algorithm (GA) method in BuildQSAR. 2D-QSAR equation was chosen by optimizing the statistical results generated along with variations of the descriptors in the model.

18 outlier compounds with residuals more than two standard deviations away from the average residual were removed. Thus, the QSAR analysis included 87 compounds, which let us to investigate the model with up to four variables such as *SlogP_VSA9*, *GCUT_SMR_0*, *PEOE_VSA-6* and *opr_nring*.

$$pEC_{50} = -0.0027\ (\pm 0.0020)\ SlogP\_VSA9$$
$$+\ 42.1146\ (\pm 15.2143)\ GCUT\_SMR\_0$$
$$+\ 0.0480\ (\pm 0.0157)\ PEOE\_VSA\text{-}6$$
$$-\ 0.1613\ (\pm 0.0973)\ opr\_nring + 32.4558\ (\pm 10.4617)$$

$n = 87$; $R = 0.831$; $s = 0.217$; $F = 21.702$; $p < 0.0001$; $Q^2 = 0.619$; SPRESS = 0.241; SDEP = 0.229.

SlogP_VSA9 which signifies sum of van der Waals surface area (in Å^2) calculation for each atom such that contribution to logP(o/w) (Li) > 0.40 is a 3D subdivided surface area descriptor. The Subdivided Surface Areas are descriptors based on an approximate accessible van der Waals surface area (in Å^2) calculation for each atom, v_i along with some other atomic property, p_i. The v_i are calculated using a connection table approximation. In the descriptions to follow, L_i denotes the contribution to logP(o/w) for atom i (Wildman and Crippen, 1999). The ranges were determined by percentile subdivision over a large collection of compounds. The negative coefficient of the descriptor indicates that an increase in the values of this descriptor decreases the antimalarial activity of the compounds. This is the reason for the low biological activity of the compound 32 which showed a high value of *SlogP_VSA9* (151.865).

GCUT_SMR_0 signifies the GCUT descriptors using atomic contribution to molar refractivity. It is an adjacency and distance matrix 2D Descriptor (Wildman and Crippen, 1999). The positive coefficient of *GCUT_SMR_0* shows that increase in the values of this descriptor is beneficial for antimalarial activity.

The next most important factor governing variation in the activity is *PEOE_VSA-6* which is a partial charge 2D descriptor and is directly proportional to the antimalarial activity. The Partial Equalization of Orbital Electronegativities (PEOE) method of calculating atomic partial charges is a method in which charge is transferred between bonded atoms until equilibrium (Gasteiger and Marsili, 1980). To guarantee convergence, the amount of charge transferred at each iteration is damped with an exponentially decreasing scale factor. The amount of charge transferred, dq_{ij}, between atoms i and j when $X_i > X_j$ is

$$dqij = (1/2^k)(X_i - X_j)/X_j^+ \tag{4}$$

where X_j^+ is the electronegativity of the positive ion of atom j; X_i is the electronegativity of atom i (quadratically dependent on partial charge); and k is the iteration number of the algorithm. The PEOE charges depend only on the connectivity of the input structures: elements, formal charges and bond orders. Descriptors using the PEOE charges are prefixed with *PEOE_*. *PEOE_VSA-6* represents the sum of van der Waals surface area (Å^2) of an atom where the partial charge of atom is less than −0.30.

The 2D descriptor *opr_nring* describes the number of rings bonds present in the compound (Oprea, 2000). The negative coefficient of *opr_nring* showed that a decrease in the values of this descriptor is beneficial for antimalarial activity.

Thus, *GCUT_SMR_0* and *PEOE_VSA-6* increases the antimalarial activity while the descriptors *SlogP_VSA9* and *opr_nring* decreases the antimalarial activity.

For the reliability of a 2D-QSAR model both Q^2 and R^2 values should be high. More often, a value of $Q^2 > 0.5$ is considered satisfactory (Ponce et al., 2004; Strazielle and Ghersi-Egea, 2005).

High correlation coefficient ($R = 0.831$) indicates good variance explanation of the model, further supported by low standard deviation ($s = 0.217$). Further, evaluation of the degree of statistical significance was accomplished by the Fischer test (F) and level of confidence ($p < 0.0001$). The validation parameters ($Q^2 = 0.619$ and SPRESS = 0.241), reflects the good predictive power of the model generated. Observed, predicted antimalarial activities and residual values of statistically significantly model obtained are shown in Table 2.

The plot of observed versus predicted activity (Fig. 1) shows a good fit with R^2 value of 0.69 and indicates that the model developed is able to predict the activity of the compounds quite well.

3.2. 3D-QSAR analysis

3.2.1. CoMFA

The predicted pEC$_{50}$ values by CoMFA model are listed in Table 3. Fig. 2 demonstrates the correlation between experimental

Table 2
Observed, predicted and residual values of the compounds with antimalarial activity.

Compounds	Observed pEC$_{50}$	Predicted pEC$_{50}$	Residual
2	7.824	7.848	−0.024
3	7.745	7.528	0.216
6	8.046	8.087	−0.041
7	7.854	7.663	0.191
8	7.658	7.572	0.085
9	8.046	7.924	0.122
10	7.745	8.061	−0.316
13	8.398	7.990	0.408
14	8.398	8.101	0.297
15	7.337	7.686	−0.348
16	7.268	7.659	−0.391
17	7.585	7.664	−0.079
18	7.959	7.809	0.150
19	7.824	7.532	0.292
21	7.398	7.627	−0.229
22	7.959	7.911	0.048
23	7.420	7.496	−0.076
24	7.509	7.474	0.034
25	7.569	7.538	0.031
26	8.000	8.021	−0.021
30	7.268	7.480	−0.213
31	6.863	7.115	−0.252
32	6.975	7.071	−0.097
33	7.495	7.603	−0.108
34	8.046	7.919	0.127
35	7.745	7.523	0.222
36	7.745	7.490	0.254
37	7.244	7.506	−0.262
38	7.824	7.803	0.021
40	7.125	7.386	−0.261
41	6.754	6.986	−0.232
42	7.658	7.341	0.317
44	6.936	6.907	0.028
45	7.260	7.154	0.106
46	7.301	7.574	−0.273
47	7.387	7.172	0.215
48	6.860	7.137	−0.277
49	7.337	7.641	−0.304
50	7.770	8.042	−0.272
51	7.886	7.580	0.306
54	7.699	7.360	0.339
55	7.180	6.989	0.191
56	7.051	6.916	0.135
57	6.928	7.218	−0.290
58	7.721	7.632	0.090
59	6.893	7.234	−0.341
60	7.046	7.198	−0.152
61	7.066	7.204	−0.139
63	7.569	7.184	0.385
64	7.398	7.223	0.175
66	7.538	7.723	−0.186
68	7.036	7.013	0.023
69	7.509	7.373	0.135
70	7.481	7.256	0.225
73	7.699	7.448	0.251
74	7.886	7.722	0.164
75	7.602	7.336	0.266
76	7.268	7.296	−0.028
77	7.699	7.559	0.140
78	8.046	7.912	0.134
79	7.770	7.503	0.267
83	6.652	6.997	−0.346
84	6.842	6.990	−0.148
85	7.721	7.748	−0.027
86	8.097	7.977	0.120
87	7.585	7.585	0.000
88	7.509	7.529	−0.020
89	7.959	7.866	0.092
90	7.886	8.090	−0.204
91	7.538	7.702	−0.164
93	7.252	7.492	−0.240
94	7.602	7.867	−0.265
95	7.409	7.452	−0.043
96	7.398	7.422	−0.024
97	7.409	7.636	−0.227
98	7.959	7.999	−0.040

Table 2 (continued)

Compounds	Observed pEC$_{50}$	Predicted pEC$_{50}$	Residual
99	7.638	7.581	0.057
100	7.553	7.541	0.012
101	7.398	7.638	−0.240
102	7.770	8.045	−0.275
104	7.959	7.579	0.380
106	8.046	7.851	0.195
107	7.387	7.446	−0.059
108	7.469	7.404	0.065
109	7.699	7.561	0.138
110	7.886	7.894	−0.008
111	7.569	7.476	0.092
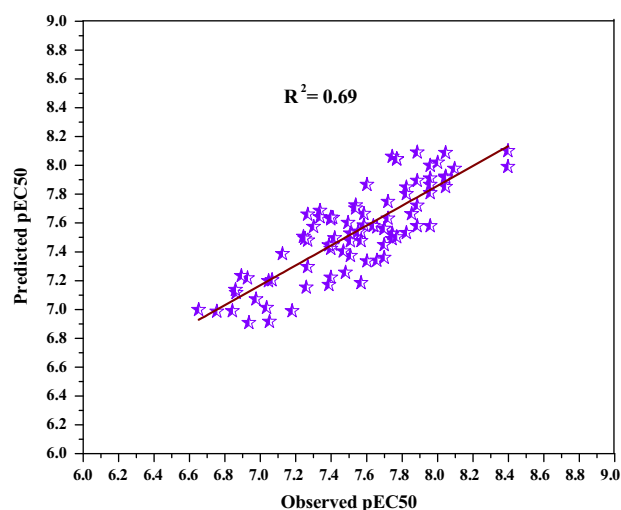
Fig. 1. Plot of actual versus predicted antimalarial activity using 2D-QSAR.

and predicted pEC$_{50}$ values by CoMFA model. It shows a R^2 value of 0.8157.

Statistical parameters derived for CoMFA model are summarized in Table 4. The derived CoMFA model illustrates a cross-validated Q^2 of 0.540 by four components. The optimal number of components (ONC) was calculated by selecting the highest Q^2 value. The non-cross-validated PLS analysis with the four components resulted in a R^2_{ncv} of 0.881, F = 157.090 and SEE of 0.214.

According to Table 4, the contributions of steric and electrostatic fields calculated by the CoMFA model are 46.7% and 53.3%, respectively, suggesting that the steric and electrostatic fields have been found to be almost equally important. The obtained high F, Q^2 and R^2_{ncv} values along with the lower SEE indicate the satisfactory predictive ability of the derived model (Table 4).

To further make sure the predictive ability of the CoMFA model an external test set of 22 compounds, which were not included in the QSAR model generation study was used. The CoMFA model showed an R^2_{pred} value of 0.518. The $R^2_{m(overall)}$ = 0.6604 was calculated and the results shows that the generated model shows a good predictive ability.

3.2.2. CoMFA contour maps

The steric and electrostatic contour maps resulted by CoMFA model based on the reference compound (compound 5) are revealed in Fig. 3. In this figure, the green contours point out the regions where presence of bulkier groups (80% contribution) would donate to enhance the biological activity while the yellow contours (20% contribution) illustrate the regions where such bulkier groups result in reduction of biological activities. Fig. 3A demonstrates the

steric field effects. The CoMFA electrostatic contour maps (Fig. 3B) are represented by red[1] and blue contours. The red contours (20% contribution) demonstrate the regions where electron-rich (electronegative) groups result in increase of biological activity whereas the blue contours (80% contribution) indicate the regions where presence of positive charge (or decreased negative charge) group would result in an increase of biological activity.

The steric contours of the CoMFA display a large green contour near R1 region demonstrating the favorable effect of bulky groups in raising the biological activities of the compounds. According to Table 1, this can be explained by comparing the activities of compounds 61 and 62 where bulk groups (–2-HO-3-MeO-Bn > –Furfuryl) at R1 substituent would result in lower EC_{50} values of 0.004 and 0.086, respectively. Same type of behavior is observed between compounds 25 and 26. The compound 26 has higher inhibitory activity ($pEC_{50} = 8.00$) and bulky characteristics than compound 25 ($pEC_{50} = 7.57$). Using the bulky substituents (–2-HO-3-MeO-Bn > –Furfuryl) R1 would lead to increase of pEC_{50} values in the compounds: 86 (having –2-HO-3-MeO-Bn group with $pEC_{50} = 8.10$) and 85 (having –Furfuryl group with $pEC_{50} = 7.72$). This effect can also be observed between compounds 34 and 35 where their higher activities can be related to the presence of –Piperonyl and –2-HO-3-MeO-Bn substituents, in which by increasing the bulky behavior of substituent (–Piperonyl < –2-HO-3-MeO-Bn) the inhibitory activities would be increased (7.74 < 8.04). As the bulkiness of the groups decreases in the order 2-HO-3-MeO-Bn > 3-F-6-MeO-Bn > Piperonyl > Furfuryl, the biological activity of the compounds decreases in the order 78 (8.04) > 80 (7.95) > 79 (7.77) > 77 (7.70), respectively. The steric contours of the CoMFA display a tiny green contour near the R2 region. This can be explained by comparing the order of activities of compounds 14 and 78. The compound 14 possesses –4-MeO-PhO substituent in contrast to the compound 78 which has only a Ph substituent at the same position and hence shows higher inhibitory activity (8.40 > 8.04). A comparison between compounds 28 and 80 reveals that compound 28 possesses 3-F-6-MeO-Bn group and displays higher inhibitory activity ($pEC_{50} = 8.15$) than compound 80 which contains a phenyl substituent as R2 ($pEC_{50} = 7.96$). As it can be seen from Fig. 3A, the steric contours map shows a small yellow contour at the R1 substituent region which exemplifies the unfavorable effect of bulky groups in some series of compounds. As shown by the pEC_{50} values, using bulky groups such as –3-F-6-MeO-Bn (compound 12 with $pEC_{50} = 5.62$) in contrast to –Furfuryl (compound 9 with $pEC_{50} = 8.04$) would result in decrease of activities. This fact can also be described by comparing compounds 72 (having 3-F-6-MeO-Bn as R1) with 69 (having Furfuryl group as R1). Replacing the R1 substituent with a bulkier group would result in decreasing of the pEC_{50} values (5.92 < 7.40).

Fig. 3B which represents the electrostatic contour plot has a blue contour near R2 group and a small blue contour in the bottom of R1 group. The small blue contour at the bottom of R1 group can be explained by comparing compounds 13 and 16 where replacing of 3-F-6-MeO-Bn in place of furfuryl is found to increase the negative charge behavior of this substituent. Consequently, the pEC_{50} values would be decreased (7.26 < 8.40). This blue contour map clearly explains why compound 9 showed higher inhibitory activities (8.04) than compound 10 (7.74). The blue contours at the R2 substituent can be understood by comparing compounds 62 (having –1-Et-Pr group with $pEC_{50} = 8.40$) and 78 (having –Ph group with $pEC_{50} = 8.04$) where using the positive charge group as R2 would lead to increasing the inhibitory activities. This fact is also

observed among compounds 105, 89 and 73 where increasing the negative charge properties (–4-CF$_3$-Ph > –4-MeO-Ph > 3, 5-Me-Bn) would result in decrease of inhibitory activities (7.70 < 7.96 < 8.05), respectively. The blue contours observed near R2 substituent can be described considering compounds 106 and 94; whereas, positive charge features increased (3,5-Me-Bn > –3-CF$_3$-Bn), the inhibitory activities (8.05 > 7.60) are also increased. The increasing biological activity can also be observed among compounds 75, 35, 79 and 51 where increasing the positive charge properties (4-CF$_3$ < –Ph < 4-F-Ph < –Ph < –PhEt) would result in increase of inhibitory activities (7.60 < 7.74 < 7.77 < 7.87), respectively. Fig. 3B demonstrated small red contours near the R2 substituent. The red contours can be explained by comparing compounds 34 and 50 where using the negative charge groups (–4-F-Ph > PhEt) would result in higher biological activities (8.05 > 7.77), respectively. The small red contour at the bottom of R1 group can be explained by comparing compounds 13 and 16 where replacing 3-F-6-MeO-Bn in place of –furfuryl would increase the negative charge behavior of this substituent, and consequently, the pEC_{50} values would be increased (compound 13; $pEC_{50} = 7.26$ < compound 16; $pEC_{50} = 8.40$). The red contour map clearly explains that why compound 78 showed higher inhibitory activities (8.05) than compound 77 (7.70).

3.2.3. CoMSIA

In addition to steric (S) and electrostatic (E) fields calculated by the CoMFA approach, hydrophobic (H), hydrogen-bond donor (D) and hydrogen-bond acceptor (A) fields can be derived using the CoMSIA method (Klebe et al., 1994). Different combinations of fields are combined to generate a total of 14 CoMSIA models. The statistical results of the constructed CoMSIA models are summarized in Table 5.

Fig. 4 demonstrates the correlation between experimental and predicted pEC_{50} values by CoMSIA model 12. It shows a R^2 value of 0.8701.

The donor and acceptor fields produced the lowest Q^2 and R^2_{ncv}, whereas the combined steric and electrostatic fields gave good Q^2 and R^2_{ncv} values. Although Q^2 for the CoMSIA model 8 show high R^2_{ncv} value the R^2_{ncv} is slightly lower. The CoMSIA model 4 gave fine Q^2 and R^2_{ncv} values but CoMSIA model 12, however, the combination of hydrophobic field provided more information and better values. Thus according to Table 5, the constructed CoMSIA model 12 with steric, hydrophobic, H-bond donor and H-bond acceptor fields could provide high statistical values for Q^2 (0.638) and R^2_{ncv} (0.946) values with the 10 optimum components. The statistical parameters calculated by CoMSIA model 12 indicate the satisfactory F value of 138.972 with the less SEE value of 0.149. The steric (S), hydrophobic (H) H-bond donor (D) and H-bond acceptor (A) field descriptor contributions were 23.1%, 44.6%, 21.5% and 10.8%, respectively.

The CoMSIA model showed an R^2_{pred} value of 0.521. The $R^2_{m(overall)} = 0.760$ was calculated and the results shows that the generated model shows a good predictive ability.

3.2.4. CoMSIA contour maps

The contour plots of the CoMSIA model-12 are presented in Fig. 5 which illustrates the steric, hydrophobic, H-bond acceptor and H-bond donor fields using the most active compound 5.

As shown in Fig. 5A, the steric field displayed a large yellow contour in the region of the R2 substituent and a large green contour around the R1 substituent. The yellow contour around the R2 substituent can be understood by comparing the compounds 51 (having PhEt group with $pEC_{50} = 7.89$) and 107 (having 3,5-Me-Bn group with $pEC_{50} = 7.39$) where the presence of bulkier size group would result in decrease of pEC_{50} values. This effect can be explained further by considering compounds 77 (having Phenyl group with $pEC_{50} = 7.70$) and 81 (having 4-tertBu-Ph group with

---

Table 3
Experimental activity and predicted activity of the compounds based on 3D-QSAR analysis (CoMFA and CoMSIA).

Compounds	Actual pEC$_{50}$ (M)	Predicted pEC$_{50}$ (M) CoMFA	Residual CoMFA	Predicted pEC$_{50}$ (M) CoMSIA	Residual CoMSIA
1	6.5031	6.681	−0.1779	6.595	−0.2279
2[a]	7.8239	7.376	0.4479	7.393	0.3419
3	7.7447	7.654	0.0907	7.622	0.1197
4[a]	6.7905	7.580	−0.7895	7.242	−0.2805
5	9.0000	8.554	0.4460	8.956	0.1090
6	8.0458	7.884	0.1618	8.155	−0.0032
7	7.8539	7.957	−0.1031	8.084	−0.2721
8	7.6576	7.755	−0.0974	7.651	−0.0384
9	8.0458	7.853	0.1928	7.848	0.1968
10	7.7447	7.954	−0.2093	7.624	0.0747
11	6.7905	7.253	−0.4625	7.041	−0.3775
12	5.6198	5.311	0.3088	5.532	0.0818
13	8.3979	8.272	0.1259	8.429	−0.0151
14	8.3979	8.466	−0.0681	8.373	0.0089
15[a]	7.3372	7.802	−0.4648	7.469	0.0982
16	7.2676	7.278	−0.0104	7.090	0.2396
17	7.5850	7.648	−0.0630	7.757	−0.1020
18	7.9586	7.782	0.1766	7.973	−0.1014
19	7.8239	7.428	0.3959	7.439	0.4699
20	6.5272	6.929	−0.4018	6.993	−0.4558
21	7.3979	7.255	0.1429	7.382	0.0309
22[a]	7.9586	7.802	0.1566	7.966	0.1186
23	7.4202	7.432	−0.0118	7.475	−0.0138
24[a]	7.5086	7.223	0.2856	7.260	0.3286
25	7.5686	7.901	−0.3324	7.511	−0.0074
26	8.0000	8.059	−0.0590	8.036	0.0060
27	5.8539	5.690	0.1639	5.743	0.0899
28[a]	8.1549	7.829	0.3259	7.438	0.7739
29	5.9586	5.825	0.1336	6.059	0.0076
30	7.2676	7.417	−0.1494	7.279	−0.0774
31	6.8633	6.739	0.1243	6.865	−0.0217
32	6.9747	6.698	0.2767	6.910	0.0487
33	7.4949	7.745	−0.2501	7.668	−0.2741
34	8.0458	8.177	−0.1312	8.161	−0.1292
35	7.7447	7.763	−0.0183	7.792	0.0707
36	7.7447	7.460	0.2847	7.496	0.2247
37	7.2441	7.486	−0.2419	7.447	−0.1769
38	7.8239	7.661	0.1629	7.727	0.0179
39	6.8962	7.086	−0.1898	6.803	−0.1098
40[a]	7.1249	7.390	−0.2651	7.113	−0.1781
41	6.7545	7.012	−0.2575	6.749	−0.0025
42	7.6576	7.267	0.3906	7.599	0.0016
43	7.5686	7.176	0.3926	7.436	0.2396
44	6.9355	6.910	0.0255	7.055	−0.1405
45	7.2596	7.091	0.1686	7.184	0.0026
46	7.3010	7.252	0.0490	7.247	−0.0930
47	7.3872	7.345	0.0422	7.353	−0.0218
48	6.8601	6.885	−0.0249	6.903	−0.2199
49	7.3372	7.455	−0.1178	7.237	0.1342
50	7.7696	7.815	−0.0454	7.820	−0.0394
51[a]	7.8861	7.216	0.6701	6.794	0.7831
52	6.8794	7.109	−0.2296	6.809	0.0514
53[a]	6.2358	6.585	−0.3492	6.702	−0.6272
54	7.6990	7.629	0.0700	7.748	−0.1300
55	7.1805	7.291	−0.1105	7.249	−0.0545
56	7.0506	7.394	−0.3434	7.065	0.0046
57	6.9281	7.124	−0.1959	7.016	0.0351
58[a]	7.7212	7.076	0.6452	7.225	0.4872
59[a]	6.8928	7.010	−0.1172	6.995	−0.0332
60	7.0458	6.995	0.0508	7.004	−0.0342
61	7.0655	7.182	−0.1165	7.013	0.1585
62	8.3979	7.998	0.3999	8.340	0.0429
63[a]	7.5686	7.341	0.2276	7.307	0.5766
64[a]	7.3979	7.721	−0.3231	7.786	−0.0651
65	6.5452	6.502	0.0432	6.478	−0.0008
66	7.5376	7.419	0.1186	7.483	0.0086
67	6.5467	6.828	−0.2813	6.628	−0.0353
68	7.0362	7.115	−0.0788	7.077	0.0242
69	7.5086	7.468	0.0406	7.541	0.0226
70	7.4815	7.314	0.1675	7.507	0.0225
71	6.2233	6.329	−0.1057	6.299	0.0343
72[a]	5.9208	5.866	0.0548	6.017	−0.0432
73	7.6990	7.918	−0.2190	7.852	−0.0430

Table 3 (continued)

Compounds	Actual pEC$_{50}$ (M)	Predicted pEC$_{50}$ (M) CoMFA	Residual CoMFA	Predicted pEC$_{50}$ (M) CoMSIA	Residual CoMSIA
74	7.8861	8.117	−0.2309	7.880	0.0001
75	7.6021	7.666	−0.0639	7.509	0.0061
76[a]	7.2676	7.504	−0.2364	7.436	−0.3214
77	7.6990	7.620	0.0790	7.673	0.1110
78[a]	8.0458	7.981	0.0648	8.116	−0.0192
79	7.7696	7.623	0.1466	7.760	0.0696
80	7.9586	7.979	−0.0204	7.958	−0.0354
81	6.1524	6.326	−0.1736	6.035	0.2054
82[a]	6.6003	7.311	−0.7107	7.057	−0.4247
83	6.6517	6.822	−0.1703	6.750	−0.0843
84	6.8416	6.801	0.0406	6.835	0.0046
85	7.7212	7.783	−0.0618	7.619	0.1142
86	8.0969	8.220	−0.1231	8.074	0.0279
87	7.5850	7.674	−0.0890	7.575	−0.0160
88	7.5086	7.560	−0.0514	7.430	−0.0524
89	7.9586	7.838	0.1206	7.943	0.2156
90	7.8861	7.832	0.0541	7.886	0.0161
91	7.5376	7.642	−0.1044	7.610	−0.0444
92[a]	7.0177	7.449	−0.4313	7.326	−0.4413
93	7.2518	7.144	0.1078	7.245	−0.0232
94[a]	7.6021	7.330	0.2721	7.328	0.1631
95	7.4089	7.422	−0.0131	7.534	−0.0731
96	7.3979	7.459	−0.0611	7.480	0.0699
97	7.4089	6.993	0.4159	7.360	0.0299
98	7.9586	7.740	0.2186	7.983	−0.1194
99	7.6383	7.557	0.0813	7.633	0.0733
100	7.5528	7.379	0.1738	7.690	0.0228
101	7.3979	7.435	−0.0371	7.533	−0.1231
102[a]	7.7696	7.422	0.3476	7.381	0.1746
103	6.1427	6.760	−0.6173	6.225	−0.1623
104	7.9586	7.427	0.5316	7.685	0.3956
105	8.0458	8.026	0.0198	8.035	−0.0482
106	8.0458	8.179	−0.1332	7.895	0.0948
107	7.3872	7.373	0.0142	7.414	0.0612
108[a]	7.4685	7.517	−0.0485	7.345	0.3295
109[a]	7.6990	7.859	−0.1600	8.227	−0.5010
110	7.8861	7.841	0.0451	7.823	0.0981
111	7.5686	7.442	0.1266	7.515	0.0966
112	6.6819	6.950	−0.2681	6.712	−0.2891

[a] Test set compounds.
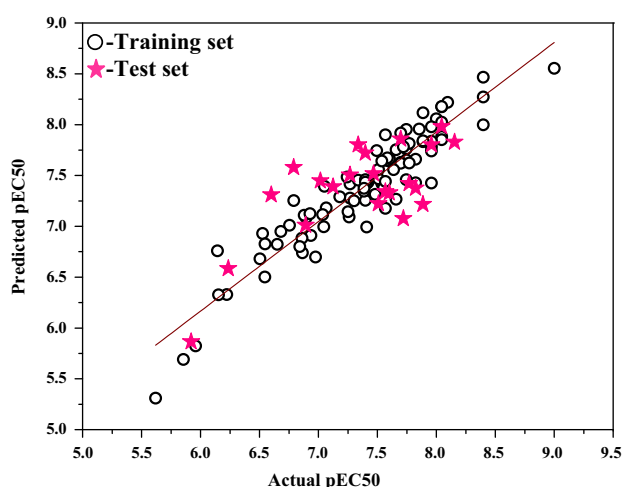
Fig. 2. Plot of actual versus predicted antimalarial activity using CoMFA model.

Table 4
Statistical results of CoMFA and CoMSIA models.

	CoMFA	CoMSIA model 12
Q^2/ONC[a]	0.540/4	0.638/10
R^2_{ncv}[b]	0.881	0.946
SEP[c]	0.437	0.385
SEE[d]	0.214	0.149
R^2_{pred}[e]	0.518	0.521
F value	157.090	138.972
Field distribution percent		
Steric	46.7	23.1
Electrostatic	53.3	–
Hydrophobic	–	44.6
H-bond donor		21.5
H-bond acceptor	–	10.8

[a] Cross-validated correlation coefficient.
[b] Non cross-validated correlation coefficient.
[c] Standard error of prediction.
[d] Standard errors of estimate.
[e] Predicted correlation coefficient for the test set.

pEC$_{50}$ = 6.15) where 4-tertBu-Ph group has bulkier size in contrast to phenyl group and, therefore, showed lower inhibitory activity. As shown by the pEC$_{50}$ values, using bulky groups such as 4-tertBu-PhO (compound 29 with pEC$_{50}$ = 5.96) in contrast to 4-MeO-Ph group (compound 89 with pEC$_{50}$ = 7.96) would result

in decrease of activities. The green contour demonstrates the favorable effect of bulky groups in increasing the biological activities of compounds. According to Table 1, this can be explained by comparing the activities of compounds 86 and 85 where using bulk groups (−2-HO-3-MeO-Bn > −Furfuryl) at R1 substituent would result in decrease of EC$_{50}$ values (0.008 < 0.019), respectively. This is also
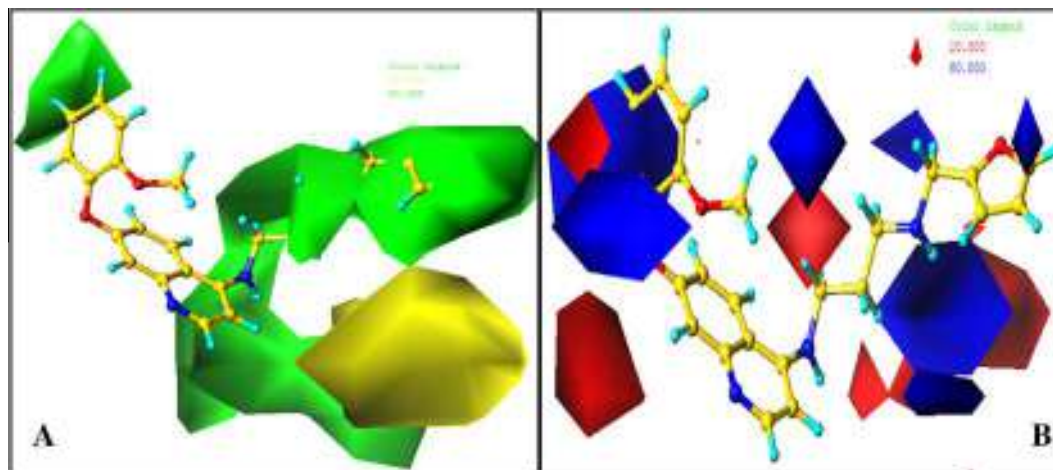
Fig. 3. Contour maps of CoMFA: (A) steric field and (B) electrostatic field based on compound 5.

observed between compounds 90 and 91 where compound 90 shows higher inhibitory activity (pEC$_{50}$ = 7.89) and bulky characteristics than compound 91 (pEC$_{50}$ = 7.54). As can be seen from Table 1, using the bulky substituents (–2-HO-3-MeO-Bn > –Furfuryl) as R1 would lead to increase of pEC$_{50}$ values in the compounds: 46 (having –2-HO-3-MeO-Bn group with pEC$_{50}$ = 7.30) and 45 (having furfuryl group with pEC$_{50}$ = 7.26). This effect can also be observed between compounds 26 and 27 where their higher activities can be related to the presence of 2-HO-3-MeO-Bn and Piperonyl substituents, namely in which by increasing the bulky behavior of substituent (2-HO-3-MeO-Bn > Piperonyl) the inhibitory activities would be increased (8.00 > 5.85).

Fig. 5B demonstrated the hydrophobic contour maps. In a hydrophobic field, orange and blue contours are highlighted areas where the orange contours represents the presence of hydrophobic substituents and using them would be favorable for better activity (favored level 80%), while blue contours indicate regions where hydrophobic groups decrease the biological activity (unflavored level 20%). Fig. 5B displays the large orange contours near R1 region and R2 region, and several small blue contours near R1 and R2 substituents.

Fig. 5C indicates that the presence of H-bond donor group would lead to enhance the inhibitory activity in cyan regions (80% contribution) while the presence of H-bond donor group would lead to decrease the inhibitory activity in purple regions (20% contribution). There is medium purple contours near R1 substituent which can be explained by comparing compounds 78 and 80 where replacing a 2-HO-3-MeO-Bn group in place of 3-F-6-MeO-Bn group would decrease the pEC$_{50}$ value (7.96 < 8.04). The H-bond donor R1 substituents (–2-HO-3-MeO-Bn > –3-F-6-MeO-Bn) would lead to decrease of pEC$_{50}$ values in the compounds: 106 (having –2-HO-3-MeO-Bn group with pEC$_{50}$ = 8.05) and 108 (having 3-F-6-MeO-Bn group with pEC$_{50}$ = 7.47). This effect can also be observed between compounds 46 and 54 where their lower activities can be related to the presence of –2-HO-3-MeO-Bn as R1 substituent, when compared to the compounds 48 and 56, respectively; having 3-F-6-MeO-Bn as R1 substituent. There are no major cyan contours near R1 and R2 substituents.

H-bonds acceptor field was also considered to be important for the activity of the ligands. The H-bonds acceptor contour maps were also provided by the CoMSIA model to facilitate structural optimization. Fig. 5D indicates that the presence of H-bond acceptor group would lead to the decrease of the inhibitory activity in red regions (20% contribution). From the Fig. 5D it is clear that

Table 5
Statistical parameters of CoMSIA models.

Model	Descriptors	$R^2_{LOO}(Q^2)$/ONC	R^2_{ncv}/SEE$_{ncv}$	F value	$R^2_{m(overall)}$	R^2_{pred}
1	S and E	0.592/8	0.962/0.124	255.632	0.762	0.391
2	D and A	0.411/4	0.671/0.355	43.351	0.339	0.392
3	S, E and H	0.593/7	0.943/0.151	193.697	0.764	0.516
4	S, E and A	0.613/8	0.962/0.124	256.727	0.766	0.393
5	S, E and D	0.603/9	0.957/0.132	198.397	0.722	0.290
6	D, A and H	0.657/10	0.944/0.152	133.561	0.754	0.493
7	D, A and S	0.453/10	0.883/0.220	59.646	0.639	0.354
8	D, A and E	0.595/9	0.958/0.131	202.186	0.718	0.261
9	S, D and H	0.606/7	0.903/0.196	109.366	0.698	0.527
10	S, E, D and A	0.609/9	0.958/0.132	200.297	0.725	0.307
11	S, E, D and H	0.616/8	0.951/0.140	198.490	0.749	0.431
12	**D, A, H and S**	**0.638/10**	**0.946/0.149**	**138.972**	**0.760**	**0.521**
13	D, A, H and E	0.648/8	0.958/0.131	228.870	0.752	0.399
14	S, E, D, A and H	0.640/9	0.963/0.123	229.875	0.763	0.094

Selected model is given in bold.

there is no magenta contour which represents the favoured region (80% contribution). There is a large red contour near R1 substituent. The red contour near R1 can be explained by comparing compounds 20 and 18 where replacing a 3-F-6-MeO-Bn group in place of 2-HO-3-MeO-Bn group would decrease the H-bonds acceptor behavior of the substituent, and consequently, the pEC$_{50}$ values would be increased (7.96 > 6.53). It can also be explained by comparing compounds 26 and 28 where replacing a 2-HO-3-MeO-Bn group which has lesser H-bond acceptor tendency in place of 3-F-6-MeO-Bn group which is a H-bond acceptor group would increase the pEC$_{50}$ value (8.05 > 8.00). The H-bond acceptor R1 substituents (–3-F-6-MeO-Bn) would lead to decrease of pEC$_{50}$ value (7.96) in the compound 104 compared with the compound 102 (having –2-HO-3-MeO-Bn group with pEC$_{50}$ = 7.77).

3.3. Molecular docking

3.3.1. Structure prediction and validation

Primary structure prediction of the protein 1CET shows that the instability index was found to be 30.26 which classify the protein as stable. The high aliphatic index (110.41) of the protein is evidence for high thermodynamic stability. The positive value of the GRAVY (0.134) supports the protein molecule to be hydrophobic. The estimated half-life is 30 h (mammalian reticulocytes, *in vitro*).

Secondary structure prediction carried out using SOPMA shows that the protein 1CET is structurally stabilized by efficient folding
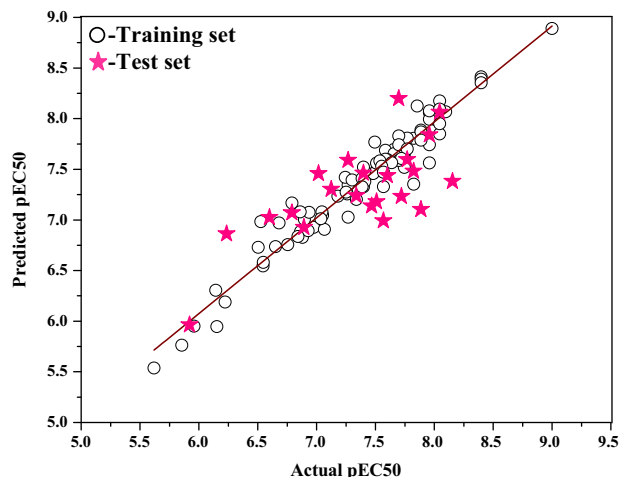
Fig. 4. Plot of actual versus predicted antimalarial activity using CoMSIA model 12.

technique. The low percentage of β-turn (7.91%) and the high percentage of α-Helix (38.29%) hold up the above factor.

Ramachandran plot (Fig. 6) shows that the protein has one outlier amino acid Gly164. The number of residues in the core region is 94.68%. The number of residues in the allowed region is 4.98% and the number of residues in the outlier region is only 0.33%.

3.3.2. Target-ligand interaction

The binding interaction of the 112 ligand molecules with the protein molecule 1CET was analyzed using Dock module in MOE 2007.09. The molecular docking results are summarized in

Table 6. The docked conformation of compounds revealed that compounds interacted with the binding pocket residues of targeted protein through several favorable interactions including polar, hydrophobic, hydrogen bonding and the weak van der Waal contacts. Compounds 6, 7, 8, 10, 15, 23, 30, 36, 38 and 39 showed good binding score with the protein 1CET.

The molecular docking interaction of compound 6 with the active site of 1CET shows that the oxygen of the methoxy group interacts (3.26 Å, 1.6 Å and 1.29 Å) indirectly with four amino acids Thr169, Ile270, Lys173 and Val166 in the active site of the enzyme. Arg185, a basic amino acid from the active site of ICET interacts with the nitrogen of the quinoline ring through a side chain hydrogen bonding interaction (3.04 Å). Strength of chemical bond between this active side residue and inhibitor is 30%. Hydrophobic interactions between the quinoline ring and the residues Arg185, Asn188, Pro184, Ala249, Glu256, Ser170, and Val268 appear to constrain the compound in close proximity with the amino acids forming the fore mentioned hydrogen bonding. An arene–cation interaction was observed between the methoxybenzene ring and basic Lys173.

The molecular docking interaction of compound 7 with the active site of 1CET is represented in Fig. 7. The molecular docking score of the compound is −13.7841 kcal/mol. The N atom attached to benzodioxole ring forms hydrogen bonds with 3 water molecules. The water molecules was found to be interacting with several important residues including Thr169, Val166, Lys173, Glu256 and Ile270. A side chain hydrogen bonding interaction was observed between basic Lys173 and O atom (3.47 Å, 10%) present in the five membered ring. An arene–cation interaction was observed between the benzene ring and the residue Lys173. Hydrophobic interactions was observed between quinoline ring
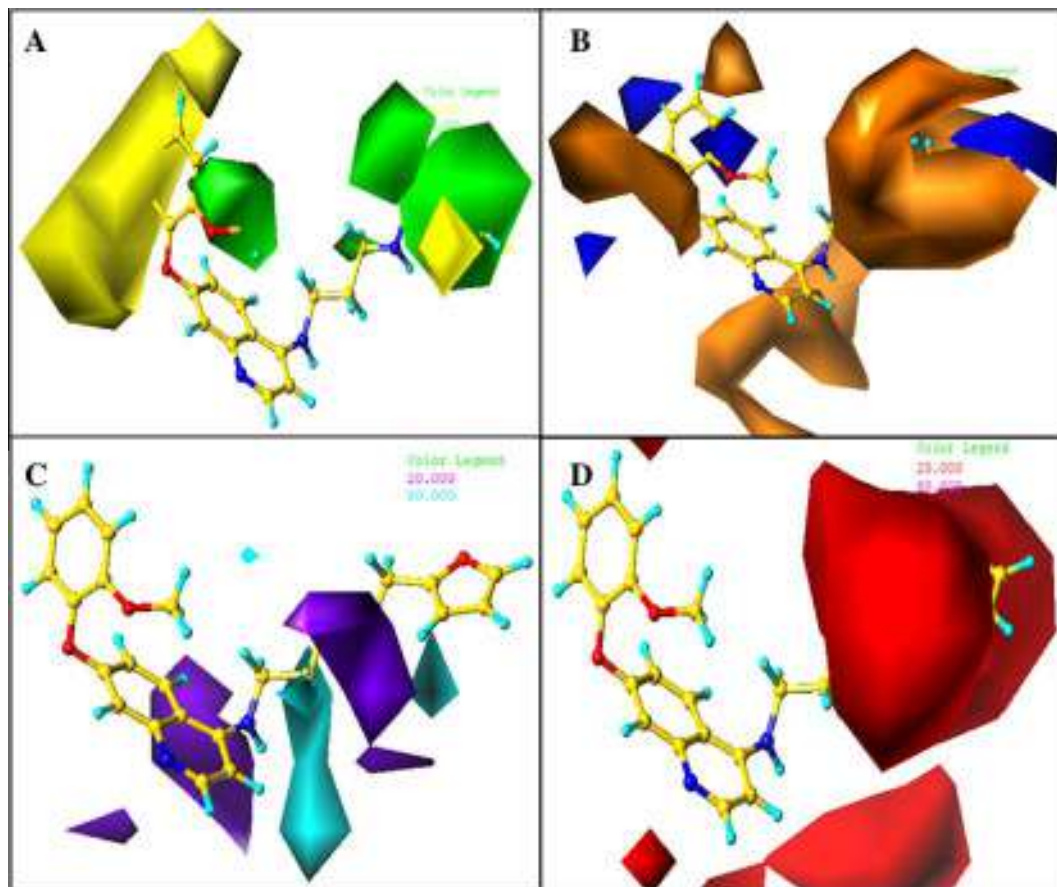
Fig. 5. Contour maps of CoMSIA: (A) steric field, (B) hydrophobic field, (C) H-bond donor field and (D) H-bond acceptor field based on compound 5.

and the sandwich of the backbone atoms of Arg185, Ala252, Tyr174, Ala249 on one side and Ser170 on the other. There are hydrophobic interactions between benzodioxole ring of the ligand and residues Asn188, Val268 and Glu256. A prominent back bone hydrogen bonding interaction was found between Val166 and the NH (2.84 Å, 14%) bonded to benzodioxole ring on one side while basic Lys173 was found to be interacting with the oxygen present in the five membered ring on the other side (3.47 Å), with very low bond strength (10%).

Compound 8 forms arene–cation interaction between basic Lys173 and fluoromethoxy benzene ring. Quinoline ring shows hydrophobic interactions with residues Tyr174, Ser170 and Ala252. The N atom attached to the fluoromethoxy benzene ring forms side chain hydrogen bonding interaction with Lys173 (2.47 Å). The polar bond is having very high bond strength (94%). It also forms interactions with residues Arg185, Val187and Glu256 through bridged water molecules. The top ranking molecular docking score was −13.2418 kcal/mol. The side chain hydrogen bonding interaction of the polar Asn188 with the oxygen of methoxy group bonded to fluoromethoxy benzene ring (2.88 Å) was found with bond strength 45%.

The binding mode observed for the compound 10 shows that the quinoline ring is located in a hydrophobic pocket surrounded by Arg185, Ser170, Lys173, Tyr175, Tyr174, Ala249 and Ala252. An arene–arene interaction was observed involving methoxy benzene ring of the ligand and polar Tyr174. The molecular docking interaction of compound 10 shows basic arene–cation interaction of methoxy phenol ring and Lys173. A side chain hydrogen bonding interaction was observed between the –OH group and Glu256 (1.26 Å) with very low bond strength 12%. Methoxy phenol ring shows hydrophobic interactions with residues Asn188, Val166, Val268, Pro184 and Arg185. The molecular docking score was found to be −13.3169 kcal/mol. Arg185 is a basic amino acid which forms a side chain hydrogen bonding interaction with NH bonded to methoxy phenol moiety with very weak bond strength (2.98 Å, 16%).

Molecular docking of compound l5 with score −13.4950 kcal/-mol showed a basic side chain hydrogen bonding interaction between O atom of the benzodioxole ring and Lys43 (2.67 Å, 77%). Quinoline ring shows arene–cation interaction with the basic residues Lys173 and Arg185 and methoxy benzene ring shows arene–cation interaction with the residue Lys173. Both Quinoline and methoxy benzene rings show hydrophobic interactions with residues Val166, Lys173, Arg185, Asn188, Leu269, Pro184, Val268 and Glu256. The N atom of the Quinoline ring shows hydrogen bond interactions with Lys173, Arg185 and Val187 through bridge water molecules. The O atom of the-methoxy group forms H-bond interactions with Ala189, Asn188 and Pro184. Benzodioxole ring shows hydrophobic interaction with Lys43, acidic Glu256, Pro184 and Val268.

In case of compound 23, a large number of interactions are present (Fig. 7). It was observed that the two oxygen of benzodioxole ring formed H-bond interactions with residues Lys173, Ala189, Ile270, Asn188 and Val268 through bridged water molecules. An arene–cation interaction was observed between quinoline ring and basic Arg185. Hydrophobic interactions between benzodioxole ring and Asn188, Leu269, Val268, Lys173 as well as the quinoline ring with Arg185, Val166 and Glu256 appear to constrain the compound in close proximity with the amino acids forming the fore mentioned hydrogen bonding. Benzodioxole ring forms an arene–cation interaction with basic Lys173. The molecular docking score of the compound 23 was −14.4918 kcal/mol. During interaction basic Lys173 behaves as a side chain acceptor residue that binds to the N atom of benzodioxole ring of inhibitor. The polar bond between the Lys173 and inhibitor is having moderate bond strength (63%). Lys173 was found making interaction with
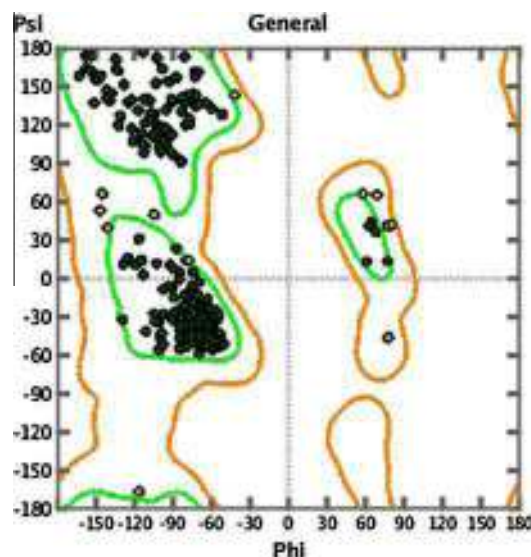
Fig. 6. Ramachandran plot (PDB 1CET) after energy and residue optimization.

Table 6
Docking results of compounds into the protein 1CET.

Compounds	E score (kcal/mol)	Amino acid residues in direct interaction	Distance (Å), bond strength (%)	Amino acid residues interaction due to water molecule
6	−13.1957	Arg185, Lys173	3.04, 30	Thr169, Ile270, Val166, Lys173
7	−13.7841	Val166 Lys173 Lys173	2.84, 14 2.56, 53 3.47, 10	Asn188, Ala189, Thr169, Ile270, Val268, Glu256, Val166, Lys173
8	−13.2418	Asn188 Lys173	2.88, 45 2.47, 94	Glu256, Val187, Asn188, Arg185, Val268
10	−13.3169	Arg185 Glu256	2.98, 16 1.26, 12	Ile270, Lys173, Glu256, Ser170, Arg185
15	−13.4950	Lys43 Arg185 Lys173	2.67, 77	Arg185, Lys173, Ala189, Asn188, His190, Val187, Pro184
23	−14.4918	Lys173 Lys173	2.75, 63 3.24, 16	Ile255, Glu256, Ala252, Asn188, Val268, Ala189, Ile270, Lys173, Thr169, Val166
30	−13.0691	Lys173 Lys173	2.92, 53 2.5, 76	Glu256, Tyr174, Asn188, Arg185, Val187, Val268, Ala189, Lys173
36	−13.5305	Lys173 Lys173	2.37, 70 2.87, 61	Ala189, Val268, Ile270, Asn188, Lys173, Val166, Thr166, Glu256
38	−15.1099	Glu256 Glu256	2, 22 1.2, 35	Lys173, Val268, Asn188
39	−13.9625	Asn188 Arg185 Lys173	2.77, 62	Glu256

(2.75 Å, 63%). A direct side chain acceptor interaction was found between basic Lys173 and oxygen atom of the benzodioxole ring (3.24 Å). The polar bond between the Lys173 and compound is having low bond strength (16%) (Fig. 8).

The binding mode observed for compound 30 shows that most of the interactions present are concentrated on the methoxy phenol ring with a molecular docking score −13.0691 kcal/mol. A stacking interaction with varied bond strength was observed between basic Lys173 and inhibitor molecule. Lys173 is interacting as a side chain donor molecule for both OH and NH groups attached to the aryl ring of the inhibitor compound (2.5 Å, 76%; 2.92 Å, 53%). Further stabilization was obtained by hydrophobic interactions with Leu269, Val268, Lys173, Arg185, Asn188, Ser170, Ala249, Ala252, Pro246, Glu256 and Tyr174.
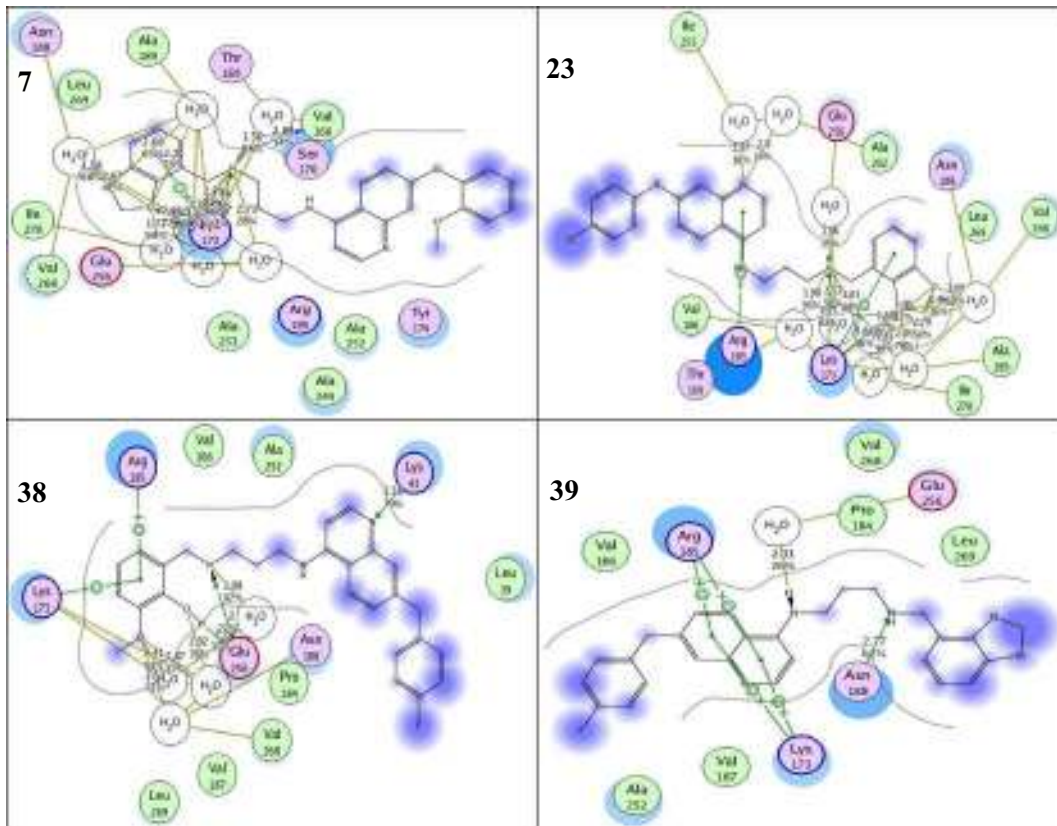
Fig. 7. The 2D interaction of the active compounds 7, 23, 38 and 39 with protein 1CET.
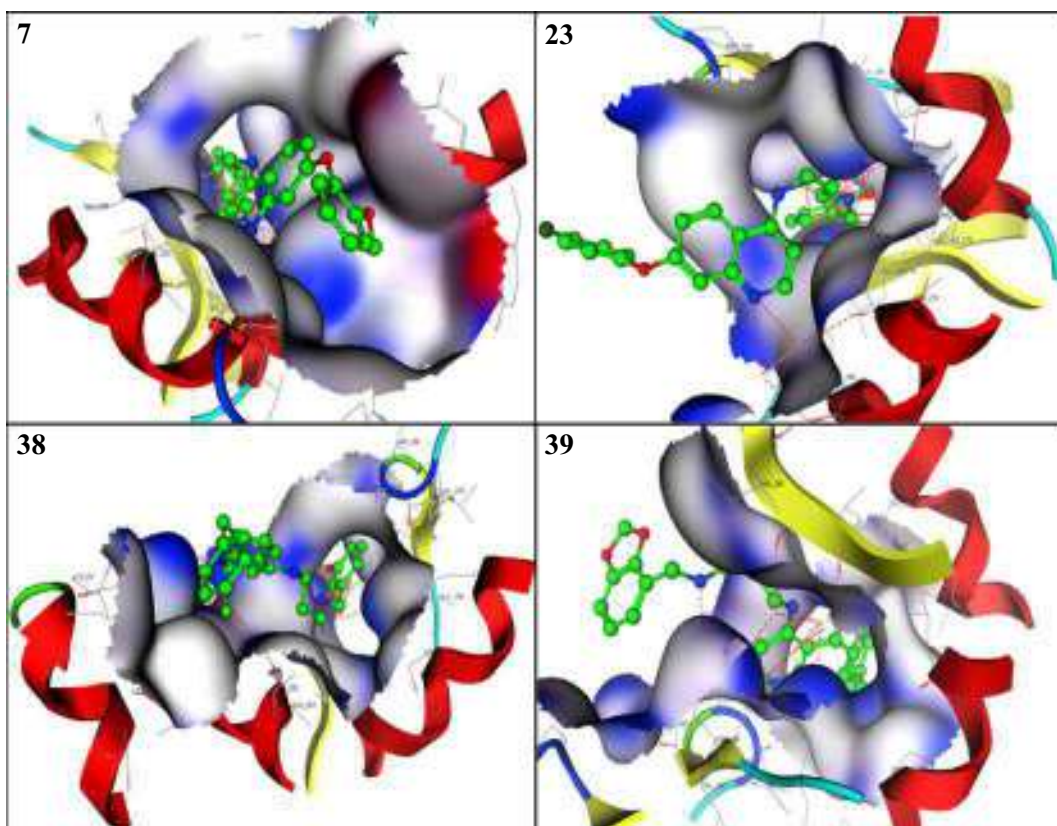
Fig. 8. The docking pose of the active compounds 7, 23, 38 and 39 with protein 1CET.

From the molecular docking analysis it appears that Lys173, Val268, Asn188, Tyr174, Glu256 etc are the residues that make compound 36 a potent inhibitor. Through different kinds of chemical interactions with the above mentioned residues, compound 36 occupies the active site of enzyme and may inhibit or lower its catalytic efficiency. An arene–arene interaction was observed between fluorobenzene ring and polar Tyr 174 amino acid. The oxygen and NH atoms attached to the other fluorobenzene ring shows side chain hydrogen bonding interactions with the basic Lys173 residue (2.92 Å, 2.5 Å). Strength of chemical bonds between this active side residue and inhibitor is 53% and 76% respectively. The molecular docking score observed was −13.5305 kcal/mol.

The binding mode observed for compound 38 (Fig. 7) shows that it binds within the binding pocket with a molecular docking score −15.1099 kcal/mol. This compound has the highest molecular docking scores of the selected compounds. An arene–cation interaction was observed between the methoxy phenol ring and basic residues Lys173 and Arg185. The N atom attached to methoxy phenol ring forms acidic side chain hydrogen bonding interaction with residue Glu256 (2 Å, 22%). A side chain hydrogen bonding interaction was also observed between acidic Glu256 and hydroxyl group of methoxy phenol ring of the compound with very low bond strength (1.2 Å, 35%). Quinoline ring shows hydrophobic interactions with residues Lys43, Leu39, Ala252 and Asn188. The nitrogen atom present in the quinoline ring shows basic side chain hydrogen bonding interaction with Lys43. The polar bond between the Lys173 and compound is having moderate bond strength (79%). The methoxyphenol ring shows hydrophobic interactions with residues Arg185, Lys173, Leu269, Val268, Glu256 and Asn188.

The binding mode observed for the compound 39 shows that the quinoline ring was located in a hydrophobic pocket surrounded by Arg185, Val166, Asn188, Lys173 and Ala252. Quinoline ring shows four arene–cation interactions with basic Arg185 and basic Lys173. The NH group attached to the benzodioxole ring forms side chain acceptor interaction with polar Asn188. (2.77 Å). The polar bond between the Lys173 and compound is having moderate bond strength (62%). Acidic Glu256 shows hydrogen bonding interaction with NH group attached to the quinoline ring (2.31 Å, 26%).

Thus the selected 7-substituted 4-aminoquinoline analogs with maximum molecular docking scores are compounds 6, 7, 8, 10, 15, 23, 30, 36, 38 and 39.

4. Conclusion

The present study on a series of 7-substituted-4-aninoquinoline analogs was carried out using 2D-QSAR, CoMFA/CoMSIA methods and molecular docking analysis. 2D-QSAR final models included *SlogP_VSA9, GCUT_SMR_0, PEOE_VSA-6* and *opr_nring* descriptors and showed a satisfactory statistical quality and predictive abilities as shown by the R^2 and Q^2 values for 2D-QSAR model. The 3D-QSAR models generated indicate that the steric, electrostatic (in CoMFA), H-bond donor, H-bond acceptor and hydrophobic (in CoMSIA) fields have important influences on the ligand–receptor interaction. The predictive ability of the CoMFA ($Q^2 = 0.540$ and $R^2_{ncv} = 0.881$) and CoMSIA ($Q^2 = 0.638$ and $R^2_{ncv} = 0.946$) models was also as good as the 2D-QSAR models. The CoMFA model and the better CoMSIA model were further validated using an external test set, with the predicted R^2 values of 0.518 and 0.521, respectively. Using molecular docking the appropriate binding conformations of these series of compounds which interact with protein 1CET, were revealed. Thus the present study provides useful guidelines for developing 7-substituted-4-aminoquinoline derivatives as potent antimalarial activity inhibitors.

References

Afantitis, A., Melagraki, G., Sarimveis, H., Igglessi- Markopoulou, O., Kollias, G., 2009. A novel QSAR model for predicting the inhibition of CXCR3 receptor by 4-N-aryl-[1,4] diazepaneureas. Eur. J. Med. Chem. 44, 877–884.

Boechat, N., Ferreira Mde, L., Pinheiro, L.C., Jesus, A.M., Leite, M.M., Júnior, C.C., Aguiar, A.C., de Andrade, I.M., Krettli, A.U., 2014. New compounds hybrids 1H-1,2,3-triazole-quinoline against *Plasmodium falciparum*. Chem. Biol. Drug Des. 84, 325–332.

Bush, B.L., Nachbar, R.B., 1993. Sample-distance partial least squares: PLS optimized for many variables, with application to CoMFA. J. Comput. Aided Mol. Des. 7, 587–619.

ChemDraw, Cambridge Software Corporation, 64-71.5.3 version, 2004.

Cramer, R.D., Patterson, D.E., Bunce, J.D., 1988. Comparative molecular field analysis (CoMFA). 1. Effect of shape on binding of steroids to carrier proteins. J. Am. Chem. Soc. 110, 5959–5967.

Dorn, A., Vippagunta, S.R., Maitle, H., Jaquet, C., Vennerstrom, J.L., Ridley, R.G., 1998. An assessment of drug–haematin binding as a mechanism for inhibition of haematin polymerisation by quinoline antimalarials. Biochem. Pharmacol. 55, 727–736.

Du, Q.S., Gao, J., Wei, Y.T., Du, L.Q., Wang, S.Q., Huang, R.B., 2012. Structure-based and multiple potential three-dimensional quantitative structure–activity relationship (SB-MP-3D-QSAR) for inhibitor design. J. Chem. Inf. Model. 52, 996–1004.

Gasteiger, J., Marsili, M., 1980. Iterative partial equalization of orbital electronegativity – a rapid access to atomic charges. Tetrahedron 36, 3219–3228.

Gasteiger, E., Hoogland, C., Gattiker, A., Duvaud, S., Wilkins, M.R., Appel, R.D., Bairoch, A., 2005. Protein identification and analysis tools on the ExPASy server. In: Walker, John M. (Ed.), The Proteomics Protocols Handbook. Humana Press, Totowa, NJ, pp. 571–607.

Geourjon, C., Deléage, G., 1995. SOPMA: significant improvements in protein secondary structure prediction by consensus prediction from multiple alignments. Comput. Appl. Biosci. 11, 681–684.

Gill, P., Murray, W., Wright, M., 1981. Practical Optimization. Academic Press, London.

Golbraikh, A., Tropsha, A., 2002. Beware of q2! J. Mol. Graph. Model. 20, 269–276.

Hwang, J.Y., Kawasuji, T., Lowes, D.J., Clark, J.A., Connelly, M.C., Zhu, F., Guiguemde, W.A., Sigal, M.S., Wilson, E.B., Derisi, J.L., Guy, R.K., 2011. Synthesis and evaluation of 7-substituted 4-aminoquinoline analogues for antimalarial activity. J. Med. Chem. 54, 7084–7093.

Klebe, G., Abraham, U., Mietzner, T., 1994. Molecular similarity indices in a comparative analysis (CoMSIA) of drug molecules to correlate and predict their biological activity. J. Med. Chem. 37, 4130–4146.

Kyaw, M.P., Nyunt, M.H., Chit, K., Aye, M.M., Aye, K.H., Lindegardh, N., Tarning, J., Imwong, M., Jacob, C.G., Rasmussen, C., 2013. Reduced Susceptibility of *Plasmodium falciparum* to Artesunate in Southern Myanmar. PLoS ONE 8 (3), e57689.

Lang Unnasch, N., Murphy, A.D., 1998. Metabolic changes of the malaria parasite during the transition from the human to the mosquito host. Annu. Rev. Microbiol. 52, 561–590.

Lin, A., 2000. QuaSAR-Descriptor. <http://www.chemcomp.com/journal/descr.htm>.

Masand, V.H., Toropov, A.A., Toropova, A.P., Mahajan, D.T., 2014. QSAR models for anti-malarial activity of 4-aminoquinolines. Curr. Comput. Aided Drug Des. 10, 75–82.

Mishra, A., Batchu, H., Srivastava, K., Singh, P., Shukla, P.K., Batra, S., 2014. Synthesis and evaluation of new diaryl ether and quinoline hybrids as potential antiplasmodial and antimicrobial agents. Bioorg. Med. Chem. Lett. 24, 1719–1723.

Molecular Operating Environment (MOE), developed and distributed by Chemical Computing Group. <http://www.chemcomp.com>.

O'Brien, C., Henrich, P.P., Passi, N., Fidock, D.A., 2011. Recent clinical and molecular insights into emerging artemisinin resistance in *Plasmodium falciparum*. Curr. Opin. Infect. Dis. 24, 570–577.

O'Neill, P.M., Bray, P.G., Hawley, S.R., Ward, S.A., Park, B.K., 1998. 4-Aminoquinolines – past, present and future: a chemical perspective. Pharmacol. Therapeut. 77, 29–58.

Oprea, Tudor I., 2000. Property distribution of drug related chemical databases. J. Comput. Aid. Mol. Des. 14, 251–264.

Podlogar, B.L., Ferguson, D.M., 2000. QSAR and CoMFA: a perspective on the practical application to drug discovery. Drug Des. Discov. 17, 4–12.

Ponce, Y.M., Garit, J.A., Torrens, F., Zaldivar, V.R., Castro, E.A., 2004. Atom, atom-type, and total linear indices of the "molecular pseudograph's atom adjacency matrix": application to QSPR/QSAR studies of organic compounds. Molecules 9, 1100–1123.

Pourbasheer, E., Riahi, S., Ganjali, M.R., Norouzi, P., 2010. QSAR study on melanocortin-4 receptors by support vector machine. Eur. J. Med. Chem. 45, 1087–1093.

Pourbasheer, E., Aalizadeh, R., Ganjali, M., Norouzi, P., 2013. QSAR study of α1β4 integrin inhibitors by GA-MLR and GA-SVM methods. Struct. Chem. 25, 355–370.

Rännar, S., Lindgren, F., Geladi, P., Wold, S.A., 1994. PLS kernel algorithm for data sets with many variables and fewer objects. Part 1: theory and algorithm. J. Chemom. 8, 111–125.

Read, J.A., Wilkinson, K.W., Tranter, R., Sessions, R.B., Brady, R.L., 1999. Chloroquine binds in the cofactor binding site of Plasmodium falciparum lactate dehydrogenase. J. Biol. Chem. 274, 10213–10218.

Riahi, S., Ganjali, M., Pourbasheer, E., Norouzi, P., 2008. QSRR study of GC retention indices of essential-oil compounds by multiple linear regression with a genetic algorithm. Chroma 67, 917–922.

Riahi, S., Pourbasheer, E., Ganjali, M.R., Norouzi, P., 2009. Investigation of different linear and nonlinear chemometric methods for modeling of retention index of essential oil components: concerns to support vector machine. J. Hazard. Mater. 166, 853–859.

Ridley, R.G., 1996. Hemozoin formation in malaria parasites: is there a haempolymerase? Trends Microbiol. 4, 253–254.

Rose, P.W., Prlić, A., Bi, C., Bluhm, W.F., Christie, C.H., Dutta, S., Green, R.K., Goodsell, D.S., Westbrook, J.D., Woo, J., Young, J., Zardecki, C., Berman, H.M., Bourne, P.E., Burley, 2015. The RCSB Protein Data Bank: views of structural biology for basic and applied research and education. Nucleic Acids Res. 43 (Database issue), D345–D356.

Sonin, D.L., Wakatsuki, T., Routhu, K.V., Harmann, L.M., Petersen, M., Meyer, J., Strande, J.L., 2013. Protease-activated receptor 1 inhibition by SCH79797 attenuates left ventricular remodeling and profibrotic activities of cardiac fibroblasts. J. Cardiovasc. Pharmacol. Ther. 18, 460–475.

Strazielle, N., Ghersi-Egea, J.F., 2005. Factors affecting delivery of antiviral drugs to the brain. Rev. Med. Virol. 15, 105–133.

Tosco, P., Balle, T., 2011. Open3DQSAR: a new open-source software aimed at high-throughput chemometric analysis of molecular interaction fields. J. Mol. Model. 17, 201–208.

Videnović, M., Opsenica, D.M., Burnett, J.C., Gomba, L., Nuss, J.E., Selaković, Z., Konstantinović, J., Krstić, M., Segan, S., Zlatović, M., Sciotti, R.J., Bavari, S., Solaja, B.A., 2014. Second generation steroidal 4-aminoquinolines are potent, dual-target inhibitors of the botulinum neurotoxin serotype A metalloprotease and P. falciparum malaria. J. Med. Chem. 57, 4134–4153.

White, N.J., Pukrittayakamee, S., Hien, T.T., Faiz, M.A., Mokuolu, O.A., Dondorp, A.M., 2014. Malaria. Lancet 383, 723–735.

Wildman, S.A., Crippen, G.M., 1999. Prediction of physiochemical parameters by atomic contributions. J. Chem. Inf. Comput. Sci. 39, 868–873.

Wiwanitkit, V., 2007. Plasmodium and host lactate dehydrogenase molecular function and biological pathways: implication for antimalarial drug discovery. Chem. Biol. Drug Des. 69 (4), 280–283.

Wold, S., Ruhe, A., Wold, H., Dunn, I.W., 1984. The collinearity problem in linear regression. The partial least squares (PLS) approach to generalized inverses. J. Sci. Stat. Comp. 5, 735–743.

ORIGINAL RESEARCH

Discovery of Rimonabant and its potential analogues as anti-TB drug candidates

J. M. Gajbhiye · N. A. More · Manoj D. Patil · R. Ummanni · S. S. Kotapalli · P. Yogeeswari · D. Sriram · V. H. Masand

Abstract Rimonabant and its analogues have been synthesized in moderate to good yields using a simple synthetic route. All the newly synthesized compounds were subjected to in vitro screening against *M. tuberculosis* and *M. smegmatis*. The most potent analogue JMG-14 exhibits MIC value of 3.13 compared to 3.25 and 50 µg/ml for ethambutol and pyrazinamide, respectively. The molecular docking reveals that pyrazole ring, number and position of halogen atoms play a crucial role in deciding interactions with MTCYP-121. These findings open up a new avenue in the search of potent anti-TB drugs with rimonabant and its novel analogue JMG-14 as lead molecules.

Graphical Abstract
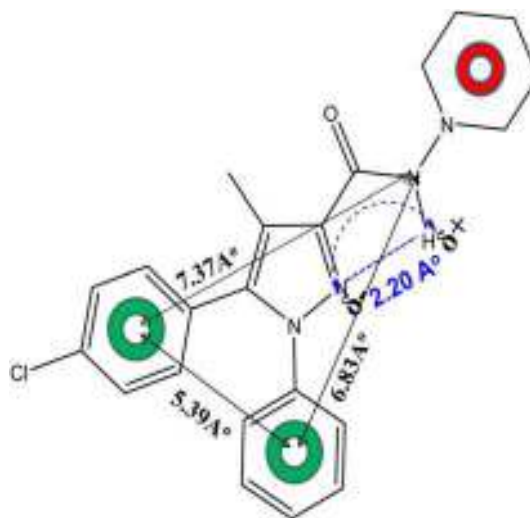
J. M. Gajbhiye (✉) · N. A. More · M. D. Patil
Division of Organic Chemistry, CSIR-National Chemical Laboratory, Pune 411008, India
e-mail: jm.gajbhiye@ncl.res.in

R. Ummanni · S. S. Kotapalli
Centre for Chemical Biology, Indian Institute of Chemical Technology, Hyderabad 500607, India

P. Yogeeswari · D. Sriram
Tuberculosis Drug Discovery Laboratory, Pharmacy Group, Birla Institute of Technology and Science, Pilani, Hyderabad Campus, Hyderabad 500078, India

V. H. Masand
Department of Chemistry, VidyaBharati College, Camp, Amravati 444602, India

Introduction

Tuberculosis (TB) is among the deadly diseases afflicting mankind, and it still remains a major public health burden in many developing countries (Corbett *et al.*, 2003). Approximately one-third of the world's population is still under the ill influence of TB. In 2011, nearly 9 million people around the world suffered from TB (WHO 2013), with 1.4 million deaths worldwide. Recent reports reveal that every year 0.2 million from 0.7 million HIV patients die due to TB,

and thus, TB is a leading killer in HIV-infected patients (Nunn *et al.*, 2005; Masand *et al.*, 2012; Shukla *et al.*, 2014). Emerging resistance to the marketed anti-tuberculosis drugs is a major concern that threatens progress made in TB care and control worldwide (Shukla *et al.*, 2014). In most of the cases, drug resistance (Chiang and Schaaf, 2010) arises due to the improper use of antibiotics in chemotherapy, administration of improper treatment regimens and failure to ensure that patient completes the whole course of the treatment (Elzinga *et al.*, 2004; Kumar *et al.*, 2013). To combat the continuous rise in multidrug-resistant TB, scientific efforts are concentrated on inventing new agents for the treatment of TB. Despite the efforts executed in laboratories and hospitals, TB is nevertheless a major challenge to medicinal chemists.

Developing a new drug is a long, expensive and tedious process, often consuming several years and resources. In addition, the regulatory approval process following the drug discovery/design involves several tests and trials. Even after completing the whole process of drug development, certain drugs such as celecoxib, sibutramine, rimonabant, though approved by the regulatory agencies, were withdrawn from the market due to the appearance of the side effects. At the current stage, it would be a highly beneficial and attractive strategy to identify a drug candidate, which has been approved as a drug by regulatory authorities, effective for the treatment of TB. This would enable a quicker introduction of the drug into the market for TB treatment. In the recent years, azoles viz. pyrazoles, imidazoles and triazoles have attracted the attention of researchers. Some clinically used drugs such as clotrimazole, fluconazole and voriconazole, which contain azole moiety, can be used to treat generalized systemic mycoses. Literature survey reveals that selected azole drugs possess potent anti-mycobacterial activity in the nanomolar range (Kumar *et al.*, 2013; Menozzi *et al.*, 2004) (Fig. 1).

It has been established (McLean *et al.*, 2002; Hudson *et al.*, 2012) that many azole compounds possessing potent anti-tubercular activity bind to MT-CYP51 and MT-CYP121, proteins with crucial role in metabolism of *M. tuberculosis*, possessing high affinity and retard the growth of *Mycobacterium bovis* and *Mycobacterium smegmatis*, the two mycobacterial species which closely resemble *M. tuberculosis*. In recent years, cytochrome P450 (CYP121) has gained popularity as an attractive target for designing potent azole-based drugs against *M. tuberculosis*, a plausible reason is that MT-CYP121, which has unique catalytic action, binds commercially available azole drugs with a higher affinity than MT-CYP51 (Menozzi *et al.*, 2004). In addition, it has no equivalent enzyme in humans. MT-CYP121 is necessary for bacterial viability since it catalyzes an unusual intramolecular carbon–carbon coupling reaction (Dumas *et al.*, 2013). The high affinity of the azole derivatives such as
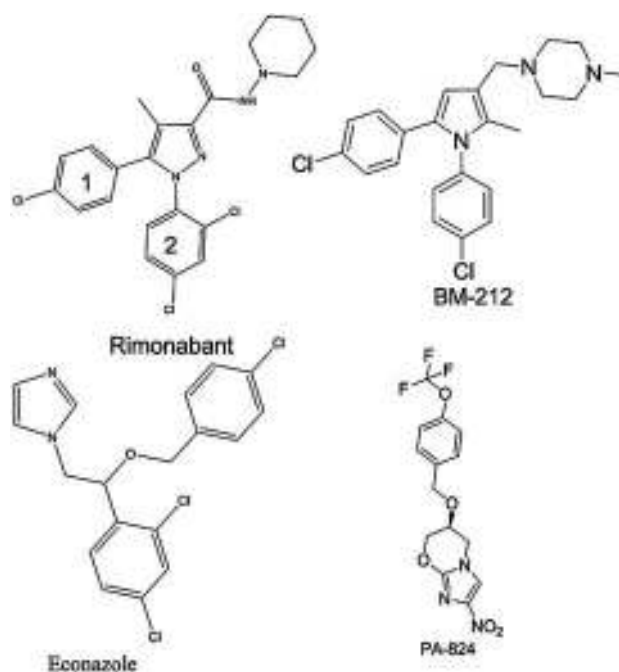
Fig. 1 Azole and pyrazole derivatives possessing anti-tubercular activity
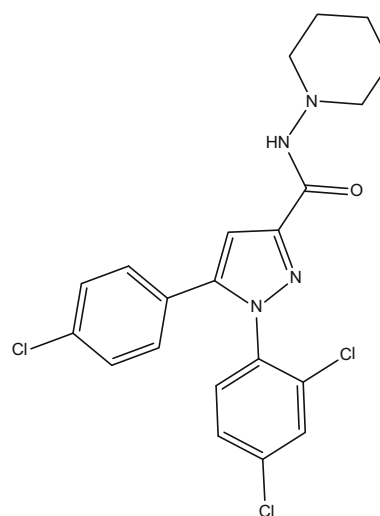
Fig. 2 2D-structure of rimonabant

clotrimazole for MT-CYP121 is attributed to their bulky, polycyclic structure, enhancing favorable interactions with the hydrophobic residues in the largely non-polar active site of the enzyme. Moreover, in many studies, the presence of halogen attached to aromatic moiety has been found to escalate antifungal and anti-mycobacterial activities (Dumas *et al.*, 2013; Sundaramurthi *et al.*, 2011; Belin *et al.*, 2009). Rimonabant (**1**) (Fig. 2), a pyrazole carboxylic acid derivative discovered by Sanofi-Synthelabo in 1994 as the first potent, orally active, selective CB_1 cannabinoid receptor antagonist and sold under several trade names as an anorectic

anti-obesity drug. Rimonabant and its analogues were also shown to have promising activities and also proved safe to human (Lange and Kruse, 2005). It was recently withdrawn (Kang and Park, 2012) from the market following post-marketing surveillance studies, which confirmed a risk of depressive disorders among users. However, modification or elimination of the side chain attached to carboxamide (Jagerovic *et al.*, 2008) which is responsible for crossing the blood–brain barrier might reduce the side effects. There are several important anti-TB drug candidates such as PA-824 and BM212, which are structurally reminiscent to rimonabant 1, and hence, we were curious to study its anti-TB properties. All these observations prompted us to develop new rimonabant analogues that may prove effective against multidrug-resistant strains of the tuberculosis pathogen.

Chemistry

The synthesis of compounds 2, 3, 7, 8, 9, 11, 12, and 13 was carried out as outlined in the Scheme 1. 4-Chloro-propiophenone (A) on condensation with diethyl oxalate in the presence of LiHMDS gave lithium salt of ethyl 4-(4-chlorophenyl)-3-methyl-4-oxydo-2-oxobuten-3-oate (B). This on condensing with 2, 4-dichlorophenyl hydrazine hydrochloride and phenyl hydrazine hydrochloride in ethanol gave hydrazones, which on refluxing in acetic acid for 24 h yielded esters 3 and 8, respectively. Subsequent reaction of B with suitable hydrazines in 50 % sulfuric acid and ethanol at 79 °C for 14 h yielded desired acids (2, 7, 9, 11, 12 and 13). These acids on subsequent treatment with thionyl chloride afforded acid chlorides. Finally, the

amidation was executed to afford the target compounds 1, 4, 5, 6, 10, 14, 15, 16, 17, 18 and 19 in moderate to good yields (Schemes 2, 3, 4). The structures of newly synthesized compounds were established on the basis of spectral and physicochemical analyses.

Results and discussion

Our initial study involved screening of rimonabant 1 against *M. smegmatis*. Interestingly, it exhibited a MIC value of 13.56 compared to 16 µg/ml for isoniazid. Therefore, its 18 analogues were synthesized (Lan *et al.*, 1999; Kotagiri *et al.*, 2007), and few of them were screened against *M. smegmatis*. They showed moderate to high activity (Table 1). Encouraged by the results, rimonabant and all the synthesized analogues were then screened for *Mycobacterium tuberculosis* (virulent strain H37Rv) in vitro (Moore *et al.*, 1999). The details of the screening data are shown in Table 1.

The precursor of rimonabant acid 2 showed improved MTB activity and ester 3 retains the activity as compared to rimonabant. Similarly, the analogues 2, 4, 7, 11 and 15–18 exhibited enhanced activity, and the analogues 3, 5, 6, 8, 10, 12 & 19 were also found to be active. Most importantly, the analogues 9 and 13 showed very good MTB activity. The analogue JMG-14 came out to be a promising lead with highest activity. Compared with one of the first-line anti-TB drug ethambutol (MIC 3.25 µg/ml), the analogue JMG-14 was found to be equally active. When compared to pyrazinamide (MIC 50.0 µg/ml), all the 18 analogues were found to be more potent. The analogue 13 also emerged as another lead molecule, which can be explored further.

2: X=Cl, R$_1$=2,4-dichlorophenyl
7: X=Cl, R$_1$=phenyl
9: X=H, R$_1$=2,4-dichlorophenyl
11: X=Cl, R$_1$=H
12: X=Cl, R$_1$=2-chlorophenyl
13: X=Cl, R$_1$=2,4-difluorophenyl

3: X=Cl, R$_1$=2,4-dichlorophenyl
8: X=Cl, R$_1$=phenyl
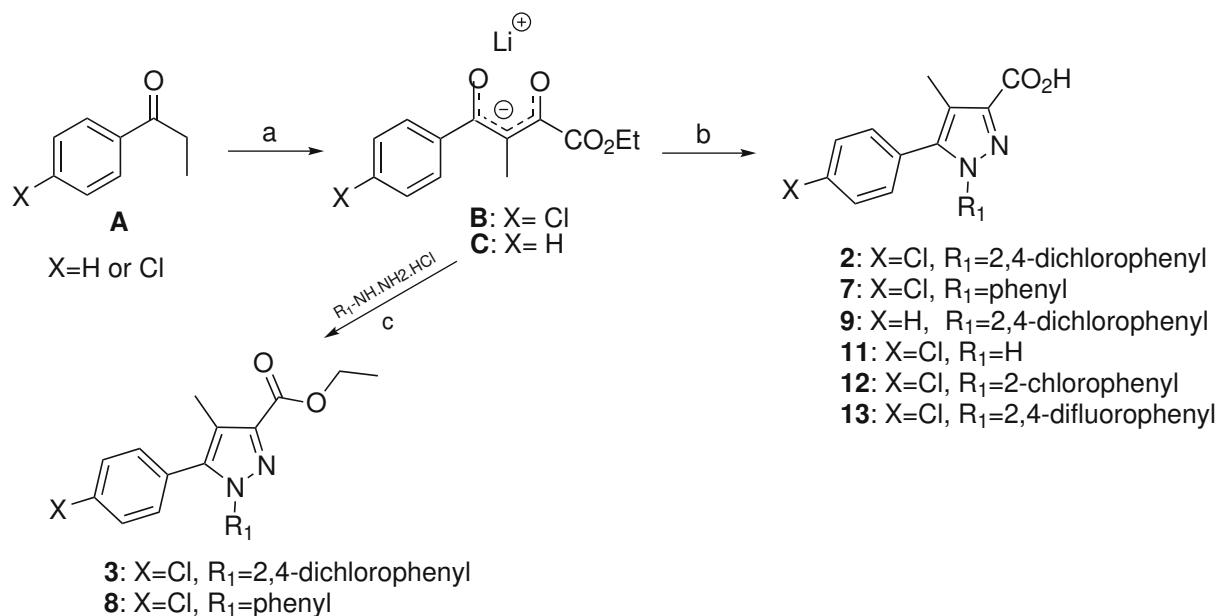
Scheme 1 Reagents and conditions: (a) LiHMDS, diethyl oxalate, methyl cyclohexane, 15–25 °C, 6th; (b) R$_1$-NH-NH$_2$·HCl, 50 % aq. H$_2$SO$_4$, EtOH, 79 °C, 14th; (c) EtOH, rt, 20 h, then AcOH, reflux, 24 h
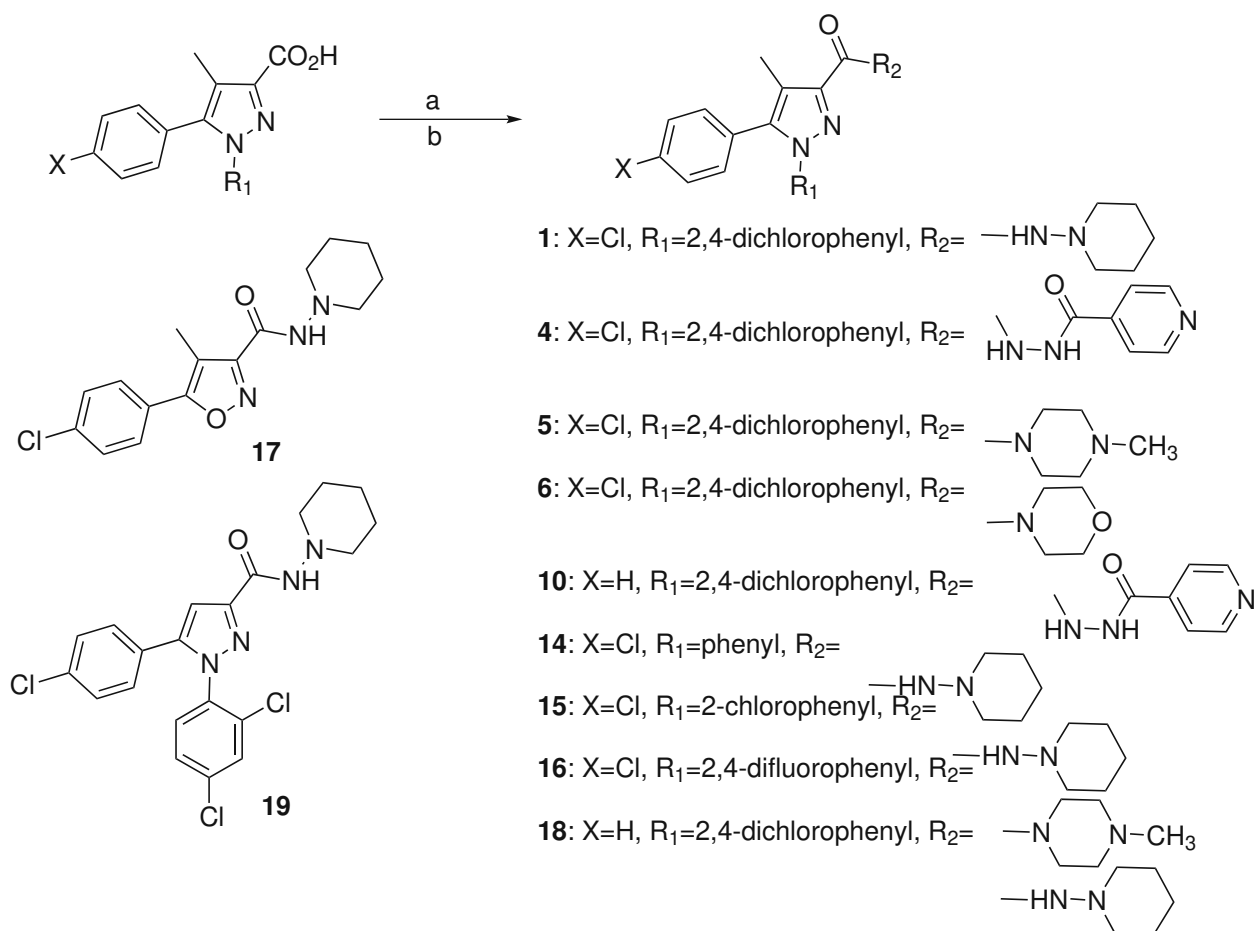
Scheme 2 Reagents and conditions: (a) thionyl chloride. DMF (cat.) toluene. 100 °C, 4 h (b) Et₃N sutiable amide. 0°-rt. 12 h

Scheme 3 Reagents and conditions: (a) LiHMDS, diethyl oxalate, methyl cyclohexane, 15–25 °C, 6h; (b) NH₂OH·HCl, 50% aq. H₂SO₄, EtOH, 79 °C, 14h; (c) thionyl chloride, DMF (cat), toluene, 100 °C, 4th; (d) Et₃N, 1-aminopiperidine, 0°-rt, 12 h

Scheme 4 Reagents and conditions: (a) LiHMDS, diethyl oxalate, methyl cyclohexane, 15–25 °C, 6h; (b) 2,4-dichlorophenylhydrazine. HCl, 50% aq. H$_2$SO$_4$, EtOH, 79 °C, 14 h; (c) thionyl chloride, DMF (cat), toluene, 100 °C, 4 h; (d) Et$_3$N, 1-aminopiperidine, 0°-rt, 12 h
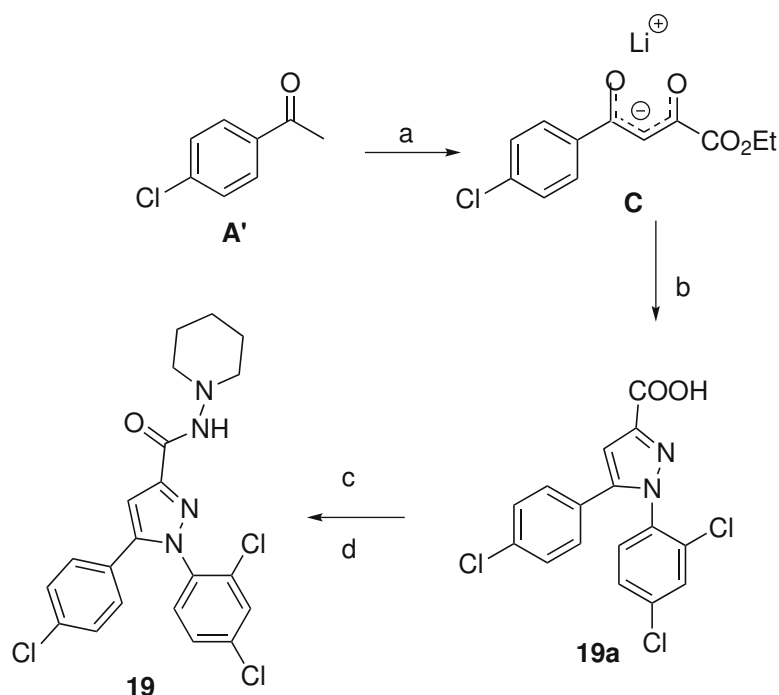
Table 1 In vitro anti-mycobacterial activity of rimonabant (**1**) and synthesized analogues

S. No.	CLogP^b	% inhibition *M. Smegmatis*	MIC (µg/ml) M. TB[a]	S. No.	CLogP^b	% inhibition *M. Smegmatis*	MIC (µg/ml) M. TB
1	6.471	99.33 MIC 13.56 µg/ml	25	13	4.981	NT	6.25
2	6.121	22.84	12.5	14	5.031	99.70	3.13
3	7.083	14.07	25	15	5.754	NT	12.5
4	5.532	19.21	12.5	16	4.526	NT	12.5
5	5.666	14.50	25	17	3.342	NT	12.5
6	5.335	NT	>25	18	5.756	32.37	12.5
7	4.681	17.70	12.5	19	6.841	NT	25
8	5.234	22.70	25	Isoniazid		16 µg/ml	0.05
9	5.407	15.73	6.25	Rifampicin		2 µg/ml	0.1
10	4.818	1.362	25	Ethambutol		NT	3.25
11	3.035	NT	12.5	Pyrazinamide		NT	50.0
12	5.404	NT	25				

NT not tested

[a] *Mycobacterium tuberculosis* H37Rv

[b] Calculated LogP using ChemDraw 12

Based on the analogue **9**, a simple replacement of chlorine by hydrogen might provide a more active analogue of **13**.

The main purpose of this study was to introduce modification on the side chain on carboxamide moiety of rimonabant and its analogues to develop new potential anti-TB agents. In the present work, diverse functional groups were introduced on the side chain of the carboxamide moiety of rimonabant to identify structure–activity relationships. It appears that the piperidinyl side chain is not must for high activity and derivatives with free acids are better candidates for further evaluation. Variation of phenyl ring attached to nitrogen (of pyrazole moiety) shows prominent effect on the activity, and this observation is further vindicated by the docking analysis. The substitution on the ring or its complete removal as well as replacement of that nitrogen with oxygen shows positive effect. Alteration on the *p*-chlorophenyl ring present on central pyrazole also influences the bioactivity. The methyl group seems to be important for the activity, since the analogue without methyl shows diminished activity.

Fig. 3 Docking pose for
a rimonabant (compound **1**) and
b most active compound **14**
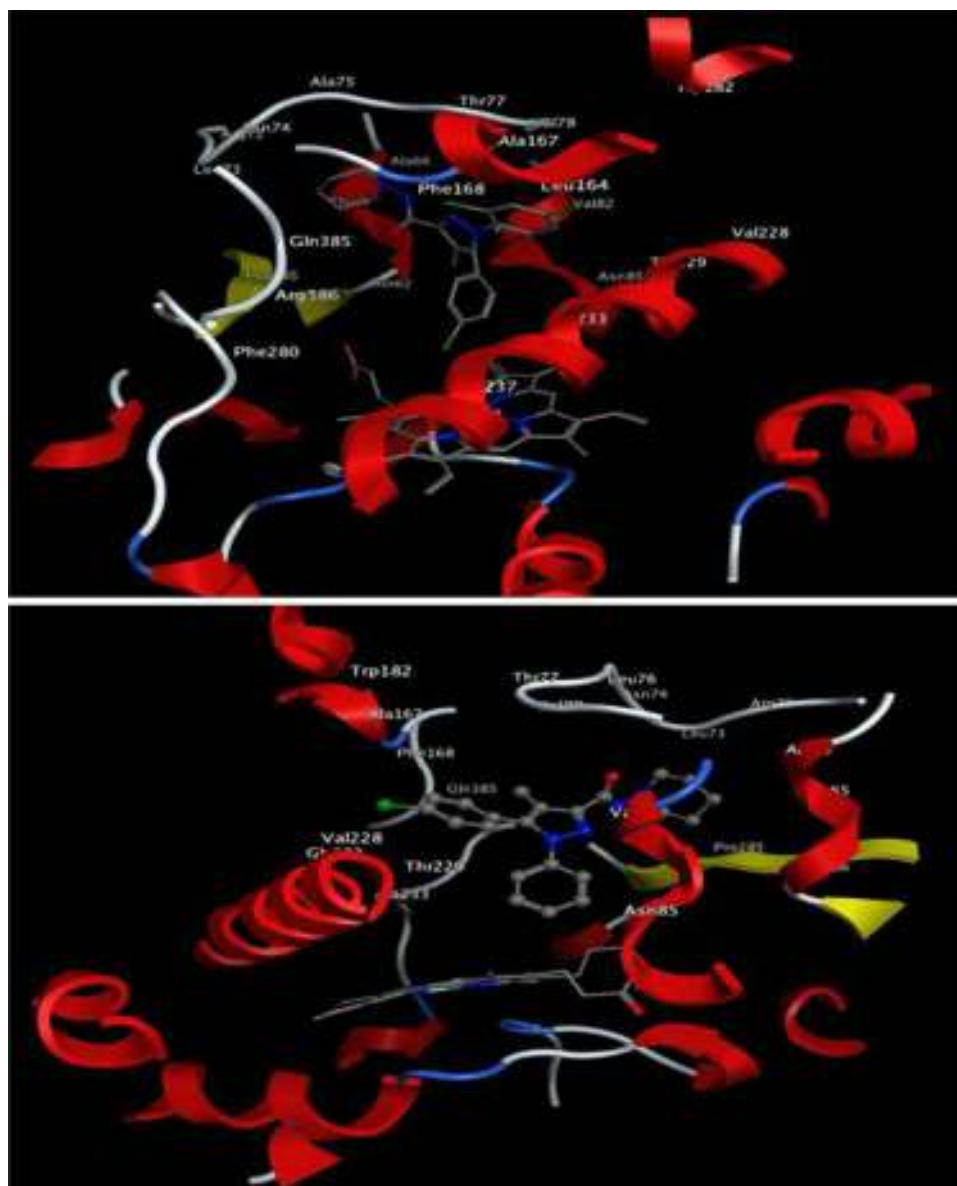
Docking analysis

Molecular docking analysis was performed to determine the structural features that steer the biological profile of Rimonabant and its novel analogues. As stated earlier (Dumas et al., 2013; Sundaramurthi et al., 2011; Belin et al., 2009), the mechanism of action for anti-TB activity involves interaction of pyrazoles with MTCYP-121; therefore, molecular docking analysis was performed to determine the structural features that govern the anti-TB of present series molecules. The docking analysis was performed for all the compounds, but for the sake of convenience, we represent the docking poses for compounds **1** and **14** as representatives. The active site of MT-CYP121, a heme-based enzyme that transfers a single oxygen atom to the substrate, comprises of Thr-77, Val-82, Val-83, Asn-85, Met-86, Ala-167, Ph-168, Thr-229, Ala-233, Ser-237, Gln-385 and Arg-386. The catalytic site is located on top of the distal side of the heme, where oxygen binds, near to I-helix (Dumas et al., 2013; Sundaramurthi et al., 2011; Belin et al., 2009).

According to the results of our docking experiments (see Fig. 3), the prominent interactions between compound **1** and the receptor are van der Waals, H-bonding and hydrophobic in nature. The compound **1** could adopt bent 'T' shape (or weird propeller shape) while interacting with the cytochrome catalytic site (1350 $\mathring{A}^3$ in size) orienting chloro atom attached to benzene ring 1 toward the iron atom of the heme group with the heterocyclic rings (pyrazole and piperidine) pointing toward polar residues. Binding of compound **1** involves numerous van der Waals contacts
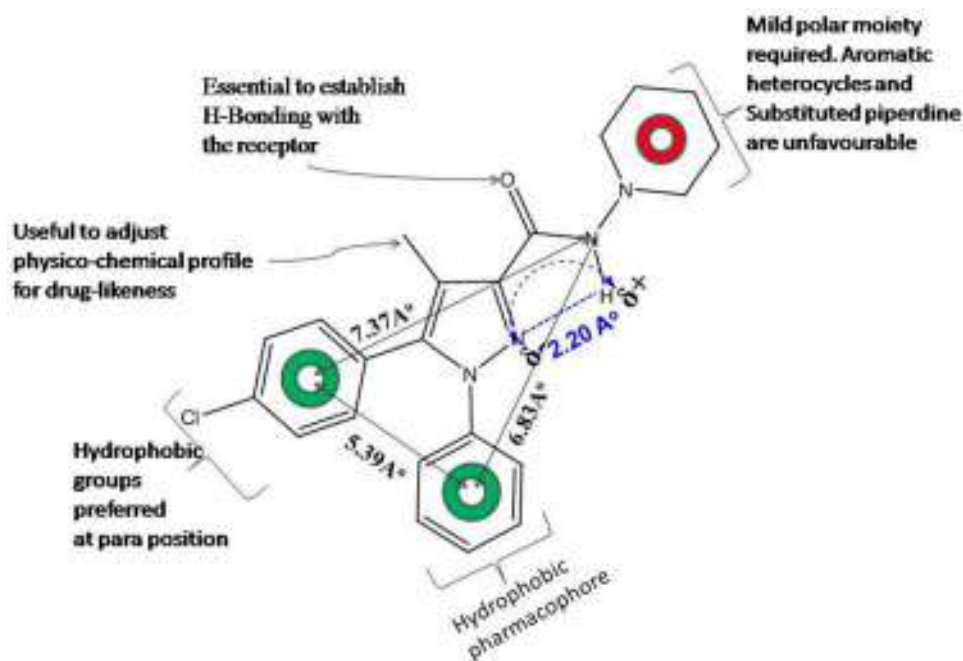
Fig. 4 Summary of SAR and molecular docking analysis for anti-TB activity of rimonabant and its analogues

with the hydrophobic side chains of Leu-76, Val-78, Val-83, Ala-167 and Phe-168. There are water-mediated H-bond network with the N (non-substituted) of pyrazole ring and with N (amide group). Furthermore, a strong H-bond between Arg-72 with N (piperidine ring) enhances the anchoring of compound **1** with CYP-121. The presence of pyrazole moiety in close proximity to Gln-385 indicates that it plays a crucial role in inhibiting the normal functioning of CYP-121.

Compound **14**, like compound **1**, adopts bent 'T' shape while interacting with CYP-121, but interacts with more number of residues of the active site than the compound **1**. The ring 2 is closer to heme moiety with ring 1 pointing toward hydrophobic residues Val-78, Phe-168, Trp-182 and Val-228. Another remarkable difference in interaction pattern of compounds **1** and **14** is due to the involvement of one and two water molecules, respectively, in enhancing the polar interactions with the receptor. The binding between the receptor and the substrate is enhanced by the water-mediated H-bonding between Thr-77 and the oxygen atom of amide group as well between Arg-72 and N (piperidine moiety).

A plausible reason for bent 'T' shape for compounds **1** and **14** is the presence of bulky Ser-237 in close proximity to phenyl ring attached to N of pyrazole moiety. Another reason could be the presence of unusually close other I-helix residues above the heme. Compounds **1** and **14** have adopted exactly opposite conformations while interacting with the receptor, and this could be attributed to the steric repulsion exerted by bulkier -Cl atoms present as substituents on the phenyl ring. Hudson *et al*. recently reported that the azoles

do not coordinate with the heme iron, as is typically observed for the azole antifungal CYP inhibitors (Hudson *et al*., 2012). Our docking experiment also concurs with this. The N $(\delta-)$/N–H $(\delta+)$ with a distance of 2.20 Å (depicted in Fig. 3), acting as polar pharmacophore, are responsible for establishing the polar contacts with the receptor.

The molecular docking and structure–activity relationships (SAR) have been summarized in Fig. 4.

Further studies being carried out in our laboratory to explore the mechanism of action of this scaffold and evaluation of these compounds for anti-bactericidal activity as well as activity under alternate growth conditions such as non-replicating growth conditions.

Pharmacology

Anti-mycobacterial activity assay

Anti-mycobacterial activity of the synthesized compounds was performed against *Mycobacterium smegmatis* MC2155 strain using growth inhibition assay by agar dilution followed by turbidimetry method. The assay was semithroughput and conducted in a 96-well plate (sterile). For *M. tuberculosis*, H37Rv strain was utilized by performing a growth inhibition assay from fresh Middlebrook 7H11 agar slants. This method is similar to that recommended by the National Committee for Clinical Laboratory Standards (NCCLS, 1995) for the determination of minimum inhibitory concentration (MIC) in duplicate.

Conclusion

For the first time, it has been shown that rimonabant could be a lead molecule for finding more potent anti-TB drug candidates. In the present work, JMG-14 is the most potent analogue of rimonabant, emerging as a suitable lead molecule, which can be further optimized using the SAR and molecular docking analyses. Currently, research work is in progress on the development of more rational analogues and their anti-TB.

Experimental

Chemistry

All the reagents and the solvents were used as received from commercial sources unless and otherwise stated. All the experiments were carried out under an atmosphere of nitrogen in round-bottom flask. Pre-coated plates (silica gel 60 PF254, 0.25 mm or 0.5 mm) were utilized for thin-layer chromatography (TLC). Column chromatographic purifications were carried out on flash silica gel (100–200 mesh) using either petroleum ether and ethyl acetate or dichloromethane and methanol as eluents. Melting points (mp) are uncorrected and were measured on an electrothermal melting point apparatus. The IR spectra were recorded on an FT-IR spectrometer. The ^{1}H and ^{13}C NMR spectra were recorded on 200/400/500 MHz and 50/100/125 MHz NMR spectrometer, respectively, in CDCl$_3$/DMSO-d_6. Mass spectra were taken on LC–MS (ESI) mass spectrometer. HRMS were scanned at NCL, Pune.

Preparation of Lithium salt of Ethyl 4-(4-chlorophenyl)-3-methyl-4-oxydo-2-oxobuten-3-oate (**B**) Methylcyclohexane (30 ml) and lithium hexamethyldisilazane (30 ml, 31.7 mmol) were introduced in a round-bottom flask under nitrogen atmosphere and cooled to 15–25 °C. A solution of 4-chloropropiophenone (A, 5.0 g, 29.65 mmol) in methylcyclohexane (12.5 ml) was slowly added with continuous stirring for 2.5 h. To this reaction mixture, diethyl oxalate (4.78 g, 32.6 mmol) was added with stirring. The reaction progress was monitored by TLC; the solid obtained was filtered, washed with methylcyclohexane (30 ml) and dried under vacuum (30 min) to afford the lithium salt (Kotagiri *et al.*, 2007) (Cream yellow solid, 5.7 g, 71.9 %).

Preparation of ethyl 5-(4-Chlorophenyl)-1-(2,4-dichlorophenyl)-4-methyl-1H-pyrazole-3-carboxylate (**3**) To a continuously stirring solution of lithium salt B (1.0 g, 3.64 mmol) in 15 ml of ethanol was added 2,4-dichlorophenyl hydrazine hydrochloride (0.777 g, 3.64 mmol) at room temperature. The shaking was carried for 20 h till

precipitate was obtained. The precipitate so obtained was filtered and washed with ethanol (10 ml) and dried under vacuum to give a pale yellow solid (1.1 g), which was dissolved in acetic acid (10 ml) and refluxed for 24 h. On completion of the reaction (TLC), the reaction mixture was poured into cold water (20 ml) and then extracted with ethyl acetate (3 × 15 ml). The combined extracts were washed with water, saturated sodium bicarbonate solution, brine and then dried under vacuum to give the crude product. It was then purified by column chromatography on silica gel using ethyl acetate/petroleum ether (1:9) as elution system to give the ester 3 (Kotagiri *et al.*, 2007), (670 mg, 45 %,) pale yellow solid.mp 128–129 °C;^{1}H NMR (CDCl$_3$, 200 MHz): δ 7.39 (d, $J = 2.02$ Hz, 1H), 7.34 (d, $J = 1.37$ Hz, 1H), 7.33–7.28 (m, 3H), 7.08 (d, $J = 8.59$ Hz, 2H), 4.51–4.41 (q, $J = 7.08$ Hz, 2H), 2.34 (s, 3H), 1.43 (t, $J = 7.08$ Hz, 3H); ^{13}C NMR (CDCl$_3$, 100 MHz): δ 162.7, 142.9, 136.0, 135.9, 135.0, 133.0, 130.9, 130.7, 130.1, 128.9, 127.7, 127.0, 119.1, 60.9, 14.4, and 9.6.HRMS-ESI (m/z) Calcd. C$_{19}$H$_{15}$O$_2$N$_2$Cl$_3$ + H)+: 409.0272 found: 409.0265.

Preparation of 1-(5-(4-Chlorophenyl)-4-methyl-1-phenyl-1H-pyrazol-3-yl)propan-1-one (**8**) Synthesis of **8** was accomplished according to the procedure applied for **3**. Pale orange solid; 595 mg, 48 %; mp 121–123 °C; ^{1}H NMR (CDCl$_3$, 400 MHz): δ 7.31–7.36 (m, 5H), 7.24–7.27 (m, 2H), 7.10 (d, $J = 8.6$ Hz, 2H), 4.48 (q, $J = 14.14$ Hz, 2H), 2.33 (s, 3H), 1.46 (t, $J = 7.07$ Hz, 3H); ^{13}C NMR (CDCl$_3$, 100 MHz): δ 163.0, 142.3, 140.9, 139.3, 134.7, 131.3, 128.9, 128.0, 127.9, 127.0, 125.4, 120.0, 60.8, 14.4, 9.7; HRMS-ESI (m/z) Calcd. C$_{19}$H$_{17}$O$_2$N$_2$ClNa: 363.0871 found: 363.0868.

Preparation of 5-(4-Chlorophenyl)-1-(2,4-dichlorophenyl)-4-methyl-1H-pyrazole-3-carboxylic acid (**2**) A mixture of lithium salt of ethyl 4-(4-chlorophenyl)-3-methyl-4-oxydo-2-oxobuten-3-oate (B, 1.0 g, 3.6 mmol), ethanol (25 ml), 2,4-dichlorophenyl hydrazine hydrochloride (0.777 g, 3.6 mmol), and 50 % sulfuric acid (10 ml) was refluxed for 6 h. After the reaction was complete (TLC), ethanol was removed under reduced pressure, and again, a second installment of 50 % sulfuric acid (20 ml) was added, followed by refluxing for 8 h. The reaction mixture was cooled to room temperature (35 °C) and was poured onto crushed ice, stirred for 15 min, filtered and washed with water (20 ml). The wet solid so obtained was stirred with water (30 ml), and the pH was adjusted to >10 with 20 % dil. NaOH. This aqueous layer was washed with petroleum ether. The aqueous layer was separated, cooled to 0 °C, and pH was adjusted to 2.0 by concentrated hydrochloric acid. Solid so obtained was filtered, washed with water (100 ml) and dried to afford 2 (Kotagiri *et al.*, 2007), (0.923 mg, 65 %), Off white solid, mp 208–209 °C; ^{1}H NMR (CDCl$_3$,

400 MHz): δ 7.44–7.41 (m, 1H), 7.35 (d, $J = 1.89$ Hz, 1H), 7.33–7.28 (m, 3H), 7.09 (d, $J = 8.47$ Hz, 2H), 2.36 (s, 3H); ^{13}C NMR (CDCl$_3$, 100 MHz): δ 166.4, 143.3, 136.2, 135.6, 135.1, 133.5, 130.8, 130.5, 129.8, 128.9, 127.8, 127.7, 126.7, 119.6, 9.6; HRMS-ESI (m/z) Calcd. $C_{17}H_{11}O_2N_2Cl_3Na$: 402.9778 found: 402.9781.

Preparation of 5-(4-Chlorophenyl)-4-methyl-1-phenyl-1H-pyrazole-3-carboxylic acid (7) Compound 7 was synthesized by the procedure applied for 2. Pale brown solid: 719 mg, 58 %; mp 203–204 °C; ^{1}H NMR (CDCl$_3$, 200 MHz): δ 7.46 (s, 1H), 7.32–7.38 (m, 5H), 7.30–7.20 (m, 2H), 7.13 (d, $J = 6.36$ Hz, 2H), 2.35 (s,3H); ^{13}C NMR (CDCl$_3$, 400 MHz): δ 165.9, 141.3, 140.9, 139.0, 134.9, 131.3, 129.0, 128.2, 127.6, 125.4, 125.1, 120.5, 9.6; HRMS-ESI (m/z) Calcd. $C_{17}H_{13}O_2N_2ClNa$: 335.0571 found: 335.0566.

Preparation of 1-(2,4-dichlorophenyl)-4-methyl-5-phenyl-1H-pyrazole-3-carboxylic acid (9) Compound 9 was synthesized by the procedure applied to 2. Cream solid: 865 mg, 59 %; mp 188–189 °C; ^{1}H NMR (CDCl$_3$, 400 MHz): δ 7.46 (s, 1H), 7.16–7.27 (m, 5H), 7.08 (s, 2H), 6.02 (s, 1H), 2.17 (s, 3H); ^{13}C NMR (CDCl$_3$, 100 MHz): δ 167.2, 145.6, 136.0, 135.1, 132.2, 131.2, 130.8, 129.6, 129.1, 128.5, 128.3, 128.2, 127.8, 118.0, 9.7; HRMS-ESI (m/z) Calcd. $C_{17}H_{12}O_2N_2Cl_2Na$: 369.0168 found: 369.0164.

Preparation of 5-(4-chlorophenyl)-4-methyl-1H-pyrazole-3-carboxylic acid (11) Compound 11 was synthesized by the procedure applied to 2. Cream solid; 387 mg, 45 %; mp 288–290 °C; ^{1}H NMR (DMSO-d_6, 500 MHz): δ 13.54 (s, 1H), 7.89, (d, $J = 8.24$ Hz, 2H), 7.77 (d, $J = 8.24$ Hz, 2H), 2.61 (s, 3H); ^{13}C NMR (DMSO-d_6, 125 MHz): δ 162.4, 132.7, 130.9, 129.4, 128.9, 128.5, 117.0, 60.5, 9.9; HRMS-ESI (m/z) Calcd. $C_{11}H_9O_2N_2ClNa$: 259.0245 found: 259.0243.

Preparation of 1-(2-chlorophenyl)-5-(4-chlorophenyl)-4-methyl-1H-pyrazole-3-carboxylic acid (12) Compound 12 was synthesized by the procedure applied to 2. Pale yellow solid: 656 mg, 52 %; mp 204–206 °C; ^{1}H NMR (CDCl$_3$, 200 MHz): δ 7.33–7.42 (m, 4H), 7.26 (d, $J = 6.41$ Hz, 2H), 7.04 (d, $J = 7.79$ Hz, 2 H), 2.32 (s, 3H);^{13}C NMR (CDCl$_3$, 100 MHz): δ 165.6, 143.3, 141.7, 136.9, 134.9, 131.9, 130.9, 130.3, 130.0, 129.8, 128.8 127.5, 126.9, 119.4, 9.6; HRMS-ESI (m/z) Calcd. $C_{17}H_{12}O_2N_2Cl_2Na$: 369.0168 found: 369.0168.

Preparation of 5-(4-chlorophenyl)-1-(2,4-difluorophenyl)-4-methyl-1H-pyrazole-3-carboxylic acid (13) Compound 13 was synthesized by the procedure applied to 2. Pale brown solid; 781 mg, 62 %; mp 196–198 °C; ^{1}H NMR (CDCl$_3$, 500 MHz): δ 9.31 (bs, 1H), 7.44 (s, 1H), 7.27 (d, $J = 8.46$ Hz, 2H), 7.03 (d, $J = 8.46$ Hz, 2H), 6.87 (s, 1H), 6.72 (s, 1H), 2.25 (s, 3H); ^{13}C NMR (CDCl$_3$, 125 MHz): δ 161.7, 157.5, 155.5, 143.1, 135.0, 130.7, 130.0, 128.9, 127.0, 123.7, 119.5, 112.1, 111.9, 104.8, 9.6; HRMS-ESI (m/z) Calcd. $C_{17}H_{11}O_2N_2ClF_2Na$: 371.0369 found: 371.0369.

Procedure for the synthesis of 5-(4-Chlorophenyl)-1-(2,4-dichlorophenyl)-4-methyl-N-(piperidin-1-yl)-1H-pyrazole-3-carboxamide 1 To a stirred solution of 2 (382 mg; 1.0 mmol) in toluene (10 ml), one drop of dimethyl formamide was added. The reaction mixture was cooled to 0 °C and thionyl chloride (140 mg: 1.2 mmol) in 2 ml toluene was added dropwise for the period of 2 min at the same temperature. The reaction mixture was allowed to attain room temperature and heated at 100 °C for 4 h. Excess of thionyl chloride and toluene was distilled off under reduced pressure. In another flask under nitrogen atmosphere was introduced 1-aminopiperidine (100 mg; 1.0 mmol) and triethyl amine (101 mg; 1.0 mmol) in 5.0 ml dichloromethane. The flask was cooled to 0 °C. To this was added a cooled solution of acid chloride dropwise at the same temperature. The resulting reaction mixture was allowed to attain room temperature, and then, it was stirred for 12 h. After completion of the reaction (monitored by TLC), the reaction mixture was diluted with water (10 ml) and organic layer was separated, washed with water (2 × 5 ml) and brine solution (5 ml), dried over Na$_2$SO$_4$ and concentrated *in vacuo*. The residue was purified by column chromatography over silica gel (ethyl acetate/petroleum ether 1:9 (v/v)) afforded pure product.

White solid: 292 mg, 63 %; mp 182–183 °C;^{1}H NMR (CDCl$_3$, 400 MHz): δ 7.63 (s,1H), 7.41–7.36 (m, 1H), 7.30–7.26 (m, 3H), 7.04 (d, $J = 8.28$ Hz, 2H), 2.93–2.78 (m, 4H), 2.35 (s, 3H), 1.78–1.70 (m, 4H), 1.48–1.37 (m, 2H);^{13}C NMR (CDCl$_3$, 100 MHz): δ 159.9, 144.4, 142.9, 136.0, 135.9, 134.9, 132.9, 130.8, 130.6, 130.3, 128.9, 127.9, 127.2, 118.2, 57.0, 25.4, 23.3, 9.3; HRMS-ESI (m/z) Calcd. $C_{22}H_{22}ON_3Cl_3 + H)+$: 463.0854 found:463.0853.

N′-(5-(4-chlorophenyl)-1-(2,4-dichlorophenyl)-4-methyl-1H-pyrazole-3-carbonyl) isonicotinohydrazide (4) Compound 4 was synthesized according to the procedure applied to 1. Off white solid: 499 mg, 59 %; mp 237–239 °C; ^{1}H NMR (CDCl$_3$, 400 MHz): δ 10.33 (s,1H), 9.44 (s, 1H), 8.71 (s, 1H), 7.74 (s, 2H), 7.41 (s, 1H), 7.30–7.32 (m, 5H), 7.05 (d, $J = 8.53$ Hz, 2H), 2.17 (s, 3H); ^{13}C NMR (CDCl$_3$, 100 MHz): δ 163.5, 161.2, 150.2, 143.3, 142.4, 136.2, 135.6, 135.2, 132.7, 130.7, 130.5, 130.3, 128.9, 128.8, 127.9, 126.7, 118.4, 30.9, 9.2; HRMS-ESI (m/z) $C_{23}H_{16}O_2N_5Cl_3 + H)+$: Calcd. 500.0442 found: 500.0443.

(5-(4-chlorophenyl)-1-(2,4-dichlorophenyl)-4-methyl-1H-pyrazol-3-yl)(4-methylpiperazin-1-yl) methanone (5) Compound 5 was synthesized according to the procedure applied to 1. Brown solid; 306 mg, 50 %; mp 111–113 °C;

^{1}H NMR (CDCl$_3$, 400 MHz): δ 7.48 (s, 1H), 7.31–7.34 (m, 3H), 7.20 (d, $J = 8.54$ Hz, 1H), 7.10 (d, $J = 8.28$ Hz, 2H), 3.99–3.80 (m, 4H), 2.61–2.45 (m, 4H), 2.37 (s, 3H), 2.24 (s, 3H); ^{13}C NMR (CDCl$_3$, 100 MHz): δ 163.2, 146.4, 141.9, 135.9, 135.7, 134.8, 133.0, 130.6, 128.9, 127.8, 127.3, 116.8, 55.5, 54.7, 47.1, 45.9, 41.9, 9.0; HRMS-ESI (m/z) C$_{22}$H$_{21}$ON$_4$Cl$_3$ + H) + :Calcd. 463.0854 found: 463.0862.

(5-(4-chlorophenyl)-1-(2,4-dichlorophenyl)-4-methyl-1H-pyrazol-3-yl) (morpholino) methanone (**6**) Compound **6** was synthesized according to the procedure applied to **1**. Cream yellow solid: 590 mg, 63 %; mp 170–172 °C;^{1}H NMR (CDCl$_3$, 500 MHz): δ 7.47 (d, $J = 2$ Hz, 1H), 7.33 (d, $J = 8.54$ Hz, 2H), 7.27–7.30 (m, 1H), 7.19 (d, $J = 8.55$ Hz, 1H), 7.09 (d, $J = 8.54$ Hz, 2H), 3.85–3.92 (m, 4H), 3.75–3.83 (m, 4H), 2.25 (s, 3H); ^{13}C NMR (CDCl$_3$, 125 MHz): δ 163.2, 146.0, 142.1, 135.9, 135.8, 134.9, 133.0, 130.6, 130.5, 130.3, 128.9, 127.8, 127.3, 117.2, 67.3, 66.9, 47.8, 42.6, 9.1; HRMS-ESI (m/z) C$_{21}$H$_{18}$O$_2$N$_3$Cl$_3$Na:Calcd. 472.0357 found: 472.0355.

N′-(1-(2,4-dichlorophenyl)-4-methyl-5-phenyl-1H-pyrazole-3-carbonyl)isonicotinohydrazide (**10**) Compound **10** was synthesized according to the procedure applied to **1**. White solid: 273 mg, 68 %; mp 167–168 °C; ^{1}H NMR (CDCl$_3$, 400 MHz): δ 10.28 (bs, 1H), 9.43 (s, 1H), 8.71 (bs, 1H), 7.75 (s, 1H), 7.41 (d, $J = 1.47$, 2H), 7.28–7.34 (m, 5H), 7.14 (d, $J = 4.40$, 2H), 7.01–7.04 (m, 1H) 2.33 (s,3H); ^{13}C NMR (CDCl$_3$, 100 MHz): δ 163.4, 161.2, 150.3, 144.4, 142.3, 138.8, 135.9, 135.8, 132.8, 130.5, 130.2, 129.5, 128.9, 128.6, 128.2, 127.8, 121.2, 118.3, 9.3; HRMS-ESI (m/z) C$_{23}$H$_{17}$O$_2$N$_5$Cl$_2$ + H)+: Calcd. 466.0832 found: 463.0830.

5-(4-chlorophenyl)-4-methyl-1-phenyl-N-(piperidin-1-yl)-1H-pyrazole-3-carboxamide (**14**) Compound **14** was synthesized according to the procedure applied to **1**. White solid; 580 mg, 65 %; mp 201–202 °C; ^{1}H NMR (CDCl$_3$, 400 MHz): δ 7.77 (bs, 1H), 7.33 (d, $J = 7.27$ Hz, 5H), 7.21 (d, $J = 7.78$ Hz, 2H), 7.08 (d, $J = 8.28$ Hz, 2H), 2.98–2.79 (m, 4H), 2.35 (s, 3H), 1.85–1.68 (m, 4H), 1.52–1.38 (m, 2H); ^{13}C NMR (CDCl$_3$, 100 MHz): δ 160.1, 143.5, 140.9, 139.3, 134.6, 131.2, 129.0, 128.9, 128.0, 127.9, 125.0, 119.1, 57.1, 25.4, 23.3, 9.3; HRMS-ESI (m/z) C$_{22}$H$_{23}$ON$_4$Cl + H)$^+$: Calcd. 395.1633 found: 395.1631.

1-(2-chlorophenyl)-5-(4-chlorophenyl)-4-methyl-N-(piperidin-1-yl)-1H-pyrazole-3-carboxamide (**15**) Compound **15** was synthesized according to the procedure applied to **1**. Yellow solid: 207 mg, 42 %; mp 248–250 °C; ^{1}H NMR (CDCl$_3$, 200 MHz): δ 7.69 (bs, 1H), 7.37–7.30 (m, 1H),7.29–7.24 (m, 2H), 7.23–7.15 (m, 3H), 6.98 (d, $J = 8.71$ Hz, 2H), 2.95–2.72 (m, 4H), 2.30 (s,3H), 1.78–1.61 (m, 4H), 1.45–1.29 (m, 2H); ^{13}C NMR (CDCl$_3$,

100 MHz): δ 160.3, 143.4, 141.1, 136.5, 135.0, 131.5, 130.9, 130.8, 130.3, 129.8, 128.8, 127.7, 126.6, 118.3, 55.7, 23.8, 21.1, 9.2; HRMS-ESI (m/z) C$_{22}$H$_{22}$ON$_4$Cl$_2$ + H)$^+$: Calcd. 429.1243 found: 429.1246.

(5-(4-chlorophenyl)-1-(2,4-difluorophenyl)-4-methyl-1H-pyrazol-3-yl)(4-methylpiperazin-1-yl) methanone (**16**) Compound **16** was synthesized according to the procedure applied to **1**. White solid; 518 mg, 84 %; mp 174–176 °C; ^{1}H NMR (CDCl$_3$, 200 MHz): δ 7.30–7.24 (m, 1H), 7.24–7.20 (m, 2H), 7.06–6.96 (m, 2H), 6.91–6.69 (m, 2H), 3.91–3.63 (m, 4H), 2.56–2.34 (m, 4H), 2.29 (s, 3H), 2.12 (s, 3H); ^{13}C NMR (CDCl$_3$, 50 MHz): δ 163.2, 146.6, 141.9, 134.8, 130.5, 129.7, 128.8, 127.4, 124.1, 116.8, 112.1, 111.6, 105.0, 104.5, 55.5, 54.7, 47.0, 45.9, 41.8, 8.9; HRMS-ESI (m/z) C$_{22}$H$_{21}$ON$_4$ClF$_2$ + H)$^+$: Calcd. 431.1445 found: 431.1447.

5-(4-chlorophenyl)-4-methyl-N-(piperidin-1-yl) isoxazole-3-carboxamide (**17**) Compound **17** was synthesized according to the procedure applied to 1. White solid: 240 mg, 45 %; mp 103–104 °C; ^{1}H NMR (CDCl$_3$, 500 MHz): δ 7.63–7.64 (d, $J = 8.24$ Hz, 1H), 7.57–7.58 (d, $J = 8.24$ Hz, 1H), 7.47–7.49 (d, $J = 8.24$ Hz, 2H), 2.99–2.81 (m, 4H), 2.45 (s, 3H), 1.85–1.71 (m, 4H), 1.53–1.41 (m, 2H); ^{13}C NMR (CDCl$_3$, 125 MHz): δ 165.8, 163.0, 157.3, 156.4, 136.1, 129.2, 126.0, 111.7, 56.9, 25.2, 23.1, 8.3; HRMS-ESI (m/z) C$_{16}$H$_{18}$O$_2$N$_3$Cl + H)$^+$: Calcd. 320.1160 found: 320.1161.

1-(2,4-dichlorophenyl)-4-methyl-5-phenyl-N-(piperidin-1-yl)-1H-pyrazole-3-carboxamide (**18**) Compound **18** was synthesized according to the procedure applied to **1**. Pale brown solid: 288 mg, 61 %; mp 172–173 °C; ^{1}H NMR (CDCl$_3$, 400 MHz): δ 7.72 (s, 1H), 7.41 (s, 1H), 7.27–7.32 (m, 5H), 7.11 (s, 2H), 3.05–2.75 (m, 4H), 2.38 (s, 3H), 1.91–1.65 (m, 4H), 1.54–1.34 (m, 2H); ^{13}C NMR (CDCl$_3$, 100 MHz): δ 160.1, 144.2, 144.0, 136.1, 135.7, 133.0, 130.6, 130.2, 129.5, 128.6, 128.6, 128.4, 127.7, 117.9, 57.0, 25.3, 23.2, 9.3; HRMS-ESI (m/z) C$_{22}$H$_{22}$ON$_4$Cl$_2$ + H)$^+$: Calcd. 429.1243 found: 429.1244.

5-(4-chlorophenyl)-1-(2,4-dichlorophenyl)-N-(piperidin-1-yl)-1H-pyrazole-3-carboxamide (**19**) Compound **19** was synthesized from the corresponding acid according to the procedure applied to **1**. Cream solid: 199 mg, 53 %; mp 139–140 °C; ^{1}H NMR (CDCl$_3$, 400 MHz): δ 7.61 (d, $J = 2.29$ Hz, 1H), 7.57 (s, 1H), 7.55 (d, $J = 2.29$ Hz, 1H), 7.53 (d, $J = 1.83$ Hz, 1H), 7.42 (d, $J = 9.15$ Hz, 2H), 7.26 (d, 2H), 7.23 (s, 1H), 3.35–3.19 (m, 4H), 2.01–1.95 (m, 4H), 1.70–1.59 (m, 2H); ^{13}C NMR (CDCl$_3$, 100 MHz): δ 158.8, 146.8, 145.6, 136.3, 135.7, 135.1, 132.8, 130.5, 130.4, 129.1, 129.0, 128.2, 127.3, 107.5, 56.8, 24.9, 22.7; HRMS-ESI (m/z) C$_{21}$H$_{19}$ON$_4$Cl$_3$ + H)$^+$: Calcd. 449.0697 found: 449.0701.

Anti-mycobacterial activity assay (Abreu *et al.*, 2012; Stigliani *et al.*, 2012; Handoko *et al.*, 2012; Tiwari *et al.*, 2012; NCCLS, 1995)

Isolated single colonies of *M. smegmatis* MC2155 (ATCC 14468) grown on 7H10 agar plate were developed overnight in Middlebrook 7H9 medium (0.47 % Middlebrook 7H9 broth base, 10 % ADS, 0.2 % glycerol and 0.1 % Tween 80) to mid-exponential phase at 37 °C. When the OD of this culture reached approximately 0.8, a secondary culture was inoculated in 5 ml Middlebrook 7H9 medium. The secondary culture was incubated overnight and allowed to grow at 37 °C to early log phase (OD600 ≈ 0.3). For the anti-mycobacterial assay, 98 µl of 1:1000-folds dilution of the secondary culture was dispensed into 96-well microtiter plate per well along with 2 µl of test compound in triplicate, and 240 µl of sterile water was added to each well of the peripheral rows of 96-well plate to minimize media evaporation during assay incubation. The final concentration of the test compound in each well was 30 µM. Bacterial growth was assessed after 32 h of incubation by measuring turbidity at 600 nm OD600 values using TECAN Infinite 200 PRO^{TM} (Tecan Instruments, Switzerland). Depending upon the percentage of growth, the percentage of inhibition was calculated at a standard concentration of 30 µM. Isoniazid and rifampicin were included in every assay plate as positive controls of growth inhibition using stock solutions of INH (10 mg/ml, HiMedia) and rifampicin (10 mg/ml, HiMedia) to achieve the final concentration of 16 µg/ml for INH and 2 µg/ml for rifampicin. Additional controls DMSO (solvent without compound) and medium without inoculums were included in all the assay plates avoiding intra-assay variability. The results were analyzed as the percentage of growth inhibition.

MIC Assay (Abreu *et al.*, 2012; Stigliani *et al.*, 2012; Handoko *et al.*, 2012; Tiwari *et al.*, 2012; NCCLS, 1995)

After the compounds were screened for percentage inhibition, the promising compounds were further screened to obtain the MIC values. Minimum inhibitory concentration (MIC) is the concentration of compound which inhibits the 90 % growth of bacteria under optimum conditions. The growth inhibition assays were carried out in the same analogy as explained above using various concentrations of the test compounds prepared by serial dilutions 100, 50, 25, 12.5 and 6.25 µM to obtain the final concentrations of 46.37, 23.18, 11.59, 5.79 and 2.89 µg/ml, respectively. From the rate of inhibition bacterial growth, the ascertained MIC of the compound was calculated. The MIC value of the test compound 1 (rimonabant) is 13.56 µg/ml (29.24 µM ± 1.47).

In vitro anti-mycobacterial activity against *M. tuberculosis* H37Rv (MTB) (Abreu *et al.*, 2012; Stigliani *et al.*, 2012; Handoko *et al.*, 2012; Tiwari *et al.*, 2012; NCCLS, 1995).

MTB H37Rv strain was obtained from National Institute for Research in Tuberculosis (NIRT), Chennai. Tenfold serial dilutions of each test compound were prepared and incorporated into Middlebrook 7H11 agar medium with OADC growth supplement. Inoculation of *M. tuberculosis* H37Rv ATCC 27294 (MTB) was prepared from fresh Middlebrook 7H11 slants with OADC growth supplement and was adjusted to 1 mg/ml (wet weight) in Tween 80 (0.05 %) saline diluted to 10–2 to achieve a concentration of ∼107 cfu/ml (culture forming units). Then, a bacterial suspension of 5 µl was spotted in 7H11 agar tubes having tenfold serial dilutions of compounds per ml. Cultures were then incubated at 37 °C for 4 weeks. The MIC values of the synthesized compounds along with the standard drugs for comparison are tabulated in Table 1.

Experimental methodology for molecular docking analysis

For molecular docking, the structures were drawn using ChemDraw 12 followed by MMFF94 optimization using the default settings. The crystallographic coordinates of CYP121 (pdb id: 2IJ7) from *M. tuberculosis* were obtained from protein data bank (www.rcsb.org). For CYP121 of *M. tuberculosis*, we opted for pdb-2IJ7 for docking, because it has been crystallized with fairly good resolution (1.90 Å) with fluconazole as a ligand. For docking analysis, the standard procedure mentioned in literature (Abreu *et al.*, 2012; Stigliani *et al.*, 2012; Handoko *et al.*, 2012; Tiwari *et al.*, 2012; Masand *et al.*, 2013) was followed using AutoDock 4.2, running under Linux Ubuntu 12.04.

References

Abreu RM, Froufe HJ, Queiroz MJ, Ferreira IC (2012) Selective flexibility of side-chain residues improves VEGFR-2 docking score using AutoDock Vina. Chem Biol Drug Des 79(4):530–534

Belin P, Le Du MH, Fielding A, Lequin O, Jacquet M, Charbonnier JB, Lecoq A, Thai R, Courcon M, Masson C, Dugavet R, Pernodet JL, Gondry M (2009) Identification and structural basis of the reaction catalyzed by CYP121, an essential cytochrome P450 in *Mycobacterium tuberculosis*. Proc Natl Acad Sci USA 106(18):7426–7431

Chiang CY, Schaaf HS (2010) Management of drug-resistant tuberculosis. Int J Tuberc LungDis 14:672–682

Corbett EL, Watt CJ, Walker N, Maher D, Williams BG, Raviglione MC, Dye C (2003) The growing burden of tuberculosis: global

trends and interactions with the HIV epidemic. Arch Intern Med 163(9):1009–1021

Dumas VG, Defelipe LA, Petruk AA, Turjanski AG, Marti MA (2013) QM/MM study of the C–C coupling reaction mechanism of CYP121, an essential cytochrome p450 of mycobacterium tuberculosis. Proteins 82(6):1004–1021

Elzinga G, Raviglione MC, Maher D (2004) Scale up: meeting targets in global tuberculosis control. Lancet 363(9411):814–819

Handoko SD, Ouyang X, Su CT, Kwoh CK, Ong YS (2012) QuickVina: accelerating AutoDock Vina using gradient-based heuristics for global optimization. IEEE/ACM Trans Comput Biol Bioinform. 9(5):1266–1272

Hudson SA, McLean KJ, Surade S, Yang Y-Q, Leys D, Ciulli A, Munro AW, Abell C (2012) Application of fragment screening and merging to the discovery of inhibitors of the mycobacterium tuberculosis cytochrome P450 CYP121. Angew Chem Int Ed 51(37):9311–9316

Jagerovic N, Fernandez-Fernandez C, Goya P (2008) CB1 cannabinoid antagonists: structure-activity relationships and potential therapeutic applications. Curr Top Med Chem 8(3):205–230

Kang JG, Park CY (2012) Anti-obesity drugs: a review about their effects and safety. Diabetes Metab J 36(1):13–25

Kotagiri VK, Suthrapu S, Mukunda Reddy J, Prasad Rao C, Bollugoddu V, Bhattacharya A, Bandichor R (2007) An improved synthesis of rimonabant: anti-obesity drug. Org Proc Res Dev 11:910–912

Kumar V, Kaur K, Gupta GK, Sharma AK (2013) Pyrazole containing natural products: synthetic preview and biological significance. Eur J Med Chem 69:735–753

Lan R, Liu Q, Fan P, Lin S, Fernando SR, McCallion D, Pertwee R, Makriyannis A (1999) Structure-activity relationships of pyrazole derivatives as cannabinoid receptor antagonists. J Med Chem 42(4):769–776

Lange JH, Kruse CG (2005) Keynote review: medicinal chemistry strategies to CB1 cannabinoid receptor antagonists. Drug Discov Today 10(10):693–702

Masand VH, Jawarkar RD, Mahajan DT, Hadda TB, Sheikh J, Patil KN (2012) QSAR and CoMFA studies of biphenyl analogs of the anti-tuberculosis drug (6S)-2-nitro-6-{[4-(trifluoromethoxy) benzyl]oxy}-6,7-dihydro-5H-imidazo[2,1-b][1,3]oxazine(PA-824). Med Chem Res 21:2624–2629

Masand VH, Mahajan DT, Hadda TB, Jawarkar RD, Chavan H, Bandgar BP, Chauhan H (2013) Molecular docking and quantitative structure–activity relationship (QSAR) analyses of indolylarylsulfones as HIV-1 non-nucleoside reverse transcriptase inhibitors. Med Chem Res 23(1):417–425

McLean KJ, Marshall KR, Richmond A, Hunter IS, Fowler K, Kieser T, Gurcha SS, Besra GS, Munro AW (2002) Azole antifungals are potent inhibitors of cytochrome P450 mono-oxygenases and bacterial growth in mycobacteria and streptomycetes. Microbiology 148:2937–2949

Menozzi G, Merello L, Fossa P, Schenone S, Ranise A, Mosti L, Bondavalli F, Loddo R, Murgioni C, Mascia V, La Colla P, Tamburini E (2004) Synthesis, antimicrobial activity and molecular modeling studies of halogenated 4-[1H-imidazol-1-yl(phenyl)methyl]-1,5-diphenyl-1H-pyrazoles. Bioorg Med Chem 12(20):5465–5483

Moore AV, Kirk SM, Callister SM, Mazurek GH, Schell RF (1999) Safe determination of susceptibility of Mycobacterium tuberculosis to antimycobacterial agents by flow cytometry. J. Clin Microbio 37(3):479–483

NCCLS-National Committee for Clinical Laboratory Standards (1995) Antimycobacterial susceptibility testing for Mycobacterium tuberculosis proposed standard M24-T. Villanova, PA

Nunn P, Williams B, Floyd K, Dye C, Elzinga G, Raviglione M (2005) Tuberculosis control in the era of HIV. Nature Rev Immunol 5(10):819–826

Shukla D, Mesfin YM, Hailemariam D, Biadglign S, Kibret KT (2014) Association between HIV/AIDS and multi-drug resistance tuberculosis: a systematic review and meta-analysis. PLoS ONE 9(1):e82235

Stigliani JL, Bernardes-Genisson V, Bernadou J, Pratviel G (2012) Cross-docking study on InhA inhibitors: a combination of Autodock Vina and PM6-DH2 simulations to retrieve bio-active conformations. Org Bio-Mol Chem 10(31):6341–6349

Sundaramurthi JC, Kumar S, Silambuchelvi K, Hanna LE (2011) Molecular docking of azole drugs and their analogs on CYP121 of mycobacterium tuberculosis. Bioinformation 7(3):130–133

Tiwari A, Saxena S, Pant AB, Srivastava P (2012) Protein-ligand interaction studies of retinol-binding protein 3 with herbal molecules using AutoDock for the management of Eales' disease. J Ocul Biol Dis Infor 5(2):40–43

www.who.int/topics/tuberculosis/en/, Global Tuberculosis Report 2013, in, 2013

www.who.int/topics/tuberculosis/en/, Tuberculosis prevalence surveys: a handbook, in, 2011

STUDIES OF ULTRASONIC AND VISCOMETRIC BEHAVIOR OF AZITHROMYCIN WITH DIFFERENT SOLVENT SYSTEMS DIOXANE-WATER AND METHANOL-WATER MIXTURE AT 305.15 K

S.A.Quazi[1], D.T.Mahajan[1], Noor Mohammad[2], M.L.Narwade[1], Vijay Masand[1], M.R. Ingle[3]

[1]Department of Chemistry VidyaBharti Mahavidyalaya, Camp, Amravati (M.S) India.
[2]Department of Chemistry Govt.Vidarbha Institute of Sci. and Humanities, Amravati (M.S) India.
[3]Department of Chemistry G.S College, Khamgaon (M.S.) India.

ABSTRACT

Antibiotic drug Azithromycin is mainly used for treatments of infectious disease caused by bacteria such as respiratory,skin,ear and sexually transmitted diseases such great importance of azithromycine in human life the densities, ultrasonic velocities and viscosities of azithromycine have been evaluated in different concentrations in 70% dioxane-water and 70% methanol-water mixtures at 305.15 K. Experimental data of sound velocities and densities of solutions in 70% dioxane-water helps to determine the various acoustical parameters such as adiabatic compressibility, apparent molal volumes, intermolecular free length, specific acoustic impedance, relative association etc. for evaluating the molecular interactions present in different solutions were studied.

Keywords: Azithromycin drug, dioxane water and viscometric measurements.

INTRODUCTION

In the fields of medicinal, industrial, biochemistry etc the study of molecular interactions between solutes molecule and solvent media has got great importance. It also helps the study of solute solvent and solvent-solvent interactions can by the measurement of relative viscosity and ultrasonic velocity of an electrolyte in solutions[1-3]. Many workers have presented the viscosity in different concentrations of ligand solutions in various solvents[4-13].The apparent and partial molar volumes of electrolyte solutions very important parameter for eluciding the ion-ions, ion-solvent and solute-solvent interactions in solution.

EXPERIMENTAL SECTION

The chemicals used were of AR grade and were purified by standard methods. Requisite amount of chemicals weighing was done by using electronic balance.By using the Pyknometers the densities of solutions were determined, which was standardized by the standard procedure. Ostwald's Viscometer was used for measurements of viscosity which was kept in elite thermostatic water bath (±0.1°C). The ultrasonic velocity of solution and solvent was determined by using single crystal interferometer (Mittal Enterprises, Model F-81) with accuracy of ± 0.03% and 2 MHz frequency.

RESULTS AND DISCUSSION

Acoustic parameters, densities and relative viscosities have been determined for all the solutions and were calculated by using different equations[14] and are presented in the following Table -I. After observing the table, the relative viscosity increases with increase in the concentration of solute that means increasing solute-solvent interactions, same results evaluated by different workers[15-19].

Table -I: Calculated Viscosities of azithromycine drug in different solvents at 305.15 K

Concentration c (mol/dm^3)	solvents			
	70% Dioxane		70% Methanol	
	ρ x 10^{-3} (kg/m^3)	ηr x 10^3 (kg/m.s)	ρ x 10^{-3} (kg/m^3)	ηr x 10^3 (kg/m.s)
0.05	0.8438	1.0591	0.8424	1.0779
0.06	0.8499	1.1260	0.8440	1.1710
0.07	0.8517	1.1812	0.8455	1.2363
0.08	0.8545	1.2446	0.8474	1.3025
0.09	0.8575	1.2890	0.8489	1.3612
0.10	0.8594	1.3450	0.8498	1.4050
0.12	0.8615	1.4083	0.8551	1.4352

Table -II: Ultrasonic velocity (U), density (ρ) and calculated values of various acoustic parameters for in 70% dioxane-water mixture at 303.15 K

Concentration c (mol/dm^3)	U (m/s^{-1})	ρ (kg/cm^3) x 10^{-3}	φv (cm^3/mole) x 10^2	φk (S) (cm^3/mole.bar)	βs (bar^{-1}) x 10^{-5}	RA	Z (cm/s.g^3) x 10^2	Lf (A^0) x 10^2
0.05	1455	0.9499	12.9511	3.8161	6.5395	0.9928	12.4869	5.8299
0.06	1444	0.9517	8.0531	1.9458	6.6317	0.9976	12.4176	5.8644
0.07	1432	0.9575	5.4608	1.3124	6.7044	1.0075	12.3939	5.8914
0.08	1412	0.9594	4.8755	1.0179	6.8935	1.0148	12.2459	5.9609
0.10	1399	0.9615	4.4797	0.8327	6.9136	1.0205	12.1615	6.0045

Table-II it can be concluded that the ultrasonic velocity decreases with increasing concentration of solute, which indicates the presence of molecular association between solute and solvent.

The values of $\varphi k(s)$, acoustic impedance (Z) and apparent molal volumes (φv) in different concentrations showed to be decreases as we increase in the concentration of solute.The of $\varphi k(s)$ show positive values the strong electrostatic force in the vicinity of ions, causing electrostatic solvation of ions[20].In case of L$_f$, β_s and R$_A$ values of concentration increases may be due to the departure of solvent molecules around the ions due to weak ion-solvent interactions.

ACKNOWLEDGEMENT

REFERENCES

[1] Sheshagiri, M.G. Rao , Ind. J. Pure and Appl. Phys., 9, 169 (1971).
[2] R.P. Varma and Surendra kumar, Ind. J. Pure and Appl. Phys., 38, 2,96 (2000).
[3] S.S. Yadav, Y.P. Singh, Rajkumar, J. Ind. Coun. Chem., 16, 2, 20 (1999).
[4] Noor,S.A.Quazi, Mahajan, Masand, Recent Trends in Material Preparation &Characterization, National Conference ISBN - 978-81-929395-2-0,24th February (2014), pp86-89
[5] S.A.Quazi, Mahajan, Masand, Noor,National Conference ISBN – 978-93-82588-41-2, Recent application mathematical tools in science May 8-3(2014),pp76-80
[6] Mistry A.A,Bhandarkar V.D and Chimankar O.P.,J.Chem.&Pharm.Research,4(1),170-174(2012)
[7] RamtekeJ.N,Adv.In appl.Sci.Res,3(3),1832-1835(2012)
[8] PalanniappanL,Asian J.Mat.Sci.,4(1),21-27(2012).
[9] Fakruddinsk,srivasa .c and Kolla.N. Int.J.Res.Chem.Env.2 (3), 164-167(2012)
[10] Narwade M.L and RamtekeA,Arch of Appl.Sci.Res.4(1),254-261(2012)
[11] DeosarkarS.D,RussianJ.Phy.Chem.(A),86(10),1507-1511(2012)
[12] Pawar R.B, Int.Res.J.2 (2), 281-291(2012)
[13] Khobragade B.G., Meshram U.P, Der. Pharm. Chemica,3(2), 376-382(2012
[14] Deepali P. Gulwade , M.L. Narwade, K.N. Wadodkar, Ind .J. Chem. Sect. A, 43 (10), 2102 (2004).
[15] BG Khobragade and ML Narwade. Acta Ciencia Indica, 1983, IX-c, 32.
[16] PB Agrawal and ML Narwade. Indian J. Chem., 2003, 42-A, 1047.
[17] BG Khobragade; ML Narwade; M Raffique and NS Quazi. Act.Cien.Ind., 2007, 33-c, 2,113.
[18] JD Mahale; SC Manoja; NG Belsare and PR Rajput. Ind. J. Chem., 2010, 29 B, 505.
[19] VS Jamode; JC Dadhichi; DD Malkhede and ML Narwade. J.Ind.Coun.of Chemist, 2005, 22-2, 35.
[20] Shishakant Ikhe and M.L. Narwade, Ind. J. Chem. (A), 44(12), 2495 (2005).

Studies of relative and specific viscosities of Aceclofenacin 70% Dioxane water mixture at different temperature

S.A.Quazi*, D.T.Mahajan, Noor Mohammad, M.L.Narwade, Vijay Masand, M.R. Ingle
Department of ChemistryVidyaBhartiMahavidyalaya, Camp, Amravati (M.S) India.
Department of ChemistryGovt.Vidarbha Institute of Sci. and Humanities, Amravati (M.S) India. Department of Chemistry, G.S college, Khamgaon.
*Corresponding author:quazi.azhar@rediffmail.com

ABSTARCT
Acelofenac drug plays their own identity in the drug, pharmaceutical and medicinal sciences in last decades. Hence, the viscometric study were carried out at 70% various percentage of solvent. The result obtained during this investigation directly focus on the dipole association of compound, intermolecular attraction between solute and solvent, dielectric constant of medium, and polarazibility.
Keywords: Acelofenac drug, dioxane water and viscometric measurements.

INTRODUCTION

Viscosity measurement is useful tools for getting information about solute-solute and solute-solvent interactions. Many workers studied interactions of binary mixtures aqueous and non-aqueous solutions in terms of β-coefficient of viscosity by using this measurement. Recently some workers presented the measurement of viscosity, refractivity index. Present paper contains viscosity measurements of Acelofenace were studied at various temperatures.

EXPERIMENTAL SECTION

All chemicals are analytical reagent (AR) grade with were obtained from Sd Fine chemicals, India which is used as such without further purification. The viscosities were measured by using Oswald's viscometer cleaned and dried, which was kept in thermostatic water bath (±0.10c) and maintaining each measurement sufficient time was allowed to maintain the temperature variation. The density of solutions were determined by a bicapillary Pyknometer and calibrated with deionised by doubly distilled water. The present study deals with the viscosity measurements of Ligand Acelofenac in 70% dioxane–water mixture at different compositions at 298°k, 300°k and 305°k respectively. The viscometric readings were taken as in literature survey. The results determined were mentioned, Aand β-coefficient values calculated in following Table.

Table: Determination of Relative and Specific Viscosities at 70% Dioxane-Water mixture

Temperature(^{0}k)	Concentration (M)	Time flow (Second)	Density (ρ) g.cm^{-3}	Relative Viscosity ηr	Specific Viscosity sp= η_r $^{-1}$	η_r - 1/$\sqrt{C}$	A-coefficient	B coefficient
298°k	0.100	97.9	1.026 0	1.5865	0.7865	2.58683	2.77	-1.7491
	0.075	95.9	1.0249	1.4913	0.6913	2.62392		
	0.050	94.2	1.0245	1.4226	0.6226	2.73055		
	0.040	91.8	1.0241	1.3503	0.5503	2.78471		
300°k	0.100	98.9	1.0247	1.5530	0.5530	1.84843	2.03	-1.8851
	0.075	96.9	1.0245	1.4985	0.4985	1.91991		
	0.050	94.2	1.0242	1.4403	0.4403	1.96019		
	0.040	92.8	1.0239	1.3987	0.3987	1.94498		
305°k	0.100	97.9	1.0243	1.4177	0.4177	1.42058	1.85	-2.8851
	0.075	96.9	1.0240	1.4166	0.4166	1.62085		
	0.050	95.2	1.0233	1.3694	0.3694	1.66059		
	0.040	91.8	1.0229	1.3446	0.3446	1.78100		

RESULT AND DISCUSSION

The relative viscosities have been analysed by Jones-Dole equation $(\eta r – 1) / \sqrt{C} = A + B \sqrt{C}$ where C is molar concentration of the ligand solution, A is the viscosity coefficient which measures solute-solute interaction and B is viscosity coefficient which measure solute-solvent interaction. The graphs are plotted between $\sqrt{C}$ versus $(\eta r – 1) /\sqrt{C}$. The graph for each system showing linear straight line which is validity of Jone's –Dole equation. The slope of straight line gave value of β coefficient. The presence of weak solute-

solvent interaction may be due to strong hydrogen bonding.

CONCLUSION

From the results, it is observed that, the concentration of ligand is directly proportional to density and relative viscosity for ligand at temperature 298°k, 300°k and 305°k for 70% dioxane-water mixture. This may be due to the weak solvation effect which shows weak molecule interaction. The A and β-coefficient values are negative indicating a weak solute-solvent interaction which is good for interactions in between the drug and the drug receptors indicate good drug activity and effect which in favors of pharmacokinetics and pharmacodynamics activity. The density and relative viscosity for ligand is inversely proportional to temperature of solution which shows weak the molecular interactions.

It indicates that when the temperature of dioxane water increases, weak solute-solvent interactions i.e. interaction of ligand (drugs) and dioxane increases, which may be stabilize the drug activity. From this it can be concluded that the drug absorption, drug transmission and drug effect of ligand is more effective at higher temperature of dioxane water.

REFERENCE

BG Khobragade; ML Narwade, M Raffique and NS Quazi, *Act.Cien.Ind.*, 2007, 2(33), 113

C.Y. Huang, Job Plot Method in Enzymology, 87, 1982, 509.

F. Karia, S. Baluja, Asian J. Chem., 12 (2), 2000, 593.

JD Mahale; SC Manoja; NG Belsare and PR Rajput, Ind. J. Chem., 2010, 29, 505.

Jones G., and Doles M., J. Am. Chem. Soc., 51, 1929, 500-503.

Jones, G. and Dole, M, J. Am. Chem. Soc., 51, 1929, 2950.

Maccarthy, Patrick, Z.D. Hillz, J. Chemical Education, 63 (3), 1986, 162.

P. Job, Amnali di chimica Application, 9 (10), 1928. 113.

Patil K.J., Manwatkar S.M., Dondge S.S., J.Ind. Chem.Soc, 4, 1994, 33.

PB Agrawal and ML Narwade, Indian J. Chem., 2003, 42-A, 1047.

R.K. Wadi, V. Kakkar, J. Ind. Chem. Soc., 39 (6), 2000, 598.

VS Jamode, JC Dadhichi, DD Malkhede and ML Narwade, J.Ind.Coun.of Chemist, 35, 2005, 22-2.

Computational POM and DFT Evaluation of Experimental *in-vitro* Cancer Inhibition of Staurosporine-Ruthenium(II) Complexes: the Power Force of Organometallics in Drug Design

Taibi Ben Hadda,[1,]* Zuhal K. Genc,[2,]* Vijay H. Masand,[3] Nadia Nebbache,[4] Ismail Warad,[5] Shehdeh Jodeh,[5] Murat Genc,[6] Yahia N. Mabkhot,[7] Assem Barakat[7] and Hector Salgado-Zamora[8]

[1] *Laboratoire Chimie Matériaux, FSO, Université Mohamed Premier, Oujda 60000, Morocco*

[2] *Faculty of Engineering, Department of Metallurgy and Materials Engineering, Adiyaman University, 02040, Adiyaman, Turkey*

[3] *Department of Chemistry, Vidya Bharati College, Camp, Amravati, Maharashtra, India*

[4] *Laboratoire de chimie appliquée, Université de Biskra, B.P. 145, RP. 07000 Biskra, Algérie*

[5] *Department of Chemistry, Faculty of Science,Taibah University, Al-Madinah Al-Munawarah, 30002, Saudi Arabia*

[6] *Department of Chemistry, Faculty of Science and Arts, Adiyaman University, 02040 Adiyaman, Turkey*

[7] *Department of Chemistry, College of Science, King Saud University, P. O. Box 2455, Riyadh-11451, Saudi Arabia*

[8] *Departamento de Química Orgánica, Escuela Nacional de Ciencias Biológicas, Instituto Politécnico Nacional, Mexico, DF 11340, Mexico*

* *Corresponding author: E-mail: taibi.ben.hadda@gmail.com, zuhalkaragoz23@gmail.com*
Tel: +212 0666134178; Fax: +212 0536500603

Abstract

A computational Petra/Osiris/Molinspiration/DFT(POM/DFT) based model has been developed for the identification of physico-chemical parameters governing the bioactivity of ruthenium-staurosporine complexes **2–4** containing an antitumoral-kinase (TK) pharmacophore sites. The four compounds **1–4** analyzed here were previously screened for their antitumor activity, compounds **2** and **4** are neutral, whereas analogue compound **3** is a monocation with ruthenium(II) centre. The highest anti- antitumor activity was obtained for compounds **3** and **4**, which exhibited low IC_{50} values (0.45 and 8 nM, respectively), superior to staurosporine derivative (pyridocarbazole ligand **1**, $150 \cdot 10^3$ nM). The IC_{50} of **3** (0.45 nM), represents 20,000 fold increased activity as compared to staurosporine derivative **1**. The increase of bioactivity could be attributed to the existence of pi-charge transfer from metal-staurosporine to its ($CO^{\delta-}–NH^{\delta+}$) antitumor pharmacophore site.

Keywords: *Cancer-Kinase* (CK), antitumor agents, ruthenium-staurosporine complexes, DFT, Petra/Osiris/Molinspiration (POM) analyses.

1. Introduction

Staurosporine derivatives (Figure 1) have been thoroughly studied in organic and inorganic chemistry. Some of these compounds have been semi-synthesized for industrial, biological, and medicinal aims. Moreover, the staurosporine derivatives are regarded as excellent agents not only for their affinity to complex the kinase enzymes[1] but also to form stable bioactive and selective complexes with the ions of ruthenium(II).[2] These com-
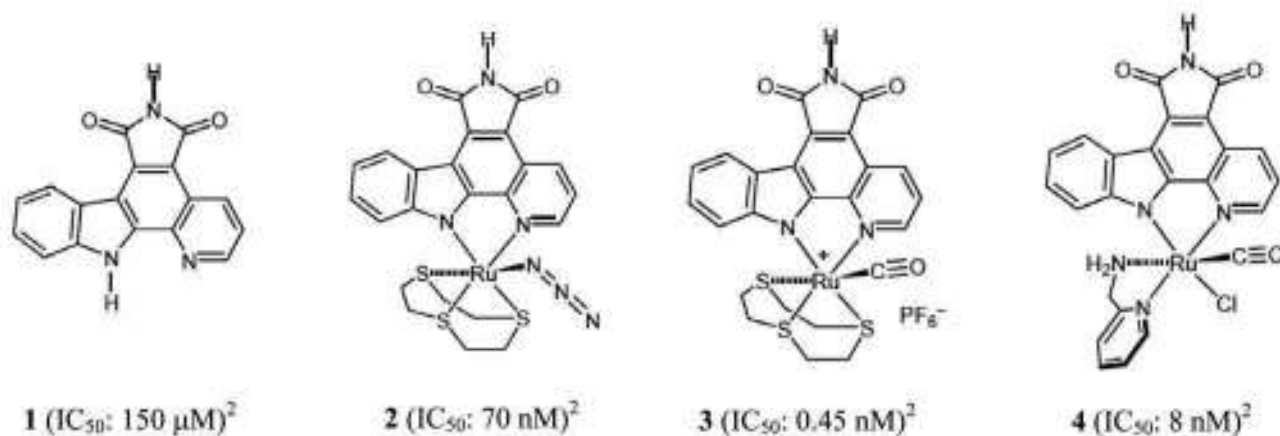
Figure 1. Molecular structure of the ruthenium-staurosporine compounds[2] studied.

plexes are so efficient that it is often projected to use them in clinics.[2,3] The protein kinase inhibition for the treatment of cancer via staurosporine and their ruthenium(II) complexes, rank as an attractive and extensively researched topic.[3–6]

Other studies on the interaction between Pd(II) and Pt(II) complexes of small molecules and DNA has been the focus of similar recent research in the scope of life science, chemistry, clinical medicine and genetics.[7,8] These studies are very useful for investigating the structure and biological function of DNA, kinases and elucidating the damage mechanism of DNA but Ru(II) complexes are less toxic than other transition metal complexes. For this reason we focalize all our attention on Ru-staurosporine complexes.

The inhibition efficiency of such drugs depends essentially on the structure of the inhibitor itself, which includes the number of active functional group centers (NH–C=O) in the molecule, the nature of the metal, and the kinase structure. The structure and the lone electron pairs in the O, N heteroatoms are important features that determine the chelation/interaction of these compounds with the metallic ion and biotargets.

The inhibition efficiency of bacteria, virus, parasite, and fungus, has been found to be closely related to drug bioavailability and molecular physico-chemical-geometric-tautomeric properties for different kinds of organic drugs.[9–22] Recently, it has been shown that the kinase inhibition by an organometallic systems under biological condition may be significantly facilitated if a ligand containing an anti-kinase pharmacophore (NH–C=O), a bidentate N,N coordinative site (staurosporine derivatives) and non-toxic metal (ruthenium) are available.[2–6]

The cancer inhibition of kinase enzymes through organic drugs has been the subject of different theoretical investigations. However, to our knowledge no group has carried out a rational correlation between experimental screenings efficiencies of anti-kinase drugs and the results of Petra/Osiris/Molinspiration (POM) analyses.

The utility of analysis of impact of coordination of drugs to transition metals on their bioactivity is of great importance in answering some fundamental questions in medicinal chemistry and biological chemistry, such as selectivity control (whether or not a given complex will be toxic). An excellent source that illustrates this concept well is the interesting work published by Eric Meggers *et al.*[2–6]

The development of theoretical scales of electrophilicity and nucleophilicity of pharmacophore site is also desirable and crucial, as a validated theoretical scale may be further used to project the global reactivity onto particular regions on the complexed drug.

There are different ways to increase the bioactivity of drugs; by modeling their bioavailability and controlling their electronic structure. A suitable theoretical concept is that proposed by Ben Hadda *et al.*[9–25] apropos of definition of pharmacophore site. The best descriptors for studying and identifying the type of pharmacophore site (antibacterial, antiviral or antitumor) are the description in detail of local electrophilicity and the nucleophilicity of each functionalized group and their spatial arrangement.

Recently, Ben Hadda *et al.* introduced some geometrical parameters, bioavailability, structural complementarily global and local (regional) nucleophilicity to establish modern definition of different pharmacophore sites.[9–25]

For these reasons, we constructed a platform of some of the key bioinformatic model in order to predict and characterize the antitumor drugs performance of the tested series of staurosporine-ruthenium(II) complexes. Our aim in this work is to give a deeper insight into the coordination effect of transition metal (ruthenium) to bioactive drug (staurosporine), on the inhibition efficiency of ruthenium-staurosporine complexes (Figure 1) using POM and DFT analyses.

2. Experimental

2. 1. DFT Method

The molecular modeling was performed using Gaussian 09 program package for calculations. In the present work, the calculations have been carried out at (DFT/B3LYP) method with 6-31+G(d,p) basis set. Electron correlations were included using Becke3-Lee-Yang-Parr (B3LYP) procedure.[26] This contains Becke's gradient exchange corrections, Lee, Yang and Parr correlation functional and/or Vosko, Wilk and Nusair correlation functional.[27]

2. 2. POM Analyses

One of the practical problems associated to the synthetic drugs is the existence of various side effects. For a molecule to be a potential drug, besides having a good biological activity, it must have good pharmacokinetic properties in biological systems. To access the pharmacokinetic profile of the synthesized molecules, we used well established *in silico* tools such as Osiris, Petra and Molinspiration, which have been validated with almost 7000 drug molecules available on the market.

3. Results and Discussion

3. 1. POM Analyses of Compounds 1–5

The analysis of theoretical toxicity risks for the staurosporine (STR) and its organic derivative **1** using the Osiris program showed that compound **1** and probably the rest of series **2–4** (Figure 2) are less toxic than standard clinical drugs (camptothecins) and can be used as therapeutic agents. From the data evaluated in Table 1, all structures are supposed to be non-mutagenic when run through the mutagenicity assessment of coordinated system and, as far as irritating and reproductive effects are concerned, all the compounds are at low risk comparable with standard drugs used. The hydrophilicity character of each compound has been expressed in terms of the cLog*P* value. It has been established that the absorption or permeation is greatly affected by the hydrophilicity (value of cLog*P*). Accordingly, when cLog*P* is higher than 5, the absorption or permeation decreases. On this basis, most of compounds **1–4** have cLog*P* values within the acceptable criteria and are active at different IC_{50} because another crucial parameter should be taken in consideration. This does not concern the geometrical conformation of phar-
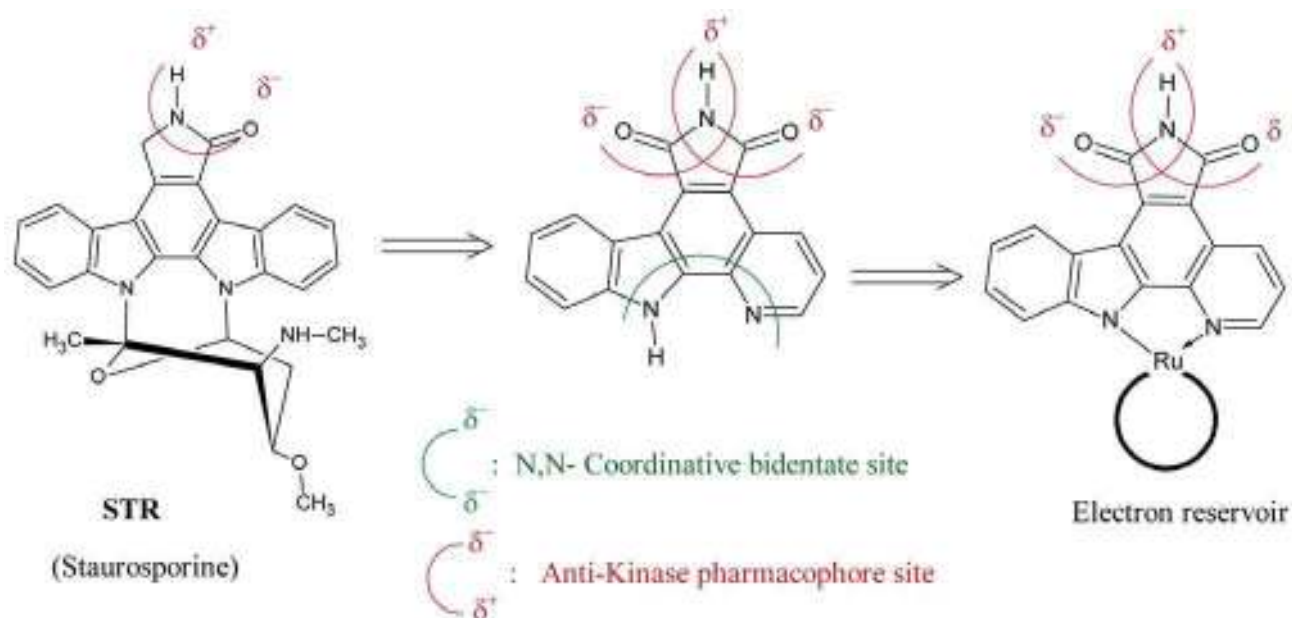
Figure 2. Series of Ru-staurosporine complexes with anti-tumoral pharmacophore site.

Table 1. Osiris calculations of toxicity risks of staurosporine (**STR**) and its derivative (**1**).

Compd.	MW	Toxicity Risks[a]				Osiris calculations[b]			
		MUT	TUM	IRRI	REP	cLog*P*	Sol	DL	DS
1	287	+++	---	+++	+++	2.41	–4.72	2.28	0.42
STR	466	+++	+++	+++	+++	4.44	–6.77	5.28	0.37

Higly toxic: (---), Slightly toxic: (+), Not toxic (+++). [a] MUT: Mutagenic, TUM: Tumorigenic, IRRIT: Irritant, RE: Reproductive effective.
[b] Sol: Solubility, DL: Druglikness, DS: Drug-Score. **STR** : Staurosporine.

Table 2. Molinspiration calculations of staurosporine derivative (**1**) and its complexes (**2**–**4**).

Compd.	Molinspiration calculations [a]				Drug-likeness [b]					
	TPSA	NONH	NV	VOL	GPCRL	ICM	KI	NRL	PI	EI
1	79	2	0	236	0.01	0.02	0.96	.48	0.21	0.56
2	109	1	1	428	0.12	0.15	0.33	–0.56	–0.02	0.42
3	76	1	1	480	0.00	0.28	0.11	0.64	0.08	0.14
4	96	3	1	394	0.04	0.18	0.25	0.70	0.25	0.28
STR	69	2	0	410	0.37	0.23	1.50	–0.18	0.35	0.86

[a] TPSA: Total molecular polar surface area; NONH: number of OH---N or O---NH interaction, NV: number of violation of five Lipinsky rules [50, 51]; VOL: volume.   [b] GPCRL: GPCR ligand; ICM: Ion channel modulator; KI: Kinase inhibitor; NRL: Nuclear receptor ligand; PI: Protease inhibitor; EI: Enzyme inhibitor. **STR** : Staurosporine.

macophore because it is fixed for all compounds **1**–**4**. The absorption, distribution characteristics and bioactivity were proved to be dependent on the geometrical parameter and the aqueous solubility of each compound. Consequently, the bad absorption of tested staurosporine-ruthe-

nium(II) complexes **2**–**4** could presumably be due to their low solubility.[28,29] Further, Table 2 shows drug-likeness of compounds **1**–**4,** not in the comparable zone with standard drugs used. We have calculated overall drug-score (DS) for compounds **1**–**4** and compared with that of standard

Compound 1

Compound 2

Compound 3
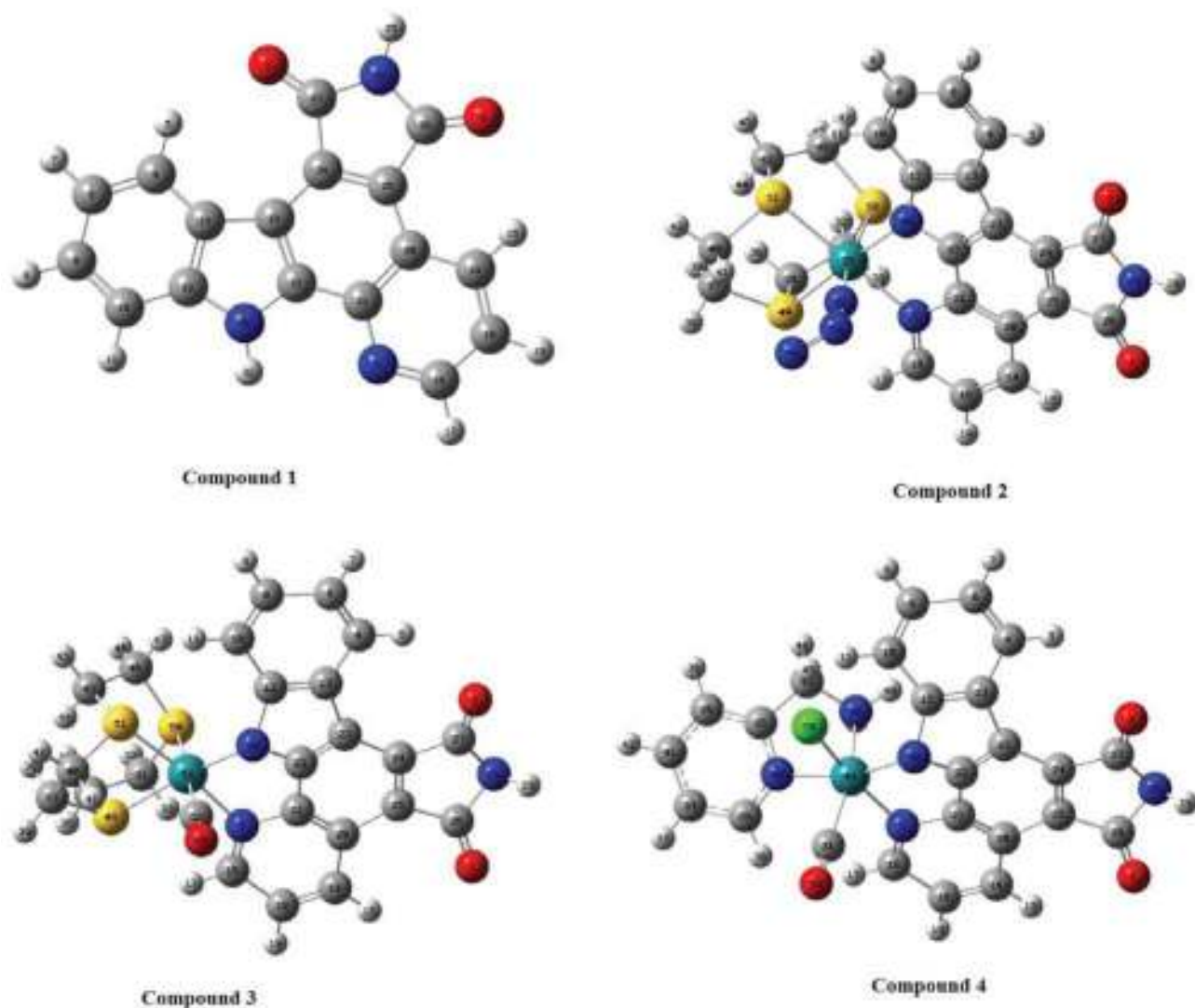
Compound 4

Figure 3. Optimized geometrical structure of compounds **1**–**4**.

drug (STR). The DS combines drug-likeness, cLog*P*, log *S*, molecular weight, and toxicity risks, in one handy value that may be used to judge the compound's overall potential to qualify for a drug. The reported compounds **2–4** showed low to moderate DS as compared with standard drug used STR (Table 1).

Incidentally, it is our opinion that DS and DL are not quite reliable since the values depend upon the program used. For this reason, supplementary DFT calculations will clarify this query.

3. 2. Frontier Molecular Orbitals

Highest occupied molecular orbital (HOMO) and lowest unoccupied molecular orbital (LUMO) are the most important orbitals to characterize the chemical reac-

tivity,[30,31] optical properties[32] and biological activity.[33] The energy gap between HOMO and LUMO is obtained by first optimization of structures **1–4** (Figure 3) as illustrated in Figure 4.

HOMO, HOMO–1, LUMO and LUMO+1 energies were calculated at B3LYP/6-311+G(d,p) and LANL2DZ theory level in order to understand influence of the structural properties of the Staurosporine and its complexes that are summarized in Table 3. As can be seen from Figures 4–7, for compound **1**, HOMO is mainly delocalized on the aromatic ring and heteroatoms except pyrrole carbonyl oxygen; however LUMO is mainly delocalized on the indole ring and heteroatoms. For compound **2**; the HOMO electrons are mainly delocalized on the Ru(II) and azido group, LUMO electrons are delocalized on the Staurosporine ring. For
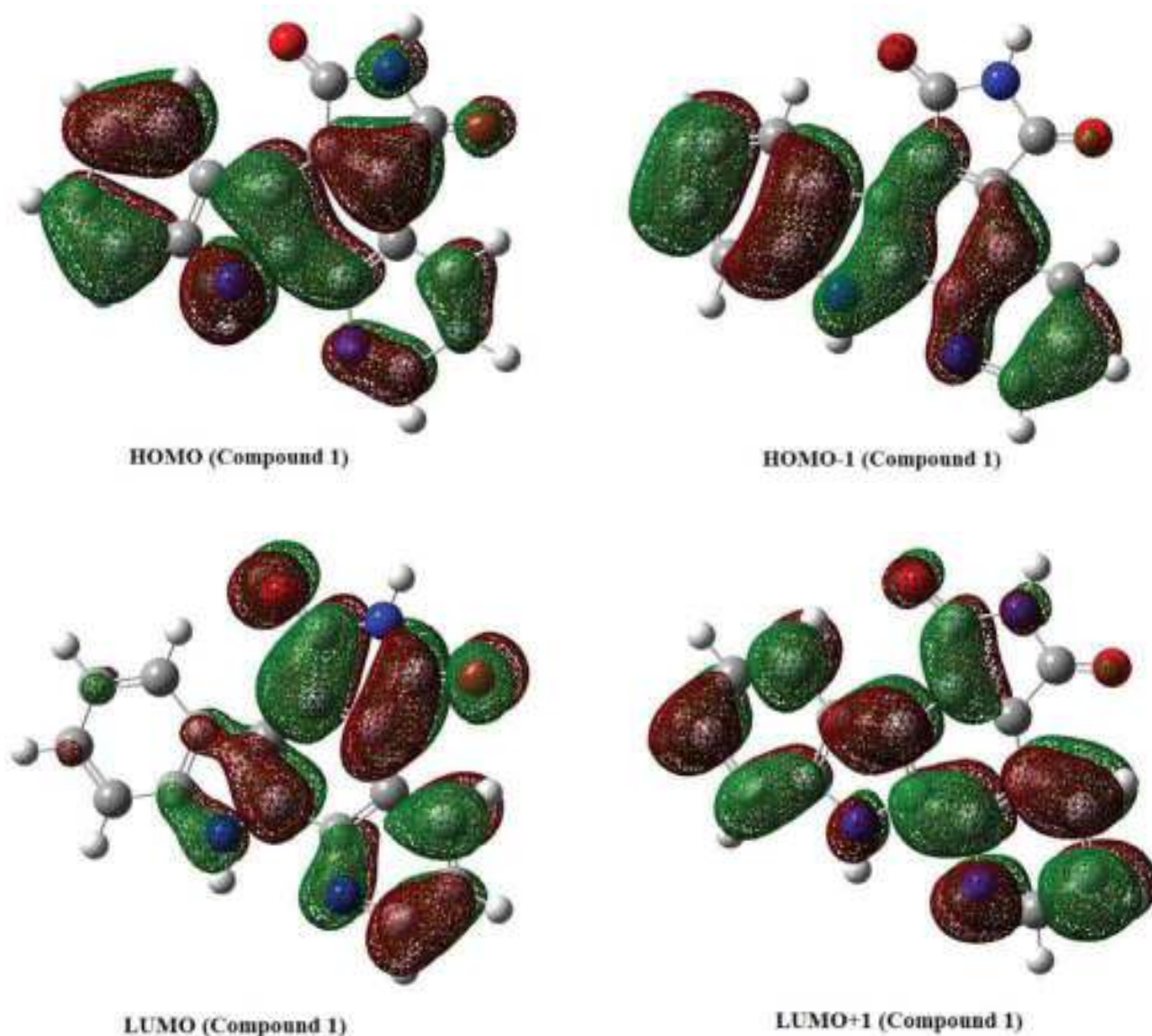
Figure 4. HOMO and LUMO molecular orbitals of the staurosporine derivative N,N-ligand (**1**) using the 6-311+G(d,p) method.

HOMO (Compound 2)

HOMO -1(Compound 2)

LUMO (Compound 2)

LUMO+1 (Compound 2)
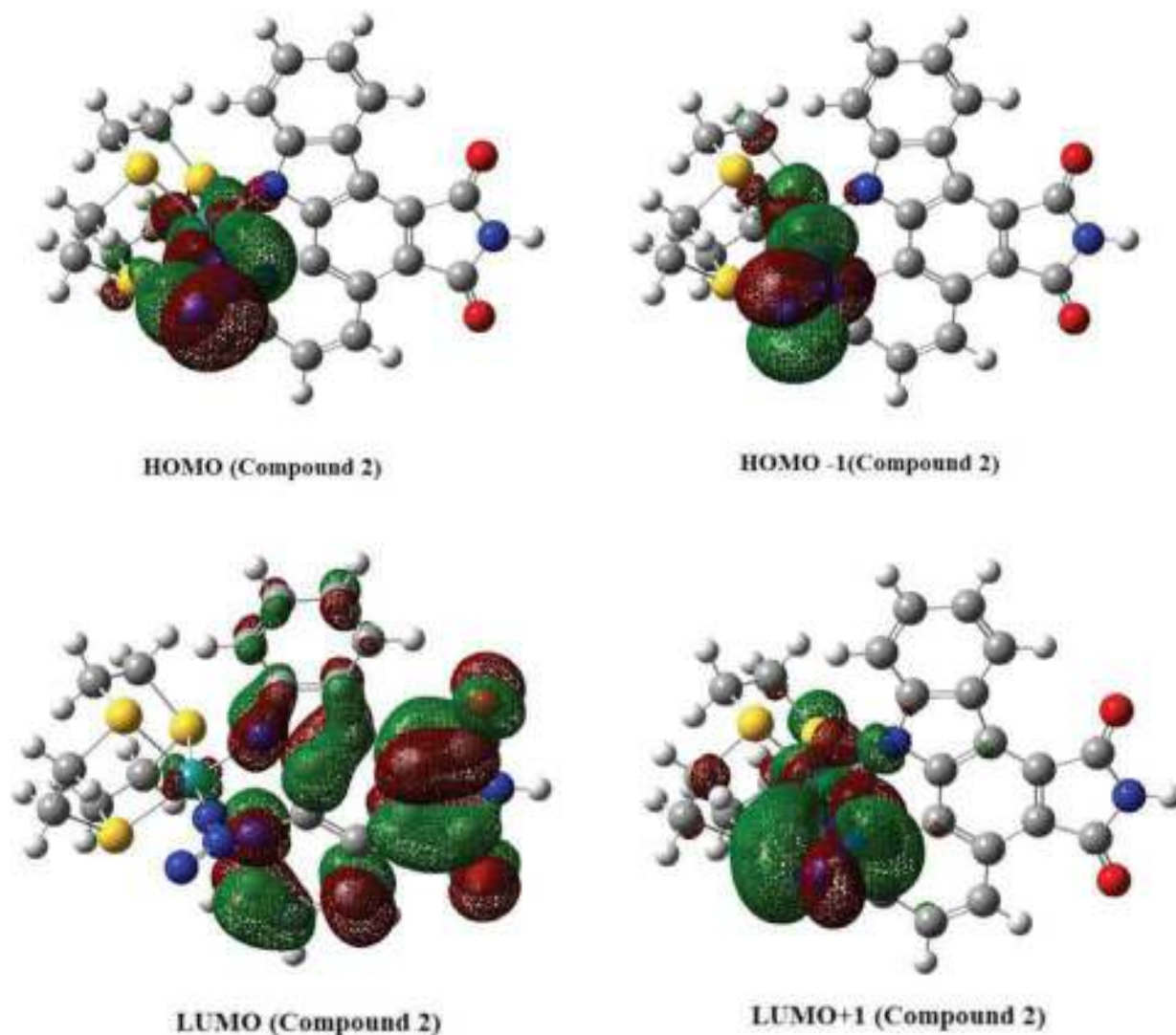
Figure 5. HOMO and LUMO molecular orbitals of the Staurosporine complex (**2**) using the LANL2DZ method.

compound **3**; the HOMO electrons are mainly delocalized on the Ru(II), oxygen atoms and pyrrole ring, while LUMO electrons are delocalized on the 1,4,7-trithiocyclononan ring. For complex **4**; the HOMO electrons are mainly delocalized on the Ru(II), –NH$_2$, indole ring, LUMO electrons are delocalized on the indole and pyridine ring. According to these results; generally HOMO and LUMO orbitals are mainly delocalized on the rings that mean p-antibonding type orbitals.

Various functional groups are the major active centers of the interraction. Indeed, the HOMO of these compounds does not contribute to an explanation of their inhibitory efficiency, but the HOMO-1 can carry out this role. In these cases, analysis of the effectiveness of kinase inhibition is based on the energy gaps (HOMO–1-LUMO+1). The chemical potential and nucleophilicity were estimated using the HOMO–1 and the LUMO (Figures 4–7; Table 3). However, the gap between the HOMO–1 and LU-

MO orbitals is an important factor that should be considered. The excellent enzyme kinase inhibitors are generally organic compounds that not only donate electrons to the positive charged amino acids of the enzyme but also accept free electrons of the imine groups of kinase enzymes.

By analyzing the HOMO–1-LUMO+1 energy gap values for these complexes (Table 3), it can be noted that for complexes **2–4**, the HOMO–1-LUMO+1 energy gaps values are lower than those obtained for ligand free (**1**). Therefore, complexes **2–4** (containing electron rich organometallic moiety) are predicted to be better kinase enzyme inhibitors with gaps HOMO-LUMO (**2**: 0.03842, **3**: 0.05054, **4**: 0.08147 a.u.) than ligand free compound **1** (containing free bidentate electron-withdrawing group) (**1**: 0.12336 a.u.) as shown in Table 3.

These results are in total agreement with the experimental results (Table 4). The HOMO-LUMO energy gaps of these complexes are consistent with the experimental

HOMO (Compound 3)

HOMO –1(Compound 3)

LUMO (Compound 3)

LUMO+1 (Compound 3)
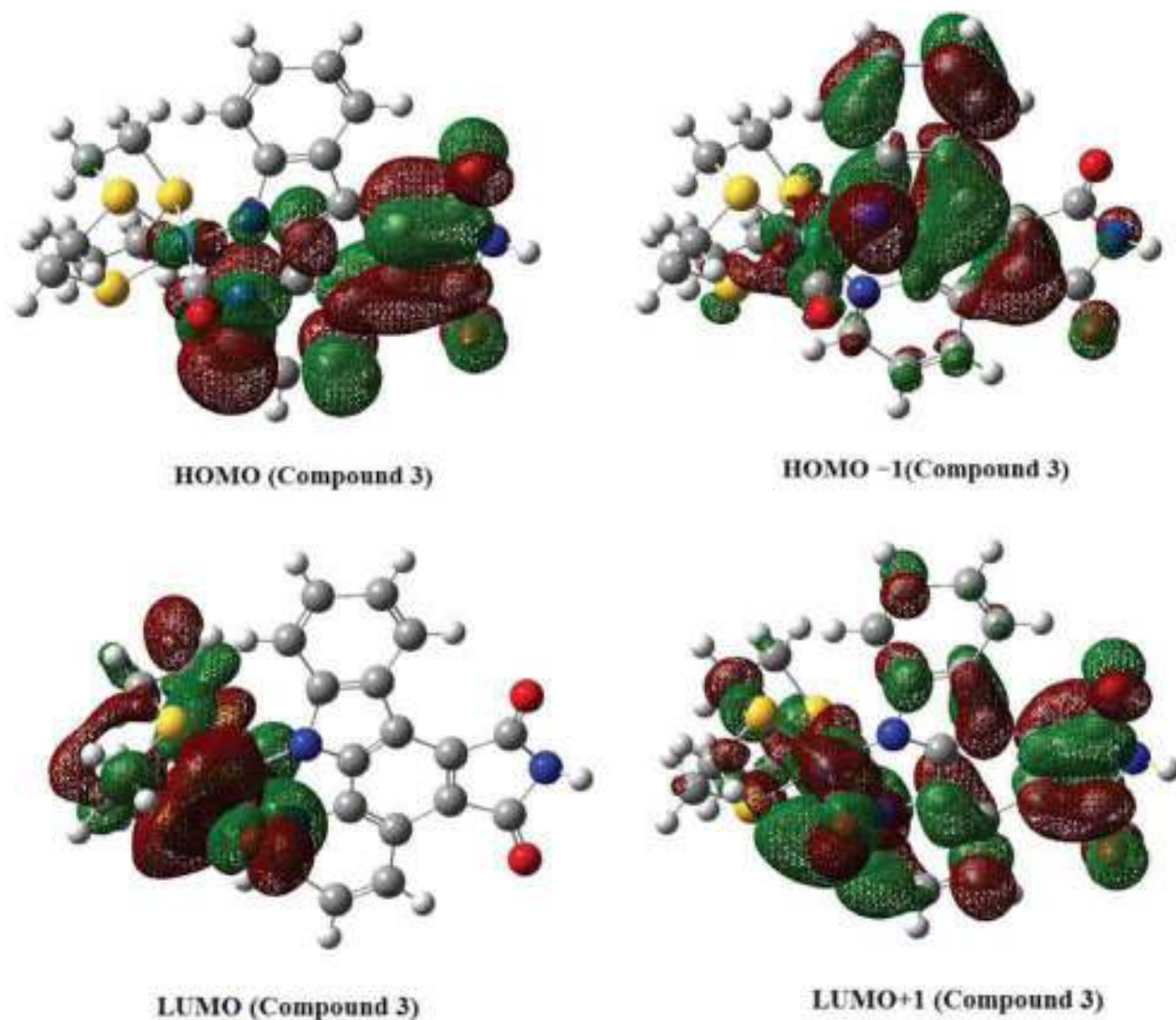
Figure 6. HOMO and LUMO molecular orbitals of the staurosporine complex (**3**) using the LANL2DZ method.

IC_{50} values given in literature[2–6] and the partial atomic charge obtained by calculations (Table 4). Furthermore, the two Oxygen atoms of the OCNHCO pharmacophore site are negatively charged, and the IC_{50} is low (more efficiency in bioactivity). The order obtained was **3 > 4 > 2 > 1** with O-charge: –0.6349, –0.56, –0.6349, –0.5383, respectively.

The structure of complex can affect the bioactivity by influencing not only the electron density of the functional pharmacophore site but also its proper bioavailability.

In order to rationalize the local bioactivity, we have calculated the local charge of each heteroatom. The results are summarized in Table 4. The local atomic charges were obtained using DFT calculations

The distribution of the electron density shows that the compounds studied **1–4** have many active centers in nucleophilicity. The areas containing the nitrogen and oxygen atoms have more opportunity to form bonds with the metallic ruthenium(II) ions, by donating electrons of the heteroatoms to the metallic ions (Table 4). However,

Table 3. HOMO, HOMO–1, LUMO, LUMO+1 and ΔE energies (a.u.)

Compd.	HOMO	LUMO	HOMO–1	LUMO+1	HOMO-LUMO	HOMO–1-LUMO+1
1	–0.22915	0.10579	–0.24174	–0.07088	0.12336	0.17086
2	–0.12373	–0.09431	–0.14660	–0.06253	0.03842	0.08407
3	–0.09299	–0.04245	–0.19200	–0.03928	0.05054	0.15272
4	–0.18283	–0.10136	–0.19945	–0.07086	0.08147	0.12859

HOMO (Compound 4)

HOMO +1(Compound 4)

LUMO (Compound 4)

LUMO+1 (Compound 4)
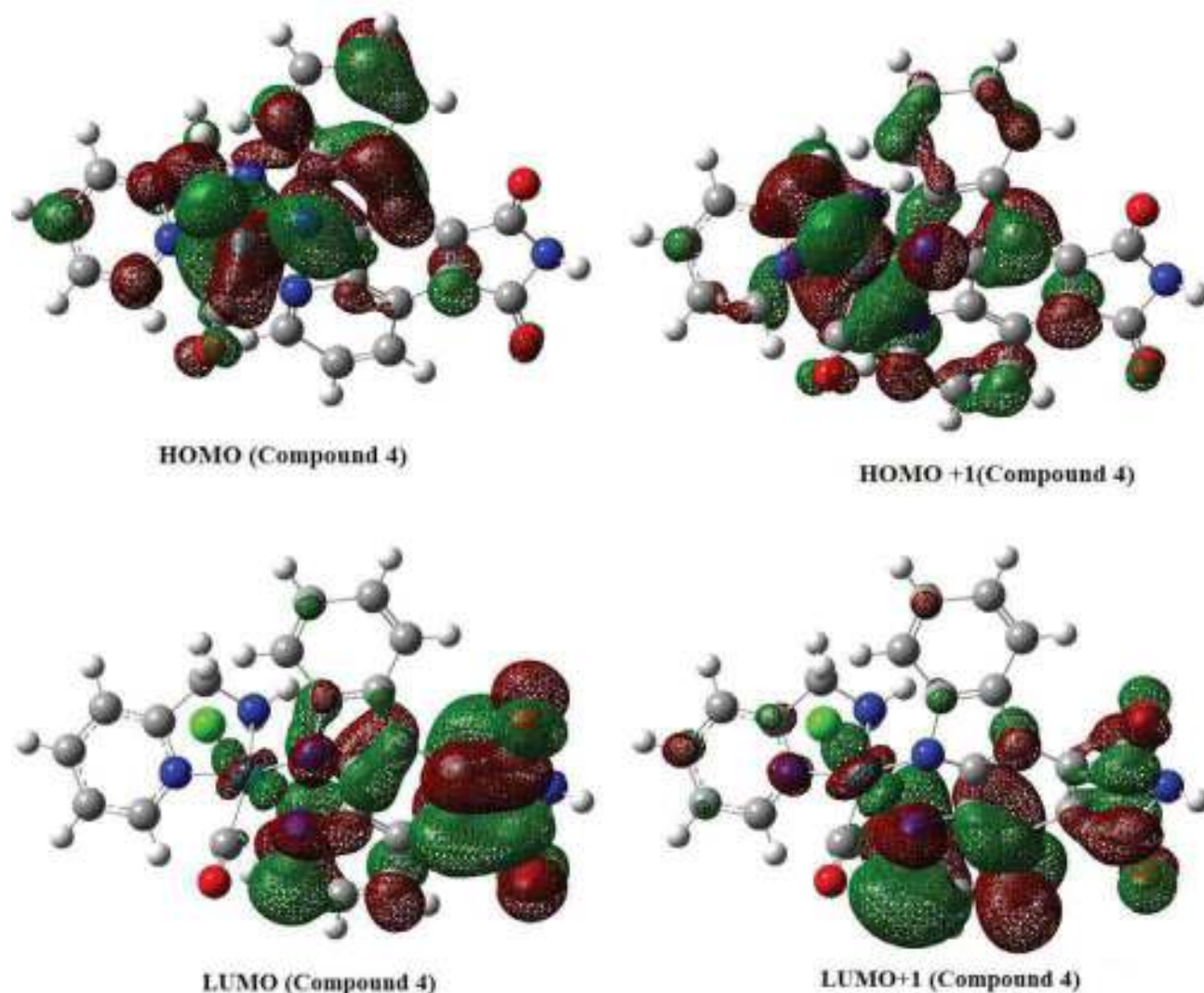
Figure 7. HOMO and LUMO molecular orbitals of the staurosporine complex (**4**) using the LANL2DZ method.

Table 4. Electronic impact on antitumor activity of (OCNHCO) pharmacophore site by coordination of drug (**1**) to electron rich organometallic moiety (**2–4**).

Compd	IC_{50} (nM)	Charge of Ru-(NN) Organometallic Moiety			Charge of OCNHCO Pharmacophore Site		
		Ru	N-1	N-2	O	N-3-H	O
1	$150 \cdot 10^3$	---	–0.3827	–0.6016	–0.5289	0.4422	–0.5383
2	70	–0.4886	–0.3827	–0.4391	–0.6292	0.4422	–0.6349
3	0.45	–1.0243	–0.4561	–0.5440	–0.6292	0.4169	–0.6349
4	8	–0.3461	–0.3979	–0.4591	–0.5808	0.2277	–0.5605

sites N1 and N2 are most favorable for electrophilic attack, in addition to oxygen in the case of **1**. It is interesting to note that the negative transferred charge of Ru(II) have important effect on the efficiency of inhibition of enzyme, like the effect of the terminal substituents on the organometallic moiety. This is in perfect agreement with the experiments (**3**: –1.0243; **2**: –0.4886; **4**: –0.3461 u.a).

4. Conclusions

The present work provided additional structure–activity and structure–cytotoxicity information for the staurosporine-ruthenium(II) complexes family. Indeed, this study proved that a simple control of nature of simple coordination to non-toxic transition metals leads to com-

pounds with high activities and reduced cytotoxicities of staurosporine as parent and clinical standard drug.

Tumor inhibition of kinase through staurosporine ligand and its complexes was elucidated by means of density functional theory (DFT)-derived reactivity indexes. The DFT calculated parameters and experimental cancer inhibition efficiency (IC_{50}) indicate that their inhibition effect is closely related to the frontier orbital energies, polarizability, electronic chemical potential and global nucleophilicity. The quantum chemistry calculations were performed at the B3LYP/6-31G(d) level. The theoretical results predicted by using DFT-based reactivity indexes, are in good agreement with experimental outcomes.

In comparing the percentages of inhibition efficiency (IC_{50}) of the studied compounds with the theoretical results, we note that their inhibitory effects are closely related to HOMO–1, HOMO–1-LUMO+1 gap, and the partial negative charge of Oxygen atoms of pharmacophore site. These parameters were calculated by the DFT method. The bioactivity decreases when HOMO–1 increases, and when the HOMO-1-LUMO+1 gap decreases. Therefore, complexes **2–4** are better kinase inhibitors (presence of donor organometallic moiety on the ligand-Ru) than free ligand **1** (presence of withdrawing nitrogen bidente groups on the staurosporine derivative ring's). The DFT calculations indicate that it is not convenient to consider only a single parameter (partial charges). However, several parameters were considered to characterize the inhibitory activity of the molecules, in particularly bioavailability (cLog*P*). The partial atomic charges of the series of complexes were discussed in a simple but precise manner.

5. Acknowledgements

6. References

1. A. Huwe, R. Mazitschek, A. Giannis, *Angew. Chem. Int. Ed.* **2003**, *42*, 2122–2138.
http://dx.doi.org/10.1002/anie.200200540

2. E. Meggers, G. E. Atilla-Gokcumen, H. Bregman, J. Maksimoska, S. P. Mulcahy, N. Pagano, D. S. Williams, *Synlett* **2007**, *8*, 1177–1189.
http://dx.doi.org/10.1055/s-2007-973893

3. E. Meggers, *Curr. Opin. Chem. Biol.* **2007**, *11*, 287–292.
http://dx.doi.org/10.1016/j.cbpa.2007.05.013

4. J. E. Debreczeni, A. N. Bullock, G. E. Atilla, D. S. Williams, H. Bregman, S. Knapp, E. Meggers, *Angew, Chem. Int. Ed.* **2006**, *45*, 1580–1585.
http://dx.doi.org/10.1002/anie.200503468

5. H. Bregman, D.S. Williams, G. E. Atilla, P. J. Carroll, E. Meggers, *J. Am. Chem. Soc.* **2004**, *126*, 13594–13595.
http://dx.doi.org/10.1021/ja046049c

6. S. P. Mulcahy, P. J. Carroll, E. Meggers, *Tetrahedron Lett.* **2006**, *47*, 8877–8880.
http://dx.doi.org/10.1016/j.tetlet.2006.10.054

7. N. Stojanović, D. Urankar, A. Brozović, A. Ambriović-Ristov, M. Osmak, J. Košmrlj. *Acta Chim. Slov.* **2013**, *60*, 368– 374.

8. M. Saeidifar, H. Mansouri-Torshizi, Y. Palizdar, M. Eslami-Moghaddam, A. Divsalar, A. A. Saboury, *Acta Chim. Slov.* **2014**, *61*, 126–136.

9. J. Sheikh, K. Hatzade, A. Bader, U. Shaheen, T. Sander, T. Ben Hadda, *Med. Chem. Res.* **2014**, *23*, 243–251.
http://dx.doi.org/10.1007/s00044-013-0621-5

10. T. Ben Hadda, S. Srivastava, B. Das, H. Salgado-Zamora, U. Shaheen, A. Bader, M. M. Naseer, *Med. Chem. Res.* **2014**, *23*, 995–103. http://dx.doi.org/10.1007/s00044-013-0707-0

11. T. Ben Hadda, M. A. Ali, V. Masand, S. Gharby, T. Fergoug, I. Warad, *Med. Chem. Res.* **2013**, *22*, 1438–1449.
http://dx.doi.org/10.1007/s00044-012-0143-6

12. T. Ben Hadda, T. Fergoug, I. Warad, *Res. Chem. Intermed.* **2013**, *39*, 1963–1971.
http://dx.doi.org/10.1007/s11164-012-0729-0

13. J. Fathi, V. Masand, R. Jawarkar, R. Mouhoub, T. Ben Hadda, *J. Comput. Method. Mol. Design* **2011**, *1*, 57–68.

14. A. Jarrahpour, J. Fathi, M. Mimouni, T. Ben Hadda, J. Sheikh, Z. H. Chohan, A. Parvez, *Med. Chem. Res.* **2012**, *21*, 1984–1990. http://dx.doi.org/10.1007/s00044-011-9723-0

15. A. Parvez, M. Jyotsna, M. H. Youssoufi, T. Ben Hadda, *Phosphorus, Sulfur, Silicon Relat. Elem.* **2010**, *185*, 1500– 1510.
http://dx.doi.org/10.1080/10426500903095556

16. Z. H. Chohan, S. H. Sumrra, M. H. Youssoufi, T. Ben Hadda, *Eur. J. Med. Chem.* **2010**, *45*, 2739–2747.
http://dx.doi.org/10.1016/j.ejmech.2010.02.053

17. Z. H. Chohan, M. H. Youssoufi, A. Jarrahpour, T. Ben Hadda, *Eur. J. Med. Chem.* **2010**, *45*, 1189–1199.
http://dx.doi.org/10.1016/j.ejmech.2009.11.029

18. A. Jarrahpour, M. Motamedifar, M. Zarei1, M. H. Youssoufi, M. Mimouni, Z. H. Chohan, T. Ben Hadda, *Phosphorus, Sulfur, Silicon Relat. Elem.* **2010**, *185* 491–497.
http://dx.doi.org/10.1080/10426500902953953

19. A. Parvez, M. Jyotsna, M. H. Youssoufi, T. Ben Hadda, *Phosphorus, Sulfur, Silicon Relat. Elem.* **2010**, *185*, 1500– 1510. http://dx.doi.org/10.1080/10426500903095556

20. B. Bennani, A. Kerbal, M. Daoudi, B. Filali Baba, G. Al Houari, A. F. Jalbout, M. Mimouni, M. Benazza, G. Demailly, M. Akkurt, S. Ö. Yildirim, T. Ben Hadda, *Arkivoc* **2007**, *16*, 19–40. http://dx.doi.org/10.3998/ark.5550190.0008.g03

21. J. Sheikh, A. Parvez, V. Ingle, H. Juneja, R. Dongre, Z. H. Chohan, M. H. Youssoufi, T. Ben Hadda, *Eur. J. Med. Chem.* **2011**, *46*, 1390–1399.
http://dx.doi.org/10.1016/j.ejmech.2011.01.068

22. Z. H. Chohan, S. H. Sumrra, M. H. Youssoufi, T. Ben Hadda, *J. Coord. Chem.* **2010**, *63*, 3981–3998.

http://dx.doi.org/10.1080/00958972.2010.523783

23. Y. N. Mabkhot, A. M. Al-Majid, A. Barakat, S. S. Al-Showiman, M. S. Al-Har, S. Radi, M. M. Naseer, T. Ben Hadda, *Int. J. Mol. Sci.* **2014**, *15*, 5115–5127.
http://dx.doi.org/10.3390/ijms15035115

24. J. Sheikh, A. Parvez, V. Ingle, H. Juneja, R. Dongre, Z. H. Chohan, M. H. Youssoufi, T. Ben Hadda, *Eur. J. Med. Chem.* **2011**, *46*, 1390–1399.
http://dx.doi.org/10.1016/j.ejmech.2011.01.068

25. Z. H. Chohan, S. H. Sumrra, M. H. Youssoufi, T. Ben Hadda, *J. Coord. Chem.* **2010**, *63*, 3981–3998.
http://dx.doi.org/10.1080/00958972.2010.523783

26. A. D. Becke, *J. Chem. Phys.* **1993**, *98*, 5648–5652.
http://dx.doi.org/10.1063/1.464913

27. C. Lee, W. Yang, R. G. Parr, *Phys. Rev. B*, **1988**, *37*, 785– 789.
http://dx.doi.org/10.1103/PhysRevB.37.785

28. C. A. Lipinski, F. Lombardo, B. W. Dominy, P. J. Feeney, *Adv. Drug Deliv. Rev.* **2001**, *46*, 3–26.
http://dx.doi.org/10.1016/S0169-409X(00)00129-0

29. C. A. Lipinski, *Drug Discovery Today: Technologies* **2004**, *1*, 337–341.
http://dx.doi.org/10.1016/j.ddtec.2004.11.007

30. Z. Karagoz, S. Tekin, S. Sandal, M. Genc, *Res. Chem. Intermed.* **2015**, DOI: 10.1007/s1164-014-1545-5.

31. J. Fleming, Frontier Orbitals and Organic Chemical Reactions, Wiley, London, **1976**, 111–155.

32. D. Sajan, K. U. Lakshmi, Y. Erdogdu, I. H. Joe, *Spectrochim. Acta* **2011**, *78A*, 113–121.
http://dx.doi.org/10.1016/j.saa.2010.09.007

33. B. Eren, A. Unal, *Spectrochim. Acta Part A* **2013**, *103*, 222–231. http://dx.doi.org/10.1016/j.saa.2012.10.055

Povzetek

Razvili smo računski model Petra/Osiris/Molinspiration/DFT(POM/DFT) za določitev fizikalno-kemijskih parametrov, ki določajo biološko aktivnost rutenij-stavrosporin kompleksov **2–4** s farmakofornim mestom antitumor-kinaze (TK). Analiziranim štirim spojinam **1–4** so bile že predhodno testirane njihove antitumorne aktivnosti; spojini **2** in **4** sta nevtralni, medtem ko je analog **3** monokation z rutenijevim(II) centrom. Največja antitumorna aktivnost je bila dosežena pri spojinah **3** in **4**, ki imata nizko IC_{50} vrednost (0.45 in 8 nM), kar prekaša derivat stavrosporina (piridokarbazol **1**, 150 · 10^3 nM). IC_{50} vrednost za **3** (0.45 nM) predstavlja 20.000-kratno povečanje aktivnosti glede na derivat stavrosporina **1**. Povečanje bioaktivnosti je možno pripisati nastanku pi-prenosa naboja s kompleksa kovina-stavrosporin na $CO^{\delta-}$–$NH^{\delta+}$ antitumorno farmakoforno mesto.

Phytochemical investigations of *Dioscorea bulbifera* linn

Ujwala G.Malode[1], Noor Mohammad[2], S.A.Quazi[3*], D.T.Mahajan[3], Vijay Masand[3]
[1]Department of Chemistry, Jagdamba Mahavidyalaya, Achalpur, Amravati (M.S) India
[2]Department of Chemistry, Govt.Vidarbha Institute of Sci. and Humanities, Amravati (M.S) India
[3]Department of Chemistry, VidyaBharti Mahavidyalaya, Camp Amravati (M.S) India
Corresponding author: E.mail:quazi.azhar@rediffmail.com

ABSTRACT

Dioscorea bulbifera Linn. Belonging to family *Dioscoreaceae* is cultivated in Maharashtra on a small scale for its edible tubers. The Plant is perennial, large climber, producing bulbils at the base of its leaves. Whole plant is medicinal being anthelmintic, aphrodisiac, diuretic and tonic. It is also used in diabetes, gonorrhea, helminthiasis and leprosy. Extract of tuber and leaves was subjected to chemical tests for the presence of phytochemical classes like carbohydrates ,proteins, amino acids, fats, oils, steroids, glycosides, alkaloids , tannins and phenolics. Due to presence of carbohydrate, proteins, amino acids, fats and starch tubers become edible. Medicinal property of the plant is due to the presence of secondary metabolites such as alkaloids, glycosides and tannins.

Key words: Tuber, *Dioscorea, bulbil*, Glycoside.

INTRODUCTION

The Plant is found commonly in India. In Maharashtra it is cultivated on a small scale in Warud and parts of Achalpur tahasils. It is a perennial large climber, Tubers very large roundish,white from inside, Stem 4 angled, Leaves opposite, broadly ovate 6-15 x 4-10 cm, base cordate, acute. The bulbils grow at the base of its leaves. Flowers greenish white. Capsules of 2 semicircular, flat lobes, seeds winged all round.Plant is anthelmintic, aphrodisiac. Cooling, diuertic, sweet and tonic. It is also used in diabetes, gonorrhoea, helminthiasis and leprosy (Ahmad, 2012). Bulbils are more important food product. It is used in the treatment of rheumatis arthritis (Kokate, 2003). The tubers are edible sweet, cooling, aphrodisiac, tonic, diuretic and anthelmintic haemorrhoids, diabetes. They are also used in heart disease (Prajapati, 2003). Phytochemical analysis and Enzyme Inhibition Assay of *Aerva javanica* for Ulcer (Abdul Wajid Khan**,** 2012). Strawberry polyphenols attenuate ethanol-induced gastric lesions in rats by activation of antioxidant enzymes and attenuation of MDA increase (Alvarez-Suarez, 2011). Protective effect of Calamintha officinalis Moench leaves against alcohol-induced gastric mucosa injury in rats (Monforte, 2012). Macroscopic, histologic and phytochemical analysis (Emam, 1999). Phytochemical studies on the herb *Aerva javanica* growing in Egypt (Garg, 1980). Aervanone, a new flavanone from Aerva persica. Antiplasmodial activity of some medicinal plants used in sudanese folk-medicine (El-Hadi, 2010). Antihyperglycaemic activity of ethanol extract of *Aerva javanica* leaves in alloxan-induced diabetic mice (Srinivas, 2009). Chemical Constituents of *Aerva javanica* (Khan, 1982)**.** Secondary transport as an efficient membrane transport mechanism for plant secondary metabolites (Kazufumi Yazaki, 2008).

MATERIALS AND METHODS

The plant parts tubers and leaves were dried in a shed under normal environmental conditions for about one week. These dried parts were broken into small pieces with the help of the cutter and grinded to a coarse powder. Coarsely grinded plant parts were extracted in Soxhlet Apparatus successively with different solvents such as Acetone, Benzene, Chloroform, Ethyl alcohol, Petroleum Ether and Distilled water. The extracts obtained were concentrated and dried. The plant extract was subjected to chemical tests for the presence of phytochemical classes like carbohydrates, proteins, amino acids, fats and oils, steroids, glycosides, alkaloids, tannins and phenolics.

RESULTS & DISCUSSIONS

Phytochemical Investigations of *Dioscorea bulbifera Linn*

Test performed	Observation	Inference	Tuber	Leaves
Carbohydrates				
Molisch test: To the test tube, few drops of Molisch's reagent was added (alcoholic α-Naphthol). 2ml of conc. Sulphuric acid was added to slowly from the side of the test tube	Violet ring is formed at junction of two liquids	Carbohydrate present	+ ve	-ve
Fehling's test: 1ml Fehling's A and 1ml Fehling's B was mixed and boiled for 1 min. To this solution was added an equal volume of test solution. And boiled for 5-10 min	First yellow , then the brick red ppt is observed	Reducing sugars present	-ve	-ve
Benedict's test: Equal volumes of Benedict's reagent and test solution was mixed in the test tube and heated to the boiling water bath for 5 min	Sol appeared green ,yellow or red	Reducing sugars present	-ve	-ve
Barford's Test: Test solution was heated with Barford's reagent on water bath.	Red ppt is obtained	Monosaccharide present	-ve	-ve
Aniline acetate test: Test solution was boiled in a test tube. Filter paper soaked in aniline acetate was held in the vapor	Filter paper did not Convert pink	Pentose sugars present	-ve	-ve
Cobalt- Chloride test: 3ml test solution was mixed with 2ml cobalt chloride. Boiled and cooled. Few drops of NaOH solution were added.	Sol appeared greenish blue and pink	Glucose and fructose present	+ve	+ve
Iodine test: 3 ml test solution and few drops of dilute Iodine Solution was mixed	Appearance of blue color	Starch present	+ve	+ve
Tannic acid: 20 % Tannic Acid and Test solution	ppt observed	Starch present	+ve	+ve

Phytochemical Investigations of *Dioscorea bulbifera Linn*

Test performed	Observation	Inference	Tuber	Leaves
Proteins				
Heat test: The test solution was heated in boiling water bath	Coagulation occurred	Protein present	+ve	+ve
Biuret test: Test solution was treated with biuret reagent (40% sodium hydroxide and dilutes copper sulphate solution)	Violet or pink color	Protein present	+ve	-ve
Amino Acids				
Million's test: Test solution was treated with Million's reagent and heated on a water bath	Brick red ppt	Amino acid present	+ve	+ve
Ninhydrin test: Test solution with Ninhydrin reagent was boiled	Purple or Bluish colour	Amino acid present	+ve	-ve
Fats and Oils				
Filter paper test	Turns oily	Fats and Present	-ve	-ve
Glycosides				
General test: 200mg of the drug with 5ml of dilute sulphuric acid was extracted by warming on a water bath, filtered and neutralized the acid extract with 5% solution of sodium hydroxide. 0.1 ml of fehlings solution A and B was added until it became alkaline (Test pH - Paper) and heated on water bath for 2min	Formation of Red ppt.	General test for glycoside Present	+ve	+ve
Test for Anthraquinone Glycosides				
Modified Borntrager's test: 200 mg of the test material was boiled with 2ml of sulfuric acid and treated with 2ml of 5% aqueous ferric chloride solution (freshly prepared) for 5min. It was shaken with equal volume of chloroform. Lower layer from chloroform was separated and shaken it with dilute. Ammonia (Half of volume of chloroform).	Ammoniacl layer showed pink to red color	Anthraquinone glycoside present	-ve	+ve
Test for cardiac glycosides				
Legal's test: Test solution was treated with pyridine made alkaline with sodium nitorprusside	Pink to red color	Cardiac glycosides present	+ve	+ve
Test for flavonoid glycosides				
Shinoda test: Test solution was treated with a fragment of magnesium ribbon and cone. HCL was added.	Appearance of Pink color	Flavonoids present	+ve	-ve

Phytochemical Investigations of *Dioscorea bulbifera Linn*

Test performed	Observation	Inference	Tuber	Leaves
Alkaloids				
Dragendorffs test: Test solution was treated with Dragendorffs reagents (potassium bismuth iodide)	Orange brown ppt	Alkaloids present	+ve	+ve
Mayer's test: Test solution was treated with Mayer's reagent (Potassium mercuric iodide)	Cream colored ppt occurred	Alkaloids present	+ve	-ve
Tannins and phenolics: Ferric chloride test test solution was treated with a few drops of 5% ferric chloride solution.	Deep Blue Green color	Hydrolysable Tannins present	+ve	-ve
To the test solution few drops of potassium dichromate solution were added	Formation Red ppt	Tannins and phenolic compound present	+ve	-ve

CONCLUSION

Phytochemical constituents such as carbohydrate, sugars, protein, amino acid and starch form reserve food. Medicinal significance is due to the presence of secondary metabolites such as glycosides, alkaloids tannins and phenolics.

ACKNOWLEDGEMENT

REFERENCES

Ahmad S, Introduction to Pharmacognosy, I.K.International Publishing House Pvt. Ltd., New Delhi, 2012, 382-386.

Kokate C.K, Purohit A.P, Gokhale SB, Pharmacognosy, Nirali Prakashan, Pune, 2003, 1-62.

Prajapati, N.D, Purohit, S.S, Sharma A.K and Kumar T, A Hand Book of Medicinal Plants, Agrobios Jodhpur, 92, 2003.

Abdul Wajid Khan**,** Saleem Jan**,** Shaista Parveen, Rahmat Ali Khan**,** Asma Saeed**,** Abdul Jabbar Tanveer and Anwar Ali Shad*,* Chemistry Central Journal, 6**,** 2012, 76.

Alvarez-Suarez JM, Dekanski D, Risti S, Radonji NV, Petronijevi ND, Giampieri F, Astolfi P, González-Paramás AM, Santos-Buelga C, Tulipani S, Quiles JL, Mezzetti B, Battino M, PLoS One*,* 6(10), 2011, 25878.

Monforte MT, Lanuzza F, Pergolizzi S, Mondello F, Tzakou O, Galati EM, Phytother Res*,* 26(6), 2012, 839-44.

Emam SS, Cairo University Faculty of Agriculture Bulletin*,* 50, 1999, 488-514.

Garg SP, Bhushan R, Kapoor RC, Phytochemistry*,* 19, 1980, 1265, 1980.

El-Hadi MA, Barki YMN,Yousif GM, Hassan SK, Environ Health Insight*,* 4, 2010, 1-6.

Srinivas KR, Reddy VM, J of Pharmacy Research*,* 2, 2009, 1259-1261.

Khan UG, Nazir T, Ahmed VU, *Fitoterapia*, 53, 1982, 75-77, 1982.

Kazufumi Yazaki, Akifumi Sugiyama, Masahiko Morita, Nobukazu Shitan, Phytochemistry Reviews, October, 7(3), 2008, 513-524.

_____

Synthesis of (E)-1-(5-chloro-2-hydroxy-4-methylphenyl)-3-(4-nitrophenyl)prop-2-en-1-one and 4-chloro-5-methyl-2-(5-(4-nitrophenyl)-4,5-dihydro-1h-pyrazol-3-yl)phenol and its derivatives

Charita B. Patil*[1]

Department of Chemistry, L.A.D. College of Women, Nagpur,
Maharashtra, India

Vijay H. Masand[2]

Department of Chemistry, Vidya Bharati Mahavidyalaya,
Amravati, Maharashtra, India- 444 602

Abstract— In the present work, a simple and efficient protocol was followed to synthesize pyrazoline derivatives. The synthetic protocol commences with acetylation of appropriately substituted phenol **1a**, followed by Fries migration to afford substituted acetophenone **2a**. The product **2a** was then condensed with properly substituted benzaldehyde to provide corresponding chalcone **3a**. The chalcone **3a** was then subjected to treatment with hydrazine hydrate to furnish 1H-pyrazoline **4a** and its derivatives **4b-d** following acetylation, benzoylation and nitrosoation in moderate to high yields. The structures of the intermediate **1a**, **2a**, **3a, and** pyrazolines **4a-d** were established using chemical reactivity, elemental and spectral analyses.

Keywords- *nitro-Chalcone, Pyrazoline, synthesis, IR, PMR*

_____*****_____

I. INTRODUCTION

The synthesis of heterocyclic molecules has enriched the understanding and knowledge of reactivity and chemistry of catalysts, reagents, reaction intermediates, medicines and toxicants [1-4]. Heterocyclic molecules bearing two or more heteroatoms are key compounds in medicinal, agriculture and other fields for synthesis of variety of compounds with diverse applications and desired toxicity/activity. Nirogen heterocycles viz. pyrazoles, imidazoles, etc. have gained the prime attention and reverence of researchers due to their therapeutic properties like anti-bacterial, anti-fungal, anti-inflammatory, etc., a few to mention [5-12, 14]. Recently, Bandgar *etal* highlighted the various methods of synthesis and applications of pyrazoline derivatives as anti-inflammatory and anti-oxidants [13].

From the literature survey [1-7], it has been found that nitro substituted chalcones have never been employed for the synthesis of respective pyrazolines using reported method. Therefore, in the present work, the synthesis of pyrazolines has been accomplished following a simple yet very efficient route. The emphasis in the present work is on developing synthetic protocol for easily scalable and competent route for pyrazolines.

II. EXPERIMENTAL SECTION

All the chemicals were of analytical grade and used as supplied. The m.p. were recorded in an open capillary and are uncorrected. The FT-IR spectra were recorded on Agilent Spectrophotometer and reported in cm^{-1}. The PMR were recorded in DMSO-d6 using TMS as an internal standard and reported in ppm.

Synthesis of chalcone 3a [1-8]**:** Appropriately substituted acetophenone 2a (0.01 mol) and nitrobenzaldehyde (0.012 mol) were dissolved in ethanol (20 ml), then the mixture was brought to boiling. To this hot solution, NaOH (0.03 mol) was added with constant stirring and solution was kept overnight.

The sodium salt obtained was decomposed by aq. HCl (1:1) in cold condition. The yellow solid obtained was filtered, washed with NaHCO3 (2%) and then with water. The product was crystallized from ethanol to get yellow crystal of (E)-1-(5-chloro-2-hydroxy-4-methylphenyl)-3-(4-nitrophenyl)prop-2-en-1-one **3a**. Yield: 80%, m.p.: 250°C. FT-IR (cm^{-1}): 3750.21 (presence of free –OH group), 1642.64 (-CO- in conjugation with -C=C-), 1574.25 (-C=C- moiety), 1514.23 and 1340.40 (asymmetric and symmetric stretch for aromatic -NO$_2$), 1050.29 (aromatic C-Cl stretch), 841.41, 788.23 and 731.47 (presence of substituted benzene ring). PMR (δ): 12.37 (phenolic -O**H**), 1.23 (-C**H**$_3$), 2.53 and 2.38 (-C**H** = C**H**-), 6.93-8.35 (multiplet, aromatic C**H**)

Synthesis of pyrazoline 4a [1-8]**:** The chalcone **3a** (0.01 mol) and hydrazine hydrate (0.012 mol) in 20 ml ethanol was refluxed for 2 hr, and the mixture was then concentrated. On cooling, the resulting solid was filtered, and crystallized from ethanol. Yield: 80%, m.p.: 220-225°C. FT-IR (cm^{-1}): 3753.20 (free –OH group), 3330.27 (-NH (2° amine)), 3078.79 (aromatic C-H stretch), 1594.24 (-C=N- of pyrazoline), 1514.53 and 1340.86 (aromatic -NO$_2$), 1442.21 (-CH$_2$- of pyrazoline ring), 1067. 31 (aromatic C-Cl stretch), 849.83, 753.46, and 729.16 (substituted benzene ring). PMR (δ): 10.93 (phenolic –O**H**), 2.29 (-C**H**$_3$), 2.53 (-C**H**$_2$), 6.86 (-N**H**) 7.21-8.23 (multiplet, aromatic C**H**).

Synthesis of 4b-d pyrazoline derivatives [4-9]**:**

Synthesis of 4b: A mixture of **4a** (0.01 mol) and acetic acid (10 ml) was refluxed for 2 hr. On cooling, the resulting solid was filtered, and crystallized from ethanol. Pale yellow solid. Yield: 75%, m.p.: 239°C.

Synthesis of 4c: An equimolar mixture of **4a** (0.01 mol) and benzoyl chloride was dissolved in dry pyridine (10 ml) and stirred at room temperature for 1 hr. The reaction mixture was treated with cold dil HCl (2N). The resulting solid was filtered, washed with water, cold NaOH (2N) and again with

279

water. The crude solid was crystallized from ethanol to give brownish-yellow solid. Yield: 75%, m.p.: 290°C.

Synthesis of 4d: A mixture of **4a** (0.01 mol) was dissolved in ice cold 2 ml HCl (1:1) and cooled to 0°C and 10% NaNO$_2$(6 ml) was added dropwise with constant stirring. The mixture was stirred for 30 minutes at room temperature. The resulting solid was crystallized from ethanol to afford the yellowish solid. Yield: 75%, m.p.: 106°C.

Results and discussion: The synthesis of targeted pyrazolines **4a-d** initiated with the acetylation of properly substituted phenol **1a**, followed by Fries migration using the literature method to provide substituted acetophenone **2a**. Further step involves treatment of **2a** with substituted benzaldehyde in the presence of NaOH in ethanol as solvent to furnish corresponding substituted chalcone **3a**. In the very next step, the chalcone **3a** was treated with hydrazine hydrate to give 1H-pyrazoline **4a**, which was then converted to **4b-d**. The synthesis scheme adopted in the present work has been depicted in figure 1.

The FT-IR of **3a** showed an absorption signal at 3750.21 indicating the presence of free –OH group. The signal at 1642.64 could be assigned to -CO- in conjugation with -C=C-. The presence of -C=C- moiety is indicated by the signal at 1574.25. The two signals of almost same intensity at 1514.23 and 1340.40 have been assigned to asymmetric and symmetric stretch for aromatic -NO$_2$. The signal at 1050.29 indicates the presence of aromatic C-Cl stretch. The peaks at 841.41, 788.23 and 731.47 point the presence of substituted benzene ring. The PMR spectrum of **3a** is with a peak at 12.37 indicating the presence of phenolic –O**H**. The peak at 1.23 is indicative of -C**H**$_3$. The peaks at 2.53 and 2.38 were correlated with -C**H** = C**H**-. The multiplet at 6.93-8.35 indicates the presence of aromatic C**H**. In addition, **3a** decolorized the bromine water and gave red colour with FeCl$_3$, thus it contains unsaturation and phenolic –OH group. Treatment of **3a** with Fe and HCl, followed by reaction with alkaline solution of β-naphthol gave orange-red dye, thereby, indicating the presence of –NO$_2$ group. Thus, on the basis of elemental analysis, chemical reactivity and spectral data (FT-IR and PMR) the compound **3a** was assigned the following structure:

3a
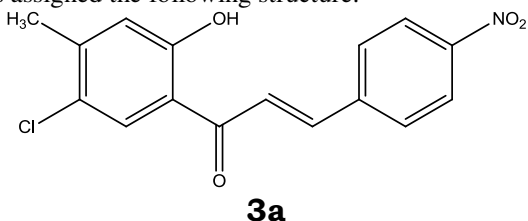
The FT-IR of **4a** showed an absorption signal at 3753.20 specifying the presence of free –OH group. The signal at 3330.27 could be assigned to –NH (2° amine) present in a ring. The peak at 3078.79 is due to the aromatic C-H stretch. The presence of -C=N- moiety of pyrazoline is indicated by the signal at 1594.24. The two signals of almost same intensity at 1514.53 and 1340.86 have been assigned to asymmetric and symmetric stretch for aromatic -NO$_2$. The 1442.21 peak indicates the presence of -CH$_2$- moiety present in the pyrazoline ring. The signal at 1067.31 arose due to the

aromatic C-Cl stretch. The peaks at 849.83, 753.46, and 729.16 point the presence of substituted benzene ring. The PMR spectrum of **4a** is with a peak at 10.93 indicating the presence of phenolic –O**H**. The peak at 2.29 is indicative of -C**H**$_3$. The peaks at 2.53 can be assigned to –C**H**$_2$. The -N**H** proton gave peak at 6.86. The multiplet at 7.21-8.23 indicates the presence of aromatic C**H**. In addition, **4a** gave red colour with FeCl$_3$, thus it contains phenolic –OH group. The treatment of **4a** with Fe and HCl, followed by reaction with alkaline solution of β-naphthol gave orange-red dye, thereby, indicating the presence of –NO$_2$ group. Thus, on the basis of elemental analyses, chemical reactivity and spectral data (FT-IR and PMR) the compound **4a** was assigned the following structure:

4a
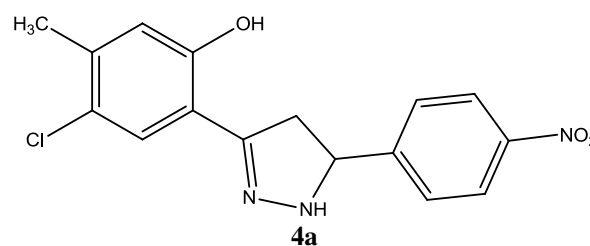
Sr.No.	Compound	Percent yield (%)	Melting point(°C)
1	3a	80	250
2	4a	80	220-225
3	4b	75	239
4	4c	75	290
5	4d	75	106

Table 1. *List of synthesized compounds, their melting points and percent yield*

Conclusion: In conclusion, a very efficient synthetic protocol has been followed to synthesize the chalcone and pyrazoline synthesis using easily scalable reactions involving use of effortlessly available starting materials and reaction conditions.

References:

[1] Sonare S.S., Doshi A.G.(1994)Synthesis of 1*H*-3-(2'-hydroxy-4-'methoxy)-5-substituted Phenyl-2-pyrazolines, Asian J. Chem. 6(2): pp 425-428

[2] Parmar P.J., Rajput S.I., Doshi A.G. (2007) Synthesis of Some Nitrosubstituted Flavanones, Pyrazolines and Their Derivatives, Asian J. Chem. 19(1): pp 493-498

[3] Parmar P.J., Rajput S.I., Doshi A.G. (2005) Synthesis of Some Pyrazolines and its Derivatives, Asian J. Chem. 17(4): pp 2539-2542

[4] Khadsan R.E., Kadu M.V., Doshi A.G., N.H. Aloolkar (2005) Synthesis and Antimicrobial Activities of 3-(2-Hydroxy-3-substituted-5-methyl

280

_____

phenyl)-(3,4-   methylenedioxyphenyl)-2pyrazoline
and Its Derivatives, Asian J. Chem. 17(3): pp 1600-
1604

[5] Bodkhe P. S., Patil K.N., Doshi A.G. (2003)
Synthesis and Characterization of 4-Aroyl Substituted
Pyrazolines and Pyrazoles, Asian J. Chem.15(3): pp
1853-1855

[6] Deshmukh A. Y., Raghuwanshi P.B., Doshi A.G.
(2002) Synthesis of 3-(4´´ -Substituted Phenyl)-5-(4´-
Substituted Phenyl)- Δ^2-Pyrazolines and Their
Derivatives, Asian J. Chem. 14(1): pp 185-189

[7] Thakare S.S., Doshi A.G., Patil S.D. (2001)
Dehydrogenation   of   1-h-3-(2"-hydroxy-3"-
substituted-5"-chlorophenyl)-5-(2'-furyl)-2-
pyrazolines and their derivatives with antimicrobial
activities, Oriental J. Chem. 17 (1): 127-130

[8] Thakare S.S., Tayade D.T. (1995) A Novel Synthesis
of Some Bromopyrazolines Asian J. Chem. 7: 891-
893

[9] Dubey R.R., Dhawas A.K., Thakare S.S. (2009)
Novel synthesis of some acetoxy aryl pyrazolines,
Asian J. Chem. 21 (8): 6233-6236

[10] C.K. Patil (2002), PhD Thesis, Sant Gadge Baba
Amravati University, Amravati

[11] C. N. Deshmukh (2003), PhD Thesis, Sant Gadge
Baba Amravati University, Amravati

[12] R. E. Khadsan (2007), PhD Thesis, Sant Gadge Baba
Amravati University, Amravati

[13] Bandgar B. P., Adsul L. K., Chavan H. V., Jalde S.
S., Shringare S. N., Shaikh R., Meshram R. J.,
Gacche R. N., Masand V. (2012) Synthesis,
biological evaluation, and docking studies of 3-
(substituted)-aryl-5-(9-methyl-3-carbazole)-1H-2-
pyrazolines   as   potent   anti-inflammatory   and
antioxidant agents. Bioorg. Med. Chem. Lett.,
22:pp5839-5844

[14] Auzzi G., Bruni F., Clauser M., Costanzo A., Pecori
Vettori L., Ademollo B. (1986). Some derivatives of
the   2-[4-pyrazolinyl]-1,3,4-thiadiazole   system,
Farmaco Sci, *41*(9): pp666-675
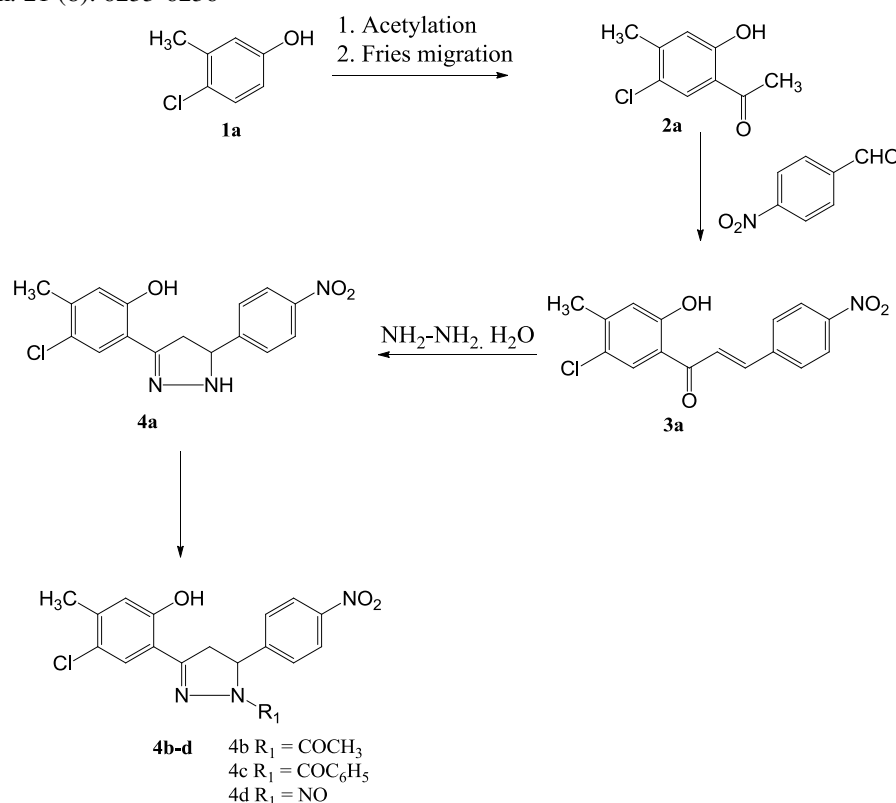
Figure 1. Synthetic scheme used in the present work for the synthesis of substituted pyrazolines

_____

EFFECT OF ADSORPTION OF TOXIC METAL IONS ON FRUIT SKIN

C.M.Deshmuk*,RohitKadam,PrachiBhartiya And C.N.Deshmukh,

Department ofChemistry,VidyaBhartiMahavidyalaya Amravati

*ShriShivaji Agriculture College,Amravati (M.S.)

ABSTRACT

The Phenomenon of higher concentration of any molecular species at the surface shows the adsorbtion.In present work study of adsorbtion of toxic metal ions such as Pb(II), Hg (II), Cd (II), Cu(II), on agricultural byproducts like Orange,Potato,Chickoo,Guava, Carrot and Banana at 25^0C has been studied at different concentrations.Rateofadsorbtion. increases with increasing the concentration of metal ions.

INTRODUCTION

The force of attraction existing between molecules in any state of matter shown an intermolecular attraction or cohesive force of attraction. Adsorption shows the collection of adsorbate on the surface of adsorbent due to cohesive force of attraction. The phenomenon of higher concentration of any molecular species at the surface shows the adsorption. M.C. Bain suggested that adsorption and absorption take place simultaneously.

The presence of toxic metal ions in industrial waste has attracted worldwide attention. Several methods such as chemical precipitation, ion exchange, ultrafiltration, electrochemical treatment etc. are suggested for the removal of these metal ions. Few workers have suggested methods for the adsorption of their ions by using inexpensive agricultural byproducts[1-2], tree barks[3-6], peanut skin[7-8] and agricultural waste material[9-10a].

We thought of using agricultural byproducts in their natural state. In the present work, an attempt has been made to study the adsorption of toxic metal ions such as Pb(II), Cd(II), Hg(II) and Cu(II) on agricultural byproducts (like Orange, Potato, Chickoo, Guava, Carrot, Banana) at 250C.

P. J. Sondawale[11] and Y. K. Meshram have studied the adsorption of Cd2+, Pb2+ and Cu^{2+} on agricultural by products such as orange skin and banana husk. Adsorption of cadmium

and leaf from aqueous solution by spent grain have been studied by K. S. Low and C. K. Lee12. Carolyn A. Burns et. al.13 has studied the adsorption of aqueous heavy metals onto carbonaceous substrates.

EXPERIMENTAL

Orange skin, Potato skin, Chickoo skin, Guava skin, Carrot skin, Banana husk, Pomegranate husk, Radish skin and Papaya skin were collected, exposed to sunlight for one week. Subsequently they were ground, exposed to sunlight for 24 hours and were preserved in air tight plastic bottles. The solution of different concentrations (0.01, 0.02, -----, 0.09 and 0.1) of Cu(II), Cd(II), Pb(II), Hg(II) were prepared in different conical flask. The absorbance of each metal ion at $\square$**max** is recorded. 1 gm of each of the adsorbent was weighed and placed in each conical flask. The flasks were corked and placed overnight. The solutions were filtered and the absorbance is measured for each of the filtrate spectrophotometrically.

The data obtained of % adsorption along with concentration for two representative systems are presented in table 9 and 10.

RESULT AND DISCUSSION

It would be seen from tables 9 and 10 that adsorption increases with respect to increase in concentration of metal ions.

The order of adsorption between metal ions and agricultural byproducts are as shown under :

1]	Orange skin	:	$Pb(II) > Cu(II) > Hg(II) < Cd(II)$
2]	Potato skin	:	$Pb(II) > Hg(II) > Cd(II) > Cu(II)$
3]	Chickoo skin	:	$Cu(II) > Pb(II) > Cd(II) > Hg(II)$
4]	Guava skin	:	$Pb(II) > Cu(II) > Cd(II) > Hg(II)$
5]	Carrot skin	:	$Pb(II) > Hg(II) > Cd(II) > Cu(II)$

It could be seen from above adsorption order that, the order of adsorption is found to same in case of potato skin and carrot skin. However, there it is also observed that the adsorption

of Pb(II) toxic metal ion on the surface of all agricultural by-products except chickoo skin. This may be the fact of more active centres on the surface of absorbent by-products.

Table 1: Adsorption of Metal on Chickoo skin

Pb(II)		Cd(II)		Cu(II)		Hg(II)		
A. Conc.	. ΔA (After A After – adsorp.)	A (AAfter – Abefore)	. ΔA (After adsorp.)	A (AAfter – Abefore)	. ΔA (After adsorp.)	. ΔA (After ABefore)	A (AAfter – adsorp.)	. ΔA (After ABefore)
0.01	1.582	1.504	1.411	1.202	1.448	1.381	1.725	1515
0.02	1.602	1.524	1.427	1.212	1.467	1.391	1.732	1.521
0.03	1.712	1.621	1.437	1.242	1.482	1.398	1.749	1.531
0.04	1.719	1.631	1.479	1.249	1.492	1.400	1.767	1.549
0.05	1.801	1.712	1.482	1.329	1.526	1.420	1.798	1.563
0.06	1.832	1.732	1.588	1.330	1.542	1.441	1.803	1.570
0.07	1.890	1.790	1.591	1.371	1.562	1.461	1.818	1.575
0.08	1.910	1.820	1.594	1.382	1.584	1.479	1.842	1.579
0.09	1.927	1.836	1.599	1.395	1.599	1.485	1.852	1.582
0.10	1.932	1.890	1.610	1.398	1.532	1.489	1.865	1.599

Table 1: Adsorption of Metal on Chickoo skin

Pb(II)		Cd(II)		Cu(II)		Hg(II)		
A. Conc.	. ΔA (After A After – adsorp.)	A (AAfter – Abefore)	. ΔA (After adsorp.)	A (AAfter – Abefore)	. ΔA (After adsorp.)	. ΔA (After ABefore)	A (AAfter – adsorp.)	. ΔA (After ABefore)
0.01	1.782	1.732	1.628	1.521	1.618	1.552	1.751	1.641
0.02	1.840	1.742	1.642	1.510	1.757	1.681	1.882	1.659
0.03	1.872	1.750	1.651	1.532	1.810	1.724	1.889	1.671

0.04	1.880	1.755	1.666	1.541	1.834	1.736	1.812	1.613
0.05	1.896	1.759	1.682	1.555	1.855	1.750	1.896	1.691
0.06	1.921	1.780	1.696	1.565	1.876	1.761	1.901	1.711
0.07	1.954	1.792	1.712	1.571	1.900	1.776	1.926	1.731
0.08	1.973	1.810	1.724	1.589	1.926	1.792	1.930	1.752
0.09	1.983	1.830	1.729	1.590	1.954	1.811	1.957	1.772
0.10	1.999	1.890	1.740	1.601	1.989	1.836	1.996	1.789

Table – 3
Values of k and n for different Adsorption Systems

S.N.	Metal ions		k	1/n
1	Orange	Pb(II)	1.1177	0.0321
		Cd(II)	2.1781	0.1142
		Cu(II)	1.8534	0.0493
		Hg(II)	1.8731	0.0327
2	Potato	Pb(II)	1.6699	0.0162
		Cd(II)	1.6782	0.0141
		Cu(II)	1.6018	0.0122
		Hg(II)	1.6220	0.01720
3	Chickoo	Pb(II)	2.4217	0.0422
		Cd(II)	1.9021	0.103
		Cu(II)	1.9212	0.0277
		Hg(II)	1.8118	0.1718
4	Guava	Pb(II)	1.711	0.0156
		Cd(II)	1.8377	0.0576
		Cu(II)	1.8141	0.0281
		Hg(II)	1.6177	0.0396

5	Carrot	Pb(II)	2.0927	0.0136
		Cd(II)	1.7871	0.0213
		Cu(II)	1.7492	0.0246
		Hg(II)	1.9171	0.0099
6	Banana	Pb(II)	1.8713	0.0326
		Cd(II)	1.481	0.0146
		Cu(II)	1.8321	0.0106
		Hg(II)	1.8214	0.0168

REFERENCES

1] Jahagirdar, D. V. and Nigal, J. N. :*Asian J. Chem.*, **9**(1), 122 (1977).

2] Roberts, E. J. and Rowland, S. P. :*Environ. Sci. Tech.*, 7552 (1975).

3] Mastri, M. S., Reuter, F. W. and Priendman, M. S. :*J. Appl. Poly.Sci.*, **18**, 675 (1975).

4] Randall, J. M., Berman, R. L., Gaterette, V. and Waiss, A. C. : *Forestprod J.*, **24**, 80 (1974).

5] Randall, J. M., Hantala, E. : Proc. 30th Industrial Waste Cont., Purdue University, 412 (1975).

6] Randall, J. M., Hantala, E. and Waiss, A. C. :Tschernitizj : Forestprod J., **26**, 46 (1976).

7] Randall, J. M., Reuter, F. W. and Waiss, A. C.: *J. Apply. Poly. Sci.*, **19**, 1663 (1955).

8] Randall, J. M. :*J. Apply. Poly.Sci.*, **2**, 353 (1978).

9] Kumar, P. and Dara, S. S. : Chemical Era, **15**, 20 (1979).

10] Kumar, P., Proger, J. : Water Tech., **13**, 353 (1980).

10a] Kumar, P. :*J. Agric. Waste*, **4**, 213 (1982).

11] Sondawale, P. J.: Ph.D. Thesis in Chemistry submitted to Amravati University, Amravati (January 2000).

12] Low, K. S., Lee, C. K. and Liew, S. C. : Process Bio Chemistry, 36, 1-2, 59-64 (2000).

13] Carolyn A. Burns; Peter J. Casi; Jan H. Harding and Russel J. Crawford: Colloids and Surface A: Physiochemical and Engg. Aspect, **155**, 63-68 (1999).

Effect Of Metal-Ligand Complex On Germination of some vegetable plants

C.M.Deshmukh *C.N.Deshmukh

Shri Shivaji College of Agriculture

Plant physiology will probably also assume an increasingly important role in agricultural research problems. As world population increases, mankind faces enormously complex problems. One of the primary tasks of the future will be to increase food, forage, fiber and wood production substantially throughout the world. Today the application of various chemical salts to soils is a basic feature of agricultural practice.

In the present work, Chalcone(an α,β-dihydroxy Ketone)treatment on Vegetable plant' is selected for study as they have both nutritional as well as medicinal value. Since organic drugs have intense biological activity and since no work is reported on the biological applications of binary complexes of Fe (III) with ligand(chalcone) and comparing with pure ligand, metal and control solution doubly distilled water to study the effect of complex, metal, ligand and control solution on germination survival, seedling height, etc. on Tomato, Chilly,Spanish &Lady finger plants in order to make suggestion whether complex, metal and ligands can be used as plant growth regulators.

The following aspects were studied in laboratory.

1) Estimation of Root / Shoot Ratio in soil & soilless media.

2) Estimation of chlorophyll contents in soil & soilless media.

EXPERIMENTAL:-

The information about the role of metal complexes in biological systems, their concentration and presence in different equilibria is of immense importance. Greshon et. al.[1, 2] reported that the activity of metal chelates is considerably increased as compared to that of the free metal and ligand alone on their complexation. The Shel et. al.[3] and

Shashindharam et. al.[4] observed the antifungal and antibacterial activities of complexes shows that they are more active as compared to free ligand and metal involved.

Rare earth ions are used as probe in bio-chemistry of calcium. Zielinski et. al.[5] showed that, Lanthanide ion could substitute the calcium ion to produce active enzyme system. Some bivalent metal ions have been reported to be useful in agriculture as plant growth regulators. Such a vast uses of lanthanide necessitate concentrating on the study of lanthanides and ligands for studying the germination pattern.

The complexes of transition metal with bis-alkyl thiourea are prepared and their herbicidal and plant growth regulating activity are tested with wheat and cucumbers by Darnall et. al.[6].

Sayed amir et.al.[7] studied effect of some heavy metals on seed germination of canola, wheat, safflower evaluate phytoremedial potential.

K. Abraham et. al.[8] also studied effect of heavy metals on seed germination of archis hypogeae. L

Shivakumar C. K. et. al.[9] also observed the presence of beneficial fungus and effect of copper and zinc metal absorption on growth and metal uptake of legumineous plants as although these metals are required in traces but are important for growth.

A. A. Ramteke et. al.[10] studied the effect of chlorosubstituted pyrrazole and their complexes on spinach at different pH.

C. Aydinalp et. al.[11] also studied heavy metal effect on seed germination and plant growth and alfalfa plant (medicago sativa)

SYNTHESIS OF CHALCONE BY KNOWN METHOD

The chalcone was prepared by known literature method and was confirmed by melting point and also the structure was confirmed by IR spectroscopy as shown in spectra.

Step I: Preparation of p-cresyl acetate from p-cresol
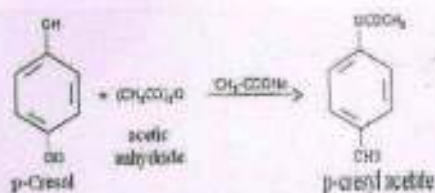
Step II: Preparation of 2-hydroxy-5–methylacetophenone from p-cresyl acetate

Step III: Preparation of chalcone from 2-hydroxy-5-methyl acetophenone
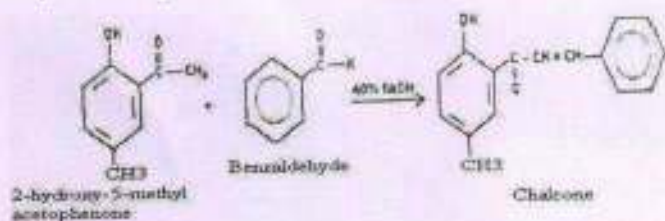
MATERIAL AND EXPERIMENTAL METHODS

- **Metal ions:-**

    The solutions of metal ion in the form of $FeCl_3$ and $MgCl2$ of 0.1 M

concentration were prepared using distilled water and the seeds of tomoto, chilly, Spanish

&lady finger were soaked in both metal solvents.

- **Ligand:-**

    The organic compound was prepared were dissolved in proper solvent and

above seeds are soaked for 2-3 hours.

Metal ion + Ligand:- The mixture of $FeCl_3$ and organic compound (chalcone) and MgCl2 and organic compound (chalcone) were dissolved in the distilled water and seeds are soaked.

Media:- For the germination of the above vegetables seeds, two types of the medias are used.

1) Soil media (media A)

2) Soilless media (media B)

EXPERIMENTS PERFORMED :-

In general practice, various chemicals are used in agricultural as an important ingredient of various pesticides, insecticides, fertilizers, etc. to improve the crop yield. Amongst several economical important plants Chilly ,tomato, Lady finger and Spanich are selected as a plants system. These plants are in ideal systems to study the germination and growth pattern. Further, their economical importance is reflected by its wide use for the dying purposes. The important uses these plants in daily life are persuasive to study its response against metal ion, ligand and its complex regarding to physiological processes; particularly germination is a vital process for the growth of plants. Therefore, these plants are selected as a plant system.

1]Healthy seeds were taken and thoroughly washed using doubly distilled water. Seeds from these healthy seeds of equal size were chosen, immersed in tested solution. These seeds soaked were taken out of each solution.the seeds are sown in germination trays of all medias.

2]Effect of ligand, metal Fe (III), complex and metal Mg (II), complex on chlorophyll in the leaves of vegetables plants were studied.

After sufficient growth, green fresh leaves were collected, as they contain chlorophyll pigments and chlorophyll content was determined spectrophotometrically given by Jahagirdar D. V.[12]

ESTIMATION OF CHLOROPHYLL IN LEAF PIGMENT:-

Procedure:-

Collect the fresh leaves weigh around 1 gm of leaves and cut them into small pieces. Add 5 ml of water and transfer the mixture to a blender. Homogenize the mixture by blending it intermittently for 3-4 minutes.

Take 0.5 ml of homogenous mixture and add 4.5 ml of 80% acetone to it. Thoroughly shake the content, centrifuge it. Collect the supernatant liquid and measure its optical density at 645 and 663 nm.

- ### Parameters:-

Plants growth is decided on the basis of parameters such as percentage of germination survival, seedling height, shoot length, root length (root length / shoot length) and thickness of young leaf having high values compared to control system. The germination was noted after 9 days and 14 days for all Plants.

After noting the survival of the plants, they were taken out of the medias. The seedling height (root length / shoot length) was measured. The average values of these parameters are presented in Table 1

RESULT AND DISCUSSION

Some attempts have been made by Bera et. al.[13] to study the effect of tannery effluent on seed germination, seedling growth and chloroplast pigment content in mungbean. Adhikari et. al.[14] have observed the effect of raw savage water on mustard. Recently Farzin M. Parabia et. al.[15] in their present investigation, effect of ligand, complex and metal ion on percentage seed germination, root length, shoot length (root / shoot ratio) has been studied.

ROOT LENGTH, SHOOT LENGTH AND ROOT / SHOOT RATIO

Germination starts when the seed shows emergence phase of growth, which begins, with penetration of embryo from the seed coat and end with development of root and shoot system. The elongation of shoot axis follows emergence of radical.

The rate and extent of elongation is subjected to a variety of controls, including nutrition, hormones and environmental factors. Though the root and shoot development start within a fraction of time but the further developments may vary according to the nutrients required for the development of root and shoot independently. Therefore, root and shoot length differs from each other.

Table 1:-Effect of Different Treatment on Vegetable Plant in Respect of Parameters in Soil and Soilless Media.

Sr. No.	Parameters	Tomato Soil Soilless		Chilli Soil Soilless		Spanish Soil Soilless		Lady finger Soil Soilless	
1	% Germination	63.6 %	70 %	65.6 %	88.6%	88%	90.4%	46 %	69.8%
2	Seedling Height(cm)	11.98	12.26	4.38	6.54	9.77	10.6	10.27	10.76
3	Shoot Length(cm)	6.44	6.46	2.84	3.86	6.04	6.29	6.69	7.0
4	Root length(cm)	5.52	5.76	1.54	2.68	3.74	4.28	3.58	3.77
5	Shoot/Root Ratio	1.11	1.15	1.84	1.44	1.68	1.50	1.86	1.88

Table 1 clearly indicates that percent germination in soilless medium is higher followed soil media.

Similarly the root length and shoot length which is called as seedling height shows a significant development of root / shoot length i.e. height of seedling highest in chalcone + Mg as compaired to over all the treatments and subsequently followed by chalcone + Fe, metal ion Mg, chalcone and control (d/w) respectively in all cases.

When we compare the performance of all the treatments for different parameters in soil and soilless media. The germination & growth parameters are studied in soil and soilless media. Soilless media shows better performance as against soil media in all the treatments.

Mg is a major constituent for the formation of chlorophyll molecule which helps in the process of photosynthesis for the production of food materials in the plant i.e. sugar synthesis. With combination of chalcone + Mg plays a pinnacle role in keeping all the system working properly. This may be the reason for the better performance.

Fe plays major role in energy transfer within the plants and also brings about chlorophyll development and formation. It is also a constituent of certain enzyme and protein. With the combination of chalcone plays a major role in keeping all the plant system working properly may be the reason for a good performance.

The germination of seed and development of the seedling is better in soilless media than the soil media. Because there is less resistance for the root development and shoot development in soilless media than the soil media may be the reason for better, overall development of the plant.

* **CHLOROPHYLL CONTENT**

Photosynthesis is the process in which the light energy will be converted into chemical energy. There are some basic requirements for the process of photosynthesis as CO_2, H_2O and light energy besides of course, the structural framework of green plant in the form of chloroplast, which is a unique cell having most important role in all the physiological reactions, starting from the absorption of light energy.

Basically, among the smallest group of coordinating pigment molecules necessary to effect a photochemical

act, the most important pigments involved in photosynthesis are chlorophyll and carotenoid.

Table 2-3 clearly shows that absorption of plant leaves is higher at 663 nm in all the treatments. These tables also clearly indicates that the amount of chlorophyll is more in chalcone + Mg. Followed by chalcone + Fe, metal ion Mg, chalcone and control (d/w) in both soil and soilless media.

Obviously the chlorophyll content is highest in chalcone + Mg in both soil and soilless medias. Because of Mg is major constituent for the formation of chlorophyll.

Table 1:-Effect of different treatment on chlorophyll content in respect to soil media

Sr.No.	Nameof vegetable plants	Treatment with Ligand	Treatment with Ligand+Mg	Treatment with Ligand+Fe	Treatment with Metal ion Mg	Treatment with distilled water
1	Tomoto	8.22×10^{-3}	10.162×10^{-3}	8.363×10^{-3}	11×10^{-3}	5.64×10^{-3}
2	Chilli	7.3×10^{-3}	25.83×10^{-3}	24.61×10^{-3}	12.67×10^{-3}	6.22×10^{-3}
3	Spanich	4.71×10^{-3}	7.65×10^{-3}	5.61×10^{-3}	8.09×10^{-3}	4.50×10^{-3}
4	Lady finger	12.7×10^{-3}	32.22×10^{-3}	21.34×10^{-3}	37.50×10^{-3}	7.095×10^{-3}

Table 2:-Effect of different treatment on chlorophyll content in respect to soilless media

Sr.No.	Name of vegetable plants	Treatment with Ligand	Treatment with Ligand+Mg	Treatment with Ligand+Fe	Treatment with Metal ion Mg	Treatment with distilled water
1	Tomoto	11.9×10^{-3}	14.8×10^{-3}	12.5×10^{-3}	19.3×10^{-3}	10.3×10^{-3}
2	Chilli	6.77×10^{-3}	16.37×10^{-3}	9.94×10^{-3}	9.88×10^{-3}	6.01×10^{-3}
3	Spanich	7.41×10^{-3}	8.45×10^{-3}	8.31×10^{-3}	9.93×10^{-3}	5.41×10^{-3}
4	Lady finger	13.13×10^{-3}	36.31×10^{-3}	25.35×10^{-3}	40.49×10^{-3}	7.1×10^{-3}

When we compare the performance of all treatments for different parameters, in soil and soilless Medias. It is clearly observed that soil less media shows better result in respect of germination percentage, development of seedling during the experimental period.

Result of effect of metal ion Mg, Chalcone, Chalcone+ Mg and control (d/W) and chalcone+ fe, on germination, seedling development clearly revels that, Chalcone +Mg shows significant better performance overall the treatments. All the parameters are considered, while finding out the results. In general order in all the parameters performance wise Chalcone+Mg stood first followed by metal ion Mg, Chalcone Chalcone+fe and control (D/W).

The germination and growth parameter are studied in soil and soilless media. The soilless media shows better performance as against the soil media in all the treatments.

Mg is major constituents for the formation of chlorophyll molecule which helps in the process of photosynthesis for the production of food materials in the plants,i.e sugar synthesis.with the combination of Mg chalcone plays a pinnacle role in keeping all the plant system working properly may be the reason for a better performance.

Mg is a secondary importance element essential for the plant growth. Which is also a constituents of many enzyme the detail information about Mg is already mention in the above para. So, keeping in view of all the characteristics of Mg plays a pivotal role for a good performance against the other treatments.

Germination of seed and development of seedling is better in the soilless media than the soil media, because there is less resistance for the root development and shoot development n the soilless media than the soil media, may be the reason for better overall development of the plant.

The analysis perform for finding out the total chlorophyll in green leaves of the plant. The results of analysis clearly indicates that metal ion Mg is having highest chlorophyll content in both soil and soilless media than the remaining treatment like Chalcone+Mg, Chalcone+fe , Chalcone and control (D/W).

REFERENCES

1] Greshon, H; Parmegiani, R., and Nicerson, W. J. : *Appl. Microbiol.*, **10**, 556 (1962).

2] Greshon, H., Parmegiani, R. : *Appl. Microbiol.*, **11**, 62 (1963).

3] Shel, A. M., Shariel, E. A., Gharib, A. and Ammar, Y. A. : *J. Ind.Chem. Soc.*, **60**, 1067 (1968).

4] Shashindharam, P. and Ramchandra, L. K. : *J. Ind. Chem. Soc.*, **62**, 920 (1985).

5] Zielinski, S. Lomosik, L. and Wojclechowska, A. : *Mh. chem.*, **245**, 6484 (1970).

6] Darnell, D. W. and Brinhawn, E. R. : *J. Bio. Chem.*, **245**, 6484 (1970).

7] Sayed Amir et. al. : *J. of Agri. Science, vol (4) No.9, (2012)*

8] K. Abrahm et. al.: peparment of environment of science S. U. University Tirupati.

9] Shivakumar C. K.: *International multidisciplinary research journal vol(2), 06-12,(2012).*

10] A. A. Ramteke et. al.: *J. of chem.. and phrm. Research vol(4) 1889-1894, (2012).*

11] C. Aydinalp et. al.:*Bulgarian J. of Agri. Science 15 (No. 4) 2009, 347-350.*

12] Jahagirdar, D. V. : Experiments in Chemistry, 1st Edition, Himalaya Publishing House (1994).

13] Bera, A. K. and Bokaria, K. : *Envir. Ecol.,* **17**(4), 958 (1999).

14] Adhikari, S., Mitra, A. and Gupta, S. K. : *J. Instr. Publ. Hlth. Engrs.,* India, **2**, 5 (1998).

15] Farzin M. Parabia et al – Current Science, Vol. (9), (2007).

Synthesis, Molecular Modeling, and Biological Evaluation of Novel 1, 3-Diphenyl-2-propen-1-one Based Pyrazolines as Anti-inflammatory Agents

Syed Nasir Abbas Bukhari[1],*, Xin Zhang[2], Ibrahim Jantan[1], Hai-Liang Zhu[2],*, Muhammad Wahab Amjad[1] and Vijay H. Masand[3]

[1]Drug and Herbal Research Centre, Faculty of Pharmacy, Universiti Kebangsaan Malaysia, Jalan Raja Muda Abdul Aziz, 50300 Kuala Lumpur, Malaysia
[2]Institute of Functional Biomolecules, State Key Laboratory of Pharmaceutical Biotechnology, Nanjing University, Nanjing 210093, China
[3]Department of Chemistry, Vidya Bharati Mahavidyalaya, Amravati, Maharashtra 444 602, India
*Corresponding authors: Syed Nasir Abbas Bukhari, snab@ukm.edu.my, snab_hussaini@yahoo.com; Hai-Liang Zhu, zhuhl@nju.edu.cn

A novel series of 1,3-diphenyl-2-propen-1-one (chalcone) derivatives was synthesized by a simple, eco-friendly, and efficient Claisen–Schmidt condensation reaction and used as precursors for the synthesis of new pyrazoline derivatives. All the synthesized compounds were screened for anti-inflammatory related activities such as inhibition of phospholipase A_2 (PLA_2), cyclooxygenases (COX-1 and COX-2), IL-6, and TNF-α. The results of the above studies show that the compounds synthesized are effective inhibitors of above pro-inflammatory enzymes and cytokines. Overall, the results of the studies reveal that the pyrazolines with chlorophenyl substitution (1b–6b) seem to be important for inhibition of enzymes and cytokines. Molecular docking experiments were performed to clarify the molecular aspects of the observed COX-inhibitory activities of the investigated compounds.

Key words: arachidonic acid, chalcones, Claisen–Schmidt condensation, flavonoids, lipopolysaccharides

Phospholipases A_2 (PLA_2) are main enzymes that are responsible for catalyzing the hydrolysis of the ester bond at the sn-2 position of glycerophospholipids. Resulting products of this hydrolysis include fatty-acids such as arachidonic acid (AA); enzymatically, this AA is further metabolized into potent pro-inflammatory mediators known as eicosanoids (prostaglandins, leukotrienes, and thromboxanes). Further, lyso-phospholipids are metabolized by PAF-acetyltransferase producing platelet activating factor (PAF) which is another pro-inflammatory mediator. Controlling or suppressing the production of the lipid mediators is one of the therapeutic strategies owing to the association and the diversity of pathological processes and involvement of lipid mediators in such processes (1).

Biotransformation of arachidonic acid into prostaglandins (PGs) and thromboxanes, which are ultimately responsible for several physiological and pathophysiological responses, is catalyzed by the cyclooxygenase isozymes (COX-1 and COX-2) (2,3). The COX-1 isozyme is responsible for the homeostatic functions such as renal blood flow regulation, initiation of labor pain, protection of the gastric mucosa, and importantly platelet aggregation. Recently, investigations have indicated a possible involvement of the COX-1 in angiogenesis thus justifying the development of new COX-1 inhibitors (4,5), while the COX-2 isozyme is involved in the production of inflammatory PGs, which is responsible for inducing pain, swelling, and fever (6–8). Other than induction of peripheral inflammation, COX-2 isozyme expression is also upregulated in several human cancers including lung, colon, prostate, gastric, hepatocellular, breast, and esophageal carcinomas (9,10).

Pro-inflammation, a widespread unwanted phenomenon, is associated with a variety of diseases including but not limited to, carcinomas and cardiovascular diseases (11–13). IL-6 and TNF-α are pro-inflammatory cytokines, which are involved in the pathogenesis of various inflammatory disorders such as endotoxemia and/or toxic shock syndrome, rheumatoid arthritis (RA), osteoarthritis, inflammatory bowel disease, and psoriasis (14–22). These cytokines play important and widespread vital roles for maintaining the normal cell physiology other than their pro-inflammatory duties. For instance, activation of T cells and other inflammatory cells, secretion of cytokines (such as IL-1, IL-6 and IL-10), and apoptosis induction can be triggered by TNF-α. Nonetheless, an over-expression of TNF-α and IL-6 could lead to the development of various inflammatory disorders and other human diseases. Numerous clinical trials for RA management have shown that targeted inhibition of cytokines, specifically TNF-α, is beneficial. Given all

above, designing, devising, and developing anti-inflammatory agents is one among the eye-catching and attractive targets which could help in inhibition of TNF-α and pro-inflammatory cytokines (23–26).

Flavonoids, either from natural or synthetic sources, have drawn continuous interest due to their abundant biological activities. Among these, chalcones and derived pyrazolines are chemical compounds which have diverse pharmacological activities. Recently, we have reported the summary of biological properties of chalcones (27,28). Although the mechanism of action of chalcone and pyrazoline derivatives have not been understood completely, however, previous studies show that these chemical compounds exert their anti-inflammatory activity partially by modulation of pro-inflammatory gene expression for instance inducible nitric oxide synthase, cyclooxygenase-2, and several other pivotal cytokines (29–32).

As an addition to our continuous search for potential anti-inflammatory drug candidates (33–35) and also due to the diverse biological activities of chalcones and pyrazolines, in this study, novel chalcones and pyrazolines were synthesized. Compounds synthesized were tested *in vitro* for anti-inflammatory activity to evaluate effects on cyclooxygenases and pro-inflammatory cytokines. To clarify the molecular basis of the observed COX-inhibitory activities, molecular docking experiments were employed.

Methods and Materials

Materials
All chemicals and reagents used in this research were of research grade with purity > 98% and used without any further purification unless otherwise mentioned in the text. For a typical work-up, washing with brine was carried out followed by drying the organic layer using anhydrous magnesium sulfate before concentration *in vacuo*. For sPLA$_2$ assay, chemicals included 5,5-dithiobis (2-nitrobenzoic acid) (DTNB), 1,2-bis(heptanoylthio)-phosphatidylcholine,
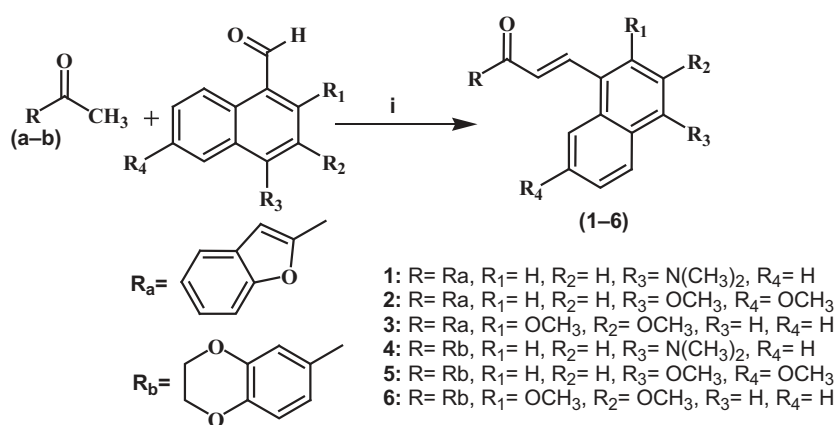
and recombinant human PLA$_2$-V from Cayman Chemicals, Ann Arbor, MI, USA. KCl, CaCl$_2$, and HCl were purchased from Merck, Darmstadt, Germany. A COX Inhibitor Screening kit from Cayman Chemicals was used for cyclooxygenase activity determination. ELISA kits (Cayman) were used for determination of TNF-α and IL-6 in the media using mouse TNF-α (Catalog No. 500850) and mouse IL-6 (Catalog No. 583371).Mouse RAW 264.7 macrophages used in the experiments were obtained from Abcam, UK (Cambridge, UK). Fetal bovine serum (FBS) and other cell culture reagents were purchased from Sigma-Aldrich (Steinheim, Germany). FBS was heat-inactivated for 30 min at 65 °C before preparation of media. LPS was purchased from Sigma and dissolved in PBS, whereas synthetic compounds were dissolved in DMSO.

General procedures
^{1}H and ^{13}C NMR spectra were recorded using a JEOL ECP spectrometer (500 MHz). Me$_4$Si was used as an internal standard, and CDCl$_3$ or DMSO-d$_6$ was employed as a solvent. Electrospray ionization mass spectrometry (ESI-MS) was used for recording the high-resolution mass spectra (HRMS) on Micro TOF-Q mass spectrometer (Bruker, Billerica, MA, USA). Microanalyses data were obtained using an elemental analyzer (Fison EA 1108, Thermo Scientific, Waltham, MA, USA). Perkin Elmer 400 (FTIR, Waltham, MA, USA) spectrometer was used to record infrared spectra by KBr disc method. Silica gel 60 (230–400 mesh) (Merck) was used to perform flash column chromatography, and precoated silica plates (kiesel gel 60 F$_{254}$, BDH) were used for carrying out thin layer chromatography (TLC). Melting points were determined on an electrothermal instrument and are uncorrected. To visualize, compounds were either illumination under ultraviolet (UV) light (254 nm) or vanillin staining was done which followed charring on a hotplate.

Synthesis of chalcone derivatives (1–6)
Synthesis steps of the chalcone derivatives are outlined in the Scheme 1. Briefly, to a 15 mL solution of the

1: R= Ra, R$_1$= H, R$_2$= H, R$_3$= N(CH$_3$)$_2$, R$_4$= H
2: R= Ra, R$_1$= H, R$_2$= H, R$_3$= OCH$_3$, R$_4$= OCH$_3$
3: R= Ra, R$_1$= OCH$_3$, R$_2$= OCH$_3$, R$_3$= H, R$_4$= H
4: R= Rb, R$_1$= H, R$_2$= H, R$_3$= N(CH$_3$)$_2$, R$_4$= H
5: R= Rb, R$_1$= H, R$_2$= H, R$_3$= OCH$_3$, R$_4$= OCH$_3$
6: R= Rb, R$_1$= OCH$_3$, R$_2$= OCH$_3$, R$_3$= H, R$_4$= H

Scheme 1: Structures and synthesis scheme of chalcones derivatives (**1–6**). Reagents and conditions: (i) NaOH, EtOH, room temperature.

respective aldehydes (10 mmol) in ethanol, respective ketones (10 mmol) were added. Reaction mixture was made alkaline by dropwise addition of 50% NaOH solution, and then the reaction mixture was stirred at room temperature (27 °C) for 2–18 h. Reaction completion was monitored by TLC. As an indicator of product formation, appearance of precipitate and color changes of the reaction mixture were observed and recorded. After completion, the reaction mixture was poured into 50 mL of the acidified ice (using concentrated HCl 1 mL). It was extracted using 50 mL ethyl acetate, washed with water (150 mL) followed by drying and concentration *in vacuo* to yield either oils or solids as the reaction product. The products obtained were further purified by recrystallization or using column chromatography.

1-Benzofuran-2-yl-3-(4-dimethylamino-naphthalen-1-yl)-propenone (1)

White powder; yield: 72%; mp: 189–190 °C; R_f = 0.38 (petroleum ether: CH_2Cl_2, 2:1); ^{1}H NMR (500 MHz, CDCl$_3$) δ: 7.87 (s, H), 7.79 (d, J = 8.0 Hz, H), 7.63 (dd, J = 7.5 Hz, H), 7.58–7.52 (m, J = 7.0 Hz, 2H), 7.48–7.44 (m, J = 8.0 Hz, 2H), 7.38 (dd, J = 6.5 Hz, H), 7.24 (t, J = 6.0 Hz, H), 7.19 (d, J = 5.5 Hz, H), 7.10 (d, J = 5.5 Hz, H), 6.92 (d, J = 8.0 Hz, H), 6.72 (d, J = 8.0 Hz, H), 3.89 (s, 6H); ^{13}C NMR (DMSO-d$_6$) δ: 32.5, 32.9, 107.8, 109.1, 113.6, 116.2, 120.8, 121.2, 121.4, 122.5, 122.9, 123.7, 123.9, 126.2, 126.5, 127.4, 127.6, 129.2, 137.5, 148.2, 148.6, 153.6, 182.8. Mass spectrometer (ESI) m/z: 342.18 [M + H]$^+$; microanalysis calculated for $C_{23}H_{19}NO_2$ (341.14): C, 80.92%; H, 5.61%; N, 4.1%. Found C: 80.87%, H: 5.92%, N: 4.48%.

1-Benzofuran-2-yl-3-(4,7-dimethoxy-naphthalen-1-yl)-propenone (2)

White crystals; yield: 64%; mp: 181–182 °C; R_f = 0.36 (petroleum ether: CH_2Cl_2, 2:1); ^{1}H NMR (500 MHz, CDCl$_3$) δ: 7.82 (s, H), 7.75 (d, J = 8.0 Hz, H), 7.69 (d, J = 7.5 Hz, H), 7.55–7.52 (m, J = 7.5 Hz, 2H), 7.47–7.41 (m, J = 8.0 Hz, 2H), 7.37 (d, J = 6.5 Hz, H), 7.27 (dd, J = 5.5 Hz, H), 7.18 (s, H), 6.90 (d, J = 8.0 Hz, H), 6.69 (d, J = 8.0 Hz, H), 3.82 (s, 3H), 3.79 (s, 3H); ^{13}C NMR (DMSO-d$_6$) δ: 52.5, 54.2, 98.7, 98.9, 106.7, 115.9, 116.5, 117.5, 120.2, 121.2, 122.5, 122.6, 122.8, 125.6, 127.6, 129.9, 133.5, 140.7, 154.0, 155.7, 158.9, 160.8, 186.2. Mass spectrometer (ESI) m/z: 359.48 [M + H]$^+$; microanalysis calculated for $C_{23}H_{18}O_4$ (358.39), C, 77.08%; H, 5.06%. Found C: 77.23%, H: 5.26%.

1-Benzofuran-2-yl-3-(2,3-dimethoxy-naphthalen-1-yl)-propenone (3)

White crystals; yield: 61%; mp: 152–153 °C; R_f = 0.31 (petroleum ether: CH_2Cl_2, 2:1); ^{1}H NMR (500 MHz, CDCl$_3$) δ: 7.84 (s, H), 7.68 (d, J = 8.0 Hz, H), 7.61 (d, J = 7.6 Hz, H), 7.54 (d, J = 7.0 Hz, H), 7.48 (d, J = 7.0 Hz, H), 7.32–7.29 (m, J = 8.4 Hz, 4H), 7.17 (s, H), 6.87 (d, J = 8.0 Hz, H), 6.73 (d, J = 7.0 Hz, H), 3.79 (s, 6H); ^{13}C NMR (DMSO-d$_6$) δ: 55.2, 56.3, 102.2, 110.6, 113.2, 116.8, 120.6, 121.8, 122.9, 123.5, 124.4, 124.7, 126.3, 126.5, 129.7, 129.8, 143.5, 146.8, 148.2, 148.8, 155.5, 162.7, 178.9. Mass spectrometer (ESI) m/z: 359.28 [M + H]$^+$; microanalysis calculated for $C_{23}H_{18}O_4$ (358.39), C, 77.08%; H, 5.06%. Found C: 77.43%, H: 5.18%.

### 1-(2,3-Dihydro-benzo[1,4]dioxin-6-yl)-3-(4-dimethylamino-naphthalen-1-yl)-propenone (4)

Pale yellow powder; yield: 49%; mp: 191–192 °C; R_f = 0.29 (petroleum ether: CH_2Cl_2, 2:1); ^{1}H NMR (500 MHz, CDCl$_3$) δ: 7.78 (d, J = 8.5 Hz, H), 7.66 (d, J = 7.0 Hz, H), 7.56 (d, J = 7.3 Hz, H), 7.41 (d, J = 6.0 Hz, H), 7.37–7.31 (m, J = 8.0 Hz, 3H), 7.15 (s, H), 7.12 (d, J = 8.0 Hz, H), 6.82 (d, J = 8.5 Hz, H), 6.61 (d, J = 7.5 Hz, H), 5.12 (m, J = 8.4 Hz, 4H), 3.72 (s, 6H); ^{13}C NMR (DMSO-d$_6$) δ: 32.2, 32.8, 82.2, 82.6, 111.3, 118.2, 119.6, 123.5, 124.3, 126.3, 127.2, 128.2, 128.8, 129.1, 129.5, 132.4, 133.4, 137.3, 146.5, 148.8, 152.4, 154.6, 190.2. Mass spectrometer (ESI) m/z: 382.62 [M + Na]$^+$; microanalysis calculated for $C_{23}H_{21}NO_3$ (359.42), C, 76.86%; H, 5.89%; N, 3.90%. Found C: 77.12%, H: 5.98%, N: 3.98%.

1-(2,3-Dihydro-benzo[1,4]dioxin-6-yl)-3-(2,3-dimethoxy-naphthalen-1-yl)-propenone (5)

Yellow solid; yield: 69%; mp: 193–194 °C; R_f = 0.37 (petroleum ether: CH_2Cl_2, 2:1); ^{1}H NMR (500 MHz, CDCl$_3$) δ: 7.87 (d, J = 8.0 Hz, H), 7.75 (d, J = 8.5 Hz, H), 7.67 (m, J = 6.5 Hz, 2H), 7.52 (s, H), 7.48–7.40 (m, J = 6.5 Hz, 2H), 7.27 (s, H), 6.91 (d, J = 8.0 Hz, H), 6.78 (d, J = 7.5 Hz, H), 5.18 (m, J = 8.0 Hz, 4H), 3.75 (s, 6H); ^{13}C NMR (DMSO-d$_6$) δ: 53.5, 53.9, 72.9, 73.2, 106.5, 114.5, 114.7, 114.8, 120.2, 122.3, 122.6, 123.4, 123.8, 126.5, 126.9, 128.8, 131.2, 142.5, 146.5, 148.8, 149.8, 152.4, 186.8. Mass spectrometer (ESI) m/z: 377.45 [M + H]$^+$; microanalysis calculated for $C_{23}H_{20}O_5$ (376.40), C, 73.39%; H, 5.36%. Found C: 73.41%, H: 5.42%.

1-(2,3-Dihydro-benzo[1,4]dioxin-6-yl)-3-(4,7-dimethoxy-naphthalen-1-yl)-propenone (6)

Yellow powder; yield: 69%; mp: 193–194 °C; R_f = 0.37 (petroleum ether: CH_2Cl_2, 2:1); ^{1}H NMR (500 MHz, CDCl$_3$) δ: 7.80 (d, J = 6.5 Hz, H), 7.79–7.70 (m, J = 7.0 Hz, 2H), 7.59 (s, H), 7.47 (d, J = 8.0 Hz, H), 7.25 (s, H), 7.15 (d, J = 6.0 Hz, H), 7.05 (d, J = 7.0 Hz, H), 6.94 (d, J = 6.5 Hz, H), 6.84 (d, J = 7.0 Hz, H), 5.14 (m, J = 8.2 Hz, 4H), 3.84 (s, 3H), 3.80 (s, 3H); ^{13}C NMR (DMSO-d$_6$) δ: 55.2, 55.9, 74.2, 774.9, 99.5, 99.8, 115.8, 116.5, 120.6, 122.2, 122.8, 123.9, 124.8, 126.5, 127.2, 128.7, 130.2, 142.5, 147.5, 148.5, 149.2, 150.4, 187.2. Mass spectrometer (ESI) m/z: 377.75 [M + H]$^+$; microanalysis calculated
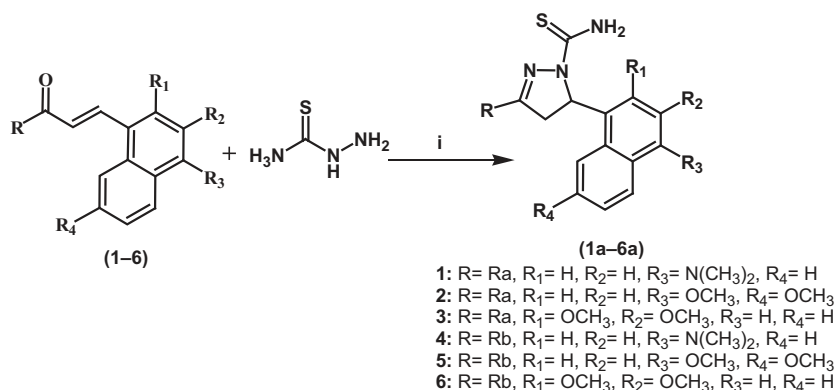
Scheme 2: Synthesis of pyrazoline derivatives (**1a–6a**). Reagents and conditions: (i) NaOH, EtOH, room temperature.

for $C_{23}H_{20}O_5$ (376.40), C, 73.39%; H, 5.36%. Found C: 73.29%, H: 5.39%.

Synthesis of disubstituted-4,5-dihydro-pyrazole-1-carbothioamides (1a–6a)

For a typical synthesis, 5 mmol NaOH solution in 1 mL was added to a mixture of 10 mmol chalcones (**1–6**) and 10 mmol thiosemicarbazide in 50 mL of ethanol under reflux for 10–18 h (Scheme 2). After designated time periods, reaction mixture was transferred onto crushed ice and the solid obtained as a result was filtered, followed by drying, recrystallization from dimethylformamide (DMF) or purification by column chromatography.

3-Benzofuran-2-yl-5-(4-dimethylamino-naphthalen-1-yl)-4,5-dihydro-pyrazole-1-carbothioic acid amide (1a)

White powder; yield: 42%; mp: 229–230 °C; $R_f = 0.48$ (petroleum ether: CH_2Cl_2, 2:1); ^1H NMR (500 MHz, CDCl$_3$) δ: 8.80 (s, D$_2$O exchangeable, 2H, NH$_2$), 7.78–7.30 (m, J = 8.0 Hz, 10H), 7.19 (s, 1H), 5.52–5.47 (dd, J = 12.0 Hz, 1H), 4.21–4.13 (dd, J = 12.0 Hz, 1H), 3.87 (s, 6H), 3.45–3.29 (dd, J = 17.5 Hz, 1H). Mass spectrometer (ESI) m/z: 415.62 [M + H]$^+$; microanalysis calculated for $C_{24}H_{22}N_4OS$ (414.52), C, 69.54%; H, 5.35%; N, 13.52%; S, 7.74%. Found C: 69.63%, H: 5.29%, N: 13.61%, S: 7.79%.

3-Benzofuran-2-yl-5-(4,7-dimethoxy-naphthalen-1-yl)-4,5-dihydro-pyrazole-1-carbothioic acid amide (2a)

White powder; yield: 39%; mp: 234–236 °C; $R_f = 0.43$ (petroleum ether: CH_2Cl_2, 2:1); ^1H NMR (500 MHz, CDCl$_3$) δ: 8.87 (s, D$_2$O exchangeable, 2H, NH$_2$), 7.89–7.29 (m, J = 8.0 Hz, 8H), 7.16 (s, 1H), 6.92 (d, J = 8.0 Hz, 1H), 5.57–5.50 (dd, J = 11.5 Hz, 1H), 4.22–4.19 (dd, J = 11.5 Hz, 1H), 3.85 (s, 6H), 3.47-3.34 (dd, J = 17.5 Hz, 1H). Mass spectrometer (ESI) m/z: 432.52 [M + H]$^+$; microanalysis calculated for $C_{24}H_{21}N_3O_3S$ (431.51), C, 66.80%; H, 4.91%; N, 9.74%; S, 7.43%. Found C: 66.97%, H: 4.98%, N: 9.73%, S: 7.41%.

3-Benzofuran-2-yl-5-(2,3-dimethoxy-naphthalen-1-yl)-4,5-dihydro-pyrazole-1-carbothioic acid amide (3a)

White solid; yield: 51%; mp: 218–220 °C; $R_f = 0.48$ (petroleum ether: CH_2Cl_2, 2:1); ^1H NMR (500 MHz, CDCl$_3$) δ: 8.81 (s, D$_2$O exchangeable, 2H, NH$_2$), 7.73–7.51 (m, J = 8.0 Hz, 9H), 7.19 (s, 1H), 5.48–5.42 (dd, J = 11.5 Hz, 1H), 4.20–4.16 (dd, J = 11.5 Hz, 1H), 3.87 (s, 6H), 3.41–3.35 (dd, J = 16.5 Hz, 1H). Mass spectrometer (ESI) m/z: 432.64 [M + H]$^+$; microanalysis calculated for $C_{24}H_{21}N_3O_3S$ (431.51), C, 66.80%; H, 4.91%; N, 9.74%; S, 7.43%. Found C: 66.85%, H: 4.98%, N: 9.85%, S: 7.48%.

3-(2,3-Dihydro-benzo[1,4]dioxin-6-yl)-5-(4-dimethylamino-naphthalen-1-yl)-4,5-dihydro-pyrazole-1-carbothioic acid amide (4a)

Pale yellow crystals; yield: 49%; mp: 201–202 °C; $R_f = 0.38$ (petroleum ether: CH_2Cl_2, 2:1); ^1H NMR (500 MHz, CDCl$_3$) δ: 8.94 (s, D$_2$O exchangeable, 2H, NH$_2$), 7.82–7.47 (m, J = 6.5 Hz, 8H), 7.12 (s, 1H), 5.42–5.32 (dd, J = 12.0 Hz, 1H), 5.12 (m, J = 8.0 Hz, 4H), 4.22–4.15 (dd, J = 12.0 Hz, 1H), 3.80 (s, 6H), 3.24–3.12 (dd, J = 16.0 Hz, 1H). Mass spectrometer (ESI) m/z: 455.64 [M + Na]$^+$; microanalysis calculated for $C_{24}H_{24}N_4O_2S$ (432.54), C, 66.64%; H, 5.59%; N, 12.95%; S, 7.41%. Found C: 66.68%, H: 5.56%, N: 12.99%, S: 7.43%.

3-(2,3-Dihydro-benzo[1,4]dioxin-6-yl)-5-(2,3-dimethoxy-naphthalen-1-yl)-4,5-dihydro-pyrazole-1-carbothioic acid amide (5a)

White powder; yield: 47%; mp: 222–224 °C; $R_f = 0.41$ (petroleum ether: CH_2Cl_2, 2:1); ^1H NMR (500 MHz, CDCl$_3$) δ: 8.90 (s, D$_2$O exchangeable, 2H, NH$_2$), 7.77–7.52 (m, J = 8.0 Hz, 7H), 7.22 (s, 1H), 5.38–5.30 (dd, J = 12.5 Hz, 1H), 5.17 (m, J = 8.0 Hz, 4H), 4.25–4.12 (dd, J = 12.5 Hz, 1H), 3.92 (s, 6H), 3.32–3.29 (dd, J = 17.0 Hz, 1H). Mass spectrometer (ESI) m/z: 450.48 [M + H]$^+$; microanalysis calculated for $C_{24}H_{23}N_3O_4S$ (449.52), C, 64.13%; H, 5.16%; N, 9.35%; S, 7.13%. Found C: 64.18%, H: 5.19%, N: 9.49%, S: 7.19%.

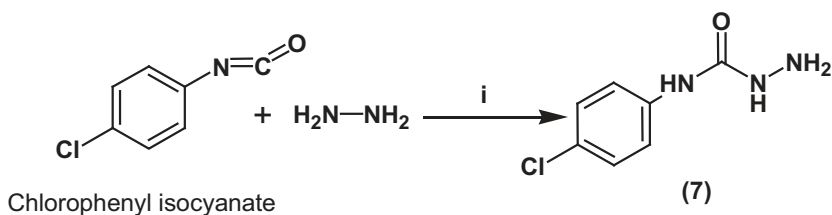**Scheme 3:** Synthesis of 4-chlorophenylsemicarbazide (**7**). Reagents and conditions: (i) NaOH, EtOH, room temperature.

3-(2,3-Dihydro-benzo[1,4]dioxin-6-yl)-5-(4,7-dimethoxy-naphthalen-1-yl)-4,5-dihydro-pyrazole-1-carbothioic acid amide (6a)

White solid; yield: 32%; mp: 227–229 °C; R_f = 0.43 (petroleum ether: CH_2Cl_2, 2:1); ^{1}H NMR (500 MHz, CDCl$_3$) δ: 8.92 (s, D$_2$O exchangeable, 2H, NH$_2$), 7.72–7.48 (m, J = 8.0 Hz, 7H), 7.28 (s, 1H), 5.44–5.28 (dd, J = 12.0 Hz, 1H), 5.09 (m, J = 8.0 Hz, 4H), 4.29–4.14 (dd, J = 12.0 Hz, 1H), 3.85 (s, 6H), 3.24–3.17 (dd, J = 19.0 Hz, 1H). Mass spectrometer (ESI) m/z: 450.74 [M + H]$^+$; microanalysis calculated for C$_{24}$H$_{23}$N$_3$O$_4$S (449.52), C, 64.13%; H, 5.16%; N, 9.35%; S, 7.13%. Found C: 64.15%, H: 5.09%, N: 9.62%, S: 7.19%.

Synthesis of 4-chlorophenylsemicarbazide (7)

For synthesizing pyrazolines (**1b**–**6b**), phenylsemicarbazide with chloro substitution were synthesized by dissolving 4-chlorophenylisocyanate (10 mmol) in diethyl ether followed by drop wise addition of hydrazine (10 mmol) and stirring for 15 min (Scheme 3). The obtained 4-chlorophenylsemicarbazide was filtered, dried, and washed with petroleum ether to get the intermediate product.

Synthesis of trisubstituted-4,5-dihydro-pyrazole-1-carboxamides (1b–6b)

10 mmol chalcone (**1**–**6**) was dissolved in ethanol (10 mL) followed by addition of 4-chlorophenylsemicarbazide (**7**) for

synthesis of trisubstituted-4, 5-dihydro-pyrazole-1-carboxamides (Scheme 4). Following this, 5 mmol NaOH in 1 mL water was added. After the reaction completion (monitored by TLC), the reaction mixture was poured onto ice and the precipitate was filtered, dried, and crystallized using suitable solvent.

3-Benzofuran-2-yl-5-(4-dimethylamino-naphthalen-1-yl)-4,5-dihydro-pyrazole-1-carboxylic acid (4-chloro-phenyl)-amide (1b)

White solid; yield: 42%; mp: 167–169 °C; R_f = 0.22 (petroleum ether: CH_2Cl_2, 2:1); ^{1}H NMR (500 MHz, CDCl$_3$) δ: 8.91 (s, NH), 7.75–7.17 (m, J = 8.0 Hz, 14H), 7.09 (s, 1H), 5.42–5.34 (dd, J = 12.0 Hz, 1H), 4.18–4.12 (dd, J = 12.0 Hz, 1H), 3.82 (s, 6H), 3.22-3.16 (dd, J = 17.5 Hz, 1H). Mass spectrometer (ESI) m/z: 510.13 [M + H]$^+$; microanalysis calculated for C$_{30}$H$_{25}$ClN$_4$O$_2$ (509.00), C, 70.79%; H, 4.95%; N, 11.01%. Found C: 70.83%, H: 4.98%, N: 10.98%.

3-Benzofuran-2-yl-5-(4,7-dimethoxy-naphthalen-1-yl)-4,5-dihydro-pyrazole-1-carboxylic acid (4-chloro-phenyl)-amide (2b)

White powder; yield: 61%; mp: 211–213 °C; R_f = 0.29 (petroleum ether: CH_2Cl_2, 2:1); ^{1}H NMR (500 MHz, CDCl$_3$) δ: 8.92 (s, NH), 7.71–7.17 (m, J = 8.5 Hz, 12H), 7.05 (s, 1H), 6.95 (d, J = 7.0 Hz, 1H), 5.27–5.12 (dd, J = 10.5 Hz, 1H), 4.17–4.10 (dd, J = 10.5 Hz, 1H), 3.78 (s, 6H), 3.42–3.28 (dd, J = 18.0 Hz, 1H). Mass spectrometer
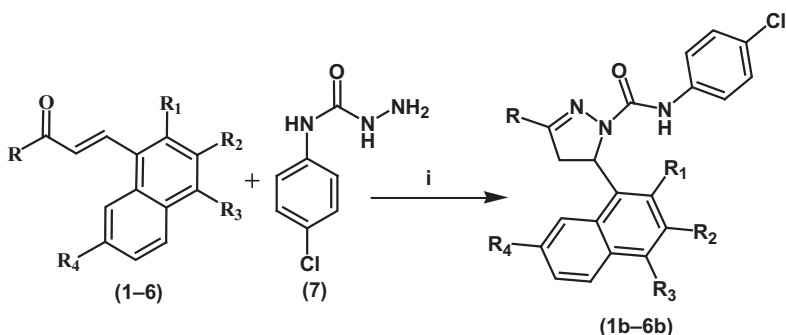
Scheme 4: Synthesis of pyrazoline derivatives (**1b**–**6b**). Reagents and conditions: (i) NaOH, EtOH, room temperature.

1: R= Ra, R$_1$= H, R$_2$= H, R$_3$= N(CH$_3$)$_2$, R$_4$= H
2: R= Ra, R$_1$= H, R$_2$= H, R$_3$= OCH$_3$, R$_4$= OCH$_3$
3: R= Ra, R$_1$= OCH$_3$, R$_2$= OCH$_3$, R$_3$= H, R$_4$= H
4: R= Rb, R$_1$= H, R$_2$= H, R$_3$= N(CH$_3$)$_2$, R$_4$= H
5: R= Rb, R$_1$= H, R$_2$= H, R$_3$= OCH$_3$, R$_4$= OCH$_3$
6: R= Rb, R$_1$= OCH$_3$, R$_2$= OCH$_3$, R$_3$= H, R$_4$= H

(ESI) m/z: 548.97 [M + Na]$^+$; microanalysis calculated for $C_{30}H_{24}ClN_3O_4$ (525.98), C, 68.50%; H, 4.60%; N, 7.99%. Found C: 68.52%, H: 4.63%, N: 7.97%.

3-Benzofuran-2-yl-5-(2,3-dimethoxy-naphthalen-1-yl)-4,5-dihydro-pyrazole-1-carboxylic acid (4-chloro-phenyl)-amide (3b)

White powder; yield: 37%; mp: 191–193 °C; R_f = 0.26 (petroleum ether: CH_2Cl_2, 2:1); ^{1}H NMR (500 MHz, CDCl$_3$) δ: 8.94 (s, NH), 7.81–7.34 (m, J = 8.5 Hz, 13H), 7.13 (s, 1H), 5.52–5.37 (dd, J = 11.0 Hz, 1H), 4.24–4.11 (dd, J = 11.0 Hz, 1H), 3.80 (s, 6H), 3.38–3.16 (dd, J = 17.0 Hz, 1H). Mass spectrometer (ESI) m/z: 527.11 [M + H]$^+$; microanalysis calculated for $C_{30}H_{24}ClN_3O_4$ (525.98), C, 68.50%; H, 4.60%; N, 7.99%. Found C: 68.48%, H: 4.62%, N: 7.94%.

3-(2,3-Dihydro-benzo[1,4]dioxin-6-yl)-5-(4-dimethylamino-naphthalen-1-yl)-4,5-dihydro-pyrazole-1-carboxylic acid (4-chloro-phenyl)-amide (4b)

Yellow powder; yield: 42%; mp: 167–168 °C; R_f = 0.21 (petroleum ether: CH_2Cl_2, 2:1); ^{1}H NMR (500 MHz, CDCl$_3$) δ: 8.94 (s, NH), 7.80–7.27 (m, J = 8.0 Hz, 12H), 7.15 (s, 1H), 5.36–5.27 (dd, J = 12.5 Hz, 1H), 5.11 (m, J = 8.0 Hz, 4H), 4.28–4.16 (dd, J = 12.5 Hz, 1H), 3.86 (s, 6H), 3.33–3.19 (dd, J = 16.0 Hz, 1H). Mass spectrometer (ESI) m/z: 528.05 [M + H]$^+$; microanalysis calculated for $C_{30}H_{27}ClN_4O_3$ (527.01), C, 68.37%; H, 5.16%; N, 10.63%. Found C: 68.39%, H: 5.14%, N: 10.68%.

3-(2,3-Dihydro-benzo[1,4]dioxin-6-yl)-5-(2,3-dimethoxy-naphthalen-1-yl)-4,5-dihydro-pyrazole-1-carboxylic acid (4-chloro-phenyl)-amide (5b)

White powder; yield: 38%; mp: 189–91 °C; R_f = 0.23 (petroleum ether: CH_2Cl_2, 2:1); ^{1}H NMR (500 MHz, CDCl$_3$) δ: 8.91 (s, NH), 7.73–7.30 (m, J = 8.0 Hz, 11H), 7.17 (s, 1H), 5.49–5.41 (dd, J = 11.0 Hz, 1H), 5.15 (m, J = 8.5 Hz, 4H), 4.28-4.09 (dd, J = 11.0 Hz, 1H), 3.88 (s, 6H), 3.39-3.24 (dd, J = 17.5 Hz, 1H). Mass spectrometer (ESI) m/z: 545.12 [M + H]$^+$; microanalysis calculated for $C_{30}H_{26}ClN_3O_5$ (544.00), C, 66.24%; H, 4.82%; N, 7.72%. Found C: 66.28%, H: 4.88%, N: 7.71%.

3-(2,3-Dihydro-benzo[1,4]dioxin-6-yl)-5-(4,7-dimethoxy-naphthalen-1-yl)-4,5-dihydro-pyrazole-1-carboxylic acid (4-chloro-phenyl)-amide (6b)

White powder; yield: 51%; mp: 227–229 °C; R_f = 0.31 (petroleum ether: CH_2Cl_2, 2:1); ^{1}H NMR (500 MHz, CDCl$_3$) δ: 8.97 (s, NH), 7.92–7.38 (m, J = 8.0 Hz, 11H), 7.11 (s, 1H), 5.42–5.27 (dd, J = 12.5 Hz, 1H), 5.12 (m, J = 8.5 Hz, 4H), 4.28–4.24 (dd, J = 12.5 Hz, 1H), 3.81 (s, 6H), 3.21–3.17 (dd, J = 17.5 Hz, 1H). Mass spectrometer (ESI) m/z: 544.97 [M + H]$^+$; microanalysis calculated for $C_{30}H_{26}ClN_3O_5$ (544.00), C, 66.24%; H, 4.82%; N, 7.72%. Found C: 66.27%, H: 4.88%, N: 7.91%.

Secretory phospholipase A$_2$-V (sPLA$_2$-V) activity assay

Human recombinant sPLA$_2$-V was used as an enzyme source. Based on the Ellman's method (36), activity of sPLA$_2$ enzyme was determined by a photometric assay. Briefly, sn-2ester bond of the substrate 1,2-bis(heptanoylthio)-glycerophosphocholine was hydrolyzed by PLA$_2$-V followed by the exposure of free thiols. These thiols activated the conversion of DTNB (5,5–dithio-bis-(2-nitrobenzoic acid) to 2-nitro-5-thiobenzoic acid, which was photometrically detected at 405 nm. After this, the assay proceeded in an aqueous buffer solution (pH 7.5) containing KCl (94 mM), CaCl$_2$ (9 mM), Tris (24 mM), and Triton-X 100 (280 BM). Before the assay was started, substrate and PLA$_2$-V was resuspended in assay buffer whereas DTNB was dissolved in an aqueous solution of Tris-HCl (pH 8) yielding an enzyme and DTNB concentrations of 100 ng/mL and 87 BM, respectively. 96-well micro titre plates containing substrate solution, DTNB, and the respective test substance were used to carry out assays at room temperature. For obtaining positive control, values substrate was added to plates with enzyme only. DMSO was used as a negative control, as it was inactive at the tested concentration in the assay (1.7% v/v).

Cyclooxygenase assay

COX Inhibitor Screening kit (Catalog No 560131) from Cayman Chemicals was used to determine the effects of the test compounds on COX-1 and COX-2 by quantifying prostaglandin E$_2$ (PGE$_2$). 100 mM Tris–HCl buffer, pH 8.0 containing 1 μM heme and COX-1 (ovine) or COX-2 (human recombinant), which was preincubated for 10 min in a water bath at 37 °C was used for reaction mixture preparation. Addition of 10 μL arachidonic acid to the reaction mixture (final concentration 100 μM) was used to initiate reaction. After 2 min reaction was stopped by addition of 1 M HCl. PGE$_2$ in the reaction mixture was determined using ELISA method. 100 mM potassium phosphate buffer (pH 7.4) was used to dilute the DMSO stock solutions of the test compounds to the desired concentration. This reaction mixture was transferred to a 96-well plate that was precoated with a mouse anti-rabbit IgG. Tracer prostaglandin acetylcholine esterase and primary antibody (mouse anti PGE$_2$) were also added to the plates followed by overnight incubation at room temperature. After overnight incubation, reaction mixtures were pipetted out and the wells were washed with 10 mM potassium phosphate buffer containing 0.05% Tween 20. After washing, 200 μL of Ellman's reagent was added to each well and the plates

Table 1: Inhibition of secretory phospholipase A$_2$-V (sPLA$_2$-V), COX-1 and COX-2 activities by synthetic compounds and their Cox-1(PDB code:1EQG) and Cox-2(PDB code: 3Q7D) docking score

Compound	sPLA$_2$-V IC$_{50}$ (μM)	COX-1 IC$_{50}$ (μM)	COX-2 IC$_{50}$ (μM)	Binding enegryΔG[b] COX-1	COX-2
1	45.22 ± 2.61	9.27 ± 1.51	25.53 ± 2.22	−37.89621	−29.4732
2	27.83 ± 1.42	14.99 ± 0.15	19.14 ± 1.52	−37.2338	−35.8670
3	12.72 ± 1.29	12.46 ± 0.08	12.24 ± 0.42	−33.8103	−42.7698
4	32.21 ± 1.91	7.06 ± 0.34	24.48 ± 1.72	−33.0058	−30.5245
5	22.78 ± 2.21	11.14 ± 1.68	18.48 ± 1.91	−29.9782	−36.5263
6	19.10 ± 2.73	8.22 ± 0.89	12.45 ± 1.40	−39.4566	−42.5523
1a	35.44 ± 3.92	4.53 ± 0.12	14.55 ± 1.78	−38.4338	−40.4554
2a	21.13 ± 1.75	7.22 ± 2.77	12.32 ± 1.89	−38.0386	−42.6865
3a	9.17 ± 1.02	8.06 ± 0.27	10.28 ± 1.61	−39.8495	−44.7298
4a	22.24 ± 0.13	1.12 ± 0.55	13.17 ± 1.99	−46.6357	−41.8345
5a	19.17 ± 3.42	3.42 ± 0.32	17.79 ± 2.06	−40.9794	−37.2143
6a	7.12 ± 1.54	2.82 ± 0.22	12.55 ± 0.28	−40.8135	−42.4512
1b	22.19 ± 1.82	1.87 ± 0.51	9.10 ± 1.12	−50.7175	−45.9235
2b	14.55 ± 1.52	2.14 ± 0.24	11.07 ± 1.67	−40.3426	−43.9378
3b	8.46 ± 2.20	0.99 ± 0.05	5.02 ± 2.35	−52.2044	−49.9890
4b	17.16 ± 1.76	0.44 ± 0.25	9.72 ± 2.45	−52.3508	−45.2812
5b	17.32 ± 0.14	1.17 ± 0.65	12.32 ± 1.89	−50.7175	−42.6890
6b	5.12 ± 0.55	0.94 ± 0.85	11.95 ± 1.35	−48.2068	−43.0565
Dexamethasone	0.62 ± 0.09	–	–	–	–
Indomethacin[a]	–	0.22 ± 0.05	3.44 ± 0.27	–	–

NDGA, Nordihydroguaiaretic acid.
Values are the mean ± SD; n = 3.
[a]30 μM concentration.
[b](kcal/mol).

were incubated at room temperature protected from light for 60 min or until the control wells yielded an OD = 0.3–0.8 at 412 nm. PGE$_2$standard curve was generated using same plate and later used to quantify the PGE$_2$ levels produced in the presence of test samples. Results of the assay were expressed as a percentage relative to a control (solvent treated samples). All the measurements were recorded in triplicate, and values were generally within 10%.

Cell treatment and ELISA assay for TNF-α and IL-6

Mouse RAW 264.7 macrophages were propagated and maintained in DMEM media, which was supplemented with 10% FBS, 100 U/mL penicillin, and 100 μg/mL streptomycin at 37 °C in 5% CO$_2$ environment. As discussed earlier, cells were pretreated with synthetic compounds or vehicle control for 2 h followed by treatment with LPS (0.5 μg/mL) for 22 h. After completion of the treatment period, the culture media and cells were collected separately. Culture media from the previous step was centrifuged for 10 min at 105 × g. Supernatant following centrifugation was stored at −80 °C until use. On the other hand, cells were washed with PBS, harvested, and lysed with cell lysis buffer (Tris–HCl 20 mM, NP40 1%, NaCl 150 mM, EDTA 2 mM, Na3VO4 200 mM, SDS 0.1%, NaF 20 mM). The cell mix in lysis buffer was shaken vigorously for 10 min at 0 °C. After lysis step, mixture was centrifuged at 15 000 × g for 30 min at 4 °C, the total protein content was determined by Bio-Rad (Hercules, CA, USA) protein assay reagents. For expressing results,

inflammatory factors in the media were normalized to the total protein content present in the viable cells.

Molecular modeling details

Automated docking studies were carried out using Discovery Studio (version 3.5, Accelrys, San Diego, CA, USA) as implemented through the graphical user interface DS-C Docker protocol. The three-dimensional structures of the aforementioned compounds were constructed using Chem. 3D ultra 11.0 software [Chemical Structure Drawing Standard; Cambridge Soft Corporation, Cambridge, MA, USA], then they were energetically minimized using MOPAC with 100 iterations and minimum RMS gradient of 0.10. The Gasteiger–Hückel charges of ligands were assigned. The crystal structures of COX-1 and COX-2 (PDB code: 1EQG and 3Q7D, respectively) complex were retrieved from the RCSB Protein Data Bank (http://www.rcsb.org/pdb/home/home.do). These pdb contain the drug bound to the receptor. All bound water and ligands were eliminated from the protein and the polar hydrogens, and the Kollman-united charges were added to the proteins.

Statistical analysis

All the experiments were conducted thrice and data represented as the mean ± standard error of mean (SEM). Graph Pad Prism 5 software was used for calculating the IC$_{50}$ values. One-way analysis of variance (ANOVA) for multiple comparisons was used for analyzing data where $p < 0.05$ was considered to be statistically significant.

Results and Discussion

Chemistry

Synthesis of all the compounds was carried out as outlined in Schemes 1–4. Claisen–Schmidt condensation reaction was employed to prepare chalcones (**1**–**6**) where equimolar aldehydes and ketones were reacted in the presence of a base. Whereas chalcones (**1**–**6**) and thiosemicarbazide were refluxed in the presence of alkaline medium to get pyrazolines (**1a**–**6a**). Compounds (**1b**–**6b**) were also synthesized by a similar reaction by refluxing chalcones (**1**–**6**) with N-(4-chlorophenyl) semicarbazide (**7**) in alkaline medium. Column chromatography and crystallization techniques were used for the purification of all synthesized compounds. Thin layer chromatography (TLC) was used to check the purity of the compounds routinely using precoated silica plates. Analytical techniques including IR, ^{1}H NMR, ^{13}C NMR, MS, and elemental analysis were used to confirm synthesis of the all the new compounds.

Inhibition of secretory phospholipase A_2-V

One among the important strategies to prevent inflammation is the inhibition of PLA_2. Table 1 lists the results obtained for all synthesized compounds for their inhibitory potential against $sPLA_2$ at concentrations of 1.25–20 μg/mL using an in vitro enzymatic photometric assay based on Ellman's method (36). In this assay, dexamethasone was used as positive control. Curcumins, chalcone derivatives (compounds bearing α, β-unsaturated carbonyl group) and other compounds which bear a pyrazoline moiety decrease $sPLA_2$ activities as shown by a number of studies carried out previously on the $sPLA_2$ isoform activities which also show that more than 70% homology was

seen among various isoforms of PLA_2 enzymes (37–39). As represented in Figure 1, a strong dose dependent inhibition of $sPLA_2$-V was shown by compounds **3**, **3a**, **6a**, **2b**, **3b**, and **6b**. IC_{50} values for all the compounds were in the range of 5.12–14.55 μM. Among all the compounds, a pyrazoline derivative **6b** showed strongest inhibition of $sPLA_2$-V with IC_{50} 5.12 μM.

Inhibition of COX-1 and COX-2

COX1 and COX2 are two isoforms of cyclooxygenase. One mechanism for anti-inflammatory action is the inhibition of the enzymes COX-1 and COX-2. The inhibitory activities of chalcone and pyrazoline derivatives on the cyclooxygenase was evaluated using the COX-inhibitor screening assay kit in vitro (37). All the compounds were tested at a concentration of 40 μg/mL for both isoforms of, that is, COX-1 and COX-2. Calculated IC_{50} values are exhibited in the Table 1. Results indicate that the newly synthesized compounds have an affinity towards COX-1. Results show that six compounds (**4a**, **1b**, **3b**, **4b**, **5b**, and **6b**) exhibited strong inhibition of COX-1 activity ranging from 82.76 to 94.44%. Indomethacin was a positive control. It was observed that majority of compounds show a better COX-1 inhibitory activity with IC_{50} values ranging from 0.44 to 3.42 μM. Similar to $sPLA_2$ inhibitory activity, strongest COX-1 inhibition was shown by a pyrazoline derivative **4b**.

In previously carried out studies, a selective COX-1 inhibitor showed an equipotent inhibition of PG formation in an inflammatory exudate to the COX-2 selective inhibitor celecoxib. However, this selective COX-1 inhibitor was ineffective in reducing increased PG levels in the cerebrospinal fluid, where non-selective COX-1/COX-2 inhibition turned out to be more effective in reducing signs of inflammation
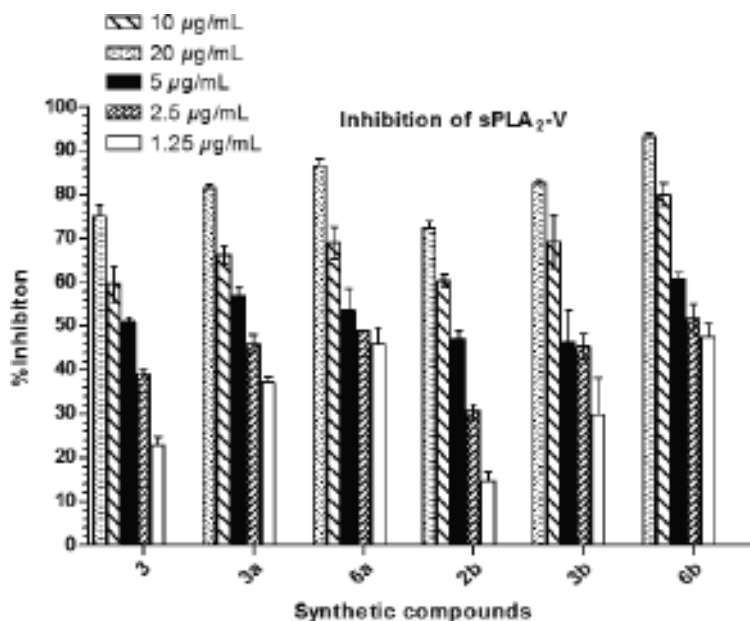

Figure 1: Concentration dependent inhibitory effects of chalcones and pyrazolines on activity of secretory phospholipase A2-V. Graph represents the % inhibition by most active compounds at different concentrations. The data shown are an average of three independent experiment and values are mean ± SD.

(40,41). Based on this and coupled with other data it could be suggested that COX-1 and COX-2 functions are not as simple as anticipated earlier and it might be a controlled by contribution from multiple other factors. It is previously known that inhibition of production of prostaglandins in inflammatory exudates could be associated with COX-1 inhibition. For that reason, a non-selective or combined COX-1 and COX-2 inhibition could turn out to be a better and efficient inhibition strategy for chronic inflammation compared to a selective inhibition of either COX-1 or COX-2.

As stated earlier that the synthesized compounds had a better affinity in suppressing the activity of COX-1 compared to COX-2. Thirteen compounds (**3**, **6**, **1a**–**4a**, **6a**, and **1b**–**6b**) demonstrated IC_{50} values <15 μM for COX-2 inhibition. Among all the compounds, the highest COX-2 inhibition was exhibited by compound **3b** which had an IC_{50} value of 5.02 μM. Similar to phospholipase inhibition, a dose dependent COX inhibition was observed; an increased inhibitory activity of compounds with increase in the concentration. Based on the results of present investigations, it may be suggested that pyrazoline derivatives could serve as COX inhibitors and show anti-inflammatory effects.

Inhibition of TNF-α and IL-6 release in LPS-stimulated macrophages

Lipopolysaccharide (LPS) is present in the outer membrane of Gram-negative bacteria, and it is an important structural component of the membrane. It is one among the well studied immunostimulators and induces a systemic inflammation response (42). Further LPS, induces the expression of pro-inflammatory cytokines, such as TNF-α and IL-6. In the present study, we evaluated the inhibitory abilities of chalcones and derived pyrazoline derivatives in mouse RAW 267 macrophages against LPS-induced TNF-α and IL-6 release. For determination of TNF-α and IL-6, the macrophages were pretreated with 10 μM compounds for 2 h followed by incubation with 0.5 μg/mL LPS for 22 h. An enzyme-linked immunosorbent assay (ELISA) was used for determination of the amount of TNF-α and IL-6 in media after normalization of the protein concentration of harvested cells from culture plates.

Figure 2 illustrates the results of the anti-inflammatory assay of tested compounds. All the compounds inhibited LPS-induced TNF-α and IL-6 expression to various degrees. Among 18 compounds tested, highest inhibition of LPS-induced TNF-α expression was shown by compounds (**1b**–**6b**) with percentage inhibition ranging from 62 to 88%. Whereas strong inhibitory effects against IL-6 release were shown by compounds **3a**, **6a**, and **2b**–**6b** as compared to the LPS-control (62–83%). Among all, compounds **3b** and **6b**, turned out to be the most potent inhibitors of LPS-induced TNF-α and IL-6 release with inhibition as high as 91% compared to the LPS-control.

Structure–activity relationship analysis of chalcone and pyrazoline derivatives

Inhibitory effects of the newly synthesized chalcone and pyrazoline derivatives on $sPLA_2$, COX (Table 1) and on
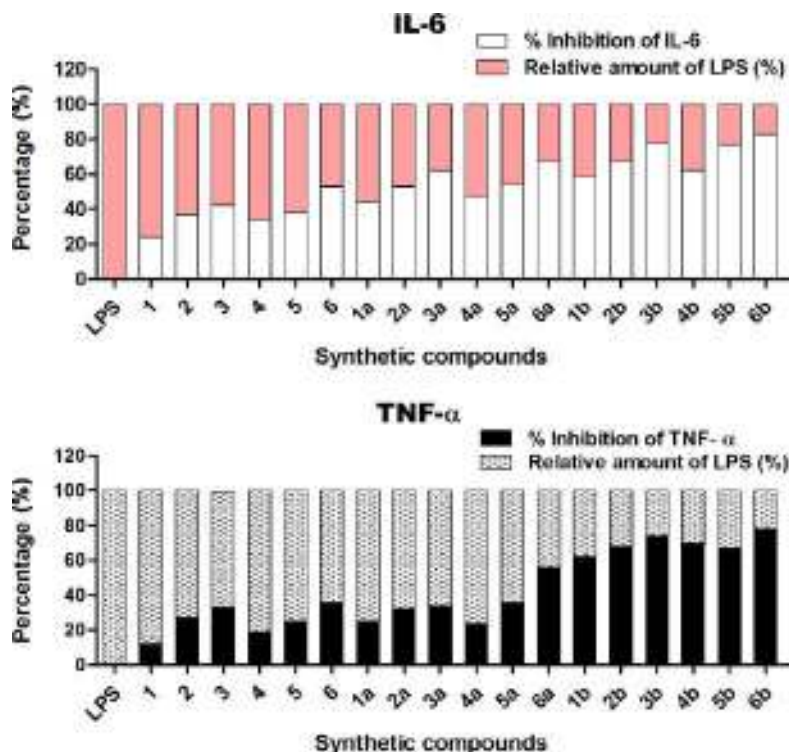

Figure 2: Chalcone derivatives and derived pyrazolines inhibited LPS-induced TNF-α and IL-6 secretion in RAW 264.7 macrophages. The results are expressed as percent of LPS control. Each bar represents mean ± SE of three independent experiments.

release of TNF-α and IL-6 (Figure 2) were evaluated. As discussed earlier, compounds **6a** and **6b** were the strongest inhibitor of secretory phospholipase A$_2$ as analysis of results along structure–activity relationship (SAR) indicate. Analysis of the results also shown that among chalcone derivatives evaluated (**1**–**6**) for inhibitory activity of sPLA$_2$, only compound **3** showed good inhibition with IC$_{50}$ value 12.72 μM. On the other hand, compound **3a** and **6a** among the 2-pyrazoline-1-carbothioamide derivatives (**1a**–**6a**) exhibited potent inhibitory activity while compound **3b** and **6b** in the series of 2-pyrazoline-1-carboxamide derivatives were the most potent inhibitors of sPLA$_2$. It leads us to suggest an interesting and notable structure–activity relationship (SAR) for these six compounds (**3**, **3a**–**b**, **6**, and **6a**–**b**), all of which bear 2,3-dimethoxy substitution pattern on naphthalene ring.

So from results, it can be observed that a comparative SAR can be carried out for chalcones and pyrazoline derivatives based upon various inhibitory activities such as COX-1, COX-2, IL-6, and TNF-α. Further, as results in Table 1 and Figure 2 show, it can be seen that highest anti-inflammatory activities were exhibited by 2-pyrazoline-1-carboxamide derivatives (**1b**–**6b**) among all newly synthesized compounds, whereas 2-pyrazoline-1-carbothioamide derivatives (**1a**–**6a**) have lesser inhibitory powers as compared to 2-pyrazoline-1-carboxamide derivatives. On the other hand, except compound **4**, all the 1,3-diphenyl-2-propen-1-one derivatives were observed to be poor inhibitors. It could be implied that anti-inflammatory activity of pyrazoline derivatives was augmented with carbothioamide moieties compared to chalcone derivatives. However, if the chlorophenyl moiety in the pyrazoline is substituted with carboxamide moiety, a more powerful inhibitor than pyrazoline derivatives with carbothioamide moieties could be obtained.

From the SAR, it can be observed that the presence of benzodioxane ring attached to an aromatic ring makes the
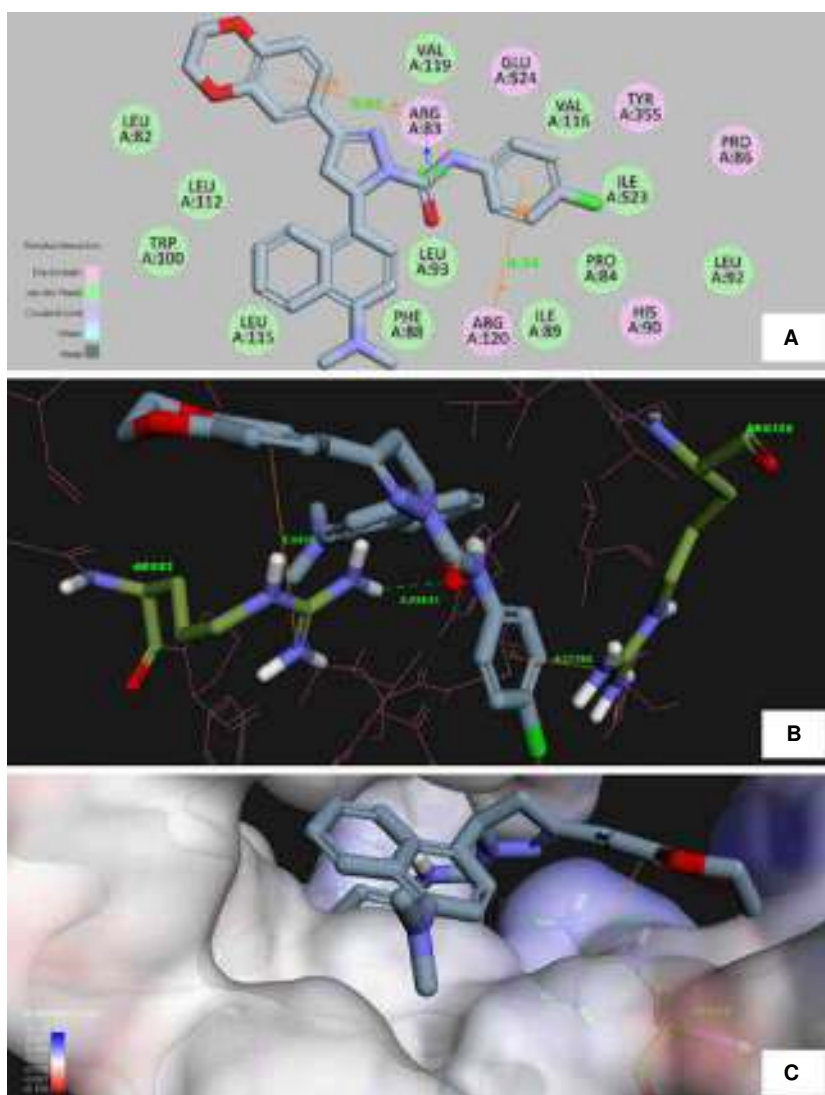

Figure 3: Compound 4b with COX-1 (1EQG.pdb) docking pose, (a) 2D image (b) 3D image (c) small molecule inserting active pocket surface image.

compounds more active than those with benzofuran ring. This can be seen, as compounds **4a**, **5a**, and **6a** show comparatively stronger inhibition of COX-1, IL-6, and TNF-α than compounds **1a**, **2a**, and **3a** which contain furan rings in their structure. Similarly, compounds which have benzodioxane ring system (**4b**, **5b**, and **6b**) were found more active for inhibition of COX-1, IL-6, and TNF-α than compounds with benzofuran ring system (**1b**, **2b**, and **3b**), although all these compounds have 2-pyrazoline-1-carboxamide as a linker. However, scenario is different in case of COX-2 inhibitory activity as compound **3b**, the most active COX-2 inhibitor, has a furan ring system compared to a benzodioxane ring system. Similarly, compound **3a**, which contains benzofuran ring system in its structure, was found to have good inhibitory activities among 2-pyrazoline-1-carbo-

thioamide derivatives (**1a–6a**). Previously, a study by Daukshas *et al.* (43) reported the importance of 1,4-dioxane ring for anti-inflammatory activity of synthesized (diaryl ketones) compounds.

Furthermore, it was observed that substitution of methoxy group at position 2 and 3 of naphthalene ring show strong anti-inflammatory properties compared to when the methoxy group is present at position 4 and 7. It was also seen from the SAR that 4-dimethylamino played an important role in COX-1 inhibition as strongest inhibitors of COX-1 among 2-pyrazoline-1-carbothioamide derivatives (**1a–6a**) were compound **4b** ($IC_{50} = 0.44$ μM) and 4a. It was reported by Tsai *et al.* (44) previously that substitution of the 4-dimethylamino on compounds results in a potent activity against the COX-2 and amyloid-β aggregation,
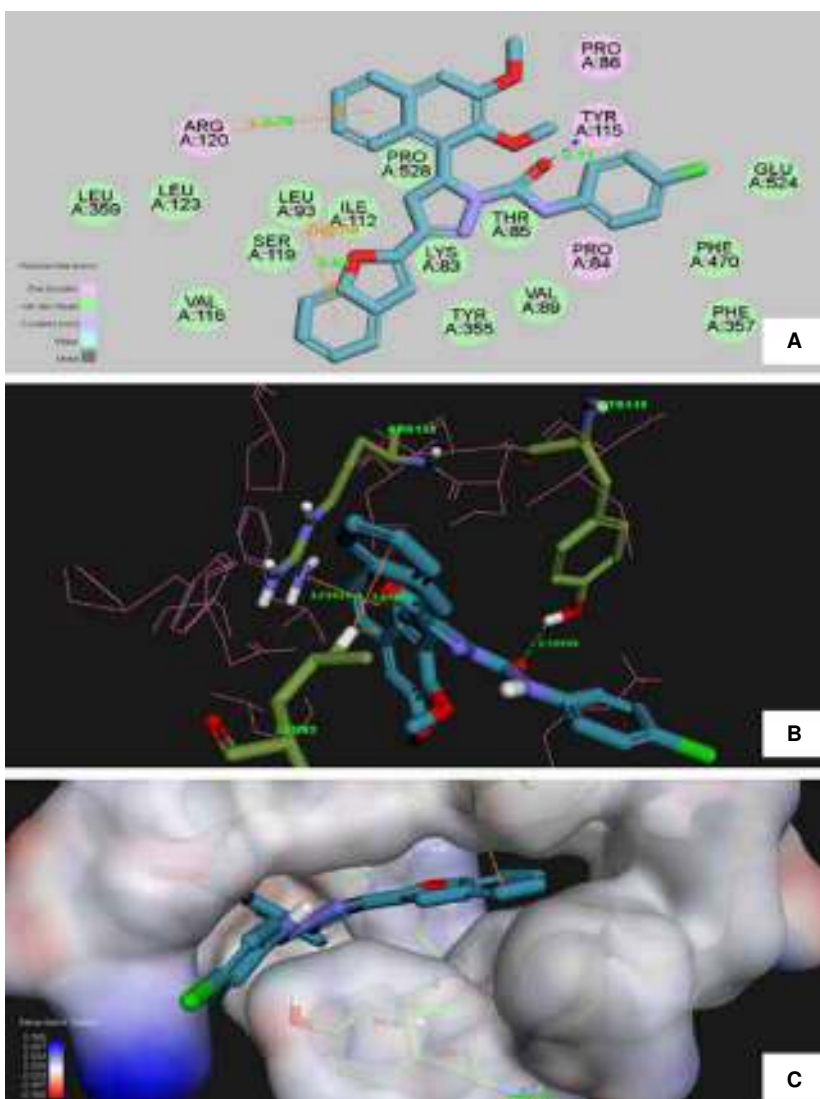

Figure 4: Compound 3b with Cox-2 (3Q7D.pdb) docking pose, (a) 2D image (b) 3D image (c) small molecule inserting active pocket surface image.

which is one of the mediators of neuro-inflammation in Alzheimer's disease.

An interesting finding among the all studies performed was the synergistic effect of some of compounds as one of pyrazoline derivative (**3b**) showed the strong inhibition of COX-1, COX-2, sPLA$_2$, and pro-inflammatory cytokines. Such kind of compounds can be very ideal candidates for the development of anti-inflammatory agents, so further research on other parameters is required to understand the mechanisms involved in the role of such compounds.

Docking studies

Docking analysis was performed for all the compounds, for the sake of convenience, docking analysis for 4b and 3b, as representatives, are reported. The binding energy of all compounds is listed in Table 1. Of the compounds studied, compound **4b** was nicely bound into the active site of Cox-2 with minimum binding energy ($\Delta G_b = -52.3508$ kcal/mol) and compound **3b** was bound into the active site of Cox-2 with binding energy $\Delta G_b = -49.9890$ kcal/mol. Compound **4b** was evaluated by molecular docking based on the binding model of the COX-1 complex structure (1EQG.pdb) (45). As shown in the Figure 3A,B, the 2D- and 3D images of the binding mode between compound **4b** and the target protein were clearly demonstrated. Figure 3C shows the small molecule was well inserted into the active pocket of the COX-1 protein. The binding mode of the most potent compound **4b** in the active pocket could be stabilized by several molecular interactions (Figure 3A,B) discussed as follows. The compound **4b** adopts bent 'T' shape in the active site of COX-1 with prominent interactions with polar ARG83, and ARG120. With rest of the residues from active site, the interactions are van der Waals forces and hydrophobic in nature. One *Cation–Pi* interaction with the length of 5.5075 Å was displayed between the benzdioxan ring of compound **4b** and the N atom of ARG83. Another *Cation–Pi* interaction can also be observed between the aniline ring of compound **4b** and the N atom of ARG120 with the length of 4.37385 Å. In addition to the two *Pi–Pi* interactions, one hydrogen bond was also formed between the backbone amino groups of ARG83 and carbonyl O atom of compound **4b** with the length of 2.09531 Å. This H-bonding between -C=O and ARG83 indicates that this group is vital for interaction with the receptor.

Molecular docking analysis for compound **3b** with COX-2 complex structure (3Q7D.pdb) (45) revealed the structural features that steer its inflammatory activity. As shown in the Figure 4, the 2D- and 3D images of the binding mode between compound **3b** and the target protein clearly demonstrated that it fits well into the active pocket of the COX-2 protein.

The binding of the most potent compound **3b** in the active pocket is due to different types of molecular interactions (Figure 4) discussed as follows. One *Cation–Pi* interaction

with the length of 3.79326 Å was displayed between the benzene ring of compound **3b** and the N atom of polar ARG120. The benzene ring of compound **3b** and the N atom of LEU93 presented another *Cation–Pi* interaction with the length of 2.60531 Å. Similar to compound **4b**, in addition to the two *Cation–Pi* interactions, one hydrogen bond was also formed between the backbone amino groups of TYR115 and carbonyl O atom of compound **3b** with the length of 2.10546 Å, signifying the importance of carbonyl group in deciding the interaction with the receptor. In addition, van der Waals forces and hydrophobic interactions enhance the interaction between the compound **3b** and the receptor.

In COX-2, the binding site is long, slender with the hydrophobic channel extending from the membrane-binding region of the protein. A second cavity branched off from the main channel that lead to the cyclooxygenase active site is observed in COX-2. A similar pocket also exists in COX-1, but it is small and less accessible due to the presence of bulkier isoleucine at position number 523. Therefore, a possible reason for the greater bending of **4b** in the active site of COX-1 compared to lesser bending of **3b** in the active site of COX-2 is relatively smaller size of active site of COX-1 than COX-2 (46).

Conclusions

In summary, a novel series of chalcones and chalcone-based pyrazolines was synthesized and assessed for their potential inhibitory activities against the sPLA$_2$-V, COX-1, COX-2 and release of pro-inflammatory cytokines including IL-6 and TNF-α. It was shown that trisubstituted-4,5-dihydro-pyrazole-1-carboxamide series with pyrazoline moiety was the most potent enzyme and cytokine inhibitors. Anti-inflammatory properties of these chalcones and pyrazoline derivatives as shown by the inhibition of enzymes and cytokines add further to the knowledge base of anti-inflammatory compounds. A number of the newly synthesized molecules in the present investigation could be further optimized and explored as lead molecules for developing novel and effective anti-inflammatory agents. Further studies which give insights into toxicity and *in vivo* anti-inflammatory activities are in progress for further understanding.

Conflict of Interest

The authors declare no competing financial interest.

References

1. Aitdafoun M., Mounier C., Heymans F., Binisti C., Bon C., Godfroid J.-J. (1996) 4-Alkoxybenzamidines as new potent phospholipase A2 inhibitors. Biochem Pharmacol;51:737–742.

2. Kurumbail R.G., Stevens A.M., Gierse J.K., McDonald J.J., Stegeman R.A., Pak J.Y., Gildehaus D., Miyashiro J.M., Penning T.D., Seibert K., Isakson P.C., Stallings W.C. (1996) Structural basis for selective inhibition of cyclooxygenase-2 by anti-inflammatory agents. Nature;384:644–648.

3. Marnett L.J. (2009) The COXIB experience: a look in the rearview mirror. Annu Rev Pharmacol Toxicol;49:265–290.

4. Kitamura T., Itoh M., Noda T., Matsuura M., Wakabayashi K. (2004) Combined effects of cyclooxygenase-1 and cyclooxygenase-2 selective inhibitors on intestinal tumorigenesis in adenomatous polyposis coli gene knockout mice. Int J Cancer;109:576–580.

5. Sano H., Noguchi T., Miyajima A., Hashimoto Y., Miyachi H. (2006) Anti-angiogenic activity of basic-type, selective cyclooxygenase (COX)-1 inhibitors. Bioorg Med Chem Lett;16:3068–3072.

6. Chakraborti A.K., Garg S.K., Kumar R., Motiwala H.F., Jadhavar P.S. (2010) Progress in COX-2 inhibitors: a journey so far. Curr Med Chem;17:1563–1593.

7. Singh P., Mittal A. (2008) Current status of COX-2 inhibitors. Mini Rev Med Chem;8:73–90.

8. Langford R.M., Mehta V. (2006) Selective cyclooxygenase inhibition: its role in pain and anaesthesia. Biomed Pharmacother;60:323–328.

9. Eberhart C.E., Coffey R.J., Radhika A., Giardiello F.M., Ferrenbach S., DuBois R.N. (1994) Up-regulation of cyclooxygenase 2 gene expression in human colorectal adenomas and adenocarcinomas. Gastroenterology;107:1183–1188.

10. Dannenberg A.J., Lippman S.M., Mann J.R., Subbaramaiah K., DuBois R.N. (2005) Cyclooxygenase-2 and epidermal growth factor receptor: pharmacologic targets for chemoprevention. J Clin Oncol;23:254–266.

11. Yang H., Gu J., Lin X., Grossman H.B., Ye Y., Dinney C.P., Wu X. (2008) Profiling of genetic variations in inflammation pathway genes in relation to bladder cancer predisposition. Clin Cancer Res;14:2236–2244.

12. McInnes I.B., Schett G. (2007) Cytokines in the pathogenesis of rheumatoid arthritis. Nat Rev Immunol;7:429–442.

13. Esch T., Stefano G. (2002) Proinflammation: a common denominator or initiator of different pathophysiological disease processes. Med Sci Monit;8:HY1–HY9.

14. Dinarello C.A. (1991) Inflammatory cytokines: interleukin-1 and tumor necrosis factor as effector molecules in autoimmune diseases. Curr Opin Immunol;3:941–948.

15. Arend W.P., Dayer J.-M. (1990) Cytokines and cytokine inhibitors or antagonists in rheumatoid arthritis. Arthritis Rheum;33:305–315.

16. Dayer J.-M., Demczuk S. (1984) Cytokines and other mediators in rheumatoid arthritis. Springer Semin Immunopathol;7:387–413.

17. Barnes P.J., Chung K.F., Page C.P. (1998) Inflammatory mediators of asthma: an update. Pharmacol Rev;50:515–596.

18. Loyau G., Pujol J.P. (1990) The role of cytokines in the development of osteoarthritis. Scand J Rheumatol Suppl;81:8–12.

19. Kirkham B. (1991) Interleukin-1, immune activation pathways, and different mechanisms in osteoarthritis and rheumatoid arthritis. Ann Rheum Dis;50:395–400.

20. Nickoloff B.J. (1999) The immunologic and genetic basis of psoriasis. Arch Dermatol;135:1104–1110.

21. Saklatvala J., Davis W., Guesdon F. (1996) Interleukin 1 (IL1) and tumour necrosis factor (TNF) signal transduction. Philos Trans R Soc Lond B Biol Sci;351:151–157.

22. Sacca R., Cuff C.A., Ruddle N.H. (1997) Mediators of inflammation. Curr Opin Immunol;9:851–857.

23. Matsui T., Kondo T., Nishita Y., Itadani S., Nakatani S., Omawari N., Sakai M. et al. (2002) Highly potent inhibitors of TNF-alpha production. Part I: discovery of new chemical leads and their structure-activity relationships. Bioorg Med Chem;10:3757–3786.

24. Kim K.J., Lee J.S., Kwak M.K., Choi H.G., Yong C.S., Kim J.A., Lee Y.R., Lyoo W.S., Park Y.J. (2009) Anti-inflammatory action of mollugin and its synthetic derivatives in HT-29 human colonic epithelial cells is mediated through inhibition of NF-kappaB activation. Eur J Pharmacol;622:52–57.

25. Esposito E., Cuzzocrea S. (2009) TNF-alpha as a therapeutic target in inflammatory diseases, ischemia-reperfusion injury and trauma. Curr Med Chem;16:3152–3167.

26. Mendis E., Kim M.M., Rajapakse N., Kim S.K. (2008) Suppression of cytokine production in lipopolysaccharide-stimulated mouse macrophages by novel cationic glucosamine derivative involves down-regulation of NF-kappaB and MAPK expressions. Bioorg Med Chem;16:8390–8396.

27. Bukhari S.N., Jasamai M., Jantan I. (2012) Synthesis and biological evaluation of chalcone derivatives (mini review). Mini Rev Med Chem;12:1394–1403.

28. Bukhari S.N., Jantan I., Jasamai M. (2013a) Anti-inflammatory trends of 1, 3-diphenyl-2-propen-1-one derivatives. Mini Rev Med Chem;13:87–94.

29. Gómez-Rivera A., Aguilar-Mariscal H., Romero-Ceronio N., Roa-de la Fuente L.F., Lobato-García C.E. (2013) Synthesis and anti-inflammatory activity of three nitro chalcones. Bioorg Med Chem Lett;23:5519–5522.

30. Bandgar B.P., Gawande S.S., Bodade R.G., Totre J.V., Khobragade C.N. (2010) Synthesis and biological evaluation of simple methoxylated chalcones as anti-cancer, anti-inflammatory and antioxidant agents. Bioorg Med Chem;18:1364–1370.

31. Kil J.S., Son Y., Cheong Y.K., Kim N.H., Jeong H.J., Kwon J.W., Lee E.J., Kwon T.O., Chung H.T., Pae H.O. (2012) Okanin, a chalcone found in the genus Bidens, and 3-penten-2-one inhibit inducible nitric oxide synthase expression via heme oxygenase-1 induction in RAW264.7 macrophages activated with lipopolysaccharide. J Clin Biochem Nutr;50:53–58.

32. Ramesh B., Sumana T. (2010) Synthesis and anti-inflammatory activity of pyrazolines. J Chem;7:514–516.

33. Bukhari S.N.A., Tajuddin Y., Benedict V.J., Lam K.W., Jantan I., Jalil J., Jasamai M. (2014) Synthesis and evaluation of chalcone derivatives as inhibitors of neutrophils' chemotaxis, phagocytosis and production of reactive oxygen species. Chem Biol Drug Des;83:198–206.

34. Ahmad W., Kumolosasi E., Jantan I., Bukhari S.N., Jasamai M. (2014) Effects of novel diarylpentanoid analogues of curcumin on secretory phospholipase A, cyclooxygenases, lipoxygenase and microsomal prostaglandin E synthase-1. Chem Biol Drug Des; 83:670–681.

35. Bukhari S.N., Jantan I., Wai L.K., Lajis N.H., Abbas F., Jasamai M. (2013b) Synthesis and effects of pyrazolines and isoxazoles on the phagocytic chemotaxis and release of reactive oxygen species by zymosan stimulated human neutrophils. Med Chem;9:1091–1098.

36. Ellman G.L., Courtney K.D., Andres V. Jr, Featherstone R.M. (1961) A new and rapid colorimetric determination of acetylcholinesterase activity. Biochem Pharmacol;7:88–95.

37. Blobaum A.L., Marnett L.J. (2007) Structural and functional basis of cyclooxygenase inhibition. J Med Chem;50:1425–1441.

38. Kim H.P., Son K.H., Chang H.W., Kang S.S. (2004) Anti-inflammatory plant flavonoids and cellular action mechanisms. J Pharmacol Sci;96:229–245.

39. Wang Y., Xu W., Shao H., Xie Y., Wang J. (2011) Design and synthesis of novel pyrazole-based Lp-PLA2 inhibitors. Chin J Chem;29:2039–2048.

40. Seibert K., Zhang Y., Leahy K., Hauser S., Masferrer J., Perkins W., Lee L., Isakson P. (1994) Pharmacological and biochemical demonstration of the role of cyclooxygenase 2 in inflammation and pain. Proc Natl Acad Sci USA;91:12013–12017.

41. Willingale H.L., Gardiner N.J., McLymont N., Giblett S., Grubb B.D. (1997) Prostanoids synthesized by cyclooxygenase isoforms in rat spinal cord and their contribution to the development of neuronal hyperexcitability. Br J Pharmacol;122:1593–1604.

42. Stoll L.L., Denning G.M., Weintraub N.L. (2006) Endotoxin, TLR4 signaling and vascular inflammation: potential therapeutic targets in cardiovascular disease. Curr Pharm Des;12:4229–4245.

43. Daukshas V.K., Gaidyalis P.G., Udrenaite É.B., Pyatrauskas O.Y., Brukshtus A.B. (1985) Synthesis and antiinflammatory activity of 6-acylsubstituted benzo-1,4-dioxanes and dihydrobenzopyrans. Pharm Chem J;19:611–614.

44. Tsai W.-J., Shiao Y.-J., Lin S.-J., Chiou W.-F., Lin L.-C., Yang T.-H., Teng C.-M., Wu T.-S., Yang L.-M. (2006) Selective COX-2 inhibitors. Part 1: synthesis and biological evaluation of phenylazobenzenesulfonamides. Bioorg Med Chem Lett;16:4440–4443.

45. Selinsky B.S., Gupta K., Sharkey C.T., Loll P.J. (2001) Structural analysis of NSAID binding by prostaglandin H2 synthase: time-dependent and time-independent inhibitors elicit identical enzyme conformations. Biochemistry;40:5172–5180.

46. Chavan H.V., Bandgar B.P., Adsul L.K., Dhakane V.D., Bhale P.S., Thakare V.N., Masand V. (2013) Design, synthesis, characterization and anti-inflammatory evaluation of novel pyrazole amalgamated flavones. Bioorg Med Chem Lett;23:1315–1321.